

Springer Proceedings in Energy

Paolo Bertoldi *Editor*

Energy Efficiency in Motor Systems

Proceedings of the 11th international
Conference EEMODS'19

 Springer

Springer Proceedings in Energy

The series Springer Proceedings in Energy covers a broad range of multidisciplinary subjects in those research fields closely related to present and future forms of energy as a resource for human societies. Typically based on material presented at conferences, workshops and similar scientific meetings, volumes published in this series will constitute comprehensive state-of-the-art references on energy-related science and technology studies. The subjects of these conferences will fall typically within these broad categories:

- Energy Efficiency
- Fossil Fuels
- Nuclear Energy
- Policy, Economics, Management & Transport
- Renewable and Green Energy
- Systems, Storage and Harvesting
- Materials for Energy

eBook Volumes in the Springer Proceedings in Energy will be available online in the world's most extensive eBook collection, as part of the Springer Energy eBook Collection. Please send your proposals/inquiry to Dr. Loyola DSilva, Senior Publishing Editor, Springer (loyola.dsilva@springer.com)

More information about this series at <http://www.springer.com/series/13370>

Paolo Bertoldi
Editor

Energy Efficiency in Motor Systems

Proceedings of the 11th international
Conference EEMODS'19

 Springer

Editor

Paolo Bertoldi
European Commission Joint Research Centre
Institute for Energy, Transport and Climate
Ispra, Varese, Italy

ISSN 2352-2534

ISSN 2352-2542 (electronic)

Springer Proceedings in Energy

ISBN 978-3-030-69798-3

ISBN 978-3-030-69799-0 (eBook)

<https://doi.org/10.1007/978-3-030-69799-0>

© The Editor(s) (if applicable) and The Author(s), under exclusive license to Springer Nature Switzerland AG 2021

This work is subject to copyright. All rights are solely and exclusively licensed by the Publisher, whether the whole or part of the material is concerned, specifically the rights of translation, reprinting, reuse of illustrations, recitation, broadcasting, reproduction on microfilms or in any other physical way, and transmission or information storage and retrieval, electronic adaptation, computer software, or by similar or dissimilar methodology now known or hereafter developed.

The use of general descriptive names, registered names, trademarks, service marks, etc. in this publication does not imply, even in the absence of a specific statement, that such names are exempt from the relevant protective laws and regulations and therefore free for general use.

The publisher, the authors, and the editors are safe to assume that the advice and information in this book are believed to be true and accurate at the date of publication. Neither the publisher nor the authors or the editors give a warranty, expressed or implied, with respect to the material contained herein or for any errors or omissions that may have been made. The publisher remains neutral with regard to jurisdictional claims in published maps and institutional affiliations.

This Springer imprint is published by the registered company Springer Nature Switzerland AG
The registered company address is: Gewerbestrasse 11, 6330 Cham, Switzerland

Introduction

This book contains selected, peer-reviewed papers presented at the 11th International Conference on Energy Efficiency in Motor Systems (EEMODS' 19) held in Tokyo, Japan, from 17 to 19 September 2019.

Energy efficiency helps to mitigate CO₂ emissions and at the same time increase the security of energy supply. This is why energy efficiency is a key priority of the EU energy policy and of the latest flagship initiative, the Energy Union. At the COP 21 meeting in Paris in 2015, countries have agreed to mitigate the impact of climate change by limiting the global temperature increase to well below 2 °C above to the pre-industrial levels and possibly stabilizing the temperature increase to 1.5 °C. Energy efficiency is a key mitigation option and it is recognized as the cleanest, quickest, and cheapest energy source.

Not only this, but energy efficiency brings several additional benefits for end users, such as lower energy costs, more reliable equipment, higher production quality, and reduced emissions.

However, in some sectors such as the industrial sector, there are still a lot of barriers against investments in energy efficiency, particularly in small and medium Enterprises. Recent European legislation under the Eco-design and Energy Efficiency Directives is trying to remove these barriers and foster investments in energy efficiency; this is complemented by innovative financing for energy efficiency, the provision of energy services by ESCOs, and national programmes.

Similar policy initiatives are also implemented in other countries around the world: Japan, USA, China, India, Australia, and Brazil.

At the same, time progress in motor technologies as well as in drives and end-use equipment offers a very high level of efficiency, for example, IE 4 class motors now available on the market.

EEMODS is the only international conference dedicated to energy efficiency in motor-driven systems. EEMODS began in 1996 in Lisbon, the last edition was organized in Rome in 2017, and in 2019, the 11th edition was hosted in Tokyo, Japan.

The conference is equally balanced between highly scientific and technical presentations on innovative motor systems component designs and test methods to achieve a high level of efficiency and more policy-oriented presentations dedicated

to how to diffuse efficient motor systems solutions and technologies in existing industrial plants. The conference topics on the technology side cover motors and fluid applications (pumps, fans, and compressors), while on the policy side they cover both regulation for equipment and more horizontal policies such as energy audits and energy management systems.

As with previous conferences in this series, EEMODS'19 provided a scientific forum to discuss and debate the latest developments in the impacts of electrical motor systems on energy and the environment, energy efficiency policies and programmes adopted and planned, standards (including ISO 50.001), and the technical and commercial advances made in the dissemination and penetration of energy-efficient motor systems. Topics covered include: technologies, research, and innovation in the areas of electric motors from life cycle costing to 3D printing to artificial intelligence/machine learning-based monitoring systems; emerging motor technologies; power electronics and drives; pump systems, including life cycle costing, energy efficiency improvements, maintenance, and operation for industrial, water supply and treatment, building, and irrigation pumps; compressed air systems; fans/exhaust systems; refrigeration systems maintenance and operation; mechanical power transmission; motors in household appliances and HVAC (residential and commercial); motors and drives for transport applications including policies, programmes, regulation, and international standards; industrial management policies and standards; motor system audit and verification; policies, programmes, and financing; analysis of motor system energy use and greenhouse gas emissions for motor systems, for e-vehicles, and related charging infrastructure; harmonization of global motor efficiency test standards; evaluation of utility programmes for improving energy efficiency in motor systems; and policy implementation, market surveillance, and enforcement mechanisms, including case studies. The conference is very international by nature and aims to attract high-quality and innovative contributions from all corners of the globe, while the papers facilitate the development of new technologies, policies, and strategies to increase energy efficiency.

Contents

Novel Design of Delta-Connected PM Synchronous Machines Considering Rotor Skewing	1
Juergen Redlich, Anton Suchan, and Bernd Ponick	
EC-Motors in a Fan Application: A Case Study	15
Kurt Stockman, Jasper De Viaene, Steve Dereyne, and Pieter Defreyne	
A Global Update on the Markets for Motors, Drives, and Motor-Driven Equipment	29
Preston Reine	
Increasing the Energy Savings of Motor Applications: The Extended Product Approach	37
Benno Weis, Benoit Leprettre, Martial Patra, Norbert Hanigovszki, Preben Holm, Tim Schuman, Michael Könen, Niels Bidstrup, and Kirk Anderson	
High-Efficiency IE4 Line-Start Synchronous Reluctance Motors	53
Francesco Parasiliti and Marco Villani	
Coordination of IEC and ISO Standards for Energy-Efficient Electric Motor-Driven Systems	67
Conrad U. Brunner, Maarten van Werkhoven, Franco Bua, and Kirk Anderson	
Surface Eddy Current Suppression on Additively Manufactured Solid Rotor Active Parts	81
Max Hullmann, Stefan Urbanek, and Bernd Ponick	
Energy Scorecard: One of the Key Executions to Transform the Market for Energy-Efficient Motors	97
Hakan Gedik	

A Novel Approach to Predict Reed Critical Frequency of Vertical Motors	103
Ravi Musinana and Harendra Singh	
Evaluation of High-Tech Electrical Steel in a High-Speed Permanent Magnet Synchronous Machine for an Aircraft Application ..	119
Mina Mirzadeh, Gerrit Narjes, and Bernd Ponick	
New Life Calculation Model for Hybrid Bearings	131
Author Magnus Arvidsson	
Programme for In-Depth Analyses of Electric Motor Systems in Industry (ProAnalySys)	147
Richard Phillips	
A Review of the United States Process for Developing MEPS, the Benefits, and How Other Economic Regions Could Benefit from Adopting Similar Approaches	165
Kirk Anderson and Rob Boteler	
Electromagnetic Design of Propulsion Motors with Superconducting Field Coils for Electrified Aircraft	175
Yusuke Ishida, Yutaka Terao, and Hiroyuki Ohsaki	
Design Methodology for a PM Electrical Variable Transmission Used in HEV	187
Florian Verbelen, Hendrik Vansompel, Ahmed Abdallah, Kurt Stockman, and Peter Sergeant	
IE3 Efficiency Class as MEPS for Industrial Motor: How Brazil Got There	203
George Alves Soares and Carlos Aparecido Ferreira	
A Decision-Making Tool Incorporating Multiple Benefits of Motor Systems' Retrofits	215
Rita Werle, Rolf Tieben, Petar Klingel, Andreas Rothen, Lea Fleischli, Victoria Pyatova, Shaun West, Kurt Ackermann, and Richard Phillips	
European Ecodesign Material Efficiency Standardization Overview for Circular Economy Aspects in Motor and Power Drive Systems	231
Martial Patra	
Comparison Between the Use of the Middle Ring and/or Skewed Bars in Induction Motor Rotor	243
Marcelo Dias da Silva, Daniel Schmitz, Carlos Manuel de Araújo Sá, Bruno Baptista, and Sebastião Lauro Nau	
Efficiency Measurement Strategy for a Planetary Gearbox with 2 Degrees of Freedom	257
Florian Verbelen, Pieter Defreyne, Peter Sergeant, and Kurt Stockman	

Development of High-Precision Efficiency Measuring Device for High Power Motor Drive Systems 271
 Masayuki Harano, Hiroki Kobayashi, Chiaki Yamaura, Kenta Ikeda, Koki Nakazawa, and Shozo Yoda

Evaluation and Application of Existing Air Curtain Effectiveness Methodology 285
 Liangzhu (Leon) Wang, David A. Johnson, and Frank Cuaderno

Promoting CO₂ Water Source Heat Pumps in Indian Industrial Sector 335
 Abdessalem Rabhi and Ananda Mohan Ghosh

Refrigeration Systems: Optimal Temperature Setpoint Regarding Air Mixing in a HVAC-R System 349
 Jérôme Jeanclos, Kamal Ejjabraoui, and François Malrait

Modeling of Radial and Tangential Roebel Bar Force Distributions in Large Electrical Machines Considering Longitudinal Transposition 367
 Amir Ebrahimi and Marius Meiswinkel

NH₃-CO₂ Brine System for Refrigeration at Cold Storages and Seafood Processing Plants in India 383
 Abdessalem Rabhi and Rudhi Sundar Pradhan

Semi-analytical Calculation of Field and Loss Distribution in the Tooth Tips of Electrical Machines. 395
 Alexander Rehfeldt, Torben Fricke, Babette Schwarz, Amir Ebrahimi, and Bernd Ponick

The Effect of Top Runner Motor (IE3) Regulation in Japan 405
 Takeshi Obata

The Market of Electric Motors, Pumps and Fans in the European Union and in Switzerland. 417
 Rita Werle, Conrad U. Brunner, Rolf Tieben, Petar Klingel, and Richard Phillips

Pilot Audit Program for Electric Motor-Driven Systems 431
 Maarten van Werkhoven and Frank Hartkamp

Operation Analysis of an Integrated Linear Flux Modulating Motor for a Direct-Driven Belt Conveyor. 439
 Alexander Hoffmann, Malte Kanus, Ludger Overmeyer, and Bernd Ponick

Performance of Copper Rotor Motor in High-Speed Applications 449
 Dong Liang, Sheng Zhou, Datong Yang, and Xu Yang

Development and Loss Evaluation of High-Speed PM Synchronous Machine	457
Mototsugu Omura, Sho Uchiyama, Keisuke Matsuo, Takashi Okitsu, Takayuki Mizuno, Koji Yamada, and Kouki Matsuse	
Regulation and Enforcement [Surveillance] Consequences	479
Rob Boteler and Kirk Anderson	
Strategies to Promote Energy-Efficient Compressed Air Systems Among Indian Companies	491
Aditi Khodke, Toshizo Maeda, Girish Sethi, and Mika Tachibana	
Transformation Program for Low-Efficiency Electric Motors and Market Surveillance Activities in Turkey	503
Mevlüt Hürol Mete	
The Public Energy Efficiency Policies Mapped and Implemented for the Industrial Motor Reconditioning Sector in Brazil.	525
Rodrigo Santos Vieira, George Alves Soares, Rodrigo Flora Calili, Glycon Garcia Junior, Reinaldo Castro Souza, and Carlos Aparecido Ferreira	
Self-Assessment Tool for the Estimation of the Savings Potential of Electric Motor Systems	537
Richard Phillips, Yannick Riesen, and Nicolas Macabrey	
Labelling of Air Compressors – Much More Than Nameplate Data	555
Peter Radgen	
Theoretical and Experimental Evaluation of Compressed Air Leakages	569
Manuel Unger and Peter Radgen	
Digitalization in Electric Motor-Driven Systems	583
Maarten van Werkhoven and Konstantin Kulterer	
Calorimetric Efficiency Determination of Power Electronic Variable Speed Drives.	595
Stan Caron, Arne Berteyn, Pieter Defreyne, Steve Dereyne, and Kurt Stockman	
Round Robin for Converter Losses: Uniform Testing Protocol and Results from Tests in Phase 1	611
Conrad U. Brunner, Emmanuel Agamloh, Andrew Baghurst, Sandie B. Nielsen, and Andrea Vezzini	
Preliminary Results from RR’C 2: Round Robin for Converter Losses, Phase 2	623
Andrea Vezzini and Sandie B. Nielsen	

Embedded Estimation of Variable Speed Drive Input Current Distortion 633
 Thomas Devos and François Malrait

Comparison of Fixed and Variable Speed Pumps Under Consideration of Manufacturer and Operator Aspects 649
 Sebastian Bold, Vincent Becker, Sven Urschel, and Jochen Schaab

New Composite Containment Shell for Magnetically Driven Pumps 665
 Nicolas Weibel, Samuel Stutz, Daniel Rougnon, and Frederic Perrottet

Hydraulic System Optimization 677
 Sandie B. Nielsen, Claus M. Hvenegaard, Otto Paulsen, and Søren Draborg

Comparison of Different Methods to Determine the Per-Phase Equivalent Circuit Parameters of Three-Phase Induction Motors Using IEC Nameplate and Catalogue Data 693
 Fernando J. T. E. Ferreira, André M. Silva, and Edson Bortoni

Experimental Study on Three-Phase Induction Motor Performance Under Supply Voltage Unbalance for Star and Delta Connections 707
 Fernando J. T. E. Ferreira, José Alberto, Edson Bortoni, and A. T. De Almeida

Conserving Energy in Compressed Air System: Practical Case Studies from Indian Industry 719
 Padmanabh Nagarkar and Prosanto Pal

Optimizing Pump and Compressor Selection for Energy Efficiency Using True-Weighted Efficiency (TWE) 741
 Trygve Dahl

Novel Design of Delta-Connected PM Synchronous Machines Considering Rotor Skewing



Juergen Redlich, Anton Suchan, and Bernd Ponick

1 Introduction

Nowadays, permanent magnet synchronous machines (PSM) for traction applications are predominantly designed with star-connected windings without neutral connection, in order to avoid additional losses as well as parasitic effects through circulating currents. Due to the increasing market share of electric vehicles, a variable modular system of electrical machines (EM) must be ensured, in order to reduce the manufacturing costs and to meet the performance requirements. Apart from the Y-connection, it is possible to use delta-connected windings to extend the operating range of an EM with a predefined cross-section.

The major drawbacks of delta-connected windings are circulating currents, which are generated in three-phase windings by the third and ninth spatial harmonics of the flux density. These harmonics have their origin either from the spatial distribution of the permanent magnets or from saturation of the stator core [1, 2]. Several methods have been proposed to reduce these harmonics [3, 4]. However, most of them are not applicable in traction applications. For example, it is claimed in [3] that a rotor with two-third pole magnet coverage will reduce the third spatial harmonic, which is obvious by the spatial distribution of the air-gap field

$$\hat{B}_{\nu'} = \frac{2\hat{B}_p}{\pi\nu'} \left[\cos(\nu'\alpha) - \cos\left(\frac{\nu'}{p}\pi - \nu'\alpha\right) \right] \quad (1)$$

with $\hat{B}_{\nu'}$ as the amplitude of the flux density of the spatial harmonic ν' and α as the pole coverage angle. To ensure $\hat{B}_{3p} \oplus 0$, α must be chosen to $\pi/6p$, which results in

J. Redlich (✉) · A. Suchan · B. Ponick
Leibniz University Hannover, Hannover, Germany
e-mail: juergen.redlich@ial.uni-hannover.de; ponick@ial.uni-hannover.de

a two-third pole magnet coverage. But this will lead to a decreased spatial fundamental of the flux density in the air-gap and to increased fifth and seventh harmonics, consequently causing undesirable high torque pulsations. In [4], it is shown that the third and ninth spatial harmonics of the flux density can also be decreased by applying a skewing angle of 120° . Nevertheless, this results in a significant reduction of the winding factor for the spatial fundamental of the flux density. The rotor design proposed in this chapter maintains a high spatial fundamental of the flux density while reducing all higher harmonics through an optimal design of coverage angle and flux barriers. Therefore, it is suitable for both, star- and delta-connected windings. Second, a calculation method will be presented to calculate skewed rotors analytically with negligible additional computational effort. Moreover, a suitable stator design considering the circulating current in delta connection due to saturation effects will be discussed. Finally, the attainable efficiency in the operating range will be evaluated.

2 Design Guidelines for PM Rotors

Based on the available installation space and the maximum permissible circumferential velocity, the initial design process of a PM rotor usually starts with the decision of how to arrange the magnets in the rotor. Several studies on PSM have been made to examine various design options and the machine behavior in the whole operating range [5, 6]. With regard to traction applications, this chapter focuses on v-shaped buried magnets within the rotor with one and two magnet layers, as these magnet topologies provide a good utilization of the reluctance torque and a suitable field-weakening behavior.

A rotor with v-shaped buried magnets, which completely avoid those harmonics whose orders are equal to a multiple of the number of phases, is practically not realizable. When dimensioning the rotor, it is assumed that the arising circulating current within the delta connection depends mainly on the third and ninth spatial harmonics of the air-gap field. For this reason, all design options of the rotor focus on minimizing these field components, while maintaining a high fundamental of the flux density and limited fifth and seventh harmonics. First of all, the magnet topology with two layers for a machine with a number of pole pairs of $p = 4$ is dimensioned. With regard to the simplified form of the air-gap field (Fig. 1), the calculation of the field distribution can be described by four parameters, where \hat{B}_1 is the flux density of the bottom magnet layer, \hat{B}_2 the flux density of the top layer, α the pole coverage angle of the bottom layer, and β the pole coverage angle of the top layer. The amplitude of a spatial harmonic of the order ν can be calculated by

$$\hat{B}_{\nu} = \frac{4p}{\pi\nu} \left[\hat{B}_1 \cos(\nu'\alpha) + \hat{B}_2 \cos(\nu'\beta) - (\hat{B}_1 + \hat{B}_2) \cos\left(\frac{\nu'\pi}{p}\right) \right]. \quad (2)$$

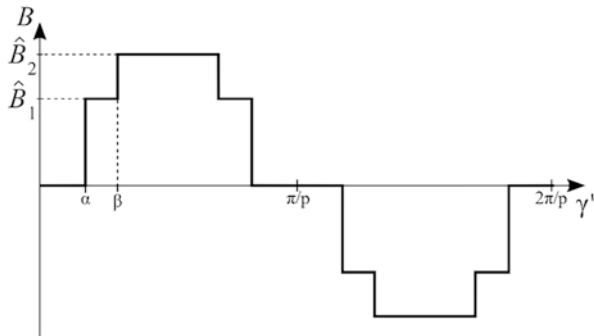


Fig. 1 Simplified form of the air-gap field considering v-shaped buried magnets with two magnet layers

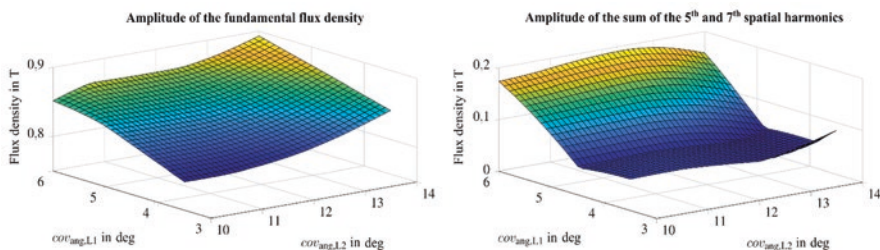


Fig. 2 Influence of the variation of the pole magnet coverage angle of the top magnet layer $\text{cov}_{\text{ang},L1}$ and the bottom magnet layer $\text{cov}_{\text{ang},L2}$ on the fundamental flux density, the fifth and the seventh spatial harmonics

Since there is no combination of the four parameters leading to $\hat{B}_{3p} \oplus 0$ and $\hat{B}_{9p} \oplus 0$, except for $\hat{B}_1 + \hat{B}_2$, the pole magnet coverage angle is firstly varied to decrease \hat{B}_{5p} and \hat{B}_{7p} (see Fig. 2) at a specified magnet height and width. As can be seen in Fig. 2, the magnet angle of the top layer has only a slight influence on the sum of \hat{B}_{5p} and \hat{B}_{7p} , whereas a reduction of the magnet angle of the bottom layer strongly affects these field shares. The drawback of the decreased fifth and seventh harmonics is a reduced fundamental flux density. Nevertheless, the coverage angles are set at the calculated minimum of $\hat{B}_{5p} + \hat{B}_{7p}$, at a value of $\text{cov}_{\text{ang},L1} = 4, 7^\circ$ and $\text{cov}_{\text{ang},L2} = 13, 6^\circ$, whereby the fundamental of the air-gap field has an amplitude of $\hat{B}_p = 0.82$ T.

In addition, choosing coverage angles which reduce the fifth and seventh spatial harmonics also affects the amplitudes of the third and ninth harmonics (see Table 1). The sum of the amplitudes of \hat{B}_{3p} and \hat{B}_{9p} is almost one-third of the fundamental. Regarding the resulting flux densities in Table. 1, it becomes obvious that the choice of a magnetic angle that limits the fifth and seventh spatial harmonics has an opposite effect on the spatial harmonics $3p$ and $9p$.

Table 1 Fundamental, third, fifth, seventh, and ninth spatial harmonics of the permanent magnet rotor with two magnet layers and optimized magnetic coverage angle for decreasing the fifth and seventh harmonics

Flux density	Amplitude	\hat{B}_v / B_p
\hat{B}_p	0.81 T	
\hat{B}_{3p}	0.0642 T	7.96%
\hat{B}_{5p}	0.0017 T	0.21%
\hat{B}_{7p}	0.0347 T	4.30%
\hat{B}_{9p}	0.1445 T	17.91%

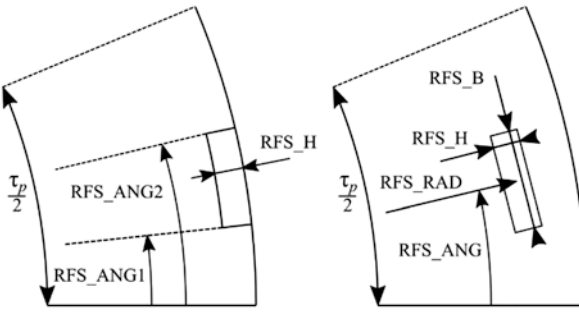


Fig. 3 Flux barriers to reduce the third and ninth spatial harmonics

When dimensioning PSM as traction motors with delta-connected windings, in addition to the reduction of the fifth and seventh harmonics, it is also essential to reduce the circulating current in order to obtain a good efficiency in the driving cycle. For this purpose, in the second step, flux barriers are used and arranged exactly at the peak value of the third spatial harmonic. The flux barriers may be applied in the rotor or on the surface of the rotor as shown in Fig. 3.

The chosen angles of $RFS_{ang,1}$ and $RFS_{ang,2}$ must be set to 7.5° and 15° , when choosing a number of pole pairs of $p = 4$. The height and width of the flux barriers is determined by a parameter study (see Fig. 4).

As a consequence, the third and the ninth spatial harmonics amplitudes can be significantly decreased, while the fundamental and the other harmonics remain unchanged (see Table 2). Considering the described design rules, it is possible to dimension PM rotors for traction applications, which are suitable for both, star- and delta-connected windings. Besides the distribution of the spatial harmonics of rotor designs with two magnet layers and flux barriers within the rotor and on the surface, Table 2 shows the distribution of harmonics of the design with one magnet layer. In contrast to the rotor design with two magnet layers, the choice of the coverage angle is only based on reducing the field shares of the third and ninth harmonics. The above mentioned opposite effect on the spatial harmonics can also be seen here.

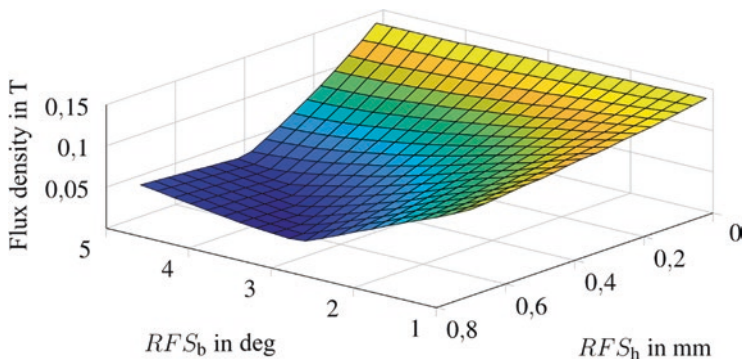


Fig. 4 Amplitudes of the sum of the third and ninth spatial harmonic at the variation of the height and width of the flux barriers

Table 2 Amplitudes of the spatial harmonics of the air-gap field of the three designed PM rotors

Rotor	\hat{B}_p	\hat{B}_{3p} / \hat{B}_p	\hat{B}_{5p} / \hat{B}_p	\hat{B}_{7p} / \hat{B}_p	\hat{B}_{9p} / \hat{B}_p
1 Magnet layer	0.82 T	0.33%	18.6%	12.7%	0.51%
2 Magnet layers with flux barriers on the surface	0.82 T	0.06%	8.01%	3.73%	1.93%
2 Magnet layers with flux barriers in the rotor	0.82 T	0.01%	8.38%	4.35%	2.38%

3 Rotor Skewing

In the design of an electrical machine (EM) for traction applications, particular attention has to be paid to decrease unwanted effects like torque ripple, vibrations, and acoustic noise. For this purpose, the PM rotor is segmented into several slices, which are shifted against each other to unlink certain spatial harmonics of the air-gap flux with the windings of the machine [7, 8]. Especially, if applying a discrete skew of the PM rotor with a skewing angle of one stator slot division, the torque harmonics due to slotting can be damped. By considering rotor skewing, the computational effort increases proportional to the number of skew segments. For evaluating the efficiency of a skewed EM as traction motor, in general, efficiency maps are used, which are calculated in the dq-current plane by 2D-FEA for every slice. The method presented in this chapter allows accounting for skewed machines with negligible additional effort. Instead of FEM calculations of several rotor slices in the whole operating range, just one slice needs to be calculated by FEM.

First of all, the number of segments, the skew angle, and the type of skewing (see Fig. 5) have to be selected. As an example, a linear skew of five segments will be derived in the following. By skewing the rotor of one stator slot division, for a machine with 48 slots and four pole pairs, the rotor segments are shifted to $\varphi_{\text{skew, mech}} = [-3^\circ \mid -1.5^\circ \mid 0^\circ \mid 1.5^\circ \mid 3^\circ]$.

Based on the torque, flux linkages, inductances, etc., calculated by FEM in the dq-current plane for the rotor segment with $\varphi_{\text{skew, mech}} = 0^\circ$, all additional d- and

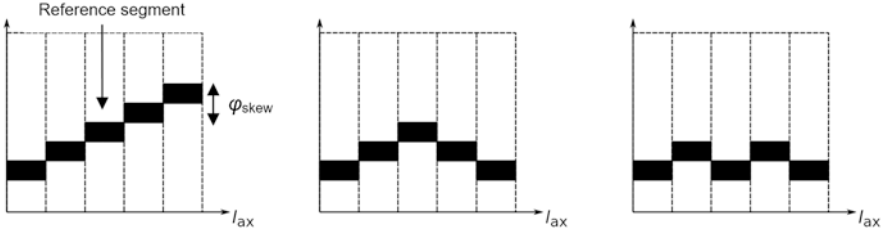


Fig. 5 Schematic drawing of a linearly skewed (left), v-skewed (middle), and w-skewed (right) rotor with five segments

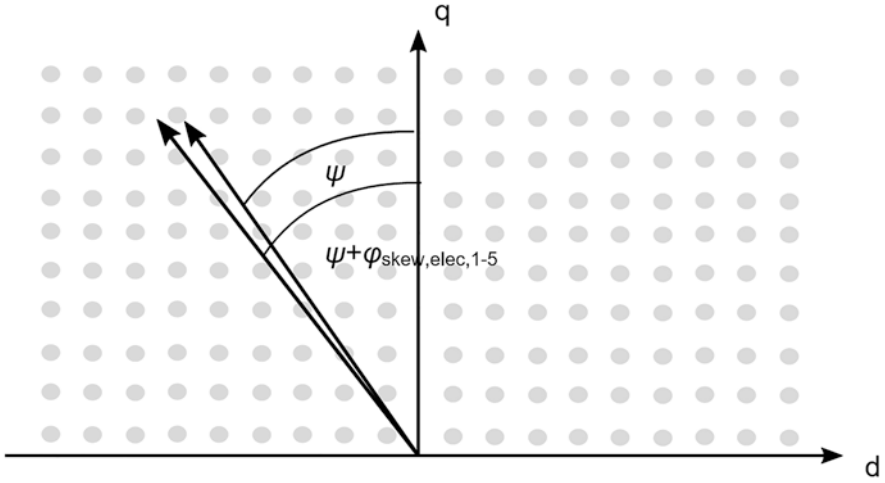


Fig. 6 Identified stator currents in the dq-current plane with the corresponding inner phase angle Ψ and the additional skew angle φ

q-currents matrices for each slice are first identified by adding the skew angle $\varphi_{\text{skew,elec}} = p \cdot \varphi_{\text{skew,mech}}$ in dependence of the slice to the initial inner phase angle Ψ of the reference segment (see Fig. 6) as per

$$\Psi = \arctan\left(\frac{I_d}{I_q}\right); \quad \Psi_{\text{new}} = \Psi + \varphi_{\text{skew,elec,1-5}}, \quad (3)$$

$$\hat{I}_1 = \sqrt{I_d^2 + I_q^2}, \quad (4)$$

$$I_{d,\text{Mat,1-5}} = \hat{I}_1 \cdot \sin(\Psi_{\text{new,1-5}}), \quad (5)$$

$$I_{q,\text{Mat,1-5}} = \hat{I}_1 \cdot \cos(\Psi_{\text{new,1-5}}). \quad (6)$$

As a consequence, four new matrices are created with corresponding d- and q-current components, whereby it should be noted that some current components may result in positive d-currents, which also have to be considered in the calculation. Operating points with negative q-currents can be created by negating the values of the second quadrant of the dq-current plane. With the additional information of the current components and the correct superimposition of every skewed segment, it is possible to calculate the resulting torque, etc. through a *spline* interpolation from the values of the reference segment.

Figure 7 shows the calculated resulting torque for a single d- and q-current component due to rotor skewing. As mentioned above, the torque ripple is significantly reduced. However, the maximum torque is also decreased about 2.5% from $T_{\text{unskewed}} = 286.5 \text{ Nm}$ to $T_{\text{skewed, FEM}} = 279.2 \text{ Nm}$ and $T_{\text{skewed, analyt}} = 279.1 \text{ Nm}$, respectively. With such simple matrix operations, it is possible to consider skewed EM with a sufficient accuracy by identifying only one slice via FEM.

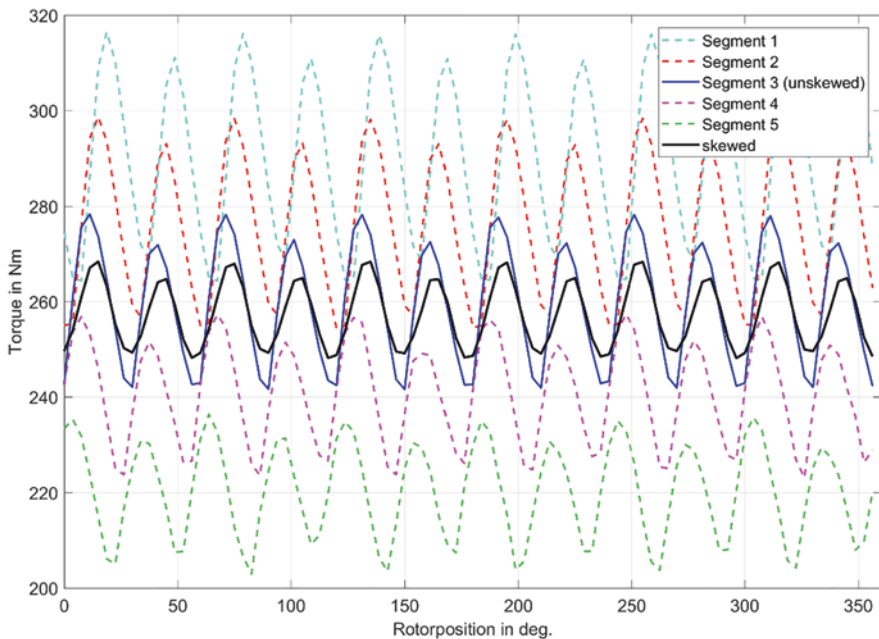


Fig. 7 Calculated torques of each segment for a single d-current and q-current component; the superimposed torque through skewing (black) in comparison to the torque of the unskewed rotor (blue)

4 Design Guidelines for the Stator

EMs as axle drives in electric vehicles are usually designed with high torque densities to achieve the required maximum torque [9] in the limited installation space. Therefore, it is necessary to design PSM with high magnetic flux provided by the permanent magnets, which results in saturated iron parts at the peak value of the flux density. The excited flux density due to iron saturation can be obtained by the air-gap permeance and the electric loading

$$\begin{aligned} \hat{B}_{2p\pm p}(v',t) &= \lambda_{\delta,2p}(v',t) \cdot \hat{V}_{\mu,p}(v',t) \\ &= \frac{R}{2p} \lambda_{\delta,2p} \cdot \hat{A}_{\mu,p} (\cos(p\gamma' - 2\pi f_1 + \varphi) + \cos(3p\gamma' - 2\pi 3f_1 + \varphi)) \end{aligned} \quad (7)$$

with $\hat{A}_{\mu,p}$ being the amplitude of the fundamental magnetizing electric loading, $\lambda_{\delta,2p}$ the air-gap permeance of the spatial harmonic $\nu' = 2p$, γ' the angular coordinate, φ the phase angle of the flux density, f the frequency, and R the bore diameter. Equation 7 describes two spatial harmonics; one is part of the fundamental field, while the other one has a pole pair number of $\nu' = 3p$ at three times of the fundamental frequency, also known as the *saturation harmonic*. This saturation harmonic causes circulating currents in delta-connected windings and has to be considered in the design process of the stator of an EM. If the teeth, which are evenly distributed over the circumference of the machine, are highly saturated at the peak value of the flux density, the third spatial harmonic has no phase displacement in relation to the fundamental, which is the main reason for the flattening of the air-gap flux density (see Fig. 8). When the most saturated part is the stator yoke, the air-gap flux density is peaked up, due to the phase opposition with the third spatial harmonic as shown in Fig. 8.

As a result of this effect, the stator can be designed with evenly saturated iron parts to compensate the third harmonic and to decrease the circulating currents, since the respective saturation harmonics have a phase opposition to each other. This can be influenced by an adaption of tooth widths and yoke height.

In order to find suitable cross-sections for these machine parts, which lead to an even saturation, a further parameter study is carried out, whereby the tooth width b_N is varied. In addition, the height of the slot is adjusted to ensure a slot area of 56.5 mm² to limit the current density S_1 , in order to be able to dissipate the losses through a water jacket cooling. To obtain different heights of the stator yoke, the outer diameter of the stator $D_{a,1}$ is also varied. Moreover, the maximum permissible flux density for the stator teeth $\hat{B}_{z,1}$ and the stator yoke $\hat{B}_{j,1}$ is assumed to be 1.9 T. The circulating current I_0 , which arises at the limiting torque curve at $n = 5000$ rpm, considering the varied parameters b_N and $D_{a,1}$, is shown in Fig. 9.

Depending on the specific choice of the cross-section of the stator yoke and the teeth, it can be stated that several design options exist, which are suitable for reducing the circulating current significantly. The smallest value is 10 A or 2.2% of the

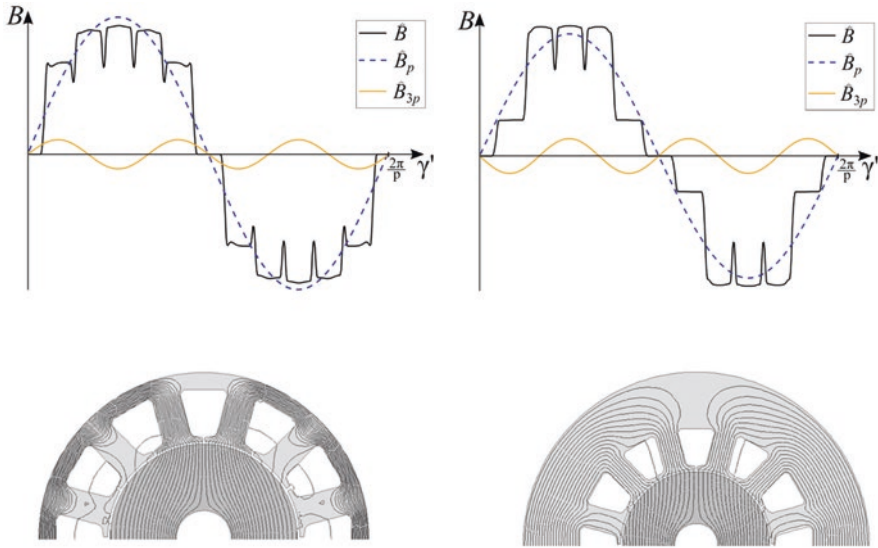


Fig. 8 Fundamental flux density and the third spatial harmonic at highly saturated stator yoke (left) and highly saturated stator teeth (right)

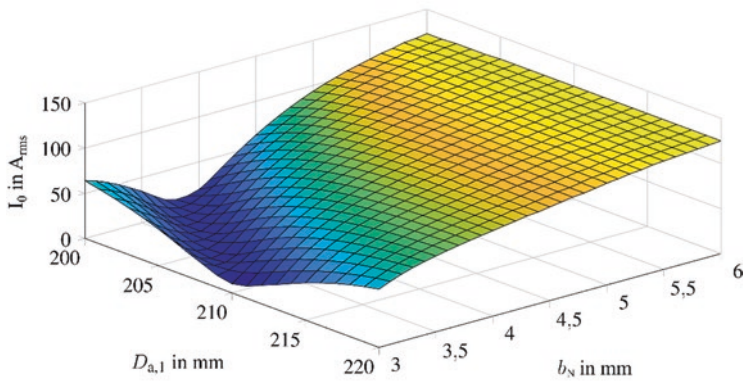


Fig. 9 Value of the circulating current with a varied stator outer diameter $D_{a,1}$ and slot width b_N at the limiting torque curve at $n = 5000$ rpm

phase current (450 A) and occurs at $D_{a,1} = 210$ mm and $b_N = 3$ mm. This examination proves the consideration that an even saturation of the stator teeth and stator yoke almost completely eliminates the saturation harmonics. It must be taken into account that the calculated circulating current can be still generated from the field distribution of the rotor. To assess the efficiency at the operating points, it is not sufficient to consider the circulating currents in the design process only. The yoke

height has a direct influence on the saturation of this machine part and thus on the occurring iron losses. The slot width in turn affects the ohmic phase resistance. In order to take these aspects into account, the ratio of the iron losses, the ohmic losses, and the mechanical power are calculated. The ratio can be determined by:

$$\frac{P_{vw,1} + P_{Fe}}{P_{mech}} = \frac{3 \cdot R_1 \cdot I_1^2 + P_{Fe,styk} + P_{Fe,sttt} + P_{Fe,stth} + P_{Fe,motot}}{2\pi \cdot T \cdot n}. \quad (8)$$

Here, the iron losses P_{Fe} are divided into several parts: styk indicates the stator yoke, sttt the tooth tips, and stth the teeth. The mechanical power is calculated from the torque T and the speed n . The circulating current is considered by the value of the phase current I_1 . The ratio is shown in Fig. 10. The increase of the loss ratio for small slot widths results from the increasing ohmic phase resistance. The higher loss ratio with large slot widths is mainly due to the increase of the circulating current. Minimum losses are achieved at slot widths between 4 mm and 5 mm. They are almost independent of the outer diameter of the stator, which is set to 220 mm. With the selected cross-sections of the active parts, the resulting flux density is 1.9 T in the teeth and 1.5 T in the yoke.

Finally, it is not sufficient to minimize the circulating current. All losses must be considered in order to achieve the highest efficiency in the operating range. Regarding the resulting efficiency map (see Fig. 11) of the designed PSM in delta connection with two magnet layers and flux barriers within the rotor, it becomes obvious that, following the described design rules, suitable PSM for traction application can be designed without a loss of efficiency in the driving cycle, compared to

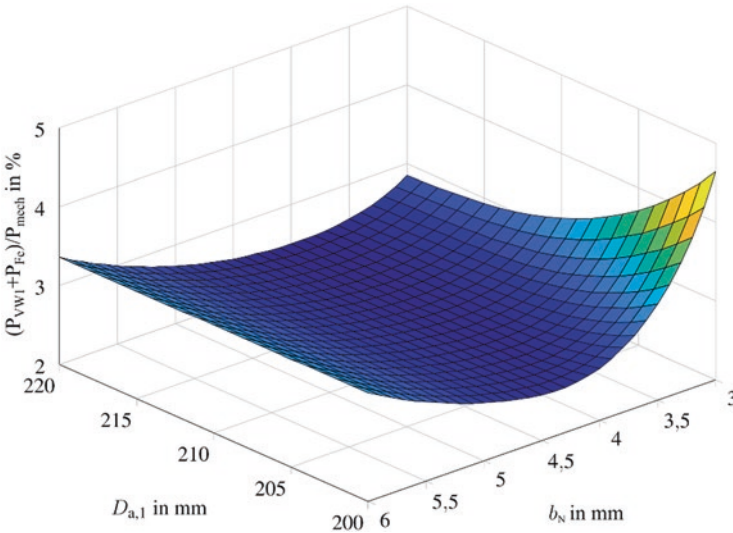


Fig. 10 Resulting ratio of the losses and the mechanical power in %, depending on the varied parameters b_N and $D_{a,1}$ at the limiting torque curve at $n = 5000$ rpm

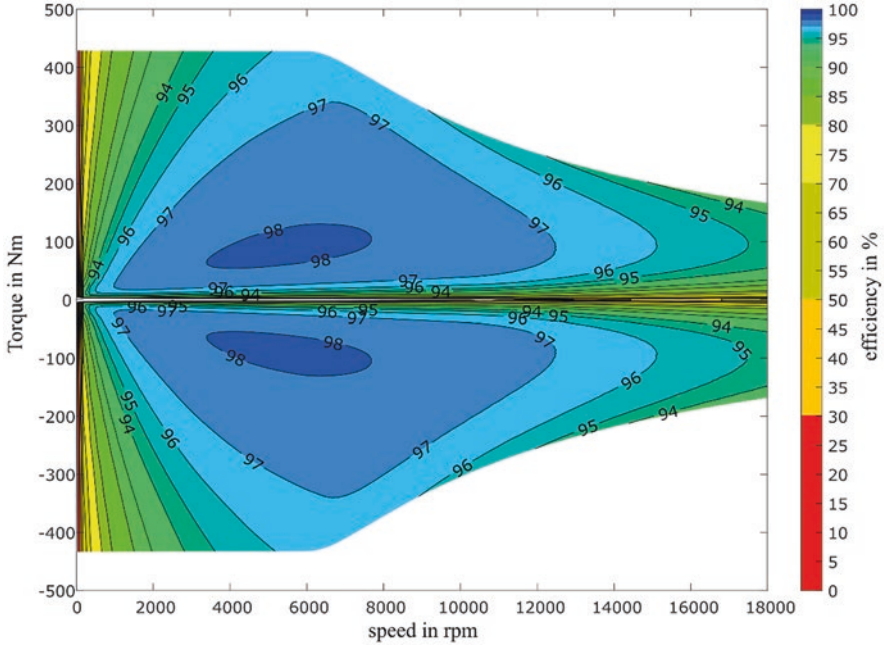


Fig. 11 Efficiency map of a PSM designed with delta-connected windings

PSM in star connection (see Fig. 12). For the EM with star-connected windings, the parallel branches are halved to attain almost the same operating range.

5 Conclusion

When dimensioning PSM as traction motors with delta-connected windings, special attention has to be paid to the arising circulating currents. Therefore, important design rules are derived in this chapter to design the stator and the PM rotor with v-shaped buried magnets. The investigations show that focusing only on the third harmonic, which is caused by the spatial field distribution of the permanent magnets or by saturation, will lead either to an increase of the fifth and seventh spatial harmonics or to higher losses in the stator. Therefore, it is recommended to use flux barriers to decrease the third and ninth harmonics and to choose the magnet angle in such a way that the fifth and seventh harmonics are also reduced while maintaining a high fundamental flux density. This approach leads to a suitable design of the PM rotor for delta-connected as well as for Y-connected windings. Furthermore, it is shown that an even saturation of the stator teeth and the stator yoke in the operating range leads to an almost complete elimination of the circulating current. Nevertheless, all losses have to be considered in order to find the best design option for EM with

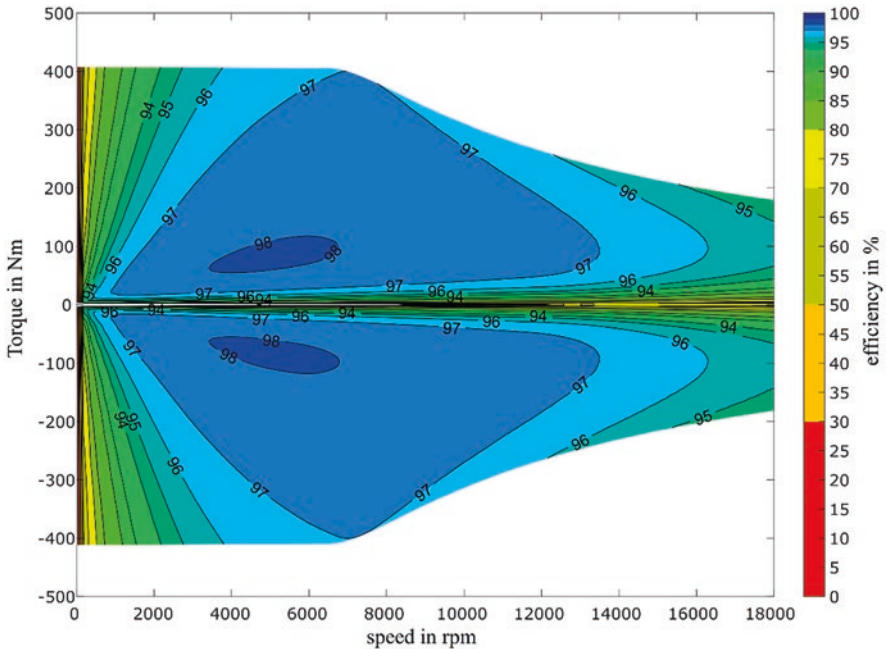


Fig. 12 Efficiency map of a PSM designed with star-connected windings

delta-connected windings. Finally, a calculation method is presented to calculate skewed machines without additional computational effort. In dependence of the skewed rotor segments, all information can be derived from the reference segment analytically. The results indicate that this method can be used to consider skewed EM in the operating range. There are only small deviations which are caused by the interpolation method. Using a higher calculation accuracy of the slice identified via FEM will reduce these deviations.

References

1. C. Dinca, U. Schäfer, Circulating currents of delta connected fractional slot machines for mass production. *Elektrotechnik & Informationstechnik* **132/1**, 68–74 (2015)
2. S.M. Raziee, O. Misir, B. Ponick, Combined star-delta winding analysis. *IEEE Transactions on Energy Conversion* **33**(1), 383–394 (2018, March)
3. R. Ni, X. Gui, G. Wang, G. Zhang, D. Xu. *Improvements in Permanent Magnet Synchronous Machines with Delta-Connected Winding*. In *IECON 2014 – 40th annual conference of the IEEE Industrial Electronics Society*, Dallas, TX, pp. 3837–3842 (2014)
4. G. Dajaku, D. Gerling, Skewing Effect on the PM Flux-Linkage High Harmonics of the PM Machines with Delta Winding. In *13th European conference on power electronics and applications*, Barcelona, pp. 1–7 (2009)

5. A. Wang, Y. Jia, W.L. Soong, Comparison of five topologies for an interior permanent-magnet machine for a hybrid electric vehicle. *IEEE Trans. Magn.* **47**(10), 3606–3609 (2011)
6. W. L. Soong, S. Han, T. M. Jahns. Design of Interior PM Machines for Field-Weakening Applications. In *International Conference on Electrical Machines and Systems (ICEMS)*, Seoul, pp. 654–664 (2007).
7. M. Bösing, *Acoustic Modeling of Electrical Drives Noise and Vibration Synthesis Based on Force Response Superposition* (ISEA, Aachen, 2013)
8. J. Pyrhönen, T. Jokinen, V. Hrabovcova, *Design of Rotating Electrical Machines* (Wiley, Chichester, 2014)
9. J. Juergens, J. Redlich, B. Ponick, Comparison of Direct and Axle Drives with Electrically Excited Synchronous Machines for Traction Applications. In *2018 IEEE Transportation Electrification Conference and Expo (ITEC)*, Long Beach, CA, pp. 49–54 (2018)

EC-Motors in a Fan Application: A Case Study



Kurt Stockman, Jasper De Viaene, Steve Dereyne, and Pieter Defreyne

1 Introduction

Since the adoption of the Ecodesign Directive 2009/125/EC in the European Union, a number of motor-related regulations have been put in place in order to stimulate the use of electric motors with higher energy efficiency. These regulations have been based on international IEC standards such as the IEC 60034-30-1 for direct on line motors, IEC 60034-30-2 for variable speed AC motors, and the IEC 61800-9 series for variable speed drives and the extended system approach.

The European fan industry also has been impacted by regulatory actions. The EC 327/2011 regulation is special, in that perspective that it does not focus on component efficiency but on the system efficiency of the entire fan unit (Fig. 1). This regulation establishes ecodesign requirements for placing on the market or putting into service of fans with an end-use as component or as sub-assembly integrated in other products. Within the regulation, efficiency values are specified for the entire fan system. The efficiency is determined as the air power produced over the electric input power of the system (Fig. 1). The regulation was launched in 2011 and has been revised in 2015. From 2020 onward, even more strict efficiency values are demanded for. As a result, the fan business in Europe has been actively in search for optimization in terms of energy efficiency. In that quest, all components of a traditional fan system have been challenged, amongst them is the electric motor and its power electronic converter for variable speed operation. Traditionally, for industrial fan units, the induction machine was the evident candidate to drive the fan. With the

K. Stockman (✉) · J. De Viaene · S. Dereyne · P. Defreyne
Department of Electromechanical, Systems, and Metal Engineering, Ghent University,
Ghent, Belgium

FlandersMake@UGent – Corelab EEDT-MP, Leuven, Belgium
e-mail: kurt.stockman@ugent.be; jasper.deviane@ugent.be; steve.dereyne@ugent.be; Pieter.defreyne@ugent.be

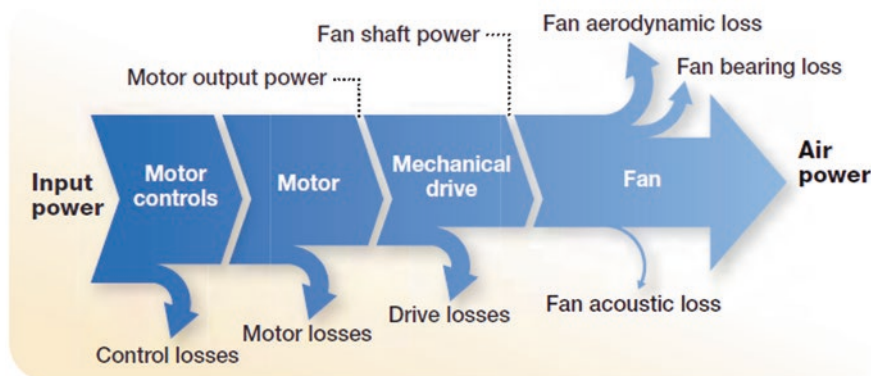


Fig. 1 Sankey diagram of a fan system

rise of IE4 technology, this induction motor has been challenged by permanent magnet machines and synchronous reluctance machines at least in the higher power ranges and for application with a high amount of operating hours. In the lower power ratings (< 11 kW), the induction motor is still the most used machine. First versions of motor regulation in Europe did not focus on small electric machines although the international standards do take small machines into account. This is overcome in the new version of the European regulation EC 640/2009 to be published in 2019.

Both the introduction of standards and regulations have triggered the research activities of motor manufacturers. Today, fan manufacturers need to select the best motor technology for their application in order to fulfill the current regulatory obligations. Especially for low power industrial fan applications EC-motors might be an interesting alternative for the induction machines. It is expected that their efficiency values outperform induction machines. This chapter shows measurement results for 3 EC-motors in the power range from 1.5 to 7 kW and compares them with IE3 induction motor technology.

This chapter is structured as follows. In Sect. 2, the operating principle of the EC-motor is explained and in Sect. 3 their marked situation is addressed. Section 4 describes the measurement results obtained in a laboratory setup. In Sect. 5, the measurement results are used to calculate the energy consumption for a fan application to show the possible energy savings. Finally some conclusion is drawn.

2 Electronically Commutated Motor

In this section, the operation and the characteristics of Electronically Commutated (EC) motors are explained. This motor type is related to the Brushless DC (BLDC) machines. BLDC machines are used in low power applications (< 400 W), such as

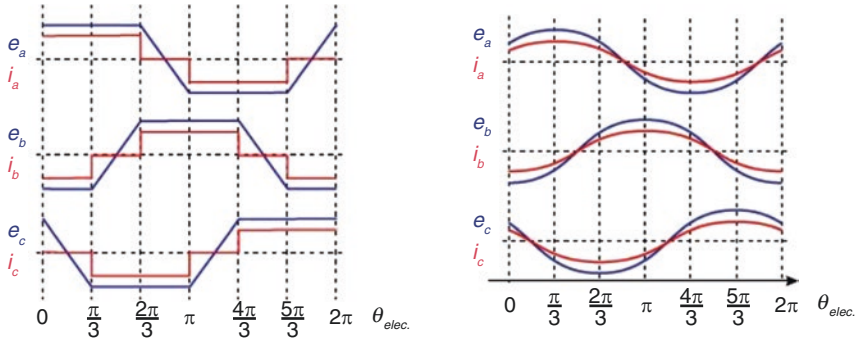


Fig. 2 Current waveforms (red) for constant torque production in a BLDC machine/EC-motor with trapezoidal and sinusoidal back-EMF (blue)

refrigerators, washing machines, and drones. Both motor types contain a stator with concentrated windings resulting in a rather low production cost of the stator. The rotor contains permanent magnet material. Originally, BLDC motors were equipped with permanent magnets that resulted in trapezoidal back-EMF voltages. By feeding the stator windings with DC currents a more or less constant torque production resulted. This principle is depicted in Fig. 2. To determine the commutation moments either Hall sensor or sensorless operation is used in the traditional BLDC motor. Most sensorless techniques are based on the zero crossing of the back-EMF voltage in a non-energized stator phase. Depending on the quality of this commutation information, torque ripple can be limited at the commutation moments. Unfortunately, tolerances in the production of the rotor results in back-EMF waveforms that deviate from their ideal shape: the back-EMF tends to be more sinusoidally shaped [1]. As a result, rotor designs occurred that intentionally resulted in more sinusoidal-induced stator voltages. In combination with sinusoidal stator currents this again results in good torque production and improved energy efficiency. As a result, a traditional three-phase voltage source inverter can be used to control such a motor. Several references show the possible gain in energy efficiency when using such sinusoidal currents [2–4]. Another advantage of the EC-motor is the option to have an outer rotor construction. This is especially interesting for fans as the fan blades can be mounted directly on the outer rotor resulting in a very compact fan unit (Fig. 3).

3 EC-Motor Market Situation

A market survey revealed that approximately 30 manufacturers of EC-motor are active worldwide. Most of these manufacturers offer only fractional horsepower machines (<400 W) that are not relevant for the industrial fan applications that are addressed in this chapter. Therefore this chapter focuses on motors with a power rating from 1 up to 11 kW and motor-rated speeds in the range from 1000 up to

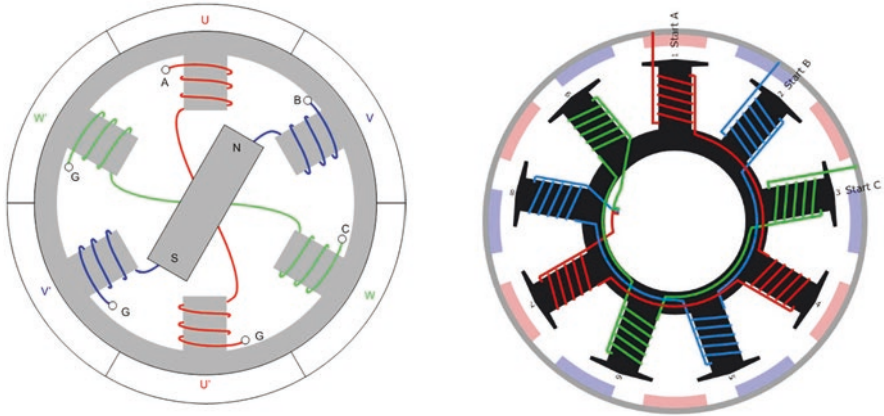


Fig. 3 Schematic overview of EC-motors with inner rotor and outer rotor construction. The stator consists of concentrated windings

3000 rpm and a rated voltage of 400 V. In this chapter, three different EC-motors were measured, two motors with a rated power of 1.5 kW and one motor with a rated power of 7 kW. For reasons of confidentiality, the motors are referred to as EC1, EC2, and EC3 in the remaining of the chapter.

4 Measurement Campaign

In this chapter, the measurement results of 3 EC-motors are compared with respect to an IE3 speed-controlled induction motor of similar power and speed rating. Efficiency maps of the motor drive combination are generated on a dedicated test bench according to the direct measurement method [5]. Figure 4 shows the test bench. The settings of the variable speed drive were only adjusted according to the motor name plates. No further drive settings were modified compared to the factory settings. Analysis of the efficiency maps clearly shows the better performance of the EC-motors in part load operation compared to the induction motor (Figs. 5, 6, 7, 8, 9, and 10).

For an operating point at 1500 rpm and 10 nm (rated power) both the 1.5 kW EC-motors outperform the IE3 IM with 8% for the EC1 and 6% for the EC2 machine, respectively. At part load operation at half speed (750 rpm) and 2.5 nm, even larger efficiency gains are obtained. It must be noted that motor EC2 has a

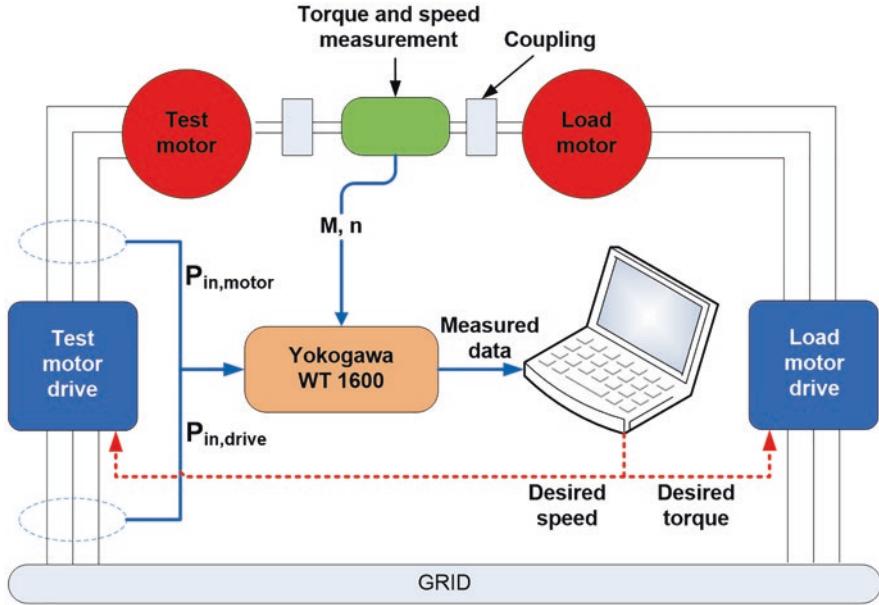


Fig. 4 Schematic overview of test bench for efficiency contour mapping based on the direct measurement principle

lower efficiency at rated load compared to EC1 but compensates this with better part load efficiency values. Table 1 summarizes the results.

5 Energy Consumption for a Fan Application

In order to quantify the energy consumption, a realistic load profile is assumed. The load profile consists of four operating points (OP). In this analysis, only the effect of the motor system is considered and the same fan is assumed. The load profile is given in Fig. 11 and is characterized by a high percentage of part load operation. The load characteristic shows a quadratic relationship between motor speed and load torque with a small amount of static torque. This load profile has been applied both to the 1.5 kW case and the 7.5 kW case.

For the 1.5 kW case, the use of both EC-motors results in a similar financial saving of about €60 compared to the IE3 induction motor case. For the 7 kW EC-motor, the gain is limited to € 84. This gain is not proportional with the increased motor

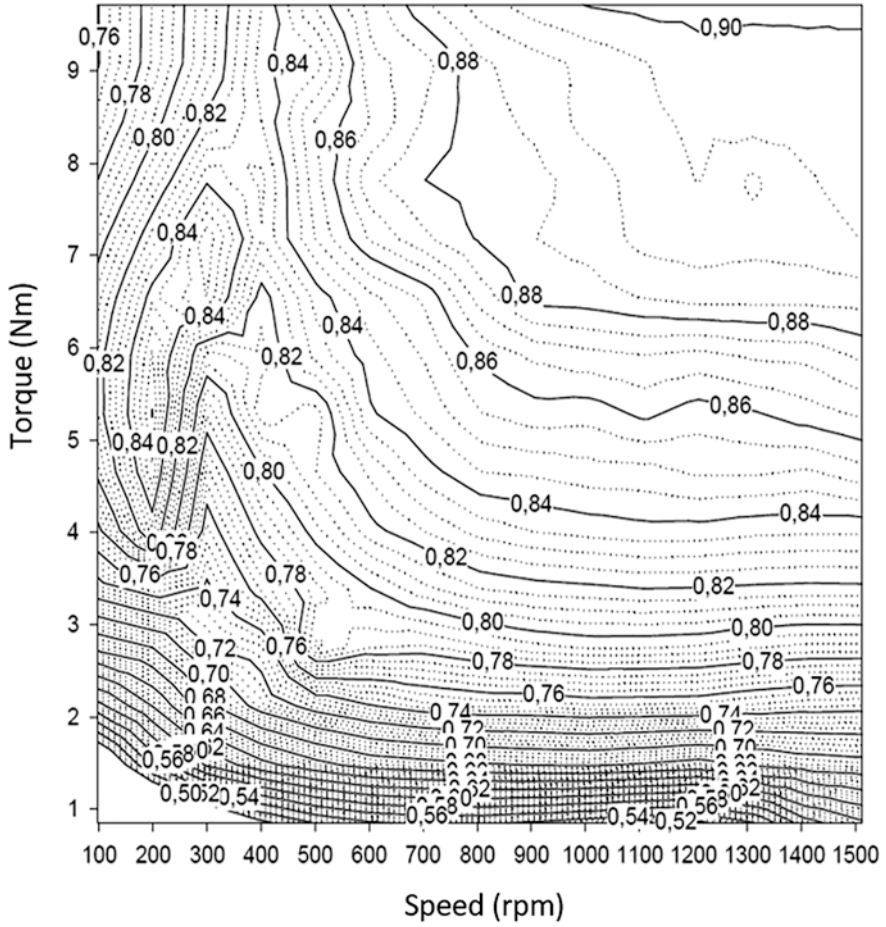


Fig. 5 Efficiency contour map for a 1.5 kW EC-motor: *motor ECI*

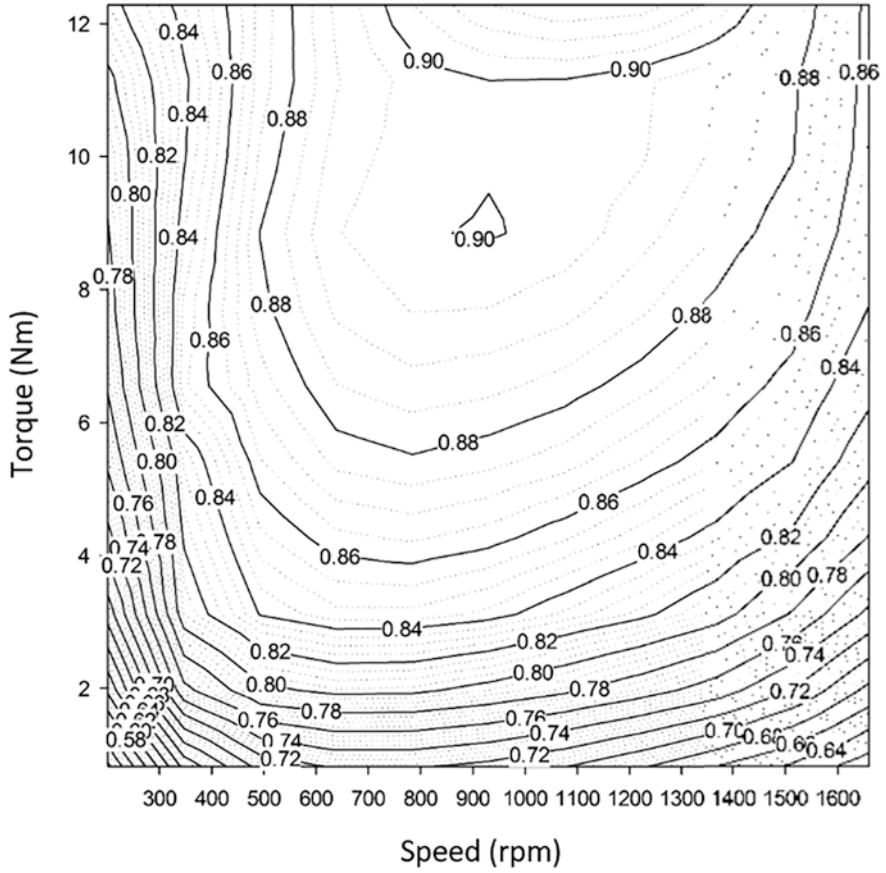


Fig. 6 Efficiency contour map for a 1.5 kW EC-motor: *motor EC2*

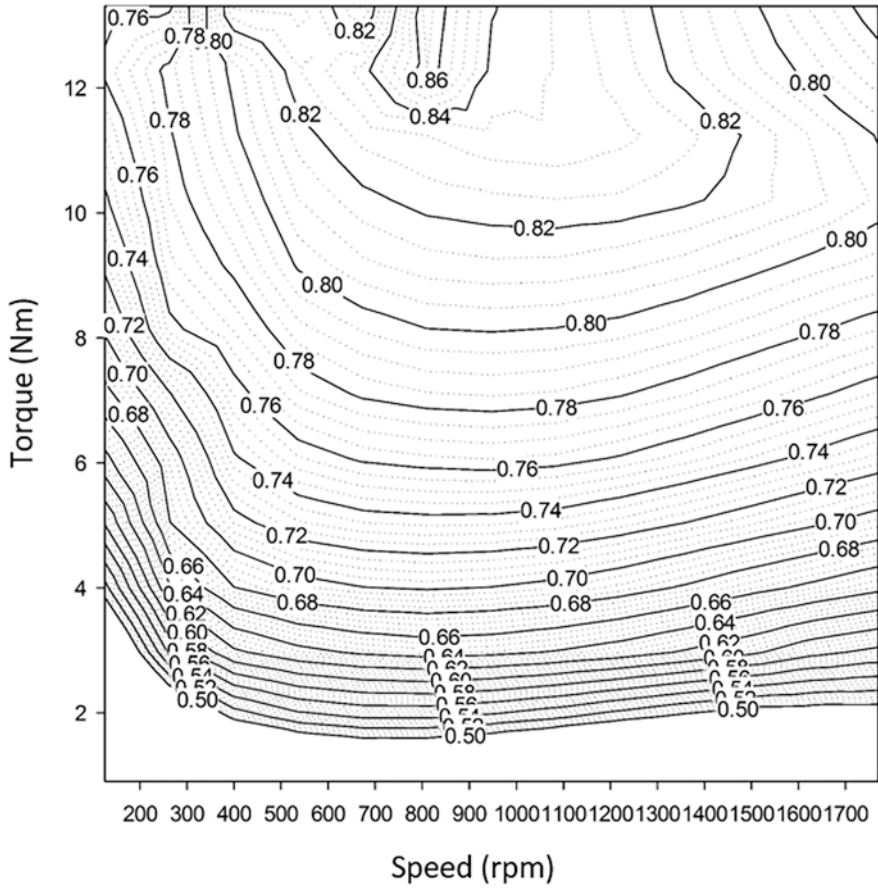


Fig. 7 Efficiency contour map for a 1.5 kW IM-motor: IE3, 4 pole

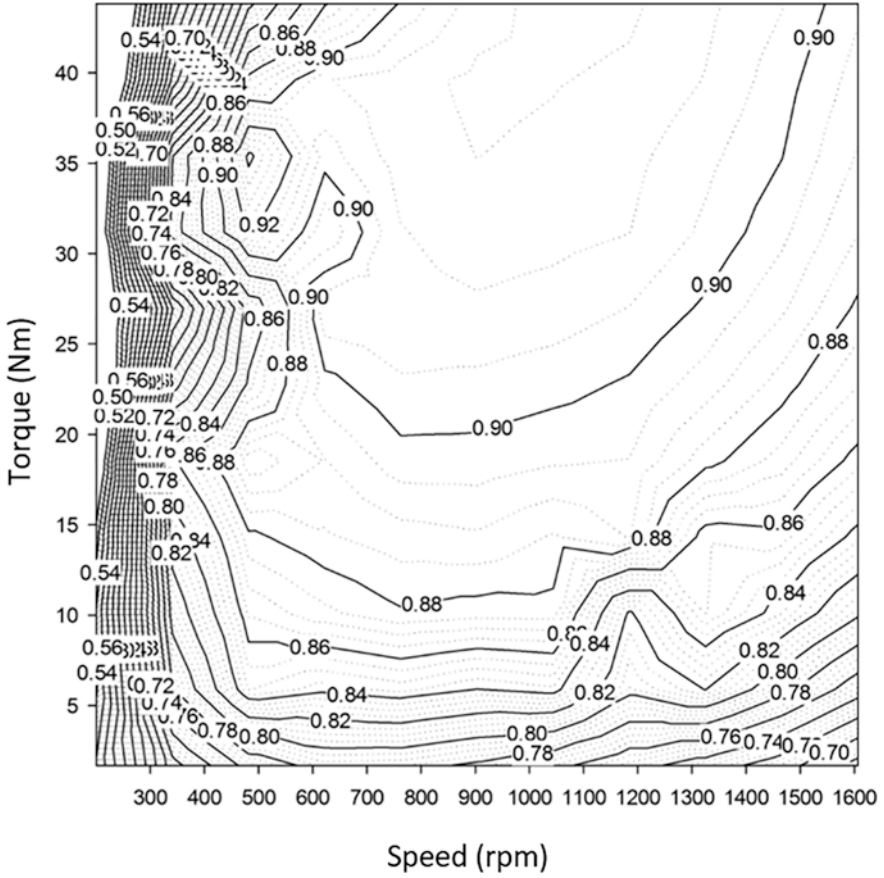


Fig. 8 Efficiency contour map for a 7 kW EC-motor: motor EC3

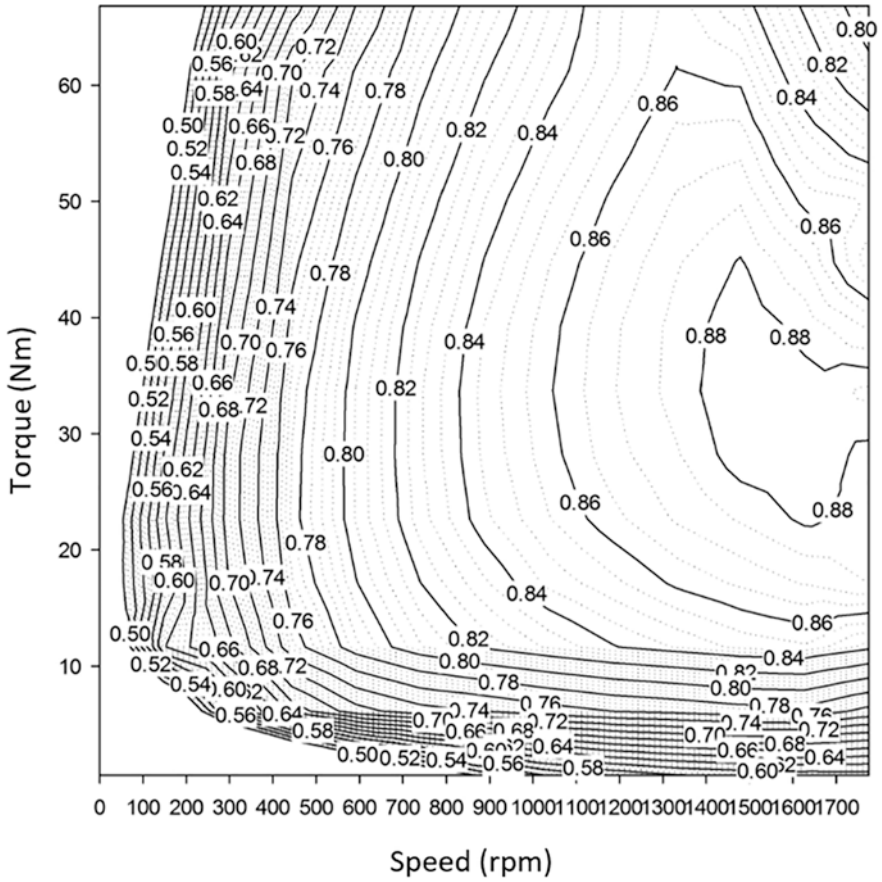


Fig. 9 Efficiency contour map for a 7.5 kW IM-motor: IE3, 4 pole



Fig. 10 Test bench with EC-motor loaded by a PMSM machine emulating a fan application

Table 1 Measurement results for 1.5 kW and 7.5 kW EC-motors compared to similar IE3 Induction motor. All motors for the same power rating driven by the same power electronic converter

Rated power	1.5 kW		
Brand	EC 1	EC2	IM
Type	EC outer runner	EC outer runner	
Power electronics	Intern	Converter 1,5 kW	Converter 1,5 kW
1500 rpm 10 nm	90.0%	88.0%	82.0%
750 rpm 2,5 nm	77.0%	82.0%	58.0%
Rated power	7 kW	7.5 kW	
Brand	EC 3	IM IE3	
Type	EC outer runner		
Power electronics	Converter 7,5 kW	DOL	Converter 7.5 kW
1500 rpm 44 nm	90.5%	88.8%	88.0%
750 rpm 11 nm	88.0%	/	80.0%

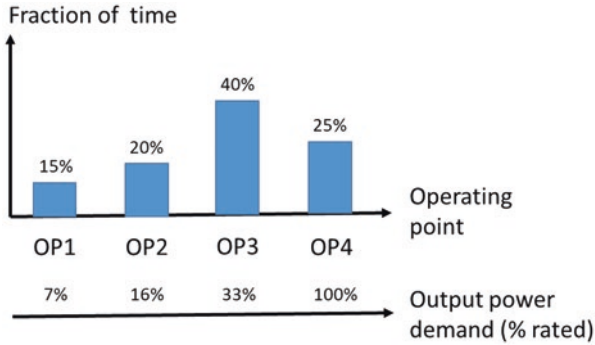


Fig. 11 Fan application load profile

Table 2 Yearly energy consumption and financial profit for the given load profile with 6000 operating hours per year and an energy cost of 0.1 €/kWh

Rated power	1.5 kW		
Brand	EC 1	EC2	IM
Yearly energy consumption	4242 kWh	4235 kWh	4844 kWh
Yearly energy cost	€ 424.2	€ 423.5	€ 484.4
Yearly profit compared to IM	€ 60.2	€ 60.9	–
Rated power	7 kW		
Brand	EC 3	IM IE3	
Yearly energy consumption	17,485 kWh	18,327 kWh	
Yearly energy cost	€ 1749	€ 1833	
Yearly profit compared to IM	€ 84.2	–	

power compared to the 1.5 kW case. It can be concluded that for the load profile of Fig. 11, the smaller the motor power, the higher the energy savings (Table 2).

6 Conclusion

In this chapter, efficiency maps for Electronically Commutated motors (EC-motors) are presented. The motors are driven with a standard three phase voltage source inverter as is typically used to control induction machines. Three EC-motors are analyzed, two 1.5 kW motors and one 7 kW motor. The results are compared with the efficiency values of IE3 induction machines of the same power rating and controlled with the same variable speed drive. Both in the rated operating point and in part load operation, the efficiency of the EC-motors outperforms the induction motor values. In the 7 kW case, the economic profit is less pronounced compared to the 1.5 kW case. For such applications, the decision to select the EC-motor will depend on the payback time which depends on the purchase cost of the machine and the possibility to mount the fan directly on the outer rotor resulting in a more compact fan design.

References

1. I. Coenen, T. Herold, C. Piantsof Mbo'o, K. Hameyer, Evaluating the influence of manufacturing tolerances in permanent magnet synchronous machines. *COMPEL Int. J. Comput. Math. Electr. Electron. Eng* **32**(5), 1552–1566 (2013)
2. P. Kshirsagar, R. Krishnan, High-efficiency current excitation strategy for variable-speed non-sinusoidal back-EMF PMSM machines. *IEEE Trans. Ind. Appl.* **48**(6), 1875–1889 (2012)
3. S.J. Park, H.W. Park, M.H. Lee, F. Harashima, A new approach for minimum-torque-ripple maximum-efficiency control of BLDC motor. *IEEE Trans. Ind. Electron.* **47**(1), 109–114 (2000)
4. J. De Viaene, F. Verbelen, S. Derammelaere, K. Stockman, Energy-efficient sensorless load angle control of a BLDC motor using sinusoidal currents. *IET Electr. Power Appl.* **12**(9), 1378–1389 (2018)
5. S. Dereyne, K. Stockman, S. Derammelaere, P. Defreyne, *Adjustable speed drive evaluation using iso efficiency maps* (EEMODS 2011, New York)

A Global Update on the Markets for Motors, Drives, and Motor-Driven Equipment



Preston Reine

1 Growth Trends in Electric Motor Systems

The worldwide market for low-voltage motors and drives is estimated to have been worth a combined \$23.8 billion, which represents a total growth of 4.1% from 2017 revenues. This growth was largely driven by a continued resurgence in the heavy industries such as metal processing, mining, and oil & gas. In fact, the process industries in general have largely benefitted since oil prices began rebounding in 2016. Leading the way in growth for low-voltage motors and drives has been the oil and gas industry; since 2016, motor and drive revenues into this sector have grown by about 14% due to rising oil prices and the ensuing capitalization of projects that had been previously delayed. IHS Markit has also reported an increasing adoption of drives, also referred to as variable frequency drives (VFDs), within key growth applications such as pumps, fans, and compressors, which account for more than 75% of motor-driven system applications (Fig. 1). These three key motor-driven systems are a main focus point because end users have increased their awareness of energy-efficient solutions. Because of this, IHS Markit has reported a significant increase in VFD adoption rates. The crucial trend in the larger industrial automation field, however, is smart manufacturing. Motors, drives, and motor-driven equipment are generally not seen as “smart” equipment, but that is rapidly changing. Product managers are working more and more closely with IIoT experts in order to bring software to the customer that will enable the proper sizing of equipment in order to optimize and ensure energy efficiency, safety, and lean manufacturing, to name a few examples.

P. Reine (✉)
IHS Markit, London, UK
e-mail: preston.reine@ihsmarkit.com

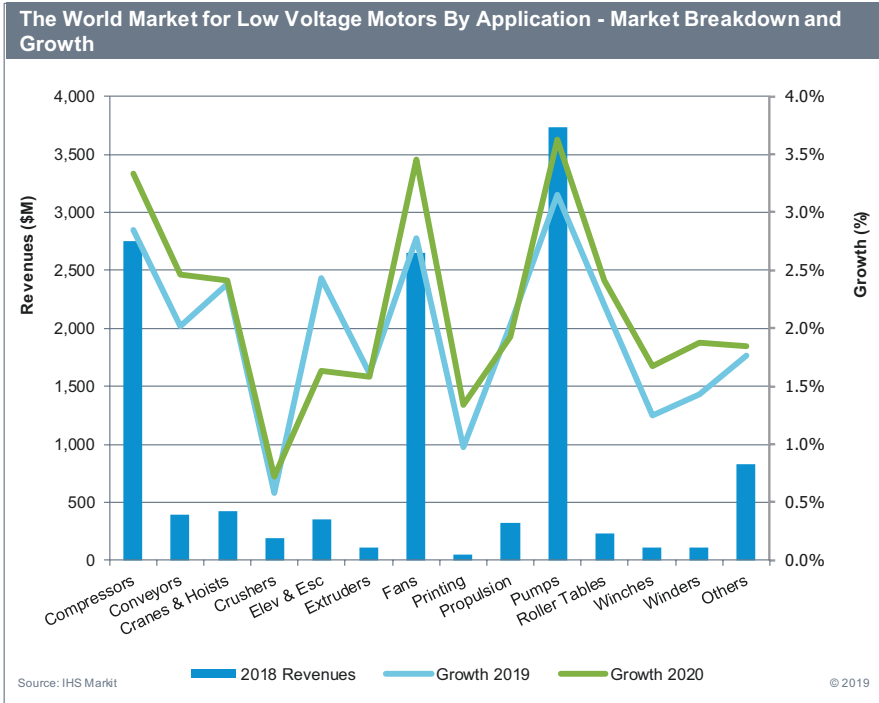


Fig. 1 Pumps, fans, and compressors account for the vast majority of electricity consumption via low-voltage motors

2 Price Tendencies for Electric Motors

For low-voltage motors specifically, price increases have been a major trend affecting the competitive environment. Many of the raw materials are bought in China, which of course puts a very heavy burden on the suppliers who rely on steel from China and other countries affected by the tariffs imparted by the United States. Due to increasing input and labor costs, many suppliers had actually announced price increases ranging from 3 to 7% before the tariffs took effect, so not all motor suppliers have passed on the cost of tariffs onto the customer; however, prices increased substantially in some developed regions, namely the United States. As a result, IHS Markit expects Vietnam and other South East Asian countries with favorable tax laws and incentives to continue to become a crucial focus for manufacturing, because aside from the tariff issue, China’s labor costs have actually increased considerably. Figure 2 highlights the growth trend of materials prices.

Key price drivers						
Percent change						
	% share	2016	2017	2018	2019F	2020F
Price		-0.9	0.9	2.7	2.2	2.0
Direct labor costs	11%	7.3	2.6	2.5	2.6	3.3
Direct material costs	81%	-1.0	5.9	5.6	0.5	0.9
Indirect product costs	8%	1.1	3.3	2.2	2.5	2.4

Source: IHS Markit 2019Q1 Forecast. Please see Cost Analyzer for more information. © 2019 IHS Markit

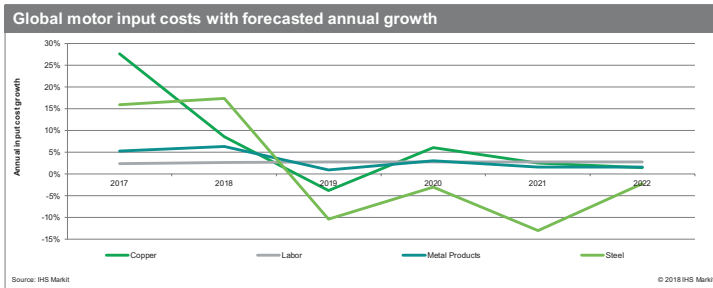


Fig. 2 If commodity prices remain low it could prevent motor suppliers from being able to increase their prices

3 Motor Efficiency

In terms of the global market size, the low-voltage motor market was estimated to be valued at less than \$12.3 billion in 2018, representing a growth of 4.6% from 2017 and 8.2% since 2016. Much of this growth was generated from price increases. Whereas energy efficiency has historically been the leading focus for motor suppliers and end users, awareness of the Industrial Internet of Things has given far more things to consider from a business model standpoint. During the economic slow-down from 2014 to 2016, many suppliers were paying less attention to growing market share and more attention on profitability through leaner manufacturing processes and increased service offerings. When commodity prices were really low and the economy was drastically slowing down, the rate of adoption for higher-efficient motors also slowed down. That is likely not driven alone by organic economic factors; in fact, IHS Markit research has shown that inorganic pressures from the government are the biggest indicator of motor efficiency sales. As seen in Fig. 3, the global share of low-voltage electric motors with an energy-efficiency designation of IE3 (NEMA Premium Efficiency) in 2016 was 17%. In 2022, IHS Markit forecasts that this allocation will increase to almost 28%. Furthermore, there has been a lot of buzz for IE4 motors. The biggest source of demand for this technology comes from pumps and compressors below 10 kW, as well as small conveyor and fan applica-

EFFICIENCY CLASS TRANSITIONS (UNITS)

Global Low Voltage Motors - Efficiency Class Transition: 2016 to 2022

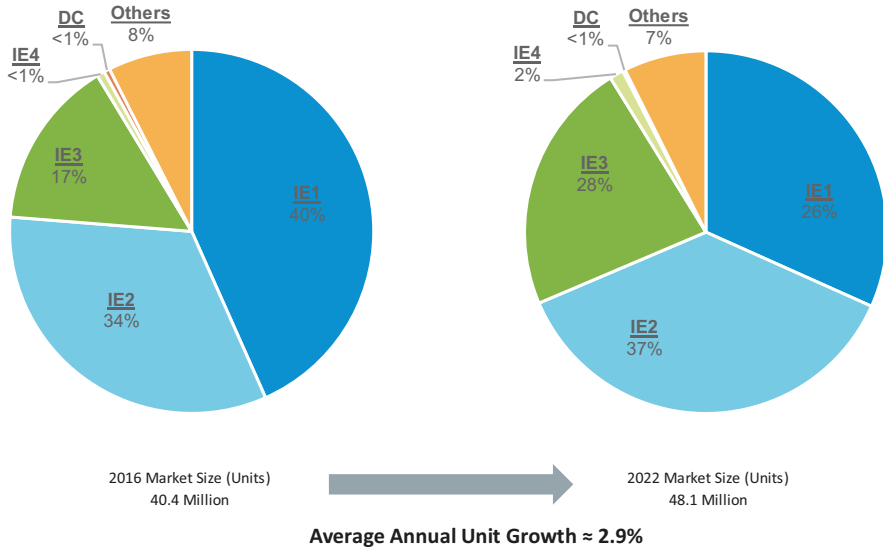


Fig. 3 IE4, super-premium efficiency motor types will grow rapidly but still account for less than 5% of motor shipments for the near future

tions. Market leaders among pump, fan, and compressor suppliers have all focused on supplying their own high-efficiency motors in order to control the increasingly specialized designs required by end users.

4 The Balance Between Organic and Inorganic Forces

As mentioned earlier, “efficiency” in and of itself can be defined and attained several different ways. For example, the United States had historically embraced the shift toward reducing carbon emissions by targeting product-specific metrics for industrial equipment such as motors, generators, pumps, fans, and compressors. Certainly, some products have received more attention than others, but the product-centric approach has slowly transitioned toward focusing on the more historically European style of improving energy efficiency, commonly referred to as the extended product approach. The extended product approach looks at full system efficiency instead of calculating energy consumption on the component level.

The above indicates how the government would look at efficiency, but the market is evolving in a manner that is independent of such standards. We have seen time after time throughout the world that the absolute leading determinant of efficient equipment being sold is government involvement, but as disruptive technologies emerge, it is possible that the industrial automation market as a whole will see new

demand metrics that are similar but unrelated to the governmental bodies' ideas of efficiency. The beginning of this trend comes from the Industrial Internet of Things, in which motors, drives, and other equipment are more broadly connected in order to monitor the condition of these assets and predict or prevent maintenance issues. Looking back at Fig. 3, it is clear that IE4 motors will not account for a significant portion of global sales any time soon. So why, after such a massive awareness of the benefits and payback opportunity with energy efficiency, does the market not take advantage of energy savings? The answer is complex, but the simplified version is that cost concerns and marginal returns are at the forefront. The jump from an IE2 motor to IE3 is significant in many applications, but the move from IE3 to IE4 can be markedly less. On top of that, most IE4 motors would require a VFD to be used in conjunction, and for the cost-conscious consumer, this can be an issue.

Even with government influence, it is clear that the process of transitioning to more efficient motors takes time. It is also clear that little progress happens without legislative endeavors, as seen in Fig. 4. After a policy is enacted, there are often loopholes that need to be shored up, which can take years to finalize and put into effect.

Cultural differences are another important factor to consider when looking at barriers and enablers of energy efficiency. Switzerland is a really good example of a country that prioritizes the utilization of energy-efficient equipment. As proof of this, despite the global average adoption rate for IE4 motors of less than 1%, IE4 motor shipments in Switzerland account for roughly 2.6% of the country [1]. Furthermore, Japan has been one of the fastest countries to transition after its adoption of standards in 2014 [2]. This is largely due to cultural and structural factors, such as commitment to sustainability and also the competitive environment having fewer players.

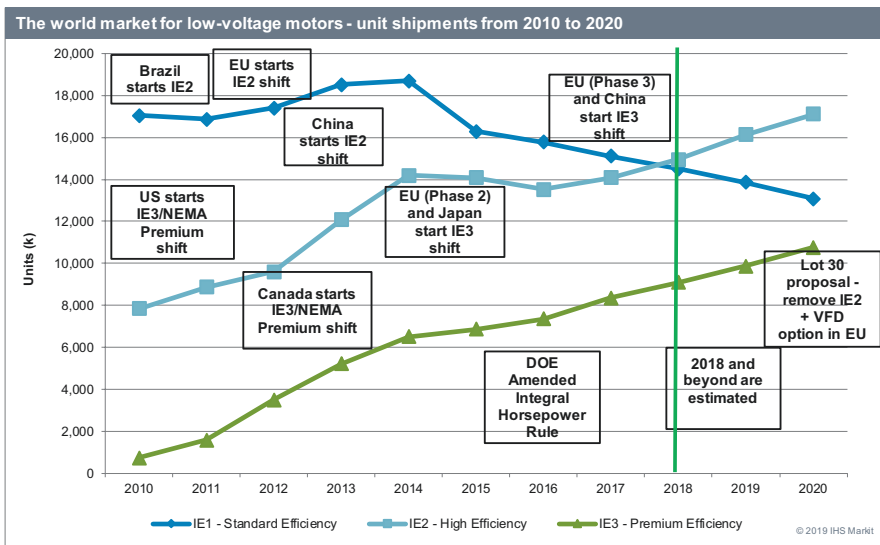


Fig. 4 It is commonplace that efficiency standards take at least 12 months for the market to recognize a significant difference

Lower-cost providers from countries with less of a focus on energy-efficiency are a threat to undercutting the progress of advanced nations. With little teeth to the worldwide legislations, there is little that can be done. This has been a problem in countries like Turkey, Mexico, and Southeast Asia. However, this pales in comparison to a major issue that suppliers have been struggling with for many years. The reason that progress is very slow without government intervention is because the company purchasing industrial automation equipment is usually not the one operating the equipment, and would therefore have little concern for operating expenses that can often be very expensive. Sure enough, motor manufacturers are combating this by investing in service offerings and IIoT solutions that can reduce downtime, and it is possible to save more money through uptime compared to the purchase of energy-efficient equipment. The key point here is that these don't have to be mutually exclusive. As the economy continues to slow down, though, it is the expectation by IHS Markit that services, lean manufacturing, and emerging smart monitoring and connectivity technologies will grow at a faster rate than the general interest in energy-efficient motors. There is plenty of room for growth in both facets.

5 VFD Market Update

Total low-voltage drive revenues in 2018 are estimated to have been worth about \$11.5 billion, representing a growth of 3.4% from 2017 revenues. This growth rate indicates a leveling out of the market after a strong year in 2017, which saw a 7% growth in revenues from 2016. This resurgence in the low-voltage drives market is largely due to a recovery in the heavy industries, much like the case with the motor market. Price pressure still exists in the low-voltage drives market, with average selling prices (ASP) falling by over 1% from 2016 to 2017. The ASP in the global low-voltage drive market was below \$550 per unit in 2017 and below \$545 in 2018. Although low-voltage motor drive revenues do not directly benefit from the positive effects of the minimum motor efficiency legislation as with low-voltage motor revenues, the overall drives market benefits from the greater focus on system efficiency. If, however, tighter minimum efficiency performance standards (MEPS) are applied to the drives themselves, this could buck the trend of selling less expensive drives. It is currently the case in the European Union that motors not attaining an efficiency rating of IE3 must be used with a VFD, but little oversight has been given to this regulation, leading to confusion for suppliers trying to understand the difference with perceived and actual demand. Moreover, this will soon be changing, now that the EU motor regulation has been finalized to take away this option. It is the opinion of IHS Markit that this will reduce the confusion and bring some much-needed standardization to the market, boosting IE3 motor sales. Still, IHS Markit research indicates strong demand for drives in the energy-intensive process industries, so declining prices likely will not offset the currently strong forecast for drive shipments, especially in Europe, where a full systems efficiency focus is commonplace. The determining factors for whether a customer opts for a more efficient motor or a less

expensive motor with a VSD largely depends on customer and application at this point. In variable speed applications, motor drives have the potential to save massive amounts of energy. In the future, as energy costs increase, the economic benefit from installing such a motor drive will also continue increasing exponentially. The greatest return on investment with regards to drives is mostly seen in pump, fan, and compressor applications, which are forecast to outperform the market average for drive applications over the next 5 years. Drives have come a long way: they can now be controlled by mobile devices; can identify problems; and can work more efficiently at various speeds and loads. In addition, they are much easier to purchase and install than in years past. IHS Markit has been tracking the penetration of connectivity, specifically related to drives. Corroborating the belief that connected devices are on the rise, an IHS Markit survey found that 69% of VFDs sold in 2016 were network-enabled, as opposed to 68% in 2015. IHS Markit predicts that this figure will expand to 76% in 2021 [3].

6 Conclusion

With the advent of more disruptive technologies permeating into the industrial automation market, suppliers are looking for more and more ways to differentiate. In many developed countries, new energy-efficiency initiatives and revisions will continue to push market growth in favor of higher-efficient motors, drives, and motor-driven equipment such as pumps, fans, and compressors. However, there is no justification to enforce standards above IE3 (NEMA Premium) rated motors, and as

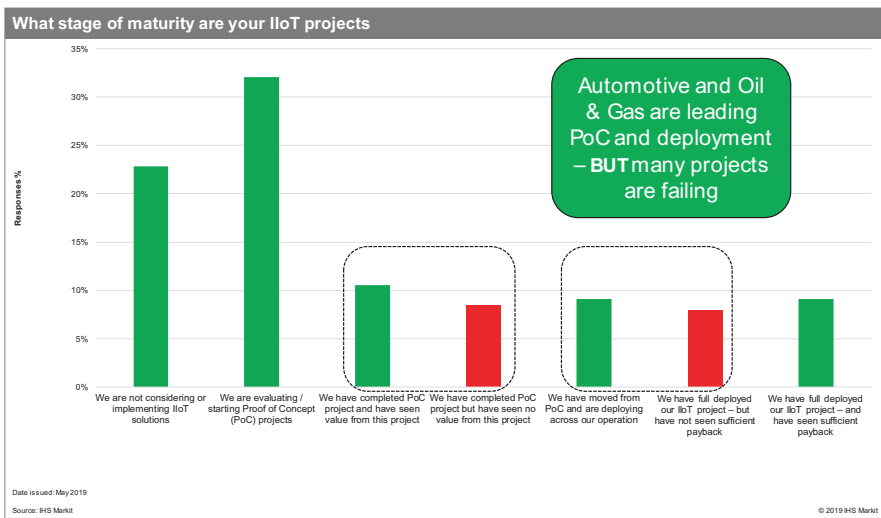


Fig. 5 Initiatives to employ IIoT will not be successful unless the organization has the necessary skillset and internal support

the market becomes more commoditized, it is likely that the successful market players will differentiate themselves by embracing IIoT. Many companies have reported that more savings have been attained with motors that are less efficient by means of properly sizing and maintaining the whole motor-driven system. Much like with IE4 motor technology, IIoT, Industry 4.0, and other transformative technologies are quite nascent in terms of practical application. Connectivity via sensors has been around for a while, but modern technology is allowing motor system end users to collect and analyze data like never before. Figure 5 shows how much room for growth there is for industrial automation original equipment manufacturers and end users that IHS Markit surveyed [4] in early 2019. The takeaway is clear; many obstacles exist to adopting this technology, but a small percentage of companies have been able to capitalize. This, along with a comprehensive adoption of energy-efficient equipment, does not have to exist separately. In other words, the market could see the utilization of advanced intelligence that helps with proper equipment sizing, condition monitoring, and predictive maintenance that can further promote energy efficiency.

References

1. Project Velani Motor Survey, A Collaboration with Swiss Federal Office of Energy, Impact Energy, and IHS Markit
2. I. Campos, IHS Markit Low-voltage Motors Intelligence Service (2018)
3. Mohsin Ali Syed, IHS Markit Industrial Communications Intelligence Service (2019)
4. A. West, IHS Markit Industrial IoT Readiness Survey (2019)

Increasing the Energy Savings of Motor Applications: The Extended Product Approach



Benno Weis, Benoit Leprettre, Martial Patra, Norbert Hanigovszki, Preben Holm, Tim Schuman, Michael Könen, Niels Bidstrup, and Kirk Anderson

1 Motor Applications Offer Huge Opportunities for Energy Savings

1.1 *Electric Motors Are a Big Source of Energy Savings*

According to The International Energy Agency [1], applications driven by electric motors account for nearly 70% of the electrical energy consumed in the industrial sector and for a significant fraction in other sectors: 20% in the commercial sector and 13% in the residential sector.

B. Weis (✉)

Siemens AG, Munich, Germany

e-mail: benno.weis@siemens.com

B. Leprettre · M. Patra

Schneider Electric, Paris, France

e-mail: benoit.leprettre@se.com; martial.patra@se.com

N. Hanigovszki · P. Holm

Danfoss, Nordborg, Denmark

e-mail: norbert@danfoss.com; Preben_Holm@danfoss.com

T. Schuman

SEW, Mountain View, USA

e-mail: tschuman@seweurodrive.com

M. Könen

KSB, Frankenthal, Germany

e-mail: michael.koenen@ksb.com

N. Bidstrup

Grundfos, Bjerringbro, Denmark

e-mail: nbidstrup@grundfos.com

K. Anderson

NEMA, Rosslyn, VA, USA

e-mail: kirk.anderson@nema.org

Motors have become essential to all business sectors and are the largest electrical energy consumers, utilizing more than twice as much as lighting. Motor applications account for about 45% of the global electricity consumption. The overall energy consumption of electric motors is more than 7000 TWh/year today.

If no effective energy-efficiency measures are implemented, the consumption and associated CO₂ emissions could increase by almost 90% by 2030. Given their paramount role in the industrial sectors, electric motors represent one of the greatest opportunities for energy savings and reduction of CO₂ emissions.

1.2 The Energy Efficiency of Electric Motor Systems Is Still Under-addressed

The efficiency of motor systems is not a major concern for most users. Although the cost of the energy used by a motor accounts for about 95% of the Total Cost of Ownership, the primary selection criteria is still by far the initial purchase price, not the cost of the energy it will use. There are three reasons for this counter-productive behavior:

- Lack of awareness of the cost of running a motor (95%) versus the cost of purchase (5%).
- Companies having different departments responsible for the investment (interested in a low purchase price) and operational costs (interest in energy efficiency).
- MEPs on components and the lack of tools for end-users to determine the true energy demand at operating points of components at other than 100% rated loads.

Consequently, the installed base includes many applications in which the motor and/or the machine connected to it are poorly sized and/or fitted to the actual requirements of the application, forming a poorly efficient application overall. The opportunities for energy savings are therefore considerable.

2 How to Increase the Energy Savings of Motor Applications?

A motor-based application is a system composed of components: power supply, motor, motor control, auxiliaries, transmission, mechanical load, process, etc. When it comes to dealing with the energy efficiency aspect of such compound systems, two approaches can be considered:

- The component approach consists of developing MEPS (Minimum Efficiency Performance Standards) for key components and then requiring each of those components to have a minimum energy-efficiency rating (typically determined at an arbitrary load point).
- The system approach consists in considering the entire application and making the overall system meet certain efficiency levels. This promotes greater energy savings and better optimization of the components used within the system, allowing the complete program to operate with greater energy savings compared with the component approach.

2.1 Current Approaches Focus on Components

Most geographical zones have a Minimum Efficiency Performance Standard (MEPS) on motor efficiency today. Old, inefficient motors still in place will progressively be replaced by more efficient motors.

While this substitution will certainly bring savings, motor MEPS limitations only focus on the energy efficiency of the motor as a component, often at or near full load operation. However, the optimization of the entire application has a much greater influence on the overall energy efficiency than the rated efficiency value of the individual components.

2.2 Components Must Be Sized Properly to Operate at an Efficient Operating Point

The operating point of a component depends on its sizing and how well it is suited to the application. As a general statement, major oversizing is to be avoided because it causes nearly all pieces of equipment to operate at an operating point where they are not optimally efficient.

For example, the efficiency of an electric motor is significantly degraded below 30% of load regardless of its energy-efficiency IE class. Yet, oversizing by a significant “margin factor” is still common practice in the industry.

The power losses when not operating a motor at an efficient-operating point are much higher than those of a less efficient motor in its nominal efficiency range, hence the recommendation to avoid oversizing.

2.3 The Control System Must Match the Requirements of the Application

Variable speed is interesting to many applications because it allows controlling the torque and speed independently. As the efficiency of a motor increases, the starting torque is reduced. By using a variable speed drive, applications can use a much higher starting torque and reduce the energy once the application is operating. This is an important feature, as the low starting torque of a high efficiency Direct on line (DOL) motor is another reason for oversizing as described above. On the other hand, the variable speed drive produces additional power losses.

It is important, from the point of view of energy efficiency, to carefully consider the use variable speed drives. The following general rules are useful to make an optimized decision:

- Applications which require full speed for almost all their operating time should use fixed speed motors.
- Applications which require speed reduction during an essential part of their operating time should use a variable speed drive.
- Applications with an essential part of their operating time at both full speed and reduced speed can minimize the losses of the variable speed drive by bypassing it with contactor when operating at full speed.
- Applications which require full but not line speed for almost all their operating time should either use a variable speed drive or a gearbox. A gearbox will add losses but the selection of the appropriate type of gearing is essential to the application to overcome those losses.

When it comes to saving energy, one of the decisions used to implement variable speed should be based on an application-level analysis of whether the drive would improve the overall efficiency. Yet, in many cases, the implementation or non-implementation of variable speed drives is based on design habits, overestimated investment cost, or preconceptions, such as electronics having poor reliability and fixed speed motor being tried and true.

2.4 A “System-level” Approach Is Needed

The actual efficiency of a motor-based application depends on how well the different pieces of equipment (motor, transmission, mechanical machine, etc.) match the requirements of the application. This involves several factors, such as:

- The operating point of the motor expressed in terms of speed and torque (or power for fixed-speed applications). For example, fixed-speed motors running at less than 30% of their rated power typically have very degraded efficiency (e.g., 70% against 95% near full load).

- The motor control system (motor starter or variable speed drive).
- The operating point of the transmission between the motor and the mechanical equipment, if any.
- The operating point of the mechanical equipment connected to the motor, e.g., a pump.
- The design speed of the system. Newer motors have less slip and run faster than older, lower efficiency motors, potentially increasing energy consumption without benefit for the application.

Failure to match the characteristics of the components to the requirements of the application can defeat the benefit of using efficient individual components (motor, control system, load machine), and lead to an overall waste of energy. Examples of solutions that typically waste energy and consequently result in poor overall system energy efficiency even if high-efficiency motors are used include:

- Using a throttling valve to permanently regulate the flow of a fluid
- Keeping components in standby mode for a long time (e.g. over the weekend)
- Using heavily oversized components to accommodate peak requirements that occur only very rarely

The Extended Product Approach is a first attempt to deal with the energy efficiency of motor-based applications through a system approach, to foster good design practice and yield tangible overall energy savings.

3 Principles of the Extended Product Approach (EPA)

The concept of Extended Product Approach has been introduced first in the EN 50598 series of European standards published in 2014 [2, 3]. Most of the content has later been included in the IEC 61800-9 Ed. 1 published in 2017, with only minor corrections and clarifications [4, 5].

3.1 What Is the “Extended Product”?

The idea behind the “Extended Product” concept is to consider other products or parameters that may influence the energy efficiency of your product.

This concept is extremely important when dealing with the energy efficiency of motor applications, because the operating points of a component (and therefore its efficiency) may be strongly influenced by other components and by the requirements of the application.

For example, if the sizing of a fixed-speed pumping application causes the associated motor to operate below 30% of rated load most of the time, the overall efficiency of the motor in this pumping system will be far from optimum.

Since the energy efficiency of a complex system is a difficult matter, a well-defined terminology is needed. In IEC 61800-9-1, an effort has been made to specify a set of terms that represent a consensus among the stakeholders writing the IEC 61800-9 series of standards. Figure 1 shows the key terms used to designate the different components of a motor application. The terms related to motors operated with variable speed drives (BDM, CDM, PDS) have been reused from other relevant IEC standards.

According to this terminology, the Extended Product is the association of of:

- The Motor System composed of:
 - The motor
 - The Motor Control System, which may be:
 - A Complete Drive Module, also called Variable Speed Drive, if the application requires varying the speed
 - or a Motor Starter (contactor, softstarter) if the application is speed-fixed.
- The Driven equipment connected to a process, composed of:
 - A mechanical transmission (coupling, gearbox, etc.)
 - A load machine (pump, compressor, etc.)

The Extended Product is therefore an arrangement of electrical and mechanical components designed to perform a task as required by the application: circulating fluids, compressing air, lifting goods, etc.

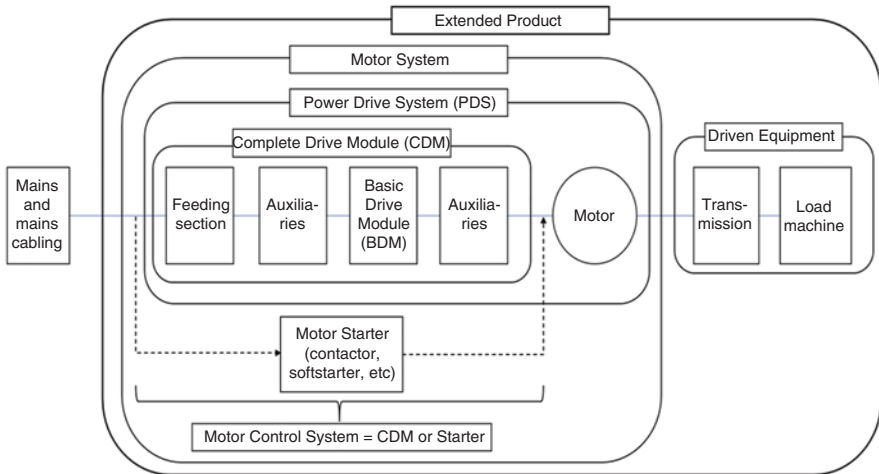


Fig. 1 Terminology: Components of a motor application

3.2 *Questions Related to the Energy Efficiency for Extended Products*

Considering an Extended Product (existing or under design), some of the questions that arise from the point of view of maximizing the energy savings include:

- Does my Extended Product consume a minimum amount of energy?
- What are the extra energy savings if I optimize the operation mode of my Extended Product compared to optimizing the individual components (e.g., CDM, motor, driven equipment)?

Answering such questions is not easy because the energy consumption of the Extended Product depends a lot on the operating points of each component, which in turn depends on the application requirements and on the selection and sizing of the components.

3.3 *The Extended Product Approach: A Generic Methodology*

The Extended Product Approach (EPA) is a generic methodology to foster the inclusion of application-level considerations (i.e., other components installed, time profile) when determining the energy efficiency of a component.

The inputs to the EPA are (see Fig. 2):

- Characteristics of the application: all information allowing to determine the operating points at which the component will operate. For a motor system this includes:
 - Mechanical power required to perform the task (lifting something, filling up a tank in a certain amount of time, etc.)
 - Need for varying the speed of the motor independently of the torque
 - Fraction of time spent in stand-by mode
 - If several levels of power or speed are required by the application, the fraction of runtime spent at each level
- Power losses of the components: the power losses of each component at the operating point(s) at which it is operated as required by the application.



Fig. 2 Principle of the extended product approach for a component

The output of the EPA is typically an Energy-Efficiency Index that characterizes its overall efficiency in the context of the application, considering all the above.

4 The Extended Product Approach for Motor Systems in IEC 61800-9

In the IEC 61800-9 series of standards, the key element is the Motor System, i.e., motors and their associated motor control system (see Fig. 1). This series is composed of two parts:

- IEC 61800-9-1 is the Extended Product Approach part (see Fig. 2). It describes the methodology for using application-related information and the power losses of a motor system to determine the overall energy-efficiency index of the motor system in the application.
- IEC 61800-9-2 describes methods for determining the power losses of motor systems at any operating point. It is specific to these components.

4.1 Step 1. Determination of the Operating Points

The first step for using the Extended Product Approach for Motor Systems from IEC 61800-9-1 is to determine the operating points of the components of the motor system.

Based on the requirements of the application (the work to be done), the selection of the different pieces of equipment forming an Extended Product can be considered:

First the load machine:

- What is the best efficient speed for the load machine to do the mechanical work?
- What is mechanical power? Is the duty continuous or intermittent?
- At variable speed, how many different operating points appear? What fraction of time will be spent at each operating point?

Then the Motor System itself:

- What do I need to operate the mechanical load?
- Is the motor well-suited to the load?
- Is it more efficient to control the speed of the motor or to use fixed speed and adjust the motor output power by its torque only?
- Do I need to manage the starting phase, e.g., in case of high-inertia load?
- If it is more efficient to change/vary the speed independently of the torque, shall I use a Drive Module or a gearbox?
- Will it need auxiliaries (e.g., additional cooling, high-frequency filters)?

Based on the above considerations, the operating points OP_k at which the Motor System will operate can be determined. These operating points may be expressed as

a percentage of the rated power for starter-based Motor Systems or as (speed, torque) couplets for Power Drive Systems.

4.2 Step 2. Determination of the Power Losses at the Operating Points: Semi-Analytical Model (SAM)

The second step is to determine what will be the power losses of the motor system in the application. This is what IEC 61800-9-2 specifies.

Considering the Motor System operating points, the IEC 61800-9-2 standard provides methods for determining the power losses at each operating point. To do this, the IEC 61800-9 series of standards introduces the Semi-Analytical Model (SAM).

From a generic point of view, a Semi-Analytical Model (SAM) is a mathematical model using a combination of measured and calculated data for determining the power losses of a component or a group of components in the Extended Product at any given operating point in a standardized manner (see Fig. 3).

A Semi-Analytical Model may for example use:

- Measured data at standardized reference operating points (in which case the manufacturers need to provide the power losses of their equipment at these points)
- Standardized mathematical models of equipment
- Formulas for interpolating the power losses between known operating points

The IEC 61800-9-2 standard specifies the Semi-Analytical Model of the Motor System. The determination of the Motor System power losses depends on the type of Motor Control System.

- If the Motor System is based on a Motor Starter (contactor, star-delta starter, softstarter), then:
 - The efficiency of the motor is considered unaffected by the Motor Control System
 - The power losses of the Motor Control System are taken as 0.1% of the motor rated power

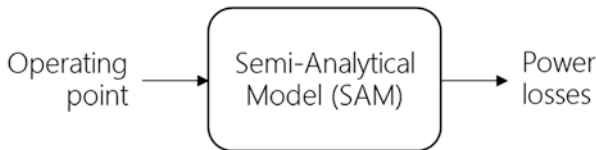


Fig. 3 Principle of the semi-analytical model of a component

- If the Motor System is a Power Drive System, i.e. based on a Complete Drive Module allowing variable speed, then:
 - The efficiency of the motor is affected by the CDM.
 - The determination of the PDS power losses needs to be done according to the SAM specified in IEC 61800-9-2. It mainly uses power losses Drive Modules and motors determined at standardized operating points (that need to be provided by manufacturers) and specified interpolation procedures.

4.3 Step 3. Determination of the Overall Energy-Efficiency Index (EEI) Using the Duty Profile

When the different operating points and the associated power losses have been obtained, the third step is to turn them into an overall Energy-Efficiency Index for the Motor System. An important factor that impacts the overall energy efficiency is how much time is spent at each identified operating point.

For example, a fixed speed motor system that continuously operates below 30% of its rated power is certainly not optimally efficient, whereas operating at a fraction of the rated power for a limited fraction of time, because the application so requires, is more tolerable.

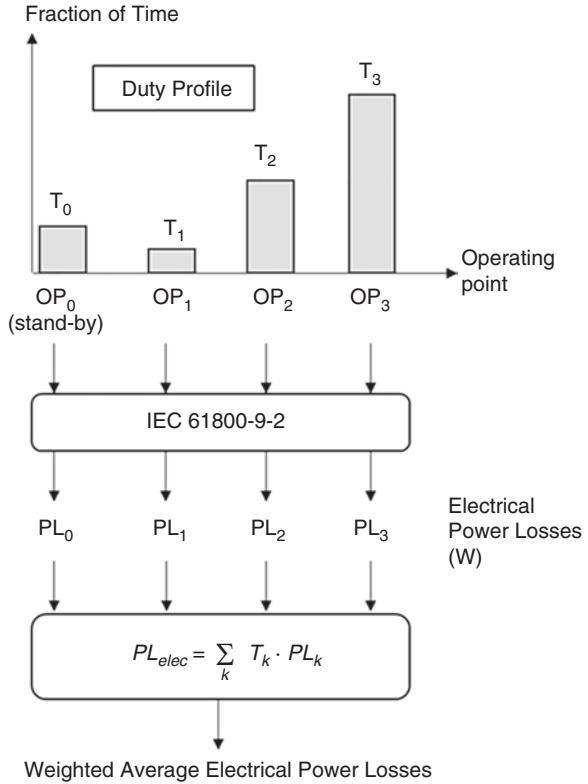
A way of describing the time aspect of the application is to use duty profiles. These profiles are histograms describing which fraction of time is spent at each operating point, including stand-by mode if relevant. This principle is described in IEC 61800-9-1.

Duty profiles may vary substantially depending on the type of application and type of mechanical load. Continuous duty applications will typically have only one operating point in the duty profile, with additional stand-by time, whereas complex applications involving variable speed may require a significant number of operating points associated to as many fractions of run time.

An overall Energy-Efficiency Index (EEI) proposed in IEC 61800-9 is the weighted average power losses, calculated as the sum of the losses at the different identified operating point, each weighted by the respective fraction of runtime spent at the operating point. This EEI is a measure of the average power lost by the Motor System over a long enough period: the smaller the better.

This process is summarized in Fig. 4. In this example, four operating points including stand-by mode have been considered relevant to describe the application.

Fig. 4 Principle of the semi-analytical model of a component



4.4 The EPA for Motor Systems Also Specifies Energy-Efficiency Classes for Components

The IEC 61800-9-2 also specifies classification schemes for CDM and PDS:

- The IE energy-efficiency class of a CDM is done by comparison to a Reference CDM whose power losses are tabulated.
- The IES energy-efficiency class of a Power Drive Systems (Motor + Complete Drive Module) is based on the comparison with a Reference Power Drive System whose power losses are tabulated in the standard.

In addition, the IEC 61800-9-2 standard specifies tests for verifying the IE class of a CDM or the IES class of a PDS.

5 The Extended Product Approach Helps Designing Efficient Motor Systems

5.1 *Comparing Potential Architectures to Select the Most Efficient Solution*

The weighted average electrical power losses can be used to characterize the energy efficiency of a Motor System for a specified application: the lesser the weighted average electrical power losses, the more efficient the motor system.

It is especially interesting to use the Energy-Efficiency Index during the design stage to compare several Extended Products representing several implementation options of an application. It allows one to decide which architecture is more efficient for the application considered, based on a fair and objective analysis instead of preconceptions or design habits. In order to achieve a sustainable result, all the various design concepts for an extended product and their expected operating points must be determined in detail in order to allow an overall loss evaluation of the different possible solutions

Suppose two Extended Products are considered for implementing a pumping application:

- An Extended Product EP1 composed of a fixed-speed motor and a throttling valve
- An Extended Product EP2 composed of a Power Drive System without throttling device

Considering the duty profile of the application, the weighted average electrical power losses can be computed for each Extended Product EP1 and EP2. The Extended Product that yields the smaller weighted average electrical power losses is more efficient and shall be preferred from the point of view of energy efficiency.

Typically,

- If the pumping application spends most of its time near 100% flow, the Extended Product EP1 based on fixed speed is more efficient.
- If the application requires the flow to be reduced to 50% most of the time, then Extended product EP2 based on variable speed is more efficient. Two cascaded system or a bypass for the variable speed drive could also be considered as further possible Extended Products.

This example is presented at a greater level of detail in IEC 61800-9-1 Annex C.

Table 1 Stakeholders of the extended product approach

Stakeholder	Possible usage
Regulatory authorities	Use the Extended Product Approach and all necessary support data to assess whether a given application is efficient enough or not. This is a way to save substantially more energy than by regulating the individual efficiencies of components (MEPS) and to focus on the practical, more relevant overall energy efficiency of Motor Systems within their applications.
Non-electrical standardization technical committees or other relevant professional organizations	Use the general guidelines of the Extended Product Approach in IEC 61800-9-1 to derive their own approach for determining the energy efficiency of the products in their scope, as relevant.
Component manufacturers (motor, CDM, PDS)	Quantify the energy-efficiency performance of their component, using the measurement /calculation principles from IEC 61800-9-2 to determine their IE or IES class and provide this information to their customers. Provide the power losses of their components (CDM, PDS) at the standardized reference operating points mentioned in IEC 61800-9-2, for use by other stakeholders, e.g. application designers.
Application designers	Use the standardized data provided by manufacturers of electrical and non-electrical equipment and follow the EPA to derive Energy-Efficiency Indices for the Motor Systems implemented in the applications under design or for the whole application under design.
Original Equipment Manufacturers	Use standardized component energy- efficiency data and follow the EPA to quantify the energy efficiency of their original equipment.

5.2 *Lots of Stakeholders Can Benefit from the Extended Product Approach*

The main stakeholders of the Extended Product Approach (IEC 61800-9-1) and the motor losses determination procedures (IEC 61800-9-2) are listed in Table 1.

5.3 *Toward a Comprehensive Approach for More Efficient Motor Applications*

The interaction of these stakeholders is expected to progressively encourage more conscious choices regarding the design and selection of energy-efficient motor-based applications.

A considerable benefit of the Extended Product Approach in the IEC 61800-9 series of standards is that it allows to determine the overall energy efficiency of a Motor System on a fair basis, considering:

- The requirements of the application (typically the different duties)
- The characteristics of the components forming the Extended Product

Alternate Extended Product configurations can be characterized and compared in terms of Motor System energy efficiency, based on a systematic approach. This is a first step toward addressing the complex topic of the energy efficiency of motor applications.

6 Extending the Extended Product Approach to the Whole Application

6.1 Compatible Approaches to Energy Efficiency Are Needed for All Components

The improvement resulting from using efficient component can be ruined by not using the component at operating points where they are efficient in the application. This is true for electrical and non-electrical components of an application.

Therefore, the Extended Product Approach for Motor Systems in the IEC 61800-9 series should be completed by equivalent approaches for characterizing the energy efficiency of non-electrical parts, typically the transmission and the mechanical load connected to the process.

Ideally, the methods for characterizing the energy efficiency of the electrical parts and for the non-electrical parts should be consistent and compatible, in the sense that:

- All methods should consider the whole application.
- All methods should produce indicators (e.g., weighted average power losses) that can be easily combined into a single indicator characterizing the energy efficiency of the whole application.

6.2 The EPA for Motor Systems Is a Good Basis

A good merit of the Extended Product Approach for Motor Systems in the IEC 61800-9 series is that it can easily be adapted to non-electrical components. The adjustments of the Extended Product Approach that can be considered to tailor it to the non-electrical world may include:

- Adapting the terminology: for example, pumping or ventilation applications may want to use flow and pressure rather than speed and torque.
- Specifying Semi-Analytical Models for the transmission, driven equipment, etc. to determine its power losses or efficiency at any given operating point. These

Semi-Analytical Models could be based on power losses or efficiency at standardized reference operating points as in IEC 61800-9-2 or other relevant data.

- Providing reference duty profiles for typical service conditions.
- Specifying how the Energy-Efficiency Index for their applications should be determined and how it should be presented to the stakeholders.

An example of such adaptation is the Extended Product Approach for pumps developed by EUROPUMP [6]. Reference duty profiles and Semi-Analytical Models have been proposed for dealing with mechanical load. Coupled with the EPA for Motor Systems in IEC 61800-9, it can be used to derive application-level energy-efficiency indicators.

The expected benefit is a significant improvement of the energy efficiency of motor-based applications for the benefit of the community.

6.3 Toward an Application-Level Energy-Efficiency Index

Assuming consistent Extended Products Approaches (EPA) are available beyond Motor Systems (which are covered by the IEC 61800-9 series of standards), i.e., for non-electrical parts of a motor-based application, the outputs of these different EPAs can be combined into an overall, application-level Energy-Efficiency Index.

For example, if all the Extended Product Approaches for the different component forming a motor-based application produce weighted average power losses as outputs, those can be directly summed up. The resulting total application power losses is a good possible Energy-Efficiency Index (EEI) for the whole application performed by the equipment considered. This concept of generalized Extended Product Approach to assess the overall, application-level energy efficiency is shown in Fig. 5.

The key inputs are the requirements of the application (the work that needs to be done). The operating points of each component will depend on the application designer's choice. Carefully sizing each component and selecting the right motor control system is especially important from the point of view of energy efficiency. It is more than just selecting nominally efficient individual components regardless of what the application requires.

It is only when we are able to easily “connect” the energy-efficiency determination procedures for all parts of the application that we can really foster the design of energy-efficient applications and achieve high-level energy savings.

The proposed generalized Extended Product Approach should be seen as a straw man presented to encourage and initiate cooperation between electrical and non-electrical technical committees and stakeholders.

Note: An extended and more detailed version of this chapter is available as an IEC SC22G Supporting Document [7].

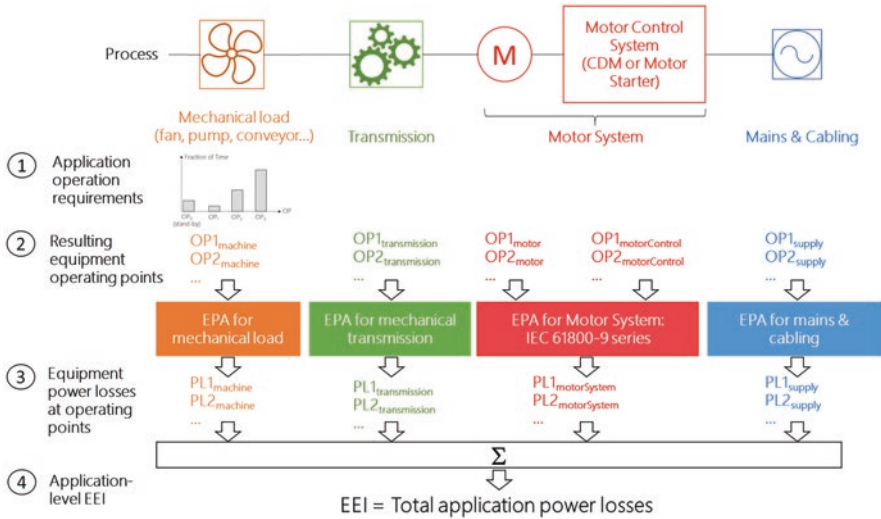


Fig. 5 Prospective application-level extended product approach

References

1. International Energy Agency, P. Waide, C. Brunner, *Energy-Efficiency Policy Opportunities for Electric Motor-Driven Systems* (2011)
2. EN 50598-1, *Ecodesign for Power Drive Systems, Motor Starters, Power Electronics & Their Driven Applications. General Requirements for Setting Energy Efficiency Standards for Power Driven Equipment Using the Extended Product Approach (EPA), and Semi Analytic Model (SAM) – EN standard* (2014)
3. EN 50598-2, *Ecodesign for Power Drive Systems, Motor Starters, Power Electronics & Their Driven Applications. Energy Efficiency Indicators for Power Drive Systems and Motor Starters – EN standard* (2014)
4. IEC 61800-9-1, *Ecodesign for Power Drive Systems, Motor Starters, Power Electronics and Their Driven Applications – General Requirements for Setting Energy Efficiency Standards for Power Driven Equipment Using the Extended Product Approach (EPA) and Semi Analytic Model (SAM) – IEC Standard Edition 1* (2017)
5. IEC 61800-9-2, *Ecodesign for Power Drive Systems, Motor Starters, Power Electronics and Their Driven Applications – Energy Efficiency Indicators for Power Drive Systems and Motor Starters – IEC Standard Edition 1* (2017)
6. EUROPUMP, *Extended Product Approach for pumps. A Europump Guide* (2014). Can be downloaded at [http://europump.net/uploads/Extended%20Product%20Approach%20for%20Pumps%20-%20A%20Europump%20guide%20\(27OCT2014\).pdf](http://europump.net/uploads/Extended%20Product%20Approach%20for%20Pumps%20-%20A%20Europump%20guide%20(27OCT2014).pdf)
7. B. Leprettre et al., *Increasing the Energy Savings of Motor Applications: The Extended Product Approach*. White paper published as an IEC SC22G Supporting Document. Can be downloaded at https://www.iec.ch/dyn/www/?p=103:227:6078631373423:::FSP_ORG_ID,FSP_LANG_ID:1416,25

High-Efficiency IE4 Line-Start Synchronous Reluctance Motors



Francesco Parasiliti and Marco Villani

1 Introduction

The demand for energy saving and the new directives on efficiency levels have shifted the interest of designers from the conventional induction motors (IM) towards new types of compact and reliable high-efficiency motors for constant speed applications, especially in the low and middle power ranges. The line-start synchronous motors represent a valid alternative to the traditional IMs, since they are able to operate without any control device: the presence of a squirrel cage embedded in the rotor core makes them capable of starting directly from the grid. These motors are mainly line-start permanent magnet motors (LSPMM). The LSPMM combines the advantages of the IM (robust construction and line-starting capability) and PM motor (high-efficiency, power factor, and torque density). One of the drawbacks of LSPMM is the price volatility of the rare earth alloys, and this has led to the reconsideration of magnet-free solutions such as the line-start synchronous reluctance motor (LSSynRM) [1–5]. The LSSynRM is potentially cost-effective and can compete with the robustness and the low price of the IM in the field of constant speed applications. Nevertheless, the rough starting transient, limitations in terms of pull-in (synchronization) capability, and low power factor are the main critical aspects that compromise its diffusion [6]. By the use of combinations of modern finite-element (FE) analysis techniques and proper optimization algorithms [5, 7], acceptable starting behaviour in the asynchronous operating region and efficient steady-state performance at synchronous speed are feasible for LSSynRM.

F. Parasiliti (✉) · M. Villani (✉)

Department of Industrial and Information Engineering and Economics, University of L'Aquila, L'Aquila, Italy

e-mail: francesco.parasiliti@univaq.it; marco.villani@univaq.it

In this chapter, a specific design procedure for LSSynRMs [5] has been used in order to reach the desired balance between the pull-in capability, starting behaviour, and steady-state performance. The procedure is applied to design two LSSynRMs, 3 kW-2pole and 4 kW-4pole, 400 V, 50 Hz. The performance of both motors, during starting and steady-state operations, was analysed by an accurate FE model and compared with that of IMs of the same size. A prototype of the 4 kW-4pole motor has been built and tested. Then, its experimental performance is presented and analysed in comparison with the IM counterpart.

2 Basic Theory

A LSSynRM can be considered a hybrid between a synchronous and an induction motor, where the contribution of the latter is required only during the starting transient. In the steady-state condition, the motor operates at synchronous speed, where the torque is due to the anisotropic rotor geometry.

The concept at the base of this motor is quite easy. However, many aspects should be taken into careful account to design a motor of this type:

1. The cage has to fit in the complex rotor geometry without affecting the optimal anisotropic shape and the efficiency of the machine at steady state. This, in turn, leads to an uncommon asymmetrical cage.
2. The capability of the motor to effectively reach the synchronous speed depends on many variables, such as the inertia and torque characteristic of the load, the shape and material of the cage, and some external factors like temperature and supply voltage.
3. The asymmetrical shape of the squirrel cage often leads to a poor locked rotor performance, characterized by evident torque fluctuations as a function of the rotor position, and by a remarkable current absorption.

The main issues in the design of line-start motors are not related to the solution of each of the previous points, but to the solution of their whole. In particular, the interventions on the rotor geometry made to improve the efficiency certainly affect the starting capability and vice-versa.

The torque-speed characteristic of an LSSynRM can be represented as in Fig. 1 [5]; it is a combination of the IM torque and that of the synchronous motor.

What really characterizes the self-starting machine is the presence of the “pull-in” torque that brings the rotor to work at synchronous speed. The breakdown torque represents the maximum performance the machine can achieve at synchronous speed.

In order to properly understand the complex phenomenon of the pull-in, it can be helpful to reason in terms of energy, instead of torque [8]: if, approaching the synchronous speed, the rotor would have enough kinetic energy, the pull-in phenomenon will correctly happen, leading to a proper steady-state condition. In the other case, the rotor will remain on the asynchronous area of the torque characteristic (or

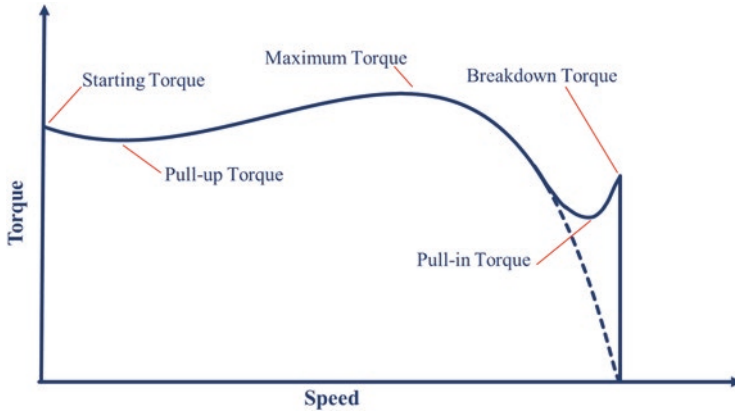


Fig. 1 Typical torque vs. speed characteristic of LSSynRM

rather operating with slip greater than zero): this working point can be considered as stable, but it leads to unacceptable fluctuation of both speed and current, due to the presence of the impulsive synchronous torque [5, 9]. These statements confirm that the pull-in capability of the motor depends on the load inertia and torque characteristic. More specifically, these lead to the definition of a critical value of load inertia [10] that the motor can effectively bring to synchronous speed, under equal mechanical, thermal, and electric conditions. Another limitation is represented by the starting torque, which is often not stable and strong as much as the torque of the IM, due to the very uncommon shape of the squirrel cage. In conclusion, LSSynRM is suitable in case of compressors, fans, pumps, blower, and other applications characterized by a low inertia and a weak locked rotor torque requirement. However, by an intense design activity, it is possible to fill the gap between the performance of LSSynRM and IM, enlarging its application field.

3 Motors Design

The technology of line-start motors is not so recent, but in the last years, it has attracted growing interest in high-efficiency applications.

Many studies have been carried out in the past: [8] introduced the topic of LSSynRM in early 1960. The principle at the base of the synchronization transient was analysed in-depth in [9] for PM motors, focusing on the critical value of load inertia. The analysis of the torque's components in a LSSynRM was proposed in [1], using a magnetic field decomposition. In [11], a FE-aided analytical method was developed to predict the starting capability of a LSPMM; for the same kind of machine, the optimal choice of the number of turns and stack length was discussed in [12]. The design of an LSSynRM, with the development of a dynamic equivalent circuit, was proposed in [2]; based on these results, the realization and testing of a

prototype with active inertia emulation were carried out in [3]. An interesting analysis of the starting transient of this kind of machine was also reported in [4].

The conventional design procedure would suggest picking up the problem starting from an analytical model of the machine. However, the analytical models are often not fully able to represent the behaviour of the motor, especially during the starting transient. The real starting capability of the machine, in terms of the maximum inertia for a given load torque characteristic, is not easy to achieve.

The problem thickens when it is necessary to fit a fully asymmetrical squirrel cage inside the rotor geometry: the actual cage's linkage flux, also considering the imbalance between the impedances of the bars, is quite challenging to represent analytically.

Thus, a reliable way in order to achieve a balance between the starting capability and the steady-state performance is to consider the FE analysis combined with suitable optimization algorithms [7] as the primary instrument for the design activity of the LSSynRM [5]. That is the procedure followed by the authors to design two LSSynRMs, 3 kW-2pole and a 4 kW-4pole, 400 V, 50 Hz for industrial applications. In the next sections, their simulation and experimental performance are presented.

3.1 3 kW-2pole LSSynRM - Design and Simulation Results

The 3 kW-2pole LSSynRM has to fall into the IE4 efficiency class according to the standard IEC 60034-30. This implies an efficiency of at least 89.1% at 50 Hz without tolerance.

The motor should replace an IE2 IM which is actually proposed for the same application. The stator core and winding topology of the corresponding IM are used for the LSSynRM, and the design is focused on the new rotor geometry. Moreover, in order to contain the product's industrialization time and cost, it is expected for it to share many existing tooling of the actual IM, such as all the components of the housing, the cooling fan, and the terminal box.

These constraints increase the difficulty of the design step, since many remarkable geometrical parameters, like the stack length, diameters, and the number of slots, cannot be modified.

The aluminium die cast process is selected for the cage, taking care of considering the same end-rings, in order to realize the die-casting process with actual industrial equipment.

The electrical steel used for the stator and rotor core is the commercial M470-50A, which represents a good compromise between cost, performance, and availability.

Another important requirement is the starting capability of the motor. It has been evaluated with a focus on the ratio K between the load inertia and the rotor's own inertia. It is commonly accepted that loads with $K > 10$ are very unlikely. Anyway, the target pull-in capacity in terms of K was chosen greater than 10, corresponding to starting a load with inertia greater than 0.035 kgm². This performance has to be achieved at steady-state temperature and constant rated load torque.

Table 1 3 kW-2pole LSSynRM requirements

Rated power	3 kW
Line voltage/frequency	400 V/50 Hz
Rated speed	3000 rpm
Rated torque	9.6 Nm
Efficiency class	IE4 (89.1%)
K (load inertia-rotor inertia ratio) at constant rated load torque	10

Table 2 3 kW-2pole LSSynRM design data

Rotor cage	Die-cast aluminium
Number of stator slots	24
Stack length	140 mm
Stator diameters (outer/inner)	152/80 mm
Turns in series per phase	132
Number of flux barriers per pole	4
Airgap	0.3 mm
Rotor inertia	$35 \times 10^{-4} \text{ kgm}^2$
Slot fill factor	0.42

Table 1 shows the main requirements of the motor design while Table 2 presents the main data of the obtained final design. Motor completely fulfils the imposed requirements.

Motor starting capability is shown in Fig. 2 in terms of speed vs time. Two cases are presented: load inertia set at 0.0175 kgm^2 (about 5 times the rotor’s inertia) and load inertia set at a critical value of 0.05 kgm^2 . A load torque/speed quadratic law has been imposed. Figure 2 highlights the successful (upper curve) and the unsuccessful (lower curve) synchronization process.

Figure 3 presents the starting capability of the motor in terms of load torque/inertia. This curve clearly identifies area of successful synchronization and area of failed pull-in. These performances have been achieved with the squirrel cage at the rated temperature of $80 \text{ }^\circ\text{C}$ and imposing constant load torque.

Figure 4 shows the motor’s efficiency, for several loads. It is higher than 88% between 50% and 125% of the rated torque.

Table 3 presents a comparison between the LSSynRM and the actual IE2 IM. The computation of the IM loss components is according to Standard IEC 60034-2-1

The efficiency improvement (almost 4 points) is mainly due to the reduction of losses in the iron core and no losses in the cage. Indeed, the losses in the cage at steady-state are not exactly null as the theory would suggest. It can be proved that also at synchronous speed the cage has eddy currents whose contribution is not effective on the torque performance itself; nonetheless, their presence introduces some additional losses, counted in the stray-load losses.

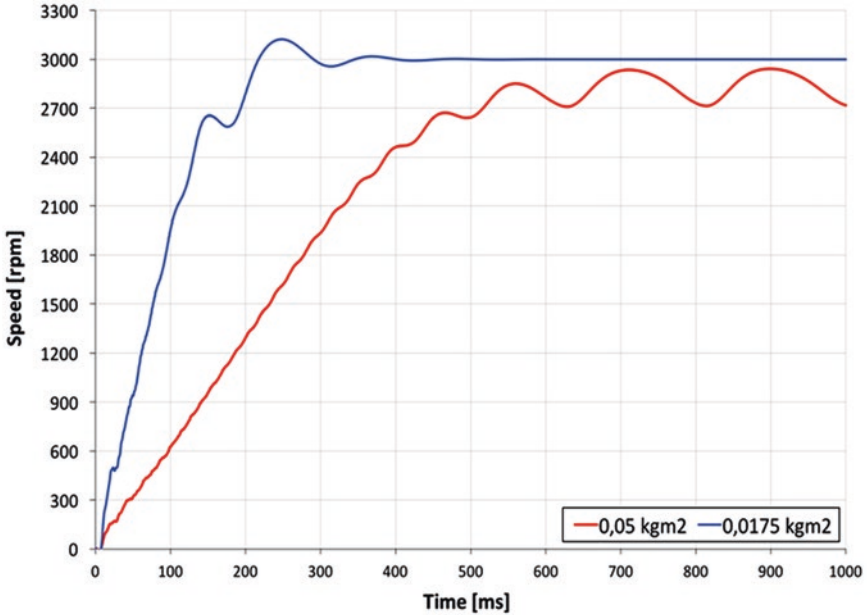


Fig. 2 3 kW-2pole LSSynRM: speed vs. time for low and high inertia loads

3.2 4 kW-4pole LSSynRM - Design, Simulation and Experimental Results

The 4 kW-4pole LSSynRM has to fall into the IE4 efficiency class according to the standard IEC 60034-30. This implies an efficiency of at least 91.1% (at 50 Hz) without tolerance. The motor is meant to replace an IE3 class IM (efficiency >88.6%) currently proposed for the same purpose, achieving a higher efficiency class without causing any increment in terms of cost.

As in the case of the 3 kW-2pole motor, the manufacturing constraints have been chosen in order to reduce the cost and time required for the industrialization of the LSSynRM: housing, cooling fan, terminal box, shaft and bearings, winding distribution and die-casting mould, cage material (aluminium) and end-rings, electrical steel (M470-50A) have to be the same as currently used for the production of the IM.

Table 4 summarizes the motor requirements and Table 5 presents the main data of the final design.

It has a stack length which is 20 mm shorter than the corresponding IE3 class IM. A saving of about 17% on the overall volume of electrical steel and 9% on the volume of copper has been achieved, with the same overall volume of aluminium.

Based on the results of the design procedure, a prototype was built, tested, and compared with the corresponding IE3 squirrel-cage IM as reported in Table 6.

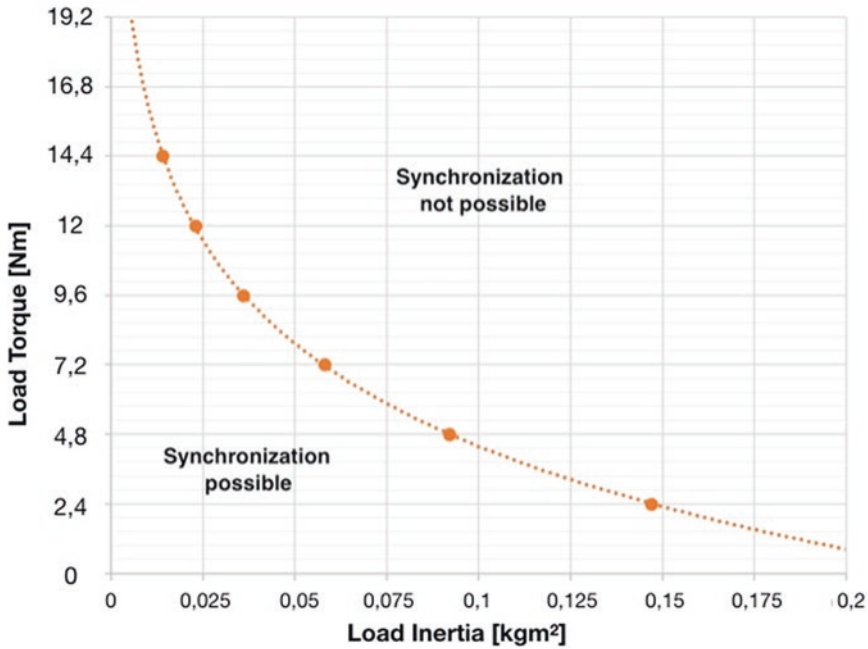


Fig. 3 3 kW-2pole LSSynRM: synchronization capability as a function of load torque and inertia

Figure 5 shows a view of the rotor core of the LSSynRM prototype while Fig. 6 shows the test bench for the evaluation of its steady-state performance. The computation of the loss components is according to Standard IEC 60034-2-1, as for the IM. Figure 7 shows the experimental efficiency vs load torque curves for the IM and the LSSynRM.

Table 7 shows the experimental results of the LSSynRM prototype locked rotor test, in comparison with the performance of the IE3 class IM.

In terms of breakdown torque, the LSSynRM prototype is able to maintain the synchronous speed up to twice the rated torque (50.5 Nm).

The requirement for the design of the LSSynRM in terms of the pull-in capability was to start a load with ten times the rotor’s own inertia, at steady-state temperature, and at constant load torque equal to the rated one (25.5 Nm). Two distinct series of tests were performed: the first at room temperature (about 20 °C), the second with the prototype at the steady-state temperature. The outcome of the test (Fig. 8) is positive, showing that the LSSynRM prototype is able to successfully start a load of almost eleven times the rotor inertia. Load inertia becomes about fourteen times the rotor inertia at room temperature.

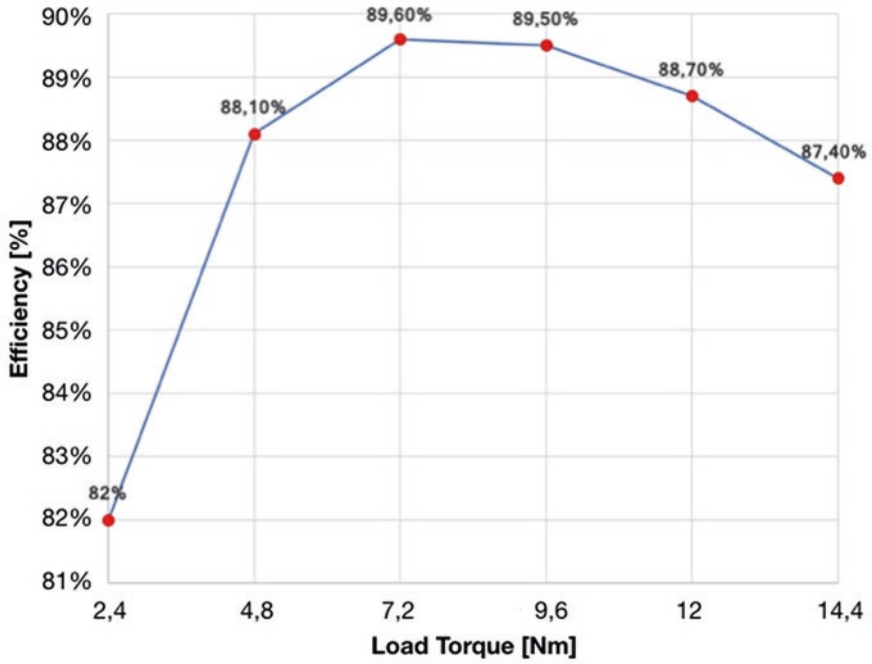


Fig. 4 3 kW-2pole LSSynRM: efficiency vs load torque

Table 3 3 kW-2pole. Comparison between the IM and the LSSynRM steady-state performance @ 50 Hz

	IM experimental	LSSynRM simulation
Line voltage	417 V	400 V
Rated torque T_n	9.8 Nm	9.6 Nm
Speed	2920 rpm	3000 rpm
Rated current I_n	6.03 A	6.44 A
Efficiency	85.9%	89.5%
Total losses	491 W	354 W
Joule losses	150 W	148 W
Cage losses	85 W	–
Core losses	180 W	110 W
Stray-load losses	56 W	71 W
F&W losses	20 W	25 W
Temperatures (winding/cage)	90–110 °C	75–80 °C
Power factor	0.80	0.75

Table 4 4 kW-4pole LSSynRM requirements

Rated power	4 kW
Line voltage / frequency	400 V/50 Hz
Rated speed	1500 rpm
Rated torque	25.5 Nm
Efficiency class	IE4 (91.1%)
K (load inertia-rotor inertia ratio) at constant rated load torque	10

Table 5 4 kW-4pole LSSynRM design data

Rotor cage	Die-cast aluminium
Number of stator slots	48
Stack length	160 mm
Stator diameters (outer/inner)	170/103 mm
Turns in series per phase	144
Number of flux barriers per pole	3
Airgap	0.3 mm
Rotor inertia	$105 \times 10^{-4} \text{ kgm}^2$
Slot fill factor	0.43

Table 6 4 kW-4pole. Comparison between the IM and the LSSynRM steady-state performance @ 50 Hz

	IM experimental	LSSynRM experimental	LSSynRM simulation
Line voltage	400 V	400 V	400 V
Rated torque T_n	26.4 Nm	25.5 Nm	25.5 Nm
Speed	1446 rpm	1500 rpm	1500 rpm
Rated current I_n	7.89 A	8.69 A	8.48 A
Efficiency	88.8%	91.6%	91.4%
Total losses	503 W	368 W	379 W
Joule losses	186 W	217 W	209 W
Cage losses	151 W	–	–
Core losses	125 W	107 W	118 W
Stray-load losses	29 W	37 W	42 W
F&W losses	12 W	7 W	10 W
Stator temperature	72 °C	53 °C	64 °C
Power factor	0.82	0.73	0.75

4 Conclusions

The chapter presents the design results of two LSSynRMs, 3 kW-2pole and 4 kW-4pole, 400 V, 50 Hz for industrial applications. Both motors have to fall into the IE4 efficiency class according to the international standard 60034-30-1. The motors are



Fig. 5 View of the rotor core of the 4 kW-4pole LSSynRM prototype

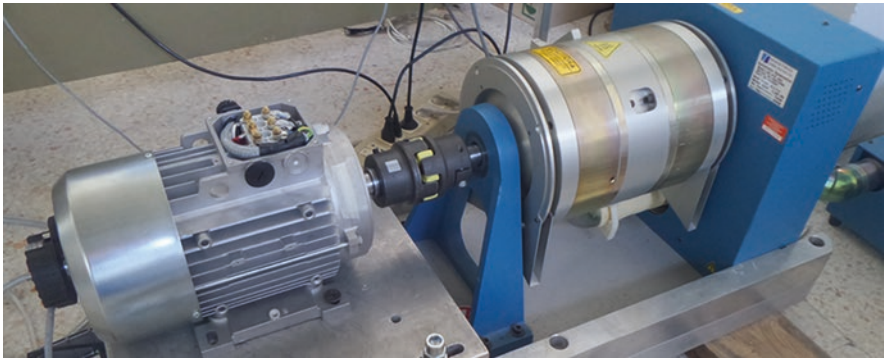


Fig. 6 Motor prototype and the test bench

meant to replace a 3 kW-2pole IE2 class IM and a 4 kW-4pole IE3 class IM currently proposed for the same purpose.

The performance, during both the starting and steady-state operations, was analysed and compared with that of the corresponding IMs by an accurate FE model.

Based on the results of the design phase, a prototype of the 4 kW-4pole motor was realized and tested.

The main result achieved with the proposed LSSynRMs is a higher efficiency than the commercial IMs one without causing any increment in terms of cost: the

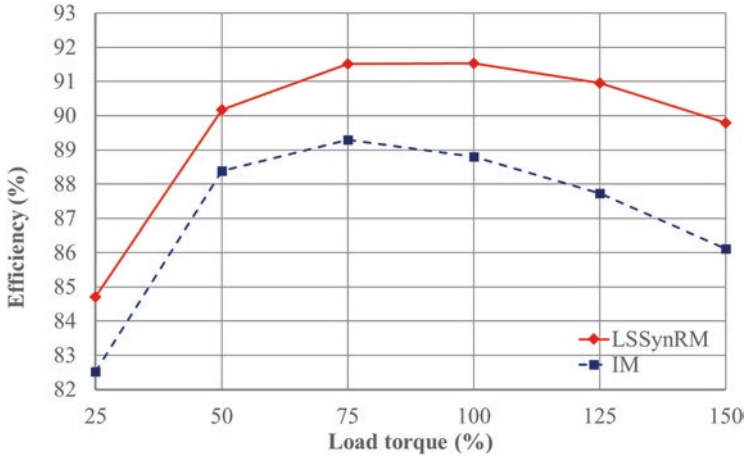


Fig. 7 Comparison between the 4 kW-4-pole IM and LSSynRM: efficiency vs. load torque, experimental results

Table 7 4 kW-4-pole. Comparison between the IM and the LSSynRM locked rotor performance @ 400 V/50 Hz

	IM experimental	LSSynRM experimental
Locked rotor torque T_{LR}	97 Nm	109 Nm
T_{LR}/T_n	3.7	4.3
Locked rotor current I_{LR}	67.2 A	63.7 A
I_{LR}/I_n	8.5	7.3

LSSynRMs are manufactured with the same tooling, components, and active materials and are able to fall completely into the IE4 efficiency class.

Despite the concerns related to the poor starting performance and the limited pull-in capabilities of the LSSynRM, the simulations and tests on the prototype demonstrate that a globally acceptable behaviour of the LSSynRM is reachable by proper design. In fact, specific tests concerning the locked rotor torque, the pull-in performance, and the starting operation demonstrate that the proposed LSSynRMs are able to start similar loads of the IM in terms of torque and inertia.

The main drawback of LSSynRM technology seems to be the poor power factor of minor concern in industrial applications where proper correction systems are often used.

In conclusion, the LSSynRM proved to be a cost-effective, mass production-ready solution for super-premium efficiency IE4 motors and is a promising alternative to the IM in a vast panorama of fixed speed industrial applications demanding high-efficiency.

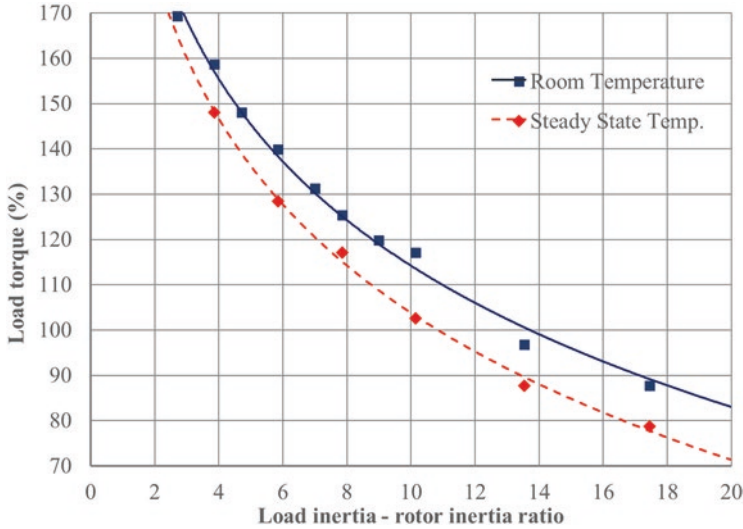


Fig. 8 4 kW-4-pole LSSynRM: synchronization capability as a function of load torque and inertia. Experimental results at room and steady-state temperature

References

1. J. Tampio, H. Kansakangas, S. Suuriniemi, L. Kettunen, J. Ikaheimo, Analysis of direct-on-line synchronous reluctance machine (DOLSynRM) start-up using a magnetic field decomposition, in Proceedings of the XXII International Conference on Electrical Machines (ICEM 2016). <https://doi.org/10.1109/ICELMACH.2016.7732517>, pp. 132–138, Sept 2016
2. M. Gamba, G. Pellegrino, A. Vagati, F. Villata, Design of a line-start synchronous reluctance motor, in Proceedings of the International Electric Machines & Drives Conference (IEMDC 2013). <https://doi.org/10.1109/IEMDC.2013.6556163>, pp. 648–655, May 2013
3. M. Gamba, E. Armando, G. Pellegrino, A. Vagati, B. Janjic, J. Schaab, Line-start synchronous reluctance motors: Design guidelines and testing via active inertia emulation, in Proceedings of the IEEE Energy Conversion Congress and Exposition (ECCE 2015). <https://doi.org/10.1109/ECCE.2015.7310340>, pp. 4820–4827, Sept 2015
4. A. Castagnini, H. Kansakangas, J. Kolehmainen, P. Savio Termini, Analysis of the starting transient of a synchronous reluctance motor for direct-on-line applications, in Proceedings of the IEEE International Electric Machines and Drives Conference (IEMDC 2015). <https://doi.org/10.1109/IEMDC.2015.7409047>, pp. 121–126, May 2015
5. M. Villani, M. Santececca, F. Parasiliti, High-efficiency line-start synchronous reluctance motor for fan and pump applications, in Proceedings of the XXIII International Conference on Electrical Machines (ICEM 2018). <https://doi.org/10.1109/ICELMACH.2018.8507230>, pp. 2178–2184, Sept 2018
6. A. Kersten, Y. Liu, D. Pehrman, Rotor design of a line-start synchronous reluctance machine with respect to induction machine for industrial applications, in Proceedings of the XXIII International Conference on Electrical Machines (ICEM 2018). <https://doi.org/10.1109/ICELMACH.2018.8507053>, pp. 393–399, Sept 2018
7. F. Parasiliti, M. Villani, S. Lucidi, F. Rinaldi, Finite-element-based multiobjective design optimization procedure of interior permanent magnet synchronous motors for wide constant-power

- region operation. *IEEE Trans. Ind. Electron.* **59**(6), 2503–2514 (2012). <https://doi.org/10.1109/TIE.2011.2171174>
8. J.F.H. Douglas, Pull-in criterion for reluctance motors. *Trans. Am. Inst. Electr. Eng. Part II Appl. Ind.* **79**, 139–142 (1960)
 9. A. Negahdari, H. Toliyat, Studying crawling effect in Line-Start Synchronous Reluctance Motors (LS-SynRM), in *EEE 25th International Symposium on Industrial Electronics (ISIE)* (2016)
 10. S.F. Rabbi, M.A. Rahman, Critical criteria for successful synchronization of line-start IPM motors. *IEEE J. Emerg. Sel. Top. Power Electron.* **2**(2) (2014). <https://doi.org/10.1109/JESTPE.2013.2295178>
 11. D. Mingardi, N. Bianchi, FE-aided analytical method to predict the capabilities of line-start synchronous motors, in *Proceedings of the IEEE Energy Conversion Congress and Exposition (ECCE 2014)*. <https://doi.org/10.1109/ECCE.2014.6954104>, pp. 5123–5130, Nov 2014
 12. D. Mingardi, N. Bianchi, L. Alberti, Optimal choice of stack length and conductors of line-start synchronous motors, in *Proceedings of the 8th IET International Conference on Power Electronics, Machines and Drives*, vol. 2016. <https://doi.org/10.1049/cp.2016.0220>, Apr 2016

Coordination of IEC and ISO Standards for Energy-Efficient Electric Motor-Driven Systems



Conrad U. Brunner, Maarten van Werkhoven, Franco Bua,
and Kirk Anderson

The IEC Advisory Committee on Energy Efficiency (ACEE) has launched with its Task Group 6 a project to promote the system approach for energy efficiency standardization outlined in IEC Guides 118 and 119, published in 2017 [2]. ACEE has the powerful instrument of Basic and Group Standards to coordinate activities of technical committees (TC) and to ensure coherence of their publications to contribute to the improvement of EMDS energy performance. Currently, some ten different IEC and ISO TCs (see also Fig. 3) are engaged in different elements of EMDS, including control and switchgear, converters, motors, belts and pulleys, gears, pumps, fans, and compressors.

A holistic approach to EMDS energy performance standardization requires a clear strategy of which energy aspects are to be considered, such as aligned operating points for efficiency tests, standard performance cycles for economic analysis, interpolation methods for the correct sizing of components and system design, etc. In order to avoid both dual and triple testing and multiple certification efforts for the manufacturer, a system approach with an integrated methodology for the alignment and coordination of each EMDS' component relevant characteristics is needed. This

C. U. Brunner (✉)
Impact Energy Inc., Zurich, Switzerland
e-mail: cub@cub.ch

M. van Werkhoven
TPA Advisors, Aerdenhout, The Netherlands
e-mail: mvanwerkhoven@tpabv.nl

F. Bua
Engineering Consulting and Design, Milan, Italy
e-mail: franco.bua@ceinorme.it

K. Anderson
NEMA, Rosslyn, VA, USA

will benefit the system integrator, industrial user, and government regulators and provide a means for effective market surveillance.

A workshop at the invitation of IEC ACEE TG6 of all the abovementioned stakeholders will be held as a side event of EEMODS'19. The goal of this project shall be discussed with all TCs involved to eventually reach consensus on the strategy and define a road map to allow mutual benefits. The overall plan on how to proceed and who will participate and lead the activities will also be part of the workshop. The IEC ACEE is an ideal platform to organize efforts among some three IEC TCs and some seven ISO TCs under a workshop format with the goal of eventually shifting from vertically oriented standardization to a horizontal approach to EMDS energy performance standardization.

1 Electric Motor-Driven Systems (EMDS)

An EDMS is a complex composite of several sequentially electrically and mechanically linked components (see Fig. 1). EMDS also represents the largest group of electric energy consumers. IEA has published in 2016 a new analysis in its World Energy Outlook [1] showing that electric motors driving pumps, fans, compressors, transport, and industrial process machines are responsible for 53% of global electricity use. For many decades, the often-repeated tune for maximizing electric energy savings in a cost-effective manner was, and still is, the coordination of the components involved in an EMDS into a well-matched system, at the design level, the manufacturing stage, as well as in the programming, control, and operation cycles. The matching of the many components, often manufactured by several diverse specialized manufacturers, requires complex engineering expertise and

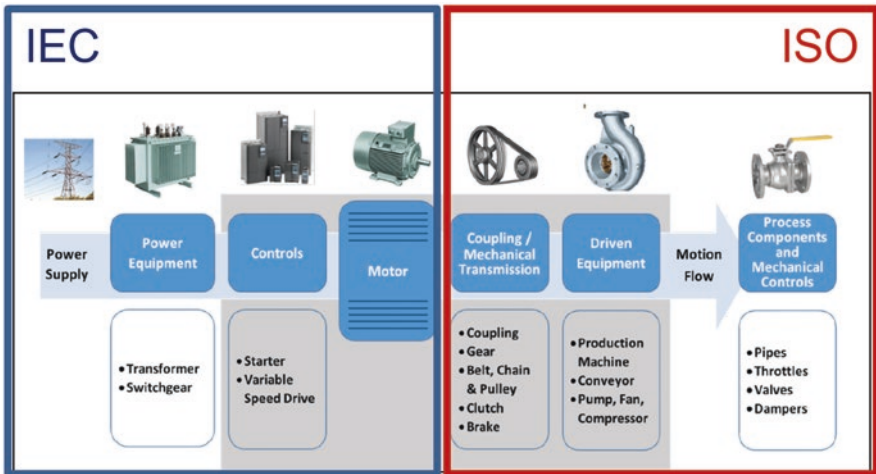


Fig. 1 The electric motor-driven system and its major components

good understanding of how each component and operating characteristic affects the overall system.

Of course, this coordination is easier for small integrated EMDS like circulator pumps, exhaust fans, and cooling compressors in refrigerators (typically below 2 kW) that are designed and manufactured by one producer who tries to make them small, light, efficient, and cost-effective. There are some outstanding success stories of an integration success like the circulator pumps where by employing advanced motors, such as new permanent magnet motor technology, the introduction of a variable frequency converter (VFC) together with better sized high efficiency pumps has transformed the market in less than a decade. The European ecodesign requirements quickly adopted this newly available technology in the regulation number 641 in 2009 [3] so that in Tier 2 from 1 August 2015 all circulators had to have an energy efficiency index (EEI) of not more than 0.23. This EEI of 0.23 was only possible to achieve by using this new technology with an integrated highly efficient circulator pump. According to the recent Topmotors Market Report 2018 [4] from 187,000 circulators sold in Switzerland in 2017, 96.8% now comply with this minimum requirement.

The energy performance of an EMDS has been highly advanced since the widespread market introduction of VFC. While only 20% of installed EMDS already use VFC [5], the market potential in closed loop pumps, fans, and many other applications with variable load and speed will eventually grow to approximately 50%. This means that the EMDS evolves to a more complex machine where not only good nominal speed/torque performance is required but also a high efficiency over a wide band of operating points has to be secured.

The integration of several components into an EMDS becomes much more difficult and complex in larger systems where the components are typically manufactured by two, three, or four different companies. The components are designed and manufactured by specialist industries with multiple applications in mind. The industrial user selects and sizes the necessary components and has them shipped to its point of use. Only then and there, when these components are assembled on the factory floor, the system comes to life. Only now its performance can be checked and – under certain circumstances – measured in situ. The electric input is relatively easy to measure with three-phase precision electric instruments while the EMDS is on standby and in operation, following a standard daily or weekly load profile. The accurate measurement of the mechanical output of the EMDS at the end of the pump or fan is much more complex. To measure the flow and head of the transported liquid of a pump or the flow and pressure of the transported gas of a fan requires previously installed measuring points and the availability of either permanently installed or mobile measurement equipment. It also requires detailed documentation of all the components with their nominal load points and the planned eventual field of required operating points.

2 Partial Load

While operating systems efficiently, partial load performance becomes much more important. Most components of an EMDS (VFC, motors, belts, pumps, fans, compressors, etc.) operate at partial load with considerably lower efficiencies. To secure energy efficiency at partial load is a challenge for all products and the entire EMDS. Also, the standardization of typical operating points at partial load for efficiency measurements is more complex because they involve several components with up to four power conversion steps with different quantities of performance indicators (see Table 1).

3 Product Standards

Most of the international product standards published by IEC and ISO that deal with energy performance still focus on efficiency of single components. ACEE case study no. 2 on electric motors [6] illustrates the number of product standards involved. Many of these components have subsequently been regulated through a national mandatory Minimum Energy Performance Standards (MEPS) based on the relevant IEC standards. One example of such interaction between regulation and standardization is the European ecodesign regulation no. 640/2009 [7] for motor efficiency that has adopted the energy efficiency classification system from IEC 60034-30-1 [8] with its IE code.

Table 1 Quantity and units of four steps of conversion in EMDS

Conversion step	Source	Input/output	Quantity	Units
1	From grid or mains	Electric input to VFC (AC)	Fundamental voltage, current, and frequency, $\cos \varphi$	V, A, Hz
			Electric power	W
2	From VFC	Electric input to motor (AC)	Voltage, current, frequency, total harmonic distortion, $\cos \varphi$	V, A, Hz, THD%
			Electric power	W
3	From motor shaft (or gear, belt, etc.)	Mechanical input to pump/fan/compressor or mechanical hoist/lift/conveyor, etc.	Torque, rotational speed	N m, rpm
			Mechanical power	W
4	From pump/fan/compressor, etc.	Mechanical output of fluid or gas of pump/fan/compressor, etc. to ducts or pipes; mechanical lift or rotation	Pressure difference (head), flow; weight, friction, acceleration	Pa (m), m^3/s , kg, m/s^2
			Mechanical power	W

Very rarely, standard makers and regulators have so far touched the complexity of publishing standards and MEPS for integrated systems (see [8]). This has a practical reason: a component can be relatively easily described in geometric terms and its performance can be measured in a testing lab based on output/input measurements. Subsequently, energy efficiency classes can be defined and given to the components.

There is also a historical reason: standardization activity has been mostly organized vertically (product oriented); one of the challenges energy efficiency poses to standardization organizations is therefore organizational and requires a coherent and effective framework to ensure the development of system-oriented standards.

The goal of the ACEE is to try and address this by creating guides that simplify the process while ensuring the committees consider all best practices, thereby improving the potential for commercially feasible market transformation and true energy savings.

4 System Standards

Top-down approach to standardization, starting at system level rather than at the product level, is not a new concept for IEC; system standards (“horizontal” standards) are increasingly required in sectors such as environment and energy efficiency.

IEC ACEE has proposed a structured approach in order to promote a systems approach for standardization in the field of energy efficiency and to ensure the consistency of standards relating to energy efficiency aspects common to several technical committees by avoiding duplication of work and contradictory requirements.

Certainly, horizontal standardization adds complexity to the consensus reaching process typical of standardization organizations. Industry has long ago claimed that their preference are standards and a MEPS for systems, several coordinated components, that allow to integrate and optimize components thus saving weight, volume, and cost. Industry is of course very interested in securing performance and compliance tests in one step (wire to water or wire to air) instead of a multitude of repeated testing requirements.

Systems are not always composed of the same components: the minimum configuration is an electric motor and one type of application. Figure 2 tries to estimate the market share of the various configurations of an EMDS. Components for motor control and mechanical equipment are not always present in an EMDS.

IEC has set up the ACEE, the responsible body to deal with energy efficiency matters which are not specific to one single technical committee of the IEC. ACEE coordinates IEC activities related to energy efficiency IEC Guide 119 [2], defines the formal procedure, and requests from the applicants a definition of the boundary, its scope of a horizontal energy efficiency aspect, and its eventual benefit. IEC ACEE receives the requests and after approval gives it to the IEC Standard Management Board (SMB) for confirmation.

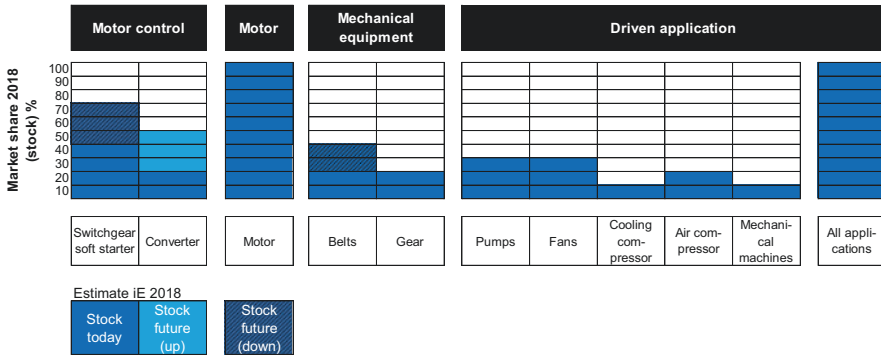


Fig. 2 Estimate of market share of the components of the various types of EMDS

A horizontal standard has (compared to a product standard) an additional pre-phase: two or more TCs together have to agree to apply to IEC ACEE in a formalized checklist to become a horizontal standard. IEC ACEE provides guidance for two different forms of horizontal standards:

- Basic energy efficiency standard (BEES): Publication covering energy efficiency aspects (EEA), applicable to products within the scope of two or more TCs. The focus of basic energy efficiency (EE) publications is the general tools and agreed methods for describing or achieving EE improvement in a defined boundary. These publications shall therefore describe EEA like measurement, calculation, and further methods like benchmarking and Key Performance Indicators (KPI) calculation for EE as described in IEC Guide 118.
- Group energy efficiency standard (GEES): Publication covering energy efficiency aspects (EEA), applicable to a specific boundary including products within the scope of two or more TCs. Group EE publications may be primarily intended as EE publications, but shall also be used by other TCs in applying their provisions. In addition, guidance shall be given to TCs on how to apply information from a group EE publication, for example, how to define boundaries for a particular application (interrelation between light fixture, motion detector, outside shading, etc.).

In order to bring together several TCs to work together, the need of a horizontal energy efficiency approach has to be clearly demonstrated, and the TCs involved must first understand the benefits of addressing these complex questions. The TCs involved have to agree on an active collaboration that serves to better follow the needs of the stakeholders involved.

- The regulators are interested to answer industry requests to provide minimum performance requirements for systems (“wire to water,” “wire to air,” etc.). The regulators need energy efficiency standards for products (existing) and systems (to be established).

- The manufacturers are interested to align their products electrically and mechanically with neighboring products and to better coordinate measuring methods and performance metrics for entire systems.
- The industrial product users are interested in guidelines for better sizing, operating, optimizing, and coordinating of products to evolve to energy-efficient systems. A set of tools is needed to calculate the system efficiency beforehand based on component performance and guidelines to measure the performance of a completed system in the factory.

IEC ACEE has accepted so far only two requests for a horizontal standard:

- IEC SMB has approved the request by TC 64 on the ACEE recommendation to allocate the following energy efficiency horizontal function “define energy efficiency measures in Low voltage electrical installations,” covered by IEC 60364–8-1 Edition 2 which will give the status of Group Energy Efficiency Publication.
- IEC ACEE has agreed to submit the request of IEC SC 22G to the IEC SMB for the recommendation to assign an energy efficiency horizontal function of “establishing a clear and simple system methodology for the comparison of the energy performance of motor systems to help product and system improvement” and assign the status of Group Energy Efficiency Publication to IEC 61800–9-1 in collaboration with IEC TC2 and IEC TC121.

5 IEC and ISO Coordination

For better coordination and to ensure coherence international standards for EMDS, some three IEC TCs and six ISO TCs need to be involved (see Fig. 3).

The goal of this coordination effort of a horizontal standard is to deal with a number of issues that are a common concern in improving the energy efficiency of EMDS, like:

- Aligned terminology, scope, and boundary for EMDS.
- Coordinated operating points and conditions for tests.
- Typical operating characteristics and time/load profiles for economy.

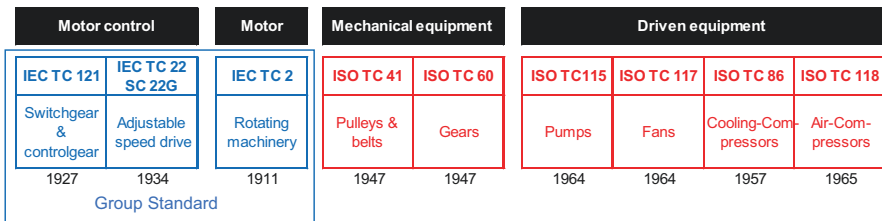


Fig. 3 Technical committees from IEC and ISO that are directly involved in product standards for EMDS (below: year of launch)

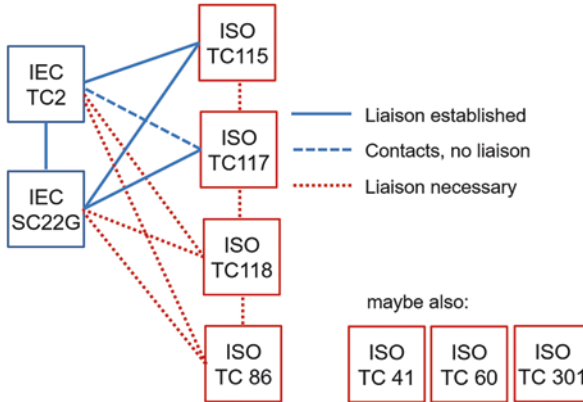


Fig. 4 Liaisons (established and planned) between the IEC and ISO TCs involved

- Ex ante: calculation method for system energy performance.
- Ex post: acceptance/testing procedure for system energy performance.
- Coordinated efficiency classification methods and metrics for product and system energy performance.
- Aligned interpolation method for losses and efficiency of system.

A first level of improved interaction between TCs is recommended through the liaison of experts as members of two interacting committees (see Fig. 4). This liaison serves to speed up the exchange of information especially with ongoing projects and helps to better understand each TC's concerns and expertise.

The coordination effort of EMDS involves a review of IEC and ISO standards (already published and under development) that include energy efficiency aspects, both in general terms, for energy performance testing, energy efficiency classification, and for basic elements like scope, performance, and tolerances (see Fig. 5, draft survey, to be extended and completed).

6 Tools and Guidance for EMDS

The assessment of the energy performance of such a system is one of the possible system attributes. System energy attributes are one of the energy efficiency aspects (EEA) addressed in IEC Guide 119.

Ex ante, a system performance calculation is required to assess the efficiency of the components involved. With the Motor Systems Tool (MST, see Fig. 6, [10]), a variety of operating points of an EMDS can be defined and their combined efficiency calculated. For VFCs, electric motors, gears, and belts as well as driven equipment like pumps and fans, a well-documented database of performance data from standards is underlaid so that a specific calculation can be made quickly. The

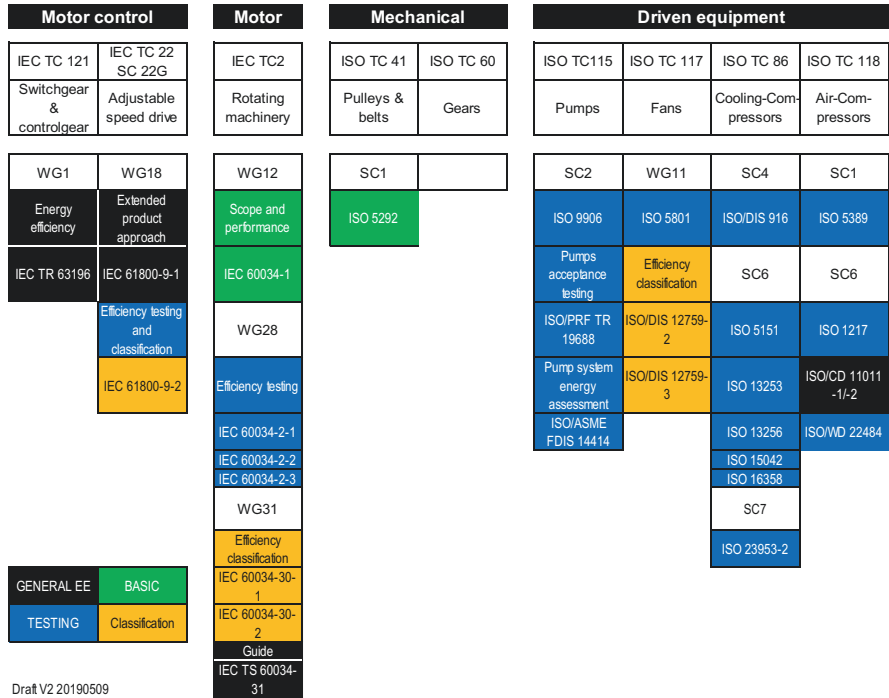


Fig. 5 Relevant energy efficiency standards for EMDS in IEC and ISO TCs (draft, to be extended and completed)

MST includes the database of motor efficiency from IEC 60034–30-1. In its latest version, the MST also includes the reference values and IE classification for VFCs of IEC 61800-9-2, Edition 1.

When used together with measured or estimated statistics of hours of load for an EMDS, the MST provides the data to calculate annual system efficiency. These results are crucial for economic decisions on the cost-effectiveness of investments in components.

Ex post, the specific energy efficiency aspect of system performance assessment under operating conditions can be approached in different moments of the EMDS life cycle. Three examples from existing standards (even though they might not be 100% replicable) serve as guidance for EMDS (see below). A good example for on-site acceptance tests are in several existing IEC standards, typically for large machines that can only be assessed once assembled in the place of final use:

- IEC 60953–2:1990
Rules for steam turbine thermal acceptance tests. Part 2: Method B – Wide range of accuracy for various types and sizes of turbines
- IEC 62381:2012
Automation systems in the process industry – Factory acceptance test (FAT), site acceptance test (SAT), and site integration test (SIT)

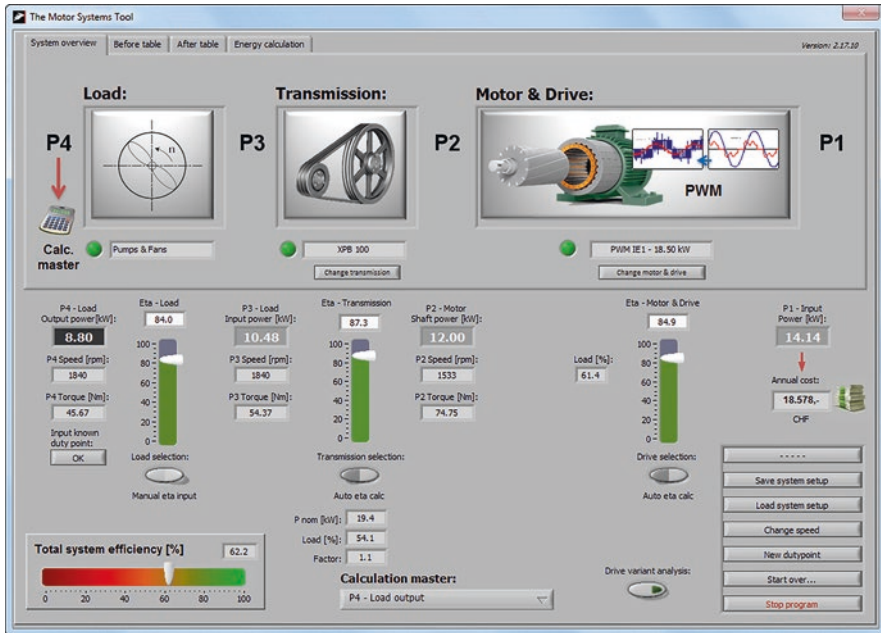


Fig. 6 The Motor Systems Tool. (Source: Danish Technological Institute, available at www.motorsystems.org)

- IEC 60193:1999

Hydraulic turbines, storage pumps, and pump turbines – Model acceptance tests

These acceptance tests serve as models for performance tests of EMDS while assembled in the final user position in a factory. It helps to define, already in the stage of specifications and contracts of products, the measuring points, the operating conditions, and the minimum requirements. It eventually serves as the base for the final acceptance protocol to check the contractual performance and efficiency data. It can also be used to check test government regulations for minimum efficiency requirements of products and systems.

7 Workshop in Tokyo

In order to bring stakeholders from industry, university, international standards, etc. to the table, an international workshop (by invitation only) will be staged by IEC ACEE Task Group 6 on 20 September 2019 as a side event of EEMODS' 19 in Tokyo.

The goals of this workshop, as part of the project to align and coordinate IEC and ISO standards for energy-efficient EMDS, are:

1. Inform participants on energy efficiency aspects in EMDS.

2. Collect information from all TCs and stakeholders:
 - (a) Existing and proposed energy efficiency standards and regulations.
 - (b) Hear needs, concerns, and interests to cooperate for energy-efficient EMDS.
3. Explain and propagate IEC Guides 118 and 119:
 - (a) Explain basic and group standards for EMDS.
 - (b) Identify energy efficiency aspects for EMDS.
4. Discuss possible ways forward:
 - (a) Liaison and joint working group?
 - (b) Group EE standard/basic EE standard?
 - (c) Start with project group, cooperation with existing TCs.
 - (d) Revise existing standard or launch a New Work Item Proposal (NP)?

The speakers (see Fig. 7) together with the invited guests will represent several ISO and IEC TCs involved and other stakeholders from industry associations, universities, and national regulators.

The invited participants will be experts from the EMDS field who can contribute to defining a good way forward including calculation tools, interpolation methods, policy guidelines and relevance for regional markets, etc.

The outcome of the informal workshop will be a list of interested experts and TCs who are willing to go forward and cooperate with the definition of basic and/or group standard(s) for EMDS.

Agenda				Speaker	Affiliation	Topic	Country
08:30 Registration				Sandie B. Nielsen	IEC TC 2, IEC SC 22G, Danish Technological Institute (DTI)	System efficiency: Software Motor Systems Tool	Denmark
09:00 Workshop starts							
Speaker	Affiliation	Topic	Country	Martin Doppelbauer	IEC TC 2 chairman, IEC SC 22G, Karlsruhe Institute of Technology (KIT)	Interpolation methods for partial load	Germany
Conrad U. Brunner	IEC ACEE TG6, Impact Energy	Welcome and goal of the IEC & ISO Workshop on energy efficient EMDS	Switzerland	Benno Weis	IEC TC 22 chairman, Siemens	The Extended Product Approach according to IEC 61800-9-1	Germany
Franco Bua	IEC ACEE TG6	Basic and Group Standards according to IEC Guides 118 and 119	Italy	Kurt Stockman	University of Gent, IEC SC 22G WG18	Gearbox and belt drive efficiency from a EMDS perspective	Belgium
Maarten van Werkhoven	IEC ACEE TG6, EMSA, TPA energy advisors	Policy Guidelines for Motor Driven Units	Netherlands	Shunsuke Matsunaga	Hitachi Industrial Equipment Systems, chairman of Inverter TC of JEMA	Impact of motor system standards on motors, inverters and application in Japan	Japan
Geoff Lockwood	ISO TC 117, EVIA, ebmpapst	Energy efficiency standards for fans, focus on Europe	UK	Kirk Anderson	IEC ACEE TG6, NEMA	What the US industry (NEMA) can benefit from aligned motor system standards?	USA
Tim Mathson	AMCA, Greenheck Fan Corp.	Regulatory policy for fans, focus on USA	USA	Jesper Jerlang	Danfoss	What can the European Industry (CEMEP) benefit from aligned motor standards?	Denmark
Benoit Leprette	IEC TC 121, Schneider Electric	Energy efficiency standards for switch-gear and controlgear	France	General discussion (100 minutes)			
Peter Gaydon	ISO TC 115, Hydraulic Institute	Regulations on pumps in the USA	USA	Conrad U. Brunner	IEC ACEE TG6, Impact Energy	Conclusions, the way forward	Switzerland
Markus Teepe	ISO TC 115, Wilo	Energy efficiency standards for pumps	Germany	17:00 Workshop ends			
Luc De Beul	ISO TC 118, Pheurop, Atlas Copco	Energy efficiency standards for air compressors	Belgium				
Lunch break (60 minutes)							

Fig. 7 Agenda of the IEC and ISO workshop on energy-efficient EMDS in Tokyo on 20 September 2019

8 Conclusion

Horizontal standards for electric motor-driven systems are needed for industry, regulators, and users. So far, few horizontal standards and MEPS exist because of lack of coordination. As the use of VFCs expands, so does the potential energy savings possible through the optimization of the components taking not only nominal loads but a variety of operating points and conditions into account at the system level.

IEC ACEE has defined the procedure to arrive at consistent group or basic standards that help to lower market barriers and improve energy efficiency. A large number of IEC and ISO TCs are involved in the standardization of different components for EMDS. Tools exist to calculate ex ante the system performance. IEC also has the precedent of acceptance tests for complex and large machines that can only be assessed in their final assembly at the factory site.

In order to move forward with the coordination and alignment of horizontal standards, ACEE has invited experts from various stakeholders for a workshop as a side event to EEMODS' 19 in Tokyo to discuss a common path forward for horizontal standards of EMDS.

The global market transformation with advanced energy efficiencies of electric motor-driven systems can only be successful with intelligent interfaces between electrical and mechanical products based on internationally agreed horizontal standards.

References

1. International Energy Agency, *World Energy Outlook 2016* (IEA, Paris, 2016)
2. IEC Advisory Committee for Energy Efficiency (ACEE), *Guide 118 Inclusion of energy efficiency aspects in electrotechnical publications*, Geneva, Switzerland, 2017 IEC Advisory Committee for Energy Efficiency (ACEE): *Guide 119 Preparation of energy efficiency publications and the use of basic energy efficiency publications and group energy efficiency publications* (Geneva, 2017)
3. European Commission, *Commission Regulation No 641/2009 of 22 July 2009 implementing Directive 2005/32/EC of the European Parliament and of the Council with regard to ecodesign requirements for glandless standalone circulators and glandless circulators integrated in products* (Brussels, 2009)
4. Impact Energy (Swiss Federal Office for Energy), *Topmotors Market Report Switzerland 2018* (Zurich, 2019)
5. Rita Werle, Conrad U. Brunner, Rolf Tieben, Swiss motor efficiency program EASY: results 2010–2014, in *Conference proceedings ACEEE Summer Study on Energy Efficiency in Industry*, (Buffalo, 2015)
6. IEC Advisory Committee on energy efficiency (ACEE), *Case study: electric motors IEC ACEE 02: 2018* (Geneva, 2017)

7. European Commission, *Commission Regulation No 640/2009 of 22 July 2009 implementing Directive 2005/32/EC of the European Parliament and of the Council with regard to ecodesign requirements for electric motors* (Brussels, 2009)
8. IEC 60034-30-1, *Rotating Electrical Machines - Part 30-1: Efficiency Classes of Line Operated AC Motors (IE code)* (Geneva, 2014)
9. Maarten van Werkhoven, Rita Werle, Conrad U. Brunner (IEA 4E Electric Motor Systems Annex), *Policy Guidelines for Motor Driven Units, Part 1: Analysis of standards and regulations, Zurich, Switzerland, 2016; Policy Guidelines for Motor Driven Units, Part 2: Recommendations for aligning standards and regulations for pumps, fans and compressors* (Zurich, 2018)
10. 4E EMSA (Danish Technological Institute), *The Motor System Tool*, version 2.17.11, October 2017. www.motorsystems.org/motor-systems-tool

Surface Eddy Current Suppression on Additively Manufactured Solid Rotor Active Parts



Max Hullmann, Stefan Urbanek, and Bernd Ponick

Nomenclature Symbols

A	Surface area
B	Flux density
C	Factor
G	Basic function
N	Number of stator slots
P	Power
S	Current density
W	Coil span
d'	Related thickness
f	Frequency
h	Height
k	Overhang factor
l	Length
m	Number of phases
n	Quantity
p	Number of pole pairs
q	Number of slots per phase and pole
r	Radius
w	Width
δ_g	Air-gap length
δ	Electromagnetic penetration depth
k	Electrical conductivity
μ_r	Relative permeability
v'	Ordinal number
p	Pole pitch

M. Hullmann (✉) · S. Urbanek · B. Ponick
Institute for Drive Systems and Power Electronics, Leibniz University Hannover,
Hannover, Germany
e-mail: max.hullmann@ial.uni-hannover.de; stefan.urbanek@ial.uni-hannover.de;
ponick@ial.uni-hannover.de

Subscripts

1	Stator
2	Rotor/test specimen
max	Maximum
min	Minimum
j	Yoke
p	Related to spatial fundamental
s	Slot
t	Tooth
δ	Electromagnetic penetration depth
λ	Wavelength
μ	Permeability
e	Eddy current

1 Introduction

Additive manufacturing (AM) allows the layered creation of components directly from 3D CAD data files without the use of forming tools. Using this technology, the implementation of complex component geometries, e.g., lattice structures, bionic structures, or freeform surfaces, offers advantages on a technical and economical scale. The processability of metal powder has been strengthening the application of AM in electromechanical engineering in recent years [1–6]. Previous studies demonstrated successfully the construction of a ferromagnetic lightweight-designed rotor for a synchronous machine and a skewed rotor structure for an induction motor using AM [7, 8]. Further examinations focused on the utilization of the AM technology for direct-driven wind turbines, an almost entirely metal-additive printed permanent magnet synchronous machine (PMSM) and a thermal design of additively manufactured induction motors with high power density [9–11].

Additively manufactured rotor active parts of synchronous machines have solid surfaces, which can be shaped, but do not consist of conventionally isolated metal sheets. Due to spatial harmonics in the air-gap field of electrical machines, additional eddy current and hysteresis losses occur in the AM rotor surface caused by the stator current time harmonics, the distribution of the stator winding, and the slotting of the stator. Inspired by several studies on eddy current suppression in rotors of electrical machines, the basic idea of reducing the influence of this undesired effect is to groove the rotor surface directly during the manufacturing process [12–16].

Hence, following a brief introduction to the AM process of rotor active parts, different rotor surface groove arrangements are examined, described and rated by 3D finite element analysis (FEA). Based on this FEA, an analytical eddy current loss prediction approach is presented. The results are further used to derive

guidelines in terms of grooving depth, grooving width, and surface grooving density for a loss-reduced design of electrical machines using the design freedom of metal additive manufacturing technologies. For experimental validation of the theoretical study, an equivalent arrangement test bench including the test bench design and 3D FEA results of the expected eddy current losses is presented in the last section.

2 Additive Manufacturing of Rotor Active Parts

Based on the investigations in [6], the rotor active parts can be manufactured by a laser beam melting (LBM) process (see Fig. 1) using a ferrosilicon alloy powder with a silicon content of 2.9%. In the first step of this process, the powder is applied in up to 25 μm thin layers by a recoater. For melting, a powerful ytterbium laser is used which creates a local melting bath where it hits the powder. The process chamber is filled with a protective gas to avoid oxidation phenomena. In addition, the building chamber is heated to reduce the laser power required. After having finished the melting process for one layer, the component platform is lowered and the next layer of powder is applied, so that this process can be repeated. In this way, any metal body can be produced with a very high material density (>99%) and a surface roughness of up to 5 μm [18]. After separation of the component from the unused powder, mechanical or heat aftertreatment may be necessary to increase the mechanic and magnetic properties. Both methods are described in [8], where a 2-h heat treatment of 900 $^{\circ}\text{C}$ increases the maximum relative permeability from approx. $\mu_r = 900$ to $\mu_r = 3000$.

3 Determination of Eddy Current Effects

In the current study, an abstracted simulation model is considered for the sake of simplicity. The basic idea is to create and move a spatial air-gap field wave relative to the observed surface of the ferromagnetic material, in order to generate eddy

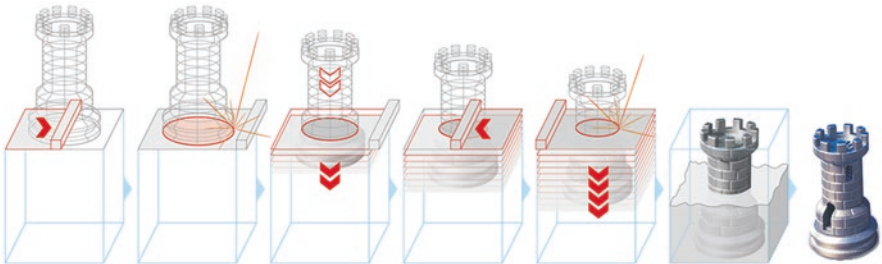


Fig. 1 Principle of laser beam melting [17]

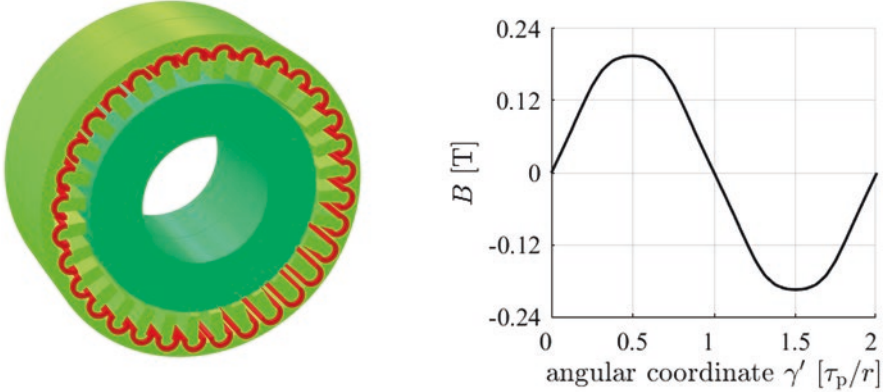


Fig. 2 Left: Abstracted simulation model with 32 poles and no grooving. The dark green rotor region represents the solid rotor surface, whereas the light green section represents the stator with the winding (red) to excite the air-gap field. The air region is hidden. Right: Radial air-gap field in the simulation model

currents. Using the 3D FEA software *Opera-3D*, the arrangement shown in Fig. 2 was created.

The model essentially consists of a stator equipped with a concentrated single-phase winding and a test specimen inside with $\mu_r = 2700$ caused by an assumed pre-saturation of 0.9 T according to a realistic machine and $\kappa = 5 \cdot 10^6$ S/m. The stator is made of an ideally magnetically and electrically conductive material and is perfectly laminated, so that eddy current effects only can appear in the rotor region. The winding is fed by a DC current, in order to create a stationary air-gap field. As mentioned above, rotating the rotor region leads to the desired relative movement of the observed surface and the air-gap field. The exact dimensions of this model are listed in Table 1.

By rotation of the test specimen with its surface velocity c and the wavelength λ , the frequency $f = c/\lambda$ of the induced voltage can be exposed. The mean eddy current power loss can thus be described by the analytical expression

$$\bar{P}_e = \sqrt{\frac{\pi\kappa}{\mu_0\mu_r}} \cdot 2rl \cdot f^{\frac{3}{2}} \cdot \frac{\lambda^2}{4} \hat{B}_\lambda^2 \quad (1)$$

with the wavelength λ corresponding to the double pole pitch $2\tau_p$ of the FEA model and the air-gap field amplitude $\hat{B}_p = 0.2$ T [19]. A comparison between the analytical and the numerical calculation for variable frequencies up to 1000 Hz is shown in Fig. 3.

Contrary to the FEA calculation, the analytical expression assumes an infinitely long current path in the axial direction, which explains the slight discrepancy.

Table 1 Dimensions of the FEA model

Name	Value
Outer radius of the test specimen	$r = 26.74 \text{ mm}$
Air-gap width	$\delta_g = 1 \text{ mm}$
Axial length	$l = 31 \text{ mm}$
Tooth height	$h_{t,1} = 7 \text{ mm}$
Tooth width	$w_{t,1} = 2.72 \text{ mm}$
Slot width	$w_{s,1} = 2.72 \text{ mm}$
Pole pitch	$\tau_p = 5.25 \text{ mm}$
Height of the stator yoke	$h_{j,1} = 10 \text{ mm}$
Height of the rotor yoke	$h_{j,2} = 12 \text{ mm}$

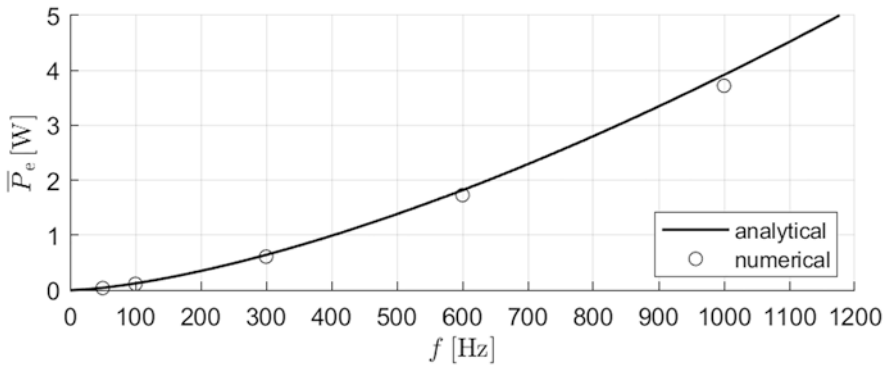


Fig. 3 Analytically calculated mean eddy current losses of the ungrooved test specimen in comparison with the FEA results of the basic model for variable frequencies with $\hat{B}_p = 0.2 \text{ T}$

3.1 Basic Research

To clearly determine the best slot arrangement for reducing eddy current losses, starting from axial slotting at 0° skewing angle, a gradually increasing skewing angle is attached to the slots until at 90° only a circumferential component is left. In order to be able to make a uniform determination, it is necessary to avoid overlapping slots within the axial direction (Fig. 4).

The FEA simulation data are presented in Fig. 5. For all investigations, a slot width of $w_{s,2} = 1 \text{ mm}$ is used with regard to the currently available AM manufacturing processes and possible real test arrangements.

Two conclusions can be derived from the data.

1. Every axial slot component leads to additional eddy current losses and every circumferential slot component leads to a loss reduction.
2. Multiple slotting causes an amplification of both effects.



Fig. 4 Design of the rotor geometry for the skewed slots. (a) 22.5° skewing (b) 45° skewing with overlapping (c) 53.5° skewing without overlapping

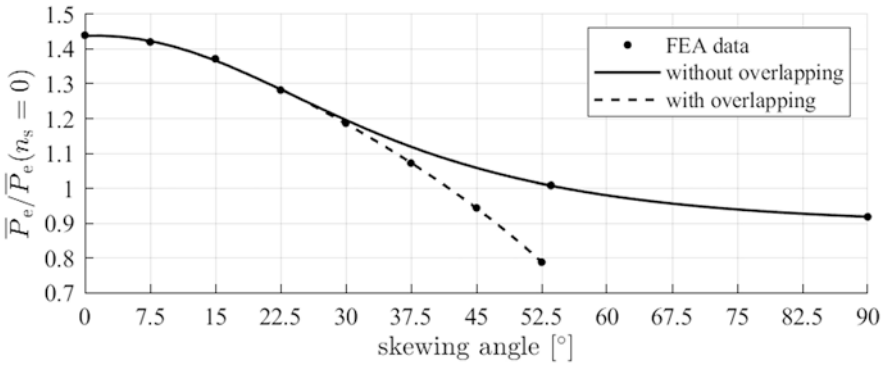


Fig. 5 Mean eddy current losses due to slotting of the test specimen related to mean eddy current losses in the specimen without slots ($n_s = 0$) with $h_{s,2} = 4$ mm, $w_{s,2} = 1$ mm, $f = 300$ Hz and $\hat{B}_p = 0.2$ T

Figure 6 shows in detail the differences between the two slot types regarding eddy current formation.

In case of an axial slot, the magnetic flux is forced to move beneath the slot, and therefore, the eddy current is extended to a larger surface and causes additional losses. In the case of the circumferential slotting, the eddy current main flow, which points into the axial direction, is interrupted, and a significantly smaller eddy current vortex occurs, since the current spreads over a larger area, and as a result, the losses will be reduced. Regarding the slot height, the FEA calculations also show that the conditions $h_s \geq 3$ mm and $h_s \geq 2.5 \cdot \delta_{\max}$ must be fulfilled, so that no eddy currents can form at the bottom of the slot, where

$$\delta_{\max} = \sqrt{\frac{1}{\mu\kappa\pi f_{\min}}} \quad (2)$$

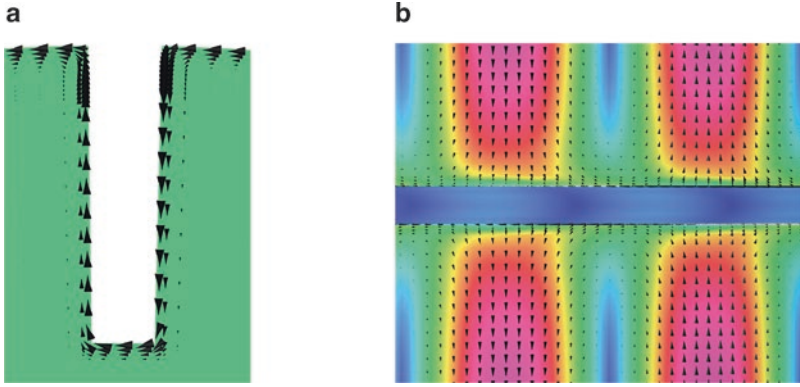


Fig. 6 Fields in a detailed view. **(a)** Magnetic flux in the cross section of an axial slot. **(b)** Eddy current flow in the area of a circumferential slot from the top view

describes the maximum analytically approximated electromagnetic penetration depth. Figure 7 shows the qualitative field and vector plot of the magnetic flux density near a circumferential slot with different heights for comparison.

3.2 Circumferential Grooving

For further investigation of the circumferential grooving, in this section, the test specimen is grooved systematically by up to $n_{s,max} = 15$ slots. The slots will be set evenly along the axial length. By reducing the cross section of the tooth in terms of pre-saturation, $\mu_{r,tooth}(n_s) \propto A_{cross}$ is stored for the remaining tooth material as a function of the number of slots for the FEA calculation (see Fig. 8).

The width of the teeth $w_{t,2}$ thus formed corresponds at $n_{s,max} = 15$ to the slot width. In Fig. 9, the results of this investigation are drawn for varying frequencies up to 1000 Hz.

Two major effects can be pointed out for the explanation of the increasing divergence of the graphs with a growing number of circumferential slots.

1. It can be related directly to the decreasing relative permeability in the teeth and explained by the analytically derived proportionality $\bar{P}_e \propto \sqrt{1/\mu_r}$. The graph for 1000 Hz clearly shows that this correlation counteracts the loss reduction, so that a local minimum exists, which occurs at $n_s \approx 11$ or $w_{t,2}/w_{s,2} \approx 2$ for the dimensioning in the present case.
2. It can be attributed to the related thickness $d(n_s, f) = w_t(n_s)/\delta(n_s, f)$ which describes the decreasing ratio between tooth width and electromagnetic penetration depth with an increasing number of circumferential slots. As a consequence, the eddy currents forming in a tooth with $d < 4$ begin to interfere with each other and therefore, the losses decrease additionally.

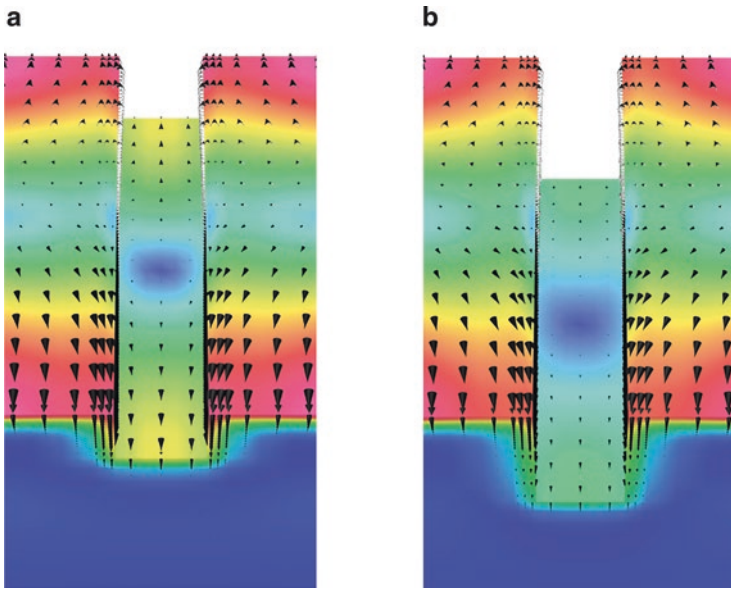


Fig. 7 Qualitative field and vectors of magnetic flux density on the specimen near a circumferential slot with $f = 300 \text{ Hz}$ and $\hat{B}_p = 0.2 \text{ T}$. (a) $h_s = 1 \text{ mm}$ (b) $h_s = 2 \text{ mm}$

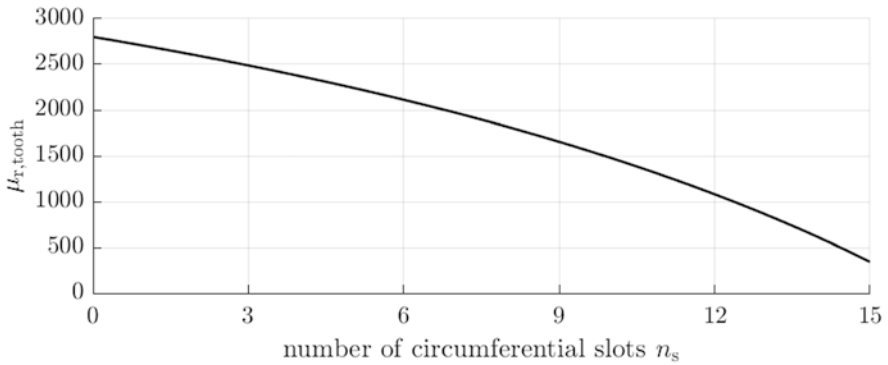


Fig. 8 Mean relative tooth permeability depending on the number of circumferential slots

3.3 Analytical Approach

Assuming that neither of the two effects will occur, a uniform basic curve $G_C(n_s)$ is then obtained independent of the frequency. This basic curve can be expressed over the axial slot density and is presented for a variable slot width in Fig. 10.

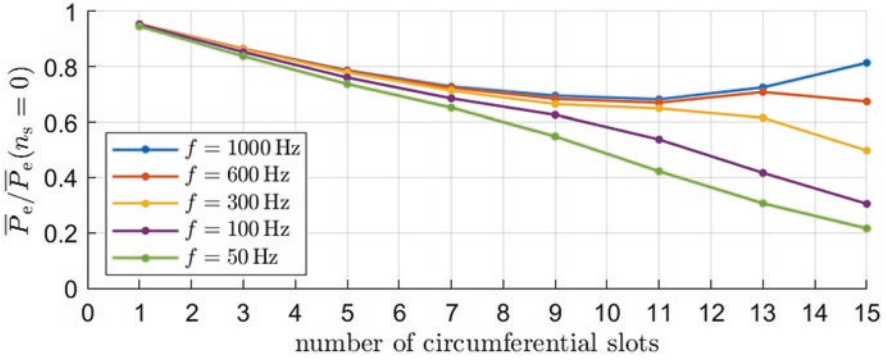


Fig. 9 Eddy current losses occurring in the test specimen as a function of the number of circumferential slots with varying frequencies taking the variable permeability in the teeth into account. The results are related to the eddy current losses of the basic model with $h_{s,2} = 4 \text{ mm}$ and $\hat{B}_p = 0.2 \text{ T}$

The comparison of the curves shows that the main contribution to an eddy current suppression is made by the interruption of the current paths. Although the slot width also reduces the eddy current losses due to the reduction of the rotor surface area, it provokes undesired tooth saturation.

In order to improve the corresponding basic function with respect to the numerical investigation, correction factors are defined to take the relative permeability and the related thickness into account. The new basic function can be expressed as

$$G_C(n_s) = G(n_s) \cdot C_\mu(n_s) \cdot C_\delta(d') \tag{3}$$

with the permeability correction factor

$$C_\mu(n_s) = \sqrt{\frac{\mu_r(n_s = 0)}{\mu_r(n_s)}} \tag{4}$$

and the related thickness correction factor

$$C_\delta(d') = \frac{\sinh(d') - \sin(d')}{\cosh(d') - \cos(d')} \tag{5}$$

Figure 11 shows both, the basic function with and without taking the correction factors into account, and compares it with the eddy current losses for selected frequencies from the previous results.

The found functions correspond with high accuracy to the results of the FEA simulations. In the range of three to nine circumferential slots, there is a small deviation from the simulation data for $f = 50 \text{ Hz}$. In the simulation, the first loss reductions compared to $G(n_s)$ are apparent from $w_{t,2}/\delta \approx 10$, but the factor $C_\delta(d')$ only

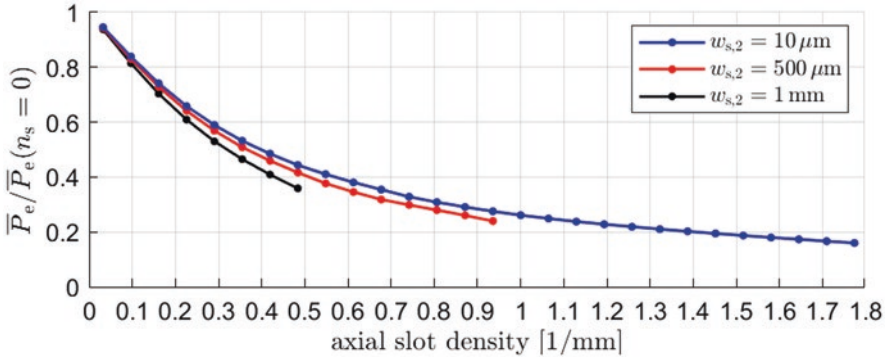


Fig. 10 Basic functions for three different slot widths

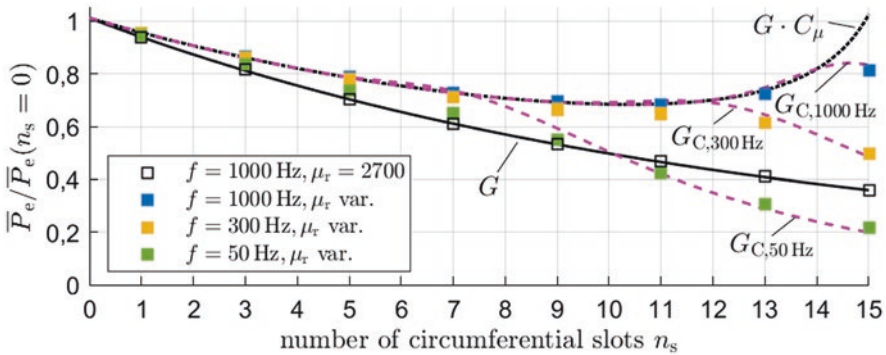


Fig. 11 Basic function including and excluding the permeability and related thickness correction factors in comparison with the eddy current losses of selected frequencies from the FEA simulation

becomes effective from a ratio of $w_{t,2}/\delta \leq 4$. If the skin effect remains so strongly pronounced for frequencies $f > 1000$ Hz that the eddy currents can flow without restriction, the eddy current losses form rapidly due to saturation and even exceed the losses occurring in the basic model.

For the additively manufactured electrical machine, the main focus should lie on the correct estimation of the relative permeability of the teeth and thus the relative thickness in view of the boundary conditions underlying the previous investigation. In addition, temperature changes and consequently changes in electrical conductivity can also have an influence on eddy current losses. Therefore, there is a need for validating the assumptions. A possible test bench design is presented in the following section.

4 Test Bench Design

Recording eddy current losses on rotating surfaces experimentally includes several practical difficulties, e.g., the implementation of the sensors or the signal routing. To extract the eddy current effects in the best possible way, a linear alternative test setup along with the test methodology is designed and presented in this chapter. With this setup, it is possible to expose additively manufactured test specimen (hereinafter named DUT) to alternating or moving magnetic fields. Therefore, the DUT, where the eddy current effects appear, is fixed on a linear stator (see Fig. 12).

Since the relative motion between the rotor and the air-gap spatial harmonics causes eddy currents on a solid rotor, a motion of the DUT is not mandatory to demonstrate the eddy current effects. With this setup, the impact of spatial harmonics with fixed wavelength and variable frequency can be investigated. The following boundary conditions and objectives have to be considered when dimensioning the active parts and the winding:

- Limited number and size of the DUTs due to the available material amount and assembly space
- The higher the number of pole pairs, the lower the impact of end winding effects
- Preferably low air-gap field and higher harmonic content to assign the appearing eddy current effects to the desired spatial harmonic
- Preferably high fundamental flux linkage amplitude to ensure a recordable quantity of expected losses

Considering these aspects, the test setup dimensions are shown in Table 2.

The laminated stator consists of a ferro-cobalt alloy to decrease the stator iron losses. The DUTs consist of the ferrosilicon, which was investigated in [8], and are solid, so that eddy currents can only appear in the DUT.

Widening the stator end teeth beyond the DUT could decrease the higher spatial harmonic content of the air-gap field, as shown in [20]. The overhang factor k_{oh} describes the enlargement of the stator end teeth in the x-direction in multiples of

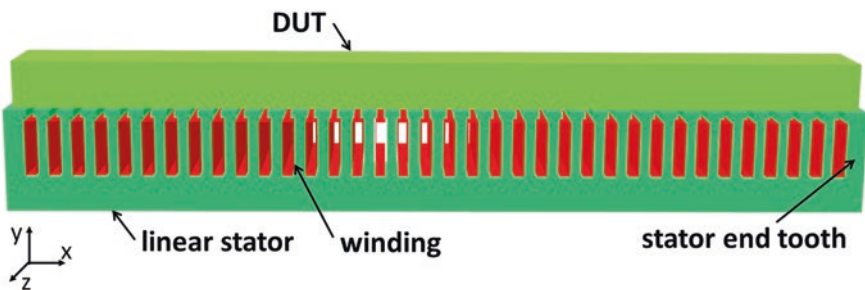


Fig. 12 Linear stator alternative test setup. Shown is the linear stator (dark green), the DUT (light green), and the winding (red). The air region is hidden

Table 2 Test setup dimensions, materials, winding data, and simulation parameters

Name	Value
DUT width (x-direction)	$w_2 = 180$ mm
DUT width (y-direction)	$h_2 = 10$ mm
DUT width (z-direction)	$l_2 = 31$ mm
DUT material	AM-FeSi material
Air-gap length	$\delta_g = 0.5$ mm
Stator width (x-direction)	$r = b_2 + 2 \cdot k_{\text{oh}} \cdot w_{t,1}$
Stator height (y-direction)	$h_{i,1} = 22$ mm
Stator length (z-direction)	$l_1 = 31$ mm
Stator teeth width (x-direction)	$w_{t,1} = 2.1$ mm
Stator material	Electr. sheet FeCo49

the stator teeth width and was set to $k_{\text{oh}} = 1$ in the present case. Referring to the objectives stated above, the aim is to minimize the harmonic leakage ratio

$$\sigma = \frac{\sum_{\nu' \neq p} \hat{B}_{\nu'}^2}{\hat{B}_p^2}, \quad (6)$$

which describes the harmonic content while comparing the flux density amplitude values of the spatial harmonics $\hat{B}_{\nu'}$ with the ordinal numbers $\nu' \neq p$ with the fundamental flux density amplitude \hat{B}_p . Simultaneously, maximizing the fundamental winding factor is the second crucial criterion. Figure 13 shows the fundamental winding factor and the harmonic leakage ratio as a function of the number of slots per pole and per phase $q = N_1/(2pm)$ and the short-pitching W/τ_p which describes the coil span W related to the pole pitch.

Due to discrete values of W , only discrete steps of W/τ_p are possible, so that the continuous line in Fig. 13 is interpolated. Nevertheless, it can be seen that choosing $q = 2$ would decrease the higher harmonics most significantly. $q > 2$ would also lead to significantly smaller stator teeth, due to the fixed DUT length. Choosing $W/\tau_p = 1$ in turn avoids a decrease of the fundamental flux linkage and avoids the need of a two-layer winding going along with additional slots (Table 3).

To comply with a maximum teeth flux density $\hat{B}_{t,1,\text{max}}$ which accompanies a minimum manufacturable stator teeth width of approx. $w_{t,1,\text{min}} = 1.5$ mm, applying the stator current density $S_{1,\text{max}}$ was achieved by primarily increasing the slot height.

Furthermore, choosing $p = 3$ leads to $l \approx \tau_p$ in the present application causing eddy currents flowing in a quadratic manner regarding the DUT air-gap faced surface. In a first step, the solid DUT without any slots is simulated using transient 3D FEA. The results are shown in Fig. 14.

The expected losses range from single watts up to several hundreds of watts depending on the stator frequency f_i . Thus, the implementation of a reliable and applicable measuring method is another challenge to overcome. In the future, additional slots will be added to the DUT in x- and z-direction with respect to the previous findings, and the impact on the eddy current losses will be observed.

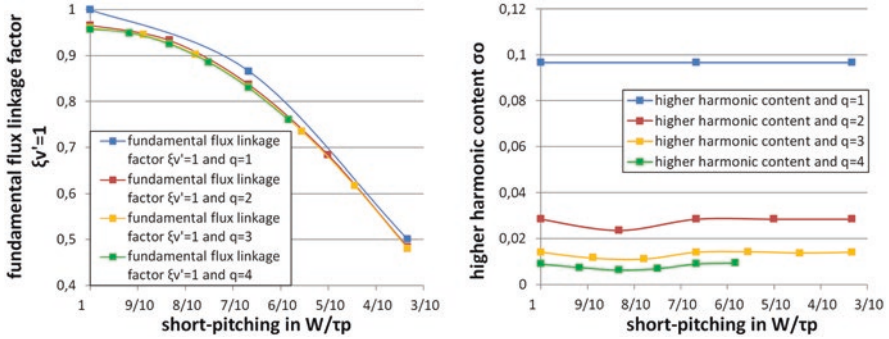


Fig. 13 Left: Fundamental flux linkage winding factor and right: higher harmonic leakage ratio depending on the number of slots per pole and per phase q and the short-pitching W/τ_p

Table 3 Winding data and simulation parameters

Name	Value
Number of poles	$p = 3$
Number of slots per pole and phase	$q = 2$
Number of slots	$N_1 = 36$
Number of phases	$m = 3$
Number of turns per coil	$w = 20$
Rated current	$I_N = 2.6 \text{ A}$
DUT conductivity	$\kappa_2 = 5 \text{ MS/m}$
Stator conductivity	$\kappa_1 = 0 \text{ S/m}$
Max. stator current density	$S_{1, \max} = 4 \text{ A/mm}^2$

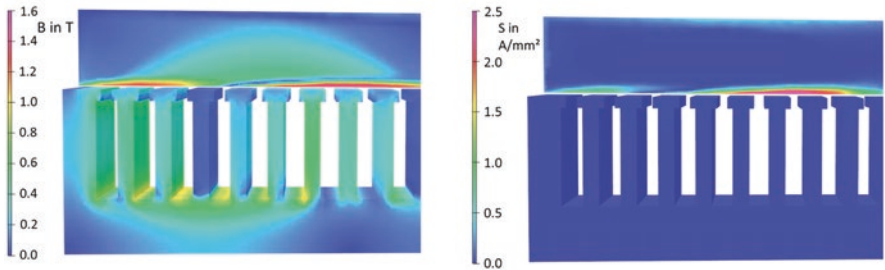


Fig. 14 Simulation results, left: flux density distribution of the non-slotted DUT and right: eddy current loss distribution for $f_1 = 50 \text{ Hz}$

5 Conclusion and Outlook

In the course of this paper, a numerical-analytical general study on eddy current loss reduction in solid surfaces using surface slots was performed. The investigations have shown that an efficient eddy current loss reduction is possible by a circumferential slotting of the rotor surface only. Based on numerically calculated base functions,

the loss reduction can be estimated quickly with the help of an analytical approach presented in this paper. Regarding manufacturing instructions, due to the assumed pre-saturation, it makes sense that the width of the teeth resulting from the slotting of the rotor should be approximately twice the slot width, in order to avoid an increase in eddy current loss compared to the unslotted rotor in the case of high frequencies ($f > 1000$ Hz). Slot height should fulfill the conditions $3 \geq h_{s,2}/w_{s,2}$ and $h_{s,2} \geq 2.5 \cdot \delta_{\max}$ in order to avoid eddy currents at the bottom of the slots.

In addition, a first test bench design was investigated and presented. Future work will deal with its implementation into reality and the measurement and evaluation of eddy current losses, in order to validate the theoretical results.

References

1. S. Lammers, G. Adam, H.J. Schmid, R. Mrozek, R. Oberacker, M.J. Hoffmann, F. Quattrone und, B. Ponick, Additive Manufacturing of a lightweight rotor for a permanent magnet synchronous machine, in *International Electric Drives Production Conference (EDPC)*, (Nuremberg, 2016)
2. E. Aguilera, J. Ramos, D. Espalin, F. Cedillos, D. Muse, R. Wicker, E. MacDonald, *3D Printing of Electro Mechanical Systems* (University of Texas, El Paso, 2013)
3. M. Garibaldi, C. Gerade, I. Ashcroft, R. Hague und, H. Morvan, The impact of additive manufacturing on the development of electrical machines for MEA Applications: A feasibility study, in *MEA2015 More Electric Aircraft*, (Toulouse, February 2015)
4. S. Lammers, F. Quattrone, R. Mrozek, Machbarkeitsstudie 3D Druck Elektromotoren, in *Forschungsvereinigung Antriebstechnik e. V. (Vol. 1189, No. 731 I)*, (2016)
5. Z. Y. Zhang, K. J. Jhong, C. W. Cheng, P. W. Huang, M. C. Tsai und I. I. W. H. Lee, „Metal 3D printing of synchronous reluctance motor,“ in *IEEE International Conference on Industrial Technology (ICIT)*, Bhubaneswar, 2016
6. A. Taube, S. Lammers, S. Urbanek, R. Mrozek und, M. Schaper, Weichmagnete 3D-Druck: Weichmagnetische Werkstoffe für die additive Fertigung von E-Motoren, in *Forschungsvereinigung Antriebstechnik e.V. (Vol. 1286, No. 731 II)*, (2018)
7. G.M. Tseng, J.K. Jhong, C.M. Tasi, W.P. Huang, W.H. Lee, Application of Additive Manufacturing for Low Torque Ripple of 6/4 Switched Reluctance Motor, in *19th International Conference on Electrical Machines and Systems (ICEMS)*, (Chiba, 13–16 Nov 2016)
8. S. Urbanek, B. Ponick, A. Taube, K.-P. Hoyer, M. Schaper, S. Lammers, T.L.D. Zimmer, Additive Manufacturing of a Soft Magnetic Rotor Active Part and Shaft for a Permanent Magnet Synchronous Machine, in *IEEE Transportation Electrification Conference and Expo (ITEC)*, (Long Beach, 2018)
9. A.C. Hayes, L. Sethuraman, L.J. Fingersh, K. Dykes, Additive Manufacturing – A New Paradigm for the Next Generation of High-Power-Density Direct-Drive Electric Generators, in *ASME 2018 Power and Energy Conference and Exhibition*, (Lake Buena Vista, 24–27 June 2018)
10. N. Urban, A. Meyer, M. Leckel, M. Leder und, J. Franke, Additive Manufacturing of an Electric Drive a Feasibility Study, in *International Symposium on Power Electronics, Electrical Drives, Automation and Motion (SPEEDAM)*, (Amalfi Coast, 2018)
11. R. Ranjan und, J. Tangudu, Thermal Design of High Power-Density Additively-Manufactured Induction Motors, in *IEEE Energy Conversion Congress and Exposition (ECCE)*, (Pittsburgh, 2014)
12. H. Yamada, M. Nanba, Eddy current loss in grooved solid poles. *IEEE Trans. Mag.* **14**(5) (1978)

13. Y. Gessese, A. Binder, B. Funieru, Analysis of the effect of radial rotor surface grooves on rotor losses of high speed solid rotor induction motor, in *SPEEDAM*, (Pisa, 2010)
14. J.-X. Shen, H. Hao, M.-J. Jin und, C. Yuan, Reduction of Rotor Eddy Current Loss in High Speed PM Brushless Machines by Grooving Retaining Sleeve. *IEEE Trans. Mag.* **49**(7) (2013)
15. H. Fang, D. Li, R. Qu, J. Li, C. Wang, B. Song, Rotor design and eddy-current loss suppression for high-speed machines with a solid-PM rotor. *IEEE Trans. Ind. Appl.* (2018)
16. S. Urbanek, B. Ponick, Surface Eddy Current Loss Reduction in Additively Manufactured Permanent Magnet Rotor Active Parts, in *IEEE International Conference on Electrical Machines (ICEM)*, (Alexandropolis, 2018)
17. EOS GmbH, EOS GmbH Homepage, [Online]. Available: https://www.eos.info/additive_fertigung/fuer_technologie_interessierte
18. DMRC, DMRC Homepage. [Online]. Available: <https://dmrc.uni-paderborn.de/de/inhalt/dmrc/verfahren/laserschmelzen/>
19. G. Müller, V.K.u.B. Ponick, *Elektrische Maschinen – Berechnung elektrischer Maschinen*, vol 6 (Wiley-VCH Verlag, Auflage Hrsg., Weinheim, 2007)
20. J.-P. Jastrzembski, *Synchrone Linear-Direktantriebe für Förderbänder* (VDI-Verlag, Düsseldorf, 2014)

Energy Scorecard: One of the Key Executions to Transform the Market for Energy-Efficient Motors



Hakan Gedik

1 Introduction

Turkey has an important place in Europe with the market size of 240 billion dollars in low-voltage electric motors. It is also estimated that there are approximately 15 million electric motors in the field.

In Turkey, 47% of total electricity consumption is from the industrial sector, with an estimated 70% of this energy consumption from electric motor-driven systems (EMDS), 90% of which use three-phase squirrel cage asynchronous motors as defined in the EU Eco-design Implementing Measure 640/2009 on electric motors as amended by Implementing Measure 4/20142.

Electric motors in Turkey, in general, are not energy efficient. The Ministry of Industry and Technology completed an electric motor inventory analysis in December 2015 which covered more than 90,000 electric motors (three-phase, ≥ 7.5 kW asynchronous motors) being operated in nearly 900 SMEs in 23 different industrial sectors in Turkey. This inventory reflects the distribution of these motors by efficiency (IE) levels, average rated power, average age, average operating time, as well as electricity consumption caused by these motors.

As a result of field studies carried out by the Ministry, it is estimated that there are a total of 3.783.694 units of 7.5 kW and above AC motors, which are currently used in industry and are considered inefficient (IE0, IE1, IE2 without variable speed drive). By means of the renewal of all of the aforementioned inefficient engines:

- Approximately 34 billion kWh of electricity will be saved. Thus, approximately 8.5 billion TL contribution will be provided to our country's economy every

H. Gedik (✉)
EMOSAD, Istanbul, Turkey
e-mail: hakan.gedik@wat.com.tr

year. The investment cost required for this engine conversion is approximately TL 14.6 billion.

- Considering the annual savings and total cost to be earned, it is estimated that the engine transformation program will return to our country's economy in about 21 months. Considering the use of DHS, this period falls to 18 months.

2 U4E and TEVMOT: Motor Replacement Program

Motors are a key product covered by United for Efficiency (U4E). U4E partners with countries (regionally and individually), and its "Integrated Policy Approach" is a model that successfully transforms markets in countries. Promotion of energy-efficient motors and solutions in this field is a high priority for U4E. At COP23 (Bonn, November 2017), at an U4E event, the Turkish Government announced its intentions to move forward with a countrywide upgrade of its installed base of industrial electric motors. The ambitious goal is for early replacement of all industrial motors to an efficiency level of IE3; currently, less than one percent of Turkey's installed base of motors are at the IE3 efficiency level. The project, named Promoting Energy-Efficient Motors in SMEs in Turkey (TEVMOT), will last 5 years until 2022 and focuses on small- and medium-sized enterprises.

TEVMOT project aims to promote significant additional investment in industrial energy efficiency in Turkey by transforming the market for energy-efficient motors used in small- and medium-sized enterprises.

This objective will be achieved by strengthening the legislative and regulatory framework related to both new and existing EE motors in Turkey, developing appropriate governance and information infrastructure, upgrading test laboratories at the Turkish Standards Institute (TSI), launching a "one-stop shop" sustainable financial support mechanism (FSM), and developing and implementing a comprehensive public awareness and training program (Fig. 1).

Project has been designed to remove barriers to sustained replacement of inefficient motors with motors that are IE3 standard and above. One of the primary barriers to sustained market transformation of the Turkish motor market has been the general absence of a trusting relationship between industrial SMEs and professionals related to providing technical assistance advice on energy efficiency; there is demand for impartial technical assistance that is not tied to one particular brand of motors (Fig. 2).

Another primary barrier is related to the lack of "user-friendly" financing products for industrial SMEs. A number of these financing products require some form of collateral, which many SMEs are unable to provide. In addition, many industrial SME applicants are unwilling or unable to navigate through the onerous paperwork required to qualify for these financial products. The project aims to promote significant additional investment in industrial energy efficiency in Turkey by transforming the market for energy-efficient motors used in small- and medium-sized enterprises.

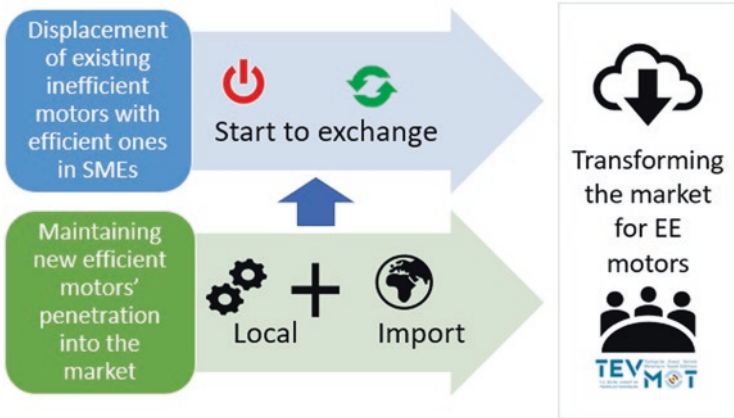


Fig. 1 Market transformation scheme



Fig. 2 TEVMOT objectives

3 EMOSAD

Electric Motor Industrialists Association (EMOSAD) was established on May 4, 2016 with the participation of the sector stakeholders in order to provide information on all kinds of subjects related to the electric motors and to carry out studies in the field of occupation.

The duty of the Association is listed below.

- The development of the electric motor industry in Turkey.
- Improve service quality.
- Increase exports.
- To make the brands of domestic member companies operating in the sector into international brands.
- To work in the areas of related technology, energy efficiency, and environmental compatibility in production.
- To contribute to the technological development of the sector.



Fig. 3 EMOSAD members (motor manufacturers)

In addition to all these, it will be among the main priorities of the association to carry out the necessary activities to fulfill the sector's energy efficiency studies, environmental compliance laws, and regulations on behalf of the members and the sector.

One of the partners of the TEVMOT project is the Electric Motor Industrialists Association (EMOSAD) which has been recently established with 11 domestic electric motor manufacturers based and operating in Turkey, and one of the outputs of the TEVMOT project will be to develop capacity of EMOSAD to better serve their members and better represent them in various international platforms and national policy-making platforms. The EMOSAD is also expected to help their members and Turkish electric motor industry to increase their shares in local electric motor market and also increase their shares in regional and other international markets. Therefore, the proposed assignment is aimed at not only helping EMOSAD better function but also for helping Turkish electric motor industry to occupy commercially better and a more reputable position in both local and international markets and platforms (Fig. 3).

4 Energy Scorecard

The most important criterion of success for TEVMOT project is to create a sustainable model. For this purpose, it would not be enough to create a framed financial model based on volunteerism. For this project to be sustainable, it should be based on a semi-mandatory model and supported by certain incentive mechanisms. EMOSAD is one of the methods we propose from this point of view.

The energy scorecard is recommended in industrial plants in order to achieve the desired result of the motor replacement program. In this model, a rating is made by

Table 1 Installed motor power

kW	No. of poles	Qty.	Total power [kW]
4	4	20	80
1,1	2	50	55
45	12	3	–
22	4	10	220
355	6	2	710

Table 2 Coefficients according to eff., VSD and operating ratio

Eff. class	Coeff for NO VSD	Coeff for VSD	Operating ratio	Coeff for operating ratio
IE0, IE1	1	2	%0–24	0.6
IE2	2	3	%25–49	0.7
IE3	3	4	%50–74	0.8
IE4	4	5	%75–100	1

Motor Usage	Status	Power (kW)	No of poles	Eff Class	Eff Value	VSD	Application	Operating time (hour/year)	Operating ratio	Qty	Total consumption (kwh/yl)	Total Class Point	Class Point	Usage weight ratio
A	B	C	D	E	F	G	H	I	J	K	L	M	N	O
Power System Compressors	In use	37	4	IE4	95,2	No	Constant torque	300	3%	1	11.660	27.983	2,4	1%
Press Cooling Unit	Spare	30	4	IE1	90,7	No	Constant pump	4760	54%	1	157.442	125.954	0,8	15%

Fig. 4 Motor and VSD report of facility

considering the existing motor inventory of the industrial plant, and tax cuts are recommended on increasing points as the motor replacement is performed.

In the application of the energy scorecard, facilities have a certain installed power of electric motors are considered. This installed power can be taken as 1000 kW initially. The following main elements are taken into account to determine the scorecard:

- Motor efficiency class (IE1, IE2, etc.)
- Whether or not the VSD is available.
- Application type (constant speed or variable speed application).
- Operating ratio (%0–24, %25–49, %50–74, %75–100).

First of all, installed electric motor power is calculated. Only motors covered by the regulation are included in this calculation. The power is based on the mechanical output power (P2) written in nameplate of the existing motors. For motors without a nameplate, the measurement is done, and output power is estimated by considering that the motor efficiency is IE1.

After that, a coefficient is given according to the efficiency class of the motor and whether there is VSD depending on the application. Another coefficient is determined according to operating time ratio (Tables 1 and 2).

These coefficients will be used to calculate the energy score. In order to calculate the energy score of the facility, the energy manager of the enterprise is asked to fill in the blue cells in the table below (Fig. 4).

Table 3 Scorecard legend

Average	Class
>4	A++
3,5–3,99	A+
3–3,49	A
2,5–2,99	B
2,01–2,49	C

After making the calculation, the scorecard point is determined.

5 Scorecard Point = Total Class Point/Total Consumption

This method can be implemented successfully if it is mandatory to upgrade the class annually until the A ++ value is reached. In addition, a variety of support should be given to enterprises that raise their class. Thus, the application continues until the replacement of the inefficient motors is realized (Table 3).

6 Conclusion

It is certain that exemplary projects will be realized by TEVMOT. There is no doubt that these projects will be realized with a well-defined finance model. However, the success of the TEVMOT project will be realized when the market transformation begins. Two issues need to be addressed for this success: sustainability and enforcement.

Simply describing a model or even applying a standard or regulation often doesn't change the market without any enforcement. Nevertheless, the most accepted version of enforcement is the one with incentives.

Since it is not possible to regulate the electric motors used in the field, energy scorecard is one of the key executions to transform the market for energy-efficient motors. Energy scorecard is a kind of enforcement with incentives and will help to sustain the TEVMOT project.

A Novel Approach to Predict Reed Critical Frequency of Vertical Motors



Ravi Musinana and Harendra Singh

1 Introduction

RCF is the first natural frequency in transverse direction of the complete motor when it is mounted vertically and fixed at base. If forcing frequency is present at the natural frequency of motor, resonance will occur, leading to high amplitudes of vibrations which is defined in the NEMA MG-1 [1] standard. NEMA simplified the motor system and stated the resulting system might have radial resonant frequency (reed frequency) same as that of rotational speed of induction machine. This system frequency can be calculated from the equation,

$$f = \frac{1}{2\pi} \sqrt{\frac{g}{\Delta_s}} \quad (1)$$

which is same as single degree of freedom system in which the static deflection of the mass (Δ_s) is related to the resonant frequency. The static deflection is lateral displacement from its original position at center of gravity if machine were horizontally mounted.

Finley et al. [2] described that in large vertical motors, the rotor critical speed may be the determining factor in the reed critical frequency of the motor alone. The effect of rotor can be determined by considering it as a separate mass and including rotor shaft flexibility in the reed frequency calculation, that is, consider the motor as a two mass two degrees of freedom system, rather than single-degree freedom system as described by NEMA MG 1–20.55 [1].

R. Musinana (✉) · H. Singh
Wolong India Technology Center, GE Industrial Motor, a Wolong Company,
Hyderabad, Telangana, India
e-mail: ravi.musinana@geim.wolong.com; harendra.singh@geim.wolong.com

This two degrees of freedom system can again be simplified into a mathematical model, which utilizes a numerical procedure by considering minimal usage of finite element analysis (FEA) to find RCF values within accuracy of $\pm 10\%$ compared to bump testing while industries are giving results with huge tolerance. This model greatly reduces the tolerance in predicting RCF at requisition stage and further suggesting the methods to take away the values from operating range.

The goals of present work are as follows:

- To predict the RCF of induction motor within $\pm 10\%$ design to test
- To reduce the time for analyzing the vertical motor during new product invention or requisition stage
- To validate the mathematical model for different frames (NEMA 320 to 500 frame size) and enclosures such as TEFC, WP-I, and WP-II
- To include components contributing stiffness to RCF
- To include components contributing mass to RCF

2 Parts and Their Sensitivity on RCF

Part of the work is determining the mass and stiffness contribution of each part, according to their effect on the reed critical frequency.

2.1 *Effect of the Stator Core as Mass and/or Stiffness Contributor*

To study the effect of the stator core, it can be modeled as point mass in first iteration at its CG, distributed mass in the second iteration and in the third iteration the stiffness value can be neglected. Lucas et al. [3] also states that determination of influence of frame over stator can be modeled as mounted in operating environment as independently, it will give erroneous result. Verma [4] suggests that parameters, for example, stator length and core thickness, influence the resonance frequency associated with given mode. The effect of stator as bonded or frictional contact with the frame, which would depend on manufacturing tolerance and process used, alters the system frequency. In our case, it is bonded, which generally results in higher value of RCF but as Verma [4] shows that in all the three models, frequency values for transverse mode were not changing indicating that frame is thick enough to overshadow the effect of stator dimensions. This clearly pointed out the stator contribution as a mass contributor and not stiffness contributor for the size of vertical motors studied.

2.2 *Effect of Upper End Shield as Mass and/or Stiffness Contributor*

To study the effect of the upper end shield, it is modeled as point mass at its center of gravity in the first iteration and in the second iteration, Upper End shield Young's modulus is reduced to very small value. The results showed negligible difference in frequency values calculated for both methods, elucidating that upper end shield contributes as mass or and not as a stiffness contributor. Consequently, all masses attached to it as well will not add to any stiffness contribution, such as ratchet, fan cover, and top hat.

2.3 *Effect of Rotor as Mass and/or Stiffness Contributor*

Rotor contribution can be found as mass/inertia contributor since no significant impact over the frequency was found when modeled as point mass in first iteration at center of gravity of rotor and in second iteration by placing point mass at coupling position with mass equal to equivalent mass for same response of system. A difference was found when rotor geometry was modeled which can be studied further.

2.4 *Effect of Lower Bearing (Drive End Side Bearing)*

Lower bearings are guide bearings which support the shaft by providing a guide way. Its stiffness can be changed to see its effect on RCF. The bearings represented by spring with stiffness varied in FEA iterations provide the frequency values as shown in Table 1.

The result indicates that natural frequency appreciably drops below stiffness value of $1.75\text{E}+08$ N/m.

Table 1 Sensitivity of stiffness of lower bearing over RCF

Stiffness (N/m)	Frequency (Hz, X-direction)	Frequency (Hz, Y-direction)
1.7513E+07	47.70	51.24
1.7513E+08	52.04	57.84
1.7513E+09	52.65	58.87

Table 2 Sensitivity of upper bearing stiffness

Stiffness N/m	Frequency (Hz) X direction	Frequency (Hz) Y direction
1.7513E+07	49.75	54.16
1.7513E+08	52.04	57.84
1.7513E+09	52.58	58.60

2.5 Effect of Upper Bearing (Non-drive End Side Bearing)

Upper bearings generally act as load bearing members. They are positioned far away from the Rigid/Massive base. They influence the frequency more than lower bearings on comparison showing sensitivity to stiffness of bearing at values lower than 1.75E+08 N/m. Values are shown in Table 2.

2.6 Effect of Contact Behavior Between P Base End Shield and Mounting Base

The boundary conditions that have been used for larger frame may not be applicable to smaller frame because of its structural and geometrical changes. So, it is necessary to come out with suitable boundary conditions which reflect the actual or test results (Fig. 1).

Various other factors such as WPI and WPII enclosure stiffness, large terminal or conduit box masses, bolt torque used for mounting bolts, and their effect on the RCF can be studied further.

3 Mathematical Modeling of Vertical Motors

3.1 Beam–Mass Schematic of Vertical Motor

Based on the parameters and sensitivity analysis carried out, the RCF model can be simplified. It is clear from the sensitivity analysis that frame and lower end shield are major contributors to the stiffness corresponding to RCF. These are together represented as one beam. Stator and rotor can be modeled as distributed masses over frame and shaft respectively. Fan cover and opposite drive end shield can be put as point mass over the beam at their center of gravity. Similarly, fan over the shaft can be represented. So, it can be concluded that the stator does not stiffen the beam span. The shaft can be modeled as a two-degree freedom beam elastically mounted over the frame. The rotor can be placed over the shaft. The fan mass can be placed over the beam.

Parts as shown in Fig. 2 are:

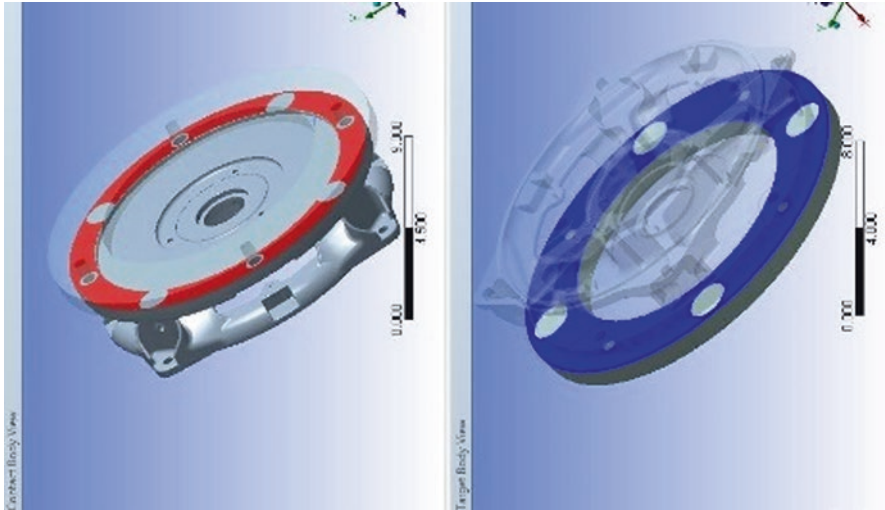


Fig. 1 Contact between DE end shield and massive base

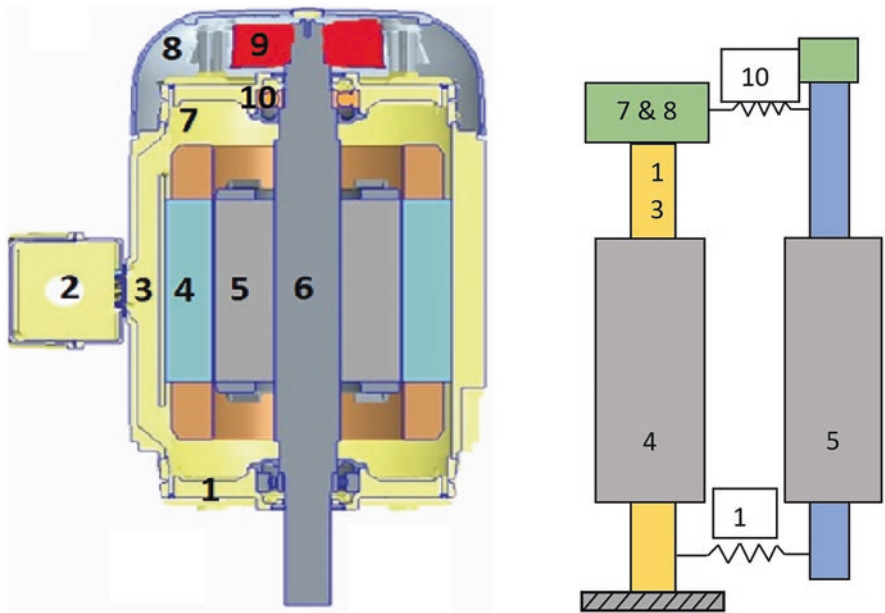


Fig. 2 Beam-mass schematic of vertical motor

(1) Drive End Shield, (2) Conduit Box, (3) Frame, (4) Stator core, (5) Rotor, (6) Shaft,

(7) Outer Drive End Shield, (8) Fan Cover, (9) Fan, (10) Upper Bearings, (11) Lower Bearings

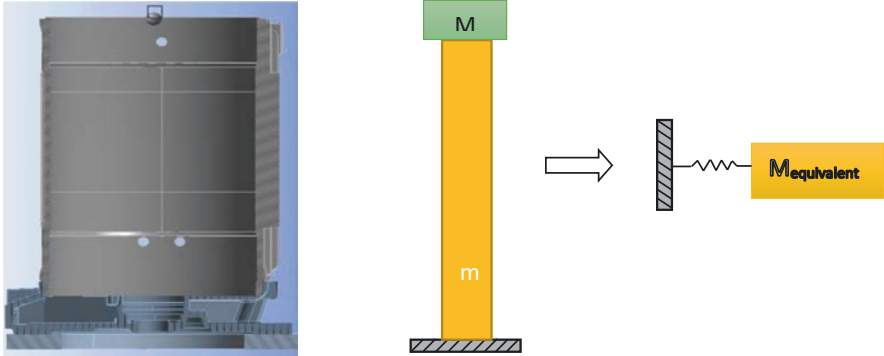


Fig. 3 Equivalent beam–mass schematic of vertical motor

The stationary or non-rotating parts can be placed over the beam because these parts do not contribute any stiffness to the vibrating structure.

Considering the sensitivity of frame, end shield, and bearings over stiffness, this model can be again simplified by taking lower end shield and frame as a beam and remaining all other parts as distributed mass over that beam with mass of each part concentrated at its own center of gravity as below in Fig. 3.

3.2 Equation of Motion

Equation of motion for two degrees of freedom mass-spring system in matrix form is given by Eq. 2 (Fig. 4)

$$\begin{bmatrix} M_S & 0 \\ 0 & M_R \end{bmatrix} \begin{Bmatrix} \ddot{X}_1 \\ \ddot{X}_2 \end{Bmatrix} + \begin{bmatrix} (K_S + K_R) & -K_R \\ -K_R & K_R \end{bmatrix} \begin{Bmatrix} X_1 \\ X_2 \end{Bmatrix} = \{0\} \quad (2)$$

where M_S is the stationary mass (frame, lower end shield, upper end shield, stator, LHC, UHC, etc.) and

M_R – rotor mass

K_S – motor frame stiffness

K_R – motor shaft and bearing stiffness

X_1 and X_2 are displacements and \ddot{X}_1 and \ddot{X}_2 are accelerations.

The frequency can be given by:



Fig. 4 Vertical motor as two degrees of freedom system

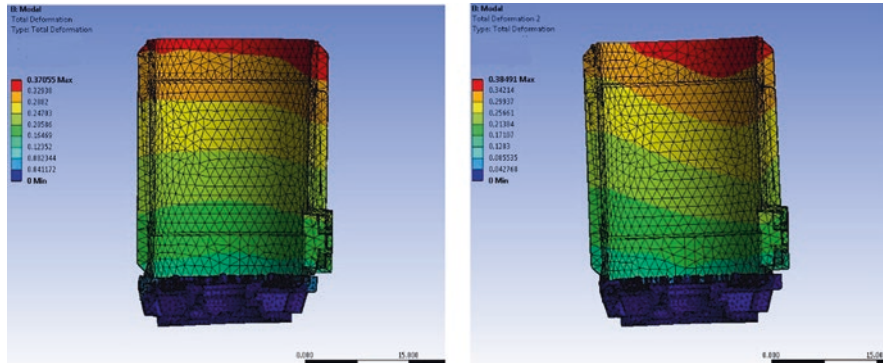


Fig. 5 RCF in conduit box direction and 90° to conduit box direction (TEFC enclosure)

$$f = \frac{1}{2\pi} \sqrt{\frac{\left((M_s * K_r) + (M_r * K_s) + (M_s * K_r) \right) \pm \sqrt{\left((M_s * K_r) + (M_r * K_s) + (M_s * K_r) \right)^2 - (4 * M_s * M_r * K_s * K_r)}}{2 * M_s * M_r}} \tag{3}$$

Now for equivalent beam–mass schematic, it is necessary to know the frame stiffness, rotor stiffness, stationary mass, and rotor mass. Stationary mass and rotary mass of motor can be calculated directly. A constant can be used for motor shaft and bearing stiffness. Since the structure of frame and lower end shield are complex, moment of inertia (I) of the structure cannot be calculated directly. To overcome the complex structure problem, ANSYS software package was used to calculate the frequency of model with frame, drive end side end shield, and a point mass at the top of the frame. Based on this simplification, the stiffness for the structure in a reverse method can be calculated

$$\omega = \sqrt{\frac{3EI}{(M + 0.243m)L^3}} \tag{4}$$

where

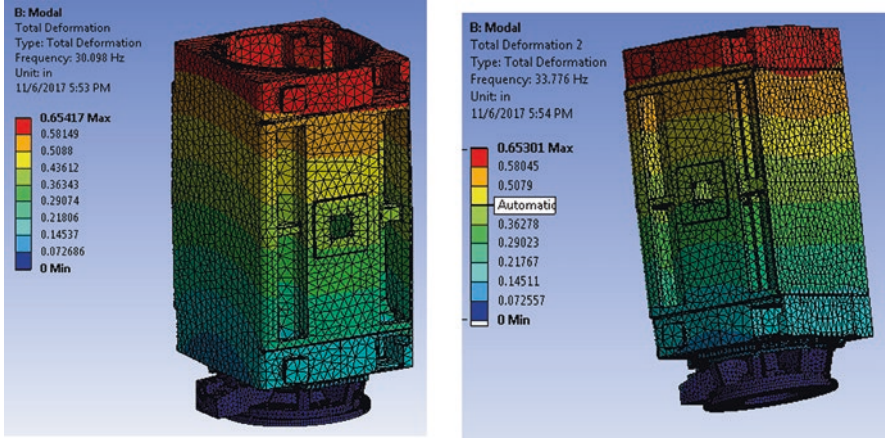


Fig. 6 RCF in conduit box direction and 90° to conduit box direction (WP-I enclosure)

E – Young’s modulus

I – moment of inertia of beam

M – mass of frame and lower end shield

m – tip mass (mass of entire motor except frame and lower end shield)

L – length of beam (frame stiffness height) (Figs. 5 and 6)

Once the moment of inertia (I) of frame and lower end shield is calculated, stiffness of beam representing frame and lower end shield can be calculated using bending equation of beam,

$$k_s = \frac{3EI}{L^3} \tag{5}$$

Here, beam considered is non-slender, homogeneous with constant cross section. Due to non-slenderness of beam, transverse shear deformation and rotation of cross section will also contribute to deflection of beam, thus equation of motion will be governed by Timoshenko Beam Theory which gives

$$EI \frac{d^4w}{dx^4} = q(x) - \frac{EI}{kAG} \frac{d^2q}{dx^2} \tag{6}$$

where w – deflection

G – shear modulus

k – Timoshenko shear coefficient and q – load

Ample amount of work has been done toward solutions of governing equation of homogeneous beam in the past. Considering work done by Ghugal and Sharma [5]

and Anderson Soares [6], deflection will be derived for beam–mass structure with cross section ($h \times L$) and with load (P) at free end and fixed at other end,

$$w(x) = \left[\frac{PL^3}{3EI} + 1.2 \frac{PL}{GA} \right] \quad (7)$$

Validation of Eq. (7) can be done by modeling beam–mass system in DyRoBeS which uses FEM as shown in figure (Figs. 7, 8 and Table 3).

3.3 Calculation of Equivalent Tip Mass

Equivalent tip mass for each mass can be calculated by multiplying equivalent mass factor to masses for same response of the system,

$$M_{eq} \text{ or } M_2 = M_1 \times \left(\frac{L_1}{L_2} \right)^n \quad (8)$$

where value of n can be calculated considering Timoshenko beam model for same response of beam for different position of masses as per Eq. (6).

A graph can be plotted to reflect the stiffness vs. tip mass following Eqs. (3, 4, and 7). This enables to calculate the frequency of motor for a range of masses (Graph 1).

Therefore, this method can be adopted to calculate K_s . Values of M_s and M_t can be calculated directly by adding weights of parts as per their state of motion. Putting all values in Eq. (2) gives RCF for that configuration of vertical motor.

4 Validation of Developed Mathematical Model

Proposed mathematical model considers various assumptions and thus needs validation by using commercial FEA packages such as ANSYS and comparison with test data.

4.1 Solution by ANSYS

Method can be validated with ANSYS by simulating full vertical motor and comparing frequency output with mathematical model output (Fig. 9 and Table 4).

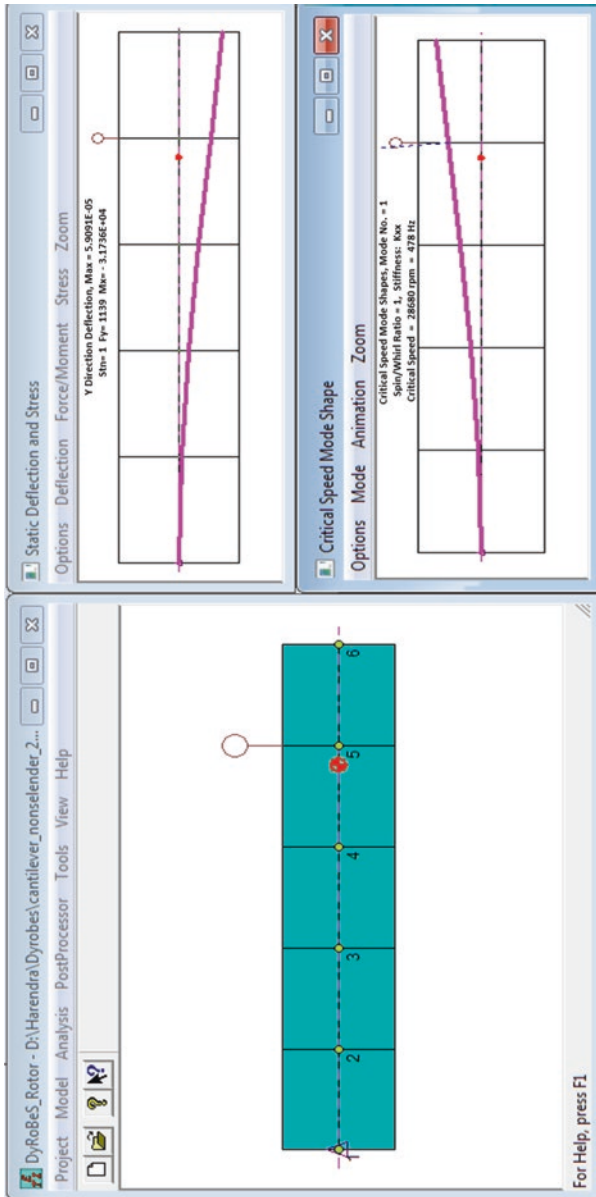


Fig. 7 Validation by DyRoBeS for in span placed mass

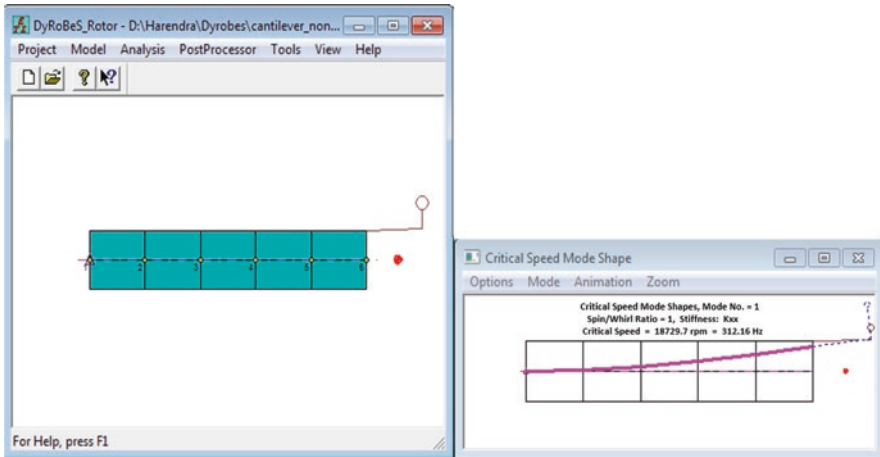


Fig. 8 Validation by DyRoBeS for out of span placed mass

Table 3 Comparison of frequency output between FEM and numerical method

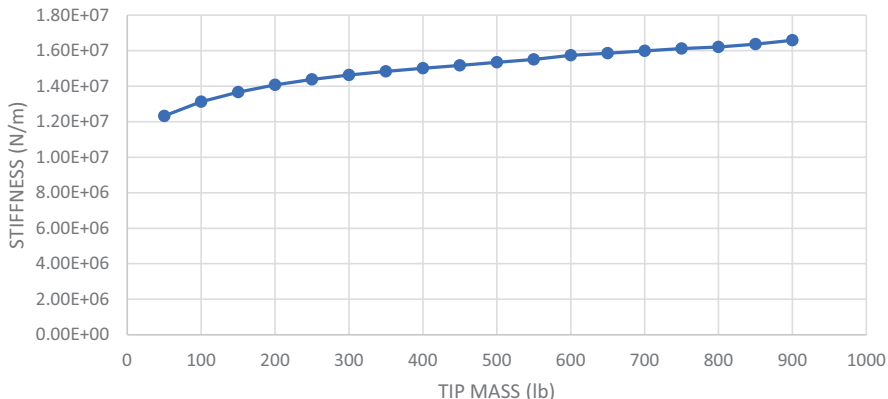
	Frequency			
	Mass in span		Mass out of span	
Numerical method	473	Hz	316.29	Hz
DyRoBeS1620	478	Hz	312.16	Hz
Error %	1.05%		1.23%	

4.2 Solution by DyRoBeS

As the frame stiffness is quite lower than bearing stiffness, the masses can be coupled with the weak spring. The corresponding model becomes as represented in DyRoBeS as Fig. 10 below and can also be solved using DyRoBeS after approximating masses at the top and calculating beam diameter by stiffness calculated by frequency mass curve.

4.2.1 DyRoBeS Gives 43.21 Hz

This falls in the same range as test data and proves the special case that the springs are stiff enough and would not contribute to the frequency much and would act as almost a rigid member.



Graph 1 Stiffness vs. tip mass at frame stiffness height

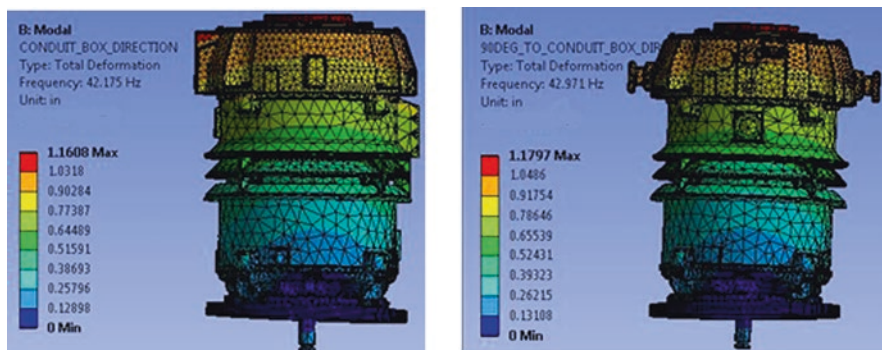


Fig. 9 WPI enclosure —natural frequency along conduit box direction and 90° to conduit box direction

4.3 Validation Across Different Enclosures

Proposed mathematical model can be validated across product range of WP-I, WP-II, and TEFC enclosure of vertical motor as below graphs.

Here FRF bump test output is compared against proposed model output for TEFC as well as WP-I product line in the direction of conduit box and opposite to conduit box direction. During testing, motors are mounted to a massive foundation as defined by NEMA MG 1 Part 7 [1] through bolts. Here massive foundation implies a cast iron base plate that is grouted into concrete foundation and has a total mass of 10 times motor weight. This foundation is sufficiently isolated from background vibration.

For accurate RCF value, motor is fully assembled with all parts including conduit box and cover, non-reverse ratchet, top cover, etc. RCF is measured at two vertical planes that project through the shaft centerline. The first plane is oriented

Table 4 RCF comparison for WP-I $\pm 10\%$ test to design ratio

RCF(Hz)	Test data	Mathematical model output	Full FEA model output	ERROR % (Test vs model)	ERROR % (Test vs ANSYS)
Conduit box	43	41.52	42.18	-3.44%	-1.91%
90° to Conduit Box	45	42.87	42.97	-4.73%	-4.51%

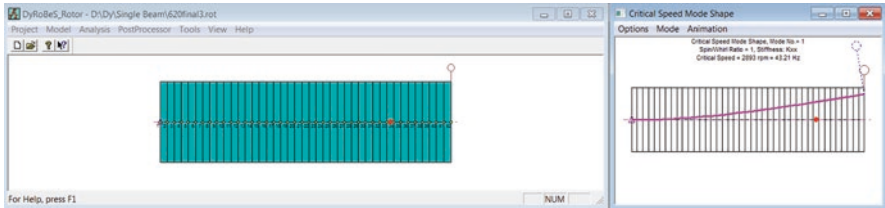


Fig. 10 DyRoBeS modeling of vertical motor

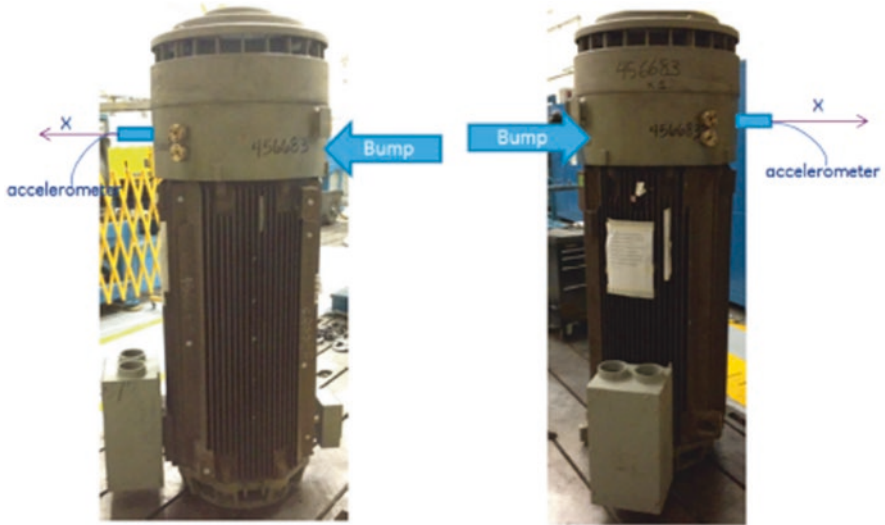
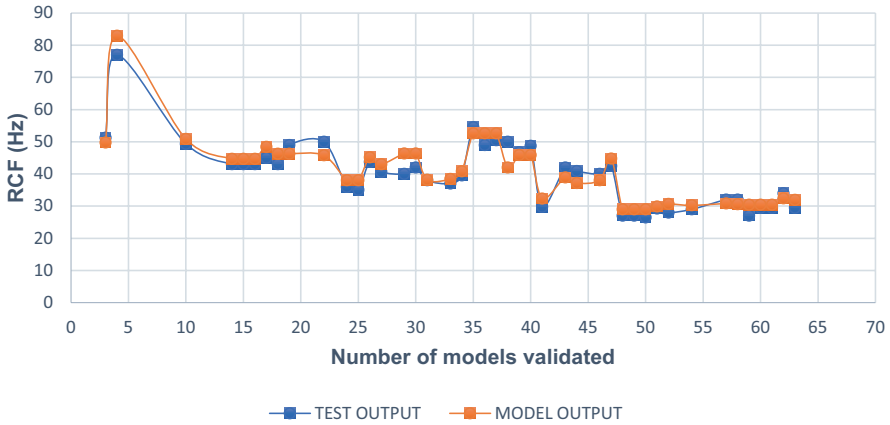


Fig. 11 FRF bump test setup

with conduit box, while the second plane is perpendicular to the first plane (Refer Fig. 11). These two planes are required to account for variation in stiffness within motor structure. Additionally, a tri-axial accelerometer and an impact hammer are used for recording FRF response and thus predicting RCF of motor.

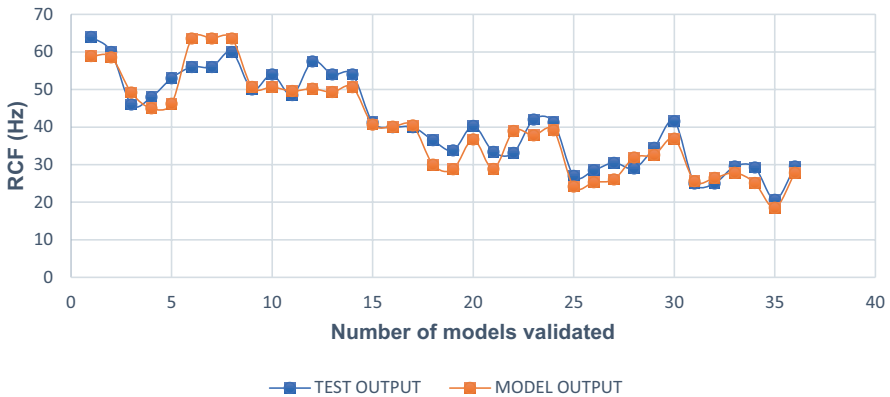
It is observed that model output is following the same trend as test with an accuracy of $\pm 10\%$ test-to-design ratio (Graph 2 and 3).

RCF COMPARISON: TEST OUTPUT vs MODEL OUTPUT



Graph 2 RCF comparison in conduit box direction for TEFC enclosure (360–500 frame sizes)

RCF COMPARISON: TEST OUTPUT vs MODEL OUTPUT



Graph 3 RCF comparison in conduit box direction for WP-I enclosure (320–500 frame sizes)

5 Conclusions

The vertical motor being a complex set of stationary elements and rotatory elements, the model is developed with vertical beam coupled with two degrees of freedom mass system represented by another beam. Running simulations lead to assume that since the lower end of the elastically attached beam is not moving, the beam can be considered as a single mass attached to the top end shield. For a simpler solution,

the problem is converted into classic example of self-weight beam with tip mass attached to it. This takes into consideration of Timoshenko beam theory as length to thickness ratio is less. Simpler approximation techniques are utilized for calculating the approximate mass. Stiffness is calculated by plotting point mass at top of frame vs. frequency curve, and subsequently assuming model to be Timoshenko type of beam. The method is again simplified and given the form of two-degree of freedom mass-spring system where, the first mass being an approximation of stationary masses and second of rotatory masses. Similarly the first spring stiffness being stiffness of frame and second of bearing stiffness at upper end shield are known. The masses are all approximated at top of frame. On comparison between bearing and frame stiffness, bearings are stiffer more than ten times the frame stiffness, subsequently the model can be converted into a single spring mass system.

This mathematical model predicts the reed critical frequency (RCF) of vibration of vertical motors with minimum use of commercial finite element packages such as ANSYS and DYROBES. Generally, finite element analysis (FEA) is used for analysis, finding the results and comparing the results with the conventional vibration methods which is also time-taking process, but with the increase in number of applications it is necessary to predict the frequency based on desired configurations of the motor at time of requisition. Thus, this mathematical model utilizes many a small computational result from traditional FEA and predicts frequency values quickly within accuracy of $\pm 10\%$ test to design ratio.

Also, this model considers weight of rotor as well as weight of stationary parts. Collectively, this model can be used to calculate total motor weight and center of gravity of motor which could be proved useful at the requisition stage.

References

1. N.E.M.A. Standard, *MG 1: Motors and Generators* (National Electrical Manufacturers Association, 2014)
2. W.R. Finley, M.M. Hodowanec, W.G. Holter, An Analytical Approach to Solving Motor Vibration Problems, in *Petroleum and Chemical Industry Conference, Industry Applications Society 46th Annual*, (IEEE, 1999), pp. 217–232
3. M. Lucas, W.T. Thomson, A study of the natural vibratory response of stator structures to improve condition monitoring strategies for induction motors. *Proc. Inst. Mech. Eng. C J. Mech. Eng. Sci.* **212**(1), 57–68 (1998)
4. S.P. Verma, R.S. Girgis, Considerations in the choice of main dimensions of stators of electrical machines in relation to their vibration characteristics. *IEEE Trans. Power Apparatus Syst.* **94**(6), 2151–2159 (1975)
5. Y.M. Ghugal, “A Hyperbolic shear deformation theory for flexure and vibration of thick isotropic beams”, *Int. J. Comput. Methods* **6**(4), 585–604 (2010)
6. A.S. Da Costaazevedo, S.D. Santoshoefel, Analysis of Rotatory Inertia and Shear Deformation on Transverse Vibration of Beams, in *Congresso Nacional de Engenharia Mecanica (CONEM)*, (ABCM, 2016), pp. 21–25
7. S.M. Han, H. Benaroya, T. Wei, Dynamics of Transversely vibrating beams Using four engineering theories. *J. Sound Vib.* **225**(5), 935–988 (1999)

8. D. Bogh, J. Crowell, R. Amstutz, IEEE 841 motor vibration. IEEE Ind. Appl. Mag. **11**(6), 32–37 (2005)
9. U. Werner, *A Plane Vibration Model for Natural Vibration Analysis of Soft Mounted Electrical Machines* (INTECH Open Access Publisher, 2011)
10. V.S. Gonçalves, *Desenvolvimento de uma metodologia numérica para a predição dos três primeiros modos de vibração de um motor elétrico fixo em base rígida* (2012)
11. S. Timoshenko, J.N. Goodier, *Theory of Elasticity* (McGraw-Hill, New York, 1951)

Evaluation of High-Tech Electrical Steel in a High-Speed Permanent Magnet Synchronous Machine for an Aircraft Application



Mina Mirzadeh, Gerrit Narjes, and Bernd Ponick

1 Introduction

With an expected compound annual growth rate of 4.7% in the number of air travel passengers between 2017 and 2036, it is of significant importance to face the challenge of providing faster and easier air travel with more environmentally compatible technologies [1]. On this line, air traffic noise pollution is recognized as an environmental concern near airports. It is one approach to decrease the emitted noise cone during the takeoff by raising the aircraft's high-lift capability [2] and thus making shorter runways possible. The additional lift is generated by turbo compressors that are distributed along the wingspan. These are powered directly by compact high-speed permanent magnet synchronous motors to save the weight of a gearbox (see Fig. 1).

As an application for an aircraft, there are several requirements that call for a compact and efficient design using an interdisciplinary approach [4] and high-tech materials for different components such as the back iron. When choosing the electrical sheet material, the iron losses, as well as the parameters for heat dissipation, the density, the tensile strength, and the cost need to be considered [5]. For the latter, the current prototype was built with silicon-iron sheets (NO20).

In the past, several authors have discussed other iron alloys, namely, cobalt-iron and nickel-iron [6, 8]. In comparison to silicon-iron steels, both show lower losses but at a price. In the case of the nickel-iron, the saturation polarization does not reach the aforementioned NO20. On the other hand, the thermal conductivity is lower and the mass density is higher, thus leading to a higher overall weight [9]. In

M. Mirzadeh (✉) · G. Narjes · B. Ponick
Institute for Drive Systems and Power Electronics, Leibniz University Hannover,
Hanover, Germany
e-mail: mina.mirzadeh@ial.uni-hannover.de; gerrit.narjes@ial.uni-hannover.de;
ponick@ial.uni-hannover.de

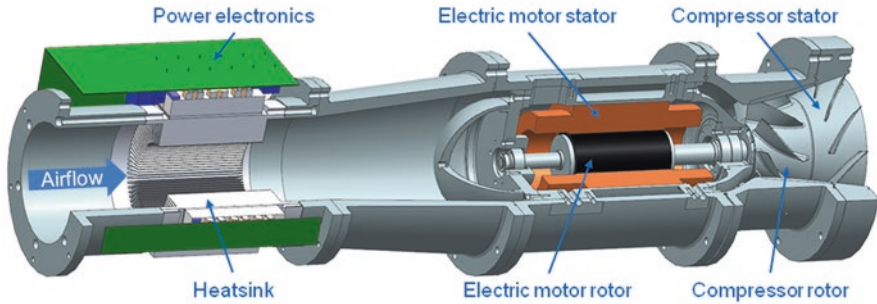


Fig. 1 Schematic of electrically powered high-lift system [3]

comparison, the cobalt-iron alloys are in between in terms of mass density but have a higher saturation polarization [10, 11]. Therefore, this alloy presents a good compromise for lower losses and possibly lower weight for the higher saturation flux density.

This paper begins with an overview of the materials used in modeling a machine. The characteristics of the three alloys and their material parameters are shown and compared regarding the use in compact machines with high power-to-weight ratios, applicable in aircraft engines. The following sections introduce the reference machine model and the design steps when using iron-cobalt electrical sheets. Later, the motivation for different variations is highlighted and the different models are discussed. Finally, the impact of the cobalt-iron alloy on the interdisciplinary design aspects is presented.

2 Material Characteristic of Electrical Sheets

Electrical steel or lamination sheets are used in a variety of applications. Electrical machines, especially those with high-performance requirements, are often designed with non-grain-oriented silicon-iron steel. In this particular case, as mentioned above, an NO20 grade was used as it provides a low loss number and the sheets are only 200 μm thick to reduce eddy current losses. Even lower loss numbers can be achieved with cobalt-iron alloys and nickel-iron alloys. These have higher contents of the respective main additive than the silicon-iron which influences every aspect of the material. The loss values also depend on the sheet thickness; therefore the comparison in Table 1 is a little off for the loss values. Nonetheless, it shows that even with this advantage in thickness for the silicon-iron sheets, the other alloys have lower losses.

The difference in saturation can also be illustrated via the B-H curves (see Fig. 2). Because of the much higher relative permeability of the cobalt-iron and its higher saturation flux density, less material is needed to carry the same flux at a given

Table 1 Specifications of different electrical steel alloys

	Silicon-iron ^a	Cobalt-iron ^c	Nickel-iron ^a
Sheet thickness in mm	0.2	0.35	0.35
Main additive content in %	2–3	49	44
Saturation polarization in T	2	2.3	1.55
Density in kg/m ³	7650	8120	8250
Specific losses in W/kg @ 1 T, 400 Hz	15 ^b	12.3 ^d	8.1 ^e
Thermal conductivity in W/m/k	31	33	14

^a[10], ^b[12], ^c[13] VACOFLEX 48, ^dSource: loss curves, ^e[14] ULTRAVAC 44 V6

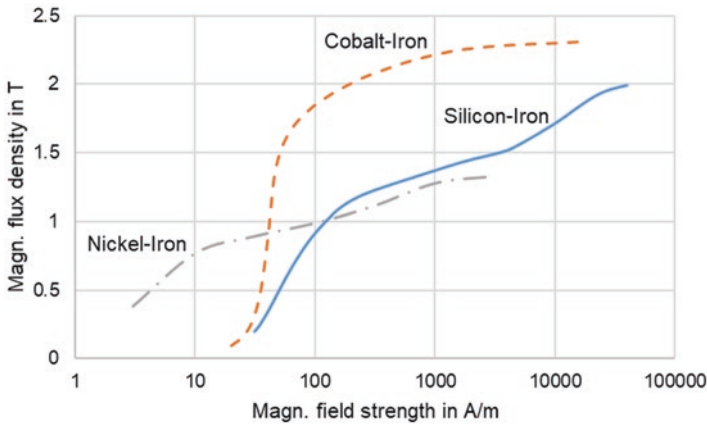


Fig. 2 B-H curves of electrical sheet alloys

operating point [7]. The reduction in material usage, however, cannot be directly mapped to lower weight because of a higher mass density.

Another aspect worth mentioning is the rise in the material cost of a machine when employing cobalt-iron sheets. As a general rule of thumb, the material cost of the core is expected to rise by a factor of 10 when switching from conventional electric sheets to cobalt-iron electrical sheets. This will contribute to a 20–25% rise in the overall cost of a PMS machine. However, these numbers are only an estimation for a non-automated manufacturing process and are highly sensitive to changes in different parameters.

3 Reference Machine Design

A permanent magnet synchronous machine (PMSM) is chosen as the reference design at an operating point of 80 kW and 60,000 rpm because it has low rotor losses and high efficiency. To save the weight of a gearbox, the PMSM directly drives the turbo compressor which calls for a low pole number to decrease the base

Table 2 Design parameters of the machine

Pole pairs	1
Outer diameter of the stator	128 mm
Bore diameter	61 mm
Shaft diameter	20 mm
Length of core	110 mm
Thickness of rotor armor	3.5 mm
Electrical sheets	NO20
Permanent magnet	SmCo

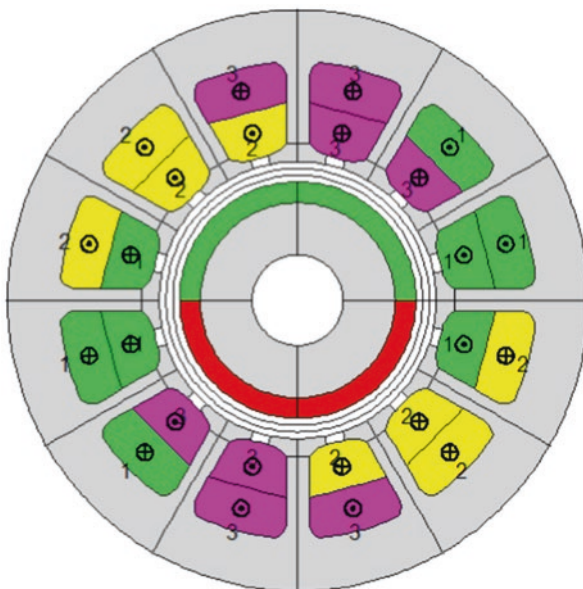


Fig. 3 Cross section of machine design

frequency and the iron losses. In Table 2, the design parameters and in Fig. 3 the cross section without the rotor armor of the machine are shown. The rotor reaches a circumferential speed of 185 m/s which the magnets' glue cannot withstand without the use of additional armoring. For this, carbon fiber-reinforced polymer was chosen because it is one of the strongest choices with a low Young's modulus and because of its characteristic of being nearly electromagnetically invisible. The flux orientation of the permanent magnets is diametral to reduce rotor harmonics.

Only the airflow of the compressor passing outside the housing can be used as a coolant which further reduces the needed mass by not requiring a cooling water circuit. Thus, the operating time is limited by the maximum temperature of the winding's insulation which is 180 °C [15] to 300 s. However, the turbo compressor is needed for additional high lift during takeoff, landing, and touchdown. Therefore, this is feasible and is even capitalized on for further mass reduction.

4 Introducing Cobalt-Iron Electrical Sheets

In the first attempt to redesign the reference machine (hereafter, Ref_NO20), the geometry and the winding are kept the same and the electrical sheet material in stator and rotor is substituted with that of VACOFLUX 48 (hereafter, Ref_VAC48). The operating point is kept through all simulations to achieve 80 kW at 60,000 rpm.

Electrical sheets made of cobalt-iron have significantly lower losses per unit mass than silicon-cobalt sheets even at 75% higher thickness (see Table 1). In addition, the copper losses should not significantly change since both machines have identical windings and the same number of conductors. The only expected difference is related to a difference in phase current amplitude. Due to better magnetization properties in cobalt-iron, Ref_VAC48 is expected to reach the operating point at lower phase current and therefore save on copper losses and consequently reach a lower temperature at its winding.

As shown in Fig. 4, the FEM analysis shows higher maximum flux density for Ref_VAC48. That brings no concern since VACOFLUX 48 has higher saturation flux density, according to Fig. 2. This promises higher achievable torques at the same speeds which also moves the rotational speed at which the maximum flux is achieved further out (see Fig. 5).

The performance parameters for both reference models are reported in Table 3 based on analytical simulations following 2D FEA modeling. The results report an improvement in the power factor and a loss reduction of more than 25%. The latter is also recognized in a lower winding temperature at the maximum operating time. However, the material's density is higher, so the overall weight of the machine has increased by 3.3%.

In conclusion, although the new machine benefits from a better power factor and lower temperature at the winding, the important parameter of weight still lacks modification. For this reason, the design parameters are specifically tuned for the

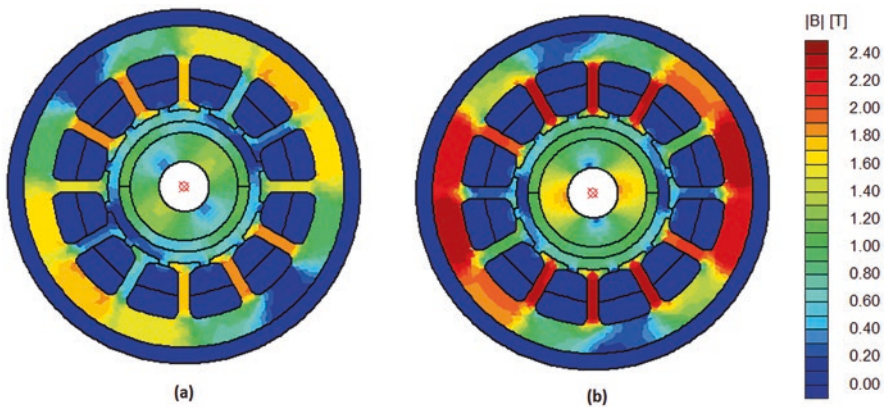


Fig. 4 Flux density distribution of (a) Ref_NO20 and (b) Ref_VAC48

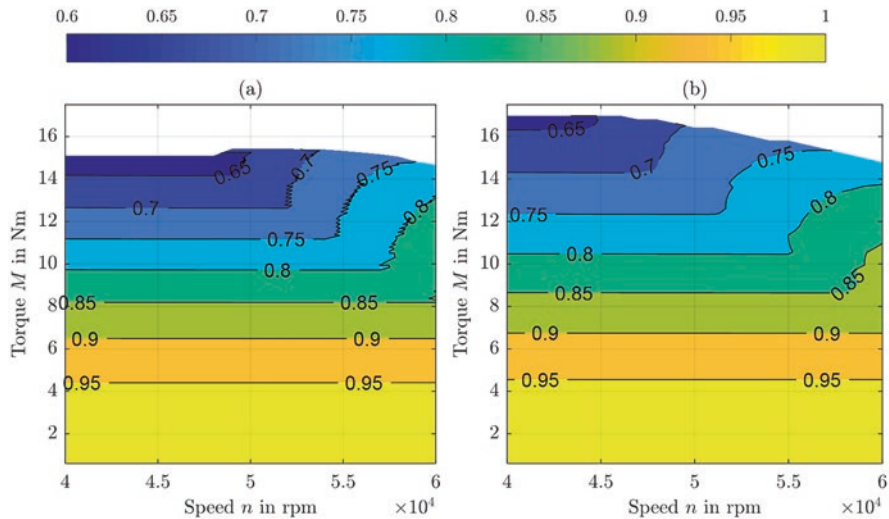


Fig. 5 Power factor of (a) Ref_NO20 and (b) Ref_VAC48

Table 3 Performance parameters' comparison

	Ref_NO20	Ref_VAC48
Power factor	0.806	0.823
Phase current in A (RMS)	144.8	141.3
Winding temperature^a in °C	168.18	154.73
Stator losses in kW	1.194	0.878
Weight in kg	10.89	11.25

^aat maximum operating time

characteristics of cobalt-iron electrical sheets in the following section to further reduce the mass.

5 Fitting the Design

As weight has direct sensitivity to the length of the machine, one impactful way is to try to shorten the machine at the cost of a lower achievable torque. When the saturation flux density of the material is not yet reached in the yoke or the teeth, thinner teeth or a thinner yoke will lead to a lower magnetic resistance which in turn raises the flux and thus compensates the loss in achievable torque. Therefore, a third variant (hereafter, 2P_VAC48) is designed with a thinner yoke, yet constant winding area.

Alternatively, an effective way to compensate for the extra weight of the stator core in the Ref_VAC48 is to cut on the copper weight. This is feasible through changing to a concentrated winding in a four-pole machine (hereafter, 4P_VAC48), as shown in Fig. 6. This would significantly increase the iron losses, especially the eddy current losses, as they depend on the frequency according to Jordan (see Eq. 1) [16].

$$P_{v,fe} = k_h \cdot f \cdot B^2 + k_e \cdot f^2 \cdot B^2. \tag{1}$$

A doubled frequency means four times the eddy current losses; thus, the cobalt-iron material has an advantage for its lower loss coefficient.

Table 4 shows the design parameters of the different machines and highlights the changes between the reference machines and the fitted ones. The maximum length is kept at 110 mm, so there wouldn't be a negative impact on the machine's rotor dynamics. The number of conductors is adjusted for the change to achieve enough flux for leakage the operating point. The results of the new designs are presented in the next section.

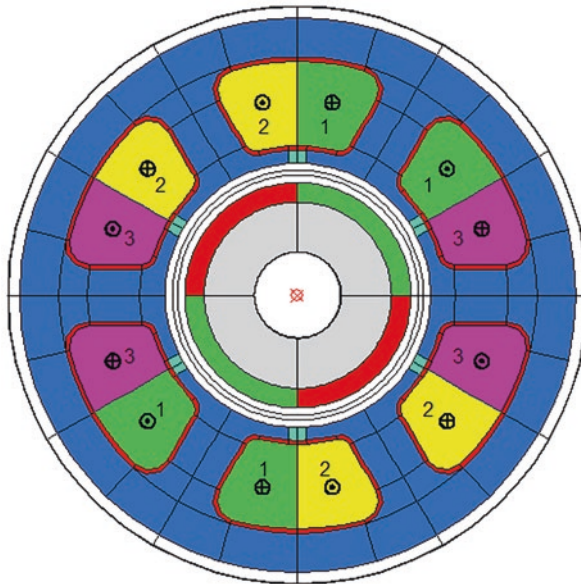
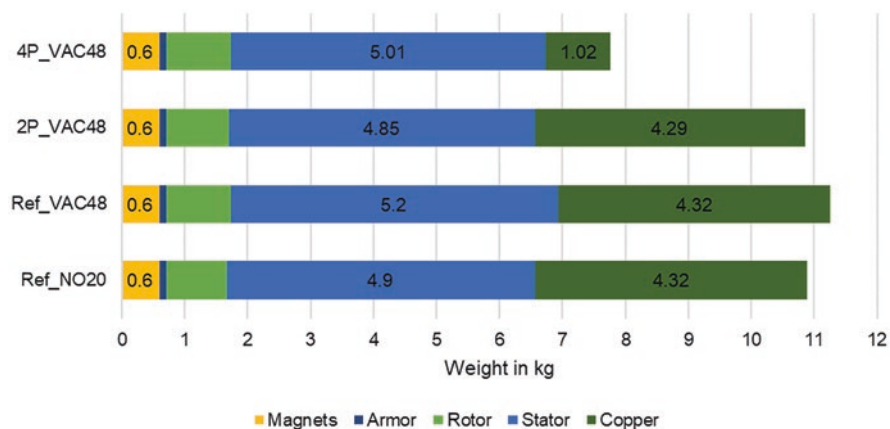


Fig. 6 Cross section of machine design 4P_VAC48

Table 4 Design parameters' comparison

	Ref_NO20/Ref_VAC48	2p_VAC48	4p_VAC48
Number of pole pairs	1	1	2
Length of the machine in mm	110	95	110
Outer diameter of stator in mm	128	126.5	128
Height of yoke in mm	11.5	10.75	11.5
Number of turns per coil	4	4	8
Tooth width in mm	5	5	12
Number of slots	12	12	6
Winding step in slots	5	5	1

**Fig. 7** Weight distribution for different machine components

6 Results and Discussion

Machines 2P_VAC48 and 4P_VAC48 are designed with the aim to provide the same performance as Ref_NO20 but with a lower weight, as it was the main downside of Ref_VAC48.

Figure 7 shows the share of each component in the total weight of the machine for all four designs. With the same rotor geometry, armor, and permanent magnet material corresponding to approximately 15% of the total weight, the importance of the stator design in the overall weight is obvious. Here lies the importance under not only the weight of electrical sheets which is directly determined by the material property but more under how much copper can be saved through an alternative winding approach. That is why no two-pole machine with distributed winding could make as much of an impact on weight reduction compared to Ref_NO20. The copper reduction in the concentrated winding of 4p_VAC48 to more than one fourth has cost-effectively reduced the overall weight of the machine by almost 30%.

In addition, copper saving directly reduces copper losses. 4P_VAC48 reports more than 40% reduction in copper losses in reference to Ref_NO20 and consequently a lower slope in end-winding temperature versus time, as illustrated in Fig. 9. The stator losses as in hysteresis and eddy current losses are also plotted in Fig. 8. These are achieved by a thermal lumped parameter model which is implemented in Matlab/Simulink [4].

From the power factor point of view, the two variants perform not more than 2% lower power factor from the reference machine. Table 5 summarizes all performance parameters for the two proposed designs in comparison to reference NO20 machine.

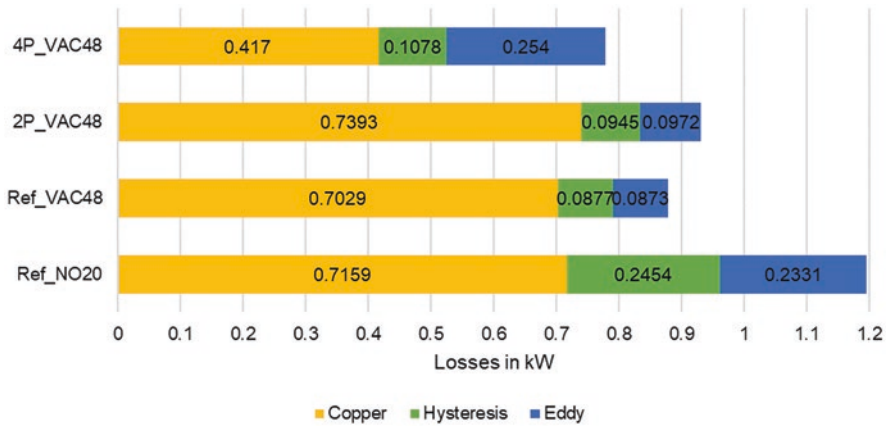


Fig. 8 Stator loss distribution

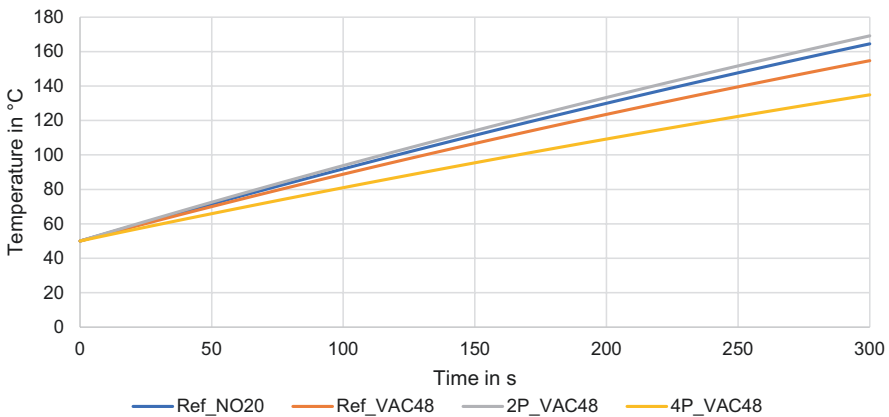


Fig. 9 End winding temperature during the operation timeframe

Table 5 Performance parameters' comparison

	Ref_NO20	2P_VAC48	4P_VAC48
Power factor	0.806	0.790	0.789
Winding temperature in °C	168	169	135
Stator losses in kW	1.194	0.931	0.779
Weight of active parts in kg	10.89	10.85	7.76
Power-to-weight ratio in kW/kg	7.35	7.37	10.31

7 Conclusion

This paper starts with different alloys of electrical steel and comparison regarding their material parameters. Ongoing from that, an electrical machine designed for a directly driven turbo compressor engine is presented as a reference design to be improved with high-tech material. Just changing the material brings an increase in the power factor. It also increases the weight by a small portion, although the aim was to reduce the weight to increase the power-to-weight ratio. Two approaches are then examined in order to reduce weight: one to just change the geometry of the reference design and the other to increase the pole pair number to see if the design with the low loss material is feasible at a higher frequency. The results clearly demonstrate that small improvement is gained by changing the geometry of the two-pole design, but the major effect is gained by combining a concentrated winding with a higher pole pair number. With this, copper losses, as well as the iron losses, are decreased resulting in better thermal behavior. Moreover, since copper has a high density of 8920 kg/m³, a much lower overall mass for the active parts is achieved. Compared to the original design, the power-to-weight ratio is increased by 40% to 10.31 kW/kg.

As an indicator for general interdisciplinary design methodologies, high-tech electrical steel is an enabler for higher frequencies, especially for aircraft applications where the overall weight is of higher significance than in other fields.

References

1. Statista GmbH, *Annual Growth in Global Air Traffic Passenger Demand from 2006 to 2019*. <https://www.statista.com/statistics/193533/growth-of-global-air-traffic-passenger-demand/>. Accessed 03/28/2019
2. R. Radespiel, W. Heinze, SFB 880 – Fundamentals of High-Lift for Future Commercial Aircraft. *CEAS Aeronaut. J.* **5**(3) (2014)
3. F. Kauth et al., Progress in Efficient High-Lift, in *Proceedings of the Applied Aerodynamics Conference*, (AIAA, Denver, 2017)
4. G. Narjes, J. Müller, A. Mertens, B. Ponick, F. Kauth, J.R. Seume, Design Considerations for an Electrical Machine Propelling a Direct Driven Turbo Compressor for Use in Active High-Lift Systems, in *Proceedings of International Conference on Electrical Systems for Aircraft, Railway, Ship Propulsion and Road Vehicles*, (IEEE, Toulouse, 2016)

5. M. Henke et al., Challenges and Opportunities of Very Light High-Performance Electric Drives for Aviation. *MDPI Energies* **11**, 2 (2018)
6. M. Palmieri, M. Perta, F. Cupertino, G. Pellegrino, High-Speed Scalability of Synchronous Reluctance Machines Considering Different Lamination Materials, in *Proc. of the IECON 2014 – 40th Annual Conference of the IEEE Industrial Electronics Society*, (IEEE, Dallas, 2014)
7. M. Weickhmann, R. Brand, M. Herget, Shifting the Limits with High End Magnetic Materials and Technologies, in *Proceedings of the IEEE International Magnetics Conference*, (IEEE, Dresden, 2014)
8. N. Boubaker, D. Matt, P. Enrici, F. Nierlich, G. Durand, Measurements of Iron Loss in PMSM Stator Cores Based on CoFe and SiFe Lamination Sheets and Stemmed From Different Manufacturing Processes. *IEEE Trans. Magn.* **55**(1) (2019)
9. A. Krings, A. Boglietti, A. Cavagnino, S. Sprague, Soft magnetic material status and trends in electric machines. *IEEE Trans. Ind. Electron.* **64**(3) (2017)
10. VACUUMSCHMELZE GmbH & CO. KG, *Soft Magnetic Materials and Semi-finished Products*. (Product Brochure, Edition 2002)
11. *Arnold Magnetic Technologies Nickel Irons and Soft Magnetics*, Product Brochure. Accessed 04.04.2019
12. Cogent Power Inc., *HI-LITE Electrical Steel for Next Generation Designs*, Brochure. Accessed 05.04.2019
13. VACUUMSCHMELZE GmbH & CO. KG, *Soft Magnetic Cobalt-Iron-Alloys*, (Product Brochure, Edition 2016)
14. VACUUMSCHMELZE GmbH & CO. KG, *Application Notes VAC ALLOYS for Motor and Generator Applications*. Accessed 05.04.2019
15. IEC 60034-1:2017, *Rotating Electrical Machines – Rating and Performance* (2017)
16. H. Jordan, *Die ferromagnetischen Konstanten für schwache Wechselfelder*, vol 1 (Elektrische Nachrichtentechnik, 1924)

New Life Calculation Model for Hybrid Bearings



Author Magnus Arvidsson

1 Introduction

When selecting bearings for any purpose, ultimately you want to be certain of achieving the required level of equipment performance and at the lowest possible cost. Robustness also is very important because the conditions in which your equipment is assembled, operated and maintained may not be precisely known and may, in fact, vary over time.

In addition to the bearing rating life, there are key factors you must consider when putting together the bearing specifications for an application, including:

- Lubricant and supply method.
- Shaft and housing fits.
- Bearing clearance class.
- Cage material and guidance.
- Dimensional stability.
- Precision requirements.
- Bearing sealing.
- Mounting method and maintenance.

To help evaluate these key factors, SKF recommends following the selection process (Fig. 1) shown in the rolling bearings' catalogue (2017) [1].

The process provides a straightforward step-by-step approach that shows the general relationship between each step. Selecting and sizing a bearing contain many other factors in addition to a life calculation.

A. M. Arvidsson (✉)
SKF, Gothenburg, Sweden
e-mail: Magnus.arvidsson@skf.com



Fig. 1 Bearing selection process

2 SKF Generalized Bearing Life Model: The Next Step in Bearing Rating Life Calculations

In general, the problems that rolling bearings are facing in E-motors, pumps and compressor are mainly due to lubrication and contamination effects and surface life. Subsurface fatigue is very rare because the loads are moderate. A new look at the surface is required nowadays with a much more flexible rating system. A system that clearly separates subsurface from surface initiated failure modes.

SKF has always been leading the development of bearing rating life models. Names like Lundberg, Palmgren, Ioannides, Harris, Bergling and others are known to engineers, who perform rating life calculations. Also most of the content in the related ISO standards like in the ISO 281 originates from SKF's research. Now SKF is ready to launch its new model SKF Generalized Bearing Life Model hybrid bearing.

3 Hybrid Bearings

Hybrid bearings (Fig. 2) have rings made of bearing steel and rolling elements made of bearing-grade silicon nitride (Si_3N_4). Silicon nitride is a ceramic (i.e. non-metallic) material characterized by high hardness, high modulus of elasticity, high temperature and chemical resistance, low density and poor conductivity and ductility. Hybrid bearings have been increasingly used in applications operating in challenging environments such as high-speed, oil-free air conditioning and refrigeration compressors, general fluid machinery, electrical machinery and gearboxes. Because the silicon nitride ceramic material is such an excellent electrical insulator, hybrid bearings can be used to effectively insulate the housing from the shaft in both AC and DC motors as well as in electrical generators. Hybrid bearings perform well under poor lubrication and solid contamination conditions compared with all-steel bearings, even though under equal load (due to higher stiffness of ceramic rolling elements) the contact stresses are higher.

In addition, silicon nitride has lower density (60%) than steel. Because of this, the effect of gyroscopic moments and centrifugal forces for angular contact ball bearings and four-point contact ball bearings is much less. For bearing performance, this means higher speed capability compared to bearings with steel balls. Cylindrical roller bearings with silicon nitride roller can run faster compared to bearings with



Fig. 2 Hybrid bearings

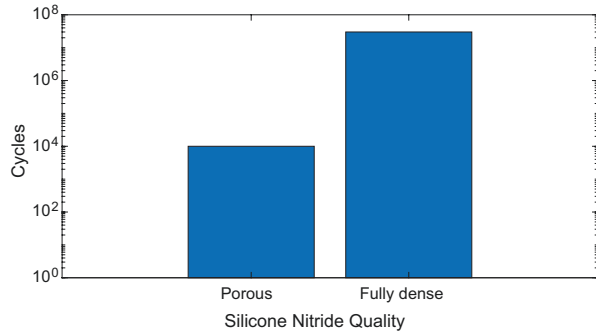
steel rollers. Another advantage, in cylindrical roller bearings with roller made of silicon nitride, is that the risk for light load skidding is lower.

Hybrid bearings provide in most cases much longer bearing service life under the same operating conditions than same-sized all-steel bearings. Hybrid bearings also perform extremely well under high accelerations, vibrating or oscillating conditions.

The use of ceramics, as bearing material, was first proposed in the 1960s for extreme temperature bearings for aero and space applications. By means of component rolling contact fatigue testing, it was established that fully dense hot-pressed silicon nitride has the best rolling contact fatigue (RCF) characteristics when compared to other ceramic materials. Significant variations in fatigue performance were also experienced from seemingly identical production batches of silicon nitride balls. In the 1980s Lorösch et al. [5] performed fatigue life testing of angular contact ball bearings. Using the best available quality of silicon nitride balls, they found that hybrid bearing RCF resistance is comparable to the one of all steel bearings tested under the same load. This despite the 12% increase in contact pressure experienced in the hybrid bearings. However, an additional test of a second batch of silicon nitride balls produced poor fatigue life indicating the criticality of the quality of the ceramic balls in achieving good fatigue life performance.

Over the years the quality and reliability of ceramic rolling elements has substantially increased. The introduction of Non-Destructive Evaluation (NDE) methods combined with the continuous progress in silicon nitride material purity and sintering technology finally allowed engineers to develop reliable and consistent RCF performance of silicon nitride balls, see Galbato et al. [6]. Due to this, in the 1990s a significant growth was observed in the use of hybrid bearings in high-speed machine tool spindles with significant benefits for the speed capability and precision of these mechanical components, Cundill [7]. Figure 3 shows the progress of

Fig. 3 Progress of ceramic rolling elements in fatigue strength



ceramic fatigue strength, Cundill [8], attributed to the improved hot-pressing hardening and cleanliness for porosity and surface defects throughout the whole manufacturing process (which now could be controlled by NDE).

It has been observed that in typical applications hybrid bearings last longer when the selection has been done according to the SKF bearing selection process.

4 Background of New Endurance Life Model

From the review of hybrid bearing development, it is found that the fatigue strength of bearing-grade silicon nitride has made tremendous strides during the last 20 years. RCF performance of silicon nitride balls has risen to two orders of magnitude since the early 1980. Fatigue life testing of hybrid bearings also shows unequivocally that the ceramic rolling element is the most reliable component in a bearing system. Nevertheless, the impact of 12% increase in contact pressure present in hybrid bearings is a characteristic that can be observed under running conditions that subsurface contact fatigue is the predominant damage mechanism dominating the performance of the bearing. Figure 2a shows the Weibull probability plot of the endurance tests performed by Foster et al. [9] of hybrid and all-steel bearing tested under the same conditions. The plot shows that under high load and favourable lubrication conditions, subsurface fatigue dominates the bearing fatigue performance. Therefore, hybrid bearings that are subjected to a high contact pressure (3.5 GPa) generate a higher failure probability, for a given running time, compared to the all-steel base line variant that was running at a pressure of 3.1 GPa (note, this is achieved with a weak statistical significance given the extent of overlapping of the 90% confidence bar as shown in the Weibull plot of Fig. 4a).

Figure 4b shows the Weibull probability plot of the endurance, comparing all steel and hybrid execution under the same test conditions. The test was performed at a lower load giving rise to a maximum Hertzian contact pressure of 2.6 GPa for the hybrid and 2.3 GPa for the all-stress variant. The test was performed under challenging environmental conditions. High temperature, thin film and raceways

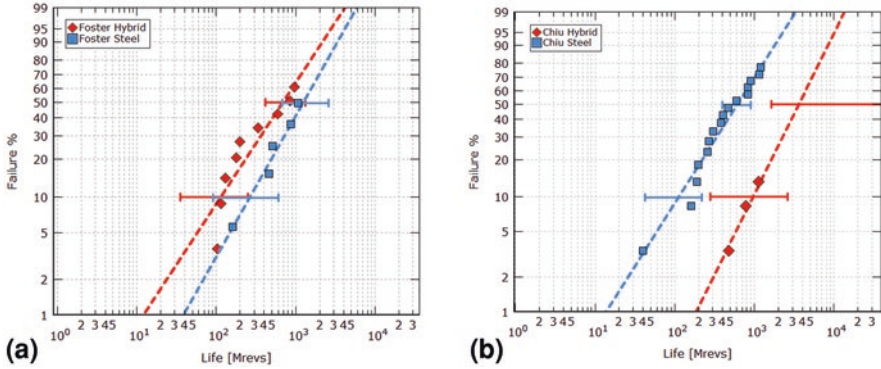


Fig. 4 (a) Endurance life of hybrid and steel 209 bearings tested at a maximum Hertzian pressure of 3.5 GPa and 3.1 GPa with good lubrication [9]. (b) Endurance life of hybrid and steel 208 bearing tested at maximum Hertzian pressure of 2.6 GPa and 2.3 GPa in a challenging environment [13]

run-in with oil contaminated with environmental particles to simulate the actual lubrication condition of the application.

5 Generalized Modelling Approach

The fundamental idea of the model [10] is to explicitly separate, in the formulation of the fatigue life, the surface from the subsurface fatigue. Traditional RCF can still be applied in the subsurface but more flexible and physically meaningful methods are used to model the surface fatigue damage.

Figure 5 illustrates how the stresses in the near surface are influenced by tribological phenomena like roughness, friction and lubrication, while the subsurface stresses can be represented, as usual, by the Hertzian stress field.

A generalized life equation was established in [11] with separate terms for the surface and the subsurface. Notice that the life L of the bearing in number of revolutions can be related to the number of load cycles N by the relation $L = N/u$, where u is the number of the load cycles taking place at each revolution.

In bearing life ratings, a standardized slope of the Weibull statistics is adopted, we can set e . The L_{10} is the 10% bearing life which implies 90% of bearing survival $S = 0.9$, and the life equation can be written as:

$$L_{10} = u^{-1} \left[\ln \left(\frac{1}{0.9} \right) \right]^{1/e} \left[\bar{A} \int_{V_v} \frac{\sigma_v - \sigma_{u.v}^c}{z^h} dV_v + \bar{B} \int_A \sigma_s - \sigma_{u.s}^c dA \right]^{-\frac{1}{e}} \quad (1)$$

Equation (1) represents the basis of a generalized bearing life model that explicitly separates the surface damage accumulation from the subsurface fatigue. The

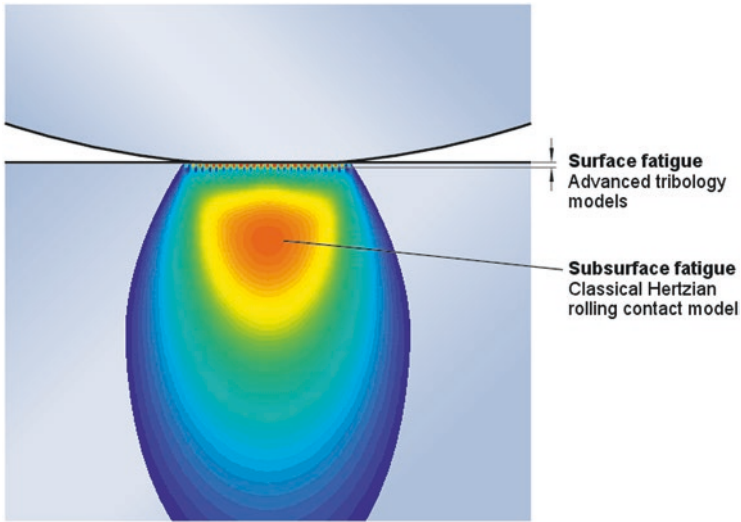


Fig. 5 Illustration of the separation of stresses between the surface and the subsurface in RCF

subsurface term of Eq. (1), represented by the volume integral, can be solved using established rolling contact fatigue methods as explained in reference [11].

However, the surface term, given by the area integral of Eq. (1), must be quantified in a radical different manner. Its assessment requires the estimation of the damage originated by the actual stress conditions of the raceway surface under a variety of operating conditions that may occur to the bearing.

This task is complex, but it offers the possibility to consistently consider, in the life estimation of hybrid bearings, the tribological phenomena that characterize the performance and endurance characteristics of the ceramic-steel raceway contact as well described in [3].

6 Surface Survival of Ceramic-Steel Interface

Equation (1) can be rewritten in a form that clearly indicates the separation between the contribution of the raceway surface to the life of the bearing:

$$L_{10} = \left[\underbrace{\frac{\bar{A} u^e}{\ln\left(\frac{1}{0.9}\right)} \int_{V_v} \frac{\sigma_v - \sigma_{u,v}^c}{z^h} dV_v}_{\text{Subsurface}} + \underbrace{\frac{\bar{B} u^e}{\ln\left(\frac{1}{0.9}\right)} \int_A \sigma_s - \sigma_{u,s}^c dA}_{\text{Surface}} \right]^{-\frac{1}{e}} \tag{2}$$

$$L_{nGM} = a_1 \left[\frac{1}{L_{n.surf}} + \frac{1}{L_{n.sub}} \right]^{-1/e} \tag{3}$$

L_{nGM} = SKF GM rating life (at 100 – n% reliability) [Mrev].

a_1 = life adjustment factor for reliability.

$L_{n.surf}$ = SKF GM surface rating life (at 100 – n% reliability) [Mrev].

$L_{n.sub}$ = SKF GM subsurface rating life (at 100 – n% reliability) [Mrev].

For the surface integral to be solved, the stresses at the surface σ_s need to be worked out. Since these stresses depend on roughness, friction, lubrication conditions, contamination, and wear.

Only a sophisticated mixed-lubrication numerical model can be used for the evaluation of this integral.

It would be unpractical to use this kind of approach for day-to-day bearing life calculations. Therefore a function was introduced to simplify the calculation; this function is the result of a parametric study using the numerical model. This function reads in terms of bearing parameters,

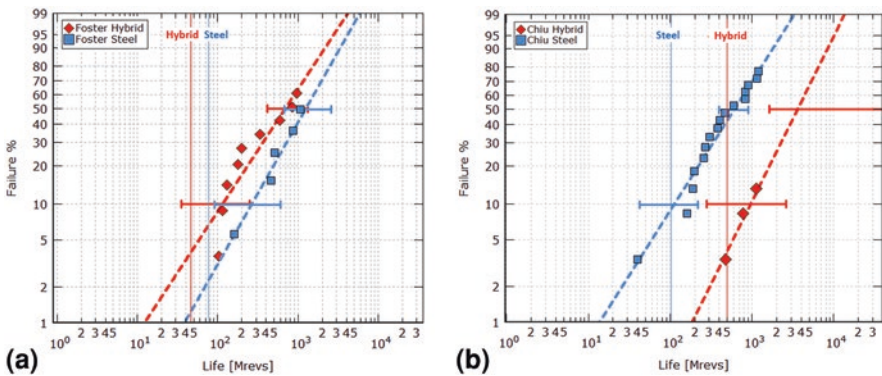


Fig. 7 (a) Endurance life of bearing size 7208 tested at a maximum Hertzian pressure of 3.5 and 3.1 GPa (hybrid and steel, respectively) and good lubrication [9]. (b) Endurance life of bearing size 7208 tested at a maximum Hertzian pressure of 2.6 and 2.3 GPa (hybrid and steel, respectively) in a challenging lubrication environment [13]

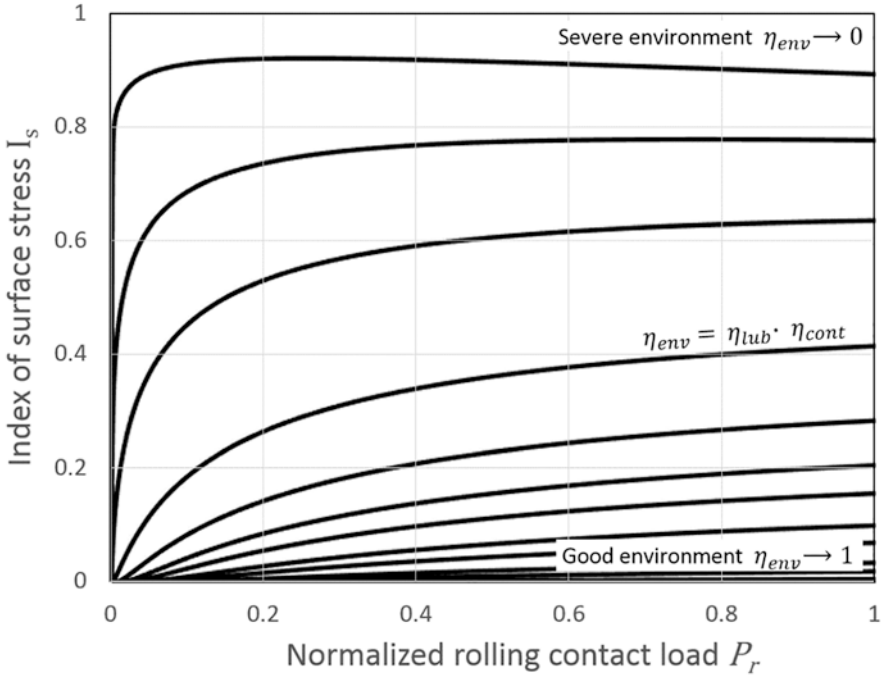


Fig. 6 Index of surface stress of hybrid bearings as function of load and environmental severity factor

$$I_s^* = \int_A \sigma_s - \sigma_{u,s}^c dA \approx c_1 \exp \left[\frac{c_2}{(P/P_u)^{c_3}} + \frac{c_4}{(P/P_u)^{c_5}} \right] \quad (4)$$

with $c_{(1...5)}$ being constants. The normalized surface integral will be called index of surface stress. Figure 7 shows a typical behaviour of this index as a function of the contact load and the effects of lubrication (η_b) and contamination (η_c), which have been combined in a new parameter called environmental severity factor $\eta_{env} = \eta_{lub}\eta_{con} = \eta_b\eta_c$. It can be seen in this figure that for the curves corresponding to very severe conditions ($\eta_{env} \rightarrow 0$) the behaviour is nearly asymptotic with respect to the load, and this is due to the competitive effect of mild wear with fatigue (Fig. 6).

High values of this index mean high surface stresses and higher impact on the surface life of the bearing.

The Generalized Bearing Life Model or GBLM takes specific values that accommodate the behaviour of the surface in hybrid bearings. The model is also validated there with the use of endurance test results.

Table 1 Bearing size 7208, hybrid and all-steel variants. Geometrical details and test loading

Parameter	Forster [9]	Chiu [10]
Ball diameter (mm)	12.7	12.7
Number of balls	11	9
Pitch diameter (mm)	60.25	60.25
Nominal contact angle (°)	22	18
Axial load (kN)	22.2	7.56
Hybrid pressure (GPa)	3.5	2.6
Steel pressure (GPa)	3.1	2.3
Environmental factor η_{env}	0.85	0.035

7 Surface Life Model

The tests were performed on a population of 72 angular contact ball bearings, size 7208. A total of 40 hybrid bearings were tested leading to 12 failures. For the all-steel variant, 32 bearings were endurance tested leading to 21 failures. Geometrical details of the test sample and related loading and stress conditions used in the endurance tests are shown in Table 1.

A major difference between the two tests is related to the loading conditions and lubrication environment in which the tests were conducted. In case of the Forster's endurance tests, the load was higher, leading to Hertzian contact pressure of 3.5 GPa for the hybrid bearing variant. Furthermore, the lubrication conditions were good. The oil circulation system was provided with good filtration, and the film thickness to composite roughness ratio was larger than two. The GBLM environmental factor resulting from the given lubrication conditions is then $\eta_{env} = 0.85$. This gives rise to a low value of the index of surface stress. Indeed, under the given loading conditions, subsurface fatigue controls the performance of the rolling contact. Therefore, the Forster's test operating conditions are of advantage to the all-steel 7208 bearing variant which operates at a lower Hertzian stress of 3.1 GPa and thus will generate lower fatigue damage per overrolling cycle.

In case of Chiu's endurance testing, the applied load was significantly lower leading to a maximum Hertzian stress of 2.6 GPa for the hybrid bearing variant. The running temperature of the tests was higher (150 oC) providing a thinner oil film to the bearing. Furthermore, the tests were conducted with induced raceway defects to reproduce the typical contamination condition encounter in many bearing applications. This was achieved by running in the bearings for 15 min in oil containing 2.5 ppm aluminium oxide particles of 20 μm size. The resulting GBLM environmental factor that characterizes the given operating conditions is, in this case, low, i.e. $\eta_{env} = 0.035$.

In case of Chiu's endurance testing, with the given loading and environmental conditions, the role of the surface fatigue strength dominates the survival of the bearing. In other words, there is a high index of surface stress; thus surface fatigue will control the fatigue performance of the bearing. The surface stress index specifically developed for hybrid bearings will play here in favour of the fatigue

performance of hybrid bearings compensating for the higher Hertzian stress (2.6 GPa), present in the ceramic-steel contact.

The running conditions discussed above of the hybrid bearing endurance testing were introduced into an ad hoc bearing life computation code with the implementation of the Generalized Bearing Life Model according to Eq. (3). The life performance of the 7208, steel variant, was also computed using an equivalent version of the GBLM as discussed in Morales-Espejel [4]. The results of the calculated 10% fatigue life corresponding to the different test and bearing variants are presented in the Weibull plots of Figs. 7a, b. The predicted endurance lives, in millions of revolutions, are shown in the plots with thin vertical lines labelled according to the corresponding bearing variant of the calculation.

The examination of the GBLM model results, related to Forster's test results, are presented in 7a. The plot shows that predicted fatigue lives for the hybrid and all-steel variants are set at about the lower end of the 90% confidence interval of the 10% failure probability of the endurance test results. This means that the Forster's endurance tests validate the GBLM model results with a high degree of statistical significance.

The model results related to Chiu's endurance tests are presented in 7b. In this case the prediction has a lower degree of statistical significance. This may be due to the low number of failures obtained for the hybrid variant and a one early failure affecting the results of the all steel test results. However, the GBLM bearing endurance results are all well below the experimental L10,50% and fully consistent with the experimental observations. Indeed, the model indicated the ability to

Table 2 Summary of application cases for the analysis

Case	Bearing	Description	Illustration
1	6310 C3	<u>Application</u> : pump <u>Load</u> : moderate – $P = 5.47\text{kN}$ ($C/P = 12$) <u>Speed</u> : 3600 rpm <u>Lubrication</u> : poor (oil bath) - $\kappa = 0.3$ (low viscosity at high temperature and water contamination) <u>Contamination</u> : moderate solid particle contamination, $\eta_c = 0.3$	Figure 8a
2	6308 2RS/ C3	<u>Application</u> : electric motor <u>Load</u> : light/mod. – $P = 2.05\text{kN}$ ($C/P = 20$) <u>Speed</u> : 3600 rpm <u>Lubrication</u> : good – $\kappa = 1.5$ (grease lubrication with rubber sealing) <u>Contamination</u> : rubber seals, $\eta_c = 0.8$	Figure 8b
3	6308 2RS/ C3	Same as (2) but $P = 5.12\text{kN}$ ($C/P = 8$)	Figure 8b
4	7217 ACD/ HC	<u>Application</u> : screw compressor <u>Load</u> : light/mod. – $P = 4.6\text{kN}$ ($C/P = 21$) <u>Speed</u> : 9600 rpm <u>Lubrication</u> : poor – $\kappa = 0.2$ (high contamination with refrigerant) <u>Contamination</u> : moderate solid particle contamination, $\eta_c = 0.4$	Figure 8c

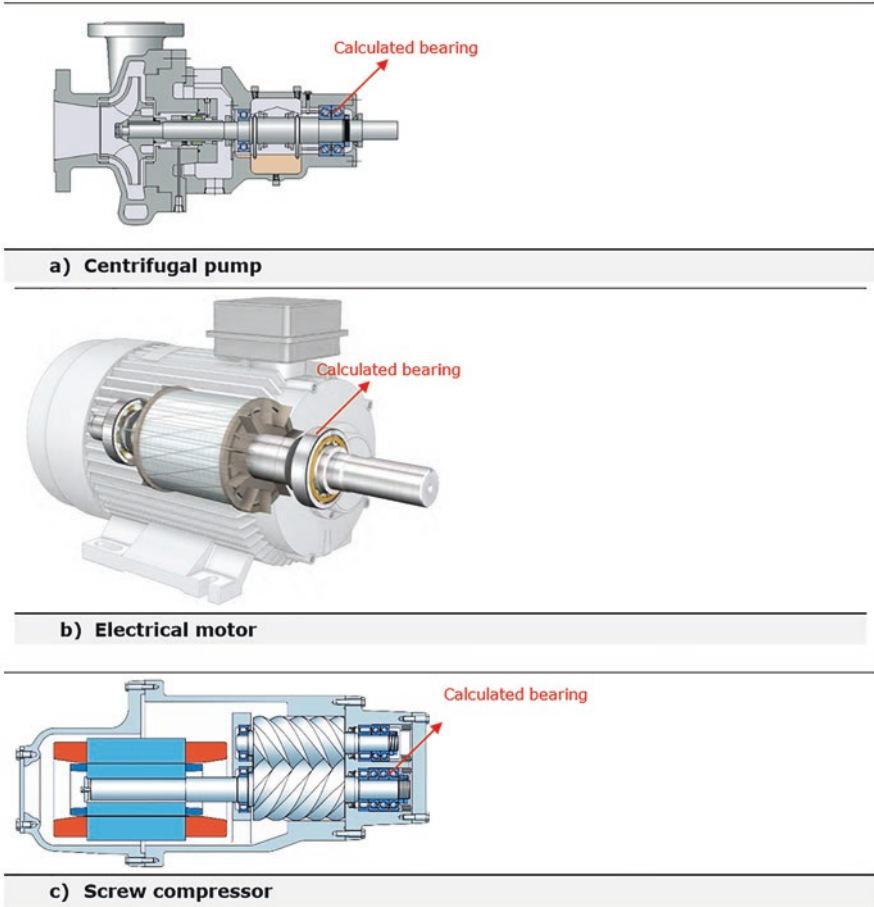


Fig. 8 Schematics of the different applications studied in this paper

represent well the significant longer rolling contact fatigue life of the hybrid variant despite the higher contact pressure present in this bearing during the test.

8 Application

In this section, some actual bearing application cases will be calculated with the GBLM (load-based) and compared with current ISO 281 calculation methodology.

Table 2 shows a summary of the different cases considered including the description of the different operating conditions. In all the applications and bearing executions, steel refers to ASTM 52100

9 Case 1: Pump

In this case the environmental severity factor results in $\eta_{env} = 0.0065$, which according to the schematics of Figs. 7a, b means very high stress for the surface. The life of these bearings will be dominated by surface-related failures. The calculated lives for the hybrid and all-steel variants are:

- L10.hyb = 3911 Mrev.
- L10.ISO = 509 Mrev.

Where L10.ISO refers to the calculated life using ISO 281:2007 [1] for all-steel bearings. Substantial advantage for the hybrid bearing.

10 Case 2: Electric Motor

The environmental severity factor for this case is $\eta_{env} = 0.48$, i.e. somehow high stress condition for the surface.

Given the low load of the bearing, the high cleanliness and good lubrication, the rolling contact fatigue life expectation of this application is very good. The rolling contact fatigue damage is therefore negligible, and fatigue life expectation reaches the asymptotic maximum of the life rating for the hybrid and the all-steel variants ($a_{ISO} = 50$) for the ISO model and an equivalent limit imposed on GBLM to keep consistency with ISO; thus the calculated lives are:

- L10.hyb = 400E3 Mrev.
- L10.ISO = 400E3 Mrev.

Actual service life of the bearing will be related to the service life of the grease. As discussed in [1] in case of hybrid bearings, grease life can be significantly extended (x4) compared with all-steel bearings.

From the point of view of electrical insulation properties and protection from electrical raceway discharge (raceway damage causing noise deterioration), the hybrid bearing keeps its advantages with respect to the all-steel execution.

Actual service life of the bearing will be related to the service life of the grease. In case of hybrid bearings grease life can be significantly extended (x4) compared with all-steel bearings.

From the point of view of electrical insulation properties and protection from electrical raceway.

discharge (raceway damage causing noise deterioration), the hybrid bearing keeps its advantages respect to the all-steel execution.

11 Case 3: Electric Motor, Higher Load

Same conditions as Case 2 but with higher load (no major changes in the environmental severity factor). The calculated lives for the hybrid and steel variants are:

- $L_{10.hyb} = 4457 \text{ Mrev.}$
- $L_{10.ISO} = 3450 \text{ Mrev.}$

Due to the higher load, the lives are substantially shorter in both cases, but remain almost the same. There is only a minor advantage by the hybrid bearing.

12 Case 4: Screw Compressor

The environmental severity factor for this case is very low $\eta_{env} = 0.001$, which implies very high surface stress condition present on the raceway of the bearing. Basically, the life of the bearings is totally dominated by the raceway surface survival. The calculated lives.

for the hybrid and all-steel variants are:

- $L_{10.hyb} = 242E3 \text{ Mrev.}$
- $L_{10.ISO} = 2.4E3 \text{ Mrev.}$

The special tribo-fatigue properties of ceramic-steel contact show here a strong and definite advantage for the hybrid bearing execution.

To illustrate the applications, Fig. 8 shows some schematics of the analysed cases.

13 Summary of Results

Table 3 shows a summary of the calculated results for the different cases. Contamination conditions can be translated into η_{con} exactly in the same way as before by using ISO 281 [1] where the contamination parameter is equivalent to ISO e_c . The ISO lubrication quality factor (κ) can be translated into and η_{lub} by using the curve described in Morales-Espejel et al. [23]. In cases 2 and 4 of Table 2, there is practically no significant advantage in fatigue life rating for the hybrid bearing

Table 3 Summary of calculation results for the different application cases of Table 2

Application case	$L_{10.hyb}/L_{10.ISO}$	η_{lub}	η_{env}
1	7.68	0.022	0.0065
2	1	0.60	0.48
3	1.29	0.60	0.48
4	100	0.0025	0.001

compared with the all-steel variant. However, other aspects might be considered for the selection criterion of hybrid bearing, such as grease life expectations, better electrical insulation properties, less noise, etc.

What the current model also clearly shows for cases 2 and 3 is that ball hybrid bearings (despite the 12% higher contact stress) are expected to have equal or better RCF life than the all-steel solution. This is because the higher contact pressure present in the hybrid bearing is compensated by the lower risk of surface fatigue of the ceramic-steel interface. For the application cases 1 and 4, in which life performance is dominated by surface-initiated fatigue, the RCF advantage of hybrid bearings is clearly predicted. This corresponds well with the field experience in the use of hybrid bearings. To illustrate the applications, Fig. 5 shows some schematics of the analysed cases.

14 Summary and Conclusions

The SKF Generalized Bearing Life Model (GBLM) that allows for the separation of surface and subsurface survival has been applied to calculate the life of hybrid bearings. SKF has developed a model and a computer tool for this calculation. With this, it has been shown that the apparent inconsistent literature test results can be explained, be understood and modelled.

For instance, in cases where hybrid bearings show less performance compared with all-steel bearings, as in the case of high load and good surface conditions (good lubrication and low contamination), this is because it is the subsurface (higher Hertzian stresses) that dominates the life of the bearings. Thus, hybrid bearings, that have higher subsurface stress, will suffer the most.

However, for the cases of low load and tough surface conditions (poor lubrication and presence of contamination), the better tribology inherent to the ceramic-steel contact (lower boundary friction coefficient and quick plastic flattening of raised edges in indentations) will dominate and provide hybrid bearing with a significant advantage compared with all-steel bearings.

The application of the GBLM model to actual application cases shows these types of behaviour. In conclusion the following can be said:

1. Hybrid bearings have an advantage over all-steel bearings when the fatigue performance is dominated by surface fatigue. In situations where the subsurface dominates performance, all-steel bearings have the performance advantage.
2. The present GBLM can model this type of behaviours efficiently.
3. Making this model available for the application engineering community will certainly open new possibilities for the use of hybrid bearings in many applications in which a performance premium over all-steel bearings is expected.

References

1. Rolling bearings catalogue, SKF Group, 86–107 (2018)
2. G.E. Morales-Espejel, A. Gabelli, A Major Step Forward in Life Modelling. SKF Evolution #4, 21–27 (2015)
3. C. Vieillard, V. Brizmer, Y. Kadin, G.E. Morales-Espejel, A. Gabelli, Benefits of Hybrid Bearings in Severe Conditions. SKF Evolution #3, 21–26 (2017)
4. G.E. Morales-Espejel, R. Hauleitner, H.H. Wallin, Pure Refrigerant Lubrication Technology in Oil Free Centrifugal Compressors. SKF Evolution #1, 26–30 (2017)
5. H.K. Lorösch, J. Vay, R. Weigand, E. Gugel, H. Kessel, Fatigue Strength of silicon nitride for high-speed rolling bearings. Trans. ASME J. Eng. Power **102**, 128–131 (1980)
6. A.T. Galbato, R.T. Cundill, T.A. Harris, Fatigue life of silicon nitride balls. Lubrication Eng. **48**(11), 886–894 (1992)
7. R.T. Cundill, High precision silicon nitride balls for bearings. Ball Bearing J. **241**, 26–32 (1993)
8. R.T. Cundill, Material selection and quality for ceramic rolling elements. Proc. of Mech. Eng. Seminar, Rolling Element Bearings – Towards the 21st Century, 31–40 (1990)
9. N.H. Forster, S.M. Peters, H.A. Chin, J.V. Poplawski, R.J. Homan, Applying Finite Element Analysis to Determine the Subsurface Stress and Temperature Gradient in Highly Loaded Bearing Contacts, in *Bearing Steel Technologies: 11th Volume, ASTM STP1600*, ed. by J. M. Beswick, (ASTM, West Conshohocken, PA, 2017), pp. 151–166
10. G.E. Morales-Espejel, A. Gabelli, A.J.C. de Vries, A model for rolling bearing life with surface and subsurface survival–tribological effects. Tribol. Trans. **58**, 894–906 (2015)
11. G.E. Morales-Espejel, A. Gabelli, A major step forward in life modelling. SKF Evolution #4, 21–27 (2015)
12. G.E. Morales-Espejel, A. Gabelli, Application of a rolling bearing life model with surface and subsurface survival to hybrid bearing cases. Proc. IMechE Part C, J. Mech. Eng. Sci, 84847 (2019)
13. Y. P. Chiu, P. K. Pearson, M. Dezzani, and H. Daverio, Fatigue Life and Performance Testing of Hybrid Ceramic Ball Bearings, Lube Eng. **52**(3), 198–204 (1996)

Programme for In-Depth Analyses of Electric Motor Systems in Industry (ProAnalySys)



Richard Phillips

1 Introduction

In 2011, the Federal Council and Parliament decided that Switzerland has to withdraw from the use of nuclear energy on a step-by-step basis. The existing five nuclear power plants are to be decommissioned when they reach the end of their safe service life and will not be replaced by new ones. As a result of this decision and various other profound changes (e.g. low electricity prices) that have been observed for a number of years, in particular in the international energy arena, the Swiss energy system will require successive restructuring in the period up to 2050. In view of this, the Federal Council developed a long-term energy policy (“Energy Strategy 2050”) based on the revised energy perspectives.¹ At the same time, it produced an initial package of measures aimed at securing the country’s energy supply over the long term. The initial package of measures concerns three sectors: households, services and industry. An extensive survey in the industry sector revealed that a large percentage of electric motor systems are oversized, too old and inefficiently operated.² Based on the savings potential of electric motor systems, Switzerland’s annual electricity consumption could be reduced by up to 5%.³

¹Botschaft zum ersten Massnahmenpaket der Energiestrategie 2050 (Dispatch to Parliament concerning the initial package of measures relating to Energy Strategy 2050), Swiss Federal Office of Energy, September 2013.

²«Easy – Lesson learned from 4 years of the Swiss EASY audit and incentive programme», Rolf Tieben et al., EEMODS 2015, Helsinki, 15–17 September 2015 under http://www.topmotors.ch/sites/default/files/2018-06/E_PB_2015_09_EEMODS15_Paper_Tieben_Werle_Brunner_EASY.pdf

³“Measures for saving electricity by electric drives: market analysis in the industry, final report,

R. Phillips (✉)
Swiss Federal Office of Energy, SFOE, Bern, Switzerland
e-mail: richard.phillips@bfe.admin.ch

The initial package of measures contains three instruments for the promotion of energy efficiency in order to facilitate the implementation of the efficiency potentials: (a) regulation, (b) voluntary measures without subsidies and (c) voluntary measures with subsidies. Energy Strategy 2050 specifies an indicative reduction target of 43% for total energy and a 13% reduction target for electricity consumption by 2035 [1].

In this paper, and in order to limit the broad scope of energy efficiency, the focus is on electric motor systems and the “Programme for In-depth Analysis of Electric Motor Systems in Industry” (ProAnalySys). This programme concerns the voluntary measures with subsidies for the analysis as a complement to the mandatory audits, the main objective of which is to reduce electricity consumption in the industrial sector. The paper contains a brief description of the consumption profile and categorisation of Swiss companies, as well as the regulation governing large and very large companies. The ProAnalySys programme and its framework are also discussed and illustrated with three pilot projects, and some conclusions are presented at the end.

2 Electricity Consumption of Swiss Companies and Applicable Regulations

The electricity statistics show that 57.4% of Switzerland’s annual consumption is attributable to the industry and services sectors [2].⁴ Switzerland has more than 400,000 companies. Their consumption is not homogeneous, and for this reason they have been classified into four groups: small, medium, large and very large companies (as shown in Fig. 1) [3].

Based on this grouping, it is interesting to note that 30% of the companies in these two sectors account for almost 90% of the overall electricity consumption. Furthermore, electric motor systems such as fans, pumps and compressors are the main consumers alongside lighting, room heating and process heat, as shown in Table 1. It is estimated that there are more than two million electric motors in the industry sector, with a total consumption of 12.0 TWh and a savings potential of between 15 and 30% [4, 5].⁵

In order to reduce the energy consumption of large and very large companies, regulations were introduced, including target agreements for very large companies

Swiss Federal Office of Energy, Bern, December 2006. The main statement of this analysis is that two million electric motors are running in the Swiss industry with a total consumption of 12 TWh p.a. and a saving potential of 25% or 3 TWh p.a. which corresponds 5% of the Swiss electricity consumption of 2018 (SFOE statistics for 2018: 57.6 TWh p.a.).

⁴“Schweizerische Elektrizitätsstatistik 2017”, Figure 2, p. 3, Swiss Federal Office of Energy, Bern, July 2018.

⁵“Massnahmen zum Stromsparen bei elektrischen Antrieben: Marktanalyse in der Industrie”, final report, Swiss Federal Office of Energy, Bern, December 2006.

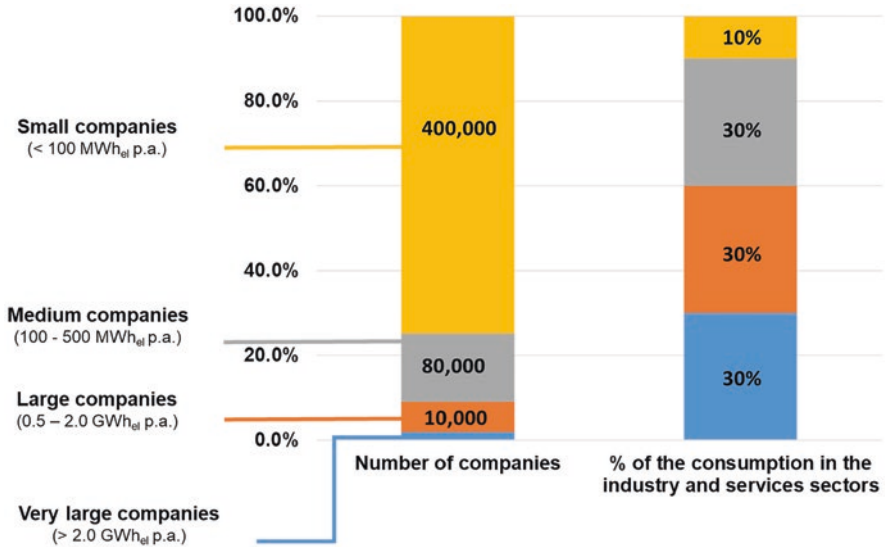


Fig. 1 The four categories of companies and their annual electricity consumption. (“Unternehmen ohne Zielvereinbarung: Auslegeordnung”, working paper, Swiss Federal Office of Energy, Bern, June 2014)

Table 1 Electricity consumption in relation to uses and sectors^a

	Energy consumption in PJ for 2017			
	Household	Services	Industries	Transport
Room heating	158.9	64.8	15.5	0.0
Hot water	32.1	11.1	2.6	0.0
Process heat	5.5	2.1	87.7	0.0
Lighting	4.9	15	5.4	0.0
Air conditioning and ventilation	4.6	16.2	0.9	0.0
ICT	4.6	4.5	0.7	0.0
Drives and processes	15.7	16.8	37.3	0.0
Mobility	0.0	0	0.0	235.8
Others	9.0	3.7	8.0	0.0

^a“Analyse des schweizerischen Energieverbrauchs 2000–2017 nach Verwendungszwecken”, Swiss Federal Office of Energy, Bern, October 2018

(electricity consumption >2.0 GWh p.a.) and legislation governing large-scale consumers (electricity consumption between 0.5 and 2.0 GWh p.a.). These regulations oblige the companies to perform an energy audit (fossil energy and electricity) and thus to compile a catalogue of measures in order to reduce their consumption, as well as their CO₂ emissions. Based on the result of the audit, they have to enter into the following commitments:

- Very large companies: to reduce their energy consumption based on a defined target over a period of 10 years, where efficiency measures with a payback shorter than 4 years for the process or 8 years for the infrastructure need to be implemented (to meet the defined target).
- Large companies: to reduce their energy consumption either by 20% over 10 years or at least 15% over 3 years by implementing (as for very large companies) efficiency measures with a payback time shorter than 4 years for the process or 8 years for the infrastructure.

Small- and medium-sized companies can only undertake a voluntary commitment, for example, through the model of target agreements for small- and medium-sized companies, where they can then save money by reducing their energy costs and can also receive a label certifying reduced CO₂ and kWh levels.

In addition to these regulations, Switzerland is also applying the same ecodesign provisions (minimum energy performance standards) as the European Union, and these will automatically apply when an installation is replaced or upgraded. However, these only concern minimum standards and the majority of audits are conducted without measurements, which means that, for example, oversized pumps will not be detected during such audits. As heat production (for heating and process purposes) and lighting account for at least two-thirds of the energy consumption in the services and industry sectors, as shown in Table 1, and as they have also often payback times shorter than 4 years, these efficiency measures are often preferred over those relating to electric motor systems.

3 In-Depth Analysis of Electric Motor Systems

Four main groups characterise the efficiency measures for electric motor systems⁶:

- Higher efficiency class of the motor
- Higher efficiency of the components
- Size reduction
- Optimisation of regulation/process optimisation

However, the impacts of these measures depend on the approach. For example, a component approach, such as just replacing the motor, does not have a strong impact (savings between 3 and maximum 10%). On the other hand, a full system approach such as optimising the process or adapting the size and regulation of the system can result in savings of up to 50%, as shown in Fig. 2 [6].

As mentioned above, mandatory audits carried out in accordance with the regulations are limited in scope for motor systems as they are performed without making any measurements. They only take very basic data into account, such as:

⁶“Massnahmen zum Stromsparen bei elektrischen Antrieben: Marktanalyse in der Industrie”, final report, Swiss Federal Office of Energy, Bern, December 2006.

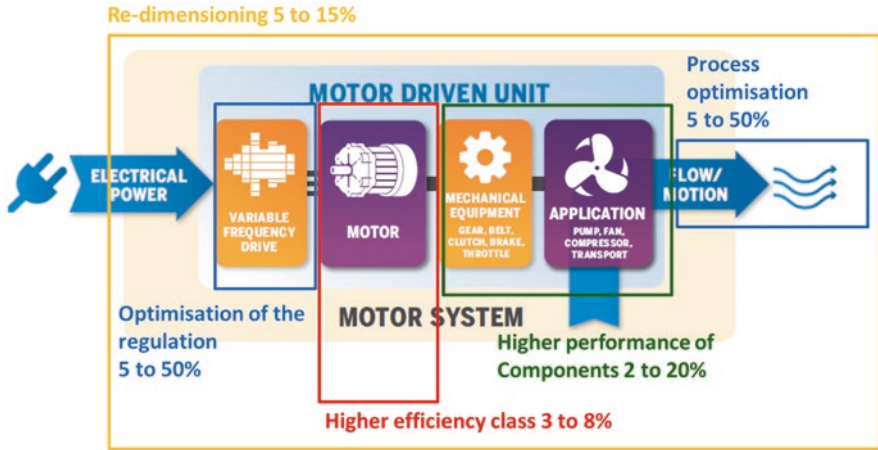


Fig. 2 Schematic representation of an electric motor system and its components, as well as the impacts of each of the four groups of efficiency measures (“Massnahmen zum Stromsparen bei elektrischen Antrieben: Marktanalyse in der Industrie”, final report, Swiss Federal Office of Energy, Bern, December 2006; “Policy Guidelines for Motor Driven Units: Part 2, Figure 1, p. 9, 4E Electric Motor Systems (EMSA), the Netherlands, February 2018)

- Power
- Running time
- Age
- Regulation mechanism

Consequently, such audits mainly concern the component level and cannot detect, for example, if a system is oversized or if a pump is not operating at its optimum working point. The regulation of the motor systems is nevertheless addressed to a certain extent. However, if the system is oversized, then the addition of a variable speed device could create other issues, such as the motor running at a too low speed (leading to its premature ageing) when performance is poor. Table 2 shows a comparison of the savings between a mandatory audit and an in-depth analysis with measurements of an 11 kW pump, which is more than 20 years old, oversized and with mechanical regulation. The mandatory audit recommends adding a VSD (variable speed drive) to replace mechanical regulation, leading to a savings potential of only 10%. However, measurements indicated that the pump was oversized, and it was also recommended to use a smaller pump leading to a savings of 37% (4.1 times higher).

For this reason, the Swiss Federal Office of Energy decided to launch a programme called ProAnalySys to support companies in their efforts to perform in-depth analyses of electric motor systems. However, certain conditions apply, for example, that the programme is only available for large and very large companies (electricity consumption >0.5 GWh p.a.) from the industrial and services sectors, because they are already in contact with energy consultants, so that they will not be overloaded with additional information about a new programme. The energy

Table 2 Savings for an 11 kW pump more than 20 years old, oversized and mechanically regulated, based on the mandatory audit (option 1) compared to a full audit with measurements (option 2)^a

	Current operating state	Option 1	Option 2
		Revision of the actual pump and installation of a VSD	New and smaller pump with VSD
Nominal power (kW)	11	11	7.5
Operating time (hours p.a.)	4000	4000	4000
Nominal flow rate (m³/h)	550	550	400
Flow rate at max. Operation (m³/h)	375	375	375
Flow rate at min. Operation (m³/h)	273	273	273
Efficiency at max. Operation	79%	79	92%
Efficiency at min. Operation	79%	79	90%
Regulation	Mechanical	Electronic	Electronic
Electricity consumption (kWh p.a.)	36,551	33,138	22,908
	Savings	9%	37%

^a“Feinanalyse Umwälzpumpen Badanlage: Schwimmbad Lättich”, Engie Switzerland, November 2018

consultants will provide the companies, which are also their clients, with the necessary information at the appropriate time. Furthermore, as a prerequisite the companies concerned must have already performed a preliminary analysis, for example, in the form of a mandatory audit, so that only those installations with a high savings potential are eligible for an in-depth analysis with measurements. The ProAnalySys programme only encompasses the following systems with a nominal power rating of at least 10 kW:

- Pumps and fans
- Compressors for refrigeration and compressed air production
- Mechanical drives (e.g. ski lifts)
- Industrial processes

Electric mobility, heat pumps and transformers are not covered by the programme, as other programmes already support these technologies.

Upon completion of the pilot phase in December 2019, the objectives of the programme are to support at least 75 analyses a year by 30 companies. Since the programme was initiated in March 2018, 13 companies have participated, and most of them have already implemented some of the identified measures.

The in-depth analysis is in fact a detailed comparison of the actual and targeted state of the electric motor system. The measurements address and assess the following parameters: operating conditions (including load management), operating points, performance ratio, partial power factor(s) as well as the load profile(s) and energy consumption.

Upon completion of the analysis, the companies receive a report containing the following information:

- A precise description of possible measures to improve efficiency
- The savings potential of the system
- The total costs of investment
- The profitability of the system
- The technical feasibility of the efficiency measures
- Practical options for implementation

The energy consultants, who are already in contact with the companies and have conducted the mandatory audits, are also authorised to perform a ProAnalySys in-depth analysis. In other words, the companies do not need to do anything themselves, as the energy consultants take care of almost everything for them in order to provide them with a “turn-key” solution. Furthermore, and at the company’s request, the energy consultants are also authorised to assist it during the implementation of the selected measures (although companies are not obliged to implement any measures since ProAnalySys is a voluntary programme). The support provided by the energy consultants during the implementation phase mainly concerns [7]:

- Preparation of the specifications (e.g. for the acquisition of a new pump equipped with a regulation system such as a VSD).
- Comparison of several offers.
- Clarification of the possibility to participate in an existing implementation programme such as the Swiss Competitive Tenders Programme.⁷

The participation procedure is as follows: the energy consultants send their request for the funding of an in-depth-analysis to the agency to which they are affiliated (there are only two in Switzerland), which checks the content and the company’s fulfilment of the framework conditions. If the request is approved, the agency forwards it to the Swiss Federal Office of Energy (SFOE) with the positive decision. In order to keep the process as simple as possible for the companies, the SFOE concludes a contract directly with the energy consultants so that they can initiate the analysis as quickly as possible. Once the analysis has been carried out, the reports and recommended efficiency measures are submitted to the companies, and copies of the reports are sent to the SFOE, which pays the subsidies after completing a quality assessment. In the case of the ProAnalySys programme, the subsidies cover 40% of the analysis costs up to a maximum of 16 thousand euros (including the support services).

⁷“Swiss Competitive Tenders for Promoting Efficient Motor Systems”, Dr. R. Phillips, EEMOD’15, Helsinki, September 2015.

4 Pilot Projects

In order to better explain the benefits and the reach of the ProAnalySys in-depth analyses, three projects are presented below from the pilot phase for three different systems: a cable railway, a refrigeration installation and a pumping system for a water tobogganing facility (Fig. 3).

4.1 Cable Railway⁸

The first pilot project concerns measurements performed on two cable railways. The first has a length of 1.6 kilometres with a height difference of 447 metres and is equipped with 100 seats. The motor drive system has an annual consumption of 295.9 MWh. The analysis started by examining the three main factors that have a significant influence on the electricity consumption of the cable railway: the lifting capacity, air drag and rolling friction. Figure 4 shows the typical distribution of these three factors at the operating conditions of 4.5 m/s with a capacity of 1000 passengers an hour. The highest losses are due to the rolling friction and air drag.

In this case, the measurement showed that the highest efficiency level is reached at 4.0 m/s (88% of the maximum speed) and at full load capacity. This means that



Fig. 3 Picture of the motor drive system of the cable railway

⁸“Energetische Feinanalyse Antriebsmotoren DKB”, FE Energieingenieur.ch, Fläsch (Switzerland), August 2018.

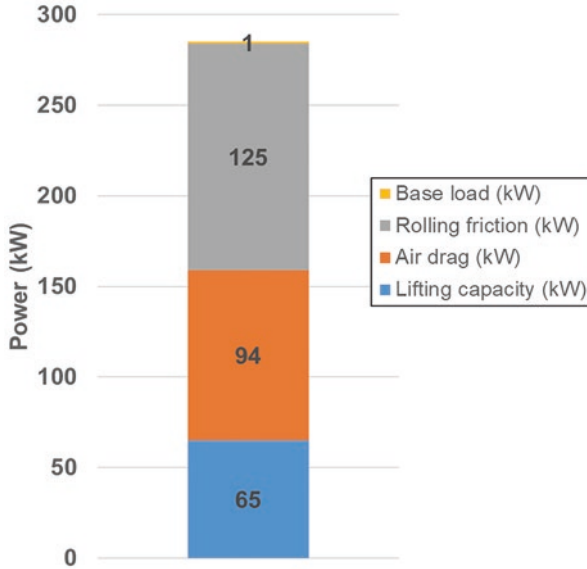


Fig. 4 Typical distribution of the air drag, lifting capacity and rolling friction at the operating conditions of 4.5 m/s and with a capacity of 1000 passengers an hour

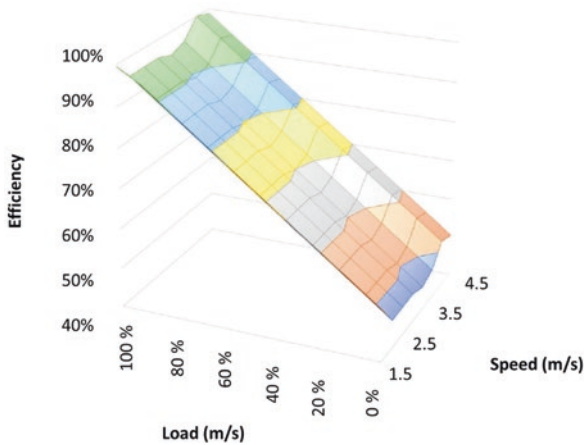


Fig. 5 Efficiency as function of load and speed of the first cable railway

the efficiency decreases when the speed is reduced, but the load increases. In other words, decreasing the speed did not significantly reduce the rolling friction, as shown in Fig. 5.

However, the reduction of the number of seats reduced the air drag: a 30% reduction of the number of seats reduced the electricity consumption by 2%.

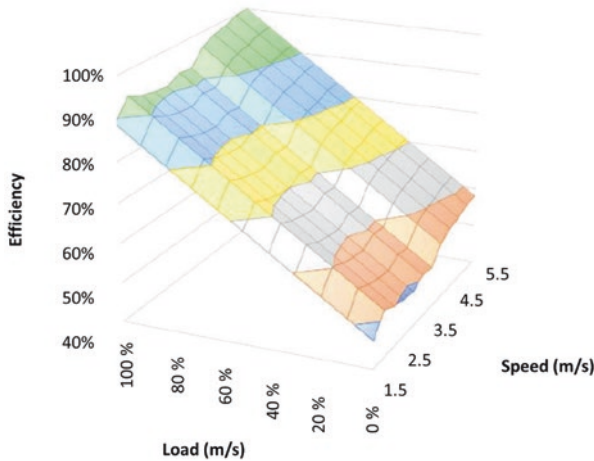


Fig. 6 Efficiency as function of load and speed of the second cable railway

Another efficiency measure concerns the replacement of the DC motor installed in 2000 with an asynchronous IE4 motor and a VSD. This results in a saving of only of 2.6%, with payback time longer than 50 years.

Ultimately, the in-depth analysis only helped implement operational optimisation with a reduction in electricity consumption by less than 2%, which represents 5900 kWh p.a.⁹ or 590 euros p.a. where the payback time for the costs of the analysis is longer than 20 years.

With the second cable railway, which was constructed in 2017, the situation was completely different. Firstly, the height difference of the installation was 200 metres lower, and secondly the proportion of the rolling friction was much higher (about 60% of the energy consumption). Although the electric motor is an IE4 class equipped with a VSD, it proved possible to adapt the speed as a function of the load, as shown in Fig. 6, and thus to reduce the consumption by 10%, which represents 53,500 kWh p.a.¹⁰ or 5350 euros p.a.. In this case, the payback time is shorter than 2 years.

4.2 Refrigeration Installation¹¹

This project concerns the analysis of a refrigeration installation in a pharmaceuticals company. The measurements of the installation provided the following information:

⁹The cable railway runs 50 days a year for 7 hours a day at an average power rating of 600 kW.

¹⁰ 1250 hours at an average power rating of 428 kW.

¹¹ «Synthèse d'analyse d'optimisation de l'installation de froid: Planair», Planair, La Sagne (Switzerland), December 2018.

- The annual consumption of the main refrigeration installation was estimated at up to 682 MWh p.a. with a running time of 6200 h p.a..
- The condensation pressure of the installation is very high and thus not optimised.
- The set point of the cooling temperature is fixed over the year, although the needs for refrigeration are variable depending on the climate as well as the process conditions.
- The regulation of the water pump for the refrigeration system is also not optimal.

Based on these findings, three efficiency measures were recommended.

The first measure concerns the complete maintenance of the cooling compressor (especially cleaning of the heat exchangers and replacement of the filters) in order to optimise the fluctuating condensation pressure (instead of keeping the condensation temperature at a constant 42 ° C all year round). This measure results in a saving of 20% of the consumption of the compressor, or a cost saving of 16 thousand euros p.a. for an investment of 4 thousand euros. Consequently, the payback¹² time for this measure is less than half a year.

The second measure concerns the optimisation of the cold set point of the system. The installation has two set points: one at 5 ° C and the other at 10 ° C. Before the measurements were carried out, the installation was set all year round at 5 ° C. However, as shown in Fig. 7, a set point at 5 ° C only makes sense during the period from May to September when dehumidification is required. The rest of the year the set point can be set to 10 ° C. Such a simple measure with an investment of 5 thousand euros results in a 2% saving of the consumption of the compressor, or 1.5 thousand euros p.a., and a payback time of 3.3 years.

The third measure concerns the implementation of a new regulation device for the distribution pump. The pump delivers an output ranging from 200 m³ per hour to 240 m³ per hour. Although it is already equipped with a VSD, which keeps the pump running at its maximum speed, the pressure difference regulates the water flow. When the pressure difference increases from 22 mCE for an output of 240 m³ per hour to 30 mCE for an output of 200 m³ per hour, then the power decreases from 24 kW to 23 kW, as shown in Fig. 8. The new regulation setting is then based on the required flow rate, allowing the pump speed to be adapted by the VSD. In this case, the speed decreases from 100% (at 240 m³ per hour) to 83% (at 200 m³ per hour), which means that the power also decreases from 24 kW to 13.0 kW (see Fig. 8). This efficiency measure required an investment of 3 thousand euros and results in savings of up to 40% of the consumption of the pump, or 7 thousand euros p.a., and a payback time of less than half a year.

¹²In this paper, the payback is the ratio between the investment costs and the energy saving costs. The investment costs are based on the offer of manufacturers' offers for the implementation of the efficiency measure(s).

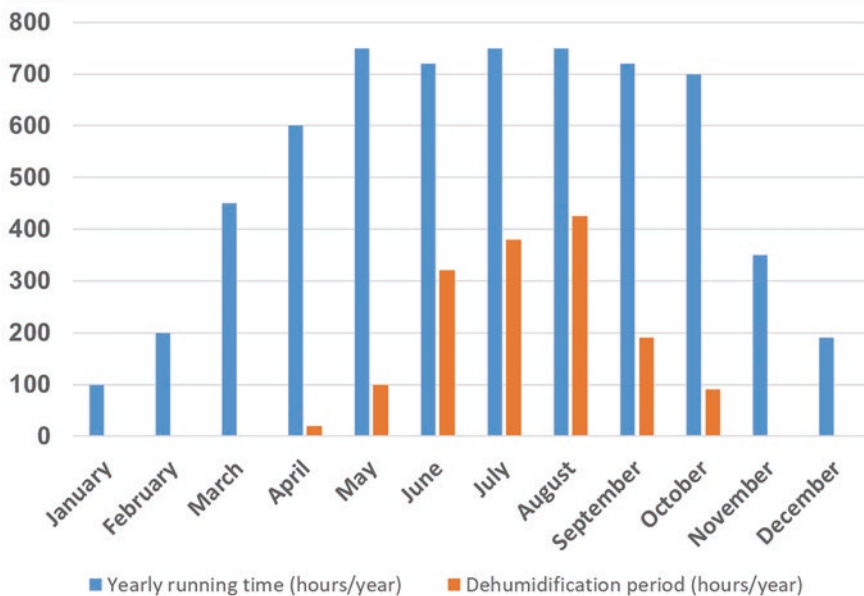


Fig. 7 Operating hours of the refrigeration installation in comparison with the period of dehumidification based on the measurements

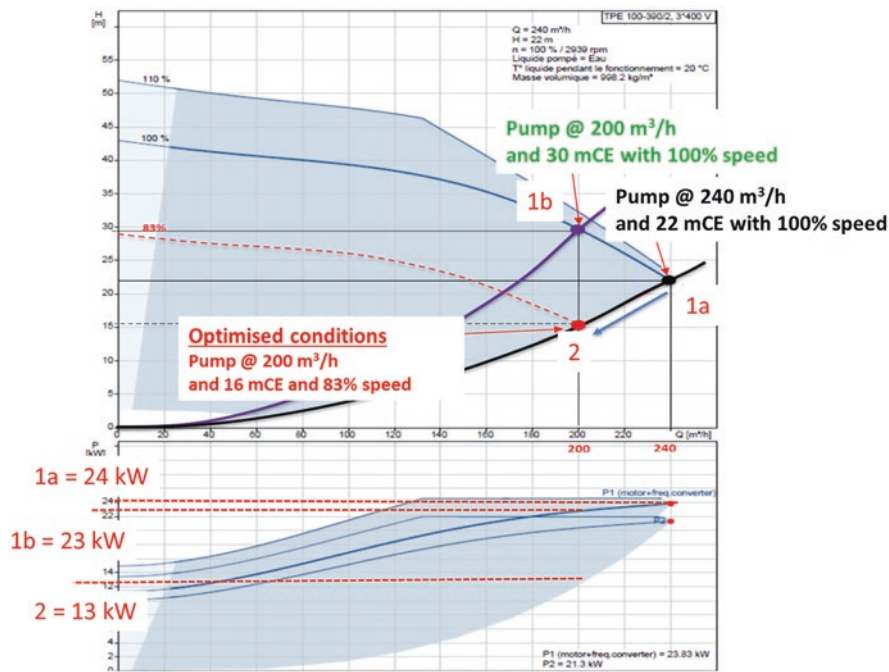


Fig. 8 Pump operation characteristics: (a) at constant speed (100%) and pressure regulated and (b) at variable speed and flow rate regulated

Each of the three measures has a payback time shorter than 4 years and they result in savings of 24.5 thousand euros a year, which means that the costs of the analysis (10 thousand euros) are paid back in less than 6 months.

4.3 Pumping System for a Water Tobogganing Facility¹³

Measurements were also carried out in an amusement park with a water tobogganing facility that was installed in the late 1970s and is open 365 days a year from 10 a.m. to 10 p.m. (4380 h p.a.). In order to deliver and maintain the supply of water for the toboggans, the park uses an impressive number of pumps. In this analysis, a specific toboggan was measured with a set of seven pumps with a nominal motor power of 13 kW each, six of which were in operation (see Fig. 9).

Of the six pumps, two were equipped with a VSD set to a constant frequency of 43 Hz, and the others were operating at their maximum speed, with the output regulated through valves, either partially (60%) or fully open (90%). The performance



Fig. 9 The pumping system that was examined comprises seven pumps with a nominal power of 13 kW, six of which are in use for more than 4000 h a year. Regulation is mainly mechanical through the use of valves

¹³ «Feinanalyse für Elektrische Antriebe ProAnalySys: Kurzbericht», Electrosuisse, Fehraltorf (Switzerland), February 2018.

Table 3 Measured performance of the set of pumps for the water toboggan in its non-optimised state

Pumps #	Throttle aperture	Flow rate	Efficiency
1	90°	102	27%
2	60°	88	24%
3 (with VSD at 43 Hz)	90°	58	18%
4 (with VSD at 43 Hz)	60°	59	18%
5	90°	106	29%
6	60°	88	25%

Table 4 Number of pumps, savings and payback time of the efficiency measures

Efficiency measures with pump replacement	Investment per pump	Pump efficiency before	Pump efficiency after	kWh before	kWh after	Savings		Payback
Three pumps without VSD	5000 euros	24–29%	70%	63,075	45,675	–17,400	–28%	13 years
One pump with VSD	9500 euros	18%	70%					

of such pumps should normally be in the range of 60 to 90% (especially at constant flow rate). The result of the measurements showed a completely different picture in which the performance of the pumps was well below expectation, with an efficiency of 30% in the best case, down to 18%, as shown in Table 3. Thus, either the pumps are oversized or too many are running at the same time. The efficiency measures in this case are to reduce either their power or their number. Based on the investment costs, it was decided to reduce the number of pumps from six to four and keep only one equipped with a VSD. As result of this measure, as we can see from Table 4, the efficiency of the pumps increased to 70%. The electricity savings are 28%, or 1.8 thousand euros a year for an investment of 24.5 thousand euros, which results in a payback time of 13 years. In total, with the analysis of the two other toboggans, the amusement park was able to save 45% of its electricity consumption, or 12.5 thousand euros p.a., with an average payback time of 6 years. The in-depth analysis costs 15 thousand euros and its payback time is less than 18 months.

5 Conclusions

Switzerland's electricity statistics show that 57.4% of its annual consumption is attributable to the industry and services sectors. Switzerland has more than 400,000 small, medium-sized and large companies. Their consumption is not homogeneous, and for this reason they have been classified into four groups: small, medium, large and very large companies. However, it is interesting to note that 30% of the companies in these two sectors account for more than 80% of the overall electricity con-

sumption. Furthermore, electric motor systems such as fans, pumps and compressors are also the main consumers alongside lighting, room heating and process heat. In fact, more than two million electric motors are in operation in the industry sector with a total consumption of 12.0 TWh and a savings potential of between 20 and 30%. In order to reduce energy consumption by large and very large companies, regulations were introduced, including target agreements for very large companies (consumption >2.0 GWh p.a.) and legislation for large-scale consumers (consumption between 0.5 and 2.0 GWh p.a.). Both regulations oblige the companies to perform a mandatory energy audit (fossil energy and electricity) and thus to compile a catalogue of measures in order to reduce their consumption, as well as their CO₂ emissions. Alongside these regulations, Switzerland is also applying the same ecodesign provisions (minimum energy performance standards) as the European Union, which will be applied automatically when a pump, fan or electric motor is replaced or upgraded. However, these are only minimum standards, and in addition, most of the conducted audits are performed without measurements, which means that, for example, oversized pumps will not be detected. As the production of heat (for heating and process purposes) and lighting account for at least two-thirds of the energy consumption in the services and industry sectors, and as they often have a payback time shorter than 4 years, these efficiency measures are preferred over those relating to electric motor systems.

There are four main groups for characterising the efficiency measures for electric motor systems: higher efficiency class of the motor, higher efficiency of the components, size reduction and optimisation of the regulation/process optimisation. However, the impacts of these measures depend on the approach. For example, a component approach such as just replacing the motor does not have a strong impact (savings between 3 and a maximum of 10%). On the other hand, a full system approach such as optimising the process or adapting the size and regulation of the system can result in savings of up to 50%. As mentioned above, audits performed in accordance with the applicable regulations are limited in scope for motor systems as they only take very basic data into account, such as power, running time, age and sometimes the regulation mechanism. Consequently, such audits mainly relate to the component level and their estimated savings potential is limited. For this reason, the Swiss Federal Office of Energy decided to launch a programme called ProAnalySys to support companies in their efforts to carry out in-depth analyses of electric motor systems. This programme only addresses large and very large companies (electricity consumption >0.5 GWh p.a.) from the industry and services sectors, as they are already in contact with energy consultants, who provide the companies, which are also their clients, with the necessary information at the appropriate time. Furthermore, as a prerequisite the companies must have already performed a preliminary analysis, for example, in the form of a mandatory audit, so that only those installations with a high savings potential are eligible for an in-depth analysis with measurements. The ProAnalySys programme covers electric motor systems with a power rating of at least 10 kW. An in-depth analysis is in fact a detailed examination of the actual versus the targeted state of the electric motor system. The measurements assess and precisely quantify the following parameters:

operating conditions (including load management), operating points, performance ratio, partial power factor(s) as well as load profile(s) and energy consumption. The energy consultants, who are already in contact with the companies and have conducted the mandatory audits, are also authorised to perform ProAnalySys in-depth analyses. In other words, the companies do not need to do anything as the energy consultants take care of almost everything for them in order to provide them with a “turn-key” solution. Furthermore, and at the request of the company, the energy consultants are also authorised to support the company with the implementation of the selected measures (although companies are not obliged to implement any measures since ProAnalySys is a voluntary programme). In order to keep the process as simple as possible for the companies, the SFOE concludes a contract with the energy consultants so that they can start the analysis as quickly as possible. Once the analysis has been carried out, the report and recommended efficiency measures are submitted to the companies, and a copy of the report is sent to the SFOE, which pays the subsidies after carrying out a quality assessment. In the case of the ProAnalySys programme, the subsidy covers 40% of the analysis costs up to a maximum of 16 thousand euros (including the support services). The pilot projects confirmed that through an in-depth analysis the savings potential can be identified with a higher degree of precision and above all that the system approach results in significant savings potential, in some cases between 45 and 50%. The payback time for the efficiency measures is quite heterogeneous: in some cases, less than 4 years, while in others it may exceed 10 years (in one case it was as high as 50 years). Ultimately it is up to the company to decide whether or not to implement recommended efficiency measures although the payback time is longer than 4 years. Next to the efficiency gains there are other advantages such as increased reliability of the system or higher product quality. Before performing a ProAnalySys in-depth analysis, it is important to ensure that the analysis is worthwhile. For example, as shown by the pilot projects, electric motor systems should be at least 10 years old with a power rating of not less than 10 kW and a running time above 1000 h a year. In the case of pumps, fans and compressors, we recommend selecting installations with a running time of at least 2500 h a year.

References

1. *Message relative au premier paquet de mesures de la Stratégie énergétique 2050 (Dispatch to Parliament concerning the initial package of measures for Energy Strategy 2050)* (Swiss Federal Office of Energy, 4 September 2013) <https://www.admin.ch/opc/fr/federal-gazette/2013/6771.pdf>
2. *Schweizerische Elektrizitätsstatistik 2017 (Swiss Electricity Statistics for 2017)*. (Swiss Federal Office of Energy, Bern, July 2018). <https://www.bfe.admin.ch/bfe/de/home/versorgung/statistik-und-geodaten/energiestatistiken/elektrizitaetsstatistik.html>
3. *Power efficiency in industry and services: Final report*. (Swiss Federal Office of Energy, Bern, February 2011)

4. W. Baumgartner et al., *Measures for Power Saving in Electric Drives: Market Analysis in the Industry* (Basic (on behalf of the Swiss Federal Office of Energy), December 2006) http://www.bfe.admin.ch/forschungelektrizitaet/01740/01748/01751/02198/html?lang=fr&dossier_id=02023 [index](#).
5. *Analyse des schweizerischen Energieverbrauchs 2000–2017 nach Verwendungszwecken (Analysis of Switzerland's energy consumption, 2000–2017, by purpose)* (Swiss Federal Office of Energy, October 2018) <https://www.bfe.admin.ch/bfe/de/home/versorgung/statistik-und-geodaten/energiestatistiken/energieverbrauch-nach-verwendungszweck.html>
6. M. van Werkhoven et al., *Policy Guidelines for Electric Motor Systems. Part 2* (Electric Motor Systems (EMSA), May 2018) https://www.motorsystems.org/files/otherfiles/0000/0200/pgmdu_part_2_may2018.pdf
7. R. Phillips, *Swiss Competitive Tenders for Promoting Efficient Motor Systems* (EEMOD'15, Helsinki, September 2015). <https://e3p.jrc.ec.europa.eu/publications/9th-international-conference-energy-efficiency-motor-driven-systems-eemods15>

A Review of the United States Process for Developing MEPS, the Benefits, and How Other Economic Regions Could Benefit from Adopting Similar Approaches



Kirk Anderson and Rob Boteler

1 An Overview of Effective MEPS Development

While regulators are responsible for reviewing the need for MEPS, they often work with others to create policies to achieve the desired energy savings. People working with regulators typically fall into one-of-three groups:

- (a) manufacturers who build products and systems,
- (b) advocates interested in accelerating the adoption of higher efficiency products in the marketplace, and
- (c) researchers that develop test methods to measure energy utilization.

While each economic region needs to consider the specific performance level, the overall process to gather feedback, develop performance levels, and implement the requirements would benefit from greater consistency and better transparency. The process for developing regulations today often varies between each economic region and often differs between national, state, and local processes within a single country. Looking at the 50+ countries with MEPS for motors, most do not publish their development process. Even if the process is public, there are instances where the process has only limited input from certain user groups, which can result in a poorly conceived regulation. In other cases, energy ministers or academia come together to create ambitious plans—many times without fully capturing the impact on products in the field, the effect these changes may have on replacement markets or completely lacking a way to enforce their policies.

K. Anderson (✉)

National Electrical Manufacturers Association, Arlington, VA, USA
e-mail: Kirk.Anderson@nema.org

R. Boteler

Nidec Motor Corp, Kyoto, Kyoto, Japan
e-mail: rob.boteler@nidec-motor.com

While the primary focus of the chapter should be on the lack of effective compliance/enforcement policies that can result in a series of negative effects. Some adverse effects include:

- (a) increased costs for legitimate producers,
- (b) higher average selling prices for buyers (without improved performance),
- (c) an incentive for bad actors who flood non-compliant products into the marketplace, and
- (d) the regulation not achieving the proposed energy savings (despite the investment).

2 History of the Process Rule

In 1975, the Energy Policy and Conservation Act of 1975 (EPCA) [1] was passed. Over the next 45 years since the enactment of this piece of legislation, it has expanded coverage nearly 70 [2] products and systems. These products include those directly mentioned in the original legislation, as well as other products, not explicitly listed in the original text, but that meet certain thresholds for national energy consumption/savings. Lastly, interested parties of stakeholders can petition the DOE to add new product classes.

In the early days of rulemakings, the DOE process was not well defined, and as a result, rules proceeded very slowly. Between 1995 and 1996, DOE sought to establish more clear practices for how to approach and conduct rulemakings. Eventually, this work resulted in a formal rulemaking process, called the Process Improvement Rule, or simply the Process Rule. The Rule was added to the Code of Federal Regulations, 10 CFR 430, Appendix A to Subpart C [3], and details the list of procedures to follow when the DOE's Office of Energy Efficiency and Renewable Energy (EERE) makes or updates energy regulations.

The DOE was tasked by Congress in the mid-2000s to review past rules and consider whether to amend them. This routine review was initially viewed as a way to refresh older and outdated regulations. Unfortunately, it became burdensome and, because of the length of time required to review regulations, was in a continual state of the rulemaking process. Industries employing several regulated components, such as lighting systems, were in constant flux, because there was always a revision to one or more related regulations. In addition, because of how the original statutes were written, the Department of Energy viewed each review as a mandate to increase the stringency of requirements, regardless of how small the incremental energy saving is.

In 2010, the rule implemented further changes to improve data gathering methods, including moving supporting data into the technical support document and establishing a standing negotiated rulemaking committee called the Appliance Standards and Rulemakings Advisory Committee (ASRAC) [4].

The ASRAC is composed of members of the public selected from applicants who are viewed as representative of impacted parties, including manufacturers, non-government organizations (e.g., energy-efficiency advocacies), as well as other technical experts. The ASRAC was charged with reviewing extant rules proposed for revision or retirement, as well as reviewing petitions for Negotiated Rulemakings (Reg Negs) and other submissions related to energy conservation standards. The ASRAC was dormant for 2017–2018 but has recently resumed limited meetings.

More recently, there have been an increased number of stakeholders requesting improvements to the Process Rule. Users cite the lengthy process to review products, even on products with already extremely high-efficiency levels, the complexity of multiple, inter-related rulemakings, and various, sometimes conflicting interpretations, made by the DOE over the past 30 years. Around 2016, a group of concerned manufacturing trade associations began a legislative push to update the Process Rule to update and improve it. Rather than have requirements imposed on it by legislation, with the chance for error that legislative compromise can sometimes cause, the DOE undertook a rulemaking to review the Process Rule and consider updates in 2018.

In February of 2019, the DOE issued opened a public request to seeking input on ways to further streamline the process. The goal was to “substantially improve the agency’s process for setting energy efficiency standards and test procedures for residential appliances and commercial equipment, enhancing transparency, accountability, and regulatory certainty for stakeholders.” In May of 2019, the DOE held 2 days of public hearings to discuss proposed changes and the comments received. As of September 1, 2019, DOE’s website included more than 137 uploaded public comments and 47,128 comments through other channels [5].

The DOE is reviewing the testimony and comments and is expected to release their findings in the next several months. The following five areas represent the majority of the comments received:

1. better defined and documented process for stakeholders to participate,
2. consistent application of the process,
3. provision stopping the process quickly if tangible energy savings are not possible,
4. assurance in order for the methods for calculating the energy savings is publicly available for review to ensure assumptions and use-cases are accurate, and finally,
5. use of consensus and industry-accepted methods (where available).

While the Process Rule is not perfect, it’s an excellent model to collect information from advocates, manufacturers, and academia/test laboratories for developing regulations. This process has been largely responsible for the United States being one of the leaders in adopting both commercially feasible and technologically advanced, and, at the same time, reducing the overall energy use for both motors and lighting, which represent roughly two-thirds of all energy consumed in the states.

3 The Process Rule Explained

Since the writing of the Process Rule in 1996, rulemakings proceed in a somewhat predictable series of steps. The entire process takes 4–5 years to complete and follows a predictable series of steps and milestone events. The DOE divides the Process Rule into four phases (see Fig. 1): a Framework Phase, the Preliminary Analysis Phase, a Notice of Proposed Ruling Making (NOPR) Phase, and the Final Rule Phase.

In addition to the formal Process Rule, two other methods exist which provide an accelerated path for developing regulations: Negotiated Rulemakings and Direct Final Rules.

3.1 Framework Phase

During the Framework Phase, the DOE publishes the basic analytical and procedural principals, along with the legal authority that guides the rulemaking. This document may also solicit feedback from various stakeholders on specific questions.

In most cases, the DOE issues a notice of intent to develop new or review existing standards or test procedures under this phase. After issuing an initial notice of intent to begin a rulemaking, the DOE releases scope and coverage documents for public feedback.

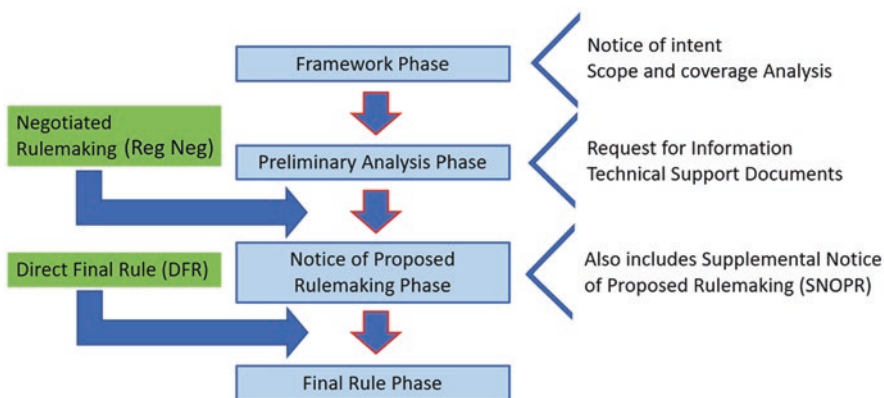


Fig. 1 Phases of the Rulemaking Process

Note: A red outline indicates a public input period. Green boxes show an alternative path to develop proposals.

3.2 Preliminary Analysis Phase

The next phase is typically where the DOE gathers the additional information. During this phase, the initial analysis for data gathering and other considerations of a rule occur. Issuance of a Technical Support Document (TSD) often results as part of this data gathering and may be issued for public comment. The TSD is essential since it does a deeper analysis of the impact based on the preliminary scope, including manufacturer production costs, consumer buying patterns, product price impacts, shipments/production estimates, and the calculated energy-savings opportunity.

Instead of following the first two phases, a separate method to develop a preliminary standard or regulation is through a Reg Neg. Any party may negotiate a rule and submit it to the DOE, although most successful Reg Neg activities have been via ASRAC oversight process.

Reg Negs are more straightforward since the parties involved are not hard-bound to perform an analysis as rigorous as the DOE. While not as rigorous, sufficient data still must be submitted to reasonably justify the energy savings and assess the national impact.

Since the requirements are drafted outside the formal notice and comment process, the DOE then posts the proposal for public comment after it has been created.

3.3 Notice of Proposed Rulemaking Phase

Once the Department believes sufficient data has been received and has analyzed it using their energy prediction model(s), a Notice of Proposed Rulemaking (NPR) is published for public review and comment. This NPR includes actual regulatory text that, if approved, is codified into U.S. law. It is common for the DOE to receive meaningful comments during this portion of the rulemaking process, in which case, the DOE may revise the NPR scope or test procedures, as needed. When this happens, a Supplemental Notice of Proposed Rulemaking (SNOPR) is published. Like a NPR, the SNOPR is published for public comment.

3.4 Direct Final Rule

As an alternative to the process described above, it is possible to issue what is called Direct Final Rule (DFR). The main benefit of using a DFR is to develop a proposed rule with a shortened development process.

Under the DFR process, a group of representative stakeholders drafts the proposed rule, submits the proposal for a new regulation, and then petitions the DOE to approve and publish it. Compared with non-DRFs, there is less opportunity to

comment on the proposal. The limited public comment is balanced by the fact that DFRs usually involve collaboration with both industry and energy advocates on products not actively regulated. This means that by adopting the proposed rule, end-users begin saving energy immediately, instead of the more common 4-to-5 years that it would take to initiate a new rule. Still, since there are times where there may be public push-back against a DFR due to some party having not been included; the DOE approves DFRs much less often.

3.5 Final Rule Phase

Once the DOE reviews all the comments, a Final Rule can be published. The Final Rule includes implementation timelines and the final text of the law. Test Procedure Rulemakings are typically faster and include fewer analytical steps since they do not require such rigorous national and manufacturing impact analyses [6]. Many DOE test procedures leverage existing industry standards and practices, either wholly or in part. That said, it is not always simple to amend or expand the standards or test procedures, even with industry support.

It is worth noting that as of this writing, few rulemakings are proceeding through the DOE. This is in part due to the regulatory-relief policies of the current presidential administration and in no small part also due to the belief that the Process Rule proceeding should be completed before starting further rulemakings. Once the Process Rule review is completed, one may expect the DOE to begin the routine reviews of test procedures and energy conservation standards with greater rates of occurrence.

Past rulemakings of note for the Motor industry include standards for integral horsepower general purpose motors [7], standards for general purpose small electric motors [8], and review of test procedures for these products [9].

4 Potential Updates to the Process Rule

As previously noted, most of the interest relate to making the process more clear (better documentation of the process) or better implementation of the existing process (more consistency with existing rules, better transparency, and use of industry standards). The one aspect which potentially represents a significant benefit, if done correctly, is creating a “fast off-ramp.”

Currently, it can take as many as 5 years to run through the rulemaking process. Since regulations are required to be reviewed every 6 years, it is possible to complete the cycle, only to begin the process once again. Furthermore, since the DOE has successfully, significantly decreased energy consumption on several products, revisiting those product areas (where the efficiencies are already high) expends a significant amount of effort from all stakeholders with only incremental benefit.

Provided the DOE finds a faster way to end the review of a rule when the potential energy savings are below a certain threshold, resources can be directed to product areas where energy savings remain.

Other areas the DOE could improve the process relates to formal interpretations. Over the last 30 years, the DOE has made a series of interpretations that, in some cases, appear to contradict another official stance/interpretation. Having the DOE use this as an opportunity to provide better clarity and more consistent interpretation would be a significant benefit for all parties.

Lastly, there is a robust dialogue on using industry consensus standards (where possible) or developing new standards. Industry spends significant engineering time and expertise to develop standards. Using ANSI or other accepted consensus processes further raises the bar to ensure the standard is both technically sound and has considered input from a variety of stakeholders. Industry standards often take many years to develop, clarifying text to ensure the exact meaning and method is as clear as possible. By using industry consensus standards, the DOE is leveraging a document that has undergone a considerable level of review, which is difficult to achieve through other processes.

5 Examples of the Process Rule and Lessons Learned

Now that we have reviewed how the Process Rule works and identified the most commonly cited weaknesses in the current process, the question is: Does existing Process Rule represent a sound model to use for regulators when working on MEPS within their own countries? Given the overall market transformation with respect to energy usage that has occurred in the United States for lighting and motors, the answer is a resounding “yes.”

One of the most challenging aspects of developing regulations is having a well-designed process; a process that allows the various interests to be fully represented, the right data and correct assumptions to be made, and a way to quickly implement a technically sound regulation. While speed and accuracy are both important, it is usually better to delay implementing a faulty regulation than publishing a poorly written regulation quickly. One reason is that most countries do not allow undoing of regulations (often referred to as backsliding). This means the effects of poorly written regulations are not easily undone.

An example of what is possible when the stakeholders work collaboratively is the amended Integral Horsepower Rule published on May 29, 2014 [10]. This was completed through the DFR using a coalition consisting of energy advocates, utilities, and representatives of industry voluntarily coming together to address gaps in the existing regulations. This group worked through two different paths of success: one where energy savings would be through increasing efficiency levels on for the existing scope of product and other where savings would be through expanding the scope to include more products to the already high-efficiency levels.

The Integral Horsepower Rule resulted in the most significant calculated energy savings in the history of DOE regulations. The rule simplified enforcement, and, since many manufacturers did not need to invest in new equipment, increased the availability of product on the market, which facilitated faster market transformation. Note: even though it used the DFR process, the process still took over 3 years from start to finish.

Even when using the current process, success is not certain. The Small Motor rule is an example of a regulation that went through the process and yet resulted in little energy savings. In addition, because of how it was implemented, it contributed to the near-collapse of the regulated product. The problem was not with the test method or efficiency levels chosen, but because the regulation lacked a practical means for enforcement. As a result, legitimate manufacturers were not able to build a cost-effective product, while overseas manufacturers were able to build non-compliant (embedded within end-products) without the fear of consequence.

6 Using the Process Rule as a Model for Other Economies

The Process Rule has been in use for nearly 25 years and helped usher efficiency requirements for roughly 70 different product classes. The existing process rule and have resulted in tremendous energy savings, some of the highest market adoption in the markets served, and spurred product innovation. Adopting this model—even acknowledging existing gaps—is still an excellent place to start for would-be regulators.

The areas noted below represent areas where further refinements would augment an already good process rather than a completely new feature. The one exception to this is a fast “off-ramp” for products that have already achieved high levels of energy savings, which does not currently exist.

Changes needed to improve the existing Process Rule:

1. **Transparent and robust process** – Developing energy regulations can potentially increase costs for consumers and eliminate classes of products from the market. As such, having a transparent process so that stakeholders understand the process and can contribute accordingly [11]. A good process should include analytics supported by science showing energy savings is possible as well as a method to get stakeholder input to ensure the economic impact aligns with the overall goal.
2. **Consistent application** – Even the best process can be undone by inconsistent application of the requirements. When regulators do not follow their documented processes, it tends to undermine the confidence of all participants. This can lead to the various stakeholders viewing one another with suspicion and exacerbate differences in interpretation of the data and polarizing of positions.
3. **Public input** – Obtaining public input on the calculation methods reduces the probability of errors or having incorrect usage assumptions. Public input is

crucial for developing regulations that balance the energy-saving goals with practical, commercially feasible, technology. When regulators access reliable information, there is a better chance to create regulations that reduce energy demands and drive innovation without market disruption.

4. Use of industry-accepted standards – The rigor to develop Industry Consensus standards is hard to match. Using these standards help to decrease the time to develop regulations, minimize costs to build a compliant product, and provide a path for better enforcement. When each regulator has a unique method, potentially incompatible requirements exist between countries. This can increase cost and create market confusion (which can create an incentive to exploit loopholes). By adopting consensus industry standards (when available), regulators invite the best chance to realize energy savings. Using international standards or having regulations include flexibility of using test methods demonstrated to provide equivalent results is also recommended practice to simplify the adoption of energy policies.

In those cases, where the existing standards are outdated, it is normally more effective to invest in improving the standards rather than creating a new, potentially conflicting, set of requirements.

On a related note, while regulation of components (like motors) has been the primary focus with nearly every country implementing MEPS, many components have efficiencies such that more energy can be saved by looking at the system where they are used rather than regulating the individual component. Where energy savings of the component has reached the point of diminishing returns, looking at the system to increase energy savings is necessary. Managing system efficiency also reduces rebound effects, since it allows end-products to optimize component selection.

5. Quick off-ramp – With the existing rule, the process takes the entire 4–5 years to determine whether tangible energy savings are present. This resulted in hundreds, or even thousands of hours of effort, only to determine that the increase in efficiency was negligible.

By having a defined threshold and a quick conclusion of non-beneficial activities, more effort can be allocated to areas where significant energy savings remain rather than following a process that results in negative-net-energy savings, incompatible designs and higher costs to consumers.

7 Conclusion

In summary, energy savings is important for everyone. The complexities associated with finding the right efficiency levels and correct test methods is difficult and, without a well-designed process, is unlikely to achieve the energy savings desired. By selecting a procedure like the Process Rule, one that requires sound technical principals and incorporates multiple points for feedback, regulators can minimize (but not eliminate) the creation of toothless policies that discourage legitimate

manufacturers from participating in the marketplace or creating unnecessary, non-value-adding procedures. If we as a global community agree on common practices (like we do for standards development), the more easily we, as a group, can align global test methods, increase enforcement of existing regulations, and enjoy the fruits of our labor, namely, reduced energy consumption and better-performing products.

References

1. The US Energy Policy and Conversation Act of 1975. <https://www.govtrack.us/congress/bills/94/s622/text>
2. List showing different products covered by DOE regulations. <https://www.regulations.doe.gov/ccms/templates>
3. Reference to 10 CFR part 430. https://www.law.cornell.edu/cfr/text/10/appendix-A_to_subpart_C_of_part_430
4. US Department description of Appliance Standards and Rulemaking Federal Advisory Committee (ASRAC). <https://www.energy.gov/eere/buildings/appliance-standards-and-rulemaking-federal-advisory-committee>
5. Process improvement rule request. <https://www.regulations.gov/docket?D=EERE-2017-BT-STD-0062>
6. Additional information on the regulatory process. <https://www.energy.gov/eere/buildings/about-appliance-and-equipment-standards-program>
7. General-purpose motor rule. <https://www.regulations.gov/docket?D=EERE-2010-BT-STD-0027>
8. Small Electric Motor rule. <https://www.regulations.gov/docket?D=EERE-2007-BT-STD-0007>
Rulemaking:homepage https://www1.eere.energy.gov/buildings/appliance_standards/standards.aspx?productid=7
9. Example of test procedure rule (for small motors). <https://www.regulations.gov/docket?D=EERE-2017-BT-TP-0047>
10. The Integral horsepower rule. <https://www.gao.gov/products/D07738#mt=e-report>
11. DOE's overview of the rulemaking process and how to participate. <https://www.energy.gov/eere/buildings/rulemakings-and-notice>

Electromagnetic Design of Propulsion Motors with Superconducting Field Coils for Electrified Aircraft



Yusuke Ishida, Yutaka Terao, and Hiroyuki Ohsaki

1 Introduction

In recent years the demand for passenger and cargo transportation aircraft has been increasing, and the reduction of carbon dioxide emissions from aircraft is required. In such a situation, aircraft electrification is currently studied worldwide [1–3]. And the electrification of propulsion system, called electrified aircraft propulsion system (EAPS), has attracted much attention. The EAPS uses electric motors to drive fans and has potential to achieve higher efficiency and less greenhouse gas emissions than conventional internal combustion propulsion systems. However, in order to realize the EAPS, electric motors are required to achieve a high output density. Since electric vehicles, such as cars and motor bikes, have become popular, the high-performance permanent magnet-type synchronous motors have been developed as compact, lightweight, and efficient machines. The permanent magnet-type synchronous motor having the world's highest output power density of 5.2 kW/kg is the model, SP260D manufactured for 260 kW applications by Siemens [3]. However, the output power density of motors to be loaded into EAPS must surpass 16 kW/kg for aircraft with more than 100 passengers [4]. Therefore, there are many technical issues for conventional motors to achieve such a high output power density. Thus, adopting superconducting motors for EAPS is considered in this study to reach the specified value for output power density.

The property of superconducting materials to have zero resistance below a critical temperature provides superconducting wires to have much higher current density than it would be possible in copper windings. The typical wound-rotor synchronous motors are composed of copper windings and iron cores. Adapting

Y. Ishida (✉) · Y. Terao · H. Ohsaki
The University of Tokyo, Tokyo, Japan
e-mail: ishida-yusuke537@g.ecc.u-tokyo.ac.jp; yterao8934@g.ecc.u-tokyo.ac.jp;
ohsaki@k.u-tokyo.ac.jp

superconducting wires to wound-rotor synchronous motors enables motors to reduce not only the amount of windings but also the amount of irons because the superconducting coils are able to achieve higher air-gap magnetic flux density without the need of iron cores of rotor and without iron teeth. Thus, high output power density synchronous motors can be realized [5].

In this study, we conducted the electromagnetic design of propulsion motors with superconducting field coils and copper armature windings, partially superconducting motor (PSCM), to be used in EAPS based on analytical equations. PSCMs have small electric loadings and relatively become heavier than fully superconducting motors (FSCMs), which have superconducting field coils and armature windings. The FSCMs have AC loss, which is proportional to frequency. Therefore, the FSCMs should be designed with a smaller number of poles. However, the PSCMs have the possibility of achieving high output density and efficiency simultaneously by increasing number of poles because the PSCMs have no AC loss at armature windings unlike the FSCMs.

The objective of this work is to verify whether PSCMs are able to attain high output density. We optimized only the output density of the PSCMs in the design dominantly. After optimization, the finite element method (FEM) analysis is carried out for the purpose of testifying that the analytical design achieves calculated output density.

2 Electrified Aircraft Propulsion System Configuration

Figure 1 shows an EAPS configuration. The hybrid AC-DC architecture is employed [6]. The whole system is composed of two turbines and generators on both wings, converters, DC bus, inverters, and several distributed PSCMs. The electric power is

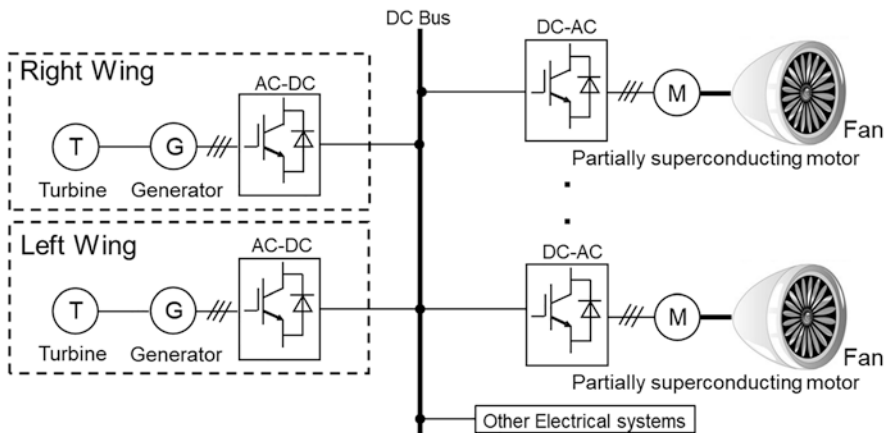


Fig. 1 Electrified aircraft propulsion system configuration

generated by the turbine and generator. The DC bus provides DC power to electrical systems in the aircraft and to the superconducting motor drive systems via converters. In order to drive the superconducting motors, DC power is converted to three-phase AC power via the inverter. The EAPS is supposed to adopt superconducting technologies. Using a superconducting DC bus power supply reduces AC loss in the cables. This improves to the efficiency of the aircraft. Several distributed superconducting motors mounted on the propulsion system provide high redundancy for the aircraft.

3 Partially Superconducting Motor Specifications

The PSCM's basic specifications we considered are summarized in Table 1. We considered that the total output power for 180-passenger class aircraft as 44 MW for takeoff [7] and all the output powers are provided from several PSCMs. Therefore, the output power of 5.5 MW means that eight motors are required to satisfy the total output power for aircraft. The line-to-line voltage is set at 1.41 kV, and this is relatively higher than that of today's aircraft considering the problem of electric breakdown in thin atmospheric pressure conditions [8]; however, there are some attempts to increase the voltage of aircraft's electric systems [6]. The rotational speed is set at 5000 rpm and this value is based on the low pressure turbine of conventional turbo-fan engines.

Figure 2 shows the basic configuration of a PSCM. The PSCM is composed of very low temperature YBCO superconducting field coils and room temperature copper armature windings. The superconducting field coils are covered with cryostat for thermal insulating. The cryostat and field coils are connected through a thin cylinder called torque tube. The torque tube should have high mechanical strength to transfer high torque from field coils to the shaft and low thermal conductivity to suppress the heat leakage into the low temperature part. The rotor rotates synchronously with the rotating field produced by armature currents in the stator, and the magnetic flux density at the field coils is not changed over time under steady-state condition except the AC field harmonics. Therefore, the YBCO wire is suitable for

Table 1 Specifications for PSCM

Description	Value
Motor output power	5.5 MW
Line-to-line voltage	1.41 kV
Torque	10,504 nm
Rotational speed	5000 rpm
Number of poles	8–14
Magnetic loading	0.4–1.2 T
Electric loading	120 kA/m
Motor diameter	<800 mm

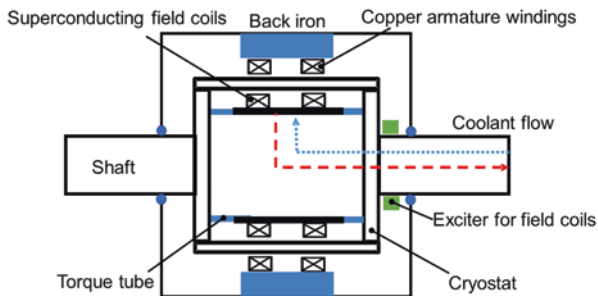


Fig. 2 Configuration of a partially superconducting motor

Table 2 Details for field coils and armature windings

Parameter	Value
Field coils	YBCO
Operating temperature	20, 65 K
Configuration	4.0 mm × 0.1 mm rectangle
Packing factor	0.95
Load factor	0.7
Armature windings	Copper
Operating temperature	300 K
Configuration	2.5 mm × 0.4 mm rectangle
Conductor current density	2.5×10^7 A/m ²
Packing factor	0.4

the field coils that have good J_c - B characteristics, mechanical strength, and large temperature margins. The details of the field coils and the armature windings are summarized in Table 2. The critical current of the YBCO wires used in this study is based on the wire from SuperPower Inc. [9]. Assumed critical current densities of the YBCO wire at different magnetic flux densities are shown in Fig. 3. The copper wire used in this study is considered to enhance its current density due to the water cooling.

As mentioned previously, the superconducting motor achieves high air-gap magnetic flux density, and the iron teeth do not serve a significant role in the motor. Thus, the stator employs three-phase single layer windings [10] with no iron teeth. This structure enables motors to close the field coils and the armature windings compared to the typical double-layer windings.

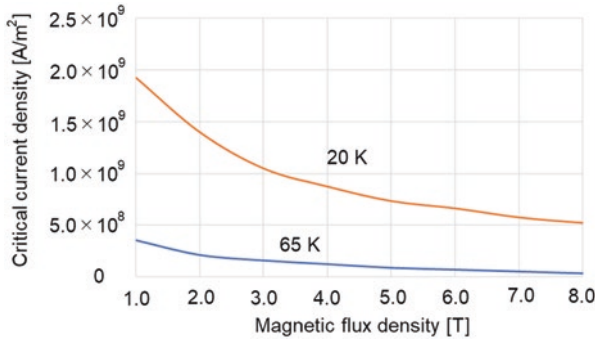


Fig. 3 Assumed critical current of the YBCO wire (4.0 mm × 0.1 mm rectangle) as a function of magnetic flux density based on a reference [9]

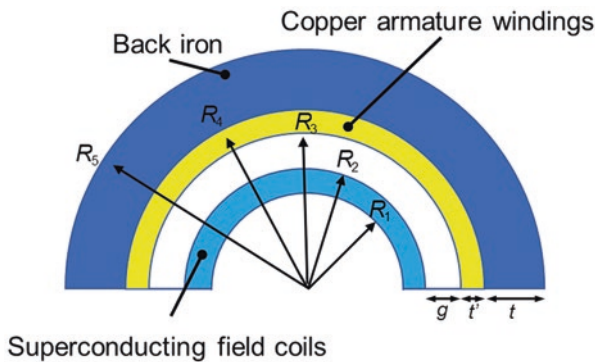


Fig. 4 Analysis model of a PSCM for EAPS

4 Output Power Density and Loss Estimate

Figure 4 shows the analytical model of the PSCM for electrified aircraft propulsion. The model is composed of field coils, armature windings, and back iron. The thickness of the components and mechanical gaps between the field coils and armature windings is t [m], t' [m], and g [m] as shown in Fig. 4. We set the g of PSCMs at 35 mm for vacuum and the cryostat wall space.

We conducted electromagnetic design based on several equations under full loaded and steady-state conditions. The PSCM's output power P_G [W] is given by

$$P_G = \frac{\pi^2}{\sqrt{2}} k_w B_m A_s D^2 I_{\text{eff}} \frac{N_{\text{rot}}}{60} \tag{1}$$

where k_w is the winding factor, B_m [T] is the magnetic loading (the amplitude of magnetic flux density from field current at the middle of armature windings), A_s [A/m] is the electric loading, D [m] is the average diameter of armature windings,

l_{eff} [m] is the effective length of the motor, and N_{rot} [rpm] is the rotational speed. This is a fundamental equation, and we calculated the motor effective length l_{eff} [m] by setting individual variables based on Table 1 conditions shown in the previous chapter.

Each radius $R_1 - R_5$ [m] is set as to satisfy the conditions used in Eq. (1). The magnetic flux density distribution generated by field current between the field coils and the back iron is calculated by following equation as a function of radial direction r [m], mechanical angle θ [rad], and harmonic number n based on references [11, 12].

$$B(r, \theta, n) = \frac{4\mu_0 J_f}{\pi n(np+2)} \sin \frac{n\pi}{2} \sin \frac{n\pi}{6} \cos \frac{n\pi}{4} \cos(np\theta) (R_2^{np+2} - R_1^{np+2}) \left(\frac{r^{np-1}}{R_4^{2np}} + r^{-np-1} \right) \quad (2)$$

In this analysis, we assumed the magnetic loading B_m [T] to the amplitude of basic sinusoidal wave ($n = 1$) at the middle of armature windings calculated by Eq. (2).

And we estimated the output power density of the PSCMs from these radius $R_1 - R_5$ [m] and the effective length l_{eff} [m] by calculating the amount of materials in Fig. 1 and densities listed in Table 3. Then, we assumed the structures of the field coils and the armature windings as shown in Figs. 5 and 6, respectively. The average lengths of the field coils l_{YBCO} [m] and the armature windings l_{Cu} [m] are defined as follows:

$$l_{\text{YBCO}} = 2l_{\text{eff}} + R_2 (\theta_{f1} + \theta_{f2}) \quad (3)$$

$$l_{\text{Cu}} = \frac{2D\pi}{mp} + 2l_{\text{eff}} + 4\theta_a l_{\text{eff}} \quad (4)$$

Table 3 Densities of the PSCM components

Description	Material	Density
Stator		
Back iron	Electromagnetic steel	7850 kg/m ³
Armature windings	Copper wire	8960 kg/m ³
Support structure	FRP	1900 kg/m ³
Rotor		
Field coils	YBCO wire	8250 kg/m ³
Shaft	SUS	7800 kg/m ³
Torque tube	FRP	1900 kg/m ³
Support structure	FRP	1900 kg/m ³
Cryostat	SUS	7800 kg/m ³

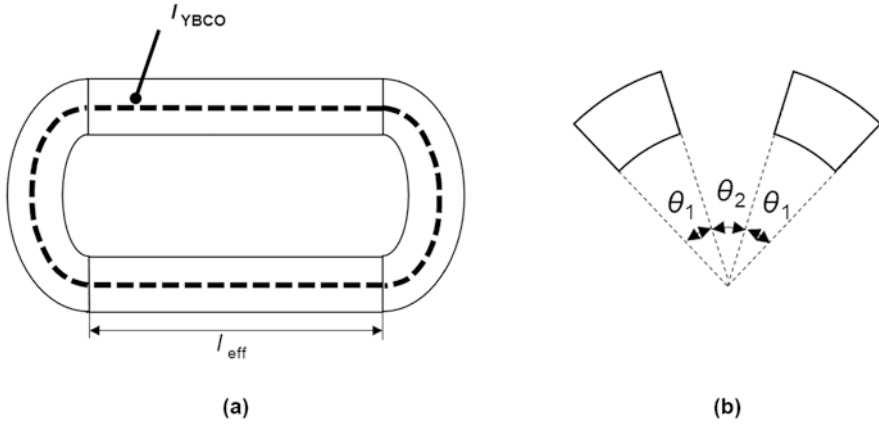


Fig. 5 Structure of the field coils. (a) is the top view and (b) is the cross section

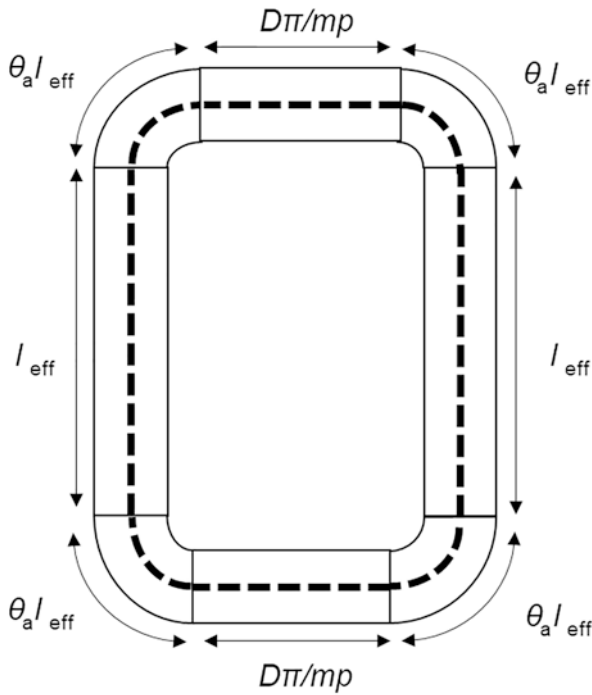


Fig. 6 Structure of the copper armature windings

where θ_{β} [rad] is the angle of one field coil, θ_{β} [rad] is the angle between the field coils, m is the number of phases ($m = 3$), p is the number of pole pairs, and θ_a is the factor at bending points.

The iron losses of the back iron and copper loss are considered in this study to estimate the efficiency of the PSCMs. The following equations represent hysteresis loss of the back iron $W_{\text{iron,hys}}$ [W/m³] and eddy current loss of the back iron $W_{\text{iron,eddy}}$ [W/m³]:

$$W_{\text{iron,hys}} = k_h \epsilon \frac{f}{100} B_{\text{iron}} \quad (5)$$

$$W_{\text{iron,eddy}} = k_e \sigma \left(\frac{f}{100} B_{\text{iron}} \right)^2 \quad (6)$$

where B_{iron} [T] is magnetic flux density at the back iron, k_h and k_e are rotation factors, ϵ and σ are coefficients. The parameters used in this paper are shown in Table 4. B_{iron} [T] is set to 2.0 T which is the maximum saturated magnetic flux density of general iron. And copper loss W_{Cu} [W] is calculated by applying Ohm's law.

5 Analysis Results

We estimated the output power densities of the 5.5 MW PSCMs with different poles and operating temperature at different magnetic loadings based on Table 1. The diameters of motors were set as to maximize the output power density below 800 mm after selecting magnetic loadings. Finally, we found the magnetic loading that achieves the highest output power density. Figures 7 and 8 show the output power densities at each operating temperature as a function of magnetic loading. Some cases, in particular, at operating temperature of 65 K have high magnetic loading and were not able to be designed in order to satisfy the required motor diameter. This is because the high magnetic loading machine requires large amount of the field coils and the back iron. In addition, the high operating temperature of the field coils leads to the increase of the amount of field coils because of the J_c - B characteristics of YBCO wires shown in Fig. 3. As shown in Figs. 7 and 8, the output power densities were improved by increasing the number of poles up to 12 because the amount of back iron was reduced. However, the output power densities of the

Table 4 Parameters for equations of iron losses

Parameter	Value
Rotation factor k_h	2.0
Rotation factor k_e	1.8
Coefficient ϵ	3.7
Coefficient σ	3.4

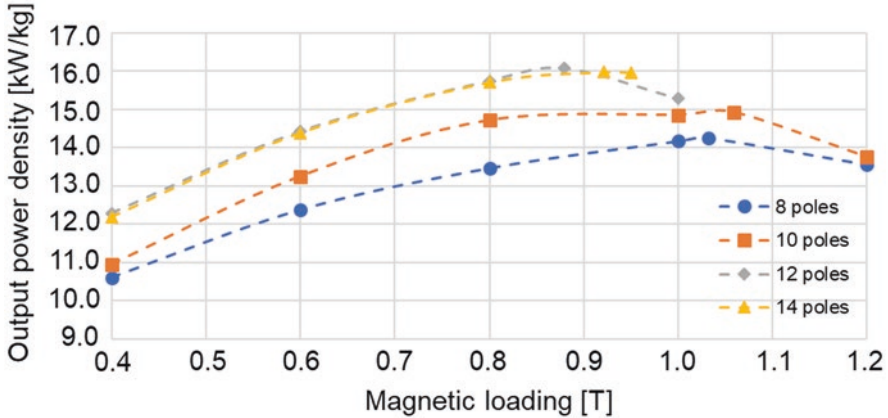


Fig. 7 Output power density of the 5.5 MW PSCMs at operating temperature of 20 K as a function of magnetic loading with different poles

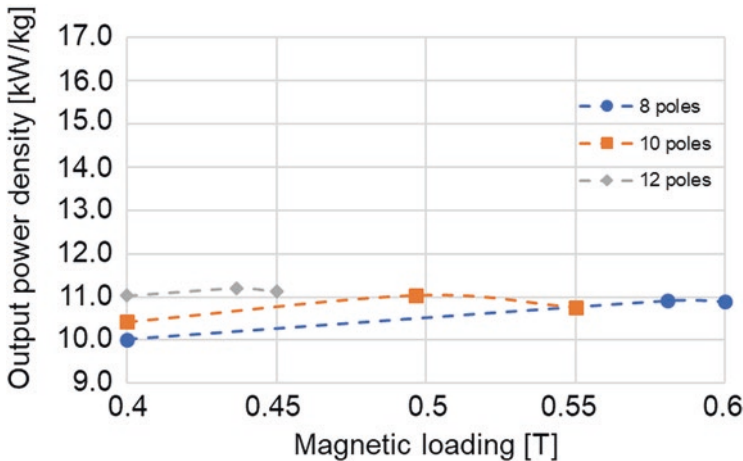


Fig. 8 Output power density of the 5.5 MW PSCMs at operating temperature of 65 K as a function of magnetic loading with different poles

14-pole PSCMs were decreased compared to the 12-pole PSCMs because the amount of the YBCO wires was increased. The output power density of 16.1 kW/kg with 12 poles at 0.88 T at 20 K and of 11.2 kW/kg with 12 poles at 0.44 T at 65 K was available. The output power density of the PSCM at 20 K attains the 16 kW/kg. However, the output power density at 65 K did not reach the required value, although, the value is much higher than that of conventional electric motors. Tables 5 and 6 show the weights and losses of PSCM components, respectively. The weight margin of 25% for the stator and the rotor is considered. The motor efficiency is calculated from the copper loss and the iron losses at the back iron. The AC loss at

Table 5 Summary of the PSCM component weights

Description	Design at 20 K	Design at 65 K
Stator		
Back iron	88.3 kg	86.9 kg
Armature windings	44.6 kg	75.4 kg
Support structure	4.3 kg	7.0 kg
25% margin	34.3 kg	42.3 kg
Rotor		
Field coils	9.0 kg	28.9 kg
Shaft	4.6 kg	6.1 kg
Torque tube	3.2 kg	4.2 kg
Support structure	10.3 kg	16.3 kg
Exciter	14.0 kg	14.0 kg
25% margin	41.0 kg	69.6 kg
Cryostat	88.7 kg	140.2 kg
Total weight	342.2 kg	491.1 kg
Output power density	16.1 kW/kg	11.2 kW/kg

Table 6 PSCM loss components

Parameter	Design at 20 K	Design at 65 K
Copper loss	52.4 kW	88.6 kW
Hysteresis loss at back iron	5.3 kW	5.2 kW
Eddy current loss at back iron	21.9 kW	21.6 kW
Efficiency	98.6%	97.9%

the field coils was not considered because the field coils only experience DC field under steady-state condition.

6 Electromagnetic Design with Finite Element Method Analysis

Two-dimensional finite element method (FEM) analysis with the electromagnetic analysis software, JMAG-Designer[®] [13], was carried out for electromagnetic design of the 5.5 MW PSCMs based on the designs that represent maximum output power density at operating temperature of 20 K and 65 K shown in the Chap. 5 to testify the designed PSCMs' output calculated output power. Figure 9 shows the one pole pitch of analysis model of a 12-pole PSCM. The analytical model is composed of the YBCO field coils, the copper armature windings, and the back iron. For simplicity, any other non-magnetic components such as cryostat wall are not taken into account in the analysis model.

Tables 7 and 8 show the comparison of the analytical and the FEM results of 5.5 MW PSCMs, whose operating temperatures of the field coils are 20 K and 65 K,

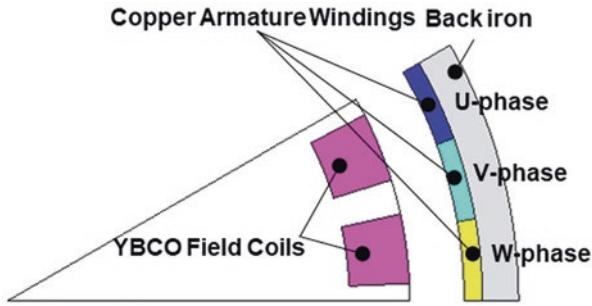


Fig. 9 One pole pitch of the analysis model of a 12-pole PSCM

Table 7 Comparison of the analytical and FEM results of 5.5 MW PSCM at operating temperature of 20 K

Parameter	Theoretical	FEM	Error
Torque	10,504 nm	10,521 nm	0.2%
Magnetic loading	0.88 T	0.92 T	4.7%
Max. of magnetic flux density at field coils	2.50 T	2.53 T	1.2%
Iron losses at back iron	27.2 kW	42.8 kW	36.4%
Output power	5.50 MW	5.51 MW	0.2%
Output power density	16.1 kW/kg	16.1 kW/kg	0.2%

respectively. Four parameters, motor torque, magnetic loading (amplitude of magnetic flux density at the middle of the armature windings), maximum of magnetic flux density at the field coils, and the iron losses at the back iron, were compared in this analysis. The output power densities of the FEM analysis were calculated from the motor torques shown in Tables 7 and 8 and the motor weight obtained by equations in the previous chapter. The errors of the motor torque, the magnetic loading, and the maximal magnetic flux density at the field coils are within the range of 7%. On the other hand, iron losses at the back iron differ over 30% between the theoretical and FEM results because Eqs. (5) and (6) calculate the iron losses at the back iron. However, the iron losses are relatively small compared to copper losses shown in Table 6. Also, the differences of the iron losses are below 0.3% compared to the total output power. Finally, the output power densities of the PSCMs are 16.1 kW/kg and 12.0 kW/kg at the operating temperature of 20 K and 65 K, respectively.

7 Conclusion

Electromagnetic design of the 5.5 MW partially superconducting motors was carried out at different operating temperatures, 20 K and 65 K. The estimated output power density results are as follows: 16.1 kW/kg at 20 K and 12.0 kW/kg at 65 K. The output power density at 20 K attains the required value. Therefore,

Table 8 Comparison of the analytical and FEM results of 5.5 MW PSCM at operating temperature of 65 K

Parameter	Theoretical	FEM	Error
Torque	10,504 nm	11,274 nm	6.8%
Magnetic loading	0.44 T	0.46 T	4.8%
Maximal of magnetic flux density at field coils	1.12 T	1.08 T	3.7%
Iron losses at back iron	26.8 kW	42.4 kW	36.9%
Output power	5.50 MW	5.90 MW	6.8%
Output power density	11.2 kW/kg	12.0 kW/kg	6.8%

partially superconducting motors operated at 20 K could be a potential candidate for the future electrified aircraft propulsion system. On the other hand, the estimated output power density at 65 K does not reach the required value, 16 kW/kg. However, it is much higher than that of the conventional electric motors.

References

1. H. Kim, J. Felder, M. Tong, J. Berton, W. Haller, *Turboelectric distributed propulsion benefits on the N3X vehicle*. *Aircr. Eng. Aerosp. Technol. Int. J.* **86**(6), 558–561 (2014). Can be downloaded at: <https://doi.org/10.1108/AEAT-04-2014-0037>
2. <https://www.airbus.com/innovation/The-future-is-electric.html>
3. <https://www.siemens.com/press/pool/de/events/2016/corporate/2016-12-innovation/inno2016-aerobaticairplane-e.pdf>
4. B. Łukasik, *Turboelectric distributed propulsion system as a future re-placement for turbo-fan engines*, in Proceedings of the ASME Turbo Expo 2017: Turbomachinery technical conference and exposition (Charlotte, America, 26–30 June 2017). ISBN:978-0-7918-5077-0. Can be downloaded at: <http://proceedings.asmedigitalcollection.asme.org/proceeding.aspx?articleid=2649486>
5. H. Ohsaki, Technology trends of superconducting rotating machines. *J. Cryog. Supercond. Japan* **47**(6), 354–361 (2012). ISSN:0389-2441
6. C. Jones, P. Norman, S. Galloway, M. Armstrong, A. Bollman, *Comparison of candidate architectures for future distributed propulsion aircraft*. *J. IEEE Trans. Appl. Supercond.* **26**(6), 1–9 (2016). Can be downloaded at: <https://ieeexplore.ieee.org/document/7407568>
7. M. Zhang, F. Eastman, W. Yuan, *Design and modeling of 2G HTS armature winding for electric aircraft propulsion applications*. *J. IEEE Trans. Appl. Supercond.* **26**(3), 1–5 (2016). Can be downloaded at: <https://ieeexplore.ieee.org/document/7428847>
8. <http://787updates.newairplane.com/787-Electrical-Systems/787-Electrical-System>
9. <http://www.superpower-inc.com/system/files/1MOr2A-03++Superpower-Inc+ASC-2016+Final.pdf>
10. S. Kalsi, K. Hamilton, R. Badcock, *Superconducting rotating machines for aerospace applications*, Meeting paper of the AIAA Propulsion and Energy Forum (Ohio, America, 9–11 July 2018). Can be downloaded at: <https://doi.org/10.2514/6.2018-4796>
11. S. Kalsi, *Applications of High Temperature Superconductors to Electric Power Equipment* (Wiley, 2011). ISBN:978-0-470-16768-7
12. Shintani T. Nitta T. and Okada T. *Explicit relations between machine constants and structure-parameters of superconducting generators*. *J. IEEJ Trans. Power Energy*, 106, 12, pp. 1075–1082, 1986. Can be downloaded at: <https://doi.org/10.1541/ieejpes1972.106.1075>
13. <https://www.jmag-international.com/jp/products/jmag-designer/>

Design Methodology for a PM Electrical Variable Transmission Used in HEV



Florian Verbelen , Hendrik Vansompel , Ahmed Abdallh, Kurt Stockman , and Peter Sergeant 

1 Introduction

Vehicle manufacturers encounter an ever-growing pressure to reduce fuel consumption and emissions, because of increasingly stringent regulations. As a result, they are forced to innovate to find new solutions which can assist in reaching the climate goals. One of these solutions is the hybrid electrical vehicle (HEV). The most important advantage of HEVs compared to classical vehicles is the higher efficiency which is due to the power split capabilities of the drivetrain. Important side effects are friction and thus wear in the planetary gears that enable the power split but also the valuable space which is taken by the added electrical machines.

A solution that eliminates the planetary gearbox and the additional electrical machines is called the electrical variable transmission (EVT) [1, 2]. The device consists of two rotors and one stator. In case of a HEV, the internal combustion engine (ICE) is connected to the inner rotor and the wheels to the outer rotor. Both shafts are electrically coupled via inverters and the DC bus, which can include a storage device. In an EVT, power can thus be transferred from the inner rotor to the outer rotor by means of an electric and/or electromagnetic path. Because the power is converted via two separate paths, the EVT can be considered as a power split device. Moreover, the EVT can also be used as an electromagnetic torque converter [3].

F. Verbelen (✉) · H. Vansompel · K. Stockman · P. Sergeant
Department of Electromechanical Systems and Materials, Ghent University, Ghent, Belgium
FlandersMake@UGent – core lab EEDT-MP, Ghent, Belgium
e-mail: florian.verbelen@ugent.be; hendrik.vansompel@ugent.be; kurt.stockman@ugent.be; peter.sergeant@ugent.be

A. Abdallh
MotionS Core Lab at Flanders Make, Lommel, Belgium
e-mail: ahmed.abdallh@flandersmake.be

The behaviour of the EVT is typically studied based on time-consuming finite element (FE) calculations. Evaluating the effect of design changes of the EVT on the performance of a considered HEV is, therefore, a tedious task. However, due to developed scaling laws for the flux, torque and losses, an existing design of the EVT can be scaled in axial and radial directions which significantly reduces the computational effort to analyse a design [4]. In this present paper, the aforementioned method is used to analyse how the design of the EVT influences the energy efficiency of the complete drivetrain given a driving cycle and vehicle parameters.

The paper is structured as follows. In Sect. 2, the topology, operating principle and control of the EVT are discussed. The scaling laws are introduced in Sect. 3, while in Sect. 4 the drivetrain and control of the considered HEV are elaborated. In Sect. 5 the results are discussed. Finally in Sect. 6 the conclusions of the research are formulated.

2 Permanent Magnet Electrical Variable Transmission

In this section, the topology of the considered EVT and the operating principle is explained as well as the control of the component.

2.1 Topology

A cross section of the considered EVT is shown in Fig. 1. The inner rotor and stator each consist of a distributed three-phase winding. The outer rotor is equipped with a single layer of rare-earth permanent magnets and a DC-field winding which are

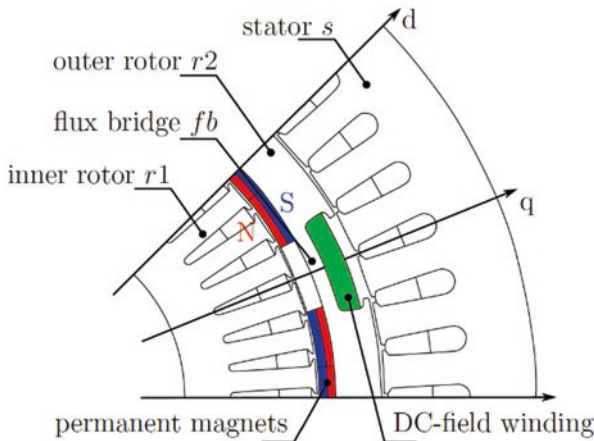


Fig. 1 Cross section of the considered PM EVT with a hybrid excitation

separated by a flux bridge. When the absolute value of the DC-field current increases, the magnetic state of the flux bridge located underneath the DC-field winding changes. The purpose of this DC-field winding is thus to modify the path of the permanent magnet flux which changes the stator flux linkage. The inner rotor field is almost not affected by the DC-field current since the magnets have a low recoil permeability of about 1.05 [5]. Using the DC-field current, it is thus possible to change the stator flux linkage while maintaining the rotor flux linkage which is particularly useful in HEV applications [1, 5].

The shafts of the inner and outer rotor form the two mechanical ports, while the windings of both the inner rotor and stator form the two electrical ports. To provide power to the inner rotor, slip rings are used. Some machine parameters are given in Table 1 for clarity.

2.2 Operating Principle

One of the main advantages of the EVT is that there is no mechanical connection between the inner rotor and the outer rotor. Moreover, in a HEV, the EVT decouples the ICE (connected to the inner rotor) and the wheels (connected to the outer rotor) in terms of speed and torque (see Fig. 4). This makes it possible to operate the ICE independently from the wheels. Consequently, the ICE can be operated in its operating point of maximum efficiency at all times. Why the EVT is decoupled in terms of speed is rather trivial: there is no mechanical link between both shafts, and as a consequence they can rotate at different speed. To explain why the EVT also decouples input and output in terms of torque, the EVT is first considered without stator. Suppose that the ICE is operating in the following operating point: T_{ICE} and N_{ICE} . Then the inner rotor should, in steady state, produce a torque equal to the opposite of the ICE torque in order to maintain the speed:

$$T_{r1} = -T_{ICE} \quad (1)$$

Table 1 Machine parameters of the considered EVT

	Stator	Outer rotor	Inner rotor
Rated mechanical power [kW]	–	120	75
Maximal speed [rpm]	–	4000	5000
Number of slots [–]	48	–	48
Number of pole pairs [–]	4	4	4
Outer radius [mm]	175	123.5	102
Inner radius [mm]	124.5	103	57
PM thickness [mm]	–	5	–
Active axial length [mm]	87	87	87
Width flux bridge [mm]	–	5	–

In order to produce this torque, currents need to be sent through the windings of the inner rotor:

$$T_{r1} = \frac{3}{2} N_p (\psi_{r1q} I_{r1d} - \psi_{r1d} I_{r1q}) \quad (2)$$

in which flux ψ and current I are related to the d - q reference frame (related to the outer rotor) and N_p is the number of pole pairs. Due to action-reaction, the electromagnetic torque on the outer rotor will produce the opposite torque. Therefore, the following is true:

$$T_{r2} = T_{ICE} \quad (3)$$

The torque at the wheels is thus the same as the torque generated by the ICE. Note that the following is of course only true in lossless conditions. To be able to modify the torque at the outer rotor, the stator is added. By sending currents through the stator windings, an electromagnetic torque is added to the outer rotor. Since the sum of the torque on all components needs to be 0, the torque on the outer rotor T_{r2} can be determined by:

$$T_{r2} = -T_s - T_{r1} = -T_s + T_{ICE} \quad (4)$$

in which the stator torque T_s is calculated as:

$$T_s = \frac{3}{2} N_p (\psi_{sq} I_{sd} - \psi_{sd} I_{sq}) \quad (5)$$

The fluxes (stator flux in the d -axis ψ_{sd} , stator flux in the q -axis ψ_{sq} , inner rotor flux in the d -axis ψ_{r1d} and inner rotor flux in the q -axis ψ_{r1q}) in (2) and (5) depend on five independent current setpoints: stator current in the d -axis I_{sd} , stator current in the q -axis I_{sq} , current in the DC-field winding of the outer rotor I_{r2d} , inner rotor current in the d -axis I_{r1d} and inner rotor current in the q -axis I_{r1q} . The relation between flux and current is determined based on FE calculations. The FE model, which forms the backbone of the EVT model, has been validated on a prototype [5].

2.3 Optimal Control

Based on (2) and (5) and knowing that the flux terms in these equations depend on five current setpoints, it is possible to deduce that an infinite number of current combinations will result in the same torque. This can also be seen in Fig. 2, which shows that a stator torque of, for example, 100 Nm can be obtained with various current combinations. Of course, only one of these combinations will result in the lowest losses.

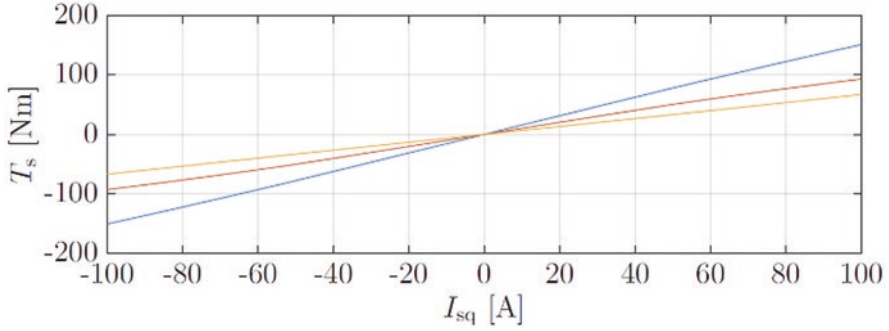


Fig. 2 Stator torque as function of stator current in the q-axis for varying DC-field current. Blue: $I_{r2d} = -10\text{A}$, red: $I_{r2d} = -5\text{A}$ and orange: $I_{r2d} = 0\text{A}$. All other currents are set to 0

The optimization routine which is written to find the optimal currents, given a specific operating point, can be summarized as follows [6]:

Find:

$$I^* = [I_{sq}^*, I_{sd}^*, i_{r2d}^*, I_{r1q}^*, I_{r1d}^*] \in \mathbb{R}^5 \quad (6)$$

with:

$$I^* = \arg \min (P_{loss}(I, N_{r1}, N_{r2})) \quad (7)$$

subjected to:

$$T_s(I^*) = T_{s,set} \ \& \ T_{r1}(I^*) = T_{r1,set} \quad (8)$$

The generated torque is calculated based on (2) and (5), and P_{loss} is equal to the sum of iron and copper losses (mechanical losses are neglected in this optimization). As solving this routine takes some time, the optimization is carried out offline after which the results are stored in a look-up table (LUT) which is consulted during operation. The LUT thus basically yields the optimal current setpoints given an operating point defined by a stator T_s and inner rotor T_{r1} torque setpoint and inner and outer rotor speed denoted by N_{r1} and N_{r2} , respectively.

3 Scaling Laws

As mentioned in the introduction, analysis of the performance of the EVT depends on the numerous FE calculations which are necessary to define the model. Therefore, the computational burden of studying the impact of design changes is high. Scaling laws, however, can be used to obtain a new design in a matter of minutes compared

to several days if FE calculations are used [4]. One way of reducing the computational effort is thus to use scaling laws.

Scaling laws allow to scale an EVT of which all current to flux relations are known in axial and radial directions. During axial scaling, the axial core length is changed while preserving the lamination cross section. The axial scaling factor K_A can therefore be calculated as:

$$K_A = \frac{l_a}{l_{a,0}} \quad (9)$$

in which $l_{a,0}$ is the axial length of the reference EVT and l_a is the length of the scaled design. Radial scaling considers a proportional change of all dimensions of the cross section. The radial scaling factor is thus equal to:

$$K_R = \frac{D}{D_0} \quad (10)$$

in which D_0 is the diameter of the reference EVT and D is the diameter of the scaled design.

In the following sections, the scaling laws as derived and validated in [4] are mentioned for clarity.

3.1 Scalable Machine Properties

The most important properties for this analysis are current, flux, torque, copper and iron losses. However, scaling laws can be derived for all machine properties including inductance, voltage, etc. [7]. Based on the Poisson's equation, it is possible to derive that the current needs to scale as follows [4, 7]:

$$I = K_R I_0 \quad (11)$$

with I_0 the current which flows in the reference machine and I the current in the scaled design. Note that both I_0 and I are arrays which contain five current setpoints $(I_{sq}^*, I_{sd}^*, i_{r2d}^*, I_{r1q}^*, I_{r1d}^*)$. If the relation in (11) is met, then the flux ψ and torque T will scale as:

$$\psi = K_A K_R \psi_0(I_0) = K_A K_R \psi\left(\frac{I}{K_R}\right) \quad (12)$$

$$T = K_A K_R^2 T_0(I_0) = K_A K_R^2 T_0\left(\frac{I}{K_R}\right) \quad (13)$$

The copper losses are calculated based on the currents flowing through the scaled EVT:

$$P_{cu} = \frac{3}{2} R_s (I_{sd}^2 + I_{sq}^2) + R_{r2} i_{r2d}^2 + \frac{3}{2} R_{r1} (I_{r1d}^2 + I_{r1q}^2) \quad (14)$$

in which the resistance of the inner rotor, outer rotor and stator scale according to the following equation:

$$R = \frac{1}{K_R^2} (K_A R_{co,0} + K_R R_{ew,0}) \quad (15)$$

in which $R_{co,0}$ is the resistance of the reference EVT in the core region, while the resistance of the end winding is denoted by $R_{ew,0}$.

Finally, the iron losses [W/kg] are determined assuming a sinusoidal air gap induction waveform, using Bertotti's model [8]:

$$P_{fe} = a \hat{B}^\alpha f + b \hat{B}^2 f^2 + c \hat{B} f \left(\sqrt{1 + d \hat{B} f} - 1 \right) \quad (16)$$

with a , b , c , d and α as magnetic core material parameters, \hat{B} the amplitude of the magnetic flux density and f the frequency. The constants have been determined based on measurements.

3.2 Scalable Control

In the previous section, it is shown how the EVT is scaled. However, setting up the optimal control is also a cumbersome task. Defining scaling laws for the optimal control (selection of the optimal currents, given the operating point) is thus also important. In [4], it is shown that this scalable control can be obtained by scaling the torque (T_{r1}^s and T_s^s , see Fig. 3) which is used as input for the LUT containing the optimal currents ($I_{sd}^s, I_{sq}^s, \triangleright$). As these currents are obtained based on the LUT of the reference machine, these currents need to be scaled back to the scaled device. Therefore, the final step is to scale the currents with K_R according to (11).

4 EVT-Based HEV

In this paper, the main application in which an EVT can be used is a HEV (see Fig. 4). The HEV that is considered, both the drivetrain and its optimal control, is presented in the following sections.

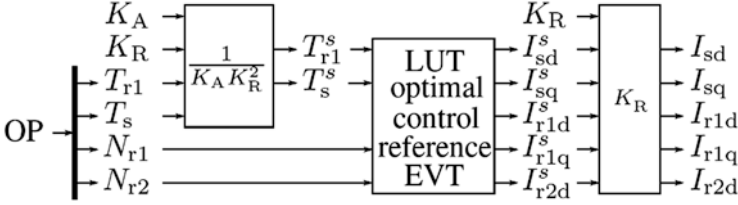


Fig. 3 Schematic of the scalable optimal control

4.1 Vehicle

Figure 4 gives a schematic overview of the complete HEV drivetrain. In accordance with previously published literature [6, 9], the inner rotor of the EVT is connected to the ICE, while the outer rotor is connected, via a gearbox, to the wheels of the vehicle. The purpose of this differential gearbox is to deliver torque to both wheels. The used ICE is a turbocharged gasoline engine (direct injection) running on a Miller cycle. The fuel map of the ICE will be used to calculate the fuel consumption for various design sizes of the EVT. The fuel consumption map of the ICE is presented in Fig. 5.

The behaviour of the vehicle is studied based on a 1-DOF model:

$$v_{car} = \int \frac{\frac{T_w}{r_w} - mfg - \frac{1}{2}v_{car}^2 \rho A_f c_d}{m} dt \quad (17)$$

in which v_{car} is the speed of the vehicle, T_w is the torque at the wheels, r_w is the wheel radius, m is the mass of the vehicle (including passengers), g is the gravitational constant, f is the rolling resistance coefficient, ρ is the density of air, A_f is the frontal cross-sectional area and c_d is the aerodynamic drag coefficient. The main parameters of this vehicle model can be found in Table 2.

To transfer the torque of the outer rotor to the wheels, a differential gearbox is used. The speed ratio of this gearbox, τ , describes the relation between the wheel speed N_w and the speed of the outer rotor N_{r2} as follows:

$$\tau = \frac{N_w}{N_{r2}} \quad (18)$$

If τ is smaller than 1, the outer rotor will rotate faster than the wheels. The wheel torque T_w , as mentioned in (9), is related to the outer rotor torque T_{r2} of the EVT by the following equation:

$$T_w = \frac{T_{r2} \eta}{\tau} \quad (19)$$

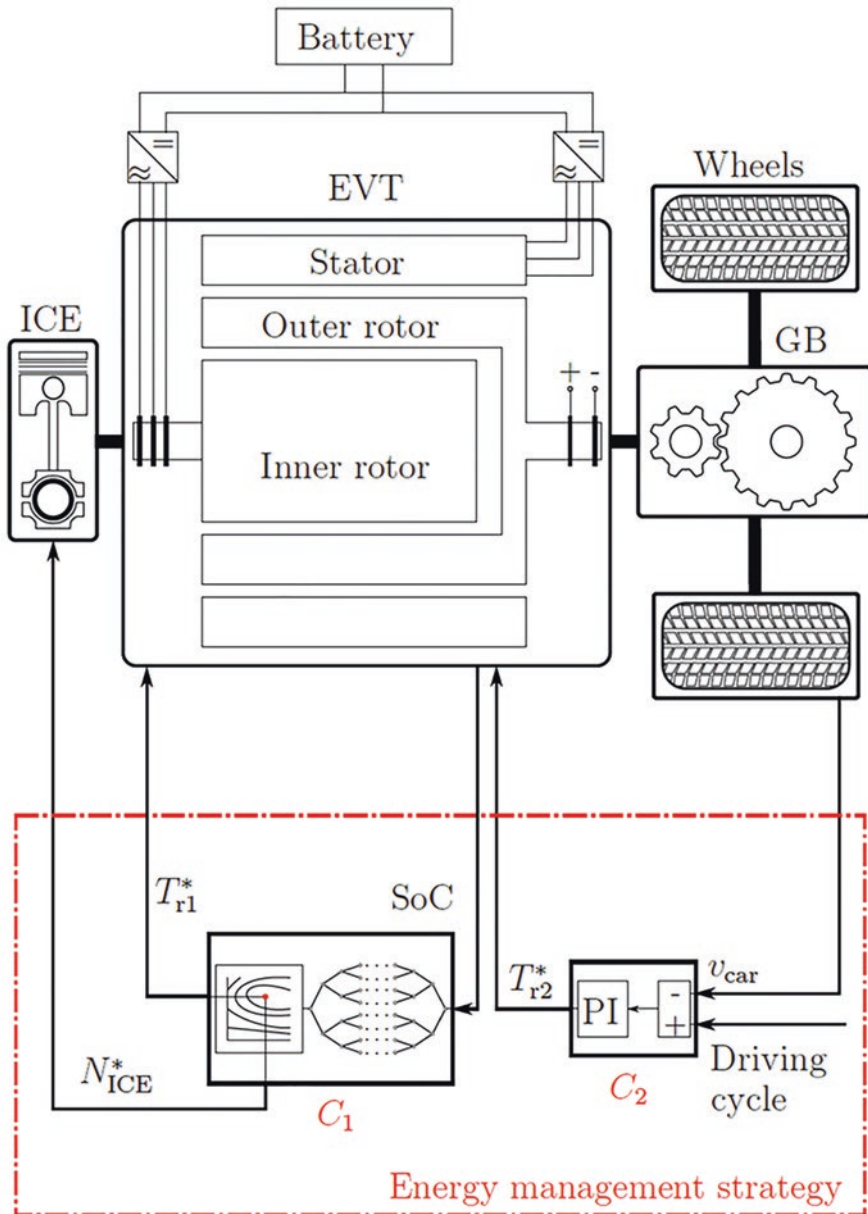


Fig. 4 Schematic of the EVT-based HEV drivetrain and simplified representation of the energy management strategy. More information concerning the energy management strategy (controllers C_1 and C_2) is given in section 3b

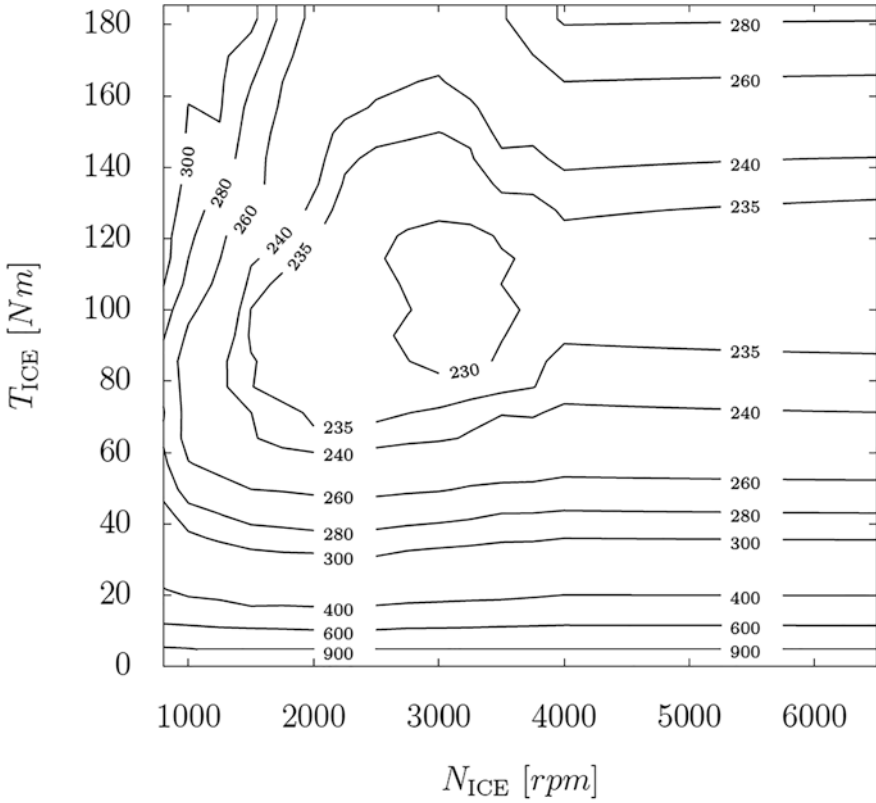


Fig. 5 Fuel consumption [g/kWh] of a turbocharged gasoline engine (direct injection) running on a Miller cycle

Table 2 Vehicle parameters

Mass m [kg]	1400
Aerodynamic drag coefficient c_d [-]	0.28
Frontal cross-sectional area A_f [m ²]	1.5
Rolling resistance coefficient f [-]	0.009
Wheel radius r_w [m]	0.3
Battery capacity C_{bat} [kWh]	1.8

in which η is the efficiency of the gearbox. Note that during braking, the efficiency term goes to the denominator as power flows from the wheels to the inner rotor. Both the wheel speed and the wheel torque are imposed by the driving cycle. The wheel speed is directly related to the vehicle speed and the wheel torque is related to the acceleration and speed of the vehicle (due to the speed dependency of, e.g. the aerodynamic drag) but also the road gradient (ignored in (9)). The selected driving cycle for this analysis is the WLTC (see Fig. 6).

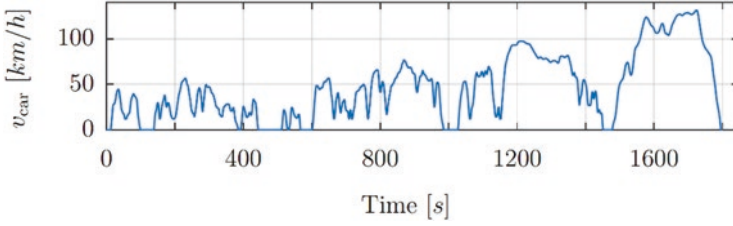


Fig. 6 Imposed vehicle speed [km/h] as function of time for the WLTC

Finally, the battery is considered as an ideal storage device (no losses) as the main goal of this paper is to show how the scaling laws can be applied. The state of charge (SoC) of the battery is calculated as:

$$SoC = SoC_0 - \frac{\int P_{bat}}{3600 C_{bat}} \quad (20)$$

with SoC_0 the state of charge at the beginning of the cycle and P_{bat} the battery power. The battery power is calculated as the sum of the electrical power of the stator $P_{e,s}$ and inner rotor $P_{e,r1}$ (including losses):

$$P_{bat} = P_{e,s} + P_{e,r1} \quad (21)$$

4.2 Control

The objective of this paper is to find the optimal size of the EVT in an EVT-based HEV. The fuel consumption of the vehicle is chosen to quantify how optimal a considered drivetrain is. The chosen operating points of the ICE (C_1 see Fig. 4), however, have a significant impact on the fuel consumption. To exclude the impact of controller C_1 , dynamic programming (DP) is applied in order to find the optimal control regardless of the drivetrain configuration.

DP has been used successfully to optimize the fuel consumption of a HEV taking into account several constraints such as the battery SoC [10–12]. Hence, the SoC at the beginning and end of the driving cycle should be the same. In this paper, the open-source toolbox provided by Sundström and Guzzella had been used as framework for the DP structure [13].

Besides controller 1 of which the output is defined based on DP, a second controller (C_2 see Fig. 4), is used to adapt the outer rotor torque in such a way that the imposed speed, defined based on the driving cycle, is achieved with a maximum error of 1 km/h [14].

5 Results

The objective is to optimize the drivetrain as depicted in Fig. 4. This comes down to optimizing the size of the EVT and the end gearbox. For the EVT, a range of possible designs defined by an axial and radial scaling factor varying from 0.8 to 1.2 are defined. For each design, the gear ratio is searched for that minimizes the fuel consumption. The fuel consumption itself is optimized based on DP. The DP algorithm is thus solved for every considered design.

The results (fuel consumption) are stored in a performance map which shows how the fuel consumption varies with the scaling factor (see Fig. 7). However, this performance could also be quantified by, for example, the maximum acceleration.

The performance map shows that, the bigger the EVT is chosen, the lower the fuel consumption becomes. This is not a surprise as bigger electrical machines tend to have lower losses due to the lower currents which are necessary to generate the same torque compared to a smaller machine. However, bigger machines come with a higher material cost. Furthermore, space is limited under the vehicle frame which limits the size of the EVT. Besides the fuel consumption, Fig. 7 also shows the cho-

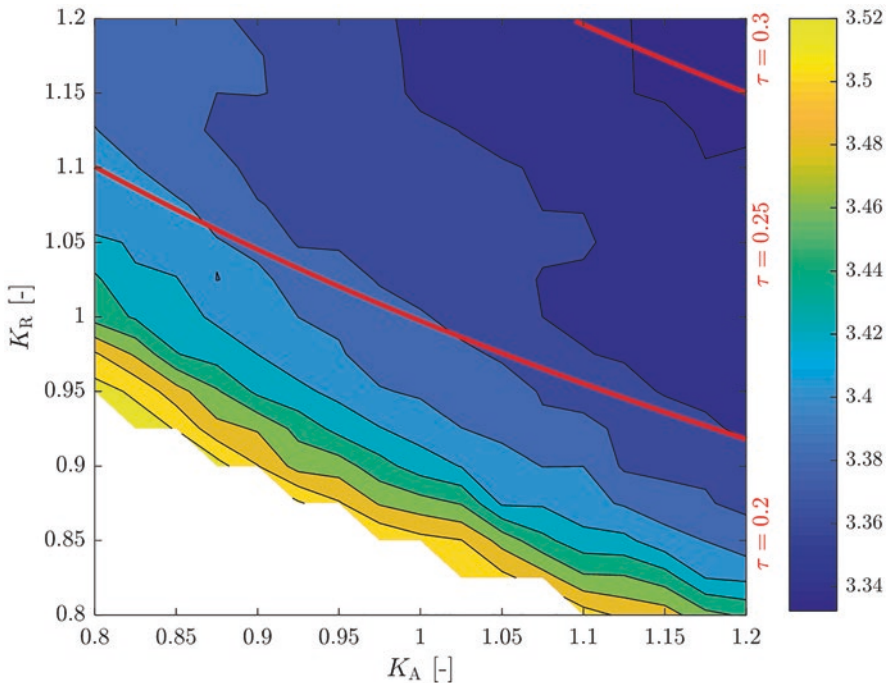


Fig. 7 Performance map showing the fuel consumption of the HEV during the WLTC for varying axial and radial scaling factor. The drivetrains that use an EVT, defined by a K_A and K_R , situated below the lowest red line use an end gearbox with a speed ratio τ equal to 0.2. Between the two red lines, τ equals 0.25 and above the highest red line τ equals 0.3

sen gear ratio for the end gearbox. The figure shows that the variation in optimal gear is rather small: it varies between 0.2 and 0.3.

To make the results in Fig. 7 a bit more tangible, the scaling factors are translated to actual dimensions (see Fig. 8). Note that the scaling factors are related to the active part of the EVT, while the total length and diameter cover also the housing. In the radial direction, the difference between the active part and housing, which includes a water jacket cooling, is rather small. However, in the axial direction, the active part is combined with a set of AC slip rings for the inner rotor and a set of DC slip rings for the DC-field winding of the outer rotor. This creates a rather significant difference between the active part and the total length of the EVT. Consequently, the variation of the axial scaling factor between 0.8 and 1.2 results only in a variation in total length of about 35 mm.

Figure 8 also shows lines of constant weight which make it possible to approximate the minimal weight (i.e. size) of the EVT for the used load cycle. As already stated, bigger and thus heavier machines result in lower losses. To quantify this, Fig. 8 can be used to calculate the fuel consumption for a given maximum weight. This comes down to finding the optimal design for a given mass. The results are presented in Fig. 9. This figure is particularly useful for manufacturers because it gives an idea of how the sizing influences the fuel consumption. It shows that

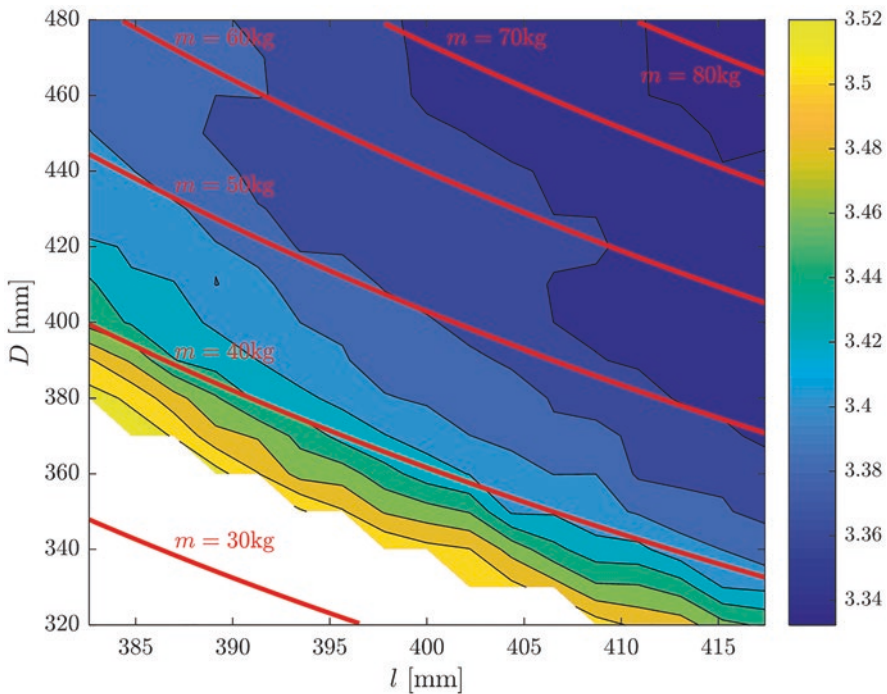


Fig. 8 Performance map showing the fuel consumption of the HEV during the WLTC for varying length and diameter of the housing. The red lines resemble designs with a constant mass

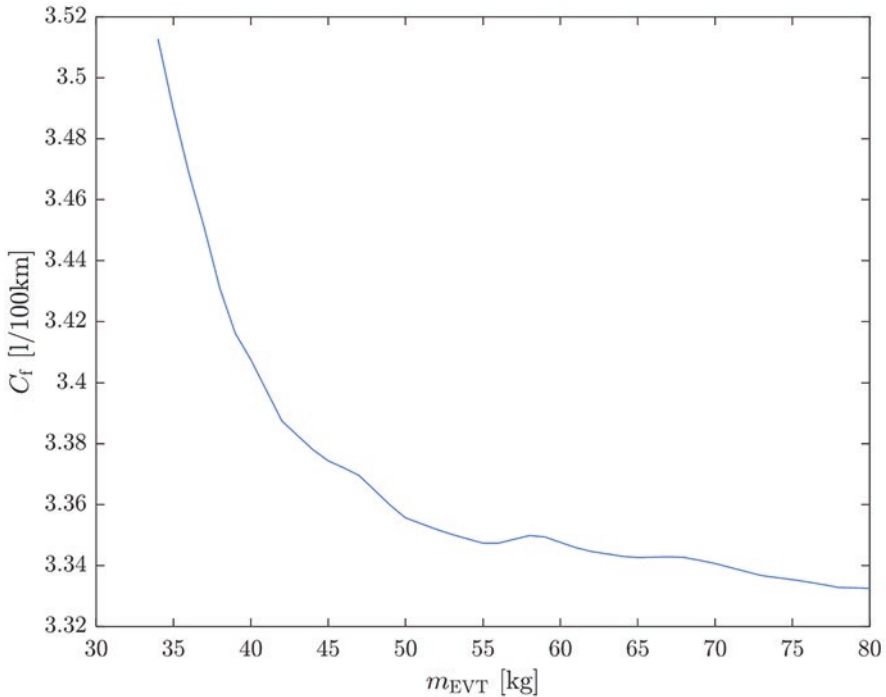


Fig. 9 Fuel consumption in l/100 km for the WLTC as function of the weight of the considered EVT design

increasing the weight beyond 50 kg results only in marginal gains in terms of overall fuel consumption. Although it is perfectly feasible to reduce the weight to 40 kg, Fig. 9 clearly demonstrates that minimizing the EVT even further has a highly negative impact on the fuel consumption.

Figure 10 shows the same information as in Fig. 9 but now as function of material cost. This figure immediately shows how high the gain is of resizing the EVT. If the design cost is, for example, estimated at 400 euro, then an increase in material cost of 100 euros will result in a decrease in fuel consumption of about 0.07 l/100 km. However, a further increase of the budget with 100 euro will only decrease the fuel consumption by 0.03 l/100 km. Again, if the manufacturer wants a product with a material cost below 400 euros, that is perfectly possible but at the cost of a higher fuel consumption per 100 km. The vehicle manufacturers can use this information to draw a conclusion about the sizing of EVT considering the trade-off between the initial cost and the running cost over the vehicle lifetime.

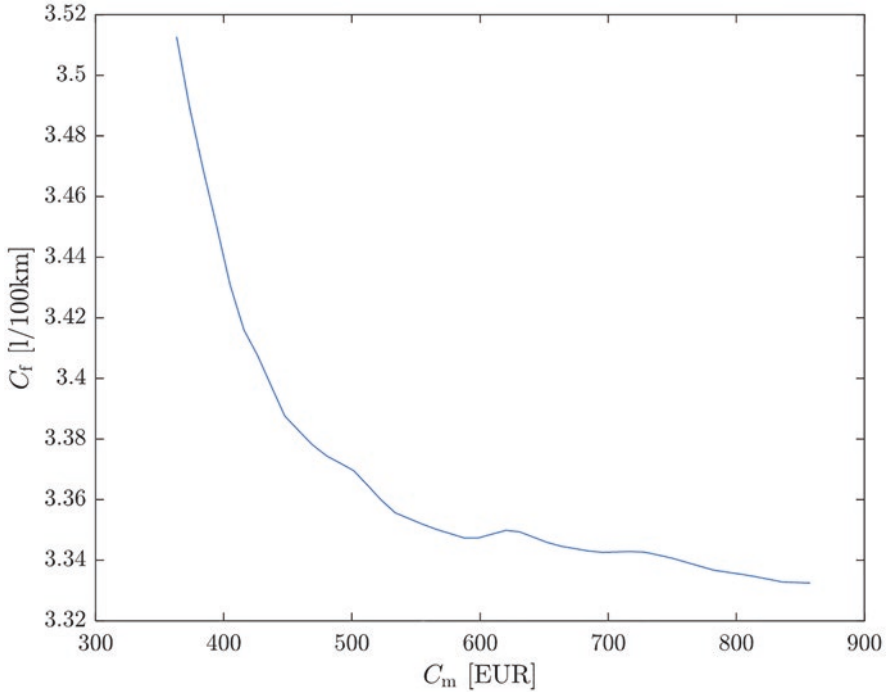


Fig. 10 Fuel consumption in l/100 km for the WLTC as function of the material cost of the considered EVT design

6 Conclusion

In this paper, a method is described to aid in the design of an electrical variable transmission based on scaling laws. The principle of a performance map is used to analyse how well the considered design, defined by an axial and radial scaling factor, performs given a load cycle. The parameter used in this paper to define the performance is the fuel consumption. The feasibility of the design in terms of dimensions can be deduced easily based on the performance map by translating scaling factors to actual dimensions. Furthermore, constraints such as maximum weight can be added as well. Finally it is demonstrated that performance in terms of fuel consumption can be calculated in terms of material cost. This is particularly useful for manufacturers as it gives an idea of how their investment is translated in fuel consumption and consequently to meet the global emission requirements.

Acknowledgement This work was carried out for the EMTechno project (project ID: IWT150513) supported by VLAIO and Flanders Make, the strategic research centre for the manufacturing industry in Belgium.

References

1. M. Hoeijmakers, Electromechanical converter, Patent US 7 164 219, 2007
2. M. Hoeijmakers, J. Ferreira, The electric variable transmission. *IEEE Trans. Ind. Appl.* **42**(4), 1092–1100 (2006)
3. S. Vanhee, Concept Study of an Electrical Variable Transmission for Off-Highway Applications, Master thesis, Ghent University, Belgium, 2015
4. F. Verbelen, A. Abdallah, H. Vansompel, K. Stockman, P. Sergeant, Sizing methodology based on scaling laws for a permanent magnet electrical variable transmission. *IEEE Trans. Ind. Electron.* **67**(3), 1739–1749 (2019)
5. J. Druant, H. Vansompel, F. De Belie, J. Melkebeek, P. Sergeant, Torque analysis on a double rotor electrical variable transmission with hybrid excitation. *IEEE Trans. Ind. Electron.* **64**(1), 60–68 (2017)
6. J. Druant, H. Vansompel, F. De Belie, P. Sergeant, Optimal control for a hybrid excited dual mechanical port electric machine. *IEEE Trans. Energy Convers.* **32**(2), 599–607 (2017)
7. S. Stipetic, D. Zarko, M. Popescu, Ultra-fast axial and radial scaling of synchronous permanent magnet machines. *IET Electr. Power Appl.* **10**(7), 658–666 (2016)
8. G. Bertotti, *Hysteresis in Magnetism: For Physicists, Materials Scientists, and Engineers* (Academic, San Diego, 1998)
9. J. Druant, H. Vansompel, F. De Belie, P. Sergeant, Efficiency of a CVT operated EVT experimentally evaluated against half-toroidal and push-belt CVTs. *IEEE Trans. Ind. Electron.* **65**(4), 3095–3103 (2018)
10. E. Vinot, R. Trigui, Y. Cheng, C. Espanet, A. Bouscayrol, V. Reinbold, Improvement of an EVT-based HEV using dynamic programming. *IEEE Trans. Veh. Technol.* **63**(1), 40–50 (2014)
11. Z. Chen, C.C. Mi, J. Xu, Energy management for a power-split plug-in hybrid electric vehicle based on dynamic programming and neural networks. *IEEE Trans. Veh. Technol.* **63**(4), 1567–1580 (2014)
12. E. Vinot, Comparison of different power-split hybrid architectures using a global optimisation design method. *Int. J. Electr. Hybrid Veh.* **8**(3), 225–241 (2016)
13. O. Sundström, L. Guzzella, A generic dynamic programming Matlab function, in *IEEE Multi-conference on Systems and Control*, 2009, pp. 1625–1630
14. UN, *Proposal for a new UN Global Technical Regulation on Worldwide harmonized Light vehicles Test Procedures (WLTP)* (Economic and Social Council, 2013), p. 235

IE3 Efficiency Class as MEPS for Industrial Motor: How Brazil Got There



George Alves Soares and Carlos Aparecido Ferreira

1 Introduction

The Brazilian market for electric motors can be characterized by the following: (1) large sales volume, about 2.7 million three-phase induction motor units; (2) strong domestic manufacturing (one manufacturer is one of the largest manufacturers in the world); and (3) the manufacturers deliver products of good quality, which can compete internationally. This big sales volume is justified by the fact that half of the domestic production is sold to national machine manufacturers and the Brazilian economy has a strong industrial basis. These characteristics make about 68% of the electric energy consumed by the industrial sector in Brazil which occurs through electric motors. This market is characterized meticulously in [2].

This significant participation in the national consumption of electric energy has justified that, since 1986, energy efficiency actions in this piece of equipment have been implemented. The first years were intended the diagnosis of technology, operation, standardization, the environment of the application, survey of educational tools, the volume of sales, type of buyers, etc. The introductory diagnosis of inefficient motors, lack of independent laboratories and training, and outdated standards from the point of view of energy performance led to the start of the Brazilian Labelling Program in 1992. In the following years, the independent and manufacturers' laboratory capacities were assembled, the standards were revised, and the

G. A. Soares (✉)

Centro de Pesquisas de Energia Elétrica, Rio de Janeiro, Brazil

C. A. Ferreira

Centrais Elétricas Brasileiras, Rio de Janeiro, Brazil

e-mail: carlosaparecido@eletrobras.com

PROCEL¹ Seal (*) and the labeling system motivated the offering of more efficient motors to the market. The first experiments with the establishment of minimum efficiencies occurred in 1998 on a voluntary basis. In 2002, the electric energy crisis caused the House of Representatives to issue law n° 12,295 /2001, delegating to the federal government the charge of determining maximum consumption or minimum efficiencies by equipment. In the same year, decree n° 4059 created the CGIEE-Energy Efficiency Index Management Committee which was in charge of making these regulations. In 2002, the first equipment regulation was published to establish IR1² as the minimum nominal efficiency for standard and IR2 for high-performance induction motors. Besides being the first one, this regulation was the unique issued by the Brazilian president [1, 9]. In 2005, the Joint Ministerial Ordinance n° 553 established that as of December 2009, the minimum nominal efficiency level for manufacturing and import was those of high-efficient motors, and in December 2010, the driving machines should also be marketed with these motors [3]. The terms “Interministerial Ordinance” and “Joint Ministerial Ordinance” are used in this paper to indicate an ordinance signed by more than one minister, in the case of motors, the Minister of Mines and Energy, Minister of Science and Technology, and the former Minister of Industry and Commerce.

In August 2017, an Interministerial Ordinance n° 1/2017 [4] was published, establishing as minimum nominal efficiency level those of the motors characterized as IR3², commonly called Premium. This ordinance comes into force in 2 years for manufacturing and importing and in 3 years for units marketed within driving machines.

It is important to clarify that the IR3 class defined by the Brazilian standard is similar to the IE3 defined by IEC 60034–30, but it also respects the strong Brazil OEM market. This ordinance embraces nominal efficiency values for two, four, six, and eight poles and powers ranging from 0.12 to 370 kW. The table is shown in [5] so it raised the efficiency values and broadened the scope. Before the referred ordinance, the powers ranged from 0.75 to 185 kW. Another important issue of this legal order is the obligation of selling repaired motors to comply with the MEPS.

The process for the enactment of the mentioned ordinance was hard and took more time than it was expected. It began by convincing CGIEE members of the importance of making this regulation and members approved the work that the Motor Technical Committee (*CT-Motores*) prepared the Regulatory Impact Study. This study is a fundamental step in the process of establishing minimum nominal efficiency. It analyzes the regulations from the point of view of energy gains for society, impacts on the supply chain, impacts on materials, and market competitiveness. This assessment is the technical basis of the legal process and its final report is bulky and full of market data. An executive summary is presented in Sect. 2.

¹Procel is the National Energy Conservation Program. Besides the Brazilian Labeling Program, Procel stimulates the best piece of equipment with a seal, on a voluntary basis.

²IR1, IR2, and IR3 are Brazilian efficiency classes which have the same values for nominal efficiencies of IE1, IE2, and IE3, except for seven cases which smaller efficiencies are allowed for motors built in smaller frames. In this paper they will have the same meanings.

2 Regulatory Impact Study

The target of the study [6] is to analyze the impact of establishing as new minimum levels of nominal efficiency the values of efficiency class IR3 (Premium) for three-phase electric induction motors two, four, six, and eight poles from 0,75 kW / 1 hp. up to 370 kW/500 hp. They must meet the required levels to be manufactured, marketed, and imported, whether sold alone or inside other machines.

The impact analysis was carried out through a qualitative analysis, in which the main impacts that could be evaluated with the available data were considered. Impacts on the steel, motor, capital goods machinery, and electric power markets were evaluated. In the steel sector, the steel supply capacity for motor manufacturers was also evaluated, considering the possibility of steel shortages and the number of suppliers. In the motor market, it was analyzed whether this action would impact the current participation of manufacturers/importers in the market share of sales. In the machinery sector, the impact of the absorption capacity of the market due to the increase of machine cost with the adoption of these motors was investigated. In the electricity sector, the energy savings for the country and its effects on the energy conservation targets set by the Federal Government were examined. Finally, the impact from the point of view of the consumer was analyzed, presenting the energy and economic gains, resulting from the acquisition of the Premium motor.

2.1 Analysis of the Impact on the Steel Market

To achieve the performance levels of the Premium motors category, the steel used to build the core of the motors is predominantly non-oriented grain silicon (GNO) produced in Brazil by only one manufacturer, with no competition in the domestic market. The semi-processed electric steels produced by the other steel mills meet the required loss levels for this line of motors for smaller frame numbers.

In the international market, large mills located in Asia (China, Taiwan, and Korea), Eastern Europe, and Germany guarantee the world supply of silicon steel with the non-oriented surplus. Regarding semi-processed electrical steel, there are no problems with internal supply, being produced by large national steel industries (CSN, Tubarão, and Usiminas), which guarantee supplies and free competition.

GNO silicon steels and the semi-processed electric steels produced in Brazil are of excellent quality, fully meeting the technical requirements for IR3 class motors.

Silicon steel, since it requires more processing, has a higher factory cost. In addition, the existence of a single manufacturer on the domestic market may burden the product, but with limited impact, due to the pressure of prices in the international market.

For this reason, there is no problem expectation of steel shortages nor any significant impact on the supply chain. Nevertheless, it is recommended to maintain market monitoring by *CT-Motores*.

2.2 Impact Analysis on the OEM Market

The OEM market in Brazil is an important economic sector that has monthly earnings of approximately US\$ 1.8 billion and employs around 720 thousand workers. Its main representative entity is ABIMAQ, Brazilian Association of Machinery and Equipment Industry, established in 1975, with the objective of acting in favour of strengthening the national Industry, activating the sector, stimulating international trade and cooperation, and contributing to improve its performance. ABIMAQ currently represents about 7800 companies from the most diverse segments of machines, in which performance has a direct impact on the other national productive sectors. This entity has been defending the modernization of the Brazilian industry to make it more competitive. From this point of view, its consulted representatives expressed their support for this measure of the increase of the minimum nominal efficiency of the motors, provided that the principle of fairness with the imported machinery was maintained, assuring equal competition in the market.

Previous experience when changing the MEPS of motors from IR1 (IE1) to IR2 (IE2) level has shown that this industry will have no problem absorbing the increasing costs of its products in the market, since the same criteria are used for imported machines which are inspected by the inspection authority and a higher technological value is added to the new driving machines.

2.3 Impact Analysis on the Motor Market

The national and international manufacturers of motors have participated in the Technical Committee of the Brazilian Labeling Program, PBE, coordinated by INMETRO (National Institute of Metrology, Standardization and Industrial Quality), and were consulted about this action and expressed their opinion about technical details of the ordinance.

The market of domestic manufacturers is very concentrated, being one manufacturer responsible for more than 75% of the national production. In terms of general participation, the entry of the manufacturers that import their products changes this participation a little. It is worth noting market share data are difficult to obtain as the class entity of these manufacturers has not disclosed these data for some years.

The acceptance of the new nominal efficiency levels should not change this market framework as it happened when to raise the efficiency levels from IR1 to IR2 in the last decade.

2.4 Analysis of the Impact on the Electricity Sector

Within the scope of CGIEE's attribution, this analysis was limited to the aspect of impact in relation to energy conservation. The methodology used to evaluate the impact on energy savings was developed by the National Energy Conservation

Programme (PROCEL). This methodology is documented in [7]. The impact was analyzed for two standard years: 2020 and 2050. This last referred year is related to the next national energy plan. Table 1 summarizes the energy and cost benefits.

The energy conservation target estimation for 2050 for the industrial sector is 160 TWh/year so this gain represents about 3% of it.

In terms of the international agreement, it is estimated that by 2030, the expected energy saving is 1830 GWh/year. This is equivalent to a 441 MW hydropower plant, which can provide energy for more than 560,000 residences in a year, meaning a city of nearly 1.9 million people. The goal of reducing energy consumption ratified by the Brazilian Government in the Paris Agreement, in the framework of the 21st Conference of the Parties (COP-21) of the United Nations Framework Convention on Climate Change (UNFCCC), is 53,000 GWh by 2030 with induced actions, and the gains from this measure will contribute to 3.52% of this target.

2.5 Impact Analysis from the Point of View of the Consumer

The energy and economic benefits to the consumer when using a Premium motor were calculated through a simple and reliable methodology. The energy saving achieved by using this type of engine instead of the high efficient satisfies the higher cost of Premium motor in a period dependent on operation time. After reaching the investment return time, energy savings will be a profit for consumers. This value is significant considering that the average useful life of the engines used in Brazilian industries is 17 years. Table 2 shows the payback time for all nominal for four poles. The assembly of this table was achieved thanks to the purchase costs, confidentially informed by Brazilian manufacturers, and market data obtained from researches.

2.6 Analysis of Impact Magnitude

A mean of summarizing the overall impact of regulatory action is to build the “Matrix of Impacts” which represents the expectation of technical staff and market. The following table presents a magnitude and probability qualitative analysis of the impacts, and the analysis of consistency revealed the coherence of the obtained data. The “+” sign means positive impact and the “-” sign negative impact (Table 3).

Table 1 Energy and cost benefits

Year	Electric energy saving (GWh/year)	Equivalent hydropower plant (MW)	Avoided investment (US\$ million)
2020	128	31	5
2050	4.762	1.142	180

Table 2 Simple payback time (PBT) for buying IR3 motor instead of IR2 on nominal load^a

P (hp)	PBT (year) 4000 h/year	PBT (year) 6000 h/year	PBT (year) 8000 h/year
1,0	2,76	1,84	1,38
1,5	1,11	0,74	0,55
2,0	2,69	1,79	1,34
3,0	2,03	1,35	1,02
4,0	1,45	0,96	0,72
5,0	2,68	1,79	1,34
6,0	3,32	2,21	1,66
7,5	2,91	1,94	1,46
10,0	3,34	2,22	1,67
12,5	2,16	1,44	1,08
15,0	3,87	2,58	1,93
20,0	3,28	2,19	1,64
25,0	3,08	2,05	1,54
30,0	3,27	2,18	1,64
40,0	2,38	1,59	1,19
50,0	2,12	1,42	1,06
60,0	3,56	2,37	1,78
75,0	3,18	2,12	1,59
100,0	3,12	2,08	1,56
125,0	5,08	3,39	2,54
150,0	5,50	3,67	2,75
175,0	3,84	2,56	1,92
200,0	4,56	3,04	2,28
250,0	5,04	3,36	2,52
300,0	7,01	4,67	3,50
350,0	6,58	4,39	3,29
400,0	6,07	4,05	3,03
450,0	5,92	3,95	2,96
500,0	5,86	3,91	2,93

^aAdopted tariff rate: US\$ 0,150/kWh

2.7 Conclusion and Recommendations of the Study

The members of the Motor Technical Committee (“CT-Motores”) recommended the implementation of the minimum levels of nominal efficiency equal to the IR3 class for three-phase induction motors due to the strong impact on the energy economy, for its contribution to meeting the targets of energy savings set by the Federal Government, by the low impacts in the steel and motor market, as well as the absorption of the cost increasing of the machine market. No significant change is expected in the market concentration of electric and steel motors or supply shortages in steel. It is also expected that the price growth of the motors in the machines will be absorbed by the market as the same criteria are required for imported

Table 3 Assessment of magnitude, probability, and consistence analysis of impacts

Impact	Magnitude	Probability	Analysis of consistency
Energy saving for the country	+3	Very high	Medium
Supply shortage of steel supply for the Premium motor in the Brazilian market	-2	Very low	High
Change in the steel supplier market participation	+1	Low	High
Change in motor manufacturer market participation	+1	Low	Medium
Absorption by the market of the increase of the prices of the machines	+2	High	High
Energy and economic gains for the consumer	+2	High	High

machines. Also, there is an evaluation conformity program for motors manufactured and imported. Besides, the new motor driving machine will be manufactured with a higher technological aggregated value to them. All these expectations are based on the lessons learned during the increasing of the minimum levels from IR1 to IR2 in the last decade.

It is worth noting that the use of Premium motors as standard motors is an international trend and that the use of such equipment will bring lower costs with electric energy to the end users, in spite of the higher acquisition cost. Before the new Interministerial Ordinance, PROCEL released a technical guide and carried out four workshops to raise awareness in the market to increase the level of users' knowledge about the benefits of these products showing the benefits of the IR3 motors in comparison to IR2 ones. One of the highlighted points was the big difference between the operational and acquisition costs for the motors' lifetimes.

3 Steps for Publication of Motor MEPS Joint Ministerial Ordinance

The process for publishing an Interministerial Ordinance is shown in Fig. 1 and may take months or years. In the case of induction motors, the process from the preparation for public consultation to the publication of the Joint Ministerial Ordinance took 9 months. The time for the development and approval by the CGIEE of the Regulatory Impact Study and the Interministerial Ordinance draft is not included in this period. The Regulatory Impact Study was presented in item 2.

The public consultation is extremely important to obtain support from the stakeholders, as well as to show the market the government's policy of increasing the level of motors efficiencies, enabling better planning by the market. In the case of induction motors, the consultation lasted about 40 days. Twenty-six contributions were received from six institutions. These contributions led to the following changes: a reduction of the deadline to take effect, the inclusion of the repaired motors that are re-marketed in the market, and the compatibility of power and pole

numbers with the Brazilian standard NBR 17.094-1 which defines the Premium motor category (IR3). The table starts now with 0.16 hp. instead of 1 hp., besides the original expansion from 250 to 500 hp. proposed by the Motor Technical Committee (*CT-Motores*) [4, 5]. Moreover, repaired motors can only be sold fulfilling the IR3 level.

Once approved by the CGIEE, an awareness and persuasion process of the decision makers of the ministry began. Because it is an Interministerial Ordinance of the Ministry of Mines and Energy (MME), Ministry of Science and Technology (MCTIC), and the former Ministry of Industry and Commerce (MDIC), this means that the ordinance is analyzed by the legal and technical areas of each ministry, with the emission of respective technical and legal opinions. After this process, the ministers may sign this regulation.

In order to be approved by each ministry, a series of meetings is held to clarify the issue from a legal and technical point of view, although representatives of these ministries are part of the CGIEE. The time for the signature of each minister is very difficult to estimate, and it depends on the documentation produced in each ministry and the agenda and understanding of the ministers.

In this case, the time length in the three ministries was about 4 months.

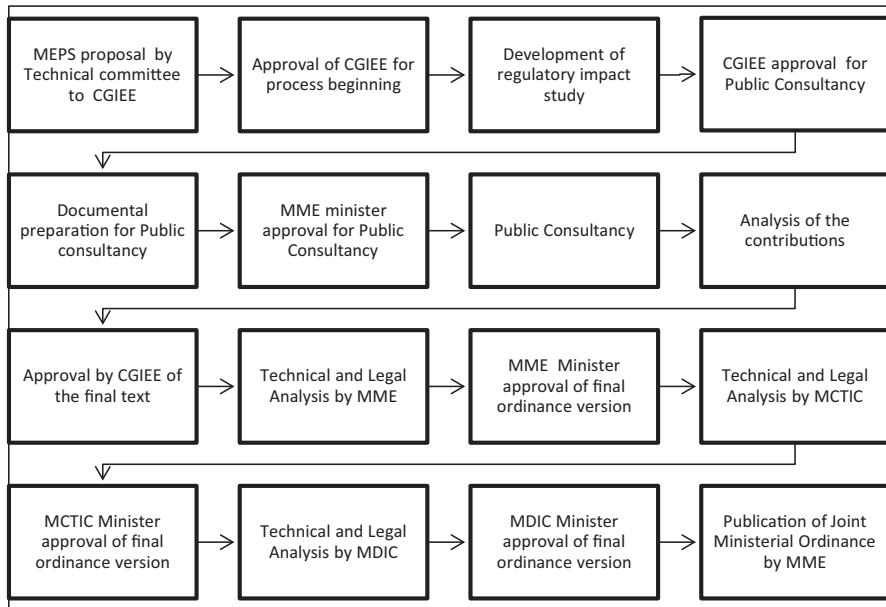


Fig. 1 Flowchart of the Interministerial Motor Ordinance publication process

4 Ordinance Benefits

The new efficiency level that takes effect in August 2019 will bring important energy and market benefits to society and will place Brazil in the top group of countries that have as minimum nominal efficiency those of the category called “Premium.” It is estimated that the saved energy accumulated in the period from 2019 to 2030 is 11,213 GWh, reaching in the year 2030, as mentioned the economy of 1830 GWh/year, equivalent to a hydroelectric plant of 441 MW, the consumption of more than 560,000 residences in a year, and to the consumption of a city of almost 1.9 million people. Estimation for 2050, the reference year for the next energy plan, is also compelling with the energy savings of 4762 GWh/year, equivalent to a hydroelectric plant of 1142 MW and the energy savings accumulated by 2050 of more than 76,000 GWh.

This regulation has innovative aspects as a greater scope: its power range goes from 0.16 hp. up to 500 hp. in all numbers of poles, and commercialized repaired motors are included.

The repaired motor sector in Brazil is huge; more than 4.5 million of units are repaired in a year and about 36% are repaired and sold. The sector is composed of 85% of small companies (up to four employees) although the big companies have quality assurance programs. There are no official repair standards nor representative association. The study [8] estimated that about 8.43 TWh of electric energy per year is wasted in the country due to the poor technical quality of motor repairing. The insertion of the repaired motor in the ordinance will reduce these losses.

The benefits to the consumer were shown in item 2.5.

5 Challenges for Effective Ordinance Implementation

The three main challenges for the enforcement of the ordinance are the effective inspection to restrain the import of motors that does not meet the established minimum levels of efficiency, the deindustrialization process that is taking place in the world economy, and the development of evaluation conformity procedures for checking the compliance of repaired motors.

Electric motors can be part of many machines. This means that there is a large number of import codes (NCM³s) that are used to import machines and their parts. The importers have to fill up a form declaring the import code for each importation. The conformity evaluation process begins by inserting for these codes the requirement of proving the compliance with the ordinance or to prove that the motor is not covered by the mentioned ordinance. To suppress the entrance of the imported motors out of specification, NCM³s that could be used to import electric motors

³NCMs are codes on a form that characterize imported products, making it easier for the IRS (the inspecting agency for products entering and leaving the country) to check whether products arriv-

were reevaluated in 2018. Besides the 24 NCMs that already demanded proof of energy performance, 67 NCMs that included motors in their descriptions were analyzed. In total, 91 codes were analyzed and the result was presented to INMETRO as the inspection authority.

The market for motor-driven machine manufacturers (OEM) is strong in Brazil and has suffered in recent years due to competition with imported machinery and, more recently, the importation of the industrialized product that does not require manufacturing in the country. This process of de-industrialization is worldwide, but in Brazil, it is very impressive because there are 7800 companies and around 720,000 employees in the machinery sector, according to ABIMAQ data. Poor import controls can lead costumers to the option of using cheaper and inefficient motors and/or machines, which would generate great resistance from the national manufacturers to the implementation of the ordinance.

With respect to inspection of repaired motors, the basic objective is to reduce the resale market of motors, without harming the market of reconditioning service (which is the one that the consumer has a failed motor and sends to the repairers). This difference is very important to be remarked as the service is a business between users and repairers. The users decide the quality of service they want to. The resale of motors happened without inspection or rules and competes with the regulated market of new motors. The difficulties encountered in the implementation of this ordinance for repairers are in the matter of proving that the minimum performance was achieved. The first step is to exclude repaired motors of the conformity evaluation process of the new motors which are manufactured or imported units of the same models and statistic tools can be used. The second step is to oversee the repairers through complaints while a new and specific evaluation procedure is elaborated. These steps are being set up by INMETRO's regulation.

Tools and procedures of market surveillance are being discussed to ensure the effectiveness of this energy efficiency regulation.

6 Conclusions

The new level established by this regulation will bring important energy and market benefits to society and will place Brazil in the group of top countries with the best international practices in Motor MEPS. This regulation will also contribute to the target of reducing energy consumption ratified by the Brazilian Government in the Paris Agreement within the framework of the 21st Conference of Parties (COP-21) of the United Nations Framework Convention on Climate Change (UNFCCC), reinforcing the country as one of the protagonists in the global effort to combat climate change.

ing in the country are within regulations and if there are any tax debts. The depth of inspection required by NCM is defined by INMETRO, the metrology institute that deals with product and testing regulations.

The analyses carried out in the scope of the study of Regulatory Impact Study have led us to believe that in terms of MEPS, IE3 level is the highest mandatory level that can be established at least in Brazil. The IE4 and IE5 levels will be consumer choices. Thus, in the coming years, efforts will be directed toward the effective implementation of the Interministerial Ordinance, mainly in curbing the importation of non-compliant motors and the sale of inefficient repaired motors. A better framework of market surveillance plays an important role to achieve this goal.

References

1. G. Soares, M. Pinheiro, R. Shindo, et al., The Target Program for Three-Phase Induction Motors, in Proceedings of Energy Efficiency in Motor Drive EEMODS – 05, Heidelberg, Germany – September 2005
2. G. Soares, C.A. Ferreira, E.A. Costa, M.A. Santos, A.P. Leme, IS IE3 Efficiency Class: A Feasible Next Step for Industrial Motor's MEPS in Brazil? in Proceedings of 8th Energy Efficiency in Motor Drive EEMODS – 13, Rio de Janeiro, Brazil – October 2013
3. MME, Ministério de Minas e Energia, "Portaria Interministerial n° 553, de 8 de dezembro de 2005, Aprova o Programa de Metas de motores elétricos de indução trifásicos, 2005
4. MME, Ministério de Minas e Energia, Portaria Interministerial n° 1, de 29 de junho de 2017, Aprova o programa de metas para motores elétricos trifásicos de indução rotor gaiola de esquilo, 2017
5. ABNT, Associação Brasileira de Normas Técnica, NBR-17.094 – Máquinas elétricas girantes Parte 1: Motores de indução trifásicos – Requisitos, 2018
6. Eletrobras Procel, Relatório Técnico PFP – 014/2015, Estudo sobre Impacto de Regulamentação de Motor Premium, Rio de Janeiro, 2015
7. Eletrobras Procel, Relatório de Resultados do Procel 2018: ano base 2017, Rio de Janeiro, 2018
8. R.S. Vieira, Evaluation of Energy Losses and Characterization of Retail and Maintenance Market Reconditioned Electric Motors in Brazil, Master's Degree Dissertation (PUC-Rio, Rio de Janeiro, 2018)
9. G. Soares, C.A. Ferreira, H.C. Furtado, A. Pedroso, A.P. Leme, Brazilian Experiences in Industrial Induction Motor's MEPS Implementation, in Proceedings of 6th Energy Efficiency in Motor Drive EEMODS – 09, Nantes, France – September 2009

A Decision-Making Tool Incorporating Multiple Benefits of Motor Systems' Retrofits



Rita Werle, Rolf Tieben, Petar Klingel, Andreas Rothen, Lea Fleischli, Victoria Pyatova, Shaun West, Kurt Ackermann, and Richard Phillips

1 Introduction

Electric motor systems are responsible for around 50% of total electricity consumption in Switzerland – and worldwide. In the industrial sector alone, their share of electricity consumption is above 70%. The average savings potential for improving motor systems is around 20–30% [1, 2].

Switzerland implements a CO₂ law and has a system of voluntary target agreements in place since approx. 20 years, with the primary purpose of saving CO₂ emissions. As electricity generation in Switzerland is almost CO₂-neutral (the bulk of this from hydropower and as of now still from nuclear power), in this context, measures for decreasing electric energy consumption were less in the focus of companies, especially measures for improving their electric motor systems.

R. Werle (✉) · R. Tieben · P. Klingel

Impact Energy, Zurich, Switzerland

e-mail: rita.werle@impact-energy.ch; Rolf.Tieben@Impact-Energy.ch; petar.klingel@impact-energy.ch

A. Rothen · L. Fleischli

act Cleantech Agentur Schweiz, Zurich, Switzerland

e-mail: a.rothen@act-schweiz.ch; l.fleischli@act-schweiz.ch

V. Pyatova · S. West

Lucerne University of Applied Sciences and Arts, Lucerne, Switzerland

e-mail: victoria.pyatova@stud.hslu.ch; shaun.west@hslu.ch

K. Ackermann

Zurich University of Applied Sciences, Winterthur, Switzerland

e-mail: acka@zhaw.ch

R. Phillips

Swiss Federal Office of Energy, Ittigen, Switzerland

e-mail: Richard.Phillips@bfe.admin.ch

Investments into improving the energy efficiency of motor systems are hindered by many different barriers; the most significant barriers include technical complexity and associated risk aversion as well as lack of resources (know-how, time, financial resources) at the end users. While investment decisions are considered to focus on financial aspects only, there are other valid reasons for improving machinery, beyond only saving energy and costs.

2 What Are Multiple Benefits?

What are the reasons for improving the efficiency of motor systems? For energy efficiency advocates, cutting energy consumption and thereby contributing to a sustainable future clearly stands at the forefront. For the affected companies, profitability considerations are on top of the agenda. However, there are also numerous other considerations – besides saving costs and energy – that can be strategically important for companies and come hand in hand with efficiency improvements.

The benefits of energy efficiency improvements are not only related to energy but also include non-energy aspects and are often referred to as multiple benefits. Non-energy benefits can have more importance than energy benefits only and ultimately help in convincing company management to invest into energy efficiency – having a positive overall impact on companies' competitiveness. Thus, multiple benefits, which include both energy and non-energy aspects, have a significant potential in triggering the (timely) replacement of existing installations [3, 4].

According to the International Energy Agency [5], there are a wide range of multiple benefits deriving from industrial energy efficiency projects (see Table 1).

Categories and benefits are not listed in order of importance. This is not an exhaustive list.

Next to the IEA, a growing body of research and projects are dedicated to the topic of multiple benefits and to the quantification of these, in an attempt of making these benefits more visible to different stakeholders, including end users (a few examples – non exhaustive [5–12]).

Researchers in Switzerland are also dedicated to this topic. The Lucerne University of Applied Sciences and Arts developed a comprehensive and standardised three-phase methodology to assess the multiple benefits of a wide range of industrial processes and energy efficiency measures. The methodology was validated based on ten case studies performed between 2016 and 2018 in the Swiss industrial sector. The study has shown that the consideration of monetisable multiple benefits may reduce the payback time of energy efficiency measures by up to 40%–85% [13]. The results are expected to inform the 'Multiple benefits for electric motor systems' project.

Table 1 Company-level benefits from industrial energy efficiency projects

Benefit	Description
<i>Competitiveness</i>	
Ability to enter new markets/ increased market share	Overcoming technical barriers to trade or overcoming market perceptions or resistance (e.g. perception about carbon dioxide [CO ₂] footprints)
	Expanded capacity or new product features that enable entrance in new markets
Reduced production costs	Reduced costs per unit or enabling the company to access and capitalise on a new complementary or substitute factor of production and in doing so opening up new opportunities for growth
Deferred plant capital investments	Optimising processes or upgrading equipment or extended equipment lifetime can defer the need for capital costs in replacing equipment. Optimising processes for energy efficiency can also lead to situations where certain equipment is redundant
Corporate risk reduction	Mitigation of corporate risk through reducing liabilities and helping to achieve or go beyond current regulatory requirements
Improved reputation, corporate image	Improved corporate image through publicising energy-efficient (sustainable) business. Improvement of corporate image through CSR that incorporates the wider range of benefits (both private benefits and public benefits)
	Better brand reputation through product or service quality improvements
<i>Production</i>	
Capacity utilisation	More efficient equipment or processes can lead to shorter process times and use of lower cost factors of production (labour and materials), which can lower production costs and enable higher product output
Improved product quality	Downstream improvements in reductions in product defects and warranty claims as well as contributing to enhanced brand reputation
Increased product value	Improved quality and consistency contribute to added value which in turn can contribute to enhanced brand reputation
<i>Operation and maintenance</i>	
Improved operation	Improved operation and process reliability leads to reduced equipment downtime, reduced number of shutdowns or system failures and can entail reduced process time (which can contribute to increased productivity); process optimisation can also reduce staff time required to monitor and operate a processing plant, which reduces overhead costs
Reduced need for maintenance	Energy efficiency projects can lead to investments in new equipment, system optimisation, optimisation or change of processes which in turn can lead to lower maintenance requirements (or avoidance of extraordinary maintenance), reduced costs for maintenance and reduced cost for maintenance materials
<i>Working environment</i>	
Improved site environmental quality	Improved work environment from improved thermal comfort, lighting, acoustics and ventilation. Improved conditions can help retain and attract skilled staff. Improved work conditions and work environment can increase labour output

(continued)

Table 1 (continued)

Benefit	Description
Increased worker health and safety	Process improvements and equipment upgrades implemented as part of energy efficiency projects can reduce the risk and incidence of work-related accidents or negative impacts on worker health. Such improvements can lead to reduced health insurance costs and medical expenses (as well as reduce corporate risk – liability in case of accidents)
<i>Environment</i>	
Reduction of air pollution and emissions	Reducing energy use or optimising processes can reduce sulphur oxides (SO _x), nitrogen oxides (NO _x), carbon monoxide (CO), chlorofluorocarbons (CFCs), hydrofluorocarbons (HFCs), as well as CO ₂ emissions and associated credit or reduced compliance costs. Process changes reduce combustion and process emissions can be important to industry when there are regulatory or compliance issues and associated cost savings include avoiding fines or taxes
Solid waste reduction	Reducing waste streams through, e.g. production improvements and product redesign, improved operation result in less waste, which reduces waste disposal/abatement costs and input materials' purchase cost
Wastewater reduction	Process optimisation, improved operation and improved maintenance can reduce water needed to run processes or water needed for cleaning purposes. Reducing wastewater has environmental benefits but can also entail reduced costs for wastewater treatment
Reduction of input materials, e.g. water	Reduction of input materials reduces upstream environmental impacts from extraction, processing and transport

Source: [5]

3 'Multiple Benefits for Electric Motor Systems': Project Background

3.1 Goal

This paper presents the project 'Multiple benefits for electric motor systems'. This project aims to develop a decision-making tool for motor systems, supporting decision-makers in small- to large-sized companies, incorporating the aspects of multiple benefits. The final product shall be a web-based tool, which is easily available and applicable for the target group.

3.2 Framework

The project is supported by the Swiss Federal Office of Energy (SFOE). SFOE is the national governmental body in Switzerland responsible for establishing Minimum Energy Performance Standards (MEPS) for energy using equipment including motor systems, market monitoring and the design and implementation of

market transformation programmes for energy efficiency via specific policy tools, such as financial incentive programmes, awareness raising, training, etc. This project was chosen to be supported via a public tender, focusing on innovative projects and approaches to advance the increased efficiency of electric motor systems.

3.3 Project Phases

The project is implemented in three phases:

1. Phase 0: In this preparatory phase, the general approach was established, taking into account technical, behavioural and financial aspects. Interviews were conducted with four organisations, laying down the groundwork.
2. Phase I: Following the preparatory phase, relevant multiple benefits will be further elaborated, identified and validated, based on interviews and data analysis. Four applications of motor systems will be analysed, namely, air compressors, cooling compressors, fans and pumps (and in addition as an option variable frequency drives).
3. Phase II: The results of Phase I will be integrated into a web-based decision-making tool.
4. Phase III: Dissemination of the tool to relevant stakeholders.

Up until now, Phase 0 has been concluded. The whole project shall be concluded by mid-2020.

3.4 Project Partners

The project is led by act (Cleantech Agentur Schweiz/Cleantech Agency Switzerland), an energy agency tasked with supporting Swiss companies in the industrial and services sectors to implement target agreements to reduce their energy consumption and CO₂ emissions. Further project partners are as follows:

- Lucerne University of Applied Sciences and Arts (HSLU): bringing in technical, organisational and methodological know-how; responsible for conducting the interviews
- Zurich University of Applied Sciences (ZHAW), bringing in insights from psychology and behavioural economics
- Impact Energy, an independent consulting company focused on energy efficiency in industry and manager of the Swiss information and networking platform Topmotors (www.topmotors.ch), bringing in technical experience from working with industrial facilities

4 Methodology

The approach taken in Phase 0 of the project is as follows:

1. Identification of the target group (see Fig. 1). Following an analysis of the electricity consumption of companies in the industrial and services sectors in Switzerland, the following categories of companies were defined as the target groups of the project:
 - (a) Small-sized companies: 0.1–0.5 GWh/a electricity consumption
 - (b) Medium-sized companies: 0.5–3 GWh/a electricity consumption
 - (c) Large-sized companies: above 3 GWh/a electricity consumption
2. Identification of the different people involved in the efficiency improvement of motor systems within a company: analysis and definition of different ‘personas’, i.e. person profiles of such people.
3. Analysis and definition of ‘trigger events’ or trigger points where actors need to take decisions with regard to their equipment as follows:
 - (a) Regular operation and planned maintenance

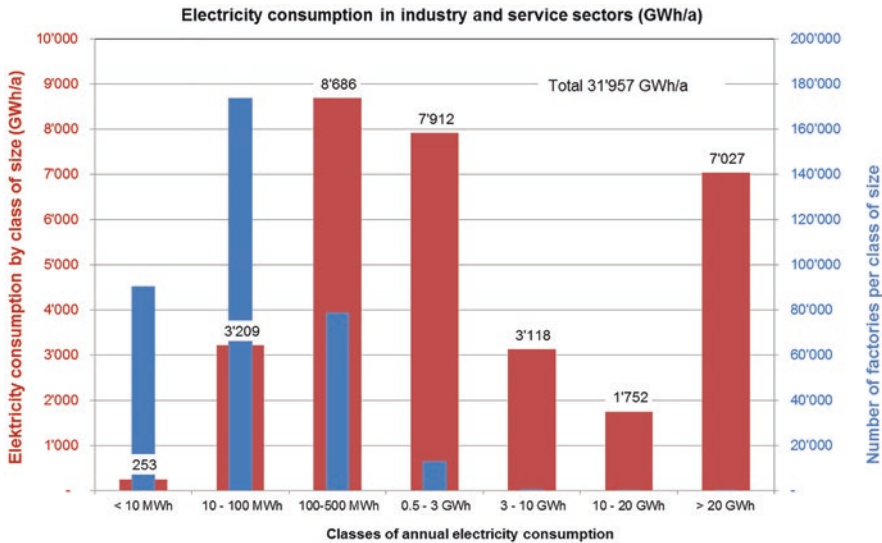


Fig. 1 Electricity consumption and number of companies in Switzerland in the industrial and services sectors. (Source: [2])

Note: the blue bar (and values on right vertical axis) shows the number of all companies within one size category, and the red bar (and values on left vertical axis) shows the total electricity consumption in GWh/a of all companies within one size category. For example, there are only a few factories which consume more than 20 GWh/a of electricity (blue bar almost not visible) and the total consumption of them within this size category amounts to 7027 GWh/a.

- (b) Changes of law (e.g. tighter energy efficiency requirements for motor systems)
 - (c) Unexpected breakdown of equipment
 - (d) Increasing capacity of one machine (upgrade)
 - (e) Modernisation of an entire facility with full system redesign
4. Analysis and identification of methodological approach for the decision-making tool.
 5. Definition of survey questions for the interviews to be conducted.
 6. Conducting first surveys (results if needed will be incorporated for subsequent interviews).

In the subsequent project Phases, the following is foreseen:

7. Conduct further interviews.
 8. Build-up of tool.
 9. Dissemination of the tool.
- (A first report is planned to be delivered at the Motor Summit 2019 Switzerland.)

5 Results

5.1 Preparation

Based on previous research [13], different multiple benefits associated with different replacement reasons were identified.

This was followed by identifying and describing the different personas involved in the efficiency improvement of motor systems within a company. The following main personas were identified:

- Persona 'engineer', further differentiating according to company sizes and responsibilities:
 - Energy manager on-site/for more sites (in case of large company with different sites)
 - Maintenance person
 - Factory or production unit manager
- Persona 'external expert', e.g. supplier (equipment manufacturer, OEM), service provider, engineering consultant
- Persona 'finance', further differentiating into:
 - Procurement
 - Chief financial officer
- Persona 'chief executive officer' (CEO)

For all personas, the following criteria were assessed and described in detail:

- Goal/motivation of actions
- Responsibilities
- Know-how: level of education, technical knowledge
- Resources (people, money, time), i.e. what resources the respective persona can utilize
- Decision power

Then, journey maps for all trigger events in all different-sized companies were drawn. The journey map represents an activity stream (journey) including the actors involved, their job/tasks and information.

The rationale behind drawing journey maps is to identify the points in time where decisions are made and to provide relevant information on the multiple benefits during these points in order to enable an investment decision that leads to increased efficiency. Figure 2 shows the journey map of an unexpected breakdown as an example including the different personas involved.

5.2 Interviews

In a next step, four interviews were conducted with persons (personas) of the following profiles, in four different organisations:

1. Chief executive officer
 - (a) Company profile: automation of chillers and in building technology
 - (b) Interviewee’s responsibilities: provides energy-efficient solutions for refrigerator systems

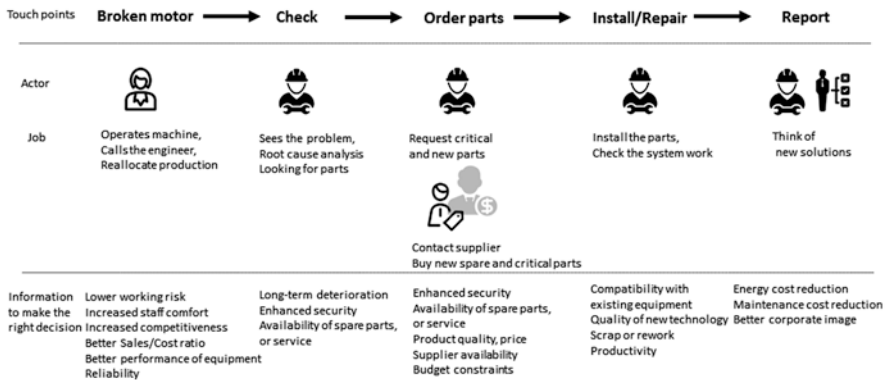


Fig. 2 Journey map in the event of a breakdown in a medium-size company: people involved and potential decision triggers. (Source: [14])

2. Energy efficiency engineer
 - (a) Organisation profile: canton (public authority)
 - (b) Interviewee's responsibilities: consults large-scale industrial energy users (>0.5 GWh/a of electricity consumption) on energy efficiency improvements, helps them to meet regulatory requirements, understands obligations and which actions to undertake and tools to use
3. Chief executive officer
 - (a) Company profile: technical service company
 - (b) Interviewee's responsibilities: works primarily with motor systems; designs technical solutions, strategy, orders and contacts
4. Chief financial officer
 - Company profile: organising luxury cruises and tours, owning different large-sized ships
 - Interviewee's responsibilities: senior finance accountant

The goal of the interviews was to identify and better understand the importance of and satisfaction with multiple benefits that decision-makers associate with more energy-efficient motors.

The interviews investigated the following:

1. Information about the interviewee: daily tasks, motivation, and relevance of work to motor systems.
2. Trigger events: on which occasions did the interviewee consider replacing or upgrading motor systems? Which benefits/risks did the interviewee associate with such replacement/upgrading?
3. Decision-making process for equipment replacement/upgrade: who is involved and what information is needed? Does the interviewee have access to that sort of information? Who would make the final decision?
4. Multiple benefits: what value does the interviewee attribute to the different multiple benefits? For this, benefits with ecological, economical, social and financial aspects were assessed.

Table 2 gives an overview of the interviewees' responses.

During the interviews, interview respondents were asked to assign points from 0 (not relevant) to 10 (highly relevant) to different multiple benefits, assessing both their importance for them and satisfaction with how much these benefits were already exploited. For example, taking the benefit of decreasing time loss due to unscheduled system failures, interview respondents found this an important benefit but were not satisfied yet with meeting it and found that an appropriate measure (motor system optimisation) would help to meet this aspect to a greater extent.

Based on the interview answers, the list of multiple benefits was classified (see Table 3) using the following main categories:

Table 2 Interviewees' responses to survey questions, summary

Interviewee	1	2	3	4
Persona	Chief executive officer	Energy efficiency engineer	Chief executive officer	Chief financial officer
Motivation	Innovation: products that are easy to commission, last long, are energy efficient	Support companies to meet the energy efficiency requirements and go beyond that	Increasing competitiveness and profitability	Increase business value
Relevance of motors in work	High (part of refrigeration system)	Medium (part of energy efficiency)	High (main focus of repair jobs)	High (capital intensive)
Trigger events	Law, government incentives or information campaign, pressure from environmental activists, scandals (machine failure > unsafe food > food poisoning)	Analyses in companies revealing savings potentials, frequent breakdowns, old equipment, high maintenance costs	Government incentives, cost reduction, frequent breakdown	Checking fixed assets (equipment) and replacement needs for budgeting, increased cost of maintenance and repair
Benefits from motor upgrade/replacement	Understanding total cost of ownership, less failure, lower maintenance costs, more floor space available	Energy efficiency, reliability of production, better performance, improved quality, higher profit	Improved production processes, reduced losses, energy cost reduction	Lower repair needs and less unplanned maintenance leading to lower costs and less administration
Risks	Lack of knowledge, conflicts of interest, replacement time after breakdown	None for performance. In financial terms: energy savings can be overestimated (prediction uncertainty)	None in terms of equipment operation. Procurement driven by saving, tend to buy at lower price	Uncertainty associated with new technology and planned investment (prediction uncertainty)
What information would be needed to decide for energy efficiency?	Benchmarking against competitors, education of engineers and managers	Government tools and support, access to information (OEMs catalogue), training. Big companies can afford energy specialist, develop tools for smaller companies	Equipment specifications (data sheet, OEMs catalogue), technical knowledge within companies	Cost and cash forecasting, price negotiation with supplier

(continued)

Table 2 (continued)

Interviewee	1	2	3	4
Personas involved in the decision-making process	Mechanic, controller, facility manager, technical manager, CEO, procurement and finance	Technicians, CEO, chief technical officer, chief financial officer	Finance and procurement	Engineer (technician), CEO, procurement, finance

- Overserved: respondents find these aspects relatively important and are very satisfied.
- Served appropriately: respondents find these aspects important and are satisfied.
- Underserved: respondents find these aspects very important but are not satisfied.

An example for quantifying the multiple benefits associated with motor replacement is shown in Fig. 3. In Fig. 3, the dark orange bar shows the total investment into a new motor, of which the individual elements are represented by the lighter orange bars:

- Purchase price of the motor (65%)
- Shipping cost (10%)
- Installation and commissioning (25%)

The dark green bar shows the multiple benefits, i.e. the sum of all relevant individual benefits. The individual benefits are represented by the lighter green bars, each calculated for the duration of 1 year:

- Energy saving (3%)
- Revenue gain (74%) through increased reliability of production (higher number of production hours thanks to increased hours of machine availability) leading to higher number of produced units
- Reduced waste (22%) through improved production process and less waste generated
- Reduced maintenance and insurance cost (1%) through improved reliability of equipment

6 Outlook

After concluding Phase 0 by now, Phase I of the project is about to be launched with further online and personal interviews, clarifying and validating the multiple benefits identified. The focus in Phase I will be on understanding the priorities set by the different interviewees to improve the classification of the multiple benefits. In Phase II, the findings will be used to elaborate the tool. First results will be presented at the See

Table 3 for the detailed list of classified multiple benefits. Motor Summit Switzerland on 4 December 2019 in Berne. The project is expected to conclude by mid-2020.

Table 3 List of identified multiple benefits and classification according to interview respondents' evaluation

Classification of benefits according to respondents' evaluation
Overserved (relatively important and respondents are very satisfied with these aspects)
Renewal of the manufacturer's warranty
Simplification through standardization
Preparation for emergency replacement (e.g. incompatibility)
Reputation through more stable system
Improvement of plant documentation
Securing the annual targets through high availability of the system
Reduction of operating costs (maintenance and repair costs)
Reduction of energy cost
Avoid non-budgeted expenditures (budget compliance)
Preservation of plant value and modernization
No unplanned write-offs in case of breakdown
Tax optimisation
Reduction of insurance costs (example: risk of loss of production)
Less failures lead to less administrative processes
Served appropriately (important and respondents are satisfied)
Opportunity for innovation
Systematic review of plant design
Improved site environmental quality
Better sustainability rating
Improve operational control
Less maintenance effort, time saving
Improved availability of spare parts and suppliers
Preservation of plant value and modernization
Performance improvement
Increase reliability of workflow / system
Avoid non-budgeted expenditures
Ability to enter new markets/ increased market share
Improved product quality
Personal profiling through innovation
Personal profiling through constant output
Possibility for process optimization
Compliance (law, regulations)
Company reputation / Green signaling
Corporate risk reduction
Increased worker health and safety
Following asset renewal program as planned

(continued)

Table 3 (continued)

Underserved (very important but respondents are not satisfied with current state)
Reduction of energy consumption
Reduce system failure
More stable process handling
Operational cost optimization
Energy cost savings as part of the cost of production
Improved and more reliable margins
Increase production reliability
Ensuring product quality
Availability of floor space
Understanding (predicting) Total Cost of Ownership
Increased product value
Less workload due to unscheduled maintenance work
Building up knowledge / further education / improving internal know-how
Increase competitiveness
Opportunity for process optimization
Decreasing time loss due to unscheduled system failures
Attractive Payback Times / Net Present Value
Investment and financing planning possible
Plannable depreciation and amortization (impact on tax , profit and cash flow payment)

Colour scheme:

Economical aspects
Social aspects
Financial aspects
Ecological aspects

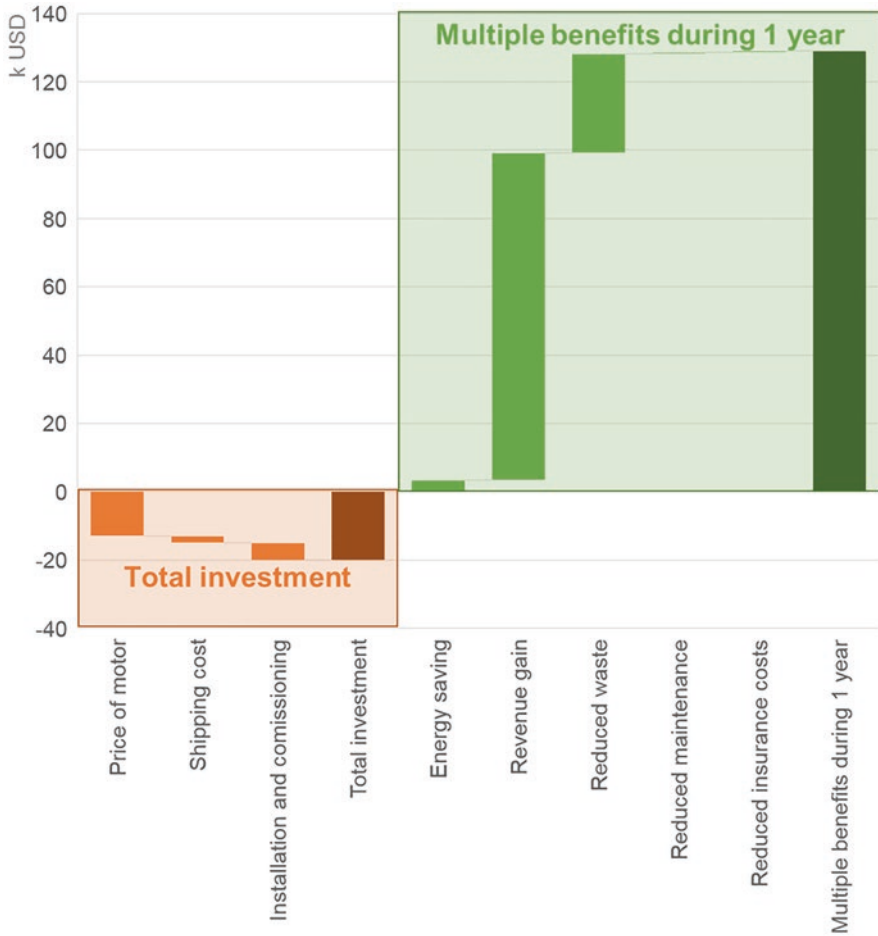


Fig. 3 Example of total investment (20,000 USD) vs. the monetary value of multiple benefits during 1 year (130,000 USD)

Acknowledgements The authors would like to thank the Swiss Federal Office of Energy for the valuable support to the project ‘Multiple benefits for electric motor systems’ and acknowledge all project partners for their important contributions.

References

1. World Energy Outlook, OECD/IEA, Paris, 2016
2. R. Tieben, R. Werle, U. Conrad, Brunner Impact Energy Inc.: EASY- Lessons Learned from Four Years of the Swiss EASY Audit and Incentive Program, in EEMODS, conference proceedings, Helsinki, 2015
3. Management as a Key Driver of Energy Performance – Final Report, 15 November 2017

4. <https://aceee.org/blog/2015/12/multiple-benefits-prove-energy>
5. International Energy Agency, Capturing the Multiple Benefits of Energy Efficiency, 2014
6. E. Gudbjerg, K. Dyhr-Mikkelsen, C. Monrad Andersen, Spreading the Word – An Online Non-energy Benefit Tool, 2014 ECEEE Industrial Summer Study
7. T. Nehler, A Systematic Literature Review of Methods for Improved Utilisation of the Non-Energy Benefits of Industrial Energy Efficiency, 2018
8. E. Andersson, T. Nehler, Energy Management in Swedish Pulp and Paper Industry – Benchmarking and Non-energy Benefits, 2018 ECEEE Industrial Summer
9. Prof Dr. C. Wagner, M. Obermeyer, A Methodology for the Assessment of Multiple Benefits of Industrial Energy Efficiency Measures, under submission (not yet published)
10. www.mbenefits.eu
11. <http://neb.uk.teknologisk.dk/>
12. www.odyssee-mure.eu/data-tools/multiple-benefits-energy-efficiency.html
13. M. Khan, T. Wuest, S. West, et al., Midlife upgrades: A Servitization-enabled, value-adding alternative to traditional equipment replacement, under submission (not yet published). CIRP J. Manuf. Sci. Technol.
14. V. Pyatova, *Multiple Benefits of Motor and Drive Systems Upgrades in Switzerland* (Lucerne University of Applied Sciences and Arts – School of Engineering and Architecture, 2019)

European Ecodesign Material Efficiency Standardization Overview for Circular Economy Aspects in Motor and Power Drive Systems



Martial Patra

Acronym

B2B	“Business-to-business” economical market
B2C	“Business-to-customer” economical market
CEN	European Committee for Standardization
CENELEC (or CLC)	European Committee for Electrotechnical Standardization
CRM	Critical raw material
ECD	Environmental conscious design. See [8].
ErP	Energy-related product
ETSI	European Telecommunications Standards Institute
IEC	International Electrotechnical Commission: International Standards and Conformity Assessment for all electrical, electronic, and related technologies
ISO	International Organization for Standardization
LLCC	Least life cycle cost
MEErP	Methodology for Ecodesign of Energy-related Products
PDS	Power drive system
VSD	Variable speed drive

1 Introduction

Environmental trends and weather changes likely go to a global warming and with the lack of natural resources make current economic models mandatory to evolve. This will impact businesses for motors, variable speed drive systems, and applicative

M. Patra (✉)
Standardization Manager, Schneider Electric, Paris, France
e-mail: martial.patra@se.com

sectors' equipment they are a part thereof like pumps, compressors, fans, conveyors, or other machinery.

For centuries, the basic economical scheme “cradle-to-grave” consisted of extraction of raw materials and natural resources from earth to produce and use products and equipment and, finally at the end of life, to go for disposal of goods in landfill. The trend is now to change for a cradle-to-cradle economic model consisting of closing the loop of the product life cycle for a more sustainable economic practice. This trend is supported more and more by new regulations published worldwide. Several regulatory initiatives are already considered or will be initiated soon.

In Europe, the European Commission circulated end of 2015 a communication document [1] to express its strategy: “Closing the loop – An EU action plan for the Circular Economy.” This paper described that the revised legislative proposals on waste treatment and the Ecodesign Directive 2009/125/EC are key regulations for impacting energy-related products (ErP), aiming to a reduced environmental footprint. It was said from that time that in industry, the resource productivity and the material efficiency improvement within the economic value chains could reduce the material input needs by one fifth to one fourth by 2030 and should represent a potential cost saving of about €630 billion per year for the European industry [2].

2 Ecodesign Standardization Request on Material Efficiency to Support Circular Economy

At the same time, end of 2015, the European Commission published a Standardization Request (M/543) [3] that is a mandate directed to the European standardization organizations for drafting a set of ecodesign horizontal standards to support the material efficiency aspects for a more circular economy. The objective of the standardization work from this request is linked to the three following objectives:

- (a) Extending product lifetime
- (b) Ability to reuse components or recycle materials from products at end of life
- (c) Use of reused components and/or recycled materials in products

The CEN, the CENELEC, and the ETSI standardization organizations agreed early in 2016 for preparing such horizontal standards for dealing with the different material efficiency topics described in the M/543 mandate that should be applicable to electrotechnological (ErP managed by CENELEC) and non-electrotechnological (ErP managed by CEN) products that are already covered by different regulations under the application of the Ecodesign Directive [4], as well as for information technology (equipment managed by ETSI). The material efficiency topics we consider are as below:

- The definition of parameters and methods relevant for assessing durability, upgradability, and ability to repair, reuse, and remanufacture products

- Provision of guidance on how standardization deliverables for assessing durability, upgradability, and ability to repair and remanufacture products can be applied to product-specific standards
- The ability to access or remove certain components, consumables, or assemblies from products to facilitate repair or remanufacture or reuse
- The reusability/recyclability/recoverability (RRR) indexes or criteria
- The ability to access or remove certain components or assemblies from products to facilitate their extraction at the end of life for ease of treatment and recycling
- The method to assess the proportion of reused components and/or recycled materials in products
- The use and recyclability of critical raw materials to the EU, listed by the European Commission
- The documentation and/or marking regarding information relating to material efficiency of the product considering the intended audience (consumers, professionals, or market surveillance authorities)

These different material efficiency aspects feed the three main principles of the circularity and are also consistent with some of the sustainable development goals defined by the United Nations [5] (in particular, Goal 12: Responsible consumption and production). The three main functions of circularity are well described by the Ellen MacArthur Foundation [6] and can be expressed as below:

1. Design and manufacture out of waste and pollution:
 - Energy savings (*now well covered for motors, VSD, pumps, and other ErP*)
 - Lowest environmental footprint associated with reference lifetime linked to conditions of use
2. Keep materials, products, and system in use:
 - Optimized conditions of use to reach the expected durability
 - Repair, reuse, and upgrade
3. Regenerate natural system:
 - Remanufacture
 - Recycle and recover

These three principles above are assessed all along the product and systems' life cycles as visible in Fig. 1. And what is important to consider is that the optimized environmental footprint for effective circularity needs a trade-off between items of the three main functions, considering the physical and digital product and system mission profiles, with risk assessment for the design by considering the functional analysis and operating conditions. Also, it should be reminded that always the safety is the priority [7].

In collaboration between CEN and CLC, a tenth standardization joint Technical Committee (CEN-CLC/JTC 10: Energy-related products – Material Efficiency Aspects for Ecodesign) has been established in 2016 for drafting a set of ten standards and technical reports within the EN 4555x series that are the following documents already published or still in work by European experts:

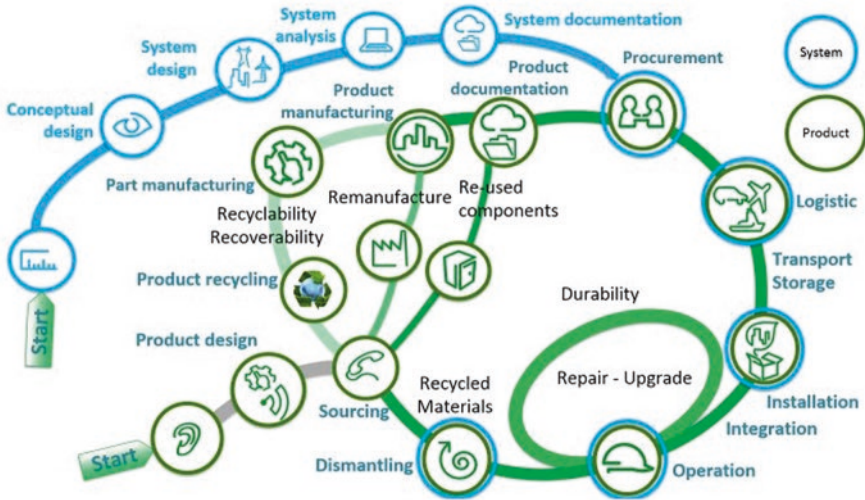


Fig. 1 Product and applicative system life cycle

- EN 45550: Terms and Definitions related to Material Efficiency of ErP
- EN 45552: Methods for assessment of durability
- EN 45553: Methods for assessment of ability to remanufacture
- EN 45554: Methods for assessment of ability to repair, reuse, and upgrade
- EN 45555: Methods for assessing the recyclability and recoverability
- EN 45556: Methods for assessing the proportion of reused components
- EN 45557: Methods for assessing the proportion of recycled material content
- EN 45558: Methods to declare the use of critical raw materials
- EN 45559: Methods for providing material efficiency information

Using a simplified product and applicative system life cycles, Fig. 2 shows how a set of material efficiency horizontal standards covers the assessment along these life cycles and interactions between their different steps.

3 Detailed Description and Purpose of the Horizontal EN 4555x Standard Series

3.1 A Set of Material Efficiency Standards Covering Assessment of ErP

First it is important to notice that the EN 4555x standard series describes some methodologies and provides some requirements for only the assessment of the individual material efficiency aspects of ErP, but does not provide requirements for a material-efficient environmental conscious design [8] (ECD) or for global circular

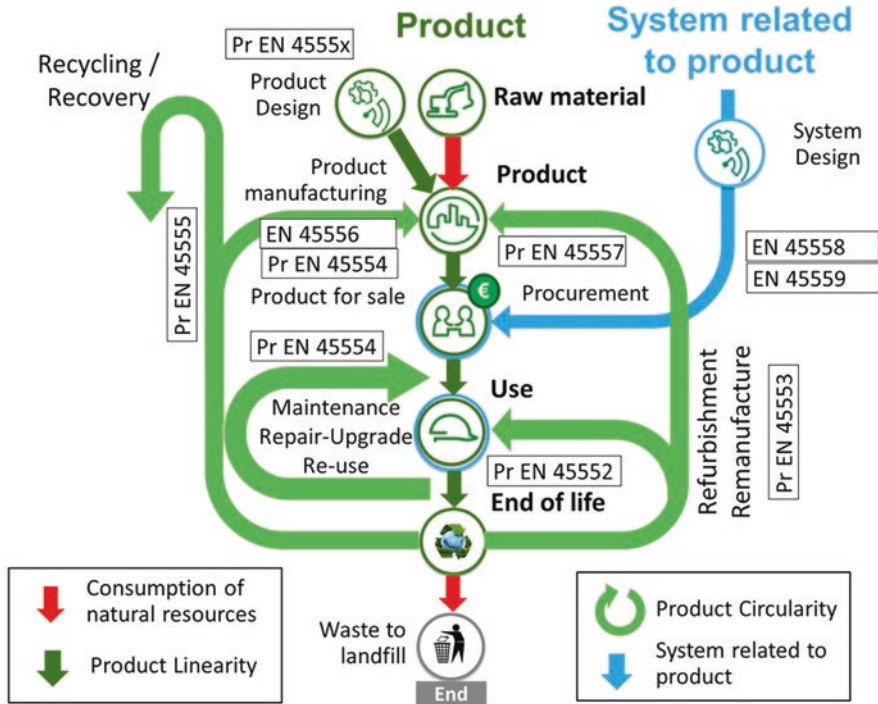


Fig. 2 Product and systems’ life cycles with circularities covered by EN 4555x series

economy aspects that are more considered today at the worldwide international level within IEC/TC 111 Committee with reference to the IEC Guide [9] 109 (environmental aspects) in collaboration with ISO/TC 207 (Environmental Management). For an optimized product and system environmental footprint, it would be critical to link and evaluate the interaction of all these Material Efficiency aspects as well as other aspects (like digitization, energy consumption, or energy saving capability) for reaching an optimized [10] design for circularity as shown in Fig. 3.

These EN 4555x European standards are horizontal (considered as generic) documents in the way they do not apply to any particular ErP but provide a common agreed methodology to assess all various ErP that are, for instance, IT or white goods for household applications (like washing machines, water heaters, televisions, or other products dedicated to the business-to-customer market) but that are also more industrial ErP equipment (like electric motors, variable speed drive systems, pumps, ventilation units, compressors, or others products dedicated to the business-to-business market).

Even if some of these material efficiency standards could be directly used for an ErP equipment, they should be, by nature, be derived for becoming product-specific standards in order to address the assessment of material efficiency aspects in a more specific way.

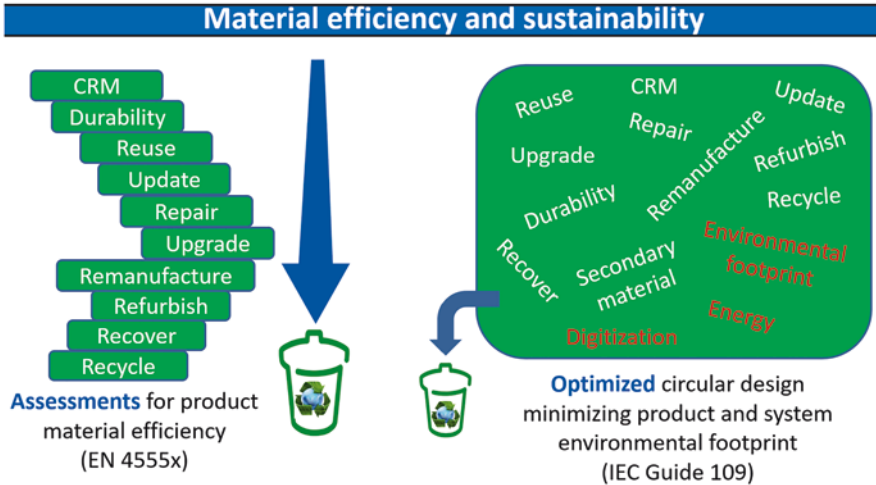


Fig. 3 Material efficiency assessment versus design optimization for circularity

3.2 Detailed Content of EN 4555x Series

Considering the particular material efficiency topics covered by each of the EN 4555x horizontal standards, their complete title, with a short abstract, consideration, and status are given below:

- **EN 45550** (Technical Report)
 Definitions related to material efficiency:
 It will be a collection of common terms that should provide a single definition of key terms used in different EN 4555x standards. But possibly two similar terms could not have a unique definition depending on the particular EN 4555x standard's context.
Status: This technical report will be submitted for voting when all other standards are approved to ensure that the definitions in the TR are exactly the same as the definitions in the other EN 4555x series.
- **EN 45552**
 General method for the assessment of the durability of energy-related products:
 The user of this horizontal standard (that should be an ErP product standardization technical committee) shall consider and select the functions that are representative of the ErP they focus on (based on the environmental and operating conditions issued from the ErP Mission profile) that will become the input for the reliability and the durability of the product. Figure 4 suggests, as example, some limiting events and actions that make the product or system moving from functional states to limiting states and finally reaching its end of life.
Status: This standard will be submitted for the final stage (formal vote) in 2019-09 and if voted positive should be published by March 2020.

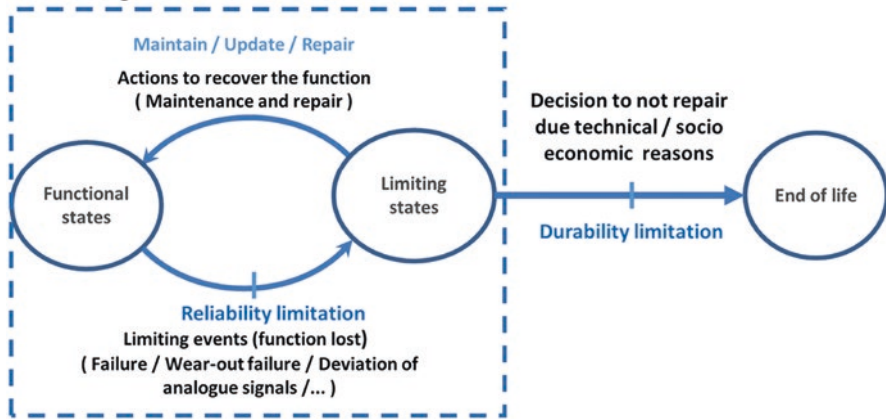


Fig. 4 Limiting events and actions impacting the ErP operating status

- **EN 45553**

General method for the assessment of the ability to remanufacture energy-related products.

This standard describes assessment and process of remanufacturability of ErP. Refurbishing (no significant changes) versus remanufacturing (significant changes) is defined, but still not clear when considered from legal aspect. “Product significant change” is controversial. A correct assessment can only be done in a product-specific way, considering specific parameters of a specific ErP. This is particularly true when considering a motor, a VSD, a complete pump, or a fan system.

Status: The formal vote on the final stage disapproved on 2019-08-16 the current version of this standard. A CEN/CLC/JTC 10 decision is waited for considering further actions.

- **EN 45554**

General methods for the assessment of the ability to repair, reuse, and upgrade energy-related products.

This standard is only generic, providing options allowing for the selection of assessment types (semiquantitative, quantitative, and qualitative assessments are possible) and criteria as appropriate for each product group. From all parts, the user shall identify the ErP-prioritized parts to be possibly repaired, reused, or upgraded.

Status: After a negative vote on the public enquiry, this standard will be submitted for the final stage (formal vote) in 2019-09 and if voted positive should be published by March 2020.

- **EN 45555**

General methods for assessing the recyclability and recoverability of energy-related products.

The user of this standard shall select the potential end-of-life treatment scenario of the product he/she considers. The ability of an ErP to be recycled and recovered depends upon factors like ErP design characteristics, combination of techniques for recycling or recovering ErP content, interaction with existing local applicable regulations, as well as industry practices, etc.

Status: This standard has been submitted for the final stage (formal vote) and has been approved on 2019-09-05. The next step is now for the publication.

- **EN 45556**

General method for assessing the proportion of reused components in energy-related products.

It is clear that this standard shall be derived in product-specific standards for determination of ratio for reused component. Also, product committees like for motors, VSD, or pump system should define the assessment criteria attached to each reused component by considering the mission profile of the ErP. In particular, specific criteria should be attached to “active components” that cannot be similar to criteria for “passive components.”

Note: Active components are, e.g., power electronic semiconductors, capacitors, and moving mechanical parts. Passive components are, e.g., resistors, inductors, static mechanical parts, etc.

Status: This standard has been approved and published on 2019-06-07.

- **EN 45557**

General methods for assessing the proportion of recycled material content of energy-related products.

The recyclability can be considered by quantity of parts that are recyclable, but the mass could be also considered, and the pre-consumer versus post-consumer content is key with documented data for relevant information. Because of various ErP equipment, product-oriented standards are necessary for this topic too.

Status: After a negative vote on the public enquiry, this standard will be submitted for the final stage (formal vote) in 2019-09 and if voted positive should be published by March 2020.

- **EN 45558**

General method to declare the use of critical raw materials in energy-related products.

This standard can be applied directly for each different ErP, as it provides a standardized format for reporting of use of critical raw material (CRM) in ErP by applying directly the EN/IEC 62474 standard for declaration. Regulated CRM are considered in the way that specific regulatory [11] requirements are set for them (in Europe, a list of 27 CRM has been published in 2017, including such CRM like antimony, cobalt, heavy rare-earth elements, tantalum, gallium, natural rubber or graphite, etc.). But non-regulated CRM can be also considered through this standard.

Status: This standard has been approved and published on 2019-03-01.

- **EN 45559**

Methods for providing information relating to material efficiency aspects of energy-related products.

This standard provides a common methodology for producing information on ErP covered by the EN 4555x series. It also describes a generic methodology for product-oriented technical committees that should create a communication strategy for their specific products like for motors, VSD, or pumps.

Status: This standard has been approved and published on 2019-03-01.

4 Consideration of Product-Specific Standards for Motors, VSD, and Their Applications

4.1 Product-Specific Standards Derived from EN 4555x Series

From the previous short descriptions of the EN 4555x horizontal standards for material efficiency aspects applicable for ErP, it is more than likely that they need to be adapted to specificities of each product, systems, or equipment. Consequently, it is supposed that every standardization product committees at European CEN and CLC or at international IEC and ISO levels would consider the benefit to prepare and draft a unique document or a complete set of similar standards for the assessment of material efficiency of ErP covered by their scope. For instance, for power electronic systems and equipment covered by IEC/TC 22 Committee, the topic of material efficiency aspects for power electronics (PDS with VSD, but also for UPS or Power supplies) will be discussed during the next TC 22 plenary meeting of 2019-10-25.

A guideline on how to consider the assessment of each material efficiency topic and the way to use each individual document has been embedded within each EN 4555x standard. Consequently, the CEN-CLC/JTC 10 Committee cancelled the project EN 45551 that was expected to become a general guideline for that purpose.

Nevertheless, because of lack of experts and for providing and explaining the global context of material efficiency for circular economy of ErP, a guideline to support the standardization work to be drafted at level of each ErP technical committee has been considered very useful. Then, the European CEN-CLC Ecodesign Coordination Group (CEN-CLC/Eco-CG) will expose this objective and will submit a call for experts for drafting a material efficiency guidance that should be used by technical committees for supporting their efforts. National committee and technical committee officers should discuss this proposal with decision during the next CEN-CLC/Eco-CG plenary meeting of 2019-12-05. If agreed, a possible Eco-CG/WG6 team would be set up for delivering such a guidance.

4.2 *Future Harmonized Standards Covering Ecodesign Regulations*

The European Commission is currently preparing an updated regulation for motor and drives (Ecodesign/EC/ENER Lot 30), implementing the Ecodesign Directive. In the most recent draft [12], no particular material efficiency requirement is included, but for the next revision of the ecodesign requirements for motors and variable speed drive systems, it should be considered the possible following request:

- *Setting additional resource efficiency requirements for products in accordance with the objectives of the circular economy, including identification and reuse of rare earth in permanent magnet motors*

This is why particular material efficiency standards for motors and for VSD could be useful as international and European harmonized standards to adapt the material efficiency horizontal EN 4555x series to the particular needs for motors, VSD, as well as for pumps and other applicative sectors' equipment.

4.3 *Future of EU Regulation Process for Ecodesign (MEErP)*

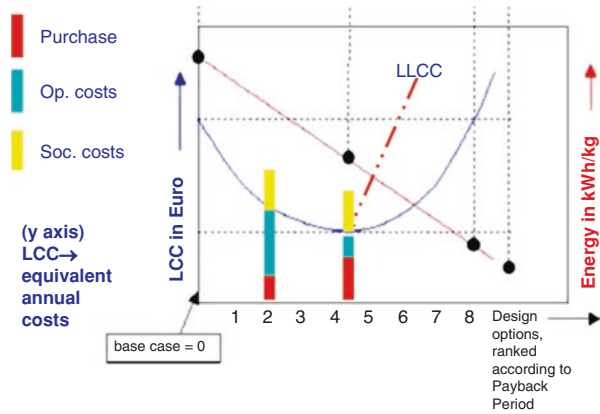
The European Commission organized last 2019-05-28 a workshop on the MEErP (the regulatory Methodology for Ecodesign of Energy-related Products). This workshop was dedicated to the reinforcement of circular economy aspects in the methodology and particularly how to consider the way the material efficiency can be assessed from the regulation point of view for implementation in the future ecodesign regulation for ErP. It was of importance and discussed the way that no contradiction should arise from material efficiency aspects but also from other aspects like the energy efficiency performance requested already from regulations for most of ErP.

Especially, consideration of the least life cycle cost analysis (LLCC) was discussed for an effective trade-off between three objectives:

- The cost that impacts manufacturers (and customers) when ErP are put on the market
- The cost (and related energy savings) that impacts the users during the ErP life operation
- The societal cost (meaning the impact on environment for air, water, ground, biodiversity), on people's health, employment, etc.

Figure 5 shows [13] by combination of the three above cost factors the equivalent overall life cycle cost (LCC) reached for optional payback periods. Studies should start to carefully consider the LCC ranking for establishment of the best regulatory proposals including material efficiency aspects.

Fig. 5 Ranking of ErP life cycle cost (LLCC) considering design options



Particularly, for motor power drive systems (PDS), it is said for a long time that the overall benefit for energy saving is obtained through the extended product approach at the applicative sector level (as described in the EN IEC 61800-9-1 standard), for instance, at pumps, fans, or compressors’ system, by using motors and VSD at the most efficient system operating point of the equipment they are used for. For instance, the energy efficiency performance objective to reach for motors has an impact on the type of materials and their quantity in the motor. If material efficiency objectives are so stringent that any new energy efficiency requirement for better performance of motors cannot be reached anymore, then compliance to regulation could be problematic, even could possibly be impossible.

Therefore, trade-offs between energy efficiency performance and material efficiency aspects should be carefully considered. And further ErP preparatory studies to be conducted by the European Commission should consider LLCC for optimization of requirements in regulations.

5 Conclusion

This paper exposed the new standardization work performed on material efficiency aspects for circular economy in Europe within the standardization organizations CEN and CENELEC under the referenced EN 4555x series. This set of eight plus one standards and technical report is established for the assessment only of ErP products as horizontal standards. Some of these material efficiency standards have been temporarily rejected for being improved but they are still considered useful.

It should be understood, for an optimal applicability, that they should be derived in product-specific material efficiency standards, for instance, for motors, for PDS, and for their applicative sectors’ equipment like pumps, fans, or compressors’ systems. Also, it is necessary to consider trade-offs between energy efficiency performance and material efficiency performance of such ErP products and systems for ensuring compliance with current and future ecodesign regulations.

References

1. European Commission Communication COM (2015) 614 final 2015/12/02: Closing the loop – An EU action plan for the Circular Economy
2. European Commission Communication COM (2014) 398 final 2014/07/02: Towards a circular economy: A zero waste programme for Europe
3. COMMISSION IMPLEMENTING DECISION M/543 of 2015/12/17 on a standardization request to the European standardization organizations as regard Ecodesign requirements on material efficiency aspects for energy-related products in support of the implementation of Directive 2009/125/EC of the European Parliament and of the Council
4. DIRECTIVE 2009/125/EC OF THE EUROPEAN PARLIAMENT AND OF THE COUNCIL of 2009/10/21 establishing a framework for the setting of Ecodesign requirements for energy-related products. (recast)
5. United Nations 17 Sustainable Development goals: <https://www.un.org/sustainabledevelopment/sustainable-development-goals/>
6. The Ellen MacArthur Foundation.: <https://www.ellenmacarthurfoundation.org/>
7. ELTEE 2018: International conference on Evolution Performance & Expected Lifetime of electrical equipment, 16–17 Oct. 2018 (EU CEN-CLC standardization on material efficiency for longer lifespan within the circular economy: By Thierry Cormenier & M. Patra; C. Garnier – Schneider Electric – France)
8. Environmental Conscious Design (ECD): covered by the joint working group “JWG ECD” for developing the standard IEC/ISO 62430: Environmental Conscious Design (ECD) – Principles, requirements and guidance. The JWG ECD is established between IEC/TC 111 Committee (Environmental standardization for electrical and electronic products and systems) and ISO/TC 207 Committee (Environmental Management)
9. IEC/Guide 109: edition 3.0 of 2012–06: Environmental aspects – Inclusion in electrotechnical product standards
10. CIRED: 25th International Conference on Electricity Distribution: Madrid, 3–6 June 2019. “MATERIAL EFFICIENCY FOR CIRCULAR ECONOMY: FROM ASSESSMENTS TO OPTIMIZATIONS”. By Mr. Thierry Cormenier – Schneider Electric – France
11. Communication from the European Commission on the 2017 list of Critical Raw Materials (CRM) for the EU. <https://eur-lex.europa.eu/legal-content/EN/TXT/PDF/?uri=CELEX:52017DC0490&from=EN>
12. Ecodesign ENER Lot 30: Draft Commission Regulation D060021/02 laying down Ecodesign requirements for electric motors and variable speed drives pursuant to Directive 2009/125/EC of the European Parliament and of the Council, amending Regulation (EC) No 641/2009 with regard to Ecodesign requirements for glandless standalone circulators and glandless circulators integrated in products and repealing Commission Regulation (EC) No 640/2009
13. European Commission workshop on “The future of the MEErP” in Brussels on 2019-05-28: Presentation of “Design options ranking and the inclusion of material efficiency aspects” by Davide Polverini (European Commission: DG GROW Unit C1: Clean technologies and products)

Comparison Between the Use of the Middle Ring and/or Skewed Bars in Induction Motor Rotor



Marcelo Dias da Silva, Daniel Schmitz, Carlos Manuel de Araújo Sá, Bruno Baptista, and Sebastião Lauro Nau

1 Introduction

Induction motors have been subject to continuous improvement since their invention more than one hundred years ago. The gains have been achieved by using better electromagnetic and insulating materials and the development of new designs for many parts of the machine, including the rotor bars and end rings.

Several designs have emerged regarding the squirrel-cage of the rotor, most of them focused on skewed bars or on the use of a middle ring. These solutions brought improvements to some performance characteristics of induction motors [1–4]. For instance, the use of only skewed bars or the use of skewed bars and a middle ring in a rotor tends to reduce significantly the electromagnetic noise produced by the motor as well as to reduce the torque ripple produced during steady state.

However, the use of these new solutions also brings some disadvantages, like the reduction of the starting and rated torque of the motor, because of the increase of the leakage flux. The increase of the leakage flux is an important issue in induction motor design. Several methods have been developed with the objective to quantify and take into account the influence of skewed bars on the leakage flux, as well as their influence on the magnetic saturation and the inter-bar currents [5–9]. To maximize the improvements provided by skewed bars and by the use of the middle ring,

M. D. da Silva (✉) · B. Baptista
WEGeuro Indústria Elétrica, Maia, Portugal
e-mail: marcelo.silva@angstrom.uu.se; brunoricardo@weg.net

D. Schmitz · S. L. Nau
WEG Equipamentos Elétricos, Jaraguá do Sul, Brazil
e-mail: daniels1@weg.net; slnau@weg.net

C. M. de Araújo Sá
Faculdade de Engenharia da Universidade do Porto, Porto, Portugal
e-mail: cas@fe.up.pt

it was discussed in [10, 11] what were the most effective details in this new skewed rotor.

Although many theoretical predictions have been done in this field, laboratory tests are not easily found. However, this chapter is based on laboratory tests. It contributes with data from steady state performance, torque-speed, and noise test at rated load produced in one motor using four different rotors. Analyzing this data set, it is possible to discuss more deeply the influence of the use of skewed bars and middle ring in rotors of induction motors, as well as compare these results with some of the predictions made in the references mentioned above.

2 Theoretical Prediction

2.1 Skewed Bars vs Straight Bars

It is expected that a motor with a straight-bar rotor will have high efficiency and low slip [2]. However, it will also present high harmonic content on the air-gap magnetic flux, a torque with a large ripple, and higher magnetic noise. The high efficiency is due to the fact that the equivalent reactance of the rotor is smaller when compared with skewed rotors.

The rotors that have skewed bars will have a lower harmonic content on the air-gap magnetic flux than the rotors with straight bars, and consequently a reduction on the electromagnetic noise produced by the motor [12]. The skew factor (k_i) for the harmonic with pair of poles λ is the ratio between the flux for straight and skewed slots. It can be expressed according to Eq. 1:

$$k_i = \frac{\sin\left(\lambda \cdot \frac{\gamma_s}{2}\right)}{\lambda \cdot \frac{\gamma_s}{2}} \quad (1)$$

where γ_s is the skew angle relative to the air gap circumference. The skew angle can also be calculated according to Eq. 2, considering the skew of the rotor bar (sk) in mm and the inner diameter of the stator (D_i) in mm.

$$\gamma_s = \frac{2 \cdot sk}{D_i} \quad (2)$$

Additionally, the skewed bars will reduce the resultant torque and can give rise to an axial force component that can reduce the service life time of the motor [2, 11]. The skewed-bar rotor will have a bigger slip for the same load than the straight-bar

rotor [2]. Due to the higher slip of the rotor, current will increase, along with additional rotor Joule (I^2R) losses. As the bars are not parallel with the shaft of the motor, the air-gap flux density has an axial variation, which will produce areas with a higher magnetic saturation in the rotor [5].

Due to the negative effects in motor efficiency produced by the skewed bars [13], the skew angle must be carefully chosen, which must not be bigger than what is necessary for the motor to meet the requirements.

2.2 Use of Middle Ring

The use of a middle ring in squirrel cage rotor allows the electrical current flowing in the bars to better adapt to the air-gap magnetic flux at every instant. This will reduce the inter-bar currents [14], and therefore improve the efficiency of the motor [2]. Additionally, the use of the middle ring will also contribute to the mitigation of the harmonic content in the air-gap magnetic flux [2]. Although, the use of the middle ring will diminish the magnetic flux density in the half-length of the rotor, because the aluminum has a magnetic permeability much smaller than the iron. This will bring a bigger no-load current and a lower power factor [2].

3 Models in Analysis

Before starting the prototype building process, it was necessary to select which designs of the squirrel cage should be tested. As the objective of this chapter is to understand the influence of the skewed bars and the middle ring on the induction motor performance, it was important to choose designs that allow the study of these two different solutions independently. The designs examined in other scientific articles about this topic, such as [2, 4], and the nowadays industrial solutions were also considered. The four selected designs are detailed in the following sections.

3.1 Skewed Bars (*skb_nr*)

This solution was widely studied in several scientific papers and used as a standard solution in some commercial induction motors. In this rotor, all the bars of the squirrel-cage present the same skew regarding the shaft of the motor. The rotor bar skew was chosen aiming to efficiently reduce the electromagnetic noise produced by the motor. It is illustrated in Fig. 1a.

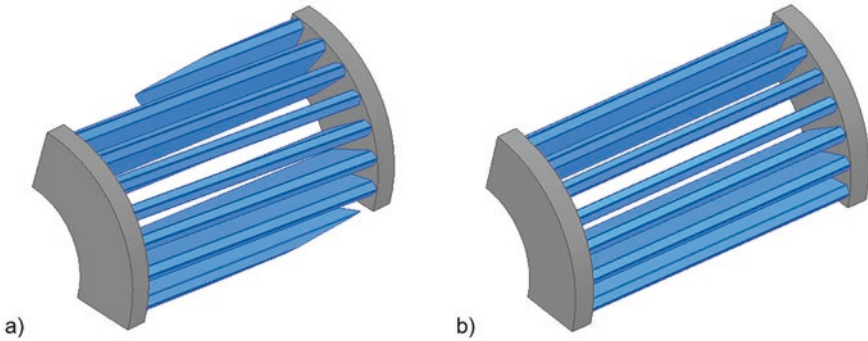


Fig. 1 Representation of a segment of a rotor. (a) Skewed bars; (b) Straight bars

3.2 *Straight Bars (stb_nr)*

This rotor was used as the control solution. The bars of this rotor are parallel to the shaft of the motor, presenting no skew angle, and connecting the two short-circuit rings located on both ends of the rotor. It is illustrated in Fig. 1b.

3.3 *Straight Bars and Middle Ring (stb_r)*

The inclusion of these rotors aims to understand the influence of the use of a middle ring in a squirrel-cage rotor. All the bars are straight and parallel to the motor shaft, but there is a middle ring that short-circuits all the bars, located at the half-length of the rotor. In this middle ring, the bars also present a stagger angle. This stagger angle is defined in the circumferential direction and measures the angular distance between two consecutive bars, each one from a different side of the middle ring. It is illustrated in Fig. 2a.

3.4 *Skewed Bars and Middle Ring (skb_r)*

This rotor uses both characteristics studied in this chapter. It has skewed bars and also a middle ring, presenting same stagger angle. With this rotor, the objective is to test the hypothesis that these two designs have a redundant effect on the performance on the steady state on induction motor. It is illustrated in Fig. 2b.

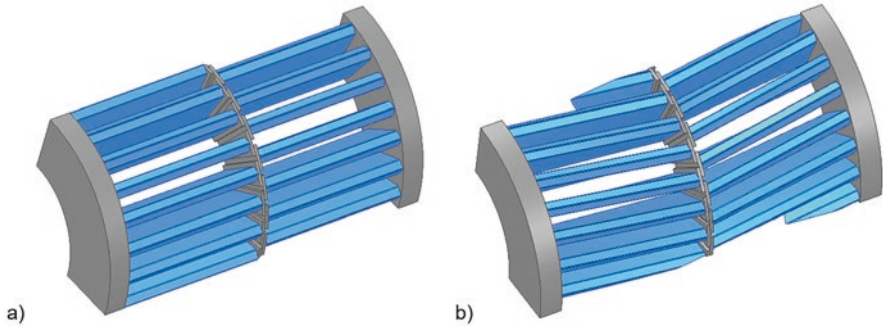


Fig. 2 Representation of a segment of a rotor. (a) Straight bars and middle ring; (b) skewed bars and a middle ring

4 Sizing of the Models in Analysis

4.1 Skew Angle

In [1, 10] it is presented that the skew angle which produces a more efficient effect on the reduction of electromagnetic noise is the one with a value similar to the stator slot pitch. To compare the performances of alternative motor designs, the skew angle was sized to be equal to one stator slot pitch.

4.2 Stagger Angle

The value of the stagger angle was defined using the same principles used for the skew angle. According to [10], it is concluded that half of the slot pitch is the optimal value of the stagger angle, so the same value is used in the design of the rotor included in this study.

4.3 Middle Ring

The process of sizing the middle ring is more complex than the process of defining the previous angles. The middle ring cannot be oversized, because it will cause an increase in the saturation of the magnetic core of the rotor.

The current, at the end of each bar, will split in two directions, corresponding to the two adjacent bars on the opposite side of the middle ring, as shown in Fig. 3. The figure of electrical current distribution was obtained from numerical simulations using the finite element method.

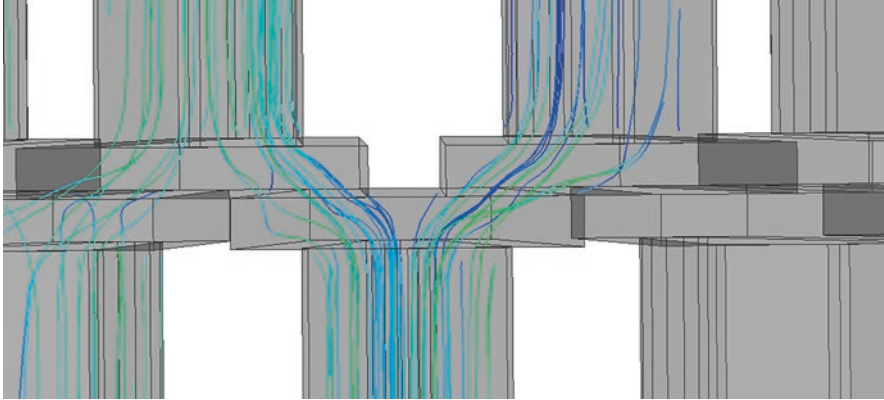


Fig. 3 Distribution of the electrical current in the middle ring

Therefore, it is important to guarantee that the cross-section of the middle ring is not smaller than the half cross-section of the bars, avoiding the increase of the rotor Joule losses.

Considering these constraints, it was decided to size the cross-section of the middle ring to avoid an increase in the rotor Joule losses, using a shape that minimizes the total volume of the middle ring.

5 Characteristics of the Machine

The motor used in this chapter was chosen taking into account the production cost and rated power of the prototypes. For the purpose of studying the distribution of the losses, the rated power could not be too low, because the difference between the losses measured with the different rotors could be significantly affected by the measuring accuracy of the equipment.

For the purpose of the laboratory tests, the same stator was used, and the rotors were changed. The stator is the same used in an ordinary three-phase induction motor with four poles and 36 slots. The stator winding is single layer with concentric coils.

Although four different rotors were tested, all of them share some characteristics, like 28 slots and aluminum single cage with deep rotor bars. The shape of the bars is also identical for these four rotors. Table 1 presents the rated characteristics of the machine tested.

Table 1 Rated characteristics of the machine

Quantity	Unit	Value
Power	<i>kW</i>	5.5
Voltage	<i>V</i>	Y 380/ Δ 220
Frequency	<i>Hz</i>	60
Current	<i>A</i>	Y 11.8/ Δ 20.4
Torque	<i>N.m</i>	30.2
Speed	<i>Rpm</i>	1740
Power factor ($\cos\varphi$)	–	0.79
Efficiency (η)	%	90.0

6 Laboratory Tests

The four prototypes described above were subjected to several laboratory tests, like performance test in steady state, torque-speed curve, and noise test at rated load. To reduce the influence of external factors on the laboratory results, the same stator was used for testing all the different rotors. The laboratory tests procedures were the same for all the different prototypes. They were done three times for each prototype, and had one prototype for each of the models analyzed, as shown in Fig. 4.

6.1 Performance Test

The performance test was based on IEC 60034–1—Rotating Electrical Machines—Part 1: Rating and Performance [15]. The input power, the rotation speed, and several components of the losses were the parameters analyzed. During the performance test of each prototype, information was collected regarding different load factors: 150%, 125%, 100%, 50%, and 25%.

6.2 Torque-Speed Curve

This test was based on the IEEE 112 – Test Procedure for Polyphase Induction Motors and Generators [16]. In this test, the objective was to trace the curve relating the torque with the rotation speed of the motor. However, due to the limitations of laboratory equipment, this test was done using 260 V (Y) at 60 Hz, instead of rated voltage.

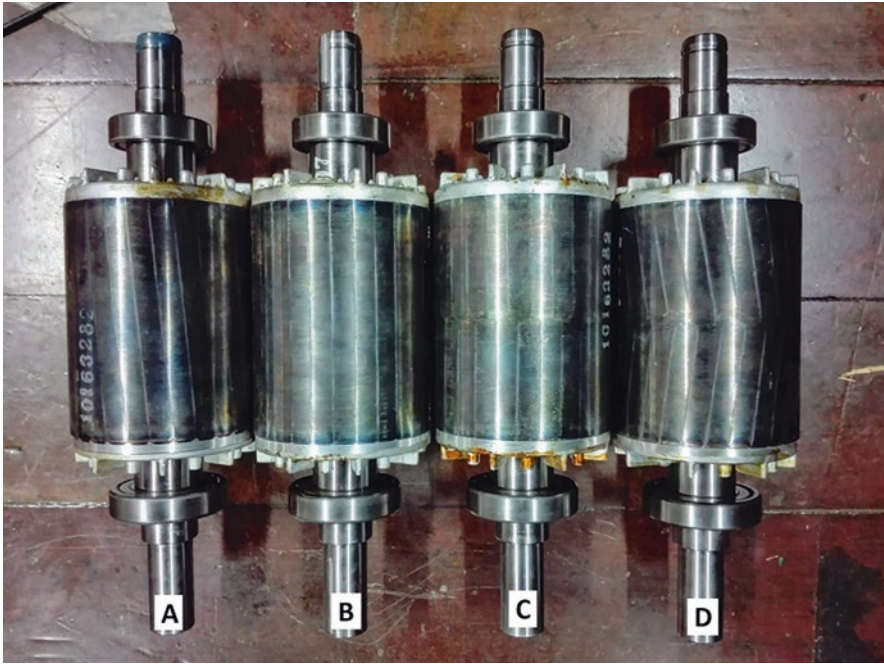


Fig. 4 Prototype for each of the models analyzed. (a) Rotor with skewed bars; (b) rotor with straight bars; (c) rotor with straight bars and middle ring; (d) rotor with skewed bars and middle ring

6.3 Noise Test

The purpose of the noise test was to measure the noise at rated load. This test procedure is similar to the back-to-back test with two induction motors. The machine under test (each selected prototype) works as a motor directly connected to the laboratory grid. The other machine is also an induction motor, but with a higher rated output power. This second machine is fed by a variable-speed drive (VSD) with torque limitation and a smaller rotation than the prototype motor. The control of torque of the second motor allows the control of the load factor of the first motor. The objective of this test is only to measure the noise of the first motor (and not the noise produced by both machines). To accomplish this goal, a special chamber was used around the second motor for acoustic isolation, and the motor inside the chamber worked without a cooling fan. Thus, only the noise produced by the first motor was measured.

In addition, the test was done in an acoustic chamber to ensure that outside noise do not interfere on the results. Figure 5 illustrates this noise test setup, except for the acoustic chamber. All conditions indicated in [17] for noise tests on a running motor in the nominal load factor were respected. The results are more useful if used for comparative analysis, instead of the absolute values alone.

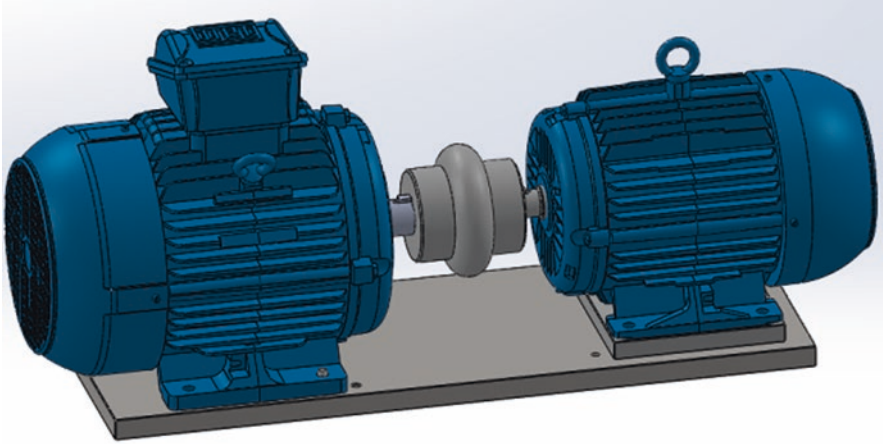


Fig. 5 Representation of the setup used for the noise test (without the acoustic chamber)

7 Results

7.1 Performance Test

Table 2 shows the overall performance test results referring to the four prototypes described in Sect. 3. The values were measured for each prototype running at rated load.

The results presented on Table 2 are the average values of the three performance tests done for each prototype. To directly compare the results between different prototypes it was necessary to ensure that the output power did not differ by more than 1% from each other. The performance test in steady state was done by continuously controlling the output power of the motor, reducing the error to minimum values.

Analyzing the rotation speed in the rated load allows to infer that the rotors with skewed bars tend to have a higher slip. Consequently, they generate more Joule rotor losses, leading to a lower efficiency.

Due to the higher slip in rotors with skewed bars, the rated torque is higher. Then the electrical current and Joule stator losses also increase and reduce the efficiency of the motor.

The higher slip in rotors with skewed bars generates higher rotor Joule losses, leading to a lower efficiency of the motor. Besides, the skewed bars also tend to raise the iron losses when compared with straight bars. In Table 2, the iron losses include both stator and rotor, and since the stator is the same for the four prototypes, the deviations are due to the presence of different rotors.

Regarding the motor power factor, the results show a tendency of not being significantly affected by the presence of a middle ring in the squirrel-cage rotor.

Table 2 Results of the performance test (load factor = 100%)

Parameter	Unit	skb_nr	stb_nr	stb_r	skb_r
Corrected absorbed power	W	6183.63	6130.51	6142.15	6188.32
Current	A	12.02	11.71	11.81	12.01
No load current	A	6.03	5.89	6.01	5.96
Speed	Rpm	1741.2	1743.7	1742.7	1738.0
Iron losses	W	90.51	83.31	82.17	89.50
Mechanical losses	W	16.84	19.07	17.55	18.34
Joule Stator losses	W	344.37	321.73	329.02	344.05
Joule rotor losses	W	187.33	178.69	182.03	197.75
Additional losses	W	47.69	30.91	34.51	41.95
Total losses	W	685.71	632.59	644.23	690.40
Efficiency	%	88.91	89.68	89.51	88.84
Power factor ($\cos\phi$)	–	0.781	0.795	0.790	0.783
Rated torque	N.m	30.15	30.11	30.13	30.21
Max. Torque	N.m	76.44	79.76	74.69	71.78
Output power	W	5497.9	5497.9	5497.9	5497.9
Temperature rise	°C	63.0	55.8	57.4	62.5

However, the difference in power factor between the skewed-bar rotors and straight-bar rotors tends to be significant and higher for the first ones.

The analysis of the results in Table 2 allows to infer how each rotor influences the electrical characteristics of the motor. The prototype having a rotor with straight bars and no middle ring (*stb_nr*) presents the highest efficiency, as predicted in [1–4]. However, the prototype having a rotor with straight bars and a middle ring (*stb_r*) presented better electrical characteristics than the one having a rotor with skewed bars and no middle ring (*skb_nr*), which indicates that this solution can be interesting for the industry purposes.

7.2 Torque-Speed Curve

Figure 6 shows the torque-speed curve for each of the tested rotors. It is possible to notice that the motors with different rotors can be split in two different groups: one with straight bars (*stb_nr* and *stb_r*) and other with skewed bars (*skb_nr* and *skb_r*). The division of the tested prototypes in these two groups shows the influence of the skew angle on the developed torque, although the inclusion of a middle ring also has an important influence, mainly for high slip (region of low rotation speed).

As expected in [1–4], both the breakdown torque and the starting torque are lower in motors having rotors with skewed bars when compared with the rotors having straight bars.

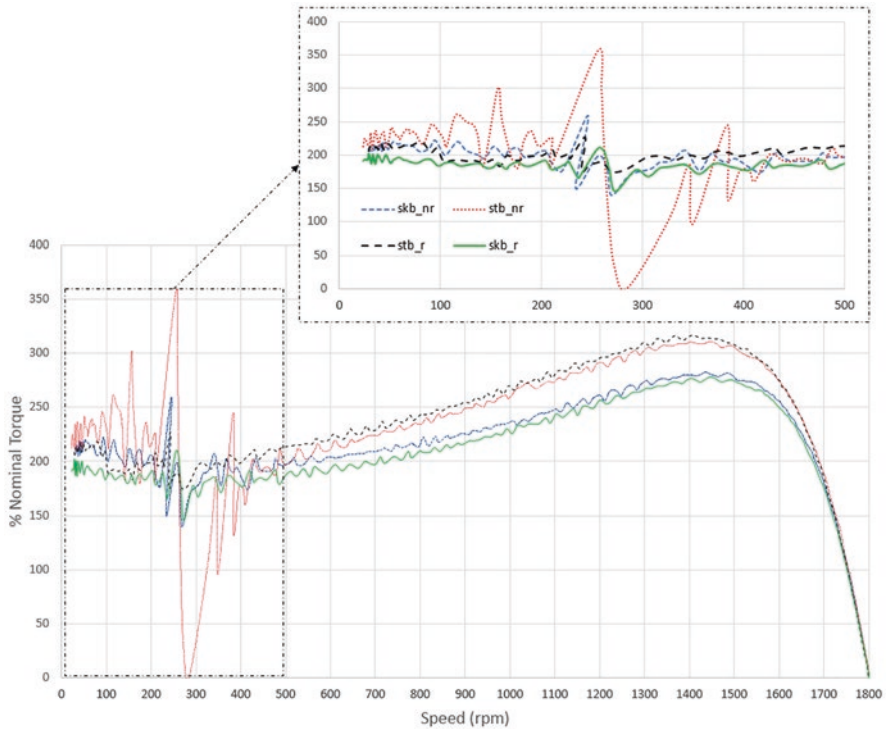


Fig. 6 Torque-speed curve of the four prototypes

For the rotors with straight bars (*stb_nr* and *stb_r*) the influence of the addition of the middle ring to the squirrel cage is relevant, mainly regarding to asynchronous torque. Seemingly, the presence of the middle ring will decrease the asynchronous torque generated by the rotor harmonics, mainly for high slip values (5^a and 7^a harmonic). This is a big advantage that makes the motors suitable for a wide range of applications. For example, the motor with a torque-speed curve as the one presented by the prototype *str_nr* would be unsuitable for application that requires a start with load.

Analyzing only the torque-speed curve results, the prototype having a rotor with straight bars and middle ring (*str_r*) seem to be a solution with the lowest asynchronous torque values, a higher breakdown and starting torque. The prototype having a rotor with straight bars and no middle ring (*str_nr*) shows the highest breakdown and starting torques, but it also shows significant asynchronous torque values. The prototype having rotors with skewed bars present very similar torque-speed curves, which may lead to the conclusion that the middle ring is not relevant in rotors that already have skewed bars.

7.3 Noise Test

During the noise test of the prototypes, several measurements were made at different conditions. The noise was measured at three different points, all equidistant from the tested motor. Besides that, the noise was measured at three moments during test. First, with only the auxiliary machine inside the acoustic chamber turned on and uncoupled from the tested motor. Second, with the auxiliary machine inside the acoustic chamber turned on and coupled to the tested motor. Third, with both machines turned on and the tested motor at rated load. Measuring the noise in these three moments enables to isolate the electromagnetic noise from the mechanical noise. The average results of the measurements at the different points are shown on Table 3.

The electromagnetic noise produced by each prototype was calculated by subtracting the noise measured at moment (b) from the one measured in (c), and it is represented in Fig. 7. A logarithmical subtract was used because the noise is expressed in dB(A).

As expected, the prototypes having rotor with straight bars present higher electromagnetic noise levels. This is expected due to the significant influence of the harmonic components in the torque produced.

Both the skewed bars and the middle ring have significant influence on the electromagnetic noise produced, and both tend to reduce it. The rotors that have skewed bars (*skt_nr* and *skt_r*) were the ones that produced less electromagnetic noise. However, the combination of the two characteristics (skewed bars and middle ring) leads to a rotor with the lowest electromagnetic noise level. The lower electromagnetic noise is due to the capacity of these two characteristics to reduce the amplitude and influence of the harmonics in the air-gap magnetic flux.

The rotor with only the middle ring and straight bars (*stb_r*) presents a significantly lower level of electromagnetic noise when compared with the rotor with straight bars and no middle ring (*stb_nr*). This shows that the capacity of the middle ring to reduce the presence of harmonics in the air-gap magnetic flux is also relevant.

Table 3 Results of the noise test

Unit	Quantity	Tested motor	skb_nr	stb_nr	stb_r	skb_r
dB(A)	Corrected absorbed power	Condition 1: Off (uncoupled)	54.7	54.7	54.7	54.7
		Condition 2: Off (coupled)	56.9	57.1	57.1	58.2
		Condition 3: On (coupled)	58.7	62.8	60.6	58.9
		Condition 3-2: Electromagnetic noise	54.0	61.4	58.0	50.6

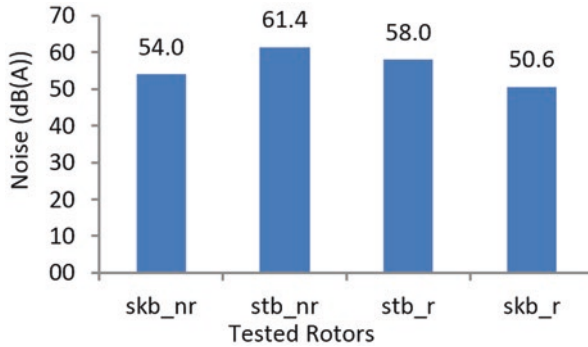


Fig. 7 Electromagnetic noise of the four prototypes

8 Conclusion

The results obtained from laboratory tests present new similarities between the rotors with skewed bars and rotors with middle ring, also they are in accordance with the relevant bibliographies.

The redundant effect of the skewed bars and of the middle ring is confirmed regarding the torque-speed curve, since the differences between the prototype *skb_nr* and *skb_r* are not relevant, particularly, in the low speed region. During the performance test, the two prototypes having rotors with skewed bars present slight differences, but in an overall assessment they look very similar. However, the noise test showed a large difference between these two prototypes, being that the rotor with skewed bars and middle ring presented the lowest noise.

Analyzing the characteristics of each prototype, the rotor with straight bars and no middle ring apparently has the most favorable electrical characteristics, being the motor that reached the higher efficiency. However, the asynchronous torque and the level of electromagnetic noise produced limit the range of application in which this rotor design can be used.

On the opposite, the rotor with skewed bars and middle ring presented the lowest level of electromagnetic noise among the four prototypes tested, but its rated load efficiency was the lowest. The developed torque is quite similar to the rotor with skewed bars and no middle ring, which is the most common industrial solution.

Both the rotor with straight bars and middle ring and the rotor with skewed bars and no middle ring presented good characteristics. The *skb_nr* presented a lower level of electromagnetic noise and the *stb_r* presented a higher torque curve with lower asynchronous torque and higher efficiency.

Based on these results, the use of a rotor with skewed bars and/or with a middle ring can lead to interesting differences on motor performance. The choice of the best option will depend on the application of the electrical motor.

References

1. S.Nau, The influence of the skewed rotor slots on the magnetic noise of three-phase induction motors. Eighth International Conference on Electrical Machines and Drives, 1997
2. Z. Ferkova, V. Kindl, Influence of skewed squirrel cage rotor with intermediate ring on magnetic field of air gap in induction machine. *Elektronika ir Elektrotechnika* **1**, 23 (2017)
3. L. Wang, X. Bao, C. Di, Y. Zhou, Influence on vibration and noise of squirrel-cage induction machine with double skewed rotor for different slot combinations. *IEEE Trans. Magn.* **52**(7), 1–4 (2016)
4. L. Wang, X. Bao, C. Di, Y. Zhou, Q. Lu, Analysis of synchronous parasitic torque in dual skew cage rotor induction motors with equivalent slot number. *IET Electr. Power Appl.* **11**(8), 1357–1365 (2017)
5. S. Williamson, C. McClay, The effect of axial variations in saturation due to skew on induction motor equivalent-circuit parameters. *IEEE Trans. Ind. Appl.* **35**(6), 1323–1331 (1999)
6. X. Bao, J. Fang, C. Di, S. Xu, A novel computational method of skewing leakage reactance for doubly skewed rotor induction motor. *IEEE Trans. Energy Convers.*, 1–1 (2018)
7. D. Dorrell, T. Miller, C. Rasmussen, Inter-bar currents in induction machines. *IEEE Trans. Ind. Appl.* **39**(3), 677–684 (2003)
8. S. Williamson, L. Lim, M. Robinson, Finite-element models for cage induction motor analysis. *IEEE Trans. Ind. Appl.* **26**(6), 1007–1017 (1990)
9. K. Yamada, Y. Takahashi, K. Fujiwara, Simplified 3-D modeling for skewed rotor slots with end-ring of cage induction motors. *IEEE Trans. Magn.* **52**(3), 1–4 (2016)
10. W. Xu, X. Bao, C. Di, L. Wang, Y. Chen, Optimal angle combination for improving electromagnetic torque in induction motor with double-skewed rotor. *IEEE Trans. Magn.* **53**(11), 1–5 (2017)
11. D. Strbac, R. Gottkehasckamp, Improvement of the operating behavior of small induction motors by finding an optimal rotor skewing angle and a harmonic distribution of the number. *IKMT 2015; 10. ETG/GMM-Symposium Innovative small Drives and Micro-Motor Systems, 2015*, pp. 1–7
12. H.D. Gersem, K. Hameyer, T. Weiland, Skew interface conditions in 2-D finite-element machine models. *IEEE Trans. Magn.* **39**(3), 1452–1455 (2003)
13. S. Williamson, C. McClay, The variation of cage motor losses with skew. *IEEE Trans. Ind. Appl.* **36**(6), 1563–1570 (2000)
14. A.M. Odok, Stray-load losses and stray torques in induction machines. *Trans. Am. Inst. Electr. Eng. Part III Power Appar Syst* **77**(3), 43–53 (1958)
15. IEC Rotating electrical machines – Part1: Rating and performance, IEC Standard 60034-1, 2017
16. IEEE Test Procedure for Polyphase Induction Motors and Generators, IEEE Standard 112, 2017
17. Acoustics – Determination of sound power levels and sound energy levels of noise sources using sound pressure – Engineering methods for an essentially free field over a reflecting plane, ISO International Standard 3744, 2010

Efficiency Measurement Strategy for a Planetary Gearbox with 2 Degrees of Freedom



Florian Verbelen, Pieter Defreyne, Peter Sergeant, and Kurt Stockman

1 Introduction

Due to increasing energy prices, the efficiency of drive trains and their individual components has gained a lot of interest. By optimizing the drive train as a whole, large savings on the long term are possible. This is called the Extend Product Approach (EPA). However, to apply EPA, knowledge of the energy efficiency of all drive train components over a wide range of operating points is vital.

For electrical components, measurement procedures and models are available to provide this important data as function of the operating point. In contrast to the latter, the provided efficiency of mechanical components is often restricted to a single operating point. In the last 5 years, a lot of effort has been spent in setting up measurement guidelines for mechanical gearboxes. The efficiency is measured and afterwards visualized as function of input speed and output torque [1, 2]. An important remark is that this method was developed for single input single output devices in which a unique power path can be defined. If another shaft is added, the method still holds, but the number of measurements to obtain an accurate description of the efficiency becomes unacceptably high. Moreover, visualizing efficiency or power losses on a 2D map is no longer possible. An example of such a gearbox is a 2 Degrees Of Freedom (DOF) planetary gearbox which is, for instance, used in hybrid electrical vehicles[3], wind turbines [4], aerospace [5], etc. Their main advantages are high efficiency, compactness, and axisymmetric arrangement.

F. Verbelen (✉) · P. Defreyne · P. Sergeant · K. Stockman
Department of Electromechanical Systems and Materials, Ghent University, Ghent, Belgium

FlandersMake@UGent – core lab EEDT-MP, Ghent, Belgium
e-mail: florian.verbelen@ugent.be; pieter.defreyne@ugent.be; peter.sergeant@ugent.be; Kurt.stockman@ugent.be; <https://www.eedt.ugent.be>; <https://www.eedt.ugent.be>; <https://www.eedt.ugent.be>; <https://www.eedt.ugent.be>

A lot of effort has already been spent to model the efficiency of the planetary gearbox. Pennestri has summarized all the work concerning efficiency evaluation in an interesting review [6]. The paper shows that the efficiency of a planetary gearbox, given a specific operating point, is determined based on the power flow (related to the operating point) and a fix efficiency value for the power path between sun & carrier and carrier & ring, denoted by path 1 and path 2 in Fig. 1, respectively. Moreover, it is shown that, although there are a lot of different mathematical expressions to calculate the efficiency, the different approaches are numerically equivalent. A completely novel approach to calculate the efficiency, based on virtual power, is introduced by Chen [7–9]. This approach has also been validated in [10] but rather on a limited dataset.

In this paper, the work of Chen [8] is used to derive equations to estimate the overall efficiency based on the power flows and efficiency values for the different/individual power paths. The individual efficiency values for the considered power paths are determined for 3 levels of accuracy: as function of load torque and input speed, purely depending on the load torque and finally they are assumed to be constant (identical to the approach in [8]). The calculated planetary gear efficiency, based on the different formulations of the efficiency of the power paths, is then compared with the measurements to determine what level of accuracy is required.

This paper is structured as follows. In Sect. 2, the equations to calculate the efficiency of the planetary gear are considered after which in Sect. 3 the measurement setup is introduced. The results of the efficiency maps of power path 1 and 2 are shared in Sect. 4 while in Sect. 5 the impact of the different efficiency formulations of the power paths on the total gear train efficiency is discussed. Finally in Sect. 6 the conclusions of the research are formulated.

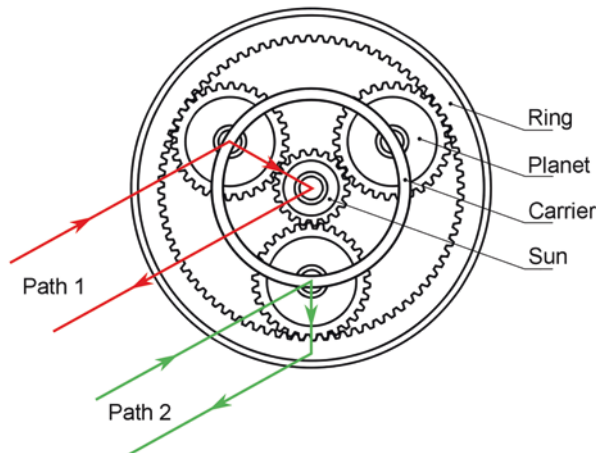


Fig. 1 Principle scheme of the planetary gear

2 Theoretical Model

The considered planetary gear consists of a sun, carrier with planets, and a ring, organized as in Fig. 1. The main parameters of the planetary gear can be found in Table 1.

As described in [8], it is possible to derive the efficiency of the 2-DOF planetary gearbox as function of the power flow (P_s, P_c, P_r), speed ratio between carrier and sun $\left(\frac{\omega_c}{\omega_s}\right)$ and 2 efficiency values that describe the efficiency of power path 1 and

$2(\eta_1, \eta_2)$. Deriving the equations for the considered planetary gear is straightforward based on the content of [8] as all the equations of a similar planetary gear are derived in that paper. Hence, only the definition of parameter C_2 (see (6)) is different compared to the original paper which is due to the slightly different configuration of the planetary gear.

Table 2 gives an overview of all the possible equations to calculate the efficiency. The first step in selecting the correct equation is to determine the power flow. Based on the power flow, it is possible to select a row in Table 2. If, for example, the power flows from the sun ($P_s < 0$) to the carrier ($P_c > 0$) and ring ($P_r > 0$), row 3 is selected. The second step is to select the correct subcase (A or B). The conditions for these subcases are given in Table 3 and depend on the speed ratio between carrier and sun. For more information concerning the derivation of the subcases and separate efficiency equations, the reader is referred to [8].

In which:

$$A = \lambda_1 + \lambda_2 - \lambda_1 \lambda_2 \tag{1}$$

$$\lambda_1 = 1 - \eta_1(T_s, \omega_p) \tag{2}$$

$$\lambda_2 = 1 - \eta_2(T_r, \omega_p) \tag{3}$$

$$k = \frac{\omega_c}{\omega_s} \tag{4}$$

$$C_1 = 1 - k \tag{5}$$

Table 1 Number of teeth of the elements

Number of teeth of the sun N_s	54
Number of teeth of the planets N_p	26
Number of teeth of the ring N_r	108
Maximum torque at the sun $T_{s, \max}$	45 Nm
Maximum torque at the carrier $T_{c, \max}$	137 Nm
Maximum torque at the ring $T_{r, \max}$	90 Nm

Table 2 Equations to calculate the efficiency as function of the power flow and a given subcase

	Subcase A	Subcase B
$P_s > 0, P_c > 0$ and $P_r < 0$	$\eta = \frac{1-A}{1-A+AC_2}$	$\eta = \frac{1}{1-AC_2}$
$P_s > 0, P_c < 0$ and $P_r > 0$	$\eta = \frac{-C_1+AC_1+C_2-AC_1C_2}{-C_1+AC_1+C_2}$	$\eta = \frac{C_1-C_2+AC_2-AC_1C_2}{C_1-C_2+AC_2}$
$P_s < 0, P_c > 0$ and $P_r > 0$	$\eta = \frac{1}{1-AC_1}$	$\eta = \frac{1-A}{1-A+AC_1}$
$P_s > 0, P_c < 0$ and $P_r < 0$	$\eta = 1 - AC_1$	$\eta = \frac{-1+A-AC_1}{-1+A}$
$P_s < 0, P_c > 0$ and $P_r < 0$	$\eta = \frac{C_1-AC_1-C_2}{C_1-C_2-AC_1+AC_1C_2}$	$\eta = \frac{-C_1-AC_1+C_2}{-C_1+C_2-AC_2+AC_1C_2}$
$P_s < 0, P_c < 0$ and $P_r > 0$	$\eta = \frac{-1+A-AC_2}{-1+A}$	$\eta = 1 - AC_2$

Table 3 Conditions of the subcases

	Subcase A	Subcase B
$P_s > 0, P_c > 0$ and $P_r < 0$	$k < 0$	Else
$P_s > 0, P_c < 0$ and $P_r > 0$	$\frac{N_s}{N_r+N_s} < k < 1$	Else
$P_s < 0, P_c > 0$ and $P_r > 0$	Else	$0 < k < \frac{N_s}{N_r+N_s}$
$P_s > 0, P_c < 0$ and $P_r < 0$	$0 < k < \frac{N_s}{N_r+N_s}$	Else
$P_s < 0, P_c > 0$ and $P_r < 0$	$k > 1$	Else
$P_s < 0, P_c < 0$ and $P_r > 0$	Else	$k < 0$

$$C_2 = \frac{(k-1)N_s}{(k-1)N_s + kN_r} \quad (6)$$

3 Measurement Setup

The measurement setup consists of a planetary gear, a belt, 3 torque sensors, and 3 electrical machines to load the shafts of the planetary gear. The purpose of the belt is to transmit torque from the ring to the load machine (and vice versa). The torque sensors are used to measure the mechanical power going through each shaft. Each shaft can be fixed to go from a 2-DOF system to a 1-DOF system. These fixing mechanisms are used to block the sun and ring in 2 separate measurements in order to set up the 1-DOF efficiency maps of power path 1 and 2. Note that the efficiency map for the power path from carrier to ring includes the efficiency of the belt. The planetary gear system as such is thus the combination of the planetary gear component and the belt. During all measurements, the temperature has been controlled at 32 ± 1 °C. This is of high importance due to the impact of temperature on the viscosity of the oil and thus the efficiency of the gearbox [11] (Fig. 2).

3.1 Measurement Accuracy

The accuracy of the measured efficiency depends on the accuracy of the torque sensors and the AD conversion of the signals. The used torque sensors are equipped with strain gauges and have a contactless signal transmission from rotor to stator.

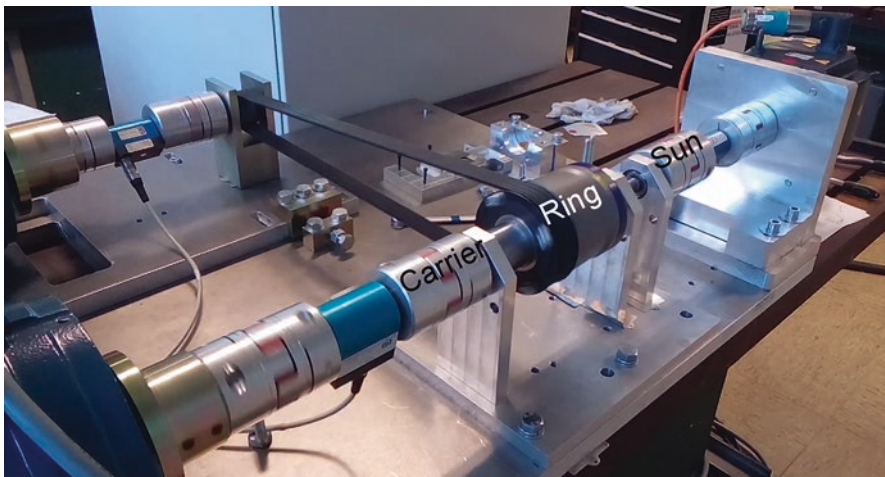


Fig. 2 Measurement setup

Table 4 Accuracy of the torque sensors

Range	Accuracy	Absolute fault	Location
50 Nm	0.2% full scale	±0.1 Nm	Sun
100 Nm	0.1% full scale	±0.1 Nm	Ring
200 Nm	0.1% full scale	±0.2 Nm	Carrier

The details in terms of range and accuracy of the 3 torque sensors that are used can be found in Table 4.

The accuracy of the AD conversion is 0.11% full scale. The range goes from 0 to 5 V for the torque sensors with a range of 50 and 100 Nm. For the torque sensor with a range of 200 Nm, the output range is 0 to 10 V.

To demonstrate how the Absolute Fault (AF) on an efficiency measurement can be calculated, an example is presented for when the ring is blocked. In this case, power flows from carrier to sun. The torque at the sun T_s equals 26 Nm, at the carrier T_c a torque of 80 Nm is applied, the speed of the sun ω_s equals 792 rpm and the speed of the carrier ω_c is equal to 264 rpm. The efficiency of this path can be calculated as:

$$\eta = \frac{P_{\text{out}}}{P_{\text{in}}} = \frac{T_s \omega_s}{T_c \omega_c} = \frac{T_s \omega_c \frac{N_s + N_r}{N_s}}{T_c \omega_c} = \frac{T_s (N_s + N_r)}{T_c N_s} = 97.5\% \quad (7)$$

The total uncertainty of this measurement depends on the uncertainty of the torque sensor and the uncertainty of the AD conversion (output of the torque sensor is an analogue signal). The accuracy of the speed measurement has no impact on measured efficiency as can be seen in (7). The total Relative Fault (RF) and AF are calculated using the following equations:

$$\text{RF}(\text{tot}) = \sqrt{\text{RF}(T_s)^2 + \text{RF}(T_c)^2} = \sqrt{\left(\frac{\text{AF}(T_s)}{|T_s|}\right)^2 + \left(\frac{\text{AF}(T_c)}{|T_c|}\right)^2} \quad (8)$$

$$\text{AF}(\text{tot}) = \text{RF}(\text{tot})\eta \quad (9)$$

According to Table 4, the AF on the torque sensor of the sun is ±0.1 Nm and of the carrier ±0.2 Nm. The AF due to the AD converter of the torque sensor of the sun is $10 \text{ V} \times 11\% = \pm 11 \text{ mV}$ which translates to ±0.055 Nm. The same can be done for the torque sensor mounted at the carrier which results in an AF of ±0.22 Nm. Based on (8) it is now possible to calculate the total relative fault RF(tot):

$$\text{RF}(\text{tot}) = \sqrt{\left(\frac{0.1 + 0.055}{26}\right)^2 + \left(\frac{0.2 + 0.22}{80}\right)^2} = 0.79\% \quad (10)$$

which yields an AF of:

$$\text{AF}(\text{tot}) = \frac{0.79}{100} \times \frac{97.5}{100} = 0.77\% \quad (11)$$

4 Measurement of 1-DOF Efficiency Map

In the following sections, the results of the 1-DOF measurements of the 2 power paths are discussed. Note that only a limited dataset is presented in the paper. Hence, the variation of the efficiency with the speed of the planets is discussed based on 4 measurements. However, the real measured dataset covers the efficiency for 18 different speed values, each for 31 torque values.

4.1 Path 1 (Sun to Carrier)

As mentioned in (2), the efficiency η_1 is a function of torque and speed. The efficiency η_1 is related to the power path between the sun and carrier (see Fig. 1) and is written as function of the torque applied to the sun T_s and the speed of the planets ω_p . As, in normal operation, the power could split toward the ring, the ring is blocked which reduces the 2-DOF planetary gear to a 1-DOF system. Hence, the only power path which remains goes from the sun to the carrier (and vice versa). Under the assumption that the direction of the power of the 1-DOF contacts has no impact on the efficiency, it does not matter which element (sun or planets) is chosen as input or output to measure the efficiency map. As the torque on the planets cannot be measured, the measurable quantity for the planets is speed. Therefore, the efficiency η_1 can be measured as function of the torque on the sun T_s (output property) and the speed of the planets ω_p (input property).

Figure 3 shows the efficiency as function of the torque applied to the sun for varying speed of the planets. As can be seen in the graph, the efficiency is fairly constant in a wide range of torque values. This can support the assumption of taking a constant value for η_1 . However, at low torque, as expected, the efficiency drops. Furthermore, the dependency with the speed is very low and only noticeable at low torque.

Based on the measured data (the complete dataset) it is possible to fit a surface (see Fig. 4). This theoretical expression is equal to:

$$\eta_1 = (a_1 + b_1 \omega_p) T_s^{(c_1 \omega_p + d_1)} + e_1 \quad (12)$$

with $a_1 = -7.558 \times 10^{-5}$, $b_1 = -0.134$, $c_1 = -5.326 \times 10^{-5}$, $d_1 = -0.7706$ and $e_1 = 0.9836$. Note that this is an empirical formula which tends to be a good fit for

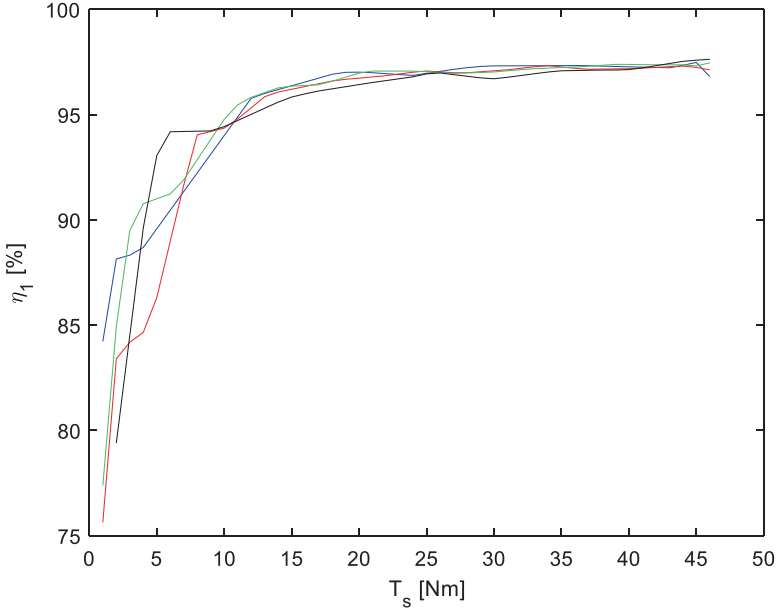


Fig. 3 Efficiency of the path going from the sun to carrier η_1 as function of the torque applied to the sun T_s for varying speed of the planets ω_p . Blue: $\omega_p = 500$ rpm, red: $\omega_p = 1000$ rpm, green: $\omega_p = 1500$ rpm, black: $\omega_p = 2000$ rpm

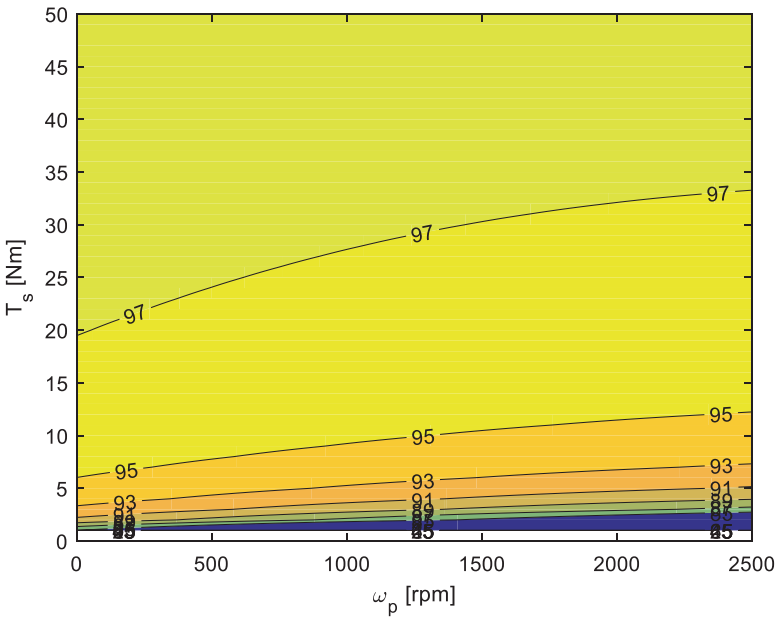


Fig. 4 Fitted efficiency of power path 1 as function of the speed of the planets and torque applied to the sun

most of the operating range. For extremely low torque values, (12) becomes useless as the efficiency goes to infinity. The advantage, however, is that, based on (12), it is easy to investigate the impact of reducing $\eta_1(T_s, \omega_p)$ to $\eta_1(T_s)$.

4.2 Path 2 (Carrier to Sun)

A similar methodology has been applied to measure the efficiency map of the second power path. Now the sun is fixed, allowing a unique power flow from carrier to ring. Figure 5 shows the results as function of torque applied to the ring for varying speed of the planets. Again, the efficiency is rather constant and almost independent of the speed of the planets. Note that the efficiency is 1–2% lower compared to the power path from sun to carrier. One of the reasons for this lower efficiency is that the efficiency of power path 2 is the combination of the efficiency of the planetary gear and the belt.

Based on the measured data it is again possible to fit a surface (see Fig. 6). This theoretical expression is equal to:

$$\eta_2 = (a_2 + b_2 \omega_p) T_s^{(c_2 \omega_p + d_2)} + e_2 \tag{13}$$

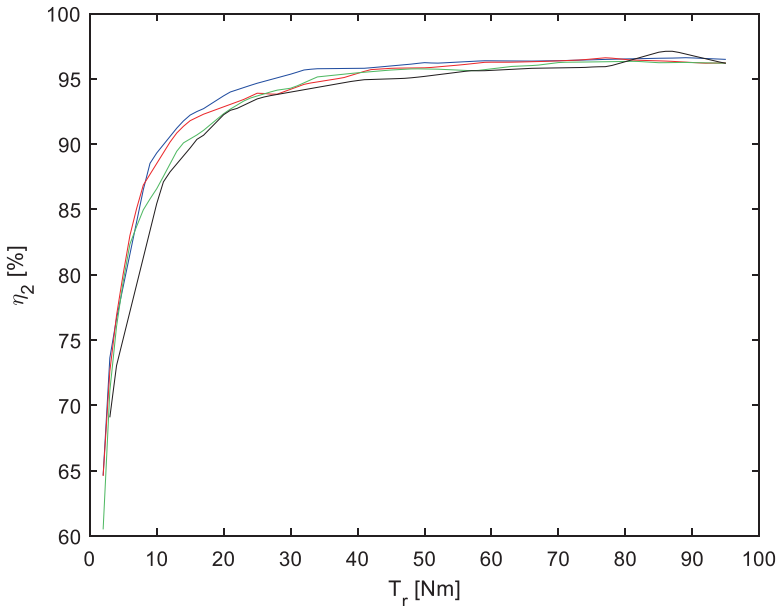


Fig. 5 Efficiency of the path going from carrier to ring η_2 as function of the torque applied to the ring T_r for varying speed of the planets ω_p . Blue: $\omega_p = 500$ rpm, red: $\omega_p = 1000$ rpm, green: $\omega_p = 1500$ rpm, black: $\omega_p = 2000$ rpm

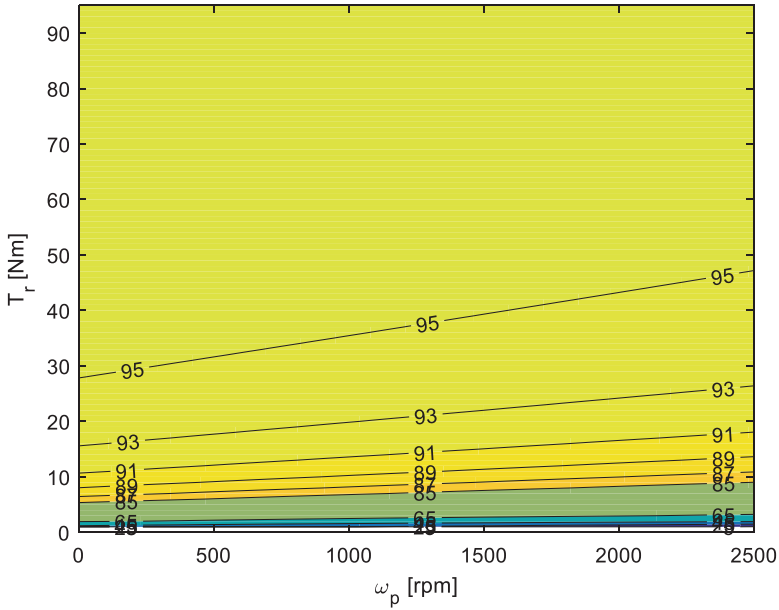


Fig. 6 Fitted efficiency of power path 2 as function of the speed of the planets and torque applied to the ring

with $a_2 = -14.2 \times 10^{-5}$, $b_2 = -0.5826$, $c_2 = -2.337 \times 10^{-14}$, $d_2 = -0.901$ and $e_2 = 0.9791$.

5 Case Study

Based on the equations written down in Table 1, (12) and (13), it is possible to calculate the efficiency for all possible operating points. Figure 7 shows the measured efficiency values of the planetary gear as function of varying speed ratio (ratio of carrier speed and ring speed) and stator torque. The ring speed was chosen constant at 200 rpm. Note that as all 3 shafts are rotating, speed cannot be excluded anymore from the equation to calculate the efficiency. Therefore, in contrast with the earlier explanation on the measurement accuracy, accuracy of the speed measurement does have an effect.

The results presented in Fig. 7 will be used as reference to benchmark the 3 cases: efficiency depending on both the load torque and input speed (case 1), efficiency as function of the load torque (case 2), and fixed efficiency (case 3). For case 1, (12) and (13) are used to calculate the efficiency of power path 1 and 2, denoted by η_1 and η_2 , respectively. For case 2, (12) and (13) are again used but at a fixed speed of the planets. This speed is arbitrarily chosen at 500 rpm. For case 3, a fixed efficiency is chosen equal to 97% and 96% for η_1 and η_2 , respectively. This decision

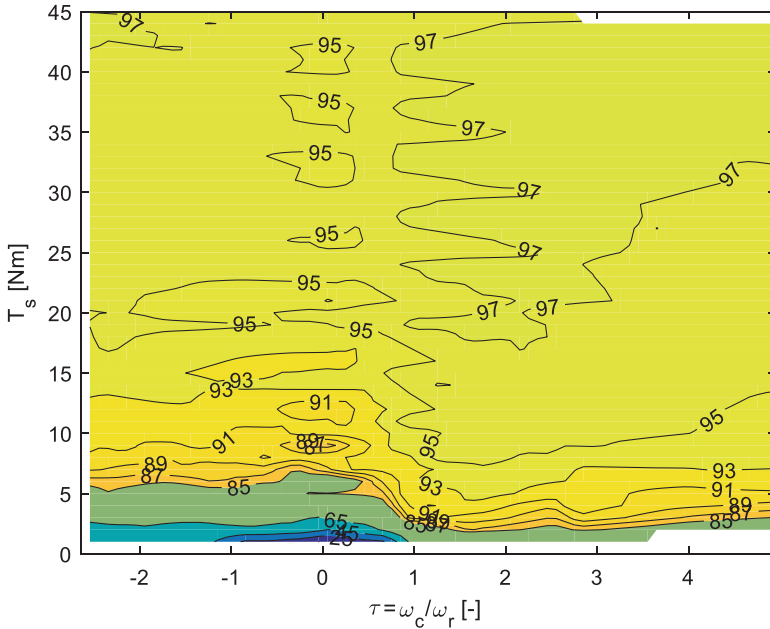


Fig. 7 Measured efficiency of the planetary gearset as function of varying speed ratio $\tau = \frac{\omega_c}{\omega_r}$ and stator torque T_s

is taken purely on the average efficiency in the operating range starting from 20 Nm until the maximum torque.

Figure 8 provides a comparison between the cases and the actual measured efficiency. The results show that the model is clearly capable of estimating the efficiency of the planetary gear, certainly for higher torque values.

Comparing the outcome based on case 1 and 2 shows that the results are almost identical. This means that there is no added value in measuring a complete efficiency map to resemble power path 1 and 2 as the variation of the efficiency with the speed is just too insignificant. However, there is a significant added value at low torque between case 2 ($\eta_{1,2}$ vary as function of $T_{s,r}$) and case 3 ($\eta_{1,2} = \text{constant}$). At higher torque, η_1 and η_2 become fairly constant (see Figs. 4 and 6), which explains why the differences between case 2 and 3 diminish for higher torque.

Based on this analysis it is possible to conclude that the efficiency of a planetary gearbox can be estimated based on 2 measurements which take into account the efficiency of power path 1 and 2 as function of the load torque. For case 2, a complete efficiency map has been set up and is presented as Fig. 9. It is clear by comparing Figs. 7 and 9 that there is a close match between measurement and model results. The average mismatch (complete operating range) between estimation and measurement is 1.7%. If torque values below 10 Nm are excluded, the average difference is below 1% which is close to the error bands of the measurements.

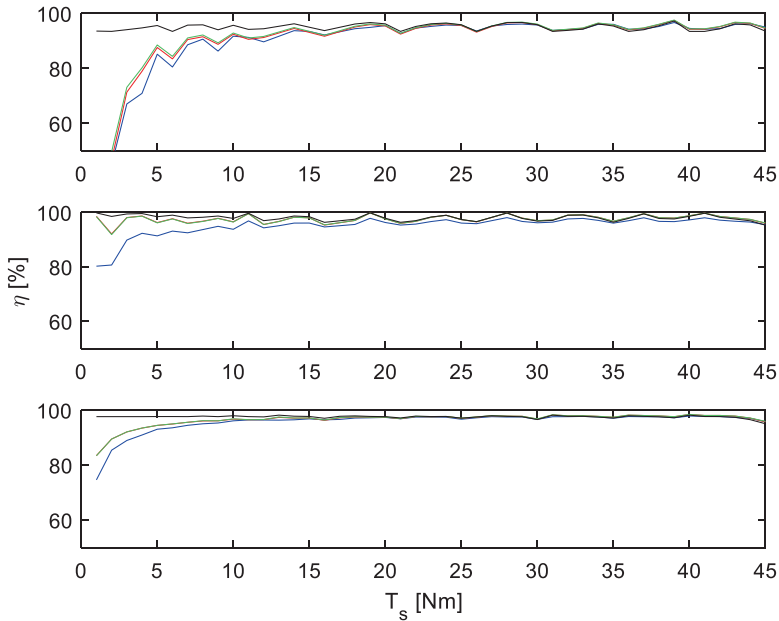


Fig. 8 Efficiency of the planetary gear for varying torque applied to the sun. (a) For a speed ratio of 0. (b) For a speed ratio of 1. (c) For a speed ratio of 2. Blue: measurement, red: case 1, green: case 2, black: case 3

6 Conclusion

In this chapter, a method is described to estimate the efficiency of a 2-DOF planetary gearbox over a wide range of operating points. The model combines the theory of virtual power with a limited set of measurements. These measurements are conducted to calculate the efficiency of 2 power paths: between sun & carrier and carrier & ring. It is shown that these efficiency terms merely depend on the load torque. The required measurement time is thus limited as the variation with speed does not have to be taken into account. The results show the good match between measured efficiency of the planetary gearbox and the estimated value. Average difference between both is 1.7% if the complete operating range is considered. The average difference drops to less than 1% if torque values below 10Nm are excluded.

Acknowledgment This work was carried out for the EMTechno project (project ID: IWT150513) supported by VLAIO and Flanders Make, the strategic research center for the manufacturing industry.

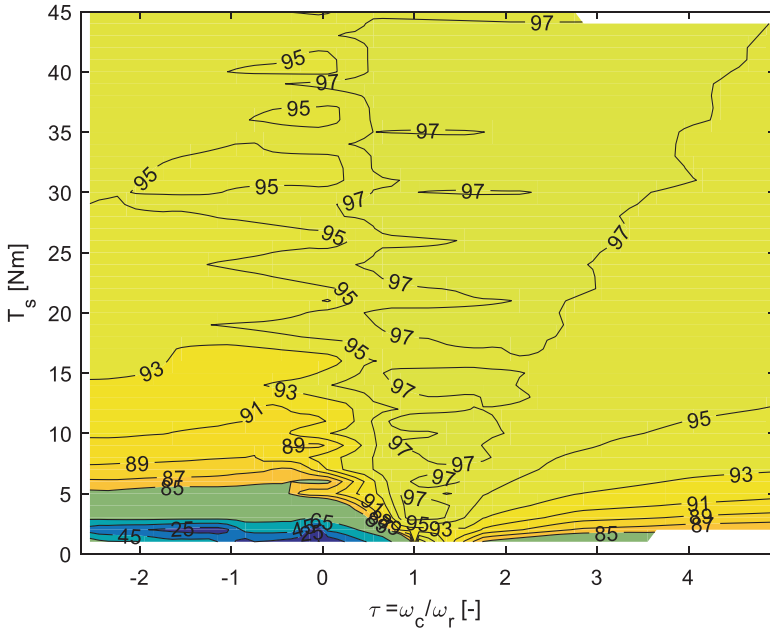


Fig. 9 Simulated efficiency of the planetary gearset for varying speed ratio $\tau = \frac{\omega_c}{\omega_r}$ and stator torque T_s

References

1. S. Dereyne, P. Defreyne, E. Algoet, K. Stockman, Construction of an energy efficiency measuring test bench for belt drives test bench setup, in *Energy Efficiency of Motor Driven Systems*, (2013), pp. 1–8
2. S. Dereyne, P. Defreyne, E. Algoet, S. Derammelaere, Efficiency measurement campaign on gearboxes, in *Energy Efficiency of Motor Driven Systems*, (2015), pp. 1–11
3. E. Vinot, R. Trigui, Y. Cheng, C. Espanet, A. Bouscayrol, V. Reinbold, Improvement of an EVT-based HEV using dynamic programming. *IEEE Trans. Veh. Technol.* **63**(1), 40–50 (2014)
4. C. Nutakor, A. Klodowski, J. Sapanen, A. Mikkola, J.I. Pedrero, Planetary gear sets power loss modeling: Application to wind turbines. *Tribol. Int.* **105**(May 2016), 42–54 (2017)
5. J.D. de Gevigney, F. Ville, C. Changenet, P. Velex, Tooth friction losses in internal gears: Analytical formulation and applications to planetary gears. *Proc. Inst. Mech. Eng. Part J J. Eng. Tribol.* **227**(5), 476–485 (2013)
6. E. Pennestri, P.P. Valentini, A review of formulas for the mechanical efficiency analysis of two degrees-of-freedom epicyclic gear trains. *J. Mech. Des.* **125**(3), 602–608 (2003)
7. C. Chen, Power flow and efficiency analysis of epicyclic gear transmission with split power. *Mech. Mach. Theory* **59**, 96–106 (2013)
8. K. Davies, C. Chen, B.K. Chen, Complete efficiency analysis of epicyclic gear train with two degrees of freedom. *J. Mech. Des.* **134**(7), 071006 (2012)
9. C. Chen, J. Angeles, Virtual-power flow and mechanical gear-mesh power losses of Epicyclic gear trains. *J. Mech. Des.* **129**(January 2007), 107–113 (2007)

10. C. Chen, J. Chen, Efficiency analysis of two degrees of freedom epicyclic gear transmission and experimental validation. *Mech. Mach. Theory* **87**, 115–130 (2015)
11. S. Dereyne, E. Algoet, P. Defreyne, K. Stockman, An energy efficiency measurement test bench for gearboxes, in *Energy Efficiency of Motor Driven Systems*, (2013)

Development of High-Precision Efficiency Measuring Device for High Power Motor Drive Systems



Masayuki Harano, Hiroki Kobayashi, Chiaki Yamaura, Kenta Ikeda, Koki Nakazawa, and Shozo Yoda

1 Introduction

Established in 1935, HIOKI E.E. CORPORATION has grown to become a world leader in consistently providing test and measuring instruments through advanced design, manufacturing, and sales and services. By currently offering over 200 main products characterized by safety and quality while meeting an expansive range of applications, we aim to contribute to the efficiency and value of our customers' work in research and development, production and electrical maintenance. HIOKI products and services are available around the world through our extensive network of subsidiaries and distributors.

As the energy measurement field is concerned, HIOKI has established its place by state-of-the-art products such as the clamp tester in 1971 and the digital power meter in 1987, both completely new to the field. In recent days, HIOKI has catered to global markets creating electric products, electronic devices, handheld devices with an ever increasing focus on improving energy efficiency and decreases power consumption. Extremely fast ON/OFF controls are being done inside the internal circuits of power converters and control devices of power units, power conditioners, and inverters. High accuracy and high bandwidth characteristics are in demand for power measurement of such controls. HIOKI is able to provide measurement systems the most suited for such measurement applications.

M. Harano (✉) · H. Kobayashi · C. Yamaura · K. Ikeda · K. Nakazawa
HIOKI E.E. Corporation, Nagano, Japan
e-mail: harano@hioki.co.jp; kobahiro@hioki.co.jp; yamaura@hioki.co.jp; k-ikeda@hioki.co.jp; koki_nakazawa@hioki.co.jp

S. Yoda
HIOKI EUROPE GmbH, Eschborn, Germany
e-mail: yodas@hioki.eu

2 Measuring the Efficiency of Inverters and Motors [1, 2]

During evaluation of motor drive systems that incorporate inverters and motors, it is possible to measure efficiency and loss by measuring the inverter's input and output power and the motor's power, and then calculating the ratio or differential between the input and output values. Figure 1 provides a measurement block diagram illustrating the measurement of the efficiency of a standard motor drive system.

The output of inverters and motors fluctuates over time. Consequently, accurate measurement is made difficult by imperfect synchronization of measurement timing and by differences in calculation methods when computing efficiency and loss by measuring the respective points with separate instruments. Accordingly, it is necessary to take all measurements simultaneously, either by using a single instrument for all of them or through the synchronized control of multiple instruments. This requirement can be met by using a power analyzer. Power analyzers provide four to six channels of power measurement along with motor analysis functionality, allowing them to measure efficiency and loss with a high degree of precision.

Looking more closely at the power calculation process, the point from which the period of the voltage/current waveform is defined becomes an error factor that affects the measurement result. Power analyzers determine the periods across which calculations are performed by detecting zero-cross events in input waveforms. However, the channel corresponding to the signal for which zero-cross events will be detected can be set as desired as the synchronization source. Setting the optimal synchronization source enables stable power measurement. For this reason, it is possible to measure efficiency and loss with a high degree of precision. For example, if the inverter is fed DC input, the calculation periods can be synchronized by setting the same synchronization source for the input and output channels, and is possible to measure efficiency and loss in a stable manner. In the example shown in

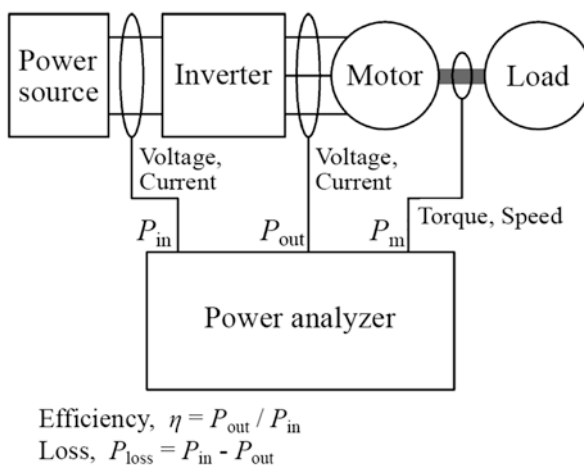


Fig. 1 Measuring the efficiency of a motor drive system

Fig. 1, power at two points and motor power at one point are being measured in a stable condition by setting the synchronization source for all channels to the inverter's output current.

2.1 *Measuring an Inverter's Input Power*

To measure efficiency and loss, it is necessary to measure the power being input to the inverter. This measurement value will serve as the basis for measuring efficiency and loss. If the values yielded by measurement of the input and output power contain an error component, it will have a significant effect on the efficiency and loss values. For this reason, it is necessary to measure the inverter's input power with a high degree of precision. For example, an error of 0.5% in the input power measured value for an inverter with an efficiency of 99% will result in an error of 50% for the loss. Although it is possible to calculate power using a general-purpose waveform recorder, one must exercise caution to ensure that a sufficient level of accuracy has been defined for the band that you wish to measure.

In general, either DC or AC commercial power is used as inverter input. Regarding DC measurement, since the DC offsets of the measurement device can become an error factor, standard power analyzers and current sensors that are susceptible to the influences of magnetization are equipped with a degaussing or zero adjust function. Before the measurement and after zeroing out the input, it is necessary to perform this function on the power analyzer and current sensor. In this way, it is possible to enable accurate DC measurement by canceling out the instrument's DC offset.

2.2 *Measuring an Inverter's Output Power*

PWM output that have been extensively used in recent years, include harmonic elements such as modulated (fundamental) wave frequencies. Consequently, power measurement must be performed over a wider band than when measuring DC or commercial frequency power. When selecting a device for high precision power measurement, it is important to carefully consider the switching frequency and the band that is needed in order to measure power. Figure 2 provides an equivalent circuit for a motor that is driven by an inverter.

Since the motor's windings have an inductance component, high-frequency current is less likely to flow to the motor. Since the inverter output voltage is a PWM waveform, it can be approximated as a rectangular wave. However, the current will take the shape of a triangular waveform. When calculating RMS values for the triangular waveform over the frequency domain, measurement can yield RMS values with an error of 0.1% or less if harmonics can be measured to the fifth order. Here the active power P_f can be expressed as a function of the voltage U_f , the current I_f , and the voltage-current phase difference θ_f as follows:

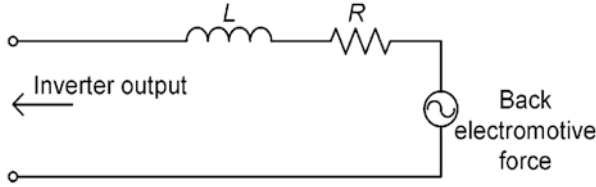


Fig. 2 Equivalent circuit for a motor (one-Phase)

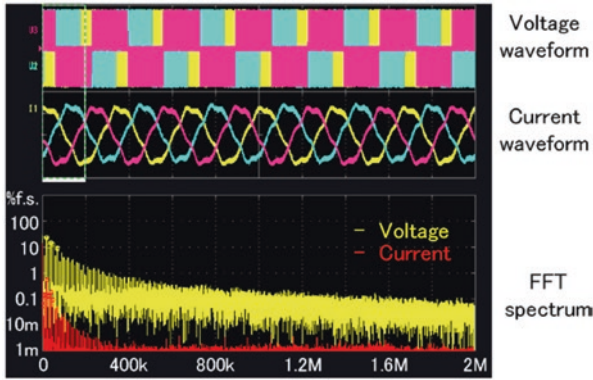


Fig. 3 Waveforms and FFT results for an actual inverter-driven motor (measured with the Power Analyzer PW6001)

$$P_f = U_f \cdot I_f \cdot \cos \theta_f \tag{1}$$

Consequently, if either the voltage or current is 0, the active power for that frequency component will be 0. Assuming measurement at a precision of 0.1%, current at seventh order and higher harmonic components can be ignored, as noted above. Therefore, the ability to measure voltage, current, and phase difference accurately within the band of five times the switching frequency is sufficient in order to measure power at the switching frequency and its harmonics with an error of 0.1% or less. However, loss in an actual motor includes the magnetic material’s core loss as well as losses from factors such as wire skin effects in addition to the resistance portion shown in Fig. 2.

Figure 3 shows the actual voltage and current waveforms of a motor driven by a SiC inverter, as well as associated FFT results. Table 1 provides detailed information about the measurement targets. Since the voltage is a PWM waveform, an examination of the FFT results reveals frequency components in excess of 1 MHz. Standard power analyzers do not provide a sufficient measurement band to measure voltage waveforms with the required degree of accuracy. Looking at the current, it is apparent that the current components do not exceed about 300 kHz. This shape derives from the fact that the motor’s inductance component makes it less likely that high-frequency current will flow, as described above.

Table 1 Specifications of measured SiC inverter and motor

Inverter		Motor		
Switching element	Switching frequency	Inductance	Resistance	Rated power output
SiC-MOSFET SCH2080KE (ROHM)	20 kHz	3.6 mH	0.9 Ω	120 W

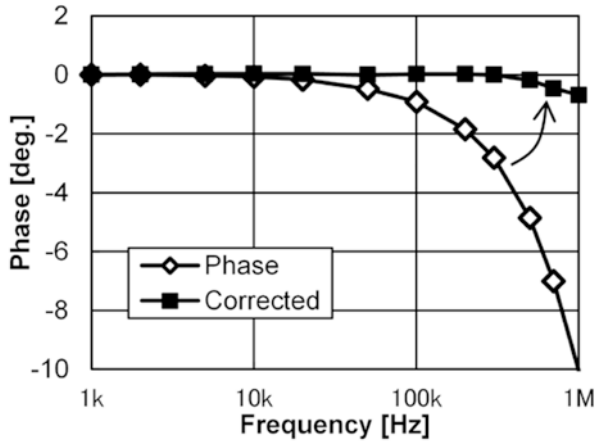


Fig. 4 Compensating a current sensor’s phase error

In this way, it is desirable to use a power analyzer with favorable characteristics for voltage, current, and phase difference characteristics in the frequency band of at least five times the switching frequency in order to allow accurate measurement of the inverter’s output power. Use of increasingly high switching frequencies for SiC inverters has the effect of requiring a higher frequency band in this regard.

In general, current sensors are used when measuring current in a motor drive system. This is due to both the ease of installing the sensor and their ability to sense relatively large currents impossible to be measured by shunt resistors. In such applications, the current sensors’ phase error becomes problematic. All current sensors exhibit a tendency toward increased phase error at higher frequencies, and this tendency becomes a source of error when measuring high-frequency power. As shown in Fig. 2, the motor windings’ inductance component is dominant at high frequencies. For this reason, power at the switching frequency and its harmonics are characterized by a lower power factor. Based on Eq. (1), phase error has an extremely large impact on power measurement error at low power factor values (θ values of approximately 90°). Consequently, it is not possible to measure loss through power measurement at a high degree of precision unless the current sensors’ phase error can be corrected. HIOKI’s Power Analyzer PW6001 provides functionality for correcting for current sensor phase error, as shown in Fig. 4. This phase shift function makes it possible to measure inverter output power more accurately.

2.3 *Measuring a Motor's Power*

In order to measure the overall efficiency and loss of a motor or motor drive system, it is necessary to measure the motor's power. To calculate motor power P_m [W] using Eq. (2), we all need to measure torque T [N · m] and Motor rpm n [rpm].

$$P_m = T \cdot 2 \cdot \pi \cdot n / 60 \quad (2)$$

The motor's rpm is measured using a tachometer or pulse encoder, while torque is measured using a torque meter. In order to measure efficiency and loss, it is necessary to measure power and motor power at the same time. Consequently, we need to use a power analyzer that can accept signals from a tachometer, pulse encoder, and torque meter as input.

3 High Precision Power Measurement [3]

Wide bandgap power semiconductors such as SiC and GaN are expected to miniaturize passive components by increasing the switching frequency and to reduce loss by low on resistance. The switching frequency of inverters mounted with these power semiconductors is becoming increasingly high, and power measurement with a wider band and higher precision than ever is required. Current measurement in a power meter (power analyzer) is generally performed by either a direct connection method or a current sensor method. Furthermore, a shunt resistor is generally used for the current detection in the former direct connection system. Table 2 shows each feature comparison.

3.1 *High Precision Power Measurement Using the Current Sensor Method*

In order to achieve high precision power measurement with high repeatability using the current sensor method described in Table 2, it is important to use the following standards as conditions for selecting the appropriate current sensor:

1. The rated current of the current sensor matches the current level of the DUT.
2. The DUT's switching frequency of the current and all of the frequency components including harmonics are within the measurable frequency bandwidth of the current sensor.
3. Measurement accuracy of the current sensor is defined across its entire measurable frequency bandwidth, and that the accuracy is sufficiently high.

Table 2 Characteristic comparison of current measurement method by power analyzer

	Direct wiring method	Current sensor method
Strengths	<p>(a) The power analyzer can measure current by itself, a very simple principle.</p> <p>(b) Appropriate for measuring very low levels of current such as standby current of electronic devices or current consumption of LED lighting.</p>	<p>(a) The DUT can be measured while still in operation.</p> <p>(b) Appropriate for measuring large currents because self-heating when measuring large currents is minimal, causing no effects to the measurement accuracy.</p>
Weaknesses	<p>(a) Conditions during measurement and actual operation conditions of the DUT differ.</p> <p>(b) Loss from routed cables due to resistance is large.</p> <p>(c) Capacitance coupling between wires and and GND can occur, leading to increased current leakage at high frequencies.</p> <p>(d) Current flow to shunt resistors can generate joule heat proportional to the square of the current, which will not only create resistance loss in and of itself, but also alter the resistance value due to self-heating, leading to worse measurement accuracy.</p> <p>(e) To minimize joule heat, a small shunt resistor with low resistance is required, and the effects of parasitic impedance will worsen the high frequency characteristics.</p> <p>(f) If wiring to the power analyzer is not done properly, contact resistance will result, leading to unexpected heating when large currents are measured, which can cause damage to the device and other associated hazards.</p>	<p>(a) Accuracy of the current sensor must be added to the accuracy of the power analyzer, making measurements at this level slightly worse than the direct wiring method in comparison.</p> <p>(b) Measurements are subject to effects from the measurement environment (effects of conductor position, external magnetic fields, and temperature).</p> <p>(c) A separate power supply to drive the current sensor is required.</p>
Layout	<p>In the direct wiring method, wires from the DUT are routed to the power analyzer to directly measure the current.</p>	<p>In the current sensor method, wires from the DUT are connected to the current sensor, and the output from the sensor (either current or voltage) is fed into the power analyzer to measure the current</p>

4. Uncertainty with respect to the current sensor’s output noise, temperature characteristics, effect of conductor position, effect of external magnetic fields, magnetic susceptibility, effect of common-mode voltage, etc., are clearly defined and sufficiently small.

In particular, it is important to note that with regard to condition (3), many general current sensors define accuracy solely for DC and 50/60 Hz signals, while accuracy for all other frequencies are only stated for typical reference. When using the current sensor method to measure power with high precision, careful attention must be paid to select both a power analyzer [2] and current sensor that exhibit the appropriate performance levels.

3.2 Power Analyzer Frequency Band and Sampling Frequency [1]

Figure 5 illustrates the relationship between sampling frequency and analog band in a typical power analyzer. The analog band of most power analyzers' input circuitry is greater than half the sampling frequency f_s (i.e., $f_s/2$). In such instruments, the voltage and current components that exist in frequencies higher than $(f_s/2)$ appear in the low-frequency domain as folding noise. This phenomenon is generally known as aliasing.

When measuring signals that include frequency components across a broad band like a PWM waveform, it becomes impossible to distinguish between the folding noise and the actual signal. HIOKI's power analyzer defines the analog band and sampling frequency based on the sampling theorem. General power analyzers other than HIOKI products specify analog band and sampling frequency that are inconsistent with the sampling theorem. When measuring wideband frequency components such as PWM waveforms, it is often not possible to clearly separate between actual harmonics and aliasing noise. For this reason, we described that "The result is that accurate analysis becomes impossible, and, for example, detection of false harmonic components more likely".

As shown in Fig. 3, inverter output voltage includes components in excess of 1 MHz. Standard power analyzers have sampling frequencies ranging from 100 kHz

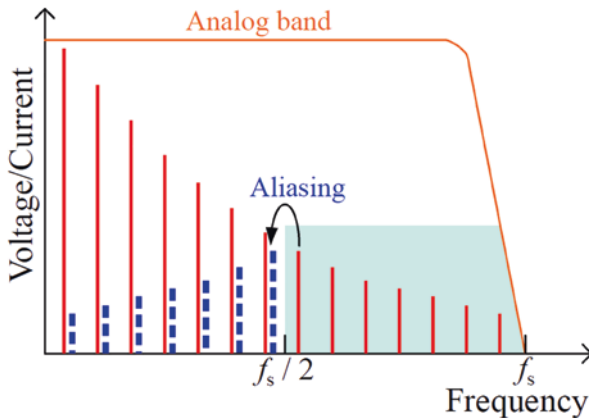


Fig. 5 Relationship between analog band and sampling frequency in a standard power analyzer

to about 5 MHz. Consequently, there are voltage components at frequencies in excess of $(f_s/2)$. In such cases, accurate measurement is not possible when the analog band and sampling frequency are related as shown in Fig. 5. To enable accurate measurement, it is necessary to limit the analog band to less than $(f_s/2)$. In other words, the band that can actually be used is less than half the sampling frequency.

In this way, when measuring and analyzing the output power of an inverter, it is necessary to use a measuring instrument that has been designed in accord with sampling principles. HIOKI's power analyzers are designed in this way. For example, the Power Analyzer PW6001 has a sampling frequency of 5 MHz versus a conventional analog band of 2 MHz/−3 dB. Consequently, the instrument is capable of simultaneous broadband power measurement, accurate harmonic analysis, and accurate FFT analysis.

4 Wide Band and Large Current Sensors [4–6]

For nearly 50 years, HIOKI has developed high performance current sensors based on proprietary technology. Figure 6 shows the classification of current sensors based on six different operating principles. HIOKI is one of the few manufacturers in the world that designs and produces its own current sensors to pair with power analyzers, power meters, and oscilloscopes.

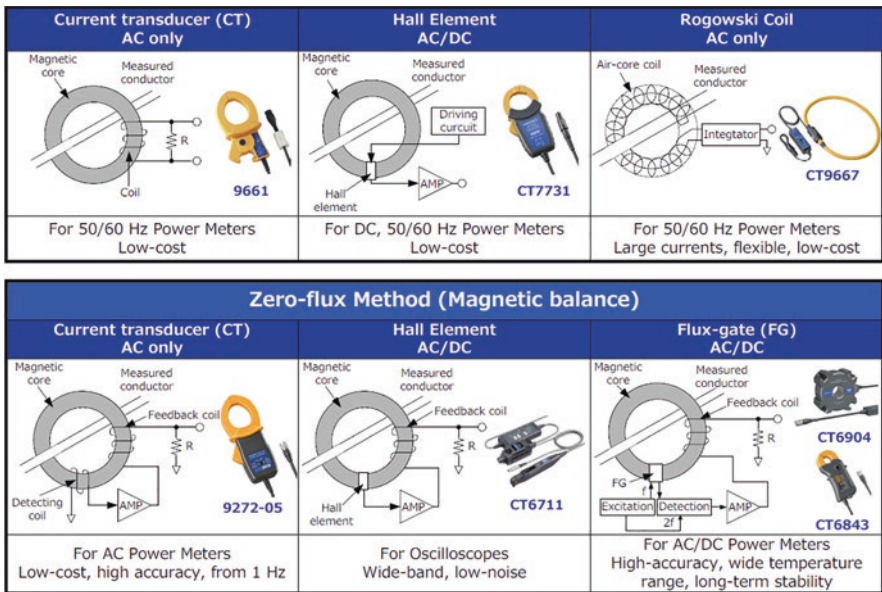


Fig. 6 Classification of current sensors by principle of operation

The AC/DC current sensor CT6877 developed in this time uses the zero flux method with a flux gate element, one of six current sensor types. This principle will be described below.

4.1 Principle of Operation of AC/DC Zero-Flux Method Using Flux-Gate (FG) Element

Figure 7 shows the principle of operation. A secondary current that is proportional to the turn ratio in the feedback winding on the secondary side of the circuit flows so as to cancel out the magnetic flux Φ produced in the magnetic core by the AC current flowing in the conductor being measured (the primary side of the circuit). In the low-frequency region starting at DC, the magnetic flux cannot all be canceled out, and some remains. The magnetic flux that remains is detected by the FG element, and a secondary current is made to flow by the amp circuit so as to cancel out the magnetic flux Φ . This secondary current flows to the shunt resistor, producing a voltage across its terminals. This voltage is the measurement circuit's output, which is proportional to the current flowing in the conductor being measured.

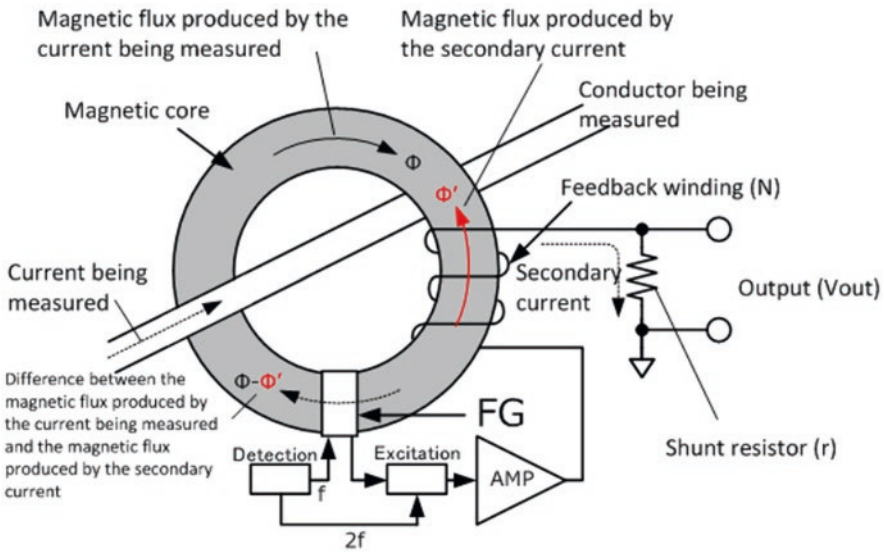


Fig. 7 Principle of operation of AC/DC zero-flux method using flux-gate (FG) element

4.2 Features Compared to Other Current Measurement Methods

1. This method delivers excellent linearity and maintains high precision down to low-level currents.
2. The method exhibits low insertion impedance since it is characterized by low operating magnetic flux levels.
3. Since the FG element that detects DC current has an extremely small offset across a broad temperature range for reasons related to its operating principle, the sensor is able to deliver high accuracy and stability.

Table 3 provides the key specifications of the CT6877

4.3 New CT Coil Structure that Achieves Wide Bandwidth Characteristics

Figure 8 shows the newly developed opposed split coil architecture and an example of its frequency characteristics (opposed split coil: a coil that increases the measurement band for current by utilizing a split winding in an opposed arrangement around

Table 3 Key specifications of model CT6877

Rated current	AC/DC 2000 A Within the frequency derating characteristics (Fig. 10)
Maximum input current	Maximum input of up to ± 3200 A peak (design value) allowed at 40 °C or less for 20 ms or less
Frequency bandwidth	DC to 1 MHz (± 3 dB typical)
Linearity	± 10 ppm typical (23 °C)
Offset voltage	± 10 ppm typical (23 °C, no input)
Accuracy (DC or basic)	$\pm 0.04\%$ rdg. $\pm 0.008\%$ f.s. (DC, 45 Hz $\leq f \leq$ 65 Hz, 0 °C to 40 °C, 80% RH or less)
Common-mode voltage rejection ratio (CMRR)	140 dB or greater (50 Hz/60 Hz), 120 dB or greater (100 kHz) (effect on output voltage/common-mode voltage)
Measurable conductor size	$\phi 80$ mm (3.15 in) or less
Output voltage	1 mV/A
Output resistance	50 $\Omega \pm 10 \Omega$
Maximum rated voltage to ground	1000 V CAT III Expected transient overvoltage 8000 V
Standard compliance	Safety EN 61010–2-030:2010 EMC EN 61326–1:2013
Operating temperature and humidity	–40 °C to 85 °C, 80% RH or less (no condensation)
Power supply	Power supplied from PW6001, PW3390, CT9555, CT9556, CT9557, or external DC power supply

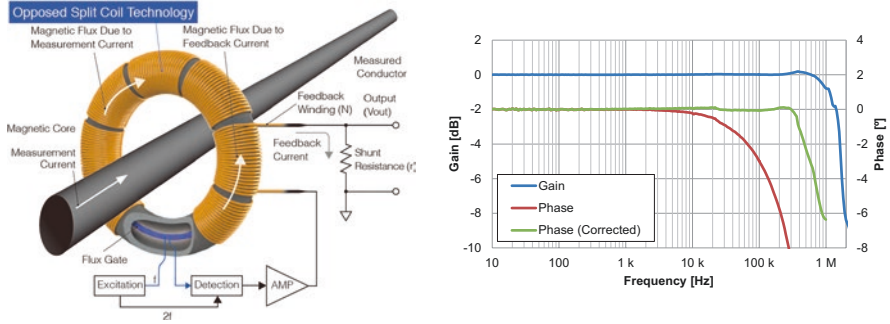


Fig. 8 CT coil structure of the CT6877 and example frequency characteristics

a magnetic core). By utilizing a new CT coil structure in a closed-loop current sensor in which feedback current is made to flow to a feedback winding so as to continuously zero out the magnetic field generated by the current under measurement, we were able to achieve wide frequency bandwidth from DC to 1 MHz. The phase values appearing in the example frequency characteristics graph illustrate the difference when the HIOKI PW6001 Power Analyzer’s phase shift function is activated. Performed properly, phase shift yields significantly better phase characteristics in the high-frequency region.

4.4 Shield Structure that Achieves Superior Noise Resistance and CMRR

Figure 9 shows the shield structure of the CT6877 and frequency characteristics with respect to CMRR. By completely shielding the opposed split coil with a solid shield crafted from aluminum, we were able to achieve exceptionally wide measurement bandwidth and noise resistance. For example, the sensor delivers a common-mode rejection ratio (CMRR) of 120 dB (1/1 million) at 100 kHz, enabling it to measure accurately with low susceptibility to surrounding electric fields.

5 Application Example

5.1 Comparison of Three-Phase Motor U-Phase Current Waveforms from an SiC Inverter

Figure 11 shows the results of observation of the U-phase voltage waveform and current waveform between the inverter and the three-phase motor. Connect five current sensors the latest model CT6875 (rated current: 500 A), CT6876 (rated current:

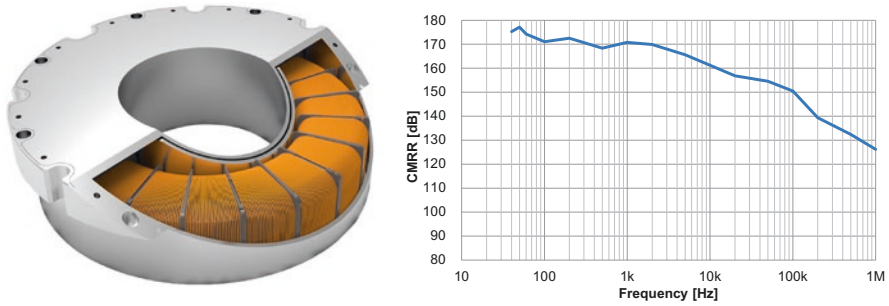


Fig. 9 Shield structure of the CT6877 and frequency characteristics with respect to CMRR

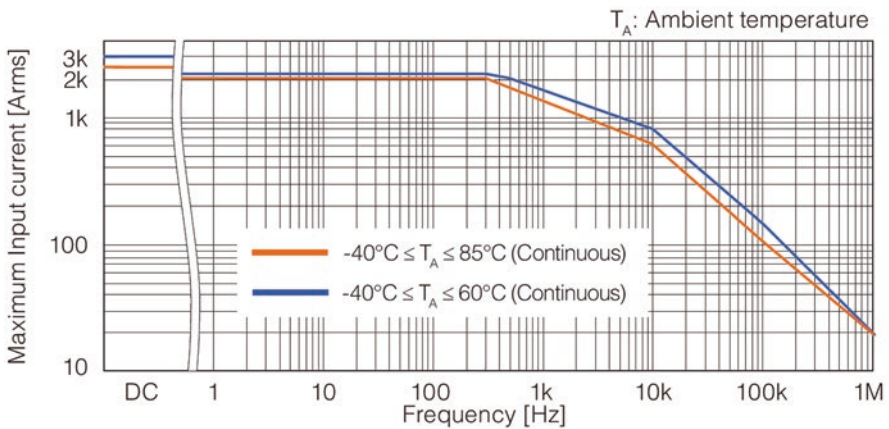


Fig. 10 Frequency derating characteristics of the CT6877

1000 A), CT6877 (rated current: 2000 A), the conventional model 9709 (rated current: 500 A), and CT6865 (rated current: 1000 A) to the power analyzer and compare the current waveforms at the same time. As a result, the latest model is observed to be less affected by noise compared to the conventional model, and it is understood that the current waveform can be accurately measured without being affected by the switching noise at a high carrier frequency (100 kHz).

6 Conclusion

This chapter discussed the importance of using a power analyzer and current sensor properly to make more accurate measurements of the efficiency of an inverter motor. In addition, the combination of the Power Analyzer PW6001 and Current Sensor

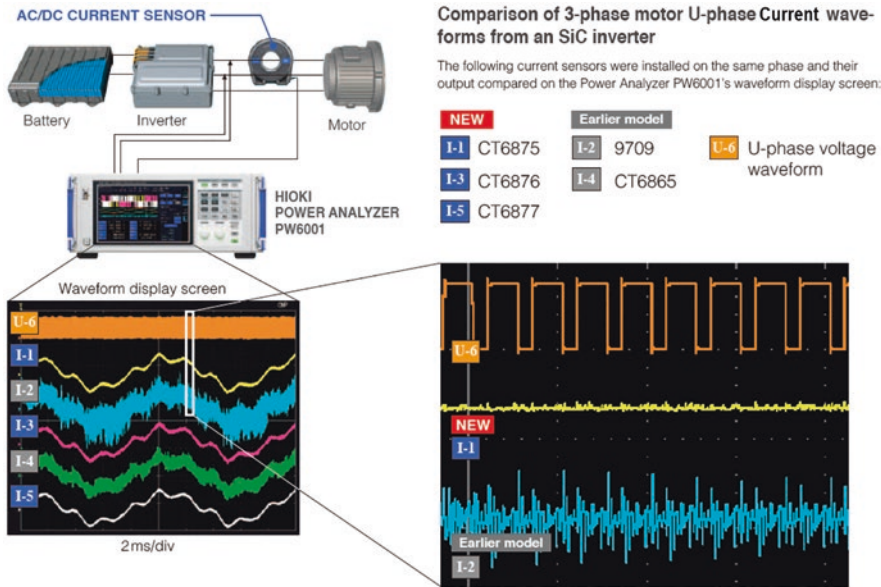


Fig. 11 Comparison of three-phase motor U-phase current waveforms from an SiC inverter

CT6877, which have excellent performance, has enabled measurements in applications that were previously difficult to measure.

In the power electronics field, frequencies will continue to increase, along with the need to perform high precision analysis of power efficiency and other factors. HIOKI is confident in our ability to contribute to the development of industrial society through the development of advanced measuring instruments.

References

1. K. Hayashi, High-precision Power Measurement of SiC Inverters. Bodo’s Power Systems. September 2016, pp. 42–47
2. H. Kondo, C. Yamaura, Y. Saito, H. Kobayashi, Effectiveness of Phase Correction When Evaluating High-Efficiency Motor Drive. Bodo’s Power Systems. November 2017, pp. 44–49
3. H. Yoda, H. Kobayashi, S. Takiguchi, Current Measurement Methods that Deliver High Precision Power Analysis in the Field of Power Electronics. Bodo’s Power Systems. April 2016, pp. 38–42
4. K. Ikeda, H. Masuda, High-precision Wideband High Stable Current Sensing Technology. Bodo’s Power Systems. July 2016, pp. 22–28
5. M. Harano, Development of a Wideband High-precision Current Sensor. Bodo’s Power Systems. November 2018, pp. 52–59
6. M. Harano, H. Yoda, K. Seki, K. Hayashi, T. Komiyama, S. Yamada, Development of a Wideband High-precision Current Sensor for Next Generation Power Electronics Applications. Proceedings of the IEEE 2018 Energy Conversion Congress and Expo (ECCE 2018) (Portland, USA, 23–27 September 2018), pp. 3565–3571

Evaluation and Application of Existing Air Curtain Effectiveness Methodology



Liangzhu (Leon) Wang, David A. Johnson, and Frank Cuaderno

Nomenclature

A	Area
A_i	Door section area of the i th section
b_0	Air curtain nozzle depth
b_v	Nozzle depth of the virtual air curtain
C_A	Airflow coefficient
C_D	Discharge coefficient
$C_{D,ac}$	Average discharge coefficient for each door operation section
D	The distance from the test point to the discharge nozzle
D_v	The distance from the test point to the virtual nozzle
$D_{D,ac}$	Discharge modifier (air curtains)
H	Door height
H_v	Door height of the virtual air curtain
q	Representative flow rate
q_i	Representative flow rate of the i th section
q_h	Representative flow rate at the air curtain level
q_l	Representative flow rate at the ground level
Q	Volume flow rate
Q_{AC}	Total volume flow rate with the air curtain installed
Q_{ACi}	Volume flow rate of the i th section
Q_{SD}	Volume flow rate of the single door
ΔP_{oi}	Pressure difference across the air curtain doors
u	Airflow velocity
u_0	Discharge velocity
u_{0i}	Average discharge velocity of the i th nozzle section
u_E	Equivalent discharge velocity
u_{Ei}	Equivalent discharge velocity of the i th nozzle section
u_{testi}	Measured airflow velocity of the i th section
u_v	Discharge velocity of the virtual air curtain

L. (Leon) Wang · D. A. Johnson (✉) · F. Cuaderno
Berner International LLC, New Castle, PA, USA
e-mail: leon.wang@concordia.ca; djohnson@berner.com; Frankc@marsair.com

W	Door width
w_i	Section width of the i th section
x	Distance to the air curtain
θ	Air curtain discharge angle
ρ	Air density
$\eta_{\left(\frac{AC}{SD}\right)}$	Efficiency factor

1 Introduction

Air infiltration and exfiltration through building entrance doors may contribute to a large part of building heating and cooling loads. In previous studies, the operational characteristics of air curtain units were investigated and the potential in energy saving was justified ([4, 5, 6, 15, 16]). The airflow patterns of the air curtain jet under different pressure differences could be categorized into three working conditions: inflow breakthrough (IB), outflow breakthrough (OB), and optimum condition (OC) [7, 13–16], corresponding to the different performances of blocking the infiltration/exfiltration between indoor and outdoor environments.

The infiltration/exfiltration flow rate reflects the sealing effectiveness of air curtain units [2, 6, 10, 11]. However, there is no efficiency evaluation method that is convenient enough to obtain the infiltration/exfiltration information through door openings. Current air curtain efficiency rating method used in Europe requires a full-scale testing in an environmental chamber [3, 8] involving a series of well-controlled test conditions, such as chamber temperature, pressure, fan power, etc. The infiltration/exfiltration flow rate through the test chamber door opening is measured to obtain the efficiency factor of the air curtain based on the test sensors. Meanwhile, another air curtain test method proposed by American National Standards Institute/Air Movement and Control Association (ANSI/AMCA) Standard 220-05 [1] or International Organization for Standardization (ISO) Standard 27327-1:2009 [12] is focused on the aerodynamic performance in terms of airflow velocity and uniformity. Without the need of the climate chamber testing, a test can be conducted in a common environment, so it is relatively simpler than the European method. However, there is a lack of method that can relate the ANSI/AMCA or ISO Standards velocity test results to the infiltration/exfiltration rate and the air curtain efficiency. If the aerodynamic performance and the infiltration rate can be related directly, the ANSI/AMCA or ISO aerodynamic test method could be directly applied to the efficiency rating, which significantly reduces the cost of testing and rating while promoting a widely accepted standardized test methodology.

In this study, the relationships between the infiltration/exfiltration rates and the pressure differences for different air curtain discharge velocities are explored and correlated based on multiple computational fluid dynamic (CFD) simulation results. A novel method to relate the air curtain aerodynamic performance data to its effectiveness was developed for the calculation of the air curtain efficiency factor.

In Sect. 2, the details and the procedure of this method are explained. Section 3 demonstrates the whole procedure by three case studies. Section 4 elaborates the validation method and the results. Finally, the conclusions and limitations of the current study are outlined in Sect. 5.

2 The Efficiency Factor Calculation Methods

2.1 The Method for Door Height Within 3 Meters

The air curtain effectiveness is often assessed by the efficiency factor $\eta_{\left(\frac{AC}{SD}\right)}$ (Eq. 1) [6] based on the ratio of the flow rate through the door opening with the air curtain (i.e., air curtain door), and without the air curtain installed (i.e., single door). The single-door flow rate Q_{SD} can be estimated by the model (Eq. 2) proposed by Yuill [17, 18] dependent on the door size and the pressure difference. It is common that the discharge coefficient for the single door, $C_D = 0.65$. For the air curtain door, the infiltration rate Q_{AC} may also depend on the air curtain jet properties. Note that hereafter, the infiltration and the infiltration/exfiltration are used interchangeably if not specified. Wang and Zhong [15, 16] developed the air curtain infiltration/exfiltration model by adding a modifier coefficient $D_{D,AC}$ (Eq. 3) to Eq. 2. The coefficients in the model, $C_{D,AC}$ and $D_{D,AC}$, can be characterized by experiments or simulation results.

$$\eta_{\left(\frac{AC}{SD}\right)} = 1 - \frac{|Q_{AC}|}{|Q_{SD}|} \tag{1}$$

$$Q_{SD} = C_D A \sqrt{\frac{2\Delta P_{oi}}{\rho}} \tag{2}$$

$$\frac{Q_{AC}}{A\sqrt{2/\rho}} = \text{sign}(\Delta P_{oi}) C_{D,AC} \sqrt{|\Delta P_{oi}|} + D_{D,AC} \tag{3}$$

The proposed air curtain effectiveness rating method estimates the infiltration rates from the aerodynamic performance measurement data to determine the air curtain effectiveness for various design parameters, for example, discharge velocity u_0 , nozzle depth b_0 , discharge angle α , and door height H .

The discharge velocities of the nozzle sections are directly related to the capability of the air curtain to protect the corresponding door sections against the indoor and outdoor pressure differences. Following ANSI/AMCA Standard 220-05 [1] or ISO Standard 27327-1:2009 [12], if x is the coordinate direction along the jet flow centerline and y is the distance to the centerline in the plane perpendicular to the x -axis, the centerline peak velocity $u_{rest,i}$ ($y = 0$) from a distance D to the nozzle sections can be measured (Fig. 1).

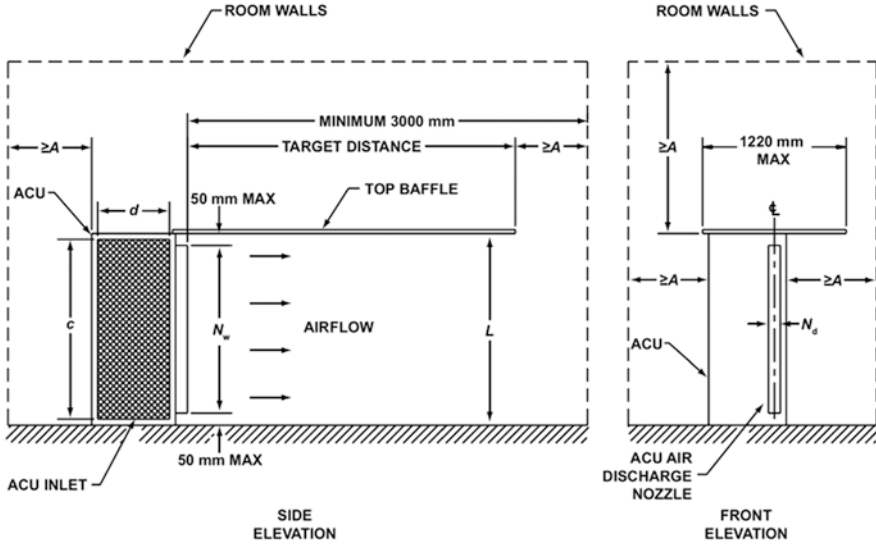


Fig. 1 Aerodynamic test setup specified in ANSI/AMCA Standard 220-05 [1]

In the standard, the air curtain vanes are adjusted to an angle of 15° (Fig. 2b). In comparison, the proposed aerodynamic test by this study is slightly different, which requires the discharge angle to be 0° (Fig. 2a).

The reason is that the proposed method needs to calculate air curtain discharge velocities based on the jet theory, which has nothing to do with the jet angle. In other words, this study assumes that the air curtain jet follows the jet theory equation (Eq. 4) in the fully developed zone ($x > 5.2 b_0$) [9]. Using the measured velocity distribution for the setup in Fig. 2a following the ANSI/AMCA Standard 220-05 or ISO 27327-1:2009, we can back-calculate (or inversely calculate) the average discharge velocity of each nozzle section $u_{0,i}$ (Eq. 5).

$$\frac{u}{u_0} = \frac{\sqrt{3}}{2} \sqrt{\frac{b_0 \sigma_2}{x}} \left[1 - \tan^2 \left(\sigma_2 \frac{y}{x} \right) \right], x > 5.2 b_0, \sigma_2 = 7.67 \tag{4}$$

$$\frac{u_{\text{test},i}}{u_{0,i}} = \frac{\sqrt{3}}{2} \sqrt{\frac{b_0 \sigma_2}{x}}, y = 0, \sigma_2 = 7.67, x = H \tag{5}$$

When the air curtain discharge velocity for each section is known, it is then possible to determine the corresponding air curtain door infiltration/exfiltration rate, Q , based on a series of standard air curtain Q - ΔP curves. These figures are obtained using the existing experimental and numerical simulation studies of previous air curtain studies, which cover a wide range of pressure differences and typical discharge velocities and angles. For a given air curtain unit with known discharge velocity and angle, and operating pressure difference, the infiltration/exfiltration

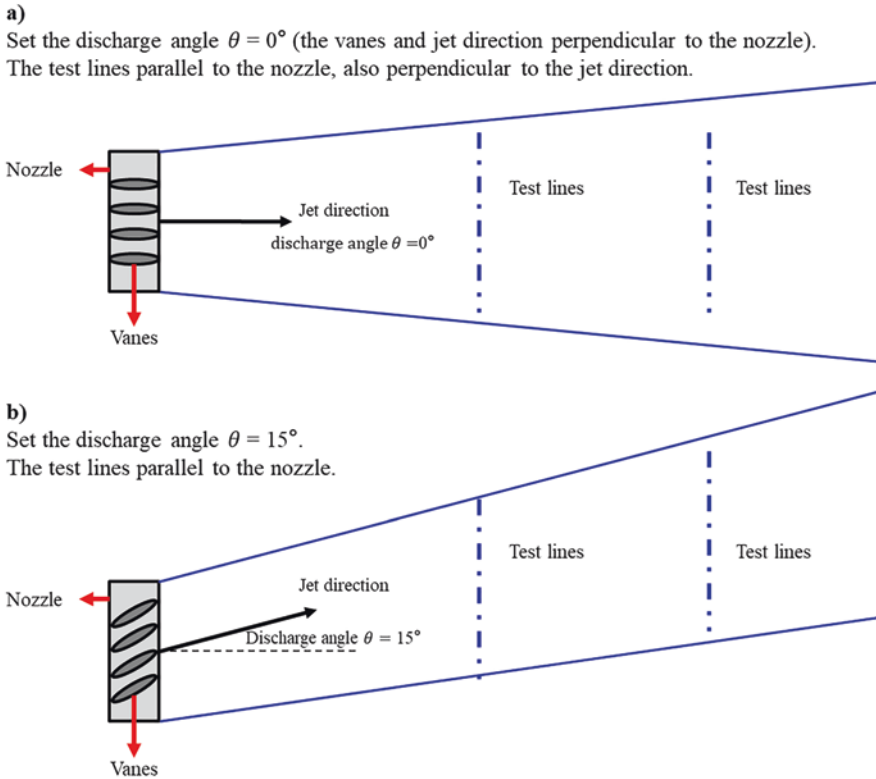


Fig. 2 Difference of the top views of (a) the proposed aerodynamic test in this method and (b) the method in ANSI/AMCA Standard 220-05 [1]

flow rate values for the air curtain can then be interpolated among these curves. The air curtain efficiency factor can then be evaluated using Eq. 1.

In this report, the scenarios of three typical discharge angles (0° , 10° , 20°), two nozzle depths (0.08 m and 0.10 m), and two door heights (2.4 m and 3 m) are considered as listed in Table 1 and the typical Q - ΔP curve figures are provided in the Appendix A. The figures for a 0.71 m height door, nozzle depth 0.0635 m, and 20° discharge angle were generated by previous research data for the validation of the proposed method.

When an air curtain supply nozzle is separated into n sections and the width of the i th ($i = 1 \sim n$) section is w_i , each nozzle section is supposed to protect a corresponding door section below with an area of $A_i = Hw_i$. Therefore, an important step is to relate the area-averaged infiltration rates of the sections to their calculated discharge velocities. The typical Q - ΔP curves have been adjusted with a representative flow rate q as defined in Eq. 6a and substituted for the volumetric flow rate Q in Fig. 3. After the value of q_i for each air curtain subsection is interpolated, the infiltration rate of the door sections can be calculated by Eq. 6b. For this study, only

Table 1 List of the typical Q- ΔP curve figures

Discharge angle (°)	Nozzle depth (m)	Door height (m)	Figure index
20	0.0635	0.71	Case [20, 0.0635, 0.71] (for validation)
0	0.08	2.40	Case [0, 0.08, 2.4]
		3.00	Case [0, 0.08, 3.0]
	0.10	2.40	Case [0, 0.10, 2.4]
		3.00	Case [0, 0.10, 3.0]
10	0.08	2.40	Case [10, 0.08, 2.4]
		3.00	Case [10, 0.08, 3.0]
	0.10	2.40	Case [10, 0.10, 2.4]
		3.00	Case [10, 0.10, 3.0]
20	0.08	2.40	Case [20, 0.08, 2.4]
		3.00	Case [20, 0.08, 3.0]
	0.10	2.40	Case [20, 0.10, 2.4]
		3.00	Case [20, 0.10, 3.0]

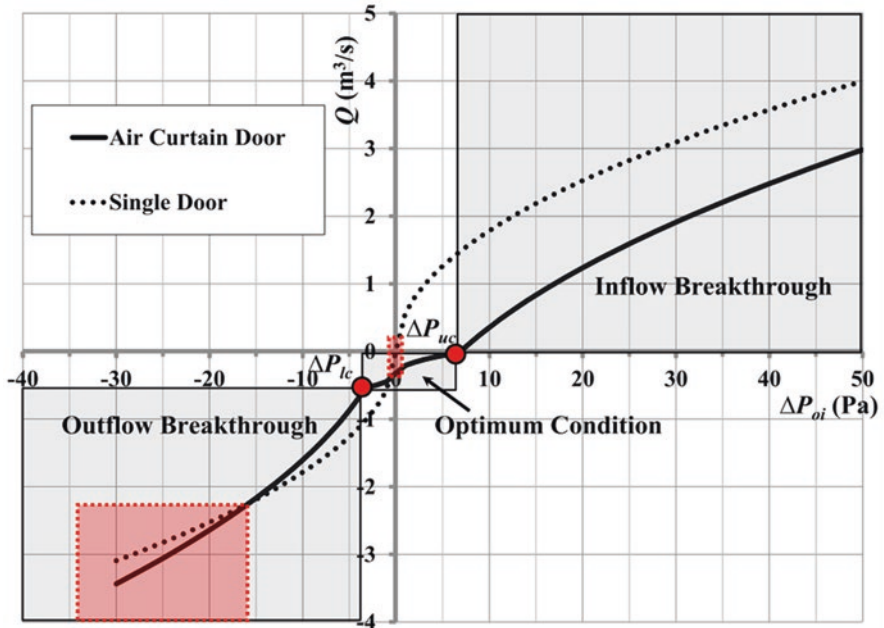


Fig. 3 Typical Q- ΔP curves in Goubran, et al. [7]

isothermal situation is investigated so the air density is considered a constant (1.2 kg/m³). Finally, the total airflow rate can be calculated by the sum of all the door sections (Eq. 7).

$$q = \frac{Q_{AC}}{A_i \sqrt{\frac{2}{\rho}}} \quad (6a)$$

$$Q_{AC,i} = A_i \sqrt{\frac{2}{\rho}} q_i \quad (6b)$$

$$Q_{AC} = \sum_{i=1}^n Q_{AC,i} \quad (7)$$

In summary, the five-step procedure to calculate the efficiency factor is as follows:

1. Separate the discharge nozzle into multiple sections and perform the aerodynamic test following ANSI/AMCA Standard 220-05 or ISO 27327-1:2009 to measure the jet flow distribution, $u_{test,i}$.
2. Calculate the discharge velocity $u_{0,i}$ for each section based on the measured velocity and the jet theory (Eq. 5).
3. Determine the representative flow rate q_i for each nozzle section from the standard Q - ΔP curves in [Appendix A](#).
4. Calculate the infiltration rate for each door section $Q_{AC,i}$ (Eq. 6), then sum them up to obtain the total airflow rate through the door Q_{AC} (Eq. 7); and calculate the infiltration rate for the corresponding single door, Q_{SD} , by Eq. 2.
5. Calculate the efficiency factor, $\eta_{\left(\frac{AC}{SD}\right)}$, (Eq. 1).

2.2 The Method for Door Height over Three Meters

In our proposed method, the important step is to determine the representative flow rate q by the standard Q - ΔP curves. Normally, a standard figure for the Q - ΔP curve is used for a specified series of products that share the similar parameters (nozzle depth b_0 , discharge angle α , and door height H). The specific scenarios in this report are listed in [Table 1](#), limited to the door height of less than three meters. To apply these standard Q - ΔP figures for the door height more than three meters, we proposed a new method based on the concept of the equivalent air curtain model as explained in [Fig. 4](#).

In an actual situation, the jet flow degrades and diverges gradually with the distance from the air curtain nozzle, implying that most of the infiltration/exfiltration, if any, should occur near the ground level rather than the higher level: that is, $q_h < q_l$.

For a door height more than three meters, if we follow the proposed method in the previous section ([Fig. 4a](#)), we need to determine q_i (Eq. 6), which is the

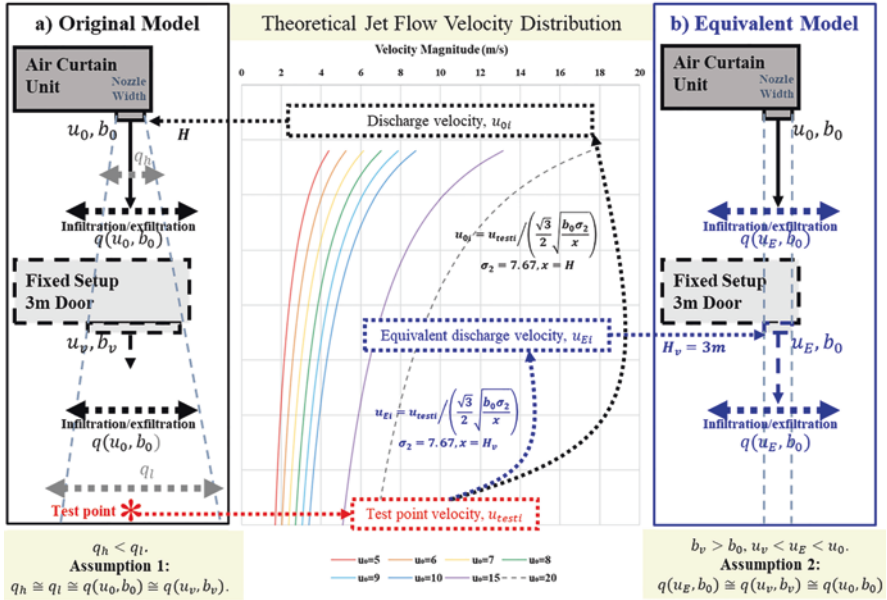


Fig. 4 (a) The original model and (b) the equivalent model for more than 3 m door height

area-averaged infiltration/exfiltration rate. The existing standard figures are based on the door height of three meters or less. For the door height over three meters, it is possible to assume that a virtual air curtain with the nozzle depth b_0 is located at the height of three meters above the floor (the equivalent model in Fig. 4b). This assumption is reasonable since for a typical air curtain, most of the infiltration/exfiltration occurs near the floor. Then, a similar five-step procedure as in Sect. 2.1 can be applied to the door higher than three meters with the following two assumptions:

1. The virtual air curtain located at 3-m height from the floor is with the nozzle depth of b_0 and the equivalent discharge velocity u_E .
2. The area-averaged infiltration rate, q_i , through the 3-m-height door section with the virtual air curtain is the same as that of the whole-door section with the actual air curtain unit.

Accordingly, the second and the third steps of the five-step procedure in Sect. 2.1 should be adjusted. In the second step, after the nozzle section is separated, the equivalent discharge velocity u_E at 3-m height should be calculated using the nozzle depth b_0 instead of the actual air curtain depth at the same height, b_v . For the third step, the standard figures for 3-m-high door should be used for the interpolation of the equivalent flow rate q_i , with the exception that the actual door height H should be used for the calculation of the total door section infiltration rate $Q_{AC, i}$ and the single-door flow rate Q_{SD} .

2.3 Resulting Calculation Procedure of Efficiency Factor

The methods are illustrated by the flowchart in Fig. 5. Note the velocity distribution is measured at the objective distance, that is, at the floor level: H (the door height) from the nozzle. For the equivalent model, the distance to the virtual air curtain unit is always 3 m. When there is no standard figure available, the existing standard figures close to the design parameters should be used by either interpolations or extrapolations.

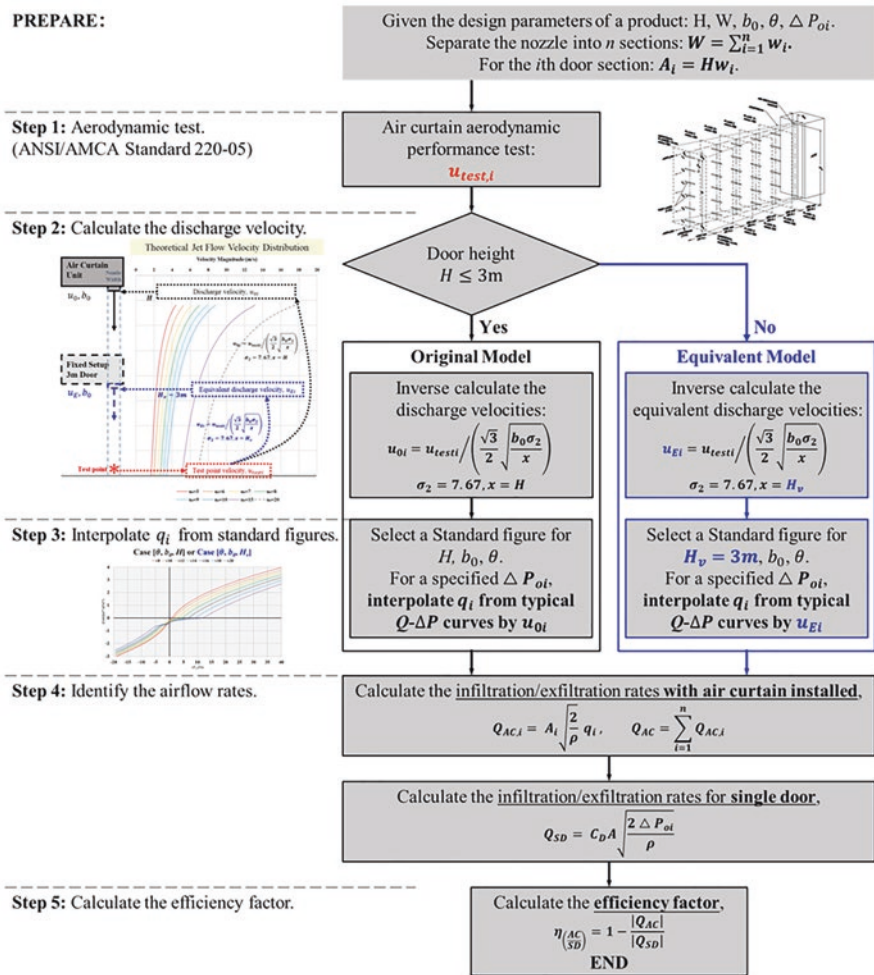


Fig. 5 Flowchart illustrating the procedure to calculate the efficiency factor

3 Case Studies and Discussions

In this section, three case studies are conducted to demonstrate the proposed efficiency factor calculation method. The first case study is for ordinary scenarios where the door height is within 3 m and corresponding standard figures are available; thus the procedure of calculation follows the original model in the flowchart in Fig. 5. The second and third case studies are for scenarios of door height more than 3 m; thus an estimation of the efficiency factor can only be carried out through the equivalent method by using the provided standard figures for 3 m doors.

The air curtain work conditions can be classified into three categories: the inflow breakthrough, optimum condition, and outflow breakthrough (Fig. 3). This classification is only based on the airflow rate through the door opening and the overall pattern of the air curtain jets. When it comes to the efficiency factor, as is defined by Eq. 1, the ratio of the absolute value of the infiltration/exfiltration flow rate with and without an air curtain installed matters. The distribution of the efficiency factor with the pressure difference will follow the theoretical pattern in Fig. 6. Some negative efficiency factor may occur in the outflow breakthrough and optimum conditions, respectively (Fig. 6). The negative efficiency factor values indicate that air curtain will have more exfiltration than single door. From considering a real-life scenario and mass balance, the exfiltration due to air curtain ought to be replaced from another source. With this concept, the correction to the $\eta_{\text{air}} \left(\frac{AC}{SD} \right)$ was made as shown by the corrected curve (i.e., dashed lines) in Fig. 6.

When the pressure difference is large enough to bend the main part of the air curtain jet, a CFD analysis shows that the air curtain jet may cause more airflow exfiltration rate through the door (Fig. 7). This phenomenon can be illustrated by the left red region in Figs. 3 and 6.

When the pressure difference is close to 0 Pa (the central red region in Figs. 3 and 6), the single-door infiltration/exfiltration flow rate is close to zero, and the corresponding efficiency factor defined by Eq. 1 would tend to become the infinity. This

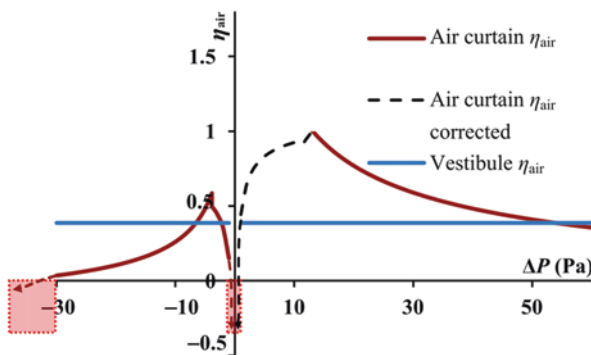


Fig. 6 Theoretical efficiency factor value distribution with different pressure difference [6]

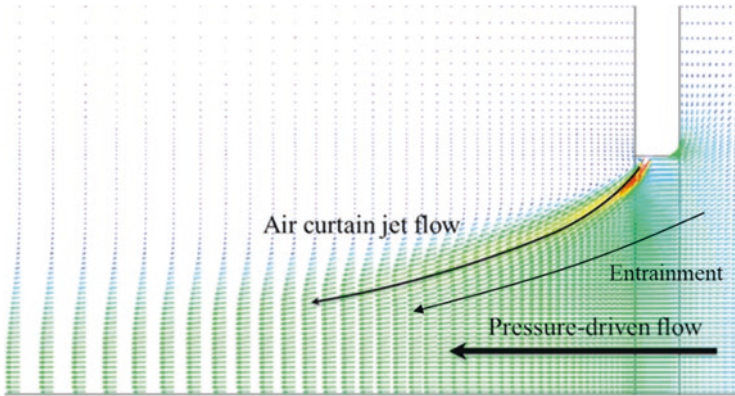


Fig. 7 Airflow pattern of fully outflow region

means that the efficiency factor in Eq. 1 becomes meaningless and trivial for this region.

3.1 Case 1: An Air Curtain for 2.4 m Door

The proposed method is demonstrated for an actual commercially available air curtain unit identified as Model A. In this case, the air curtain has a nozzle width of 1.98 m and a depth of 0.08 m, a discharge angle of 20° outward, and is designed for installation on a 2.4-m-high door.

Multiple CFD simulations were conducted to obtain the typical Q - ΔP curves, as shown in Fig. 3 based on the leakage model for air curtains (Eq. 3), for seven discharge velocities from 8 m/s to 20 m/s. The air curtain nozzle is separated into 20 sections. The width of the nozzle sections and the corresponding door sections are listed in Table 2.

In the first step, the velocity distributions at 2 m from the nozzle were measured ranging from 3.47 m/s to 4.84 m/s. Please note that the velocity distribution data provided from the manufacturer are only available up to 2 m instead of the door height of 2.4 m. Therefore, the current calculation is based on the velocity at 2 m. It is also recommended that when applying the method developed in this report, to avoid interpolations/extrapolations, the velocity distribution measurements should be available at least up to the door height where an air curtain is intended to be installed. In the second step, the corresponding discharge velocity for each section was calculated according to the jet theory in Eq. 5, where the distance x from the test points to the nozzle is 2 m. In the third step, it requires to identify the representative infiltration rates q value from the modified typical Q - ΔP curves. The discharge velocities of the sections in this case are in the range of 7.2 m/s and 10.1 m/s, so only

Table 2 Average flow rates of each nozzle section for Model A

Section number	Measured velocity (m/s)	u_0 (m/s)	Nozzle section width (m)	Door section area (m ²)	Average flow rate q_i (Pa ^{0.5}) for different pressure differences				
					25 Pa	9 Pa	1 Pa	-1 Pa	-9 Pa
1	4.84	10.1	0.1275	0.306	2.64	1.10	-0.15	-0.53	-2.03
2	4.11	8.6	0.095	0.228	2.81	1.31	-0.10	-0.58	-2.06
3	4.02	8.4	0.095	0.228	2.84	1.34	-0.09	-0.59	-2.07
4	4.53	9.4	0.0975	0.234	2.72	1.20	-0.12	-0.56	-2.05
5	4.27	8.9	0.0975	0.234	2.78	1.27	-0.11	-0.57	-2.06
6	3.89	8.1	0.095	0.228	2.87	1.38	-0.08	-0.60	-2.08
7	4.04	8.4	0.095	0.228	2.84	1.34	-0.09	-0.59	-2.07
8	4.4	9.2	0.095	0.228	2.75	1.22	-0.12	-0.56	-2.05
9	3.79	7.9	0.095	0.228	2.89	1.40	-0.08	-0.61	-2.08
10	4.1	8.5	0.0975	0.234	2.83	1.32	-0.10	-0.59	-2.07
11	3.84	8.0	0.0975	0.234	2.88	1.39	-0.08	-0.61	-2.08
12	4.49	9.4	0.095	0.228	2.72	1.20	-0.12	-0.56	-2.05
13	3.75	7.8	0.095	0.228	2.91	1.42	-0.08	-0.61	-2.08
14	4.37	9.1	0.095	0.228	2.76	1.24	-0.12	-0.57	-2.05
15	3.86	8.0	0.095	0.228	2.88	1.39	-0.08	-0.61	-2.08
16	4.02	8.4	0.0975	0.234	2.84	1.34	-0.09	-0.59	-2.07
17	3.9	8.1	0.0975	0.234	2.87	1.38	-0.08	-0.60	-2.08
18	4.17	8.7	0.095	0.228	2.80	1.29	-0.10	-0.58	-2.06
19	3.47	7.2	0.095	0.228	2.97	1.50	-0.06	-0.63	-2.10
20	3.94	8.2	0.1075	0.258	2.86	1.36	-0.09	-0.60	-2.07
Total value			1.96	4.704					

the curves of 8 m/s, 10 m/s, and 12 m/s in Fig. 17 were used for the calculation of q_i . The results for these three steps are shown in Table 2.

In the fourth step, the airflow rate through each door section $Q_{AC,i}$ can be calculated according to the door section areas and the local air density. By summing up the volumetric flow rate through each door section, the total airflow rates Q_{AC} are calculated to be 16.96 m³/s, 7.90 m³/s, -0.59 m³/s, -3.52 m³/s, and -12.42 m³/s under the pressure difference of 25 Pa, 9 Pa, 1 Pa, -1 Pa, and -9 Pa, respectively. For the pressure difference of -9 Pa, the airflow rate with an air curtain may exceed that of a single door, which is only -11.72 m³/s. The air exchange rate Q_{SD} of a single door is calculated by Eq. 2.

Finally, the efficiency factor $\eta_{\left(\frac{AC}{SD}\right)}$ can be found using Eq. 1. The results show that this air curtain unit has the ability to block 13% infiltration for the 25 Pa pressure difference, and 33% at 9 Pa pressure difference. The best efficiency is achieved for 1 Pa with 85%. For -1 Pa and -9 Pa, the corresponding efficiency factor reduced to 10% and -6%, respectively. The air curtain may step into the negative efficiency at the pressure difference of -9 Pa (Fig. 7). This is an example to show that, for a large outward discharge angle (20°), the air curtain can still perform well to separate

Table 3 Volume flow rate through the door and the air curtain efficiency for Mode A

Section number	u_0 (m/s)	Volume flow rate Q_i m ³ /s under different pressure differences				
		25 Pa	9 Pa	1 Pa	-1 Pa	-9 Pa
1	10.10	1.03	0.43	-0.06	-0.21	-0.79
2	8.60	0.82	0.38	-0.03	-0.17	-0.60
3	8.40	0.83	0.39	-0.03	-0.17	-0.60
4	9.40	0.81	0.36	-0.04	-0.17	-0.61
5	8.90	0.83	0.38	-0.03	-0.17	-0.62
6	8.10	0.84	0.40	-0.02	-0.18	-0.60
7	8.40	0.83	0.39	-0.03	-0.17	-0.60
8	9.20	0.80	0.36	-0.03	-0.16	-0.60
9	7.90	0.84	0.41	-0.02	-0.18	-0.61
10	8.50	0.85	0.40	-0.03	-0.18	-0.62
11	8.00	0.86	0.42	-0.02	-0.18	-0.62
12	9.40	0.79	0.35	-0.04	-0.16	-0.60
13	7.80	0.85	0.41	-0.02	-0.18	-0.61
14	9.10	0.80	0.36	-0.03	-0.16	-0.60
15	8.00	0.84	0.41	-0.02	-0.18	-0.61
16	8.40	0.85	0.40	-0.03	-0.18	-0.62
17	8.10	0.86	0.41	-0.03	-0.18	-0.62
18	8.70	0.82	0.38	-0.03	-0.17	-0.60
19	7.20	0.87	0.44	-0.02	-0.18	-0.61
20	8.20	0.94	0.45	-0.03	-0.20	-0.68
Total Q_{AC} m ³ /s		16.96	7.90	-0.59	-3.52	-12.42
Total Q_{SD} m ³ /s		19.53	11.72	3.91	-3.91	-11.72
Efficiency factor		0.13	0.33	0.85	0.10	-0.06

the indoor and outdoor environments when the outdoor pressure is much higher than indoor (25 Pa pressure difference), but this protection can be easily destroyed by a small negative pressure difference (-9 Pa). The results for the last two steps are shown in Table 3.

3.2 Case 2: An Air Curtain for 5 m Door

The air curtain unit described in Model B is designed for a 5-m-high door, with a nozzle width of 0.9 m and a depth of 0.08 m, and the discharge angle of 10° outward. The standard figures for door height of 3 m, nozzle depth of 0.08 m, and discharge angle of 10° were used for the calculation of q_c . The air curtain nozzle is separated into nine sections equally, with the nozzle section width of 0.1 m and the door section area of 0.5 m².

Table 4 lists the results of the first three steps. In the first step, the measured velocity distribution at five meters from the nozzle was from 3.56 m/s to 4.57 m/s following the standard. In the second step, the corresponding equivalent discharge velocities at 3 m for each section were calculated to be in the range of 9.08 m/s and 11.67m/s according to the jet theory in Eq. 5. In the third step, the typical Q - ΔP curves in Fig. 21 for 3 m door are used for the interpolation of q_i for each nozzle section.

Table 5 summarizes the results of steps 4 and 5. In the fourth step, the airflow rates through each door section $Q_{AC,i}$ are calculated according to the real door section areas (0.5 m²). By summing up the volumetric flow rate through each door section, the total airflow rates Q_{AC} are calculated to be 16.58 m³/s, 8.00 m³/s, -0.04 m³/s, -2.43 m³/s, and -11.11m³/s under the pressure difference of 25 Pa, 9 Pa, 1 Pa, -1 Pa, and -9 Pa, respectively. The air exchange rate Q_{SD} of a single door is calculated by Eq. 2 using the real door size (4.5 m²). In the fifth step, the efficiency factor $\eta \left(\frac{AC}{SD} \right)$ can be calculated by Eq. 1. The results show that this air curtain unit has the ability to block 11% infiltration for the 25 Pa pressure difference, and 29% at 9 Pa pressure difference. The best efficiency is also achieved for 1 Pa with 99%. For -1 Pa and -9 Pa, the corresponding efficiency factor reduced to 35% and 1%, respectively.

3.3 Case 3: An Air Curtain for 8 m Door

The air curtain unit Model C is designed for an 8-m-high door, with a nozzle width of 2.4 m, a depth of 0.2 m, and a discharge angle of 15° outward. As the size of this air curtain is too large for the aerodynamic test, it is separated into three modules equally along the nozzle width. Each of them has a nozzle width of 0.8 m. The

Table 4 Average flow rates of each nozzle section for Model B

Section number	Measured velocity (m/s)	Equivalent u_E (m/s)	Nozzle section width (m)	Door section area (m ²)	Average flow rate q_i Pa ^{0.5} for different pressure differences				
					25 Pa	9 Pa	1 Pa	-1 Pa	-9 Pa
1	4.32	11.02	0.1	0.5	2.82	1.33	-0.03	-0.39	-1.91
2	4.06	10.38	0.1	0.5	2.88	1.39	-0.02	-0.42	-1.93
3	4.06	10.38	0.1	0.5	2.88	1.39	-0.02	-0.42	-1.93
4	3.56	9.08	0.1	0.5	2.98	1.50	0.04	-0.48	-1.98
5	3.81	9.73	0.1	0.5	2.93	1.44	0.00	-0.45	-1.96
6	3.56	9.08	0.1	0.5	2.98	1.50	0.04	-0.48	-1.98
7	3.81	9.73	0.1	0.5	2.93	1.44	0.00	-0.45	-1.96
8	4.57	11.67	0.1	0.5	2.77	1.27	-0.04	-0.35	-1.88
9	4.57	11.67	0.1	0.5	2.77	1.27	-0.04	-0.35	-1.88
Total value			0.9	4.5					

nozzle partitioning method and the dimensions of nozzle sections are illustrated in Fig. 8. The three modules have been further separated into five nozzle sections in the same way according to the standard, and the test results for each module are the same. For the whole air curtain nozzle, there are 15 sections in total, among which sections 1, 5, 6, 10, 11, and 15 have a section width of 0.28 m (door section area 2.24 m²), and the rest of them 0.08 m (door section area 0.64 m²). Because the test results and the dimensions of each module are the same, the efficiency factor of the whole unit is the same with one of the modules. Therefore, the calculation procedure demonstrated below will be carried out for only one module and the results of the efficiency factors can represent for the whole unit.

The velocity distribution data at 8 m to the nozzle are used for the calculation. The calculation procedure is demonstrated in Fig. 9. Since the nozzle depth of this unit is 0.2 m, the airflow rate calculation will be performed twice for the nozzle depth of both 0.08 m and 0.1 m, and then followed by an extrapolation process to

Table 5 Volume flow rate through the door and the air curtain efficiency for Model B

Section number	Equivalent u_E (m/s)	Volume flow rate Q , m ³ /s under different pressure differences				
		25 Pa	9 Pa	1 Pa	-1 Pa	-9 Pa
1	11.02	1.80	0.85	-0.02	-0.25	-1.22
2	10.38	1.84	0.89	-0.01	-0.27	-1.23
3	10.38	1.84	0.89	-0.01	-0.27	-1.23
4	9.08	1.90	0.96	0.03	-0.31	-1.26
5	9.73	1.87	0.92	0.00	-0.29	-1.25
6	9.08	1.90	0.96	0.03	-0.31	-1.26
7	9.73	1.87	0.92	0.00	-0.29	-1.25
8	11.67	1.77	0.81	-0.03	-0.23	-1.20
9	11.67	1.77	0.81	-0.03	-0.23	-1.20
Total Q_{AC} m ³ /s		16.58	8.00	-0.04	-2.43	-11.11
Total Q_{SD} m ³ /s		18.69	11.21	3.74	-3.74	-11.21
Efficiency factor		0.11	0.29	0.99	0.35	0.01

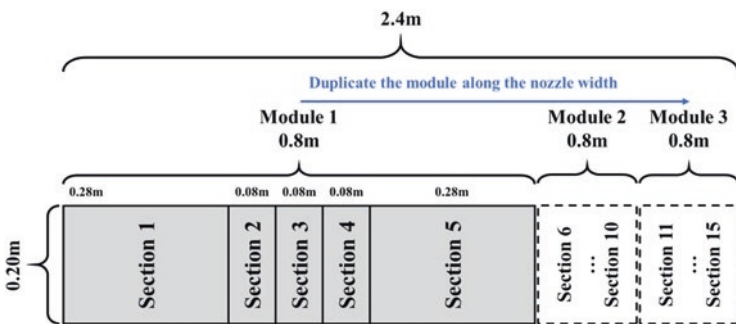


Fig. 8 Dimensions of Model C and the nozzle partitioning method in the aerodynamic test

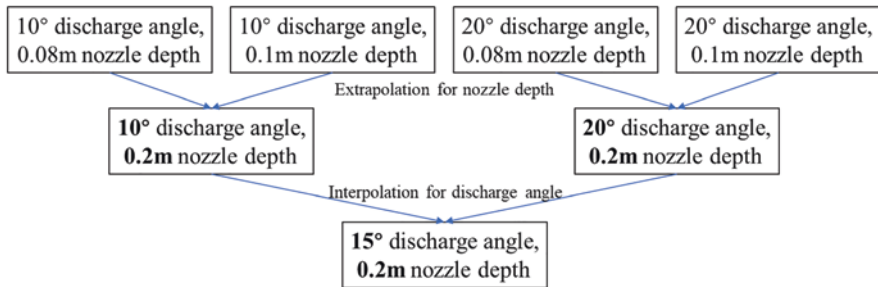


Fig. 9 Procedure to calculate three discharge angles for a nozzle depth of 0.2 m

calculate for the nozzle depth of 0.2 m. The discharge angles of 10° and 20° outward will be calculated directly from the provided standard figures, while the 15° outward calculation will be an interpolation by the results of the previous two discharge angles.

In the first step, the velocity distribution at 8 m to the air curtain nozzle is measured to be uniform, which is 7.62 m/s for all the nozzle sections. In the second step, the corresponding equivalent discharge velocities at 3-m height are calculated to be 19.46 m/s by the jet theory Eq. 5.

In the third step, the typical Q - ΔP curves in Figs. 21, 22, 23, and 24 are used for the identification of the representative flow rate q for the discharge angles of 10° (Tables 6 and 7) and 20° (Tables 8 and 9), respectively.

In the fourth step, the airflow rates through each door section $Q_{AC,i}$ for the two discharge angles and two nozzle depths are calculated according to the real door section areas (Tables 10, 11, 12, and 13).

In the final step, the airflow rates for the nozzle depth of 0.2 m are first extrapolated by the results of 0.1 m and 0.08 m, and then the airflow rates for discharge angle of 15° are interpolated by the results of 10° and 20°. The air exchange rate Q_{SD} of a single door is calculated by Eq. 2 using the real door size (6.4 m²). Thus, the efficiency factor can be calculated for the setup of 0.2 m nozzle depth and 15° discharge angle. The efficiency factors are 85%, 65%, -3%, -51%, and 43%. The best efficiencies for the three discharge angles are achieved for 25 Pa. When the pressure difference is 1 Pa and -1 Pa, the efficiency factor drops to negative at the near-zero pressure difference area as discussed in Fig. 6 (Tables 14, 15, and 16).

3.4 Discussions

In Case 1, the efficiency factors of the air curtain for door height of 2.4 m are calculated following the calculation procedure in Fig. 5 using the original model. In the other two cases, the door heights are more than 3 m, so the equivalent model is

Table 6 Average flow rates of each nozzle section for a module of Model C using the standard figure for 0.08 m nozzle depth, 10° discharge angle, and 3 m door

Section number	Measured velocity (m/s)	Equivalent u_E (m/s)	Nozzle section width (m)	Door section area (m ²)	Average flow rate q_i Pa ^{0.5} for different pressure differences				
					25 Pa	9 Pa	1 Pa	-1 Pa	-9 Pa
1	7.62	19.46	0.28	2.24	1.87	0.12	-0.20	-0.42	-1.48
2	7.62	19.46	0.08	0.64	1.87	0.12	-0.20	-0.42	-1.48
3	7.62	19.46	0.08	0.64	1.87	0.12	-0.20	-0.42	-1.48
4	7.62	19.46	0.08	0.64	1.87	0.12	-0.20	-0.42	-1.48
5	7.62	19.46	0.28	2.24	1.87	0.12	-0.20	-0.42	-1.48
Total value			0.8	6.4					

Table 7 Average flow rates of each nozzle section for a module of Model C using the standard figure for 0.1 m nozzle depth, 10° discharge angle, and 3 m door

Section number	Measured velocity (m/s)	Equivalent u_E (m/s)	Nozzle section width (m)	Door section area (m ²)	Average flow rate q_i Pa ^{0.5} for different pressure differences				
					25 Pa	9 Pa	1 Pa	-1 Pa	-9 Pa
1	7.62	19.46	0.28	2.24	1.52	-0.04	-0.27	-0.50	-1.32
2	7.62	19.46	0.08	0.64	1.52	-0.04	-0.27	-0.50	-1.32
3	7.62	19.46	0.08	0.64	1.52	-0.04	-0.27	-0.50	-1.32
4	7.62	19.46	0.08	0.64	1.52	-0.04	-0.27	-0.50	-1.32
5	7.62	19.46	0.28	2.24	1.52	-0.04	-0.27	-0.50	-1.32
Total value			0.8	6.4					

Table 8 Average flow rates of each nozzle section for a module of Model C using the standard figure for 0.08 m nozzle depth, 20° discharge angle, and 3 m door

Section number	Measured velocity (m/s)	Equivalent u_E (m/s)	Nozzle section width (m)	Door section area (m ²)	Average flow rate q_i Pa ^{0.5} for different pressure differences				
					25 Pa	9 Pa	1 Pa	-1 Pa	-9 Pa
1	7.62	19.46	0.28	2.24	1.63	-0.01	-0.28	-0.53	-1.97
2	7.62	19.46	0.08	0.64	1.63	-0.01	-0.28	-0.53	-1.97
3	7.62	19.46	0.08	0.64	1.63	-0.01	-0.28	-0.53	-1.97
4	7.62	19.46	0.08	0.64	1.63	-0.01	-0.28	-0.53	-1.97
5	7.62	19.46	0.28	2.24	1.63	-0.01	-0.28	-0.53	-1.97
Total value			0.8	6.4					

Table 9 Average flow rates of each nozzle section for a module of Model C using the standard figure for 0.1 m nozzle depth, 20° discharge angle, and 3 m door

Section number	Measured velocity (m/s)	Equivalent u_E (m/s)	Nozzle section width (m)	Door section area (m ²)	Average flow rate q_i , Pa ^{0.5} for different pressure differences				
					25 Pa	9 Pa	1 Pa	-1 Pa	-9 Pa
1	7.62	19.46	0.28	2.24	1.24	-0.10	-0.36	-0.62	-1.92
2	7.62	19.46	0.08	0.64	1.24	-0.10	-0.36	-0.62	-1.92
3	7.62	19.46	0.08	0.64	1.24	-0.10	-0.36	-0.62	-1.92
4	7.62	19.46	0.08	0.64	1.24	-0.10	-0.36	-0.62	-1.92
5	7.62	19.46	0.28	2.24	1.24	-0.10	-0.36	-0.62	-1.92
Total value			0.4	3.2					

Table 10 Volume flow rate through the door and the air curtain efficiency for a module of Model C using the standard figure for 0.08 m nozzle depth, 10° discharge angle, and 3 m door

Section number	Equivalent u_E (m/s)	Volume flow rate Q_i , m ³ /s under different pressure differences				
		25 Pa	9 Pa	1 Pa	-1 Pa	-9 Pa
1	19.46	5.36	0.35	-0.58	-1.21	-4.23
2	19.46	1.53	0.10	-0.17	-0.35	-1.21
3	19.46	1.53	0.10	-0.17	-0.35	-1.21
4	19.46	1.53	0.10	-0.17	-0.35	-1.21
5	19.46	5.36	0.35	-0.58	-1.21	-4.23
Total Q_{AC} m ³ /s		15.31	0.99	-1.67	-3.46	-12.09

Table 11 Volume flow rate through the door and the air curtain efficiency for a module of Model C using the standard figure for 0.1 m nozzle depth, 10° discharge angle, and 3 m door

Section number	Equivalent u_E (m/s)	Volume flow rate Q_i , m ³ /s under different pressure differences				
		25 Pa	9 Pa	1 Pa	-1 Pa	-9 Pa
1	19.46	4.36	-0.11	-0.77	-1.43	-3.78
2	19.46	1.25	-0.03	-0.22	-0.41	-1.08
3	19.46	1.25	-0.03	-0.22	-0.41	-1.08
4	19.46	1.25	-0.03	-0.22	-0.41	-1.08
5	19.46	4.36	-0.11	-0.77	-1.43	-3.78
Total Q_{AC} m ³ /s		12.47	-0.32	-2.19	-4.07	-10.81

implemented. The standard figures are used for the interpolation of the q_i values for each door section, which cover a great number of scenarios.

In Case 3, the efficiency factor for 0.2 m nozzle depth and 15° discharge angle is not included in the provided standard figures. It is a well-demonstrated example to calculate by multiple interpolation and extrapolation operations of the other scenarios.

Table 12 Volume flow rate through the door and the air curtain efficiency for a module of Model C using the standard figure for 0.08 m nozzle depth, 20° discharge angle, and 3 m door

Section number	Equivalent u_E (m/s)	Volume flow rate Q , m ³ /s under different pressure differences				
		25 Pa	9 Pa	1 Pa	-1 Pa	-9 Pa
1	19.46	4.68	-0.04	-0.80	-1.52	-5.63
2	19.46	1.34	-0.01	-0.23	-0.43	-1.61
3	19.46	1.34	-0.01	-0.23	-0.43	-1.61
4	19.46	1.34	-0.01	-0.23	-0.43	-1.61
5	19.46	4.68	-0.04	-0.80	-1.52	-5.63
Total Q_{AC} m ³ /s		13.36	-0.10	-2.29	-4.34	-16.09

Table 13 Volume flow rate through the door and the air curtain efficiency for a module of Model C using the standard figure for 0.1 m nozzle depth, 20° discharge angle, and 3 m door

Section number	Equivalent u_E (m/s)	Volume flow rate Q , m ³ /s under different pressure differences				
		25 Pa	9 Pa	1 Pa	-1 Pa	-9 Pa
1	19.46	3.54	-0.27	-1.03	-1.79	-5.51
2	19.46	1.01	-0.08	-0.29	-0.51	-1.57
3	19.46	1.01	-0.08	-0.29	-0.51	-1.57
4	19.46	1.01	-0.08	-0.29	-0.51	-1.57
5	19.46	3.54	-0.27	-1.03	-1.79	-5.51
Total Q_{AC} m ³ /s		10.10	-0.78	-2.94	-5.11	-15.73

Table 14 Extrapolation for the 0.2 m nozzle depth with a discharge angle of 10°

Pressure difference (Pa)	25	9	1	-1	-9
Q_{ac} for 0.08 m nozzle depth (m ³ /s)	15.31	0.99	-1.67	-3.46	-12.09
Q_{ac} for 0.1 m nozzle depth (m ³ /s)	12.47	-0.32	-2.19	-4.07	-10.81
Q_{ac} for 0.2 m nozzle depth (m ³ /s)	-1.73	-6.87	-4.79	-7.12	-4.41

Table 15 Extrapolation for the 0.2 m nozzle depth with a discharge angle of 20°

Pressure difference (Pa)	25	9	1	-1	-9
Q_{ac} for 0.08 m nozzle depth (m ³ /s)	13.36	-0.1	-2.29	-4.34	-16.09
Q_{ac} for 0.1 m nozzle depth (m ³ /s)	10.1	-0.78	-2.94	-5.11	-15.73
Q_{ac} for 0.2 m nozzle depth (m ³ /s)	-6.20	-4.18	-6.19	-8.96	-13.93

Table 16 Interpolation for the 15° discharge angle by the results of 10° and 20°

Pressure difference (Pa)	25	9	1	-1	-9
Q_{ac} for 20° (m ³ /s)	-6.20	-4.18	-6.19	-8.96	-13.93
Q_{ac} for 10° (m ³ /s)	-1.73	-6.87	-4.79	-7.12	-4.41
Q_{ac} for 15° (m ³ /s)	-3.97	-5.53	-5.49	-8.04	-9.17
Q_{sd} (m ³ /s)	26.58	15.95	5.32	-5.32	-15.95
Efficiency factor	0.85	0.65	-0.03	-0.51	0.43

This report provides 12 standard figures with 7 curves of different velocities, covering a wide range of practical situations for many design scenarios by applying interpolations and/or extrapolations.

4 Validation of the Method

4.1 Validation Setup

To confirm the effectiveness of the new method, the results from the proposed method are compared with the experimental and simulation data from previous studies. The only factor affecting the efficiency factor calculation value is the infiltration/exfiltration flow rate, so the results are compared in terms of the flow rates. The configuration of the experiments and the simulations were elaborated by Goubran et al. [7]. The air curtain has a nozzle depth of 0.0635 m and an outward discharge angle of 20°. It was installed in the lab chamber with a door height and width of 0.71 m and 0.61 m, respectively. The CFD model used the User Defined Function (UDF) to specify the similar air curtain nozzle boundary condition based on the measured velocity profile. The typical Q - ΔP curves (Fig. 10) were prepared by setting the air curtain nozzle as the uniform velocity inlet in the simulation from 8 m/s to 18 m/s. Then, we can repeat the procedure as described in Sect. 2.1 to calculate the total airflow rates Q_{AC} through the door.

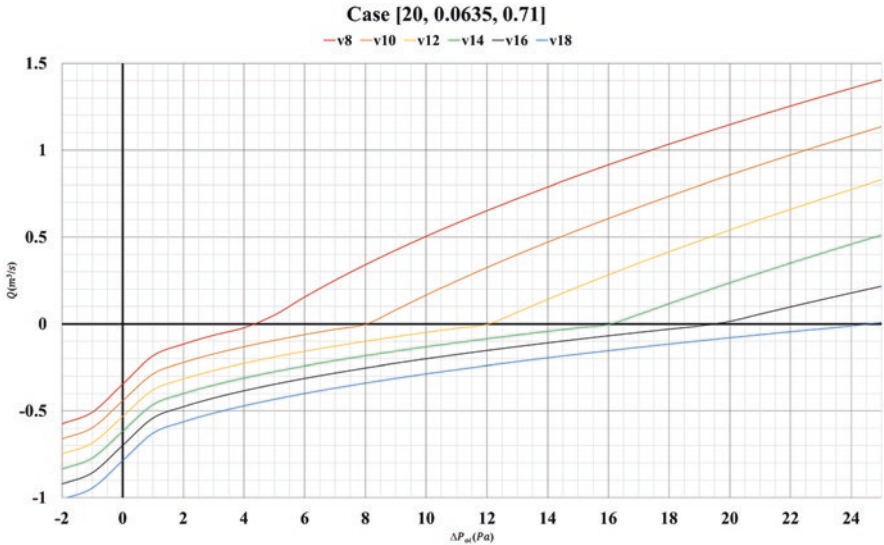


Fig. 10 The standard figure of the typical Q - ΔP curves for 0.71 m door, 0.0635 m nozzle depth, and discharge angle of 20°

The air curtain nozzle is separated into 12 sections. Each section has a width of 0.0508 m and the corresponding door section area is 0.036 m². Two average discharge velocities, 13.75 m/s and 9.1 m/s, were tested, and the measured discharge velocity distribution for each nozzle is listed in Table 17. The measured discharge velocities for each section were used to interpolate from Fig. 10; thus the corresponding representative flow rate q_i and the infiltration rate $Q_{AC,i}$ for different pressure differences can be obtained. By summing up the flow rates $Q_{AC,i}$ through all the door sections, the total airflow rates Q_{AC} through the opening are calculated.

4.2 Validation Results

The calculated airflow rates are compared in Fig. 11 with the previous results in Goubran et al. [7]. A good agreement between the previous CFD simulation data and the experimental data ensured validity of the CFD method. The new method extends the empirical infiltration model based on more CFD simulation results. Thus, it can well capture the trend for the inflow breakthrough condition and the optimum condition, and most of the points are located between the CFD data and the experimental data. Instead of considering the air curtain supply jet as a uniform airflow, the separation of the air curtain nozzle can partly conserve the airflow distribution along the door width.

Figure 12 exhibits the correlation of the proposed method with the experimental and CFD simulation data. The calculated flow rates by the method are close to both experimental and simulation data for the inflow breakthrough region. In the optimum condition, the jet flow reached the ground and caused some uncertainties for

Table 17 Section separation for the air curtain unit and measured discharge velocity

Section number	Section width (m)	Door section area (m ²)	Discharge velocity average 13.75 m/s	Discharge velocity average 9.1 m/s
1	0.051	0.036	13.55	9.41
2	0.051	0.036	16.07	10.33
3	0.051	0.036	16.97	10.86
4	0.051	0.036	14.67	9.71
5	0.051	0.036	10.95	7.52
6	0.051	0.036	8.34	5.67
7	0.051	0.036	8.42	5.24
8	0.051	0.036	11.28	6.57
9	0.051	0.036	15.32	9.11
10	0.051	0.036	17.94	11.56
11	0.051	0.036	17.25	12.40
12	0.051	0.036	14.24	10.82
Nozzle width	0.61	0.43		

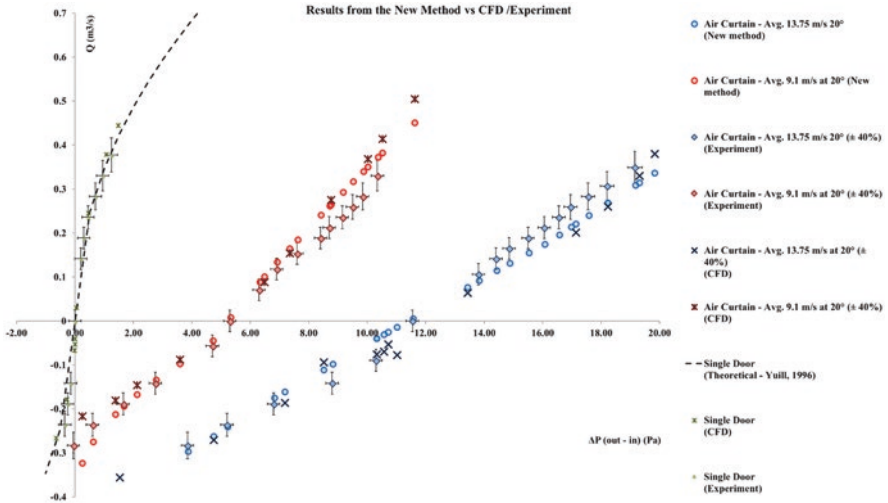


Fig. 11 Results comparison of the new method and previous experimental data and CFD simulation data [7]

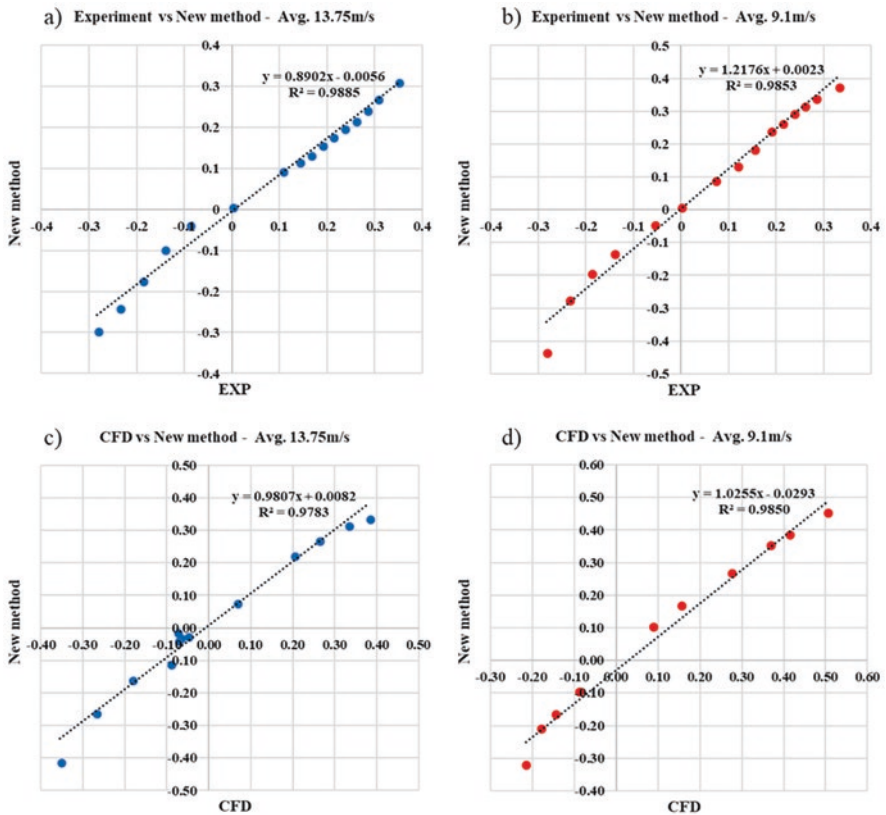


Fig. 12 Correlation of the new method with the (a, b) experimental data and (c, d) CFD simulation data for the average supply velocity of (a, c) 13.75 m/s case and (b, d) 9.1 m/s case

both the experimental and the CFD simulations, resulting in bigger discrepancies at this region. The R^2 coefficient of the 13.95 m/s cases are 0.989 and 0.978 for the experiment and the CFD results, respectively. For the 9.1 m/s cases, it is 0.985 and 0.985. In general, the high R^2 coefficient reflects the reliability of this new method.

5 Conclusions

A new approach to calculate the air curtain efficiency factor is established in this project by using a series of typical Q- ΔP curves. This provides an effective way to avoid complex experimental tests whereas at the same time to evaluate the effectiveness of air curtain products to reduce infiltration/exfiltration at building entrances under different ambient conditions, which only needs the measured data of air curtain velocity distribution and degradation following the ANSI/AMCA or ISO Standards. The typical Q- ΔP curves for 12 design scenarios are provided in the form of standard figures in this report for 3 discharge angles (0° , 10° , 20°), 2 nozzle depths (0.08 m and 0.10 m), and 2 door heights (2.4 m and 3 m). For the scenarios of doors higher than the door height of 3 m, an equivalent method based on the concept of the virtual air curtain unit is developed. The procedure to calculate the efficiency factor is demonstrated by the case studies of three off-the-shelf air curtain units.

Note that, the main logic of the proposed method is to identify the uniformity and the aerodynamic strength of the air curtain jet through the aerodynamic test and use the standard Q- ΔP curve figures to determine the infiltration/exfiltration rates through the air curtain door. For the successful application of the method, users should pay attention to the following tips.

1. In the aerodynamic test, the discharge angle of the air curtain should be 0° , based on which the jet theory equation for the inverse calculation of the discharge velocity was originally developed.
2. The measured data at the objective distance, which is preferred to be the door height, should be used for the inverse calculation of the discharge velocity.
3. When a design scenario (e.g., door height, jet velocity, or angle) is out of the scope of the provided standard figures, interpolations/extrapolations among the existing curves should be performed to obtain the closest results.
4. The proposed method is assumed to be applicable to non-isothermal and wind conditions, should the total pressure difference under both conditions include the stack and/or wind effects and can be obtained or measured, which may need to be further confirmed.

Finally, the proposed method is validated by the data from the previous studies, and a reasonable agreement of the results exhibits the validity of the method.

Appendices

Appendix A

Please note the y-axis is the q_i (originally defined in Eq. 6) with the unit of $\text{Pa}^{0.5}$: $q_i = Q_i / \left(A_i \sqrt{\frac{2}{\rho}} \right)$

The x-axis is the pressure difference ΔP with the unit of Pa (Figs. 13, 14, 15, 16, 17, 18, 19, 20, 21, 22, 23, and 24).

Appendix B

Please note the data in Appendix B is used for the generation of the standard curves in Appendix A (Tables 18, 19, 20, 21, 22, 23, 24, 25, 26, 27, 28, and 29).

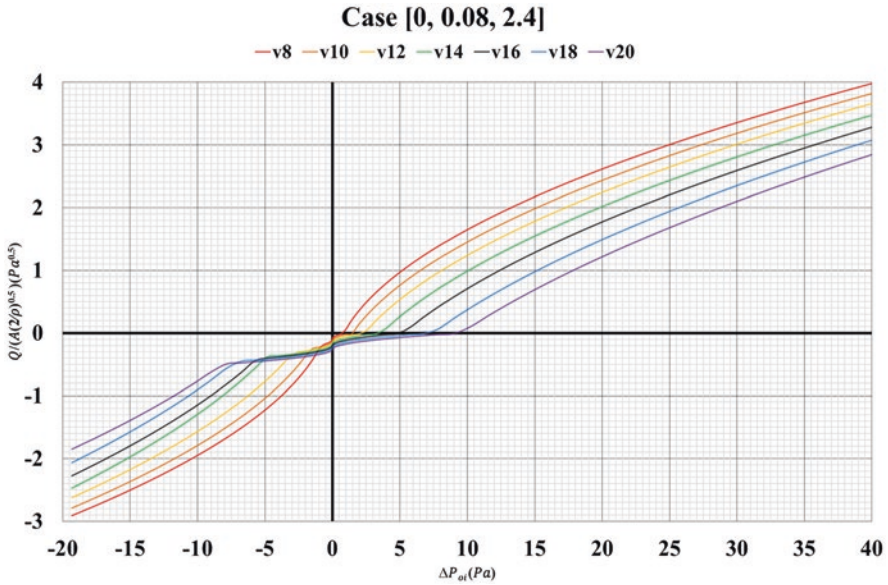


Fig. 13 The standard figure of the typical Q- ΔP curves for 2.4 m door, 0.08 m nozzle depth, and discharge angle of 0°

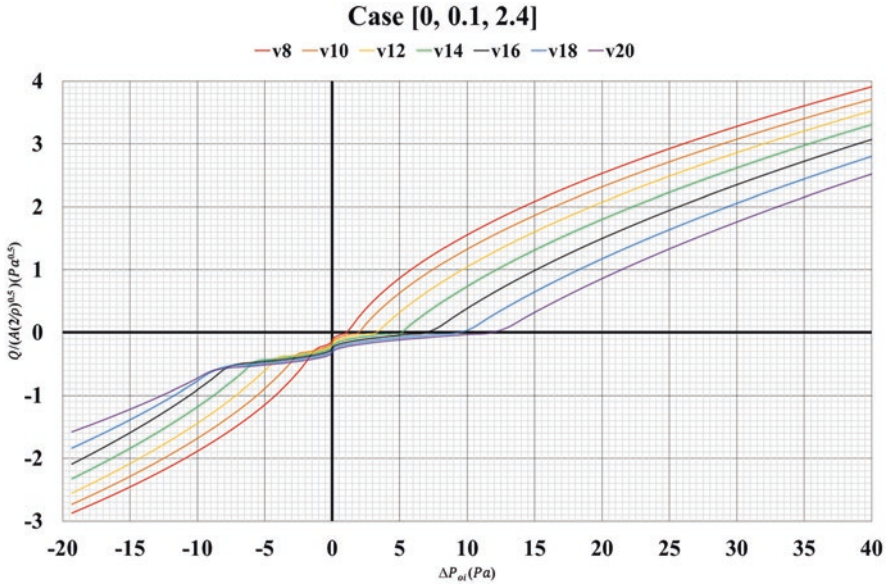


Fig. 14 The standard figure of the typical Q- ΔP curves for 2.4 m door, 0.1 m nozzle depth, and discharge angle of 0°

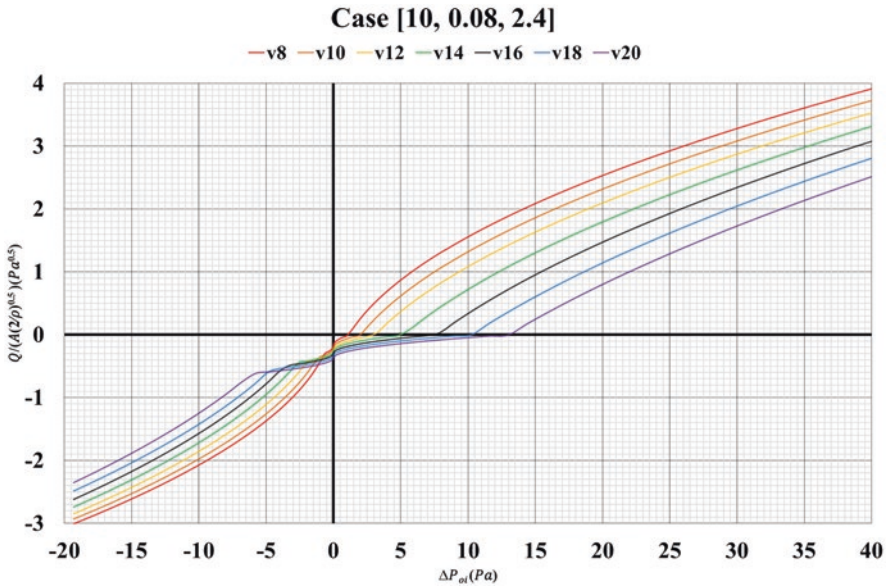


Fig. 15 The standard figure of the typical Q- ΔP curves for 2.4 m door, 0.08 m nozzle depth, and discharge angle of 10°

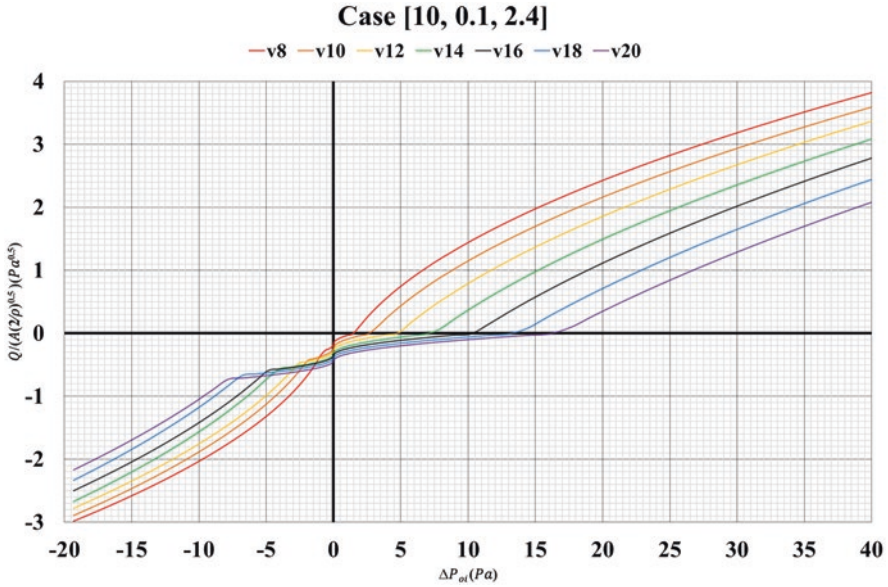


Fig. 16 The standard figure of the typical Q- ΔP curves for 2.4 m door, 0.1 m nozzle depth, and discharge angle of 10°

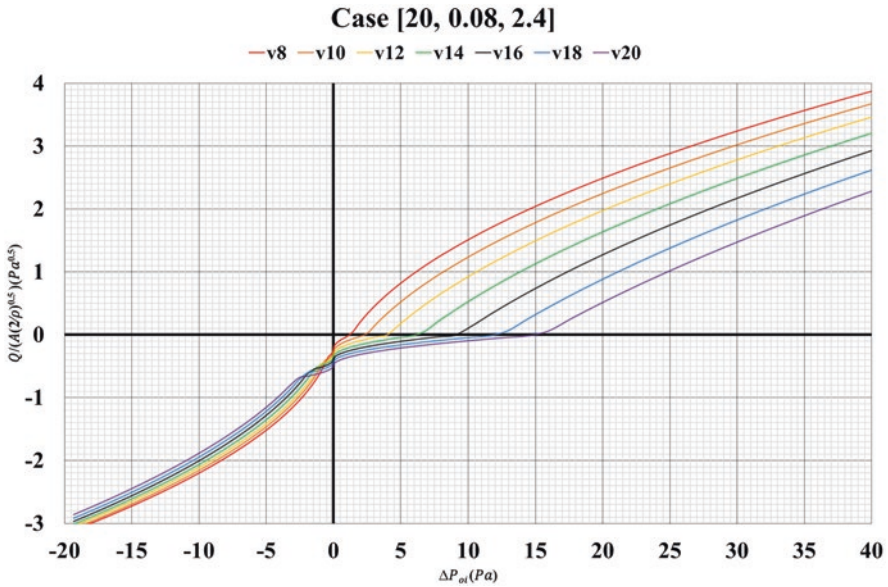


Fig. 17 The standard figure of the typical Q- ΔP curves for 2.4 m door, 0.08 m nozzle depth, and discharge angle of 20°

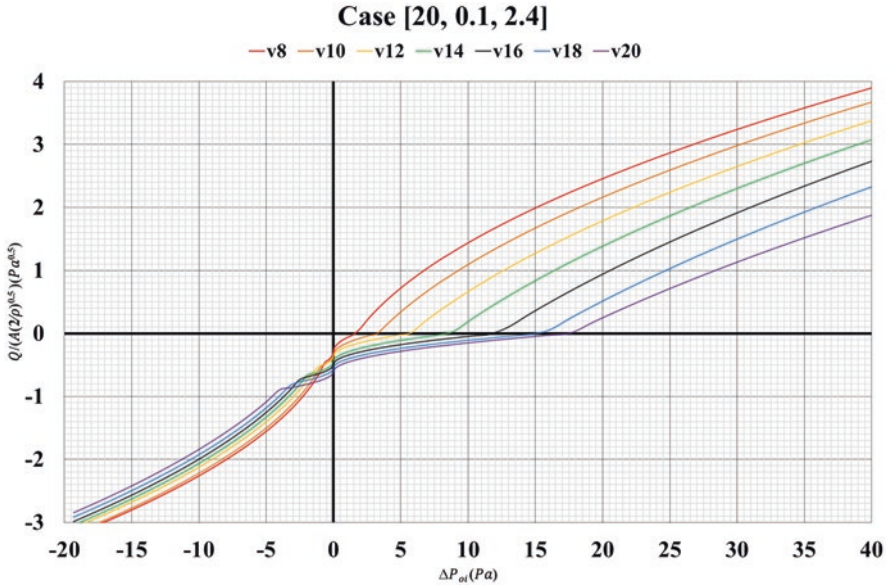


Fig. 18 The standard figure of the typical Q- ΔP curves for 2.4 m door, 0.1 m nozzle depth, and discharge angle of 20°

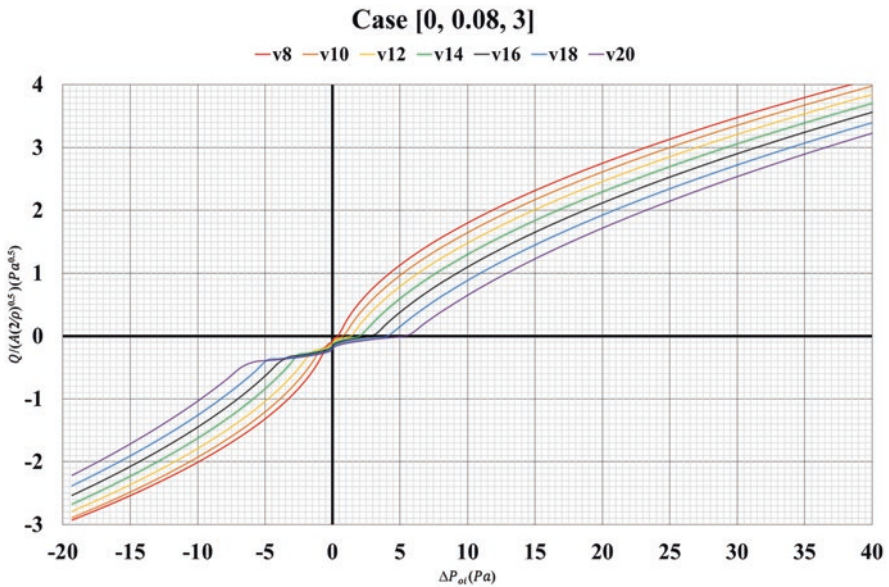


Fig. 19 The standard figure of the typical Q- ΔP curves for 3 m door, 0.08 m nozzle depth, and discharge angle of 0°

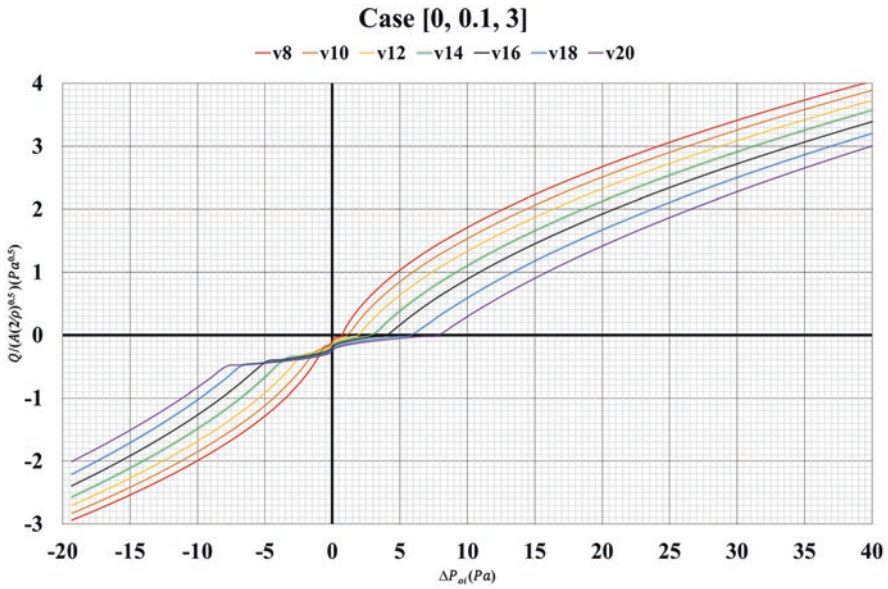


Fig. 20 The standard figure of the typical Q- ΔP curves for 3 m door, 0.1 m nozzle depth, and discharge angle of 0°

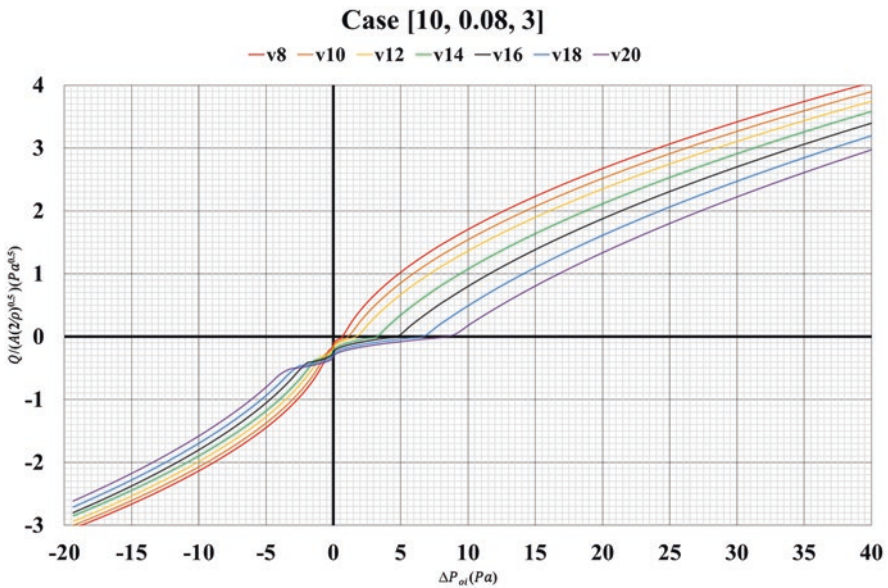


Fig. 21 The standard figure of the typical Q- ΔP curves for 3 m door, 0.08 m nozzle depth, and discharge angle of 10°

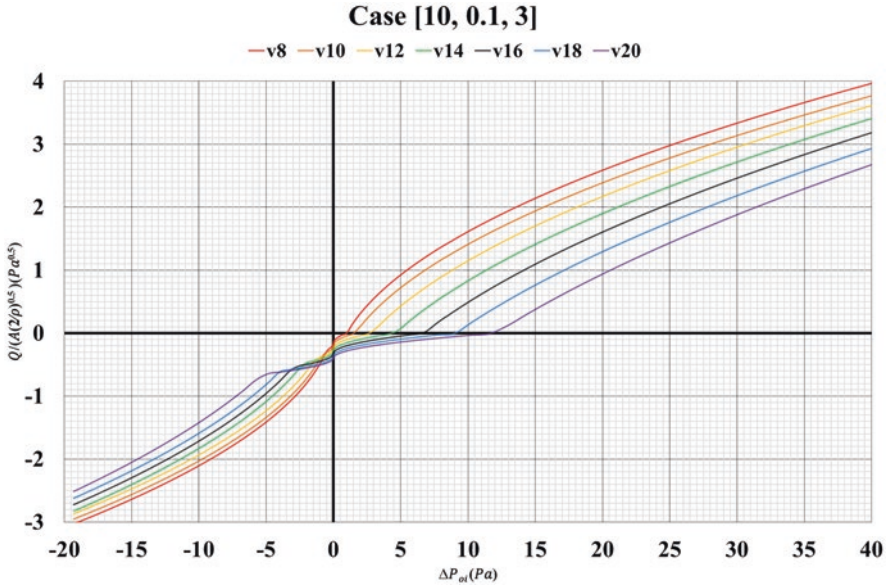


Fig. 22 The standard figure of the typical Q- ΔP curves for 3 m door, 0.1 m nozzle depth, and discharge angle of 10°

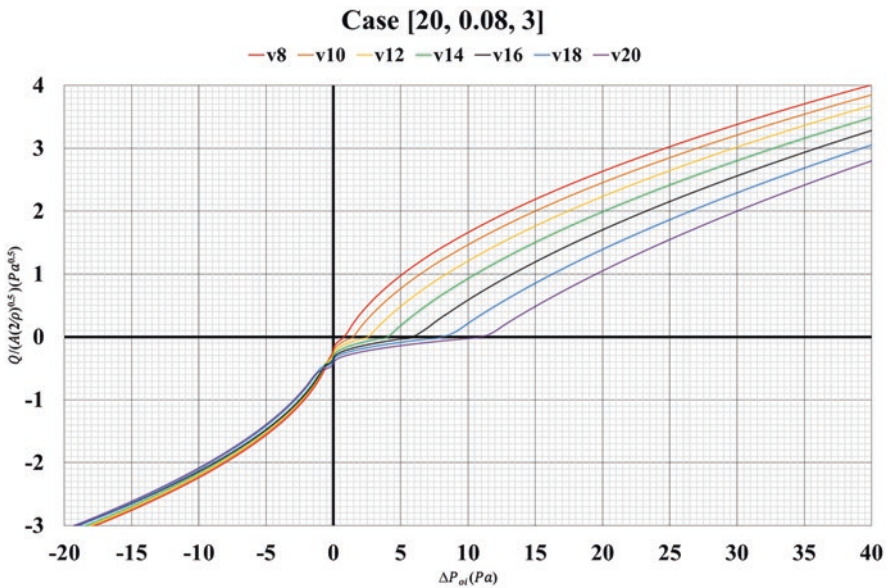


Fig. 23 The standard figure of the typical Q- ΔP curves for 3 m door, 0.08 m nozzle depth, and discharge angle of 20°

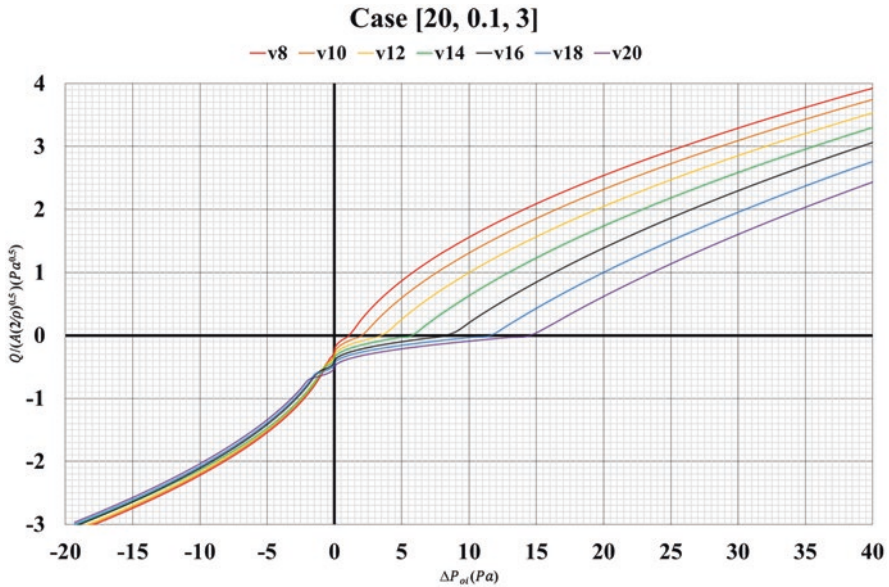


Fig. 24 The standard figure of the typical Q- ΔP curves for 3 m door, 0.1 m nozzle depth, and discharge angle of 20°

Table 18 Original data of the standard curves for 2.4 m door, 0.08 m nozzle depth, and discharge angle of 0°

ΔP Pa	8 m/s	10 m/s	12 m/s	14 m/s	16 m/s	18 m/s	20 m/s
40.96	4.03	3.87	3.71	3.53	3.34	3.14	2.91
38.44	3.88	3.72	3.56	3.38	3.18	2.97	2.73
36.00	3.74	3.57	3.41	3.22	3.02	2.80	2.56
33.64	3.59	3.42	3.25	3.06	2.85	2.62	2.38
31.36	3.44	3.27	3.10	2.90	2.69	2.45	2.21
29.16	3.29	3.12	2.95	2.75	2.53	2.28	2.03
27.04	3.15	2.97	2.80	2.59	2.37	2.11	1.86
25.00	3.00	2.83	2.64	2.43	2.20	1.94	1.68
23.04	2.85	2.68	2.49	2.28	2.04	1.77	1.51
21.16	2.71	2.53	2.34	2.12	1.88	1.60	1.33
19.36	2.56	2.38	2.19	1.96	1.72	1.43	1.15
17.64	2.41	2.23	2.03	1.81	1.55	1.26	0.98
16.00	2.26	2.08	1.88	1.65	1.39	1.09	0.80
14.44	2.12	1.93	1.73	1.49	1.23	0.92	0.63
12.96	1.97	1.78	1.57	1.33	1.06	0.74	0.45
11.56	1.82	1.63	1.42	1.18	0.90	0.57	0.28
10.24	1.68	1.48	1.27	1.02	0.74	0.40	0.10
9.00	1.53	1.33	1.12	0.86	0.58	0.23	-0.01
7.84	1.38	1.18	0.96	0.71	0.41	0.06	-0.02

(continued)

Table 18 (continued)

ΔP Pa	8 m/s	10 m/s	12 m/s	14 m/s	16 m/s	18 m/s	20 m/s
6.76	1.23	1.03	0.81	0.55	0.25	-0.01	-0.04
5.76	1.09	0.88	0.66	0.39	0.09	-0.03	-0.06
4.84	0.94	0.73	0.50	0.23	-0.01	-0.04	-0.07
4.00	0.79	0.58	0.35	0.08	-0.03	-0.06	-0.09
3.24	0.65	0.43	0.20	-0.01	-0.04	-0.08	-0.11
2.56	0.50	0.28	0.05	-0.03	-0.06	-0.10	-0.12
1.96	0.35	0.14	-0.01	-0.05	-0.08	-0.11	-0.14
1.44	0.20	-0.01	-0.03	-0.07	-0.10	-0.13	-0.16
1.00	0.06	-0.02	-0.05	-0.08	-0.12	-0.15	-0.17
0.64	-0.01	-0.04	-0.07	-0.10	-0.13	-0.16	-0.19
0.36	-0.03	-0.06	-0.09	-0.12	-0.15	-0.18	-0.21
0.16	-0.06	-0.08	-0.11	-0.14	-0.17	-0.20	-0.22
0.04	-0.08	-0.10	-0.13	-0.16	-0.19	-0.21	-0.24
0.00	-0.10	-0.12	-0.15	-0.18	-0.20	-0.23	-0.26
-0.04	-0.12	-0.15	-0.17	-0.20	-0.22	-0.25	-0.27
-0.16	-0.14	-0.17	-0.19	-0.21	-0.24	-0.27	-0.29
-0.36	-0.16	-0.19	-0.21	-0.23	-0.26	-0.28	-0.31
-0.64	-0.19	-0.21	-0.23	-0.25	-0.28	-0.30	-0.32
-1.00	-0.26	-0.23	-0.25	-0.27	-0.29	-0.32	-0.34
-1.44	-0.42	-0.25	-0.27	-0.29	-0.31	-0.33	-0.36
-1.96	-0.57	-0.36	-0.29	-0.31	-0.33	-0.35	-0.37
-2.56	-0.73	-0.52	-0.31	-0.33	-0.35	-0.37	-0.39
-3.24	-0.89	-0.69	-0.40	-0.34	-0.37	-0.38	-0.41
-4.00	-1.04	-0.85	-0.57	-0.36	-0.38	-0.40	-0.42
-4.84	-1.20	-1.01	-0.74	-0.38	-0.40	-0.42	-0.44
-5.76	-1.35	-1.17	-0.91	-0.56	-0.45	-0.44	-0.46
-6.76	-1.51	-1.33	-1.08	-0.76	-0.63	-0.45	-0.47
-7.84	-1.67	-1.50	-1.25	-0.95	-0.81	-0.56	-0.49
-9.00	-1.82	-1.66	-1.43	-1.14	-1.00	-0.75	-0.62
-10.24	-1.98	-1.82	-1.60	-1.33	-1.18	-0.94	-0.80
-11.56	-2.13	-1.98	-1.77	-1.52	-1.36	-1.13	-0.97
-12.96	-2.29	-2.14	-1.94	-1.71	-1.55	-1.32	-1.15
-14.44	-2.44	-2.31	-2.11	-1.90	-1.73	-1.51	-1.32
-16.00	-2.60	-2.47	-2.28	-2.09	-1.91	-1.69	-1.50
-17.64	-2.76	-2.63	-2.45	-2.28	-2.10	-1.88	-1.67
-19.36	-2.91	-2.79	-2.63	-2.47	-2.28	-2.07	-1.85

Table 19 Original data of the standard curves for 2.4 m door, 0.1 m nozzle depth, and discharge angle of 0°

ΔP Pa	8 m/s	10 m/s	12 m/s	14 m/s	16 m/s	18 m/s	20 m/s
40.96	3.96	3.77	3.58	3.37	3.13	2.87	2.59
38.44	3.82	3.62	3.43	3.21	2.97	2.70	2.41
36.00	3.67	3.47	3.27	3.04	2.80	2.52	2.23
33.64	3.52	3.32	3.11	2.88	2.63	2.34	2.05
31.36	3.37	3.17	2.96	2.72	2.46	2.17	1.87
29.16	3.22	3.02	2.80	2.55	2.29	1.99	1.69
27.04	3.07	2.87	2.64	2.39	2.12	1.82	1.52
25.00	2.92	2.72	2.49	2.23	1.95	1.64	1.34
23.04	2.77	2.57	2.33	2.07	1.78	1.47	1.16
21.16	2.63	2.42	2.17	1.90	1.61	1.29	0.98
19.36	2.48	2.27	2.02	1.74	1.44	1.11	0.80
17.64	2.33	2.12	1.86	1.58	1.27	0.94	0.62
16.00	2.18	1.96	1.70	1.42	1.10	0.76	0.44
14.44	2.03	1.81	1.55	1.25	0.93	0.59	0.26
12.96	1.88	1.66	1.39	1.09	0.76	0.41	0.08
11.56	1.73	1.51	1.23	0.93	0.59	0.23	-0.01
10.24	1.59	1.36	1.08	0.77	0.42	0.06	-0.03
9.00	1.44	1.21	0.92	0.60	0.25	-0.01	-0.05
7.84	1.29	1.06	0.76	0.44	0.08	-0.03	-0.06
6.76	1.14	0.91	0.61	0.28	-0.01	-0.05	-0.08
5.76	0.99	0.76	0.45	0.11	-0.03	-0.07	-0.10
4.84	0.84	0.61	0.29	-0.05	-0.05	-0.08	-0.12
4.00	0.69	0.46	0.14	-0.03	-0.07	-0.10	-0.14
3.24	0.54	0.31	0.00	-0.04	-0.08	-0.12	-0.15
2.56	0.40	0.16	-0.02	-0.06	-0.10	-0.14	-0.17
1.96	0.25	0.00	-0.04	-0.08	-0.12	-0.16	-0.19
1.44	0.10	-0.02	-0.06	-0.10	-0.14	-0.18	-0.21
1.00	-0.01	-0.04	-0.09	-0.12	-0.16	-0.19	-0.23
0.64	-0.03	-0.07	-0.11	-0.14	-0.18	-0.21	-0.24
0.36	-0.05	-0.09	-0.13	-0.16	-0.20	-0.23	-0.26
0.16	-0.08	-0.11	-0.15	-0.18	-0.22	-0.25	-0.28
0.04	-0.10	-0.13	-0.17	-0.20	-0.23	-0.27	-0.30
0.00	-0.12	-0.16	-0.19	-0.22	-0.25	-0.28	-0.31
-0.04	-0.15	-0.18	-0.21	-0.24	-0.27	-0.30	-0.33
-0.16	-0.17	-0.20	-0.23	-0.26	-0.29	-0.32	-0.35
-0.36	-0.19	-0.22	-0.25	-0.28	-0.31	-0.34	-0.37
-0.64	-0.22	-0.25	-0.27	-0.30	-0.33	-0.36	-0.39
-1.00	-0.24	-0.27	-0.29	-0.32	-0.35	-0.38	-0.40
-1.44	-0.31	-0.29	-0.31	-0.34	-0.37	-0.39	-0.42
-1.96	-0.47	-0.31	-0.33	-0.36	-0.38	-0.41	-0.44
-2.56	-0.63	-0.34	-0.35	-0.38	-0.40	-0.43	-0.46

(continued)

Table 19 (continued)

ΔP Pa	8 m/s	10 m/s	12 m/s	14 m/s	16 m/s	18 m/s	20 m/s
-3.24	-0.79	-0.51	-0.38	-0.40	-0.42	-0.45	-0.48
-4.00	-0.95	-0.68	-0.40	-0.42	-0.44	-0.47	-0.49
-4.84	-1.11	-0.86	-0.57	-0.44	-0.46	-0.48	-0.51
-5.76	-1.27	-1.03	-0.75	-0.47	-0.48	-0.50	-0.53
-6.76	-1.43	-1.20	-0.93	-0.66	-0.50	-0.52	-0.55
-7.84	-1.59	-1.37	-1.11	-0.84	-0.56	-0.54	-0.57
-9.00	-1.75	-1.54	-1.29	-1.03	-0.75	-0.63	-0.62
-10.24	-1.91	-1.71	-1.47	-1.22	-0.95	-0.80	-0.75
-11.56	-2.07	-1.88	-1.65	-1.40	-1.14	-0.98	-0.89
-12.96	-2.23	-2.05	-1.84	-1.59	-1.33	-1.15	-1.03
-14.44	-2.39	-2.22	-2.02	-1.77	-1.52	-1.32	-1.17
-16.00	-2.55	-2.39	-2.20	-1.96	-1.71	-1.50	-1.30
-17.64	-2.71	-2.56	-2.38	-2.15	-1.90	-1.67	-1.44
-19.36	-2.87	-2.73	-2.56	-2.33	-2.09	-1.84	-1.58

Table 20 Original data of the standard curves for 2.4 m door, 0.08 m nozzle depth, and discharge angle of 10°

ΔP Pa	8 m/s	10 m/s	12 m/s	14 m/s	16 m/s	18 m/s	20 m/s
40.96	3.97	3.79	3.59	3.38	3.14	2.88	2.58
38.44	3.82	3.63	3.43	3.21	2.97	2.70	2.40
36.00	3.67	3.48	3.28	3.05	2.79	2.52	2.21
33.64	3.52	3.33	3.13	2.88	2.62	2.34	2.03
31.36	3.37	3.18	2.97	2.72	2.45	2.16	1.85
29.16	3.23	3.03	2.82	2.56	2.28	1.98	1.66
27.04	3.08	2.87	2.66	2.39	2.10	1.80	1.48
25.00	2.93	2.72	2.51	2.23	1.93	1.62	1.29
23.04	2.78	2.57	2.35	2.06	1.76	1.44	1.11
21.16	2.63	2.42	2.20	1.90	1.58	1.26	0.92
19.36	2.48	2.26	2.04	1.74	1.41	1.08	0.74
17.64	2.33	2.11	1.89	1.57	1.24	0.90	0.55
16.00	2.18	1.96	1.74	1.41	1.06	0.72	0.37
14.44	2.04	1.81	1.58	1.24	0.89	0.54	0.18
12.96	1.89	1.66	1.43	1.08	0.72	0.36	0.00
11.56	1.74	1.50	1.27	0.92	0.54	0.18	-0.02
10.24	1.59	1.35	1.12	0.75	0.37	0.00	-0.04
9.00	1.44	1.20	0.96	0.59	0.20	-0.02	-0.06
7.84	1.29	1.05	0.81	0.43	0.02	-0.04	-0.08
6.76	1.14	0.90	0.65	0.26	-0.02	-0.06	-0.10
5.76	0.99	0.74	0.50	0.10	-0.04	-0.08	-0.12
4.84	0.85	0.59	0.34	-0.01	-0.06	-0.10	-0.14
4.00	0.70	0.44	0.19	-0.03	-0.08	-0.12	-0.16

(continued)

Table 20 (continued)

ΔP Pa	8 m/s	10 m/s	12 m/s	14 m/s	16 m/s	18 m/s	20 m/s
3.24	0.55	0.29	0.04	-0.05	-0.10	-0.15	-0.18
2.56	0.40	0.14	-0.02	-0.08	-0.12	-0.17	-0.20
1.96	0.25	0.00	-0.05	-0.10	-0.15	-0.19	-0.22
1.44	0.10	-0.03	-0.08	-0.12	-0.17	-0.21	-0.25
1.00	-0.01	-0.06	-0.10	-0.15	-0.19	-0.23	-0.27
0.64	-0.04	-0.09	-0.13	-0.17	-0.21	-0.25	-0.29
0.36	-0.07	-0.12	-0.16	-0.19	-0.23	-0.27	-0.31
0.16	-0.11	-0.15	-0.19	-0.21	-0.25	-0.29	-0.33
0.04	-0.14	-0.18	-0.21	-0.24	-0.27	-0.31	-0.35
0.00	-0.17	-0.21	-0.24	-0.26	-0.30	-0.33	-0.37
-0.04	-0.20	-0.24	-0.27	-0.28	-0.32	-0.35	-0.39
-0.16	-0.23	-0.27	-0.30	-0.30	-0.34	-0.37	-0.41
-0.36	-0.26	-0.29	-0.32	-0.33	-0.36	-0.39	-0.43
-0.64	-0.30	-0.32	-0.35	-0.35	-0.38	-0.41	-0.45
-1.00	-0.43	-0.35	-0.38	-0.37	-0.40	-0.43	-0.47
-1.44	-0.58	-0.45	-0.41	-0.39	-0.42	-0.46	-0.49
-1.96	-0.73	-0.61	-0.43	-0.42	-0.44	-0.48	-0.51
-2.56	-0.88	-0.76	-0.59	-0.44	-0.47	-0.50	-0.53
-3.24	-1.03	-0.92	-0.75	-0.58	-0.49	-0.52	-0.55
-4.00	-1.19	-1.07	-0.91	-0.75	-0.58	-0.54	-0.57
-4.84	-1.34	-1.23	-1.07	-0.92	-0.75	-0.59	-0.59
-5.76	-1.49	-1.38	-1.24	-1.08	-0.92	-0.77	-0.61
-6.76	-1.64	-1.54	-1.40	-1.25	-1.09	-0.94	-0.74
-7.84	-1.79	-1.69	-1.56	-1.41	-1.26	-1.11	-0.92
-9.00	-1.95	-1.85	-1.72	-1.58	-1.43	-1.28	-1.10
-10.24	-2.10	-2.00	-1.88	-1.75	-1.60	-1.46	-1.28
-11.56	-2.25	-2.16	-2.04	-1.91	-1.77	-1.63	-1.46
-12.96	-2.40	-2.31	-2.20	-2.08	-1.94	-1.80	-1.64
-14.44	-2.55	-2.47	-2.36	-2.24	-2.11	-1.97	-1.82
-16.00	-2.70	-2.62	-2.53	-2.41	-2.28	-2.15	-2.00
-17.64	-2.86	-2.78	-2.69	-2.58	-2.45	-2.32	-2.18
-19.36	-3.01	-2.93	-2.85	-2.74	-2.62	-2.49	-2.36

Table 21 Original data of the standard curves for 2.4 m door, 0.1 m nozzle depth, and discharge angle of 10°

ΔP Pa	8 m/s	10 m/s	12 m/s	14 m/s	16 m/s	18 m/s	20 m/s
40.96	3.88	3.65	3.43	3.15	2.85	2.51	2.15
38.44	3.73	3.50	3.26	2.98	2.67	2.33	1.97
36.00	3.58	3.34	3.10	2.81	2.49	2.14	1.78
33.64	3.43	3.19	2.94	2.63	2.31	1.95	1.59
31.36	3.28	3.03	2.77	2.46	2.13	1.76	1.40
29.16	3.13	2.88	2.61	2.29	1.95	1.58	1.22
27.04	2.98	2.72	2.45	2.12	1.77	1.39	1.03
25.00	2.83	2.57	2.29	1.95	1.59	1.20	0.84
23.04	2.68	2.42	2.12	1.78	1.41	1.02	0.66
21.16	2.53	2.26	1.96	1.60	1.23	0.83	0.47
19.36	2.38	2.11	1.80	1.43	1.05	0.64	0.28
17.64	2.23	1.95	1.63	1.26	0.87	0.46	0.10
16.00	2.07	1.80	1.47	1.09	0.69	0.27	-0.01
14.44	1.92	1.64	1.31	0.92	0.51	0.08	-0.03
12.96	1.77	1.49	1.15	0.75	0.33	-0.01	-0.05
11.56	1.62	1.34	0.98	0.57	0.15	-0.03	-0.07
10.24	1.47	1.18	0.82	0.40	0.00	-0.05	-0.10
9.00	1.32	1.03	0.66	0.23	-0.02	-0.08	-0.12
7.84	1.17	0.87	0.49	0.06	-0.05	-0.10	-0.14
6.76	1.02	0.72	0.33	-0.02	-0.07	-0.12	-0.16
5.76	0.87	0.56	0.17	-0.04	-0.09	-0.14	-0.18
4.84	0.72	0.41	0.01	-0.06	-0.11	-0.16	-0.20
4.00	0.57	0.25	-0.02	-0.09	-0.13	-0.18	-0.22
3.24	0.42	0.10	-0.05	-0.11	-0.15	-0.20	-0.24
2.56	0.27	-0.01	-0.07	-0.14	-0.18	-0.22	-0.26
1.96	0.12	-0.04	-0.10	-0.16	-0.20	-0.24	-0.29
1.44	-0.01	-0.07	-0.12	-0.18	-0.22	-0.27	-0.31
1.00	-0.03	-0.09	-0.15	-0.21	-0.24	-0.29	-0.33
0.64	-0.06	-0.12	-0.18	-0.23	-0.26	-0.31	-0.35
0.36	-0.09	-0.15	-0.20	-0.25	-0.28	-0.33	-0.37
0.16	-0.11	-0.18	-0.23	-0.28	-0.31	-0.35	-0.39
0.04	-0.14	-0.21	-0.25	-0.30	-0.33	-0.37	-0.41
0.00	-0.17	-0.23	-0.28	-0.33	-0.35	-0.39	-0.43
-0.04	-0.19	-0.26	-0.30	-0.35	-0.37	-0.41	-0.46
-0.16	-0.22	-0.29	-0.33	-0.37	-0.39	-0.43	-0.48
-0.36	-0.25	-0.32	-0.35	-0.40	-0.41	-0.46	-0.50
-0.64	-0.28	-0.35	-0.38	-0.42	-0.44	-0.48	-0.52
-1.00	-0.37	-0.37	-0.40	-0.45	-0.46	-0.50	-0.54
-1.44	-0.52	-0.40	-0.43	-0.47	-0.48	-0.52	-0.56
-1.96	-0.67	-0.44	-0.45	-0.49	-0.50	-0.54	-0.58
-2.56	-0.83	-0.60	-0.48	-0.52	-0.52	-0.56	-0.60

(continued)

Table 21 (continued)

ΔP Pa	8 m/s	10 m/s	12 m/s	14 m/s	16 m/s	18 m/s	20 m/s
-3.24	-0.98	-0.77	-0.63	-0.54	-0.54	-0.58	-0.63
-4.00	-1.14	-0.93	-0.79	-0.57	-0.57	-0.60	-0.65
-4.84	-1.29	-1.09	-0.96	-0.70	-0.59	-0.62	-0.67
-5.76	-1.44	-1.26	-1.12	-0.88	-0.75	-0.65	-0.69
-6.76	-1.60	-1.42	-1.29	-1.06	-0.92	-0.67	-0.71
-7.84	-1.75	-1.59	-1.46	-1.24	-1.10	-0.83	-0.73
-9.00	-1.91	-1.75	-1.62	-1.42	-1.27	-1.02	-0.90
-10.24	-2.06	-1.91	-1.79	-1.60	-1.45	-1.21	-1.08
-11.56	-2.22	-2.08	-1.95	-1.78	-1.62	-1.40	-1.26
-12.96	-2.37	-2.24	-2.12	-1.96	-1.80	-1.58	-1.45
-14.44	-2.52	-2.41	-2.29	-2.14	-1.97	-1.77	-1.63
-16.00	-2.68	-2.57	-2.45	-2.32	-2.15	-1.96	-1.81
-17.64	-2.83	-2.73	-2.62	-2.49	-2.32	-2.15	-1.99
-19.36	-2.99	-2.90	-2.78	-2.67	-2.50	-2.34	-2.17

Table 22 Original data of the standard curves for 2.4 m door, 0.08 m nozzle depth, and discharge angle of 20°

ΔP Pa	8 m/s	10 m/s	12 m/s	14 m/s	16 m/s	18 m/s	20 m/s
40.96	3.93	3.73	3.52	3.27	3.00	2.69	2.35
38.44	3.78	3.58	3.36	3.10	2.82	2.50	2.16
36.00	3.63	3.43	3.20	2.93	2.64	2.32	1.97
33.64	3.48	3.27	3.04	2.76	2.46	2.13	1.78
31.36	3.33	3.12	2.88	2.59	2.28	1.94	1.59
29.16	3.18	2.96	2.72	2.42	2.10	1.75	1.40
27.04	3.03	2.81	2.56	2.25	1.92	1.57	1.21
25.00	2.88	2.65	2.40	2.08	1.74	1.38	1.02
23.04	2.73	2.50	2.24	1.91	1.57	1.19	0.83
21.16	2.58	2.35	2.08	1.74	1.39	1.00	0.64
19.36	2.44	2.19	1.92	1.58	1.21	0.82	0.45
17.64	2.29	2.04	1.75	1.41	1.03	0.63	0.25
16.00	2.14	1.88	1.59	1.24	0.85	0.44	0.06
14.44	1.99	1.73	1.43	1.07	0.67	0.25	-0.02
12.96	1.84	1.58	1.27	0.90	0.49	0.07	-0.04
11.56	1.69	1.42	1.11	0.73	0.31	-0.02	-0.07
10.24	1.54	1.27	0.95	0.56	0.14	-0.04	-0.09
9.00	1.39	1.11	0.79	0.39	-0.01	-0.07	-0.12
7.84	1.24	0.96	0.63	0.22	-0.03	-0.09	-0.14
6.76	1.09	0.80	0.47	0.05	-0.06	-0.11	-0.17
5.76	0.94	0.65	0.31	-0.02	-0.08	-0.14	-0.19
4.84	0.79	0.50	0.15	-0.05	-0.11	-0.16	-0.21
4.00	0.64	0.34	0.00	-0.07	-0.14	-0.19	-0.24

(continued)

Table 22 (continued)

ΔP Pa	8 m/s	10 m/s	12 m/s	14 m/s	16 m/s	18 m/s	20 m/s
3.24	0.50	0.19	-0.03	-0.10	-0.16	-0.21	-0.26
2.56	0.35	0.03	-0.07	-0.13	-0.19	-0.24	-0.29
1.96	0.20	-0.03	-0.10	-0.16	-0.21	-0.26	-0.31
1.44	0.05	-0.06	-0.13	-0.19	-0.24	-0.29	-0.34
1.00	-0.03	-0.10	-0.16	-0.21	-0.26	-0.31	-0.36
0.64	-0.07	-0.13	-0.19	-0.24	-0.29	-0.34	-0.39
0.36	-0.11	-0.17	-0.22	-0.27	-0.32	-0.36	-0.41
0.16	-0.15	-0.20	-0.25	-0.30	-0.34	-0.39	-0.44
0.04	-0.19	-0.24	-0.29	-0.32	-0.37	-0.41	-0.46
0.00	-0.23	-0.27	-0.32	-0.35	-0.39	-0.43	-0.49
-0.04	-0.27	-0.31	-0.35	-0.38	-0.42	-0.46	-0.51
-0.16	-0.31	-0.34	-0.38	-0.41	-0.44	-0.48	-0.54
-0.36	-0.34	-0.38	-0.41	-0.43	-0.47	-0.51	-0.56
-0.64	-0.46	-0.41	-0.44	-0.46	-0.50	-0.53	-0.59
-1.00	-0.61	-0.53	-0.48	-0.49	-0.52	-0.56	-0.61
-1.44	-0.75	-0.68	-0.64	-0.55	-0.55	-0.58	-0.64
-1.96	-0.90	-0.83	-0.79	-0.71	-0.63	-0.61	-0.66
-2.56	-1.05	-0.98	-0.94	-0.86	-0.78	-0.71	-0.68
-3.24	-1.19	-1.13	-1.09	-1.02	-0.94	-0.87	-0.81
-4.00	-1.34	-1.28	-1.24	-1.17	-1.10	-1.03	-0.97
-4.84	-1.49	-1.43	-1.39	-1.32	-1.25	-1.19	-1.12
-5.76	-1.64	-1.58	-1.54	-1.48	-1.41	-1.34	-1.28
-6.76	-1.78	-1.73	-1.69	-1.63	-1.56	-1.50	-1.44
-7.84	-1.93	-1.88	-1.84	-1.78	-1.72	-1.66	-1.60
-9.00	-2.08	-2.03	-1.99	-1.94	-1.88	-1.82	-1.76
-10.24	-2.23	-2.18	-2.14	-2.09	-2.03	-1.97	-1.91
-11.56	-2.37	-2.33	-2.30	-2.25	-2.19	-2.13	-2.07
-12.96	-2.52	-2.49	-2.45	-2.40	-2.35	-2.29	-2.23
-14.44	-2.67	-2.64	-2.60	-2.55	-2.50	-2.45	-2.39
-16.00	-2.81	-2.79	-2.75	-2.71	-2.66	-2.60	-2.55
-17.64	-2.96	-2.94	-2.90	-2.86	-2.82	-2.76	-2.71
-19.36	-3.11	-3.09	-3.05	-3.01	-2.97	-2.92	-2.86

Table 23 Original data of the standard curves for 2.4 m door, 0.1 m nozzle depth, and discharge angle of 20°

ΔP Pa	8 m/s	10 m/s	12 m/s	14 m/s	16 m/s	18 m/s	20 m/s
40.96	3.96	3.73	3.44	3.14	2.81	2.40	1.94
38.44	3.80	3.57	3.27	2.96	2.61	2.20	1.77
36.00	3.65	3.41	3.10	2.78	2.42	2.01	1.59
33.64	3.49	3.24	2.93	2.60	2.23	1.81	1.42
31.36	3.33	3.08	2.75	2.41	2.03	1.62	1.24
29.16	3.18	2.92	2.58	2.23	1.84	1.42	1.07
27.04	3.02	2.75	2.41	2.05	1.65	1.22	0.89
25.00	2.87	2.59	2.24	1.87	1.45	1.03	0.71
23.04	2.71	2.43	2.07	1.68	1.26	0.83	0.54
21.16	2.56	2.26	1.90	1.50	1.07	0.64	0.36
19.36	2.40	2.10	1.73	1.32	0.87	0.44	0.19
17.64	2.25	1.94	1.55	1.14	0.68	0.25	0.01
16.00	2.09	1.78	1.38	0.96	0.49	0.05	-0.03
14.44	1.94	1.61	1.21	0.77	0.29	-0.02	-0.06
12.96	1.78	1.45	1.04	0.59	0.10	-0.05	-0.08
11.56	1.62	1.29	0.87	0.41	-0.01	-0.08	-0.11
10.24	1.47	1.12	0.70	0.23	-0.04	-0.10	-0.14
9.00	1.31	0.96	0.52	0.04	-0.07	-0.13	-0.17
7.84	1.16	0.80	0.35	-0.02	-0.10	-0.16	-0.20
6.76	1.00	0.63	0.18	-0.05	-0.13	-0.19	-0.23
5.76	0.85	0.47	0.01	-0.08	-0.15	-0.21	-0.26
4.84	0.69	0.31	-0.03	-0.11	-0.18	-0.24	-0.29
4.00	0.54	0.15	-0.06	-0.14	-0.21	-0.27	-0.32
3.24	0.38	0.00	-0.09	-0.17	-0.24	-0.30	-0.34
2.56	0.22	-0.04	-0.12	-0.20	-0.27	-0.33	-0.37
1.96	0.07	-0.08	-0.15	-0.23	-0.30	-0.35	-0.40
1.44	-0.02	-0.12	-0.18	-0.27	-0.32	-0.38	-0.43
1.00	-0.07	-0.15	-0.21	-0.30	-0.35	-0.41	-0.46
0.64	-0.11	-0.19	-0.24	-0.33	-0.38	-0.44	-0.49
0.36	-0.16	-0.23	-0.27	-0.36	-0.41	-0.46	-0.52
0.16	-0.20	-0.27	-0.30	-0.39	-0.44	-0.49	-0.55
0.04	-0.24	-0.30	-0.33	-0.42	-0.46	-0.52	-0.57
0.00	-0.29	-0.34	-0.36	-0.45	-0.49	-0.55	-0.60
-0.04	-0.33	-0.38	-0.39	-0.48	-0.52	-0.58	-0.63
-0.16	-0.38	-0.42	-0.42	-0.51	-0.55	-0.60	-0.66
-0.36	-0.42	-0.45	-0.45	-0.54	-0.58	-0.63	-0.69
-0.64	-0.46	-0.49	-0.48	-0.57	-0.61	-0.66	-0.72
-1.00	-0.61	-0.55	-0.52	-0.60	-0.63	-0.69	-0.75
-1.44	-0.77	-0.70	-0.60	-0.63	-0.66	-0.71	-0.78
-1.96	-0.92	-0.86	-0.75	-0.66	-0.69	-0.74	-0.80
-2.56	-1.07	-1.01	-0.91	-0.82	-0.74	-0.77	-0.83

(continued)

Table 23 (continued)

ΔP Pa	8 m/s	10 m/s	12 m/s	14 m/s	16 m/s	18 m/s	20 m/s
-3.24	-1.22	-1.17	-1.06	-0.98	-0.90	-0.83	-0.86
-4.00	-1.38	-1.32	-1.22	-1.14	-1.06	-0.99	-0.89
-4.84	-1.53	-1.48	-1.38	-1.30	-1.22	-1.15	-1.06
-5.76	-1.68	-1.63	-1.53	-1.46	-1.39	-1.31	-1.22
-6.76	-1.83	-1.79	-1.69	-1.61	-1.55	-1.47	-1.38
-7.84	-1.99	-1.94	-1.84	-1.77	-1.71	-1.63	-1.54
-9.00	-2.14	-2.10	-2.00	-1.93	-1.87	-1.79	-1.71
-10.24	-2.29	-2.25	-2.16	-2.09	-2.03	-1.96	-1.87
-11.56	-2.44	-2.41	-2.31	-2.25	-2.19	-2.12	-2.03
-12.96	-2.60	-2.56	-2.47	-2.41	-2.35	-2.28	-2.20
-14.44	-2.75	-2.72	-2.62	-2.57	-2.51	-2.44	-2.36
-16.00	-2.90	-2.87	-2.78	-2.73	-2.67	-2.60	-2.52
-17.64	-3.06	-3.03	-2.94	-2.88	-2.83	-2.76	-2.68
-19.36	-3.21	-3.18	-3.09	-3.04	-2.99	-2.92	-2.85

Table 24 Original data of the standard curves for 3 m door, 0.08 m nozzle depth, and discharge angle of 0°

ΔP Pa	8 m/s	10 m/s	12 m/s	14 m/s	16 m/s	18 m/s	20 m/s
40.96	4.15	4.03	3.90	3.76	3.62	3.46	3.29
38.44	4.00	3.88	3.75	3.61	3.46	3.30	3.12
36.00	3.86	3.73	3.60	3.46	3.31	3.14	2.96
33.64	3.71	3.59	3.45	3.31	3.15	2.98	2.80
31.36	3.57	3.44	3.30	3.15	3.00	2.82	2.63
29.16	3.42	3.29	3.15	3.00	2.84	2.66	2.47
27.04	3.28	3.15	3.00	2.85	2.69	2.50	2.31
25.00	3.13	3.00	2.85	2.70	2.53	2.35	2.15
23.04	2.99	2.85	2.70	2.55	2.37	2.19	1.98
21.16	2.84	2.70	2.55	2.39	2.22	2.03	1.82
19.36	2.70	2.56	2.41	2.24	2.06	1.87	1.66
17.64	2.55	2.41	2.26	2.09	1.91	1.71	1.49
16.00	2.41	2.26	2.11	1.94	1.75	1.55	1.33
14.44	2.26	2.12	1.96	1.78	1.60	1.39	1.17
12.96	2.12	1.97	1.81	1.63	1.44	1.24	1.01
11.56	1.97	1.82	1.66	1.48	1.28	1.08	0.84
10.24	1.83	1.67	1.51	1.33	1.13	0.92	0.68
9.00	1.68	1.53	1.36	1.18	0.97	0.76	0.52
7.84	1.54	1.38	1.21	1.02	0.82	0.60	0.35
6.76	1.39	1.23	1.06	0.87	0.66	0.44	0.19
5.76	1.25	1.08	0.91	0.72	0.51	0.28	0.03
4.84	1.10	0.94	0.76	0.57	0.35	0.13	-0.01
4.00	0.96	0.79	0.61	0.42	0.19	0.00	-0.03

(continued)

Table 24 (continued)

ΔP Pa	8 m/s	10 m/s	12 m/s	14 m/s	16 m/s	18 m/s	20 m/s
3.24	0.81	0.64	0.46	0.26	0.04	-0.02	-0.05
2.56	0.67	0.50	0.32	0.11	-0.01	-0.04	-0.07
1.96	0.52	0.35	0.17	-0.01	-0.03	-0.06	-0.08
1.44	0.38	0.20	0.02	-0.02	-0.05	-0.08	-0.10
1.00	0.23	0.05	-0.02	-0.04	-0.07	-0.09	-0.12
0.64	0.09	-0.01	-0.04	-0.06	-0.09	-0.11	-0.13
0.36	-0.01	-0.03	-0.06	-0.08	-0.11	-0.13	-0.15
0.16	-0.03	-0.06	-0.08	-0.10	-0.13	-0.15	-0.17
0.04	-0.05	-0.08	-0.10	-0.12	-0.15	-0.16	-0.19
0.00	-0.07	-0.10	-0.12	-0.14	-0.16	-0.18	-0.20
-0.04	-0.09	-0.12	-0.14	-0.16	-0.18	-0.20	-0.22
-0.16	-0.11	-0.14	-0.16	-0.18	-0.20	-0.22	-0.24
-0.36	-0.13	-0.16	-0.18	-0.20	-0.22	-0.24	-0.25
-0.64	-0.25	-0.18	-0.20	-0.22	-0.24	-0.25	-0.27
-1.00	-0.39	-0.24	-0.22	-0.24	-0.26	-0.27	-0.29
-1.44	-0.54	-0.40	-0.24	-0.26	-0.28	-0.29	-0.31
-1.96	-0.69	-0.55	-0.36	-0.28	-0.29	-0.31	-0.32
-2.56	-0.84	-0.71	-0.52	-0.30	-0.31	-0.32	-0.34
-3.24	-0.99	-0.87	-0.68	-0.47	-0.33	-0.34	-0.36
-4.00	-1.14	-1.02	-0.85	-0.64	-0.43	-0.36	-0.37
-4.84	-1.29	-1.18	-1.01	-0.81	-0.60	-0.38	-0.39
-5.76	-1.44	-1.33	-1.17	-0.98	-0.78	-0.56	-0.41
-6.76	-1.59	-1.49	-1.33	-1.15	-0.95	-0.74	-0.50
-7.84	-1.74	-1.65	-1.49	-1.32	-1.13	-0.93	-0.69
-9.00	-1.89	-1.80	-1.66	-1.49	-1.31	-1.11	-0.88
-10.24	-2.04	-1.96	-1.82	-1.66	-1.48	-1.29	-1.07
-11.56	-2.19	-2.11	-1.98	-1.83	-1.66	-1.47	-1.26
-12.96	-2.34	-2.27	-2.14	-2.00	-1.84	-1.65	-1.45
-14.44	-2.49	-2.43	-2.30	-2.17	-2.01	-1.84	-1.65
-16.00	-2.63	-2.58	-2.47	-2.34	-2.19	-2.02	-1.84
-17.64	-2.78	-2.74	-2.63	-2.51	-2.36	-2.20	-2.03
-19.36	-2.93	-2.89	-2.79	-2.68	-2.54	-2.38	-2.22

Table 25 Original data of the standard curves for 3 m door, 0.1 m nozzle depth, and discharge angle of 0°

ΔP Pa	8 m/s	10 m/s	12 m/s	14 m/s	16 m/s	18 m/s	20 m/s
40.96	4.09	3.94	3.79	3.63	3.45	3.26	3.07
38.44	3.94	3.80	3.64	3.48	3.29	3.10	2.90
36.00	3.80	3.65	3.48	3.32	3.13	2.93	2.73
33.64	3.65	3.50	3.33	3.16	2.98	2.77	2.55
31.36	3.50	3.35	3.18	3.01	2.82	2.60	2.38
29.16	3.36	3.20	3.03	2.85	2.66	2.44	2.21
27.04	3.21	3.05	2.88	2.70	2.50	2.27	2.04
25.00	3.06	2.90	2.73	2.54	2.34	2.11	1.87
23.04	2.92	2.75	2.58	2.38	2.19	1.94	1.70
21.16	2.77	2.61	2.42	2.23	2.03	1.78	1.53
19.36	2.62	2.46	2.27	2.07	1.87	1.61	1.36
17.64	2.47	2.31	2.12	1.92	1.71	1.45	1.19
16.00	2.33	2.16	1.97	1.76	1.55	1.28	1.01
14.44	2.18	2.01	1.82	1.60	1.40	1.12	0.84
12.96	2.03	1.86	1.67	1.45	1.24	0.95	0.67
11.56	1.89	1.71	1.52	1.29	1.08	0.79	0.50
10.24	1.74	1.56	1.37	1.14	0.92	0.62	0.33
9.00	1.59	1.42	1.21	0.98	0.76	0.46	0.16
7.84	1.45	1.27	1.06	0.82	0.61	0.29	0.00
6.76	1.30	1.12	0.91	0.67	0.45	0.13	-0.02
5.76	1.15	0.97	0.76	0.51	0.29	0.00	-0.04
4.84	1.01	0.82	0.61	0.36	0.13	-0.02	-0.05
4.00	0.86	0.67	0.46	0.20	0.00	-0.04	-0.07
3.24	0.71	0.52	0.31	0.04	-0.02	-0.06	-0.09
2.56	0.57	0.37	0.16	-0.01	-0.04	-0.08	-0.11
1.96	0.42	0.23	0.00	-0.03	-0.06	-0.10	-0.12
1.44	0.27	0.08	-0.02	-0.05	-0.08	-0.12	-0.14
1.00	0.13	-0.01	-0.04	-0.07	-0.10	-0.13	-0.16
0.64	-0.02	-0.03	-0.06	-0.09	-0.12	-0.15	-0.18
0.36	-0.03	-0.06	-0.09	-0.12	-0.14	-0.17	-0.19
0.16	-0.05	-0.08	-0.11	-0.14	-0.16	-0.19	-0.21
0.04	-0.07	-0.10	-0.13	-0.16	-0.18	-0.21	-0.23
0.00	-0.10	-0.12	-0.15	-0.18	-0.20	-0.23	-0.25
-0.04	-0.12	-0.15	-0.17	-0.20	-0.22	-0.25	-0.27
-0.16	-0.14	-0.17	-0.19	-0.22	-0.24	-0.26	-0.28
-0.36	-0.17	-0.19	-0.21	-0.24	-0.26	-0.28	-0.30
-0.64	-0.19	-0.21	-0.24	-0.26	-0.28	-0.30	-0.32
-1.00	-0.33	-0.24	-0.26	-0.28	-0.30	-0.32	-0.34
-1.44	-0.49	-0.29	-0.28	-0.30	-0.32	-0.34	-0.35
-1.96	-0.64	-0.45	-0.30	-0.32	-0.34	-0.36	-0.37
-2.56	-0.79	-0.61	-0.39	-0.34	-0.36	-0.38	-0.39

(continued)

Table 25 (continued)

ΔP Pa	8 m/s	10 m/s	12 m/s	14 m/s	16 m/s	18 m/s	20 m/s
-3.24	-0.95	-0.77	-0.55	-0.36	-0.38	-0.39	-0.41
-4.00	-1.10	-0.93	-0.72	-0.46	-0.40	-0.41	-0.42
-4.84	-1.25	-1.09	-0.89	-0.64	-0.42	-0.43	-0.44
-5.76	-1.41	-1.25	-1.05	-0.81	-0.57	-0.45	-0.46
-6.76	-1.56	-1.41	-1.22	-0.99	-0.75	-0.49	-0.48
-7.84	-1.71	-1.56	-1.38	-1.16	-0.94	-0.68	-0.49
-9.00	-1.87	-1.72	-1.55	-1.34	-1.12	-0.87	-0.68
-10.24	-2.02	-1.88	-1.71	-1.52	-1.30	-1.06	-0.87
-11.56	-2.17	-2.04	-1.88	-1.69	-1.48	-1.25	-1.06
-12.96	-2.33	-2.20	-2.05	-1.87	-1.67	-1.44	-1.25
-14.44	-2.48	-2.36	-2.21	-2.04	-1.85	-1.64	-1.44
-16.00	-2.63	-2.52	-2.38	-2.22	-2.03	-1.83	-1.63
-17.64	-2.79	-2.68	-2.54	-2.40	-2.21	-2.02	-1.82
-19.36	-2.94	-2.84	-2.71	-2.57	-2.40	-2.21	-2.01

Table 26 Original data of the standard curves for 3 m door, 0.08 m nozzle depth, and discharge angle of 10°

ΔP Pa	8 m/s	10 m/s	12 m/s	14 m/s	16 m/s	18 m/s	20 m/s
40.96	4.10	3.95	3.80	3.64	3.46	3.26	3.04
38.44	3.95	3.80	3.65	3.48	3.29	3.09	2.86
36.00	3.80	3.65	3.50	3.32	3.13	2.92	2.69
33.64	3.66	3.50	3.35	3.17	2.96	2.75	2.51
31.36	3.51	3.36	3.20	3.01	2.80	2.57	2.33
29.16	3.36	3.21	3.05	2.85	2.64	2.40	2.16
27.04	3.21	3.06	2.90	2.69	2.47	2.23	1.98
25.00	3.06	2.91	2.74	2.53	2.31	2.06	1.80
23.04	2.92	2.76	2.59	2.37	2.14	1.89	1.62
21.16	2.77	2.61	2.44	2.21	1.98	1.72	1.45
19.36	2.62	2.46	2.29	2.06	1.82	1.55	1.27
17.64	2.47	2.31	2.14	1.90	1.65	1.38	1.09
16.00	2.33	2.17	1.99	1.74	1.49	1.21	0.92
14.44	2.18	2.02	1.84	1.58	1.32	1.04	0.74
12.96	2.03	1.87	1.69	1.42	1.16	0.87	0.56
11.56	1.88	1.72	1.54	1.26	0.99	0.69	0.39
10.24	1.73	1.57	1.39	1.10	0.83	0.52	0.21
9.00	1.59	1.42	1.24	0.95	0.67	0.35	0.03
7.84	1.44	1.27	1.09	0.79	0.50	0.18	-0.02
6.76	1.29	1.12	0.94	0.63	0.34	0.01	-0.04
5.76	1.14	0.97	0.79	0.47	0.17	-0.02	-0.06
4.84	1.00	0.83	0.64	0.31	0.01	-0.04	-0.08
4.00	0.85	0.68	0.49	0.15	-0.02	-0.07	-0.10

(continued)

Table 26 (continued)

ΔP Pa	8 m/s	10 m/s	12 m/s	14 m/s	16 m/s	18 m/s	20 m/s
3.24	0.70	0.53	0.34	0.00	-0.05	-0.09	-0.13
2.56	0.55	0.38	0.19	-0.03	-0.07	-0.11	-0.15
1.96	0.41	0.23	0.04	-0.05	-0.09	-0.13	-0.17
1.44	0.26	0.08	-0.02	-0.08	-0.12	-0.16	-0.19
1.00	0.11	-0.01	-0.05	-0.10	-0.14	-0.18	-0.21
0.64	-0.01	-0.04	-0.08	-0.13	-0.16	-0.20	-0.23
0.36	-0.04	-0.07	-0.11	-0.15	-0.19	-0.22	-0.26
0.16	-0.07	-0.10	-0.14	-0.18	-0.21	-0.25	-0.28
0.04	-0.10	-0.13	-0.16	-0.21	-0.23	-0.27	-0.30
0.00	-0.13	-0.16	-0.19	-0.23	-0.26	-0.29	-0.32
-0.04	-0.16	-0.19	-0.22	-0.26	-0.28	-0.31	-0.34
-0.16	-0.19	-0.22	-0.25	-0.28	-0.30	-0.33	-0.37
-0.36	-0.23	-0.25	-0.28	-0.31	-0.33	-0.36	-0.39
-0.64	-0.38	-0.29	-0.31	-0.33	-0.35	-0.38	-0.41
-1.00	-0.53	-0.44	-0.34	-0.36	-0.38	-0.40	-0.43
-1.44	-0.68	-0.59	-0.48	-0.39	-0.40	-0.42	-0.45
-1.96	-0.82	-0.74	-0.63	-0.54	-0.42	-0.45	-0.47
-2.56	-0.97	-0.89	-0.79	-0.69	-0.54	-0.47	-0.50
-3.24	-1.12	-1.04	-0.94	-0.85	-0.70	-0.58	-0.52
-4.00	-1.27	-1.19	-1.10	-1.00	-0.87	-0.74	-0.61
-4.84	-1.42	-1.35	-1.25	-1.15	-1.03	-0.91	-0.78
-5.76	-1.57	-1.50	-1.40	-1.31	-1.19	-1.07	-0.94
-6.76	-1.72	-1.65	-1.56	-1.46	-1.35	-1.23	-1.11
-7.84	-1.86	-1.80	-1.71	-1.62	-1.51	-1.40	-1.28
-9.00	-2.01	-1.95	-1.86	-1.77	-1.67	-1.56	-1.45
-10.24	-2.16	-2.10	-2.02	-1.93	-1.83	-1.73	-1.61
-11.56	-2.31	-2.25	-2.17	-2.08	-2.00	-1.89	-1.78
-12.96	-2.46	-2.40	-2.33	-2.24	-2.16	-2.05	-1.95
-14.44	-2.61	-2.55	-2.48	-2.39	-2.32	-2.22	-2.12
-16.00	-2.76	-2.70	-2.63	-2.54	-2.48	-2.38	-2.28
-17.64	-2.90	-2.85	-2.79	-2.70	-2.64	-2.55	-2.45
-19.36	-3.05	-3.00	-2.94	-2.85	-2.80	-2.71	-2.62

Table 27 Original data of the standard curves for 3 m door, 0.1 m nozzle depth, and discharge angle of 10°

ΔP Pa	8 m/s	10 m/s	12 m/s	14 m/s	16 m/s	18 m/s	20 m/s
40.96	4.02	3.82	3.67	3.47	3.25	3.00	2.75
38.44	3.87	3.67	3.52	3.31	3.08	2.82	2.56
36.00	3.72	3.53	3.36	3.14	2.91	2.65	2.37
33.64	3.57	3.38	3.20	2.98	2.74	2.47	2.18
31.36	3.42	3.23	3.05	2.82	2.57	2.29	2.00
29.16	3.28	3.08	2.89	2.66	2.40	2.12	1.81
27.04	3.13	2.93	2.74	2.49	2.23	1.94	1.62
25.00	2.98	2.78	2.58	2.33	2.06	1.76	1.43
23.04	2.83	2.63	2.43	2.17	1.89	1.59	1.25
21.16	2.68	2.48	2.27	2.00	1.72	1.41	1.06
19.36	2.53	2.33	2.11	1.84	1.55	1.23	0.87
17.64	2.38	2.19	1.96	1.68	1.38	1.06	0.69
16.00	2.23	2.04	1.80	1.52	1.21	0.88	0.50
14.44	2.09	1.89	1.65	1.35	1.04	0.70	0.31
12.96	1.94	1.74	1.49	1.19	0.87	0.53	0.12
11.56	1.79	1.59	1.34	1.03	0.70	0.35	-0.01
10.24	1.64	1.44	1.18	0.87	0.53	0.17	-0.03
9.00	1.49	1.29	1.02	0.70	0.36	0.00	-0.05
7.84	1.34	1.14	0.87	0.54	0.19	-0.02	-0.08
6.76	1.19	0.99	0.71	0.38	0.02	-0.05	-0.10
5.76	1.05	0.84	0.56	0.21	-0.02	-0.07	-0.12
4.84	0.90	0.70	0.40	0.05	-0.05	-0.10	-0.14
4.00	0.75	0.55	0.25	-0.02	-0.07	-0.12	-0.17
3.24	0.60	0.40	0.09	-0.04	-0.10	-0.14	-0.19
2.56	0.45	0.25	-0.01	-0.07	-0.12	-0.17	-0.21
1.96	0.30	0.10	-0.04	-0.10	-0.15	-0.19	-0.23
1.44	0.15	-0.01	-0.07	-0.12	-0.17	-0.22	-0.26
1.00	0.00	-0.04	-0.10	-0.15	-0.20	-0.24	-0.28
0.64	-0.03	-0.07	-0.13	-0.18	-0.22	-0.26	-0.30
0.36	-0.06	-0.10	-0.16	-0.20	-0.25	-0.29	-0.32
0.16	-0.09	-0.13	-0.18	-0.23	-0.27	-0.31	-0.35
0.04	-0.13	-0.16	-0.21	-0.25	-0.30	-0.34	-0.37
0.00	-0.16	-0.20	-0.24	-0.28	-0.32	-0.36	-0.39
-0.04	-0.19	-0.23	-0.27	-0.31	-0.34	-0.38	-0.41
-0.16	-0.22	-0.26	-0.30	-0.33	-0.37	-0.41	-0.44
-0.36	-0.25	-0.29	-0.33	-0.36	-0.39	-0.43	-0.46
-0.64	-0.34	-0.32	-0.36	-0.39	-0.42	-0.45	-0.48
-1.00	-0.49	-0.41	-0.38	-0.41	-0.44	-0.48	-0.51
-1.44	-0.64	-0.56	-0.44	-0.44	-0.47	-0.50	-0.53
-1.96	-0.79	-0.71	-0.59	-0.46	-0.49	-0.53	-0.55
-2.56	-0.94	-0.86	-0.75	-0.57	-0.52	-0.55	-0.57

(continued)

Table 27 (continued)

ΔP Pa	8 m/s	10 m/s	12 m/s	14 m/s	16 m/s	18 m/s	20 m/s
-3.24	-1.09	-1.01	-0.90	-0.73	-0.60	-0.57	-0.60
-4.00	-1.23	-1.16	-1.05	-0.89	-0.76	-0.61	-0.62
-4.84	-1.38	-1.31	-1.20	-1.05	-0.92	-0.78	-0.64
-5.76	-1.53	-1.46	-1.35	-1.21	-1.09	-0.95	-0.74
-6.76	-1.68	-1.61	-1.51	-1.37	-1.25	-1.12	-0.92
-7.84	-1.83	-1.76	-1.66	-1.54	-1.41	-1.28	-1.10
-9.00	-1.98	-1.91	-1.81	-1.70	-1.58	-1.45	-1.27
-10.24	-2.13	-2.06	-1.96	-1.86	-1.74	-1.62	-1.45
-11.56	-2.28	-2.21	-2.11	-2.02	-1.91	-1.79	-1.63
-12.96	-2.43	-2.36	-2.26	-2.18	-2.07	-1.95	-1.81
-14.44	-2.58	-2.50	-2.42	-2.34	-2.23	-2.12	-1.98
-16.00	-2.73	-2.65	-2.57	-2.50	-2.40	-2.29	-2.16
-17.64	-2.88	-2.80	-2.72	-2.66	-2.56	-2.46	-2.34
-19.36	-3.03	-2.95	-2.87	-2.83	-2.72	-2.62	-2.52

Table 28 Original data of the standard curves for 3 m door, 0.08 m nozzle depth, and discharge angle of 20°

ΔP Pa	8 m/s	10 m/s	12 m/s	14 m/s	16 m/s	18 m/s	20 m/s
40.96	4.07	3.91	3.74	3.55	3.35	3.12	2.87
38.44	3.92	3.76	3.58	3.39	3.18	2.94	2.68
36.00	3.77	3.61	3.43	3.23	3.01	2.76	2.49
33.64	3.62	3.45	3.27	3.07	2.83	2.58	2.30
31.36	3.47	3.30	3.11	2.90	2.66	2.40	2.11
29.16	3.32	3.15	2.96	2.74	2.49	2.22	1.92
27.04	3.18	3.00	2.80	2.58	2.32	2.04	1.74
25.00	3.03	2.85	2.64	2.42	2.15	1.86	1.55
23.04	2.88	2.70	2.49	2.26	1.98	1.68	1.36
21.16	2.73	2.55	2.33	2.10	1.81	1.50	1.17
19.36	2.58	2.40	2.17	1.93	1.64	1.33	0.98
17.64	2.43	2.25	2.02	1.77	1.47	1.15	0.79
16.00	2.29	2.10	1.86	1.61	1.30	0.97	0.60
14.44	2.14	1.95	1.71	1.45	1.13	0.79	0.42
12.96	1.99	1.80	1.55	1.29	0.96	0.61	0.23
11.56	1.84	1.65	1.39	1.12	0.79	0.43	0.04
10.24	1.69	1.50	1.24	0.96	0.62	0.25	-0.02
9.00	1.54	1.35	1.08	0.80	0.45	0.07	-0.04
7.84	1.40	1.20	0.92	0.64	0.28	-0.02	-0.07
6.76	1.25	1.05	0.77	0.48	0.11	-0.04	-0.09
5.76	1.10	0.89	0.61	0.32	-0.01	-0.07	-0.12
4.84	0.95	0.74	0.46	0.15	-0.04	-0.09	-0.14
4.00	0.80	0.59	0.30	0.00	-0.07	-0.12	-0.17

(continued)

Table 28 (continued)

ΔP Pa	8 m/s	10 m/s	12 m/s	14 m/s	16 m/s	18 m/s	20 m/s
3.24	0.65	0.44	0.14	-0.03	-0.09	-0.14	-0.19
2.56	0.51	0.29	0.00	-0.06	-0.12	-0.17	-0.22
1.96	0.36	0.14	-0.04	-0.09	-0.15	-0.20	-0.24
1.44	0.21	0.00	-0.07	-0.13	-0.18	-0.22	-0.27
1.00	0.06	-0.04	-0.11	-0.16	-0.21	-0.25	-0.29
0.64	-0.03	-0.08	-0.14	-0.19	-0.23	-0.27	-0.32
0.36	-0.07	-0.12	-0.17	-0.22	-0.26	-0.30	-0.34
0.16	-0.11	-0.16	-0.21	-0.25	-0.29	-0.32	-0.37
0.04	-0.16	-0.20	-0.24	-0.28	-0.32	-0.35	-0.39
0.00	-0.20	-0.24	-0.28	-0.31	-0.35	-0.38	-0.42
-0.04	-0.25	-0.28	-0.31	-0.34	-0.37	-0.40	-0.44
-0.16	-0.29	-0.32	-0.35	-0.37	-0.40	-0.43	-0.47
-0.36	-0.36	-0.36	-0.38	-0.40	-0.43	-0.45	-0.49
-0.64	-0.51	-0.47	-0.45	-0.43	-0.46	-0.48	-0.52
-1.00	-0.65	-0.62	-0.59	-0.56	-0.59	-0.51	-0.54
-1.44	-0.80	-0.76	-0.74	-0.71	-0.73	-0.64	-0.62
-1.96	-0.94	-0.91	-0.89	-0.86	-0.87	-0.79	-0.77
-2.56	-1.09	-1.06	-1.04	-1.01	-1.02	-0.94	-0.91
-3.24	-1.24	-1.21	-1.18	-1.16	-1.16	-1.09	-1.06
-4.00	-1.38	-1.35	-1.33	-1.30	-1.30	-1.24	-1.21
-4.84	-1.53	-1.50	-1.48	-1.45	-1.45	-1.39	-1.36
-5.76	-1.68	-1.65	-1.63	-1.60	-1.59	-1.54	-1.51
-6.76	-1.82	-1.80	-1.77	-1.75	-1.73	-1.69	-1.66
-7.84	-1.97	-1.95	-1.92	-1.90	-1.88	-1.84	-1.81
-9.00	-2.11	-2.09	-2.07	-2.04	-2.02	-1.99	-1.96
-10.24	-2.26	-2.24	-2.22	-2.19	-2.16	-2.14	-2.11
-11.56	-2.41	-2.39	-2.36	-2.34	-2.31	-2.29	-2.26
-12.96	-2.55	-2.54	-2.51	-2.49	-2.45	-2.44	-2.41
-14.44	-2.70	-2.68	-2.66	-2.64	-2.59	-2.59	-2.56
-16.00	-2.85	-2.83	-2.81	-2.79	-2.74	-2.74	-2.71
-17.64	-2.99	-2.98	-2.96	-2.93	-2.88	-2.89	-2.86
-19.36	-3.14	-3.13	-3.10	-3.08	-3.02	-3.04	-3.01

Table 29 Original data of the standard curves for 3 m door, 0.1 m nozzle depth, and discharge angle of 20°

ΔP Pa	8 m/s	10 m/s	12 m/s	14 m/s	16 m/s	18 m/s	20 m/s
40.96	3.98	3.80	3.59	3.37	3.13	2.83	2.51
38.44	3.83	3.65	3.43	3.20	2.95	2.64	2.31
36.00	3.68	3.49	3.27	3.03	2.77	2.45	2.12
33.64	3.53	3.34	3.11	2.86	2.59	2.26	1.92
31.36	3.38	3.19	2.95	2.69	2.41	2.07	1.72
29.16	3.23	3.03	2.79	2.52	2.23	1.88	1.53
27.04	3.08	2.88	2.63	2.35	2.05	1.69	1.33
25.00	2.93	2.72	2.47	2.18	1.87	1.50	1.14
23.04	2.78	2.57	2.31	2.01	1.69	1.31	0.94
21.16	2.63	2.42	2.15	1.85	1.50	1.12	0.74
19.36	2.48	2.26	1.99	1.68	1.32	0.93	0.55
17.64	2.34	2.11	1.83	1.51	1.14	0.74	0.35
16.00	2.19	1.95	1.67	1.34	0.96	0.55	0.16
14.44	2.04	1.80	1.51	1.17	0.78	0.36	-0.01
12.96	1.89	1.65	1.35	1.00	0.60	0.17	-0.03
11.56	1.74	1.49	1.19	0.83	0.42	0.00	-0.06
10.24	1.59	1.34	1.03	0.66	0.24	-0.03	-0.08
9.00	1.44	1.18	0.87	0.49	0.06	-0.06	-0.11
7.84	1.29	1.03	0.71	0.33	-0.02	-0.08	-0.14
6.76	1.14	0.88	0.55	0.16	-0.05	-0.11	-0.16
5.76	0.99	0.72	0.39	0.00	-0.08	-0.13	-0.19
4.84	0.84	0.57	0.23	-0.03	-0.10	-0.16	-0.22
4.00	0.69	0.42	0.07	-0.06	-0.13	-0.19	-0.24
3.24	0.54	0.26	-0.02	-0.09	-0.16	-0.21	-0.27
2.56	0.39	0.11	-0.05	-0.13	-0.19	-0.24	-0.30
1.96	0.24	-0.01	-0.09	-0.16	-0.22	-0.27	-0.32
1.44	0.09	-0.05	-0.12	-0.19	-0.25	-0.29	-0.35
1.00	-0.02	-0.09	-0.16	-0.22	-0.27	-0.32	-0.38
0.64	-0.06	-0.13	-0.19	-0.25	-0.30	-0.35	-0.40
0.36	-0.11	-0.17	-0.23	-0.28	-0.33	-0.37	-0.43
0.16	-0.15	-0.21	-0.26	-0.31	-0.36	-0.40	-0.45
0.04	-0.19	-0.25	-0.30	-0.34	-0.39	-0.43	-0.48
0.00	-0.24	-0.29	-0.33	-0.37	-0.42	-0.45	-0.51
-0.04	-0.28	-0.33	-0.36	-0.40	-0.44	-0.48	-0.53
-0.16	-0.33	-0.37	-0.40	-0.43	-0.47	-0.51	-0.56
-0.36	-0.37	-0.41	-0.43	-0.46	-0.50	-0.53	-0.59
-0.64	-0.49	-0.45	-0.47	-0.49	-0.53	-0.56	-0.61
-1.00	-0.63	-0.60	-0.57	-0.59	-0.56	-0.58	-0.64
-1.44	-0.78	-0.75	-0.71	-0.73	-0.63	-0.61	-0.67
-1.96	-0.93	-0.89	-0.86	-0.87	-0.78	-0.76	-0.71
-2.56	-1.07	-1.04	-1.01	-1.02	-0.93	-0.91	-0.86

(continued)

Table 29 (continued)

ΔP Pa	8 m/s	10 m/s	12 m/s	14 m/s	16 m/s	18 m/s	20 m/s
-3.24	-1.22	-1.19	-1.16	-1.16	-1.08	-1.05	-1.01
-4.00	-1.37	-1.34	-1.31	-1.30	-1.23	-1.20	-1.16
-4.84	-1.52	-1.48	-1.46	-1.45	-1.38	-1.35	-1.31
-5.76	-1.66	-1.63	-1.60	-1.59	-1.53	-1.50	-1.46
-6.76	-1.81	-1.78	-1.75	-1.73	-1.68	-1.65	-1.61
-7.84	-1.96	-1.93	-1.90	-1.88	-1.83	-1.80	-1.76
-9.00	-2.10	-2.07	-2.05	-2.02	-1.98	-1.95	-1.91
-10.24	-2.25	-2.22	-2.20	-2.16	-2.13	-2.10	-2.06
-11.56	-2.40	-2.37	-2.34	-2.31	-2.28	-2.25	-2.21
-12.96	-2.54	-2.52	-2.49	-2.45	-2.43	-2.40	-2.37
-14.44	-2.69	-2.66	-2.64	-2.59	-2.58	-2.55	-2.52
-16.00	-2.84	-2.81	-2.79	-2.74	-2.73	-2.70	-2.67
-17.64	-2.98	-2.96	-2.94	-2.88	-2.88	-2.85	-2.82
-19.36	-3.13	-3.11	-3.08	-3.02	-3.03	-3.00	-2.97

References

1. AMCA, *ANSI/AMCA Standard 220-05 Laboratory Methods of Testing Air Curtain Units for Aerodynamic Performance Rating* (Air Movement and Control Association International, Inc., Arlington Heights, 2012)
2. ASHRAE, *ASHRAE Handbook—HVAC Applications* (American Society of Heating, Refrigerating and Air Conditioning Engineers, Atlanta, 2015)
3. M.V. Bellegheem et al., Heat transfer through vertically downward-blowing single-jet air curtains for cold rooms. *Heat Transf. Eng.* **33**, 1196–1206 (2012)
4. S. Goubran, D. Qi, W.F. Saleh, L.L. Wang, Comparing methods of modeling air infiltration through building entrances and their impact on building energy simulation. *Energy Build.* **138**, 579–590 (2017a)
5. S. Goubran, D. Qi, L.L. Wang Annual energy saving impact of air curtains in commercial reference buildings. Proceedings of ISHVAC-COBEE, Tianjin, China, 2015
6. S. Goubran, D. Qi, L.L. Wang, Assessing dynamic efficiency of air curtain in reducing whole building annual energy usage. *Build. Simul.* **10**, 497–507 (2017b)
7. S. Goubran, D. Qi, L.L. Wang, R. Zmeureanu, Experimental study on the flow characteristics of air curtains at building entrances. *Build. Environ.* **105**, 225–235 (2016)
8. H. Hammink, L. Hendriksen, Determination of the Climate Separation Efficiency of Biddle Air Curtains Doorflow HP-200 and Indac S200 under Laboratory Conditions, Netherland: Indac, S, 2011
9. F. Hayes, Heat transfer characteristics of the air curtain: A Plane jet subjected to transverse pressure and temperature gradients. PhD Thesis ed. s.l.: University of Illinois, USA, 1968
10. F.C. Hayes, W.F. Stoecker, Design data for air curtains. *ASHRAE Trans.* **75**(2), 168–180 (1969a)
11. F. Hayes, W. Stoecker, Heat transfer characteristics of the air curtain. *ASHRAE Trans.* **75**(2), 153–167 (1969b)
12. ISO, *ISO Standard 27327-1 Part 1 - Laboratory methods of testing for aerodynamic performance rating* (International Organization for Standardization, Geneva, 2009)
13. D. Qi, S. Goubran, L.L. Wang, R. Zmeureanu, Parametric study of air curtain door aerodynamics performance based on experiments and numerical simulations. *Build. Environ.* **129**, 65–73 (2018)

14. D. Qi, S. Goubran, R. Zmeureanu, L.L. Wang, Effect of People on Infiltration of Building Entrance with Air Curtains. Proceedings of ISHVAC-COBEE, Tianjin, China, 2015
15. L.L. Wang, Z. Zhong, An approach to determine infiltration characteristics of building entrance equipped with air curtains. *Energy Build.* **75**, 312–320 (2014a)
16. L.L. Wang, Z. Zhong, Whole building annual energy analysis of air curtain performance in commercial building. s.l., eSim, 2014b
17. G.K. Yuill, *Impact of high use automatic doors on infiltration* (ASHRAE, Atlanta, 1996)
18. G.K. Yuill, R. Upham, H. Chen, Air leakage through automatic doors. *ASHRAE Trans.* **106**(2), 145–160 (2000)

Promoting CO₂ Water Source Heat Pumps in Indian Industrial Sector



Abdessalem Rabhi and Ananda Mohan Ghosh

1 Introduction

The Institute for Global Environmental Strategies (IGES) and The Energy and Resources Institute (TERI) have been conducting joint projects to promote Japanese low-carbon technologies (LCTs) in the Indian industrial sector over nearly a decade [1].¹ This paper draws on their findings regarding the promotion of electric CO₂ water source heat pumps (hereafter EHP).

Since their introduction for residential and commercial use in 2001, the EHP were regarded as the next generation of low-carbon technologies [2]. EHP for industrial use have been piloted as first of their kind at two dairy plants in India in 2013, by IGES and TERI as part of a Science and Technology Research Partnership for Sustainable Development (SATREPS) project² [3]. Results from the two pilot projects revealed that a potential of 30–50% primary energy saving is possible by using EHP. The feasibility studies conducted by IGES and TERI subsequently at other sites too showed similar achievement is possible; hence EHP are alternative technology solutions that offer ecological and financial benefit for Indian industries that require both hot water and cold water regularly.

¹<https://pub.iges.or.jp/pub/jitmap-promoting-japanese-low-carbon>

²SATREPS is a Japanese government program structured as a collaboration between the Japan Science and Technology Agency (JST) and the Japan International Cooperation Agency (JICA).

A. Rabhi (✉)

Institute for Global Environmental Strategies (IGES), Hayama, Japan
e-mail: rabhi.abdessalem@mx.iges.or.jp

A. M. Ghosh

The Energy and Resource Institute (TERI), New Delhi, India
e-mail: amghosh@teri.res.in

Although various schemes are available in India that can be used to promote EHP, including the financing under the credit scheme initiated by Japan International Cooperation Agency (JICA) and Small Industries Development Bank in India (SIDBI), it was not possible to replicate the implementation of EHP so far even at the sites where they have been piloted. The authors argue that this is mainly due to existing barriers in terms of (1) high initial investment cost, (2) lack of awareness about EHP, and (3) limited technical capacity on how to operate and maintain EHP.

With support from the Ministry of the Environment, the Government of Japan (MOEJ), IGES and TERI jointly launched the Japan–India Technology Matchmaking Platform (JITMAP) in July 2016 to support business matchmaking between LCT providers from Japan and their recipients from India. JITMAP activities vary from organizing seminars for promoting particular LCTs and training workshops for improving energy managers' and auditors' understanding of the LCTs, to conducting feasibility studies of the LCTs at selected factories and arranging business talks with top management of selected companies and meetings with policymakers and regulators to discuss supporting policies. The authors argue that JITMAP could be used as a multistakeholder approach to promoting EHP as well.

The rest of the paper is organized as follows: the second section highlights the need for CO₂ heat pumps. The third section reports the findings from a case study on the feasibility of introducing EHP at a chocolate factory in India. The fourth section proposes an approach to adopt EHP more widely in India, and the fifth section concludes.

2 CO₂-Based Heat Pumps

2.1 An Overview

EHP are capable of generating heating and cooling output simultaneously. Both cooling and heating streams have separate primary and secondary paths with necessary equipment to generate designed output. They are operated with the help of electrical power, and main equipment consists of a reciprocating compressor, water heater (gas cooler), supercritical tank, expansion valve, and water cooler. In a heat pump cycle when a liquid evaporates, it usually takes heat from its environment. Conversely, when vapor condenses and liquefies, it releases heat. This characteristic is utilized in the process called the heat pump cycle. In this cycle, coolant circulated by the compressor is repeatedly evaporated and condensed to produce heating and cooling effects as per the design configuration.

The main operations in the primary circuit of the EHP cycle are mentioned below (Fig. 1):

1. Compression of refrigerant (CO₂)—it is compressed to supercritical level at very high pressure and temperature.
2. Cooling of refrigerant (CO₂)—high enthalpy of the refrigerant is transferred for heating.

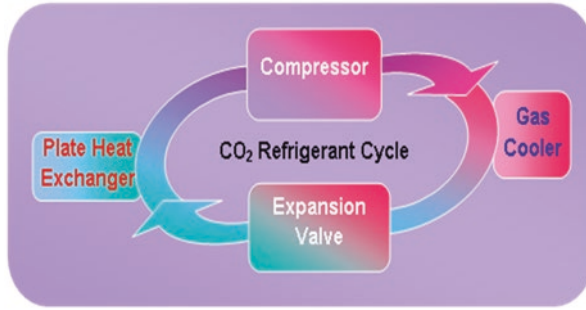


Fig. 1 Refrigeration cycle of EHP

3. Expansion of refrigerant (CO₂)—cooled refrigerant at low temperature and pressure passes through specially designed expansion valve for further reduction of pressure and temperature.
4. Evaporation of refrigerant (CO₂)—evaporation absorbs the required enthalpy from the desired cooling stream.
5. The evaporated refrigerant (CO₂) is again returned for compression to complete the cycle.

2.2 Need for CO₂-Based Heat Pumps

The hydrochlorofluorocarbons (HCFCs) and the hydrofluorocarbon (HFC) have been widely used as refrigerants for heat pumps; they are being phased out due to their harmful environmental impact as agreed under the Montreal Protocol and its Kigali Amendment.³ The concerns with HCFC and HFC refrigerants have led to an interest in other chemicals that can be used as refrigerants, one of which is the carbon dioxide (CO₂), which is a natural refrigerant and has an ozone depletion potential (ODP) of zero and a global warming potential (GWP) of one [4]. Consequently, there has been considerable interest in CO₂-based heat pumps, and three types are commercially available (Table 1).

2.3 CO₂ Water-to-Water Heat Pumps (EHP): Basic Concept

This paper focuses on the CO₂ water-to-water heat pumps (EHP) that generate hot water and cold water simultaneously using the trans-critical cycle of the natural refrigerant CO₂ instead of chemical refrigerants typically used in other heat pumps.

³<https://www.buildinggreen.com/blog/heat-pump-using-carbon-dioxide-refrigerant>

Table 1 Types of CO₂-based heat pumps

Heat source		Purpose
Air	Air-to-water heat pumps	Hot water at 65–90 °C
Water	Water-to-water heat pumps	Hot water at 65–90 °C + cold water
	Water-to-air heat pumps	Hot air at 80–120 °C + cold water

Source: Egashira Hiroyuki (2017) [5]

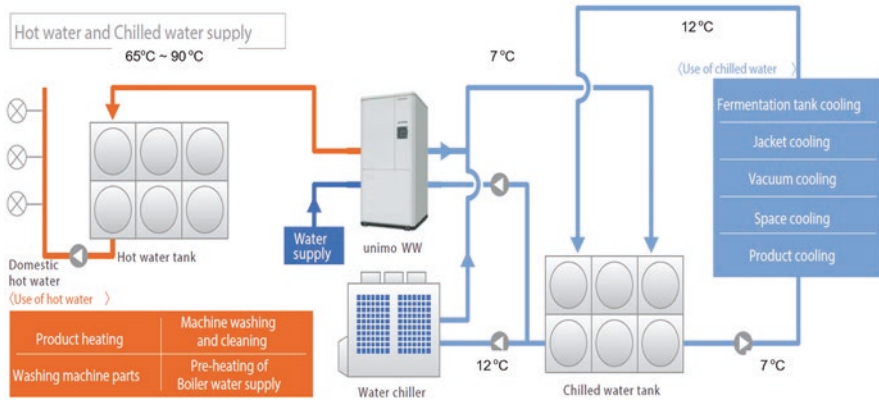


Fig. 2 Example of the application of the CO₂ water-to-water heat pump. (Source: Mayekawa Mfg. Co. Ltd. [6])

One of the examples of the EHP application is depicted in Fig. 2. The EHP extracts energy from a water supply source to generate hot water up to 90 °C and simultaneously precool the water entering the chiller from 12 °C to 7 °C.

From a performance standpoint, the big difference with EHP is that they can produce much higher water outlet temperatures up to 90 °C given that CO₂ is a “trans-critical” refrigerant and does not entirely change phase like other refrigerants [4]. Their operational characteristics are different from conventional systems (such as electric/gas/oil boilers or electric heaters). With traditional systems, 1 kW input of energy provides less than 1 kW of output energy or heat. With EHP, the coefficient of performance (COP) could be up to 8 in the case of heat recovery type [7] (Table 2).

EHP are ideal for applications that require both heating (high-quality hot water) and cooling constantly. They can produce hot water up to 90 °C, and precool water up to −9 °C (brine diversion type); therefore, they are applicable for various industries (Fig. 3).

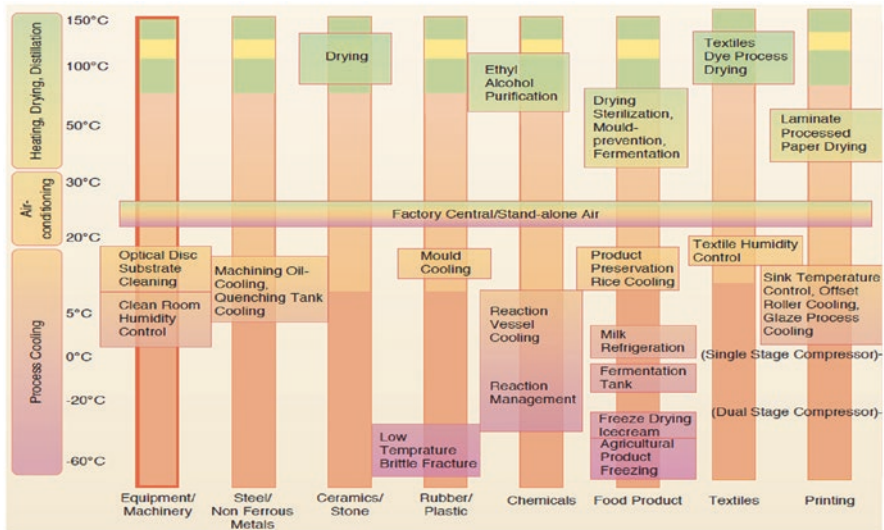
Table 2 Examples of CO₂ water-to-water heat pumps and their operation ranges

Capacity	Brine type	Cold water type	Heat recovery type
Heating capacity [kW]	49.9	82.1	101.8 (COP = 4.4)
Cooling capacity [kW]	35.0	61.7	82.3 (COP = 3.6)
Power consumption [kW]	18.4	21.8	23.1
COPt (total)	4.6	6.6	8.0
Condition	Supplied water (17 °C → 65 °C) Brine (-5 °C → -9 °C)	Supplied water (17 °C → 65 °C) Cold water (12 °C → 7 °C)	Supplied water (17 °C → 65 °C) Heat source water (22 °C → 17 °C)

Operation range	Water heater (Heater)	Water cooler (heat absorber)		
		Brine diversion type	Cold water diversion type	Heat recover type
Inlet temp. (°C)	5 ~ 40 (5 ~ 65*)	-5 ~ 37	10 ~ 37	10 ~ 37
Outlet temp. (°C)	65, 90	-9 ~ 32	5 ~ 32	5 ~ 32
Difference between Inlet and outlet temp. (°C)	≥ 25	5 ~ 10		
Flowrate (L/min)	8 ~ 5	≥ 100		

Source: Troy Davis and John Bush (2016) [7]

*At 90 C set point



Source: IEA Heat pump program [8]

Fig. 3 Range of applicability of heat pumps. (Source: IEA Heat pump program [8])

3 Case Study of Installing EHP in India

3.1 Background

IGES in collaboration of the Kyoto University, from Japan side, and TERI, from Indian side, had jointly conducted a 4-year research project to promote the application of Japanese low-carbon technologies in Indian Small and Medium Enterprises (SME).⁴ EHP were among the technologies studied under the project. Pilot projects about EHP were implemented at a chocolate factory in Anand, Gujarat, and dairy plant in Chandigarh, Punjab. Below is a report about the pilot project implemented at a chocolate factory in Anand, Gujarat.

3.2 The Proposed EHP System

The proposed EHP system included the EHP unit and heat exchanger. The EHP unit was to simultaneously cool water from 15 °C to 10 °C, and to heat the soft water from 35 °C to 90 °C. The heat exchanger unit was to heat soft water from 30 °C to 35 °C and to cool water supplied to feed water tank from 90 °C to 65 °C (Fig. 4). The specification of the introduced system is given in Table 3.

3.3 Summary of Key Findings

3.3.1 Potential for Replicating EHP

The annual fuel saving and CO₂ emission reduction are as shown in Figs. 5 and 6, respectively. The actual saving is shown in solid line, whereas the dotted line shows the estimated savings if the EHP were running all over the year, which was not the case in 2013 and 2015. In 2013 the EHP operated only for 5 months given it was installed in August 2013, and in 2015 EHP were not in use for about 4 months for maintenance purpose. The latest data from the site were received in July 2017, hence the actual saving in 2017 is also just for about 7 months. Overall, the authors found that the annual fuel saving is up to 69,970 kg, and the annual CO₂ emission is up to 181 tons/year.

Subsequently, IGES and TERI conducted feasibility studies at three sites in 2014.⁵ Results showed that 30–50% of primary energy saving is possible by using EHP at these sites as well.

⁴Funded by the JICA-JST Science and Technology Research Partnership for Sustainable Development (SATREPS) scheme.

⁵One at a food processing plant (Uttar Pradesh); two at dairy plants (Haryana).

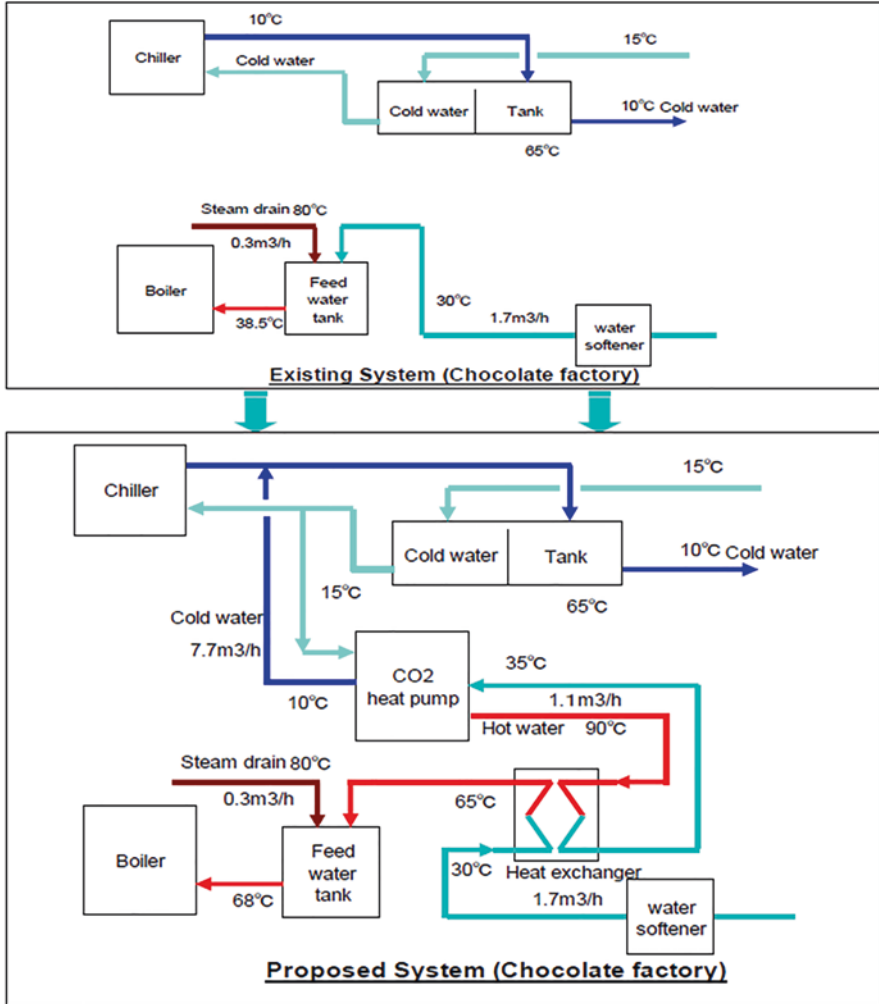


Fig. 4 Diagram of the initial and the proposed EHP systems. (Source: Amit Vyas, 2017 [9])

Assuming that EHP will be implemented at about 50 other dairy units in Punjab and Gujarat, the authors found that the replication could result in primary energy saving of 952 toe/year, and CO₂ emissions reduction of 3128 tons/year [3]. Based on the assumption of installing EHP at all dairy units in India, the authors found that the primary energy saving is approximately 30 million liters of crude oil equivalent, and CO₂ emission reduction is about 60,000 tons each year. These are rough estimations but still can provide an approximate picture of the impact of deploying EHP at a broader level in India.

Table 3 Specifications of the proposed EHP system

Sr. no	Parameter	Value
1	Connected electrical load	
	Compressor	24 kW
	Assorted auxiliaries	10 kW
2	Heating capacity	
	Water flow rate	1200 kg/hour
	Heating capacity	59.6 kW
	Delta T	55 °C
3	Cooling capacity	
	Water flow rate	8800 kg/hour
	Chilling capacity	37.6 kW
	Delta T	3.8 °C
4	Refrigerant (ODP type)	CO ₂
	COP of EHP	3.98
	COP of existing chiller	2.3
	Existing boiler efficiency	75%
	Primary energy saving	>35%
	Primary avoided CO ₂ emission	>40%
	Annual operating hour	6000 hours/year
	Primary energy saving	48 toe/year
	Primary avoided CO ₂ emission	100 tons/year
	SPP if operated for 7000 hours/year	<5 year

Source: Amit Vyas (2017) [9]

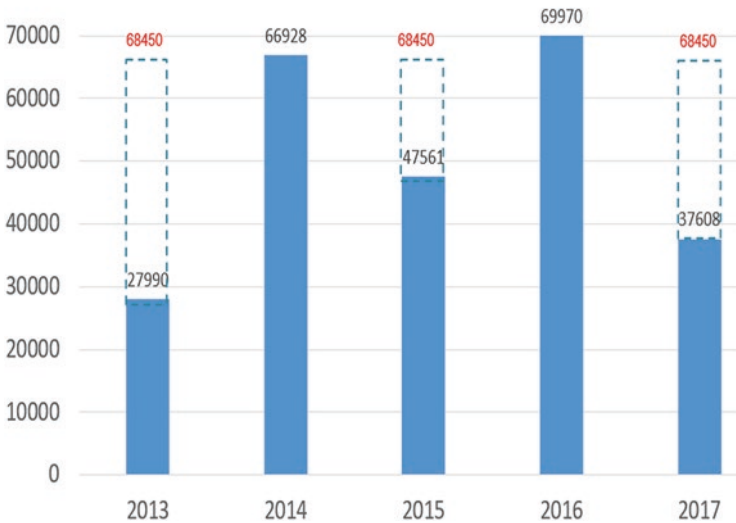


Fig. 5 Annual fuel saving (in kg). (Source: Authors, based on figures from Amit Vyas’s presentation at ISAP2017, Yokohama Japan)

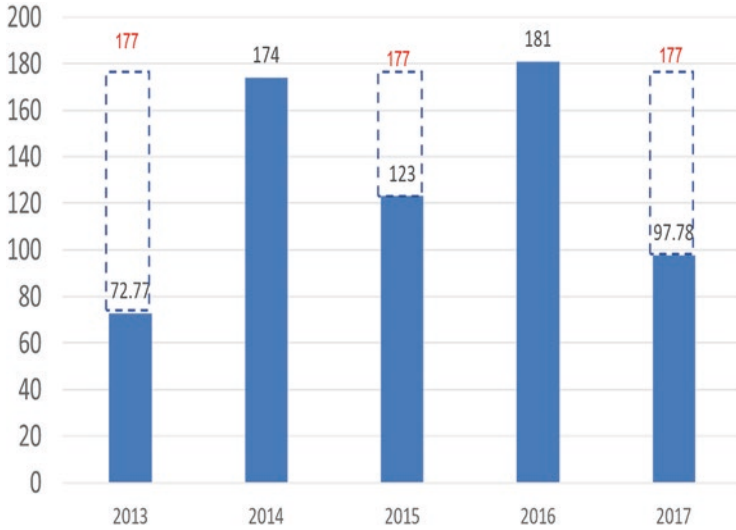


Fig. 6 Annual CO₂ emission reduction (tons/year). (Source: Authors, based on figures from Amit Vyas’s presentation at ISAP2017, Yokohama Japan)

3.3.2 Barriers to Deployment of EHP in Indian Industrial Sector

High Investment Cost

Compared to oil and gas boilers, EHP have relatively higher investment costs. The estimated payback period of the installed EHP is about 5 years, whereas companies with whom the authors interacted expect lower payback periods of less than 2 or 3 years.

Limited Awareness About EHP

EHP for industrial use are new to the market in India. Therefore, there is still insufficient awareness about their financial and environmental benefits among Indian industries. Mainly, end users are not aware and not able to identify the long-term benefits of EHP, including operation and maintenance costs, payback period, and return on investment.

Limited Technical Capacity to Run and Maintain EHP

The integration of EHP into industrial processes requires knowledge of the capabilities of industrial heat pumps, as well as knowledge about the process itself. Only a few local service providers and decision-makers in the industry have this combined

knowledge, which enables them to integrate EHP most suitably. For instance, due to limited technical capacity to run and maintain EHP, the EHP implemented at a dairy plant in Chandigarh did not run as initially expected.

4 Approaches to Promote EHP in the Indian Industrial Sector

The introduction of EHP in India can happen on a business-to-business basis. However, the authors call for benefitting from the existing initiatives and ongoing partnerships between Japan and India to faster the introduction process further.

4.1 Overcoming the Financial Barrier

Key measures to bring the cost of EHP down are to be taken by the manufacturers of EHP themselves, such as by manufacturing the EHP (or part of them) in India. By doing so, they would bring the cost of EHP significantly down and make it affordable to some extent. To overcome any remaining financial barriers, the authors suggest for benefitting from existing financial schemes. For instance, based on IGES-TERI's suggestion, EHP were added to the JICA-SIDBI two-step loan scheme [9]. Besides the JICA-SIDBI two-step loan, several other programs are also available (Table 4).

4.2 Overcoming the Limited Awareness and Technical Capacity Regarding EHP

The authors propose using the Japan–India Technology Matchmaking platform, which was initiated by IGES and TERI, with support from the Ministry of the Environment, Government of Japan.⁶ JITMAP intends to support business match-making between LCT providers from Japan and their recipient from India mainly, though not only, in the form of awareness enhancement, networking, access to financial schemes, and arrangement of policy and regulatory discussions through partnership among various stakeholders (research institutes, business associations, financing and supporting agencies, and government agencies) from India and Japan (Fig. 7).

⁶Activities in Gujarat State in particular are supported also by Hyogo Prefectural Government, Japan, through the activities of the IGES Kansai Research Centre as they have signed a Memorandum of Understanding (MOU) with the State Government of Gujarat.

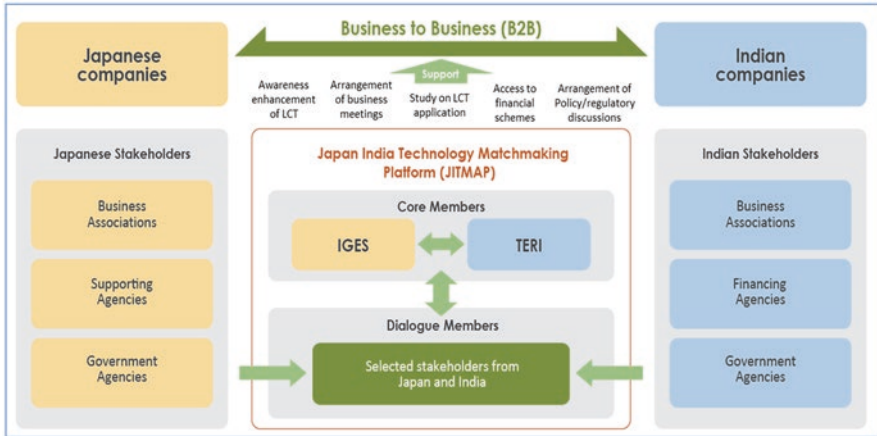
Table 4 Examples of financing options that can be used to promote EHP in India

Subsidy schemes	Source of financing	Brief description	To know more, visit
Credit-Linked Capital Subsidy Scheme (CLCSS) for technology upgradation	Ministry of Micro, Small and Medium Enterprises (MSME), Government of India	Facilitate technology upgradation in MSME by providing an upfront capital subsidy of 15% (on institutional finance of up to Rs 1 crore availed by them) for induction of well-established and improved technology in the specified 51 subsectors/products approved	http://www.dcmsme.gov.in/schemes/sccredit.htm
Technology and Quality Upgradation (TEQUP) support for MSME		Grant assistance to the extent of 25% of the project cost for implementation of energy efficient technologies (EET) subject to a maximum of 10 lakh is provided; MSME to be audited for energy consumption by a qualified energy auditor and project/machines installed in the units should lead to a minimum 15% reduction in energy consumption	http://msme.gov.in/WriteReadData/DocumentFile/technology&quality10.pdf
Technology Upgradation Fund Scheme (TUFS)	Ministry of Textiles, Government of India	Facilitate induction of state-of-the-art technology by the textile units; under the amended TUFS effective from January 13, 2016, only capital subsidy is provided (subject to a cap of Rs 30 crore) for eligible units in the textile sector	http://texmin.nic.in/schemes/technology-upgradation-fund-scheme
Scheme for technology upgradation/ establishment/modernization for food processing industries	Ministry of Food Processing Industries, Government of India	Assist processing industries in the form of grant subject to 25% of the plant and machinery and technical civil work subject to a maximum of Rs 50 lakh in general areas and 33.33% up to Rs 75 lakh in difficult areas	http://www.mofpi.nic.in/

Source: Authors, based on various sources (More schemes are available at <<https://udyamitra.in/SubsidySchemes#/Central>>)

JITMAP can support the promotion of EHP through:

1. Enhancing the awareness about EHP by introducing them to Indian industries through its dissemination workshops
2. Developing the technical capacity about EHP among local service providers, energy managers, and energy auditors through its training programs
3. Arranging business meetings and facilitating onsite feasibility studies about EHP through its extensive network



Source: Abdesslem Rabhi and Prosanto Pal 2019 [D]

Fig. 7 Schematic diagram of JITMAP as a supporting mechanism to promote business matching. (Source: Abdesslem Rabhi and Prosanto Pal, 2019 [10])

4. Sharing and discussing the findings and case studies with relevant stakeholders, including financing agencies and policymakers, directly through stakeholder meetings or indirectly through uploading the results at the JITMAP website

5 Conclusion

The industrial sector in India is responsible for a very considerable proportion of greenhouse gas emissions in India, as elsewhere. Heat pumps are a vital technology in the solution to break this trend. Using CO₂ as the refrigerant and achieving a high coefficient of performance, EHP offers both ecological and financial benefits. The results from piloting EHP at two dairy plants in India, by IGES and TERI, revealed that a potential of 30–50% primary energy saving is possible, with ultimate reduction in CO₂ emissions up to 180 tons/year.

EHP replication seems to be challenging due to three critical barriers in terms of (1) high initial investment cost, (2) lack of awareness about EHP, and (3) limited technical capacity on how to operate and maintain EHP.

To overcome the financial barriers, the authors recommend the use of existing financial schemes, including the financing under the credit scheme initiated by Japan International Cooperation Agency (JICA) and Small Industries Development Bank in India (SIDBI). To overcome the lack of awareness and to develop the technical capacities regarding EHP, the authors recommend to use the Japan–India Technology Matchmaking Platform, which was initiated by IGES and TERI with the support of MOEJ to promote Japanese low-carbon technologies in India.

Acknowledgments The content of this paper and the conclusions and the recommendations mentioned in it should be understood to be those of the authors and not attributed to IGES or TERI. Therefore, the authors should be responsible for the accuracy and relevance of the content.

Many thanks go to colleagues and supervisors at IGES and TERI, who contributed to it through suggestions and comments, namely to Prof. Yutaka Suzuki, Toshizo Maeda, Mika Tachibana, and Aditi Khodke (from IGES), and Girish Sethi (from TERI).

Special thanks go to Hiroyuki Egashira and Shidehara Kitayama from Mayekawa MFG. Co. Ltd. for their valuable technical inputs. Authors also thank Amit Vyas, Managing Director, Chocolate Plant Amul, Mogar, Anand, and H.S. Grewal, General Manager, Verka Milk Plant, Milkfed, Chandigarh, for their cooperation.

References

1. A. Rabhi, JITMAP: Promoting Japanese low carbon technologies and best practices in India. Presentation at the 2nd JITMAP dialogue meeting, Pune, India, 2018
2. Emerging Technologies. Summary report available at <http://e3tnw.org/ItemDetail.aspx?id=389>. Last accessed 18 Aug 2019
3. SAMEEEKSHA, SAMEEKSHA Newslett 4(4), Dec 2013 P5. TERI, Delhi, 2013
4. A Heat Pump Using Carbon Dioxide as the Refrigerant. Article available at <https://www.buildinggreen.com/blog/heat-pump-using-carbon-dioxide-refrigerant>. Last accessed 13 Aug 2019
5. E. Hiroyuki, Introduction of the water source heat pump. Presentation was given to Indian end-users during the onsite investigation (available upon request to authors), 2017
6. Mayekawa USA brochure available at <https://www.mayekawausa.com/pdf/brochures/Unimo-WW.pdf>. Last accessed 22 Aug 2019
7. T. Davis, J. Bush, Presentation at ACEEE Hot Water Forum available at https://aceee.org/sites/default/files/files/pdf/conferences/hwf/2016/Davis_Session1B_HWF16_2.22.16.pdf. Last accessed 10 May 2019, 2016
8. IEA Heat pump program. Policy paper available at http://www.jeh-center.org/asset/00032/Annex35/03%20Final%20Report_policy%20paper.pdf. Last accessed 12 Aug 2019
9. A. Vyas, Impact of implementing EHP at the Amul Chocolate factory. Presentation at ISAP2017, Yokohama, Japan, 2017
10. A. Rabhi, P. Pal, Japan–India technology matchmaking platform: approach to promote Japanese low carbon technologies in Indian industries. *J. Resour. Energy Dev.* **16**(1), 9–18 (2019)

Refrigeration Systems: Optimal Temperature Setpoint Regarding Air Mixing in a HVAC-R System



Jérôme Jeanclos, Kamal Ejjabraoui, and François Malrait

1 Introduction

The ability to manage energy consumption and cost has become increasingly important in recent years. In addition to budget concerns and environmental pressures, building owners and facility managers face the negative effect that rapidly growing demand has had on the reliability of service provided by utilities. As HVAC-R equipment typically accounts for a large portion of a facility's electricity use, solutions for managing these systems are essential to achieving control of energy usage. Typically, the HVAC-R equipment consumes the largest amount of energy in a facility, so the ability to analyze HVAC-R usage data can lead to great savings in energy and cost. These facts add up to an emerging need for a solution that enables logical control over energy using assets.

The aim of this chapter is to define optimization of energy usage in rooftop unit systems considering the constraints (user comfort, air outdoor, etc.). Note that in this chapter humidity will be considered, which will influence results in case of humid climates because of its latent loads.

First, we will provide an overview of rooftop units, and how we can split this kind of system into parts to well understand and analyze them. In the second part, we will provide a mathematical representation of each loop in the system (evaporator air loop and fluid refrigerant loop), variables specified by the system manufacturer will be highlighted (fans flow rate, compressor speed, air mixing). Simulation-based results will support the theoretical demonstration. The chapter ends with a conclusion and perspectives.

J. Jeanclos (✉)

Sherpa Engineering for Schneider Electric, Nanterre, France
e-mail: jerome.jeanclos@hotmail.fr

K. Ejjabraoui · F. Malrait

Industrial Automation Business, Schneider Electric, Rueil-Malmaison, France
e-mail: kamal.ejjabraoui@se.com; francois.malrait@se.com

2 Annotations and Definition

2.1 Nomenclatures

The following table gives different nomenclature used in this chapter:

Variable name	Definition	Unit
P_{cool}	Cooling capacity coming from the evaporator	W
P_{heat}	Cooling capacity coming from the condenser	W
P_w	Compressor power (or power consumed)	W
P_{in}	Power entering in a volume	W
x	Air mixing (100% = 100% outdoor air)	%
ΔT	Differential temperature between outdoor and the room	°C
HeatIn	The power entering in the room	W
$Q_{m\ ev}$	Air mass flow rate (evaporator air loop)	kg/s
$Q_{m\ cd}$	Air mass flow rate (condenser air loop)	kg/s
h_j	Specific enthalpy (see Note ¹ for “j”)	J/kg
w_j	Absolute humidity (see Note ¹ for “j”)	kg/ kgas
$P_{w,j}$	Partial pressure of water vapor (see Note ¹ for “j”)	Pa
T_j	Temperature (see Note ¹ for “j”)	°C
RH_j	Relative humidity (see Note ¹ for “j”)	%
$p_{w\ sat}$	Partial pressure of water vapor @ Saturation	Pa
c_{pa}	Specific heat capacity of the air	J/(K. Kg)
c_{pw}	Specific heat capacity of the water vapor	J/(K. Kg)
h_{we}	Evaporation heat of water at 0 °C	J/kg
p_a	Atmospheric pressure	Pa
OH_R	Overheating reference	°C
ω	Compressor speed	rad/s
S	Section area of the expansion valve	m ²
P_i	Refrigerant absolute pressure (see Note ² for “i”)	Pa
h_i	Refrigerant specific enthalpy (see Note ² for “i”)	J/kg
T_i	Refrigerant Specific enthalpy (see Note ² for “i”)	°C
$Q_{m\ ref}$	Refrigerant mass flow	kg/s
m_{ref}	Total refrigerant mass in the refrigeration loop	kg

Note¹: The index “j” can be (**mix**: air mixed, **out.**: outdoor air (new air), **ev**: evaporator, **ro**: room air)

Note²: The index “i” can be (**1**: before compressor, **2**: after compressor, **3**: before expansion valve, **4**: after expansion valve)

3 Rooftop Unit (RTU) System Description

This paper will focus on the rooftop unit, because in this system the limitation of the temperature differential is the most frequent. In a rooftop unit, the system can be represented as follows:

This system can be separated into three subsystems: the refrigeration loop, the condenser air loop, and the evaporator air loop.

In a more schematic way, Fig. 1 can be represented, with interesting variables, as follows:

$Heat_{in}$ (W) represents the power entering the room (due to the sun, an open door, body heat, etc.) and OH_R ($^{\circ}C$) represents the overheating limit specified by the rooftop manufacturer to the refrigeration loop system.

4 Problem Description and Objective

The air registers (dampers) seen in Fig. 1 are the physical components which mix the return and the outdoor air before the evaporator. This phenomenon is represented by the mixing ratio variable x seen in Fig. 2.

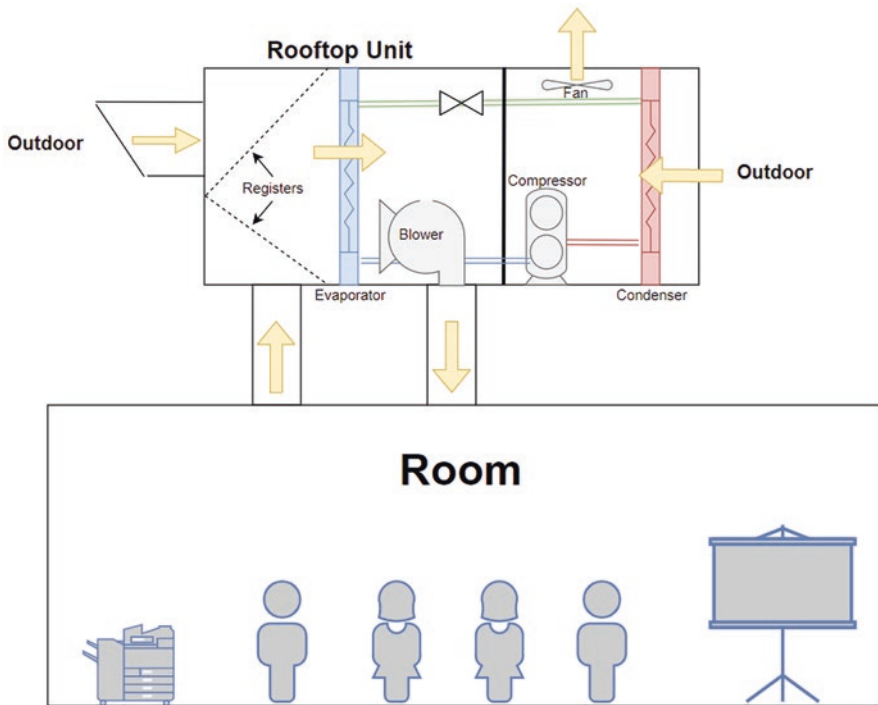


Fig. 1 Rooftop unit system

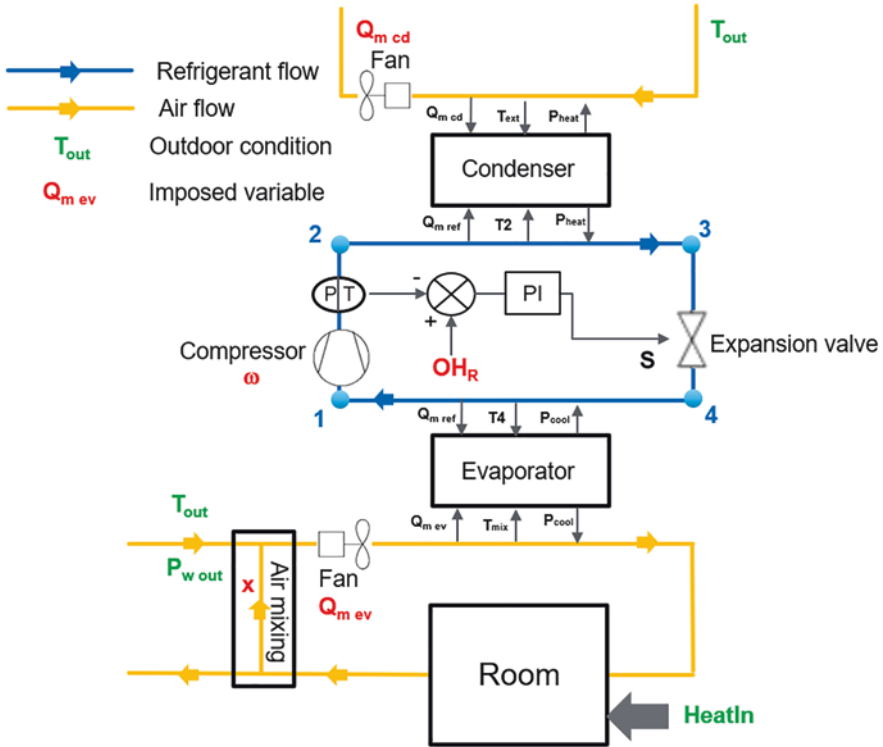


Fig. 2 Schematic of a rooftop unit

On the other side, rooftop unit manufacturers can limit the temperature differential between the outdoor and the interior setpoint to limit energy consumption (ΔT_{max}). In that case, the comfort of the user may be impacted if the outdoor temperature is high.

The goal of this chapter is to check the impact of the mixing air and temperature difference on the energy consumption, and to propose an optimized way to limit the energy consumption and to provide the best comfort for the user with a maximum ΔT_{max} .

For that, the study will be separated in two parts:

- Analyzing the evaporator air loop: Determine the cooling capacity P_{cool} regarding the air mixing x and the temperature differential ΔT .
- Analyzing the refrigeration loop: Determine the power consumption P_w regarding the cooling capacity P_{cool} .

5 Evaporator Air Loop Analysis

5.1 Characterization

To check the influence of the air mixing, we will focus on the evaporator air loop, and then extend to the compressor consumption.

The evaporator air loop can be modeled as a loop consisting of three volumes (mixing chamber, evaporator chamber, and the room). Each volume can be characterized by the following variables where some values have relationships to each other:

- RH: relative humidity (%)
- p_w : partial pressure of water vapor (Pa)
- T: Temperature ($^{\circ}\text{K}$ or $^{\circ}\text{C}$)
- h : Specific enthalpy (J/kg)

The air mass flow ($Q_{m, ev}$) delivered by the blower is supposed to be constant (no high pressure drops).

In the evaporator air loop, the air mixing variable x is comprised of a split in the blower air mass flow between the outdoor air and the return air.

Finally, the evaporator air loop is represented as follows:

P_{cool} (W) is the cooling capacity coming from the refrigeration loop.

As a reminder, the goal of the study is to evaluate the effect of the mixing air variable x on the cooling capacity of the system P_{cool} for a given $\Delta T = T_{out} - T_{ro}$.

5.2 Energy Balance and Water Vapor Mass Balance in a Moist (Humid) Air Volume

5.2.1 Energy Balance

The energy of a moist air volume at constant pressure is the enthalpy H (J), which can be specific (not dependent of the mass of air on a given volume). This moist air specific enthalpy h (J/kg) is defined by the following equation [1]:

$$h = c_{pa} * T (^{\circ}\text{K}) + 0.62198 * \frac{P_w}{P_a} * (c_{pw} * (T (^{\circ}\text{C})) + h_{we}) \quad (1)$$

Furthermore, a power transfer in moist air can be defined as follows:

$$P_{in} = Q_m * h \quad (2)$$

Thus, for each volume, we can define an energy balance equation:

$$\sum P_{out} - \sum P_{in} = \sum Q_{mout} * h_{out} - \sum Q_{min} * h_{in} = 0 \tag{3}$$

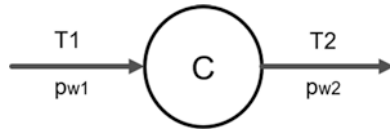
5.2.2 Water Vapor Mass Balance

Condensation Condition Definition

The partial pressure of water vapor of a volume (p_w) cannot be above the saturation partial water vapor ($p_{w\ sat}$), which is defined as a function of temperature:

In a steady state, the partial pressure of water vapor of a volume will be equal to the partial water vapor entering the volume.

We give an example of a volume with an airflow input and an airflow output:



T_2 and p_{w2} are, respectively, the temperature and the partial vapor water of the volume C (because the airflow output is coming from the volume).

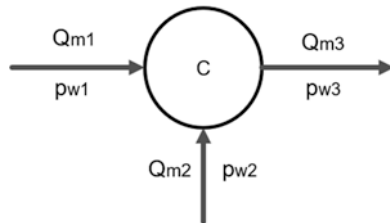
Thus, if $p_{w1} \leq p_{w\ sat}(T_2)$, there will be no condensation, and then $p_{w2} = p_{w1}$.

On the contrary, if $p_{w1} > p_{w\ sat}(T_2)$, there will be condensation, and then $p_{w2} = p_{w\ sat}(T_2)$.

Water Vapor Mass Balance without Condensation

In a steady state, and in case of no water condensation, the water vapor mass balance is null; the amount of water vapor entering in a volume is the same of the amount of water vapor rejected.

We provide an example of a chamber with three water vapor input/output:



By using the mass balance, we have:

$$Q_{mw1} + Q_{mw2} = Q_{mw3} \tag{4}$$

where

- Q_{mw} water vapor mass flow (kg/s)
- Q_m moist air mass flow (kg/s)

The absolute humidity is defined by the following formula [2]:

$$w = \frac{m_w}{m_a} = 0.62198 * \frac{P_w}{P_a} \quad (5)$$

Then, the mass of the water vapor can be expressed as:

$$m_w = 0.62198 * \frac{P_w}{P_a} * m_a \quad (6)$$

We can express the water vapor mass flow rate as a function of the air mass flow rate:

$$Q_{mw} = 0.62198 * \frac{P_w}{P_a} * Q_m \quad (7)$$

Then, replacing with the expression defined in (7) in the Eq. (4), we obtain:

$$0.62198 * \frac{P_{w1}}{P_a} * Q_{m1} + 0.62198 * \frac{P_{w2}}{P_a} * Q_{m2} = 0.62198 * \frac{P_{w3}}{P_a} * Q_{m3} \quad (8)$$

It yields the following equality with no condensation:

$$P_{w1} * Q_{m1} + P_{w2} * Q_{m2} = P_{w3} * Q_{m3} \quad (9)$$

5.3 Energy and Mass Balances Applied to the Evaporator Air Loop

All the following energy balances will be done in steady state, therefore, $\sum P_{out} - \sum P_{in} = 0$.

Based on the “evaporator air loop” schematic defined in Fig. 3, the objective is to define the cooling capacity P_{cool} needed to maintain the room temperature T_{ro} at a given value.

Because the air temperature will be the lowest at evaporator outlet (T_{ev}), it is assumed there may be condensation only in the evaporator volume.

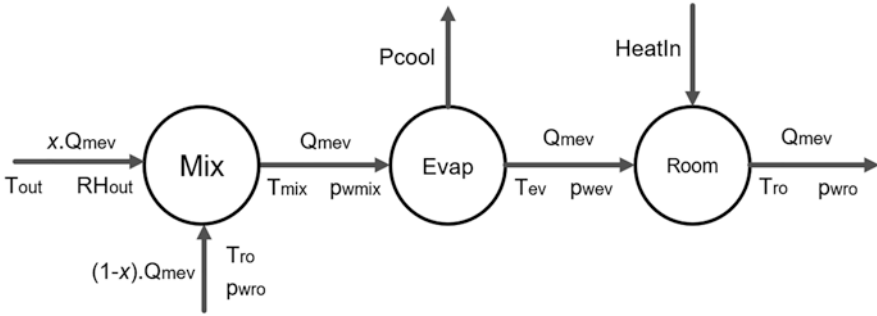


Fig. 3 Evaporator air loop schematic

5.3.1 Energy Balance Analysis on “Mixing Chamber” Volume

The application of the energy balance at the mixing chamber allows us to express T_{mix} as a function of (T_{out} and T_{ro}) and the partial pressure $p_{w_{mix}}$ as a function of ($p_{w_{out}}$ and $p_{w_{ro}}$).

The energy balance equation is defined as follows:

$$\sum P_{in} - \sum P_{out} = 0 \Rightarrow x * Q_{mev} * h_{ext} + (1 - x) * Q_{mev} * h_{ro} - Q_{mev} * h_{mix} \quad (10)$$

It yields:

$$T_{mix} = x * T_{ext} + (1 - x) * T_{ro} \quad (11)$$

With no condensation condition and using the Eq. (9) defined above, we obtain:

$$p_{w_{ext}} * x * Q_{mev} + p_{w_{ro}} * (1 - x) * Q_{mev} - p_{w_{mix}} * Q_{mev} = 0 \quad (12)$$

Then,

$$RH_{ext} * p_{sat(T_{ext})} * x + p_{w_{ro}} * (1 - x) - p_{w_{mix}} = 0 \quad (13)$$

It yields:

$$p_{w_{mix}} = RH_{ext} * p_{wsat(T_{ext})} * x + p_{w_{ro}} * (1 - x) \quad (14)$$

5.3.2 Energy Balance Analysis on “Room” Volume

The application of the energy balance at the “room” volume allows us to express T_{evout} as a function of (T_{ro} and Heat_{In}).

The energy balance equation is defined as follows:

$$\sum P_{in} - \sum P_{out} = 0 \Rightarrow Q_{mev} * c_{pa} * (T_{evout} - T_{ro}) + Heat_{In} \quad (15)$$

The temperature at the outlet of the evaporator can then be expressed as follows:

$$T_{evout} = \frac{Q_{mev} * c_{pair} * T_{ro} - Heat_{In}}{Q_{mev} * c_{pa}} \quad (16)$$

If we consider that there is no condensation in the “room” volume, this allows us to assume that:

$$P_{wro} = P_{wev} \quad (17)$$

5.3.3 Energy Balance Analysis on “Evaporator” Volume

The application of the energy balance at the “evaporator” volume allows us to express P_{cool} as a function of T_{ro} , T_{out} , and $Heat_{In}$.

$$\sum P_{in} - \sum P_{out} = 0 \Rightarrow Q_{mev} * h_{mix} - Q_{mev} * h_{evout} - P_{cool} \quad (18)$$

By replacing h_{mix} and h_{evout} with the explicit equation of the specific enthalpy defined on the Eq. (1), we found:

$$P_{cool} = Q_{mev} * \left(c_{pa} * T_{mix} + 0.62198 * \frac{P_{wmix}}{P_a} * (c_{pw} * (T_{mix}) + h_{we}) - \left(c_{pa} * T_{evout} + 0.62198 * \frac{P_{wevout}}{P_a} * (c_{pw} * (T_{evout}) + h_{we}) \right) \right) \quad (19)$$

If $p_{wmix} < p_{wsat}(T_{mix})$, there is no condensation, and thus:

$$P_{wevout} = P_{wmix} \quad (20)$$

If not, there is condensation, and thus:

$$P_{wevout} = P_{wsat}(T_{evout}) \quad (21)$$

5.3.4 Equation Resolution:

- Specified by user/manufacturer variables: x , Q_{mev} , T_{ro} .
- Outdoor conditions: T_{out} , RH_{out} , $Heat_{In}$

- Constants: $p_a, h_{we}, c_{pa}, c_{pw}$
- Unknown variables: $p_{w\text{ ro}}, T_{\text{mix}}, p_{w\text{ mix}}, P_{\text{cool}}, T_{\text{ev}}, p_{w\text{ evout}}$

Since the equation system is composed of six equations and six unknown variables, the system can be solved.

To solve this equation system, it is necessary to define $P_{w\text{ sat}}(T_{\text{evout}})$ and $P_{w\text{ sat}}(T_{\text{out}})$. For that, empirical values seen in Fig. 4 has been model as a second order equation [3].

Because T_{evout} and T_{out} are not in the same range of temperature, the second order equation can be different to improve precision:

$$p_{w\text{ sat}}(T_{\text{ext}}) = psat11 * T_{\text{ext}}^2 + psat12 * T_{\text{ext}} + psat13 \tag{22}$$

and

$$p_{w\text{ sat}}(T_{\text{evout}}) = psat21 * T_{\text{evout}}^2 + psat22 * T_{\text{evout}} + psat23 \tag{23}$$

With coherent equation simplification, P_{cool} can be expressed as:

$$P_{\text{cool}} = a1 * \Delta T * x + a2 * x + a3 \tag{24}$$

Because of the condition on condensation, the coefficient will not be the same:

- With condensation ($p_{w\text{ mix}} < p_{w\text{ sat}}(T_{\text{evout}})$), the coefficients $a1, a2,$ and $a3$ will be expressed as follows:

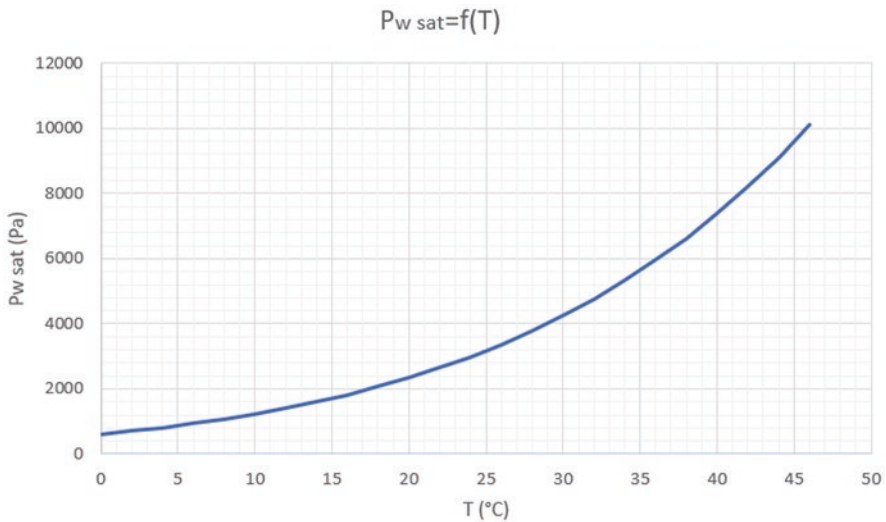


Fig. 4 Saturation partial vapor water versus temperature

$$a1 = Q_{mev} \times c_{pa} + Q_{mev} \times 0.62198 * \frac{h_{we}}{P_a} \times \left(psat22 + 2 \times psat21 \times \left(T_{ext} - \frac{HeatIn}{Q_{mev} * c_{pa}} \right) \right)$$

$$a2 = Q_{mev} \times 0.62198 \times \frac{h_{we}}{P_a} \times \left[\left(RH_{ext} * psat11 - psat21 \right) \times T_{ext}^2 + \left(RH_{ext} \times psat12 - psat22 + 2 \times psat21 \times \frac{HeatIn}{Q_{mev} \times c_{pa}} \right) \times T_{ext} + \left(RH_{ext} \times psat13 - psat21 \times \left(\frac{HeatIn}{Q_m \times c_{pa}} \right)^2 - psat22 \times \frac{HeatIn}{Q_{mev} \times c_{pa}} - psat23 \right) \right]$$

$$a3 = Heat_{in}$$

- Without condensation ($p_{w\text{mix}} > p_{wsat}(T_{evout})$), the coefficients a1, a2, and a3 will be expressed as follows:

$$a1 = Q_{mev} \times c_{pa}$$

$$a2 = 0$$

$$a3 = Heat_{in}$$

Note: We can see that without condensation, in case of dry climate, the exterior humidity has no significant impact on results. This implies that for dry climate areas, a humidity sensor will be of no use because there will never be condensation in the system.

5.3.5 Simulation Results

Based on the equation for the cooling capacity of the evaporator (24), we can analyze and simulate the impact of both the differential temperature and mixing coefficient against the cooling capacity for a specific external condition (T_{out} , RH_{out} , and $Heat_{in}$). Fig. 5 illustrates an example with the following outdoor and specified variables ($Q_{mev} = 0.6 \text{ kg/s}$; $HeatIn = 4000 \text{ W}$; $RH_{out} = 55\%$; $T_{out} = 40^\circ\text{C}$)

Because of the change of equation depending on water vapor condensation, there is a discontinuity on the graph.

We can also deduce a maximum $\Delta T_{max} = T_{out} - T_{ro}$ for a given maximum cooling capacity:

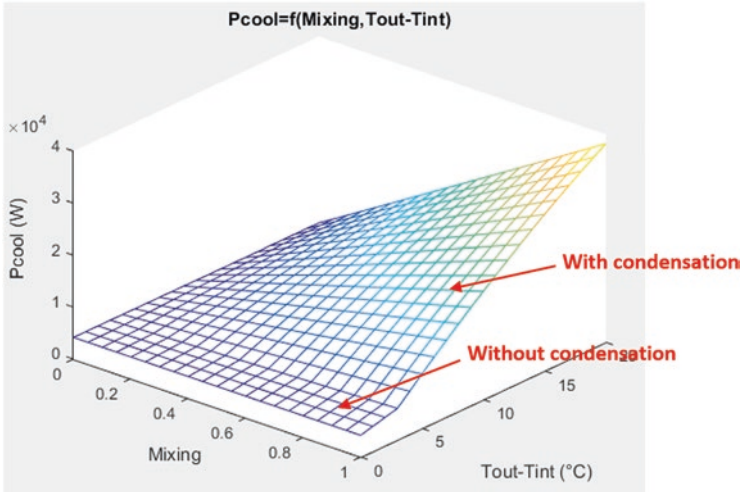


Fig. 5 Cooling capacity for given outdoor conditions

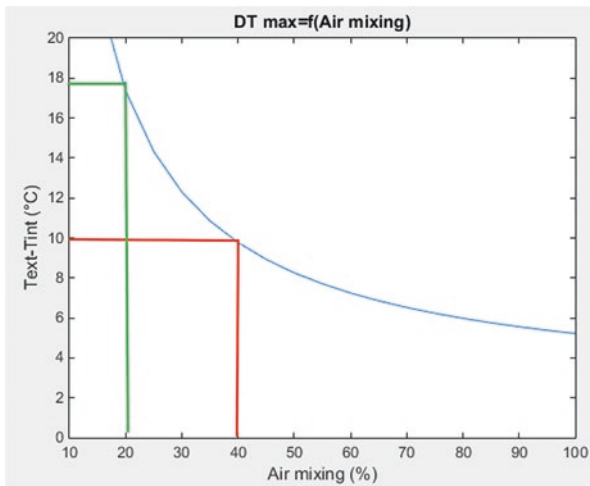


Fig. 6 Maximum difference temperature versus air mixing

$$\Delta T_{\max} = \frac{P_{cool\max} - a3 - a2 * x}{a1 * x}$$

Thus, a minimum room temperature can be defined with the information from a rooftop unit with an energy economizer mode where the maximum cooling capacity is defined by the manufacturer.

Another example on how we can define the maximum temperature difference as a function of mixing coefficient and maximum cooling capacity is illustrated in

Fig. 6. If a rooftop unit manufacturer defined a maximum cooling capacity as $P_{cool\ max} = 11160\ W$ with the outdoor conditions from the previous example, the maximum temperature difference would be defined by this curve.

Here the outdoor temperature is $40\ ^\circ C$. For a 20% air mix, the minimum room temperature will be defined as $40 - 18 = 22\ ^\circ C$. And for a 40% air mix, the minimum room temperature will be defined as $40 - 10 = 30\ ^\circ C$.

Note: Because the condensation at the evaporator will imply a lot more energy consumption, it could be relevant, in that case, to limit the air renewal by decreasing the air mixing x .

6 Refrigeration Loop Analysis

6.1 Equation System Resolution

To identify the relation between the cooling capacity P_{cool} and the power consumption P_w , the refrigeration loop presented in Fig. 2 should be solved. Nevertheless, contrary to the evaporator air loop, the system cannot be solved analytically. Indeed, an implicit loop analysis is necessary.

For fixed outdoor conditions, a given compressor speed will generate a given cooling capacity. Then, in respect to the cooling capacity determined by the evaporator air loop analysis,

- The corresponding compressor speed should be deduced for a variable speed compressor
- The on/off compressor ratio should be deduced for a fixed speed compressor

This solved system will determine the mean power consumption P_w for a given cooling capacity P_{cool} required by the evaporator air loop.

Fig. 7 represents the refrigeration loop system in terms of exchanged variables.

This refrigeration loop system can be solved following the process on Fig. 8. We get an iterative process with the two variables P_1, P_2 pressures. The inputs are ω compressor speed, $DT+$ overheating, cooling power P_{cool} , heating power P_{heat} . The refrigerant mass m is an internal constant. The outputs are the condenser and the

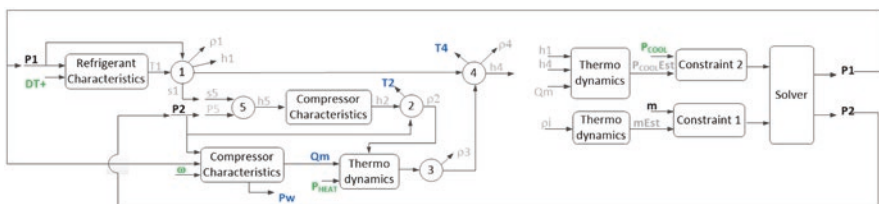


Fig. 8 Refrigeration loop system solving

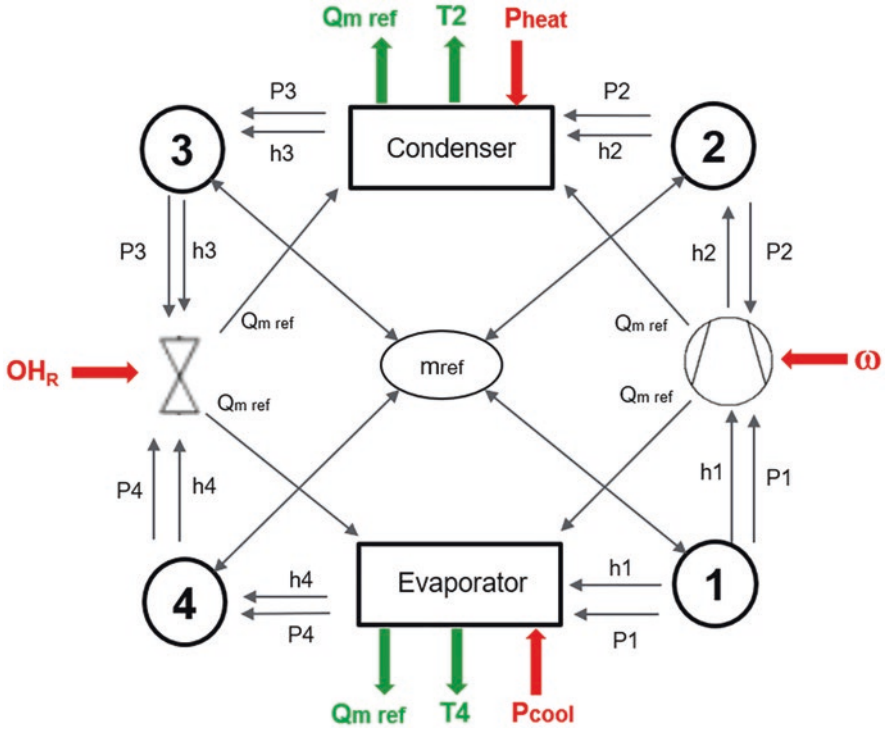


Fig. 7 Refrigeration loop system model

evaporator temperature as well as the flow. We may consider also the mechanical power as an output of the calculation.

6.2 Simulation-Based Results

PhiSim® software (multi-physical software, extension of Simulink) has been used to solve the system equation and then obtain results.

The specified variables are:

$$Q_{m_{ev}} = 0.6 \text{ kg / s}$$

$$Q_{m_{cd}} = 2.35 \text{ kg / s}$$

$$\text{Heat}_{in} = 4000 \text{ W}$$

$$RH_{out} = 55\%$$

$$T_{\text{out}} = 40^{\circ}\text{C}$$

$$\text{OH}_R = 10^{\circ}\text{C}$$

$$x = 20\%$$

6.2.1 Simulation with Compressor at Variable Speed

In this case, regulating the compressor speed to not exceed $P_{\text{cool max}} = 11160 \text{ W}$ will lead to a compressor speed of 2000 RPM, and the room temperature to stabilize at 21.2°C (the relationship between the cooling capacity and the room temperature has been calculated with equations, see Fig. 6).

In this case, the consumed power P_w obtained by simulation is **4845 W**.

Note: The difference between Fig. 6 (22°C) and the simulation result (21.2°C) is due to approximation in equations exposed in evaporator air loop analysis.

6.2.2 Simulation with Compressor at Fixed Speed

As discussed previously, in the case of fixed speed regulation, the cooling capacity required will be obtained with an on/off cycle on compressor. Here, the speed in working condition is at 3000 RPM (Fig. 9).

The compressor is then “On” for 82% of a period of the cycle.

With those given outdoor conditions, the instantaneous cooling capacity delivered by the compressor is about 13,800 W. $13800\text{W} * 0.82 \approx 11160\text{W}$; results are consistent.

Furthermore, the instantaneous power consumption $P_w = 7515\text{W}$. Thus, the mean power consumption will be about $7515 * 0.82 = \mathbf{6162\text{W}}$.

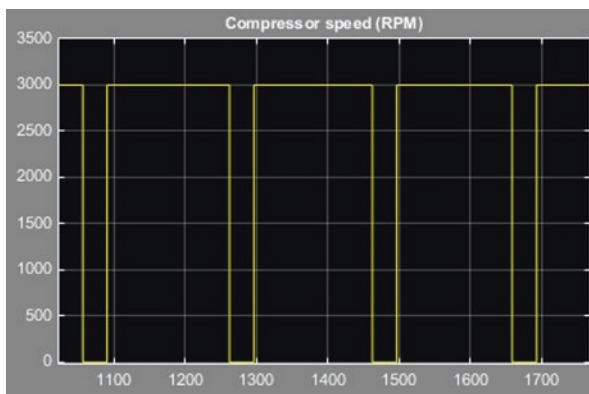


Fig. 9 Compressor speed cycle for a fixed speed compressor

The variable speed technology allows an energy consumption gain of about 27% compared to a fixed speed compressor, for the same cooling capacity requested.

6.3 Another Example

Let us study a system with those specific variables:

$$Q_{\text{mev}} = 0.6 \text{ kg / s}$$

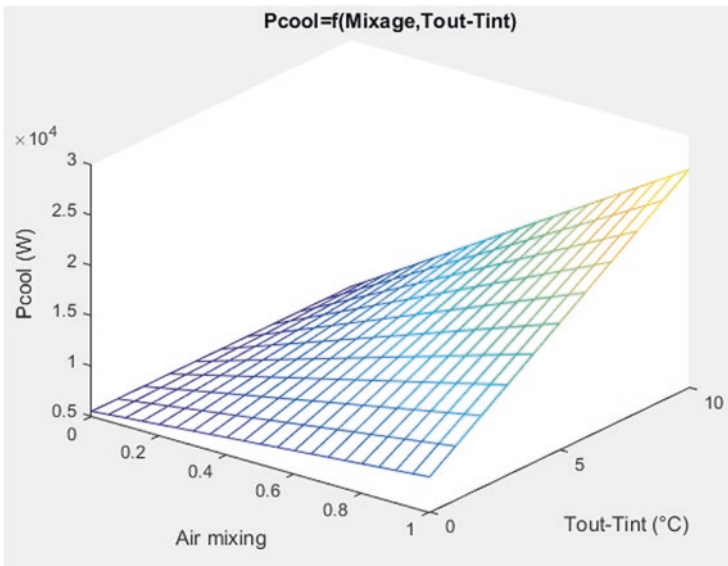
$$Q_{\text{mcd}} = 2.35 \text{ kg / s}$$

$$\text{Heat}_{\text{in}} = 5500 \text{ W}$$

$$\text{RH}_{\text{out}} = 65\%$$

$$T_{\text{out}} = 30^\circ \text{ C}$$

$$\text{OH}_R = 10^\circ \text{ C}$$



The maximum temperature differential will be in relation with the maximum cooling capacity and the current air mixing.

Now, to see effect of variable speed compressor compared to fixed speed compressor, let us assume that the differential temperature is 10 °C ($T_{\text{room}} = 20 \text{ °C}$) and that the fixed compressor speed is 6000RPM. The same methodology for simulation-based results is used:

	P_w – Fixed compressor speed	P_w – Variable compressor speed	Consumption gain
$X = 0.2$	7040 W	2972 W	–57%
$X = 0.4$	9600 W	5495 W	–42%
$X = 0.6$	12,800 W	11,000 W	–16%

We can see in this case the variable speed compressor technology can bring a significant energy saving in the system, which can be combined with the limitation of cooling capacity limiting the temperature differential.

7 Conclusion

In the first section, we presented an overview of a rooftop unit (RTU) system and how it can be modeled by three subsystems (evaporator air loop, condenser air loop, and fluid refrigerant loop). We then presented the purpose of the study on such a system and how we can associate the energy consumption with the mixing feature and the speed of compressor, evaporator fan, and condenser fan. We have limited our study only to the impact of the mixing feature and the differential of temperature on the total capacity cooling and then the compressor power consumption.

In the second section, by using theoretical demonstration, we obtained an explicit equation of the cooling capacity as a function of mixing ratio “ x ” and the differential temperature ΔT . We then analyzed the impact of the mixing air and temperature difference on the maximum cooling capacity resulting in the determination of the energy consumption.

In the third section, we used the fluid refrigerant loop to find the relationship between the maximum cooling capacity that maintains comfort in the room and the compressor power consumption. A method is then proposed to optimize a way to limit the energy consumption and provide the best comfort for the user with a maximum ΔT_{max} . Based on simulation, we have demonstrated that for a certain maximum cooling capacity and air mixing ratio, we can optimize the power consumption of the compressor with variable speed compared to fixed speed.

Therefore, with a maximum cooling capacity defined by the manufacturer, the user comfort will be optimized regarding the air mixing ratio, with an energy consumption limitation.

References

1. Markku J. Lampinen: *Thermodynamics of Humid Air*, University of Oxford (UK), 1998. ISBN 1-874370-20-6.
2. U.S. Department of Energy: *Doe Fundamentals Handbook Thermodynamics, Heat Transfer, and Fluid Flow Volume 1 of 3*. United States of America. June 1992
3. B. Hardy, *ITS-90 Formulations for Vapor Pressure, Frostpoint Temperature, Dewpoint Temperature, and Enhancement Factors in the Range - 100 to + 100 C* (Thunder Scientific Corporation, Albuquerque)

Modeling of Radial and Tangential Roebel Bar Force Distributions in Large Electrical Machines Considering Longitudinal Transposition



Amir Ebrahimi and Marius Meiswinkel

1 Introduction

Studying large electrical machines is an ongoing important topic due to the very different electromagnetic phenomena and modeling uncertainties caused by their immense dimensions. Despite decades of developing calculation methods for megawatt generators, there are still varieties of problems and aspects to be studied [1]. The necessity of extending our understanding of operational characteristics of large generators can be described considering design and operational challenges of these systems. Regarding design aspects, a more comprehensive model results into a better design with more optimization possibility. Regarding reliability, a comprehensive model describes the multi-physical relations between several parameters more sophisticatedly and results in more deterministic lifetime models and improves the maintenance management and reduces outages and costs. Roebel bar forces are a suitable example to explain this fact. The slot stray fluxes generate double frequency radial and tangential forces on the Roebel bars in large generators. These vibrations could lead to bar deformation, deterioration of isolation and fixation materials in the slot, and in the worst case, it results in sub-conductor or conductor short circuits to the stator core or to each other. A comprehensive model of Roebel bar forces helps to understand the behavior of these forces for a better design of slot materials and a sophisticated anticipation of Roebel bar condition.

Since these forces are much less than the radial double frequency forces acting on the stator core and teeth, they are not comprehensively considered in the literature. In general, a simplified formulation based on the Lorentz force formulation is given for the slot ground force estimation. The tangential force on the slot wall is usually neglected. Grabner et al. gives an analytical approximation of displacement

A. Ebrahimi (✉) · M. Meiswinkel
Leibniz University, Hannover, Germany
e-mail: ebrahimi@ial.uni-hannover.de

of Roebel bar and mechanical stress in the slot of large generators [2, 3]. Pantelyat et al. investigates the forces on the slot wedges [4].

In this chapter, an investigation on the tangential and radial Roebel bar forces considering bar transposition is proposed. In the first section, the origination and formulation of Roebel bar forces are given. After that the tangential and radial stray fluxes in the slot are described, and the impact of the field and stator current on these fluxes are explained. This section is followed with an investigation on the impact of the load angle and power factor on the slot fluxes. At the end, the radial and tangential forces are estimated both for a single transposed sub-conductor and for a Roebel bar. Finally, these values are calculated and discussed for a real hydrogenerator.

2 Roebel Bar Forces

The origin of Roebel bar forces is widely independent from the generator type. Nevertheless, to concretize the investigation and generate specified and comparable results, the origination of Roebel bar forces in a salient pole hydrogenerator is studied in this chapter.

2.1 Salient Pole Synchronous Generator with Roebel Bar

Schematic of one pole pitch of a salient pole generator is indicated in Fig. 1. The main parts of the generator are: rotor pole with damper winding, rotor rim, tee head attachment, pole winding, stator yoke and teeth, and the stator windings (Roebel bars). The DC current in the rotor winding generates a magnetic flux which closes its path mainly through rotor body, air gap, teeth, and yoke. The shaft of the generator is connected to a prime mover (in this case a hydroturbine). The shaft rotation creates a rotating magnetic field in the air gap and induces a three-phase voltage in

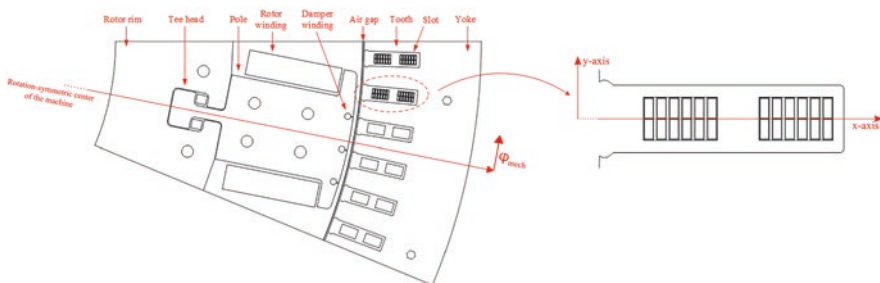


Fig. 1 Schematic of a salient pole generator; (a) left: one pole pitch, (b) right: one slot with sub-conductors

the stator windings. The parameters of the generator simulated in this chapter are summarized in Table 1.

The rotor winding generates an almost sinusoidal field across the air gap. Considering the spatial distribution of the air gap flux density, one can observe breakdowns in the flux density under the slots. The average air gap flux density can be estimated with carter factor. A small portion of the air gap flux lines enters into the slot radially and takes a circular path and enters the tooth tangentially. The conductor in the slot also generates fluxes across the slot with a dense concentration at the slot opening. These two flux densities are responsible for the radial and tangential forces on each sub-conductor in a Roebel bar.

Alternating current creates an alternating flux in the conductor material and causes a skin effect. To reduce the eddy current losses in the conductors, the conductors are divided into sub-conductors, which are connected together just at the beginning and at the end of the winding. To eliminate the circulating currents in the sub-conductors, every parallel-connected sub-conductor has to be surrounded exactly by the same amount of slot stray flux [5]. This is done by transposing the sub-conductors and use of Roebel bars. A schematic of the Roebel bar is illustrated in Fig. 2.

2.2 Lorentz Force and Maxwell Stress Tensor

The tangential (y-direction) and radial (x-direction) stray fluxes densities in the slot generate a radial and a tangential force on the current-conducting Roebel bar acting on the slot ground and slot wall, respectively. The reformulation of Lorentz force describes these forces. Assuming $q = \rho V$ and substituting with $\vec{J} = \rho \vec{v}$ in the Lorentz force definition $\vec{F} = q\vec{v} \times \vec{B}$, the force can be given by:

$$\vec{F} = \iiint \vec{J} \times \vec{B} dV \tag{1}$$

The variables in Eq. 1 can be determined using Finite Element Methods (FEM) in the slot of a generator. However, the current density \vec{J} and the flux density \vec{B} are

Table 1 Machine parameter

Parameter	Value
Rated voltage	550 V Y
Rated current	768 A
Rated torque	18.6 KNm
Rated speed	375 rpm
Number of poles	16
Number of slots	96
Max. Power	880 kW

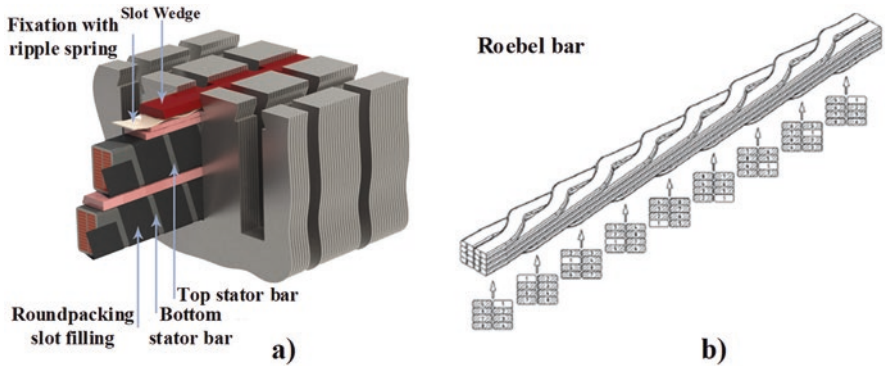


Fig. 2 Cross section of the stator with conductors in a slot; (a) two layer conductors and (b) transposed Roebel bar. (Source of images: (a) <https://www.fortum.se> (b) M. Znidarich, “Hydro Generator High Voltage Stator Windings”)

not constant along the z-direction in the generator because of the cooling ducts. Therefore, it is necessary to divide the conductor along the z-direction into smaller segments (1 mm). The force on the segment $d\vec{s}$ of the conductor is given by:

$$\vec{F} = A\vec{J} \times \vec{B}(s)d\vec{s} \tag{2}$$

where A is the cross section of the sub-conductor. Since the length of the sub-conductors is much more than its cross section, Eq. 2 can be simplified by:

$$\vec{F} = \sum IA\vec{J} \times \vec{B} \tag{3}$$

To consider the transposition of the sub-conductors in the z-direction, all three components of the current density should be estimated. This can be given by [6]:

$$\vec{J} = \begin{pmatrix} J_x \\ J_y \\ J_z \end{pmatrix} = \begin{pmatrix} \cos\beta & 0 & \sin\beta \\ \sin\alpha \sin\beta & \cos\alpha & -\sin\alpha \cos\beta \\ -\cos\alpha \sin\beta & \sin\alpha & \cos\alpha \cos\beta \end{pmatrix} \begin{pmatrix} 0 \\ 0 \\ J_z \end{pmatrix} \tag{4}$$

where α and β are the unit area vectors in y and x direction given by:

$$\alpha = \arcsin\left(\frac{dy}{dz}\right), \beta = \arcsin\left(\frac{dx}{dz}\right) \tag{5}$$

FEM programs mostly estimate the magnetic forces based on Maxwell Stress Tensor (MST). Therefore, it is necessary to compare these two force calculation methods. The MST can also be derived from Lorentz force using Maxwell

equations and Vector Potential formulation [7]. The modified (MST) method used in FEM programs (e.g., FEMM) applies multiple integrating lines in a path including the sub-conductors. This path is selected merely in materials with the unit permeability due to the derivation of MST. The MST formulation to calculate the forces on the conductors in FEMM is given by [8]:

$$F_j^{\Omega a} = \frac{1}{\mu_0} \int_{\Gamma-\partial\Omega_b} (g_- - g_+) \left[(B \cdot n) B - \frac{1}{2} B^2 n \right] ds + \sum_{k=1}^q \frac{1}{\mu_0} \int_{\Omega_{bk}} \left[\frac{1}{2} B^2 \Delta g - (B \cdot \Delta g) B \right] dV \quad (6)$$

where Ω_{bk} are the inner integrating loops in Ωa and g is a piecewise differentiable function [9]. The difference between Lorentz force and MST for calculating conductor forces in a slot is just 0.01%. Hence, all forces in this chapter are estimated with Lorentz force formulation.

3 Radial and Tangential Flux Density Distribution in the Slot

Since conductor forces occur with respect to the radial and tangential components of flux density in the slot B_x and B_y , the distribution of these flux densities is described in this chapter. Considering Fig. 3a–c, it can be observed that B_x is higher in the slot opening region, since B_x is mainly caused by the rotor current. The influence of the rotor field on the B_x is less than the winding current at the upper conductor. The clockwise rotating magnetic field originated from the current of the upper conductor (shown with red circle in Fig. 3a), causing an increase in B_x at the upper side of the conductor which can also be observed in Fig. 3c. After half electric period, this magnetic field will be higher at the lower side of the conductors. As it can be observed from Fig. 3d–f, the influence of the rotor field in B_y is negligible. The tangential flux in a slot is mainly due to the phase currents. It generates a force F_y on the slot wall. B_y is bigger at the slot opening. The kink in the Fig. 3e shows the influence of the radial field around the conductor on the tangential field in the slot. Each sub-conductor causes a kink in the flux density distribution. Furthermore, the flux lines leave the lower side of the slot perpendicularly but enter the tooth on the upper part of the slot with an angle.

Flux density distribution should also be analyzed for a mix slot in which the upper and lower bars belong to two different phases. It can be shown that the behavior of the radial and tangential flux densities in a slot remains similar to a normal slot in which both the upper and the lower conductors belong to the same phase. It can also be observed that B_x is the same for a normal and a mix slot, since B_x originates mainly from the rotor field. The behavior of B_y remains also similar to a normal slot; however, the amplitudes are less for a mix slot.

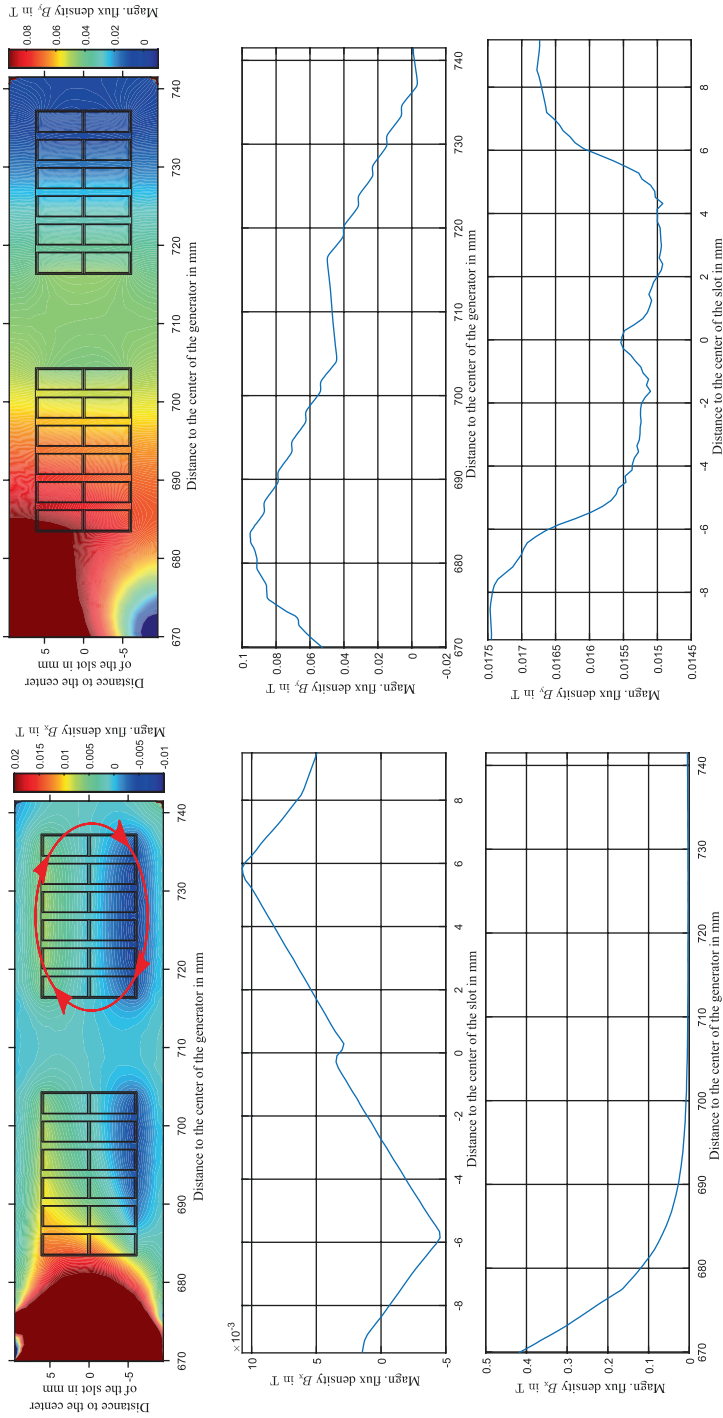


Fig. 3 Flux density distribution in the slot: (a) B_x distribution in a slot, (b) B_x as a function of slot width at the distance of 729 mm to the center of the machine, (c) B_x as a function of slot height, (d) B_y distribution in a slot, (e) B_y as a function of slot height, (f) B_y as a function of slot width

3.1 Impact of Field Current on the Flux Density Distribution in the Slot

Field current is mainly responsible for generating B_x . This can be observed in Fig. 4. B_x is calculated for different rotor positions and currents. The kinks in the diagrams in Fig. 4a are due to the asymmetrical damper winding on the surface of the pole. Also the influence of rotor core saturation can be observed in Fig. 4. More interesting is the behavior of B_y . The increase in the flux density can be explained by the stator core saturation. In this case, the teeth are saturated and the difference between the slot and tooth reluctance is less. Therefore, more flux lines enter into the slot, rotate, and enter the tooth through the slot wall. To describe the behavior of the flux density in Fig. 4c, we need to consider the relative position of the rotor to the middle of the slot. As the rotor rotates counterclockwise (Fig. 1), B_y increases at first, and then decreases as the middle of the pole is aligned with the middle of the slot (same B_y to the left and right side of the slot). After that, the rotor starts leaving the slot area and the second maxima happens since the south pole enters the slot area. This double frequency phenomenon develops the main part of the forces on the Roebel bar in the slot.

3.2 Impact of the Stator Current on the Flux Density Distribution in the Slot

The influence of the phase current on B_y is linear, since B_y mainly depends on the phase current. However, B_x in a slot with let say phase “w” is 90° leads to the phase current. To explain this, we need to consider the two other phases. When the current in phase “w” is maximum, the field lines of this phase goes through the phases “-u” and “v”. This field develops a considerable B_y in the slot with phase “w”. When the current in phase “w” is zero, the currents in phase “u” and “w” generate a magnetic. Consequently, this field contributes considerably to B_x in the slot with phase “w” which is the field passing through the same slot reason for 90° leading behavior of B_x and the phase current angle.

4 Impact of Operation Points on the Roebel Bar Forces

4.1 Impact of Load Angle on the Flux Density Distribution in the Slot

The load angle δ is defined as the angle between phase voltage V and the induced voltage E and is an important parameter for determining the torque of a salient pole machine given by:

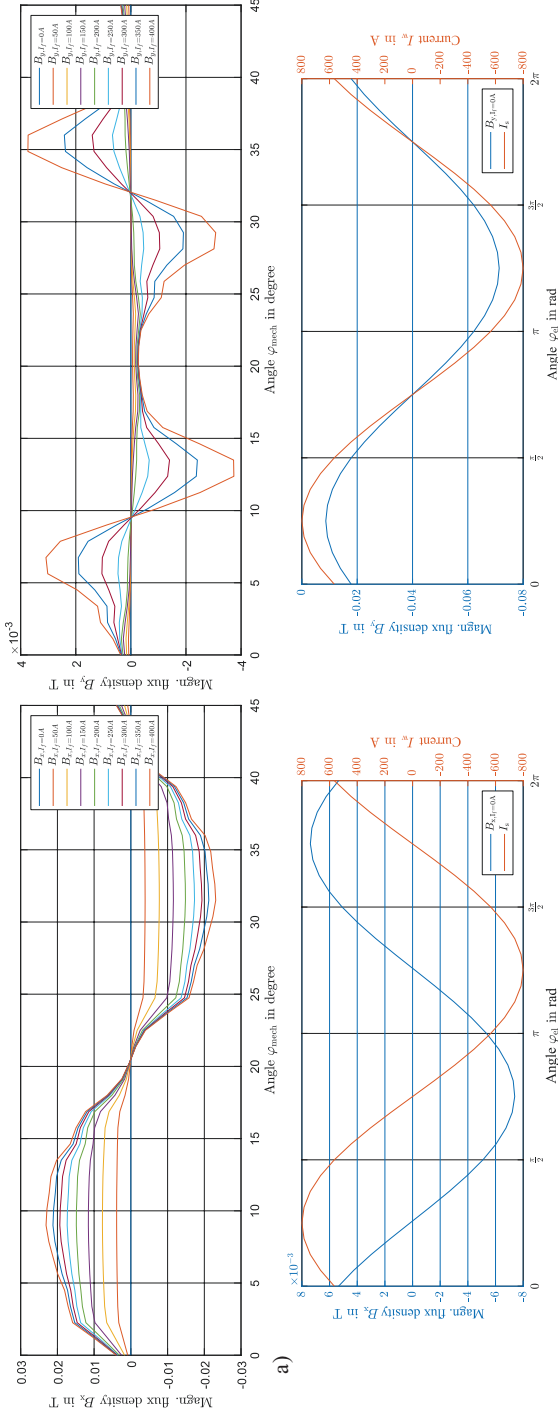


Fig. 4 Impact of the field current on the flux density distribution in the slot

$$T = \frac{m}{2\pi n_0} \left(\frac{VE}{X_d} \sin(-\delta) + \frac{V^2}{2} \left(\frac{1}{X_q} - \frac{1}{X_d} \right) \sin(-2\delta) \right) \quad (7)$$

where X_d and X_q are the inductances in the d- and q-axis. Since B_y mainly depends on the phase current, it is expected that the load angle has no major impact on the forces acting in the direction of the slot ground F_x as it can be observed in Fig. 5b. F_x is a double frequency force acting on the slot ground with a constant polarity.

On the other hand, the radial flux density in the slot B_x depends mainly on the load angle as it can be observed from Fig. 5c ($\varphi_{el} = p\varphi_{mech} + \delta$). The change in the amplitude is caused by the salient pole. The total MMF current can be calculated by transforming the rotor current I_f to the stator side I'_f and adding them to the stator current ($I_m = I_s + I'_f$). Now the total MMF can be given by:

$$V_m = \frac{\sqrt{2}}{\pi} \frac{m_s}{p} N_s k_w I_m \cos \left(\frac{x_r}{\tau_p} \pi \right) \quad (8)$$

where N_s and k_w are the stator winding number and factor. τ_p is the pole pitch and x_r is the distance to the middle of the pole. Thus, it is possible to give an approximation of the air gap flux density with:

$$B_h(x_r) = \mu_0 \frac{V_m(x_r)}{\delta(x_r)} \quad (9)$$

where $\delta(x_r)$ describes the air gap reluctance. Equation 9 describes the air gap flux density referring to the rotor position which can be referred to the stator with:

$$x_r = \frac{2\pi r_r}{360^\circ} (\varphi_{mech}) \quad (10)$$

Based on Eq. 9, estimated flux densities for different load angles create an idealized form of the fields indicated in Fig. 5c. One way to generate the exact B_x diagrams of Fig. 5c is to apply conformal mapping to Eq. 9.

4.2 Impact of Power Factor on the Flux Density Distribution in the Slot

Power factor relates to the angle between stator current and voltage, and it could be also shown that it is connected to the load angle with:

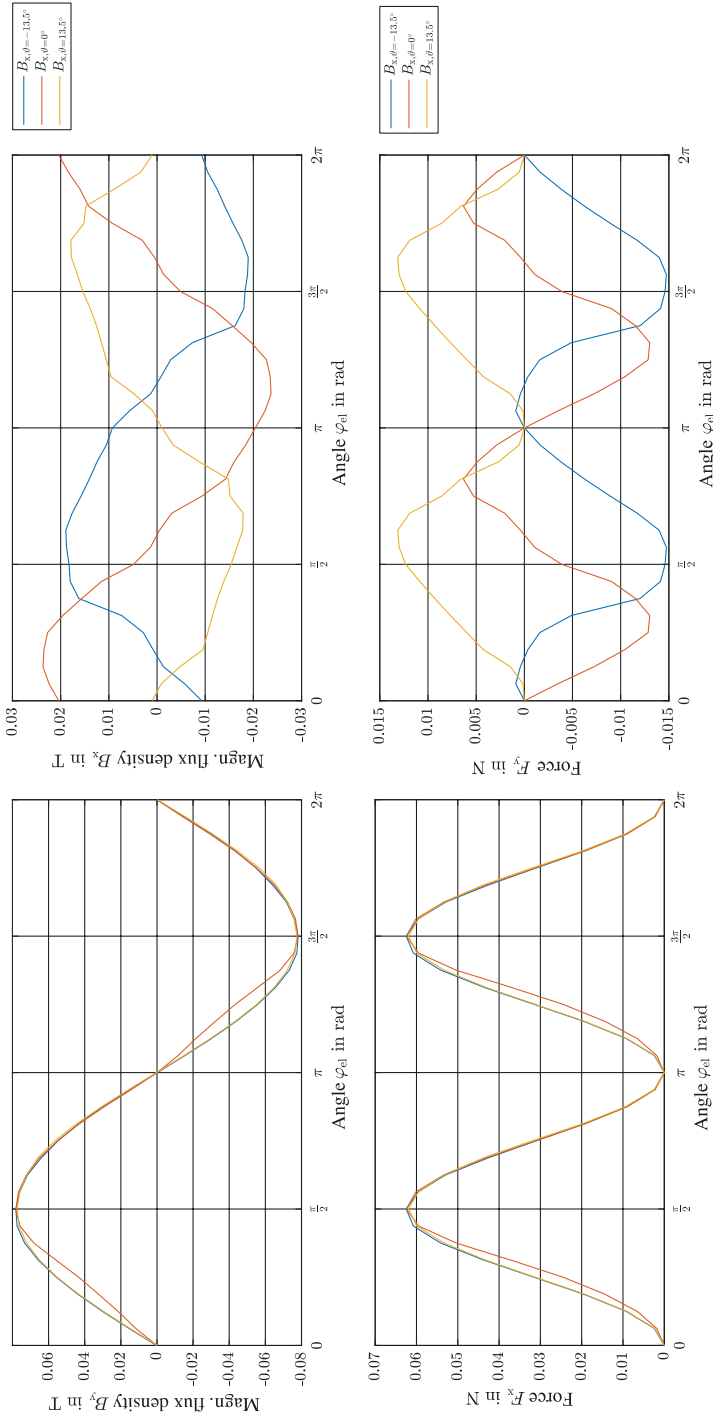


Fig. 5 Impact of load angle on Roebel bar forces: (a) B_y vs. δ , (b) F_x vs. δ , (c) B_x vs. δ , (d) F_y vs. δ

$$\tan(\delta) = \frac{r_s I_m \sin(\varphi) + \omega_e L_q I_m \cos(\varphi)}{V_m + r_s I_m \cos(\varphi) - \omega_e L_d I_m \sin(\varphi)} \tag{11}$$

According to Fig. 6b, power factor shifts F_x but does not change its amplitude. Since B_y is mainly caused by the phase currents, its magnitude remains constant and just a phase shift in the radial force can be observed. However, the tangential forces are more subject to variation since the B_x component of the flux density in the slot depends on the rotor position. Considering the relation between the load and power angle described by Eq. 11, the power factor influences the tangential Roebel bar forces more drastically. While the force is positive for $\cos(\varphi) = 0$, it is shifted down for other values as it can be observed in Fig. 6a.

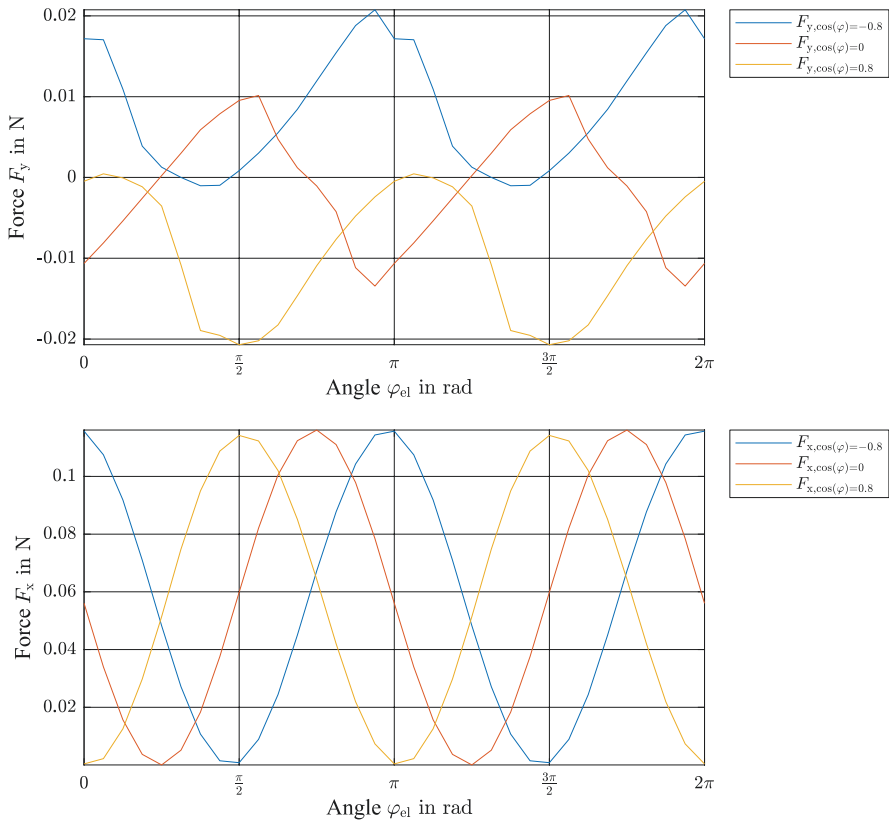


Fig. 6 Radial and tangential Roebel bar forces as a function of power factor

5 Radial and Tangential Forces on the Roebel Bar

5.1 Sub-conductor Forces

As mentioned in Sect. 3, the flux density in a slot is not constant across the slot and varies across different positions in the slot. Therefore, the radial and tangential forces on the sub-conductors are also functions of their position in the slot. Generally, it can be said that the sub-conductors closest to the slot opening experience much more radial and tangential forces than the sub-conductors near to the slot ground. The force distribution is similar to Fig. 3. To estimate the total force on a sub-conductor, a transient 3D-FEM model of a generator with sub-conductors is constructed (Fig. 7).

The simulation results for a rotor field current of 260 A and the stator current of 800 A are indicated in Fig. 8.

The results are similar to 2D simulation. However, the 3D-FEM estimated forces are less than the multiplication of 2D-FEM results with the length of the machine.

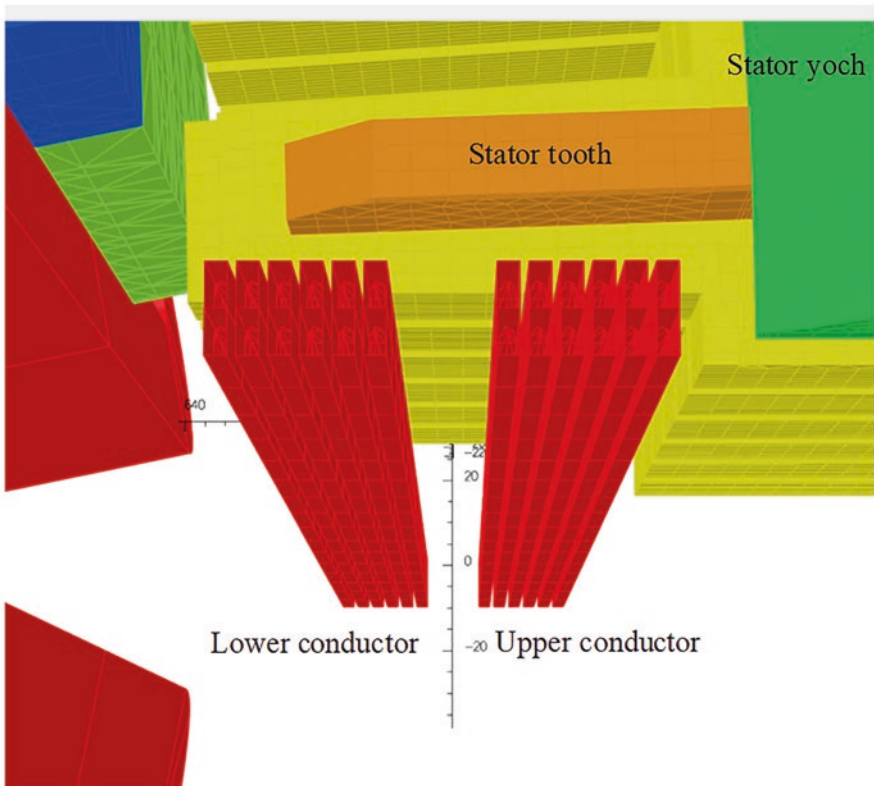


Fig. 7 3D-FEM Model for calculating the sub-conductor forces

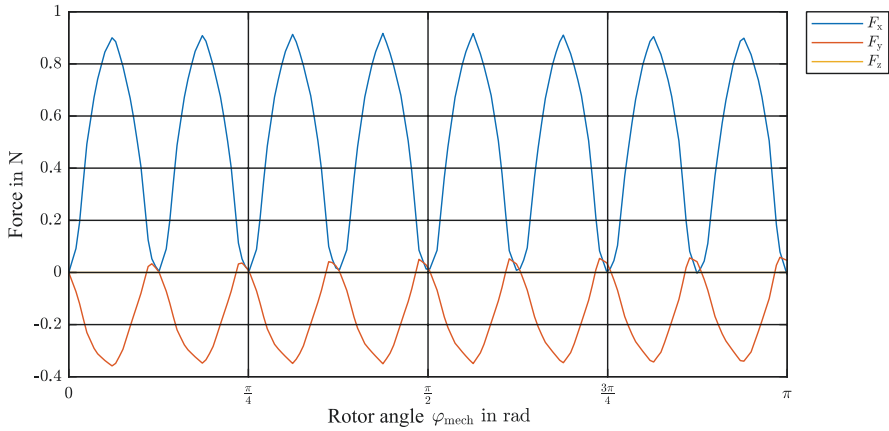


Fig. 8 Total sub-conductor forces as a function of mechanical angle

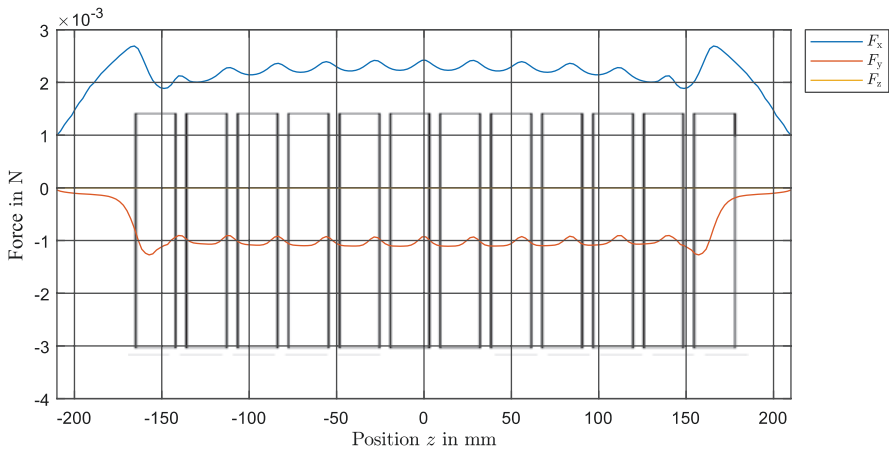


Fig. 9 Sub-conductor forces as a function of the positions along the z-axis

To explain this, one should consider each segment of a sub-conductor along the z-axis. The 3D behavior of sub-conductor forces are determined by several factors. The breakdowns in the F_y component relate to the cooling ducts in the stator. The magnetic reluctance in the cooling ducts is much bigger than that in the stator core. Hence, the air gap flux density under cooling ducts is less than in the active part of the machine which can be estimated with Carter factor. Therefore, the B_x component of the flux density is less and consecutively the F_y component breaks down in this region. More interesting is the impact of the cooling ducts on the slot ground forces. Under the cooling ducts, the flux lines take a circular path and enter into the stator core along the z-direction, perpendicularly to the radial fluxes in the tooth. This circulation of flux lines increases B_y and, consecutively, F_x is even more than the active region, which can be observed in Fig. 9.

The same effect can also be observed at the end region. Due to an increase in radial and tangential components of the flux density in this region relating to the fringing effect, an increment in the tangential and radial forces can be recognized (Fig. 9). Although the force development in a slot has the same behavior in 2D and 3D, for correct estimation of sub-conductor forces a 3D calculation is essential.

5.2 The Impact of Transposition

As it can be recognized in Fig. 3, the flux density distribution in the slot is not homogenous and hence the position of the sub-conductor in a slot has an impact on the forces acting on this sub-conductor. The current density in each segment (1 mm) is estimated with the method described in Sect. 2.2. The integral volume is the volume of the sub-conductor segment. B_x and B_y components of flux density in the slot along the z-axis are calculated with the 3D-FEM. While the sub-conductors closest to the rotor experience much more forces, the forces near the slot ground are much less. The rotor has almost no influence in the slot ground region; however, the radial component of the conductor field acts on the sub-conductors. While the lower conductor is pushed through the upper slot wall, the upper conductor is pushed through the lower slot wall. Figure 10 shows the forces acting on single sub-conductor as a function of positions along the z-axis. A difference between a Roebel bar and a straight bar can be recognized comparing to Fig. 9. Considering F_x , there is a sudden increment in the force, because in this moment the sub-conductor changes its position. The position of a sub-conductor changes along the z-axis. The radial forces decrease as the sub-conductor moves through the slot ground. Due to this change of position, a small F_z component can be recognized in Fig. 10. The same is also valid for F_y ; however, a change in the force polarity can be observed in the middle of the machine since the sub-conductor transposition moves through the other half of the bar.

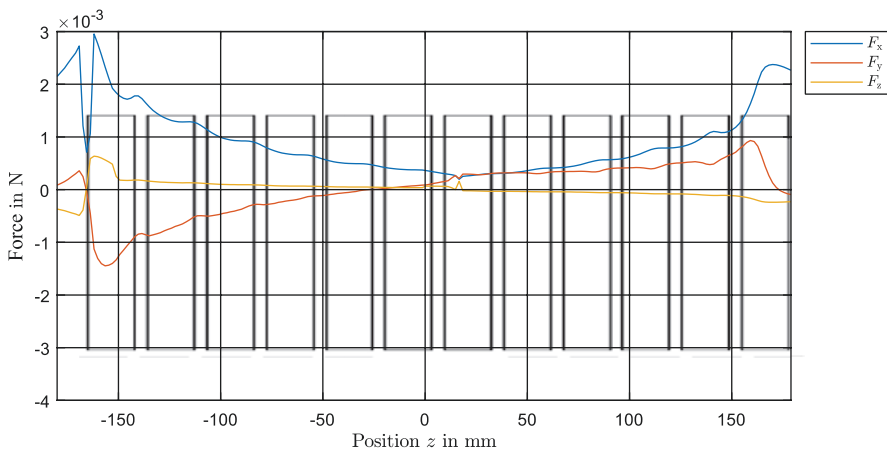


Fig. 10 Forces acting on single sub-conductor as function of positions along the z-axis

For a real generator with a diameter of 18 m, 2253 A current in the stator bar and 1.2 T air gap flux density, the forces against the slot wall would be 23 N for the lower conductor and 5 N for the upper conductor. Approximately $F_x = 60 \text{ N}$ acts on the upper conductor with double frequency. This should be considered by design of isolation and fixation materials in the slot.

6 Conclusion

A comprehensive study of Roebel bar forces in large generators is proposed in this chapter. The impact of the radial and tangential flux lines in the slot and the radial cooling ducts on the three-force Roebel components are investigated. Moreover, the impacts of load angle and power factor on these forces are studied. The estimations are performed with a 3D-FEM model, and the effect of Roebel bar transposition is considered. The behavior of the forces along the machine length is investigated. The radial and tangential Roebel bar forces for a real hydrogenerator are estimated. Since the relation and amplitude of radial and tangential forces change in different operation points, a mechanical analysis should be performed to estimate the mechanical deterioration of Roebel bar, fixing and isolation materials due to the radial and tangential Roebel bar forces.

References

1. A. Ebrahimi, *Characterization of a Large Electrical Machine Test Bench for Advanced Investigations on Wind and Hydro Generators*, 4th IEEE Southern Power Electronics Conference, Dermatol. Sin., pp. 1–6, December 2018
2. C. Grabner, E. Schmidt, *Analytical Approximation of the Displacement Process of Roebel Bars*, Conference Record – IAS Annual Meeting (IEEE Industry Applications Society), February 2002
3. C. Grabner, H. Köfler, *Mechanical Stress Behavior Inside Slots of Large Hydro Generators*. <https://doi.org/10.24084/repqj01.313>
4. M.G. Pantelyat, O. Biri, A. Stermecki, *Electromagnetic Forces in Synchronous Turbogenerator Rotor Slot Wedges*, *Proceedings of the Joint INDS'11 & ISTET'11*, Austria, July 2011
5. J. Pyrhönen, et al., *Design of Rotating Electrical Machines*. Wiley, ISBN: 978-0-470-69516-6
6. O. Marti, M. Gonçalves, *Lecture notes PHYS2200.0*, Darmstadt, Ulm University, Institute for Experimental Physics, 2018, <http://wwwex.physik.uni-ulm.de/lehre/ap-2015/ap-2015.pdf>
7. A. Ebrahimi, *Hybrid Analytical Modeling and Optimization of Surface Mounted Permanent Magnetic Synchronous Motors Considering Spatial Harmonics*, Dissertation, ISBN: 978-3-8440-5026-4
8. D. Meeker, *Finite Element Method Magnetics*. Version 4.2, 2018, <http://www.femm.info/wiki/Files/files.xml?action=download&file=manual.pdf>
9. S. McFee, J.P. Webb, D.A. Lowther, A tunable volume integration formulation for force calculation in finite-element based computational magnetostatics. *IEEE Trans. Magn.* **21**, 439–442 (1988)

NH₃-CO₂ Brine System for Refrigeration at Cold Storages and Seafood Processing Plants in India



Abdessalem Rabhi and Rudhi Sundar Pradhan

1 Introduction

Under its Nationally Determined Contributions (NDC), the Government of India (hereafter India) pledged to reduce its Greenhouse Gas (GHG) emissions intensity per unit of GDP by 33 to 35%, from 2005 levels, by 2030 [1]. India has also targeted to completely phase out the use of hydrochlorofluorocarbons (HCFCs) by 2030, and to cut 85% of the use of Hydrofluorocarbons (HFCs) by 2047 (over the 2024–2026 levels) [2]. To meet these targets, India has to grasp opportunities in every possible sector, especially in the industrial sector, which accounts for about 58% of total final energy consumption in the country [3].

The refrigeration systems, particularly in the seafood processing industries, are one among the prominent sectors that are studied in this chapter. For instance, India is the second-largest producer of seafood products in the world after China. It has 29,556 million tons of processing capacity with 567 processing plants and 612 registered cold storages with a capacity of 325,604 MT [4].¹ India exported 10,85,378 MT of seafood during the first 10 months of the FY 2017–18 as against 9,54,744 MT a year earlier, registering a growth of 13.68% in quantity and 10.11% in value [5]. The seafood industry is expected to increase even further in the coming years. Hence, more processing plants and cold storages are expected to be installed.

¹<http://mpeda.gov.in/MPEDA/#>

A. Rabhi (✉)

Institute for Global Environmental Strategies (IGES), Hayama, Kanagawa, Japan
e-mail: rabhi.abdessalem@mx.iges.or.jp

R. S. Pradhan

The Energy and Resource Institute (TERI), New Delhi, India
e-mail: rudhi.pradhan@teri.res.in

Therefore, it is essential to enhance the awareness of their owners and managers about the latest technologies options that they could consider.

This chapter is addressed to seafood processing plants and cold storages that are using HFC (R404a) refrigerant in their refrigeration systems and looking for better alternative technology solutions to improve their competitiveness while protecting the environment and ensuring the safety of their workers. It proposes to them to use the ammonia (NH₃)–carbon dioxide (CO₂) secondary (brine) refrigeration system (hereafter NH₃-CO₂ system) by highlighting the safety, energy efficiency, and cost aspects of such proposed technology. The chapter also introduces a comprehensive framework of partnership among specific relevant stakeholders that could be considered to adopt the proposed NH₃-CO₂ system in India, as part of the Japan-India Technology Matchmaking Platform (JITMAP) that has been initiated to promote Japanese low-carbon technologies (LCT) in India.

The rest of the chapter is organized as follows: the second section highlights the need for natural refrigerants as an environmentally friendly alternative to synthetic refrigerants. The third section outlines the concept of the proposed NH₃-CO₂ system and its benefits. The fourth section reports the findings from a case study on the feasibility of introducing the proposed technology at cold storage in India. The fifth section offers a framework to adopt the proposed technology more widely in India, and the sixth section provides the conclusion.

2 Switching to Natural Refrigerants as an Environmentally Friendly Alternative to Synthetic Refrigerants

2.1 Why Switch to Natural Refrigerant?

Synthetic refrigerants, such as chlorofluorocarbons (CFCs) and hydrochlorofluorocarbons (HCFCs), hurt the earth's atmosphere. They destroy the protective ozone layer. The ozone-friendly successors, namely, the hydrofluorocarbons (HFCs), contribute to global warming up to 4000 times more than CO₂. Even though they are specified as greenhouse gases (GHG) under the Kyoto Protocol, they are still widely used in refrigeration appliances [5]. Due to their harmful impact on the environment, CFC has been banned since 1996; HCFCs and HFCs are being phased out over the next decades as agreed under the Montreal Protocol and its Kigali Amendment. The legislative pressure on the refrigeration, air-conditioning, and heat pump (RACHP) sectors will continue to increase. Switching to more sustainable options, therefore, becomes more attractive to both manufacturers and users.

Table 1 Summary: Harmful and climate-friendly refrigerants

	Ozone depletion potential	Global warming potential	Status
<i>Synthetic refrigerants</i>			
CFC	High	Very high	A total ban in 1996
HCFC	Very low	Very high	Being phased out as agreed under the Montreal protocol and its Kigali amendment
HFC	Zero	Most high	
<i>Natural refrigerants (natural five)</i>			
HC	Zero	Negligible	“Future-proof” as it is unlikely that any new environmental legislation will prohibit or severely limit their use
CO ₂	Zero	Negligible	
NH ₃	Zero	Zero	
Water	Zero	Zero	
Air	Zero	Zero	

Source: Authors, based on the table available at <<http://www.refrigerantsnaturally.com/natural-refrigerants/>>, last accessed 22-7-2019

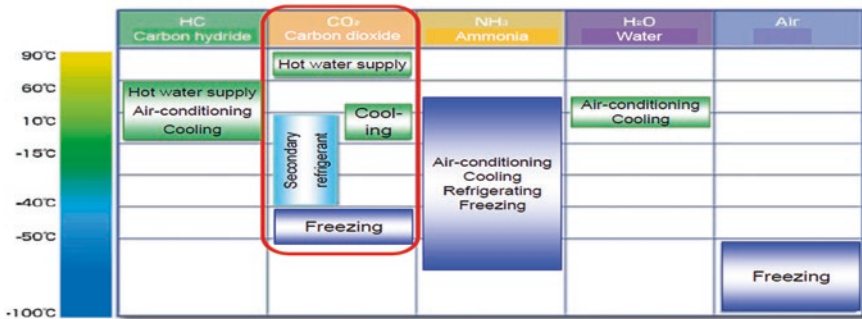


Fig. 1 Temperature range that can be met by natural refrigerants. (Source: Egashira Hiroyuki 2018 [6])

Natural refrigerants, namely, hydrocarbons (HC), carbon dioxide (CO₂), ammonia (NH₃), water (H₂O) and air (also called “the natural five”) are sustainable alternatives to synthetic refrigerants. Their emissions have no, or only a negligible, impact on the environment, even if they escape to the atmosphere (Table 1).

Natural refrigerants are less expensive compared to other synthetic refrigerants with low global warming potential. Hence, there is an increasing trend towards applying them as environmentally friendly alternatives. Natural refrigerants are also considered “future-proof” as it is unlikely that any new environmental legislation will prohibit or severely limit their use.² Applying natural refrigerants can satisfy any needs for freezing, cooling, and heating from –100 °C up to 120 °C (Fig. 1); Therefore, they can be considered as the best alternatives to synthetic refrigerants.

²<http://www.refrigerantsnaturally.com/natural-refrigerants/>

3 NH₃-CO₂ Secondary System

3.1 Basic Concept

NH₃-CO₂ secondary (brine) system (hereafter NH₃-CO₂ system) uses NH₃ and CO₂ as primary and secondary refrigerants, respectively, to provide highly efficient cooling systems for the refrigeration industry. The basic concept is that the expanded primary refrigerant (NH₃) evaporates through one side of a heat exchanger, where CO₂ condenses on the other side within a secondary cycle. CO₂ is circulated via pumping into the evaporators. Consequently, liquid CO₂ extracts heat and returns to the NH₃-CO₂ heat exchanger [7] (Fig. 2).

The NH₃ and CO₂ charges are distributed in the following way, as separated by inside the production area and outside the production area (machinery room):

Table 2 Ammonia and CO₂ charge distribution inside and outside the production area

Outside the production area	In the production area
Ammonia/CO ₂ brine system (with small ammonia charge at a centralized/self-contained location)	Small CO ₂ piping
	CO ₂ evaporative coils
	No ammonia inside the facility or around the products

Source: Alexandra Maratou and Nina Masson 2013 [7]

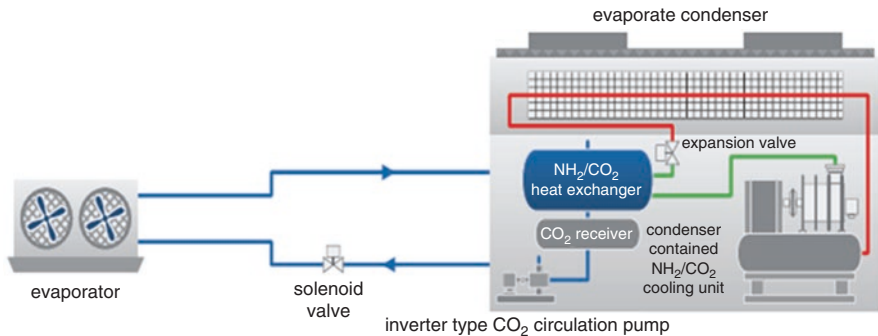


Fig. 2 Outline of the NH₃-CO₂ secondary system. (Source: Alexandra Maratou and Nina Masson 2013 [7])

3.2 *Benefits of NH₃-CO₂ Secondary System*

Among the natural refrigerants, NH₃ has the best physical and thermal properties with proved application [8]; however, they are generally considered to be more dangerous compared to the NH₃-CO₂ systems. This danger is due to NH₃ being a more toxic refrigerant compared to CO₂, and a high-charge conventionally pumped NH₃ system exposes a large portion of the building to NH₃ via piping, heat exchangers, and vessels. For seafood processing plants and cold storage owners looking for better alternatives technology solutions that take safety, environmental protection, and energy conservation into consideration, then an NH₃-CO₂ system is a more viable option [9]. NH₃-CO₂ systems are gaining momentum in many developing countries [10]. Among their benefits, the following could be enumerated:

1. Lower capital costs: Using CO₂ instead of NH₃, for lower temperatures, takes advantage of CO₂'s unique physical properties, resulting in smaller pipes, smaller pumps, less insulation, and less installation labor when compared to two-stage ammonia systems. CO₂ brine systems have at least 15% lower life-time cost when installation, energy, and maintenance costs are considered.
2. Ammonia charge reduction: An NH₃-CO₂ system allows designers to limit the NH₃ charge to the machine room. Only CO₂ is present in the processing and storage areas. For large low-temperature freezing systems, the reduction in NH₃ charge can be up to 90% compared to an NH₃ only system.
3. Reduced compliance costs: In many cases, NH₃-CO₂ systems can be designed with NH₃ charge below the threshold quantity (TQ), as stated by the Occupational Safety and Health Administration (OSHA) and the Environmental Protection Agency (EPA) programs, giving owners the opportunity to reduce the costs associated with PSM and RMP compliance.
4. Safety: Undoubtedly, the advantage of using CO₂ as a secondary refrigerant is safety: For instance, the NH₃ charge is reduced by up to 90% compared to an NH₃ only system and is confined to the machinery room. Besides, in the case of refrigerant leakage within the storage space, where only CO₂ refrigerant is circulated, the products stored in the cold storage facility are not affected.

4 A Case Study in India

4.1 *Outline*

To explore the potential of introducing NH₃-CO₂ system in India, IGES and TERI along with Japanese expert investigated nine (9) sites located in Andhra Pradesh, India. The investigation was part of a broader project to promote low-carbon technologies in India, supported by the Ministry of the Environment, the Government of Japan (MOEJ). It was found that seven (7) among the nine (9) visited sites are currently using HFC

(R404a)-based refrigerant, whereas two (2) are using NH₃ screw compressors. This chapter reports the findings from the feasibility study conducted at cold storage using HFC (R404a) with a storage capacity of 3000 metric tons. The details about the existing system's outlines, the characteristics of the freezer room's compressor, and the assumptions made to calculate the heat load are given in Tables 3, 4, and 5 respectively.

Table 3 Outline of the existing system

Freezer rooms			
Room temp:	−18 deg.C.		
No. of room	7 rooms		
Room size (m)	L: 8.5	W: 20.5	H: 12.5
Pallet per room	350 pallet		
Estimated capacity	28.8 kW		
Compressors (model: Carlyle 06CC899F200)	8 sets (1set stand-by)		
Chilled and loading area			
Room temp:	5 deg.C.		
No. of room	3 rooms		
Room size (m)	L: 8.5	W: 20.5	H: 12.5
Pallet per room	350 pallet		
Compressors (model: Carlyle 06EM799601)	4 sets (1set stand-by)		

Table 4 Characteristics of freezer rooms' compressors

Refrigeration load/room	26.1 kW
Amp/set	34 amp
BkW expected to be:	19 kW
From manufacturer's software	
Model	06CC899F200
Condensing temp	45 deg.C
Evaporating temp	−25 deg.C
Capacity	33.18 kW
BkW	19.38 kW

Table 5 Parameters/assumptions used to calculate the heat load/room

Ambient temp:(deg.C)	36 deg.C
Loading area temp: (deg.C)	10 deg.C
Room temp (deg.C)	−18 deg.C
Insulation material	PUF
Insulation thickness (mm)	Ceiling 150 mm
	Wall 150 mm
	Floor 100 mm
Incoming products	
Products incoming temp.(deg.C)	Frozen products
Products incoming temp.(deg.C)	−10 deg.C
Incoming weight MT/day	24 MT/day

Note: Heat load/room is calculated to be 28.8 kW; therefore full load is 28.8 kW × 7 rooms = 201.6 kW

4.2 Calculation and Findings

The comparison of installed power and the comparison of the brake kW (BkW) are provided in Tables 6 and 7, respectively.

Based on the calculations, it was found that the proposed NH₃-CO₂ system can give better performance than R404a-based refrigeration system at all loads (Fig. 3).

For instance, by considering the BkW (including the motors for condenser fans, pump motors, and evaporators fan motors), at maximum loading of 201.6 kW, energy saving at 60%, 80%, and 100% loads are 24.6%, 30.24%, and 29.08% respectively. Consequently, the CO₂ emission reduction ranges from 119 ~ 241 tCO₂/year. By considering the running hours to be 18 h/day and the power cost 6.3 Rs/KWh, then the energy cost saving ranges from 9 ~ 18 million Rs/year (Table 2), which makes the payback period of the proposed system within 4 years, assuming the production of critical components in India.

Table 6 Comparison of installed power

Capacity	236.7 kW			240.5 kW			
Existing				NH ₃ -CO ₂ system N62K × 5 sets			
Equipment	Q'ty	Motor	Total	Equipment	Q'ty	Motor	Total
Compressor	8	22.5	180	Compressor	5	30	150
Unit cooler	7	2.48	17.36	Unit cooler	7	2.48	17.36
Air cooled condenser	2	22.4	44.8	CO ₂ pump	1	2.2	2.2
				Eva. Condenser	1	5.15	5.15
Installed motor kW	242.16						174.7

Note: Motor sizes and brake kW (BkW) of unit coolers and air-cooled condensers are based on the assumed selection based on the required capacity

Table 7 Comparison of BkW at full load operations

Capacity	236.7 kW			240.5 kW			
Existing				NH ₃ -CO ₂ System N62K × 5sets			
Equipment	Q'ty	BkW	Total	Equipment	Q'ty	BkW	Total
Compressor	7	19.38	135.66	Compressor	5	22.1	110.5
Unit cooler	7	1.96	13.72	Unit cooler	7	1.96	13.72
Air cooled condenser	2	14.4	28.8	CO ₂ pump	1	1.76	1.76
				Eva. Condenser	1	4.12	4.12
Total BkW at full load	178.18				130.1		

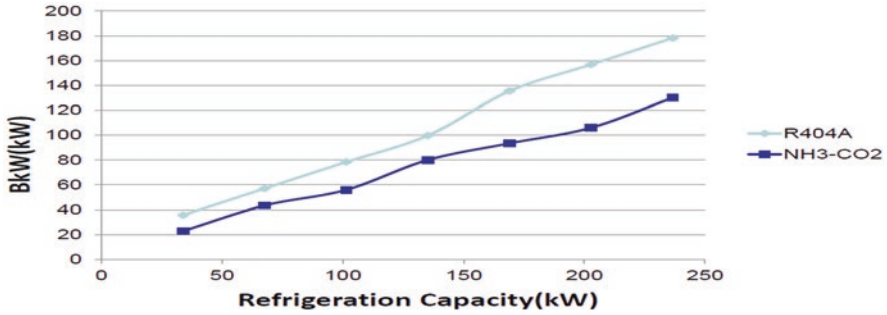


Fig. 3 NH₃-CO₂ system provides better performance at all load. (Source: Feasibility study on NH₃-CO₂ system, IGES-KRC 2019)

5 A Framework to Adopt the NH₃-CO₂ System more Widely in India

Based on feedback from the Japanese and Indian experts, who conducted the feasibility study, there is a significant scope to introduce the NH₃-CO₂ systems in seafood plants and cold storages in India in general and in Andhra Pradesh in particular. For instance, 70 out of 605 cold storages and 57 out of 562 seafood-processing plants in India are located in Bhimavaram and Vizag cities in Andhra Pradesh (AP).³

The introduction of the NH₃-CO₂ system can happen on a business-to-business basis while supported through other ongoing partnerships between Japan and India to promote low-carbon technologies in the industrial sector. For instance, IGES and TERI have initiated a Japan-India Technology Matchmaking Platform to encourage business-to-business matching with support from the Ministry of the Environment, Government of Japan.⁴ JITMAP supports business-to-business (B2B) matching mainly, and not only, in the form of: awareness enhancement, networking, access to financial schemes, and arrangement of policy and regulatory discussions through partnership among various stakeholders (research institutes, business associations, financing and supporting agencies, and government agencies) from India and Japan (Fig. 4).

³http://e-mpeda.nic.in/registration/Rpt_Region_Wise_Storages_With_Capacity.aspx

⁴Activities in Gujarat State, in particular, are supported also by Hyogo Prefectural Government, Japan through the activities of the IGES Kansai Research Centre as they have signed a Memorandum of Understanding (MOU) with the State Government of Gujarat.

Table 8 Summary of impacts

Load %	Existing BkW	NH ₃ -CO ₂ BkW	BkW difference	Running hour/month	Saving/month in INR	Saving/year in INR
100	156.1	110.6	45.4 (29.08%)	540	154,588.-	1,855,065.-
80	127.3	88.8	38.5 (30.24%)	540	130,951.-	1,571,420.-
60	90.8	68.3	22.4 (24.6%)	540	76,287.-	915,449.-

Source: Feasibility study on NH₃-CO₂ system, IGES-KRC report (Feb. 2019) (Could be shared upon sending request to authors)

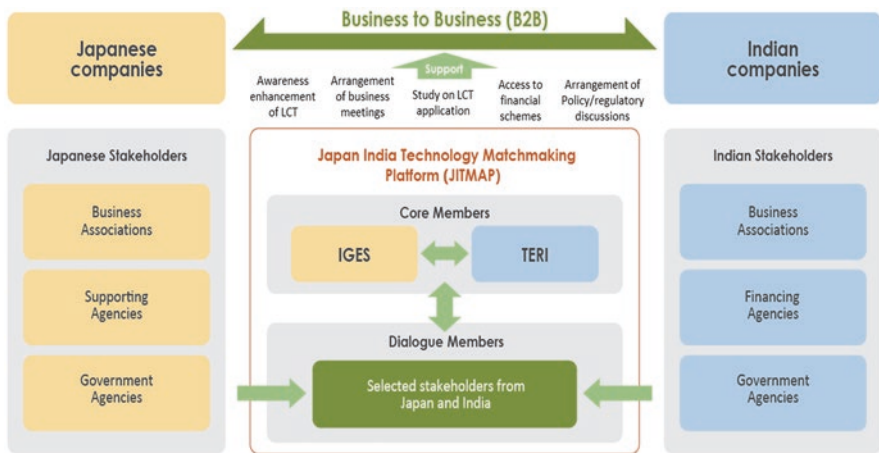


Fig. 4 Schematic diagram of JITMAP. (Source: Abdesslem Rabhi and Prosanto Pal 2019 [11])

JITMAP can support the promotion of NH₃-CO₂ system through the following:

1. Introduce it to seafood plants and cold storage owners through its dissemination workshops.
2. Train energy managers and energy auditors about it through its training programs.
3. Arrange business meetings and facilitate onsite feasibilities studies about it through its vast network.
4. Share and discuss the findings and case studies with relevant stakeholders, including financing agencies and policymakers, directly through stakeholder meetings or indirectly through uploading the findings at the JITMAP website (jitmap.org/).

The NH₃-CO₂ system is applicable to the case where there are strict requirements for NH₃ charging volume [12]. While the Association of Ammonia Refrigeration in India (AAR) is discussing with the central pollution control board on stricter regulations regarding the use of NH₃ in rural areas in India, discussions

with Pollution Control Boards at the state level (PCB) may also be needed to share with them/propose to them ways to enforce current policies/regulations or to incentivize businesses to use natural refrigerants. Businesses on their own may not have the chance to meet with PCB, hence using other channels such as JITMAP could be of good help to them.

6 Conclusion

India is the second-largest producer of fish in the world after China. The seafood industry is expected to increase even further in the coming years; hence, more processing plants and cold storages are expected to be installed. Seafood processing plants and cold store owners are under constant pressure to produce more while spending less on operations. This chapter is addressed to those who are looking for guidance on selecting technology solutions that provide investment security at high efficiency and safety levels. It proposes to them to use the NH₃-CO₂ system for refrigeration.

While NH₃ systems could be the best option for them to save energy, however, when considering safety issues NH₃-CO₂ systems could be an alternative viable option. The feasibility study about installing the NH₃-CO₂ system at a cold storage in India revealed that up to 30% of energy saving is possible. Consequently, cost-saving ranges from 9 Million ~18 million Rs/year, which makes the payback period within 4 years, assuming the localization of its critical components in India.

It is obvious that the technology can be promoted on the business-to-business level. As a complementary measure, the chapter proposes to consider the support being provided under the Japan-India Technology Matchmaking platform (JITMAP), which is part of an overall collaboration between Japan-India to promote low-carbon technology in Indian industries. JITMAP activities in terms of workshops, training of trainers, feasibility studies, and facilitating stakeholder meetings with various relevant stakeholders (business, financing agencies, and government agencies) could be of great help to promote this technology at seafood processing plants in India.

Acknowledgments The content of this chapter, the conclusions, and the recommendations mentioned in it should be understood to be those of the authors and not attributed to IGES or TERI. Therefore, the authors should be responsible for the accuracy and relevance of the content.

Many thanks go to colleagues and supervisors at IGES and TERI, who contributed in it through suggestions and comments, namely, to Prof. Yutaka Suzuki, Toshizo MAEDA, Mika Tachibana and Aditi Khodke (from IGES), and Girish Sethi (from TERI). Special thanks go to Hiroyuki Egashira, Sales Department, Asian Regional Headquarters, Mayekawa MFG. Co. Ltd. for his valuable technical inputs.

Appendix: Region-Wise Processing Plants and Storage Premises (as on 10-04-2019)

No..	Centre	Processing plants		Cold storage		Chilled storage		Dry fish storage		Other storage		Total	
		No	Capacity (MT)	No	Capacity (MT)	No	Capacity (MT)	No	Capacity (MT)	No	Capacity (MT)	No	Capacity (MT)
1	RO Kochi (Kerala)	106	3834.02	131	65,376.40	1	861.00	3	22.70	8	2612.90		68,873.00
2	SRO Quilon (Kerala)	16	579.20	26	8795.50	0	0.00	0	0.00	0	0.00		8795.50
3	RO Vizag (Andhra Pradesh)	14	646.90	25	13,244.00	1	50.00	2	3030.00	0	0.00		16,324.00
4	SRO Bhimavaram (Andhra Pradesh)	43	2222.27	45	20,834.00	2	1786.00	10	871.00	0	0.00		23,491.00
5	RO Chennai, (Andhra Pradesh and Tamil Nadu)	42	2681.94	46	41,010.00	1	804.00	7	1268.00	2	1246.00		44,328.00
6	SRO Tuticorin (Tamil Nadu)	36	978.10	37	17,950.20	7	726.00	5	1922.00	6	752.00		21,350.20
7	SRO Goa	16	1079.26	16	7386.50	0	0.00	0	0.00	2	1400.00		8786.50
8	SRO Mangalore (Karnataka)	44	4049.66	27	13,045.70	0	0.00	4	5050.00	18	10,289.00		28,384.70
9	SRD Ratnagiri Maharashtra	12	1454.90	8	7876.00	1	706.00	4	5810.00	4	5810.00		20,202.00
10	RO Mumbai, (Maharashtra and Gujarat)	47	3416.30	52	39,157.10	1	10.00	3	460.00	0	0.00		39,627.10
11	RO Veraval, Gujarat	88	4467.06	93	45,269.00	0	0.00	13	1196.00	0	0.00		46,465.00
12	SRO Porbandar, Gujarat	27	1496.68	24	14,033.80	4	1386.80	4	484.00	1	5.00		15,909.60
13	SRO BBSR (Odisha)	32	1128.80	31	16,864.00	17	10,568.00	0	0.00	1	2000.00		29,432.00
14	RO Kolkata (West Bengal)	44	1521.06	51	14,761.93	0	0.00	15	1367.58	1	60.00		16,189.51
	Total	567	29,556.15	612	325,604.13	35	16,897.80	70	21,481.28	43	24,174.90		388,158.11

Source: Authors' compilation, based on data available at <<http://mpeda.gov.in/MPEDA/#>>, last accessed 23 Apr. 2019

References

1. UNFCCC. 2019. INDC portal, available at <https://www4.unfccc.int/sites/submissions/indc/Submission%20Pages/submissions.aspx>. Last accessed 23 Apr 2019.
2. MOEF&CC. 2018. MOEF&CC home page available at <http://www.ozonecell.com/viewsection.jsp?lang=0&id=0,166,399>. Last accessed 23 Apr 2019.
3. MSPI (Ministry of Statistics and Programme Implementation, Government of India). 2018. Energy Statistics, 25th issue, MSPI Central Statistic Office, New Delhi. Available at http://www.indiaenvironmentportal.org.in/files/file/Energy_Statistics_2018.pd. Last accessed on 23 Apr 2019.
4. MPEDA (Marine Product Export Developing Agency). 2019. Available at <http://mpeda.gov.in/MPEDA/#>. Last accessed 12 Apr 2019.
5. Article available at <https://www.financialexpress.com/market/indias-seafood-exports-up-13-7-in-april-january/1155153/>. Last accessed 02 Aug 2019.
6. E. Hiroyuki, *Japanese energy-efficient technologies for seafood. Presentation at a dissemination workshop held in Bhimavaram, Andhra Pradesh* (Mayekawa Mfg. Co. Ltd, 2018)
7. A. Maratou, N. Masson, *Examples of NH₃-CO₂ secondary systems for cold store operators*. Available at: http://www.shecco.com/files/news/guide_nh3-final.pdf. Last accessed 02 Aug 2019, 2013.
8. Asano Hideyo and Mugabe Nelson. 2013. Actual energy conservations by using the NH₃-CO₂ refrigeration system. Proceeding for the third ICSERA2013. ICRERA2013-3-C-2. Available at <https://mayekawa.com.au/494/wp-content/uploads/2013/12/Actual-Energy-Conservations-by-using-NH3-CO2.pdf>. Last accessed 23 Apr 2019.
9. R. Peterson. *Six Reasons to Consider a CO₂/NH₃ Cascade Refrigeration System*. Article available at http://stellarfoodforthought.net/six-reasons-to-consider-a-co2nh3-cascade-refrigeration-system/?doing_wp_cron=1564728381.0453319549560546875000. Last accessed 02 Aug 2019, 2014.
10. D. Yoshimoto, *Mayekawa develops new NH₃/CO₂ system for China market*. Article available at http://r744.com/articles/8882/mayekawa_develops_new_nh3_co2_system_for_china. Last accessed 02 Aug 2019, 2019.
11. Abdessalem RABHI, P. Pal, Japan–India technology matchmaking platform: approach to promote Japanese low carbon technologies in Indian industries. *Journal of Resources Energy, and Development (JREAD)* **16**(1), 9–18 (2019)
12. Shenzhen Sunicorn Technology Co.,Ltd. Ammonia/CO₂ secondary refrigerant refrigeration system for vegetable. Article available at <http://commercialcoldroom.buy.lightneasy.org/pz63cb784-ammonia-co2-secondary-loop-refrigeration-system-for-vegetable-processing.html>. Last accessed 02 Aug 2019.

Semi-analytical Calculation of Field and Loss Distribution in the Tooth Tips of Electrical Machines



Alexander Rehfeldt, Torben Fricke, Babette Schwarz, Amir Ebrahimi, and Bernd Ponick

1 Introduction

Iron losses in electrical machines depend on various parameters, such as the flux density's amplitude, frequency and whether the magnetization is of rotating, alternating or elliptical nature. As described in [1, 2], the losses can be separated into eddy current losses, hysteresis losses and excess losses:

$$P_{fe} = P_{eddy} + P_{hyst} + P_{exc}. \quad (1)$$

The latter two show a distinct dependency on the type of magnetization. As described in [3, 4], there are three types of magnetization: rotating magnetization, alternating magnetization and elliptical magnetization, the latter being a superposition of rotating and alternating magnetization, as displayed in Fig. 1.

Finite element analysis shows that rotating magnetization as well as a high-time harmonic distortion are present in the tooth tip area and, therefore, important to consider for a precise iron loss calculation. Figure 2 shows the relationship of total losses due to alternating and due to rotating magnetization as a function of the flux density as per unit value of the alternating loss energy at 1 T measured on a three-phase single sheet tester. For low-flux density values, the rotating magnetization produces losses twice as high than alternating magnetization. At higher flux density

A. Rehfeldt (✉) · T. Fricke · A. Ebrahimi · B. Ponick
Institute for Drive Systems and Power Electronics, Leibniz University Hannover,
Hannover, Germany
e-mail: alexander.rehfeldt@ial.uni-hannover.de; torben.fricke@ial.uni-hannover.de;
ebrahimi@ial.uni-hannover.de; ponick@ial.uni-hannover.de

B. Schwarz
Vo/th Hydro Holding GmbH & Co. KG, Heidenheim, Germany
e-mail: babette.schwarz@voith.com

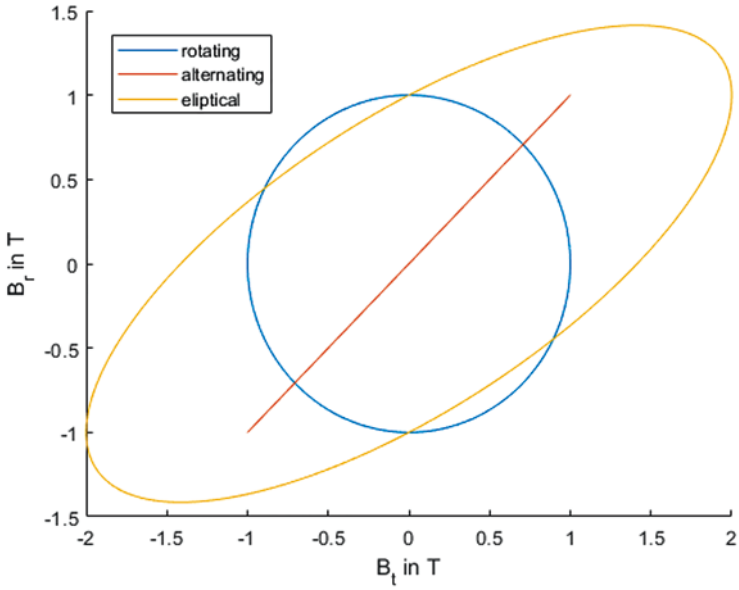


Fig. 1 Rotating, alternating and elliptical magnetization

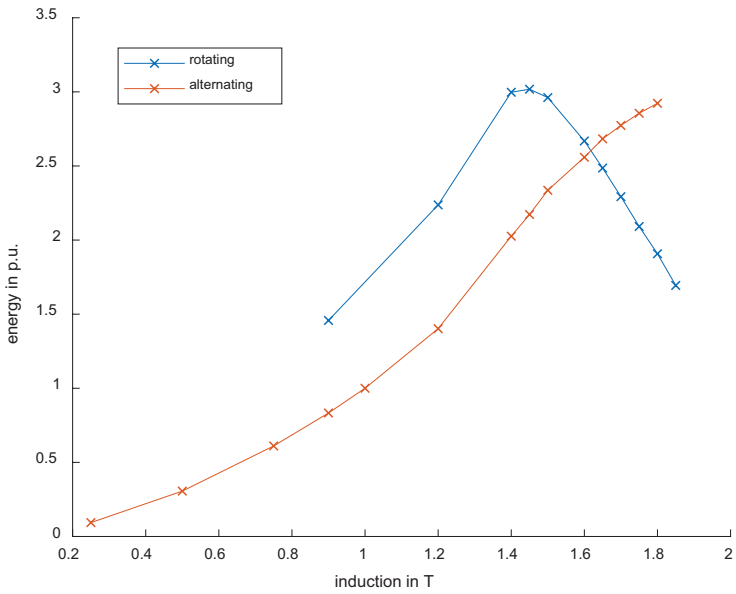


Fig. 2 Measured loss energy for rotating and alternating magnetization

values, the ratio drops and the hysteresis and excess losses in case of rotating magnetization converge to zero at high saturation.

2 Loss Model

Considering the effect of rotating magnetization in the iron loss model is crucial. In [5], an approach is presented, in which the rotational magnetization is incorporated using the relationship between alternating and rotational magnetization for each loss component:

$$W^{ROT} = R_{hyst}(J) \cdot W_{hyst}^{ALT}(J, f) + R_{exc}(J) \cdot W_{exc}^{ALT}(J, f) + 2 \cdot W_{eddy}^{ALT}(B, f). \quad (2)$$

The factors R_{hyst} and R_{exc} are independent of the frequency and only depend on the polarization J . To consider elliptical magnetization, the calculated results for alternating and rotating magnetization are interpolated as a function of the ratio of minor and major axis of the ellipse. The “circularity” c of the magnetization is defined as

$$c = \frac{r_{minor}}{r_{major}}. \quad (3)$$

The ratio is $c = 1$ for purely rotating magnetization and zero for alternating magnetization. After calculating the ratio, the losses of the elliptical magnetization can be calculated as

$$W_{ellip}(c) = W_{alt} \cdot (1 - c) + W_{rot} \cdot c. \quad (4)$$

Various measurements with different flux density values, frequencies and magnetization types are used to determine the loss coefficients, which have been executed on a single sheet tester capable of impressing arbitrary flux density values in both spatial directions.

For eddy currents, a solely analytical approach is used based on the common equation for calculating eddy currents in soft magnetic iron sheets:

$$W_{eddy} = \frac{\pi^2 \sigma d^2}{6} f B^2. \quad (5)$$

$$W_{hyst}^{ALT} = k_h B^2. \quad (6)$$

In the next step, the hysteresis losses for alternating and for rotating magnetization can be identified by extrapolating the measured losses to $f = 0$. The results of alternating magnetization are used to interpolate the hysteresis loss coefficient.

The factor R_{hyst} is calculated by dividing the rotating hysteresis losses by the alternating hysteresis losses. This results in rotating hysteresis losses:

$$W_{hyst}^{ROT} = R_{hyst} (J) k_h B^2. \quad (7)$$

The excess losses are obtained by subtracting the calculated eddy and hysteresis losses from the measurements. Similar to the hysteresis losses, the alternating excess losses are used to determine the excess loss coefficient:

$$W_{exc}^{ALT} = k_{exc} B^2 f^{0.5}. \quad (8)$$

In order to obtain the excess losses for rotating magnetization, the factor R_{exc} is determined by dividing rotating and alternating excess losses. The rotating excess losses can be written as

$$W_{exc}^{ROT} = R_{exc} (J) k_{exc} B^2 f^{0.5}. \quad (9)$$

3 Field Calculation

In this section, a semi-analytical field calculation approach is presented to calculate the flux density distribution in open-circuit operation of a synchronous machine. The approach is split into two consecutive field calculation routines. First, the flux density distribution normal to the tooth surface is obtained by employing the Laplace equation combined with Schwarz-Christoffel mapping. Subsequently, the flux density distribution inside the tooth is calculated with a reluctance network.

3.1 Schwarz-Christoffel Mapping

The Schwarz-Christoffel mapping algorithms used in this chapter are the same as the ones described in a previous paper [6].

Therefore, only an overview of the approach is given in this chapter. Schwarz-Christoffel mappings can be used to map from an infinite half plane into an arbitrary geometry by solving the mapping equation:

$$\underline{z} = f(\underline{w}) = \int (\underline{w} - \underline{w}_1)^{\frac{\alpha_1}{\pi} - 1} \cdot (\underline{w} - \underline{w}_2)^{\frac{\alpha_2}{\pi} - 1} \dots (\underline{w} - \underline{w}_n)^{\frac{\alpha_n}{\pi} - 1} d\underline{w}, \quad (10)$$

using the nomenclature shown in Fig. 3.

To achieve a mapping from a rectangle (the canonical domain), where the Laplace equation can easily be solved, into the desired geometry, the mapping prob-

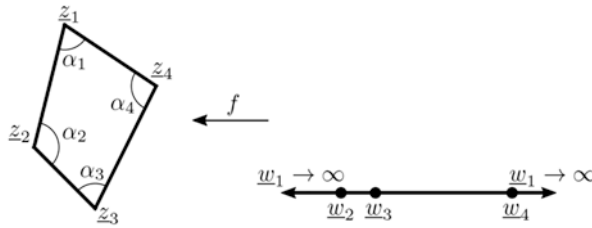


Fig. 3 Nomenclature around Schwarz-Christoffel mappings

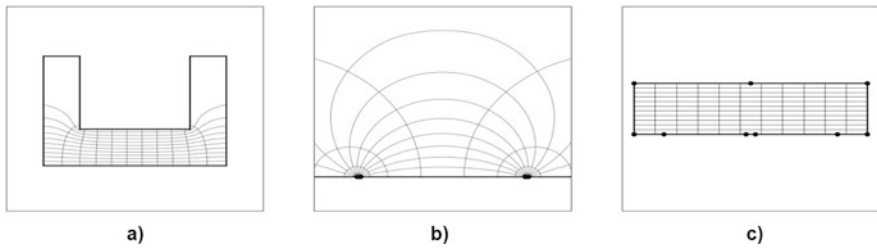


Fig. 4 Mapping between a rectangle and a symmetrical arbitrarily shaped physical domain. (a) Physical domain. (b) Intermediate domain. (c) Canonical domain

lem is split into two distinct mappings as seen in Fig. 4. The first mapping from the canonical to the intermediate domain can be found in the relevant literature [7] and relies on elliptic integrals. The second mapping from the intermediate to the physical domain poses a greater challenge and is thus approached by integrating the mapping function numerically. This numerical approach was pioneered by Reppe [8] and refined by Driscoll [9]. A more detailed explanation of the mapping approach used in this chapter can be found in a previous paper [6].

3.2 Solving the Laplace Equation

$$\frac{\partial \Phi}{\partial x^2} + \frac{\partial \Phi}{\partial y^2} = 0 \tag{11}$$

After transforming the teeth outline into a series of rectangles as shown in Fig. 5, the Cartesian Laplace equation is solved for each harmonic with the basic potential function

$$\Phi(x,y) = \sum_{i=0}^n \sin k_i x (A_i \sin h k_i y + B_i \cos h k_i y). \tag{12}$$

Solving the Laplace Equation

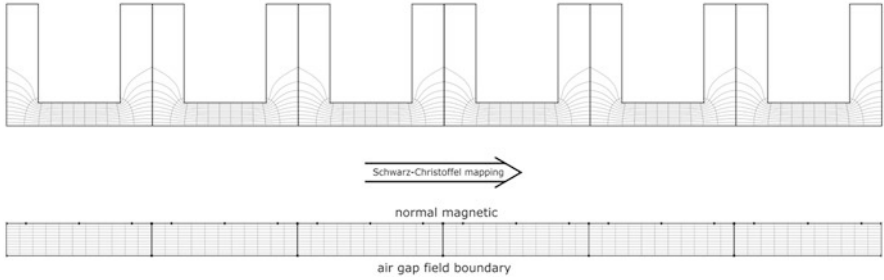


Fig. 5 Schwarz-Christoffel mapping of the tooth region

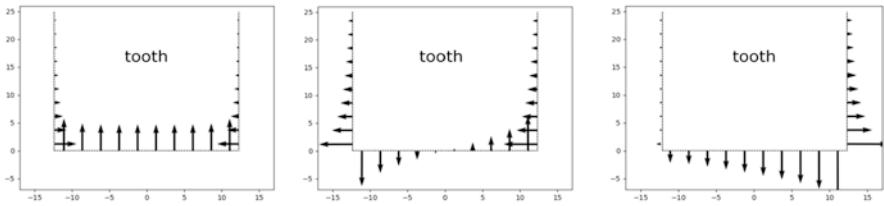


Fig. 6 Normal component of flux density on the tooth surface

By differentiating the magnetic potential in x - and y -direction, the x - and the y -component of the flux density distribution can be determined as

$$B_x = \frac{\partial\Phi}{\partial y}, B_y = \frac{\partial\Phi}{\partial x}. \tag{13}$$

The boundary condition at the tooth surface is normal magnetic, as the permeability of the stator core is considered to be infinite in the analytical approach ($\mu \rightarrow \infty$). The inner boundary condition is determined by the air-gap flux density. The air-gap flux density distribution is computed by an analytical approach. The air-gap field is disassembled using a Fourier transform, and the field results are superimposed due to the linearity of the approach. Figure 6 shows the results for three exemplary instants of time.

3.3 Magnetic Reluctance Network

After having obtained the normal component of the flux density at the edge of the tooth, a reluctance network of the tooth is used to determine the flux density distribution inside the tooth. Figure 7 shows the reluctance network used to model a tooth.

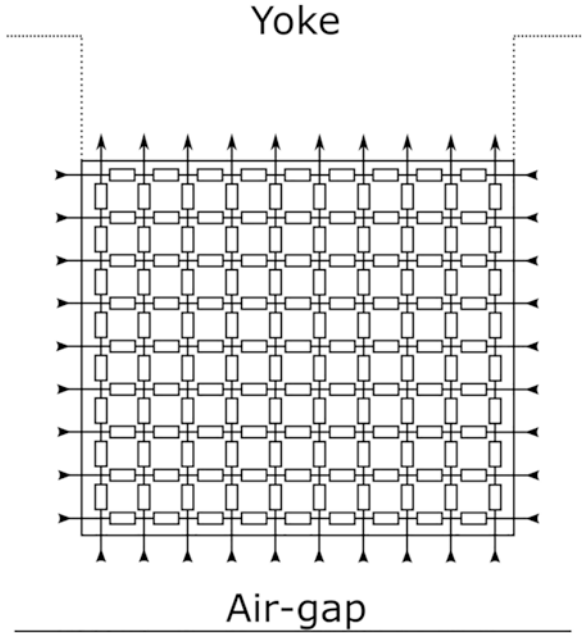


Fig. 7 Reluctance network of tooth tip

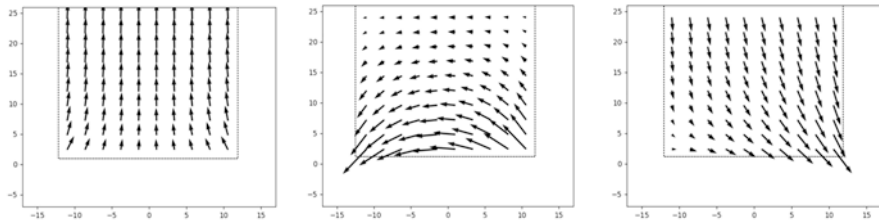


Fig. 8 Flux distribution inside of a tooth

FEA investigations have shown that the effect of rotating magnetization is limited to a small area of the tooth tip. Therefore, it is sufficient to investigate the radial height of about one tooth width. Outside of this region, the flux density is only directed radially (Fig. 8).

4 Transient Calculation

As the flux density distribution is time-dependent, the field distribution is calculated for multiple time steps. The process of Schwarz-Christoffel mapping as well as inverting the admittance matrix of the magnetic network is only dependent on the

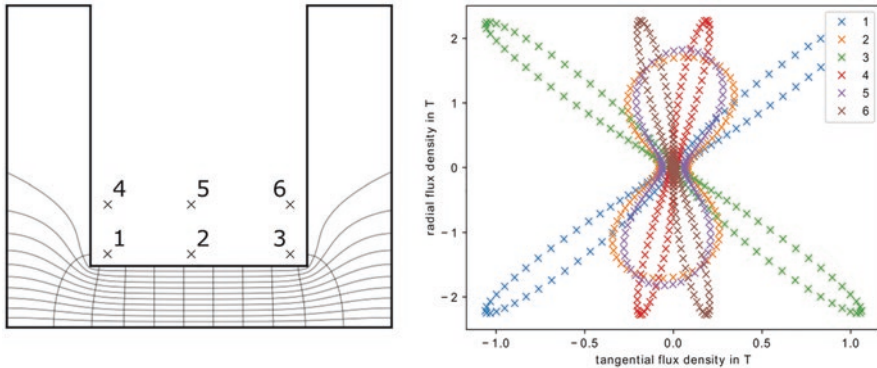


Fig. 9 Flux loci at different positions in the tooth tip

geometry and, therefore, only has to be conducted once for each geometry. This results in a very quick calculation for multiple time steps, that is, rotor positions. To validate the field results calculated with the presented approach, FEA results are used.

Figure 9 shows the analytically calculated flux loci for different positions in the tooth tip. It is apparent, that the flux loci are strongly dependent on the position. The impact of rotating or rather elliptical magnetization is limited to an area near the tooth tip. The comparison of the iron losses for FEA and the semi-analytical approach shows a difference of about 3%. Therefore, the total losses in the tooth area calculated with a 2D transient FEM calculation and a similar loss model have been used. Although the analytical field calculation is based on a linear approach, the agreement is very good, despite a high degree of saturation. This is due to the fact that the correct amount of air-gap flux is inserted into the model so that neglecting the non-linear material properties only results in a slightly different distribution of the flux density.

Additionally, the approach provides the possibility to incorporate the anisotropy of iron losses. The iron loss model described in [5] has to be adapted to include a dependency of the alternating loss components on the spatial direction.

5 Conclusion

The presented semi-analytic spatial field distribution calculation in the tooth tips of synchronous machines proved to be in good agreement with FEA calculation results. The presented approach based on conformal mapping, the Laplace equation and a reluctance network in the tooth is a computationally inexpensive method of calculating the spatial and time-dependent field distribution. In future work, the iron loss model will be adapted to include anisotropic material properties. Furthermore, the effect of punching will be investigated and possibly incorporated into the iron loss model.

References

1. G. Bertotti, General properties of power losses in soft ferromagnetic materials. *IEEE Trans. Magn.* **24**(1), 621–630 (1988)
2. Z. Neuschl, Rechnerunterstützte experimentelle Verfahren zur Bestimmung der lastunabhängigen Eisenverluste in permanentmagnetisch erregten elektrischen Maschinen mit additionallem Axialfluss (2007)
3. H. Kapeller, D. Dvorak, J. V. Gragger, F. Müllner, H. Neudorfer, Modeling of iron losses in an induction machine based on a magnetic equivalent circuit in Modelica. In *Proceedings of the IEEE International Electric Machines and Drives Conference (IEMDC)*, (Miami, FL, USA, May 2017), pp. 1–8
4. Y. Guo, J.G. Zhu, J. Zhong, H. Lu, J.X. Jin, Measurement and modeling of rotational core losses of soft magnetic materials used in electrical machines: A review. *IEEE Trans. Magn.* **44**(2), 279–291 (2008)
5. C. Appino, M. Khan, O. de la Barrière, C. Ragusa, F. Fiorillo, Alternating and rotational losses up to magnetic saturation in non-oriented steel sheets. *IEEE Trans. Magn.* **52**(5), 1–4 (2016)
6. A. Rehfeldt, T. Fricke, D. Emmrich, B. Ponick, *Semi-Analytical Calculation of Field Distribution in Yoke/Tooth Transition in Electrical Machines* (IEMDC, 2019)
7. W.J. Gibbs, *Conformal Transformations in Electrical Engineering* (Chapman & Hall, London, 1958)
8. K. Repp, “Berechnung von Magnetfeldern mit Hilfe der konformen Abbildung durch numerische Integration der Abbildungsfunktion von Schwarz–Christoffel”, ser. Siemens Forschungs- und Entwicklungsberichte, vol. 8 (Springer, 1979)
9. T.A. Driscoll, S.A. Vavasis, Numerical conformal mapping using cross-ratios and Delaunay triangulation. *SIAM J. Sci. Comput.* **19**(6), 1783–1803 (1998)

The Effect of Top Runner Motor (IE3) Regulation in Japan



Takeshi Obata

1 Background

1.1 Motor Market in Japan

Figure 1 shows annual production volumes and the total output capacity of motor in Japan [1]. From 2009, the aggregation of hermetic motors for air-conditioning has been transferred from “AC three-phase” to “Others”. From 2012, the breakdown of “Others” was divided into “PM motor” and “Others”. The number of production has decreased significantly in 20 years from 2000, and the cause is that AC single-phase motors have decreased by 14 million or more. Motor production reached a major turning point in 2009. The impact of the 2008 economy shock has remarkably reduced overall motor production and output capacity. In particular, the number of AC three-phase motors decreased significantly from 2009 onwards. However, the number of “other” AC motors (referred to as “Others (PM)” and “Others” in Fig. 1) are superior in efficiency to the mentioned AC three-phase motors, and their production has started to increase substantially after 2009. The total output capacity of the motor maintains at the 22 million kW level, and it can be seen that the single-phase motor and the three-phase motor have been shifted to the PM motor.

Figure 2 shows the composition of motor types in 2008 [2], and Fig. 3 shows that of 2017. The composition ratio of the three-phase motor, which was 44% in 2008 and 85% in output capacity, has fallen to 26% in 2017 and 57% in output capacity. On the other hand, it can be seen that the transition from three-phase motors to PM motors is progressing, as the proportion of PM motors in 2017 has increased by 32% and 26% in output compared to those in 2008. .

T. Obata (✉)

The Japan Electrical manufacturer’s Association (JEMA) (Hitachi Industrial Equipment Systems Co., Ltd.), Tokyo, Japan

e-mail: obata-takeshi@hitachi-ies.co.jp

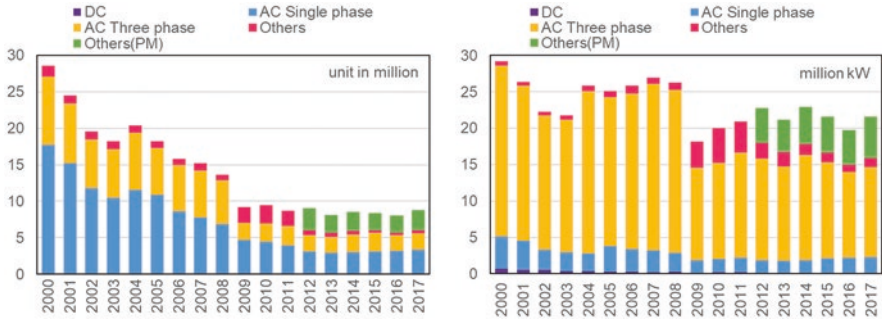


Fig. 1 Production volumes and total output capacity of motor

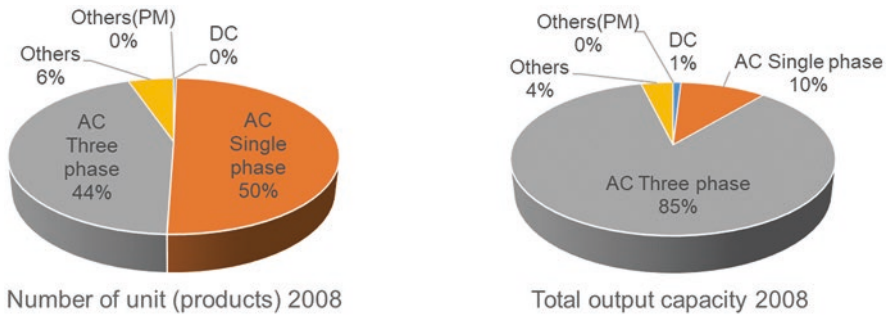


Fig. 2 Composition of motor types in 2008

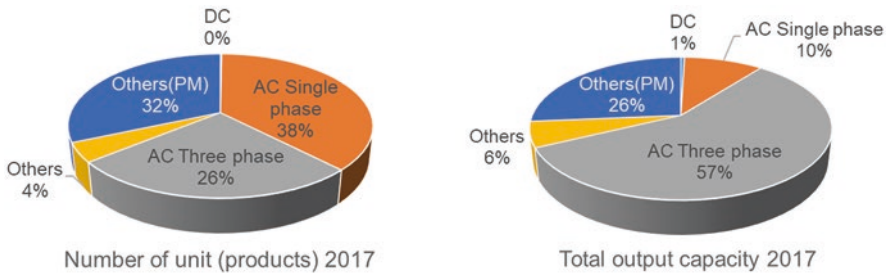


Fig. 3 Composition of motor types in 2017

2 Top Runner Standard for Three-Phase Induction Motor

The Decree, Ministerial Ordinance and Notification of the Energy Conservation Act were enforced on November 1, 2013, and the target year started on April 1, 2015 [3]. Japanese manufacturers and importers are required to ensure that the average efficiency value of motors shipped in 1 year does not fall below the efficiency regulated value set for each category.

2.1 Outline of Regulation

The applicable three-phase induction motor is a motor that meets the following condition specified by Japanese Industrial Standard JIS C 4034-30 “Efficiency class of single-speed three-phase cage induction motor (IE code)”.

- (a) Rated frequency (based frequency): 50 Hz ± 5%, 60 Hz ± 5%, and could drive both 50 Hz ± 5% and 60 Hz ± 5%.
- (b) Single speed.
- (c) Rated voltage: Up to 1000 V.
- (d) Rated output: Between 0.75 kW and 375 kW.
- (e) Poles: 2P 4P 6P.
- (f) Duty type: S1 (continuous duty) or S3 (intermittent periodic duty).
- (g) Capable of operating direct on-line.

But there are some exceptions.

- (1) Motors completely integrated into a machine (e.g. pump, fan and compressor) that cannot be tested separately from the machine.

*Motors with flanges, feet and/or shafts with special mechanical dimensions are included.

- (2) Inverter drive motors are out of scope in JIS C 4034-30.

*If these motors could operate direct on-line, they are included in the coverage.

Also, Fig. 4 shows the exceptions of Top Runner regulation.

There are two major methods for verifying whether motor efficiency meets the standard. One is the minimum energy performance standard (MEPS). Another is

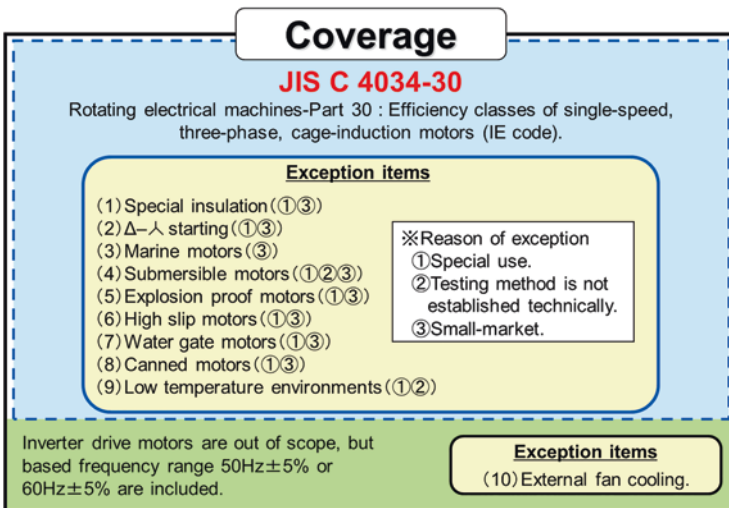


Fig. 4 Exceptions of Top Runner regulation

category (class) average standard (CAS). The former is the most widely used method in the world, and the minimum value is determined, and if it cannot be exceeded, measures are taken to stop the shipment of the product. In this method, the tolerance is set as shown in the upper part of Fig. 6, and a motor whose efficiency is less than the value (average value – tolerance) cannot be distributed.

The latter is a scheme in which the regulated efficiency (see Fig. 5) can be achieved by a weighted average efficiency of shipments for each category. According to this method, if there is a demand for a motor with emphasis on performance other than the efficiency, it can be shipped to the market even if the efficiency of the motor is inferior to a regulated value (for example, an IE1 class motor). The regulated

60Hz				50Hz					
Category	Rated output power		Regulated efficiency [%]	Category	Rated output power	Regulated efficiency [%]	Category	Rated output power	Regulated efficiency [%]
	from	to							
1	0.75kW	≤ 0.925kW	85.5	14	0.75kW	82.5	27	37kW	93.9
2	> 0.925kW	≤ 1.85kW	86.5	15	1.1kW	84.1	28	45kW	94.2
3	> 1.85kW	≤ 4.6kW	89.5	16	1.5kW	85.3	29	55kW	94.6
4	> 4.6kW	≤ 9.25kW	91.7	17	2.2kW	86.7	30	75kW	95.0
5	> 9.25kW	≤ 13kW	92.4	18	3kW	87.7	31	90kW	95.2
6	> 13kW	≤ 16.75kW	93.0	19	4kW	88.6	32	110kW	95.4
7	> 16.75kW	≤ 26kW	93.6	20	5.5kW	89.6	33	132kW	95.6
8	> 26kW	≤ 33.5kW	94.1	21	7.5kW	90.4	34	160kW	95.8
9	> 33.5kW	≤ 41kW	94.5	22	11kW	91.4	35	200~375kW	96.0
10	> 41kW	≤ 50kW	95.0	23	15kW	92.1	36	Others	Defined by eguation
11	> 50kW	≤ 100kW	95.4	24	18.5kW	92.6			
12	> 100kW	≤ 130kW	95.8	25	22kW	93.0			
13	> 130kW	≤ 375kW	96.2	26	30kW	93.6	Regulated efficiency : IE3		

Fig. 5 Efficiency classification and regulated efficiency

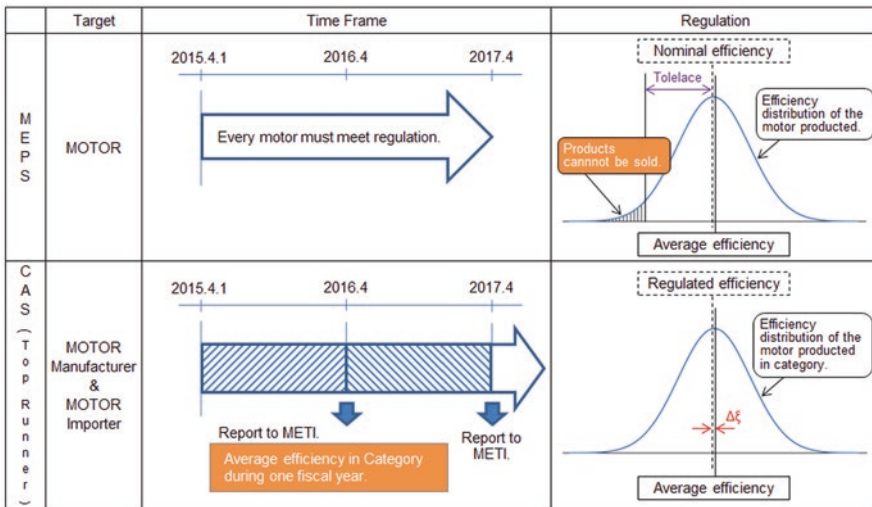


Fig. 6 Difference between MEPS and CAS (Top Runner)

value may be achieved as an average value by shipping a motor having higher efficiency than the regulated value with products in the same category.

The Top Runner scheme is a method in which the degree of technological progress assumed in the future is added as an efficiency improvement part as a regulated value based on the value of the most efficient motor existing in the market at the time of setting the regulated value. As a matter of course, although the target regulated value is high, the above-mentioned regulated value CAS is adopted as an evaluation method of achievement. Therefore, as shown in the lower part of Fig. 6, it is necessary that the average efficiency weighted by the shipment quantity exceeds the regulated in each category.

2.2 Results of Top Runner Scheme

As the regulation was implemented by April 1, 2015, each company has had to report their efficiencies over the FY2015, 2016 and 2017. The Agency for Natural Resources and Energy (extra-ministerial of The Ministry of Economy, Trade and Industry – METI) says that all motor makers have met the efficiency standard. However, since the reports of each company are not disclosed, it is unclear how the actual spread of IE3 motors in Japan is and how much CO₂ reduction by the improvement of energy efficiency has been achieved. In this report, with the cooperation of member companies, the situation of switching to IE3 motor and the CO₂ reduction effect will be studied at The Japan Electrical Manufacturers' Association (JEMA, general incorporated association), which is a group of motor manufactures.

First, we will check the proportion of JEMA member companies in Japan overall, where the statistics of METI and the scope of aggregation agree. Table 1 compares the statistics of a standard three-phase motor (0.2–37 kW) and a non-standard three-phase motor (0.07–75 kW). On average from 2010 to 2017, the proportion of JEMA statistics accounts for 70% of the figures of METI statistics. In other words,

Table 1 Statistics of three-phase induction motor

Monthly average	JEMA Self-report A (Unit)	METI Dynamic statistics of production B (Unit)	Cover ratio A/B (%)
FY2010	166,769	204,247	82
FY2011	177,565	241,991	73
FY2012	157,633	246,985	64
FY2013	163,129	217,518	75
FY2014	182,463	246,232	74
FY2015	141,904	224,330	63
FY2016	139,643	208,306	67
FY2017	150,340	230,008	65
Avg	159,931	227,452	70

Standard three-phase (0.2–37 kW) shipment + Non-Standard three-phase (0.07–75 kW) production Monthly average

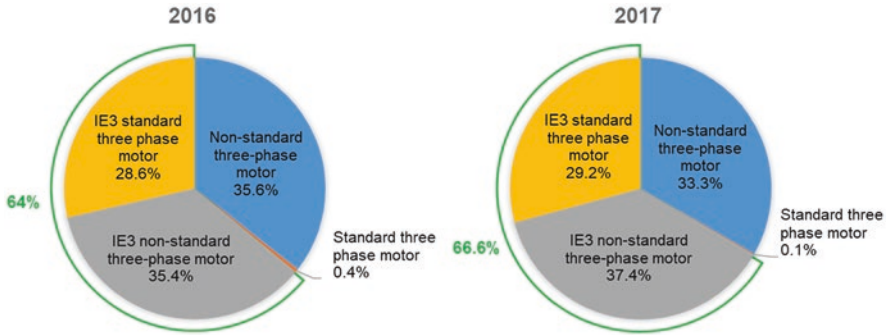


Fig. 7 IE3 ratios of 0.75 to 75 kW motor in FY 2016 and 2017 by JEMA member self-reporting

it accounts for 70% of shipments in Japan, and the analysis of JEMA member reports is effective as an analysis of the Japanese market [4].

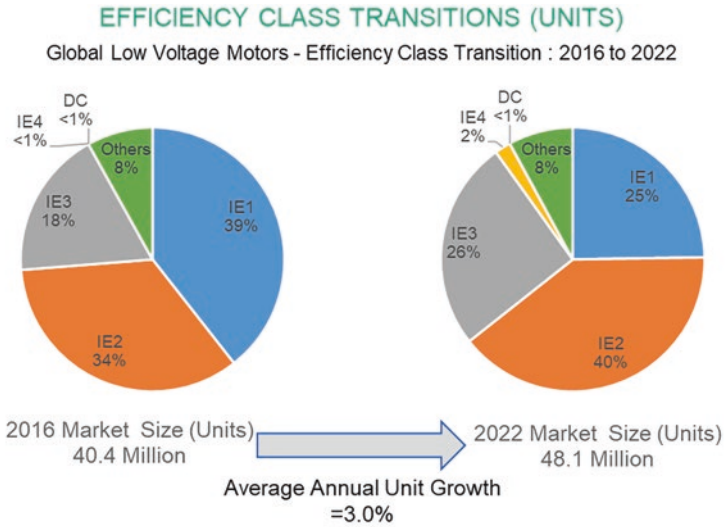
2.2.1 Ratio of IE3 Motors

Figure 7 shows IE3 ratios of 0.75 to 75 kW motor in FY 2016 and 2017 by JEMA member self-reporting. This figure shows that the IE3 ratio in the Japanese motor market is 64% in FY2016 and 66.6% in FY2017. On the other hand, Fig. 8 shows the global distribution by motor efficiency. This figure shows that the IE4 ratio is less than 1%, the IE3 ratio is 18%, and both are less than 19%. Therefore, IE3 penetration in Japan is considered to be in the leading area internationally, even though the start of regulation was delayed.

2.2.2 Consideration of the Cause Why IE3 Does Not Progress

The percentage of motors to which the IE3 motor is not applied is 33% in 2017. Among these motors, the ratio of the special motors of the items (1) to (10) in Fig. 4 is several percent. It is difficult to apply IE3 motor in these fields. In addition, the number of motors completely incorporated into machines in Sect. 2.1 is counted as the number of motor productions, and it is considered that many machines incorporate IE1 motors. Also, even if the IE3 motor is mounted, it is not counted as IE3 motor number because it is not subject to regulation.

One of the main cases that is not subject to IE3 regulation is shown in Fig. 9. In this figure, case 2 described in “about the explanation of the three-phase induction motor”, which was notified in 2015, is shown. Case 2: Company A incorporates an industrial motor manufactured by itself into another machine and ships it as a component, that is, in the case of self-manufacture. In case 2, although the number of motors produced is counted, even if the IE3 motor is used, it is not counted as the number of IE3 motors because it is out of regulation. Therefore, in this case, the IE3



IE1 motors drastically reduced in shipments from 2014 to 2017 (46% share to 37%, respectively), largely due to increased focus on efficiency in Western Europe, North America, and China.

Compliance, emerging technologies are potential headwinds going forward

Fig. 8 Ratio by motor efficiency class. (Source: IHS Markit “Current trends in the market for industrial motors and drives” Motor Summit 2018 International, Zurich Switzerland, 14/15 November 2018)

[Case2] The same company (company A) incorporates the industrial motor manufactured in Japan into another machine and ships it as a component (self-manufacture)

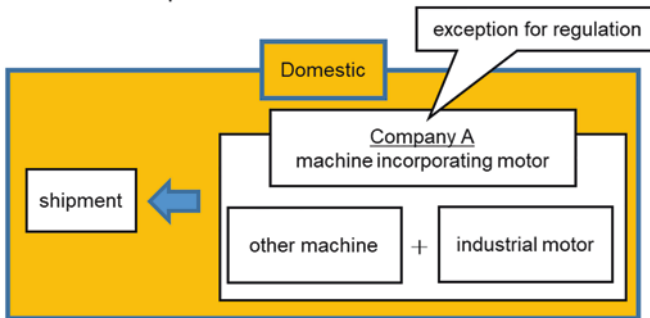


Fig. 9 Case 2: self-manufacture

ratio is pushed down. However, the actual energy consumption efficiency is not a problem because it exhibits the efficiency of the IE3 motor and contributes to energy saving, which is the original purpose.

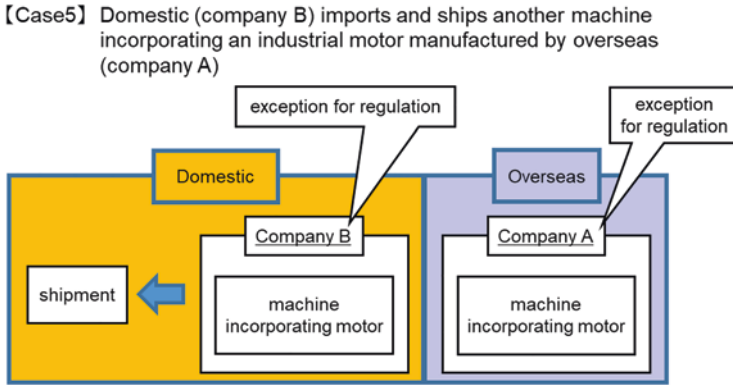


Fig. 10 Case 5: import of machine incorporating motor

Another major case that is not subject to IE3 regulation is shown in Fig. 10. Case 5: A domestic company B imports and ships a machine incorporated with an industrial motor manufactured by a foreign company A. Therefore, in this case, even if the machine is equipped with the IE1 motor and is not subject to regulation, inefficient motors will continue to be used.

However, the subcommittee of the Comprehensive Resources and Energy Research Committee Energy Conservation Standards makes recommendations on energy conservation in the final report (June 2013) [5]. Based on these recommendations, the following two points are requested by those engaged in the business of manufacturing, importing or selling energy consumption equipment:

1. Strive to manufacture and to import machines incorporating a three-phase induction motor with high energy efficiency.
2. Strive to provide appropriate information so that the buyer can select a machine incorporating a three-phase induction motor with excellent energy-saving performance.

Furthermore, under the Energy Conservation Law, not only motor efficiency regulations but also factories and offices that use energy are obliged to reduce the energy consumption rate by 1% or more every year. For this reason, inefficient machines are likely to be eliminated in the market.

2.2.3 Energy-Saving Achievement Level

Table 2 shows the energy efficiency achievement of the Top Runner scheme motor. Since the Top Runner regulation adopts CAS instead of MEPS, the calculation of the number of shipments and the average energy efficiency includes motors that do not satisfy the regulation efficiency alone, including the IE1 motor. The average efficiency weighted by each output and unit achieved the average value of the standard efficiency defined in the Top Runner standard, and the achievement rate was

Table 2 Top Runner motor energy-saving achievement level

Yearly total number				
	Shipment	Energy efficiency	Top Runner standard efficiency	Standard achievement ratio
FY	(Unit)	(%)	(%)	(%)
2015	679,073	89.3	87.7	101.8
2016	755,353	89.3	87.6	101.9
2017	844,338	89.2	87.7	101.6

101.6% in the value of FY2017. Therefore, the energy efficiency value by Top Runner regulation is also improved 1.6% (101.6% -100% = 1.6%) on average from IE3 level.

The efficiency values assumed at the time of considering Top Runner regulations are as follows.

Average efficiency per unit weighted average in FY2010 (base year): 81.1%.

Average efficiency per unit expected in FY2015 (target year): 87.1%.

The effect when all approximately 100 million motors prevailing in the country are replaced by IE3 is 15.5 billion kWh per year, approximately five million t-CO₂.

[Source: Comprehensive Resource and Energy Survey Committee Energy Conservation Standards Subcommittee Three-phase Induction Motor Judgment Subcommittee Final Report].

The energy-saving effect is calculated based on the premise that shipments for 15 years are widespread in Japan, and approximately 100 million motors will be replaced by IE3. In addition, the average operating time at that time: 4263 h, the operating load factor was 64%. (CO₂ emission basic unit: 0.34 kg-CO₂ / kWh).

[Source: Agency for Natural Resources and Energy “2009 Energy Consumption Equipment Survey Report”].

The target effect for the year is 15.5 billion kWh/15 year = 1.033 billion kWh, about five million t-CO₂/15 year = about 333,000 t-CO₂: 0.333 million t-CO₂.

Using these, we will roughly verify the energy-saving results for FY2017. From JEMA survey results, IE3 motor shipment total output capacity in FY2017.

Total output capacity = 3,972,696 kW.

The efficiency value of 81.1% in 2010, the base year, is defined as *Efficiency1*. When the efficiency stays at *Efficiency1*, the annual energy required to operate the IE3 motor is defined as *Input Energy1*. First, the *Input Energy1* is calculated using the relationship of.

$$Input = \frac{Output}{Efficiency}$$

$$Input\ Energy1 = \frac{Total\ output\ capacity \times Average\ operating\ time \times Operating\ load\ factor}{Efficiency1}$$

$$= \frac{3,972,696 \times 4,263 \times 64\%}{81.1\%} = 13,364,717,572 \text{ kWh}$$

On the other hand, the efficiency in FY2017 has actually improved to 87.7% (see Table 2). This efficiency value is defined as *Efficiency2*. The annual energy required to operate the IE3 motor when the efficiency value is improved is defined as *Input Energy2*. Next, the *Input Energy2* is calculated.

$$\begin{aligned} \text{Input Energy2} &= \frac{\text{Total output capacity} \times \text{Average operating time} \times \text{Operating load factor}}{\text{Efficiency2}} \\ &= \frac{3,972,696 \times 4,263 \times 64\%}{87.7\%} = 12,358,934,950 \text{ kWh} \end{aligned}$$

The required amount of electric power is reduced from *Input Energy1* to *Input Energy2* by improving the motor efficiency. That is, the energy-saving effect is the difference between *Input Energy1* and *Input Energy2*. This is expressed as follows.

$$\begin{aligned} \text{Energy - saving effect} &= \text{Input Energy1} - \text{Input Energy2} \\ &= 13,364,717,572 - 12,358,934,950 \\ &= 1,005,782,622 \text{ kWh} : 1.01 \text{ billion kWh} \end{aligned}$$

Furthermore, the CO₂ reduction effect is calculated using the value of above energy-saving effect and CO₂ emission basic unit: 0.34 kg-CO₂ / kWh.

CO₂ reduction effect: 1,005,782,622 * 0.34 = 341,966,092 kg-CO₂: 342,000 t-CO₂

In other words, the CO₂ reduction effect is 0.342 million t-CO₂. This means it achieved the target effect of 0.333 million t-CO₂.

Although it is approximate, the initial energy-saving effect has been achieved. Although the number of IE3 motors manufactured is decreasing, this is because low-power models with inefficiency have been replaced by PM motors. The efficiency value has also improved as the ratio of high-power models with high efficiency value has increased. Therefore, the target energy-saving effect was achieved.

Figure 11 shows the transition of energy-derived CO₂ emissions. The CO₂ reduction amount of manufacturing sector from 2016 to 2017 is five million t-CO₂, and contribution by IE3 motor is an effect of 0.342 / 5 * 100 = 6.8%. It shows that Top Runner motor regulation is effective for CO₂ reduction in manufacturing sector.

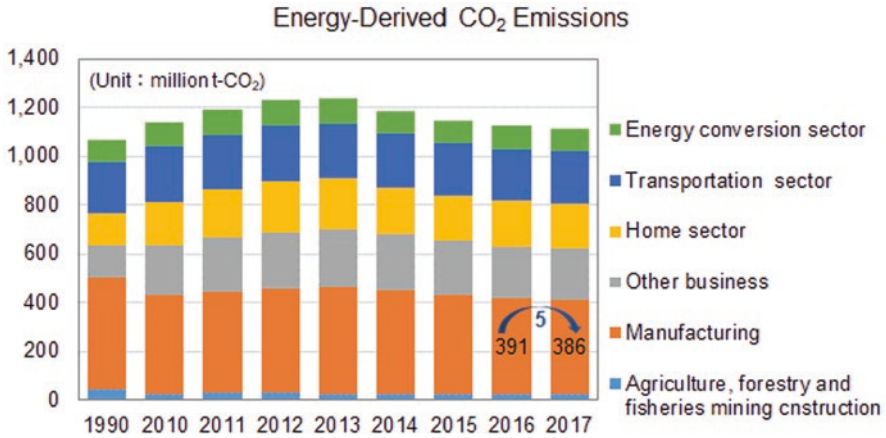


Fig. 11 Transition of energy-derived CO₂ emissions

3 Conclusion

1. The Top Runner regulation of the motor started from FY2015 promotes the switch to IE3 motor. In addition, the transition to a PM motor with energy-saving effects of both high efficiency and variable speed drive (VSD) is also in progress.
2. As a result of analysis by JEMA member companies that account for about 70% of the motor market in Japan, the switching ratio to IE3 motor is 66.6%. Despite the delayed start of regulation, the application rate of IE3 motors in the Japanese market has improved.
3. The energy efficiency value by the Top Runner regulation is also improved 1.6% on average from IE3 level.
4. The CO₂ reduction amount from 2017 shipment of Top Runner motor is 0.342 million t-CO₂. It achieved the target reduction: 0.333 million t-CO₂.
5. Next stage: There is still a share of 33% of motors in Japan which do not comply to the regulation. The target is to bring built-in motors and motors installed in other facilities into the Top Runner motor regulation.

References

1. Ministry of Economy, Trade and Industry *YEARBOOK OF CURRENT PRODUCTION STATISTICS MACHINERY Rotating electrical machineries* (2017)
2. Y. Shibata, *The Status Quo of Electric Motor Energy Standard Setting and “Top Runner” Experience in Japan* (EEMODS 2013)
3. O. Takeshi, *Motor Drive and Energy Conservation Activities in Japan* (EEMODS 2011)
4. “Top Runner Program” (March 2015). https://www.enecho.meti.go.jp/category/saving_and_new/saving/enterprise/overview/pdf/toprunner2015e.pdf
5. “Final Report by Three-phase Induction Motor Evaluation Standards Subcommittee, Energy Efficiency Standards Subcommittee of the Advisory Committee for Natural Resources and Energy”, (June 28 2013, Ministry of Economy, Trade and Industry, Japan)

The Market of Electric Motors, Pumps and Fans in the European Union and in Switzerland



Rita Werle, Conrad U. Brunner, Rolf Tieben, Petar Klingel,
and Richard Phillips

1 Background

Motor systems represent a large share of global and Swiss electricity consumption (around 50%) [2]. More than half of this is for industrial applications and building technology in the service sector including infrastructure facilities, commercial applications, etc. In the industrial sector, motor systems are responsible for more than 70% of electric energy consumption in Switzerland and worldwide [2, 7].

The Swiss Topmotors programme, managed by Impact Energy, has been promoting efficient motor systems, pumps, fans, compressors, transport and process machines since 2007 with the support of the Swiss Federal Office of Energy (SFOE).

2 Goal

The SFOE is the public regulator for establishing and implementing minimum energy performance standards (MEPS) for energy-using products and for their market surveillance. The SFOE closely monitors market developments for all energy-using products. In the case of motor systems, it is especially focused on motors, circulator pumps, water pumps and fans which are subject to MEPS. It is important to monitor

R. Werle (✉) · C. U. Brunner · R. Tieben · P. Klingel
Impact Energy Inc., Zurich, Switzerland
e-mail: rita.werle@impact-energy.ch; cub@cub.ch; rolf.tieben@impact-energy.ch;
petar.klingel@impact-energy.ch

R. Phillips
Impact Energy Inc., Zurich, Switzerland

Swiss Federal Office of Energy, Berne, Switzerland
e-mail: richard.phillips@bfe.admin.ch

the market transformation towards energy-efficient equipment and especially the effect of MEPS, to verify the success and effectiveness of policy instruments, sharpen their scope and advance the requirements if necessary [3, 4, 5, 6].

The Topmotors Market Report was first launched in 2017 to research the sales, the efficiency (MEPS compliance), the availability and the price of electric motors and the price of VFDs in Switzerland [1]. The goal was to cover at least 50% of the market with available data. The Topmotors Market Report is published annually to inform the SFOE and all interested stakeholders on the status of the market development. This chapter summarizes the findings of the second Topmotors Market Report 2018 [9].

3 Scope

The Topmotors Market Report 2018 covers sales data from 2017 of electric motors and price data from 2017 for motors and VFDs. In addition, it also covers market data on the sale of circulators, water pumps and fans in Switzerland and in the European Union from 2017.

In Switzerland, MEPS are in effect in line with the Efficiency ordinance (EnEV) for motors, circulators and water pumps and are fully synchronized with the respective European Ecodesign Directive (see Table 1).

From 1 January 2017, the following criteria apply to electric motors within the scope of MEPS in Switzerland, as laid out in Annex 2.7 of the Swiss Energy Efficiency Ordinance:

- Scope:
 - Motors with nominal output power of minimum 0.75 kW up to maximum 375 kW.
 - 2-, 4-, 6- poles
- Minimum requirement (energy efficiency class as defined in IEC 60034-30-1) of either:
 - Efficiency class IE3.
 - IE2 sold in combination with a VFD.

As before, the energy efficiency of electric motors has been defined and is measured since 2014 by IEC 60034-30-1 from 0.12 kW to 1000 kW for 2-, 4-, 6-, and 8-pole motors under 1000 V.

Table 1 MEPS in the European Union and in Switzerland

Product	European Union: Ecodesign directive, regulation no./year	Switzerland: Efficiency ordinance (EnEV), Annex no.
Motor	640/2009	2.7
Circulator	641/2009	2.8
Water pump	547/2012	2.9
Fan	327/2011	2.6

4 Methodology

In order to ensure impartial, scientific and anonymous market research, the SFOE mandated Impact Energy to conduct the market research. Impact Energy commissioned IHS Markit, a global market research agency with know-how expertise and experience for industrial products. IHS Markit's primary task was interacting with the industrial companies that manufacture, import or sell the products to large end users, original equipment manufacturers (OEMs) and wholesalers. It is not possible to ascertain how many of these products were purchased as standalones or eventually integrated into machines and exported abroad from Switzerland.

The survey was sent out with a questionnaire in spring 2018 to a total of 59 companies involved in motors, pumps, fans and VFDs in Switzerland. Useful answers for the research could be derived from 18 leading companies (including all large international manufacturers), three of which are manufacturing in Switzerland. The direct findings of the survey cover around 60% of the market volume. The full market data is an estimate based on the survey and calculated data from Switzerland and other European countries. The sales data were collected by IHS Markit and anonymized. Companies surveyed were informed about the purpose of the research, clearly stating that the data gathered would be kept confidential and used in an anonymous manner. The subsequent data evaluation work by Impact Energy was based on anonymous files.

The reliability of the data gathered is satisfactory, as it covers more than the planned 50% of the market. At the same time, it must be evaluated critically, as the research findings are based on self-declared data by manufacturers complemented by IHS Markit estimates for the entire Swiss market based on larger samples in Europe.

The findings for motors and VFDs, which were surveyed for the second time in 2018, show consistent data. For pumps and fans, which were surveyed for the first time in 2018, data consistency can only be verified in coming years. The goal for the coming years is to increase the quality and reliability of the raw data and their evaluation, which can also be achieved by having more companies participate in the survey.

The motors' electric energy consumption was estimated:

- Average configuration of 4500 operating hours per year.
- Annual average load factor of 0.7.
- The respective efficiency of each class.

As the available data on the size of pumps and fans is scarce, it is not possible to calculate their energy consumption.

5 Motors in Switzerland

The total number of electric motors sold in Switzerland in 2017 was 177,786 (see Table 2).

It is interesting to see how the number and electricity consumption of all motors sold in 2017 in Switzerland compare (see Figs. 1 and 2). While 59.4% of the motors sold were below 0.75 kW, these only account for 5.1% of the total electricity consumption of motors in Switzerland. At the same time, 40.5% of motors sold were between 0.75 and 375 kW and accounted for 82.4% of the total electricity consumption of motors in Switzerland, being clearly the most significant size group in terms of electricity consumption.

Figure 3 shows the distribution of motors sold by efficiency class. For the smaller motors falling outside the scope of the MEPS (e.g. below 0.75 kW), the units sold were on average of lower efficiency (e.g. higher share of IE2 and IE1 motors).

Table 2 Quantities for 2017, motor output and electricity consumption by size (all numbers of poles)

Motors sold in Switzerland 2017 Nominal output power (kW)	Quantity		Motor output (mech.)		Electricity consumption	
	Number	Share	MW _{mech}	Share	GWh/a	Share
0.12–0.75 kW	105,641	59.4%	40	4.0%	175	5.1%
> 0.75–375 kW	71,931	40.5%	829	82.9%	2827	82.4%
> 375–1000 kW	214	0.1%	131	13.1%	430	12.5%
Total	177,786	100.0%	1'000	100.0%	3'432	100.0%

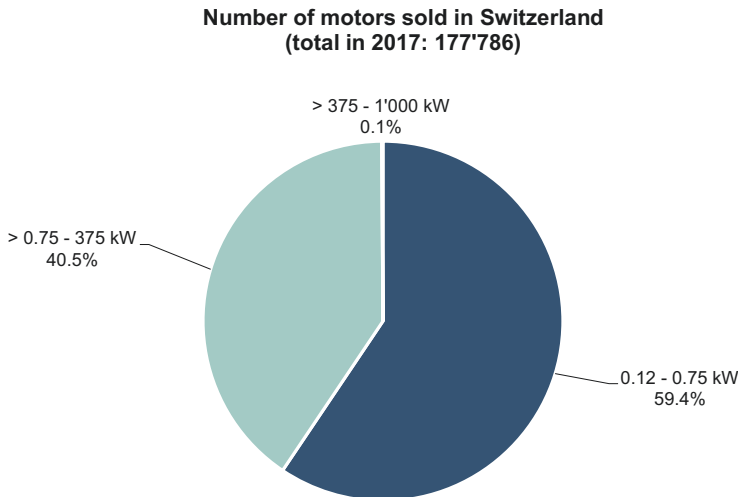
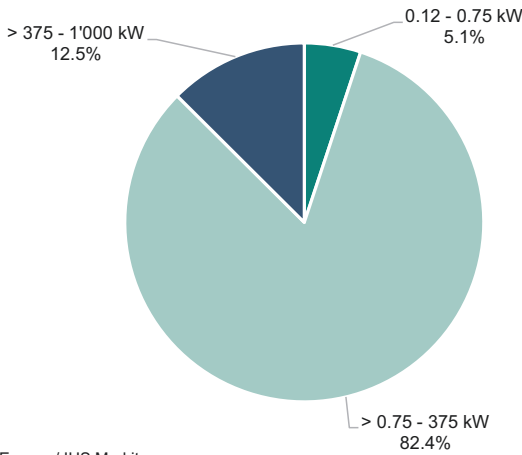


Fig. 1 Number of motors sold in Switzerland in 2017 by size

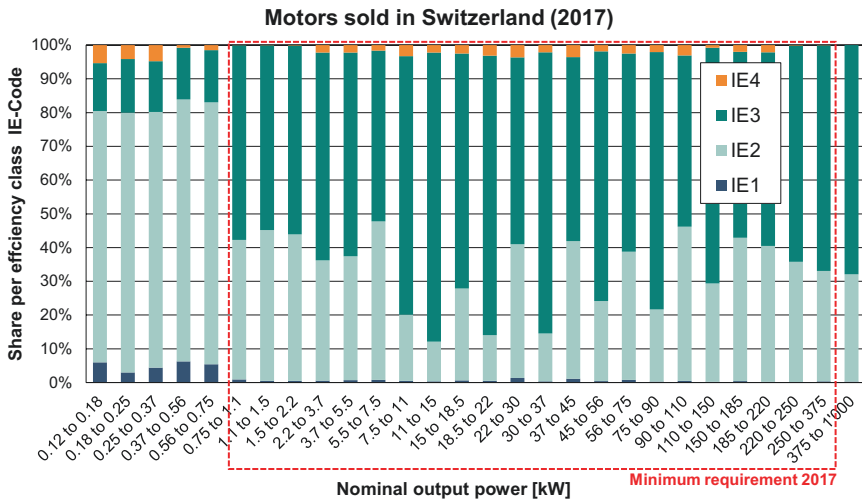
**Electricity consumption of motors sold in Switzerland
(total in 2017: 3'432 GWh/a)**



© 2018 Impact Energy / IHS Markit



Fig. 2 Motors sold in Switzerland in 2017: electricity consumption by size



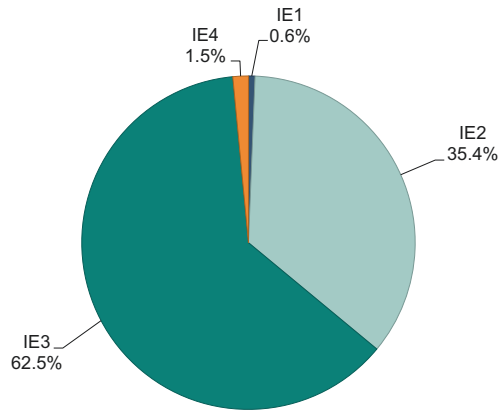
© 2018 Impact Energy / IHS Markit



Fig. 3 Efficiency class by size of motors sold in Switzerland in 2017

From the total 177,786 motors sold in 2017, 70,143 (39.5%) were within the scope of MEPS (0.75–375 kW nominal output power and 2-, 4-, 6-poles). The motors in scope account for 81.0% of electricity consumption of all motors sold. Out of the motors in scope, it is assumed that 57,292 or 81.7% met the 2017 MEPS.

**Efficiency of motors sold in Switzerland
(in scope in 2017 0.75 kW to 375 kW)**



© 2018 Impact Energy / IHS Markit

TOPMOTORS

Fig. 4 Motors sold by efficiency class within the scope of MEPS in Switzerland in 2017 (0.75–375 kW, 2-, 4-, 6-poles)

The detailed findings are as follows (see Fig. 4):

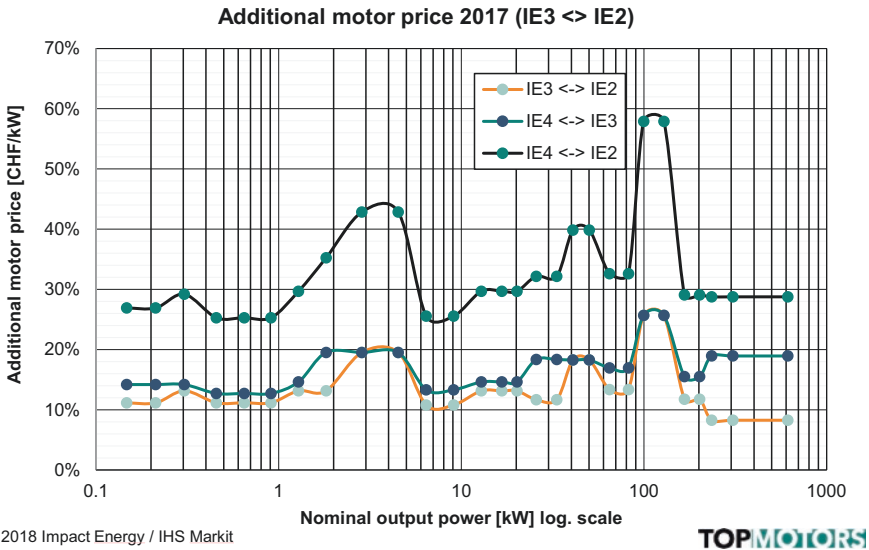
1. It should be emphasized that some of the motors sold in 2017 did not have to comply with the MEPS as they were outside the scope (e.g. not capable of continuous operation, brake motors, designed to operate in potentially explosive atmospheres, etc.) as defined in the Ecodesign Regulation No. 640/2009.
2. 0.6% of the motors sold were IE1; those under the scope of MEPS did not comply with the MEPS.
3. 64.0% of the motors sold were IE3 and IE4 and complied with the MEPS.
4. 35.4% of the motors sold were IE2. It cannot be accurately determined to what percentage they met the MEPS, while it is assumed that they did so to a large extent, taking into account the following assumptions and considerations:
 - (a) It is assumed that 50% of the IE2 motors were sold together with a VFD (according to the regulation in effect, IE2 in combination with a VFD is acceptable as a substitute for IE3) and hence complied to the MEPS.
 - (b) Some of the motors are not under the scope of MEPS as mentioned in point 1.

6 Motor and VFD Prices in Switzerland

The Topmotors Market Report 2018 gives the motor and VFD prices for the year 2017 (Table 3 and Fig. 6).

Table 3 Average specific motor prices USD/kW by efficiency class for 2017 (linear average value for 28 size classes)

Specific price 2017 (USD/kW)		
IE2	IE3	IE4
180	204	237



© 2018 Impact Energy / IHS Markit



Fig. 5 Additional motor price by size category

The price premium for more efficient motors (IE3 and IE4) as compared with standard motors (IE2) was surveyed by motor size. Motor prices were subdivided into 28 size categories. The three curves compared are shown in Fig. 5:

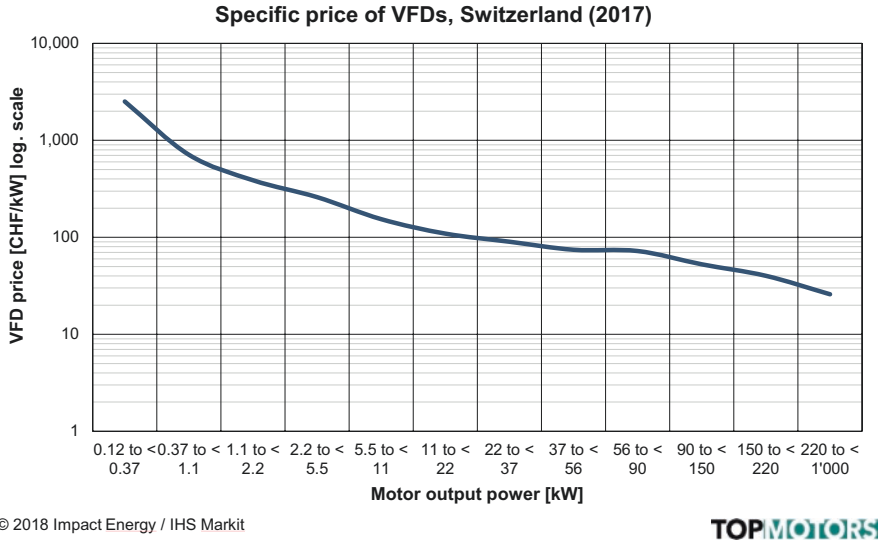
- IE3 as compared with IE2.
- IE4 as compared with IE3.
- IE4 as compared with IE2.

The cost differential varies significantly depending on nominal output power. The highest price premiums are for 1.5–5 kW and for 90–150 kW (Fig. 5).

The average specific prices of VFDs rose by 5% in 2017 compared to 2016 (see Table 4).

7 Circulators in Switzerland and in the EU

Glandless circulators are used to circulate water in a closed circuit, primarily in heating systems but also in cooling systems and other types of systems (they are not used for drinking water or waste water). In accordance with the EU’s 2009 Ecodesign



© 2018 Impact Energy / IHS Markit



Fig. 6 Specific price of VFDs in Switzerland in 2017

Table 4 Average specific VFD prices in 2016 and 2017 (linear average value for 12 size classes)

Price of Variable Frequency Drives (USD/kW) average	
2016	356.6
2017	374.3
Additional price 2017/2016	+5.0%

Regulation No. 641, a glandless circulator is a circulator where the shaft of the motor is directly coupled to the impeller and the motor is immersed in the pumped medium.

The Ecodesign Regulation for glandless circulators with hydraulic power between 1 and 2500 W has been in force in Europe since 2013. The Regulation was tightened in 2015. The implementation of this Regulation in Europe, and subsequently in Switzerland, prompted a major development in the market, which had a significant impact on energy considerations. The original technology was launched in Switzerland in 1993 by Jürg Nipkow.¹ The minimum requirements can only be met by using an integrated, high-efficiency pump, consisting of a variable frequency drive (VFD), permanent magnet motor and an efficient impeller.

In 2017, 398,870 circulators (integrated and non-integrated) were sold in Switzerland. Of these, 98.4% had an energy efficiency index (EEI) of ≤ 0.23 , that is,

¹Jürg Nipkow, Klein-Umwälzpumpe mit hohem Wirkungsgrad, Swiss Federal Office of Energy, 1994

Table 5 Pump sales in Switzerland and in the EU in 2017: circulators (integrated and nonintegrated)

	CH – compliance: 98.4%		EU – compliance: 91.3%	
	Switzerland		European Union	
Circulator	Number	Share	Number	Share
EEI > 0.23	6,236	1.6%	1,566,384	8.7%
EEI ≤ 0.23	392,634	98.4%	16,341,983	91.3%
Total	398,870	100.0%	17,908,367	100.0%
CH as share of EU	2.2%			

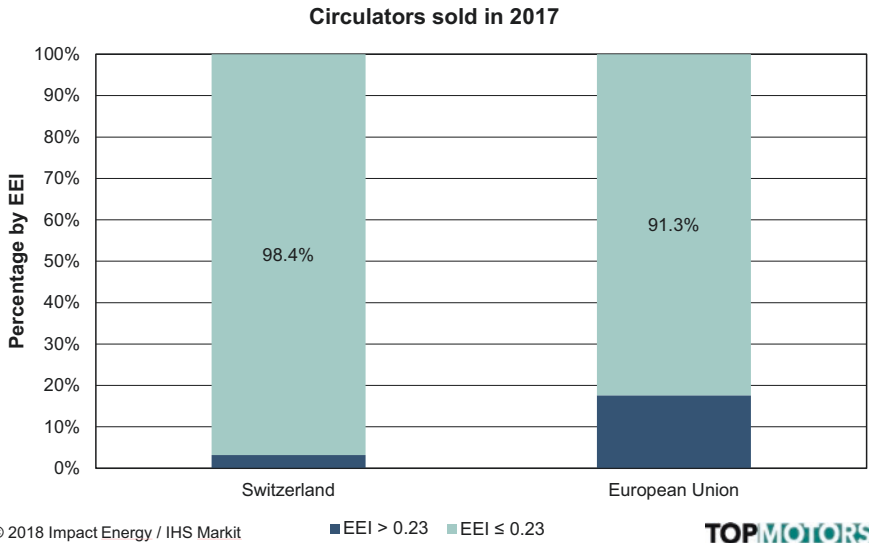


Fig. 7 Share of sales of circulators according to EEI (≤ 0.23 is the minimum requirement for Switzerland and the EU)

they satisfied the minimum requirements of Annex 2.8 of the Swiss Energy Efficiency Ordinance (EnEV) for circulators with less than $2500 W_{hydr}$. The share of circulator sales in Switzerland is equivalent to 2.2% of the units sold in the European circulator market.

In 2017, 17,908,367 circulators (integrated and non-integrated) were sold in the European Union. Of these, 91.3% had an EEI of ≤ 0.23 , that is, they satisfied the prevailing minimum requirements of EU Ecodesign Regulation 641/2009 (Table 5).

The market transformation towards new, high-efficiency circulators can be described as exemplary. The development of the new technology of efficient circulators was followed by a rapid transformation of the market, first supported by a voluntary labelling programme. The circulator market was completely changed by a new, efficient technology within 20 years (Fig. 7).

8 Water Pumps in Switzerland and in the EU

Glanded water pumps are used in many different ways to transport liquids. Clean water is paramount (i.e. neither wastewater nor drinking water), axial, multistage and submersible pumps are used. The terminology of the five types of water pumps with a capacity of less than 150 kW, as specified by EU Ecodesign Regulation No. 547/2012 and also referred to in Annex 2.9 of the EnEV, are not yet very common among pump manufacturers and retailers (although this Regulation was adopted in 2012 and has been in force since 2013). According to IHS Markit, therefore, the relevant findings must be treated with some caution.

A distinction is made between the following five types of water pumps in the Regulation:

- ESOB: end suction own bearing.
- ESCC: end suction close coupled.
- ESCCi: end suction close coupled inline.
- MS-V: vertical multistage.
- MSS: submersible multistage.

In 2017, 51,577 water pumps were sold in Switzerland. The vast majority of them met the minimum requirement of a minimum efficiency index (MEI) of ≥ 0.4 as set out in Annex 2.9 of the EnEV. Some pumps were even available with the higher MEI value of 0.7. Most of the pumps (91.0%) were smaller than 10 kW, and frequently were smaller than 2 kW. The share of water pump sales in Switzerland is equivalent to 1.9% of the units sold in the European water pump market (Table 6).

A surprisingly high proportion (39.8%) of water pumps sold in Switzerland are submersible multistage pumps (MSS); in the EU, the figure is as high as 45% (Fig. 8). These permanently installed or mobile pumps are used for a wide range of purposes, such as supplying water, irrigation (e.g. in agriculture), construction, swimming pools and aquariums. They are also used by fire services and disaster management personnel. This is clearly an important market segment. However, no ISO standards currently exist for submersible pumps, nor are there any IEC standards for electric motors in submersed applications.

Table 6 Pump sales in Switzerland and in the EU in 2017: water pumps

Water pump	Switzerland		European Union	
	Number	Share	Number	Share
< 10 kW	46,934	91.0%	2,335,671	85.4%
> 10 kW	4643	9.0%	400,717	14.6%
Total	51,577	100.0%	2,736,388	100.0%
CH share EU	1.9%			

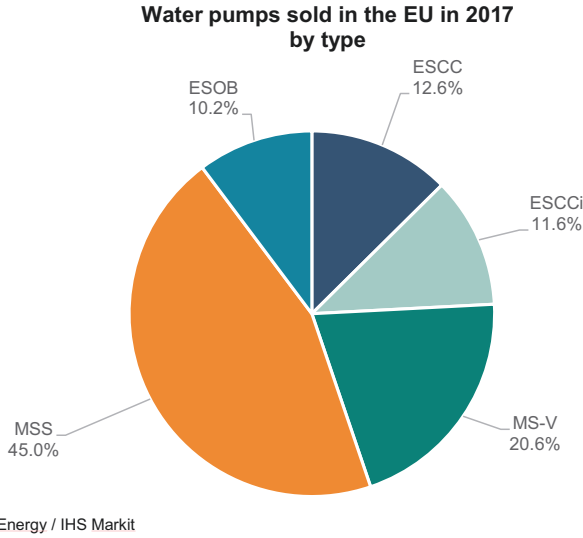


Fig. 8 Water pumps sold in the EU in 2017 by type

In 2017, 2,736,388 water pumps were sold in the EU. Of these, 85.4% were smaller than 10 kW. There are no precise figures for the share of pumps that meet the minimum requirement of a MEI of ≥ 0.4 as specified by EU Ecodesign Directive No. 547/2012.

9 Fans in Switzerland and in the EU

A distinction is made between the following six fan types in the EU Ecodesign Regulation No. 327/2011:

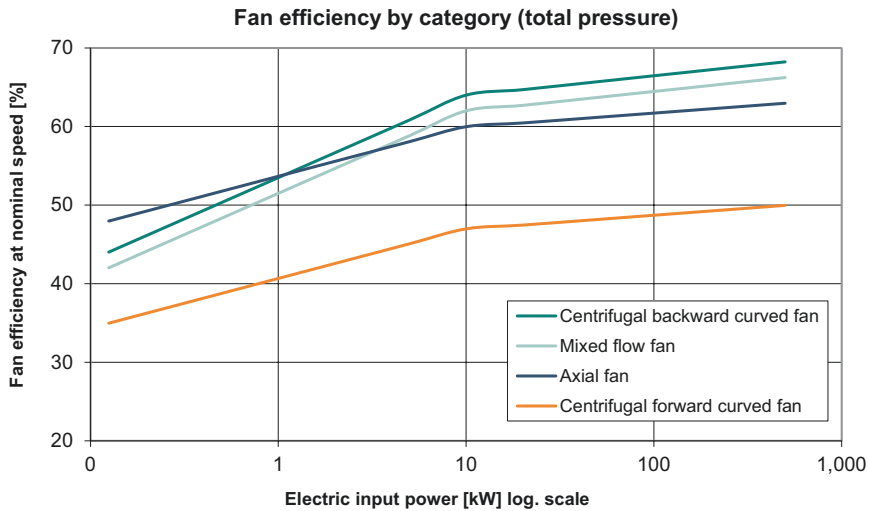
- Axial fans.
- Centrifugal forward-curved fans and centrifugal radial-bladed fans.
- Centrifugal backward-curved fans without housing.
- Centrifugal backward-curved fans with housing.
- Mixed flow fans.
- Cross flow fans.

In 2017, 115,647 fans were sold in Switzerland. Of these, 83.4% were smaller than 10 kW. Approximately, 30% of the fans were used in homes, 50% were used in the service sector and 20% was used in industry. The fans sold in Switzerland account for 1.0% of all fans sold in the EU.

In 2017, 11,616,614 fans were sold in the EU. Of these, 82.5% were smaller than 10 kW (Table 7). Approximately 32% of the fans were used in households, 49% were used in the service sector, and 19% were used in industry. The share of fans that meet the minimum requirements set out by EU Ecodesign Regulation No. 327/2011 is not known.

Table 7 Total fan sales in Switzerland and in the EU in 2017

Fan	Switzerland		European Union	
	Number	Share	Number	Share
< 10 kW	96,415	83.4%	9,587,536	82.5%
> 10 kW	19,232	16.6%	2,029,078	17.5%
Total	115,647	100%	11,616,614	100%
CH share EU	1.0%			



© 2018 Impact Energy



Fig. 9 Fan efficiency by type and size at maximum speed in accordance with EU Ecodesign Regulation No. 327/2011

Axial fans have the largest market share in Switzerland with 56% (54% in the EU). The more efficient, backward-curved fans have a market share of some 19% in Switzerland (18% in the EU).

Figure 9 shows the fan efficiency of the four different basic fan types (Fig. 9).

10 Observations and Recommendations

This study is the second of its kind to be conducted in Switzerland. The motor section in the Topmotors Market Report 2017 was enhanced and refined. The section on pumps and fans is new, as is the comparison with EU data.

The findings for the development of elements subject to minimum requirements in Switzerland are promising and must be monitored annually. The high share of IE3 and IE4 motors as well as the very high level of circulators is a positive confirmation of the ongoing market transformation. The available data for water pumps and fans are less clear to judge the state of the market transformation.

For motors, the expected entry into force of a revised Regulation no. 640 of the Ecodesign Directive means changes from 2021 (and in a second tier from 2023), establishing minimum requirements also for smaller (from 0.12 kW) and larger (up to 1000 kW) motors as well as for VFDs.

For pumps and fans, this data, which has been collected for the first time, and the development of market shares, should be pursued in the coming years. In the case of fans in particular, market stimulation is needed for promoting the use of backward-curved fans with increased efficiency.

11 Outlook

The third Topmotors Market Report 2019 is currently under preparation and will be published in 2020, including data on motors and VFDs in Switzerland and in the European Union as well as the analysis on pumps and fans in both Switzerland and in the European Union.

References

1. Swiss Federal Office of Energy: Topmotors Market Report 2017, Berne Switzerland 2018
2. P. Waide, C.U. Brunner, et al., *Energy-Efficiency Policy Opportunities for Electric Motor-Driven Systems*, International Energy Agency (IEA) (Paris, France, 2011)
3. K. Kulterer, R. Werle, P. Lackner, et al., *Policy Guidelines for Electric Motor Systems – Part 2: Toolkit for Policy Makers*, October 2014
4. 4E Energy efficiency roadmap for electric motors and motor systems, November 2015
5. van M. Werkhoven, R. Werle, C. U. Brunner: *4E EMSA Policy Guidelines for Motor Driven Units – Part 1: Analysis of standards and regulations for pumps, fans and compressors*, October 2016
6. van M. Werkhoven, R. Werle, C. U. Brunner: *4E EMSA Policy Guidelines for Motor Driven Units – Part 2: Recommendations for aligning standards and regulations for pumps, fans and compressors*, May 2018
7. R. Tieben, R. Werle, C.U. Brunner, EASY- Lessons learned from four years of the Swiss EASY audit and incentive program, in *Proceedings of the International Conference on Energy Efficiency in Motor Driven Systems, Helsinki, Finland, 15.–17, (September 2015)*
8. C. Barthel, J. Nipkow, B. Schäppi, et al.: Energy+ pumps – Technology procurement for very energy efficient circulation pumps, first results of the current IEE-project, in: ECEEE Summer Studies, conference proceedings, La Colle sur Loup, Côte d'Azur, France, 2007
9. Swiss Federal Office of Energy: Topmotors Market Report 2018, Berne Switzerland, 2019

Pilot Audit Program for Electric Motor-Driven Systems



Maarten van Werkhoven and Frank Hartkamp

1 Background

Efficient electric motor-driven systems (EMDS) can deliver an important contribution to achieving national energy savings and CO₂ emission reduction targets. In the Netherlands the savings potential on industrial electricity consumption is more than 15%, or 24.7 PJ [1]. This is equivalent to 6% of the national electricity consumption in the Netherlands. The International Energy Agency shows an industrial savings potential of 24% in the long term [2].

These saving opportunities require additional policies: that is, going beyond the current EU Ecodesign Guidelines for electric motors, for example, and further than the existing measure lists¹ from the national energy saving policy, where the realization of system savings for drives has lagged behind.

According to the current EU MEPS for electric motors (Ecodesign Directive), new motors must meet minimum efficiency requirements IE2 + frequency inverter or IE3 in the power range 0.75–375 kW. MEPS for fans, clean water pumps, and circulation pumps are also in force; a directive is being prepared for air compressors. The current MEPS are at the level of products [3]; system optimizations can bring greater savings especially when high-efficient components are used as well, i.e., IE4 motors, VSDs, controls, and high-efficient applications like pumps, fans,

¹The Dutch government uses a “Standard Savings Measure List” to specify savings measures per sector. Companies have to comply to this list, i.e., assess the economic and technical viability of these measures for their company and report back to the MSA.

M. van Werkhoven (✉)
TPA Advisors, Amsterdam, The Netherlands
e-mail: mvanwerkhoven@tpabv.nl

F. Hartkamp
Netherlands Enterprise Agency RVO, The Hague, The Netherlands
e-mail: frank.hartkamp@rvo.nl

and compressors in utilities and in process applications. These components can be used cost-effectively in many situations [4] (see Fig. 1).

The Dutch Knowledge Network for efficient electric motor-driven systems (KEEA, a collaboration between three trade associations and government: Techniek Nederland, FEDA, HPG and RVO²) sees good opportunities for achieving greater savings: by applying the system approach to electric motor systems and helping industry to apply this approach and harvest the savings. The positive experiences with the Dutch Green Deal in motor systems (2012–2015) together with the KEEA network and experiences from international research and audit programs form the basis for this.

The Dutch government coalition agreement (2017) has set ambitious goals for a new national climate and energy agreement: a 49% reduction in CO₂ emissions in 2030. In its analysis of the coalition agreement, a Dutch governmental advisory body (PBL) indicated that additional policies must be developed for around 50% of this objective for 2030. In addition, for short-term results, the so-called Intensification Program for Energy Challenges 2020 (IP2020) needs to focus on concrete extra energy savings for the coming years.

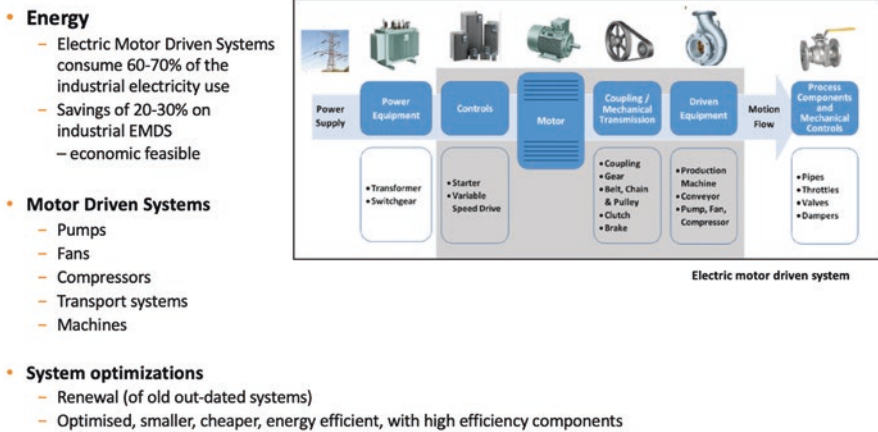


Fig. 1 Electric motor-driven systems, system optimization

²Techniek Nederland = industrial service companies, FEDA = manufacturers, suppliers of motor system components and automation, HPG = manufactures and suppliers of pumps, RVO = Netherlands Enterprise Agency

2 Audit Program

The main objective of this program is to achieve energy savings and CO₂ emission reduction on short term within the participating industrial companies by conducting a series of 150 audits and to guide the companies during the first implementation. The audits will provide:

- Insight into the overall savings potential within motor systems on short term
- Five concrete business cases for (a group of) motor systems
- Identification of next steps for transition toward efficient motor systems for the next 1–3 years

The program is split into a pilot audit program, including 30 audits and an assessment of potential of the next 120 audits, and the viability of the start of a voucher system for this audit series.

The audit consists of four audit steps (see Fig. 2).

The audit methodology is directly derived from the EMSA publication “Energy Audit Guide for Motor Driven Systems” [5]. This guide is structured along the Energy Audit Standard ISO 50002 and includes organizational and technical tasks. For each step the relevant standards and tools are specified. The designated tools are brand independent and include calculations which are based on IEC standards and objective research data. The tools are made available through the Swiss Topmotors’ program (SOTEA, ILI, and STR - adjusted for Dutch purposes), through IEA 4E EMSA (the Motor Systems Tool), and through the Dutch program management (TCO calculation tool for business cases and the standard format for the Audit report) [6, 7].

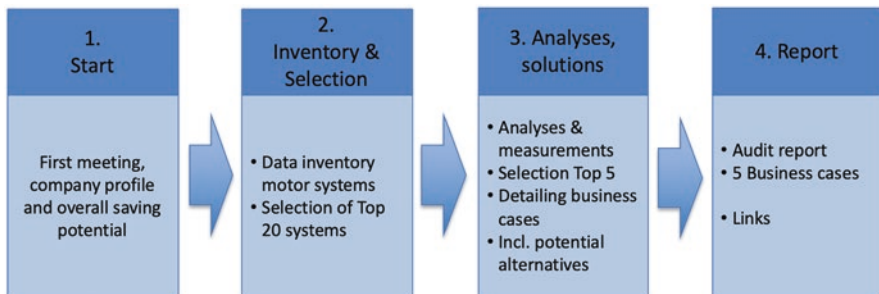


Fig. 2 Audit steps 1 to 4

2.1 Organization, Roles, and Stakeholders

The knowledge network is the initiator of this pilot audit program and provides the audit program’s project management. The audits will be conducted by members of the network partners, i.e., service companies, consulting services, and suppliers. The industrial companies, the targeted auditees, are identified as the top 800 of energy-consuming industrial companies in the Netherlands. For the marketing and communication of the program, a number of sources and approaches will be used, e.g., governmental digital newsletters, specific digital networking groups, specific meetings for selections of companies (workshops), and direct consulting by the network partners themselves.

The auditors will all participate in a start-up training consisting of two dedicated workshops on the methodology, the communication, and available tools and audit report format, thus delivering capacity building to the network partners and creating a level playing for the customers, the industrial companies.

In collaboration with the Ministry of Economic Affairs and Climate (EZK) and the Dutch Enterprise Agency (RVO), research will be done into financial instruments for supporting the investments into efficient electric motor-driven systems. Focus will be on the Energy Investment Allowance (EIA), as well as into the potentials for an energy efficiency investment fund. The latter is currently under development by different stakeholders among which several Dutch pension funds, banks, and financial institutions. This fund could actually deliver an important contribution to the “conversion” from saving measure (building the business case, step 1 to 4) into realization (the engineering and implementation) (see Fig. 3).

The audit program has a small subsidy available (for the auditor) per completed audit.

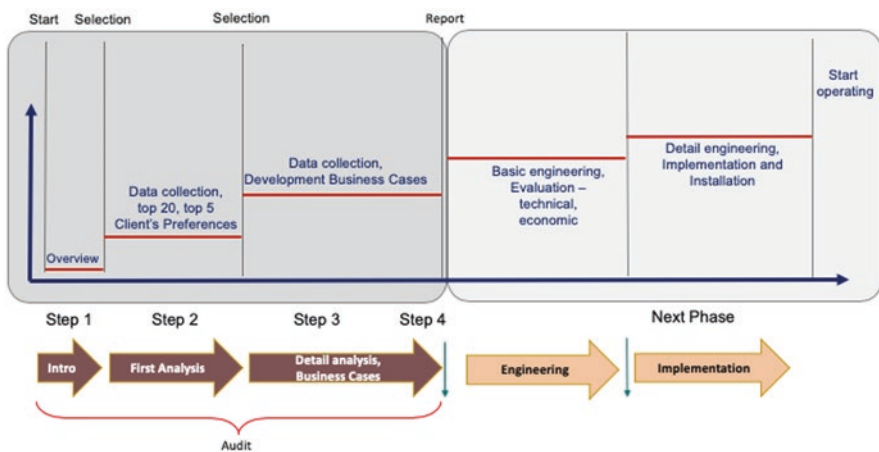


Fig. 3 Audit steps 1 to 4 and next phase: engineering and implementation

A successful audit requires a close cooperation between the auditor and the auditee, for obtaining the necessary data, granting access to the installations (operation), selecting measures, making analyses and taking measurements, etc. Depending on the available information, manpower, and expertise, the audit can be carried out effectively and efficiently.

In communications with the targeted industrial companies, the following arguments for participating as auditee are presented as well as the minimum:

Why?

- Compliance with National Environmental Law and CO₂ reduction targets.
- Lowering operational cost (OPEX) through lower energy and maintenance cost, direct effect on net profit margin and profitability
- Lowering (un)planned downtime
- Concrete contribution to companies' sustainability targets

What does it take?

- Commitment by management and employees.
- Effort by employees (s) for delivering data, site visit(s), and analysis in cooperation with auditors.
- No out-of-pocket cost; fiscal allowance scheme (through EIA) applicable.
- Lead time: 2–3 months.
- See further details in “Participation form” Industry (part of audit concept).

2.2 Success and Fail Factors

As the pilot program demands cooperation by a number of parties active in different sections of the supply chain and industry, the pilot aims to identify a number of factors that are critical for success or that ensure failure. For the pilot audit program itself including the audit concept, some of those factors, currently identified, are:

- Communications: being able to communicate clearly the (1) audit proposition to the target industrial companies and (2) the independency of the sender, i.e., independency of promoting one technical solution, one component brand, and such.
- Data availability: in the very early stage of the audit, auditor and auditee need to assess the actual availability of data on electricity use and especially the electric motor-driven systems. The status has direct effect on the cost of the audit, feasibility, and lead time.
- Split responsibilities between the different entities within large companies: management, operations, procurement, and maintenance. Each entity has its own responsibilities and performance targets which do not always lead to converging interests concerning energy efficiency and lowest TCO in operation. Well-identified “governance” within the audit project is therefore essential.

- The audit results need to be presented in such a way both the technical officials and the financial officials have access to the key data of the business cases.
- Capacity building: as the pilot carries in itself the goal of performing a total of 150 audits in the years ahead, the group of participating auditor companies needs to develop its knowledge and experience. Only then they will be able to serve the large number of industrial companies as envisaged.
- Cooperation: the assessment of the different types of motor-driven systems demands for specific knowledge of, e.g., pumps, fans, motors, transmissions, process automation, and such. Depending on the actual specifics of the production facility, the auditor needs to compose a project team with the appropriate skills and knowledge.

2.3 Cost and Benefits

The audits will lead to the identification of energy savings potential and CO₂ emission reduction potential at the participating industrial companies; they will specify a number of business cases ready for direct implementation, and they're aiming to function as a starting point for continued savings for the coming years. The benefits – savings potential – of the 150 audits, including the practical business cases for industrial companies as a start, are estimated to amount to 0.8–1.2 final PJ and 125–190 kton CO₂ emission reduction. Note: this is the savings potential at a 100% implementation rate. To achieve the full benefits, the companies need to develop an implementation scheme for the coming 5 years at least. The benefits of the business cases are twofold: the demonstration of sound savings measures within the company and the urge to give these cases a follow-up, by the uptake of next analysis rounds.

The direct savings by the first business cases will be assessed in the pilot, as well as the value of the subsidy for the participating company, i.e., does the subsidy actually add to the decision by industrial companies to participate in this program, and is the subsidy a sufficient benefit for the auditors to actually do their auditing work? One special point of interest in the evaluation of the pilot program will be into the question whether there is a need felt within the industrial companies and the audit companies themselves for, for instance, a certification scheme or register for auditors.

The pilot audit program is executed in the Netherlands. The Netherlands has an industry which is internationally oriented and competes on the world market. The concept and methodology applied in this pilot should be applicable to many other industrial markets around the globe, given a comparable state of development of the “supply chain” and it's interest to cooperate on the subject of industrial energy efficiency.

3 Training

In parallel with the development and start of the pilot audit program, a training has been developed for employees from industry, service companies, and manufacturers. The Dutch Knowledge Network for efficient electric motor-driven systems (KEEA) initiated the development of this training course and assisted the Dutch training company NCOI in the actual development of the curriculum and practical cases.

The training covers a technical curriculum on the different fields of a motor-driven system, like mechanics, electrotechnics, energy systems, and automation. A second part has special focus on personal social skills including awareness and training of presentation skills. The program covers a practical assignment in an industrial facility, as well as classical education (5 days) and e-learning modules, in details:

Energy savings section

- Energy management
- Electrical engineering
- Mechanical engineering
- Industrial automation and digitization
- Climate technology and system analysis

Audit section

- Audit method (ISO50002)
- Writing skills
- Presentation techniques

Advise skills

- Communication skills
- Convince and influence
- Dealing with resistance. Personal development plan

Afterward participants will be able to perform expert audits based on the audit methodology according to the ISO50002 standard for energy audits with a specification on electric motor-driven systems.

The first training has started early July 2019.

4 Planning

Some first audit results are expected to be available for presentation in September/October 2019. The overall assessment of the pilot audit program is planned for end of 2019.

References

1. J. Sipma, ECN, Savings potential in Electric motor driven systems in the Netherlands, April 2017
2. International Energy Agency, *World Energy Outlook 2016* (IEA, Paris, 2016)
3. Maarten van Werkhoven, Rita Werle, Conrad U. Brunner (IEA 4E Electric Motor Systems Annex), Policy Guidelines for Motor Driven Units, Part 1: Analysis of standards and regulations, Zurich, Switzerland, 2016; Policy Guidelines for Motor Driven Units, Part 2: Recommendations for aligning standards and regulations for pumps, fans and compressors, Zurich, Switzerland, 2018
4. A.D. Almeida, *ISR University of Coimbra, Motor Summit* (Zurich, 2016)
5. Konstantin Kulterer (IEA 4E Electric Motor Systems Annex), Energy Audit Methodology for Motor Driven Systems based on international Standards and Tools, 2017
6. R. Tieben, C.U. Brunner, R. Werle, Lessons Learned from Four Years of the Swiss EASY Audit and Incentive Program; EEMODS'15, 15 September 2015
7. 4E EMSA (Danish Technological Institute), *The Motor System Tool, version 3.17.01*, June 2019., www.motorsystems.org/motor-systems-tool

Operation Analysis of an Integrated Linear Flux Modulating Motor for a Direct-Driven Belt Conveyor



Alexander Hoffmann, Malte Kanus, Ludger Overmeyer, and Bernd Ponick

1 Introduction

Considering a common case as shown in Fig. 1, a belt conveyor is made up of two drums and an endless belt. To support the carrying side of the belt, a low-friction table is located underneath it. One of the drums is used to introduce the feeding force; the other drum is needed to apply the necessary force to span the belt. When the belt is strained, the force F_1 can be observed as shown at the top right and bottom right of Fig. 1. The vectors are perpendicular to the actual direction of the forces to visualize the distribution along the belt. The force F_1 is equally distributed along the belt and has no direct contribution to the moving force. The movement of the belt is introduced by the force F_2 , which is provided by the geared motor and transmitted by the drum and the friction between drum and belt. The described forces are significant, restricting the capability to scale the system to greater belt lengths. Therefore, a distribution of the forces is considered to improve the scalability of the system [1]. For this reason, the application of one or several linear motors being distributed along the belt is suggested. As a result, the force to strain the belt can be reduced as indicated by the lower force F_1 at the bottom right of Fig. 1 compared to the top right of the same figure. The conducted research is supported by the German Research Foundation under the label PO 1002/8–1.

A. Hoffmann (✉) · B. Ponick

Institute for Drive Systems and Power Electronics, Leibniz University Hannover, Hanover, Germany

e-mail: alexander.hoffmann@ial.uni-hannover.de; ponick@ial.uni-hannover.de

M. Kanus · L. Overmeyer

Institute of Transport and Automation Technology, Leibniz University Hannover, Hanover, Germany

e-mail: malte.kanus@ita.uni-hannover.de; Ludger.Overmeyer@ita.uni-hannover.de

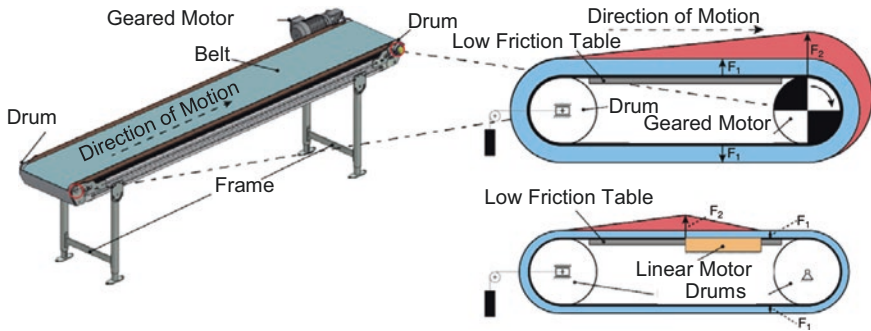


Fig. 1 Force distribution inside the belt of a conveyor when driven by a conventional geared motor attached to a drum (top right) and for a linear motor directly attached to the belt (bottom right). The distribution of the forces F_1 and F_2 is indicated by the colored areas which are raised by the corresponding vectors [2]

The first section of this article covers the reduction of a motor segment into a 2D parametric model. A genetic optimization algorithm is applied in the second section to maximize the feeding force of the motor. To meet modern actuator requirements, a method is presented in the third section to reduce the force ripple significantly. The last section presents the efficiency map of the designed integrated linear flux modulating motor. Further details on the design, operation, and the appearance of the motor are given in [3]. An illustration of a motor segment is given below.

2 Parametric Model

To carry out parametric simulations and to find optimal geometry properties for the linear motor's active parts, a fully parametric model of one single phase is built. By utilizing mathematical constraints, the number of geometrically independent variables can be reduced from 10 to 7. Due to the high number of remaining variables, a 2D representation of the linear flux modulating motor is used, which is indicated in Fig. 2. During this stage, the permanent magnet is neglected, and the achieved results are transferred to the 3D geometry.

The yoke and the teeth are made out of laminated electrical steel, grade M330-50A. Cold-forming steel is selected for the runner elements, in this case DC01. Each of the four concentrated coils consists of 220 turns of 1.13 mm-thick copper wire. All four coils of one phase are connected in series, and all phases are in star connection. Since a nonlinear magnetostatic problem is solved, the material of the coil former and the isolation can be neglected.

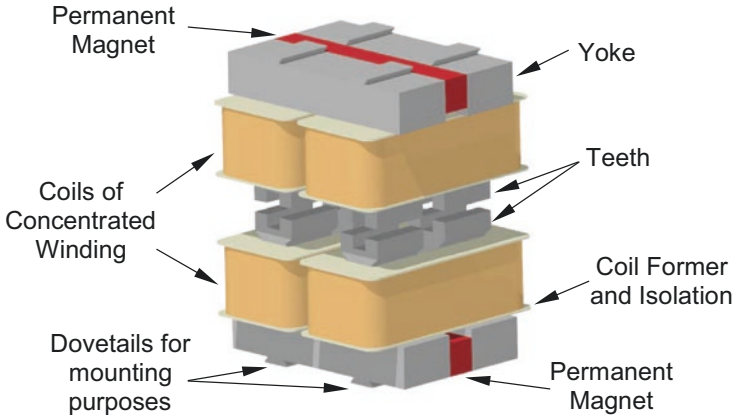


Fig. 2 Illustration of a single motor segment of the linear flux modulating motor with annotations. The permanent magnets are indicated in red, and parts made of laminated electrical steel are indicated in gray

3 Model Optimization

To investigate the behavior of the 2D representation in Fig. 2 for different sets of parameters, a genetic optimization algorithm is used. A set of parameters consists of seven parameters, as shown in Fig. 2. Since the number of simulations depends heavily on the number and discretization of the parameters, a conventional parameter investigation is not an option. The number of required simulations to cover the majority of possible designs would be 10^7 , allowing a discretization of ten steps for each parameter. In order to reduce the number of simulations significantly, a genetic optimization algorithm is used. The genetic algorithm is a stochastic search technique based on the mechanism of natural selection and natural genetics [4]. After each simulation, the resulting feeding force is evaluated against the optimization criteria, which is done to maximize the feeding force. In addition, an adaption of the parameters based on the genetic algorithm is executed [5]. Figure 3 shows the optimization process of the feeding force for each evaluation. The ordinate indicates the resulting feeding force normalized to the resulting feeding force of the non-optimized geometry. Both geometries are limited to the same net surface area. Therefore, a direct comparison is appropriate. After 500 evaluations, no further improvements are visible, and a local maximum can be found at evaluation 484. The increase in feeding force is significant and is 1.9 times higher than the force of the non-optimized geometry.

A visualization of the parameters for different stages of optimization is given in Fig. 4. The greatest change can be recognized for w_3 which describes the width of the teeth at the air gap.

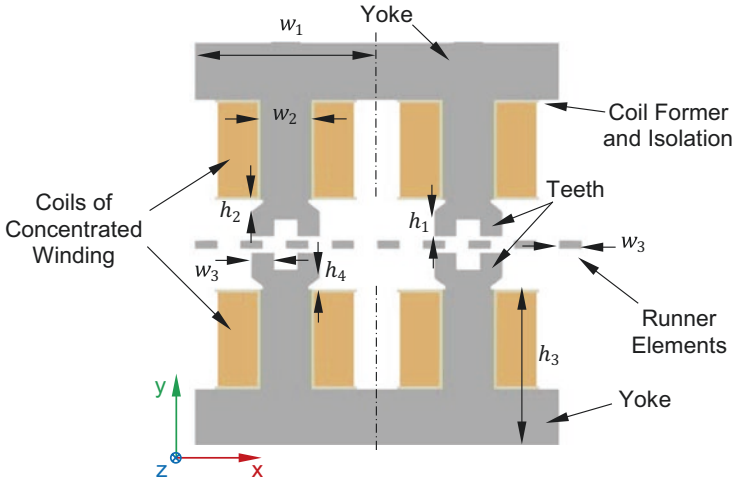


Fig. 3 Fully parametric 2D representation of a single phase of the motor segment of the linear flux modulating motor with annotations

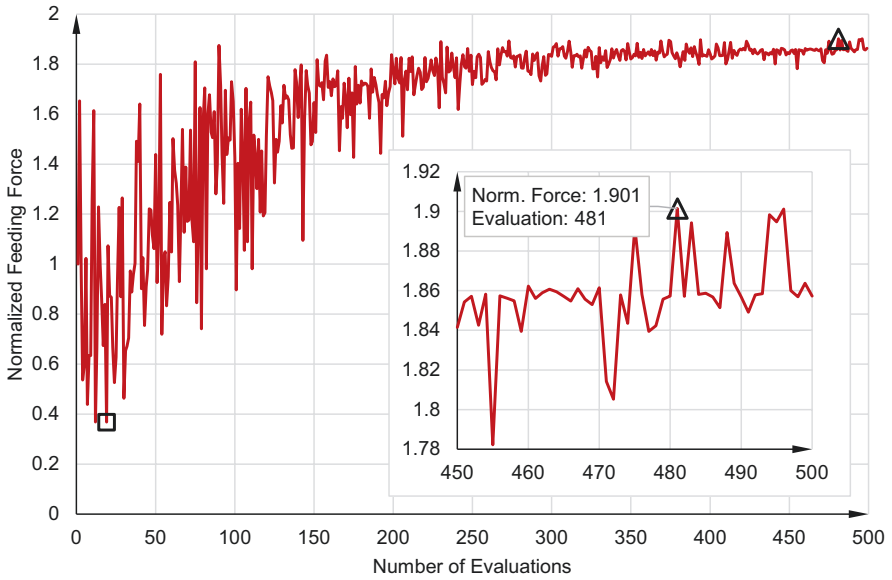


Fig. 4 Normalized feeding force for 500 evaluations with different parameter sets based on a generic algorithm. The maximum is indicated with a triangle and minimum with a square

4 Feeding Force Ripple Reduction

A crucial requirement of modern actuators is a limited force ripple [6]. Several strategies are known to fulfill this requirement for linear permanent magnet synchronous machines by introducing additional teeth or by current control during operation [7]. A systematic approach for the novel linear flux modulating motor is shown, which consists of two steps. The first step utilizes the known 2D representation from Fig. 2 and introduces a new parameter a . The new parameter can vary during the interval of $\{a \in R \mid 0 < a < 2\}$, changing the width of a runner element τ_{re} with respect to the tooth pitch τ_i , as can be seen in Fig. 5 and Eq. (1). All remaining parameters are kept unchanged after the optimization done by using the genetic algorithm from the previous section.

$$\tau_{re} = a \frac{\tau_i}{2} \tag{1}$$

Due to symmetrical conditions, it is sufficient to calculate the force in dependence of time $F_s(t)$ for one motor segment and a finite number of variations of a . In order to measure the quality of the solution with respect to the resulting force ripple, $F_s(t)$ is compared to the ideal force $F_i(t)$ in

$$F_i(t) = \hat{F}_i \cos^2 \left(2\pi v_x \frac{1}{\tau_i} t \right) \tag{2}$$

where v_x is the velocity in x-direction. The ideal force describes the force required by one motor segment to achieve steady linear motion in a setup with m_1 motor

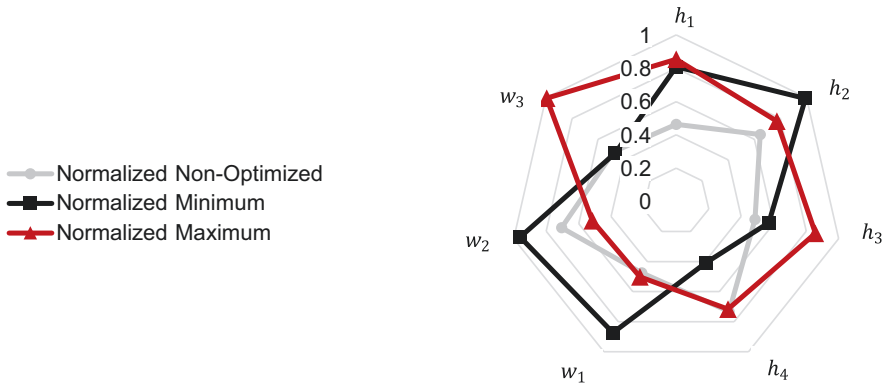


Fig. 5 Variation of geometry parameters during the optimization process for three distinguished solutions

segments neglecting force ripple. The combined force of a setup with m_1 motor segments can be calculated using

$$F(t, m_1) = \sum_{k=0}^{m_1-1} F\left(t - \frac{k}{m_1} \tau_t\right). \tag{3}$$

To measure the result with respect to the ideal condition of Eq. (2), the root-mean-square error is calculated using

$$\text{RMSE} = \sqrt{\frac{1}{T} \sum_{t=0}^T (F_s(t) - F_i(t))^2}, \tag{4}$$

where $F_s(t)$ is the result of a 2D FEM simulation. In order to find the best solution, resulting in a balance between a low force ripple and a high feeding force, the quality criterium

$$\Gamma = \sqrt{(\text{RMSE}')^2 + \widehat{F}'_s{}^2} \tag{5}$$

is used. This applies, when RMSE' is equal to one minus the normalized root-mean-square error from Eq. (4) and \widehat{F}'_s represents the peak force normalized for all simulation results. The results are presented in Fig. 6, showing the complexity of finding an ideal set of parameters when nonlinear material and transient conditions are applied. This is done for different air-gap widths δ below, while the ideal value of parameter a is indicated when applying the quality criterium from Eq. (5). It should be pointed out that no edge effects are taken into account at this stage. Therefore, this step is advisable to narrow down the number of required 3D simulations towards an optimized a (Fig. 7).

In order to consider the edge effect, the simulations are repeated in a second step in a 3D environment. The number of required simulations can be narrowed down by taking the results from step one into consideration. The accomplished reduction of force ripple is indicated in Fig. 8 compared to the previous design. As pointed out in

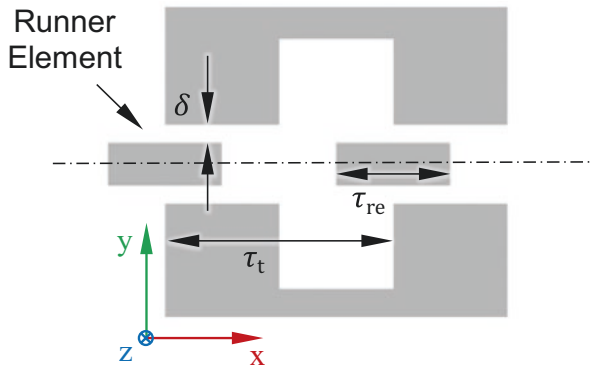


Fig. 6 Variation of the runner element width with respect to the tooth pitch

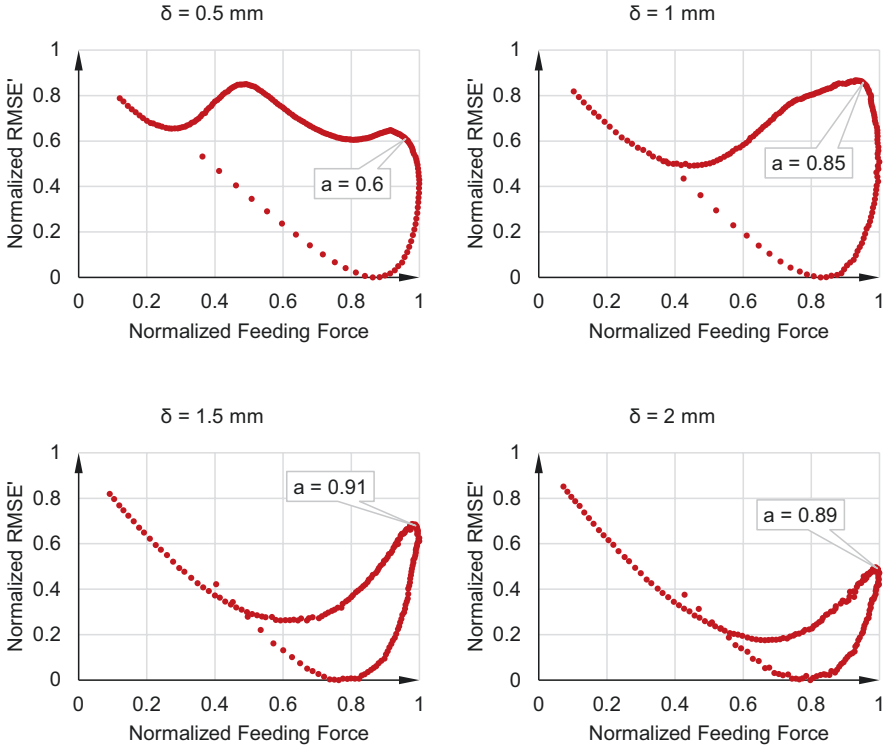


Fig. 7 Results of a 2D optimization in order to find a trade-off between feeding force, force ripple, and time-intensive 3D FEM simulations

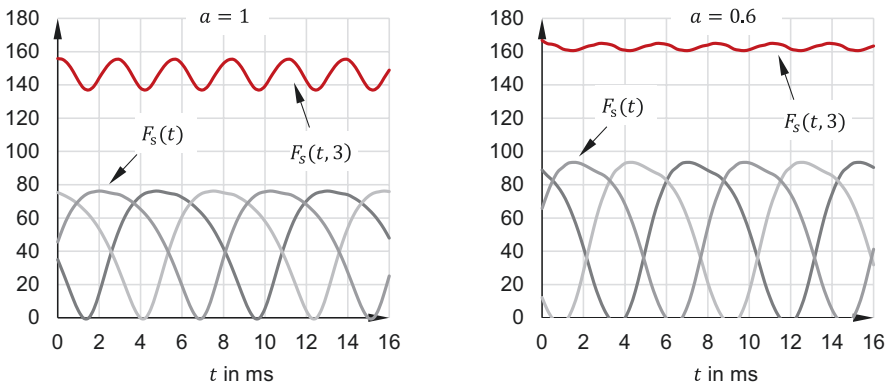


Fig. 8 3D simulation results showing the feeding force of each motor segment $F_s(t)$ and the combined force $F_s(t, 3)$ for $a = 1$ and $a = 0.6$

Table 1 Evaluated simulation results of $F_s(t, 3)$ before and after force ripple reduction for a 3D geometry, as can be seen in Fig. 8

	a = 1	a = 0.6	Divergence
Maximum	155.8 N	166.7 N	+10.9 N
Minimum	136.9 N	160.6 N	+23.7 N
Average	146.6 N	162.9 N	+16.3 N
Peak to peak	18.9 N	6.1 N	-12.8 N
Rel. Ripple	6.4%	1.9%	-4.5%

Table 1, the maximum and the minimum force could be improved, which leads to an average increase in feeding force of almost 10%. The introduced approach also reduced the force ripple significantly from 6.4% to 1.9%. It should be mentioned that the case of $a < 1$ has two additional advantages for the stated application of a direct-drive belt conveyor. First, this is a reduction of runner element material by 40% which results in less mass and fewer friction losses. Second, a more robust structure of the belt could be achieved, since a higher number of filaments, supporting the structure of the belt, will be kept intact.

5 Efficiency Analysis for All Points of Operation

Furthermore, a study is provided, giving an insight into the efficiency of the designed integrated linear flux modulating motor for a direct-drive belt conveyor. The results are obtained by 3D simulations, taking electromagnetic loss effects into consideration and neglecting losses through Coulomb friction. Iron losses inside the laminated areas of yoke and teeth are taken into account by applying the Bertotti formula [8].

$$p_{v,fe} = k_h fB^2 + k_c (fB)^2 + k_e (fB)^{1.5}, \quad (6)$$

which separates the iron losses $p_{v,fe}$ into three quantities, i.e., hysteresis losses, eddy current losses, and excess losses. Eddy current losses and ordinary ohmic losses are calculated by using

$$p_{v,o} = \frac{1}{\sigma} \int_V J^2 dV. \quad (7)$$

during the stage of postprocessing, since the current density J is available for all time steps inside all runner elements and the concentrated winding. In a last step, the efficiency (disregarding friction) can be calculated for all points of operation which is indicated in Fig. 9 below. It can be seen that the efficiency tends to be higher than 90% at speeds above 0.5 m/s and for a feeding force below 73 N. The motor is initially designed for a phase current of 3 A; therefore, the iron is saturated

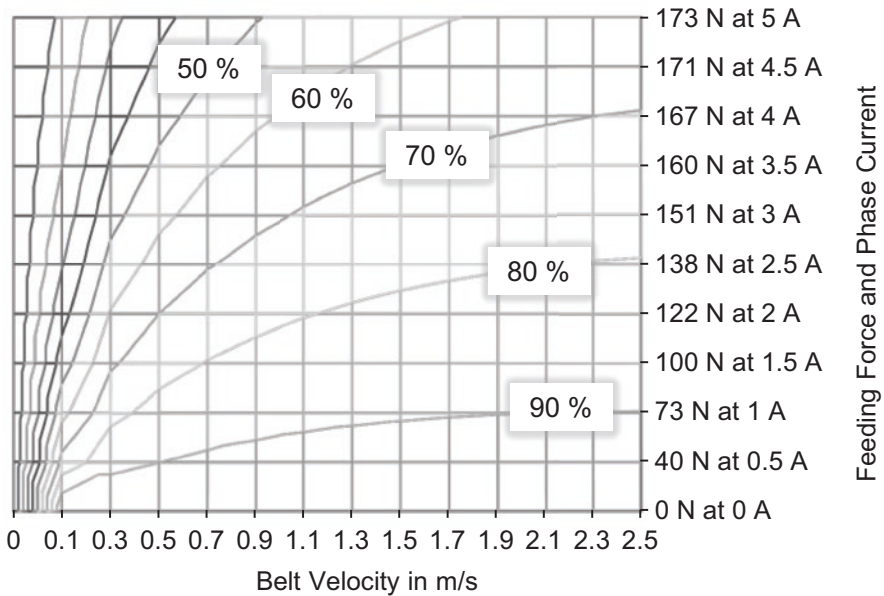


Fig. 9 Motor efficiency distribution for all points of operation up to 2.5 m/s belt velocity and 173 N feeding force at 5 A phase current

at this stage. This circumstance leads to a reduced increase of feeding force per ampere for higher phase currents. Moreover, the belt velocity does not contribute in the same way to the motor efficiency as the phase current does. The motor efficiency is fairly independent of the belt velocity above 1.5 m/s. This can be explained by taking a look at the distribution of losses between current-driven losses and iron losses. The proportion of iron losses to overall losses is approximately one third, while current-driven losses are just about two third of the sum total. An even distribution would lead to a higher overall efficiency, but it would compromise the feeding force. It might be beneficial to perform an efficiency-based optimization rather than a feeding force-based one, like in the stated case.

6 Conclusion

The presented operation analysis of a novel integrated linear flux modulating motor for a direct-driven belt conveyor shows the application of a genetic algorithm for the purpose of geometric optimization. As a result, the feeding force is increased by a factor of 1.9. A second section deals with the reduction of force ripple and divides the approach into two steps: first a 2D simulation to narrow down the number of 3D simulations and a second step consisting of a small number of 3D simulations to take the edge effect into account. The force ripple was significantly reduced by

4.5% in addition to an average gain in feeding force by 10%. The mentioned adjustment of the width of the runner elements is another advantage of the novel direct-driven belt conveyor. A reduction of runner element width ultimately reduces the weight of the belt. In this case, the mass introduced by runner elements is decreased by 40%. The last section delivers an efficiency analysis for all points of operation and discusses the downside of feeding force maximization with respect to efficiency optimization. Overall, the concept of a direct-driven belt conveyor proved to be capable to pave the way toward new material flow models.

References

1. J. Jastrzembki, B. Ponick, Design of a novel direct driven conveyor by a linear synchronous motor, in *2009 35th Annual Conference of IEEE Industrial Electronics, Porto*, (2009), pp. 1092–1096
2. Transnorm Systems GmbH, Technical Datasheet Gurtförderer BC11, Product Information, Harsum, Germany, 2013
3. A. Hoffmann, M. Kanus, L. Overmeyer, B. Ponick, *Design of an Integrated Linear Flux Modulating Motor for a Direct-Drive Belt Conveyor* (IKMT, Würzburg, 2019)
4. P. Guo, X. Wang, Y. Han, The enhanced genetic algorithms for the optimization design, in *International Conference on Biomedical Engineering and Informatics, Yantai*, (2010), pp. 2990–2994
5. G. Bramerdorfer, J.A. Tapia, J.J. Pyrhönen, A. Cavagnino, Modern electrical machine design optimization: Techniques, trends, and best practices. *IEEE Trans. Ind. Electron.* **65**(10), 7672–7684 (2018)
6. J. Jastrzembki, B. Ponick, Different methods for reducing detent force in a permanent magnet linear synchronous motor, in *IECON 2010 – 36th Annual Conference on IEEE Industrial Electronics Society, Glendale, AZ*, (2010), pp. 823–828
7. Y. Mieno, K. Shinohara, Current waveforms for high torque to current ratio in surface mounted permanent magnet synchronous motors, in *Proceedings of Second International Conference on Power Electronics and Drive Systems*, vol. 2, (Singapore, 1997), pp. 542–547
8. G. Bertotti, General properties of power losses in soft ferromagnetic materials. *IEEE Trans. Magn.* **24**(1), 621–630 (1988)

Performance of Copper Rotor Motor in High-Speed Applications



Dong Liang, Sheng Zhou, Datong Yang, and Xu Yang

1 Introduction

High-speed motor is one of the important directions of motor development. The physical size of high-speed motors is much smaller than that of low-speed motor with the same output power, which means high-speed motor has higher energy density and can save the material cost. High-speed motor can connect the load directly without traditional transmission, which can improve the system efficiency and reduce the noise.

Because of these advantages, high-speed motors have been widely used in many applications. According to their functions, they can be divided into two categories: high-speed generators and high-speed motors. High-speed generators are widely used in aviation, new energy vehicles, ships, and other industries because of their high efficiency, high power density, and smaller size. High-speed motors are widely used in blowers, centrifugal compressors, shrinkage, high-speed machine tools, high-speed grinders, and other applications.

In order to ensure the mechanical strength of the high-speed motor rotor, it is required that there should be no brushes and sliding rings in the rotor. There are many types of motor that can be used for high-speed operation including switched reluctance motor, squirrel cage induction motor, solid rotor induction motor, permanent magnet synchronous motor, brushless DC motor, and so on.

D. Liang (✉) · S. Zhou
International Copper Association, Beijing, China
e-mail: daniel.liang@copperalliance.asia

D. Yang
Beijing Rong Xin Ya De Technology Co. Ltd., Beijing, China

X. Yang
Yunnan Copper Die-casting Technology Co. Ltd., Kunming Shi, China
e-mail: Victor.zhou@copperalliance.asia

In most of the cases, permanent magnet synchronous motor, induction motor, and switched reluctance motor are usually selected for high-speed operation. For permanent magnet motors, it has high efficiency and power factor, but the huge centrifugal force produced by the high speed gives big challenge to the rotor, which should be protected by a surrounding protective sleeve. For the switched reluctance motors, it has robust structure under high speed, but its electromagnetic performance is not good enough. For induction motors, it has good mechanical strength and electromagnetic performance, and its simple structure, low cost, and ease of control make it the main type of high-speed motor [1].

The working principle of high-speed induction motor is the same as that of low-speed induction motor. It relies on increasing the frequency of power supply to achieve high-speed operation. Compared with low-speed motor, the main challenge comes from two aspects: firstly, the high strength requirement of rotor caused by the centrifugal force produced by high-speed motor rotation; and secondly, reducing the working temperature of high-speed motors. The high-speed motor has higher power density compared with low-speed motor; the physical size of high-speed induction motor is smaller, so the energy density of high-speed induction motor is high and heat dissipation is difficult. The heating problem seriously affects the stable operation and service life of high-speed induction motor. In the design process of high-speed motor, it is important to reduce the loss of motor as much as possible, so as to reduce the heat source and increase the life of motor. At the same time, by using external cooling, including water cooling and air cooling, the operating temperature of motor is further reduced, and the stability and service life of motor are improved.

2 Copper Rotor Motor

Currently, the rotors of low-speed squirrel cage induction motors are produced by aluminum die casting technique. That is mainly because of the low cost of aluminum rotors. As is well known, copper has better electrical and mechanical performance compared with aluminum. Table 1 gives some fundamental properties of copper and aluminum. From the table we can find that copper's electrical resistivity is only 60% than that of aluminum, and the coefficient of thermal expansion of copper is 75% than that of aluminum. These properties make copper is an ideal material for rotors.

Table 1 The fundamental properties of copper and aluminum

	Electrical Resistivity ($\Omega \cdot m$), 20 °C	Melting Point (°C)	Density (g/ cm ³)	Coefficient of Thermal Expansion($10^{-6}/K$), 20 °C
Copper	1.73×10^{-8}	1084.62	8.96	17.5
Aluminum	2.85×10^{-8}	660.32	2.7	23.2

Compared with aluminum rotor, copper rotor can reduce the total motor loss and hence increase the overall motor efficiency. The data show that copper rotors can reduce the low-speed induction motor energy consumption by 15–25% and increase the efficiency by 2–5% [2]. Copper rotors can be used to produce high efficiency and even super premium efficiency motors without enlarging the motor frame size. Redesigning of motor's rotor and stator is required in line with the property of cast copper rotors, which can maximize the motor efficiency to reach higher or even super premium energy efficiency. By using copper rotor technology, the whole series IE3 efficiency grade induction motors were developed successfully [3, 4].

The YZTE4 (IP55) series IE4 efficiency three-phase induction motors (Frame size 80–180) have been developed by using copper rotor technology in line with IEC60034-30-1 Standard [5]. These motors possess many remarkable features such as IE4 super premium efficiency, low noise, little vibration, large margin of safety in temperature rise, popular shape, and safe and reliable operation.

Moreover, copper rotor is more suitable to improve the small motor performance compared with large-sized motor. It is reported that by changing copper rotors, the efficiency of 1.1 kW induction motors can be improved from 86.4% to 88.1%. Together with the optimization of the structure design and the electromagnetic design, the motor's efficiency could reach 89.4% [6], which exceed the IE4 efficiency.

For high-speed induction motors, the operating temperature is very important to motor stability and the service life. The rotor plays a very important role during energy conversion when motor is operating. In order to alleviate the problem of heat dissipation of the rotor, effective method should be taken in the design to weaken the heating problem of each part of the rotor.

Because of its high-speed rotation, sometimes the cooling hole inside the rotor is not available when considering the strength of the rotors. Therefore, reducing the rotor loss so as to reduce the rotor temperature is very important for the design of the high-speed motors.

As mentioned, copper rotor can reduce the rotor loss and reduce the motor operating temperature subsequently. It is very suitable for high-speed induction motors to reduce the operating temperature and improve the performance.

Copper has better mechanical characteristics compared with aluminum; the tensile strength of pure copper is around 220 MPa and that of aluminum is only 90 MPa. The high tensile strength of copper rotor can meet higher speed. Considering both thermal performance and mechanical performance, copper rotor is the best choice for high-speed induction motors to reduce the operating temperature and improve the performance.

3 Copper Rotor for Spindle Motor

As the key component of computer numerical controlled (CNC) machine tools, electric spindle has a very big market potential. Under high-speed cutting condition, the load on the spindle is large. The spindle motor and the spindle bearing produce a lot of heat, which will make the spindle elongation and increase the pre-tightening force. That will increase the friction heating of the spindle bearing, and seriously reduce the processing accuracy of the machine tool. Therefore, the electric spindle should have stable thermal performance. Electric spindle generates heat continuously in the process of rotation. There are two main heat sources: motor loss heat generation and bearing friction heat generation [7]. It is necessary to minimize the heat generation of these two main heat sources to improve the performance of electric spindle.

The spindle motor was required to have high efficiency, low loss, and high energy density. On the other hand, the strength and robustness of the structure should be guaranteed in the design of the spindle motor. There are two kinds of motors that are widely used in the electric spindle, permanent magnet synchronous motor and asynchronous induction motor. At present, most of the electric spindles use asynchronous induction motor, which has high speed, low cost, easy maintenance, and relatively mature control system.

As mentioned, copper rotor has less rotor loss compared with aluminum rotors. And copper has high tensile strength than aluminum, which means copper rotor is more robust than aluminum rotor. These make copper rotor to be the best choice for induction motor of electric spindle. By using copper rotor, the heating of rotor can be significantly reduced, the power density of motor can be increased, and the life of spindle can be prolonged.

A spindle motor was selected to compare the performance between copper rotor and aluminum rotor. Table 2 gives the parameters of the spindle motor.

One spindle motor used aluminum rotor, and the other was changed to copper rotor. Both spindle motors were operated for 180 min to test the operating temperature; the results are shown in Fig. 1.

Through the experimental data, it can be found that the operating temperature of the spindle motor has been significantly reduced when the copper rotor is used. After 180 min of operation at rated speed, the temperature rise of the copper rotor spindle motor decreases by 11 °C. That means the thermal stability of the electric spindle has been greatly improved, which is of great help to the spindle's life and operation reliability.

Generally speaking, the resistivity will be increased along with the temperature rise. Table 3 gives the values of the resistivity of copper and aluminum at different temperatures. From the table we can find that at 20 °C, the difference is 1.12×10^{-8} ,

Table 2 The parameters of spindle motor

Rated Power (kW)	Rotation Speed (r/min)	Voltage (V)
11	36,000	350

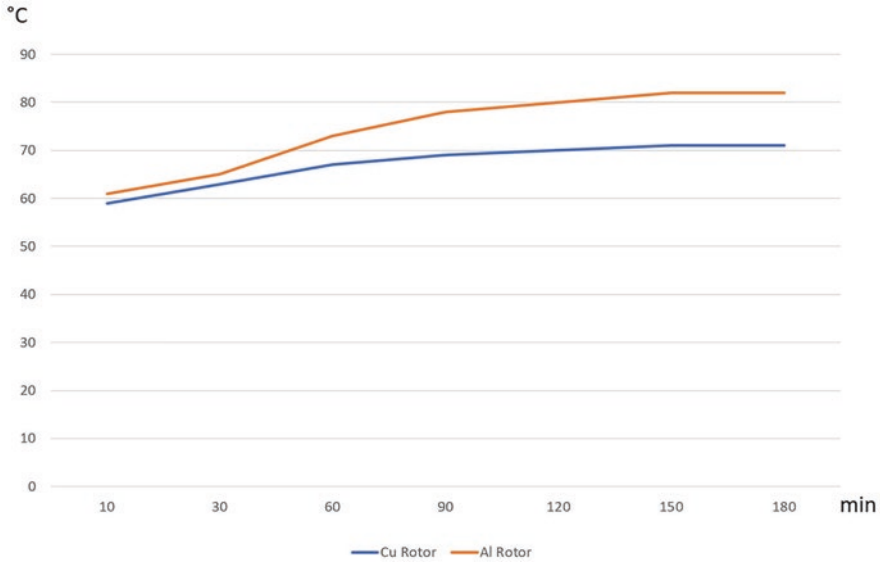


Fig. 1 The operating temperature between copper rotor and aluminum rotor

Table 3 The electrical resistivity of copper and aluminum rotors under different temperature

	20 °C ($\Omega\cdot m$)	50 °C ($\Omega\cdot m$)	80 °C ($\Omega\cdot m$)	110 °C ($\Omega\cdot m$)
Copper	1.73×10^{-8}	1.94×10^{-8}	2.16×10^{-8}	2.37×10^{-8}
Aluminum	2.85×10^{-8}	3.21×10^{-8}	3.57×10^{-8}	3.93×10^{-8}
Difference	1.12×10^{-8}	1.27×10^{-8}	1.41×10^{-8}	1.56×10^{-8}

and at 110 °C, the difference increased to 1.56×10^{-8} . Due to the linear relationship between electrical resistivity and temperature rise, the higher the temperature, the bigger the resistivity. That means the copper rotor advantage will be increased under the higher operating temperature, which is proved by the experimental data.

Besides improving the thermal performance of spindle motors, the copper rotor could increase the energy density and other performances. The copper rotor spindle motors were produced by Beijing Rong Xin Ya De Technology Co. Ltd. in collaboration with Beijing Chao Tong Bu Motor Co. Ltd. The prototypes were tested and compared with the aluminum rotor spindle motors. Table 4 compares the copper and aluminum rotors. The aluminum rotor spindle motor and the copper rotor spindle motor have the same physical size.

For the experimental data, we can find that the rated torque has been improved from 35 N•m to 45 N•m, which is 28.6% improvement. That means the spindle motor power density has been improved a lot by using copper rotor.

From the prototype development and performance analysis, it can be concluded that copper rotor will give advantages to spindle motor as follows.

Table 4 The electrical resistivity of copper and aluminum rotors under different temperature

	Copper Rotor	Aluminum Rotor
Rated power (kW)	11.8	11
Rated voltage (V)	305	315
Rated torque (N•m)	45	35
Rated speed (rpm)	2500	3000
Maximum speed (rpm)	12,000	12,000
Efficiency (%)	88.9	88.8
Power factor	0.87	0.86
Winding temperature rise (K)	51	42

1. Lower temperature rise: Copper has lower electric resistivity, which means copper rotor has less rotor losses compared with aluminum rotor. Copper rotor spindle motor has high efficiency and small slip, which will reduce the motor operating temperature, enhance the thermal performance of electric spindle, and prolong the service life. Copper rotor reduces the additional losses at high frequency, which is helpful in improving the performance of electric spindle motors especially under high speed.
2. High energy density: Copper rotor motor has smaller physical size compared with aluminum rotor motor with the same power and efficiency. That makes the spindle motor more compact and increases the energy density of the spindle motor.
3. High speed: Copper has high tensile strength than aluminum, which makes copper rotor more robust than aluminum rotors. The use of copper rotor can increase the maximum speed and the speed under constant power region of the spindle motor.
4. Good performance: Copper has higher density, which makes the output torque rigidity of motor better than that of aluminum rotor. Copper rotor has better resistance to load variation. Under the variable speed working condition, it has low speed and high speed at the inflection point of speed characteristic curve.

4 Copper Rotor for Traction Motors

According to statistics, the sales of electric vehicles in China in 2017 are about 777,000, and the production volume of electric vehicles only accounts for 2.8% of that of the total car. According to the plan of “energy saving and new energy vehicle technical roadmap,” the sales of China’s car will reach 30 million, 35 million, and 38 million in 2020, 2025, and 2030, respectively, and the sales of electric vehicles will account for 7%, 20%, and 40% of the total car sales, respectively.

According to this, the sales of electric vehicles in 2020, 2025, and 2030 will reach 2.1 million, 7 million, and 15.2 million, respectively, and the growth rate of electric vehicles will reach 25.5% from 2017 to 2030 in China [8].

That makes the electric vehicle (EV) driven motor a very big potential market. The copper rotor induction motor is one of the solutions for driven motor of new energy vehicles. With copper rotor, the induction driven motor could be designed with high efficiency, high speed, high energy density, and high overload performance.

Copper rotor motor has advantage during high speed and it has wider speed range. Although the permanent magnet has better starting performance, the copper rotor motor has better overall performance during high speed. That is because the permanent magnet motor needs the coil to increase the counter current to weaken the magnetic field during high speed, which causes the waste of energy and affects the motor efficiency.

Another advantage of copper rotor motor is overload performance when compared with permanent magnet motors. During the middle and high rotating speed range, the excellent overload performance makes the copper rotor induction motor very competitive.

Take four-pole driven motor as an example; the maximum speed is 15,000 rpm, power density up to 4 kW/kg, and service factor could be four times, which is better than the permanent magnet motor.

Table 5 gives the technical parameters for one type of copper rotor driven motor for electrical vehicles.

At present, although the market share of copper rotor traction motor is not big, the future market prospects are good. The asynchronous motor with copper rotor is not only more efficient than the aluminum rotor motor, but also has irreplaceable advantages compared with the permanent magnet motor. For example, permanent magnet materials are prone to loss of excitation in short circuit, high temperature, and intense vibration environments, and the cost is usually expensive. Copper rotor motor has very excellent performance in this respect. Copper rotor traction motor for new energy vehicles has a bright future.

Table 5 Parameters of 160 kW copper rotor traction motor

	Tested Results
Rated power (kW)	160
Peak power (kW)	300
Nominal torque (N•m)	511, at the rate > 1 h
Peak torque (N•m)	1700, at the rate of 0.5 min
Rated speed (rpm)	3000
Maximum speed (rpm)	7000
Maximum efficiency (%)	96.2
Rated voltage (V)	380
Cooling type	Water
Weight (kg)	280
Dimension (mm)	Φ420 × 520
Temperature rise (K)	65.1

5 Conclusion

Copper has better electric and mechanical characteristics compared with aluminum. Copper rotor can help motor to improve the efficiency, reduce the operating temperature, increase the energy density, improve the reliability, and prolong the service life.

For high-speed motors, in which the temperature rise and energy density are more important than other applications, copper rotor could play a very important role to help the designer to meet these requirements.

Copper rotor is one of the best solutions for high-speed induction motor to improve the performance.

References

1. J. Hong, Research on electromagnetic design method of high speed induction motor. Harbin Inst. Tech. (2006)
2. Z. Sheng, Copper and motor efficiency. *China Electr. Equip. Ind.*, 31–35 (2011)
3. Y. Xu, Y. Jianbin, Technical performance analysis of casting copper rotor high efficiency three-phase asynchronous motor. *Electr. Mach. Control Appl.*, 4–8 (2012)
4. L. Zhiqiang, H. Jian, Consideration about development of premium efficiency copper rotor three phase asynchronous motor series. *Electr. Mach. Control Appl.*, 17–21 (2010)
5. H. Jian, Y. Binglei, Development of IE4 super premium efficiency motor series products. *Electr. Mach. Control Appl.*, 56–61 (2018)
6. Z. Yanzhi, L. Quanfeng, H. Houjia, F. Hui, Energy efficiency analysis of small premium industrial synchronous motors. *J. Shanghai Dianji Univ.* **21**(6) (2018)
7. S. Yusu, C. Weifang, Simulation and experimental study on temperature field and thermal deformation of electric spindle. *Mach. Electron.*, 18–28 (2018)
8. All China Market Research Co. Ltd., *The Market Study of Chinese Electrical Vehicles* (2018), p. 25

Development and Loss Evaluation of High-Speed PM Synchronous Machine



Mototsugu Omura, Sho Uchiyama, Keisuke Matsuo, Takashi Okitsu, Takayuki Mizuno, Koji Yamada, and Kouki Matsuse

1 Introduction

Permanent magnet (PM) synchronous motors have been widely used in various industrial applications due to their compact size and high efficiency [1, 2]. For high-speed applications such as industrial blowers and compressors, we have developed a 250 kW–20,000 min⁻¹ high-speed PM motor using an active magnetic bearing (AMB) [3–6].

When the high-speed motor is utilized in such a way, the system can be replaced by using a speed-increasing gear with the direct drive system to eliminate the gear. Thus, in this way, the system size can be made compact, costs can be lowered, system efficiency can be improved, and maintenance time can be reduced.

On the other hand, the high-output power density that is produced due to compacting the size while maintaining output power via high-speed rotation can bring about high loss density or high heat-generating density. It is necessary to reduce the motor loss and choose an appropriate cooling method. Therefore, many studies have been implemented, including development of various types of high-speed motors [7–14], examination of loss reduction [15–19], and research on magnetic bearings [20, 21].

In this paper, we present the characteristics of the prototype (250 kW–20,000 min⁻¹) and the results of the loss separation and fundamental windage loss verification.

M. Omura (✉) · S. Uchiyama · K. Matsuo · T. Okitsu · T. Mizuno · K. Yamada
Meidensha Corporation, Tokyo, Japan
e-mail: omura-m@mb.meidensha.co.jp; uchiyama-s@mb.meidensha.co.jp; matsuo-ke@mb.meidensha.co.jp; okitsu-ta@mb.meidensha.co.jp; mizuno-t@mb.meidensha.co.jp; yamada-ko@mb.meidensha.co.jp

K. Matsuse
Meiji University, Tokyo, Japan
e-mail: matsuse@meiji.ac.jp

2 Development and Specification of Prototype Motor

Table 1 lists the specifications, and Fig. 1 shows the general view of the prototype motor [18]. The rated output power is 250 kW at a maximum rotational speed of 20,000 min^{-1} , and there are two poles. Forced air cooling (via a separately installed air blower) was utilized to cool the motor. As the rotor shaft is levitated by the AMB, contactless rotation can be realized. In addition, a surface permanent magnet (SPM) has been adopted for the rotor structure, and the PMs mounted on the surface of the shaft have been retained by the sleeve. In this prototype motor, carbon fiber-reinforced plastic (CFRP), which has features of high stress with light weight and low conductivity, has been applied as the material for the sleeve for enduring centrifugal force at 160 m/s over the circumferential speed to reduce the rotor eddy current losses.

Figure 2 shows the AMB structure. Radial magnetic bearings with floating the rotor that follow electromagnetic principle make it possible to rotate so as to avoid contact. Also, the axial magnetic bearing controls the axial position of the rotor based on the same principle. The rotor positions of radial and axial magnetic bearings are detected by a position sensor. Position information returned to controller is used for control of the rotor position by an active magnetic bearing as shown in Fig. 3. In case of an emergency, touchdown bearings are mounted on the outside of the radial magnetic bearings.

Figure 4 is a high-frequency inverter manufactured by MEIDEN. This inverter is a sister model of the high functional universal inverter VT240S, with its highest frequency enhanced to 800 Hz (200 V/400 V system). It enables sensorless control of high-speed PM motors. In case of two pole motors, the maximum rotation speed is 48,000 rpm, and the maximum rated output is 475 kW.

An LC filter is inserted between the inverter and motor to reduce the motor loss by smoothening the current waveform.

Figure 5 is a system configuration diagram from a commercial power supply to an inverter and motor.

Figure 6 is an example of the current waveform in the prototype motor. From this figure, it can be seen that clean sinusoidal current flows through the motor.

Table 1 Specifications of the prototype motor

Motor type	PM motor
Rated output [kW]	250
Rated rotational speed [min^{-1}]	20,000
Number of poles	2
Frequency [Hz]	333.3
Rated torque [N·m]	119.4
Cooling system	Forced air cooling
Bearing	Active magnetic bearing
Magnet type	Nd-Fe-B

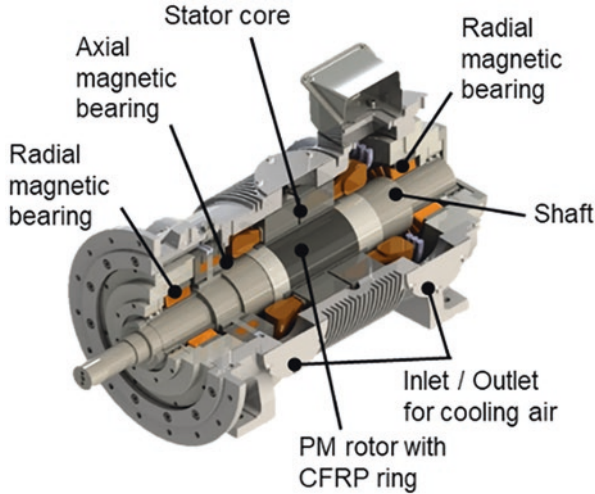


Fig. 1 Cross-sectional configuration

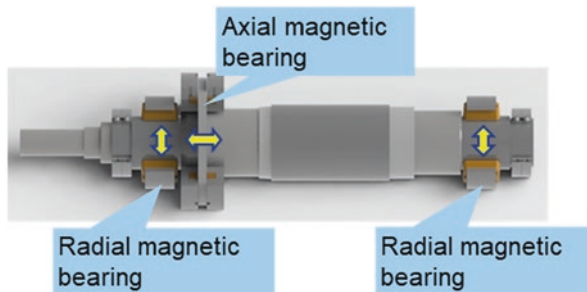


Fig. 2 AMB structure

3 Performance Evaluation

The motor loss consists of copper loss, iron loss, mechanical loss, and stray load loss. With high-speed motors, an increase in stator iron loss and mechanical loss is expected as the frequency increases. In examining various characteristics such as motor efficiency and temperature, these loss evaluations are considered to be extremely important themes.

Here, to create basic data for pursuing an effective loss reduction measure, each loss ratio will be experimentally clarified by the method shown below

- Copper loss: $3 \times (\text{current effective value})^2 \times \text{winding resistance}$
- Iron loss: No load iron loss (separate from single motor no-load input)
- Mechanical loss: Measure with a non-magnetized rotor (windage loss, AMB iron loss)

Fig. 3 AMB control principle

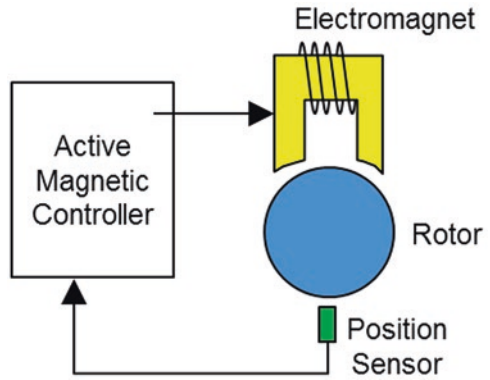


Fig. 4 High-frequency inverter

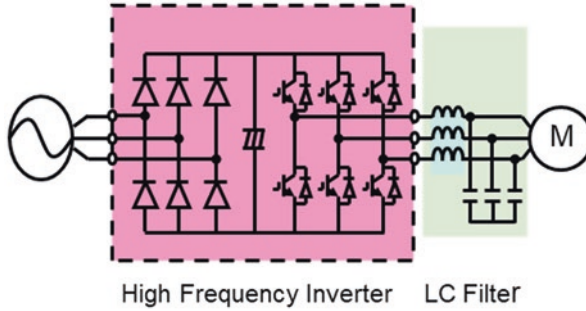


Fig. 5 AMB control principle

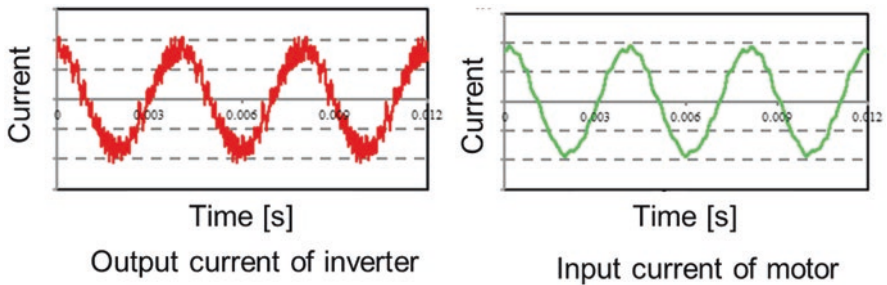


Fig. 6 AMB control principle

- Stray load loss: (input current at motor load) – (copper loss, iron loss, mechanical loss)

The load test is conducted with the same motor connected directly.

3.1 Loss Separation in No-Load Test

We performed the loss separation in a no-load test. When driving a PM motor in a no-load state, the iron loss due to only the magnetic flux generated by the PM will occur in the stator core. Therefore, the mechanical loss can be determined by the difference of two input powers: the one for the single motor is measured in a no-load state and the other from the total amount of two identical coupled motors. The one rotor is magnetized, and the other one is non-magnetized, measured in a back-to-back state (See Fig. 7).

As the rotor shaft is levitated by the magnetic force generated by the AMB, there will not be any friction loss in this motor due to contact between the rotor shaft and bearing. Hence, the mechanical loss will include the windage loss in the air gap and the iron loss that occurred in the AMB. Furthermore, the iron loss in the stator core

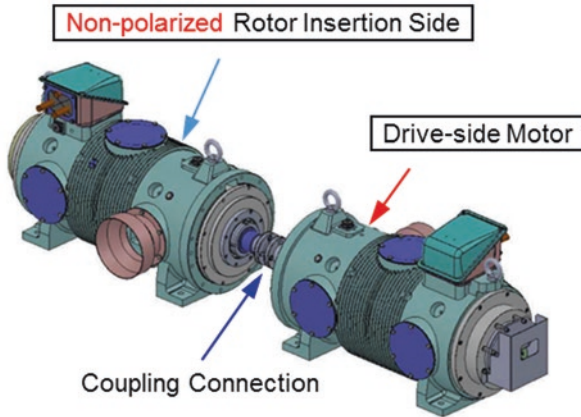


Fig. 7 Mechanical loss measurement test

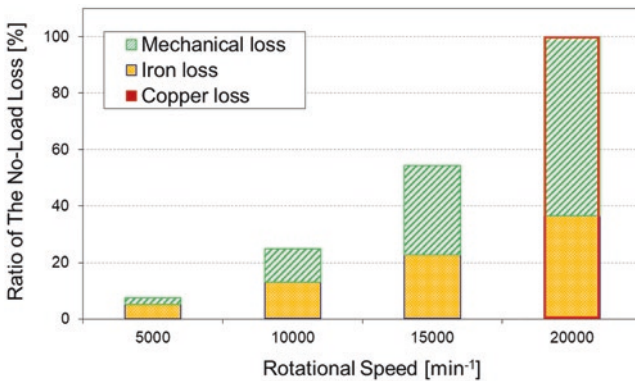


Fig. 8 Result of the loss separation in no-load test

can be determined by subtracting the mechanical loss and the measured copper loss (I^2R) in the winding coil from the no-load loss of the single motor.

Figure 8 shows the result of the loss separation at the speed of 5000 min⁻¹ intervals in the no-load test. In Fig. 8, each loss was standardized with the loss at a maximum rotational speed of 20,000 min⁻¹. As a result of the loss separation, the ratio of the mechanical loss increases as the rotational speed becomes higher and is about 64% at a speed of 20,000 min⁻¹. It can be seen that the ratio of the copper loss is very small because the current is small in the no-load state. Accordingly, it will be an issue of reducing the mechanical loss for improving the efficiency of the high-speed motor.

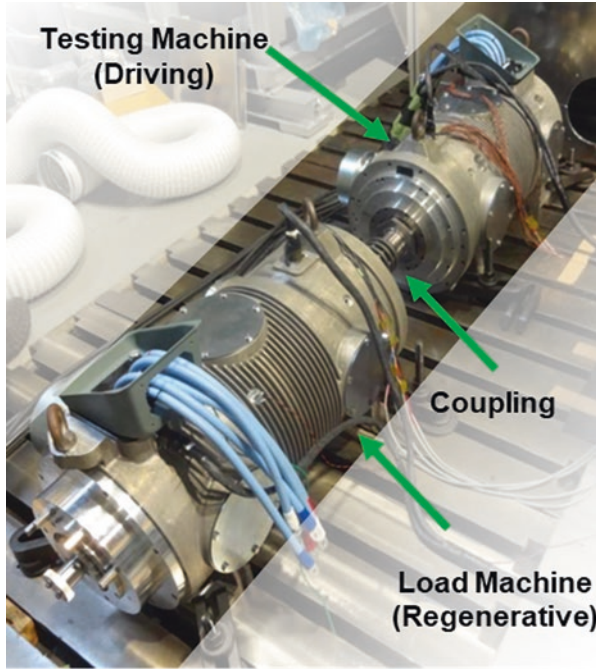


Fig. 9 Setup of the back-to-back test

3.2 Load Test by Back-to-Back Test

By coupling the two same prototype motors, we carried out the back-to-back test to measure the electrical characteristics and calculate the motor efficiency. Figure 9 shows a view of the back-to-back test. In the test, we measured the input power W_{in} of the drive motor and the regenerated power W_{out} of the regeneration motor by using the power meter, and the relation of W_{in} and W_{out} with the output power W_{trq} would be expressed as follows.

$$W_{in} = W_{trq} + (\text{loss of the drive motor}) \quad (1)$$

$$W_{out} = W_{trq} - (\text{loss of the regeneration motor}) \quad (2)$$

Assuming each loss generated in both drive and regeneration motor would be almost the same, W_{trq} is derived as the following equation.

$$W_{trq} = (W_{in} + W_{out}) / 2 \quad (3)$$

By the above method, we measured the electric characteristics while changing the rotational speed and load factor and calculated the motor efficiency.

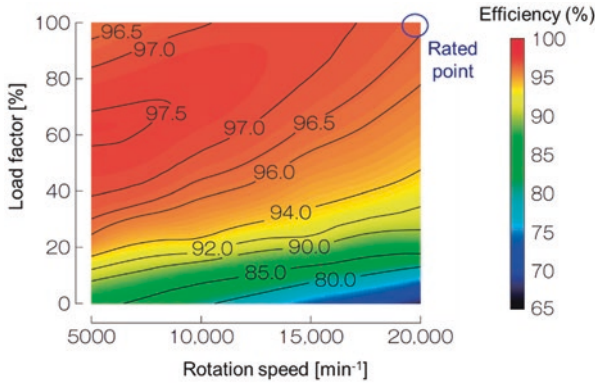


Fig. 10 Efficiency map of the prototype

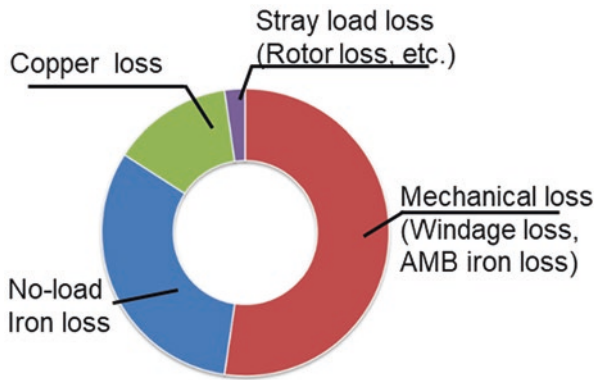


Fig. 11 Loss separation at rated load

Figure 10 shows the efficiency map of the drive motor. The efficiency at the rated point is 96.6%, and it is confirmed that the efficiency tends to decrease in the region of higher rotational speed.

Based on the test results from the no-load test and load test, the results of loss separation at the rated load are shown in Fig. 11. The mechanical loss accounts for about 55% of the total. In order to achieve high efficiency, it is necessary to clarify the factors causing mechanical loss and to take measures to reduce the same.

3.3 Consideration of Loss Analysis of Retaining Ring

The retaining ring is located at the outermost part of the rotor. It has a possibility of decreasing efficiency or demagnetization by heating because an eddy current is caused by space harmonics due to stator slots or time harmonics due to the distorted

current waveform. Therefore, it is necessary to quantitatively grasp the loss of the retaining ring and the influence of the temperature [20].

The authors conducted a magnetic field analysis and actual measurement on a holding ring (hereinafter referred to as a titanium ring) made of a titanium alloy (Ti-6Al-4V) having a high specific strength and a low conductivity and a holding ring made of CFRP. Losses were compared and evaluated when applied to high-speed motors.

3.3.1 Loss Analysis of Retaining Ring

Figure 12 shows a magnetic field analysis model for the retaining ring loss analysis. Loss generated in each part of the rotor was analyzed and compared by changing the material of the retaining ring to titanium, CFRP. When using the titanium ring, the axial division number of the retaining ring is increased so that the eddy current loss occurring in the retaining ring can be reduced (see Table 2).

Figure 13 shows the analysis results of the loss generated in the rotor at the rated load (250 kW–20,000 min⁻¹).

The ring conductivity differs by a parallel or vertical direction from the carbon fiber. As resin is filled around the fiber, the value gets much lower than that of a titanium ring.

The loss represents the loss of the rotor of condition A as 100%. In Condition A, significant eddy current loss occurs in the titanium ring, and it can be confirmed that the ring loss occupies the value of 67% of the total rotor loss. In condition B, the conductivity of the CFRP ring is lower than that of the titanium ring as described above. Therefore, it can be confirmed that the eddy current loss generated in the ring is very small. From the comparison of both conditions, the loss of the rotor for condition B is about 35% of the loss of the rotor for condition A.

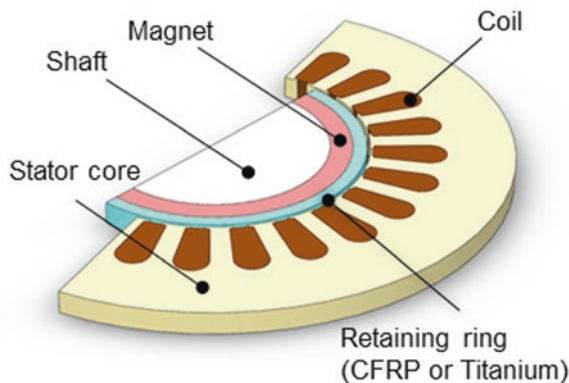


Fig. 12 Magnetic field analysis model

Table 2 Loss analysis pattern

	Ring Material	No. of Ring Division	Conductivity [$\times 10^5$ S/m]
A	Titanium alloy (Ti-6Al-4V)	20	5.8
B	CFRP	5	//: 0.23 ⊥: 0.000046

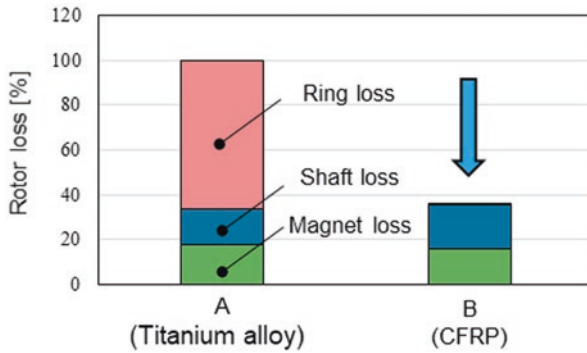


Fig. 13 Analysis result of rotor loss

From the above results, the CFRP ring seems to be superior in terms of loss reduction.

3.3.2 Ring Loss Measurement Test

According to the method of loss separation described above, loss at the rated load was measured with a motor using each ring. From the result, the stray load loss W_{str} , including the loss of the retaining ring, was calculated by (4).

$$W_{str} = W_{total} - W_m - W_c - W_{ni} \tag{4}$$

W_{total} is total loss at load, W_m is mechanical loss, W_c is copper loss, and W_{ni} is no-load core loss.

According to the result shown in Fig. 13, loss occurring at the magnet and shaft is respectively equal. So, if you suppose that the CFRP ring's eddy current loss is 0, the eddy current loss of the titanium ring can be calculated as a difference of each stray load loss by the following formula (5).

$$W_{Ti} = W_{str_Ti} - W_{str_Cf} \tag{5}$$

W_{Ti} shows the eddy current loss of the titanium ring. W_{str_Ti} and W_{str_Cf} show the stray load loss of the motor when the titanium or CFRP ring is respectively applied.

Figure 14 shows the eddy current loss calculated by the formula (5) using the measured value and eddy current loss acquired by the magnetic field analysis on the

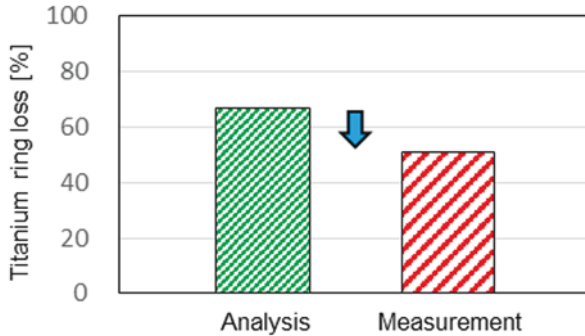


Fig. 14 Comparison of titanium ring loss

titanium ring. Figure 14 indicates that the eddy current loss of the titanium ring is around 15% larger in the analysis compared to the measurement. A possible reason for this would be an error caused by an assumption when formula (5) was derived or due to alteration of the conductivity caused by the temperature increase when measured.

3.3.3 Temperature Evaluation of the Retaining Ring

To evaluate the influence of the retaining ring on the temperature, we performed a continuous operation under the rated load condition and checked the temperature increase of the magnet during steady operation. The magnet temperature was estimated using the change rate of the induced voltage both before and after the operation as well as the temperature coefficient of the residual flux density of the magnet. As a result, the CFRP ring motor took a value whose temperature increase from the magnet was around 30 K lower than that of the titanium ring motor. This result shows that the heating caused by the eddy current loss of the retaining ring has a significant influence on the magnet temperature. Therefore, the CFRP ring can be considered to be suitable for rotor retention of the high-speed motor because its heating and eddy current are smaller compared to the titanium ring.

3.4 Fundamental Consideration of Windage Loss and Iron Loss

It is necessary for realizing high efficiency to decrease windage loss because windage loss is one of the main losses in rated operation. However, it is very difficult to calculate windage loss accurately in advance, though many researches about windage loss calculated by using relationship of friction moment coefficient and rotational Reynolds number have been reported.

As a first step of understanding windage loss characteristic, amount and position of generating windage loss were confirmed by calculating windage loss of the motor based on calculation formula. Secondly, windage loss generated in motor core part was measured in loss evaluation machine, and the calculated and measured values were compared to figure out fundamental windage loss characteristics.

3.4.1 Windage Loss of the Prototype Motor

Calculation Formula of Windage Loss

The prototype motor is a kind of radial gap motor. Hence, it can be considered that the motor structure is replaced as a simple model in double cylinder shape. In double cylinder model, outer cylinder keeps stop like a stator and inner cylinder rotates like a rotor. Windage loss is generated in the circumferential surface of the both cylinders and the top and bottom surface of inner cylinder under its condition.

Firstly, windage loss generated in the circumferential surface of the both cylinders when inner cylinder rotates in rotational angular velocity ω [rad/s] was derived by equation quoted from [22] proposed by Wendt, F. Rotational angular velocity ω is calculated by (6). N expresses rotations per minute.

$$\omega = 2\pi \frac{N}{60} \quad (6)$$

Circumferential speed u_i [m/s] is calculated by (7).

$$u_i = r_i \omega \quad (7)$$

r_i is outer diameter of the rotor. Reynolds number Re_r is defined as (8).

$$Re_r = \frac{u_i d}{\nu} \quad (8)$$

d is gap length from outer diameter of the rotor to inner diameter of the stator [m]. ν is coefficient of kinematic viscosity [m²/s]. Coefficient of friction moment C_{Mr} is shown as empirical formula (9) and (10). η expresses radius ratio as shown in (11).

$$C_{Mr} = 3.68 \frac{(1-\eta)^{0.25} \eta^{3.5}}{(1+\eta)^4} Re_r^{-0.5} \quad (400 < Re_r < 10^4) \quad (9)$$

$$C_{Mr} = 0.584 \frac{(1-\eta)^{0.25} \eta^{3.5}}{(1+\eta)^4} Re_r^{-0.3} \quad (10^4 < Re_r < 10^5) \quad (10)$$

$$\eta = \frac{r_i}{r_o} \quad (11)$$

C_{Mr} is another defined as shown in (12). Windage loss P_{wr} is calculated as shown in (13) by using torque M_r derived by (9), (10), and (12).

$$C_{Mr} \equiv \frac{M_r}{2\pi\rho r_m^4 \omega^2 L} \quad (12)$$

$$P_{wr} \equiv M_r \omega \quad (13)$$

ρ is fluid density [kg/m^3], L is the height of cylinder (core thickness) [m], and r_m is the length from gap central to diameter center of cylinder model [m].

Secondly, windage loss generated in the top and bottom surface of the rotor was derived by equation quoted from [23] proposed by Schlichting. Reynolds number Re_z is defined as (14).

$$Re_z \equiv \frac{u_i r_i}{\nu} \quad (14)$$

Coefficient of friction moment CM_z depends on critical Reynolds number. Critical Reynolds numbers are shown in (15) to (17). S indicates gap length from cylindrical surface to wall surface [m].

$$Re_{z1} = \left(\frac{1}{2.67} \times 2\pi \frac{r_i}{s} \right)^2 \quad (15)$$

$$Re_{z2} = \left(\frac{2.67}{0.0622} \right)^{\frac{1}{0.3}} \quad (16)$$

$$Re_{z3} = \left(\frac{1}{0.0622} \times 2\pi \frac{r_i}{s} \right)^{1.25} \quad (17)$$

Coefficient of friction moment CM_z is shown as an empirical formula and calculated by (18), (19), or (20) if Re_{z2} is larger than Re_{z3} and, if not, by (21) or (22).

Case 1: $Re_{z2} > Re_{z3}$

$$C_{Mz} = 0.0622 Re_z^{-0.2} \quad (Re_{z2} < Re_z) \quad (18)$$

$$C_{Mz} = 2.67 Re_z^{-0.5} \quad (Re_{z1} < Re_z < Re_{z2}) \quad (19)$$

$$C_{Mz} = 2\pi \frac{r_i}{s} Re_z^{-1} \quad (Re_z < Re_{z1}) \quad (20)$$

Case 2: $Re_{z2} < Re_{z3}$

$$C_{Mz} = 0.0622 Re_z^{-0.2} \quad (Re_{z3} < Re_z) \quad (21)$$

$$C_{Mz} = 2\pi \frac{r_i}{s} \text{Re}_z^{-1} (\text{Re}_z < \text{Re}_{z3}) \quad (22)$$

The coefficient of friction moment CM_z is defined as shown in Eq. (23). Windage loss P_{Wz} was calculated from (24) using torque M_z derived from (18) to (22).

$$C_{Mz} \equiv \frac{M_z}{\frac{1}{2} \rho \omega^2 r_i^5} \quad (23)$$

$$P_{Wz} \equiv M_z \omega \quad (24)$$

From above derivation, total windage loss P_W is derived from (25) as sum of windage loss P_{Wr} derived by (13) and P_{Wz} (24).

$$P_W = P_{Wr} + P_{Wz} \quad (25)$$

Windage loss derived from (25) is calculated under the ideal condition that rotor is column, the stator is cylinder, and there is no interaction between the cylindrical surface and the top and bottom surface of double cylinder model.

Windage Loss Breakdown

Windage loss was calculated based on above calculation formula. Cross-section structure of the rotor and stator is shown in Fig. 1. The rotor that includes magnetic bearing part is shown in Fig. 2. Cooling style of the motor is forced-air cooling. Here, windage loss was calculated as simple coil-end shape and constant inner air temperature.

Table 3 shows windage loss breakdown against total loss. It is denoted the total windage loss of the machine is 100%. The ratio of windage loss generated by axial magnetic bearing part was the largest because the largest outside diameter of the rotor in the rotary part of axial magnetic bearing made circumference speed fast and a disc face has large area. The ratio of windage loss generated by motor core part was second largest. It is because outside diameter of rotor in motor core part is the

Table 3 Windage loss distribution (calculation)

Part	Calculation value [%]
Axial magnetic bearing	51.5
Core	21.0
Coil end	15.4
Radial magnetic bearing	8.2
Touchdown bearing	3.9
Total windage loss	100

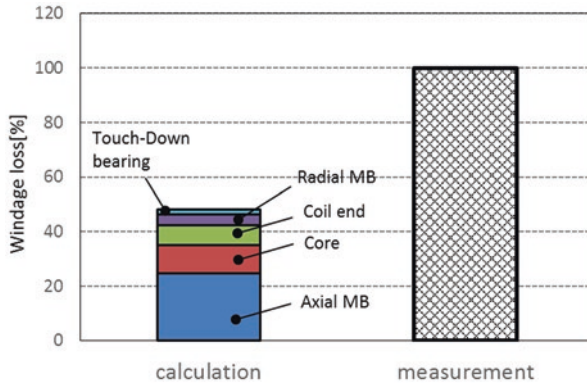


Fig. 15 Calculation and measurement value of windage loss

largest except of axial magnetic bearing part and thickness of laminating steel is thick.

Figure 15 shows windage loss value derived from calculation and measurement. Windage loss was measured by rotating a rotor core of the generating side that was not magnetized in back-to-back test. In Fig. 15 expresses total measured windage loss of the machine as 100%. From this result, measured value was only 48% of calculation value. There can be some considered factors which are as follows.

Factor 1: No influence of operation environment reflects for calculation formula of windage loss.

Calculation formula of windage loss was considered as ideal double cylinder model. Since this model assumes which, there is no influence for generating windage loss caused by friction of component shape, especially roughness of laminating steel, slot openings, case inner surface and coil end, reflected for calculation formula.

Factor 2: Uncertain viscosity, density, and flow of inner fluid.

Inner fluid of the motor is air. Windage loss was calculated using constant fluid physical property of coefficient of kinematic viscosity and density. Although forced-air cooling is performed in the experiment, the change of fluid physical property inside the motor by forced-air cooling cannot be considered in the calculation formula.

3.4.2 Windage Loss Measurement

Difference between calculation and measurement value about windage loss was confirmed in the preceding section. However, it is not necessary to be able to apply this characteristic to all motors because there are many kinds of motor that has various shapes and volumes and does not have the same operating environment. In this

section, windage loss is verified against loss evaluation machine which imitates only double cylinder structure in the motor.

Loss Evaluation Machine Structure

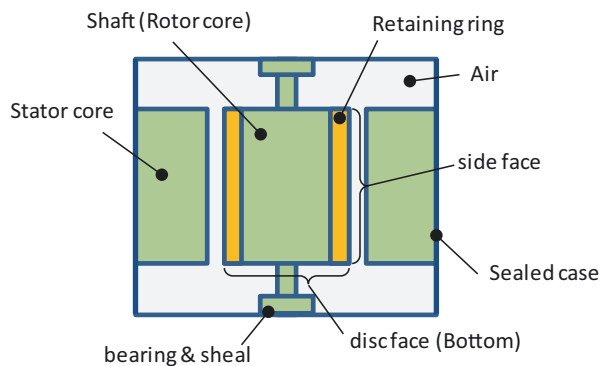
The structure of the loss evaluation machine is shown in Fig. 16. As a specimen, the machine has a rotor core and a stator core which are in the same size as those of the prototype motor. The rotor core is not magnetized. The stator core has no coils two-stator core are prepared for the experiment; one has some grooves in slot openings on the inner surface, while the other does not have. Machinery loss that includes bearing loss and windage loss of the machine can be measured by rotating the rotor core from the outside.

Decompression Experiment

Decompression experiment using the loss evaluation machine was performed in the purpose of extracting only windage loss from machinery loss that includes not only windage loss but also bearing loss and seal loss.

As the specimen of the machine is shown in Fig. 16, CFRP rings were used as retaining rings for the rotor core. Ball bearings and seals were implemented at both ends of the shaft. A two-stator core made of iron in cylinder shape was prepared for this experiment in order to remove disturbance. One has some grooves in slot opening in inner surface, while the other does not have. In its experiment, the specimen part of the machine is sealed, and machinery loss was measured in decompression condition by using vacuum pump. Machinery loss in absolute vacuum condition can be estimated from its experimental result because the amount of loss generating in the specimen is proportional to inner pressure. In absolute vacuum condition, machinery loss is expressed as the sum of bearing loss and seal loss. Therefore, windage loss can be derived by subtracting machinery loss calculated in absolute vacuum condition from that calculated in atmospheric pressure condition.

Fig. 16 Structure of loss evaluation machine



Experimental Result

Decompression experiment was performed under the condition shown in Table 4. Figure 17 shows the relationship between inner pressure inside the specimen and mechanical loss. Mechanical loss measured before decompression expresses 100% in Fig. 17. From this result, it could be said that mechanical loss was proportional to inner pressure. Mechanical loss under absolute vacuum condition was 53% of the mechanical loss measured before decompression from approximation. Since mechanical loss under absolute vacuum includes only bearing loss and seal loss, windage loss can be estimated in the value of 47% of total mechanical loss.

Likewise, another experiment was performed in the condition of replacing the stator core for the other one that has some grooves imitating slot shape, and windage loss was also calculated. Windage loss calculated from experimental data in each condition is shown in Table 5 when the calculation value of windage loss as 1. In Experiment 1, a rotor with retaining ring that is made of CFRP and a stator without grooves were used. In Experiment 2, a rotor with retaining ring that is made of CFRP and a stator with grooves were used.

Windage loss generated in experiment 1 in which CFRP rings and stator core that has no grooves were implemented was 1.19 times as calculation value. It can be considered that one of the reasons about the difference between these values is the increase of friction caused by rotor surface roughness.

Windage loss generated in experiment 2 in which CFRP rings and stator core that has some grooves were implemented was 1.36 times as calculation value. Its value is larger than that of experiment 1. From difference of condition in each experiment, it can be considered that grooves in slot opening are one of the reasons why windage loss increases.

From the above results, the construction of theory equation about windage loss for each motor is required in consideration of the shape and roughness of surface in contact with fluid in order to calculate windage loss accurately.

Table 4 Decompression experiment condition

Rotor Surface	CFRP (Rough Surface)
Stator surface	No grooves (Smooth surface)
Inner fluid	Air
Cooling	No cooling
Decompression	0 ~ -0.08 [MPa]
Loss from specimen	Windage loss
	Bearing loss
	Seal loss

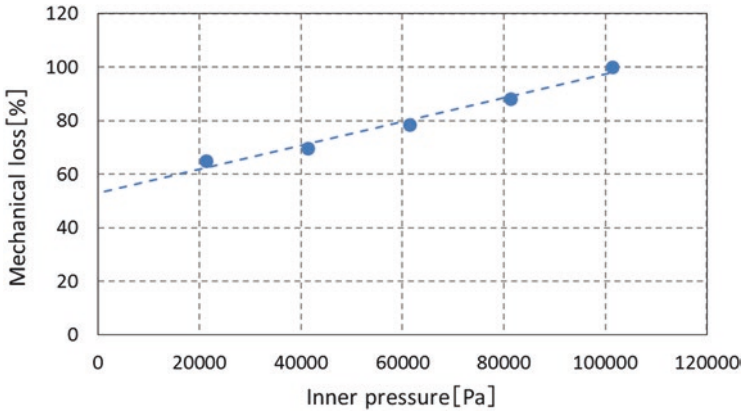


Fig. 17 Relationship between inner pressure and machinery loss

Table 5 Windage loss on surface condition

Specimen condition	Rotor surface	Stator surface	Windage loss [P.U.]
Calculation (Ideal condition)	Smooth	Smooth	1.00
Experiment 1	CFRP (rough)	No grooves in slot openings	1.19
Experiment 2	CFRP (rough)	Some grooves in slot openings	1.36

4 Cooling System and Heat Run Test

4.1 Cooling System

We carried out the heat run test at the rated point for measuring steady temperature inside the motor. Figure 18 shows the configurations of the air cooling system in the test. At this time, two cooling systems were evaluated by installing one 3.7 kW–50 Hz cooling blower for exhausting air. In system A, inlet air would be flowing through to a ventilation hole of the direct-coupled side and passing through the other ventilation hole of the non-direct-coupled side. In system B, in contrast, inlet air would be flowing through to ventilation holes on both the direct-coupled side and the non-direct-coupled side and passing through ventilation holes opposite both sides. Additionally, the center ventilation hole was opened for inlet air in system B.

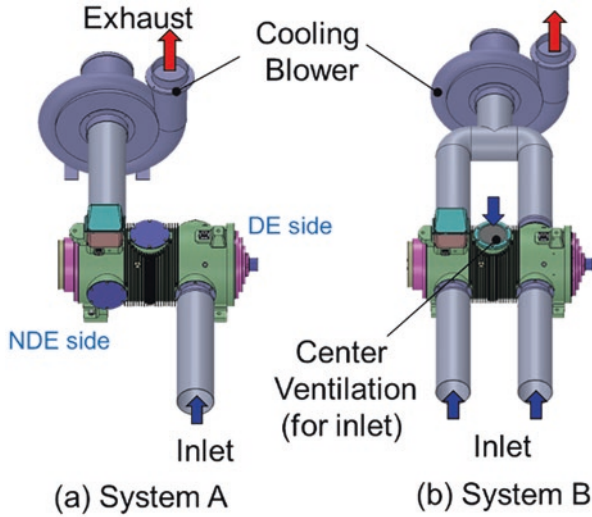


Fig. 18 Air cooling system in heat run test

4.2 Temperature Test Result

To measure the coil temperature during the operation, a plurality of thermocouples was mounted inside the coil as shown in Fig. 19a. Furthermore, the temperature of the rotor magnet was estimated as an average temperature by calculation with the temperature coefficient of residual flux density $\%/K$ of the magnet, and the decrease rate in the induced voltage was measured before and after the operation. Figure 19b shows the temperature increases in the coils and the magnet. As a result of measurements, the temperature increases in both the coils, and the magnet in system B is lower than that in system A.

4.3 Flow Analysis

Flow in the ventilation system has a significant influence on the temperature increase of each part of the motor. We conducted computer fluid analysis (CFD) to evaluate the cooling system. Figure 20 shows the analysis result for the air flow inside the motor. From this analysis result, it is possible to clarify the state of air flow inside the motor.

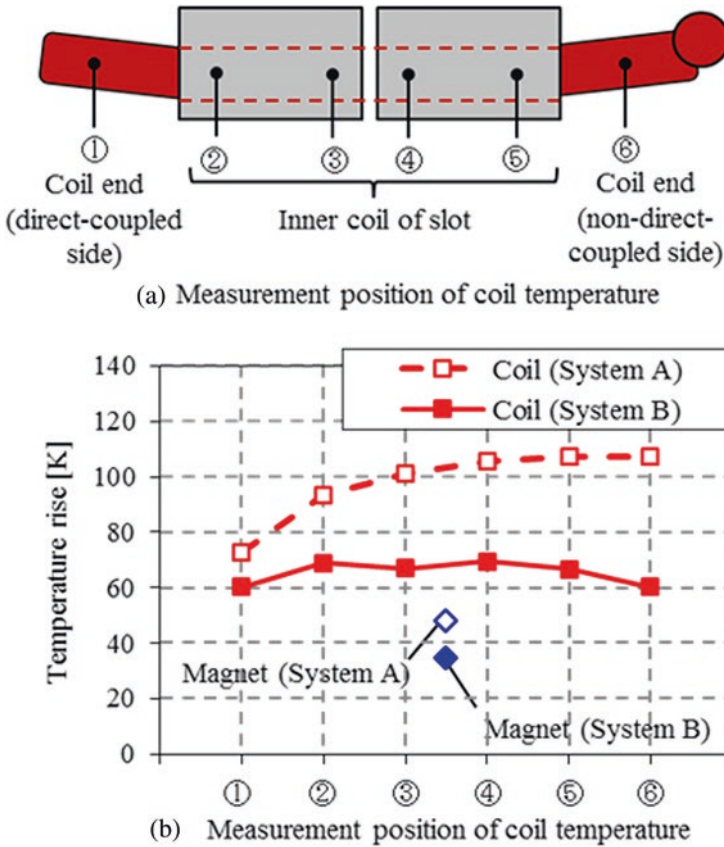


Fig. 19 Temperature increase in heat run test

5 Conclusion

In this paper, we evaluated the performance of the prototype for a 250 kW–20,000 min⁻¹ high-speed PM motor. As the result of the evaluation, it was found that the motor efficiency is 96.6% at the rated point and the mechanical loss could be considered to be dominant loss, especially in the high-speed region. Furthermore, fundamental verification about windage loss was performed. Calculation and measurement of windage loss in the loss evaluation machine were conducted and compared. From comparison, influence of surface shape of the rotor and stator for windage loss and accuracy of calculation formula were confirmed. In addition, we compared two air cooling systems by carrying out a heat run test at the rated point and confirmed that system B could have sufficient cooling performance for the motor.

In the future, we will verify the design accuracy by performing comparisons with the results from loss separation found at this time and confirming more accurate

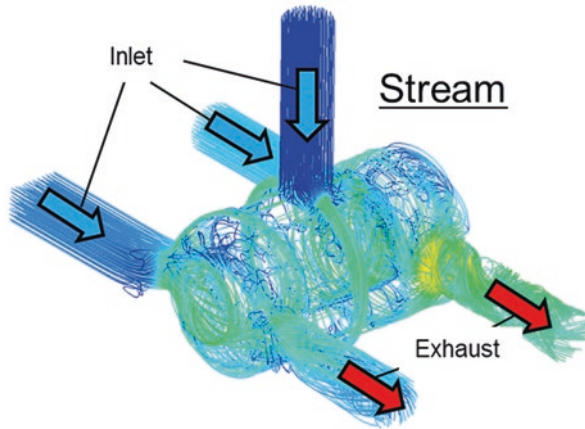


Fig. 20 Air flow inside motor

calculation formula for the motor in operation environment to improve efficiency and work on development of further high-speed and large output power motors.

References

1. Investigating R&D Committee on New Technologies for Industry Applications of PM motors, Trend of New Technologies toward their Spread, IEEJ Technical Report, No. 1207, 2010 (in Japanese)
2. IEEJ, Current Situations and Future Issues of Adjustable-Speed AC Drives, Technical Report No. 1326, p. 64, 12, 2014 (in Japanese)
3. T. Okitsu, S. Uchiyama, K. Matsuo, D. Matsuhashi, Performance evaluation of high speed PM motor 250kW-20,000rpm. *Meiden-jihō* **352**(3), 30–33 (2016) (in Japanese)
4. S. Uchiyama, K. Matsuo, T. Onishi, T. Okitsu, D. Matsuhashi, Characteristic evaluation of 250kW – 20,000min⁻¹ High-speed Motor, in *Proceedings of IEEJ 2016*, vol. 5, (Sendai, 2016), pp. 35–36. (in Japanese)
5. M. Omura, K. Matsuo, S. Uchiyama, T. Okitsu, D. Matsuhashi, Loss comparison of rotor retaining ring in a high-speed motor, in *Proceedings of IEEJ 2017*, vol. 5, (Toyama, 2017), pp. 55–56. (in Japanese)
6. Meidensha Catalogue, *Ultra-High Speed PM & Medium Voltage Drive* (Meidensha Corporation, 2016)
7. T. Fukao, A. Chiba, Super high-speed drives-introduction. *Proc. Natl. Conv. IEEJ*, S.21.1-4,3 (1998). (in Japanese)
8. R.R. Moghaddam, *High Speed Operation of Electrical Machines, a Review on Technology, Benefits and Challenges* (IEEE ECCE, 2014), pp. 5539–5546
9. M. Rahman, A. Chiba, T. Fukao, Super high speed electrical machines-summary, in *IEEE, Power Engineering Society General Meeting*, vol. 2, (2004), pp. 1272–1275
10. B. Sarlioglu, T. Jahns, D. Ionel, Design and Manufacturing of PM Electric Machines, *IEEE ECCE 2015*, Tutorial, p. 196
11. E. Schubert, B. Sarlioglu, Mechanical Design Method for a High-Speed Surface Permanent Magnet Rotor, *IEEE ECCE 2016*, p. 6

12. D. Matsuhashi, K. Matsuse, High Power High Speed Motor Drives for Industry Application, IEEE PEDES 2016, Plenary speech, India, 16 Dec 2016
13. K. Matsuse, D. Matsuhashi, New technical trends on adjustable speed AC motor drives. *Chin. J. Electr. Eng.* **3**(1), 1–9 (2017)
14. C. Babetto, G. Bacco, G. Berardi, N. Bianchi, *High Speed Motors: A Comparison between Synchronous PM and Reluctance Machines* (IEEE ECCE, 2017), pp. 3927–3934
15. B. Sarlioglu, T. Wu, *Design and Analysis of Electrical Machines Including High-Speed Types* (IEEE IECON Tutorial, 2014), p. 176
16. J. Luomi, C. Zwyssig, A. Looser, J.W. Kolar, Efficiency Optimization of a 100-W 500000 – r/min Permanent-Magnet Machine Including Air-Friction Losses. *IEEE Trans. Ind. Appl.* **45**(4), 1368–1377 (2009)
17. H. Fang, R. Qu, J. Li, *Rotor Design for a High-Speed High-Power Permanent-Magnet Synchronous Machine* (IEEE ECCE, 2015), pp. 4405–4412
18. P. Mellor, R. Wrobel, D. Salt, A. Griffio, *Experimental and Analytical Determination of Proximity Losses in a High-Speed PM Machine* (IEEE ECCE, 2013), pp. 3504–3511
19. P.B. Reddy, T.M. Jahns, T.P. Bohn, *Modeling and analysis of Proximity Losses in High-Speed Surface Permanent Magnet Machines with Concentrated Winding* (IEEE, ECCE, 2010), pp. 996–1003
20. A. Smirnov, N. Uzhegov, T. Sillanpaa, J. Pyrhonen, O. Pyrhonen, High-speed electrical machine with active magnetic bearing system optimization. *IEEE Trans. Ind. Electron.* **64**(12), 9876–9885 (2017)
21. Z. Fu, D. Jiang, R. Qu, Design of four-axis magnetic bearing for high speed motor, in *IPEMC-ECCE Asia*, (2016)
22. V.F. Wendt, Turbulente Stromungen zwischen zwei rotierenden konaxialen Zylindern. *Arch. Appl. Mech.* **4**(6), 577–595 (1933)
23. Schlichting, *Boundary Layer Theory* (McGraw-Hill Press, New York, 1979)

Regulation and Enforcement [Surveillance] Consequences



Rob Boteler and Kirk Anderson

1 Current Regulations Covering Motors and Motor-Driven Systems

1.1 *Small Motors [Fans, Pumps, Pool Pumps, Compressors, and Others]*

Motor and motor-driven systems are regulated in two distinct manners. The first is a legacy method that looks at the motor in isolation from the system it is driving. This method relies on tested or computed efficiency obtained at 100% load conditions under controlled laboratory conditions. The accuracy of these tests has been and continues to receive great attention from many in the energy arena. This method can produce very precise results under regulatory parameters. The weakness of this method comes with downstream accuracy of forecasted savings when motors become part of a system operating under real applications with load variations and power quality variables. The second, and newer method, is the systems approach. As regulators now realize that the systems approach offers not only a much greater energy saving opportunity but also a more meaningful metric, “power management” that adds elements of application to create an energy index. This method is similar to how automobiles are regulated (i.e., miles per gallon or liters per 100 km). This approach considers the entire system [automobile] into the metric instead of focusing on a single operating point of a single component [the automobile engine].

R. Boteler (✉)
Nidec Motor Corporation, St Louis, MO, USA
e-mail: rob.boteler@nidec-motor.com

K. Anderson
NEMA, Washington, DC, USA
e-mail: kirk.anderson@nema.org

The changes in the global motor supply chain since the first motor MEPS in 1992 are staggering. Because of a new distributed supply chain, motor regulations now need robust market surveillance/enforcement policies to ensure delivery of the energy savings projected by the regulator. The task now before regulators to avoid creating unfair competitive situations in the market is truly monumental. In the USA, manufacturers and importers are viewed as the same by federal code. This places responsibility for motor MEPS compliance with the motor manufacturer who imports motors or a system builder who imports a system (e.g., pump, compressor, meat grinder, etc.) that includes all motors covered by regulation. This paper will discuss the proposed import declaration procedure put forth by the US Department of Energy in 2017.

The concern for future small motor regulation has been accelerated by a test standard NOPR [notice of proposed rulemaking] issued by the DOE in 2017. NEMA commented on the test methods included within the NOPR as to their applicability to a wider range of small motors including the addition of several previously unregulated motor technologies. It was in this evaluation that the consideration for global motor supply chain became a greater concern. And it is for this reason that NEMA again asked DOE and CBP [customs and border patrol] for clear and concise enforcement procedures of current and future motor performance regulations.

1.2 Global Motor Supply Chain

The need for better border enforcement has been exacerbated by changes in the global motor supply chain brought about by the Internet. A recent Internet search showed 618,000,000 total hits with “electric motor for sale” which included 135,000,000 AC for sale and 107,000,000 DC, to over 1.2 billion hits depending on the terminology searched.

Research shows over 250 motor suppliers soliciting business on the Internet from Asia. These companies ship through various importers or direct to OEM’s within regulated markets. The absolute numbers of Internet hits are not as important as the fact that the overall supply chain of regulated motors has seen this transition occur since the first motor efficiency regulations over 20 years ago. How does a regulatory body deal with this situation and not place domestic suppliers at severe disadvantage to foreign competition?

With the expansion of online industrial retailers, OEMs, end users, distributors, and contractors now have access to a thousand or more suppliers. This availability combined with limited means of identifying compliant products and even less enforcement elevates enforcement to a new level of importance for motor efficiency regulations.

It is estimated that both the EU and US markets for small motor <5 HP single phase exceed 10 million units per year each. The global supply of small motor sales falls into three categories, one sold to OEMs, two manufactured by OEMs for use in

their equipment, or three sold to distribution/contractor. Of the 10 million estimate units, 80–90% enter the end-user market embedded inside a piece of equipment. Of the embedded units it is estimated that 75–85% are imported as a component of the equipment. Therefore approximately 70% or more of the units sold in the EU or USA are imported (Fig. 1).

To understand the impact of enforcement/surveillance on realized energy savings, one must consider the scope covered product currently within motor efficiency standards. In general, the EU, USA, Canada, Brazil, Australia, and Mexico have standards that cover AC induction motors from ¼ horsepower to 500 horsepower. This range of products is very broad thus encompassing virtually all electrically powered systems used in commercial, industrial, and residential application. The global supply of goods allows motors to reach regulated markets through several different channels. As noted previously, most electric motors are sold to an OEM [original equipment manufacturer] who incorporates the motor into a device to drive the device. The lower the power level of the motor, the more likely it only sold as a replacement by the OEM. Larger motors in higher power levels are generally available from multiple manufacturers/suppliers to the replacement market.

The existing US small motor rule [EISA 2010] [1] determined that over 4 million units [general purpose open drip proof] ship per year would be covered by the rule in the USA. The DOE based their analysis on data supplied by NEMA motor manufacturers, a search of Internet catalog data and consultant research. The DOE included imports in the calculations done to determine the market. DOE estimated 750,000 polyphase, 3.1 million CSIR, and 163,000 CSCR motors were sold in the base year 2010. The technical support document then broke these estimates down to five applications: pumps, fans, compressors, conveyors, and general industrial and

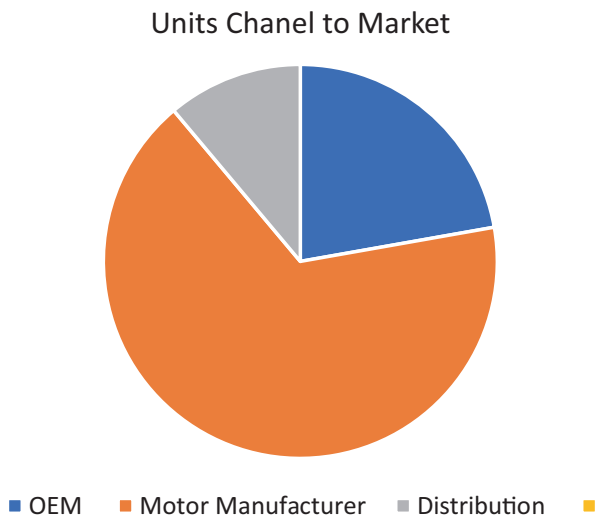


Fig. 1 Units estimated split by channel

miscellaneous. It is important to consider the applications identified to recognize the likelihood that covered motors will enter the market embedded within the application as an imported device. OEMs producing these systems sell a large percentage of their product with the motor attached or embedded making it very likely that imported pumps, fans, compressors, or conveyor drives will include a small motor as part of the imported “system.” We will come back to this assumption later to estimate the effect on DOE forecasted energy and GHS reduction models (Fig. 2) [2].

In drafting the EISA small motor rule in June of 2010, the motor manufacturers were joined by several energy advocacy groups in discussing the need for border enforcement and provided recommendations for procedures and methods to address the concerns. These groups include ACEEE [American Council for an Energy-Efficient Economy], NEEA [Northwest Energy Efficiency Alliance], and Earthjustice. The excerpt below is a summary of the rule:

DOE received a number of comments pertaining to the enforcement of today’s final rule and what steps DOE will take to enforce these efficiency standards. Regal-Beloit, A.O. Smith, and WEG all expressed the concern that some manufacturers, most notably from overseas, may not comply with the standards, and they wished to see a plan for how these standards would be enforced. A joint comment submitted by PG&E, SCE, SCGC, and SDGE also stressed the importance of developing a plan for enforcement. Emerson agreed with the joint commenters that a lack of enforcement would put the domestic manufacturers who comply with today’s standard at a disadvantage in the marketplace because they would incur the costs necessary to increase efficiency. Additionally, DOE received comments offering suggestions for how to improve the enforcement of today’s rule. Regal-Beloit commented that DOE should require a marking on the motor to indicate that it complies with the efficiency standard, such as is done with NEMA Premium motors. Regal-Beloit also suggested that DOE perform some sort of audit of the motors on the market to ensure compliance with today’s rule. Earthjustice requested that the final rule outline a specific date on which DOE will layout plans for enforcement of the small electric motor standards. NEMA’s reiterated these concerns about enforcement and outlined several steps DOE should take to ensure proper compliance.

Table 9.2.1 Application Shares by Equipment Type

No.	Application	Equipment Category		
		Polyphase	CSIR	CSCR
1	Air and gas compressors	17.3%	14.9%	14.9%
2	Conveyors	13.3%	11.9%	11.9%
3	General industrial machinery	11.3%	12.5%	12.5%
4	Industrial and commercial fans and blowers	7.3%	6.9%	6.9%
5	Pumps and pumping equipment	50.7%	53.7%	53.7%
	TOTAL	100%	100%	100%

Fig. 2 EISA small motor rule application breakdown

1.3 NEMA Recommendations to DOE

First, NEMA recommended that DOE expands its present compliance certification number system that is used for electric motors to include small electric motors.

Second, it recommended a means to notify DOE of potential violations.

Third, it suggested maintaining a Web site that lists manufacturers and OEMs who have submitted compliance certificates.

Fourth, it supported penalties for repeat violations of the law. Finally, NEMA stressed the importance of securing the appropriate funds for implementing and maintaining an enforcement program (NEMA, No. 24 at pp. 26–27). NEEA and NPCC also commented on the importance of appropriating funds for enforcement of today's standards.

1.4 DOE's Reply to NEMA, Advocates, and Electric Power Utilities

While it is uncommon for a standard rulemaking to address issues of enforcement, DOE would like to highlight its intention to outline concrete steps for enforcing today's efficiency standards. Given the numerous rulemakings that the agency must promulgate pursuant to its court consent decree and statutory requirements, DOE plans to issue this supplemental notice as expeditiously as possible to invite comment from interested parties and to ensure that the motor industry has sufficient time to adjust to any new provisions that DOE proposes.

EISA forecasted GHG reductions shown below for two covered categories of small electric motors: (1) polyphase and (2) capacitor start. The estimated negative impact of having no border enforcement reduces the polyphase savings by 30% or more, while the single-phase capacitor start forecast drops by an estimated 40% due to the higher percentage of single-phase imports. This percentage is low because of the current narrow definition of covered product [open drip proof general purpose]. Should a broader definition become regulated the percentages could reach as much as 70% of imported small motors (Fig. 3).

2 Changes to the Global Supply Chain

The changes to the supply chain that have occurred over the past 20 years have forever altered the way regulators must address the global supply chain's impact on regulations. In the early 1990s, when the USA was drafting the very first motor efficiency regulation, the Department of Energy considered how it could best police imports of covered product. The Department discussed this point with motor manufacturers as well as OEMs who integrate motors into their system. The DOE agreed

Changes to the global supply chain

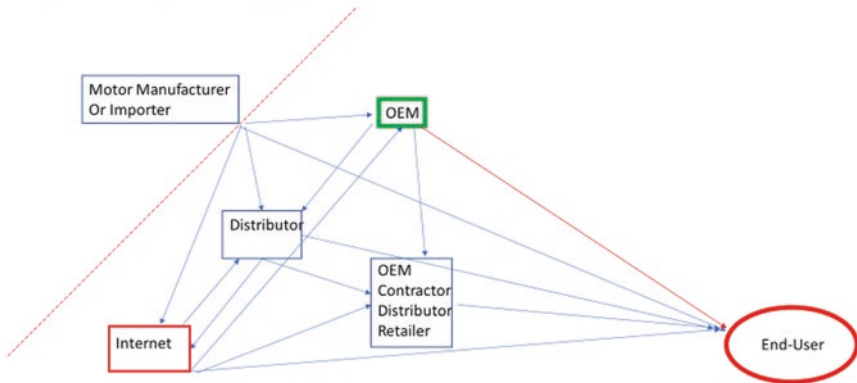


Fig. 3 Today's global motor supply chain product flow

with motor manufacturer to include a “CC compliance number” requirement. The DOE rule required motor manufacturers and motor importers to submit test performance data to meet compliance requirements demonstrating compliance. Once DOE reviewed the data submitted for acceptance, the DOE would then issue a unique CC compliance number to each manufacturer/importer. The manufacturer/importer was required to include this unique identifier on each unit's permanent nameplate. By having each motor identified with the compliance number, the registered motor supplier could be tied back to test data submitted to DOE. It was assumed by the motor manufacturers that with this in place, a border DOE enforcement process could take place. Unfortunately, in actual practice this has not been the case.

Motor manufacturers were somewhat naive in their assumption that there was a coordinated effort between DOE and CBP [customs and border patrol] to create procedures and provide resources using the CC as a tool to identify compliant and noncompliant product, which would ultimately protect compliant motor and motor system suppliers from unfair competition. Motor manufacturers have been concerned since the original EPCA regulations issued in 1992 for CBP to initiate a process that enforced the DOE motor efficiency regulations. To date, there have been no procedures issued by CBP to enforce DOE motor efficiency rules.

In subsequent regulations, EISA [Energy Independence and Security Act] small motor rule, NEMA again questioned DOE's intent to engage with CBP. NEMA members expected DOE, as the creator of motor regulations, to have an interest in border enforcement that policed the border assuring that the energy savings predicted by the rule were achieved. For many years, the DOE response given the motor manufacturers was to instruct NEMA to contact CBP directly and work out a plan for motor efficiency regulation border enforcement.

2.1 What Has the Current Global Supply Chain Done to Achieving Estimated Energy Savings?

Since 1992, electric motors have been subject to minimum energy performance standards. The DOE has worked closely with manufacturers and trade associations to define covered products, establish efficiency performance levels, and select or create test methods. DOE has included sampling requirements and penalties for noncompliance.

As the number of suppliers has increased, and distribution channels evolved, NEMA believes there is an increasingly greater number of noncompliant motors that are being imported, most commonly embedded inside a piece of equipment.

In the past, government agencies, such as the DOE, have released motor performance regulations that were not vetted with CBP for border enforcement. It is NEMA's view that there needs to be enforcement of federal regulations on covered products and products containing covered products embedded within.

Presently there is no specific statutory requirement to establish comprehensive administrative enforcement requirements including a detailed product description, performance and label requirements, as well as resource requirements with CBP for government agencies that establish regulations. Lacking this, the energy savings originally sought will be lost and an increasing number of noncompliant products will enter the market.

NEMA believes including a well-defined border enforcement plan requirement within motor energy performance regulations that covers both finished goods and embedded products fits with the administration's item five "impact of any lessening of competition" (Fig. 4).

As regulations consider additional motor products, lower output power levels will have a difficult time reaching an energy savings level that satisfies the proposed efficiency requirements for regulation. Higher output power levels have gone through multiple rulemakings over the past 25 years and have less energy savings opportunities remaining. NEMA members believe the future energy savings will be delivered by the motor-driven system. Regardless of how DOE chooses to regulate [component or system], NEMA motor members believe there is ample reason for DOE to establish a border enforcement plan to ensure that manufacturers making compliant product remain competitive now and in the future.

Current regulations cover higher output motors (1–500HP or 0.75–375 kW) that have a relatively lesser number of imports when compared with the smaller and lower output power motors (below 1HP or 0.75 kW). Should regulation expand to include a larger scope of smaller and lower output power motors the percentage of motors embedded in imported motor-driven equipment will be the greater number of motors manufactured in the USA. Regulators will need to adjust energy savings estimates based on their ability to manage the effect of the global supply on results.

To allow a regulation to exist without a well-developed enforcement plan will cause harm to the economy. The risks to deploying regulations without inter-agency coordination [DOE and CBP] are not in the interest of manufacturers or those who

Energy Policy & Conservation Act of 1975 Factors	DOE Analysis
1. Economic impact on consumers and manufacturers	Life-cycle cost analysis Manufacturer impact analysis
2. Lifetime operating cost savings compared to increased cost for the product	Life-cycle cost analysis
3. Total projected savings	National impact analysis
4. Impact on utility or performance	Engineering analysis Screening analysis
5. Impact of any lessening of competition	Manufacturer impact analysis
6. Need for national energy conservation	National impact analysis
7. Other factors the Secretary considers relevant	Environmental assessment Utility impact analysis Employment impact analysis

Fig. 4 Seven elements used to evaluate a motor efficiency regulation

use electric or small electric motors. By not enforcing a regulation at the border, the motor consumer essentially pays an added tariff for regulated products that the off-shore supplier avoids.

The US Department of Energy acknowledged this issue and released a NOPR [notice of proposed rulemaking] in 2016 to address motor efficiency rule border enforcement. The DOE issued a pre-NOPR that outlined an import declaration procedure designed to create an enforcement method that employed existing CBP protocols relying on existing UTSC codes to identify imported motor-driven systems that have embedded motors.

3 Certification Report Proposed to Be Added to Motors and Motor Systems When Imported

The import declaration will require a certification report that provides specific information for each basic model, including the product or equipment type, the brand name, and the basic model number, as well as specific energy use information (10 CFR 429.12(b)).

Importers are currently required to submit certifications on product-specific templates to DOE’s Compliance and Certification Management System (CCMS), which assigns each certification submission a unique attachment identification number (10 CFR 429.12(h)) processing infrastructure. Specifically, EO [executive order] 13659 requires applicable government agencies to use CBP’s International Trade Data

System (ITDS) and its supporting systems, such as the Automated Commercial Environment (ACE), to create a “single window” through which businesses will electronically submit import-related data for clearance. EO 13659 was established to provide a simpler, more efficient portal for trade use, to the benefit of both the trade and those government agencies [DOE and CBP] with related authorities and responsibilities.

In this Import Declaration NOPR, DOE proposes to require that importers of covered products or equipment subject to an applicable energy conservation standard set forth in 10 CFR Part 430 or 431 and falling under specified classifications of the Harmonized Tariff Schedule of the USA provide a certification of admissibility *for each shipment of such products or equipment before their arrival* at a US port of entry. Importers of such covered products or equipment are *currently required to submit annual certification reporting to DOE* that the products or equipment they intend to import are compliant with all applicable energy conservation standards, using CCMS.

DOE proposes that if an importer has already submitted its required certification report to DOE, the importer would provide a certification of admissibility with only the information necessary to tie the shipment back to its most recent CCMS submission. Any importer that has not already filed its required annual certification would be required to provide more detailed information regarding the covered product or equipment contained in the shipment. The requirement for a certification of admissibility would apply to all covered products and equipment subject to a DOE energy conservation standard set forth in 10 CFR Part 430 or 431. The requirement would apply to all such products and equipment contained in the shipment, either as a final product or a component part of a final product. For example, an importer would need to submit an electronic record for all covered electric motors as defined in 10 CFR 431.12, provided that the electric motor is subject to a standard, regardless of whether the electric motor will be imported as a stand-alone product or as a component part of another product not subject to DOE regulations (e.g., a treadmill). DOE has provided a list of UTC codes to be included in the ACE data requirement. This list is extensive and subject to editing as the extent of covered motor products content is determined. Below is a partial sample of the HTS codes under consideration by the Department of Energy to be subject to the import declaration requirement. This sample represents approximately 15% of the total HTS codes to be covered.

3.1 HTS Code (2014) HTS Product Description (2014) Partial Listing of Products to Be Included

8402 Steam or other vapor-generating boilers (other than central heating hot water boilers capable also of producing low-pressure steam); super-heated water boilers; parts thereof

8403 Central heating boilers (other than those of heading 8402) and parts thereof

8413 Pumps for liquids, whether or not fitted with a measuring device; liquid elevators; parts thereof

8414 Air or vacuum pumps, air or other gas compressors, and fans; ventilating or recycling hoods incorporating a fan, whether or not fitted with filters; parts thereof

8415 Air-conditioning machines, comprising a motor-driven fan and elements for changing the temperature and humidity, including those machines in which the humidity cannot be separately regulated; parts thereof

8416 Furnace burners for liquid fuel, for pulverized solid fuel or for gas; mechanical stokers, including their mechanical grates, mechanical ash dischargers, and similar appliances; parts thereof

8417 Industrial or laboratory furnaces and ovens, including incinerators, non-electric, and parts thereof

8418 Refrigerators, freezers, and other refrigerating or freezing equipment, electric or other; heat pumps, other than the air-conditioning machines of heading 8415; parts thereof

8419.11.00 Instantaneous gas water heaters

8419.19.0020 Instantaneous water heaters, nonelectric

8419.81.50 Cooking stoves, ranges, and ovens

8421.12.0000 Clothes dryers (centrifugal)

8422.11.00 Dishwashing machines, of the household type

8422.19.00 Dishwashing machines, other

8422.90 Parts of dishwashing machines

8427.10 Self-propelled trucks powered by an electric motor

8428 Other lifting, handling, loading, or unloading machinery (e.g., elevators, escalators, conveyors, teleferics)

8429 Self-propelled bulldozers, angledozers, graders, levelers, scrapers, mechanical shovels, excavators, shovel loaders, tamping machines, and road rollers

8430 Other moving, grading, leveling, scraping, excavating, tamping, compacting, extracting, or boring machinery, for earth minerals or ores; pile drivers and pile extractors; snowplows and snowblowers

8431 Parts suitable for use solely or principally with the machinery of headings 8425 to 8430

8432 Agricultural, horticultural, or forestry machinery for soil preparation or cultivation; lawn or sports ground rollers; parts thereof

If the import shipment contains any listed products or equipment, the importer would be required to state whether the product or equipment has been certified to DOE as compliant with all applicable energy conservation standards and, if so, the CCMS ticket number, the CCMS attachment identification number assigned to the certification submission, and the line number in the submission corresponding to the basic model certified. EPCA [Energy Policy and Conservation Act] currently authorizes the Secretary of Energy to require importers of covered products and equipment “to submit information or reports to the Secretary” with respect to energy efficiency, energy use, or water use of covered products and equipment (42 U.S.C. 6296(d)

(1)). 10 CFR Part 429 requires, among other things, that importers submit a certification report to DOE prior to distributing their products in US commerce, and the failure to properly certify covered products and covered equipment subject to DOE energy conservation standards is a prohibited act under those regulations (10 CFR 429.12, 429.102(a)(1)). Part of the certification report is a statement whereby the manufacturer (including an importer) certifies that the basic models listed in the certification report comply with the applicable energy conservation standard and have been tested according to the applicable test requirements (10 CFR 429.12).

If any covered product or equipment contained in the shipment has not been certified to DOE through CCMS, the importer would be required to include in its certification of admissibility (1) the type of product or equipment, (2) the brand name of the covered product or equipment, (3) the individual model number of the covered product or equipment, (4) the original equipment manufacturer (OEM) of the covered product or equipment, and (5) a contact name and e-mail address for the importer of record.

Currently, 10 CFR Part 429 uses the terms “individual model number,” “manufacturer’s individual model number,” and “manufacturer’s model number” interchangeably and, of the three terms, only defines the term “manufacturer’s model number.” For clarity, DOE proposes to replace the term “manufacturer’s model number” with the term “individual model number” in the definitions at 10 CFR 429.2. which is defined as follows:

Manufacturer’s model number means the identifier used by a manufacturer to uniquely identify the group of identical or essentially identical covered products or covered equipment to which a particular unit belongs. The manufacturer’s model number typically appears on the product nameplates, in product catalogs, and in other product advertising literature.

Forecasted savings impact of current EISA small motor rule is a 40% deduction for a lack of border enforcement (Fig. 5).

Polyphase	CO2- MT	NOX-KT	Hg- Tons
DOE rule	15.4	11.0	.085
Import affect neg %	30	30	30
Lost savings	4.62	3.3	.0255
Cap Start	CO2-MT	NOX- KT	Hg –Tons
DOE rule	96.8	69.5	.408
Import affect neg %	40	40	40
Lost savings	38.72	27.8	.163

Fig. 5 EISA small motor rule greenhouse gas reduction

4 In Conclusion

The global motor supply chain has changed so greatly over the past 20 years that to effectively regulate motor efficiency and deliver estimated energy saving is much more difficult than in the past. Potential savings from motors as components has become a much smaller percentage of the overall motor-driven system potential. NEMA identified the lack of border enforcement as early as 1996 to the Department of Energy as having a major impact on motor efficiency regulation results. In 2016, the Department of Energy acknowledged the need to enforce motor efficiency rules on all motor market channels and released a comprehensive enforcement plan to correct this long-standing issue as in import declaration NOPR. DOE agreed that a lack of enforcement results in energy savings not being achieved by federal rules. The current administration has placed this NOPR on hold as an active rulemaking. NEMA supports DOE's import declaration NOPR to implement requirements on both certification compliance and enforcement and will continue to work with DOE to establish a valid import process applied to all current and future motor rules. NEMA will continue to explore motor system opportunities as an additional way to achieve greater energy savings including border enforcement.

References

1. US Department of Energy – 2009_11_25 Technical _Support Document chapter 9
2. US Department of Energy – 2010 10 CFR part 431 Energy Conservation Standards for Small Motors – Final Rule page 41 “ section B Enforcement”

Strategies to Promote Energy-Efficient Compressed Air Systems Among Indian Companies



Aditi Khodke, Toshizo Maeda, Girish Sethi, and Mika Tachibana

1 Background

The Government of India is committed to reducing its greenhouse gas emissions intensity of its GDP by 33–35% by 2030 from 2005 level as stated in the Intended Nationally Determined Contributions submitted to the United Nations Framework Convention on Climate Change in October 2015 [1]. The industrial sector in India accounts for 58% of the total commercial energy consumption [2], and there is substantial scope for improving the energy efficiency across large- as well as small- and medium-scale enterprises (SMEs) [3, 4]. Technology transfer from industrialised countries to other emerging countries is a recommended mechanism by the United Nations to reduce carbon emissions systematically. Acknowledging this potential, the Institute for Global Environmental Strategies (IGES), Japan, and The Energy and Resources Institute (TERI), India, have been jointly facilitating low carbon technologies (LCT) transfer from Japan to India since 2011. This paper summarises the lessons learned from these activities, particularly the ones for promoting energy-efficient compressed air system in the last 4 years that have been supported by a project for assessing the effectiveness of LCT transfer by Ministry of the Environment, Government of Japan.

A. Khodke (✉) · T. Maeda · M. Tachibana
Institute for Global Environmental Strategies (IGES), Hayama, Japan
e-mail: khodke@iges.or.jp; maeda@iges.or.jp; tachibana@iges.or.jp

G. Sethi
The Energy and Resources Institute (TERI), New Delhi, India
e-mail: girishs@teri.res.in

2 Introduction

Air compressors are among the most commonly used technologies across various manufacturers in India. According to a market forecast report, air compressor market in India is estimated to grow at a compound annual growth rate of 9% by 2019 from its baseline value of 550 million USD in 2014 [5]. Air compressors account for a significant amount of energy consumption across these manufacturers, but it is seldom considered a primary contributing factor of the production cost [6]. The energy-saving potential is larger when a whole compressed air system (CAS), including the distribution pipes, pressure tanks, air guns, and air compressors, is examined, rather than only the air compressors [6, 7]. An energy audit is the first step to identify such potential [8].

In India, the Bureau of Energy Efficiency (BEE), Ministry of Power, and the designated agencies in each state (SDAs) are responsible for promoting energy efficiency. Overview of SDA policies among India's most industrialised states, such as Maharashtra, Gujarat, and Tamil Nadu, shows that subsidised energy audits are prevalent. Some SDAs such as the one from Maharashtra have a detailed checklist for energy audit of CAS [9]. However, in many other states, the audit tends to be general without any particular technology-specific guidance. At national level, the Indian government provides subsidy to install inverter compressor across energy-intensive sectors such as textile [10], but the applicability of such subsidy is limited for other sectors. Likewise, Energy Saving Equipment List (ESEL) that highlights potential energy savings through the adoption of energy-efficient air compressors is also provided [11].

Despite the existing schemes and subsidies, lack of access to the information and the cumbersome application process limit the companies, particularly the SMEs, from fully availing the opportunity [12, 13]. Besides, lack of knowledge about financial benefits of installing energy-efficient technologies further hinders their deployment as observed through United Nations Industrial Development Organization's (UNIDO) ongoing energy-efficiency programme targeting SMEs in India [14].

Taking into account the information and awareness barriers, as well as the scope for improving CAS energy efficiency through strategic interventions, the authors addressed these barriers through a packaged approach that was derived through their field interventions in India. This paper elaborates further on this approach by structuring the argument in three parts. First, it draws examples of common barriers and drivers for adopting energy efficiency across the industrial sector; second, it provides an overview of successful energy-efficiency programmes for CAS in selected countries; third, it explains the interventions made by the authors for promoting energy efficiency of CAS in India and then summarises policy recommendations for further enhancement.

3 Barriers and Drivers for Industrial Energy Efficiency

Information and awareness gap impedes the promotion of industrial energy efficiency, as accentuated in the seminal work by Sorrell et al. (2011) [15]. For example, in India information about the government's energy-efficiency schemes is readily available on the Internet through the websites of the Ministry of Micro, Small and Medium Enterprises, Ministry of Commerce and Industry, and State-Designated Agencies (SDAs). However, more than two-thirds of the SMEs in India do not use the Internet according to the study by KPMG-Google (2017) [16]. Other common barriers include perceived risk, lack of knowledge about the capital and operational cost, limited access to capital, subjective decision-making by the end users [15], and limited time to investigate energy-efficient technologies [17]. The scale of the company is also a determinant for access to the right information: some SMEs have better access, while others do not [18]. Barriers for energy efficiency are often a combination of these multiple factors, and their cumulative effect discourages the companies from adopting efficient technologies [15].

On the other hand, the drivers for adopting energy efficiency can be categorised as regulatory, voluntary, and external factors.

In Japan, the large-scale companies with over 1500 kl of annual energy consumption are subject to set 1% per year emission reduction target and are obliged to report the progress every year to the Ministry of Economy, Trade and Industry (METI) [19]. In India, under the Perform Achieve and Trade (PAT) scheme, energy-intensive industries identified by the Bureau of Energy Efficiency are mandated to take energy-saving target based on a unit (facility)-wise benchmarking. The PAT scheme is undertaken in phases, and in each phase, the number of companies is expanded, and as of phase three, 737 companies are mandated to take energy conservation measures [20]. In Japan, along with regulations, government interventions through subsidies tend to be effective. The Ministry of Economy, Trade and Industry (METI) provides energy audit subsidies for SMEs; over 36% of the companies achieved their energy-saving targets [21]. In India, some SDAs provide subsidies for energy audits, but the number of beneficiaries of these schemes was not found on the SDA websites.

Examples of voluntary drivers include setting a long-term corporate energy-efficiency strategy for gradually replacing less efficient equipment, training in-house energy managers to design the strategy based on monitoring and evaluation of energy data, and facilitating their interaction with decision-makers as exemplified in a study on Swedish SMEs [17]. Sources of information on energy-efficiency options, subsidies, and access to energy auditors are some of the other drivers [22].

External factors, such as rising energy prices, persuade companies to adopt energy-efficient technologies [23].

Nevertheless, both the barriers and drivers are company-specific [18, 22]. Companies prefer a tailored approach that provides comprehensive information on the energy-efficient technologies, including the installation cost, energy-saving potentials, and other benefits.

4 Programmes on CAS Efficiency

Some countries have developed dedicated schemes to promote energy efficiency of compressed air system (CAS) by leveraging the drivers and thereby overcoming the barriers. For example, 'Druckluft Effizient' was launched in Germany from 2001 to 2004; this programme was sponsored by the German Energy Agency GmbH (DENA) monitored by Fraunhofer Institute for Systems and Innovation Research (ISI) and conducted by partnering with CAS suppliers. The programme had two objectives: CAS benchmarking and auditing. Free energy audits were conducted as part of this programme. The interested companies sent baseline data about their CAS operations, and the experts shortlisted the companies that had high energy-saving potentials. In many of the visited companies, the experts were able to suggest low-cost energy-efficiency measures [24]. This programme resulted in a 53% technology implementation rate and is considered one of the successful energy-efficiency programmes across the European Union [25].

Similarly, New Zealand has a dedicated CAS efficiency programme in which an independent company, Energy Nz, conducts free energy audits [26]. The industries above energy consumption of 75 kw-installed capacity could avail these free audits. To implement the suggestions of the audits, the programme assists in availing government financial assistance [26]. In the development stage of the CAS efficiency programme in New Zealand, various suggestions were made by the academia that included a demand-based approach to audits which includes inspection of air leaks, inappropriate usage, peak demand management, pressure settings, and distribution inefficiencies [7].

Compressed air challenge (CAC) started in 1997 in the USA to make the air compressor users more aware of the energy efficiency that could enable them to make informed choices when expanding their business. CAC does so by organising training programmes and disseminating information on CAS. Over 20 years the programme has trained 3900 people. As an outcome of this programme, about 76% of the participants took CAS-specific actions within 1 year. In the initial stage, the programme strengthened its outreach mechanisms through widely read industrial magazines and later through webinars [8].

CAS programmes in different countries illustrate that subsidised energy audits, assistance to implement suggestions, training energy personnel, and context-specific outreach mechanisms were effective in promoting CAS energy efficiency.

5 Approaches to Promote Energy-Efficient CAS in India

In India, there is no specific energy-efficiency programme for compressed air system (CAS) yet. Nevertheless, the air compressor market is experiencing high growth. Hence, authors opted to leverage on the growing market by reaching out to companies that have extensive CAS usage and potential for energy savings. To

reach out to the right end users, authors approached industrial clusters formed by the agglomeration of similar manufacturing companies in the same geographical area. A similar approach was echoed in the intermediate findings of UNIDO’s ongoing project in India [14].

Through the business networks of the industrial clusters, authors reached out to 30 companies, including 16 SMEs and 14 large companies in ten cities across five states, and the national capital region. Organisational profile of these business networks varied from state to state: in Gujarat and Punjab, business associations representing various industrial sectors of SMEs were shortlisted, whereas in Maharashtra, an independent business organisation that commonly organises industrial exhibitions and publishes magazine was appropriate, and in Tamil Nadu, a business association formed by representatives from a specific sector was selected. Despite the different organisational structures, it was observed that they are all effective in identifying potentially interested companies, as well as disseminating information and collecting feedback from them. Unlike commonly observed communication barriers across technology deployment processes [27], these business networks are effective in communicating with the members in their local language through cluster meetings and other means. It resonates with the findings of Cagno and Trianni (2013) about the significance of the source of information – companies learn from their peers [22].

To provide technical advice to the companies, authors engaged a CAS expert to carry out preliminary energy audits. The expert studied how CAS is being managed at each company and suggested better operational and maintenance measures and replacement of some of the equipment. Later the activities were expanded to the training of energy personnel to improve their understandings on the management of the entire CAS and then to organising awareness workshops to reach out to more potential end users.

1. Preliminary Energy Audits

Since 2011, 30 preliminary audits were carried out at nine textile, five pharmaceutical, two automobile, six auto components, six casting, and two forging companies. The geographic coverage included Gujarat, Karnataka, Maharashtra, National Capital Region (NCR), Punjab, and Tamil Nadu (Fig. 1). Among the visited

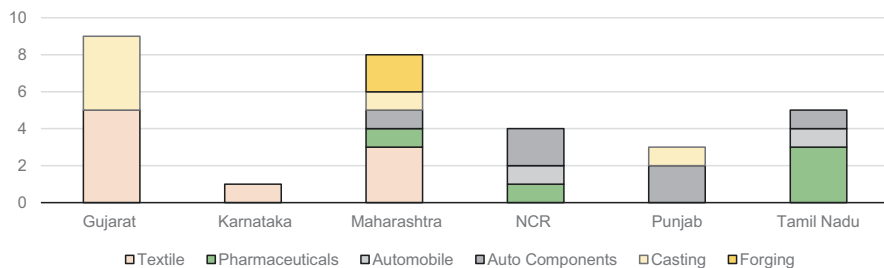


Fig. 1 Distribution of audited companies across different states and sectors (Source: Authors)

companies, the ratio of energy consumption by the compressed air system ranged from 5% to 35%: maximum was observed at a forging company whereas the minimum at a pharmaceutical company.

Recommendations by the expert covered comprehensive management of CAS in four categories: equipment, accessories, better operating practices (BOPs), and maintenance, as pointed out in Fig. 2. Among them, adopting BOPs showed high applicability and potential for energy saving, including simple measures such as improving ventilation of the air compressor room, addressing air leaks, and adjusting the pipe layout [6, 7]. Adjusting pressure setting and undertaking a regular periodic inspection of the receiver tank and filters were also recommended at many sites.

In 18 cases, installation of a new compressor was suggested. As most of the companies had frequent loading and unloading fluctuation during the operation, application of inverter compressors was recommended. In the pharmaceutical, textile, and auto component companies, oil-free inverter compressors were recommended due to the requirement of high air quality as well as to meet the Good Manufacturing Practice (GMP)¹ standards in specific cases. At two large companies where multiple boosters were installed, changing from a mechanical booster (pressure valve) to booster compressor was recommended. In one textile company, installation of a centrifugal compressor was suggested for the proposed plant expansion, and in

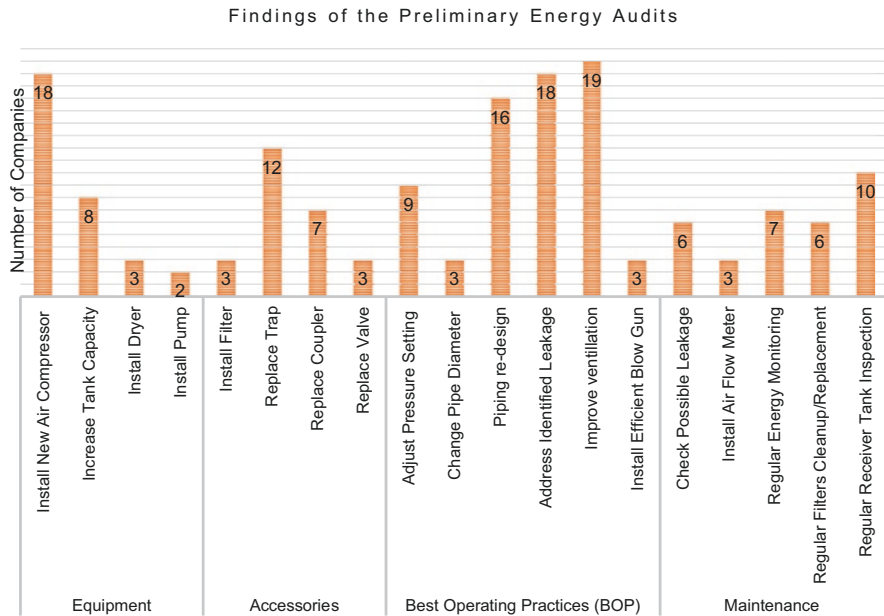


Fig. 2 Scope for energy efficiency in CAS based on the findings from 30 audited companies (Source: Authors)

¹ Good Manufacturing Practice (GMP) is a quality performance certification applicable across the pharmaceutical industries.

another case for a plant using a dated compressor, changing to any new and affordable compressor was recommended.

After the audit, one forging and two textile companies installed new inverter compressors within 1–3 years, and one of them decided after conducting a detailed energy audit by an accredited auditor. Most of the companies implemented the recommended BOPs within 1 year.

The audit was specific to the compressed air system, and the findings and recommendations, which were shared with the hosting company promptly after the audit, were also site-specific. As a result, uptake of recommendations was high, particularly for BOPs, which exemplifies appreciation of such service by the companies. In this way, to avoid common concerns raised by existing studies [7, 12], authors' interventions differentiated from general audits accompanied with general recommendations and other supplier-led audits which would often end up with specific product recommendation.

2. Training of Energy Personnel

Since 2016, authors organised four CAS-specific training programmes which have trained over 200 energy personnel, including energy managers of companies, local air compressor suppliers, individual energy consultants, and energy auditors. These programmes aimed to improve knowledge on the CAS as a whole covered not only the basics of the management but also various points to detect energy wastage as listed in Fig. 2. Practical solutions with a rough estimation of energy-saving potentials based on audit experiences of the expert in a wide range of industrial sectors were discussed with the participants. Provision of such a specific training programme by an expert seemed to be limited as the participants appreciated training opportunity and discussed their technical concerns. Demand for such a service at large-scale companies was also confirmed as following a preliminary audit, one large company requested for a specially arranged in-house training for the company's energy and utility personnel. There were also requests for similar specific training for other commonly applicable technologies, such as chillers, boilers, and motors. From these experiences, it was inferred that there is a strong need for similar technology-specific training programmes.

Also, as the energy auditors are an essential gateway for energy efficiency, not only their quality but also their quantity matters. According to the BEE website (accessed on 17 April 2019), there are only 262 accredited energy auditors compared to over 55 million micro-, small-, and medium-sized enterprises in India. Geographical distribution of these auditors is also an issue: they are mostly concentrated in industrial states and big cities. Considering the potential for energy efficiency in a variety of industries, both large-scale and SMEs, the sheer number of energy auditors needs to be increased along with their widespread distribution. To enable such business environment, regulation for energy-efficiency needs to be further strengthened covering not only among energy-intensive but also other large companies and SMEs. Furthermore, raising awareness of SMEs through the provision of right information, such as subsidies for energy audit and capital investment, is also essential to create such a market.

3. Awareness Workshops

Authors organised seven workshops in four states in collaboration with business networks of selected industrial clusters. The workshops aimed to address commonly asked questions of compressed air system (CAS), such as capital and operational costs, payback period, energy-saving potential, and other benefits for installing new equipment [28]. Over 300 representatives from SMEs and large companies participated in these workshops.

Feedback from two recent workshops in 2018 showed that more than 75% of the participants improved their knowledge of CAS. After the workshops, there were requests from the participants to conduct preliminary energy audits, and some of them contacted air compressor suppliers to discuss the procurement conditions. The result exemplifies that these companies are willing to consider energy-efficient technologies and provision of the right information can trigger their action.

During the preliminary audits, it was observed that local suppliers of air compressors usually advise SMEs about CAS installation. The SMEs usually make decisions based on the upfront cost and after-sales services. Compared to large-scale companies which usually deal with compressor manufacturers directly and make decisions based on long-term performance and running cost, among the SMEs generally these long-term benefits are not well considered. Informative workshops, which could change the mindset of energy managers, can be an entry point for letting the SMEs consider energy efficiency.

6 Conclusion

Authors have attempted to provide a comprehensive service for promoting energy efficiency of compressed air system (CAS) for Indian manufacturers through carrying out preliminary audits at selected companies and organising awareness workshops and training programmes in collaboration with industrial clusters. Through these activities, it was found that:

Energy Audit Technology-specific energy audits are highly effective in improving the energy efficiency of CAS. Energy-saving potentials were identified by the expert in the operation and maintenance of the system at most of the audited companies, and many of these companies implemented recommendations within 1 year. Replacement of the equipment and accessories, including air compressors and traps, was also recommended at about half of the audited companies, and some of them replaced them within 1–3 years.

Training of Energy Personnel There is a demand for CAS-specific training programmes for energy personnel, such as energy auditors, energy managers of companies, local suppliers, and consultants. Improving their capacity in auditing the entire compressed air system, rather than air compressors alone, will enable them to provide useful recommendations for the end users. There is also a demand for similar

technology-specific training programmes for other commonly applicable technologies, including chillers, boilers, and motors.

Awareness Workshops It was observed that understanding about the energy-saving potential of compressed air system among energy managers and business owners of companies especially that of SMEs can be changed through provision of right information at awareness workshops. Improving their understanding of short- and long-term benefits through provision of financial information such as payback period is essential to improve the acceptance of energy-efficient technologies.

Outreach Mechanism Collaborating with industrial cluster-level business network was effective particularly in communicating with, and outreaching to, SMEs compared to large-scale companies which can be easily reached out through connection of State-Designated Agencies (SDAs).

As a policy recommendation, the authors underscore the following points:

1. Compressed air system (CAS) has a substantial potential for energy savings through implementing better operating and maintenance practices, as well as by installing appropriate air compressors. To provide such site- and technology-specific energy audit service, energy auditors and other service providers need specific training. There is a demand for not only for CAS but also for other commonly applicable energy-saving technologies.
2. Provision of the right information on compressed air system, such as payback period in consideration of the capital and operational costs and long-term economic, environmental, and social benefits, can alter the mindset of energy managers of private companies. Awareness workshop is an important opportunity to provide such information.
3. Organising all these three components, CAS-specific energy audit, training of energy personnel, and awareness workshop, is a recommendable package for promoting specific energy-saving technology in a comprehensive manner. The utilisation of business networks of industrial clusters to reach out to SMEs willing to implement energy-saving technologies and disseminate right information is also recommendable.
4. The number of energy auditors needs to be increased along with expanding their spatial distribution to cater to the potential demand. To sustain such business market, regulation for energy saving needs to be strengthened further by covering not only energy-intensive but also other large companies and SMEs, and support for energy efficiency needs to be expanded including subsidies for energy audits and capital investment.

Acknowledgement The content of this paper should be considered as the opinions of the authors and not of IGES or TERI. The findings of this paper are part of IGES and TERI's LCT dissemination project. This project has been supported by various organisations in Japan, including the Ministry of the Environment, Japan International Cooperation Agency, Japan Science and Technology Agency, and Hyogo Prefectural Government.

The authors thank Mr. Tsukasa Saito, compressed air system expert, for providing the details of the preliminary energy audits and his inputs for writing this paper. Similarly, the authors thank Prof Yutaka Suzuki, Dr. Rabhi Abdessalem, Mr. Prosanto Pal, and two anonymous reviewers for their valuable feedback.

The authors report no conflict of interest.

References

1. Government of India, India's intended nationally determined contribution: UNFCCC, 2015. [Online]. Available: <https://www4.unfccc.int/sites/submissions/INDC/Published%20Documents/India/1/INDIA%20INDC%20TO%20UNFCCC.pdf> [Accessed: 19-Apr-2019]
2. Ministry of Statistics and Programme Implementation, Energy Statistics 2018 (Twenty Fifth Issue), New Delhi, 2018. [Online]. Available: http://www.indiaenvironmentportal.org.in/files/file/Energy_Statistics_2018.pdf. [Accessed: 19-Apr-2019]
3. D. Gielen, P. Taylor, *Indicators for Industrial Energy Efficiency in India*, vol 34 (Energy, 2009), pp. 962–969
4. Ministry of Micro, Small, and Medium Enterprises, Annual report 2017–2018, 2018. [Online]. Available: <https://msme.gov.in/sites/default/files/MSME-AR-2017-18-Eng.pdf>. [Accessed: 19-Apr-2019]
5. ValueNotes, Industrial Compressors Industry in India 2014–2019 – ValueNotes Strategic Intelligence, 2014. [Online]. Available: <https://www.valuenotes.biz/insights-publications/publications/industrial-compressors-industry-in-india-2014-19/>. [Accessed: 10-Apr-2019]
6. R. Saidur, N.A. Rahim, M. Hasanuzzaman, A review on compressed-air energy use and energy savings. *Renew. Sust. Energ. Rev.* **14**(4), 1135–1153 (2010)
7. J.R. Neale, P.J.J. Kamp, Compressed air system best practice programmes: What needs to change to secure long-term energy savings for New Zealand? *Energy Policy* **37**(9), 3400–3408 (2009)
8. A. Mckane and B. Medaris, The Compressed Air Challenge: Making a Difference for US Industry, Energy Efficiency in Motor Driven Systems (EEMODS), pp. 33–40, 2003
9. Maharashtra Energy Development Agency (MEDA) (Govt of Maharashtra Institution), “Save Energy Program.” [Online]. Available: https://www.mahaurja.com/meda/data/energy_conservation/SaveEnerProg.PDF. [Accessed: 19-Apr-2019]
10. Ministry of Textiles, Amended Technology Upgradation Fund. [Online]. Available: http://texmin.nic.in/sites/default/files/revised_atufs_guideline_02082018.pdf [Accessed: 23-Aug-2019]
11. JICA-SIDBI, Energy Saving Equipment List (ESEL). [Online]. Available: http://foundryinfo-india.org/pdf/Energy_Saving_Equip_List_Version8.2.pdf [Accessed: 23-Aug-2019]
12. D. Ghosh, J. Roy, Approach to energy efficiency among micro, small and medium enterprises in India: Results of a field survey, Work. Pap. 08, 2011, UNIDO, 2011
13. P. Veeraboina, G.Y. Ratnam, Analysis of the opportunities and challenges of solar water heating system (SWHS) in India: Estimates from the energy audit surveys & review. *Renew. Sust. Energ. Rev.* **16**(1), 668–676 (2012)
14. UNIDO, Independent Mid-term Evaluation Promoting energy efficiency and renewable energy in selected micro, small and medium enterprises (MSME) clusters in India, p. 87, 2018
15. S. Sorrell, A. Mallett, S. Nye, Barriers to industrial energy efficiency: a literature review. United Nations Industrial Development, Working Paper 10/2011, 2011
16. N. Atroley, A study by KPMG in India and Google January 2017, no. January, pp. 1–29, 2017
17. P. Rohdin, P. Thollander, Barriers to and Driving Forces for the Implementation of Manufacturing Simulation in the Swedish Foundry Industry, in Proceedings of the 2006 Winter Simulation Conference, no. 31, pp. 2302–2302, 2006

18. A. Trianni, E. Cagno, Dealing with barriers to energy efficiency and SMEs: Some empirical evidences. *Energy* **37**(1), 494–504 (2012)
19. Energy Conservation Center Japan, Complimentary Energy Conservation Audit Cases in FY2016, 2016
20. Bureau of Energy Efficiency, Pathways for Accelerated Transformation in Industry Sector, 2017. [Online]. Available: <https://beeindia.gov.in/sites/default/files/Final%20Booklet%2029-9-2017.pdf> [Accessed: 17-Apr-2019]
21. Energy Conservation Center Japan, The Energy Conservation Benchmark, 2018. [Online]. Available: <https://www.asiaeec-col.eccj.or.jp/infocus180702/>. [Accessed: 17-Apr-2019]
22. E. Cagno, A. Trianni, Exploring drivers for energy efficiency within small- and medium-sized enterprises: First evidences from Italian manufacturing enterprises. *Appl. Energy* **104**, 276–285 (2013)
23. S. Bhattacharya, M. Cropper, Options for Energy Efficiency in India and Barriers to their Adoption: A Scoping Study, SSRN, 2010
24. P. Radgen, The Compressed Air Campaign “Druckluft effizient”: a Collaborative Action to Achieve Market Transformation in Germany. In *Energy Efficiency in Motor Driven Systems (EEMODS)*, pp. 397–402, 2003
25. M. Unger, P. Radgen, Energy Efficiency in Compressed Air Systems – A review of energy efficiency potentials, technological development, energy policy actions and future importance, In *Energy Efficiency in Motor Driven Systems (EEMODS)*, pp. 207–233, 2017
26. Energy NZ, Fully Funded Compressed Air System Energy Audits, 2009
27. DJ. Teece, Technology Transfer by Multinational Firms : The Resource Cost of Transferring Technological Know-How, In *The Transfer And Licensing Of Know-How And Intellectual Property: Understanding the Multinational Enterprise in the Modern World*, pp. 1–22. 2008
28. E. Worrell, J.A. Laitner, M. Ruth, H. Finman, Productivity benefits of industrial energy efficiency measures. *Energy* **28**(11), 1081–1098 (2003)

Transformation Program for Low-Efficiency Electric Motors and Market Surveillance Activities in Turkey



Mevlüt Hürol Mete 

IEEAP has three policy areas. Policy 1 is the transformation of inefficient AC electric motors through replacing low-efficiency electric motors with high-efficiency ones as well as promoting wider use of variable-frequency drivers (VFDs). This policy would be achieved through:

- The preparation of an inventory of 7.5 kW and higher-capacity AC motors used in industry.
- Strengthened enforcement of secondary legislation concerning shift to high-efficiency motors. This will be achieved through the preparation of legislation on minimum efficiency requirements for electric motors and streamlining the conduct of inspections on the production and import of electric motors.
- The larger use of equipment increasing the efficiency of motors (such as variable speed drives, soft-starters, harmonic filters).
- Establishment of a motor testing laboratory for market surveillance activities.
- Conducting studies on taxation incentives aimed at expanding the use of high-efficiency motors.

In this study, the components of this transformation program will be introduced and information and statistics about market surveillance activities for electric motors will be presented.

M. H. Mete (✉)
Ministry of Industry and Technology, Ankara, Turkey

1 Background

The growth of GHG emissions in Turkey has been globally one of the highest, increasing from 188 million tons CO₂ in 1990 to 459 million tons CO₂ in 2013. According to Turkey's INDC, this can be attributed to the 230% increase of Turkey's GDP between 1992 and 2012, a 30% increase in its population since 1990, and annual increases in energy demand of 6–7%. According to the Ministry of Energy and Natural Resources (MoENR) of the Government of Turkey (GoT), demand for electricity power has been steadily increasing for the past decade; electricity demand in 2014 was 255.5 TWh, an increase of 3.7% from 2013. Moreover, the electricity growth forecast of Turkish Electric Transmission Company (TEIAS) is an electricity consumption increase of 72% from 2013 to 2023. With limited domestic reserves of fossil fuels, Turkey is highly dependent on energy imports with more than 70% of its energy needs and 60% of its electricity based on fossil fuel consumption.

While Turkey was a party to the Kyoto Protocol, it did not have targets due to the fact that it is not in Annex B and that its national conditions include rapid industrialization and urbanization and a low per capita GHG emission rate. In the successor agreement to the Kyoto Protocol, adopted in Paris in 2015, Turkey's INDC states that the country will adopt GHG emission reduction targets along with all other nations that will include a 21% reduction in GHG emissions from the business-as-usual level by 2030 that will enable the country to adopt low carbon development initiatives to limit the increasing global temperatures below 2 °C. One of these low carbon development initiatives will be the implementation of the Strategy on Energy Efficiency or, more specifically, the National Strategy and Energy Efficiency Improvement Action Plan under 10th Development Plan that targets the industrial sector. Another important plan to be implemented under the INDC is to increase energy efficiency in industrial installations and provide financial support to energy efficiency projects.¹

Efforts to increase energy efficiency in Turkey have intensified over the past 15 years. While there have been progress in decreasing the energy intensity of the industrial sector, the sector has been the highest energy-consuming sector in Turkey for many years. This has been the case notwithstanding reductions in industrial outputs from the economic crisis. Since 1990, industrial primary energy consumption has increased an average of 4% per annum, a growth rate higher than the country's overall energy consumption.

In Turkey, 47% of net electricity consumption is from the industrial sector,² with an estimated 70% of this energy consumption from electric motor-driven systems (EMDS), 90% of which use three-phase squirrel cage asynchronous motors as defined in the EU Eco-design Implementing Measure 640/2009 on electric motors

¹ http://www4.unfccc.int/submissions/INDC/Published%20Documents/Turkey/1/The_INDC_of_TURKEY_v.15.19.30.pdf

² TEDC (TEDAS), Electricity Distribution and Consumption Statistics of Turkey, 2015

as amended by Implementing Measure 4/2014³. Electric motors in Turkey, in general, are not energy efficient. Moreover, it is estimated that electric motors in Turkey vary considerably in efficiencies; for example, there can be a 3–5% difference between the efficiencies of an IE1 and IE3 15 kW motors assuming the IE1 motor has not been rewound.⁴ Based on DGP's motor inventory analysis,⁵ industrial IE1 motors are generally rewound two to three times (likely from old or burnt-out wires) at local shops with a loss of 2–5% per re-winding, raising the difference of efficiencies between the IE1 and IE3 motors to 5–15%. In this case, these motors may consume an amount of energy equivalent to its purchase cost in about 5–6 months (assuming an 8-hour daily operation of the motor).⁶ A typical electric motor causes an energy cost of more than 50 times its purchase cost during its 20 years of service life.

MoIT recognizes the opportunity to transform the market for electric motors toward energy-efficient electric motors and electric motor driver systems (EMDS) and has made energy efficiency a priority of industry, development, and climate change policy. The Strategy on Energy Efficiency (SEE), in this context, sets an overall target of reducing Turkey's energy intensity (energy consumption per unit of GDP) by 20% by year 2023 from the levels of 2011. Promoting EE in Turkey's industrial and service sectors is among the top-priority actions outlined in the SEE. In addition, the GoT has adopted and transposed the EU Directive 2012/19/EU on waste electrical and electronic equipment into Turkish regulations that obligate electric motor manufacturers to recycle discarded inefficient motors.

The developmental challenge for Turkey on this transformation program is to achieve substantial energy savings in an industrial sector where more than 90% of the enterprises are SMEs.⁷ SMEs in Turkey have traditionally had difficulties in obtaining access to finance primarily due to their creditworthiness, inability to provide sufficient collateral, and their lack of capacity to articulate their specific needs for financing to banks. Turkish commercial banks have historically been reluctant to offer EE financing product lines since they associated such funding with higher transaction cost and higher risk. Moreover, these banks typically had limited internal capacity to properly assess, develop, and EE market financing instruments.

MoIT have had and currently operate support programs to assist SMEs to improve their access to loans at concessional interest rates from banks contracted with KOSGEB⁸ and the involvement of the Credit Guarantee Fund (KGF) that is

³These are defined in Communiqué on Eco-Design Requirements for Electric Motors (OG No. 28197 of 7 February 2012)

⁴IEC 60034-30 Efficiency Table

⁵DGP Electric Motor Inventory – Preliminary Analysis Report from December 2015

⁶For motors that are used less than 2000 hours annually, price of the motor would be equivalent to the electricity consumed over a much longer period (3 years or more), making the installation of an EE motor less feasible

⁷The KOSGEB definition of an SME is “an enterprise with up to 249 employees and an annual turnover of up to 125 million Turkish Lira.”

⁸KOSGEB – Small and Medium Enterprises Development Organization of Turkish Republic, a

supported by the Turkish Treasury (KGF provides guarantees up to 80% of the loan amount). Despite these programs, these de-risked credit support schemes have been underutilized by industrial SMEs for the purposes of financing EE motor investments. Primary barriers to the wider adoption of EE electric motors in Turkey include:

- *The low level of awareness amongst SME personnel on the benefits of energy efficiency.* As a result, there is a lack of importance placed on energy efficiency by most SMEs. Decisions by these personnel on motor investments almost always involve lowest cost options (not lifecycle costs)⁹ and optimizing production through minimization of downtime risks.
- *The general lack of liquidity of SMEs to pay up front and financing costs for energy-efficient motor investments.* Most SMEs do not have available cash for such investments and are unable to make any down payments on new equipment.
- *SME aversion on the use of external engineers such as ESCOs and equipment suppliers to improve their energy efficiency.* Many of these engineers are generally linked to preferred equipment suppliers. As such, general SME perceptions are that these engineers may not offer the best solutions for their operations. In addition, they feel that there are higher risks of operational disruptions if the equipment replacement does not function as designed. Overcoming this barrier will require the development of a trusting relationship between a trusted and independent equipment supplier and the end-user SME.
- *Inefficient coordination in the implementation of the EE Law that slows the pace of legislative changes.* Since the majority of institutional effort to implement the EE Law falls under the responsibilities of MoIT (who in this instance have oversight of industrial issues and implementing EE), improving the coordination between MoIT and other line agencies such as MENR is required; this would ensure efficient development and implementation of EE policies, regulations, and government-supported programs.

2 The Adaptation Process of the Eco-Design Regulation for Electric Motors in Turkey

The Eco-design Directive for Energy-Using Products (2005/32/EC) was published in the EU Official Journal on 22 July 2005. This Directive was amended to include energy-related products (2009/125/EC) and published in the EU Official Journal on 31 October 2009. Thereafter, some regulations related to some product groups on

public organization affiliated with MoIT

⁹Most industrial SMEs are reluctant to give up their inefficient motors, either selling them for scrap metal or re-wiring them for continued usage in their processes

the implementation of this directive were also published. Eco-design Regulation for Electric Motors **640/2009/EC** is one of these.

The related regulation has been adopted in Turkey, pursuant to Turkey's obligation to align with the EU Acquis Communautaire based on the Customs Union Agreement between EU and Turkey.

This regulation was amended (**4/2014/EU**) by the European Commission. The Annex 1, subject matter, and scope of **640/2009/EC** were amended by a regulation dated 7 January 2014 published in EU OJ. **4/2014/EU** was also translated into Turkish and promulgated with its publication on Turkish OJ after the compilation of the opinions of the related parties. The process in Turkey has been continuing in parallel with the EU since 15 March 2015.

3 Electric Motors Inventory Analysis

The action entitled "to prepare an inventory of AC electric motors being used in Turkish industry with a power rate 7.5 kW and higher" stated in the IEE Action Plan. Based on this statement, MoIT-DG for Productivity has compiled the inventory information of 887 industrial enterprises (which have annual electricity consumption above 50 toe) in 62 provinces of Turkey. In this context, the "Inventory Analysis Report" on electric motors used in manufacturing industry has been prepared. The project's principal objectives were to create a detailed portrait of the inventory of motor systems currently in use in Turkish industrial facilities and estimate motor system energy use and potential for energy savings.

For sampling process, electricity consumption data of more than 100.000 manufacturing firms were used. Then, the population was determined which includes firms have annual electricity consumption of more than 50 toe (0.0021 PJ). Sector, scale, and location data of approximately 10.000 firms have been analyzed and sample distribution has formed.

Then, field studies have started. Eight hundred eighty-seven companies in manufacturing industry from 62 provinces have been visited. Data of more than 95.000 electric motors which have power of more than 7.5 kW have been collected. Besides these, for crosscheck process, domestic production data and motors import data for the last 10 years have been used. And for sectoral generalizations, data about number of employees, electricity consumptions, and real assets of companies have been benefited.

4 Findings

- As a result of the studies conducted on electric motors with a power rate 7.5 kW or above in 887 industrial enterprises, data on 93.139 AC electric motors have been acquired. And some findings have been generated based on the reviews according to some parameters.
- Average rates/numbers of motors have calculated for the parameters of:
 - Motor age (avg. 12 years)
 - No. of rewiring (avg. 2.4 times)
 - Efficiency level (88% of the analyzed motors are IE1 or below)
 - Annual working hours (5.400 hours)
 - Load factor (77%)
 - Distribution of motors by application (pumps 26%, fans 25%, conveyor systems 11%)
- Potential electricity savings have been calculated (1.5 billion \$).
- Current stock for motors has been estimated (overall estimate is 4.3 million motors with power of >7.5 kW).
- Potential of VSD market was found.
- Cost for transformation and return of investment have been calculated on sectoral level.

5 GEF Project: “Promoting Energy-Efficient Motors in Small- and Medium-Sized Enterprises” (TEVMOT)

A new GEF Project titled “Promoting Energy-Efficient Motors in Small and Medium Sized Enterprises” has been coordinated by MoIT in collaboration with UNDP. The Project aims to promote significant additional investment in industrial energy efficiency in Turkey by transforming the market for energy-efficient motors used in small- and medium-sized enterprises. This objective is planned to be achieved by strengthening the legislative and regulatory framework related to both new and existing electric motors in Turkey, developing appropriate governance and information infrastructure, upgrading test laboratories at the Turkish Standards Institute, launching a sustainable financial support mechanism, and developing and implementing a comprehensive public awareness and training program.

There are five main components in this Project:

- Strengthening policy and institutional frameworks for energy-efficient electric motors
- Capacity building for relevant stakeholders to promote the benefits of EE motors
- Upgraded Turkish Standards Institute Test Laboratory and strengthened monitoring, verification, and enforcement

- Support the development of a one-stop-shop financial support mechanism to support EE motors replacement and procurement of new EE motors in Turkey
- Knowledge management and M&E

TEVMOT supports the strengthening of the legislative and regulatory framework both for new and existing energy-efficient motors in Turkey. As a step of the said transition, TEVMOT Project aims to achieve a “market transformation” in Turkey through replacing old, inefficient electric motors at SMEs with new, energy-efficient motors. This means taking the first step for the transition by replacing the AC motors currently used in industry with energy-efficient motors that will contribute \$1.5 billion to the Turkish economy and ensure sustainability.

Scheduled to end in June 2022, TEVMOT Project rolled out various technical work and activities to make a market transformation in electric motors. Experts from the Ministry, technical experts of the project, project partners, and a broad range of national and international stakeholders continue to make significant contributions in the phases of design, implementation, and evaluation of such actions.

TEVMOT builds a national database of electric motors with a view to developing a market monitoring system. In this context, technical experts of the project are already engaged in comprehensive work coordinated by the Directorate-General for Industry and Productivity of Ministry of Industry and Technology in cooperation with the Directorate-General for Industrial Product Safety and Inspection; Directorate-General for Product Safety and Inspection of Ministry of Trade; Ministry of Energy and Natural Resources; Turkish Statistical Institute (TURKSTAT); Association of Electric Motor Producers (EMOSAD); Energy Efficiency and Management Association (EYODER); and Organized Industrial Zones Senior Organization (OSBÜK).

TEVMOT held a technical consultative meeting on 18 October 2018 for the market players (manufacturers, suppliers, importers, and users) to strengthen the investment environment for electric motors in close collaboration with Ministry of Energy and Natural Resources to design minimum energy performance standards (MEPS) in line with EU Directives and international best practices. With support from technical experts of the project, the participants reviewed and assessed the relevant national and international legislation on the updates of eco-design implementation measures and new legislation.

Turkish Standards Institute’s (TSI) Electrical Testing Laboratory upgraded with TEVMOT support. TEVMOT initiated work to upgrade the testing systems and auxiliary equipment of the Electric Motors Testing Laboratory at Gebze Electro-technical Laboratory Directorate of TSI in order to ensure effective market surveillance, inspection, and legal compliance of energy-efficient electric motors in Turkey and strengthen testing procedures.

TEVMOT introduces innovative solutions of international caliber to increase the use of energy-efficient electric motors. In the context of technical work of the relevant project partners, experts, and Energy Efficiency Consulting Companies (EVDs), TEVMOT develops an audit methodology specific to motors in terms of system efficiency at SMEs to ensure replacement of accurately identified motors.

6 One-Stop-Shops at OIZs to Accelerate Investments by SMEs

The plan is to engage in motor energy efficiency audits by “Energy Efficiency Consulting Companies” (EVDs) with TEVMOT support at the SMEs identified through one-stop-shops which are located at OIZs and operate in the manufacturing industry. Based on the audit results, inefficient electric motors at the enterprises will be replaced by new energy-efficient motors. A specific TEVMOT Financing Model has been developed to provide financial support to such investment by SMEs. The work on the financing model and “bring in your old motor, take away the new, let the motor pay itself” campaign is underway with feedbacks and contributions of the stakeholders.

Field work at the selected pilot organized industrial zones (OIZs) is at the heart of TEVMOT’s activities. The pilot intends to enable the energy management units (EMUs) of OIZ to establish and operate one-stop-shops (OSS). The one-stop-shops will collaborate with such project stakeholders as KOSGEB and TurSEFF as well as various bank and financing alternatives to achieve a rapid, easy market transformation. Pilot applications and SME financing support will start in 2020.

7 Kayseri Organized Industrial Zone (OIZ) Pilot Project

SMEs’ access to finance which is valued by the similar country programs as a primary concern to achieve success is considered as a basic factor of Turkey’s transformation program of inefficient electric motors as well. Taking this into consideration, credit interest support program has been developed by MOIT’s Directorate General for Productivity and KOSGEB (SME Administration of Turkey).

Before the promotion of this transformation program throughout the country, it is planned to implement a pilot project in one province. Within this context, Kayseri OIZ has been selected where energy-efficiency audits of 130 SMEs were carried out by an ESCO.

Within this scope, KOSGEB designed a new program, namely, Credit Interest Support Programme for the Transformation of Inefficient Electric Motors. According to this program, a support of 85.000 USD from banks, identified by KOSGEB, is available per SME, and for pay back, the installments are based on a scheme of non-payment for the first 12 months followed by quarterly payments in a total period of 36 months, and if required by the banks, 80% of the amount is to be paid by KGF (Credit Guarantee Fund).

Credit Interest Support Program started to be implemented in 2016 after a protocol was signed between KOSGEB, MOIT, Kayseri OIZ Directorate, and the banks. Credit program was covering new motor or VFD purchases of SMEs. Unfortunately, only one application – by a plastic firm for an amount of 80.000 USD credit – was received within the context of the program.

Program implementation together with the arising difficulties, problems, and precautions against them was evaluated, and a survey has been carried out among the SMEs in Kayseri OIZ and that have been asked about the program. And these are the summary of results regarding the reasons of lack of application:

- Firms do not want give the scrap motors (60%).
- EE motors are not in their short-term investment plan (52%).
- Electricity consumption/share of motors is low (40%).
- Do not want a new credit line (37%).
- Do not want to pay for energy audits (35%).
- Using EE motors already (26%).
- Do not believe the benefits (or profits) of transformation (20%).
- Do not want to allocate time/stop the production (16%).
- Thinks that procedures are complicated/bureaucracy is high (12%).
- Unaware of the support program (3%).

8 Stakeholders of the Program

Transformation of the Turkish motors market involves a wide range of stakeholders, which includes the SMEs, electric motor manufacturers, organized industrial zones (OIZs), their energy management units (EMUs), energy-efficiency consultants (EECs) such as EVDs, and financial institutions (public and private sector).

9 SMEs

The focal point of the transformation program is the small and medium-sized enterprises (SMEs). In line with the official Turkish definition, an SME is an enterprise with up to 249 employees and an annual sales revenue of up to 125 million Turkish Lira (appx. 23 million USD). The industrial sector in Turkey comprises mainly of SMEs. With most of the electric motors on the Turkish market being used in the industrial sector, more than 98% of Turkey's industrial sector is mainly comprised of SMEs. Out of Turkey's more than 2.6 million SMEs, there are an estimated 355.312 SMEs in the industrial sector. The SMEs in the industrial sector produce more than 46% of the sector's outputs. The challenge lies in convincing SMEs to utilize more efficient motors in their industrial processes to save energy as opposed to their current alternative of resorting to the cheapest options of restoring operations of a motor, mainly through the rewinding of the motor.

There are many barriers that are limiting SMEs to engage with electric motor replacement. Despite the availability of energy efficient motors in Turkey for the past decade, the level of awareness among SMEs is limited. The limitations of this awareness are mainly related to knowledge on the benefits of energy efficiency

within an industrial enterprise. Managers of SMEs who make investment decisions have limited awareness of the differences and benefits of IE2, IE3, and IE4 motors. Moreover, SMEs do not regard energy efficiency as important when their main concerns are related to optimizing production and minimizing risks of interruptions. As such, if an SME experiences reduced production from a malfunctioning motor, the manager makes the decisions opting for lowest-cost solutions without consideration of lifecycle costs. This typically involves the replacement of this malfunctioning motor with a spare electric motor that is stored onsite. While a spare electric motor may not have the required capacity, the broken electric motor is then repaired in a clandestine repair shop, where it is rewired and losing 2–3% efficiency with each rewiring. Changing this *modus operandi* will require a change in behavior via full-scale awareness raising. Many industrial SMEs are located within OIZs who employ energy managers within energy management units (EMUs) who provide advice to member SMEs, with less than 1.000 toe¹⁰ (0.0419 PJ) annual energy consumption, on energy-related matters.

In general, industrial SMEs experience a lack of liquidity to pay the upfront costs for an energy-efficient motor investment. This is a primary cause of difficulties in financing SMEs. With their small-scale operations, limited own funds, and limited capacity to borrow money, these SMEs have limited awareness of de-risked credit support that does exist in Turkey.¹¹ If a SME has money available to invest either own means or bank credit, the SME typically will invest in increasing production rather than improving efficiency. As such, most industrial SMEs generally are unwilling to pay the replacement of this equipment with upfront costs for an energy-efficient motor or measures. Furthermore, replacing electric motors results in downtimes, duration of which varies depending on the complexity of the electric motor-driven systems. These downtimes can lead to significant interruptions in production. With SME unwillingness to make investments in energy efficiency measures, any feasible financial mechanism involving an SME investment in an energy-efficient motor cannot include a down payment.

SME distrust in the use of external engineers, ESCOs, and equipment suppliers to improve their energy efficiency stems from the fact these experts and engineers are generally linked to preferred equipment suppliers. Due to their small scale,¹² SMEs typically do not have dedicated energy managers that understand and are able to convince management to engage with external parties to replace electric motors. Given the risk aversion of SMEs due to their lack of liquidity, general SME perceptions are that these engineers and experts may not offer unbiased energy efficiency solutions for their industrial enterprise.

¹⁰toe is tonne of oil equivalent

¹¹KOSGEB and KGF provide financial support specifically to SMEs

¹²If the annual energy consumption of a company is more than 1000 toe, the company is required to appoint an energy manager. However, in the case of smaller companies, these energy managers are not fully dedicated and often perform the role of energy manager on top of their other role in the company

10 Motor Manufacturers

There are several international and domestic producers of electric motors active in Turkey. The main domestic electric motor manufacturers are Gamak, Wat Motor (Arcelik), Volt Motor, Aemot, and Emtas. There are also imported motors produced by Siemens, ABB, AEG, SEW Leroy Somer, ATB Group, and the VEM Group with low voltage motors. According to foreign trade statistics for 2011, Turkey's motor imports were valued at 793 million USD and exports at 134 million USD.¹³ There have been efforts spearheaded by Arcelik to form a Turkish Electric Motors Manufacturing Association (TEMMA). The members of the TEMMA will be contributing their knowledge of EU eco-design standards for motors and the manufacturing of various models of energy-efficient motors. Through TEMMA, they will provide to DGP their applied knowledge of motor eco-design standards that can be manufactured in Turkey.

These manufacturers have indicated their interest in supporting an increased share of energy-efficient motors through motor replacements. From this perspective, some of these manufacturers have engaged with banks on vendor finance for other products and could be convinced to enter into a similar agreement if the terms are right. Further discussion with these manufacturers to explore possible arrangements is advised.

11 Organized Industrial Zones

Organized industrial zones are designed to allow companies to operate within an investor-friendly environment with ready-to-use infrastructure and social facilities. The existing infrastructure provided in the zones typically includes roads, water, natural gas, electricity, communications, waste treatment, and other services. Provision of electricity to the SMEs at a lower rate is included in the utilities. In many cases, the OIZ generates their own electricity supply for the OIZ tenants. In addition to receiving revenues from OIZ tenants to administer and maintain the zone, OIZs generate revenue from electricity sales as well as some government support. OIZs are also allowed to finance investments to increase effectiveness of their electricity service.

Under the Energy Efficiency Law (No. 5627), all organized industrial zones with more than 50 enterprises will need to establish an energy management unit (EMU) to support companies that consume less than 1.000 toe (0.0419 PJ) of energy consumption with increasing energy efficiency. Several OIZs have limited awareness of or incentive to explain energy efficiency benefits for its members. Some, particularly

¹³From Ministry of Trade <https://www.ekonomi.gov.tr/portal/content/conn/UCM/uuid/dDocName:EK-051195;jsessionId=o6kkc58sWboZAbc4oH59QGa9wWevSE-uxFoOxI7dzY6LvshigN9r!1249264818>

those that own their own electricity generation installations, have the perception that energy efficiency may reduce their income from sale of energy to its tenants. As a result, most of the EMUs are not empowered and do not have the capacity to support SMEs to unlock their energy efficiency potential. More progressive OIZs, however, have the perception that their role is to offer energy at lowest cost. These OIZs typically already assist their SMEs with lowering their energy use. There are EMUs within OIZs that do provide quality assistance to SME tenants on all energy-related issues. More importantly, their relationship with SME tenants is one built on trust where the EMU provides independent advice.

To involve OIZs in a market transformation program for energy-efficient motors, their reluctance will need to be addressed particularly if the zones are to have a central role in the finance of the electric motor replacements. OIZs do have credit lines in place with banks to finance a wide range of projects related to maintaining and building new infrastructure as a service to their SME tenants such as roads, waste collection, and energy supply. For these credit lines, they are providing collateral. Borrowing additional funds for the replacement of electrical equipment, capitalizing its EMU to purchase equipment, and implementing a motor replacement program with SMEs for a monthly fee would probably have limited impact on their current credit arrangements. However, during initial consultation, even the more progressive zones have indicated a reluctance to utilize borrowing capacity to fund energy efficiency measures at SMEs. Further exploration of OIZ's willingness to finance energy efficiency is advisable, especially if tailored guarantees can be applied to cover SME default risk.

12 Financial Institutions

A financial institution or bank is an institution that provides financial services for its clients or members. There are about 50 banks active in Turkey. Many Turkish financial institutions offer financial products dedicated to energy efficiency investments.

13 Energy Service Companies

ESCOs are companies that provide both technical and financial services to implement energy efficiency projects on energy performance-based contracts (EPCs). As the ESCO guarantees performance, their remuneration is directly linked to the amount of energy saved by the project. The ESCO assumes the technical and performance risks associated with the project. If the energy savings are not achieved, the ESCO does not get paid. This is what differentiates ESCOs from other energy efficiency consultants that sell energy efficiency equipment. The typical services that an ESCO offers are:

- Identification, development, and design of the energy efficiency project
- Financing or acquiring the financing of the energy efficiency project
- Installation of energy efficiency technology/equipment
- Measuring, monitoring, and verification of the project's energy savings

Globally, many ESCOs are implementing a variety of energy efficiency measures, including high-efficiency lighting, heating and air conditioning, efficient motors, industrial process improvement, cogeneration, variable speed drives, waste heat recovery, and centralized energy management systems. ESCOs can be vendor-based or consultancy-based. Consultancy or technically based ESCOs are often consulting firms that have a general expertise in engineering or energy efficiency. Vendor or technology-based ESCOs are often energy technology suppliers, sometimes with a connection to a particular energy efficiency equipment manufacturer.

In many developing countries, ESCOs undertake more traditional fixed-fee energy efficiency contracts. These contracts do not include guarantees or performance-based remuneration element. They do not take performance risks, arrange financing, or undertake monitoring. These companies are technically not ESCOs, although they are still referred to as ESCOs leading to much confusion. This is also often the case with Turkish ESCOs or EVDs. In most cases, Turkish ESCOs or EVDs do not have performance risk nor arrange finance.

However, according to the ESCO Association of Turkey, there are a few ESCOs operating in Turkey, many with side businesses other than providing ESCO services. The state of ESCOs in Turkey can be described as follows:

- Viable ESCO transactions involve clients with energy loads that are steady, allowing the ESCO to correctly establish a baseline to base remuneration from an energy performance contract (EPC). For example, an ESCO contract could consist of the installation of energy-efficient lighting in a shopping complex where the hours of usage of the lighting can be correctly established.
- There are few if any ESCOs with industrial clients given the difficulties and variances in determining industrial SME energy demand baselines. Much of this is due to variations in industrial production output, frequency, and intensity in the use of the equipment and the type of products being manufactured, making the baseline for each factory unique, complex, and difficult to measure. In this regard, the ESCO has insufficient data and control to guarantee performance under EPC contacts.
- Many ESCOs in Turkey do not have sufficient experience to act as a full ESCO that would include finance measures and executing energy performance contracts.
- Nearly all ESCOs in Turkey do not have collateral and thus have limited borrowing capacity.
- Viable ESCOs in Turkey are often linked with multinational companies. However, these ESCOs have a perceived bias toward certain electric motor models and lack independent technical opinions reducing the confidence of the SME on the technical advice of these ESCOs.

These characteristics of ESCOs in Turkey are somewhat consistent with the EU's ESCO Market Report.¹⁴ Some of the ESCO characteristics of this report apply to Turkish ESCOs including:

- Low level of awareness among SME clients of ESCO services
- Lack of supporting legislative framework for ESCO services including a tendering process and the lack of exposure in Turkey to an energy performance contract
- Difficulties in accessing financing (mainly due to limited availability of collateral)
- Perceptions of high business and technical risks in the ESCO model that are related to:
 - Perceived risk that energy efficiency interventions might compromise core business-related production processes
 - Competition of energy efficiency investments with other investments related to the core business
 - Aversion to outsourcing energy management of an enterprise
 - Required long commitments of ESCO contracts that lead to a lack of flexibility
- Lack of trust in the ESCO model due to the lack of standardization that is related to:
 - Lack of homogeneity in ESCO offers
 - Lack of competition due to the nascent nature of the ESCO industry
 - Lack of experience of ESCOs, their clients, and participating financial institutions
 - Lack of reference ESCO projects from which new clients can draw confidence
 - Lack of clarity in EPC contract definitions leading to failed EPC contracts
 - Insufficient standardized measurement and verification protocols
 - Complex and nonstandardized EPC contracts

In summary, the application of the ESCO business model to replace electric motors in Turkish industrial SMEs would not be practical since the business model would introduce several risks, which may prove to be too cumbersome to overcome.

¹⁴Bertoldi, P., Boza-Kiss B., Panev, S., Labanca, N., ESCO Market Report 2013, JRC Science and Policy Reports

14 Financial Structures

SMEs in Turkey have traditionally had difficulties in obtaining access to finance primarily due to their lack of creditworthiness and inability to provide sufficient collateral. With SMEs representing a significant proportion of the country's economic production, MoIT has established a number of support programs through MoIT (KOSGEB, Techno-entrepreneurs, SAN-TEZ) and TÜBİTAK (TEYDEB).

Turkish banks have historically been reluctant to offer energy efficiency financing product lines since they associated such funding with higher transaction cost and higher risk. Moreover, banks typically had limited internal capacity to properly assess, develop, and market financing instruments for energy efficiency. However, ever since 2009, MoIT together with a number of development banks and organizations collaborated to mobilize significant amount of private sector funds for the purposes of reducing GHG emissions while driving sustainable economic growth in Turkey. Some examples are KOSGEB financial support, dedicated energy efficiency credit lines, and leasing of energy-efficient equipment. In addition, and although not specifically directed to energy efficiency investments, SMEs can apply for guarantees to support their loan application.

14.1 *KOSGEB Financing Support*

KOSGEB has programs that provide a number of financial products targeting SMEs to access bank loans at concessional interest rates from banks contracted with KOSGEB. While more than 16,000 SMEs utilize the program between 2010 and 2014 to access more than 2.7 billion USD in bank loans, the scheme has been underutilized by the industrial sector for the purposes of financing energy efficiency investments.

One relevant KOSGEB program is the pilot project entitled “Interest Support for Investment Loan” that was commenced in 2016 to support SMEs in their plans to invest and replace inefficient electric motors with IE3 or IE2 motors with variable speed drives. In addition to KOSGEB and MoIT (DGP), the Credit Guarantee Fund (KGF) and nine commercial banks are designated to provide services to SMEs for this interest rate support. The credit loan to be granted under this pilot project is a maximum of 55.000 USD per enterprise. This pilot project is scheduled for completion in late 2016 at which time the performance of the project would be evaluated for its uptake by SMEs and possible further implementation.

14.2 Dedicated Energy Efficiency Credit Lines

Credit lines are set up at local banks from extended credit lines from multilateral or bilateral development banks, specifically for on-lending to industrial borrowers for the implementation of energy efficiency and renewable energy investments. Typically, these credit lines are supported by a comprehensive technical assistance package that underpins demand for the facility, helps potential borrowers prepare loan applications, and familiarizes local bank officers with sustainable energy investment opportunities. This assistance is provided free-of-charge by a project implementation team consisting of international and local experts supported by grant funding provided by donors.

For example, the European Bank for Reconstruction and Development (EBRD) provides funds under the Turkey Private Sector Sustainable Energy Finance Facility, or TurSEFF. The local banks use the credit line to provide commercial loans, at their own risk, to borrowers with eligible investment opportunities, which include load-matching variable speed motor controls. Currently 390 million USD has been disbursed, and a further 265 million USD is available for financing. One of the eligible types of financing under TurSEFF is vendor finance; this financing modality allows a manufacturer or vendor of equipment to borrow money from one of the banks to provide finance for the sale of their equipment. The end-user would pay for the equipment with a monthly annuity payment to cover interest and repayment of the principal until the equipment is fully paid off. While 10% of TurSEFF's portfolio has been financed using vendor finance, the facility does not focus on electric motors; rather, it provides finance for their "list of eligible materials and equipment" (LEME) that can be only accessed from a "list of eligible suppliers and installers" (LESI). Since SME access to these credit lines is voluntary and approved by commercial banks on a case-by-case basis, SMEs have not accessed these credit lines for motor replacements.

15 Market Surveillance Activities and Testing Facilities

Another part of the transformation program is market surveillance. Market surveillance activities are carried out by the Ministry of Industry and Technology (MoIT)-DG for Safety and Inspection of Industrial Products.

Electric Motors Transformation Programme has been coordinated by Ministry of Industry and Technology (MoIT) in Turkey. DG for Safety and Inspection of Industrial Products (DGSIIP) is responsible for market surveillance of electric motors as other industrial products.

In this context, DGSIIP has been carrying out an audit program for motors since 2015. And these are the steps of electric motors market surveillance activities:

- A Project Team consisting of internal and external stakeholders has been identified.

- Control lists have been established in line with the requirements of the existing legislation.
- Important economic actors in the market have been identified.
- It has been determined where, how, and with whom the audits will be conducted (auditors pool has been created).
- Training needs analysis and training planning and organization activities have been completed.
- Procedures and principles regarding the form of supervision have been established.
- Audit follow-up form, minutes, and auditor reporting format and content have been designed.
- Test inspection substructure and capacity are determined.
- Two motor companies with good practice were visited with the participation of determined project team, auditors, and Turkish Standards Institute (TSI) authorities.
- Electric Motors Test Laboratory of TSI, which is the conformity assessment body, was visited by the project team, the auditors, and the TSI authorities, and an evaluation workshop was organized.
- Inspection activities are to be carried out in the import and domestic markets for electric motors, the Ministry of Trade and the Turkish Standards Institute have set up a sub-working group to include the authorities, and the Import Inspection Procedures and Principles have been prepared. As of July 2016, audits have been started at the import stage.
- In the audits conducted, the procedures and basic studies for the measures to be implemented within the framework of the Energy Efficiency Law No. 5627 concerning the detected nonconformities have been completed.

16 Pilot Audits

- Pilot audits (testing for compliance of motors) were carried out in Ankara. Audits were carried out in a total of 18 firms including electric motor, fan and compressor manufacturers, importers, and sellers in organized industrial zones (OIZs) of Ankara.
- A total of 12 IE2 efficiency class electric motor samples were taken from 7 brands within the inspection and sent to the TSI Electric Motors Test Laboratory, and the 3 samples were left as the witness samples.
- The test results were sent to the DGSİIP by TSI and are evaluated within the scope of eco-design directives.
- According to the results obtained from the pilot audits, the design of the audit program was reexamined.

Within the scope of Phase 1 audits of the project, which was carried out in 2016, inspections were carried out at firms that were in producers, importers, and sellers

in Kocaeli and Istanbul provinces. In Phase 1 inspections, samples from 10 different brands of samples were taken from 15 different model samples and sent to Turkish Standards Institute for testing and inspection. In addition, inspection orders were given for six models belonging to three brands. During the first phase inspections, 53 deficiencies of 12 different brands were detected. Furthermore, as a result of the inspections carried out, the sale of electric motors with a total of 389 IE1 efficiency levels is prohibited.

Under Phase 2, audits were planned at two separate levels in 2017. This plan focuses on import product inspections. However, for the purpose of analyzing the users, it is planned to perform the inspection for the purpose of establishing the best practice model for the inspection of the electric motors and taking the effective measures and the activities within the scope of the targets.

16.1 Future Plans

- Specialization of auditors, the development of supervisors' audit capacity for this product group and the establishment of a pool of expert inspectors
- Completion of effective audit model work on internal market inspections
- Formation of the conformity assessment process
- Identification of the legislative compliance level and harmonization issues of the sector, use of audits as a tool to increase the level of conformity
- Sectoral analysis (market actors, supply flow to the market, user profile and shape, product profile, and usage quantities)
- Developing a common understanding and cooperation between the sector and DGSİIP
- Upgraded Turkish Standards Institute (TSI) test laboratory and strengthened monitoring, verification, and enforcement

17 Testing Facilities

To ensure market transformation toward the use of more efficient energy-related products (ERPs), the Government of Turkey has supported the development of electrical and electronic equipment testing labs under the Turkish Standards Institute (TSI). In addition to having a number of testing labs for white appliances and other household equipment, TSI also established an electric motor testing laboratory in August 2015 that has been accredited by TURKAK to TS EN/IEC 60034-1 and TS EN/IEC 60034-2-1. The laboratory has a capacity to test up to 220 motors annually up to 90 kW.

Turkish Standards Institute (TSI) currently operates several test laboratories for the testing of electronic equipment as part of a proactive market surveillance plan to ensure compliance of new and existing electronic products to adopted MEPS. Current TSI motor testing laboratories have the capacity to test motors between 0.75 and 90 kW for 2, 4, and 6 pole induction motors. According to new investment plans, electric motor testing facility of TSI will be upgraded, and test capacity will increase to 375 kW in 2019.

18 Market Surveillance and TEVMOT Sample Selection

One of the work packages of the TEVMOT Project is about market surveillance and scanning of the electric motors market. Test samples need to be representative of those in the market place, i.e., should be sourced from market leaders, importers, new entrants, and those suppliers judged to be higher risk of supplying non-compliant products. The samples selected will need to cover different types, characteristics, and power ratings to represent the national electric motor market as much as possible.

The types, rated power range, number of samples, and testing schedule of the motors that will be required for testing are given in Table 1. This is a provisional listing since the final scope of the program should be decided through agreement between the TEVMOT Project Management Unit and the Directorate-General for Safety and Inspection of Industrial Products (DGSIIIP) and by taking into consideration of the current market data and the annual inspection program of the DGSIIIP.

The selection of sizes of motors given in Table 1 for Program A attempts some reflection of the market distribution in Turkey.

The selection of sizes of motors given in Table 1 for Program B is focused on those sizes of motors that are not in the scope of the current regulations but are expected to be included in the scope of the revised regulations. Note that these revisions are expected to include performance requirements for variable speed drives, hence their inclusion in Program B.

It may be possible to reduce the number of models tested in Program A if, by coincidence, motors of similar sizes, sources, etc. are already being tested as part of DGSIIIP's routine market surveillance activities. In such cases, the results of market surveillance testing could be used for program purposes too.

Table 1 Provisional list of motor sizes for testing

Types of motor	June	August	September	October	November	December	Total number of samples
2019 program A – establishment of indicative baseline							
13 units; 7.5–11 kW (2–4 poles)	13						13
20 units; 12–22 kW (2 to 4–6 poles)		10	10				20
7 units; 23–37–50 kW (4–6 poles)				7			7
3 units; 38–55 kW (4–6 poles)					3		3
2 units 56 kW and above (6 poles)						2	2
Total (2019) Program A							45
Types of motor							
	February	April	June	August	October	December	Total number of samples
2020 program A – establishment of indication of performance improvement (if any)							
13 units; 7.5–11 kW (2–4 poles)	13						13
20 units; 12–22 kW (2 to 4–6 poles)		10	10				20
7 units; 23–37–50 kW (4–6 poles)				7			7
3 units; 38–55 kW (4–6 poles)					3		3
2 units 56 kW and above (6 poles)						2	2
Total (2020) program A							45
2020 program B – Establishment of an indicative baseline for the categories of motors covered by the revised regulations expected to be introduced in 2021 and 2022							
2-, 4-, or 6-pole three-phase motors 375–1000 kW*					5		5
VSDs for operating in range 0.75–1000 kW					5	5	10
Three-phase motors > 0.12–0.75 kW					5	5	10

19 Conclusion

Energy demand in Turkey is increasing, and transition to energy efficiency is becoming inevitable for all sectors. By investing in energy efficiency, it is possible to meet Turkey's future energy demand and reduce greenhouse gas emissions that cause climate change. This may also be a potential driving force for Turkish economic growth.

Accounting for 47.2% of net electricity consumption in Turkey and mostly using inefficient motors, the Turkish manufacturing industry is expected to enjoy considerable decrease in electricity consumption if the market is transformed by using energy-efficient motors. In this context, the "Programme for Transition to Energy-Efficient Electric Motors in Industry" in line with the Energy Efficiency Law, Energy Strategy Plan, and 10th Development Plan set important objectives; and various activities were started with the initiative of Turkish Ministry of Industry and Technology.

"Industrial Energy Efficiency Action Plan" (IEE) within the context of the "Energy Efficiency Improvement Programme" which is one of the primary transformation programs of the 10th Development Plan has been coordinated by the Ministry of Industry and Technology (MoIT). One of three key policy areas of this Action Plan outlines the goal of "increasing energy efficiency through replacing low-efficiency AC electric motors" for which MoIT has formulated national standards on electric motors following EU Commission Regulation (EC) No 640/2009 on electric motors.

The transformation program aims to promote significant additional investment in industrial energy efficiency in Turkey by transforming the market for energy-efficient motors used in industrial enterprises. This objective will be achieved by strengthening the legislative and regulatory framework related to both new and existing energy-efficient motors, developing appropriate governance and information infrastructure, upgrading test laboratories, launching sustainable financial support mechanisms, and developing and implementing a comprehensive public awareness and training activities.

For Turkey, an energy-dependent country, increasing energy efficiency has a vital proposition. The transformation of electric motors is seen as one of the shortest cuts to increase energy efficiency. In the forming of this program, examples of successful countries were examined, and the components of the program were determined. The most important components at this point are legislation, creating alternatives for financing, making inventories, building awareness, establishing test infrastructure, pilot projects, and market surveillance. MoIT's efforts in this direction continue to be multidimensional and aim to maximize the benefits of converting low-efficiency electric motors used in industry.

The Public Energy Efficiency Policies Mapped and Implemented for the Industrial Motor Reconditioning Sector in Brazil



Rodrigo Santos Vieira, George Alves Soares, Rodrigo Flora Calili, Glycon Garcia Junior, Reinaldo Castro Souza, and Carlos Aparecido Ferreira

1 Introduction

In 2001, there was an electric energy crisis in Brazil [1] due to the low investments in transmission lines in the national interconnected system, water scarcity and the absence of certainty energy planning [1]. The electric energy rationing plan created policies to expand energy supplies and energy efficiency by the government to prevent such events.

One of the most important policies was the creation of Law n° 10295 of 2001, called the Energy Efficiency Law [2], which established the attribution of federal government to promote the increase of equipment's efficiencies through mandatory MEPS. Later on there were several regulations derived from it.

R. S. Vieira (✉) · R. F. Calili
Pontifícia Universidade Católica do Rio de Janeiro – PUC-Rio, Posgraduate Programme in Metrology, Rio de Janeiro, Brazil
e-mail: calili@puc-rio.br

G. A. Soares
Centro de Pesquisas de Energia Elétrica – Eletrobras Cepel, Rio de Janeiro, Brazil
e-mail: gealsoares00@gmail.com

G. G. Junior
International Copper Alliance – Latin American, Procobre Brasil, Rio de Janeiro, Brazil
e-mail: glycon.garcia@copperalliance.org.br

R. C. Souza
Pontifícia Universidade Católica do Rio de Janeiro – PUC-Rio, Postgraduate Programme in Metrology, Rio de Janeiro, Brazil
e-mail: reinaldo@puc-rio.br

C. A. Ferreira
Eletrobras – Procel, Rio de Janeiro, Brazil
e-mail: carlosaparecido@eletrobras.com

One of the government's most incisive energy efficiency efforts was in electric motors. The reason for this initiative was the high consumption of electric power by driving systems within the Brazilian industry, being equivalent to 25% of the consumption of the whole country [3]. Therefore, this motor-driven system is one of the most important and strategic for load control due to its impact on consumption and generation of electric energy.

The first public policy of minimum energy efficiency levels in electric motors was established in 2002. Its scope was induction three-phase electric motors, with alternating voltage up to 600 V, 60 Hz, 2, 4, 6 and 8 poles and from 1 to 250 hp. The policy has established a minimum nominal efficiency for electric manufactured motor, imported or commercialized in Brazil. The Decree 4508 of 2002 [4] imposed that the motors should have efficiency at least IR1 (IE1), which was started to be valid in the date of its publication. In 2005, a new program of minimum efficiency target was established by Interministerial Ordinance 553 [5]. It determined the new MEPS of IR2, quite similar to IE2, for 2009.

There are also other important reasons to save energy, as the world population is growing; the energy consumption per person also increases as people need to accumulate technologies for their comfort needs and the global warming caused by the emission of greenhouse effect gases increases [6]. This way, Brazil, aligned with the countries that signed the UN climate convention in Paris, presented the nationally determined contribution (INDC), establishing a commitment to the future of the global climate by helping to reduce global temperature by 2 °C [7].

Brazil has promised to promote renewable energy sources, increasing its participation in the national energy matrix to 45% in 2030 (not including hydroelectric plants) and also reducing energy consumption by 10% [7].

However, the waste of energy in motor-driven systems is linked not only to the performance of new electric motors but also to the operation of old motors, which do not receive suitable maintenance and to the failed motors that were repaired to get back into operation. There are several theoretical studies that claim that the loss of efficiency is 2% at each reconditioning [16] and that the average lifespan of Brazilian motors from 1 to 250 HP is about 17 years. It is noteworthy that in a good reconditioning the efficiency drop is minimal, but for most of the repairing companies found by Vieira [3, 8], the quality of the service is low. In this article, the words "repaired" and "reconditioning" mean that a failed electric motor is repaired in a company in order to return it to its owner or to be resold.

Several countries in the world are also concerned about the impacts of the services offered by this repairing sector. An example is the study carried out by Associations of the United States and the United Kingdom to understand the best practices that this sector can adopt in the day-to-day work and also to evaluate the quality level of the current service [9].

Interested in evaluating the impact of the sale of second-hand reconditioned electric motors compared to the sale of new motor, in 2013 the Brazilian Electrical and Electronic Industry Association (ABINEE) and International Cooper Association – ICA requested a study to PUC-Rio [10] in order to understand it and measure the energy impact to the country caused by the resale of reconditioned motors. It was

also found out a poor known, unstructured area with no official technical standard to follow, professionals with low level of training and services practices that directly impacts the Brazilian energy matrix.

The Committee of Indicators and Levels of Energy Efficiency (CGIEE), coordinated by the Ministry of Mines and Energy (MME), realized the importance of better understanding and structuring the sector and approved the creation of a Working Group of Reconditioned Motors. This group was officially created in April 2017 with the participation of 13 important institutions representing the government, manufacturers, consumers, universities and research centers.

This chapter aims to present the development of the work performed by the work group of reconditioned motors, as well as their achievements and barriers.

2 Working Group of Reconditioned Electric Motors

The work group of reconditioned motors (WG) counts with the participation of governmental institutions such as ELETROBRÁS (which runs PROCEL- the National Energy Conservation Program), CEPEL (Research Center) and INMETRO (National Metrology Institute), educational institutions such as PUC-Rio (university) and SENAI (organization for training professional of industries), class associations such as ABINEE (motor manufacturers) and the International Copper Association (ICA), and consumer representatives such as CNI (industries state federations representation) and ABRACE (large consumers representation), as well as other institutions. The purpose of this group is to map the entire reconditioned motor sector in order to know the impacts created by it in several areas, and to implement governmental policy actions to improve the sector.

At the first moment, based on a study of PUC-Rio, in 2013 [10], the WG specified six areas of action: Sector Identification, Regulatory, Normative, Consumer Awareness, Qualification / Training and Representativeness of the category. The actions developed in each of these areas are shown below.

2.1 Sector Identification

The first study [10] about RM Sector in Brazil was done in the 2013. As a result, it was noted that there was little acquired knowledge about this area. A major RM resale market was quickly identified. This led the study to focus further on motor resale. The outcome that the number of reconditioning motors was twice the new ones inspired the insertion in the Interministerial Ordinance in 2017, the obligation to achieve minimum efficiency level also for repaired motors. A small entry of new international engines was also seen, in the order of 4% of market share. So, as the 2013 study detected several new market distinctions and it had to be focused on electric motors resale, further studies needed to be carried out.

The first study [10] about RM Sector in Brazil was done in 2013. It was verified a large number of repaired motors being resold and it was observed that the majority of companies that are carrying out this resale are small one. There were no official technical standards for good practices of repairing. The staffs of small companies have received few trainings. Most of the small companies and some medium companies did not use appropriate equipment and performed bad technical procedures which introduced additional losses. The new import motors were responsible for 4% of market share. There was no representative association. The need for a detailed survey embracing more states of the federation and a methodology to better classify the repairing services and sale was also found out.

An assessment was commissioned for PUC-Rio in 2017, settled in 2019 [8] through the funding from International Copper Association, expanding the strands of the 2013 study. In this study, the market of reconditioned motors was split into two parts, the service, which means the motor was repaired and went back to the costumers, and the sale, which means the motor was repaired and sold in the market.

This new study was published in 2019 by ICA. The first step was to better understand the market in terms of the companies' size, gender, educational skills and age of the employees. Three large national official databases were analyzed using data identification techniques. Table 1 shows the total number of companies in the conservative scenario and how the market is strongly composed by small companies.

To map the techniques and equipment used in the companies, a survey was carried out in 40 repairing companies spread throughout the national territory, focusing on the five most representative states: São Paulo (SP), Minas Gerais (MG), Bahia (BA), Rio Grande do Sul (RS) and Rio de Janeiro (RJ), as it can be seen in Table 2. Together, these states account for over 66% of companies in the country. For these companies, a form was applied and, in the compilation of the results, descriptive statistics and important information were extracted to determine the losses in the sector.

The methodology [3] to determine the additional losses inserted in the motors due to inappropriate repairing techniques and equipment was very original and used a lot of data, such as:

- Bibliography survey about repair losses;
- Age, average power, load factor of reconditioning motors by companies' size;
- Number of repairs by companies' size;
- Type of losses affected by type of failure;
- Factors that may increase losses due to company quality;
- Number of motors that are repaired more than once.

Table 1 Number of companies in Brazil and distribution according to size

Company size	Number of companies	Percentage
Small (up to 4 employees)	5584	85.9%
Medium (from 5 to 50 employees)	849	13.1%
Big (over 51 employees)	70	1.1%
Total	6503	100.0%

Table 2 Number of companies in Brazil, distribution in the states and quantity of samples selected

Description	Number of companies	In percentage	Selected sample quantity
Distributed in the states			
In SP	2408	37.0%	15
In MG	667	10.3%	10
In RS	539	8.3%	6
In RJ	449	6.9%	3
In BA	259	4.0%	6
Total in these states	4322	66.5%	40
Total companies in Brazil	6503	100.0%	–

Market Share of three phase motors

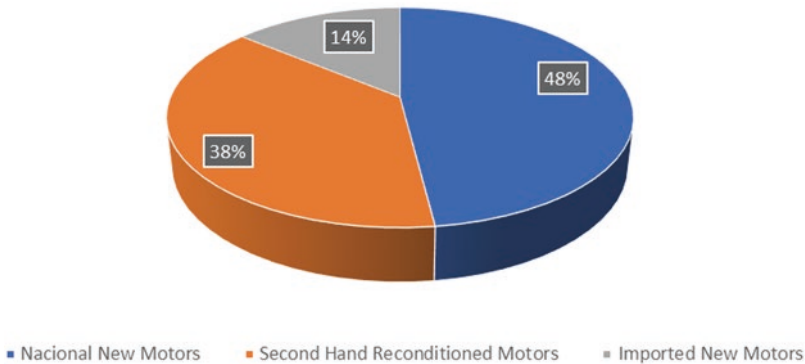


Fig. 1 Market share of three-phase motors in Brazil

As there was a lot of uncertainty in the data and calculation, scenarios were built, and the medium scenario estimated that about 8.43 TWh of electric energy per year are wasted in the country due to poor technical quality of motor repairing. This value of waste is correlated with the fact that the majority (about 86% of a total of 6503 companies) of the reconditioning companies are small, with less than 4 employees, where they usually have low technical quality and few specific tools for the job.

The market share of new three-phase motor sold in Brazil in 2016 presented in Fig. 1 shows the importance of the regulation of repaired motors. They are responsible for 38% of the sale and compete with the manufactured motor, which are under regulation and conformity evaluation process. The total number of motors sold was 2.7 million in this year.

Another important point raised by the research in the companies was the increasing entrance of imported new motors in the country which did not meet the required specifications, presenting low cost of acquisition, low quality, being a disposable product and with probably lower capability than the ones demanded in national

regulation. The repair companies reported motors made of poor quality materials and also the manufacturers' names are not mentioned in the list of participant manufacturers of the conformity evaluation program. The research of 2013 pointed out 4% of the market share, while the research of 2017 [8] identified that 14% of the engines sold are imported, as it can be seen in Fig. 1.

It was noticed that these motors were entering the country, without being submitted to inspection, possibly using NCMs¹ (registration of the imported product) that does not require proof of minimum yields. To suppress the entrance of these imported motors out of specification, NCMs that could be used to import electric motors, were reevaluated in 2018. Besides the 24 NCMs that already demanded proof of energy performance, 67 NCMs that included motors in their descriptions were analyzed. In total, 91 codes were analyzed and the result was presented to INMETRO as the inspection authority.

Regarding the 2013 level of sales by companies, a reduction in some stores and a sudden increase in others were observed. The difference is the marketing strategy. The successful stores built online sales websites for repaired motors, boosting sales [3, 8].

Another action for identification of the sector was the inclusion of a small application about motor repairing in the governmental program "*Brasil mais produtivo*" that aims small industries. The purpose of the application is to collect data to guide the government in decision-making and policy creation, so that energy misuse is reduced in this industrial segment. With this larger sample data, it is expected to build a better understanding about what are the driving factors that lead the final consumer choices: repair, buy a repaired motor or buy a new motor.

2.2 Regulatory

The WG worked with the Ministry of Mines and Energy to publish in July 2017 the Interministerial Ordinance 01 [11] that established IR3 efficiency class as MEPS for electric motors three-phase induction with alternating voltage up to 600 V, 60 Hz, from 2 to 8 poles and from 1 to 500 hp. The ordinance is valid for motors sold in Brazil including manufactured, imported and commercialized so it also includes repaired motors which were resold. This interministerial Ordinance n° 01/2017 replaces the interministerial Ordinance n° 553/2005 and started to be valid in August 29, 2019. It is expected to save 11.2 TWh between 2019 and 2030, being equivalent to the consumption of 560,000 Brazilian houses within a year by the implementation of this ordinance, only considering the market of new motors.

¹ NCMs are codes on a form that characterize imported products, making it easier for the IRS (the inspecting agency for products entering and leaving the country) to check whether products arriving in the country are within regulations and if there are any tax debts. The depth of inspection required by NCM is defined by INMETRO, the metrology institute that deals with product and testing regulations.

The intention is to reduce the resale market of motors, without harming the market of reconditioning service (which is the one that the consumer has a failed motor and sends to the repairer). This difference is very important to be highlighted because the reconditioning service between owner of the motors and the maintenance company is legal, but the resale of motors happened without inspection or rules and competed with the regulated market of efficient motors. Many times companies took motors totally deteriorated, repaired and brought motors back to the market completely inefficient.

The difficulties faced in the implementation of this ordinance for repairer are in the matter of proving that the minimum performance was achieved, since the dynamometer for measuring the motor performance is expensive and unfeasible for most Brazilian repair shops, where 85% of them are of small size (have up to 4 employees), according to Table 1.

For the implementation of the Ordinance, it is important to exclude the repaired motors from the need for the Inmetro certification, which is imposed on new motors manufactured or imported, making the process cheaper and removing bureaucracy for the RM sector. Therefore, the inspection of the RM sector will be the best tool to guarantee the quality of the service. Due to the continental dimensions of the country and the number of repair companies, the follow-up of complaints during after-sales will possibly be chosen as the most effective means. These steps are being defined by an INMETRO regulation.

Furthermore, the costs of inspection of these companies would be very high, especially for approximately 6503 identified companies, spread across a country that has continental proportions. One of the alternatives under analysis is educating the costumers to report the shops, which sell nonconforming second-hand motors to address the inspection.

2.3 Standardization

The first challenging point bounced in the standardization area was the organization of multilateral team for the development of the first Brazilian standard for motors repair, which will standardize all process of repairing to ensure a good-quality service. The purpose of this standard is to present in general the techniques needed to have a quality in reconditioning, showing basic calculations step-by-step and tests that should be done on the motors. This standardization is based on IEC 60034-23 Rotating electrical machines – Part 23: repaired, overhaul and reclamation [12, 13] with adaptations to the Brazilian reality plus items of the South African standard SANS 10242-1 [14]. This standard was completed in February 2021, with name ABNT NBR 16929:2021 – Rotating electrical machines - Repair, overhaul, reclamation or modification, being an ally for the implementation of Joint Ministerial Ordinance n° 01/2017 [11].

One of the challenges for elaboration of this standard is in the adaptation of the international standards to the Brazilian reality motors. Another difficulty is to keep

a high level of participation in standards working meeting, specially, the one that represents medium and small repairers and users. The big players such as big repairers, big manufacturers and big clients go more often to these meetings.

2.4 Consumer Awareness

In the same 2019 study [3, 8], a smaller qualitative survey was conducted on 10 consumers in the state of Rio de Janeiro (RJ), divided into two residential, four commercial and four industrial consumers, according to Table 3. An application was applied in which their answers were analyzed and used to write a booklet directed to consumers. This booklet was launched on August 15th, 2019, and its distribution through the new courses being developed and WG workshops will begin after COVID-19 Pandemic ends [17]. As a result, it was discovered that most consumers chose the repaired motor, due to lower cost compared to buying a new motor, and does not calculate the impact of performance loss of the repaired motor. Additionally, most do not know the motor history, how many times the motor failed or went through maintenance, nor care about the quality of the repairing companies or the repairing procedure adopted.

Therefore, in this booklet the repair process, precautions that must be considered when hiring the service and the calculation that helps deciding whether buying a new motor or repair the old one is better are explained. It also shows some precautions that must be taken in motor maintenance so its performance is not jeopardized.

Another action of the WG was holding workshops to warn consumers and repairers about the importance of qualification and quality of service, types of failures, impact of the failures in the efficiencies, new technical standards in elaboration and new regulation. In the second semester of 2018 until the first semester of 2021, two workshops in Rio de Janeiro, one in São Paulo, one in Minas Gerais and one in Bahia were held and others are planned after the COVID-19 Pandemic ends [17].

PROCEL has a newsletter that broadcasts the main news about the use of conscious energy, with the intent of promoting the WG actions. This newsletter will be made available for the WG to post news about the developed programs, along with small articles for consumer awareness.

Table 3 Consumers selected for this small qualitative research

Consumer type	Selected consumers			
Residential	Condominium of 100 apartments	Condominium of 1000 apartments	–	–
Commercial	University	Hospital	Merchants association	Hotel
Industrial	Petrochemical	Pharmaceutical laboratory	Steel mill	Cleaning materials industry

After the publication of repair standard in February 2021, a new guide for good practice for repairing will be developed based on the standards with a more colloquial language.

2.5 *Qualification/Training*

Current qualifications are provided by the manufacturers to their technical assistance networks. They train and build capacity of these companies. The study [8] noticed a need to reestablish a professional qualification program for motor repair workers whose companies do not belong to those networks, around 67%. SENAI, as the technical and vocational educational representative in the country, took the repair course out of its catalogue. As a result of WG efforts, SENAI organized a workshop and agreed to offer the course with updated arrangement including energy efficiency concepts and techniques.

In December 2018, a meeting was held with motor manufacturers, WG members and SENAI to draft content for the new motor repairing course, offered as a skilled labor program at SENAI. The content included the important points raised by a PUC-Rio 2019 study, and energy efficiency topics. The course was implemented in September 2019. In August 2019, SENAI decided to add once again the repair course in its catalogue to be offered across the country.

2.6 *Category Representativeness*

The implementation of public policies demands a communication channel between repairers and the government, so the initiatives promoted by the public policies can reach more effectively their goals, and also be evaluated if they are fair to the sector. The government incentives can be better identified with participation of the repair shops in order to obtain higher quality services performed by the companies. Repairing companies have no organization that represents them.

To generate representativeness, the WG verified that the best way was to create an electric motor repairer association. The invitation to form the organization was extended to all participants during the workshops, many of them showed interest, but none took a leadership role. The Mines and Energy Ministry provided full support for the formation, inviting some companies and associations to spearhead the project. To accelerate interactions between the WG and corporate representatives and stimulate discussions, a social network group was built. However, not so far a company committed to the creation of this organization.

2.7 Other Actions

A PUC-Rio 2019 data [3, 8] raised several topics that deserve additional studies. Therefore, PROCEL - National Program for Energy Conservation included in its action plan some activities to insert reconditioning theme in other projects. They are the ones that follow:

- Study of Brazilian industrial motor-driven systems – the intention is to understand the reality of current industrial motors; checking lifetime, number of reconditioning, maintenance, operation conditions, applied load etc.; additionally, to also understand energy saving opportunities;
- Inclusion of repair issues in technical international standards – An example was the Brazilian contribution in the reviewing of standard ISO 50004 [15], including the subject of motor repair as an example of energy management;
- Restructuring the “*Lamotriz*” network – the test laboratories network of electric motors developed by the government in 14 universities will be remodeled, promoting researches about motors, repairing evaluation, mechanical transmission, start-up and load to improve motor-driven systems performance;
- “*Programa Aliança*” – It will analyze energy efficiency in large energy-intensive industries to study the benefits that energy efficiency can bring to the nation, allowing governmental actions to stimulate industrial energy efficiency adoption;
- Evaluation of repair techniques in the efficiency of induction motors – the objective is to measure the impact in motor performance caused by repairing done by Brazilian companies in failed motors. Several size and efficiency classes of motors, different types of faults and service quality of repair companies will be tested to consider a mean loss percentage in the Brazilian market.

3 Conclusion

The sector of RM in Brazil is a very important player in terms of energy consumption. The innovative methodology estimated that around 8.43 TWh are lost due to inappropriate service quality in this sector. Brazilian sales market for repaired motors is huge, around 38% of all motor sales in 2016. Despite its relevance, it has not received proper attention of public policies. The sector is composed mostly of small companies, around 86% of 6053 corporations spreading across the country. Most lacking trained staff and proper equipment. One way to increase the quality of this service is to advance the offer of the courses for these teams. It is crucial to highlight that in Brazil, there are excellent maintenance companies that usually compose the manufacturers’ technical assistance network. These companies attend

maintenance courses offered by the manufacturers and have quality assurance programs.

The Ministerial Ordinance n° 01/2017 that came into force in August 2019, expanded the MEPS for repaired motors. The conformity evaluation process is in discussion but this expansion was the first step to reduce the sale of inefficient repaired motor without harming the repair service business.

Consumers' awareness is another relevant point to be worked. Industrial consumers do not log maintenance history, and when the motors fail they do not always require good quality services. Workshops, guide, booklet and computational programs are tools to leverage this awareness and to raise the capacity of the staffs.

The formation of the WG allowed several policies to be enacted during its 2 years of existence. Studies to better understand the sector, law drafting, workshops and educational material and regulations and technical standards were implemented. Due to the WG's studies and actions, governmental energy efficiency programs like PROCEL noticed the relevance of the subject and invested in more studies to enhance the knowledge about motors and their reconditioning. The repair motor technical standard being drafted will allow more acts to stimulate the sector.

These efforts make possible the reduction of inappropriate practices that waste electric energy and increase the unneeded energy generation.

References

1. nytimes.com, Energy Crisis in Brazil Is Bringing Dimmer Lights and Altered Lives, June 6, 2001. [Online]. Available: <https://www.nytimes.com/2001/06/06/world/energy-crisis-in-brazil-is-bringing-dimmer-lights-and-altered-lives.html>
2. BRAZIL, Presidency of the Republic, Civil House, "Law 10 295 of October 17, 2001 – Energy Efficiency Law", Brazil, 2001
3. R.S. Vieira, *Evaluation of Energy Losses and Characterization of Retail and Maintenance Market Reconditioned Electric Motors in Brazil*, master's Degree Dissertation (PUC-Rio, Rio de Janeiro, 2018)
4. BRAZIL, Federative Republic of Brazil, "Decree No. 4,508 of December 11, 2002. Defines the Minimum Energy Efficiency Levels of National or Imported Three-Phase Squirrel Cage Rotor Induction Electric Motors for Sale or Use in Brazil", (2002)
5. MME, Ministry of Mines and Energy, "Interministerial Ordinance No. 553 of December 8, 2005. Approves the Three-Phase Induction Electric Motor Targets Program," (2005)
6. P. Nejat, F. Jomehzadeh, M.M. Taheri, M. Gohari, M.A.M. Majid, A global review of energy consumption, CO₂ emissions and policy in the residential sector (with an overview of the top ten CO₂ emitting countries). *Renew. Sustain. Energy Rev.* **43**, 843–862 (2015)
7. BRASIL, Federative Republic of Brazil, "Intended Nationally Determined Contribution (iNDC)," (2015)
8. R.C. Souza, R.F. Calili, R.S. Vieira, R.S.D. Teixeira, *Market Research on Refurbished Engines, a Proposal for the Regulator*, Technical Report for International Cooper Association (PUC-Rio, Rio de Janeiro, 2019)

9. EASA, Eletrical Apparatus Service Association Inc.; AEMT, Association of Electrical and Mechanical Trades, The effect of repair/rewinding on motor efficiency. EASA/AEMT Rewind Study and Good Practice To Maintain Motor Efficiency. Good Practice Guide to Maintain Motor Efficiency (2003), pp. 1–82
10. R.C. Souza, B.F. Dantas, D. Reis, H. Sant’Anna, R.F. Calili, W.d.C. Fagundes, *Final Report – Market Research on Refurbished Engines, A Proposal for the Regulatory Agency* (PUC-Rio, Rio de Janeiro, 2013)
11. MME, Ministry of Mines and Energy, “Interministerial Ordinance No. 1 of June 29, 2017, Approves the Target Program for Three-Phase Squirrel Cage Induction Electric Motors,” (2017)
12. IEC, International Electrotechnical Commission, “IEC 60034-23 – Rotating Electrical Machines. Part23: Repair, Overhaul and Reclamation,” (2003)
13. IEC, International Electrotechnical Commission, IEC 60034-23 – Rotation Electrical Machines. Part 23: Repair, Overhaul and Reclamation, (2019)
14. SANS – South African National Standard, SANS 10242-1:2017. The rewinding and refurbishing of rotating. Part 1: Low-voltage three-phase induction (2017)
15. ISO, International Organization for Standardization, ISO 50004, Energy management systems – Guidance for the implementation, maintenance and improvement of an energy management system, (2014)
16. A.J. Bazurto, E.C. Quispe, R.C. Mendoza, Causes and failures classification of industrial electric motor. Proceedings of the 2016 IEEE ANDESCON, ANDESCON 2016 (2017)
17. The New York Times, Coronavirus in Brazil: What You Need to Know. March 27, 2021. [Online]. Available: <https://www.nytimes.com/article/brazil-coronavirus-cases.html>. Accessed May 16, 2021

Self-Assessment Tool for the Estimation of the Savings Potential of Electric Motor Systems



Richard Phillips, Yannick Riesen, and Nicolas Macabrey

1 Introduction

In 2011, the Federal Council and Parliament decided that Switzerland has to withdraw from the use of nuclear energy on a step-by-step basis. The existing five nuclear power plants are to be decommissioned when they reach the end of their safe service life, and will not be replaced by new ones [1]. As a result of this decision and various other profound changes (e.g. low electricity prices) that have been observed for a number of years, in particular in the international energy arena, the Swiss energy system will require successive restructuring in the period up to 2050. In view of this, the Federal Council developed a long-term energy policy (“Energy Strategy 2050”) based on the revised energy perspectives.¹ At the same time, it produced an initial package of measures aimed at securing the country’s energy supply over the long term. The initial package of measures concerns three sectors (households, services and industry), as well as the production of electricity based on new renewable sources (sun, wind and geothermal energy) and energy efficiency.

Electric motor systems in all sectors account for almost half of Switzerland’s electricity consumption. However, the industry and services sectors remain dominant. For this reason, companies with electricity consumption higher than 0.5 GWh p.a. must complete a mandatory audit and undertake commitments in target

¹Botschaft zum ersten Massnahmenpaket der Energiestrategie 2050 (Dispatch to Parliament concerning the initial package of measures relating to Energy Strategy 2050), Swiss Federal Office of Energy, September 2013.

R. Phillips (✉)
Swiss Federal Office of Energy, SFOE, Bern, Switzerland
e-mail: richard.phillips@bfe.admin.ch

Y. Riesen · N. Macabrey
Planair SA, La Sagne, Switzerland
e-mail: yannick.riesen@planair.ch; nicolas.macabrey@planair.ch

agreements. However, the main driver for the regulations governing large and very large companies is the reduction of CO₂ emissions. Electricity produced in Switzerland has lower CO₂ emissions than efficiency measures, so most companies tend to implement efficiency measures relating to heat production based on non-renewable sources. As a consequence, the savings potential of electric motor systems remains dormant. Furthermore, efficiency measures for electric motor systems often remain second choice in the target agreements, because the payback time for such measures is in many cases longer than 4 years. However, an extensive survey in the industry sector revealed that a large percentage of electric motor systems are oversized, too old and inefficiently operated. Based on the savings potential of electric motor systems, Switzerland's annual electricity consumption could be reduced by up to 5%.

This chapter presents a new “all-in-one” tool for estimating the savings potential of electric motor systems such as pumps, fans, compressors for the production of compressed air and refrigeration. The tool is based on the one hand on an empirical approach relating to statistical data obtained from in-depth analyses, and on the other hand on a three-step approach: quick check, preliminary analysis and extended analysis. This methodology enables companies to quickly identify those installations with the highest savings potential, and especially those that are good candidates for in-depth analyses with measurements.

2 Electricity Consumption and Savings Potential of Electric Motor Systems

Electric motor systems in all sectors account for almost half of Switzerland's electricity consumption. Furthermore, the industry and services sectors account for two-thirds of this consumption. The main electric motor systems in operation in the industry sector are fans, pumps and compressors, as shown in Table 1 [2].

Table 1 Energy consumption of electric motor systems in the households, industry and services sectors (“Analyse des schweizerischen Energieverbrauchs 2000–2017 nach Verwendungszwecken”, Swiss Federal Office of Energy, Bern, October 2018)

Usage	Households	Services	Industry
Heat pump – room heating	1.50 TWh	0.55 TWh	0.00 TWh
Heat pump – hot water	0.25 TWh	0.00 TWh	0.00 TWh
Ventilation	1.27 TWh	4.50 TWh	0.25 TWh
Drives and process	4.36 TWh	4.66 TWh	10.36 TWh
Total I	7.38 TWh	9.71 TWh	10.61 TWh
Total II	27.7 TWh (or 48% of Switzerland's annual electricity consumption)		

A study from the early 2000s already pointed out that around 2 million motors are in operation in Switzerland's industry sector and that their savings potential is estimated at up to 30% based on following four sets of measures:²

- Higher motor efficiency
- Higher efficiency of the components
- Optimisation of the operating conditions
- Process optimisation

However, these measures have varying impacts and savings potentials [3]. The savings potential depends on the degree and extent of the system approach, as shown in Fig. 1 [4].

The replacement of a single component such as a motor with a more efficient model does not result in significant savings (possibly 8–10% in the best case). However, optimisation of the system based on specific needs can result in savings of 45–50%.³

It is also important to bear in mind that a savings potential of up to 30% means that almost all possible efficiency measures have to be implemented. However, the implementation of the various measures greatly depends on economic aspects such as the payback time. Unfortunately, companies tend to implement measures with a payback time shorter than 4 years without taking into account the total cost of ownership. In other words, they completely ignore the fact that the investment and

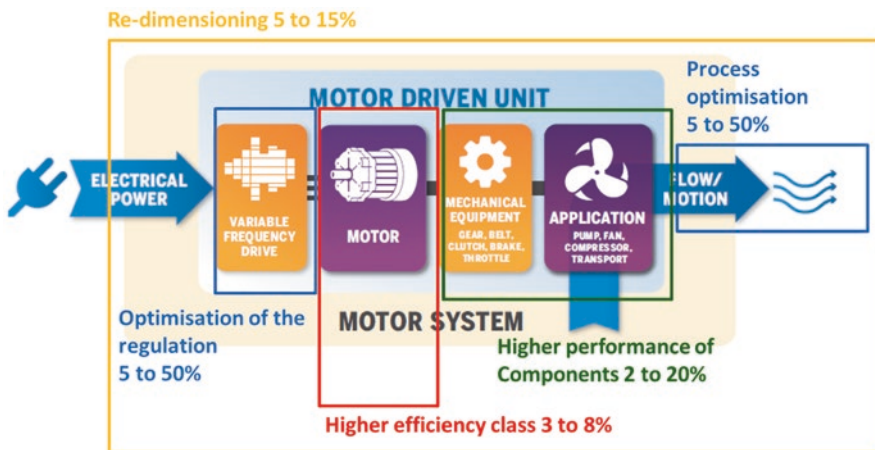


Fig. 1 Schematic representation of an electric motor system and its components, as well as the impacts of each of the four sets of efficiency measures ("Policy Guidelines for Motor Driven Units: Part 2, Figure 1, p. 9, 4E Electric Motor Systems (EMSA), The Netherlands, February 2018)

²"Massnahmen zum Stromsparen bei elektrischen Antrieben: Marktanalyse in der Industrie", final report, Swiss Federal Office of Energy, Bern, December 2006.

³"Programme for In-depth Analyses of Electric Motor Systems in Industry (ProAnalySys)", Dr. R. Phillips, EEMOD'19, Tokyo, 17–19 September 2019.

maintenance costs are less than 10% of the overall cost of the installation over its lifetime.⁴ Unfortunately, a significant proportion of the potential lies in “non-viable” measures that have a payback time longer than 4 years and which are now outside of the regulation, as explained below. However, the aim of this chapter is to present an “all-in-one” tool designed to help companies assess the savings potential of their electric motor systems. The chapter also explains that the methodology is based on a step-by-step approach that gives rise to a catalogue of basic measures that are classified on the basis of their savings potential. Companies can then decide which efficiency measures they want to implement or examine more closely (for example by means of an in-depth analysis).

3 Regulations for Swiss Companies

Swiss companies with an electricity consumption above 0.5 GWh p.a. or heat consumption exceeding 5.0 GWh p.a. have to enter into a commitment within the scope of a target agreement based on a mandatory audit. The commitment is binding over a period of up to 10 years for very large companies. However, large companies can choose between two other options: a) 20% in 10 years or at least 15% in 3 years. Accredited energy consultants conduct the mandatory audit in which efficiency measures to reduce heat as well as electricity consumption are taken into account. In the industry and services sectors, heat for room heating, hot water and process purposes accounts for almost two-thirds of the total energy consumption.⁵ However, the companies are only obliged to implement efficiency measures with a payback time shorter than 4 years. In addition, the target agreements that apply in the case of very large companies are mainly driven by the reduction of CO₂ emissions in order to gain exemption from the CO₂ tax. For all these reasons, efficiency measures for electric motor systems are often regarded as second priority. Alongside the mandatory audits there are also the minimum energy performance standards for pumps, fans and electric motors. However, in most cases these standards are based on a component approach, which means that their impacts and the mandatory audits to assess the savings potential of electric motor systems are limited as they do not take into account, for example, whether a system or installation is oversized or operating at its optimal efficiency level. Furthermore, process and operational optimisations are also not addressed. Consequently, to make companies aware of the savings potential of their electric motor systems, several tools have been developed, for example by motor, pump and fan suppliers, as well as by neutral Internet platforms such as topmotors.ch or by the Swiss Federal Office of Energy (SFOE) itself. Most

⁴“Elektrische Antriebssysteme mit kleinerem Stromverbrauch”, Armin Braunwalder, *Electrorevue*, No. 25, p. 30, 2012. http://www.topmotors.ch/sites/default/files/2018-06/D_PB_2012_25_Electrorevue_Topmotors.pdf

⁵“Analyse des schweizerischen Energieverbrauchs 2000–2017 nach Verwendungszwecken”, Swiss Federal Office of Energy, Bern, October 2018.

of these tools are based on the affinity laws and only focus on one or two technologies at most. Furthermore, they are also divided into several segments depending on the depth of the analysis. Figure 2 depicts the “four-step” approach that was developed by Topmotors and permits a preliminary estimation of the savings potential through to the implementation of the identified efficiency measures.

The next chapter describes a new all-in-one tool that enables a preliminary assessment of the savings potential of electric motor systems.

4 All-in-One Software Tool

Based on the “four-step” approach from Topmotors, a new integrated tool has been developed which comprises three steps (excluding implementation): a quick check, a preliminary analysis and an extended analysis. To ensure that the company only invests its time when and where this is beneficial, the quick check is based on a set of questions, most of which can be answered with “yes” or “no”, and takes less than 10 minutes to complete. The first question concerns the annual electricity consumption. For companies with consumption below 100 MWh p.a., the tool terminates. These companies do not have enough incentives to examine and implement efficiency measures as their annual energy costs are below 20,000 euros, which means that their cost savings through energy efficiency are irrelevant. Upon completion of the quick check, the company receives a recommendation to either proceed to the next step or quit the tool if the savings potential appears to be too low (for example, if most of their installations are less than 5 years old or the size and number of their electric motors are too low).

After the quick check, the next step is the preliminary analysis, where the main electric motor systems, such as pumps, fans and compressors for refrigeration and compressed air, are listed on the basis of the following input data:

- Nominal power of the motor in kW
- Efficiency class of the motor
- Year of construction
- Operating hours per annum (or load profile)
- Variable load (if applicable, it should be mentioned whether the regulation mechanism is mechanical or electronic)

Based on the input data, the annual consumption is calculated as follows:

$$E_{el} = P \times t \times \text{load}_{\text{factor}} \quad (1)$$

where

E_{el} is the electricity consumption in kWh p.a.

P is the nominal power of the motor in kW

T is the operating time in hours p.a.



Fig. 2 The “four-step” approach developed by Topmotors, ranging from the estimation of potential through to the implementation of efficiency measures (<http://www.topmotors.ch/en/content/motor-systems-check>)

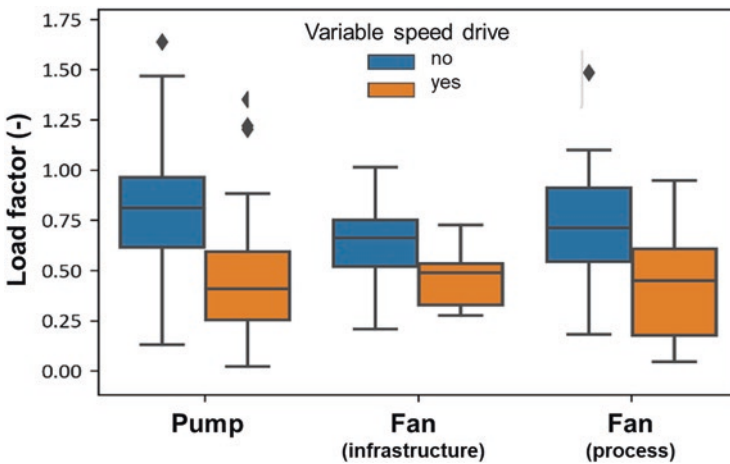


Fig. 3 Statistical data of the load factor for pumps and fans depending on the variability and regulation of the load

$Load_{factor}$ is a variable parameter that depends on the operating mode of the system (constant or variable load).

The load factor depends on the variability of the load and on its regulation, as shown in Fig. 3: 60% for constant load, 50% and 40% respectively for variable load with mechanical and electronic regulation.

Once the electricity consumption has been calculated, the four sets of efficiency measures can be used for estimating the savings potential:

- Higher efficiency class of the motor (up to 10% as shown in Fig. 4 under “Savings - New motor”)
- Technological improvement (up to 3% as shown in Fig. 4 under “Savings - More efficient drive”)
- Redimensioning (8% savings in all cases)
- Implementation of a VSD (20% for fans and between 10% [lifting] and 20% [circulation] for pumps)

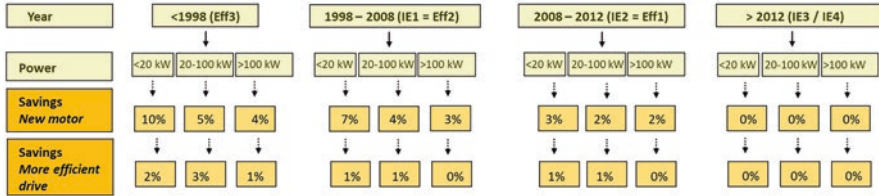


Fig. 4 Estimation of the savings potential depending on the power and the age of the installation for the efficiency measures: (a) higher efficiency class of the motor and (b) technological improvement

The savings percentages shown in Fig. 4 are based on the statistical data from 170 analyses carried out at 28 different industrial sites (savings estimates for 114 pumps, 38 fans [infrastructure] and 45 fans [process]).

5 Preliminary Analysis

The results of an in-depth analysis based on measurements will now be compared with calculated examples of the preliminary analysis using the tool [5].

The first example is a lift water pump with a power rating of 13 kW, which was installed in 1990 (see Fig. 5), and which is in operation 4380 hours a year. The load is variable over time and the regulation is manual (using a throttle). Based on the methodology presented above, the savings potentials are estimated as follows:

- 10% by changing the motor (age <1998 and power rating <20 kW)
- 2% through technological improvement (age <1998 and power rating <20 kW)
- 8% through redimensioning
- 10% with the use of a VSD (for lifting pumps)

In total and based on the software tool, the calculated consumption of the pump is 28,470 kWh p.a. (13 kW x 4380 hours p.a. x 0.5) and the estimated savings are 30%, or a reduction in consumption by 8500 kWh p.a.. The measurements of the in-depth analysis indicated an annual reduction in consumption by 10,875 kWh p.a.⁹ The difference between the tool calculation and the measurements corresponds to +/- 28%.

The calculation model contains a specific module for refrigeration installations, where the savings potential also depends on (a) the temperature profile, (b) the regulation of the condensation temperature (fixed or variable) and (c) use or non-use of the free-cooling system. Figure 6 shows the additional savings specific to refrigeration motor systems.

For example, a cooling installation more than 20 years old with a compressor with a power rating of 113 kW which is operated for 4000 hours per annum (temperature profile B) with no free cooling, a “stop and go” regulation of the compressor and a fixed condensation temperature results in an annual calculated consumption



Fig. 5 13 kW lifting water pump installed in 1990, with a variable load regulated by a throttle (“Feinanalyse für Elektrische Antriebe ProAnalySys: Kurzbericht”, Electrosuisse, Fehraltorf (Switzerland), February 2018)

of 452,000 kWh with the following savings potentials based on the tool’s methodology:

- 3% by changing the motor
- 2% through technological improvement
- 8% through regulation
- 15% by implementing a variable condensation temperature
- 30% by implementing free cooling

The software tool then estimates the savings at up to 58%, or a reduction in electricity consumption by up to 263,000 kWh p.a. The measurements of the in-depth analysis of the installation indicate a reduction in consumption by 345,000 kWh

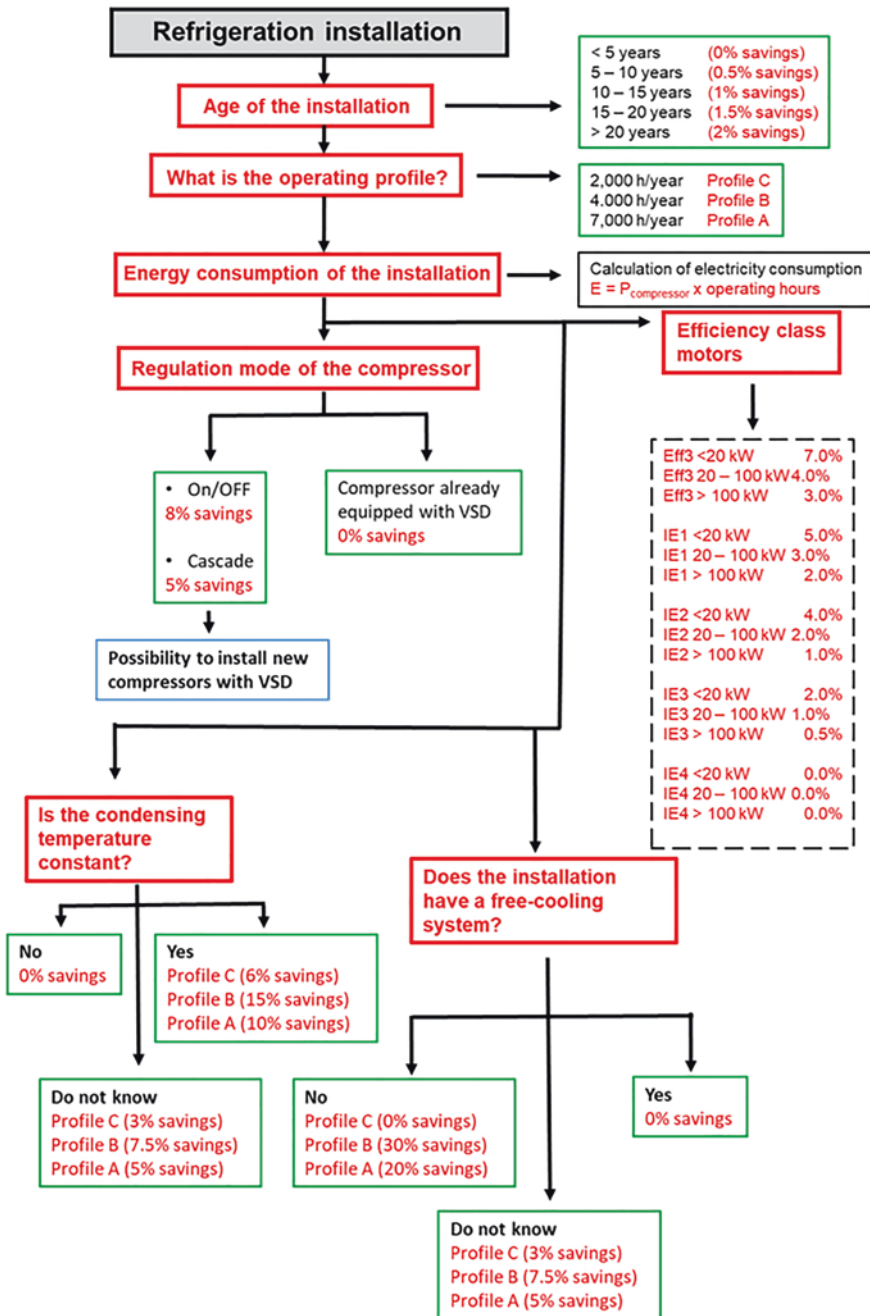


Fig. 6 Estimation of the savings potential for refrigeration installations depending on the power rating and the age of the installation for a set of efficiency measures: (a) higher efficiency class of the motor, (b) technological improvement, (c) regulation of the compressor, (d) management of the condensation temperature and (e) use of a free-cooling system

p.a.⁶ In this case the difference between the calculation and the measurements corresponds to $\pm 31\%$.

The tool also contains a module for compressed air production systems. The savings resulting from the elimination of air leakages based on four states of the compressed air distribution network are specific to this module:

- Leak-proof (leakage rate below 10%: 0% savings)
- Almost leak-proof (leakage rate between 10 and 15%: savings 5%)
- Poorly leak-proof (leakage rate between 15 and 20%: savings 10%)
- Not leak-proof at all (leakage rate above 20%: savings up to 40%)

What is also specific to the calculation module for compressed air is the savings based on the pressure reduction with 3.5% electricity savings per reduction by 0.5 bar. (Fig. 7)

The next example concerns a compressed air system with a power rating of 11 kW, which is used in a car workshop where the compressor was renewed in 2010 [6, 7]. Based on some measurements of the compressor, it appears that it is permanently operating with a load factor estimated to be around 40–50%. All the data were entered in the calculation tool with additional inputs such as an estimation of the state of the compressed air distribution network (which was assessed as “not leak-proof at all”), as well as the fact that pressure has not been optimised and the compressor was also not equipped with a VSD. The tool calculated an annual consumption of 68,400 kWh (11 kW \times 8700 \times 0.72⁷), but the figure was 40,000 kWh

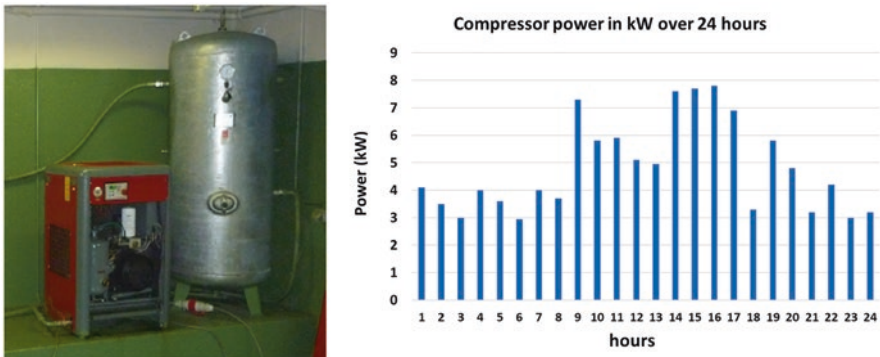


Fig. 7 Left: 11 kW compressed air production installation installed in 2010. Right: Power distribution over time (here 24-hour measurements) (“Druckluftoptimierung Autogarage”, Rolf Gloor, final report, July 2016. <https://www.google.ch/url?sa=t&rct=j&q=&esrc=s&source=web&cd=1&ved=2ahUKewiR973544niAhXJURUIHb2VBywQFjAAegQIABAC&url=https%3A%2F%2Fpubb.bdb.bfe.admin.ch%2Fde%2Fpublication%2Fdownload%2F9314&usg=AOvVaw1cuWPCYrJcIG3Skz6kCnuy>)

⁶“Stromeffizienz-Analyse”, Thomas, Grieder, DM Energieberatung, interim report, March 2019.

⁷The average load of the compressor is 50%. This gives a compressor power of 0.65, which has to be divided by 0.9 in order to calculate the motor power. This then results in a load factor of 0.72 ($=0.65 / 0.9$).

based on the measurements. As result, the tool calculated a saving of 70% or a reduction in consumption by 28,000 kWh p.a.:

- 4% by reducing the air pressure of at least 0.5 bar
- 40% for the suppression of air leaks
- 26% for improved regulation with the aid of a VSD

The in-depth analysis of this installation resulted in a savings potential of 14,000 kWh p.a., mainly based on the suppression of air leaks. The compressor is too new to already be replaced and the pressure cannot be reduced at present. Consequently, the savings potential has been estimated at 35%, which is close to the 40% calculated by the tool for air leakage only.

6 Extended Analysis

As pointed out above, the savings potential calculated by the tool is a rough estimation with a degree of precision of $\pm 30\%$ (though this can also be as high as $\pm 50\%$). This is attributable to the limited amount of information available, which is also the purpose of the tool, i.e. to quickly obtain an initial (approximate) estimation based on readily available data. However, when more data are available it is then possible to extend the analysis in order to make the estimation of the savings potential more precise. For example, for fans, as well as for pumps, it is possible to include the following additional data:

- The ratio between the nominal output (provided by the supplier) and the maximum output used during the operation of the fan/pump (this information should be provided by the user of the fan/pump)
- Nominal power at the shaft of the fan/pump
- The temporal load profile (at 25%, 50%, 75% and 100% load)

Based on the ratio of Q_{\max} and Q_{nom} , the redimensioning is estimated more precisely (instead of the overall 8%) as shown in Fig. 8. Because the shaft power of the fan is now known, it can be used for estimating the consumption instead of the nominal power of the motor. The maximum power at the shaft of the fan is then corrected based on the following equation:

$$P_{\text{max, fan}} = (0.5162(Q_{\max} / Q_{\text{nom}}) + 0.4455) * P_{\text{nom, fan}} \quad (2)$$

where

Q_{\max} is the maximum airflow rate during operation in m^3/h

Q_{nom} is the nominal airflow rate indicated by the supplier in m^3/h

$P_{\text{nom, fan}}$ is the nominal power of the fan indicated by the supplier in kW

Extended analysis

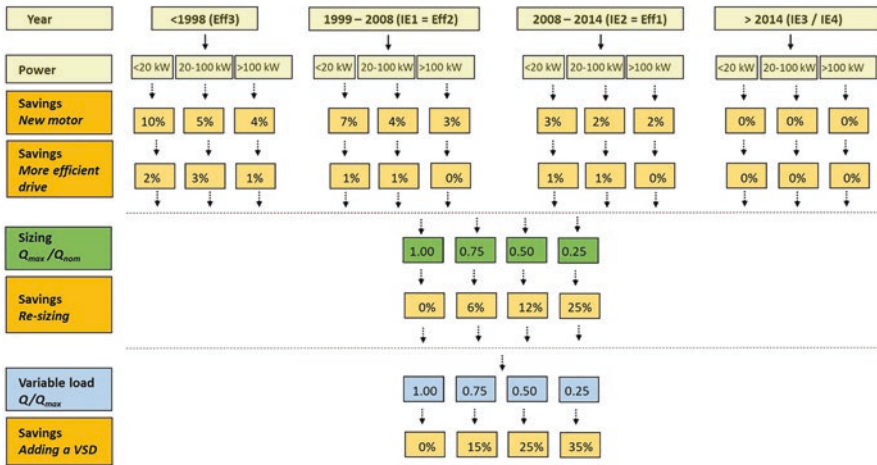


Fig. 8 Savings estimation based on the additional data provided for the tool for the extended preliminary analysis

$P_{max,fan}$ is converted to motor power $P_{max,motor}$ by taking an average efficiency ratio of 90%. This value ($P_{max,motor}$) allows a more precise estimation of the savings potential due to the implementation of a VSD as a function of the load profile.

Let us take a practical example with a fan with a motor with a nominal power of 45 kW installed in 1998 (efficiency class Eff3/IE0), which is used as a cooler in an extraction process that is in operation for 6150 hours a year. The airflow as well as the pressure vary, but the regulation is mechanical, using valves. It appears that the nominal power of the fan is 39 kW and the ratio Q_{max} / Q_{nom} is 49%, which means that the installation is poorly regulated and oversized. Based on Eq. (2) the maximum power of the fan is 27.3 kW, which then induces a motor power of 30.3 kW ($27.3 \text{ kW} / 0.9$) at Q_{max} . The calculation of the motor power at partial load is made using the same method with Eq. (2):

- 0% – 25% = 0.0–22.0 kW
- 25% – 50% = 22.1 kW - 24.8 kW
- 50% – 75% = 24.8 kW - 27.5 kW
- 75% – 100% = 27.5 kW - 30.3 kW

In this example, the time distribution of the load profile is:

- 0% – 25% during 1950 hours p.a.
- 25% – 50% during 1700 hours p.a.
- 50% – 75% during 1250 hours p.a.
- 75% – 100% during 1250 hours p.a.

The actual energy consumption can then be estimated as follows:

$$E = 22.0 \text{ kW} * 0.93 * 1950 \text{ h} + (22.0 + 24.8) / 2 \text{ kW} * 1700 \text{ h} + (24.8 + 27.5) / 2 \text{ kW} * 1250 \text{ h} + (27.5 + 30.3) / 2 \text{ kW} * 1250 \text{ h} \\ = 148,930 \text{ kWh p.a.}$$

Figure 8 enables the estimation of the savings potential as follows:

- Redimensioning with 12% reduction, or 18,646 kWh p.a.
- Use of a VSD with 20% savings, or 28,691 kWh p.a.
- Savings = $22.0 \text{ kW} * 0.93 * 1950 \text{ h} * \mathbf{0.35} + (22.0 + 24.8) / 2 \text{ kW} * 1700 \text{ h} * \mathbf{0.25} + (24.8 + 27.5) / 2 \text{ kW} * 1250 \text{ h} * \mathbf{0.15} + (27.5 + 30.3) / 2 \text{ kW} * 1250 \text{ h} * \mathbf{0.0}$
=28,961 kWh p.a.
- Efficiency improvement of the components with 8% savings, or 11,914 kWh p.a.

In total, savings of 40% or 76,851 kWh p.a. Table 2 compares the results between the preliminary and the extended analysis. Although the relative savings potentials are fairly close, in this case the preliminary analysis underestimates the absolute savings potential by one-fifth.

The in-depth analysis of this installation confirmed that the fan is effectively oversized and it runs inefficiently at relatively high power (39.0 kW), although the airflow varies between 2.0 m³/s and 4.0 m³/s, as shown in Fig. 9.

The solution is to replace the fan by a smaller one equipped with a VSD and a new synchronous IE4 22 kW motor. Figure 10 shows the operating curve of the new fan, where its efficiency is increased and its power reduced to 7.8 kW at 2.0 m³/s and 22.0 kW at 4.0 m³/s, as shown in Fig. 10. The new solution will save 56%, or 90,800 kWh p.a. In other words, the degrees of precision of the savings estimation of the preliminary and extended analysis are +/- 45% and +/- 35% respectively. Although the extended analysis increases the precision of the estimated savings potential, the margin of error is still significant. Nonetheless, the tool remains suitable for determining which motor systems are worth subjecting to an in-depth analysis.

Table 2 Comparison of the savings estimations between the preliminary and the extended preliminary analysis for a fan with a nominal power of 39 kW, installed in 1988, in operation for 6150 hours a year, with the load varied through mechanical regulation (no VSD)

	Preliminary analysis		Extended analysis	
	%	kWh _{el} p.a.	%	kWh _{el} p.a.
Consumption (kWh _{el} p.a.)		138,375		148,930
Higher efficiency of the components	8	11,070	8	11,914
Redimensioning	8	11,070	12	18,646
Addition of a VSD	20	27,675	20	28'961
Total savings	36	49,815	40	59,500

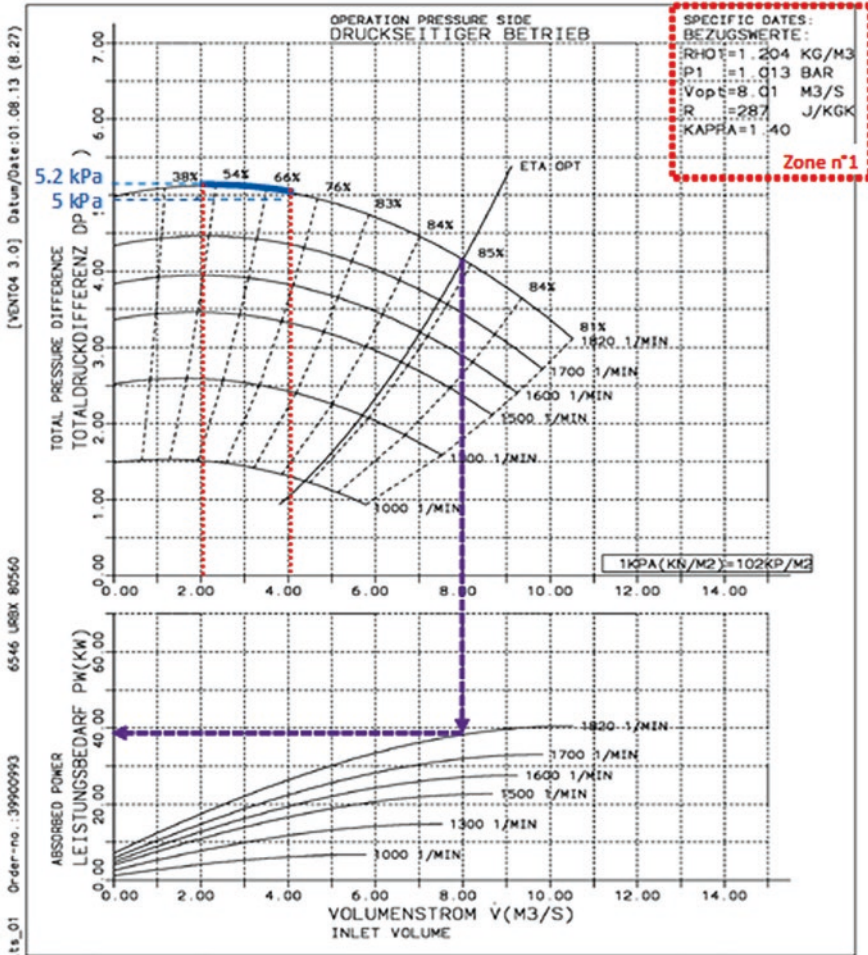


Fig. 9 Actual situation of a fan with a motor with a nominal power of 45 kW, installed in 1988 (efficiency class IE0) with variable airflow from 2.0 m³/s up to 4.0 m³/s; regulation is carried out by opening or closing a valve

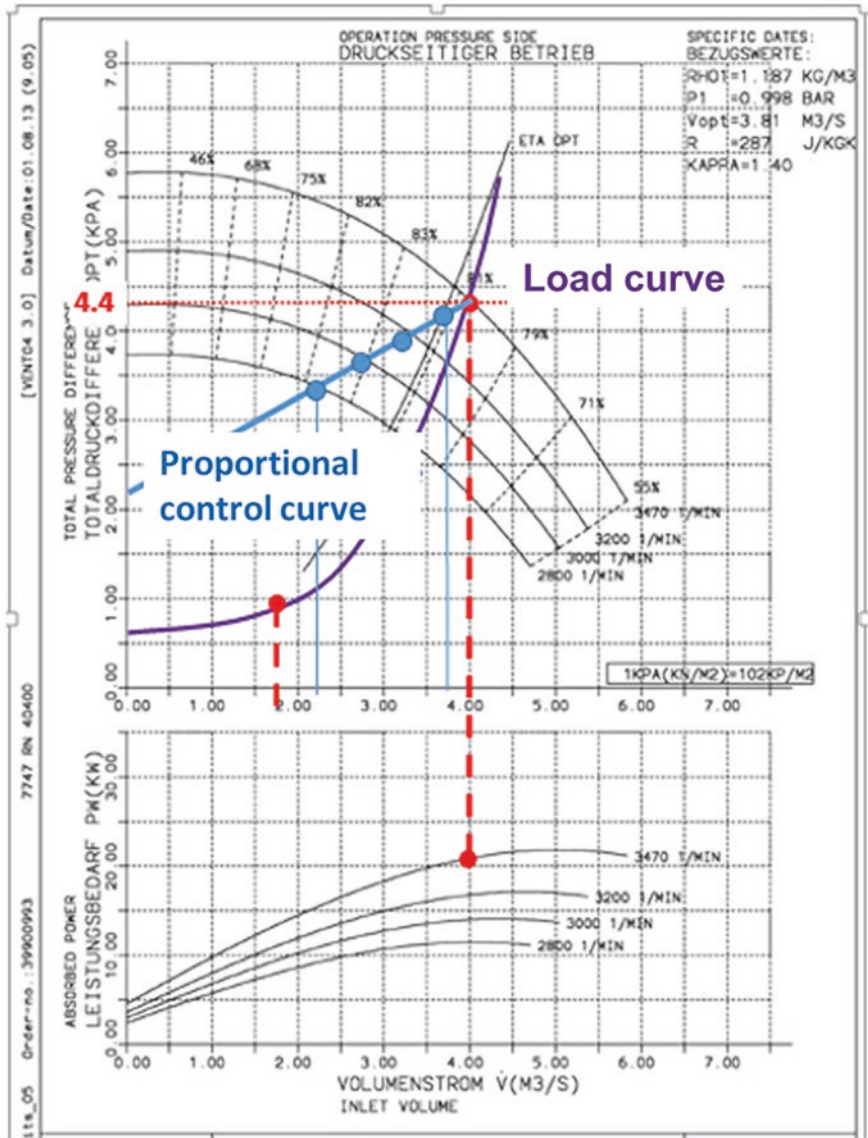


Fig. 10 Characteristics of the new fan with a lower nominal power (22 kW) and equipped with a VSD, based on the results of the in-depth analysis

7 Conclusions

There are more than 2 million electric motors in use in the industry sector, for which a savings potential of up to 30% has been estimated based on four groups of efficiency measures: higher motor efficiency, higher efficiency of the components, optimisation of the operating conditions and process optimisation.

Swiss companies with an electricity consumption higher than 0.5 GWh p.a. or heat consumption exceeding 5.0 GWh p.a. have to enter into target agreements based on mandatory audits. However, in both the industry and the services sectors, heat for room heating, hot water and process purposes accounts for almost two-thirds of the total energy consumption. Furthermore, in the case of very large companies, the implementation of efficiency measures is mainly driven by the reduction of CO₂ emissions in order to gain exemption from the CO₂ tax. For all these reasons, efficiency measures relating to electric motor systems are often regarded as second priority. Alongside the mandatory audits there are also minimum energy performance standards for pumps, fans and electric motors, but their impacts are limited. Consequently, to make companies aware of the savings potential of their electric motor systems, several tools have been developed, most of which are based on the affinity laws and only focus on one or two technologies at most.

Based on the “four-step” approach similar to that developed by Topmotors, a new integrated tool has been developed that comprises three steps (excluding implementation): a quick check, a preliminary analysis and an extended analysis. The tool can be downloaded directly from the Internet (<https://velani-tool.ch/>). It addresses companies with an electricity consumption of at least 100 MWh p.a. The input data for the preliminary analysis performed by the tool are:

- Nominal power of the motor in kW
- Efficiency class of the motor
- Year of manufacture
- Operating hours per annum (or load profile)
- Variable load (if this applies it should be indicated whether the regulation mechanism is mechanical or electronic)

Based on these data, the annual consumption is then calculated and the four sets of efficiency measures permit the estimation of the savings potential. This is based on a statistical approach where data from 170 analyses at 28 different industrial sites (114 pumps, 38 fans [infrastructure] and 45 fans [process]) were collected.

The results obtained with the tool for pumps, fans, compressed air and refrigeration installations were compared with those resulting from in-depth analyses. In most cases, the degree of precision of the estimation was $\pm 45\%$ (worst case). We may therefore conclude that, despite the limited amount of input data, the preliminary analysis can still provide some approximate estimations that are accurate enough for companies to select those systems for which it is beneficial to invest time and money in an in-depth analysis.

The tool can also be used for performing an extended analysis if specific data are available, such as:

- The ratio between the nominal output (indicated by the supplier) and the maximum output used in the operation of the pump/fan (this information should be provided by the user of the pump/fan)
- Nominal power at the shaft of the fan/pump
- The temporal load profile (at 25%, 50%, 75% and 100% load)

An extended analysis provides a more precise estimation of the potential, especially for the absolute value. However, its accuracy in comparison to results provided by an in-depth analysis is still quite limited, with an improvement of $\pm 10\%$ in its precision compared to the preliminary analysis.

The tool is therefore a useful aid for a company to obtain an initial estimation of the savings potential of its electric motor systems with a reasonable amount of effort based on accessible data. However, it remains a rough estimate, the main objective of which is to be able to identify those systems with a high savings potential, and thus to select the systems for which it is worth investing additional time and effort for determining their potential more precisely. Ultimately, only an in-depth analysis with measurements can provide an accurate estimation of the savings potential. In addition, the tool was designed to remain conservative in its estimations.

References

1. *Message relative au premier paquet de mesures de la Stratégie énergétique 2050 (Dispatch to Parliament concerning the initial package of measures for Energy Strategy 2050)*. Swiss Federal Office of Energy, 4 September 2013. <https://www.admin.ch/opc/fr/federal-gazette/2013/6771.pdf>
2. *Analyse des schweizerischen Energieverbrauchs 2000–2017 nach Verwendungszwecken (Analysis of Switzerland's energy consumption, 2000–2017, by purpose)*. Swiss Federal Office of Energy, October 2018. <https://www.bfe.admin.ch/bfe/de/home/versorgung/statistik-und-geodaten/energiestatistiken/energieverbrauch-nach-verwendungszweck.html>
3. *Measures for power saving in electric drives: Market analysis in the industry*, W. Baumgartner et al., Basic (on behalf of the Swiss Federal Office of Energy), December 2006. http://www.bfe.admin.ch/forschungelektrizitaet/01740/01748/01751/02198/index.html?lang=fr&dossier_id=02023
4. *Policy Guidelines for Electric Motor Systems. Part 2*. Maarten van Werkhoven et al., Electric Motor Systems (EMSA), May 2018. https://www.motorsystems.org/files/otherfiles/0000/0200/pgmdu_part_2_may2018.pdf
5. *Programme for In-depth Analyses of Electric Motor Systems in Industry (ProAnalySys)*, Dr. R. Phillips, EEMODS'19, Tokyo, 17–19 September 2019. Forthcoming
6. *Elektrische Antriebssysteme mit kleinerem Stromverbrauch (Electric motor systems with lower power consumption)*, Armin Braunwalder, Electre revue, No. 25, p. 30, 2012. http://www.top-motors.ch/sites/default/files/2018-06/D_PB_2012_25_Electre revue_Topmotors.pdf
7. *Druckluftoptimierung Autogarage (Compressed air optimisation in a car garage)*, Rolf Gloor, final report, SFOE, July 2016. <https://www.google.ch/url?sa=t&rct=j&q=&esrc=s&source=web&cd=1&ved=2ahUKewiR973544niAhXJURUIHb2VBywQFjAAegQIABAC&url=https%3A%2F%2Fpubdb.bfe.admin.ch%2Fde%2Fpublication%2Fdownload%2F9314&usg=AOvVawIcuWPCYrJclG3Skz6kCnuy>

Labelling of Air Compressors – Much More Than Nameplate Data



Peter Radgen

1 Introduction

Compressed air is one of the key utilities used in industry. The application and use of compressed air is easy, is safe, and offers many benefits in handling and transporting of materials. Therefore, without compressed air supply, industrial production would stand still. In Europe about 80–100 TWh [1] of electricity is used annually for compressed air generation in industry. Typically, 7–10% of all electricity consumption is going into the production of compressed air. Despite significant efforts to improve the energy efficiency of compressed air systems [2–4], the economic energy-saving potential in compressed air systems remains very significant [5].

The study of Radgen et al. [1] undertaken about 20 years ago for the European Commission ignited a number of energy efficiency campaigns in Europe. The study identified and quantified the typical energy-saving potential in compressed air systems, which are reiterated in Table 1. Based on this study, about 50% of the energy efficiency potential is related to compressed air leaks. This translates into 16% of the compressed air produced being wasted without delivering any useful value. Understanding of the quantification of compressed air leakage is still not well developed. There are nearly no data available in the scientific literature which present credible results for this issue. Whereas ultrasonic devices can be used to identify the location of leaks, the quantification of the leaking airflow is rather erratic and based on the ultrasonic noise level. They do not take the effects of the shape of the leakage and the material of the leaking equipment into account.

P. Radgen (✉)
Institute for Energy Economics and the Rational Energy Use (IER), University of Stuttgart,
Stuttgart, Germany
e-mail: peter.radgen@ier.uni-stuttgart.de

Table 1 Energy-saving potential in compressed air systems

Energy-saving measure	% applicability (1)	% gains (2)	Potential contribution (3)
<i>System installation or renewal</i>			
Improvement of drives (high-efficiency motors, HEM)	25%	2%	0.5%
Improvement of drives (adjustable speed drives, ASD)	25%	15%	3.8%
Upgrading of compressor	30%	7%	2.1%
Use of sophisticated control systems	20%	12%	2.4%
Recovering waste heat for use in other functions	20%	20%	4.0%
Improved cooling, drying, and filtering	10%	5%	0.5%
Overall system design, including multi-pressure systems	50%	9%	4.5%
Reducing frictional pressure losses	50%	3%	1.5%
Optimising certain end use devices	5%	40%	2.0%
<i>System operation and maintenance</i>			
Reducing air leaks	80%	20%	16.0%
More frequent filter replacement	40%	2%	0.8%
TOTAL			32.9%

Source: reproduced from [1]

(1) % of CAS where this measure is applicable and cost effective

(2) % reduction in annual energy consumption

(3) potential contribution = applicability * reduction

The second largest energy-saving potential in compressed air systems is related to the compressor package. Savings can be achieved either by improving the drives, using variable frequency drives, or by improving the compressor element itself or recovering the heat of compression. Especially since 2000, significant progress in the energy efficiency of electric drives was achieved. At the time of the first study in 1999, efficiency classes for electric motors had been EFF1, EFF2, and EFF3, with EFF1 being the best in class motors. Since then, the efficiency of electric motors has further increased. Today the motor efficiency is specified by the new efficiency classes according to IEC 60034-30-1:2014, labelled IE1, IE 2, IE3, IE4, and IE5, with IE5 having the highest efficiency. The EFF1 classification is about equivalent to the current efficiency class IE2, which highlights the significant progress in electric motors made during the last 20 years.

Whereas the improvement of the energy efficiency in electric motors is very visible by the labelling of electric motors and the minimum energy performance standards defined for electric motors worldwide, the energy efficiency progress in motor-driven system, especially air compressors, is mostly invisible. To this day, there is no labelling or minimum energy performance standard of air compressor packages legally entered into force, neither in Europe nor in the USA. So far, only China has introduced a minimum energy performance standard for air compressors in 2009 [6].

As electric motors are an integral part of air compressor packages, they have benefited from the energy efficiency improvements of the drives, so air compressors have gradually improved over time as well. Due to the legal requirement, compressor manufacturers have upgraded their compressor packages to IE3 motors, with some manufacturers even applying IE4 motors.

2 Air Compressor Efficiency

The first step when talking about energy efficiency is to define the system boundary. A typical air compressor package does not only include the air compressor element itself but also a transmission between the electric motor and the compressor and the electric motor itself. It typically includes a controller, heat exchangers and a fan driven by the main motor and/or an additional motor to drive the fan. If the compressor has a variable frequency drive, it includes a frequency converter. Last but not least, some compressor packages include additional air treatment equipment such as a refrigerant dryer and an air receiver. To ensure a valuable comparison of different air compressors, it is necessary to define the scope of the air compressor package. Figure 1 shows the system boundary of an air compressor package with the in- and outgoing flows of energy and materials. Nearly all compressor packages are sold as ready-to-use units, so they only need to be connected to the electricity grid, the compressed air, and the condensate system as well as to the inlet air duct and the compressed air piping network. However, not all units have all elements integrated; therefore, when comparing energy efficiency, the different scope of the compressor packages needs to be taken into account.

The efficiency of the compression element alone would therefore be of little interest for the compressed air user, as it will indicate only a part of the efficiency of the compressor package. In practice, the international standard for acceptance test

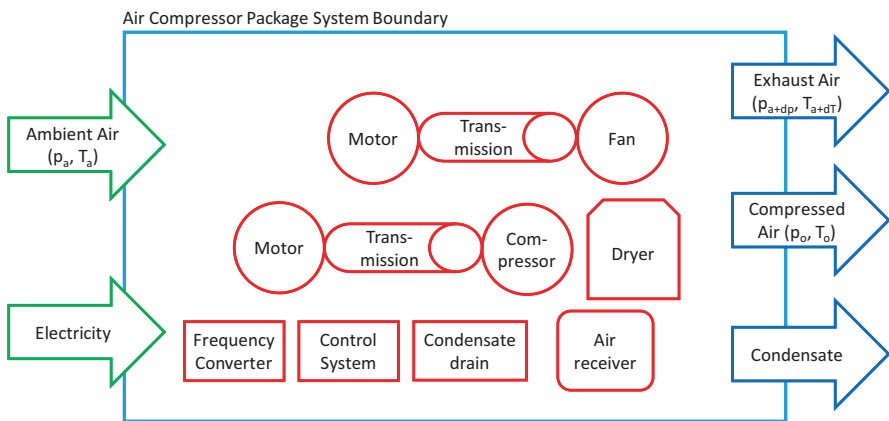


Fig. 1 Air compressor system boundary and components

for displacement compressors ISO 1217 [7] includes in Annex C a simplified acceptance test for electrically driven packaged displacement compressors and in Annex E variable speed drive compressors. The key data obtained are packaged compressor power input and the volume flow at a given system outlet pressure. From the measured input and output variables, the efficiency ratio of the air compressor package in kWh/m³ or kW/(m³/min) can be obtained.

The minimum energy requirement for the compression can be calculated based on the laws of thermodynamic for an ideal (reversible) isothermal compression. This is the lower limit in regard to performance but can never be reached by any sort of industrial equipment. Real compressor packages typically have much higher values of specific performance. The performance of compressors decreases when the compressed air pressure outlet increases. It should be noted that the energy requirement of an air compressor is not linked to the pressure difference between the air entering and leaving the compressor but to the pressure ratio. Figure 2 shows the specific performance range for poor and good compressors. The performance chart in Fig. 2 does not include the energy demand for drying, so it is only valid for a compressor without refrigeration dryer.

The calculations behind the chart are more than 15 years old, so the good range should be narrowed, taking the efficiency improvements of electric motors into account. The smaller the difference between the real specific performance and the specific performance for an isentropic (ideal adiabatic) compression, the better the compressor package.

In Germany, the replacement of air compressors is subsidised by the BAFA under the support programme for energy efficiency and process heat from renewable

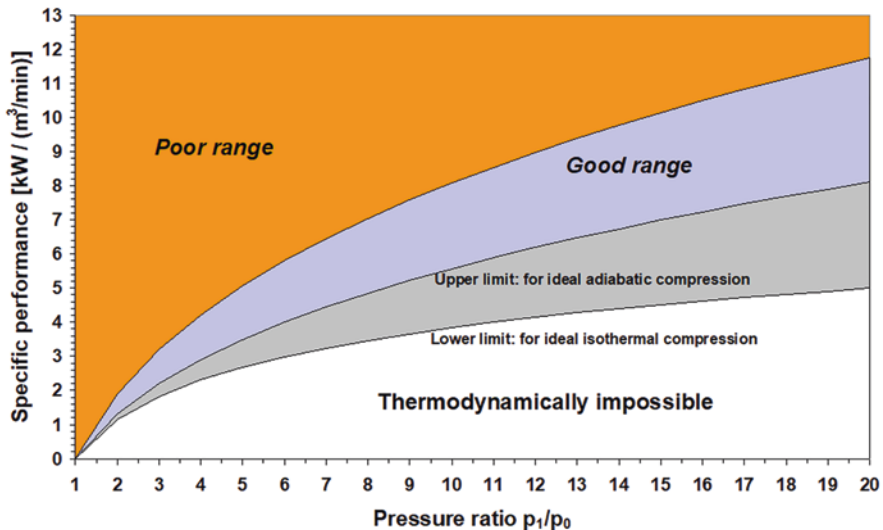


Fig. 2 Specific performance of air compressor systems [8, own translation]

energy in industry: Module 1 (cross-cutting technologies). For air compressors to be eligible for funding, they must achieve at least the minimum efficiency values according to pressure and motor size tabled in the funding guidelines [13].

The graphical representation of the requirements for selected motor sizes is shown in Fig. 3. The larger the compressor, the lower the maximum allowed specific power consumption for the compressor which is in line with expectation. Surprisingly, the requirements for oil-free compressors are less stringent than for the oil-injected compressors. Although oil-free compressors are disadvantaged by the higher compression temperature, their advantage of typically having two stages with intercooling seems to be neglected. The boundary lines for good efficiency as shown in Fig. 1 have been included for better comparison.

Instead of using the specific performance, the efficiency of compressors can be described by the isentropic efficiency η_c , which is the isentropic compressor work divided by the compressor work of the real device. The higher the isentropic efficiency, the better the compressor but it can never reach 100%. As for the specific power consumption, the isentropic efficiency will depend on the pressure ratio, so a single value would not be sufficient. The key disadvantage for the user is, however, that from the isentropic efficiency, they cannot calculate directly the energy consumption, but this is easily possible with the specific power consumption.

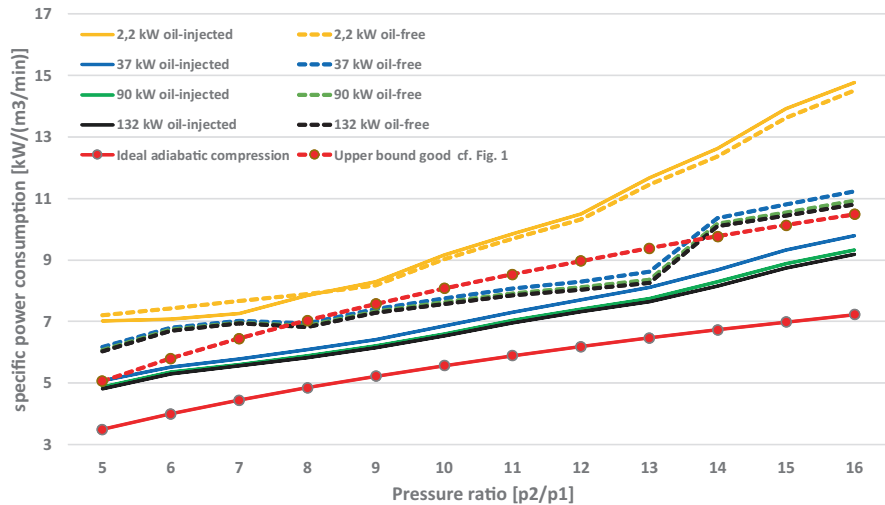


Fig. 3 Minimum efficiency for air compressors to be eligible for funding under the German support programme. (Datasource: [13], own calculation)

3 Compressor Nameplate Data

Despite a clearly defined standard to calculate and indicate the energy efficiency of a compressor package, the manufacturers do not publish detailed data sheets about the performance of the compressor packages. By scanning the sales brochures of compressor manufacturers, there is no information on the efficiency of the compressor included. In some cases, the manufacturers might highlight the use of IE4 motors for the compressor package, which is the application of motors with efficiencies above the minimum requirement (currently IE2 with frequency converter or IE3 without frequency converter). The typical sales brochure in Europe only present data on the power of the installed compressor drive motor and the maximum volume flow at a defined system pressure. Both values are typically based on an air inlet pressure of 1 bar and an inlet temperature of 20 °C. However, with these values given by the manufacturer, the efficiency of the compressor package cannot be calculated. The installed power of the main drive motor is only an indication of the energy demand of the compressed air package. The drive motor could be over- or under-loaded by design, and the electricity consumption of the fan motor, the control, and a frequency controller if installed are adding to the overall electricity consumption as well.

As an example, the following data are taken from a sales brochure of a compressor manufacturer:

Working pressure 8 bar_e; free air delivery 9.3 m³/min = 155 l/s; Installed motor power 55 kW.

By measuring the power consumption of the compressor package at 9 bar total pressure, a shaft power of 60.6 kW and an efficiency of the main motor of 93% were obtained. In addition, the shaft power and the efficiency of the separate fan motor were measured and have led to a power consumption of 1.7 kW and an efficiency of the fan motor of 84%, respectively. The total power input into the compressor package at the stated conditions therefore is $P_{in} = 60.6 \text{ kW} / 0.93 + 1.7 \text{ kW} / 0.77 = 67.4 \text{ kW}$ (note the consumption of the control system was neglected). This is significantly above the value one would estimate when looking into the sales brochure. The real power consumption is about 22.5% higher than someone would expect from the information given in the sales brochure.

In addition, another important information is missing in the brochure, which is the power consumption in idle mode. The fluctuating compressed air demands requiring the compressor to switch on and off to adapt to the flow. Switching the air compressor on and off or more precisely the electric motor will stress the motor by increasing the temperature due to the high startup currents. This limits the number of possible starts per hour to avoid the overheating of the motor. Typically, motor manufacturers fix the maximum start per hour for each motor. Others will monitor the temperature inside the motor and make the stop behaviour dependent on the temperature level. The larger the motor, the lower the number of allowed motor starts per hour. In practical applications, the compressor package is therefore not switching between start and stop but between load and unload to avoid overheating

of the motor. If the compressor is unloaded, it is no longer delivering compressed air but still consumes electricity, as the drive is still turning the compressor and the fan and the control system is continuously working. In unloaded mode, the shaft power was measured to be 10.5 kW and the efficiency is 84%. The lower efficiency of the motor in idle mode is driven by the motor efficiency being dependent on the load factor. At lower load, the efficiency of the motor is significantly decreasing. In idle mode the compressor package is still requiring a power input of $P_{in} = 10.5 \text{ kW} / 0.84 = 12.5 \text{ kW}$.

The specific power of the analysed compressor package is therefore $67.4 \text{ kW} / 9.3 \text{ (m}^3\text{/min)} = 7.24 \text{ kW}/(\text{m}^3\text{/min)}$. Compared to the specific performance of compressors shown in Fig. 1, the analysed compressor package performs not very well.

Unfortunately, due to the missing publication of compressor performance data in Europe, it is very difficult to compare air compressors in regard to their efficiency. This was encountered already during the EuP study on air compressors [9]. Getting an overview of the typical efficiencies in the market is impossible with the available database. However, the data is principally available from the manufacturers. In the USA the Compressed Air and Gas Institute (CAGI) in cooperation with many key players in the compressed air market is running a performance verification programme. In the framework of this programme, a standard data sheet is available for each tested compressor. In this data sheet, the relevant energy data, e.g. the total package input power at zero flow, the total package input power at rated capacity and full-load operating pressure, and the total package input power at rated capacity and full-load operating pressure, is included. Even if mainly the same compressor models are sold on the market in Europe, the values cannot easily be adapted for Europe, as the US frequency of 60 Hz compared to the European standard of 50 Hz is leading to a higher speed of the drive motor and therefore an operation of the compressor at a different operating point. Figure 4 is reproducing a figure from [9], highlighting the broad range of isentropic efficiencies of fixed speed oil-injected compressor packages. Often compressor packages with similar free air delivery will have the same motor power installed, hiding the fact that the compressor package efficiencies can vary significantly.

The EuP study [9] however was not recommending energy labelling for compressors or defining the minimum data set to be made public for any compressor package. The reasoning behind this recommendation was driven by the fact that compressed air equipment of larger size is purchased by energy professionals being aware that they need to request the data from the manufacturer. In the author's views, this assumption seems to be overoptimistic, as small- and medium-sized companies will normally not have an expert in compressed air and compressor replacements are not required every year. In this regard, there is a lack of experience on the buyer's side and the customer might not be aware about the large differences between the different products on the market.

Experience with the labelling of other products such as circulators has however demonstrated that the introduction of a mandatory energy labelling can be a game changer. Such labelling could boost competition and could trigger the development

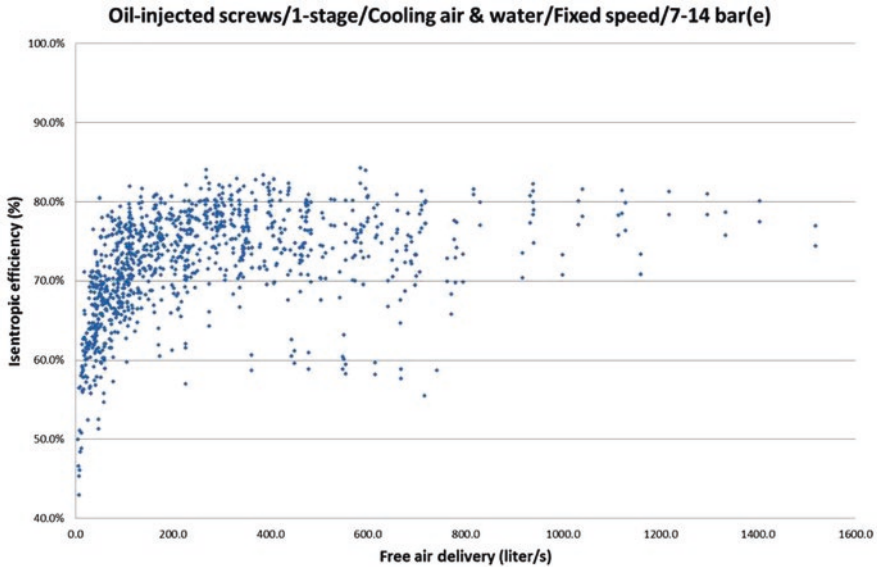


Fig. 4 Typical efficiency ‘cloud’ showing the range of efficiency for specific volume flow ranges (based on CAGI data) (taken from [9])

of new and more efficient products. This effect might not be limited to smaller products but might work as well for larger products.

Even if the compressor data sheets are not easily available from the manufacturers in Europe, potential customers requesting the full data sheets typically will receive this data from the manufacturers, but they will need to overcome the manufacturer’s resistance to disclose the data. Even in the US, the CAGI data [10] is covering only part of the delivery programme of the manufacturers, as the required testing is an added cost for them and they have to pay for the independent third party for testing and verification. In Europe, there is no voluntary or obligatory third party for the testing required, so the data sheets are typically based on the manufacturers’ own measurements without an external verification. At the University of Stuttgart [11], some performance verification measurements based on ISO 1217 Annex C had been performed to verify the manufacturers’ compressor data, pinpointing some weaknesses in the ISO standard. In chapter 6.2.i of the ISO standard 1217, it is stated that ‘Before readings are taken, the compressor shall be run long enough to ensure that steady-state conditions are reached so that no systematic changes occur in the instrument readings during the test’. However, no clear definition regarding the minimum time lapse before taking the measurement and when steady-state conditions are reached is given in the standard. As the compressor package is typically warming up during the performance test, the air inlet temperature into the compressor element is increasing, and the free air delivery is going down over time until the compressor package is warmed up completely. Figure 5 shows a typical result from the testing of a compressor package according

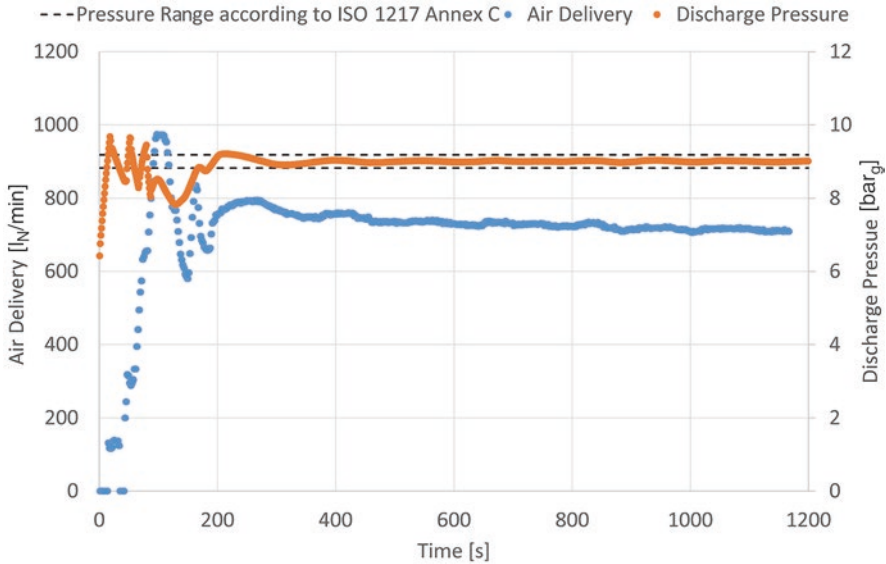


Fig. 5 Development of compressor efficiency during performance measurements according to ISO 1217 Annex C [11]

to ISO 1217 Annex C. The first 200 seconds of metre readings represents the startup of the compressor where the discharge pressure and the air delivery are quickly increasing. Before starting the performance measurement procedure, the outlet pressure should be stable within a small pressure band defined by the standard and is shown as dotted lines in the diagram. At the point in time when the pressure is sufficiently stable to perform the measurements, the air delivery has still not reached its final value and is still going down with further warming up of the compressor. So using the time interval between 200 and 400 s for the determination of the compressor performance, the calculated performance will be significantly higher compared to calculation using the time interval from 800 to 1000 s. The value of the compressor fully warmed up will represent the real performance of the compressor in the field much better. To avoid such loopholes, it might be worthwhile to consider some revision to the standard to clearly specify when stable operation is reached. Furthermore, the standard does not require measuring the power consumption in idle mode, even if this is an important parameter for a standard compressor package without frequency control.

So far, we only have discussed the issues of fixed speed air compressors, which have a different efficiency value for every operating pressure and an energy consumption at no load operation. For variable frequency drive compressors, even more data is required to fully describe the energy efficiency range of the compressor package. For variable speed drive compressors, the efficiency at different rotational speeds and operational pressures is required to obtain the performance curves of the compressor. Figure 6 shows the specific power consumption of a variable frequency

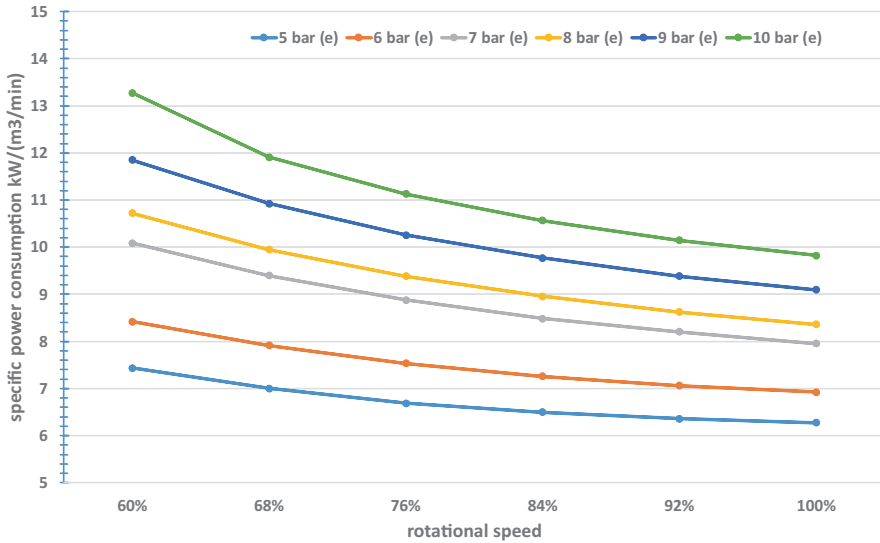


Fig. 6 Specific power consumption of a variable frequency drive oil-injected screw compressor

drive, oil-injected screw compressor for outlet pressures from 5 to 10 bar_e. As expected the higher the outlet pressure, the higher the specific power consumption.

Furthermore, it is increasing with part load operation at reduced speed. The efficiency of a variable speed drive compressor can aggravate significantly at part load operation. The maximum efficiency point is often not at 100% rotational speed as can be seen in the example but closer to 80%, and the performance curve will have a parabolic form. The real performance depends on the interactions between the compressor, the drive, the transmission, and the frequency converter and can be different depending on the compressor model. The specific power consumption in part load worsens for the presented variable frequency compressor between 18% at 5 bar_e and 35% at 10 bar_e.

So an important question to be discussed when comparing the use of a variable frequency drive with a fixed speed compressor changing between load and no load operation is which system performs better, taking the part load operation into account. The no load power of the air compressor is 1.3 kW. If the compressor is not delivering any cubic metre of air, it is however consuming energy. So instead of reducing the speed, the compressor could switch between full load and no load operation. The lower the air demand, the higher the share of no load operation. Figure 7 shows the comparison between the specific power for both compressors at 5 and 8 bar_e, respectively. Whereas for the pressure of 5 bar_e the specific power consumption is slightly lower for the variable frequency compressor, at 8 bar_e the fixed speed compressor performs much better at part load conditions. Therefore, the selection of the best compressor depends not on the air requirements or on the system pressure alone. In fact, this makes labelling of air compressors much more challenging than the labelling of household appliances, which are all operating at

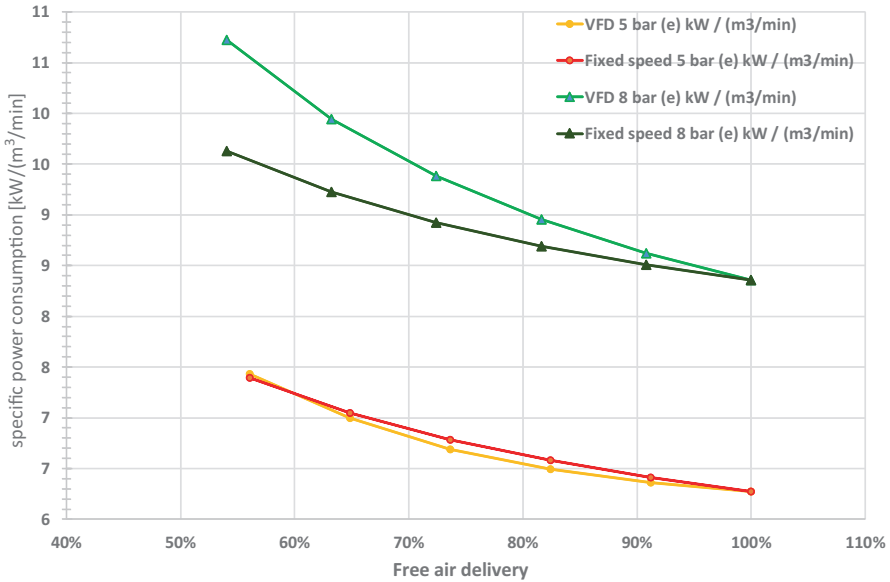


Fig. 7 Comparison of specific power consumption of a variable frequency drive oil-injected screw compressor with a fixed speed compressor at 5 and 8 bar_c.

the same conditions under full load. One single number or indicator is therefore not a useful approach for the classification of the energy efficiency of air compressors. Neither the specific power consumption nor the isentropic efficiency at a single operating point will describe the performance sufficiently. Instead, a legal requirement to make a full compressor package data sheet public for each air compressor package sold in Europe would drive the market towards higher-efficiency products and make it easier for customers to compare the compressor models of different manufacturers. The requirement for publication would also facilitate market surveillance in Europe and would pave the way for third-party certification of compressor performance data.

4 Compressor Efficiency Versus Compressed Air System Efficiency

Labelling of air compressor had been widely discussed in the context of the Energy Using Products Directive and the preparatory studies for air compressors [9, 12]. So far, the European Commission has implemented neither any labelling requirements nor minimum energy efficiency standards. One key aspect for valuing the pros and cons of labelling and minimum energy performance standards is the possible effect on the energy and emissions savings due to the implementation of measures on air

compressors. The overall saving potentials as presented in Table 1 made clear that focusing on the compressor alone would enable only to address a part of the saving potential. The largest energy efficiency potential can be realised by a system approach. Therefore, instead of labelling and regulating air compressors alone, the focus should be on the compressed air system. The analysis of the efficiency of air compressors needs to be done carefully and detailed to be of practical use. Analysing compressed air systems is even more complex due to the further increased number of impact factors, making it highly complex to compare or to regulate systems.

The largest opportunities to improve compressed air systems are related to leakage reduction and the use of waste heat from the compressor. Understanding how the overall amount of leakages can be quantified is available but there is still a lack in the basic understanding of the airflow from individual leakage spots. Up to date, there is no scientific understanding about the flows and how they can be quantified. The heat produced during the compression is still wasted most of the time instead of being used for space heating and sanitary hot water preparation. There is even a significant number of compressors installed being prepared for heat recovery but will never be connected to the heat consumers. Both measures will have a much stronger impact on the energy demand than the improvement of the compressor package alone. The challenge however lies in the broad number of companies to be addressed and the broad variety of framework conditions. Therefore, an important first step could be to make the performance curves of air compressor packages freely available. This will likely only happen if this would be enforced by legislation. In the author's view, this would be the most cost-effective step in regard to regulation in improving the energy efficiency in compressed air systems.

References

1. P. Radgen, E. Blaustein, *Compressed Air Systems in the European Union* (LOG_X Publishing, Stuttgart, 1999)
2. Radgen, P.; Agricola, A.; Zelinger, M.: Final Report Compressed Air Campaign Germany (in German). Download at: <https://www.druckluft-effizient.de/downloads/Abschlussbrochuere-druckluft-effizient.pdf>
3. Radgen: Compressed Air campaign Switzerland (2005–2008) (in German). Swiss Federal Office of Energy (SFOE), Project Report No. 101226, Bern, 2008
4. Compressed Air Challenge. <https://www.compressedairchallenge.org/>
5. M. Unger, P. Radgen, Energy Efficiency in Compressed Air Systems – A review of energy efficiency potentials, technological development, energy policy actions and future importance, in *Proceedings of the 10th international conference on energy efficiency in motor driven system (EEMODS 2017)*, EUR 29 101 EN, (Publications Office of the European Union, Luxembourg, 2018). <https://doi.org/10.2760/345473>
6. GB 19153–2009, *Minimum Allowable Values of Energy Efficiency and Energy Efficiency Grades for Displacement Air Compressors* (China National Institute of Standardization, 2009)
7. ISO 1217, *Displacement Compressors – Acceptance tests* (ISO 1217:2009(E), Geneva, 2009)
8. *Fact about compressed air – II Thermodynamics* (In German). <https://www.druckluft-effizient.de/downloads/fakten/fakten-00-09.pdf>, August 2003

9. M. Elburg, R. Boorn, *Ecodesign Preparatory Study on Electric motor systems/Compressors*, ENER Lot 31, Final report. Van Holsteijn en Kemna B.V ((VHK) for the European Commission, Brussels/Delft, 3 June 2014)
10. CAGI: Performance Verification of Air Compressors. <https://www.cagi.org/performance-verification/overview.aspx>. Last visited 01.06.2019
11. P. Radgen, M. Unger, *Results of Performance Measurements of Air Compressors According to ISO 1217 Annex C* (Unpublished test results, IER, University of Stuttgart, 2019)
12. M. Elburg, R. Boorn, *Preparatory study on Low pressure & Oil-free Compressor Packages*, ENER Lot 31, Final Report, Van Holsteijn en Kemna B.V ((VHK) for the European Commission, Brussels/Delft, 7 June 2017)
13. BAFA: Modul 1 – Querschnittstechnologien Bundesförderung für Energieeffizienz in der Wirtschaft – Zuschuss. Version 1.3, 15.07.2019. https://www.bafa.de/SharedDocs/Downloads/DE/Energie/eew_modul1_qst_merkblatt_tma.pdf

Theoretical and Experimental Evaluation of Compressed Air Leakages



Manuel Unger and Peter Radgen

1 Introduction

The use of compressed air (CA) is common in almost every industrial sector and requires a significant share of the overall electricity consumption. The energy demand for compressed air usually takes about 10% of the overall industrial electricity consumption of a country, while potentials for cost-efficient energy efficiency measures are still high. Leakages contribute to inefficiencies in compressed air systems in a significant way. Despite the high energetic relevance of leakages in compressed air systems, typical leakage rates of 15–25% exist, while there is a clear lack in scientific publications [1].

This chapter gives a review of scientific publications and illustrates the span of published leakage rates for standard geometries. A simple method for calculating leakage rates is introduced. Additionally, a test bench for high-precision leakage measurements is introduced and results for several artificial leakages (circular holes and slots) are presented.

2 CA Leakages in the Literature

Counting brochures by manufacturers and guidelines for energy efficiency published by energy agencies, there are many publications on compressed air leaks. Usually, these publications have a different focus and just briefly introduce the topic. Most publications underline the importance of leakage losses by referring to

M. Unger (✉) · P. Radgen

Institute for Energy Economics and the Rational Energy Use (IER), University of Stuttgart, Stuttgart, Germany

e-mail: manuel.unger@ier.uni-stuttgart.de; peter.radgen@ier.uni-stuttgart.de

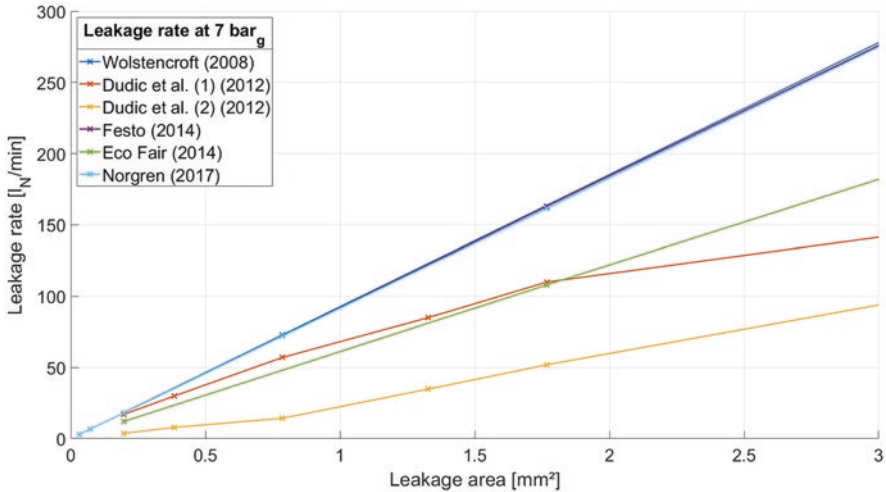


Fig. 1 Published leakage rates at 7 bar_g [2–7]

the leakage of holes with certain diameters, either as an air loss per minute or cash per year. However, these publications rarely meet scientific standards, as information on the calculation or the experimental setup are missing. Thus, these publications will not be explained in detail in this publication, the stated leakage losses can be found in Fig. 1.

Only a few scientific papers exist on leakage losses through specified geometries; this chapter reviews the most relevant.

2.1 Experimental Evaluations

Dudic et al. (2012) published two papers on the experimental evaluation of compressed air leakages. They focused on circular leakages in different materials (steel and PUN) and the quantification of leakages via ultrasound and thermography. Since the focus of these publications is on the quantification of leakages, certain key information are missing. The authors do not show the experimental setup, no statement if the tightness of the setup has been checked and there is no information on the stability of the leakage pressure and how it was controlled [2, 3].

The published values depending on the leakage area can be seen in Fig. 1. At first glance, leakages in steel pipes seem to have a higher leakage rate, than in PUN pipes. This high sensitivity to the material is not explained in the publications. Most likely, the differences occur because the orifices differ due to a lack in manufacturing quality and control [2, 3].

In 2008, Wolstencroft published his master thesis on ultrasonic air leak detection. The thesis, due to its length, is more comprehensive than the introduced papers.

The experimental setup shows that the leakage pressure is regulated manually by a throttle valve and digitally read close to the actual leak. Volume flow is measured either with analog rotameters for small rates or digitally by a differential pressure flow meter. Wolstencroft measured a variety of artificial leakages (slots and holes), highlighting the importance of quality control of the manufactured leaks (deviations up to 25%, laser cutting) [4].

The setup and work of Wolstencroft are generally interesting, while leaving room for improvement. Since the leakage pressure is manually regulated, fluctuations in the air supply will directly influence the leak pressure resulting in unstable conditions. Additionally, analog rotameters usually have a low precision and cause reading errors. Experimental data for circular holes is shown in Fig. 1. In comparison to the evaluations by Dudic et al. the leakage rates are much higher (up to 70%) [4].

2.2 Summary

A deeper look at the published literature on leakage rates through artificial leaks shows that most published literature can be identified as “non-scientific”, only few scientific papers deal with this topic and show tremendous deviations of up to 70% on the leakage rates. Figure 1 compares six different publications on leakage rates and illustrates this problem.

3 Theoretical Calculation of CA Leaks

3.1 Ideal Gas

The leakage rate of a CA leak can be calculated using the ideal gas approach (Eq. 1).

$$pV_{\text{Air}} = m_{\text{Air}} R_{\text{Air}} T \quad (1)$$

$$\rho_{\text{Leak}} = \frac{p_{\text{Leak}}}{T_{\text{Leak}} R_{\text{Air}}} \quad (2)$$

Using Eq. 2 and differentiate Eq. 1, the leakage mass flow can be written as the product of density (ρ) and volume flow (\dot{V}_{Air}):

$$\dot{m}_{\text{Air}} = \rho_{\text{Leak}} \dot{V}_{\text{Air}} \quad (3)$$

The product of leakage orifice Area (A_{Leak}) and the mean velocity of the air at exhaust of the leak (c_{Leak}) calculate the volume flow (Eq. 4).

$$\dot{V}_{\text{Air}} = A_{\text{Leak}} c_{\text{Leak}} \quad (4)$$

The temperature (T_{Leak}) and pressure (p_{Leak}) of the air at the exhaust of the leak are needed to calculate the air density under ideal gas conditions (Eq. 2). As long as the shape of the leakage differs from a laval nozzle, the so called critical pressure will adjust at the exhaust, it is a direct result of reaching the sonic flow speed. Thus, p_{Leak} can be written as:

$$p_{\text{Leak}} = \left(\frac{2}{\kappa + 1} \right)^{\frac{\kappa}{\kappa - 1}} p_{\text{supply}} = 0,5283 p_{\text{supply}} \geq p_{\text{amb}} \quad (5)$$

However, pressure ratios (ambient pressure to supply pressure) greater than 0,5283 would lead to slight vacuum which is non-physical, thus $p_{\text{Leak}} \geq p_{\text{amb}}$. Assuming an isentropic expansion of the air, the leak temperature can be calculated as follows:

$$T_{\text{Leak}} = \left(\frac{p_{\text{Leak}}}{p_{\text{supply}}} \right)^{\frac{\kappa - 1}{\kappa}} T_{\text{supply}} = 0,5283^{\frac{\kappa - 1}{\kappa}} T_{\text{supply}} \quad (6)$$

Looking at Eq. 6 shows, the temperature of the air at the exhaust of the leakage depends solely on the temperature of the CA before the leakage, due to the critical pressure. Finally, the leakage velocity (c_{Leak}) has to be calculated using Eq. 7.

$$c_{\text{Leak}} = \sqrt{\frac{2\kappa}{\kappa - 1} R_{\text{Air}} T_{\text{supply}} \left(1 - \left(\frac{p_{\text{Leak}}}{p_{\text{supply}}} \right)^{\frac{\kappa - 1}{\kappa}} \right)} \quad (7)$$

For pressure ratios (ambient pressure to supply pressure) smaller than 0,5283, Eq. 7 can be simplified to Eq. 8, because the leakage velocity equals the sonic flow velocity.

$$c_{\text{Leak}} = \sqrt{\kappa R_{\text{Air}} T_{\text{Leak}}} \quad (8)$$

Figure 2 shows the results of calculating a leakage with a diameter of 1 mm. From 1 to 1.89 bar_a, the leakage flow rate is not linear, since sonic flow velocity is yet to be reached. Reaching sonic flow velocity, the normalized flow rate increases linear due to the linear increase of the pressure which affects the density. The normalized leakage flow resembles the mass flow of the leakage, the actual leakage flow (without any normalization) keeps constant after reaching sonic flow velocity.

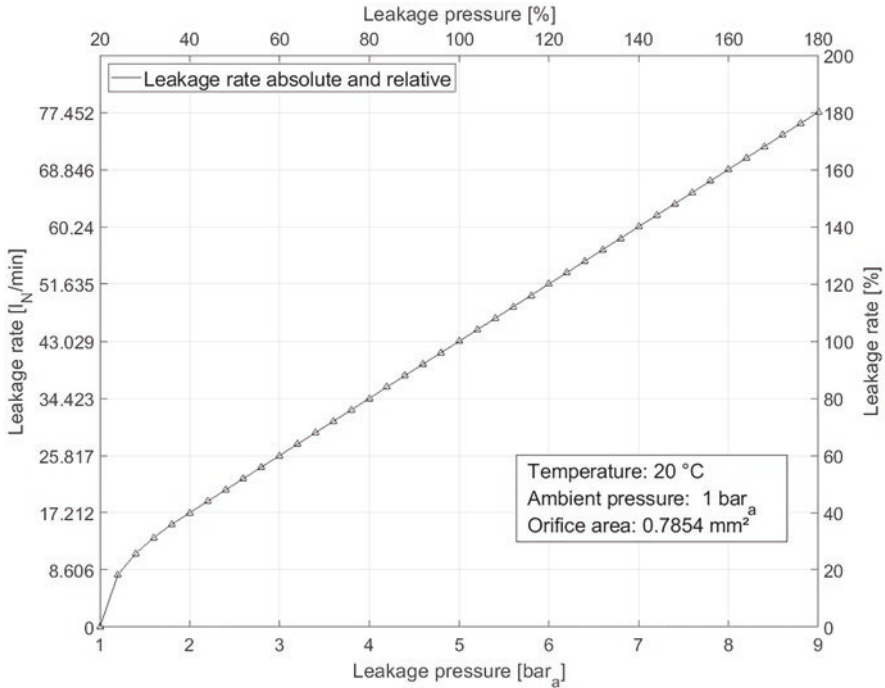


Fig. 2 Analytical results for the leakage normalized flow rate of a 1 mm leakage

3.2 Simulation Model

A matlab simulation model is developed to enable leakage rate simulations. As a first step, all equations from Sect. 3.1 have been implemented. Additionally, the simulation model is constantly enhanced with new functions. As of now, the simulation model can vary one input factor during simulation (temperature, pressure, orifice area/diameter) to evaluate the sensitivity.

CA consist of ambient air, therefore water, oil and other particles make up a small share of the CA. In a first effort, the simulation model is linked with the substance database REFPROP to achieve two goals:

- Use actual fluid properties instead of assumptions.
- Enable adding the calculation of leakage rates of moist air.

Results show: Adding water dry air slightly increases the leakage rate. However, this increase is far less than 1% and thus irrelevant. Modelling shares of oil or particles will not be implemented, since their concentration is usually way less than water.

4 Experimental Evaluation of CA Leaks

To investigate CA leakages, a test bench was developed. The setup allows precise measurement of leakage losses. It is designed to allow a variety of different measured parameters such as temperature, pressure and dew point, as well as different measurement techniques.

4.1 Experimental Setup

The experimental setup is shown in Fig. 3. CA enters through a low-loss coupling at the top of the test bench, it passes a dew point sensor and the first pressure sensor before it arrives at the proportional valve. The different flow meters are located after the proportional valve, because the dew point sensor itself has a small leakage rate to improve its response time plus the proportional valve can use its exhaust to ensure proper control. The test bench has multiple options for flow metering:

- Two separate thermal flow meters with different ranges.
- Three different nozzles for flow metering via differential pressure.

The design considers sufficient inlet sections for the thermal flow meters. After the flow meters, the temperature of the CA is measured. Shortly before the actual leak is the second pressure sensor that displays the leak pressure. The artificial leak is mounted via flange on the test bench.

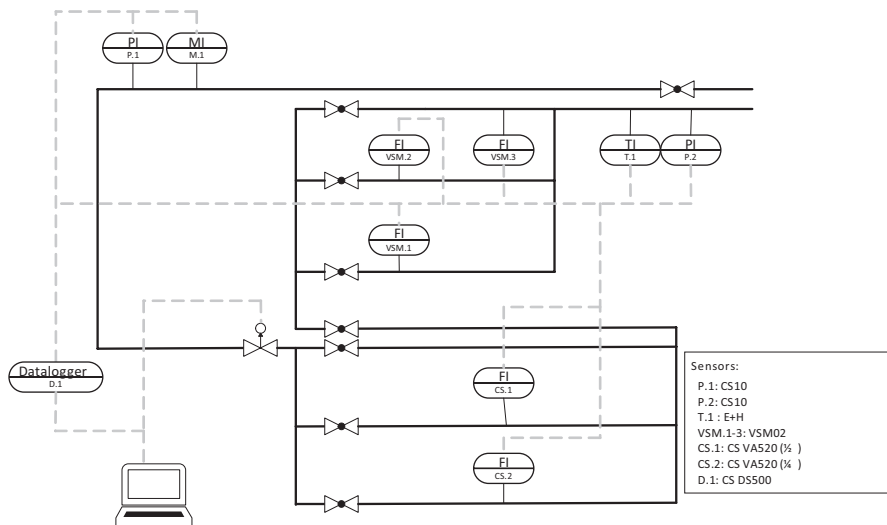


Fig. 3 Experimental setup

Table 1 Measuring equipment: range and measurement accuracy

Device	Measuring Range	Measurement accuracy
VSM02 (Optiserve)	0.2 l _N /min – 3000 l _N /min	±1% m.v.
VA520 ¼" (CS instruments)	0 l _N /min – 105 l _N /min	±1% m.v. ±0.3% e.v.
VA520 ½" (CS instruments)	0 l _N /min – 1500 l _N /min	±1% m.v. ±0.3% e.v.
CS 10 (CS instruments)	0 bar _g – 10 bar _g	≤0.5% e.v.

On a regular basis, the test bench is checked for internal leakages. The test bench is therefore held under pressure for several days (weekend) and pressure readings are taken to evaluate the losses. The internal leakages are smaller, 0.0005 l_N/min, and therefore negligible.

The test bench is designed to enable high-precision measurements on CA leakages and the respective influencing factors. The main core component to ensure reliable findings is the differential pressure flow meter, thus the flow meter was calibrated and shows deviations of smaller than ±1% of the measured value. All measuring equipment used in the setup are listed in Table 1.

All measuring equipment are read digitally and then processed using a self-written virtual instrument (VI) in LabView. The electrical proportional valve regulates the pressure at its outlet from 1 to 11 bar_a according to the alternate current 4 to 20 mA. It is therefore used to control the test bench and enable the user to regulate the pressure right before the leakage. The regulation is implemented in the same VI by a digital fuzzy controller that calculates the necessary alternate current due to the current pressure near the leakage and the pressure gradient. The regulation concept ensures stable pressure conditions at the leakage even during unstable conditions on the pressure supply of the test bench, as they usually occur in a compressed air system.

4.2 Manufacturing of Artificial Leakages and Quality Control

As a first step, the setup is used to evaluate artificial leakages with circular shape and slots. The artificial leakages are manufactured using milling machines (slots) and stood drills (circular), using aluminium disks with a thickness of 0.5 mm. Reamers are used to ensure low manufacturing tolerances for circular holes. Slots are manufactured using small milling cutters (0.8 mm and 1 mm). All artificial manufactured leaks can be seen in Table 2.

Since the tolerance of the manufactured slots is high, an optical procedure was developed to determine the exact orifice area of the leak for quality control. The artificial leak is illuminated and photographed from a predefined distance and angle. The pictures are evaluated using the software ImageJ, which enables measuring surfaces via brightness selection. As a reference, a precisely manufactured circular hole (reamer) is used. Figure 4 shows two illuminated manufactured leaks and the identified orifice area using the stated method, the yellow line is generated based on

Table 2 List of manufactured leaks

Type	Amount	No.	Dimensions	Orifice area
Circular hole	3	D-010-01	1 mm	0.785 mm ² (calc.)
		D-010-02		
		D-010-03		
Circular hole	3	D-020-01	2 mm	3.142 mm ² (calc.)
		D-020-02		
		D-020-03		
Circular hole	3	D-030-01	3 mm	7.069 mm ² (calc.)
		D-030-02		
		D-030-03		
Slot	2	10-0725-01	1 mm × 7.25 mm	7.12 mm ² (meas.)
		10-0725-02	1 mm × 7.25 mm	7.79 mm ² (meas.)
Slot	2	08-0895-01	0.8 mm × 8.95 mm	7.46 mm ² (meas.)
		08-0895-02	0.8 mm × 8.95 mm	7.66 mm ² (meas.)
Slot	2	08-040-01	0.8 mm × 4.0 mm	3.52 mm ² (meas.)
		08-040-02	0.8 mm × 4.0 mm	3.16 mm ² (meas.)

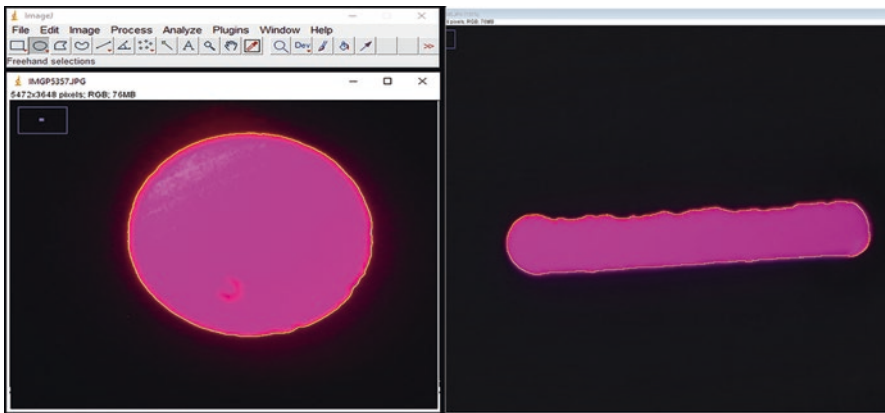


Fig. 4 (Left) orifice area of a 3 mm circular hole. (Right) orifice area of a 1 × 7.25 mm slot

the different brightness of the picture and indicates the shape of the orifice. The amount of pixels surrounded by this line can be calculated and therefore used to measure the area. It is important to clean all manufactured leakages since this procedure is very sensitive to contamination.

4.3 Test Procedure

The manufactured and quality-checked leakages are mounted on the flange of the test bench, the screws have to be tightened that the seal rests flat and ensures proper tightness. The supply for compressed air has to be checked and the supply valve to be opened. The user has to decide which flow meters shall be used during the procedure and open the respective ball valves. However, simultaneous usage of parallel measuring sections must be avoided for accurate findings.

As explained in Sect. 4.1, a self-written program in LabView is used to control the test bench and the pressure near the leakage. The test procedure consists of readings at several predefined pressures for a sufficient amount of time (steady state conditions). The program allows implementing standard test procedures (pressure and measuring time), so all tests are conducted under the same conditions and eliminate human errors. Pre-tests showed that steady state conditions, which we defined as the deviation and fluctuation of actual pressure from the target pressure of smaller 0.01 bar, are reached after 30 s. The differential pressure flowmeter reacts instantly on volume flow changes. The resulting test procedure is shown in Fig. 5. The procedure runs automated via LabView.

5 Results and Discussion

All measured leakage rates are given as standard volume flow rates according to DIN 1945-1 (20 °C, 1 bar_a, dry air). The artificial leaks (see Table 2) are divided into circular orifices and slots. All leaks are measured on the test bench with the procedure described above. Every artificial leakage runs three times through this process, the mean value of these runs represents the result. Exemplary, Table 3 shows leakage rates for all measurement runs of a circular leakage with a diameter of 3 mm. Deviation from the mean value is smaller 0.3%, which proves that all measuring equipment are working properly, pressure control is working fine and steady state conditions have been reached. The biggest share of the small differences between the runs can be attributed to changing CA temperature (difference between run 1 and 3: 0.8 K). The results for all other measured artificial leakages have similar results and will not be presented.

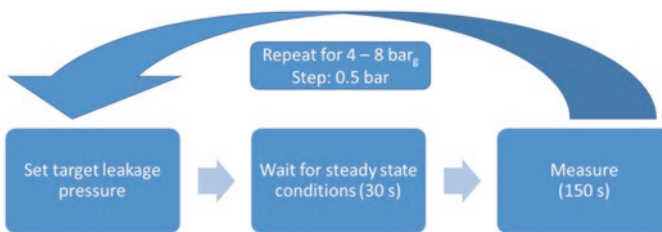


Fig. 5 Test procedure

5.1 Circular Orifices

Circular artificial leakage with diameters of 1 mm, 2 mm and 3 mm are measured. For each diameter, three artificial leakages have been manufactured and measured. Figure 6 shows the results of three different circular leakages. The deviation between the leakages is smaller 0.3% and thus smaller than the measurement precision, it proves a high manufacturing quality. As diameters decrease, the deviation in leakage flow rates increases, because of a more challenging manufacturing. For leakages with a diameter of 2 mm deviation is smaller 1.6%, for leakages with a diameter of 1 mm the deviation is about 4%. A clear linear relation between leakage pressure and leakage rate can be identified in all measurements.

The leakage rate is very sensitive to changes in the geometry/area. Errors during manufacturing can be easily identified by the measurement on the test bench. An example for this is the leakage D-010-01; it is a circular leakage with a diameter of

Table 3 Leakage rates of all runs plus mean leakage rate of D-030-03

System pressure [bar _g]	Leakage rate [l _N /min]			
	Run 1	Run 2	Run 3	Mean
4.00	360.34	360.41	359.95	360.23
5.00	434.76	434.10	433.20	434.02
6.00	507.51	507.19	506.56	507.09
7.00	580.86	579.93	579.77	580.19
8.00	653.41	652.98	652.94	653.11

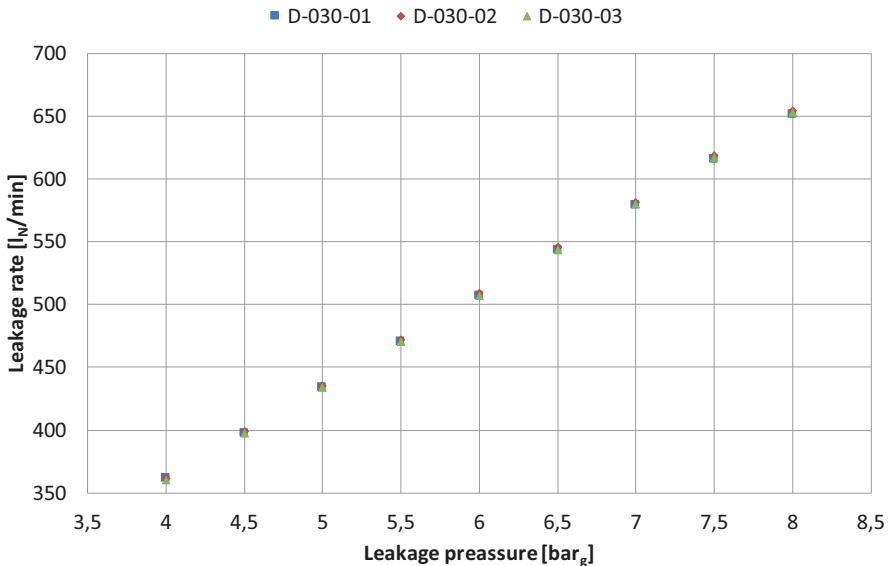


Fig. 6 Leakage rate of three different circular leakages

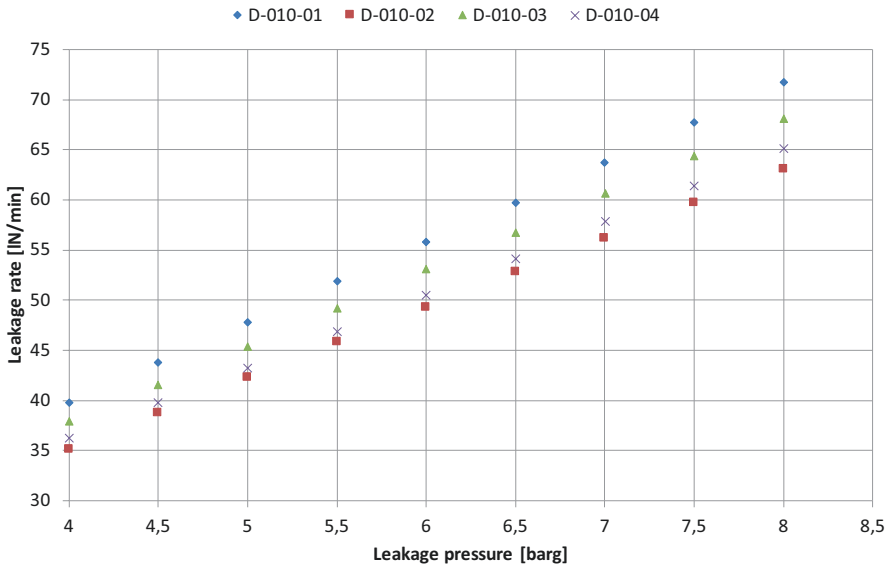


Fig. 7 Measuring results of a countersunk hole in comparison to non-countersunk

1 mm. On one side of the disk, the hole is clearly countersunk, leading to a significant increase in the leakage rate. The leakage D-010-04 has been manufactured as a replacement (Fig. 7).

All measured and averaged leakage rates can be found in Table 4. Comparing the stated leakage rates to their respective orifice areas shows a clear linear relation; this differs from the results of Dudic et al. (compare Fig. 1).

5.2 Slots

Several slots have been manufactured and measured. Since manufacturing slots with a milling machine is much less precise than drilling with a reamer, the respective orifice areas need to be measured (see Table 2). To compare the leakage rates of slot with each other, the results have to be normalized on the same orifice area. Figure 8 shows the effect of normalization: The deviation of the results decreases tremendously from about 10% to 0.5%.

Normalizing the areas on $3.142 \text{ mm}^2/7.069 \text{ mm}^2$ additionally enables the comparison to the circular holes of 2 mm and 3 mm. Comparing 08-040 with D-020 shows a decrease in the leakage rate of about 13%; this can be explained by increasing friction on the edges (longer edges than a circle), additionally constriction effects are assumed. This theory can be emphasized by looking at all normalized leakage flow rates for slots (Table 5). Slot 10-0725 (1 mm × 7.25 mm) is normalized on the same area as slot 08-0895 (0.8 mm × 8.95 mm), while being wider and shorter, having a higher leakage rate.

Table 4 Leakage rates for circular holes

Leakage pressure [bar _g]	Leakage rate [l _N /min]		
	3 mm (7.069 mm ²)	2 mm (3.142 mm ²)	1 mm (0.785 mm ²)
4.00	361.15	157.83	36.43
4.50	397.81	173.78	40.04
5.00	434.68	189.38	43.65
5.50	471.16	205.50	47.29
6.00	507.73	221.13	50.95
6.50	544.10	236.90	54.54
7.00	580.45	252.69	58.24
7.50	617.24	268.55	61.85
8.00	652.97	284.41	65.44

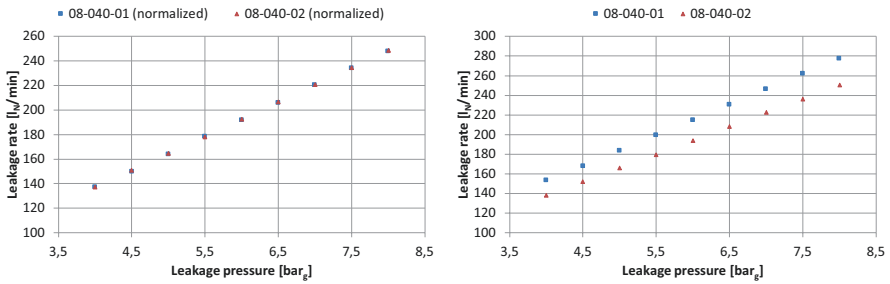


Fig. 8 Leakage rate of a slot (8 mm × 4.0 mm). (left) normalized on 3.142 mm² (right) non-normalized

Table 5 Normalized leakage rates for artificial slots

Leakage pressure [bar _g]	Leakage No./Leakage rates (normalized) [l _N /min]		
	08-40	10-0725	08-0895
4.00	137.19	331.95	287.93
4.50	150.40	365.69	316.80
5.00	164.39	399.57	346.09
5.50	178.21	432.91	375.53
6.00	192.31	466.85	404.82
6.50	206.44	500.20	434.20
7.00	220.56	533.76	463.33
7.50	234.27	566.93	492.42
8.00	248.28	600.05	521.81
Normalization	3.142 mm ²	7.069 mm ²	7.069 mm ²

Table 6 Comparison of calculated leakage rates and measurements at 7 bar_g

Leakage pressure [bar _g]	Leakage rate [l _N /min]			Calculated/measured
	7.069 mm ²	3.142 mm ²	0.785 mm ²	
7.00	580.45	252.69	58.24	Measured
7.00	619.80	275.47	68.87	Calculated
Difference	-6.22%	-8.27%	-15.43%	

5.3 Comparison Theoretical and Experimental Leakage Rates

Table 6 compares experimental data for circular holes with analytically calculated leakage rates according to the procedure described in this chapter. Experimental leakage rates are lower than the prediction, with differences growing for smaller orifice areas. Since the calculation is based on ideal gas and an ideal isentropic expansion, as well as a uniform velocity profile, this method tends to overestimate.

6 Conclusion

Leakages in compressed air systems contribute in a significant way to the poor energy efficiency. However, very little scientific research does exist on this topic, published leakage rates for standard geometries deviate of up to 70%. This chapter explains a simple method for calculating leakage losses based on ideal gas equation and isentropic expansion. A more detailed simulation model for CA leakages is introduced, showing only small effects of varying water contents in the air. In comparison to the experimental evaluation, the calculations tend to overestimate the leakage rates for circular holes by 6–15%.

A test bench for high-precision measurement of CA leakages has been developed and commissioned. The test bench shows no internal leakages and enables measuring manufactured leakages. This chapter presents leakage rates for circular holes and slots. Circular holes have a higher leakage rate, due to lower friction and constriction. Experiments prove a clear linear relation between orifice area and leakage rate, as well as leakage pressure and leakage rate. The identified leakage rates are higher than the average and median rates of all investigated publications.

References

1. M. Unger, P. Radgen, Energy efficiency in compressed air systems – A review of energy efficiency potentials, technological development, energy policy actions and future importance, in *Proceedings of the 10th International Conference on Energy Efficiency in Motor Driven Systems (EEMODS' 2017)*, ed. by P. Bertoldi, (Rom, 2018), pp. 207–233
2. S. Dudić, I. Ignjatović, D. Šešlija, V. Blagojević, M. Stojiljković, Leakage quantification of compressed air using ultrasound and infrared thermography. *Measurement* **45**(7), 1689–1694 (2012)
3. S. Dudic, I. Ignjatovic, D. Seslija, V. Blagojevic, M. Stojiljkovic, Leakage quantification of compressed air on pipes using thermovision. *Therm. Sci.* **16**(suppl. 2), 555–565 (2012)
4. H. Wolstencroft, Ultrasonic Air Leak Detection: An Investigation to Improve Accuracy of Leak Rate Estimation, 2008, Checked on [May 24, 2019], Available from: <https://researchcommons.waikato.ac.nz/bitstream/handle/10289/6780/thesis.pdf?sequence=1&isAllowed=y>
5. eco fair, Efficient Compressed Air Systems, 2014
6. Norgren, Energy Saving. The Norgren guide to saving energy in compressed air systems, Checked on [August 15, 2017], Available from: <http://cdn.norgren.com/pdf/ENERGY.pdf>
7. Festo, Effizienz@Festo, 2014, Checked on [July 19, 2019], Available from: https://www.festo.com/net/SupportPortal/Files/640431/EEF_de_V13_M.pdf

Digitalization in Electric Motor-Driven Systems



Maarten van Werkhoven and Konstantin Kulterer

1 Electric Motor-Driven Systems (EMDS) and Electricity Use

Electric motor-driven systems in industrial plants, infrastructure applications and buildings drive pumps, fans, compressors and other equipment. All motor systems consume annually about 10,700 TWh and are responsible for 53% of the global electric energy consumption (Fig. 1).

About 70% of this is used by pumps, fans and compressors, which are the focus of this study [1]. In industry electric motor-driven systems consume appr. 70% of the total industrial electricity consumption (Fig. 2).

An EDMS is a complex composite of several sequentially electrically and mechanically linked components (Fig. 3). New and existing technologies offer the potential to reduce the energy demand of motor systems across the global economy by 20% to 30%.

2 Digitalization in Industry: Scope

The term digitalization is used in a large number of policy documents and initiatives. Digitalization describes the increasing application of digital technologies (*i.e.* IT) throughout the economy, including energy, to achieve desired results, such as

M. van Werkhoven (✉)
TPA Advisors, Amsterdam, The Netherlands
e-mail: mvanwerkhoven@tpabv.nl

K. Kulterer
Austrian Energy Agency, Vienna, Austria
e-mail: konstantin.kulterer@energyagency.at

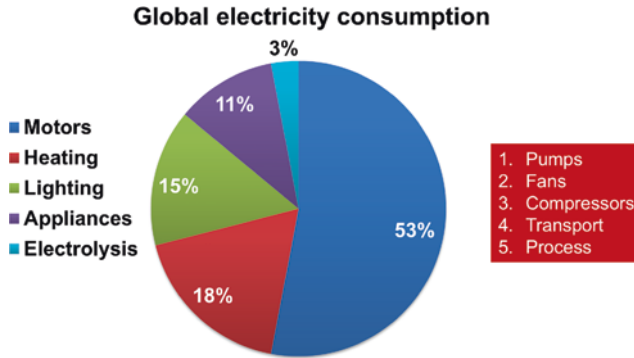


Fig. 1 Global electricity consumption

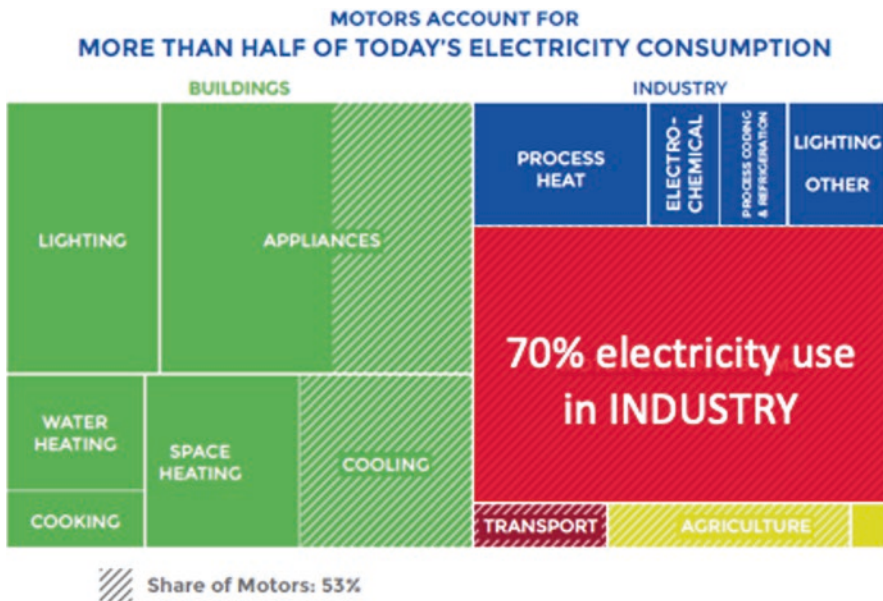


Fig. 2 Global electricity consumption and percentage electricity consumption electric-driven systems of total industrial electricity consumption

improved safety, efficiency and productivity. In other words, the use of digital technologies to change a business process and enhance efficiency and revenue. It is the process of moving to a digital business¹ [2].

¹Note: Digitization is then defined as: the process of changing from analogue to digital form, also known as digital enablement. Said another way, digitization takes an analogue process and changes it to a digital form without any different-in-kind changes to the process itself.

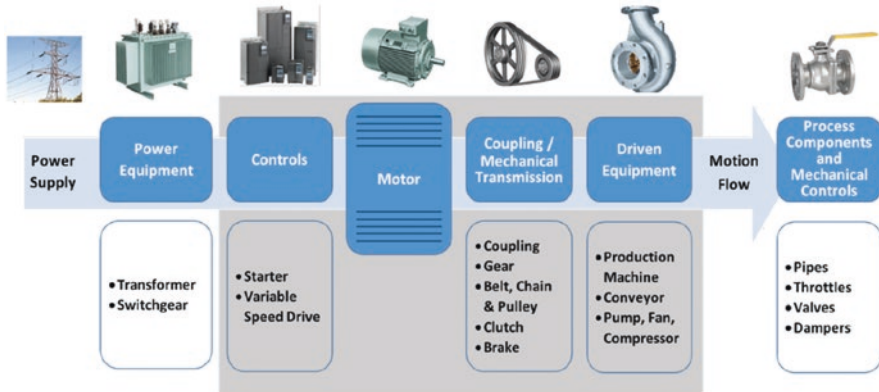


Fig. 3 The electric motor-driven system and its major components

2.1 Smart Manufacturing/Industry 4.0

For the industrial sector, digitalization is often referred to as Industry 4.0 and Smart Manufacturing (hereafter used as synonym). These concepts describe a form of industrial value creation that is characterized by digitalization, automation and networking of all actors involved in value creation, and that influences processes, products and business models of industrial companies [3]. To put it differently: combining production methods with the most modern information and communication technology. The driving force behind this development is the rapidly increasing digitalization of the economy and society [2].

To differentiate between today’s automation and smart manufacturing, the following three basic functions can be considered as the foundation for smart manufacturing [4]:

- Connected.
- Access to logic (data analytics and simulation).
- Use of logic to optimize energy use (anticipatory).

Technologies relevant for Industry 4.0 comprise the following five fields [3]:

- Internet and communication technology.
- Sensors and actuators.
- Automation, manufacturing technology and robotics.
- Embedded systems, analytics and systems engineering.
- Human-machine interfaces.

2.2 Digitalization in the Industry

The IEA distinguishes the following themes for digitalization in the industry [5], see Fig. 4:

- Inside the factory.
 - Industrial Equipment: Smart sensors, 3D printing, Industrial Robotics,
 - Analytics: Process control systems, Data analytics & Decision Support, Digital Twin factories, Artificial Intelligence.
- Outside the factory.
 - Connectivity: Remote controlled operations, Connected industrial equipment, Connected supply value chains.

Some key elements in the developments in digitalization are the speed (e.g. Moore's Law) at which it takes place, the global effects of it and the vast number of leading entities and receiving entities as well. Some find their way at an autonomous pace, others are boosted or stimulated through (inter)national research consortia and/or companies, and start-ups. All stakeholders, especially industry and governments, have a great interest in the assessment of 'relevant' developments, in terms of technologies, key players, applications and effects on trade/economics, safety and climate.

A further definition of this field of industrial digitalization and a differentiation towards 'domains' and 'technologies' does not bring definite answers yet; see Fig. 5, which shows a draft clipping up of industrial into domains and technologies.

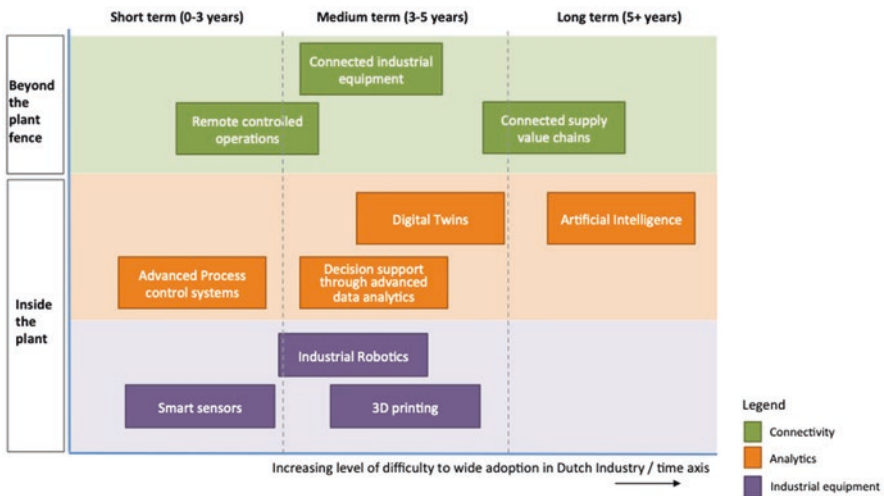


Fig. 4 Scope of digitalization in industry – inside and outside the factory; adapted for Dutch industry [5]

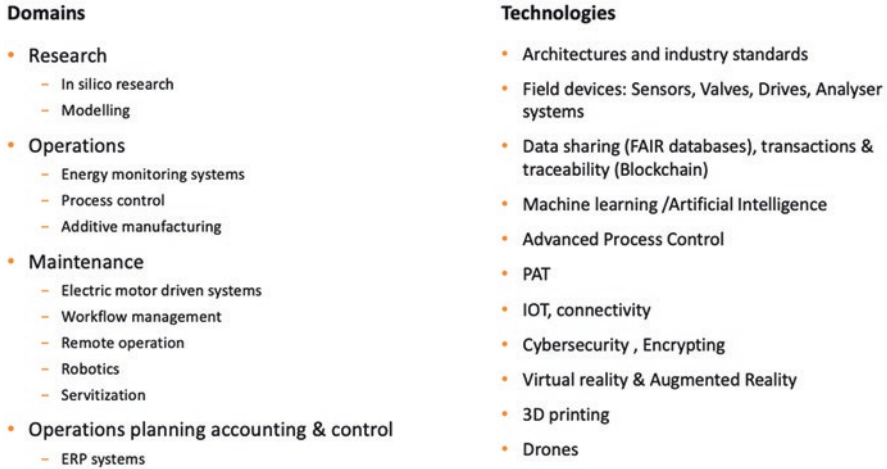


Fig. 5 Clipping up the field of industrial digitalization into domains and technologies – draft

Depending on the sector, state of development and country as well, the found definitions and scopes differ from a minor to a greater extent.

This one aspect (i.e. further definition of this field of industrial digitalization) needs to be further investigated in the coming period, see paragraph 5, in order to enable a more in-depth focus on those technologies that are relevant to energy efficiency and climate goals and governmental involvement.

3 Advantages of Industry 4.0 – Business Views

Smart Industry can contribute to solving social issues, for example, through lesser downtime in the production process, higher efficiency (climate and raw materials), new production technology for sustainable agriculture and robotics for support of healthcare staff.

Related to electric motor-driven systems in industry, the next generation of sensors, control and communication technologies, that gather, manage, interpret, communicate and act upon disparate and often large volumes of data, can improve device, process, facility or organization performance [4].

In general, the following goals of Industry 4.0 can be summarized [6]:

- Resource productivity and efficiency.
- Agility and responsiveness.
- Value-added services and business model innovation.
- Speed of market introduction.
- Adaptability to customer requirements.

The elements of higher efficiency and reduction of production cost (highlighted in the following section) are acknowledged by the following two Austrian studies:

1. Main goals for investments in digital technology are [7]:
 - More flexible response to changing needs (65%).
 - Faster adjustment to fluctuations in demand (39%).
 - Expansion of the product portfolio (37%).
 - Reduction of production costs/efficiency increase (36%).
 - Greater proximity to the customer/local production (35%).
 - Individualization/personalization of production (21%)
2. Main motives for Industry 4.0 measures in companies that already deal with Industry 4.0 [8].
 - Increase of internal efficiency (80%).
 - Transparency in the processes e.g. in production (71%).
 - Cost reductions (54%).
 - Competitive edge through modern products (48%).
 - Strengthening the interface to the customer (44%).
 - Increase in sales through new business models (39%).
 - Increase in sales through additional services, e.g. Predictive Maintenance (38%).
 - Possibilities for economic individualized production (lot size 1) (37%).

Reduction of production costs/efficiency increase proves to be a medium level goal for companies in general to invest in digital technologies. Companies that already work with digitalization (Industry 4.0) put the goals increase of internal efficiency, transparency in the processes and cost reductions at the top of their list of motives for further digitalization.

4 Digitalization and Energy Efficiency in EMDS

The potential energy effects of applying digitalization in industry (Industry 4.0 systems) include the following [4]:

- A. Efficient component instead of standard product.
- B. Component works only when needed to fulfill the requirement (instead of switching on/off).
- C. Process only works if necessary – as far as necessary to fulfill the production target (instead of switching on/off).

Components of Digitalization	Energy effects	category					
		A	B	C	D	E	F
Actuators, sensors	Communication with other sensors and with systems at a higher level increases the level of information and offers possibilities for analysis and condition monitoring.				X		X
Robotica and automation technologies	The energy effect is rather negative, but it also depends on the robot's standby consumption and the time to make the processes faster and thus reduce the specific energy consumption.						
Additive production technology (3D-printing)	In general, the goal is customization instead of mass production, whereby the energy consumption per piece can be higher than with mass production. The energy effect depends on the technology used so far. Theoretically, energy efficient design can be applied with better results.						
Big Data Data Mining Data Analytics Cloud based data analytics	The evaluation of process data makes enables the identification of weaknesses and failures. The goal is to achieve process and quality improvements by collecting and analyzing data. Improved methods for evaluation and validation.				X		
Automated process control Online monitoring	Time registration of process-relevant data in real time and its evaluation can bring slight energy savings. An immediate error message makes intervention in the production process possible; Waste percentages and material use are minimized. Demand-oriented control (e.g. automatic temperature control) for heat treatment increases quality together with lower gas consumption.		X	X	X		X
Human/machine interface, cooperation Augmented reality	Auxiliary systems assist people in the energy efficient operation of the machine, e.g. KPIs at SCADA. Augmented Reality can facilitate maintenance processes.		X	X			X
Digital Twins/digital shadow	An image of the process, equipment makes it possible to create a real-time evaluation basis for all relevant data and enables predictions of future states and provides information about the current status. Enables the development of more efficient processes and sub-	X					X
Comining process/production, material, energy, emission data	The business information system stores all available data (energy, material consumption), enables evaluation over longer periods, and potential savings are to be recognized.				X		X

Fig. 6 Components of digitalization and its energy effects

- D. Attitudes based on past experience rather than best guess settings.
- E. Smart Design (instead of conventional design).
- F. Connected systems and business units instead of isolated systems.

The table above (Fig. 6) shows for some major industrial technology areas the components of industrial digitalization; for each set of components a link is given to the listed energy effects (A to F) at the right side of the table. Most components/technologies include multiple possible energy effects.

Three Cases of Digitalization in Industry [5]

The following cases show some main characteristics of examples of digitalization in industry.

Case 1: 100% Predictable Maintenance

Technology: Monitoring the condition of installations, through sensing (on electric motors and applications), data analysis and decision tools. Systems establish links between equipment failure behavior and the data that can predict this failure. This involves a combination of process, machine, instrument and environmental data.

Location: Chemelot Limburg, the Netherlands.

Development phase: from start up to upscaling. Invest in the development of services, technology and the market.

Advantages: The timely prediction of a possible malfunction has a positive effect on the safety, reliability and availability of the installation. In addition, the fixed and variable maintenance costs decrease due to timely intervention. Preventing downtime is an important profit point. Example savings of 100 k EUR per line.

Energy and CO₂: Due to timely signaling of pollution (heat exchangers), leaks and the like, devices can continue to run at the right operating points.

Impact industry: Process industry is an important target group due to high costs of unplanned downtime, long operating times and high energy consumption installations. Development of technology and services make wider application possible in other industries.

Case 2: Resource Efficiency Process Industry

Technology: Advanced process control systems for optimum resource efficiency. Provide decision support to operators and managers through methods and tools for process monitoring and optimal dynamic planning, planning and control of factories, industrial sites and clusters under dynamic market conditions. The next phase is the move to automated closed-loop solutions for optimum energy and resource efficient production.

Location: EC project CoPro.

Development phase: Development and demonstration.

Energy and CO₂: Some sub-projects report concrete savings, for example 3–5% cost savings on a production line in a refinery; equals to 1 to 5 million euros per year savings, with a 3.4% reduction in greenhouse gases.

Case 3: Digital Twin

Technology: Use of a digital copy of/for the design and process modeling, simulation, control, maintenance and management registration of installations.

Location: Various locations, including BASF Germany chemical group.

Development phase: In initial applications (demonstration), continuing R&D.

Advantages: Far-reaching optimization of processes through digital design based on minimal materials and energy required. Can be used for existing installations and new designs.

Energy and CO₂: Example BASF where first a detailed kinetic model of the expanded polystyrene (EPS) batch process was developed and then improved with dynamic optimization techniques. The company noted a 30% reduction in batch time, which led to significant energy savings.

Impact industry: Wide scope; field is under development, with connections to sensing, artificial intelligence, servitization, both service industry and process engineers.

Energy Savings Potentials

Research into the potential contribution of digitalization to the reduction of energy use, CO₂-emissions and raw material consumption is scarce, due to the new cross-cutting nature and complexity of the material and possibly also the speed of innovation.

Saving effects associated with digitalization show examples or exemplary proof in the order of average 5–20% energy efficiency improvements in industry; some examples are given from the following studies [9]:

Manufacturing Industry

- Digital technologies can improve energy efficiency by 25% in the context of smart manufacturing [10] (Smart Manufacturing Leadership Coalition, US-based).
- In the manufacturing industry (German based) the reduction in energy consumption (electrical energy) achieved through digital transformation measures ranked mostly in the range of up to 25%. Based on Sensitec's experience, the same study estimates potential savings in electricity through real-time control of the production line of between 10% and 20% [9].
- The use of big data and advanced analytics (in the manufacturing industry) can result in a 20–25% increase in production volume and a 45% reduction in downtime, which in turn minimizes standby losses, saving energy for operating the equipment [9, 11].

Industry

- The study of the World Economic Forum 2019 indicates an increase in energy efficiency for selected applications of Industry 4.0 from 2% to 50% [6].
- The application of energy-efficient electric motor systems and digitalization show savings of approximately 18–26% on the industrial electricity use [5] (Dutch industry), see Fig. 7.
- Conversely, the German Federal Environmental Agency in Germany calculated the electricity consumption caused by information and communication technologies (ICT) in Germany in 2014 at 75.2 TWh (corresponding to a share of approximately 10% of the total German electricity consumption), of which 9.6 TWh is accounted for by industry [12].
- Globally, a first assessment (by the Global e-Sustainability Initiative (GeSI) in the Smarter 2030 report) shows that the IT-induced emission reductions potential through advanced applications in other sectors like industry and buildings can amount up to 9.1 billion tonnes by 2030, which is a factor 7.2 higher as the 1.3 billion tonnes emissions as accounted for by IT at that point [12].

The technologies with an impact on energy efficiency and CO₂ emissions reduction in industry are listed in Fig. 8 – example for Dutch Industry:

- Smart Sensors.
- Digital Factory (Digital Twins and Artificial Intelligence).
- Servitization.
- Advanced Process Controls.
- Decision support & Data analytics (Artificial Intelligence).

It concerns technologies for ‘in the factory’ and the associated preconditional or enabling technologies such as data analytics and decision support systems. Examples of applications are Energy Management 2.0 and Condition-Based Monitoring. In the Servitization domain, technologies are linked to services and associated business models. The list of potential promising applications is long and growing, where the cases give a first impression.

5 Next Steps

The preceding paragraphs give a first detailing of scope in domains, technologies, sectors and potentials – in energy efficiency, economic benefits and emissions reduction. The ongoing interest by the IEA 4E EMSA partners is into identifying the potential impact and possible or needed policy measures to stimulate the development and implementation of digital technologies towards more efficient motor systems in industry, as well as to identify potential negative effects – like potential extra emissions.

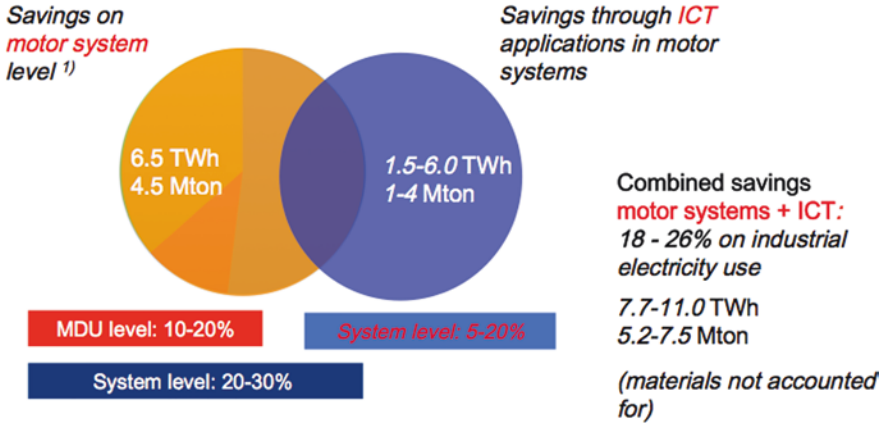


Fig. 7 Savings in Dutch industry through efficient electric motor systems and digitalization

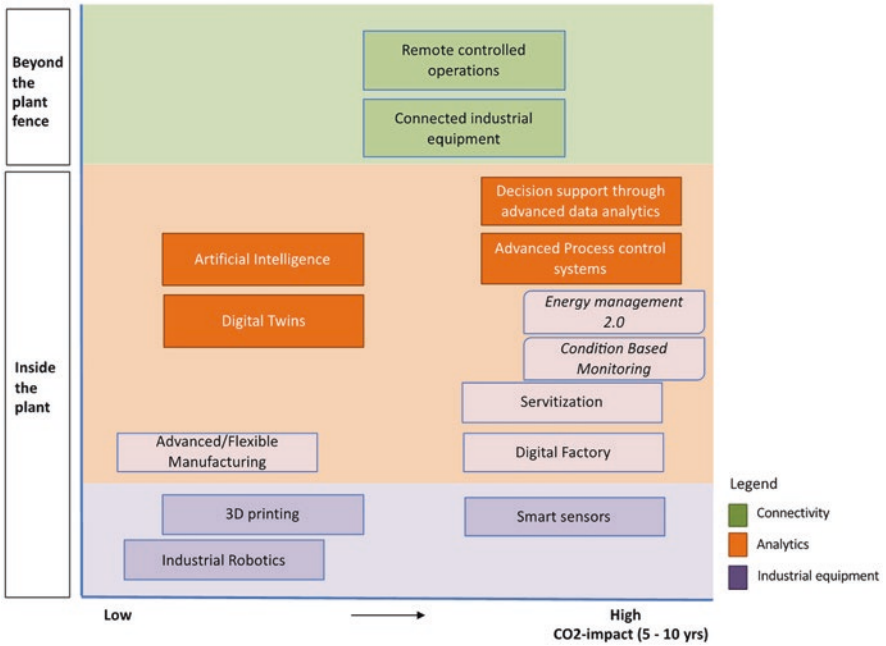


Fig. 8 Components of digitalization and its energy effects

First assessments indicate a significant contribution of digitalization to industrial energy efficiency, i.e. an improvement of energy efficiency of 20–25% and an increase of operational efficiency of 25%.

Examples of related digital technologies and products are sensors and big data analysis, decision tools and new testing tools. The application of digital twins and artificial intelligence will enhance energy and motor management and maintenance and systems efficiency strategies.

On short term an identification of possible (research) steps will be made by partners. Special focus will be on a further definition of relevant technologies, assessment of their potential and the need (or not) for policy involvement i.e. potential related actions by governments and their related bodies. The economic and climate-related benefits define the main value (importance) in these assessments.

References

1. International Energy Agency: World Energy Outlook 2016, IEA Paris, 2016
2. Digitalization and the future of energy, DNV GL, 2019
3. Industrie 4.0 Lösungen für Effiziente Motorsysteme, Konstantin Kulterer, 2019
4. E. Rogers, E. Junga, Intelligent Efficiency Technology and Market Assessment, American Council for an Energy-Efficient Economy (ACEEE), 2017
5. Exploration of Growth Markets and CO₂ reduction in industry, Focus on IT applications (digitalization) and Electric Drives, EZK/TPA advisors, 2018 (in Dutch)
6. World Economic Forum: Fourth Industrial Revolution, Beacons of Technology and Innovation in Manufacturing, in collaboration with McKinsey & Company, January 2019
7. EY-research: Industry 4.0 in Austrian SMEs (in German: EY-Umfrage: Industrie 4.0 im österreichischen Mittelstand, Befragungsergebnisse), Ernst & Young, 2018
8. Industry 4.0 – German Industry 4.0 Index 2018 by (in German: Staufen AG, Staufen Digital Neonex GmbH: Deutscher Industrie 4.0 Index 2018), Staufen AG, 2018
9. VDI ZRE (Zentrum für Ressourceneffizienz): Ressourceneffizienz durch Industrie 4.0, Potenziale für KMU des verarbeitenden Gewerbes, 2017
10. Smart Manufacturing Leadership Coalition (SMLC), Implementing 21st Century Smart Manufacturing. Workshop Summary Report, University of California, Los Angeles, 2011
11. McKinsey Digital: Industry 4.0 – How to navigate digitalization of the manufacturing sector, McKinsey & Company, München, 2015
12. Global e-Sustainability Initiative (GeSI), Reger, Kosch, 2017

Calorimetric Efficiency Determination of Power Electronic Variable Speed Drives



Stan Caron, Arne Berteyn, Pieter Defreyne, Steve Dereyne,
and Kurt Stockman

1 Introduction

Variable speed drives come with very high efficiency values, which makes it particularly difficult to accurately measure their low power losses. To address the efficiency of these converters or Complete Drive Modules (CDM), the IEC has developed the international standard IEC 61800-9-2 Ed. 1.0 b:2017 [1].

Three types of testing of CDM for IE classification are mentioned in the standard, i.e. the single component loss determination, the well-known input–output approach and the calorimetric measurement methodology. With the single component loss determination method, the loss is calculated. Detailed information on the components inside of the drive should be provided by the manufacturer to calculate the power loss, but this is usually not the case. This method is also called the semi-analytic model approach. The input–output method measures the electrical power extracted from the grid and the electrical output power delivered by the drive by using high-end power analyzers. The last method mentioned in the standard is the calorimetric method which determines the power loss by measuring the heat loss or power dissipation of the CDM.

In the IEC 61800-9-2 standard, constant uncertainty is assumed for the single component loss determination and the calorimetric measurement [1]. The uncertainty of the single component loss determination method depends on the datasheet

S. Caron (✉) · P. Defreyne · S. Dereyne · K. Stockman

Department of Electromechanical Systems and Materials, Ghent University, Ghent, Belgium

Member of Energy Efficient Drive Trains Partner of Flanders Make, Ghent, Belgium

e-mail: Stan.Caron@ugent.be; Pieter.Defreyne@ugent.be; Steve.Dereyne@ugent.be; Kurt.Stockman@ugent.be

A. Berteyn

Department of Electromechanical Systems and Materials, Ghent University, Ghent, Belgium

e-mail: Arne.Berteyn@ugent.be

of the CDM, which can be unavailable or not accurate. The uncertainty of the input–output method rises exponentially with respect to the increasing efficiency [1]. These aspects make the calorimetric approach attractive to overcome the uncertainty problems when accurate measurements of very high efficiency drives (>97%) are required.

2 Calorimeter Concept

The calorimetric measurement is a straightforward measurement method in which the losses are determined by measuring the heat loss of a device under test (DUT). The DUT is mounted in an insulated box which is heated up due to the power loss of the DUT. By measuring temperature changes, the amount of power or heat is determined as shown in (1). The power is absorbed by a cooling gas or liquid. The absorbed power (P) is thus equal to the mass flow rate (\dot{m}) multiplied by the average specific heat of the liquid or gas (c_p) and the difference of temperature between the inlet and outlet (ΔT).

$$P = \dot{m}c_p\Delta T \quad (1)$$

Different calorimetric concepts have been developed to be able to measure power electronic variable speed drives with a high accuracy [2]. There are two main approaches, i.e. direct and indirect calorimetry. Direct calorimeters measure the heat directly by measuring the parameters in (1) while indirect calorimeters determine the power loss indirectly by implementing an auxiliary heater. All of the types are explained in [2]. These types each have their own advantages and disadvantages but to achieve effective measurements with a calorimeter three main requirements must be met: a steady mass flow is needed, heat leakage has to be minimized and the coolant temperature has to be measured or controlled [2].

In this chapter an air-cooled indirect balanced calorimeter test bench is introduced. The measurement consists of two tests: the main and balance test. During the main test, a DUT is powered and heating up the chamber. The balance test requires an additional heater. In this test the power of the heater is adjusted to achieve the same temperature rise of the coolant as during the steady state in the main test [3]. Both tests are performed in the same calorimetric chamber. Therefore this chamber contains both the DUT and the heater. The biggest advantage of this method is that the coolant properties do not change much because the main and balance tests are executed sequentially. Hence, measuring the coolant properties is not critical anymore. The measurement of electric DC power is easier than measuring the coolants properties which makes indirect calorimeters as the balance type interesting. However, due to the variation of the specific heat capacity when barometric pressure and air humidity change, the accuracy of the power measurement could be influenced [4]. This is taken into account in the test bench construction.

As mentioned in [2], the heat leakage through the walls of the box should be minimized. To minimize the heat leakage, thick insulated walls can be used to construct the box. However, due to thick insulation the thermal mass of the setup increases resulting in a longer time to reach a thermal equilibrium [5]. One of the main disadvantages of calorimetric measurement is the test duration. So this aspect should be considered carefully. Equation (1) is expanded when the heat leakage is added to the formula, shown in (2)

$$P_{\text{loss,DUT}} = \dot{m} * c_p * \Delta T + P_{\text{walls}} \quad (2)$$

with P_{walls} the power loss through the walls.

In the balance calorimeter concept, the mass flow rate (\dot{m}), the average specific heat capacity (c_p) and temperature difference (ΔT) are not used to calculate the power loss of the device under test (P_{DUT}). The power of the resistive heater (P_{heater}) replaces the first part in (2) which results in (3) when calculating the power loss of the DUT. Notice that Eq. (3) is only accurate when the thermal conditions during the main test are identical compared with the balance test. A compensation power (P_{comp}) can be added to (3) when there are differences in specific heat capacity during the thermal equilibria of the main and balance tests, resulting in (4). The difference in heat leakage through the walls ($P_{\text{diff,walls}}$) should be added to (3) because the power leakage is almost never exactly the same during the main and balance test due to fluctuations of the ambient air temperature. If the heat leakage would be constant during the whole measurement, the power loss of the DUT should be equal to the heater power.

$$P_{\text{loss,DUT}} = P_{\text{heater}} + P_{\text{diff,walls}} \quad (3)$$

The heater can be used during the main test to increase the power in the box and thus decrease the measurement rate. The loss of the DUT is equal to (4) if every power is added to the power loss equation

$$P_{\text{loss,DUT}} = P_{\text{heater,bal}} - P_{\text{heater,main}} + P_{\text{diff,walls}} + P_{\text{comp}} \quad (4)$$

with $P_{\text{heater,bal}}$ and $P_{\text{heater,main}}$ the power dissipated by the heater during the balance and main tests, $P_{\text{diff,walls}}$ the difference in power leakage through the walls and P_{comp} the compensation power due to variation of the thermal equilibria during the whole measurement.

To determine the efficiency with a calorimetric measurement, (5) is taken into account.

$$\eta_{\text{DUT}} = \frac{P_{\text{out}}}{P_{\text{in}}} = \frac{P_{\text{in}} - P_{\text{loss,DUT}}}{P_{\text{in}}} \quad (5)$$

with P_{in} the power input extracted from the grid, P_{out} the output power delivered to the motor and $P_{loss,DUT}$ the power loss of the device under test.

3 Test Bench Setup

In this chapter a balanced calorimetric setup with air as medium is proposed to test small electronic drives for AC motors in a power range from 1 kW up to 7,5 kW. An efficiency and power loss determination is performed on a 2,2 kW drive using the input–output and calorimeter method. These measurements are executed simultaneously in order to compare the results.

Figure 1 shows a schematic overview of the test bench. The variable speed drive on the drive side of the setup is measured by the input–output method with a PM6000 power analyzer. Thus, the input power extracted from the grid and the output power delivered to the drive motor are measured.

The calorimetric measurement is performed at the same time. This setup consists of several parts (Fig. 1). The box is constructed from insulation plates of 200 mm thick made out of polyurethane (PUR) with a thermal conductivity value (λ) of 0,022 W/mK and a thin layer of aluminium on both sides. These plates have three benefits, i.e. the insulation value is very good so heat leakage is minimized, the plates are rigid and it is easy to make a box out of it and the aluminium layer

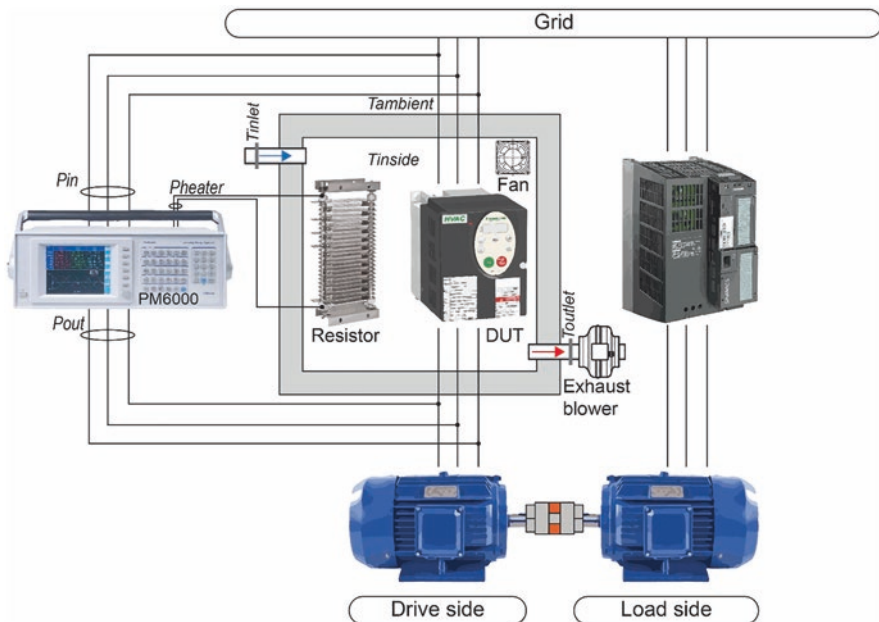


Fig. 1 Balance calorimeter test bench setup

increases heat conduction and the temperature is better distributed along the surface of the inside walls [2]. The outer dimensions of the box are $1,08\text{ m} \times 1,08\text{ m} \times 1,28\text{ m}$. The volume of the box has to be chosen so that it is large enough for the DUT, a heater, additional fans, temperature sensors and extra room for air displacement.

There are two holes in the box for the air inlet and outlet tubes with diameters of 40 mm for the inlet and 125 mm for the outlet, positioned in such a way that the distance of the airflow is as long as possible in the chamber. The inlet tube is located in the upper deepest corner of the box and the outlet tube is located in the lower corner near the front opening. This is to prevent separation of the air into layers of different temperature [3].

The inlet air is sucked out of a large basement because the air properties vary less than in the laboratory where the calorimeter is placed. In this setup, the air properties are assumed to be constant, but if variations in temperature occur, a compensation power is added to the power loss. The outlet air is blown into the ambient, which causes the laboratory to warm up and thus causes instabilities in the power leakage through the walls. Therefore, the difference in power leakage during the main and balance tests is also added to the power loss, as seen in (3).

The temperature of the inlet and outlet air is measured with four temperature sensors each. The average of those four sensors is then used to calculate the mean inlet and outlet temperature. The inside temperature, on the other hand, is measured by a grid of six sensors while the ambient temperature is measured with one sensor outside the calorimeter. All of the temperature sensors used in this setup are A class, four wire pt100's with a tolerance of $\pm 0,15\text{ }^{\circ}\text{C}$.

Other parts in the calorimetric setup are the inside fans and the exhaust blower. 12 Vdc fans are placed in the box to mix the air in such a way that the temperature is homogenous in the whole box. The inside fans are enabled during the main and balance test.

To move the air through the inlet tube, the calorimetric chamber and the outlet tube, an exhaust blower is attached to the outlet tube. When the blower in the outlet tube exhausts the air, a small vacuum occurs inside the chamber and therefore the air is circulating from the basement into the chamber and out into the ambient [5]. The blower is an electronically commutated motor of 85 W, powered by the grid of 230 Vac. The nominal rotation speed is 3200 rpm with a mass flow rate of approximately $415\text{ m}^3/\text{h}$. The blower speed is controlled by an analogue signal of 0–10 V.

During the balance test a heater is needed which is a resistor in this setup. There is a heat sink mounted on top of the resistor to improve the heat transfer to the air. The $6,8\ \Omega$ resistor is powered by a controlled DC voltage of 0–65 V. Therefore the maximum possible heat dissipation is 500 W, which defines the range of the calorimeter in theory. In practice, the range is around 350 W due to the maximum flow rate of the air in the setup.

In Fig. 1 the load side of the test bench can be seen as well. If the drive motor is connected to the load motor, the motor-generator cycle is complete and multiple setpoints can be measured.

4 Measurement Procedure

A thorough measurement procedure (Fig. 2) is proposed to achieve accurate and reproducible results with the calorimetric test bench. The balance type of calorimetry consists of a two-step measurement procedure, i.e. the main and balance test phase. Before efficiency or power loss determination tests of a drive can be performed, the DUT is be mounted. Then the setup must be calibrated in order to accurately determine the power leakage.

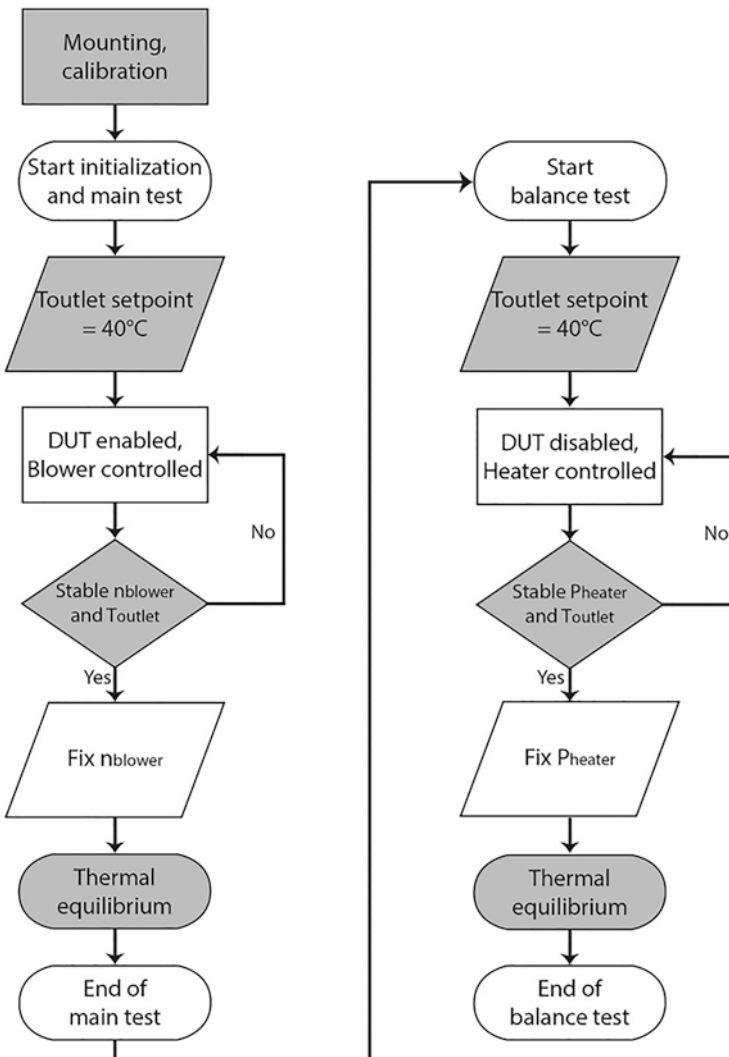


Fig. 2 The flowchart of the measurement procedure

During the calibration, a constant amount of power is dissipated in the box by the heating element while a high end power analyzer with a basic uncertainty of 0,02% measures the input power. Both the inlet and outlet tubes are stuffed with insulation material. Thus, the heat circuit of the box is a closed circuit and the heat can only be lost through the walls of the calorimeter. The power loss through the walls (P_{walls}) is equal to (6).

$$P_{\text{walls}} = U_{\text{walls}} S_{\text{walls}} \Delta T_{\text{walls}} \quad (6)$$

U_{walls} is the overall heat transfer coefficient of the chamber. This coefficient depends on the insulation thickness (d) and the thermal conductivity (λ) of the applied insulation material, as seen in (7).

$$U_{\text{walls}} = \frac{\lambda}{d} \quad (7)$$

The surface area of the calorimetric box is S_{walls} and ΔT_{walls} is the temperature difference between the inside temperature of the chamber and the ambient temperature. The overall heat transfer coefficient of the chamber and the surface area are assumed to be constant. Therefore, if the temperature over the wall is measured, the power leakage can be calculated. A calibration should be performed to determine the correlation between the temperature over the walls and the power leakage.

The difference in temperature over the walls of the calorimeter with respect to the heater power is seen on the calibration curve (Fig. 3). The curve is obtained by performing a linear fit on the results. The linear equation of the curve is used to determine the power leakage when the temperatures are measured, as shown in Eq. (8). The worst case or maximum error on the linear fit is 0,76 W.

$$P_{\text{walls}} = 0,707 * \Delta T_{\text{walls}} - 1,77 \quad (8)$$

The start of the actual measurement is the next step in the flowchart (Fig. 2). The initialization and main test are performed first. The calorimeter has a specific thermal mass which increases the measurement rate. During the initialization, the heating element produces extra heat in the calorimeter to decrease the test duration and overcome the thermal inertia problem. In practice, the heater produces 400 W the first 10 min of the test. After the initialization, the DUT, inlet and outlet tubes, the perforated plate, cables and insulation are heated up.

While the initialization is performed, the main test is already executed simultaneously. The DUT is powered on and the drive motor is controlled with a constant speed and loaded by the load side of Fig. 1. The drive is heating up the air inside the box because of its power loss. During the main test, the exhaust blower speed is PID controlled to reach a constant outlet air temperature of 40 °C. The blower sucks air into the inlet tube, through the calorimeter and out into the ambient. To maintain a minimum air circulation through the setup, the lower limit of the rotation speed is set on 15% of the maximum speed.

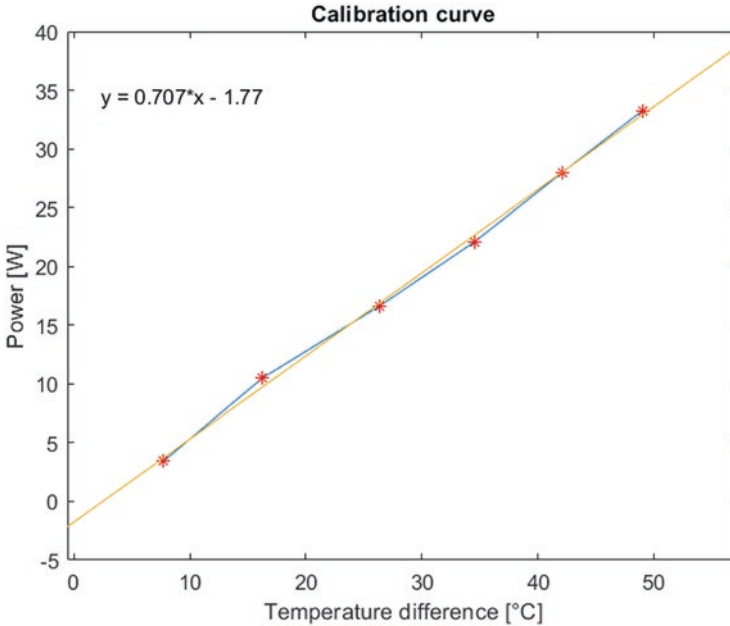


Fig. 3 Calibration curve of the calorimeter setup

It should be noticed that the drive and load motor should also reach a thermal equilibrium. Therefore during the beginning of the test, the power loss of the DUT varies. The settling time of the electric motors is much smaller than the settling time of the calorimeter, hence, this is neglected.

After a while the exhaust blower speed settles ($\Delta n_{\text{blower}} < 20$ rpm) while the DUT is losing a constant amount of power and the outlet air remains equal to 40 °C ($\Delta T_{\text{outlet}} < 0.1$ °C). The rotation speed of the blower is fixed. A steady state or thermal equilibrium is reached. The inside and ambient temperature should also be stable to ensure a constant thermal condition of the calorimeter. 15 min of the thermal equilibrium are saved and analyzed before the main test is finished. Data points are saved every 10 s.

The second phase of the measurement is the balance test. The blower is rotating at fixed speed, which is the value obtained from the thermal equilibrium during the main test. The outlet temperature setting value remains 40 °C. Next, the DUT is switched off and the heating element should then produce enough heat to achieve the same thermal conditions as during the main test. The power source of the heater is controlled during the balance test with a PID controller. Therefore, the heater is actually mimicking the DUT while the PID controller is searching for the same amount of power that the DUT was dissipating during the main test. When the temperatures and heater power are stable, the power source control of the heater is fixed and a new thermal equilibrium is achieved. The balance test is finished. The thermal conditions of both the main and balance test should be compared to conclude if the

measurement has been successful. If necessary, a compensation power should be implemented to correct the results.

If the power loss of a DUT is very low, an extra power can be produced during the main test with the heater. Hence, the duration to reach the thermal equilibrium decreases but the uncertainty rises because the heater power has to be measured during both the main and balance test. The power loss of the inside fans is neglected because the fans are enabled throughout the whole measurement.

5 Measurement Uncertainty

The measurement uncertainty of the input–output measurement method depends completely on the uncertainty calculation of the power analyzer. During the measurements in this chapter, the PM6000 of Voltech is used with a base accuracy of 0,02%. Compared to the input–output method, the uncertainty determination of a calorimeter is not so obvious.

The main interesting subject about the calorimetric concepts is the uncertainty of the measurement. The goal of this method is to achieve a higher accuracy compared with the direct method, especially when high efficiency devices are tested. As mentioned in [6], there is no standard method to calculate the uncertainty of calorimetric measurements. Therefore, comparing results of publications about this type of calorimetry is difficult. Also, a clear explanation of how the uncertainty should be calculated is not found. Hence, in this chapter the uncertainty calculation of a measurement is explained clearly.

The measurement uncertainty consists of two types e.g. the A-type and B-type uncertainties [7]. The A-types occur because of fluctuations in the measured values. They are derived from the standard deviation (s) of the mean (x). If the standard deviation is low, the variations on the mean are small and thus more accurate results are obtained. To calculate the standard A-type uncertainty of a measurement, Eq. (9) is implemented

$$AF_A(x) = \frac{s}{\sqrt{n}} \quad (9)$$

with n the amount of readings and $AF_A(x)$ the A-type absolute fault of the mean.

The A-type standard uncertainties are included in the results but not shown in detail.

B-type uncertainties depend on other causes than the A-type uncertainties as the uncertainties due to the measurement instruments and other parameters. In this balance calorimeter setup, the accuracy depends on the uncertainty of the temperature sensors and the power analyzer. The uncertainty due to the change of the air properties between the main and balance test is implemented in the uncertainty calculation. The humidity and pressure are not measured, therefore, the uncertainty of the

air variation only depends on the temperature sensors. This could decrease the measurement accuracy [3].

The temperature sensors are accurate up to $\pm 0,15$ °C. The uncertainty of the reading is also equal to $\pm 0,15$ °C which makes the total uncertainty of the temperature measurements equal to (10)

$$AF_B(T) = \sqrt{\left(\frac{0,15^\circ\text{C}}{\sqrt{n_s}}\right)^2 + (0,15^\circ\text{C})^2} \quad (10)$$

where n_s is the number of sensors. The uncertainty of the different temperature measurements are found in Table 1.

To measure the DC power dissipated by the balance heater, the PM6000 power analyzer is applied. (11) is used to calculate the total uncertainty on the measured power loss of the DUT, while (12) shows the uncertainty equation for the efficiency determination. It is important to notice that the accuracy of the efficiency determination also depends on the input power measurement, as seen in (5).

$$AF(P_{\text{loss,DUT}}) = \sqrt{AF(P_{\text{heater,bal}})^2 + AF(P_{\text{heater,main}})^2 + AF(P_{\text{diff,walls}})^2 + AF(P_{\text{comp}})^2} \quad (11)$$

$$RF(\eta_{\text{DUT}}) = \sqrt{RF(P_{\text{in}})^2 + RF(P_{\text{in}} - P_{\text{loss,DUT}})^2} \quad (12)$$

The uncertainty of the heater power (P_{heater}) is calculated as stated in the data-sheet of the PM6000.

Next, the uncertainty of the power leakage through the walls should be calculated, which is not evident. As shown in (6) the power loss depends on the overall heat transfer coefficient, the surface area and the temperature difference of the walls. The overall heat transfer coefficient and the surface area are assumed to be constant. The temperature difference over the walls, however, is not constant and is being measured. To calculate the total power leakage, the calibration curve in (8) is taken into account. The uncertainty is therefore depending not only on the error of the linear fit of the curve but also on the uncertainty of the temperature difference measurement. Hence, the relative fault on the power leakage is equal to (13)

Table 1 Accuracy of the temperature measurements

Temperature measurement	Number of sensors	Uncertainty
Inlet	4	$AF(T_{\text{inlet}}) = 0,17$ °C
Outlet	4	$AF(T_{\text{outlet}}) = 0,17$ °C
Inside	6	$AF(T_{\text{inside}}) = 0,16$ °C
Ambient	1	$AF(T_{\text{ambient}}) = 0,21$ °C

$$RF(P_{\text{walls}}) = \sqrt{RF(\text{Curve}_{\text{error}})^2 + RF(\Delta T_{\text{walls}})^2} \quad (13)$$

Hence, the uncertainty of the difference in power leakage through the walls of the main ($P_{\text{walls,main}}$) and balance ($P_{\text{walls,bal}}$) test is equal to (14).

$$AF(P_{\text{diff,walls}}) = \sqrt{AF(P_{\text{walls,main}})^2 + AF(P_{\text{walls,bal}})^2} \quad (14)$$

If the thermal properties during the main and balance test are perfectly the same, the sum of the heater and the difference in leakage power through the walls is equal to the power loss of the DUT but this is never exactly the case [3]. The variation of humidity, pressure or temperature changes the specific heat capacity. As seen in (1), variations of the specific heat have an influence on the absorbed power. The percentage variation due to the temperature change is measured and therefore the variation on the power is calculated. This results in a compensation power (P_{comp}), which is usually small. Hence, the uncertainty of P_{comp} is almost negligible.

Thus, the absolute fault on the power loss of the DUT can be calculated with (11). The uncertainty calculation is still not complete because the humidity and pressure of the inlet air are not measured, but these would be very small and can therefore be neglected, especially when the standard uncertainty is multiplied with a coverage factor (k) [7]. The expanded uncertainty when a normal distribution is applied with a coverage factor of two gives a 95% level of confidence that the error lies in that interval [8]. The uncertainty on the power loss would then be equal to (15)

$$AF(P_{\text{loss,DUT}}) = k * \sqrt{AF(P_{\text{heater,bal}})^2 + AF(P_{\text{heater,main}})^2 + AF(P_{\text{diff,walls}})^2 + AF(P_{\text{comp}})^2} \quad (15)$$

with k the coverage factor.

6 Measurement Results

Two tests are executed and the results are processed. The first test is at the full load and speed and the second test at 100% load and 25% speed. The input–output and calorimetric measurements are performed simultaneously and compared. In Fig. 4, the temperatures, heater power, blower speed and power leakage through the walls of the test at nominal load and speed are shown. The progress of the measurement is clearly visible on these plots with at first the initialization (1), then the main test (2) and at last the balance test (3).

In Table 2, the measurement results of the 100% load and speed test are shown. It is noticed that the temperature rise of the air during both tests is almost identical while the temperature difference over the walls changes. Therefore a difference in

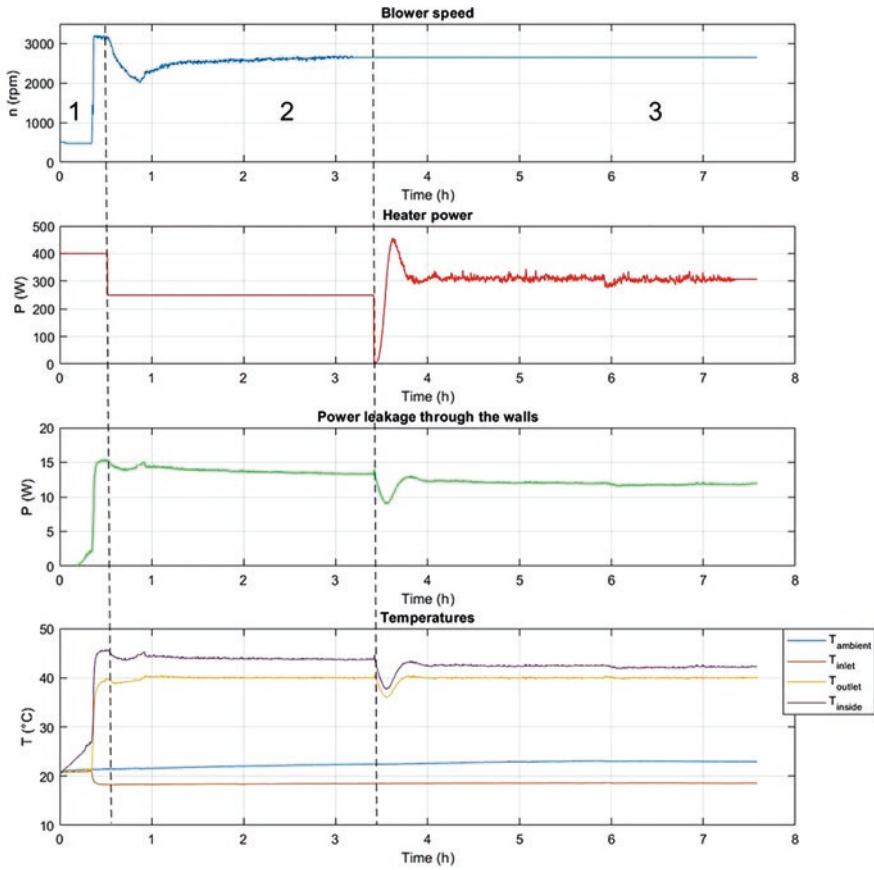


Fig. 4 Blower speed, heater power, leakage power and temperature plots of 100% load and 100% speed test. The initialization (1), the main test (2) and balance test (3) are indicated on the figure

power leakage through the walls 1,44 W is determined. This difference is compensated when the results are processed in Table 3. It should also be noticed that the heater dissipates heat during the two measurement phases to decrease the test duration. An uncertainty due to the extra heater power in the main test is added to the total uncertainty. There are also variations in air temperature during the measurement. A compensation power of 1,27 W is added to the power loss.

In Table 3, the measurement results of the two tests at 100% load and speed and at 100% load and 25% speed are shown. During the first test, the difference in power loss determined by both methods is 5,21 W. The efficiency difference is much smaller due to the fact that the input power is taken into account when the efficiency is calculated. The difference in power loss of the second test is only 0,22 W. The uncertainty of the measured power loss with the calorimeter is remarkably much lower than when the direct or input–output method is applied.

Table 2 Measurement results of 100% load and 100% speed test

	Main test	Balance test	Difference
T_{inlet} (°C)	18,45	18,56	0,11
T_{outlet} (°C)	39,99	40,01	0,02
ΔT_{rise} (°C)	21,54	21,45	0,09
T_{inside} (°C)	43,72	42,20	1,51
$T_{ambient}$ (°C)	22,40	22,93	0,53
ΔT_{walls} (°C)	21,31	19,27	2,04
P_{heater} (W)	247,72	307,19	59,47
P_{walls} (W)	13,30	11,86	1,44
P_{comp} (W)		1,27	
P_{input} (W)	2277,26		
P_{output} (W)	2209,87		

Table 3 Measurement results of direct and calorimetric measurements

		100% load, 100% speed		25% load, 100% speed	
		Value	Uncertainty	Value	Uncertainty
Input – Output measurement	P_{in}	2277,26 W	$\pm 8,01$ W	564,90 W	$\pm 3,07$ W
	P_{out}	2209,87 W	$\pm 9,52$ W	501,88 W	$\pm 2,24$ W
	$P_{out-in+DUT}$	67,39 W	$\pm 12,44$ W or $\pm 18,46\%$	63,01 W	$\pm 3,80$ W or $\pm 6,04\%$
	$\eta_{out/in}$	97,04%	$\pm 0,56\%$	88,84%	$\pm 0,70\%$
	Measurement duration	30 min		30 min	
Calorimetric measurement	$P_{heater,main}$	247,72 W	$\pm 0,66$ W	200,68 W	$\pm 0,58$ W
	$P_{heater,bal}$	307,19 W	$\pm 0,75$ W	258,81 W	$\pm 0,68$ W
	P_{heater}	59,47 W	$\pm 1,00$ W	58,14 W	$\pm 0,90$ W
	$P_{diff,walls}$	1,44 W	$\pm 1,12$ W	1,68 W	$\pm 1,10$ W
	P_{comp}	1,27 W	$\pm 0,02$ W	2,96 W	$\pm 0,05$ W
	$P_{loss,DUT}$	62,18 W	$\pm 1,48$ W or $\pm 2,39\%$	62,79 W	$\pm 1,42$ W or $\pm 2,26\%$
	η_{calo}	97,27%	$\pm 0,51\%$	88,89%	$\pm 0,87\%$
	Measurement duration	8 h		4 h	

The uncertainty of the power loss determined with the direct method is 12,44 W for the first test and only 1,48 W when the calorimetric method is used. The uncertainty of the power loss with the direct method in the second test is 3,80 W and for the calorimetric result 1,42 W. It should be noticed that the uncertainty on the power loss determined by the calorimeter does not change much when the DUT is more efficient. On the other hand, the input–output method is more accurate when the DUT is less efficient, as can be seen in the results in Table 3 [1].

The difference in uncertainty on the efficiency between both methods is not that large because the input power is taken into account to calculate the efficiency value.

It should be noticed that the measurement duration of the calorimetric tests is much longer than when the input–output method is performed.

7 Conclusion

In this chapter a calorimeter test bench for the efficiency determination of power electronic variable speed drives is presented. This is an indirect balanced type with air as medium to test drives in a power range from 1 kW up to 7,5 kW. First, a short introduction into the international standard IEC 61800-9-2 [1] is given. Secondly, the calorimeter concept is explained according to the balanced type. The test bench setup is also shown and discussed. Next, a flowchart with the measurement procedure is proposed to obtain correct results. Afterwards a measurement uncertainty calculation is shown and at last two tests are executed on the 2,2 kW drive and their results are presented.

The overall goal of this chapter is to examine and optimize the calorimetric approach and to be able to obtain accurate results. The construction of a calorimeter is an intensive and difficult job. Compared to a power analyzer, it is cheaper in this power range but a lot of men hours are needed to finish such a construction.

The calorimetric approach is very time-consuming compared to the input–output measurements but this way of power loss determination is far more accurate when the power loss of a complete drive module is determined for IE classification compared to the direct approach. The calorimetric setup reaches a standard uncertainty of 2,39% or 1,48 W on the power loss while the direct method reaches 18,46% or 12,44 W during the same test on the same power loss. The accuracy of the calorimeter could even be increased when the heater would not be enabled during the main test.

It can be concluded that an uncertainty calculation for calorimetric measurements is not evident to execute because no standard method exists and comparing results with other publications is difficult. Therefore in this chapter a thorough uncertainty calculation is presented.

A disadvantage of this setup is the variation of the ambient temperature. The power leakage through the walls varies due to this problem. The solution is to control the ambient air but this is not done yet. In general, the variation of the thermal conditions creates the largest uncertainty. This can be solved by measuring the air properties accurately and by controlling the inlet temperature of the air.

References

1. Adjustable speed electrical power drive systems – Part 9–2: Ecodesign for power drive systems, motor starters, power electronics & their driven applications – Energy efficiency indicators for power drive systems and motor starters. Ed. 1. IEC 61800-2-9, March 2017

2. W. Cao, H. Zhang, G.M. Asher, X. Huang, I. French, J. Zhang, M. Short, Calorimeters and techniques used for power loss measurements in electrical machines. *IEEE Instrum. Meas. Mag.* **13**(6), 26–33 (2010)
3. A. Kosonen, L. Aarniovuori, J. Ahola, J. Backman, J. Pyrhönen, M. Niemelä, Loss definition of electric drives by a calorimetric system with data processing. *IEEE Trans. Ind. Electron.* **61**(8), 4432–4442 (Aug. 2014)
4. H. Kärkkäinen, L. Aarniovuori, M. Niemelä, J. Pyrhönen, Induction Motor Efficiency Verification Using a Balance-Type Calorimeter Equipped with a Mass Flow Meter, in 20th European Conference on Power Electronics and Applications (EPE'18 ECCE Europe), Riga, Latvia, Sept 2018
5. L. Aarniovuori, A. Kosonen, M. Niemelä, J. Pyrhönen, Calorimetric measurement of variable-speed induction motor, in 20th International conference on Electrical Machines (ICEM), Marseille, France, Sept 2012, pp. 870–876
6. L. Aarniovuori, H. Kärkkäinen, A. Kosonen, J. Pyrhönen, Z. Liu, W. Cao, Overview of calorimetric systems used in loss determination of electric motors and drives, in IECON 2017 – 43rd Annual Conference of the IEEE Industrial Electronics Society, Beijing, 2017, pp. 2110–2115
7. Joint Committee for Guides in Metrology, Evaluation of Measurement Data – Guide to the Expression of Uncertainty in Measurement (GUM), 2008
8. NIST, Uncertainty of Measurement Results, Dec. 2017, [Online], Available: <https://physics.nist.gov/cuu/Uncertainty/index.html>. Accessed 23 Apr 2018

Round Robin for Converter Losses: Uniform Testing Protocol and Results from Tests in Phase 1



Conrad U. Brunner, Emmanuel Agamloh, Andrew Baghurst,
Sandie B. Nielsen, and Andrea Vezzini

1 Electric Motor-Driven Systems: Efficiency

The complete Electric Motor-Driven System (EMDS) consists of the following four major elements:

- Motor control, such as switch gear, control gear and variable frequency converters (IEC 61800-9-2) [1].
- Electric motor (IEC 60034-2-1 [2], IEC 60034-30-1 [3]).
- Mechanical equipment, like belts and gears (respective ISO standards from TCs 41 and 60).
- Application, such as pumps fans and compressors (respective ISO standards from TCs 86, 117, 117, 118).

C. U. Brunner (✉)
Impact Energy Inc., Zurich, Switzerland
e-mail: cub@cub.ch

E. Agamloh
Advanced Energy, Raleigh, NC, USA
e-mail: eagamloh@advancedenergy.org

A. Baghurst
CalTest, Port Elliot, SA, Australia

S. B. Nielsen
Danish Technological Institute (DTI), Taastrup, Denmark
e-mail: sbn@dti.dk

A. Vezzini
Bern University of Applied Sciences (BFH), Bern, Switzerland
e-mail: andrea.vezzini@bfh.ch

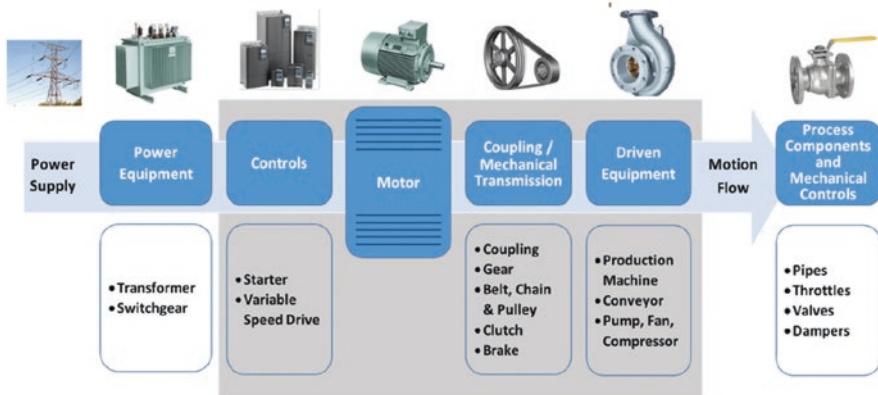


Fig. 1 The complete Electric Motor-Driven System. (Source: IEC TS draft 60034-31, edition 2, 2019)

In many applications, only the motor and the applications exist. The system energy efficiency of the EMDS is always the product of the efficiencies of the four component efficiencies (Fig. 1).

The need to change the fixed speed of an electric motor that is defined by its pole number, has existed for a long time. Many machines used mechanical or hydraulic means (gears, transmissions, etc. still used in automobile engines today) to adapt the motor speed to the necessary speed of the application and to easily accelerate. Also, early on, DC motors had the capacity to vary their speed, which was necessary for instance to start and accelerate an electric train.

The use of electronic VFCs based on pulse-width-modulation (PWM) are considered a major innovative element for energy savings in EMDS. The VFC has added to the EMDS the possibility of easily and continuously varying the rotating speed. Sensors for continuous measurement of the demand of the application (pressure, temperature, flow, etc.) can be used as an input signal to control the rotating speed of the application by varying the input frequency of the electric motor. Thus, process control can be adapted to the necessary load, acceleration and deceleration can be easily adjusted and the energy efficiency can be highly improved by reducing losses. The elimination of dampers and throttles that were used to mechanically reduce the flow pump systems makes for big savings both in installation cost and energy consumption.

A number of international manufacturers have expanded and perfected their portfolio with all types and sizes of VFCs.

2 Converter Losses

The use of a converter does have tremendous advantages. But it does not come for free:

- The VFC induces considerable added investment costs (roughly in the same order of magnitude as the motor of the same output size).
- The VFC has an added loss at nominal speed.
- The VFC also has considerable losses through reduced efficiency at part load at reduced speed and frequency.
- The electric motor efficiency is reduced due to the non-sinusoidal current and voltage delivered from the PWM power supply.

Thus, the use of VFCs in an application is always an optimization procedure that considers the added costs and the added energy losses vs. the lower energy use in the EMDS.

3 The Genesis of IEC 61800-9-2

Since the publication of the European ecodesign regulation no. 640 for electric motors [4] in 2009 that allows to also use IE2 plus VFC instead of a required IE3 motor, the discussion was launched to better understand VFC efficiencies.

One of the first data set of VFC efficiencies in full and part load was published by the US Department of Energy as part of their Tip Sheets in 2008 [5]. The first publication to specify a testing protocol and an efficiency classification for converters in IEC standards was published at EEMODS 2009 [6]. The need arose to define an efficiency classification similar to the motor IE code (IEC 60034-30-1 [3]). In order to speed up this process, the European Commission issued shortly after the regulation for motor efficiency in 2010 a mandate to Cenelec (M/476) [7] to define:

Procedures and methods for measuring the energy efficiency, efficiency classes, load and speed profiles and associated characteristics of variable speed drives and/or of Power Drive Systems (PDS) equipped with variable speed drives, as appropriate.

Contrary to the parallel issued EC mandate for electric motors (M/470 in 2010), which was immediately handed to IEC, CENELEC decided to keep the VFC mandate at the European level and to setup a working group to deal with it. In 2014 CENELEC published a first version of EN 50598-2 [10] that included an efficiency classification scheme and a calculation model for VFC losses. Subsequently, IEC took over and published a slightly improved version in IEC 61800-9-2, edition 1, in 2017.

The published standard contained a calculation method and a test method as well as reference losses for comparing and classifying VFCs into IE classes. The calculation method was criticized by industry experts as being arbitrary and not useful for other industrial programs, the test method was considered incomplete and not applicable for check testing by market surveillance authorities. The reference VFC losses were considered to be way too high compared to market products and arbitrarily set without a transparent scientific base.

In September 2017, an international group of experts met at EEMODS'17 in Rome and decided to setup a Round Robin Program to develop an improved test method and to provide statistically relevant data of converter losses. The group decided to cooperate both with the team of experts in IEC SC 22G WG18 and to agree on a management platform provided by 4E EMSA to secure independence and funding by the involved governments. The Australian, Danish, Swiss and US governments provided the majority of funding for the RR'C through their respective agencies.

4 Round Robin RR'C

The RR'C program is divided in two phases:

Phase 1

From November 2017 to the end of February 2019
phase 1 serves as a pilot phase of the RR'C with a small number of laboratories and converters to elaborate a testing method. The published final Report of the RR'C phase 1 is available at www.motorsystems.org.

Phase 2

From beginning of March 2019 to the end of 2020
phase 2 tries to provide sufficient evidence of a larger number of converters to serve as a basis to define reference losses and efficiency classes.

With the project management from EMSA (phase 1: Conrad U. Brunner, Impact Energy), the co-financing from the four EMSA member countries Australia (AU), Denmark (DK), Switzerland (CH) and USA, the following four independent motor testing laboratories have been involved in the definition of the UTP and the converter testing of RR'C phase 1 (see Fig. 2): Advanced Energy, CalTest, Danish Technological Institute (DTI) and Bern University of Applied Sciences (BFH).

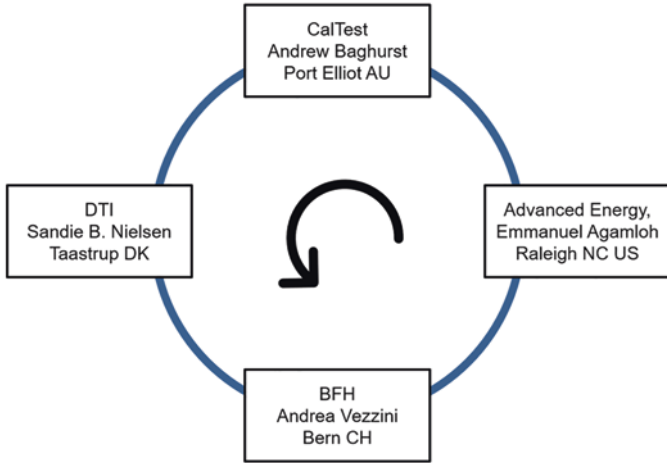


Fig. 2 The Round Robin circle with the four testing laboratories

5 The Uniform Testing Protocol (UTP)

The testing needed a much more clearly defined basis and procedural sequence as given in IEC 61800-9-2, edition 1. The nominal and the Zero load points got special attention. The 17 operating points (see Fig. 3) are spread over the entire field of frequency and current. They were chosen for this scientific exercise only (the number will eventually be reduced to the most important points). Tests at 50 Hz and 60 Hz, with 1-phase and 3-phase motors and using IE1, IE2 and IE3 motors were conducted. Also, the use of VFC auxiliaries, filters, cooling fans, cables, the setting of the converter “out-of-the-box”, etc. had to be defined in order to get highly repeatable results. It was also tested whether “any motor” could be used as a load for the tests, and whether motor size needed to precisely match converter output rating was important.

The choice of the 17 operating points has shown not to be feasible for currents below 50%. Therefore, the tables of results only show 100%/75%/minimum current values and therefore do not follow strictly the 17 points of the UTP.

The UTP test method is based on the idea that the VFC acts as a power source to the motor and there are three types of loss dependencies; namely loss which is load independent, loss which is proportional to load current, and loss which is proportional to load current squared. It is therefore possible to characterize total converter losses by means of a quadratic equation in load current, with the constant term representing standby losses (see Fig. 4).

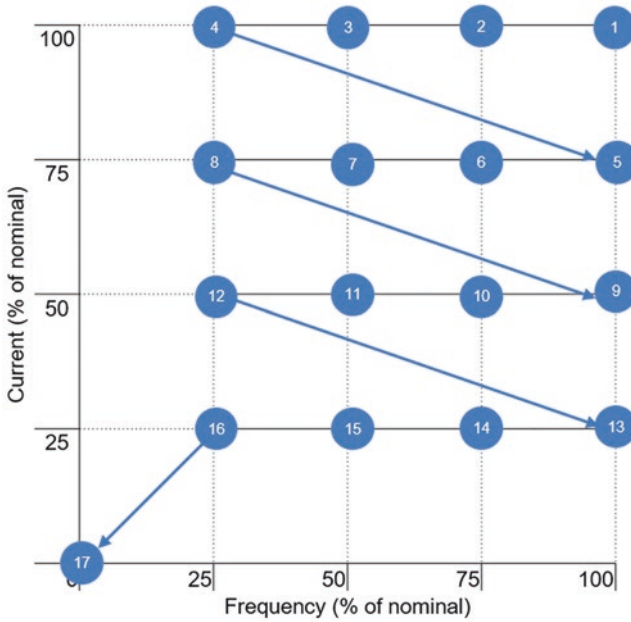


Fig. 3 17 operating points of the converter tests according to the UTP in phase 1

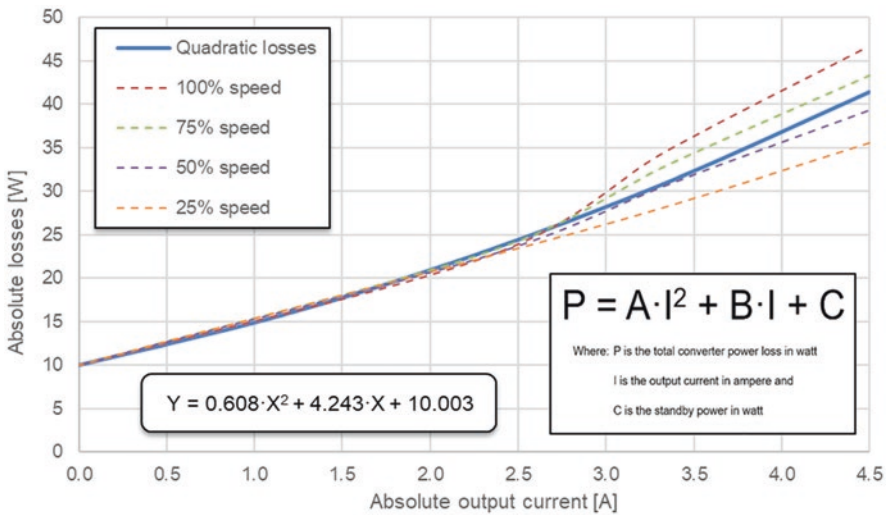


Fig. 4 Quadratic equation for curve fit of the relation between output current and losses

A Standard Reporting Format (SRF) was defined that included a data table and a quadratic curve fit (Fig. 5) to demonstrate the consistency of the test results and to allow the interpolation for any intermediary load point.

Converter tested: **650-21140010-0F0PR0-A1** Nominal current: **3,40**

Load Point		Supply			Output				Calculation	
Frequency % / 50 Hz	Current % rated	V (V)	I (A)	Power (W)	Flux V (V)	V _(rms) (V)	I (A)	Power (W)	Eta (%)	Losses (W)
100%	100%	230	7,51	1071	232	3,80	1034	96,6	36,5	
	75%	229	5,20	695	239	2,66	670	96,4	24,8	
	Min.	231	1,18	139	255	1,66	125	89,7	14,3	
75%	100%	231	6,01	825	212	3,40	793	96,1	32,2	
	75%	230	4,28	564	214	2,56	541	95,8	23,6	
	Min.	230	1,03	114	224	1,72	99	86,8	15,0	
50%	100%	231	4,44	591	174	3,49	561	95,0	29,6	
	75%	232	3,15	405	177	2,59	383	94,6	21,9	
	Min.	230	0,82	88	183	1,69	73	83,3	14,7	
25%	100%	231	2,40	309	122	3,48	283	91,4	26,5	
	75%	231	1,81	220	123	2,57	200	90,9	20,2	
	Min.	230	0,73	76	127	1,62	62	81,3	14,2	
0,0%		230	0,13	9	1	0,10	0	-0,5	9,0	
Stopped		230	0,10	4,6	0	0,00	0	0,0	4,6	

Resulting quadratic equation:

x^2	x^1	x^0	R^2
0,76	4,87	4,59	0,999

Example:

Amps
3,40

A² losses:
29,9 W

Fig. 5 Test results presented in table in Standard Reporting Format

Owner	Brand	Size [kW]	RR'C No.	CalTest	DTI	BFH	AE
Australia	ABB	1.1	01A	X	X	X	X
	ABB	11.0	01B	X			
Denmark	Schneider	2.2	02A		X	X	X
	Parker	0.75	02B		X	X	X
Switzerland	Lenze	5.5	03A	X		X	X
	ABB	5.5	03B	X		X	X
	ABB	2.2	03C			X	
USA	Schneider	2.2	04A	X	X		X
	Schneider	3.0	04B	X	X		X

Fig. 6 List of tested products and the testing laboratories

In the SRF, all test results were reported in data table in Fig. 5 that documents input and output, shows the efficiency (eta), the absolute losses (W) in four frequencies plus zero and stopped. It also calculates the parameters directly for the quadratic equation in Fig. 4.

6 Results from VFC Tests in RR'C Phase 1

The goal of the tests in phase 1 was to check the repeatability of the UTP method. The testing program in phase 1 included nine converters from 0.75 kW to 11 kW from four different manufacturers (see Fig. 6). A total of 58 tests were conducted by four independent laboratories, using 24 different load motors from 12 different manufacturers. The motors were in efficiency classes of IE1, IE2 and IE3. The tests were run at 50 Hz and 60 Hz line frequencies.

To further the knowledge on converter losses a number of special tests were also run to find out about the feasibility of the selected load motor by type, size, poles, efficiency class, etc. Some of these results (2-pole, larger size motors, etc.) showed higher deviations and some of these results were not included in the final compilation and evaluation of repeatability of the test results. However, the insights gained from those deviations helped to inform the criteria for selecting motors for phase 2.

A sample result table on a 2.2 kW 3-phase Schneider VFC comparing all nine tests conducted by three labs are shown in Fig. 7:

This converter was tested both at 3.91 A and 5.1 A nominal currents, using different load motors with IE1, IE2 and IE3 efficiency class. The colors indicate “red” higher and “green” lower losses or deviations from mean values. The losses at 4.6 A, the defined “nominal” output current corresponding to a standard 2.2 kW 4-pole motor, shows very good agreement.

The statistics at the 4.6 A load point are as follows:

Mean value: **52.4 W** with a standard deviation of **1.87 W**

The averaged efficiency of the converter at this operating point was measured to **98.0%**.

For reference it should be noted that the testing standard for converters IEC 61800-9-2, edition 1, has a suggested reference IE1 converter loss for a 3.3 kVA unit (2.2 kW informative) of 237 W. This would lead to a relative value of $52.4/237 \approx 0.22$. In the specific case with this converter, the reference becomes even higher. Considering the calculated rated apparent power of this converter which is, $S_R = \sqrt{3 \cdot U_R \cdot I_R} = 1.73 \cdot 460 \cdot 4.6 = 3.66$ kVA, the reference losses would then be 299 W, corresponding to a relative value of 0.18.

The compiled test results of all the 58 tests on the nine converters are shown in see Fig. 8.

For the sample of nine converters between 0.75 and 11 kW the losses range from 30 W to 221 W. The Standard Deviation is between 0.3 W and 4.3 W, which amounts to between 0.39% and 3.56%. Overall, the achieved repeatability is very good. With the more stringent definition of the load motor (IE2 or IE3, 4-pole), the results will be even better in the future.

	AE1	AE2	CalTest1	DT11	DT12	AE1	AE2	DT11	DT12		
	IE3	IE3	IE2	IE2	IE1	IE3	IE3	IE1	IE2		
Equations	-0.72	-0.74	-0.79	-0.96	-0.84	0.04	-0.27	-0.36	-0.31		
	13.50	13.65	13.58	13.88	13.49	10.44	11.32	11.87	11.65		
Absolute Current	6.73	6.77	5.80	5.67	5.60	6.68	6.74	5.61	5.57		
	1.00	1.00	1.00	1.00	1.00	1.00	1.00	1.00	1.00		
1.80	28.7	28.9	27.7	27.5	27.2	25.6	26.3	25.8	25.5	27.0 W	± 1.7 W
1.93	30.1	30.4	29.1	28.9	28.5	27.0	27.6	27.2	26.9	28.4 W	± 1.7 W
2.06	31.5	31.8	30.4	30.2	29.9	28.4	29.0	28.6	28.3	29.8 W	± 1.7 W
2.20	32.9	33.2	31.8	31.5	31.2	29.8	30.3	29.9	29.7	31.1 W	± 1.8 W
2.33	34.2	34.5	33.1	32.8	32.5	31.2	31.7	31.3	31.0	32.5 W	± 1.8 W
2.46	35.6	35.8	34.4	34.0	33.7	32.6	33.0	32.6	32.3	33.8 W	± 1.8 W
2.59	36.9	37.1	35.7	35.2	34.9	34.0	34.3	33.9	33.7	35.1 W	± 1.7 W
2.72	38.1	38.4	36.9	36.4	36.1	35.4	35.6	35.2	35.0	36.4 W	± 1.7 W
2.86	39.4	39.7	38.1	37.5	37.3	36.8	36.9	36.5	36.3	37.6 W	± 1.7 W
2.99	40.6	40.9	39.3	38.6	38.4	38.2	38.2	37.8	37.6	38.8 W	± 1.7 W
3.12	41.8	42.1	40.4	39.6	39.5	39.6	39.5	39.1	38.9	40.1 W	± 1.6 W
3.25	43.0	43.3	41.6	40.6	40.6	41.1	40.7	40.4	40.2	41.3 W	± 1.6 W
3.38	44.2	44.4	42.6	41.6	41.6	42.5	42.0	41.6	41.4	42.4 W	± 1.5 W
3.51	45.3	45.6	43.7	42.6	42.7	43.9	43.2	42.8	42.7	43.6 W	± 1.5 W
3.65	46.4	46.7	44.8	43.5	43.6	45.3	44.5	44.1	43.9	44.7 W	± 1.6 W
3.78	47.5	47.7	45.8	44.4	44.6	46.7	45.7	45.3	45.1	45.9 W	± 1.7 W
3.91	48.5	48.8	46.8	45.3	45.5	48.1	46.9	46.5	46.4	47.0 W	± 1.8 W
4.00	49.2	49.5	47.4	45.8	46.1	49.1	47.8	47.3	47.2	47.7 W	± 1.8 W
4.30	51.5	51.7	49.5	47.6	48.1	52.3	50.5	49.9	49.9	50.1 W	± 2.4 W
4.60	53.6	53.8	51.5	49.2	49.9	55.6	53.2	52.5	52.6	52.4 W	± 3.2 W
4.90	55.6	55.8	53.3	50.6	51.6	58.8	55.8	55.1	55.2	54.6 W	± 4.1 W
5.20	57.5	57.6	55.0	51.9	53.1	62.1	58.4	57.5	57.7	56.8 W	± 5.1 W

Fig. 7 Collected results of converter No. 04A – Schneider 2.2 kW

Brand	Size [kW]	RR'C No.	Supp.	UTP rated		Span [W]	Max [W]	Min [W]	Std. dev. [W]	% of mean
				Current [A]	Loss [W]					
Parker	0,75	02B	1 ph	3,40	30,3	± 0,5	30,9	29,9	0,3	1,08%
ABB	1,10	01A	1 ph	4,50	41,6	± 0,8	42,4	40,8	0,5	1,23%
Schneider	2,20	04A	3 ph	4,60	52,4	± 3,2	55,6	49,2	1,9	3,56%
Schneider	2,20	02A	3 ph	4,75	57,4	± 1,6	58,9	55,6	1,2	2,04%
ABB	2,20	03C	3 ph	4,90	63,1	± 1,3	64,0	61,4	1,2	1,84%
Schneider	3,00	04B	3 ph	8,65	58,1	± 0,8	59,1	57,5	0,6	0,97%
Lenze	5,50	03A	3 ph	12,00	124,3	± 0,7	125,0	123,7	0,5	0,39%
ABB	5,50	03B	3 ph	12,00	126,2	± 6,3	130,8	118,3	4,3	3,39%
ABB	11,00	01B	3 ph	21,40	220,9	± 1,0	221,9	219,9	0,9	0,39%

Fig. 8 List of aggregated results of all tests

The key results of the RR'C tests in phase 1 show:

- The UTP is a valuable test method that returns highly repeatable results from tests in different laboratories.
- It was shown that selection of the load motor has some sensitivity with respect to power rating and number of poles, whereas manufacturer and efficiency class are less important. Based on this finding, it is suggested that load motors must be (kW) sized to the converter in question and fulfill energy class IE2 or IE3. All load motors must be 4-pole asynchronous motors.
- The tests can be equally conducted at 50 Hz and 60 Hz fundamental frequency without any impact on the losses.

- High-precision measuring instruments from at least two different manufacturers have been used without any influence on the results.
- In the tested group of nine converters from 0.75 kW to 11 kW, the maximum span between minimum and maximum loss at full load was between 0.5 W and 6.3 W. The relative span was between 0.39% and 3.56%. The standard deviation was between 0.3 W and 1.9 W.
- The measured converter losses were all less than one-third of the reference losses of IE1 in IEC 61800-9-2, edition 1.

7 Recommendations and Conclusions

The recommendations for the improvement of the converter testing method for phase 2 include the following:

- The nominal and rated output current in ampere of any converter must be clearly defined. A solution has been introduced to use the reference output current in the standard.
- The converters can be tested with any asynchronous motor to return reasonable results. But it is recommended to use IE2 or IE3 and only 4-pole motors of the same nominal rating as the converter to keep repeatability of the test results high.
- The no load/off point must be precisely defined to return repeatable results. Auxiliaries like fans can distort the measured results.
- So far, the 17 operating points have been chosen because of the scientific necessity to have the measurements covering the entire operating field. The necessary operating points for the tests will be reappraised for practical reasons to be required in IEC 61800-9-2, edition 2. In RR'C phase 2, only 13 operating points will be used.
- For phase 2 of the RR'C it is recommended to include converters with all typical accessories, filters, 4Q, etc. to evaluate the influence of these factors on the losses. Matrix converters shall also be included.
- The comparison of losses and performance in basic drive modules and in complete drive modules (including auxiliaries) shall be more clearly distinguished in phase 2.

And, the cooperation between IEC SC 22G WG 18 and 4E EMSA proved to be both inspiring and productive and will be continued in RR'C phase 2.

References

1. IEC 61800-9-2, edition 1: Adjustable speed electrical power drive systems – Part 9-2: Ecodesign for power drive systems, motor starters, power electronics and their driven applications – Energy efficiency indicators for power drive systems and motor starters, Geneva, Switzerland, 2017

2. IEC 60034-2-1, edition 2: Rotating electrical machines – Part 2–1: Standard methods for determining losses and efficiency from tests (excluding machines for traction vehicles), Geneva, Switzerland, 2014
3. IEC 60034-30-1, edition 1: Rotating electrical machines – Part 30–1: Efficiency classes of line operated AC motors (IE code), Geneva, Switzerland, 2014
4. European Commission (EC), Commission Regulation No. 640/2009 of 22 July 2009 implementing Directive 2005/32/EC of the European Parliament and of the Council with regard to ecodesign requirements for electric motors, Brussels, Belgium, 2009
5. U.S. Department of Energy, Advanced Manufacturing Office, Motor Systems Tip Sheet #11, Adjustable Speed Drive, Part-Load Efficiency, Washington DC, USA, 2008 (edition 1), 2012 (edition 2)
6. A.T. de Almeida, P. Angers, C.U. Brunner, M. Doppelbauer, Motors with Adjustable Speed Drives: Testing Protocol and Efficiency Standard, in Conference proceedings EEMODS'09, Nantes, France, 2009
7. European Commission, Mandate M/476 CENELEC for Standardisation in the field of variable speed drives and/or Power Drive System products, Brussels, Belgium 2010
8. E. Agamloh, A. Baghurst, C.U. Brunner, S.B. Nielsen, A. Vezzini, EMSA IEC WG 18, Round Robin of Converter Losses, Report of Results of Phase 1, Zurich, Switzerland, March 2019. Available at: www.motorsystems.org
9. S.B. Nielsen, A. Vezzini, Preliminary results from (RR'C) round robin for converter losses, phase 2, in EEMODS'19 conference proceedings, Tokyo, Japan, 2019
10. CENELEC EN 50598-2, Ecodesign for power drive systems, motor starters, power electronics & their driven applications – Part 2: Energy efficiency indicators for power drive systems and motor starters, Brussels, Belgium, 2014. (withdrawn)

Preliminary Results from RR'C 2: Round Robin for Converter Losses, Phase 2



Andrea Vezzini and Sandie B. Nielsen

1 Goal

The main goals of an international Round Robin test (RR'C) for converters are:

- The test method described in IEC 61800-9-2:2017 [1] (edition 1) for converters (and in IEC TS 60034-2-1:2013 [2] for motors driven by converters) have not been used for sufficient time to know their accuracy and repeatability.
 - Clarify and verify test method.
- The test laboratories around the world using this test method are not yet familiar with it.
 - Check laboratory performance.
- The performance of the converters and their losses need to be verified vs. the catalogue data.
 - Provide scientifically based and documented evidence.
- Different products from different manufacturers need to be tested as to defining the reference and IE1/IE2 or eventual higher levels.
 - Clarify spread of product performance by different manufacturers.

A. Vezzini (✉)
Bern University of Applied Sciences, Bern, Switzerland
e-mail: andrea.vezzini@bfh.ch

S. B. Nielsen
Danish Technological Institute, Taastrup, Denmark
e-mail: sbn@dti.dk

The results of the Round Robin test will build the key evidence for the revision of IEC 61800-9-2 ed. 2, especially the design of an updated and solid testing procedure, which in the current version is often referred to as being vague and ambiguous, and also the provision of sufficient solid and impartial measured background data for a potential correction of the current level of the reference values for losses inside converters

2 Organization

The organization of RR'C in Phase 2 profits from the near completion of Phase 1 where a vast body of evidence was gathered by four international testing laboratories (Advanced Energy/USA, CalTest/Australia, DTI/Denmark and BFH/Switzerland). We thank the four involved laboratories for their work and the governments of the USA, Australia, Denmark and Switzerland for providing the necessary funding.

The RR'C Task Force and its leadership from 4E EMSA, IEC SC 22G WG18 and industry has been selected and mandated at the EEMODS'17 meeting in Rome on 6 September 2017. The cooperation between IEC WG18 and 4E EMSA has been clarified at the IEC WG18 meeting on 26–28 February 2018 in Tampa, FL, the USA.

The setup looks like the following:

- Project management from the 4E EMSA group.
- Advisory group consisting of representatives from independent laboratories worldwide.
- Steering committee from 4E EMSA management and Swiss representative.
- Industry contact group consisting of representatives from the largest manufacturers.

3 Preparation

The RR'C workshop on 13 November 2018 at the Motor Summit in Zurich has served as a first opportunity for an intermediate report on the results of the RR'C Phase 1 and the clarification of the plan for Phase 2. Also, the IEC SC 22G WG18 meeting on 18–22 February 2019 in Australia served both for the final reporting of the results of the RR'C Phase 1 and the launch of RR'C Phase 2. The timeline of Phase 2 has already been synchronized with the preparation of IEC 61800-9-2, edition 2. The preparation phase for RR'C Phase 2 included the following tasks:

- Product definition and selection to include a representative sample of typical converter types, sizes, frequencies and phases, etc. The goal is to select enough products in the entire range of 0.12 kW up to 1000 kW to get the necessary information on reviewing the reference losses and the IE-classes.

- Workshop regarding organizational issues as well as testing procedures (UTP).
- Discussion with IEC WG18 to include the results in IEC 61800-9-2, edition 2 (next WG18 meeting in February 2019 in Australia).

4 Phase 2

Phase 2 includes the following tasks:

- Setup phase 2 (collect converter data and planning of testing schedule).
- Full converter testing campaign in about 10–12 testing labs with some 60–80 products based on the UTP, edition 2.
- Analysis and report of the results.
- Publication of results.

The bulk of the testing work in Phase 2 will be between spring of 2019 and summer of 2020. After that, the evaluation and reporting in the fall of 2020 will take the rest of the program's time. For budgetary reasons the testing might be continued in 2021.

5 Timeline

1 May 2019 – 31 December 2020 (full testing phase)

- Phase 2: start March 2019.
- Phase 2: final report to EMSA/WG18 October 2020.
- Phase 2: results dissemination December 2020.

6 Test Laboratories in Phase 2

A group of independent test laboratories, qualified for converter tests, have been selected to be invited to participate in Phase 2. As a result of a questionnaire, sent to all labs in August 2018, there is positive responses by 18 September 2018 for the participation in the Round Robin Phase 2 from the following seven laboratories (details see Annex 1):

- Canada.
 - Hydro Quebec, Laboratoire des Technologies de l'Énergie, Shawinigan, Québec.

- China.
 - China National Center for Quality Supervision and Test of Electrical Control and Distribution Equipment, Tianjin City.
- Denmark.
 - Danish Technological Institute (DTI), Aarhus.
- Germany.
 - Karlsruhe Institute for Technology (KIT).
- Japan.
 - Fuji Electric Co., Ltd., Suzuka-shi, Mie.
- Switzerland.
 - Bern University of Applied Sciences (BFH), Biel.
- USA.
 - Advanced Energy, Raleigh NC.
- Australia.
 - CalTest, Port Elliot SA 5212.

We have also invited four industry laboratories that are capable of testing their own large size converters on the factory site (200–1000 kW) according to the UTP. So far, we have positive responses to participate in stationary tests with an expert of the Task Force attending from:

- Denmark.
 - Danfoss Drives, Graasten.
- USA.
 - Rockwell, Mequon, Wisconsin, USA.

Currently pending are the responses and the details of the cooperation from ABB and Siemens to participate in the stationary tests for large converters.

7 Product Selection

The product selection will be decided by the following criteria:

- Converter type: hardware and software.
- Grid feeding phases, frequency.
- Converter power range, general purpose products.
- Number of relevant manufacturers.

- Number of products per size.

Phase 2 includes a total of circa 60–80 converters in the power range of from 0.12–1000 kW from 5 to 8 manufacturers to form a representative sample of converters used in the global market for motor driven units (Table 1).

The total number of products to be tested is dependent on the availability of the products, the capability of the test laboratories, the cost and available resources to cover the cost. The four classes of converter sizes are chosen to reflect the power and the market share of the respective groups.

The estimate is for about a minimum of 60 converters between 0.12 and 1000 kW to be tested and evaluated in about 6 to 8 countries and their respective independent laboratories plus some industry laboratories. The converter sizes will be distributed between the labs according to their available capacity and testing equipment (see Fig. 1). This table will be updated once the feedback of the participating labs has been consolidated.

In order to satisfy the rules of a Round Robin (and to save money and time) the current plan is not to have all products go through tests in all the seven labs. All products between 0.12 kW and 110 kW (around 50) are to be tested normally by three labs. A total of circa 160 tests are anticipated (circa 15–25 tests per lab) (Fig. 2).

To have the necessary testing capacity, which only few manufacturers have (and to also save time and money), the test of these bigger machines is not following the formal Round Robin rules, but they will be tested only stationary at the manufacturer’s testing lab.

Currently, for the testing of larger machines between 200 kW and 1000 kW (maybe a total of 6–8), the involvement of Danfoss and Rockwell is confirmed, the discussion is ongoing with ABB. The RR'C project management will send one of the independent laboratory testing engineers as auditor to monitor these tests and to make sure that they are executed according to the Uniform Testing Protocol of the RR'C.

Separately, a batch of promised additional industry test results following the UTP will be used to gain statistical evidence.

Table 1 Proposed minimum selection of converters for tests, by size (preliminary)

RR'C	Converter tests	Output power range		Number of products under test
		from [kW]	to [kW]	
Budget Phase 2 Details by size	Products size			
1	Small	0.12	5	18
2	Medium	11	30	21
3	Large	37	110	15
4	Very large	200	1000	6
	Total (average)			60

Available converter testing capacity											
RR'C Phase 2	Round Robin (small and intermediate machines)							Stationary tests (large machines)			All
Output power (kW)	1	2	3	4	5	6	7	8	9	10	
	TRIED, CN	DTI, DK	BFH, CH	Advanced Energy, USA	Hydro Québec, CA	Fuji Electric, JP	KIT, GE	Danfoss, DK	ABB, FI	Rockwell, USA	
	CHAI Qing	Sandie B. Nielsen	Andrea Vezzini	Emmanuel Agamloh	Pierre Angers	Ikuya Sato	Alexander Stahl	Norbert Hanigovszki	Henri Kinnunen	Jiangang Hu	Total (Labs)
0.12 to <0.18											3
0.18 to <0.25											3
0.25 to <0.37											4
0.37 to <0.56											5
0.56 to <0.75											6
0.75 to <1.1											6
1.1 to <1.5											8
1.5 to <2.2											8
2.2 to <3.7											8
3.7 to <5.5											8
5.5 to <7.5											8
7.5 to <11											8
11 to <15											8
15 to <18.5											8
18.5 to <22											8
22 to <30											7
30 to <37											7
37 to <45											7
45 to <56											5
56 to <75											5
75 to <90											4
90 to <110											4
110 to <150									pending		3
150 to <185											3
185 to <220											1
220 to <250											1
250 to <375											1
375 to 1000											1
Number of products	10	?	20	20	5	17	5	4	?	3	84

Fig. 1 Testing capacity: Converter size (results from questionnaire, September 2018)

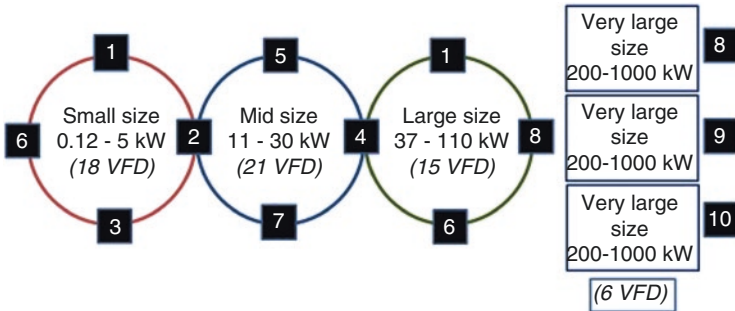


Fig. 2 Four subgroups of laboratories for the Round Robin

8 Uniform Testing Protocol (UTP)

8.1 Background

To speed up and to reach early convergence, the advisory group is charged with the design of a complementary Uniform Testing protocol, which includes all current knowledge for improvement. It will include among others:

- Choice of requirements of load motor. Testing with IE2 or IE3 load motor.

- Timing and sequence of tests on x operating points in partial speed and torque.
- Necessary accuracy of measurement instruments for electric input and output of the.
- Converter and the mechanical output of the load motor.
- Standby and control losses.
- Testing in 50 Hz and 60 Hz grids under the respective nominal voltage.
- PWM frequency of converter under test applied.

8.2 Test Program

The test program according to the UTP must be defined (coordinate with IEC WG18 and IEC WG28):

- Selection of load motor(s).
- Measurement of losses at defined operating points and in standby.
- Number of tests per converter at each location.

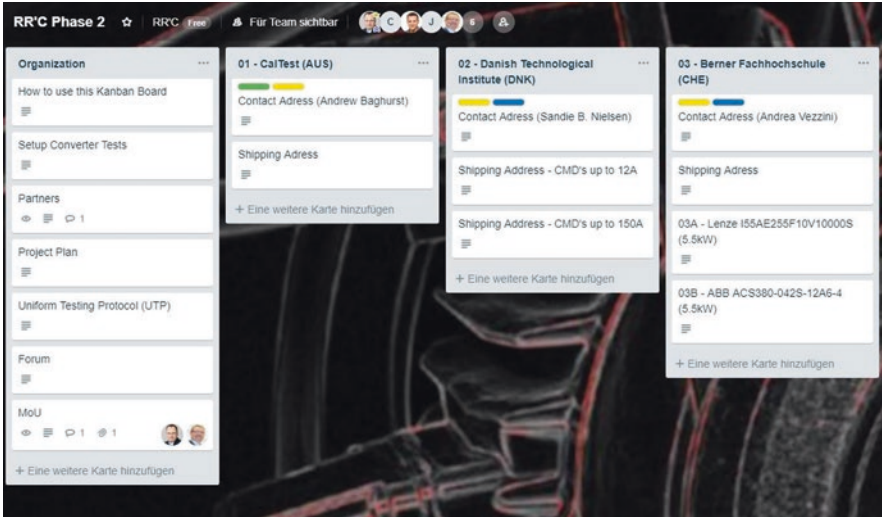
9 Management and Collaboration Tool

Phase 2 will be coordinated with the help of Trello.

Trello is an online collaboration tool that organizes your projects into boards. In one glance, Trello tells you what's being worked on, who's working on what, and where something is in process.

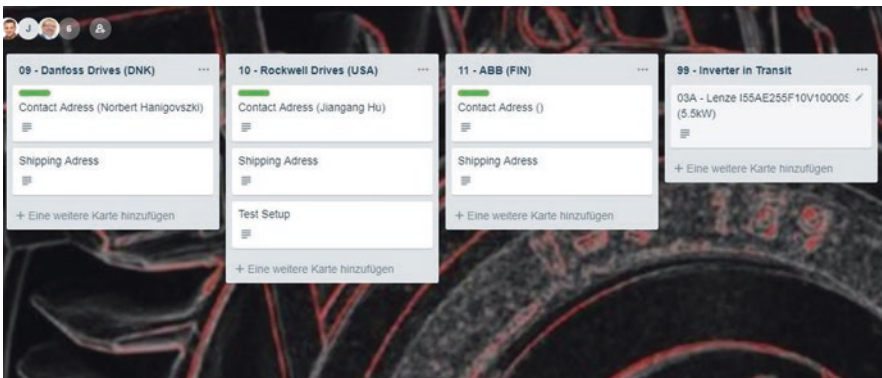
Trello can be compared with a white board, filled with lists of sticky notes, with each note representing one of the devices under test. Each of those sticky notes (DUTs) has photos, attachments from other data sources, documents and a place to comment and collaborate with other team members.

The lists are representing the current position of the DUTs. This can be either in a laboratory or in transit.



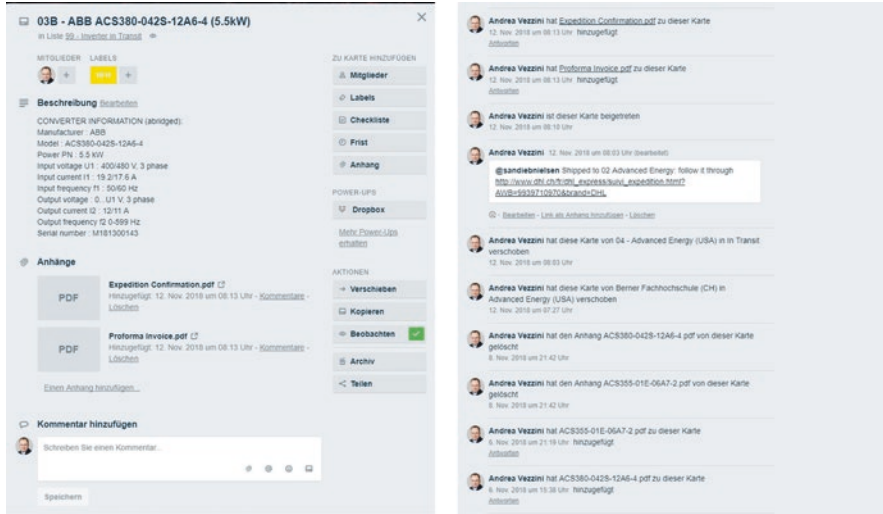
Part of the Trello whiteboard shows that the inverters Nr. 03A and 03B are currently at Berner Fachhochschule. Details about the contact person and the shipping address are also attached to the same list.

Once the tests at Bern University of Applied Sciences have been finished, the inverters are shipped to the next lab and the sticky note is moved to the new list called “99 – Inverter in transit”.



Special list where all the DUTs currently shipping (in transit) are placed. This allows to track the status of the shipping

Additionally, the shipping documents as well as the expedition confirmation are attached to the note as seen on the next picture. This allows the receiving laboratory to check how long the shipment will take and prepare the reception of the DUTs



In this example BFH has directly addressed DTI (by using the identifier @sandiebnielsen) to give a link where the shipment can be tracked.

An introduction to Trello has been given during the workshop at the next WG18 meeting in February 2019 in Australia).

10 Results and Evaluation

The RR'C Task leader decides on the program and timeline in detail. They prescribe an Excel data sheet to be filed for every test of every product. The data are accumulated, verified (plausibility check), evaluated and described in a report (anonymous manufacturers). A fully transparent documentation will be made and available for the laboratories, manufacturers, the IEC WG18- and EMSA-members involved. A short report with the key results will be made publicly available.

11 Cost and Financing

The cost of the RR'C consists of the following components:

- Converters: acquisition of the products for tests.
- Shipment of products between the test labs.
- Testing work at each lab.
- Project management, evaluation, reporting and publication.

The financing is based on the following concept of burden sharing:

- The manufacturers of the converters to be tested and the necessary motors for the test are invited to provide their products free of charge (leasing agreement or with a discount) for the RR'C.
- The governments, hosting the testing and research laboratories, are invited to carry the testing costs in their nationally assigned independent laboratories and the shipment costs. The industry labs involved are invited to provide their work as in-kind contribution to the RR'C.
- EMSA and its member countries are invited to share the cost of the project management, the evaluation, the reporting to EMSA and IEC WG18 and the publication.

The final plan for RR'C Phase 2 has been discussed at the EMSA meeting in Zurich on 12/13 November 2018 and at the RR'C workshop on 13 November 2018. The RR'C 2 was confirmed in February 2019 at the IEC WG18 meeting in Melbourne, Australia.

References

1. IEC 61800-9-2, edition 1, Adjustable speed electrical power drive systems – Part 9–2: Ecodesign for power drive systems, motor starters, power electronics and their driven applications – Energy efficiency indicators for power drive systems and motor starters, Geneva, Switzerland, 2017
2. IEC 60034-2-1, edition 2, Rotating electrical machines – Part 2–1: Standard methods for determining losses and efficiency from tests (excluding machines for traction vehicles), Geneva, Switzerland, 2014

Embedded Estimation of Variable Speed Drive Input Current Distortion



Thomas Devos and François Malrait

1 Introduction

The Total Harmonic Distortion (THD) of the drive input current is an indicator of the EMC and of the efficiency of the drive. Different standards refer to this indicator or to another one: the Total Harmonic Current (THC), for electromagnetic compatibility, which is defined at nominal set point. But with variable speed drives, the application can work at different operating speed and load torque points (some operating points are defined in [3]). Moreover, for robustness consideration, the system (drive, motor) can be oversized. In this context, it is necessary to consider the THDI not only at nominal drive power but also in different areas of the speed/torque map.

By calculating the THD of the input drive current online, the drive gives an additional information to the customer. It could be done with extra input current measurements (which increase the cost of the product) or without addition of sensors, by the knowledge of the drive topology model, component values and motor set point. Different DC bus topologies exist for the drives, which can be active (Electronic Smooth Inductance) or passive (DC choke or C-less for example), and the evolution of the THDI for the same power can be drastically different according to the topology of the drive.

In first step, a reminder of the different definitions and the description of the different DC bus topologies is done. Then, the estimation of the THD is presented, first with the global system view and then the analysis of the inputs signals of the DC bus model. The study of the dynamic model of the DC bus is performed to calculate the stability conditions. These conditions define an area in the speed / torque map where the THD estimator analysis is valid. Simulations are done on the comparison of the different drive DC bus topologies chosen (DC choke, ESI and C-less) at two

T. Devos (✉) · F. Malrait

Industrial Automation Business, Schneider-Electric, Pacy-sur-Eure, France
e-mail: thomas.devos@se.com; francois.malrait@se.com

different operating points corresponding to 100% and 25% of the nominal drive power. To finish, the complete harmonic calculation is done in the frequency domain considering the continuous mode (current of the DC choke always positive) and the stability of the DC bus model is studied. A proposition of a simplified THDI estimator working both in continuous or discontinuous mode is done, with accuracy below 2% in continuous mode corresponding on the normal operation of the drive.

2 Definition and Measures

2.1 Total Harmonic Current and Total Harmonic Distortion

The standard IEC 61000-3-12 [2] on electromagnetic compatibility defines the limits for harmonic currents produced by equipment connected to public low-voltage systems with input current $>16\text{A}$ and $\leq 75\text{A}$ per phase. It gives global limitations on THC and PWHC, and also limitations on each current harmonic.

The standard IEC61800-3 [1] is dedicated to EMC requirements and specific test methods for adjustable speed electrical power drive systems.

The test conditions and electromagnetic compatibility vocabulary are described respectively in standard IEC 61000-4-7 and 60050 (chapter 161).

One of the performance indicators of the standard 61000-3-12 [2] is the total harmonic current on the drive input current for harmonic mitigation. THC also has an impact on the energy efficiency on the drive input with possible additional losses.

The total harmonic current is defined as $\text{THC} = \sqrt{\sum_{n=2}^{40} I_n^2}$. The different limits are defined according to a reference current whose determination is also described in the standard.

The total harmonic distortion is described in IEC 61800-3 and calculated by:

$$\text{THD} = \sqrt{\sum_{n=2}^{40} \left(\frac{I_n}{I_1} \right)^2}$$

where I_i represents the magnitude of i th harmonic, referenced to the mains frequency. These both indicators are linked by a ratio dependent on the reference current chosen compared to the value of the fundamental frequency.

2.2 Drive Topologies

In this section, three different drive topologies of DC bus are described:

- DC choke.
- C-less.
- Electronic smooth inductance (ESI).

The drive is composed of three power conversion elements, which can be seen in Fig. 1:

- The rectifier (AC/DC converter).
- The DC bus (DC/DC converter).
- The inverter (DC/AC converter).

In this chapter, only the diode or thyristor bridge is considered for the rectifier.

The three different DC/DC converter topologies are described in Fig. 2. The DC choke and C-less topologies are modelling with same schema (Fig. 2a), but with different values of components. The schema of the ESI (Electronic Smooth Inductance) is shown on Fig. 2b.

Simulations are performed on a 7.5 kW/400 V drive and motor. The values of inductances and resistances used for the mains are defined in Table 1. The values of the DC/DC converters parameters are defined in Table 2.

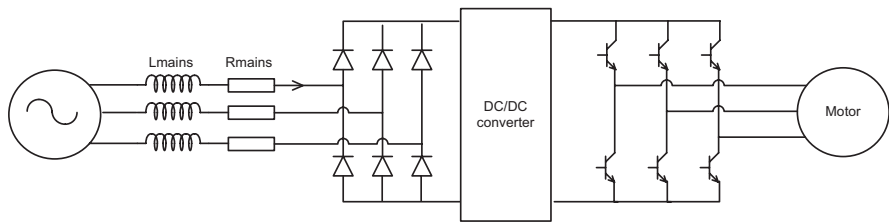


Fig. 1 Drive schematic

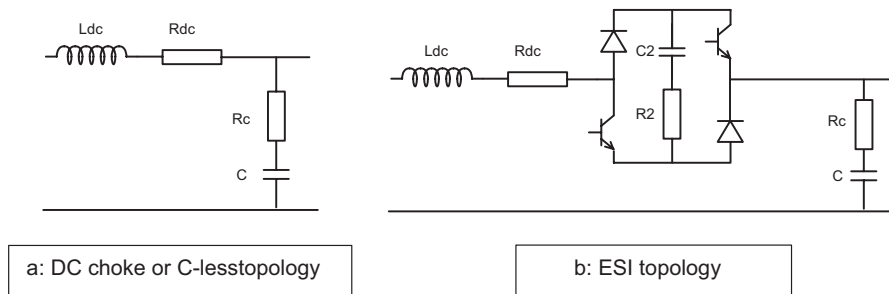


Fig. 2 DC/DC converters topology

Table 1 Component values of mains

Lmains	Rmains
50 μH	7 $\text{m}\Omega$

Table 2 Component values of DC/DC converter

Topology	Ldc	Rdc	C	Rc
DC choke	3.19 mH	155 $\text{m}\Omega$	1000 μF	113 $\text{m}\Omega$
C-less	1 μH	1 $\mu\Omega$	66 μF	100 $\text{m}\Omega$
ESI	300 μH	53 $\text{m}\Omega$	390 μF	40 $\text{m}\Omega$

3 Estimation

In this part, we present the total harmonic distortion calculation and estimation. We focus first on power systems models, with a special attention on its input/output representation. Secondly, we show results in simulation how the THD changes according to operating point. We end this part by presenting a model usable to estimate THD.

3.1 System View

We consider a power system view of Drive interfacing mains supply voltage and electric motor. We identify three sub-systems (Fig. 3)

- Rectifier,
 - Input: DC current, mains supply voltages.
 - Output: Rectifier voltage, mains supply currents.
- DC/DC ‘filtering’ converter.
 - Input: Rectifier voltage, DC bus current.
 - Output: DC current, DC bus voltage.
- Inverter.
 - Input: DC bus voltage, Motor currents.
 - Output: DC bus current, Motor voltages.

We focus on DC/DC filtering converter dynamic models. To do so, we start by a functional modelling of rectifier, and the rectifier voltage V_r in particular. Then, we focus on functional modelling of inverter, and the DC bus current I_o in particular.

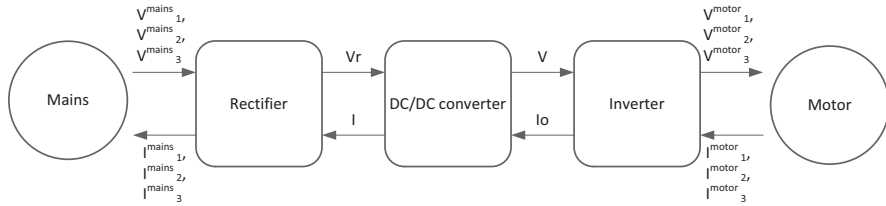


Fig. 3 System view

3.2 Rectifier and Input Voltage V_r

The voltage V_r depends on the mains and the DC current I . If the DC current is zero, the diode rectifier is going in blocking state. The input voltage V_r is no more linked to the mains and is equal to DC bus voltage. When the voltage V_r becomes higher than mains voltage, diodes are switched on. This is called the continuous case, i.e. the current I is positive. In this case, V_r can be calculated from the input voltages. It corresponds to

$$V_r(t) = \max(V_1(t), V_2(t), V_3(t)) - \min(V_1(t), V_2(t), V_3(t))$$

With V_i the voltages $V_i(t) = V_{\text{mains}} \cos\left(\omega_0 t - \frac{(i-1)2\pi}{3} + \frac{\pi}{6}\right)$, $i = 1, 2, 3$, the signal $V_r(t)$ can be expressed as:

$$V_r(t) = \sqrt{3} \cdot V_{\text{mains}} \cdot (\cos(\omega_0 t) f(t)) * p(t)$$

Where $f(t)$ is a rectangular window of width $\frac{T}{6} = \frac{\pi}{3\omega_0}$ (T period of the input voltages) and $p(t)$ is an impulse train of period $\frac{T}{6}$.

The Fourier transform of the rectangular window of width $T/6$ is $F(j\omega) = \frac{2 \sin\left(\frac{\pi\omega}{6\omega_0}\right)}{\omega}$, and the transform of the impulse train of period $T/6$ is $P(j\omega) = \frac{6\omega_0}{2\pi} \sum_k \delta(\omega - 6k\omega_0)$.

Based on previous formula, we can write V_r as:

$$V_r(j\omega) = \sum_k \hat{v}_k \delta(\omega - 6k\omega_0)$$

With Fourier coefficients

$$\hat{v}_k = \sqrt{3}V_{\text{mains}} \frac{6\omega_0}{2\pi} \left(\frac{\sin\left(\frac{(6k-1)\pi}{6}\right)}{(6k-1)\omega_0} + \frac{\sin\left(\frac{(6k+1)\pi}{6}\right)}{(6k+1)\omega_0} \right)$$

Which can be simplified by: $\hat{v}_k = \sqrt{3}V_{\text{mains}} \frac{3\omega_0}{\pi} \left(\frac{(-1)^{k+1}}{36k^2 - 1} \right)$

The mains currents are expressed accordingly to the switch on diode. Let us define *u* the index (1–3, or) of the maximum of ($V_1(t)$, $V_2(t)$, $V_3(t)$) and *d* the index (1–3, or) of the minimum of ($V_1(t)$, $V_2(t)$, $V_3(t)$). When the system is in the continuous case, I_u is equal to DC current I , and I_d is equal to $-I$. When the system is in discontinuous case, the mains currents are equal to 0.

3.3 Inverter and Output Current I_o

The current I_o of the DC bus is coming from the inverter. The motor voltages are generated by the inverter with pulse width modulation (Fig. 4).

From a reference voltage V_k^{motoref} , we calculate a modulating ratio $\alpha_k = \frac{2V_k^{\text{motoref}}}{V}$ that is compared to a special triangular signal to generate real voltage. Let us define $h(t)$ the inverse triangle starting from 1, decreasing up to -1 at $\frac{T_{\text{pwm}}}{2}$ and increasing again from $\frac{T_{\text{pwm}}}{2}$ up to T_{pwm} . The real motor voltage may be expressed as $V_k^{\text{motor}} = \text{sign}(\alpha_k - h(t)) \frac{V}{2}$.

We have to consider that if $\text{sign}(\alpha_k - h(t))$ is equal to 1 then the current is going through top DC bus phase (no current from this phase goes to bottom DC bus phase), and if $\text{sign}(\alpha_k - h(t))$ is equal to -1 then the current is going through bottom DC bus phase (no current from this phase goes to up DC bus phase).

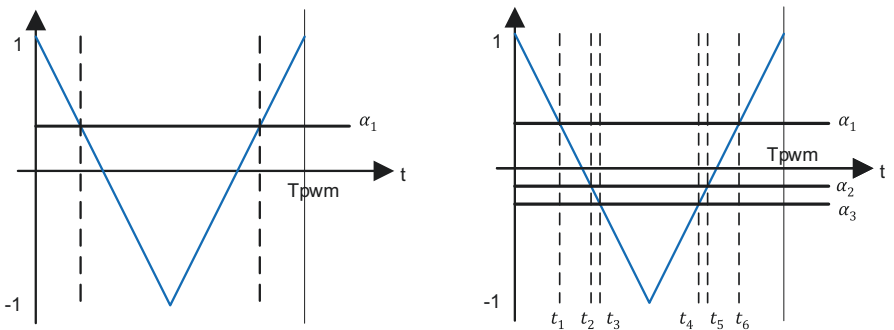


Fig. 4 PWM generation

For top DC bus phase, we get:

$$\begin{aligned}
 I_o &= \sum_{k=1}^3 \frac{1 + \text{sign}(\alpha_k - h(t))}{2} I_{\text{mot } k} \\
 &= \frac{1}{2} \sum_{k=1}^3 \text{sign}(\alpha_k - h(t)) I_{\text{mot } k}
 \end{aligned}$$

For bottom DC bus phase, we get:

$$\begin{aligned}
 I_o &= -\sum_{k=1}^3 \frac{1 - \text{sign}(\alpha_k - h(t))}{2} I_{\text{mot } k} \\
 &= \frac{1}{2} \sum_{k=1}^3 \text{sign}(\alpha_k - h(t)) I_{\text{mot } k}
 \end{aligned}$$

Another way to get this result is to write the equilibrium of power within inverter converter:

$$\begin{aligned}
 VI_o &= \sum_{k=1}^3 V_k^{\text{motor}} I_k^{\text{motor}} \\
 &= \sum_{k=1}^3 \text{sign}(\alpha_k - h(t)) \frac{V}{2} I_k^{\text{motor}}
 \end{aligned}$$

So, the current I_o is defined by this direct calculation from motor currents.

$$I_o = \frac{1}{2} \sum_{k=1}^3 \text{sign}(\alpha_k - h(t)) I_k^{\text{motor}}$$

We do not consider voltage compensation and overmodulation strategy. They do not change in average the total power shared between inverter and motor.

By definition, the average of the quantity $\text{sign}(\alpha_k - h(t)) \frac{V}{2}$ on a pwm period is equal to V_k^{motorref} . We can rewrite motor voltage and DC bus current as follows:

$$\begin{aligned}
 V_k^{\text{motor}} &= V_k^{\text{motor ref}} + (\text{sign}(\alpha_k - h(t)) - \alpha_k) \frac{V}{2} \\
 I_o &= \frac{\sum_{k=1}^3 V_k^{\text{motor}} I_k^{\text{motor}}}{V} = \frac{P_o}{V}
 \end{aligned}$$

PWM method is introducing high-frequency perturbation on the motor voltage, as well as on the DC bus current.

Considering a PWM carrier frequency higher than 40 times the mains frequency, we decide not to take this high frequency into account.

For the next parts, we could either consider inverter as a DC current source I_o or as a power source P_o .

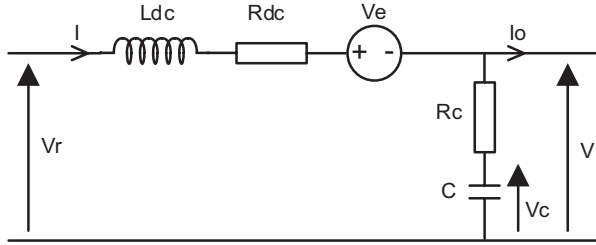
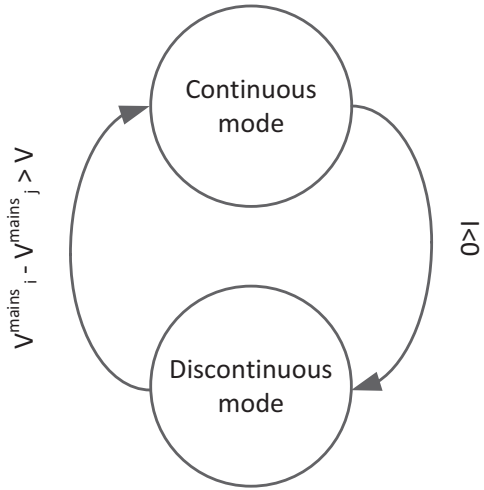


Fig. 5 Common DC bus schematic

Fig. 6 Dynamic models principle



3.4 Dynamic Model

The three topologies can be modelled by a unique circuit. We will not consider in this chapter the control part of the ESI. So, it can be simplified by a voltage source. The voltage source generates a voltage whose mean value is null and compensates the oscillations of the output rectifier voltage (Fig. 5).

In case of C-less or DC choke topology, the voltage source is not considered, i.e. $V_e = 0$.

The dynamic model is depending on the conduction mode of the rectifier (Fig. 6).

In case of discontinuous mode, the equations of the system are in a state-space representation

$$C \frac{dV_c(t)}{dt} = -I_o(t)$$

$$I(t) = 0$$

The DC bus voltage is given by

$$V(t) = V_c(t) - R_c I_o(t)$$

In case of continuous mode, the equations of the system are in a state-space representation

$$C \frac{dV_c(t)}{dt} = I(t) - I_o(t)$$

$$L_{dc} \frac{dI(t)}{dt} = -V_c(t) - (R_c + R_{dc}) I(t) + R_c I_o(t) + V_r(t) - V_e(t)$$

The DC bus voltage is given by

$$V(t) = V_c(t) + R_c (I(t) - I_o(t))$$

We have a second-order differential equation for the DC bus current.

$$L_{dc} C \frac{d^2 I(t)}{dt^2} + (R_{dc} + R_c) C \frac{dI(t)}{dt} + I(t)$$

$$= C \frac{d}{dt} (V_r(t) - V_e(t)) + R_c C \frac{dI_o(t)}{dt} + I_o(t)$$

The current of the DC bus is depending on two inputs: $V_r - V_e$ and I_o . In case of passive filter, V_e is equal to 0 and the rejection of V_r depends only on the parameters value.

We may calculate the equilibrium trajectory of the dynamic systems using the superposition principle. Each variable may be decomposed on a base of sinus and cosinus functions at each multiple of mains frequency. Let us define $V_r(t) = \sum_k VC_r^k \cos(k\omega_0 t) + VS_r^k \sin(k\omega_0 t)$, $I_o(t) = \sum_k IC_o^k \cos(k\omega_0 t) + IS_o^k \sin(k\omega_0 t)$,
 $V_c(t) = \sum_k VC_c^k \cos(k\omega_0 t) + VS_c^k \sin(k\omega_0 t)$, and

$I(t) = \sum_k IC^k \cos(k\omega_0 t) + IS^k \sin(k\omega_0 t)$. We get the following relations between

variables:

$$VC_c^k = A_o^k (-R_{dc} IC_o^k - kL\omega_0 IS_o^k + VC_r^k)$$

$$- B_o^k (kL\omega_0 IC_o^k - R_{dc} IS_o^k + VS_r^k)$$

$$VS_c^k = -B_o^k (-R_{dc} IC_o^k - kL\omega_0 IS_o^k + VC_r^k)$$

$$- A_o^k (kL\omega_0 IC_o^k - R_{dc} IS_o^k + VS_r^k)$$

$$IC^k = Ck\omega_0 VS_c^k + IC_o^k$$

$$IS^k = -Ck\omega_0 VC_c^k + IS_o^k$$

with

$$A_O^k = \frac{1 - k^2 LC \omega_0^2}{(1 - k^2 LC \omega_0^2)^2 + (k(R_c + R_{dc}) \omega_0)^2}$$

and

$$B_O^k = \frac{k(R_c + R_{dc}) \omega_0}{(1 - k^2 LC \omega_0^2)^2 + (k(R_c + R_{dc}) \omega_0)^2}$$

The dynamic system is stable in case of I_o current source. In case of power source P_o , the stability conditions on a linear tangent system are

$$\frac{1}{R_{dc} - R_c} > \frac{I_o}{V_C + R_c(I - 2I_o)}$$

and

$$\frac{R_{dc} + R_c}{\frac{L}{C} - R_c^2} > \frac{I_o}{V_C + R_c(I - 2I_o)}$$

In case of continuous mode, the DC current I can be expressed for I_o current source.

$$I(t) = I_o + \sqrt{3} \cdot \omega_0 \cdot C \cdot V_{\text{mains}} \cdot \left(A \cdot \cos\left(\omega_0 \cdot t + \frac{\pi}{3}\right) + B \cdot \sin\left(\omega_0 \cdot t + \frac{\pi}{3}\right) + C_1 \cdot e^{-\frac{v}{\sqrt{LC}}} + C_2 \cdot e^{-\frac{qt}{\sqrt{LC}}} \right)$$

With

$$x = \frac{(R_{dc} + R_c) \cdot C}{\sqrt{LC}}, v = \frac{x}{2} - j \frac{\sqrt{4 - x^2}}{2}, q = \frac{x}{2} + j \frac{\sqrt{4 - x^2}}{2}$$

And

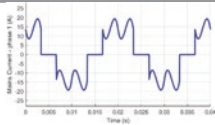
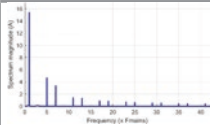
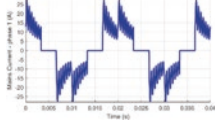
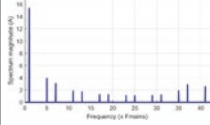
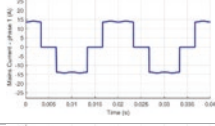
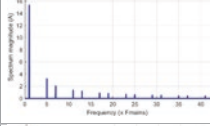
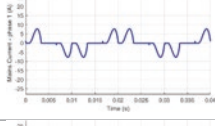
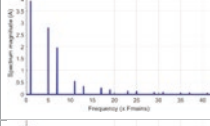
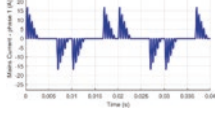
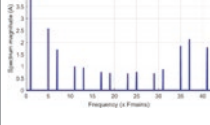
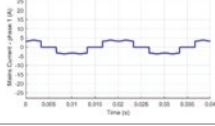
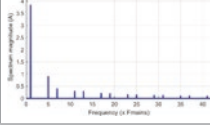
$$A = \frac{(R_{dc} + R_c) \cdot C \cdot \omega_0}{(1 - LC \omega_0^2)^2 + ((R_{dc} + R_c) \cdot C \cdot \omega_0)^2},$$

$$B = \frac{1 - LC \omega_0^2}{(1 - LC \omega_0^2)^2 + ((R_{dc} + R_c) \cdot C \cdot \omega_0)^2}$$

$$C_1 = - \frac{\omega_0 \sqrt{LC} A + qB}{j\sqrt{4-x^2} \left(1 - e^{\frac{q\omega_0 \pi}{\sqrt{LC}^3}} \right)}$$

$$C_2 = \frac{\omega_0 \sqrt{LC} A + vB}{j\sqrt{4-x^2} \left(1 - e^{\frac{q\omega_0 \pi}{\sqrt{LC}^3}} \right)}$$

Table 3 Comparison between topology (signal form, harmonics, THDI)

Topology	Power	Current shape	Fourier transformation	THDI
DC choke	100%			40.7%
C-less	100%			46.2%
ESI	100%			29.6%
DC choke	25%			88.9%
C-less	25%			120.2%
ESI	25%			29.6%

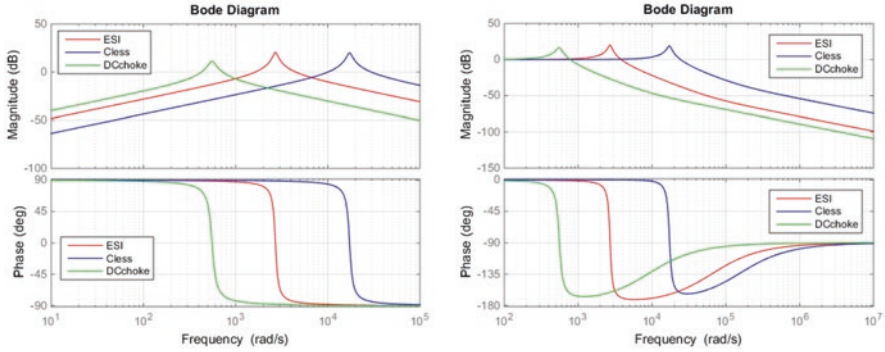


Fig. 7 Bode diagram of the transfer functions

3.5 Simulation

For simulation, we consider a mains supply with characteristics such as 50 μH inductive effect and 7 mΩ resistive effect. We collect data for two operating points in Table 3. For 100% motor power, we are in a continuous mode, while 25% is in discontinuous mode.

3.6 Harmonics Calculation

3.6.1 Frequency Domain Calculation

Considering $I > 0$ for the validity of the dynamic model, we can write the two transfer functions and their bode diagrams. It corresponds to $I = H(s)V_r + G(s)Io$.

$$H(s) = \frac{Cs}{L_{dc}Cs^2 + (R_{dc} + R_c)Cs + 1}$$

$$G(s) = \frac{rCs + 1}{L_{dc}Cs^2 + (R_{dc} + R_c)Cs + 1}$$

We can plot the bode diagram of the transfer functions for the different studied topologies (Fig. 7).

The Fourier transformation of the current I can be calculated based on the transfer functions and the Fourier coefficients of V_r and Io . As the switching frequency has been neglected as we consider switching frequency higher than 40 times nominal frequency, we have:

$$I(j\omega) = \sum_{k \in \mathbb{Z}} i\hat{1}_k \delta(\omega - 6k\omega_0) + \sum_{k \in \mathbb{Z}} i\hat{2}_k \delta(\omega - 6k\omega_0)$$

With Fourier coefficients

$$i\hat{1}_k = H(j6k\omega_0)\hat{v}_k \quad \text{and} \quad i\hat{2}_k = G(j6k\omega_0)\hat{I}o_k$$

Considering now the transfer between the DC bus current $I(t)$ and the line current $I_1(t)$. The current $I_1(t)$ of one particular branch of the bridge is related to the DC bus current as follows:

$$I_1(t) = (I(t) \cdot f(t)) * p_1(t)$$

Where $f(t)$ is the same rectangular window of width $\frac{T}{6} = \frac{\pi}{3\omega_0}$ (T period of the input voltages) and $p_1(t)$ is an impulse train of period T . We can write p_1 as:

$$p_1(t) = \sum_{m \in \mathbb{Z}} p_2(t - mT)$$

With $p_2(t)$ the unitary pattern of the signal. It encodes the symmetry property and the zero-average value of the current signal $I_1(t)$.

The pattern $p_2(t)$ is equal to: $p_2(t) = \delta\left(t + \frac{T}{6}\right) + \delta\left(t + \frac{T}{3}\right) - \delta\left(t - \frac{T}{6}\right) - \delta\left(t - \frac{T}{3}\right)$.

The Fourier transformation of the signal $p_1(t)$ is:

$$P_1(j\omega) = \frac{1}{T} \sum_{k \in \mathbb{Z}} \hat{p}_1(k) \delta(\omega - k\omega_0)$$

With
$$\hat{p}_1(k) = \int_{-\frac{T}{2}}^{\frac{T}{2}} p_2(t) e^{-jk\omega_0 t} dt = 2 \left(\sin\left(\frac{k\pi}{3}\right) + \sin\left(\frac{k2\pi}{3}\right) \right)$$

For $k = 6n + 1$, $\hat{p}_1(k) = 2\sqrt{3}$, and for $k = 6n - 1$, we have $\hat{p}_1(k) = -2\sqrt{3}$.

At the end, the Fourier transformation of the signal $I_1(t)$ is

$$I_1(j\omega) = (I(j\omega) * F(j\omega)) \cdot P_1(j\omega)$$

$$I_1(j\omega) = \left[\sum_k H(j6k\omega_0) \hat{v}_k \frac{2}{\omega - 6k\omega_0} \sin\left(\frac{(\omega - 6k\omega_0)\pi}{6\omega_0}\right) + \sum_k G(j6k\omega_0) \hat{I}o_k \frac{2}{\omega - 6k\omega_0} \sin\left(\frac{(\omega - 6k\omega_0)\pi}{6\omega_0}\right) \right] \cdot P_1(j\omega)$$

Substituting the expression of $P_1(j\omega)$, we obtain:

$$\begin{aligned}
 I_1(j\omega) = & \frac{\omega_0}{2\pi} 2\sqrt{3} \left[\sum_n \sum_k H(j6k\omega_0) \mathbb{V}_k \frac{2}{(6(n-k)+1)\omega_0} \sin\left(\frac{(6(n-k)+1)\pi}{6}\right) \delta(\omega - (6n+1)\omega_0) \right. \\
 & - \sum_n \sum_k H(j6k\omega_0) \mathbb{V}_k \frac{2}{(6(n-k)-1)\omega_0} \sin\left(\frac{(6(n-k)-1)\pi}{6}\right) \delta(\omega - (6n-1)\omega_0) \\
 & + \sum_n \sum_k G(j6k\omega_0) \mathbb{I}_k \frac{2}{(6(n-k)+1)\omega_0} \sin\left(\frac{(6(n-k)+1)\pi}{6}\right) \delta(\omega - (6n+1)\omega_0) \\
 & \left. - \sum_n \sum_k G(j6k\omega_0) \mathbb{I}_k \frac{2}{(6(n-k)-1)\omega_0} \sin\left(\frac{(6(n-k)-1)\pi}{6}\right) \delta(\omega - (6n-1)\omega_0) \right]
 \end{aligned}$$

Which can be simplified as:

$$\begin{aligned}
 I_1(j\omega) = & \frac{\omega_0}{2\pi} 2\sqrt{3} \left[\sum_n \sum_k H(j6k\omega_0) \hat{v}_k \frac{(-1)^{n-k}}{(6(n-k)+1)\omega_0} \delta(\omega - (6n+1)\omega_0) \right. \\
 & + \sum_n \sum_k H(j6k\omega_0) \hat{v}_k \frac{(-1)^{n-k}}{(6(n-k)-1)\omega_0} \delta(\omega - (6n-1)\omega_0) \\
 & + \sum_n \sum_k G(j6k\omega_0) \hat{I}_k \frac{(-1)^{n-k}}{(6(n-k)+1)\omega_0} \delta(\omega - (6n+1)\omega_0) \\
 & \left. + \sum_n \sum_k G(j6k\omega_0) \hat{I}_k \frac{(-1)^{n-k}}{(6(n-k)-1)\omega_0} \delta(\omega - (6n-1)\omega_0) \right]
 \end{aligned}$$

In previous equation, the two transfers $H(j6k\omega_0)$ and $G(j6k\omega_0)$ are depending on DC bus parameters (capacitor, resistance, inductance).

The two inputs of the THDI calculation are the voltage V_r and the output current I_o . If we consider an output current source, I_o is constant as we neglect the igt commutations as the switching frequency is higher than the 40th current harmonic. In this case, the second part of the previous equation can be simplified. If a power source is considered, the current I_o depends on the voltage V_r and we have to consider the complete equation.

As expected, only harmonic in $2n + 1$ or $2n - 1$ is not equal to 0. The complete calculation of the THDI can be done as every parameter is known. The accuracy of the estimation will depend on k , the number of harmonic coefficients which are considered. Moreover, this study is valid only for continuous mode. The study in discontinuous mode is more complex. For the online drive calculation, another approach can be used by simplifying the equation and approximate the THDI. It is described in the next section.

3.6.2 Approximation

We must separate the continuous mode from the discontinuous mode. We can determine a minimum power as a limit for continuous mode. This power depends on the mains supply according to a simple second-order polynomial function

$$P_{LIM} = a_2 \cdot V^2 + a_1 \cdot V + a_0$$

where V is the ratio of mains voltage by nominal mains voltage, and P a power expressed in kW.

In each part, we can define a function of V and P that allows estimating THDi

$$THD_{EST} = (b_1 \cdot V + b_0) \cdot \frac{P + c_2 \cdot V^2 + c_1 \cdot V + c_0}{P + d_1 \cdot V + d_0}$$

We get

DC Choke	a2	a1	a0	b1	b0	c2	c1	c0	d1	d0
Continuous	2,86	0,15	-0,04	-0,89	2,62	22,59	-27,27	9,12	0,17	-0,89
Discontinuous				0,49	3,79	1,21	0,74	0,10	1,04	-0,36

and

C-less	a2	a1	a0	b1	b0	c2	c1	c0	d1	d0
Continuous	3,61	0,89	-0,36	-0,77	2,53	23,60	-26,40	8,54	0,17	-0,92
Discontinuous				0,33	1,60	8,17	2,48	0,11	1,69	-0,79

We get an estimation with an accuracy lower than 2% of THDi on continuous mode, which is the normal operating condition (Figs. 8 and 9).

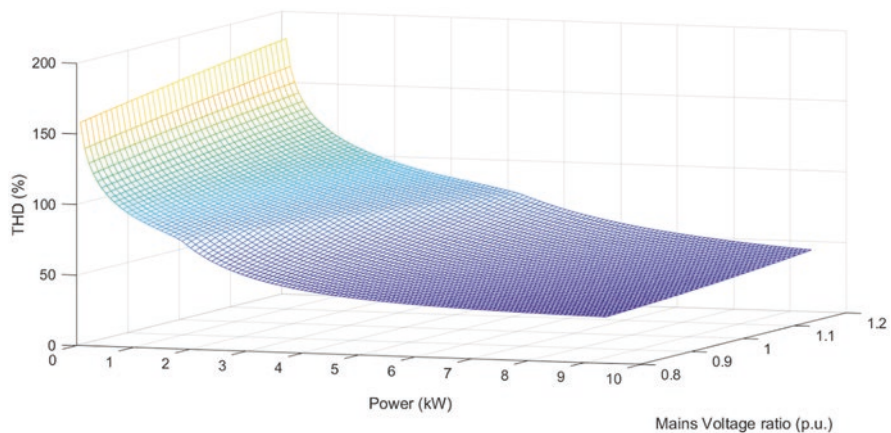


Fig. 8 THD estimation for DC choke

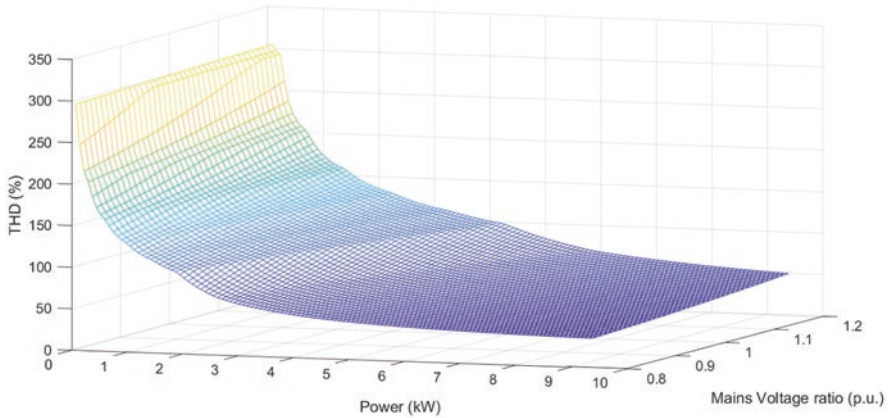


Fig. 9 THD estimation for C-less

4 Conclusion

This chapter has proposed the study of the THD of the drive input currents for three different DC bus topologies (DC choke, C-less and ESI). The analysis of the stability of the DC bus has been performed to enclose the area of model validity. The frequency analysis of the THD determine each harmonic of the input current in function of the input voltage, output power or current and DC bus parameters. At the end, a simplified estimator has been proposed to evaluate the THD in continuous (DC bus current always positive) or discontinuous mode (DC bus current goes to 0) online in the drive and give this additional information to customer. Simulations have been done on the three DC bus topologies to compare their respective THDI, and the form of the signals for two different operating points (100% and 25% of nominal power).

References

1. IEC 61800-3 Edition 3.0 2017-02 Adjustable speed electrical power drive systems – Part 3: EMC requirements and specific test methods
2. IEC 61000-3-12 2011-12 Limits for harmonic currents produced by equipment connected to public low-voltage systems with input current $>16\text{A}$ and $\leq 75\text{A}$ per phase
3. IEC 61800-9-1 Edition 1.0 2017-03 Adjustable speed electrical power drive systems – Part 9–1: Ecodesign for power drive systems, motor starters, power electronics and their applications – General requirements for setting energy efficiency standards for power driven equipment using the extended product approach (EPA) and semi analytic model (SAM)

Comparison of Fixed and Variable Speed Pumps Under Consideration of Manufacturer and Operator Aspects



Sebastian Bold, Vincent Becker, Sven Urschel, and Jochen Schaab

1 Introduction

Successful mastery of the energy turnaround requires consideration of the three pillars: energy generation, distribution and storage, and consumption. There is still enormous potential for savings, especially in the area of electrical energy consumption. All across the EU, pumps consume 22% of electric motor energy in industrial sector and 16% in services sector [1]. Areas of application are e.g. in cooling, heating and drinking water systems or the transport of liquid foodstuffs and chemicals.

The characteristics of hydraulic systems are determined by many factors, such as pipe length and material, number of adapters, pumps and valves, mostly under variable load [2]. Although individual components are optimized with regard to their efficiency, most pump systems operate at suboptimal efficiency for different reasons. Regardless of the transported medium, users require a defined hydraulic operating point, consisting of head and flow, to run their processes. For this task, pumps with different principles, such as centrifugal pumps and displacement pumps, are available in various sizes. If the desired operating point is not reached by a characteristic curve of any pump, various methods are applied to adjust the operating point. Among experts it is generally accepted that speed control is in nearly all cases the most energy-efficient method of adjusting operating points [3–5]. Nevertheless, only about 10% of all pumps are equipped with variable speed drives (VSD) [6].

S. Bold · V. Becker · S. Urschel (✉)
University of Applied Sciences Kaiserslautern, Kaiserslautern, Germany
e-mail: sebastian.bold@hs-kl.de

J. Schaab
KSB SE & Co. KGaA, Frankenthal, Germany
e-mail: sven.urschel@hs-kl.de

2 State of the Art

In order to satisfy customer requests, pump manufacturers create a product portfolio to cover a range of hydraulic values as large as possible. This product portfolio contains a selection of standard pumps whose dimensions are specified by a standard. In addition, the manufacturers offer sizes that deviate from the standard sizes and are referred to as oversizes and undersizes.

For new plants or applications, aggregates from the product portfolio are used. The following steps are taken to select the most suitable pump unit:

At first the process needs to be identified. The values of the static head, dynamic head, flow and liquid details have to be determined. With this knowledge it is possible to eliminate variants which are not suitable for the process. At last, economic calculations are done for the remaining variants at different operating conditions, allowing the user to choose the best variant.

If the requested operating point does not lie on the pump curve, a procedure for setting the operating point is required. Five different methods are used in industry for setting operating points. Each of the methods mentioned is based on changing either the system curve or the pump curve in such a way that the intersection point corresponds to the desired customer operating point. Figure 1 shows the procedures and their influence on the system and pump curve. The system curve of the process is shown in blue and the pump curve in yellow. The new curve, which was created by applying the method, is shown in brown dashed lines. In addition, the desired operating point, consisting of the requested flow (Q_{des}) and head (H_{des}) is marked in the diagram.

There are a number of procedures for setting the operating point that can be chosen:

- (a) Use of a throttle valve: In this case, a throttle valve is used to increase the flow resistance of the pipe network. The addition of the flow resistances of the pipe network and the throttle valve results in a steeper overall system curve. The point of intersection of the overall system curve and the pump curve results in

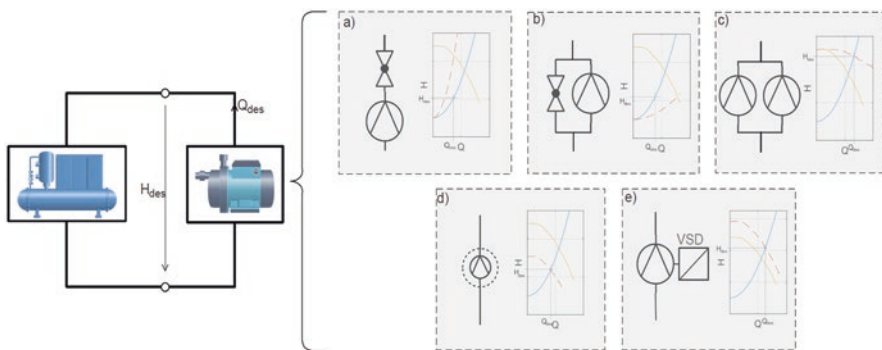


Fig. 1 Methods for adjusting the hydraulic operating point of a process

the new operating point of the pump, which should not be confused with the operating point of the system.

- (b) Use of a bypass valve: By connecting a valve in parallel, the opposite effect to throttling is achieved and the overall system resistance is reduced. The reason for this is that the medium can now flow both through the bypass and through the system of pressure to the suction port of the pump.
- (c) Parallel operation of two or more pumps: Parallel operation can be achieved by connecting several pumps in parallel on the one hand and by using twin pumps on the other. This allows the nominal flow and head of the system to be increased [7].
- (d) Impeller trimming: Impeller trimming means reducing the impeller diameter of a pump and thus reducing the rotating speed at the impeller outlet of a centrifugal pump.
- (e) Speed control: The use of a VSD to drive the motor enables the setting of an individual speed. This speed can be higher or lower than the rated speed of the motor within certain limits. The position of the pump curve at changed speed can be predicted with the aid of affinity laws. The operating point desired by the customer can thus be easily achieved by adjusting the speed.

With the manipulation of the characteristic curves, however, unwanted effects can occur. On the one hand the effects affect the operation and on the other hand the manufacture of the pumps. Table 1 lists unwanted effects that can occur when a certain procedure is used.

Users demand reliability, easy and fast commissioning and increasingly a high efficiency as well as the possibility to react to plant modifications by readjusting the operating point and at the same time the lowest price possible. For manufacturers, this means reducing costs by eliminating extensive warehouses and additional production steps as well as lowering materials input.

3 Content of the Study

The selection of the method for adjusting the flow in pump systems is often the subject of controversy. On the one hand, this is due to the many possibilities and their individual advantages and disadvantages, and on the other hand, there is little information available on the topic.

The aim of this work is to make a contribution so that users and manufacturers of pumps can assess the advantages and disadvantages of the methods mentioned. The

Table 1 List of unwanted effects

Operation of a pump	Production of a pump
Additional losses	Additional storage costs
Additional equipment	Additional manufacturing costs
Cavitation	Additional material costs

analysis focuses on the operation of pumps with VSD and its advantages and disadvantages.

In order to be able to make precise statements, a concrete application scenario was created. Two adjacent pump sizes were selected from a pump type series of a pump manufacturer. These two mains-powered pumps form Device Under Test (DUT) 1 and 2. As the third DUT (DUT3), the smaller pump is driven via a VSD (see Fig. 2 and Table 2). To ensure the highest possible comparability, the same motor was used for all three DUTs.

These configurations are compared by measuring the pump units in a hydraulic test bench. In order to investigate the differences of the results, the induction motor (IM) was also measured on a motor test bench. The results of the investigations can be divided into three sections A, B and C. Independently of the first three studies, D examines how VSD operation affects resource efficiency.

- A. DUT2 is compared with DUT3 as the first examination. The question is answered how the use of a VSD and the associated increased speed affects the efficiency of the pump unit. For this purpose, the pump curve of DUT2 is recorded and the pump curve of DUT3 at a stator frequency of 63 Hz, for example. The efficiencies along the pump curve are determined and compared.
- B. In the second study, DUT1 is compared with DUT3. The pump curve of DUT1 was recreated by setting the speed with DUT3. Thus, a direct comparison of the efficiencies can be carried out at each operating point. The advantages and disadvantages of replacing a bigger pump with a smaller pump with increased speed will be investigated.

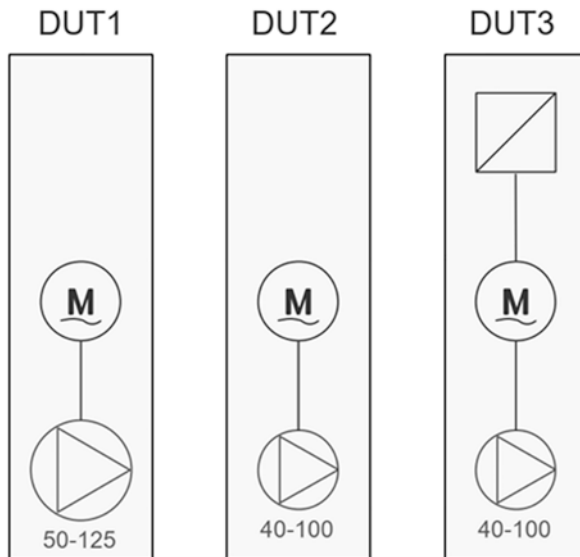


Fig. 2 Display of the examined DUTs

Table 2 Pump configurations

	DUT1	DUT2	DUT3
Variable speed drive	None	None	IE2 class frequency inverter (370 W)
Motor	IM (180 W, 1370 rpm)	IM (180 W, 1370 rpm)	IM (180 W, 1370 rpm)
Pump	Inline 50–125 ^a ($\eta_{\text{BEP}} = 67.0\%$)	Inline 40–100 ($\eta_{\text{BEP}} = 60.6\%$)	Inline 40–100 ($\eta_{\text{BEP}} = 60.6\%$)

^aInline «Nominal Pump Size»-«Impeller diameter»

- C. In addition, measured values were recorded in the complete operation range between the pump characteristics of DUT1 and 2 with the aid of DUT3. These results can be used to make comparisons to the operating point setting. In concrete terms, the speed control (DUT3) is compared with the setting of the operating point with DUT1 and a throttle valve.
- D. Here the savings potential of a VSD pump series is investigated by a simulation study. The goal of this simulation study was to find out if it is possible cover a certain Q-H range with a reduced total number of pump sizes. The study was carried out using a pump model that allowed the application range to be extended by increasing the speed. It was taken into account that in a physical system the speed cannot be increased arbitrarily without cavitation occurring. Pumps which are operated at critical speeds are excluded. To determine the occurrence of cavitation the NPSH value is calculated.

4 Experiments and Calculation Methods

This section deals with the process and methodology needed to achieve the above objectives. In the first two sections, the test objects, the structure, the equipment and the measurement procedure are described. The last part of this section deals with the calculation methods required for the investigations.

4.1 Measurements on the Pump Test Bench

The measurements described in this section are based on three pump configurations, consisting of different components (see Table 2). When selecting the pumps two criteria were taken into account. At first both pumps are to be operated on the existing pump test bench with a maximum power of 2.2 kW. Secondly, the difference between the two pumps should only be one power stage.

All DUTs are measured on a pump test bench. The structure of the experimental setup is shown in Fig. 3. The hydraulic circuit consists of a pipeline with a nominal diameter of DN100, two control valves connected in parallel and a water tank. Due to the large nominal diameter, a high flow rate can be set, especially for small pumps.

The pump test bench allows the measurement of the electrical power as well as the hydraulic power of the test objects. Therefore, the pump unit efficiency can be determined at all adjustable operating points. The electrical power is calculated with a wattmeter from the grid voltage and the motor current. The flow and the head of the pump are measured to calculate the hydraulic power. The control valves are used to set the operating point.

4.2 Measurements on the Motor Test Bench

Since a torque sensor cannot be mounted between the impeller and the motor, the motor is also measured on a motor test bench. The motor test bench can be used to measure a wide variety of drives with a maximum power of 7.5 kW. The motor is measured once at the mains and once with VSD. The VSD parameters are identical to those of the first test section. Figure 4 shows the structure of the motor test bench; the devices used and their characteristics are shown in Table 3.

With the help of the motor test bench, the motor can be put into the same states as it had during the measurement on the pump test bench. After warming up, the

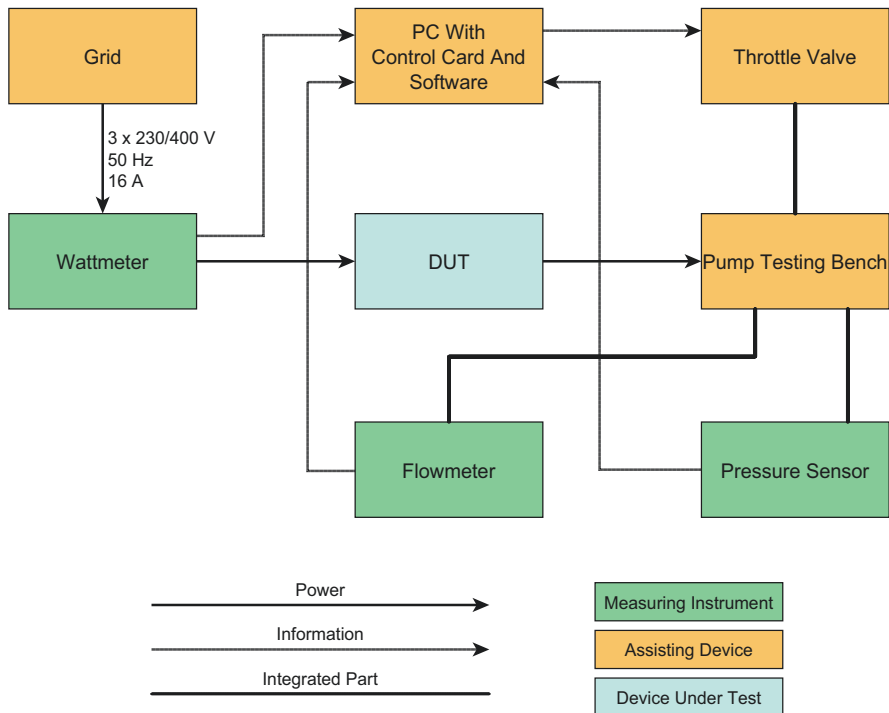


Fig. 3 Structure of the measurement configuration of the pump test bench

operating point is set via the load machine. The condition is monitored by measuring the speed, input voltage and power consumption. In addition, the mechanical quantities can now be recorded via the torque measuring shaft. With the additional information from the torque measuring shaft, the efficiency of the drive can be determined individually.

4.3 Calculation Fundamentals

This section describes all the calculation principles required for carrying out and evaluating the investigations.

Different models are used in the investigation. The affinity laws, see Eq. 1, are used to calculate the pump curves at changed speed [8]. The index ref. indicates that

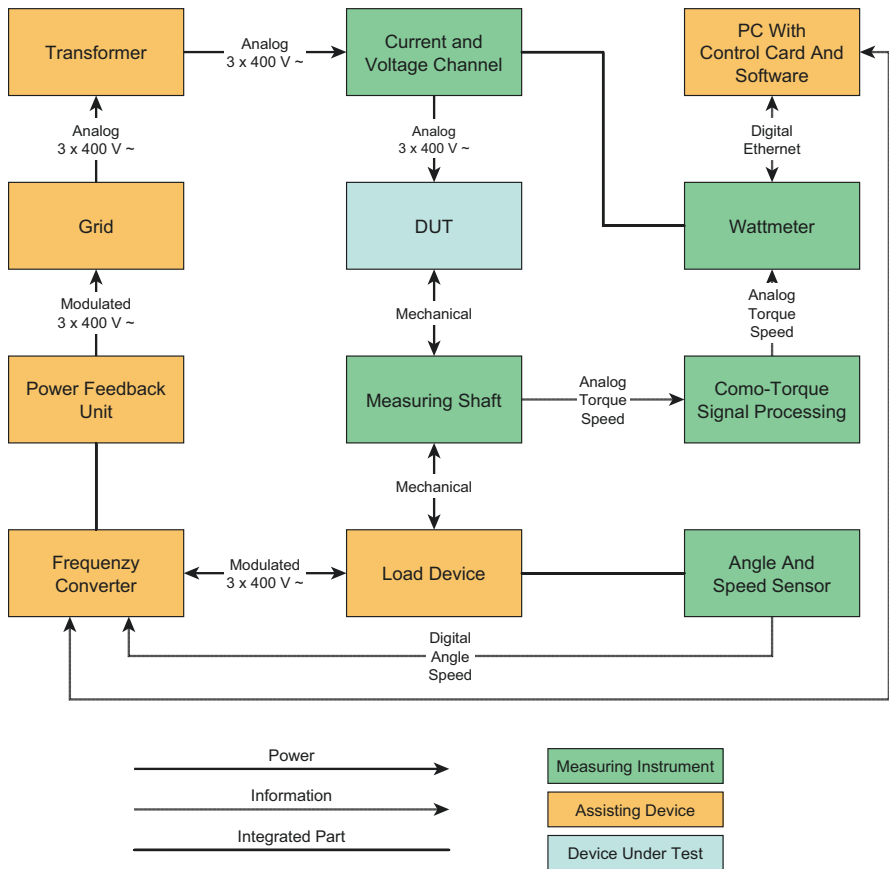


Fig. 4 Structure of the measurement configuration of the motor test bench

Table 3 List of used measuring instruments

Instrument name	Manufacturer	Product number	Measuring range
<i>All measurements</i>			
Watt meter	Yokogawa	WT3000E	0–1000 V
Watt meter	Yokogawa	WT3000E	0–30 A
<i>Pump test bench</i>			
Flow rate sensor	ABB	FER 100	0.25–200 m ³ /h
Differential pressure sensor	WIKA	DPT-10	0–3 bar
Measurement card	NI	USB-6363	
<i>Motor test bench</i>			
Torquemeter	Kistler	4503B	5 nm
Measuring amplifier	CoMo Torque	Type 4700BP0UN	±10 mV DC, 700 mA
Measurement card	NI	USB-6363	

the value can be read from the reference curve. Index i is the newly calculated value at a speed n_i . Q is the flow, H the head and P the shaft power of a pump.

$$Q_i = Q_{\text{ref}} \cdot \left(\frac{n_i}{n_{\text{ref}}} \right) \quad H_i = H_{\text{ref}} \cdot \left(\frac{n_i}{n_{\text{ref}}} \right)^2 \quad P_i = P_{\text{ref}} \cdot \left(\frac{n_i}{n_{\text{ref}}} \right)^3 \quad (1)$$

The Net Positive Suction Head (NPSH) parameter is of great importance for the operation of a pump. It enables a statement to be made about the safety against the effects of cavitation during operation. Pump manufacturers specify a minimum value for the NPSH in the pump data sheet, the NPSH required (NPSH_r). The specification of the NPSH_r value means a cavitation-induced head drop of 3%. Therefore, the data sheets often contain the NPSH₃ [9].

The NPSH_r value can be scaled depending on the speed and the diameter D of the impeller, just like the head of a pump, see Eq. 2 [10].

$$\text{NPSH}_{r,i} = \text{NPSH}_{r,\text{ref}} \left(\frac{n_i}{n_{\text{ref}}} \right)^2 \left(\frac{D_i}{D_{\text{ref}}} \right)^2 \quad (2)$$

There are no general rules for capturing the influence of the Reynolds number Re on the efficiency η of geometrically similar pumps. With the help of a scale-up equation, it can be predicted how an increase of the impeller diameter or of the speed influences the efficiency of a pump. However, approximation equations have been developed over time, such as the Ackeret¹ equation, see Eq. 3 [11].

¹Named after Jakob Ackeret (1898–1981); Swiss Aerodynamicist.

$$\frac{1-\eta_i}{1-\eta_{\text{ref}}} = 0.5 \cdot \left[1 + \left(\frac{\text{Re}_{\text{ref}}}{\text{Re}_i} \right)^{0.2} \right] \quad (3)$$

The Reynolds number depends on the impeller diameter, speed and kinematic viscosity ν , see Eq. 4.

$$\text{Re} = \frac{\pi \cdot D^2 \cdot n}{\nu} \quad (4)$$

If a throttle valve is used to set the operating point, the hydraulic losses are calculated from the difference between the head of the pump at its operating point and the required head of the system (see Fig. 1), multiplied by the flow through the system, see Eq. 5 [12].

$$P_{\text{loss}} = Q \cdot (H_{\text{Pump}} - H_{\text{des}}) \quad (5)$$

The basis for this simulation study is a given pump type series. Here the characteristic Q - H , H - P and Q -NPSH curves are used. For a given set of customer request points covering a certain area of the Q - H plane, two scenarios are calculated. First, for each customer point the most efficient fixed speed pump is selected out of a subset of all feasible pumps operating at this customer point. Whether a pump is feasible for a certain customer operating point depends on the part load and over load boundaries as well as the resulting NPSH at this point. Second, for each customer point a pump with variable speed is selected. Here, by selecting an individual speed, the customer point is matched. Again, the same criteria for finding the best pump are applied; now the speed limits of the pump and drive are a further criteria.

The overall efficiency is calculated from two partial models. The first submodel is an efficiency model for the pump. This model follows the affinity laws for speed changes and respects the changed pump efficiency by Ackeret. The second submodel is a data-driven model for the calculation of the motor efficiency. The method was taken from the standard DIN EN 50598-1. This standard describes a procedure that can be used to interpolate the efficiency from eight measurements. A similar approach is used for describing the inverter efficiency.

5 Results and Analysis

After the execution of the experiments and the methods for evaluation are described, the results will be presented and discussed in this section. The results of the four investigations are shown and analyzed.

5.1 Efficiency of a Pump Running at Increased Speed

This section deals with the properties of pumps at increased speed. Figure 5 shows the measurement results of DUT2 and DUT3. On the left are the pump curves, in the middle the efficiency of the pump units and on the right both drive (motor and VSD) and pump efficiency. DUT3 is fed with an increased stator frequency, for example 63 Hz.

First of all, the characteristic curves of DUT2 are compared with the manufacturer’s data sheet and a high degree of agreement is found. The measured efficiency at the best efficiency point (BEP) is 59%, compared to the manufacturer’s specification of 60.6%.

What is immediately noticeable is the lower efficiency of the pump unit of DUT2 compared to DUT3. This is due to the low efficiency of the motor, which is only operated at partial load. For example, in the place of the pump’s BEP (7 m³/h), the motor power is only 46% of the rated power. With increasing speed (DUT3) the motor load increases and with it the efficiency of the pump unit. As expected (Eq. 1), the pump curve of DUT3 is higher than that of DUT2. The efficiency of the pump of DUT3 is also 1% higher than that of DUT2, which is due to the efficiency scale-up by increasing speed and thus the Reynolds number [13].

The course of the NPSH₃ value of DUT2 is taken from the manufacturer’s data sheet. The course of the NPSH₃ value of DUT3 was simulated using Eq. 2. This shows, demand for input pressure increases with increasing speed up to a flow of

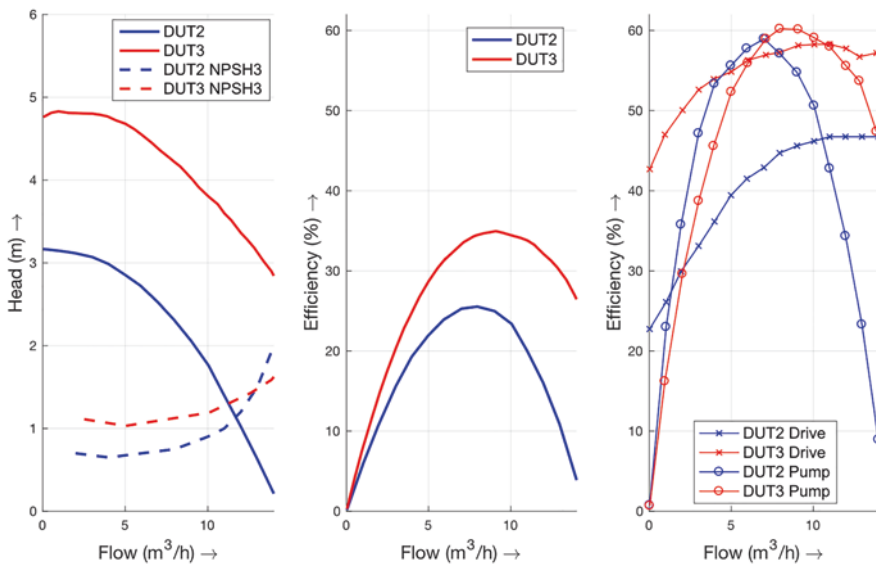


Fig. 5 Pump and NPSH₃ curves (left) and pump unit efficiency (middle) and drive (motor + VSD) and pump efficiency (right) of DUT2 and DUT3 (63 Hz)

about 13 m³/h. From this flow onwards, the pressure requirements are lower, due to the improved flow characteristics caused by the increased speed.

In summary, it can be said that in the selected configuration, an increase in speed results in an increase in overall efficiency, which is mainly due to the increase in the efficiency of the drive.

5.2 Replacing Bigger Pump with Smaller Pump at Increased Speed

In this section, a direct comparison is made between a smaller pump with VSD (DUT3) and a larger pump (DUT1). A direct comparison means that the pump curve of DUT1 is recreated by setting the speed of DUT3. The pump characteristics of the two configurations are shown in Fig. 6.

In comparison to the manufacturer’s datasheet, the efficiency of DUT1 was found to be about 3% lower. One reason for this could be the modification of the pump.

As was to be expected, both pump curves of DUT1 and 3 lie on top of each other. If the pump unit efficiencies are evaluated, the better efficiency of DUT3 in the range 0 to 9 m³/h can be seen. In this range, the efficiency can be up to 2.8% higher. For flow above 9 m³/h, the efficiency of the DUT1 is higher and the ratio improves with increasing flow in favor of DUT1. The use of a different pump configuration is

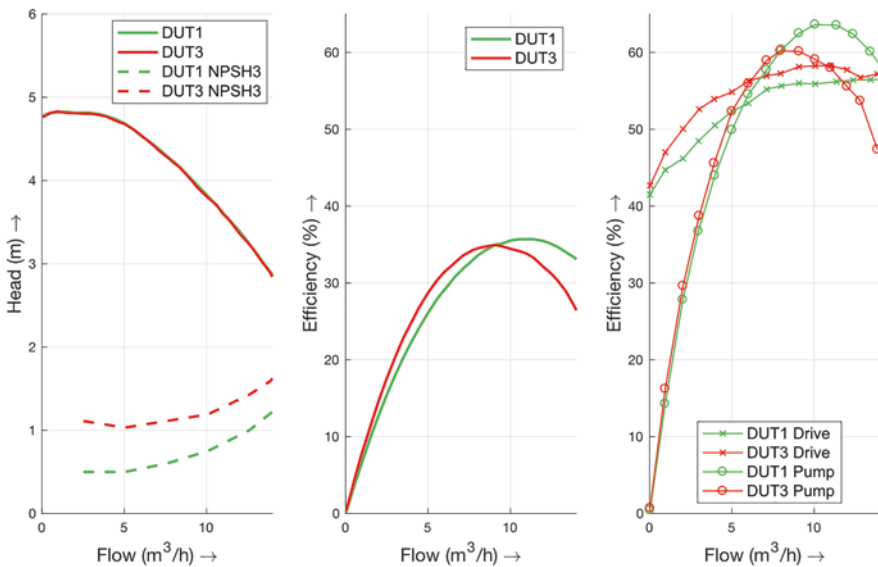


Fig. 6 Pump and NPSH₃ curves (left) and pump unit efficiency (middle) and drive (motor + VSD) and pump efficiency (right) of DUT1 and DUT3

recommended in this area. Since the overall efficiency is made up of pumps and motor efficiency, these are now analyzed separately.

First the pump efficiency is considered. The pump efficiency at the best point of DUT1 is 3.4% higher than that of DUT3. This can be explained, among other things, by the use of Eqs. 3 and 4 when DUT2 is used as the basis for the application of the Ackeret equation (see Table 2 for the pump parameters). First, the increase in efficiency of DUT2 is calculated by increasing the speed (DUT3) and then the increase in efficiency of DUT2 is calculated by increasing the diameter (DUT1). Although the results do not fully correspond to the measurement results, the tendency is recognizable (see Table 4).

With approximately the same output power, the efficiency of the motor of DUT3 is consistently higher than that of DUT1. The maximum difference is about 4.2%. An attempt will be made to explain the observations for the drive with a simple loss model. The model considers the stator copper, rotor copper, iron, friction and fan losses. If the higher iron losses due to the higher stator frequency and the higher friction and fan losses due to the higher speed are taken into account in DUT3, the current heat losses must have a decisive influence on the observed courses [14].

The NPSH₃ value curve shows that the smaller pump with higher speed (DUT3) requires about twice the minimum inlet pressure than the larger pump at mains frequency (DUT1). This must be taken into account when dimensioning the components.

In summary, this measurement shows that even without using a throttle or a bypass, the use of a VSD can be advantageous over a standard pump. The design of the motor and pump components is decisive for efficiency here. In addition, the NPSH value must be taken into account when designing the hydraulic system.

5.3 Operating Point Adjustment via VSD

In this section, the operating point adjustment via VSD is compared with that via throttle valve. For this purpose, measured values from DUT3 were recorded over the entire operating range between the pump curves of DUT1 and DUT2 by setting the speed. This is compared with the efficiency if the same operating point was reached with the aid of DUT1 using a throttle valve. The difference of the measured pump unit efficiency is calculated at each operating point of DUT3 and DUT1, taking into account the throttle losses (Eq. 5).

The advantages of being able to adjust the speed are already evident in the illustration (see Fig. 7). DUT3 has a higher efficiency than DUT1 with the exception of

Table 4 Comparison of measured and calculated pump efficiencies

DUT	Speed	Measured η_{BEP}	Calculated η_{BEP}
DUT3	1850 rpm	60.2%	61.5%
DUT1	1370 rpm	63.6%	62.4%

a narrow area at the top right. The closer the operating point is to the pump curve of DUT2, the greater the difference in efficiency. The difference can be up to 6%. The reason for this is that the throttle losses increase the greater the pressure drop at the valve.

There are two reasons why the result is not even more drastic. One reason is the poor efficiency of the motor in the lower operating range. As shown in Investigation A, the motor efficiency in this range is 10% below compared to the upper working range (see Fig. 5). The second reason is pump efficiency. At the nominal point of DUT1 and DUT2, the efficiency of DUT1 is already 6.4% higher than that of DUT2 (see Table 2). The efficiency of DUT1 is also not achieved by efficiency scale-up, as shown in investigation B. Taking these two points into account, the advantage of DUT3 over DUT1 would be up to 12% higher than can be seen in Fig. 7.

In summary, this application case shows that a VSD pump is advantageous in terms of efficiency over throttling the flow with a valve. The greater the pressure drop across the throttle valve, the more profitable it is to use a VSD pump.

5.4 Reduction of Pump Sizes Due to Speed Adjustment

A simulation study was created to evaluate how the two design methods (a: trimming the impeller and using a fixed speed drive, b: individual fixed speed by using a VSD) can be compared to a real-world scenario. To achieve meaningful results, a large number of real customer operating points were used to avoid distortions that

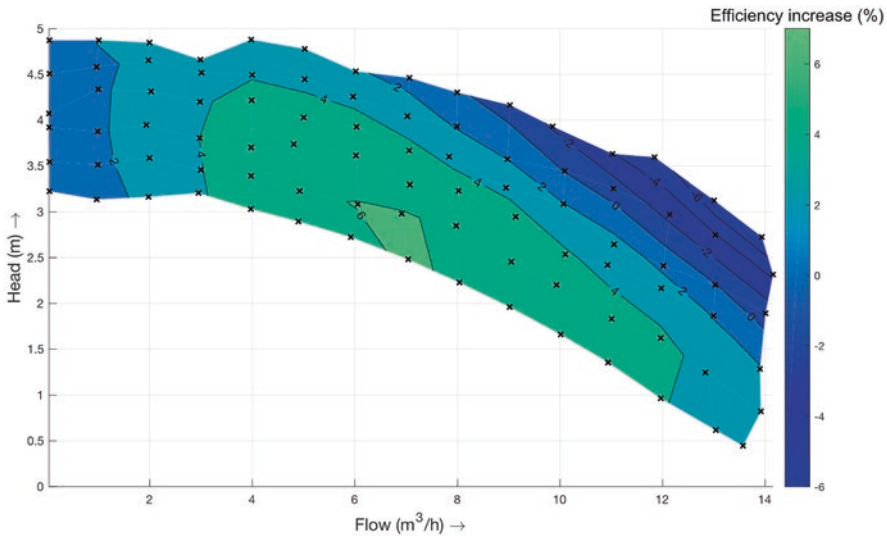


Fig. 7 Efficiency Increase using VSD pump (DUT3) compared to throttle controlled pump (DUT1)

would result from the selection of only a few operating points. The selected set of operating points corresponds in its statistical properties to the customer requirements for an entire series of pumps. The most suitable pump is calculated for each individual operating point, once after the impeller trimming approach and once after the new individual fixed speed approach.

The evaluated results from the pump simulation according to different design methods are shown in Fig. 8. The series under consideration comprises 26 sizes, of which only 21 are actually required to optimally cover the here considered range from 1 to 80 m³/h flow and from 1 to 30 m head. The limits of the approach are an NPSH value of 5 m and a maximum speed of 4200 rpm.

If the design is based on a drive with VSD, the total number of sizes can be reduced to 6 due to the variable frequency. Instead of covering the requested Q - H area with a large number of physical pump sizes with fixed speed drives, now a small number of pump sizes is used which cover the same Q - H area by continuous speed adjustment. By this, 71% of the pump sizes can be saved without any loss in efficiency. However, the frequency inverter, needed to realize a continuous speed range, as an additional device must be accepted. The required VSD, however, has only minor technical requirements, since it only has to be able to output a voltage with a variable frequency, sensor channels and complex control strategies are not required. Manufacturers should also be able to calculate the operating point of the IM and parameterize the VSD accordingly. If this procedure is assumed, the extensive commissioning of the VSD at the customer's site is not necessary. How the

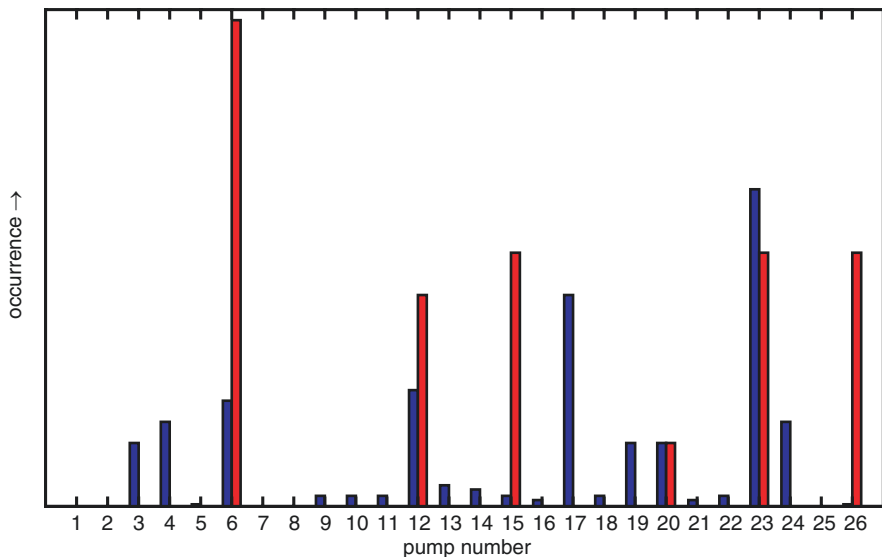


Fig. 8 Occurrence of pump number considering fixed speed pumps (blue) and variable speed pumps (red)

measure affects the costs of a pump unit and the entire series must be investigated in further work. However, significant savings can be made in warehousing.

6 Conclusion

This chapter examines the importance of VSD-driven pumps for users and manufacturers.

In order to answer the question which advantages VSD pumps have for users, a concrete application case with three pump configurations is examined. The first result shows that by using a VSD, smaller pumps can be used to serve the required operating points while improving the efficiency of the pump unit. This is advantageous for the users of pumps, who can thus save part of the required energy. The result of the second study shows that it may even be more efficient to replace a larger pump with a smaller VSD-driven pump. The result depends strongly on the selected motor and pump. The biggest advantage of a VSD pump is that the operating point can be adjusted flexibly. The operating point adjustment by means of the VSD pump is compared with that of the throttle valve. It turns out that in the almost complete Q - H range the VSD pump is more efficient than the conventional setting.

A further result is that, from a technical point of view, the majority of sizes can be saved in the series under consideration. The question remains as to how economical the concept of fewer sizes is by using a VSD. There are lower storage costs as well as savings in logistics and the additional costs of a technically simple drive.

The concept of variable speed pumps using a low-cost VSD is technically superior to other flow adjustment methods and has benefits for users and manufacturers.

Acknowledgements This research is part of the activities of the project “Application development of innovative resource and energy-saving circulation pumps for heating, air-conditioning, drinking water and solar systems” (Eco-Pump-Drive) with the project number 033R154, which is financially supported by the Federal Ministry of Education and Research in Germany. The project was funded under the $r +$ Impuls funding measure (Impulses for Industrial Resource Efficiency). The authors would like to take this opportunity to thank all the supporters who made this work possible.

References

1. A.T. de Almeida, P. Fonseca, H. Falkner, P. Bertoldi, Market transformation of energy-efficient motor technologies in the EU. *Energy Policy* **31**, 563–575 (2003)
2. F.J.T.E. Ferreira, J.A.C. Fong, A.T. de Almeida, Ecoanalysis of variable-speed drives for flow regulation in pumping systems. *IEEE Trans. Ind. Electron.* **58**(6), 2117–2125 (2011). <https://doi.org/10.1109/TIE.2010.2057232>
3. M. Pemberton, Variable speed pumping: Myths and legends. *World Pumps*, 22–24 (2005)

4. R. Saidura, S. Mekhilefb, M.B. Ali, A. Safari, H.A. Mohammed, Applications of variable speed drive (VSD) in electrical motors energy savings. *Renew. Sust. Energ. Rev.* **16**, 543–550 (2012)
5. V. Vodovozov, I. Bakman, Performance improvement of pumps fed by the variable speed drives. *Electr. Control. Commun. Eng.* **4**, 45–50 (2013)
6. G. Wohlauf, S. Thomas, W. Irrek, O. Hohmeyer, Erhöhung der Effizienz im Bereich der Umwälzpumpen in Industrie und Gewerbe, Handel, Dienstleistung (inklusive öffentlicher Bereich und Versorgungswirtschaft), Final report, 2005
7. J. Viholainen, J. Tamminen, T. Ahonen, J. Ahola, E. Vakilainen, R. Soukka, Energy-efficient control strategy for variable speed-driven parallel pumping systems. *Energy Effic.*, 1–15 (2012)
8. L. Gevorkov, V. Vodovozov, Study of the centrifugal pump efficiency at throttling and speed control, in *2016 15th Biennial Baltic Electronics Conference*, (BEC, Tallinn, 2016), pp. 199–202
9. KSB, NPSH, <https://www.ksb.com/centrifugal-pump-lexicon/npsH/191284/>, 28.07.2019
10. J.F. Gülich, *Centrifugal Pumps*, 3rd edn. (Springer, Heidelberg/Dordrecht/London/New York, . ISBN 978-3-642-40113-8, 2014)
11. M. Hess, P. Pelz, Comparison of Measurements on Axial Fans and Performance Prediction Using Common Scale-Up Methods at Part and Overload, in *Proceedings of FEDSM2009 ASME Fluids Engineering Division Summer Meeting*, 2009
12. M. Al-Khalifah, G. McMillan, Control valve versus variable-speed drive for flow control, *International Society of Automation*, 2013, [online] Available: <http://isa.org/>
13. KSB, Efficiency scale-up, Online: <https://www.ksb.com/centrifugal-pump-lexicon/efficiency-scale-up/328172/>, 25.07.2019
14. S. Bold, J. Dolgirev, S. Urschel, Resource and Energy Efficient Synchronous Reluctance Machine for Small Power Applications, in *2018 21st International Conference on Electrical Machines and Systems*, (Jeju, ICEMS, 2018), pp. 582–587. <https://doi.org/10.23919/ICEMS.2018.8549270>

New Composite Containment Shell for Magnetically Driven Pumps



Nicolas Weibel, Samuel Stutz, Daniel Rougnon, and Frederic Perrottet

1 Introduction

The invention of magnetically driven pumps dates back to the 1940s. However, the magnets available at that time were Aluminum–Nickel–Cobalt (AlNiCo) based with a maximum density of magnetic energy (BH_{\max}) of some 50 kJ/m^3 . In the 1970s, Samarium–Cobalt ($\text{Sm}_2\text{Co}_{17}$) magnets were invented with BH_{\max} of some 300 kJ/m^3 and finally in the 1980s, Neodymium–Iron–Boron ($\text{Nd}_2\text{Fe}_{14}\text{B}$) magnets offered energy densities above 400 kJ/m^3 . Thanks to these much stronger magnets, it was possible to produce coupling systems with significantly higher torque values, capable of driving large pumps with more than 500 kW. To separate the outer magnets, connected to the motor and running in a dry environment, from the inner magnets, connected to the impeller and immersed in the pumped fluid, a shell is needed, the so-called containment shell. Traditionally, this shell is made from stainless steel or other metals with low electric conductivity such as Inconel or titanium. However, any electrically conductive material placed between the rotating magnets will generate eddy currents. These currents generate heat in the shell due to the Joule's effect. It is therefore important to have a continuous flow of liquid along the shell to drive off the produced heat. Unfortunately, this heat generation makes traditional magnetically driven pumps inefficient with losses that can exceed 20% of the power delivered by the motor. Furthermore, any upset condition that leads to a fluid starvation would quickly destroy the pump if it runs dry. For these two reasons, i.e., low efficiency and poor robustness to upset conditions, magnetically driven pumps only represent approximately 3–4% of today's rotating pump market (Fig. 1).

N. Weibel (✉) · S. Stutz · D. Rougnon · F. Perrottet
Greene, Tweed & Co., Kulpsville, PA, USA
e-mail: nweibel@gtweed.com; sstutz@gtweed.com; drougnon@gtweed.com; fperrottet@gtweed.com

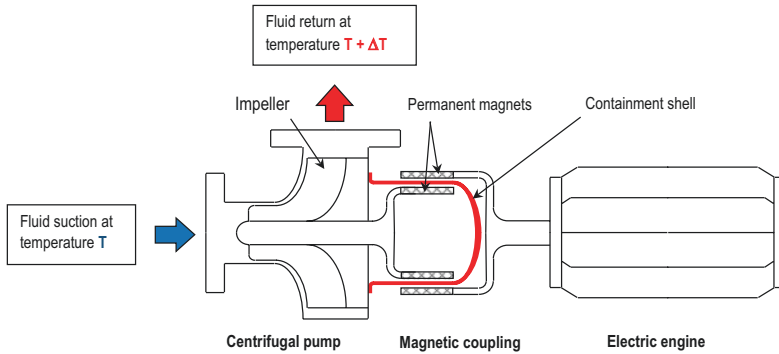


Fig. 1 Schematic of a magnetically driven, single stage, centrifugal pump

The advantage of a magnetically driven pump is that no dynamic seal is involved, making these pumps almost maintenance-free. Another advantage is that they conform to the zero-emission requirement as needed for an increasing list of toxic, explosive, and carcinogenic fluids. The majority of magnetically driven pumps are therefore installed in refineries and chemical plants for the more challenging fluid-handling operations. Other applications are found in difficult-to-maintain areas, such as offshore platforms, nuclear plants, or super tankers to stir the oil during transportation. While for some of these applications, the lower efficiency is of little concern, the risk of pump damage in case of an upset condition can have catastrophic and very expensive consequences. As a result, a new kind of containment shell material was engineered, called Xycomp®, which practically eliminates the eddy currents, and hence makes magnetically driven pumps as efficient and reliable as standard mechanically sealed pumps but with the added advantage of zero emission and prolonged mean time between maintenance (MTBM).

2 Xycomp® Pump-Shells

Xycomp® pump-shells are made of an advanced composite with 60% long carbon fibers and 40% polyetheretherketon (PEEK), a highly chemically resistant polymer originally engineered by the NASA for the space race in the 1970s. This composite is non-fragile even at cryogenic temperatures and has shown upper continuous service temperatures for containment shells of 180 °C (350 °F). Its high strength and stiffness, combined with a very low electric conductivity, make it an ideal candidate for pump-shell applications [1]. The manufacturing process is, however, a manual lay-up of a non-woven fabric, which requires skilled labor leading to shells that are typically 50% higher in cost than high-end metallic shells used in the API market with 40 bar pressure rating. For lower pressure applications, as found in the

ANSI/ASME market, an alternative is to manufacture shells based on a chopped C/PEEK composite called Xycomp® DLF. The shells can be produced with more automation opportunities, offering a cost-competitive option to pump OEMs. This option has been used in the Aerospace market for more than 10 years for parts near the engine, to replace complex shaped Inconel or titanium parts [2, 3]. Based on our experience, we developed Xycomp® DLF containment shells. These shells offer approximately 40% lower service pressure at a price closer to, or even below, that of metallic shells (Fig. 2).

3 Internal Testing

To validate the performance of Xycomp® shells, we performed a large number of tests as needed to build trust amongst the pump OEMs and end users.

3.1 Burst Pressure

According to API 685, every shell produced must be exposed to a pressure 1.5 times the maximum service pressure for a duration of 30 min and show no leak. To ensure passing the proof test with significant safety, and to accommodate the variability inherent to composite materials, shells are designed with a burst pressure of approximately 2.5 times the service pressure.

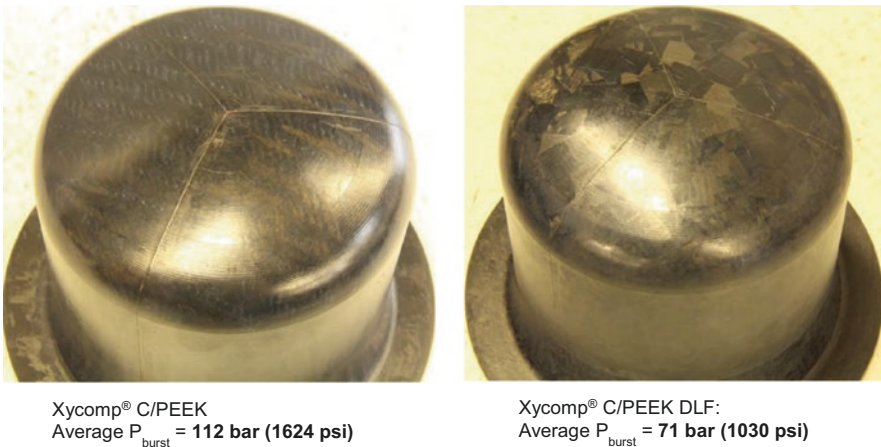


Fig. 2 Average burst pressures of Xycomp® & Xycomp® DLF pump-shells with an identical design

3.1.1 Room Temperature Burst Pressures

To validate the design, before shells are offered to pump-OEMs, 10 shells are tested up to burst pressure (Fig. 3).

3.1.2 Cryogenic Temperature Burst Pressures

To evaluate the lower temperature limit, shells have been pressurized up to burst once immersed and filled with liquid nitrogen at $-196\text{ }^{\circ}\text{C}$ ($-321\text{ }^{\circ}\text{F}$) using helium gas. As helium has limited solubility in nitrogen, and as its liquefying temperature is significantly lower than that of nitrogen, it was possible to pressurize the shells up to their burst pressure.

The shell shown in Fig. 4 had a burst strength of 82 bar. A second shell had a small crack at 80 bar but could not be burst due to excessive leakage. Indeed, sealing off against helium gas a relatively large shell at $-196\text{ }^{\circ}\text{C}$ ($-321\text{ }^{\circ}\text{F}$) was technically challenging. However, the safety factor above two against the service pressure was sufficient to establish the trust amongst pump OEMs.

3.1.3 Elevated Temperature Burst Pressures

To define the maximum service temperature, creep tests at maximum service pressure for up to 10,000 h have been performed at $120\text{ }^{\circ}\text{C}$ ($248\text{ }^{\circ}\text{F}$), $160\text{ }^{\circ}\text{C}$ ($320\text{ }^{\circ}\text{F}$), $180\text{ }^{\circ}\text{C}$ ($356\text{ }^{\circ}\text{F}$), and $204\text{ }^{\circ}\text{C}$ ($399\text{ }^{\circ}\text{F}$). After more than a year of creep testing, the shells were tested for their residual strength at exposure temperature.



Fig. 3 Room temperature burst pressures of different shell sizes and geometries

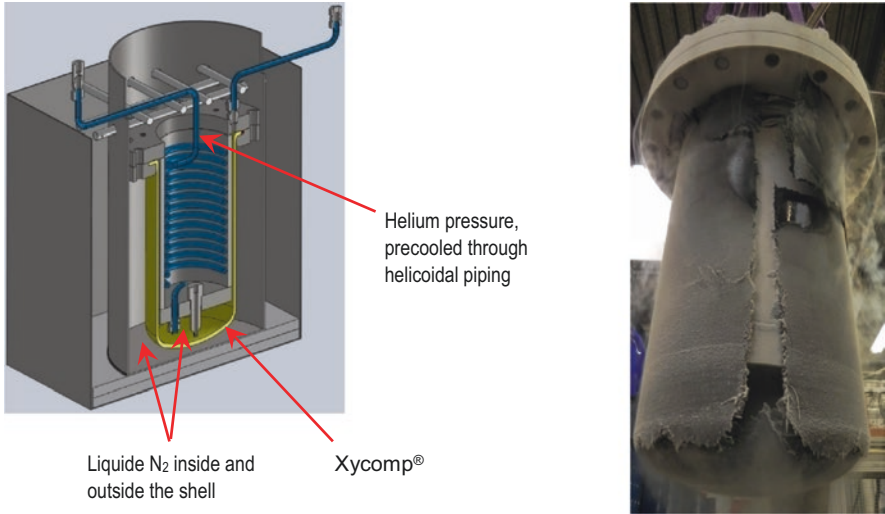


Fig. 4 Cryogenic burst testing jig and burst shell

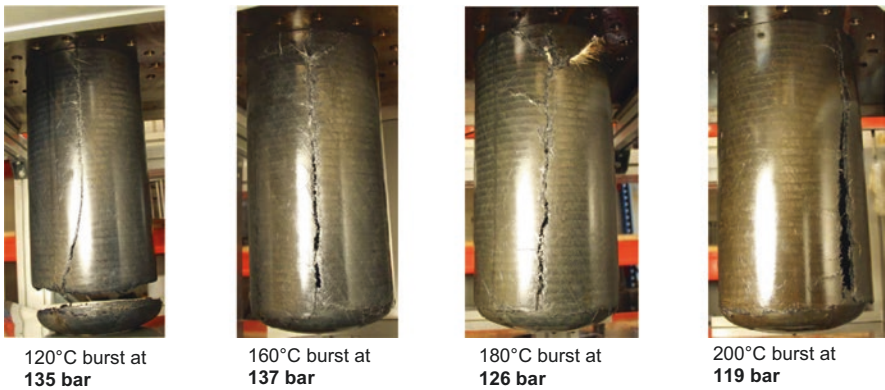


Fig. 5 High-temperature burst strength

The average burst pressure, at room temperature, of the shells shown in Fig. 5 is 120 bar. As shown, there is no strength reduction with temperature; however, a change in failure mechanism was observed. Indeed, looking at Fig. 3, the burst shells in the upper right corner show six dome failures and four rim failures. In other words, failures are located at the transition radius at either end of the cylindrical portion of the shell. This is due to the stress concentration in this area built in during processing as the through thickness CTE (coefficient of thermal expansion) is much larger than the in-plane CTE, hence building up internal stresses during the cooling from the liquid state down to room temperature. At elevated temperature, this stress concentration is relaxed. At 120 °C (248 °F), a temperature just below the glass

transition temperature (T_g) of PEEK, both failure modes are observed with a dome and hoop crack combined. At higher temperatures, above T_g , the hoop crack is dominant.

3.2 Creep Testing

Four shells have been exposed to over 40 bar pressure at 120 °C (248 °F), 160 °C (320 °F), 180 °C (356 °F), and 204 °C (399 °F) for 10,000 h, with data acquisition on seven diameters measured along the cylindrical portion of the shell after 1, 3, 10, 30, 100, 300, 1000, 3000, and 10,000 h. The temperature was measured at the top and base of the shell. The oil inside the shell was constantly stirred using a magnetic agitator to ensure a homogeneous temperature throughout the shell. Continuous data acquisition demonstrated that the maximum temperature gradient within any given shell never exceeded 2 °C (36 °F). To guarantee a minimum pressure of 40 bar, the actual pressure was set to 43.5 bar as the daily thermal fluctuations led to pressure variation of up to ± 1.5 bar (Figs. 6 and 7).

To capture permanent deformation, the shells were periodically taken out of the creep testing jig, cleaned, dried, and measured on a coordinate measuring machine (CMM) measuring seven diameters based on 420 acquisition points (60 points per diameter). The average permanent deformation is shown by the increased diameters represented in Fig. 8. The dotted lines show the growth slope, indicating the expected permanent deformation extrapolated to 20 years for the 120 °C, 160 °C, and 180 °C



Fig. 6 Creep testing jig set-up. Four shells are simultaneously tested above 40 bar at 120 °C (248 °F), 160 °C (320 °F), 180 °C (356 °F), and 204 °C (399 °F) for 10,000 h

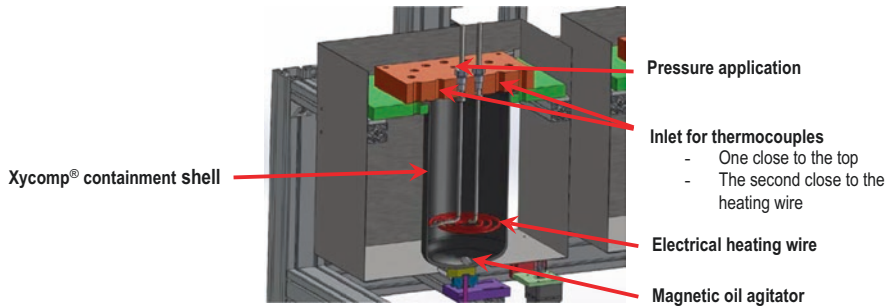


Fig. 7 Details of the testing jig shown in Fig. 6

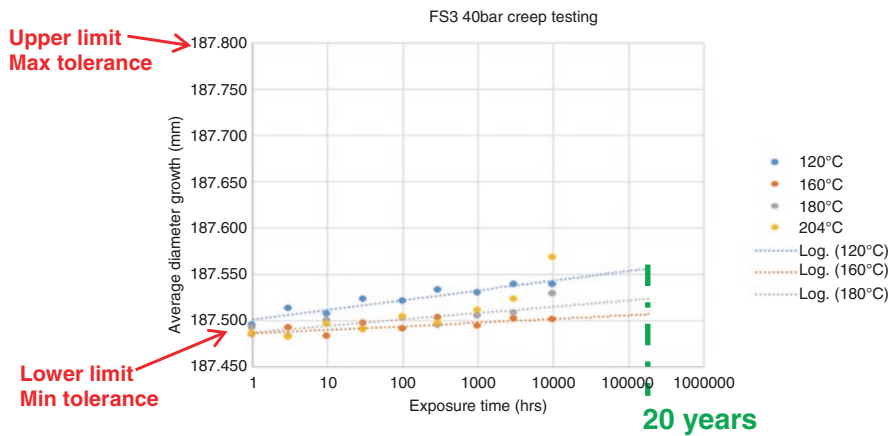


Fig. 8 Permanent diameter growth after 10,000 h exposure to 40 bar pressure. For temperatures up to 180 °C, an extrapolation is shown to 20 years

shells. For the 204 °C shell, the curve starts to bend into a non-linear shape, which indicates an acceleration in creep. Therefore, no extrapolation is presented up to 20 years for that temperature.

For the three lower temperatures, the extrapolation to 20 years indicates an expected permanent diameter increase of no more than 0.05 mm, which is only a fraction of the available maximum tolerance level of 0.30 mm, which means that the shell remains fully functional. Also, for comparison, when the shell is pressurized to 40 bar, this diameter will expand by 0.38 mm and just prior to burst, at 120 bar, by 1.14 mm.

The maximum service temperature for Xycomp® DLF shells is also 180 °C (356 °F), as demonstrated by a large creep testing campaign conducted over 2 years to obtain the master data curve for DLF creep properties [4].

3.3 *Fatigue Testing*

Fatigue testing was performed to ensure that over time no strength reduction appears, even when pumps are periodically started and stopped. Assuming a maximum of five starts and stops per day for a duration of 20 years, tests have been conducted up to 36,000 cycles between ambient pressure and maximum service pressure. Inspection was performed after 1, 10, 100, 1000, 10,000, and 36,000 cycles (Fig. 9).

To inspect a possible progressive damage, a dye penetration inspection has been used which revealed certain crack-like surface features. It is to be noted that dye penetration inspection techniques are common for metallic inspections but are normally not used for composites. Nevertheless, it allowed us to monitor these surface features after progressively larger numbers of pressure cycles (Fig. 10).

Seven surface cracks have been spotted and were observed over the entire testing program. As shown in Fig. 11, there is no indication that any of them grew during the 36,000 cycles. Note that there is a significant scatter due to the test method.



Fig. 9 Fatigue testing jig

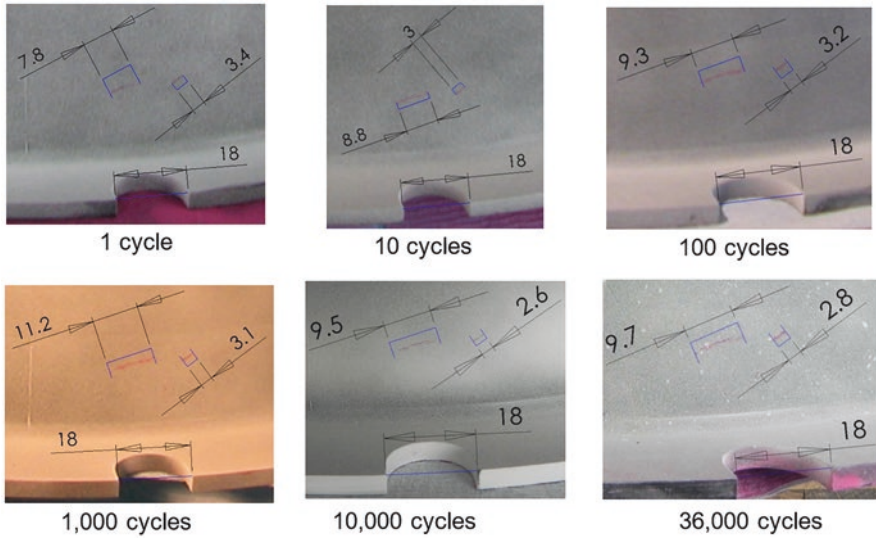


Fig. 10 Pictures of the same section of the containment shell after various number of cycles showing the surface crack length measured using a dye penetration inspection

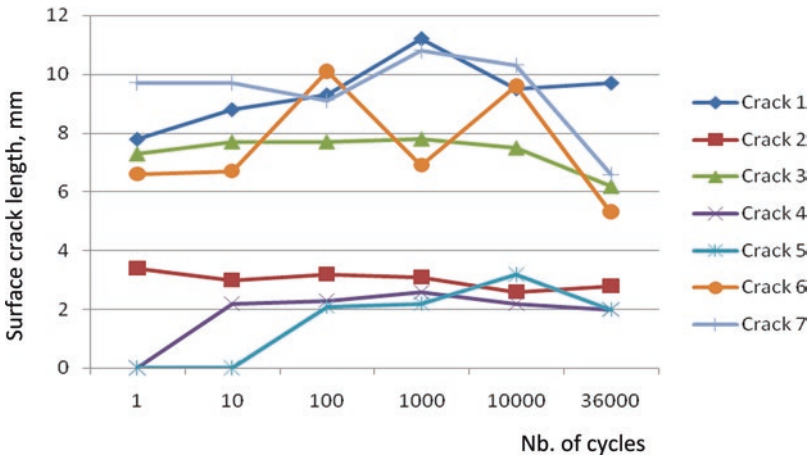


Fig. 11 Surface crack lengths evolution as a function of pressure cycles

4 Other Tests

Other tests have been performed, e.g., thermal shock, to demonstrate that even when pouring liquid nitrogen into a room temperature shell, or pressing a shell into a bath of liquid nitrogen, no damage is caused as demonstrated by a subsequent helium gas tightness test. Another test is a fire test, where an empty shell is exposed to a 1000 °C

(1832 °F) flame for 15 min. We demonstrated that a 2-mm-thick shell was sufficient to avoid flame burn-through.

To assist OEMs when they design the pump assembly, we simulated the stiffness of our shells using FEA tools based on an Abacus code. To validate the simulations, shells were pressurized with water in a jig placed on a CMM and showed good correlation between actual and predicted values. For example, a radial deformation was predicted at 0.35 mm and was found to be 0.33 mm on the actual shell. The length elongation of the same shell was predicted at 0.85 mm and turned out to be of 0.90 mm. Another important information needed by an OEM during the design phase is thermal expansion. Using Digital Image Correlation (DIC) equipment, very accurate coefficient of thermal expansion (CTE) could be measured. For Xycomp® shells, the OD CTE is of 5.6 $\mu\text{m}/\text{m}/^\circ\text{C}$ and the axial length CTE is of 6.8 $\mu\text{m}/\text{m}/^\circ\text{C}$.

5 OEM Testing

Our customers have also performed significant testing to demonstrate the safety and superiority of the Xycomp® shell compared to either metallic or ceramic containment shells. They created an advertisement movie [5] to demonstrate how robust the Xycomp® shell is against impact, one of the drawbacks of ceramic shells, which are often damaged during installation. Furthermore, they have run sand through a pump to evaluate shell erosion and concluded that the erosion rate was three times slower on Xycomp® shells than on Inconel shells. Finally, they published a case study about a quite challenging fluid to be pumped, namely Trichlorosilane (TCS). This liquid has a high density of 1342 kg/m^3 , a low boiling point of 31.8 °C (89 °F), combined with a very low specific heat capacity of 820 $\text{J}/\text{kg}/^\circ\text{C}$ (compared to water at 4180 $\text{J}/\text{kg}/^\circ\text{C}$). Because of the combination of these three properties, TCS is very challenging to pump, with a high risk of cavitation if the vapor pressure limit is reached. Indeed, fluid temperature measurements have shown that if a pump is lined with an Inconel shell, the temperature of TCS increases by 50 °C (122 °F) as it runs through the pump, whereas the same pumping conditions will only generate a temperature increase of 4.5 °C (40 °F) when the pump is lined with a Xycomp® shell. Due to the low boiling point, several catastrophic failures were observed in the field until Xycomp® shells were used as a retrofit solution and no further failure has been observed since [6].

5.1 Dry Running

An OEM did a full-scale test to evaluate the difference between a metallic containment shell and a Xycomp® shell in an upset condition of fluid starvation. The metallic shell was sectioned by the (thermally) expanding magnets within 3 min. Additionally, the heat from the eddy currents evaporated the remaining liquid,

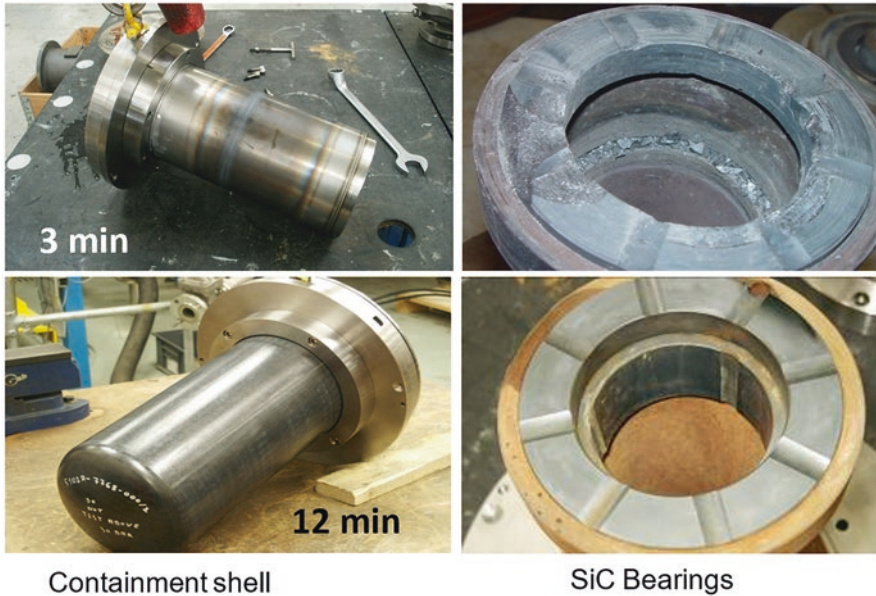


Fig. 12 Top section: Damaged metallic shell and SiC Bearing after a 3-min dry running test. Bottom section: Undamaged Xycomp® shell and intact SiC Bearing after a 12-min dry running test

which caused the SiC bearings to shatter and destroy the entire pump. The Xycomp® shell run for 12 min in the same condition of fluid starvation, before the test was stopped to inspect the pump. The inspection showed that no damage had occurred to any parts of the system (Fig. 12).

6 Conclusions

Ten years after the first Xycomp® shell sold on the market, nearly 1000 pumps are running with Xycomp® shells worldwide. It was a very slow market penetration curve, as the magnetically driven pump market is extremely conservative due to the probable very high cost of in-service failure. Today, Xycomp® and Xycomp® DLF pump-shells have proven to be a highly reliable product, offering significantly more safety in-service than any metallic or ceramic shell can offer.

Xycomp® shells are well suited for the API 685 market, with service pressure above 40 bar (above 580 psi), a temperature range from $-120\text{ }^{\circ}\text{C}$ ($-184\text{ }^{\circ}\text{F}$) to $180\text{ }^{\circ}\text{C}$ ($356\text{ }^{\circ}\text{F}$), and diameters above 300 mm (12 in.). They feature thin walls, high impact, and thermal shock resistance and practically eliminate the major issue of traditional magnetically driven pumps, namely the eddy currents generated by metallic shells. For a lower pressure market, Xycomp® DLF shells are highly cost competitive even to metallic shells, while still offering all of the above advantages.

If the elimination of eddy currents is key to the significantly improved reliability, it also comes with another great benefit: much lower running cost, saving the end user as much as 25% electricity. As an example, when switching from an Inconel shell to a Xycomp® shell, one pump of the size shown in Reference [5] will save the end user as much energy as that which 50 people consume, based on the average European electricity consumption.

Acknowledgment We would like to acknowledge Sundyne HMD Kontro Company for their trust placed in our product and to bring it first to market.

References

1. N. Weibel, T. Bieler, Magnetic-coupled pumps: the containment shell. EEMODS'09, Paper #46, 6 May 2009
2. T.L. Greene, Discontinuous long-fiber composites for complex shaped metal replacement. CMAX 2014, Orlando, FL, 13–16 October 2014
3. T.L. Greene, C. Wonderly, M.H. Kilic, B. Keller, Complex-shape metallic aircraft engine bracket replacement using compression molded discontinuous long fiber thermoplastic composites. CMAX 2015, Texas, 26–29 October 2015
4. S. Stutz, N. Weibel, Creep of discontinuous long fiber C/PEEK above T_g. ITHEC 2018. 4th International Conference and Exhibit on Thermoplastic Composites, Bremen, Germany, 30–31 October 2018
5. <https://www.youtube.com/watch?v=Uh8Lgi2bJ9A>
6. I. Guthrie, N. Weibel, S. Stutz, Case study – “using engineered composite materials in seal-less magnetic drive pumps to eliminate eddy current losses and improve reliability”. 45th Turbomachinery & 32nd Pump Symposia, Houston, TX, 12–15 September 2016

Hydraulic System Optimization



Sandie B. Nielsen, Claus M. Hvenegaard, Otto Paulsen, and Søren Draborg

1 Introduction

Optimizing hydraulic systems is primarily about choosing the right size or sizes of pumps in the right configuration and the appropriate control strategy for the pumps, thereby achieving maximum energy efficiency of the entire system (Fig. 1).

Hydraulic systems driven by electric motors are in widespread use in industry. Hydraulic components include pumps, hydraulic motors, cylinders for linear movements, and hence a large variety of valves.

For an incompressible fluid, the hydraulic power is:

$$P = QV \cdot \Delta p$$

Where

P is the mechanical power in W

Q_v is the fluid flow in m^3/s

Δp is the pressure difference in N/m^2

Hydraulic power components have generally a high efficiency when sized correctly. For motors and cylinders, often over 90%. Therefore, system losses are mostly related to the system design. The cheapest and still very common system runs at constant speed and with a constant flow. Oil not used pass at a simple overflow valve, so flow and pressure are independent of the actual load, and hence also the load at the electric motor. This may in some cases lead to very poor efficiency.

S. B. Nielsen (✉) · C. M. Hvenegaard · O. Paulsen · S. Draborg
Energy & Climate Division, Department of Energy Efficiency & Ventilation, Danish
Technological Institute, Taastrup, Denmark
e-mail: sbn@dti.dk; cmh@teknologisk.dk; otp@teknologisk.dk; sdg@teknologisk.dk

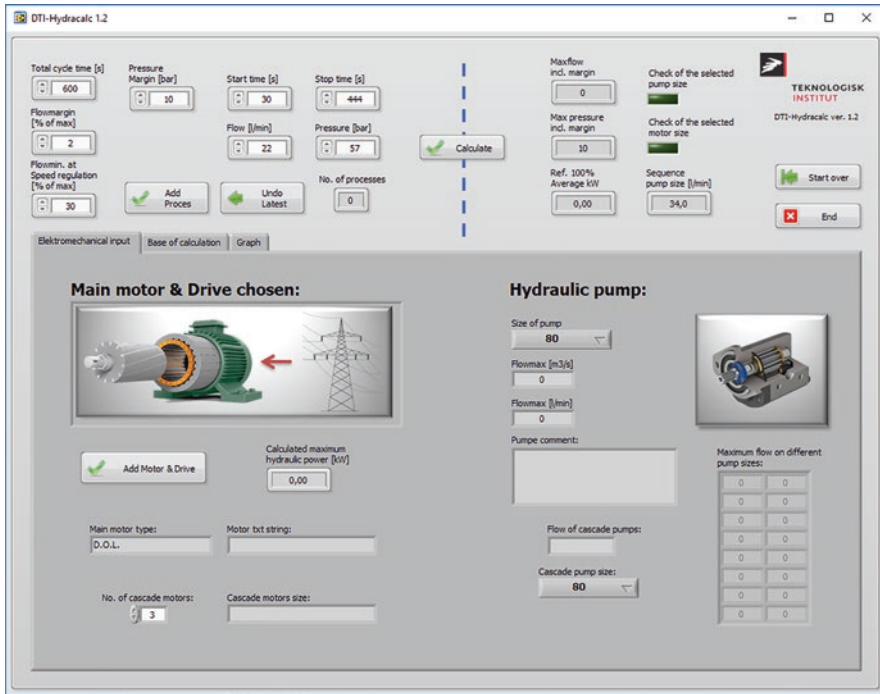


Fig. 1 Main screen of hydraulic optimization tool

This is especially the case, when one motor pump serves many processes with different demands for flow and pressure.

Modern hydraulic system component offers many possible control strategies:

- Control of motor speed and hence the pump capacity
- Control of pump displacement
- Control of the overflow-valve

For a given system, the minimum hydraulic power is found when the pump pressure matches the highest process pressure, without any pressure drop in the control valves and when the oil flow matches the sum of the flow demand for the individual processes. This control is called “load sensing system.” When the pump efficiency and motor efficiency is included in the calculation, it sometimes changes the optimal result. The optimization tool hence can be used for analyzing the possible solutions for new as well as possible energy savings in existing systems.

1.1 Basic Considerations

The optimization tool based on the starting point for the calculations is the application of a table with flow and pressure as a function of time, which corresponds to Fig. 2 [1].

The application is based on systems with one pump and systems with several identical pumps. Basically, an overall assessment of the structure must always be carried out. If there are large variations in simultaneous pressure requirements, it will always be the highest pressure that determines the operation and even with Load Sensing or EFM (Electrohydraulic Flow Matching – speed control) there will be limitations on the achievable energy economy. In such cases, several separate pumps, such as a high pressure and a low-pressure pump. If the developed calculation tool is to be used in such cases, the calculations can be repeated with the processes divided into different pressure systems.

Input to the developed calculation tool is made based on a detailed review of the processes the plant serves. In the tool, values for flow and pressure need be entered for each of the processes operated by the hydraulic system. Values must be entered for one total process cycle, including a possible idle period. Furthermore, a pressure margin and a flow margin are defined, although not all systems require this. For example, a speed-controlled motor/pump after flow will not necessarily require flow and pressure margin beyond the process requirement.

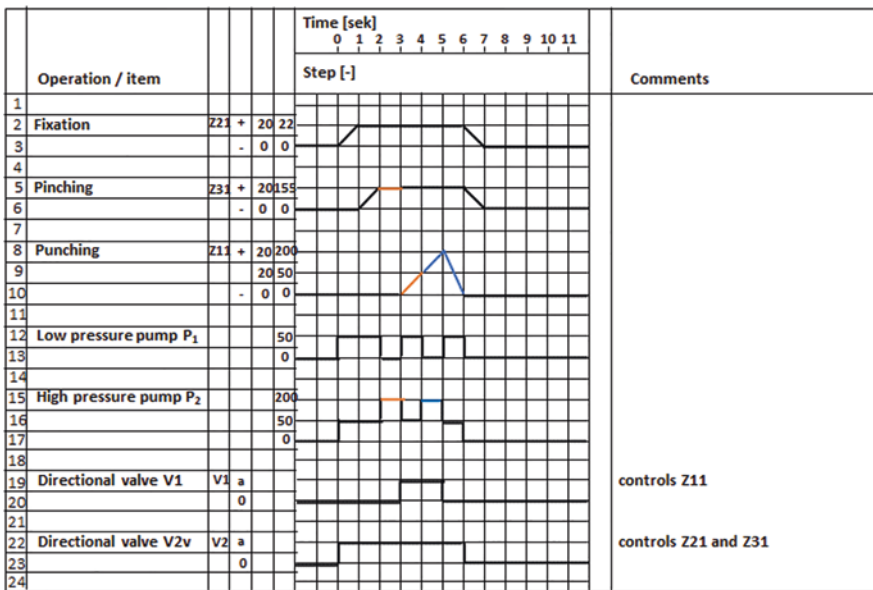


Fig. 2 Table of flow and pressure as a function of time

In the development of the tool, mathematical expressions for hydraulic components are set up based on data from data sheets and performance curves. An advanced energy calculator part has been developed that can handle the various forms of control that are normally used in the industry. The developed calculation tool can handle a total of 10 different types of control. The tool can be used both for analysis of existing plants and even planning new installations.

0. Separate pump for each process. This is an idealized system where pumping work is exactly the same as the need for each consumption point. Here, the work performed is equal to the energy supplied to the pump near the friction loss. The hydraulic system efficiency here is 100%. This system structure is the reference for the efficiency of other systems.
1. V1: Constant flow and pressure control. Pump and motor run constantly, but the over-current valve is continuously adjusted to the maximum working pressure and there is pressure relief at idle. Motor and pump run at approximately constant speed. If the flow requirement does not vary so much, but the pressure requirement varies, this system is suitable.
2. V2: Constant motor speed and variable displacement pump. The overflow valve is set to constant high pressure, but the flow is adjusted so that only a small amount of control or nothing runs out of the overflow valve. Motor and pump run at approximately constant speed. If the pressure requirement varies slightly, and the flow requirement varies greatly, this system is suitable.
3. V3: Load sensing. Constant speed of the pump and the displacement of the pump are controlled by load-sensing signals for pressure and flow. Here, both flow and pressure are adapted to the need: The pressure is adapted to the highest pressure, typically with a small margin, and the displacement is adapted to the flow requirement typically with a small overflow. This system can achieve a high hydraulic efficiency and is suitable for systems with large variations in both pressure and flow requirements. The pump displacement will typically be controlled down to near zero.
4. V4: Speed control of pump with constant displacement and pressure. The pump is equipped with a speed-adjustable motor so that the speed is regulated according to the flow requirement and the over-flow valve is set at the highest possible pressure plus a pressure margin. Optionally, a small control flow must flow through the overflow valve. The system can also be realized electronically without flooding. The control range will be limited by the lowest possible speed. It is important that the motor torque is still high at low speeds (as opposed to what applies to the operation of fans and pumps). The system is suitable for small variations in pressure requirements and large variations in flow.
5. V5: Constant speed for the pump and constant pressure and flow. An often-used primitive system. At constant flow and pressure, a pump with constant displacement is selected, e.g., a georotor or gear pump and a constant-speed engine. The overflow valve is set to the highest pressure + a pressure margin. This system will provide the lowest system efficiency. Motor and pump, on the other hand, can be dimensioned to run at maximum efficiency.

6. V6: Constant speed for the pump and flow but with pressure relief. The system described in V5 can be supplemented with a pressure relief device, so that the pump is short-circuited at idle, almost typically a pressure of 5–10 bar. This can give great improvement in processes with long idle time and reduce the cooling requirement accordingly. Motor and pump run at approximately constant speed. The pump will typically run at high power input.
7. Speed adjustment using load sensing. The flow is adjusted to the need, possibly except for a small control flow. The pressure is adjusted to the current maximum pressure demand. In the case of LS systems with variable pump displacement and constant rotation, higher engine and pump efficiency levels can be achieved in some cases.
8. V8: Step control with constant pressure adjusted on the overflow valve, flow matching by stepwise operation of motor/pump. Only one engine and pump combination are defined. Up to four similar motor and pump combinations can be defined. Each of them runs with both constant flow and constant counterpressure and thus constant power consumption.
9. V9: Step control with pressure adjusted to actual maximum, flow matching by stepwise operation of motor/pump. Up to four similar motor and pump combinations can be defined. Each of them runs with constant flow and with a back pressure adjusted to maximum need + a small margin.

1.2 Pump Model

The basic calculations in the hydraulic part of the tool are based on the fundamental hydraulic Eq. 1. But a model for the efficiency of hydraulic pumps is needed.

An axial piston pump model based on Kawasaki's K3VL pump series has been developed. K3VL pumps are available in nominal displacements ranging from 28 to 200 cm³/rev and can provide a pressure up to 350 bar [2].

Input to the model is flow and pressure and output is the efficiency. The pumps have variable displacement, so fundamentally the speed is constant, and the capacity is varied by varying the displacement. However, the physics of efficiency is the same for pump types with fixed displacement; so as a compromise, the same model is used for fixed displacement and variable speed.

1. The basic assumption is that the volumetric efficiency only depends on the pressure and displacement (and the size of the pump).
2. It is assumed that the *not transported* volume of liquid expressed by the volumetric efficiency is also pressurized to the pump's output pressure.
3. In addition, it is assumed that the mechanical efficiency can be expressed by a constant friction torque that depends only on the pump size and the pressure. This is an approximation, since some of the torque will depend on the speed.

All together deviations are found between the developed pump model and the curves underlying the model of up to 4% at low pressure and slight displacement, and 1–2% at high pressure and flow.

When desired pressure p and flow Q_v is known, the hydraulic power is calculated by:

$$P_{\text{hyd}} = p \cdot Q_v [W],$$

where P is the pressure [Pa] and Q_v is the flow [m³/s].

The torque corresponding to the hydraulic work is then:

$$M_{\text{hyd}} = P_{\text{hyd}} / \omega,$$

where ω is the angle speed [s⁻¹].

The shaft power is:

$$P_{\text{axle}} = (M_0 + M_{\text{hyd}}) \cdot \omega$$

The efficiency is:

$$\eta = P_{\text{hyd}} / P_{\text{shaft}}$$

The correlation between the pump size, the pressure, and the volumetric efficiency is found by linear regression; however, displacement ratio (displacement) is included with its reciprocal value.

It is a reasonable assumption that the physics of hydraulic pumps are generally represented by this model. It is therefore allowed to extrapolate this model to larger displacement at 200 cm³. In case other types of pumps are used, the results are qualitative, and it is then recommended to check the efficiency compared to the model used here (Fig. 3).

1.3 Motor and Drive

In the Hydraulic Optimization Tool, it is necessary to choose a motor and a drive. The motor calculator from the well-known Motor Systems Tool is used for that [3].

When clicking on “Add Motor & Drive” the screen in Fig. 4 appears.

It is possible to choose an asynchronous motor (standard motor) and drive. By default it is assumed that there is no frequency converter, i.e., the motor is started directly (Direct On Line – D.O.L).

It is also possible to choose if the motor is supplied by a soft starter and a frequency converter.

K3VL80

Pump Efficiency (%)

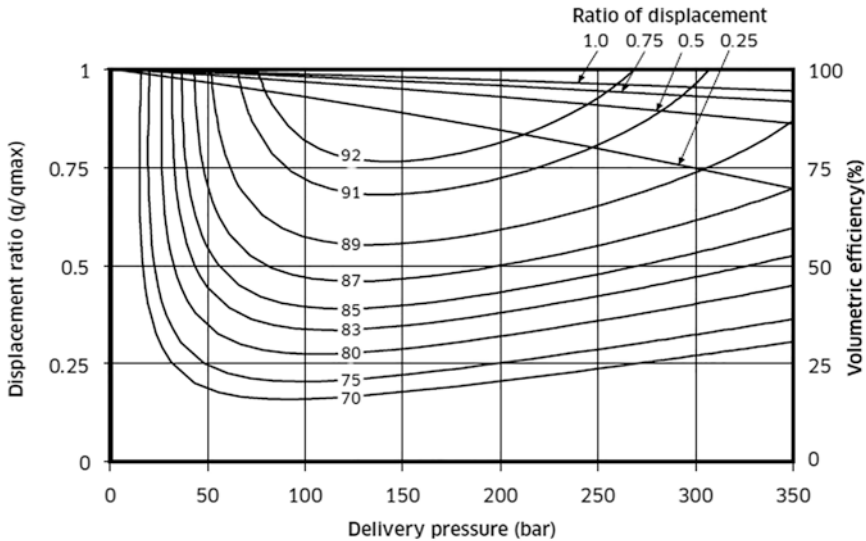


Fig. 3 Efficiency chart for one of the Kawasaki pumps that is a background for the pump model [2]

It is also possible to choose a permanent magnet motor (PM-motor) and a synchrony reluctance motor (SynRM-motor). The two last motor types always have a drive included (frequency converter).

Finally, it is possible to choose an asynchronous motor with data according to IEC 61800-9-2, Annex A and Annex D [4].

2 Example

There are four processes as given in Table 1.

The data are entered in the start screen. The “result” screen gives the graph as in Fig. 5.

When motor and drive are chosen, the result now is as in Fig. 6.

In Fig. 6, average power P1 the input electrical power to the drive and the efficiency is chosen. The best efficiency is achieved with speed control and constant pump displacement. In this case, this LS control is 26% lower.

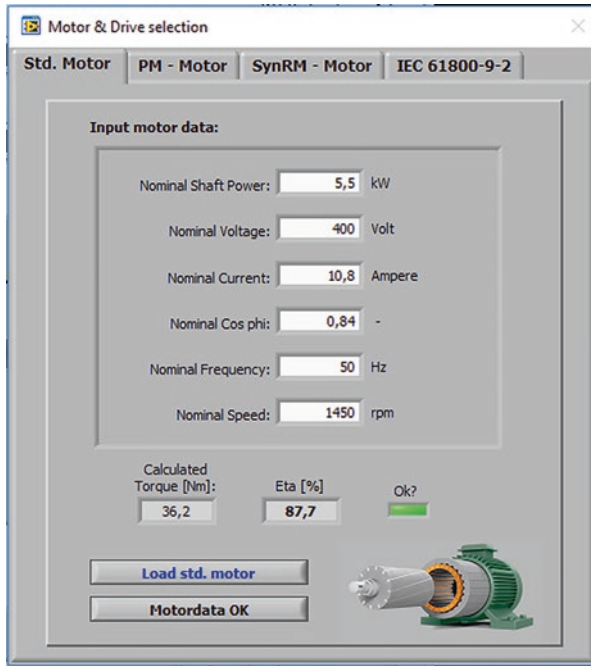


Fig. 4 Choosing a motor and a drive

Table 1 Definition of the processes. It could be movement, fixing the item, processing the item, and release of the item

Process number [-]	1	2	3	4
Start [s]	0	1.5	50	100
End [s]	12	90	100	200
Flow [l/min]	20	10	30	0
Pressure [bar]	100	50	200	0

It is possible to see more detailed results and it will show that the LS system has a larger efficiency than the speed control, but this advantage is cancelled by the decreasing pump efficiency, when the displacement is reduced. Compared to the simplest system, the speed control reduces the power to 11% and the oil cooling demand by 41 kW. Also, it is seen that flow control is better than pressure control, which is often the case.

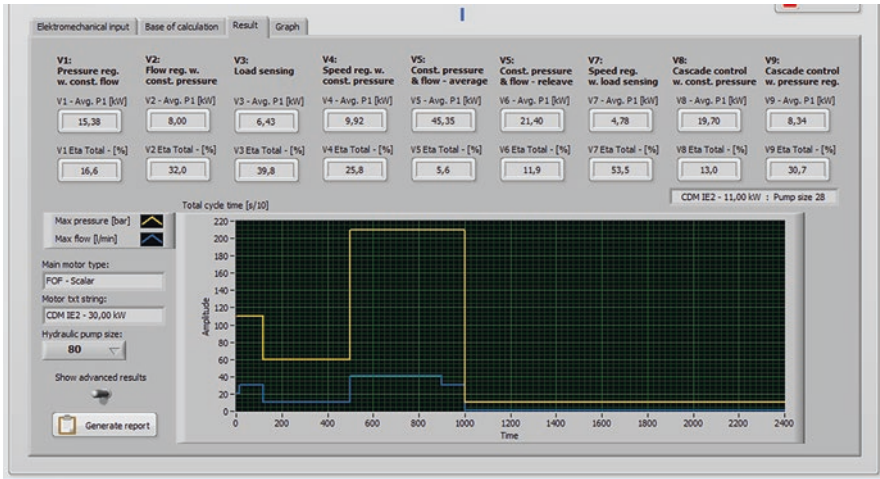


Fig. 5 The total flow in a graph

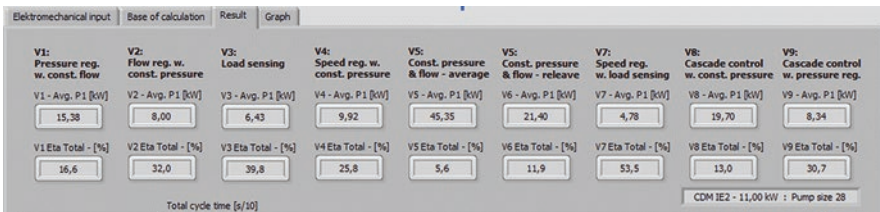


Fig. 6 Results when motor and drive are chosen

3 An Example from the Field

Below is an example of use of the Hydraulic Optimization Tool in practice. The example originates from NLMK Dansteel and deals with a heating furnace for baby slabs.

Baby slabs are transported after cutting and marking to the natural gas fired furnace, where they are heated for approx. 4 h to about 1.200 °C, which is the roller temperature. The temperature is computer controlled and cannot exceed 1.325 °C (Figs. 7, 8, 9, and 10).

The hydraulic system of the furnace is equipped with four identical Bosch Rexroth A4VS0-250 DR hydraulic pumps with 110 kW motors at 1.485 rpm.

The pumps are variable displacement axial piston pumps. The three pumps supply the system on each supply tube (east, center, and west), and one pump is in reserve. The spare pump can supply each of the three supply pipes (switching with manually operated valves). The “center” pump is usually the most heavily loaded hydraulic pump. The furnace has a hydraulic pump for each of the three tracks/beams, called east, center, and west.



Fig. 7 Slabs entering the furnace



Fig. 8 Hydraulic pump 55 kW



Fig. 9 Lifting cylinder



Fig. 10 Cylinder for the horizontal movement

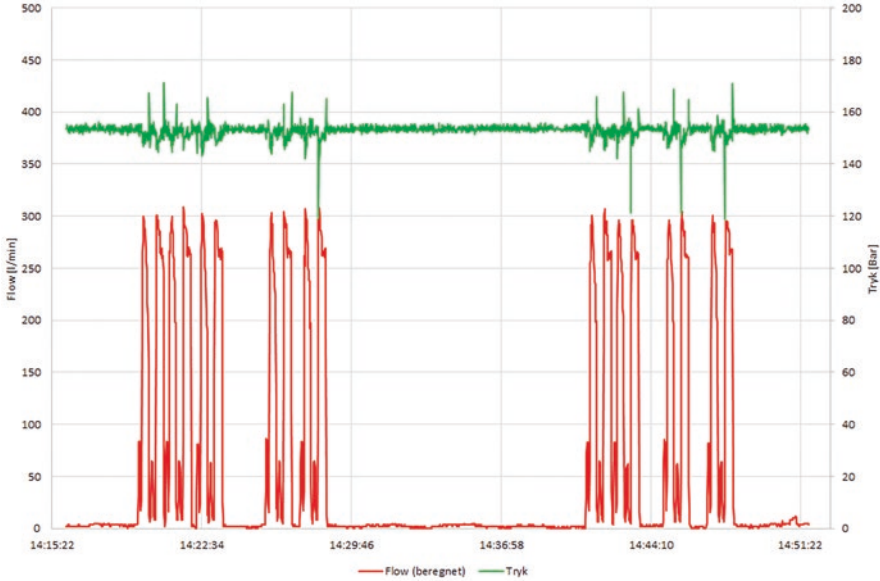


Fig. 11 Calculated flow as well as measurements of pressure and power input on a variable displacement pump

The hydraulic system is used solely for lifting, driving forward, and lowering the individual beam.

The beams can run individually, or synchronously. Synchronous operation is used if the slab is so large that it lies over several beams or there is a risk of collision between the slots.

The movements are done with two lifting cylinders (main and auxiliary cylinders) and a cylinder for the horizontal movement.

Figures 11 and 12 show calculated flow as well as measurements of pressure and power input on a variable displacement pump

Figure 11 shows that the flow varies between 0 and 300 l/min, while the pressure is largely constant at 155 bar.

Figure 12 shows that the power input varies between 16 and 100 kW. The 16 kW is a basic load which is present even at a flow of 0 l/min.

As can be seen, displacement reductions cause significant reductions in power input. The pump type is therefore suitable for systems with varying flow requirements.

Figure 13 shows a simplified operating profile of the hydraulic pump based on the measurements of flow and pressure.

The pump has six cycles every 20 s where it supplies approx. 276 l/min at a pressure of 160 bar and six cycles of 9 s where it supplies approx. 82 l/min at a pressure of 160 bar.

Then it runs for 120 s with a flow of 0 l/min at a pressure of 160 bar.

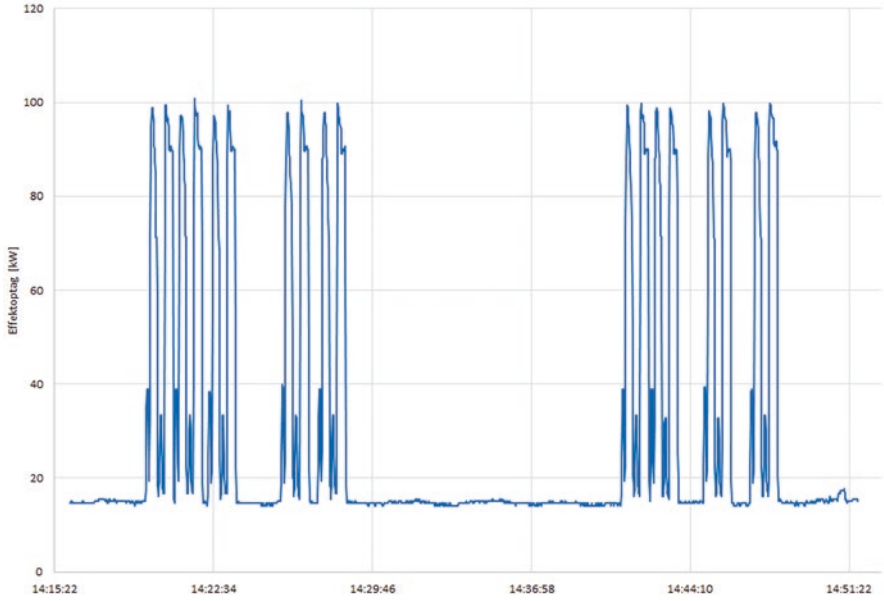


Fig. 12 Power input

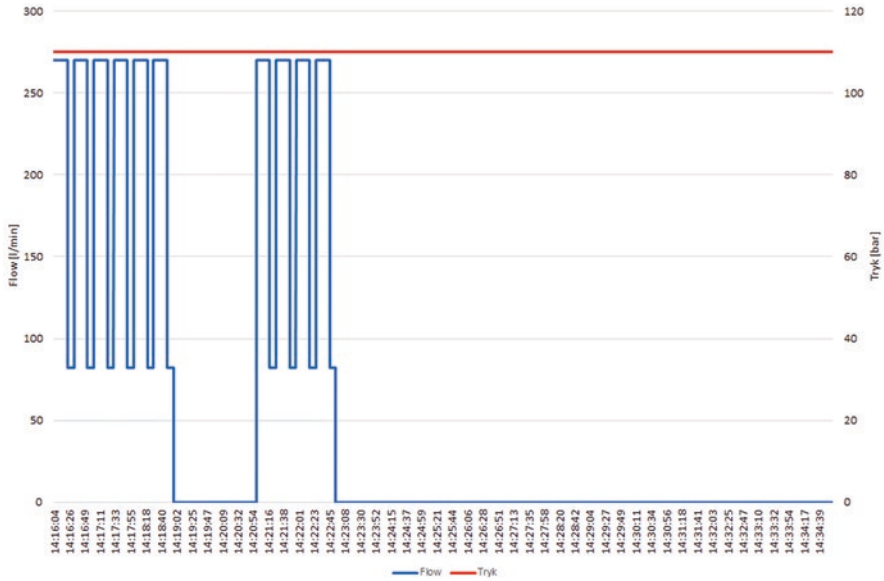


Fig. 13 Operating profile of the hydraulic pump based on the measurements of flow and pressure

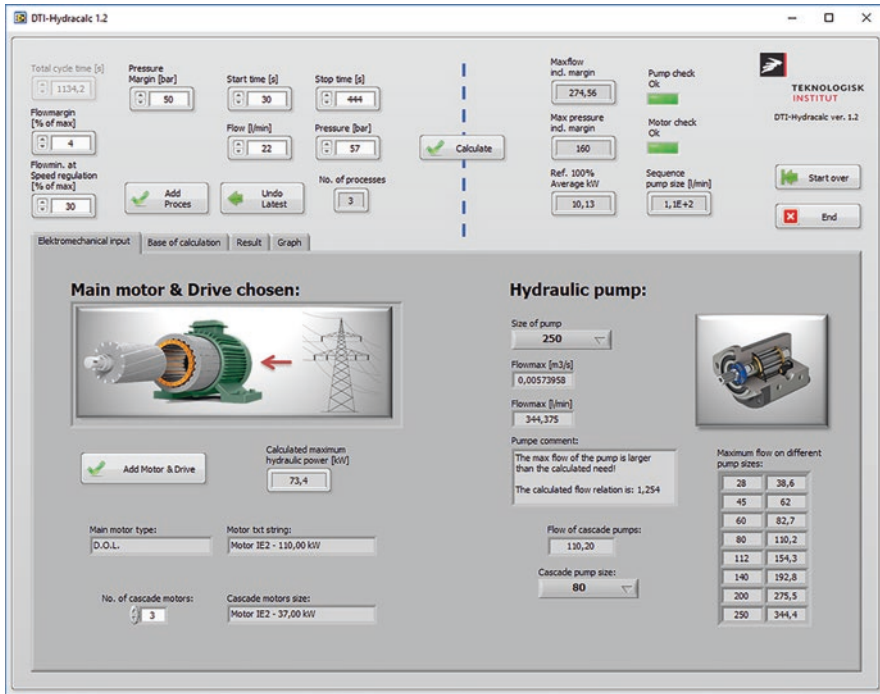


Fig. 14 Electromechanical inputs

The pump then has four cycles of 20 s where it supplies approx. 276 l/min at a pressure of 160 bar and four cycles every 9 s where it supplies approx. 82 l/min at a pressure of 160 bar.

Then it runs for 720 s with a flow of 0 l/min at a pressure of 160 bar.

Figure 14 shows the electromechanical inputs. An IE2 electrical motor of 110 kW and a hydraulic pump of 250 cm is used.

Figure 13 shows the calculation basis. The calculation basis is downloaded as a text file via the button “Download data”. These data correspond to Fig. 13.

Furthermore, a flow margin of 4% and a pressure margin of 50 bar have been entered (Fig. 15).

Figure 16 shows the result of the calculations. As can be seen, flow control at constant pressure, which is now used, and load sensing are the most energy-efficient control methods.

The total efficiency of these types of control is 34%.

The pump is actually too large, as it can provide approx. 344 l/min. A calculation shows that if the pump is changed to 200 ccm, the total efficiency of flow control at constant pressure could be improved to 38.5%.

The reason for the relatively low total efficiency is the period of 720 s, when the pump does not deliver any flow but runs at idle. If the pump could be stopped, the overall efficiency could be improved to approx. 54%.

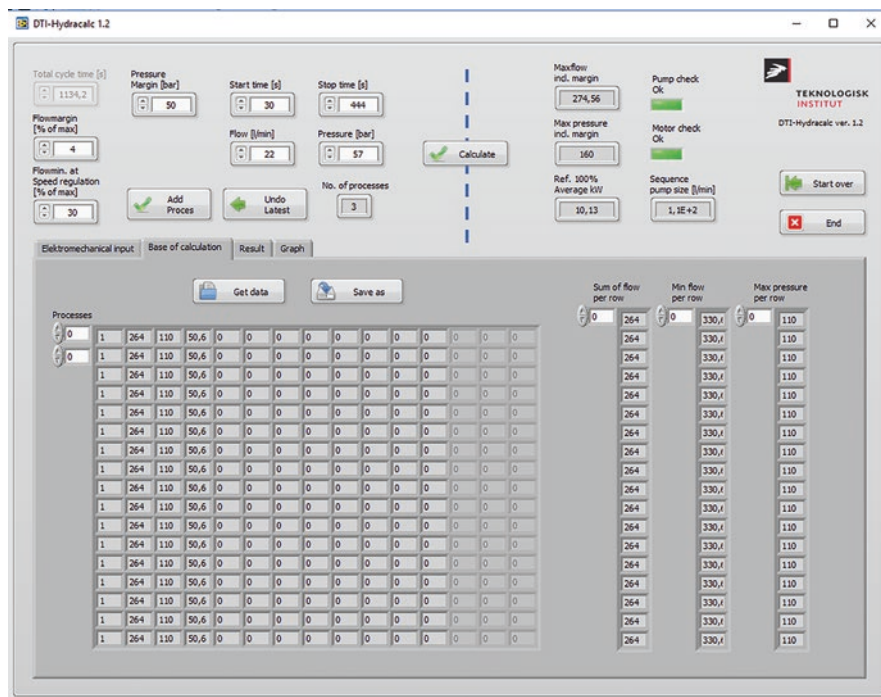


Fig. 15 Calculation basis

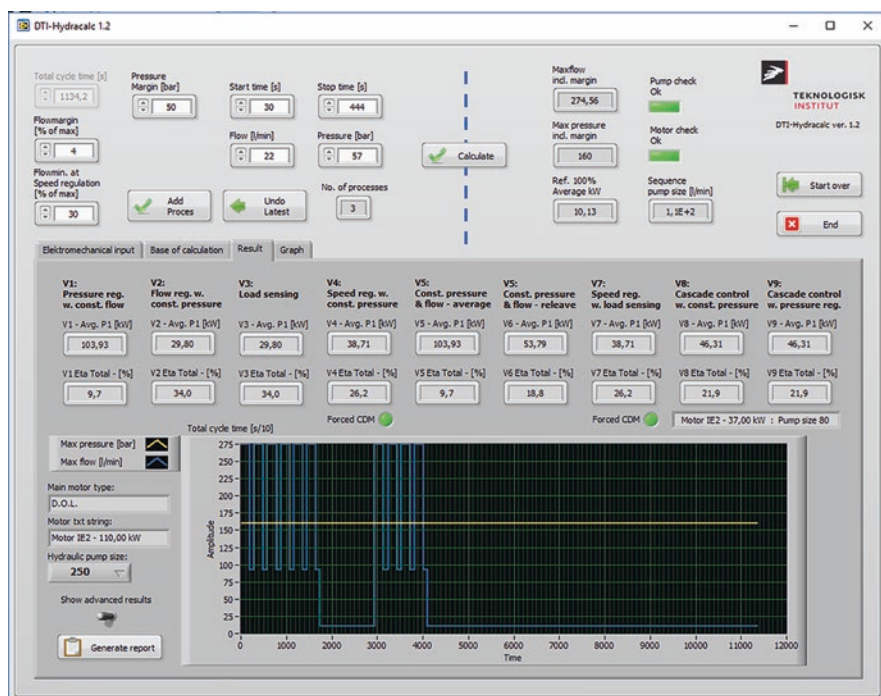


Fig. 16 Result of the calculations

4 Conclusion

The Motor System Tool has been extended by a module for industrial stationary hydraulic systems.

The tool includes total models for hydraulic processes, hydraulic pumps, for motors and for drives.

The input for the model is in general the total oil flow (excluding the flow in the overflow-valve) and the maximum pressure as a function of time. The time step is 1/10 s. The tool calculates the total efficiency and the efficiency of drive, motor, pump for nine different strategies for control of the system.

The tool can be used for design of new systems and for analyses of existing systems. The tool is also valuable for training and demonstration purposes, as it combines the thermodynamics of hydraulic systems with data for hydraulic pumps and electric motors.

References

1. Hydraulik Ståbi (Hydraulics Handbook). Teknisk Forlag A/S 1996. Peter Winfeld Rasmussen. isbn: 87-571-1325-9
2. Kawasaki: www.kpm-eu.com
3. Motor Systems Tool: <http://motorsystems.org>
4. IEC 61800-9-2

Comparison of Different Methods to Determine the Per-Phase Equivalent Circuit Parameters of Three-Phase Induction Motors Using IEC Nameplate and Catalogue Data



Fernando J. T. E. Ferreira, André M. Silva, and Edson Bortoni

1 Introduction

Nowadays, more than 85% electric motors used in the industry are three-phase squirrel-cage induction motors (SCIMs).

The per-phase equivalent circuit (EC) of SCIMs [1], shown in Fig. 1, is used to simulate their performance and to set motor control parameters in variable-speed drives.

Deterministic approaches can be used to compute the EC parameters using the locked-rotor and no-load tests [1] and/or the IEC motor nameplate data, which contains rated voltage, current, power factor, and speed values, as well as the efficiency values at 100%, 75%, and 50% load levels. The additional data presented in the manufacturer catalogues may also be used, which typically includes the power factor and efficiency at 100%, 75%, and 50% load levels, for three different line-to-line voltages, typically 380, 400, and 415 V, for low-voltage, 50-Hz SCIMs, as well as the locked-rotor to nominal current and torque ratios.

However, there are several aspects that can introduce significant errors in the computed values since, some of the EC parameters vary with the saturation level, skin effect, and temperature rise at different load levels, phase voltages and/or frequencies. For example, due to the skin effect in the rotor cage, the EC with constant parameters is unable to provide good results for the starting and pull-down torque regions. Nevertheless, for fixed frequency and voltage, in most cases, the EC with

Fernando J. T. E. Ferreira · A. M. Silva
Department of Electrical and Computer Engineering, Institute of Systems and Robotics,
University of Coimbra, Coimbra, Portugal
e-mail: ferreira@deec.uc.pt

E. Bortoni (✉)
Universidade Federal de Itajubá, Itajubá, Brazil
e-mail: bortoni@unifei.edu.br

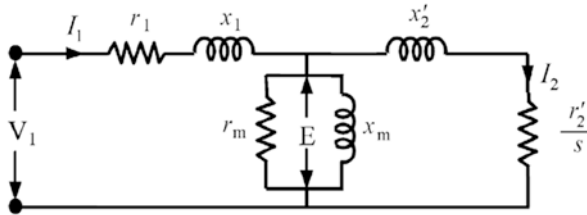


Fig. 1 Per-phase equivalent circuit of SCIMs (r_1 – stator resistance; x_1 – stator leakage reactance; r_2' – rotor resistance referred to the stator; x_2' – rotor leakage reactance referred to the stator; r_m – core loss resistance; x_m – magnetizing reactance; V_1 – phase voltage; E – phase magnetizing branch voltage or induced electromotive force; I_1 is the phase current) [1]

constant parameters can be used to simulate with good accuracy the performance of SCIMs in the steady-state operating region (between no-load and full load), i.e., from zero to nominal slip, if the parameters are properly set.

Due to saturation and skin effect, the EC using constant parameters is unable to give good results, mainly for the starting and pull-down torque regions.

In this chapter, a new method based on a stochastic approach is applied to determine the EC parameters of IE1-, IE2-, IE3-, and IE4-class SCIMs on the basis of motor nameplate and catalogue data, and the simulated motor efficiency, power factor and current curves, as a function of slip, are compared to those obtained with two deterministic methods, namely, the IEEE 112 F/F1 standard [2] method (traditional method), based on the no-load and locked-rotor tests, and the method proposed in [3, 4] (Bortoni's method), based on the motor nameplate and catalogue data.

2 Deterministic Methods to Determine EC Parameters

2.1 Traditional Method Based on the No-Load and Locked-Rotor Tests

The traditional method to determine the EC parameters proposed in the main induction machine testing standards [2, 3], consists in performing two experimental tests, namely, the no-load and the locked-rotor tests [1].

In the no-load test, the machine is fed with rated voltage and frequency, and the shaft is free of any load. In this condition, the voltage, current, and active power are measured.

In the short-circuit test, the machine is fed with reduced voltage and rated frequency. The motor has its shaft locked and the supply voltage is increased until the line current reaches the nominal value. In this condition, the voltage, current, and active power are measured.

The per-phase stator winding resistance is measured at room temperature and corrected to the operating temperature.

The EC parameters are then determined using a set of equations [1, 2].

In this chapter, the IEEE 112 F/F1 standard [8] method was used as the traditional method to determine the EC parameters.

2.2 Bortoni's Method Based on the IEC Nameplate and Catalogue Data

In order to obtain good results for the starting and pull-down torque regions, Bortoni et al. proposed a deterministic method to obtain the EC parameters, described in [3, 4]. The Bortoni's method is based in full catalogue information and does not rely in any kind of experimental tests or measurements.

In order to consider saturation and skin effect in the rotor parameters, a suitable function is selected, instead of using a double branch approach in the EC, normally used in electromagnetic transient software [5, 6].

3 New Proposed Method Based on a Stochastic Approach

Deterministic approaches to determine the electrical EC parameters of SCIMs are based on elaborated calculations, aiming at meeting the machine's physical characteristics for a more accurate representation. More recent approaches embody the parameters variation with slip for more accurate results [7–11]. Sometimes, obtaining the required data to use these methodologies is not possible or involves complex experimental setups.

The nature of the procedure to identify the EC parameters is intrinsically of a nonlinear optimization problem. In [12], an induction motor is modeled by a triple-cage circuit to accurately consider skin effect. The model's many parameters are estimated by a small-signal model of the machine by using the Differential Evolution metaheuristic. In [13], a sparse grid optimization algorithm is used to determine, with accuracy, the EC parameters of SCIMs for a more efficient motor control. The cost function is evaluated regarding the stator currents of the motor model. In this method, the variation of the EC parameters is restrained, thus a previous knowledge of the machine is required.

The proposed stochastic method to solve the EC parameters of SCIMs employs the Differential Evolution metaheuristic. The required data to obtain the EC parameters is only based on that provided in the IEC nameplate/catalogue of SCIMs. Thus, the proposed stochastic algorithm requires the motor efficiency, slip, and power factor (PF) for one or more operating points. The algorithm's cost/objective function is the minimization of the normalized differences between the nameplate/catalogue and motor model values of efficiency, shaft power, and power factor for three operating points:

$$\min F(x) = \sum_{j=1, \dots, \text{points}} \frac{\widetilde{f}_1^j(x) + \widetilde{f}_2^j(x) + \widetilde{f}_3^j(x)}{3}, \quad (1)$$

where

$$\widetilde{f}_1^j(x) = \frac{|\eta^j - \eta^j(x)|}{\eta^{j, \max}}; \widetilde{f}_2^j(x) = \frac{|P_2^j - P_2^j(x)|}{P_2^{j, \max}}; \widetilde{f}_3^j(x) = \frac{|\text{PF}^j - \text{PF}^j(x)|}{\text{PF}^{j, \max}}, \quad (2)$$

and

η^j is the nameplate efficiency for the j^{th} operating point, $\eta^j(x)$ is the x candidate efficiency value for the j^{th} operating point, and $\eta^{j, \max}$ is the maximum efficiency value taken into account all individuals and the nameplate values; P_2^j is the nameplate shaft power for the j^{th} operating point, $P_2^j(x)$ is the x candidate shaft power value for the j^{th} operating point, and $P_2^{j, \max}$ is the maximum shaft power value taken into account all individuals and the nameplate values; and PF^j is the nameplate power factor for the j^{th} operating point, $\text{PF}^j(x)$ is the x candidate power factor value for the j^{th} operating point, and $\text{PF}^{j, \max}$ is the maximum power factor value taken into account all individuals and the nameplate values. The normalization is needed to give equal relevance to the three machine quantities evaluated.

Thence, the optimization problem's decision variables vector is given by

$$x = [r_1, x_1, x_m, r_m, x_2, r_2'], \quad (3)$$

where r_1 is the stator winding phase resistance, x_1 is the winding phase leakage reactance, x_m is the magnetization reactance, r_m is the core loss resistance, x_2 is the rotor leakage reactance referred to the stator, and r_2' is the rotor resistance referred to the stator.

The optimization problem is unconstrained, thus several different solutions may be possible for the given operating points. If the optimizer is given more operating points, the resulting motor EC parameters are closer to their realistic values. Otherwise, a previous knowledge of the machine is necessary to select the more adequate parameters which result from several runs of the algorithm.

In this stochastic approach, the variation of the EC parameters with the rotor slip, namely the rotor leakage inductance and rotor resistance, is not considered. Although, it can be promptly included for more accurate results, as it is done in the Bortoni's method.

4 Comparison of Results

In this section, the proposed method, based on a stochastic approach, is applied to obtain the EC parameters of four 7.5-kW, 400-V, 50-Hz SCIMs of IE1, IE2, IE3, and IE4 classes and the results are compared with those obtained with the

previously referred deterministic methods in terms of simulated efficiency, power factor, and current curves, as a function of slip, for a slip varying between 0% and 5%. For reference, the efficiency, power factor, and current at 50%, 75%, and 100% load levels provided in the motor nameplate/catalogue, as well as the experimental efficiency, power factor, and current at six different load levels obtained experimentally in a motor test bench.

In Table 1, the EC parameters obtained with IEEE 112 F/F1 method, Bortoni's method, and proposed stochastic method are presented.

In the Figs. 2, 3, 4, 5, 6, 7, 8, 9, 10, 11, 12, and 13, the simulated efficiency, power factor, and current curves, as function of the motor slip, using the EC parameters provided in Table 1 for the IE1-, IE2-, IE3-, and IE4-class motors, are presented. Considering the three nameplate/catalogue values for efficiency, power factor, and current, which were the base to adjust the stochastic algorithm, for all the presented cases, the proposed method presents the best fit to those reference values.

Table 1 EC parameters of IE1-, IE2-, IE3-, and IE4-class SCIMs obtained with three different methods

Motor class	EC parameter	Method		
		IEEE 112 F/F1	Stochastic	Bortoni's
IE1	r_1	2.17	0.669	0.908
	x_1	4.15	0.835	0.685
	x_m	99.7	29.076	26.27
	r_m	1518.2	287.063	346.9
	x_2'	4.15	0.245	2.341
	r_2'	2.18	0.5642	0.485
IE2	r_1	2.17	0.698	0.716
	x_1	4.28	2.438	0.767
	x_m	120.7	39.911	37.62
	r_m	3123.9	492.488	508.08
	x_2'	4.28	0.413	1.98
	r_2'	2.14	0.531	0.46
IE3	r_1	1.59	0.729	0.678
	x_1	3.76	1.388	0.632
	x_m	113.3	29.748	29.848
	r_m	2983	926.815	869.88
	x_2'	3.76	0.069	2
	r_2'	1.76	0.477	0.46
IE4	r_1	1.23	0.516	0.37
	x_1	3.24	0.631	0.504
	x_m	93.9	28.93	30.967
	r_m	2558.4	852.877	696.78
	x_2'	3.24	0.936	1.953
	r_2'	1.88	0.382	0.329

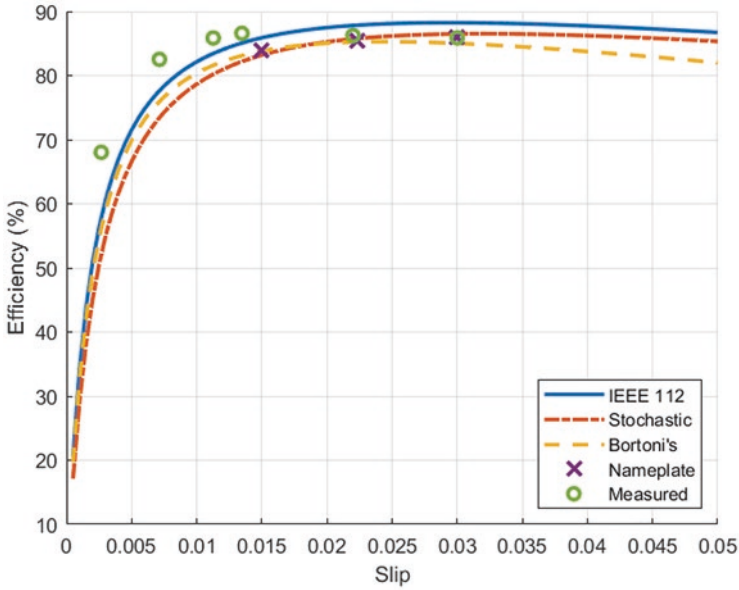


Fig. 2 IE1-class SCIM: simulated motor efficiency-slip curves, nameplate efficiency values for 100%, 75%, and 50% load levels, and experimental efficiency values for six different load levels

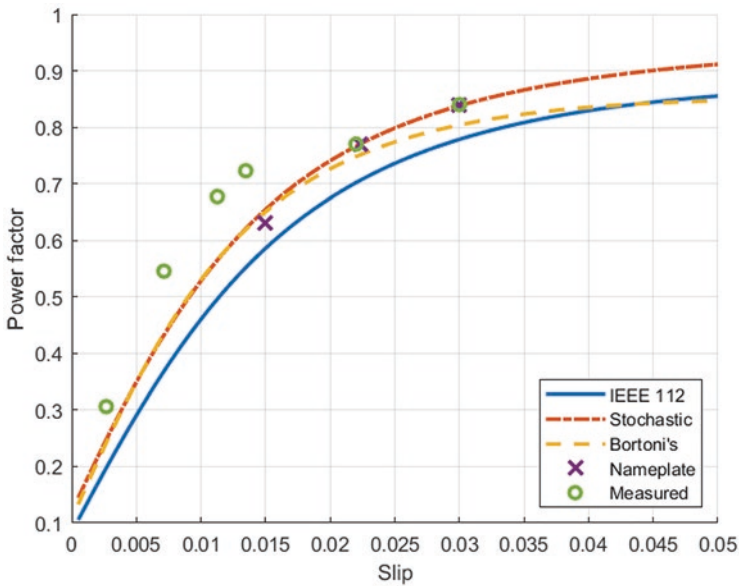


Fig. 3 IE1-class SCIM: simulated motor power factor-slip curves, nameplate/catalogue power factor values for 100%, 75%, and 50% load levels, and experimental power factor values for six different load levels

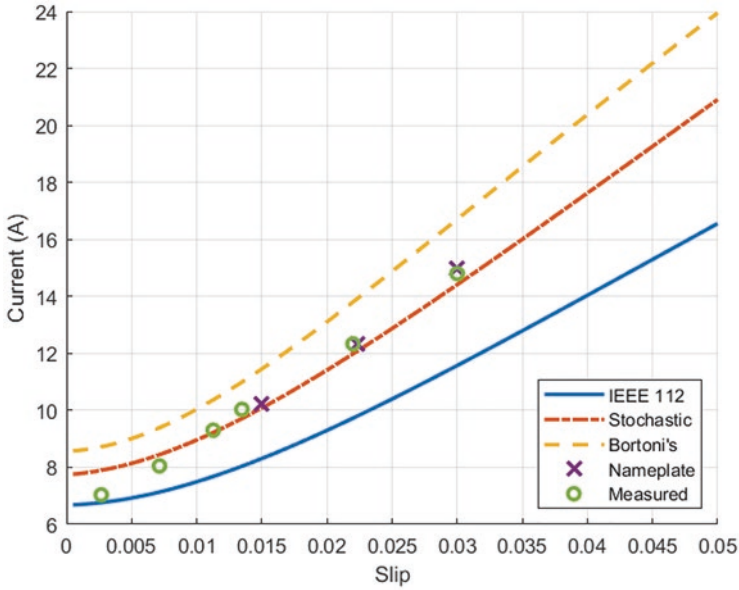


Fig. 4 IE1-class SCIM: simulated motor current-slip curves, nameplate/catalogue current values for 100%, 75%, and 50% load levels, and experimental current values for six different load levels

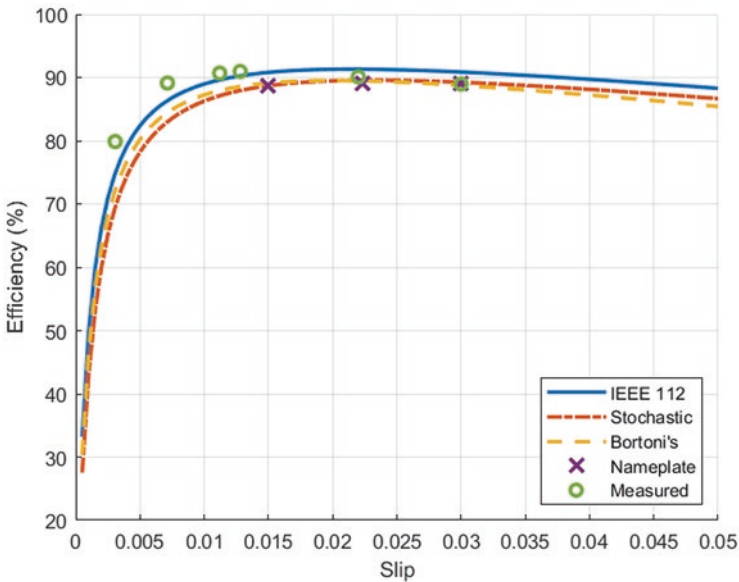


Fig. 5 IE2-class SCIM: simulated motor efficiency-slip curves, nameplate efficiency values for 100%, 75%, and 50% load levels, and experimental efficiency values for six different load levels

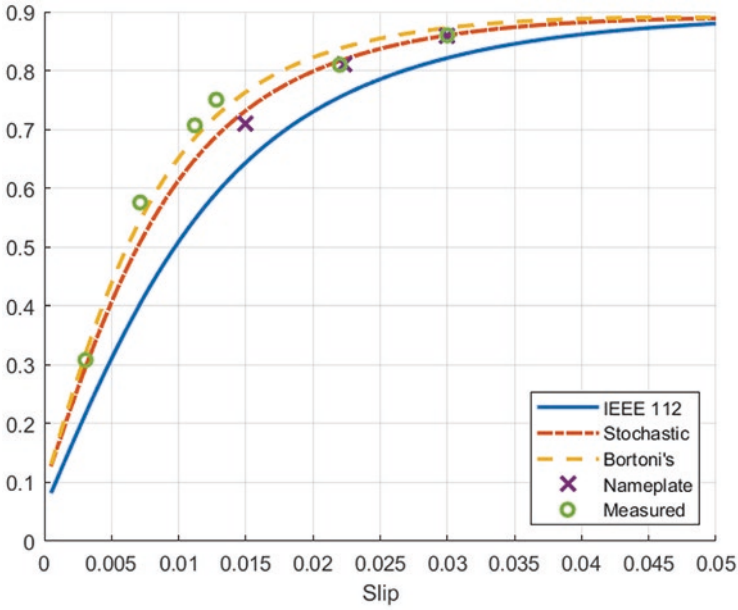


Fig. 6 IE2-class SCIM: simulated motor power factor-slip curves, nameplate/catalogue power factor values for 100%, 75%, and 50% load levels, and experimental power factor values for six different load levels

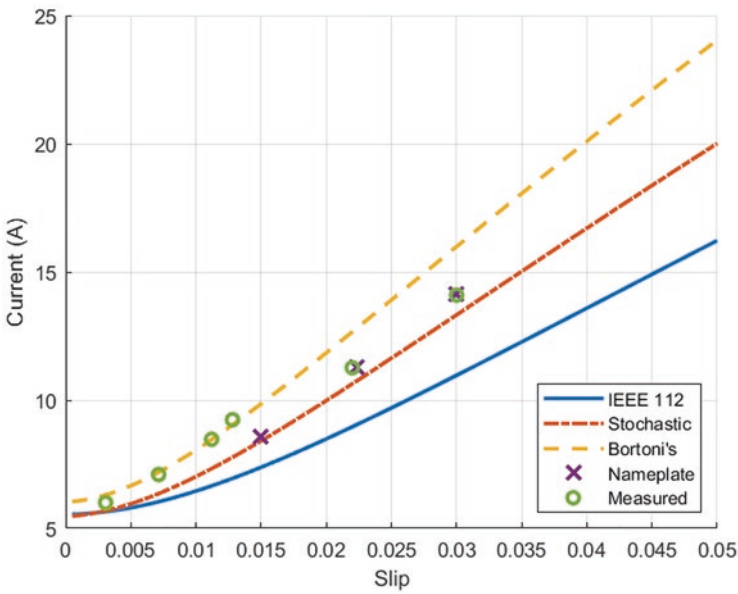


Fig. 7 IE2-class SCIM: simulated motor current-slip curves, nameplate/catalogue current values for 100%, 75%, and 50% load levels, and experimental current values for six different load levels

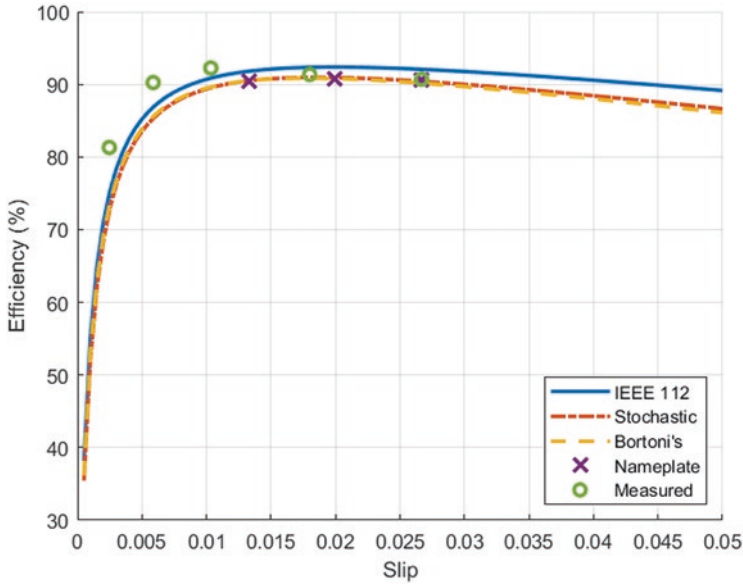


Fig. 8 IE3-class SCIM: simulated motor efficiency-slip curves, nameplate efficiency values for 100%, 75%, and 50% load levels, and experimental efficiency values for six different load levels

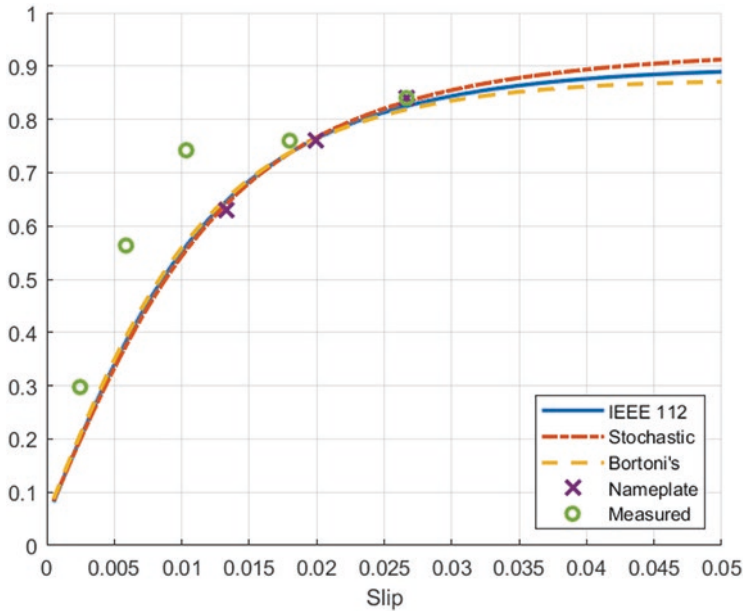


Fig. 9 IE3-class SCIM: simulated motor power factor-slip curves, nameplate/catalogue power factor values for 100%, 75%, and 50% load levels, and experimental power factor values for six different load levels

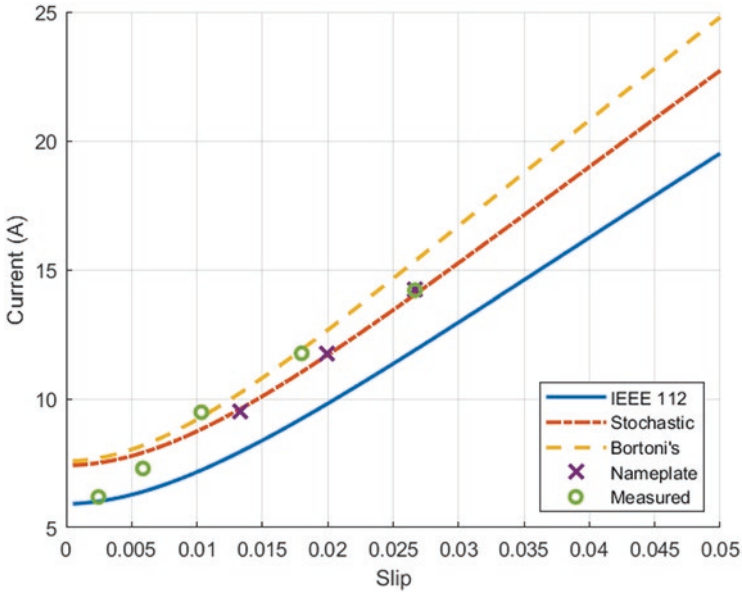


Fig. 10 IE3-class SCIM: simulated motor current-slip curves, nameplate/catalogue current values for 100%, 75%, and 50% load levels, and experimental current values for six different load levels

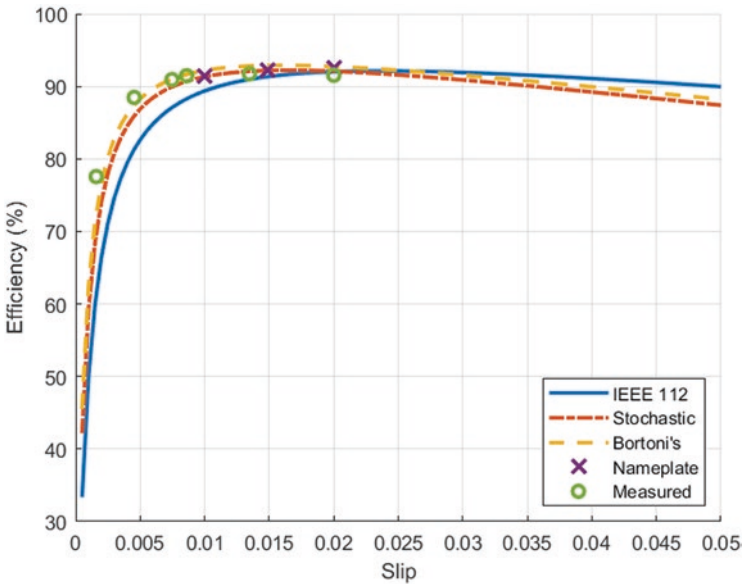


Fig. 11 IE4-class SCIM: simulated motor efficiency-slip curves, nameplate efficiency values for 100%, 75%, and 50% load levels, and experimental efficiency values for six different load levels

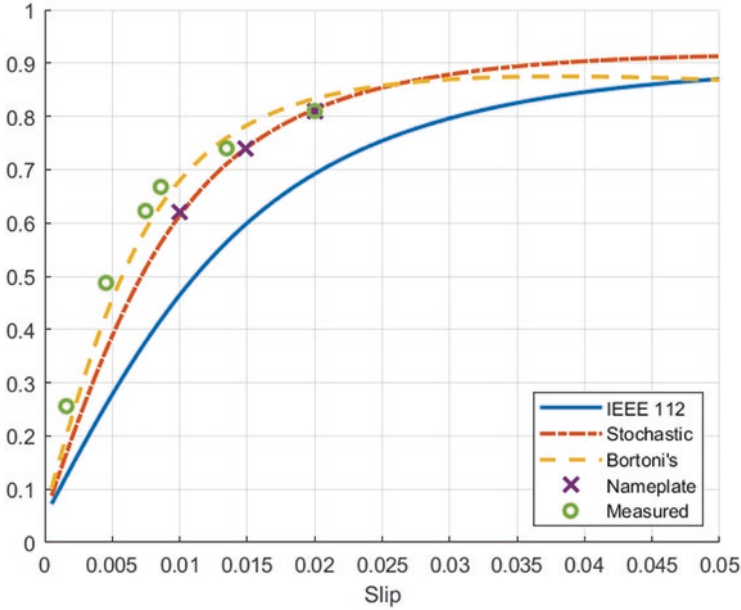


Fig. 12 IE4-class SCIM: simulated motor power factor-slip curves, nameplate/catalogue power factor values for 100%, 75%, and 50% load levels, and experimental power factor values for six different load levels

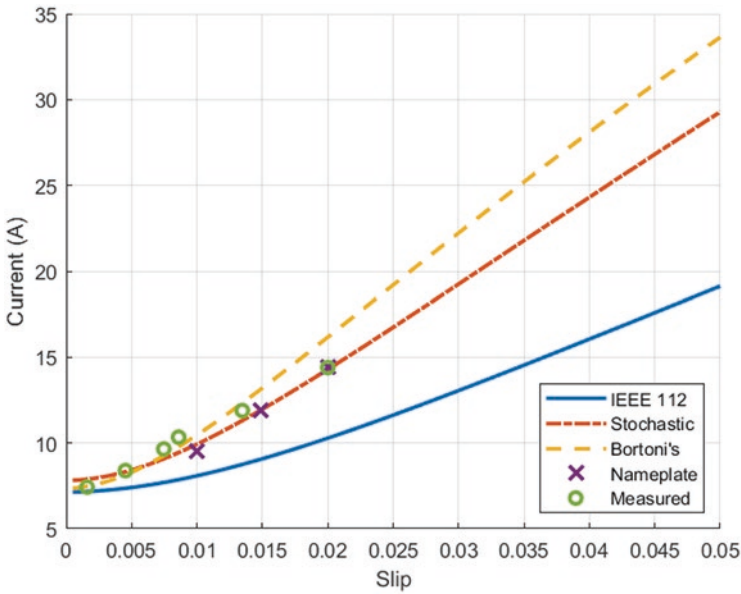


Fig. 13 IE4-class SCIM: simulated motor current-slip curves, nameplate/catalogue current values for 100%, 75%, and 50% load levels, and experimental current values for six different load levels

5 Conclusions and Future Work

On the basis of the presented results, considering only the IEC motor nameplate/catalogue data, it can be concluded that the proposed method based on a stochastic approach is relatively fast and leads to better simulated results than the other presented deterministic method (IEEE 112 F/F1) for a slip equal or lower than the nominal value (operation between no-load and full load), presenting the best fit with the motor nameplate/catalogue efficiency, power factor, and current values for 50%, 75%, and 100% load levels, respectively.

As future work, more data sets (e.g., efficiency and power factor at different voltages, locked-rotor to nominal current and torque ratios, no-load test, locked-rotor test, load tests, etc.) will be used in the proposed method to obtain the variation of the EC parameters with the slip, phase voltage, and stator/rotor temperature rise, extending the use of the EC to different voltages and to a slip between 0% and 100%.

Acknowledgments Prof. Edson Bortoni would like to thank the support of FAPEMIG, INERGE, CAPES, and CNPq, for their continued support in conducting the research.

References

1. A.E. Fitzgerald, C. Kingsley, S.D. Umans, *Electric Machinery* (McGraw-Hill, Boston, 2003)
2. IEEE 112, *Standard Test Procedure for Polyphase Induction Motors and Generators*, 2017
3. IEC 60034-2-1, *Rotating Electrical Machines – Part 2–1: Standard Methods for Determining Losses and Efficiency from Tests (Excluding Machines for Traction Vehicles)*, 2nd edn, June 2014
4. J.M.C. Guimarães, J.V. Bernardes Jr., A.E. Hermeto, E.C. Bortoni, Parameter determination of asynchronous machines from manufacturer data sheet. *IEEE Trans. Energy. Convers.* **29**(3), 689–697 (Sept 2014)
5. E.C. Bortoni, J.V. Bernardes Jr., P.V.V. da Silva, V.A.D. Faria, P.A.V. Vieira, Evaluation of manufacturers strategies to obtain high-efficient induction motors. *Sustain. Energy Technol. Assess.* **31**, 221–227 (2019)
6. L. Monjo, F. Córcoles, J. Pedra, Saturation effects on torque- and current–slip curves of squirrel-cage induction motors. *IEEE Trans. Energy Convers.* **28**(1), 243–254 (Mar 2013)
7. D. Lindenmeyer, H.W. Dommel, A. Moshref, P. Kundur, An induction motor parameter estimation method. *Electr. Power Energy Syst.* **23**, 251–262 (2001)
8. L. Monjo, H. Kojooyan-Jafari, F. Córcoles, J. Pedra, Squirrel-cage induction motor parameter estimation using a variable frequency test. *IEEE Trans. Energy Convers.* **30**(2), 550–557 (June 2015)
9. H. Kojooyan-Jafari, L. Monjo, F. Córcoles, J. Pedra, Using the instantaneous power of a free acceleration test for squirrel-cage motor parameters estimation. *IEEE Trans. Energy Convers.* **30**(3), 974–982 (Sept 2015). <https://doi.org/10.1109/TEC.2015.2399697>
10. J. Pedra, On the determination of induction motor parameters from manufacturer data for electromagnetic transient programs. *IEEE Trans. Power Syst.* **23**(4), 1709–1718 (Nov 2008)
11. M.S. Zaky, M.M. Khater, S.S. Shokralla, H.A. Yasin, Wide-speed-range estimation with online parameter identification schemes of sensorless induction motor drives. *IEEE Trans. Ind. Electron.* **56**(5), 1699–1707 (May 2009)

12. H. Van Khang, W. Pawlus, K.G. Robbersmyr, Identification of parameters and harmonic losses of a deep-bar induction motor. 2017 Seventh International Conference on Information Science and Technology (ICIST), Da Nang, 2017, pp. 194–199
13. F. Duan, R. Živanović, S. Al-Sarawi, D. Mba, Induction motor parameter estimation using sparse grid optimization algorithm. *IEEE Trans. Ind. Inf.* **12**(4), 1453–1461 (Aug 2016)

Experimental Study on Three-Phase Induction Motor Performance Under Supply Voltage Unbalance for Star and Delta Connections



Fernando J. T. E. Ferreira, José Alberto, Edson Bortoni,
and A. T. De Almeida

1 Introduction

Nowadays, more than 85% electric motors used in the industry are three-phase squirrel-cage induction motors (SCIMs) [1, 2]. Despite star and delta being the most common connection modes, other modes are possible if the motor has two sets of windings sharing the same slots [3–5]. Typically, line-fed SCIMs with rated power higher than 4 kW have a six-terminal star/delta winding, with the delta as the nominal connection (for rated voltage) to allow the star-delta starting. However, with the wide availability and relatively low cost of electronic soft-starters, SCIMs can be designed by manufacturers or during a rewinding service, to have a three-terminal winding with single connection mode (star or delta) for rated voltage.

Supply voltage unbalance (SVU) is common in industrial plants, particularly in developing countries, easily reaching 3–5%. It is well-known that SVU leads to a significant decrease in the efficiency and lifetime of SCIMs [6–16]. The lifetime reduction is associated with the increase of the maximum temperature rise in the stator windings (asymmetric heating due to asymmetric phase currents) and of the mechanical vibration levels.

Several studies analyze the tolerance of the different connection types to voltage unbalance [13, 14], but there is a lack of experimental studies. In this chapter, an experimental study comparing the performance of a SCIM under SVU at no-load and full-load, for star and delta connections, is presented. This study evidences the

Fernando J. T. E. Ferreira · J. Alberto · A. T. De Almeida
Department of Electrical and Computer Engineering, Institute of Systems and Robotics,
University of Coimbra, Coimbra, Portugal
e-mail: ferreira@deec.uc.pt; jalberto@deec.uc.pt; adealmeida@isr.uc.pt

E. Bortoni (✉)
Universidade Federal de Itajubá, Itajubá, Brazil
e-mail: bortoni@unifei.edu.br

differences in terms of maximum phase current and voltage deviation in relation to the nominal phase current and voltage and the expected winding temperature rise in the slots. SVU is obtained by reducing one of the supply phase voltages, using a programmable voltage source. Moreover, the estimated derating curves for both connection modes are compared to the NEMA derating curve.

2 Experimental Setup

In the experimental tests, a 4-kW, 4-pole, 36-slot SCIM with reconfigurable stator windings and flux search coils (Fig. 1b) was used, in which an imbricated double-layer full-pitch winding was implemented. The star (star-series) and delta (delta-series) connection modes (Fig. 2b, c) were tested under SVU. The motor was fed by a programmable power source (Fig. 1a), and the supply phase voltages were changed so that the voltage at the terminals of the flux search coils and consequently the air-gap flux level was kept constant for the two tested connection modes (star and delta). The voltage at the terminals of the search coils was measured with a digital oscilloscope (Rigol DS1054). The motor line-to-line voltages, line currents, torque, and speed were measured using a digital power meter (Yokogawa WT1030M). The motor phase voltages and currents were measured with a portable digital multimeter/voltmeter (TENMA 72-8720) and clamp ammeter (TENMA 72-2985).

The supply phase voltages used for the no-load test for star and delta connections were 300 V and 173 V, respectively. Taking these values as a reference, one of the phase voltages of the AFX3300 power source was reduced down to 80%. For the full-load tests, using the same reference voltages, the motor mechanical load (output shaft power) was increased using a hysteresis brake (Fig. 1b) in order to reach the SCIM nominal speed (1445 rpm).



Fig. 1 Experimental setup: (a) programmable power source (AFX3300); (b) induction motor with reconfigurable stator windings mechanically coupled with a hysteresis brake

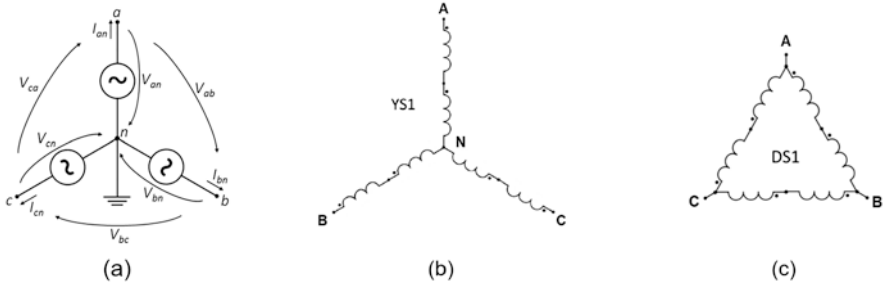


Fig. 2 (a) voltage source connection; (b) star-series connection; (c) delta-series connection

The SVU was quantified using the phase voltage unbalance ratio (PVUR), defined by [17]:

$$PVUR = \frac{\max(|V_{AN} - V_{avg}|, |V_{BN} - V_{avg}|, |V_{CN} - V_{avg}|)}{V_{avg}}, \tag{1}$$

with

$$V_{avg} = \frac{1}{3}(V_{AN} + V_{BN} + V_{CN}), \tag{2}$$

where V_{AN} , V_{BN} , and V_{CN} are the motor phase voltages.

In the same way, the phase current unbalance ratio (PCUR) can be calculated by:

$$PCUR = \frac{\max(|I_{AN} - I_{avg}|, |I_{BN} - I_{avg}|, |I_{CN} - I_{avg}|)}{I_{avg}}, \tag{3}$$

with

$$I_{avg} = \frac{1}{3}(I_{AN} + I_{BN} + I_{CN}), \tag{4}$$

where I_{AN} , I_{BN} , and I_{CN} are the motor phase currents.

For the delta connection, the voltages V_{AN} , V_{BN} , and V_{CN} are replaced by V_{AB} , V_{BC} , and V_{CA} , in (1) and (2). In the same way, I_{AN} , I_{BN} , and I_{CN} are replaced by I_{AB} , I_{BC} , and I_{CA} in (3) and (4).

Moreover, to test the winding temperature rise in each slot of the motor due to SVU, it was assumed that the winding temperature would rise with the square of the current (Joule losses). So, the per unit (p.u.) winding temperature rise in each slot, $\Delta\theta_{slot(p.u.)}$, was calculated by:

$$\Delta\theta_{\text{slot(p.u.)}} = \frac{I_{\text{inner, unb.}}^2 + I_{\text{outer, unb.}}^2}{I_{\text{inner, bal.}}^2 + I_{\text{outer, bal.}}^2}, \tag{5}$$

where $I_{\text{inner, unb.}}$ and $I_{\text{outer, unb.}}$ are the RMS values of the currents on the inner and outer layer of the windings in the same slot in case of unbalanced supply voltage, and $I_{\text{inner, bal.}}$ and $I_{\text{outer, bal.}}$ are the currents in the same conductors but in case of balanced supply voltage.

Finally, in order to compare the performance of the motor with the derating curves defined by the NEMA MG1 standard [17], for each connection mode (star and delta) and different values of voltage unbalance, the mechanical load was reduced, until the maximum phase current equals the value of phase current in the case of balanced supply voltage.

3 Experimental Results

3.1 No-Load Test

As referred earlier, one of the power supply phase voltages (V_{an}) was reduced gradually down to 80% of the reference voltage values and the phase voltages and currents were measured for each case. In Figs. 3, 4, 5, and 6, the experimental results at no-load are shown.

Regarding the values of the voltages, it is possible to see in Fig. 3a, b that for the lowest supply phase voltage reduction, and the star connection, the motor phase voltage V_{AN} drops down to about 87% for the star connection, while both motor phase voltages V_{AB} and V_{CA} drop down to 90% for the delta connection. Moreover, from Fig. 4, it can be observed that delta connection has only a slightly lower PVUR value compared to the star connection (0.070 vs. 0.076).

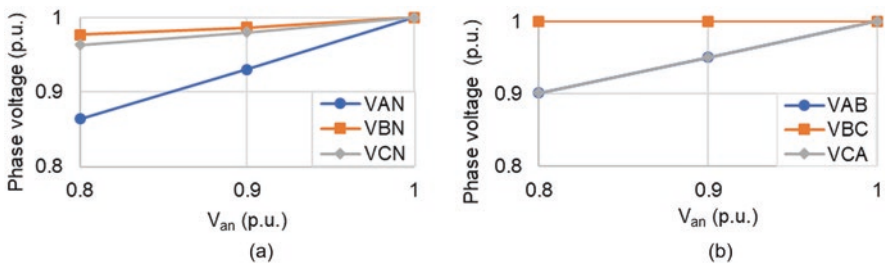


Fig. 3 Values of motor phase voltages for different values of supply phase voltage V_{an} , at no-load, for: (a) star connection; (b) delta connection

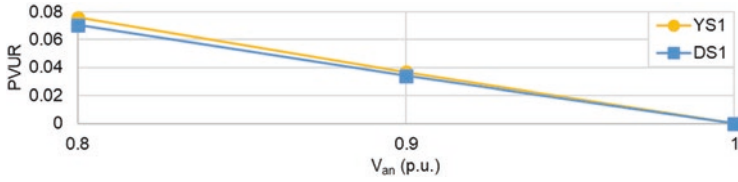


Fig. 4 PVUR for different values of supply phase voltage V_{an} , at no-load

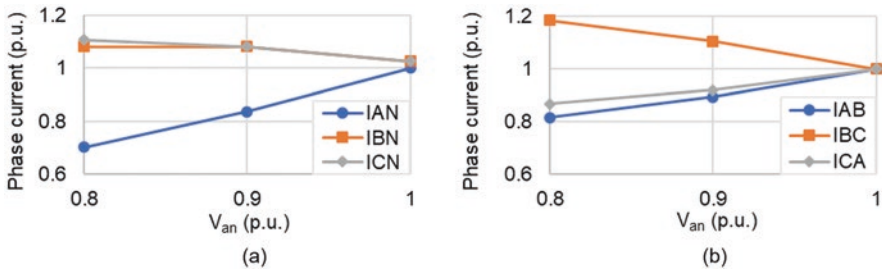


Fig. 5 Values of the motor phase currents for different values of supply phase voltage V_{an} , at no-load, for: (a) star connection; (b) delta connection

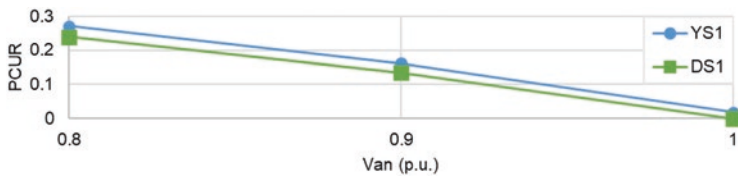


Fig. 6 PCUR for different values of supply phase voltage V_{an} , at no-load

From Figs. 5a, b, it can be observed that the delta connection has a higher increase of the current in the unbalanced supply case (1.18 p.u. vs. 1.11 p.u.). However, the star connection shows a higher value of PCUR, as seen in Fig. 6.

In Table 1, the symmetric components of motor phase current are presented for the no-load test, as well as the $PCUR_{sc}$, which is calculated as the quotient between the negative-sequence component (I^-) and the positive-sequence component (I^+).

Table 1 Symmetric components of motor phase currents for the no-load test

	Star connection				Delta connection		
V_{an} (p.u.)	1.0	0.9	0.8	V_{an} (p.u.)	1.0	0.9	0.8
I_{AN} (p.u.)	1.00	0.84	0.70	I_{AB} (p.u.)	1.00	0.90	0.82
I_{BN} (p.u.)	1.00	1.08	1.11	I_{BC} (p.u.)	1.00	1.10	1.18
I_{CN} (p.u.)	1.00	1.08	1.11	I_{CA} (p.u.)	1.00	0.92	0.87
I^+ (p.u.)	1.00	0.99	0.95	I^+ (p.u.)	1.00	0.97	0.94
I^- (p.u.)	0.00	0.16	0.26	I^- (p.u.)	0.00	0.14	0.25
PCUR _{sc}	0.00	0.162	0.274	PCUR _{sc}	0.00	0.144	0.266

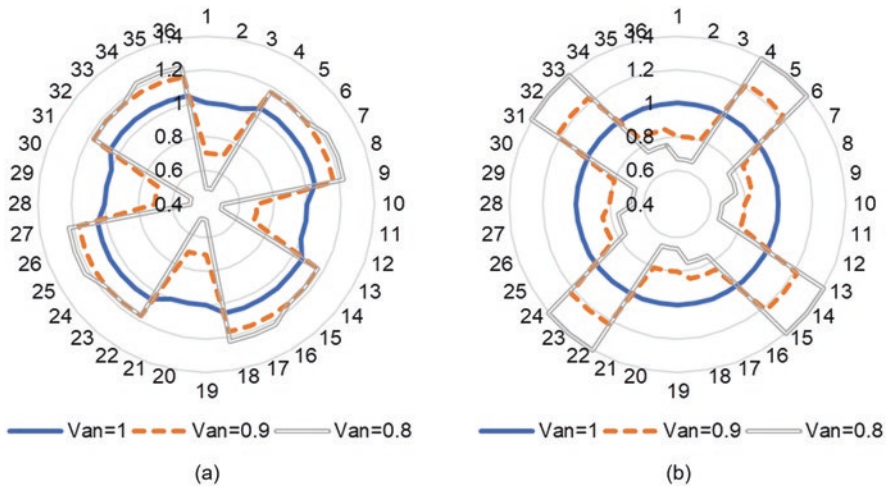


Fig. 7 Expected temperature rise (p.u) in each slot (1–36), for different values of V_{an} , at no-load for: (a) star connection; (b) delta connection

Equation (5) was used to estimate the per-unit winding temperature rise in each slot under unbalanced voltage supply. The results are shown in Fig. 7.

As seen in Figs. 7 and 8, despite the star connection a larger number of slots experience an increase of temperature above nominal values (e.g. slots 4–9), the delta connection shows higher values of maximum temperature rise (1.4 p.u. vs. 1.22 p.u.).

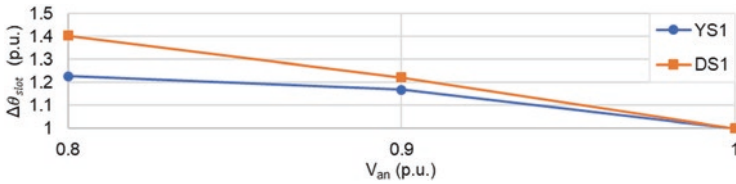


Fig. 8 Maximum temperature rise (p.u.) in the motor windings (p.u.) for different values of V_{an} , at no-load

Table 2 Symmetric components of motor phase currents for the full-load test (1445 rpm)

	Star connection				Delta connection		
V_{an} (p.u.)	1.0	0.9	0.8	V_{an} (p.u.)	1.0	0.9	0.8
I_{AN} (p.u.)	1.00	1.07	1.14	I_{AB} (p.u.)	1.00	1.07	1.14
I_{BN} (p.u.)	1.00	0.96	0.96	I_{BC} (p.u.)	1.00	0.84	0.70
I_{CN} (p.u.)	1.00	0.86	0.74	I_{CA} (p.u.)	1.00	0.98	0.98
I^+ (p.u.)	1.00	0.96	0.93	I^+ (p.u.)	1.00	0.96	0.92
I^- (p.u.)	0.00	0.12	0.23	I^- (p.u.)	0.00	0.13	0.25
$PCUR_{sc}$	0.0	0.125	0.247	$PCUR_{sc}$	0.0	0.135	0.272

3.2 Full-Load Test

As referred earlier, using the hysteresis break shown in Fig. 1b, the load of the motor was increased until the motor reached its nominal speed, 1445 rpm. Using that load as a reference, one supply phase voltage was reduced gradually down to 80% of its reference value, and motor phase voltages and currents were measured. The experimental results are presented in Figs. 9, 10, 11, and 12.

Regarding the values of the motor phase currents compared in Fig. 11, there are significant differences in relation to the no-load operation (Fig. 5). It can be seen that the maximum increase of the current is approximately the same for both the types of connections (1.14 p.u.). However, contrarily to the no-load operation, in the full-load operation, the value of the PCUR for the delta connection is higher than that for the star connection (0.26 vs. 0.21).

In Table 2, the symmetric components of motor phase current are presented for the full-load test, as well as the $PCUR_{sc}$, which is calculated as the quotient between the negative-sequence component (I^-) and the positive-sequence component (I^+).

Concerning the temperature rise, as it can be seen in Fig. 13 and confirmed in Fig. 14, the peak temperature rise is almost the same in the two connections modes: 1.31 p.u. for star and 1.29 p.u. for delta. Yet, by observing thoroughly Fig. 13, the star connection could be better because the slots next to the most affected ones (e.g., slots 1–3) have lower temperature rise values. As an example, slots 4–6 in star

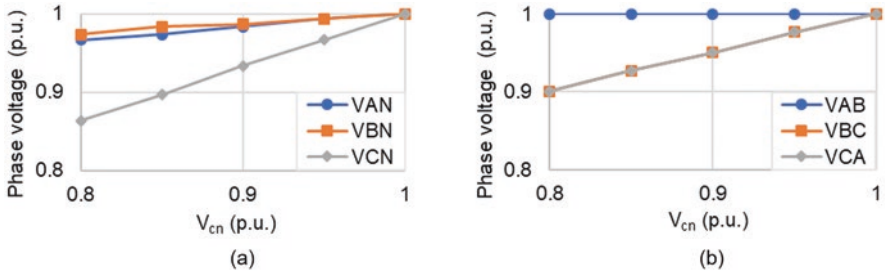


Fig. 9 Values of motor phase voltages, for different values of V_{cn} , at full-load (1445 rpm), for: (a) star connection; (b) delta connection

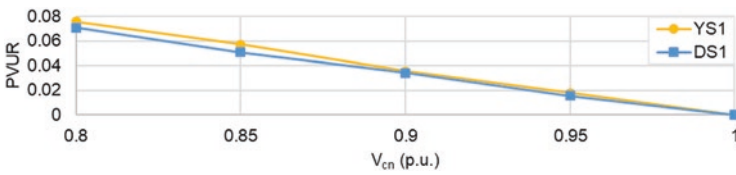


Fig. 10 PVUR for different values of V_{cn} , at full-load (1445 rpm)

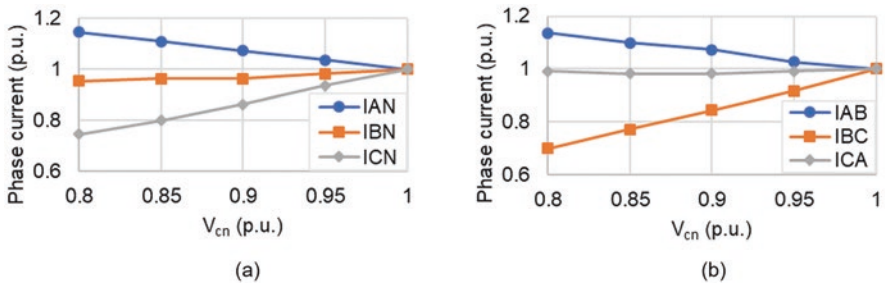


Fig. 11 Values of the motor phase currents, for different values of V_{cn} , at full-load (1445 rpm): (a) star connection; (b) delta connection

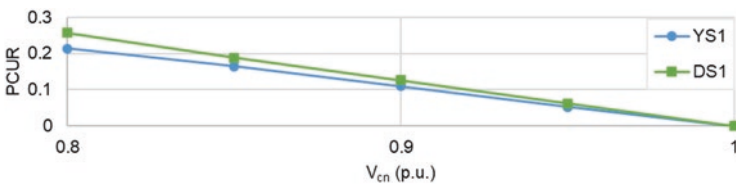


Fig. 12 PCUR for different values of V_{cn} , at full-load (1445 rpm)

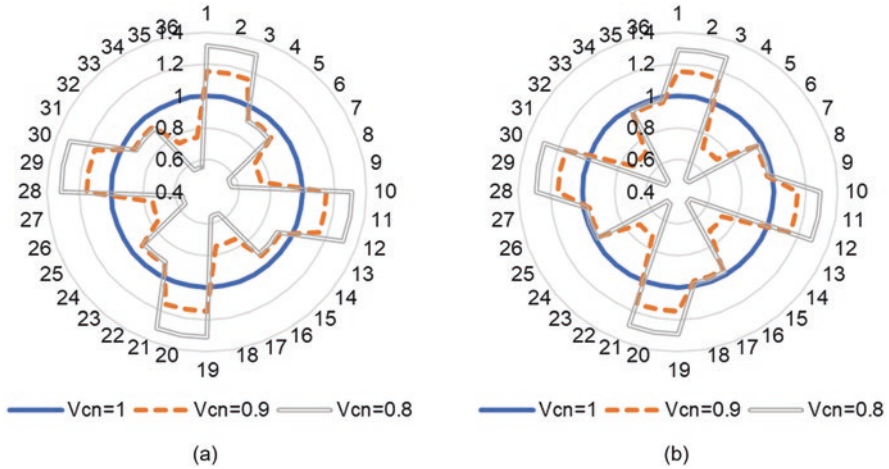


Fig. 13 Expected temperature rise (p.u) in each slot (1–36), for different values of V_{cn} , at full-load (1445 rpm), for: (a) star connection; (b) delta connection

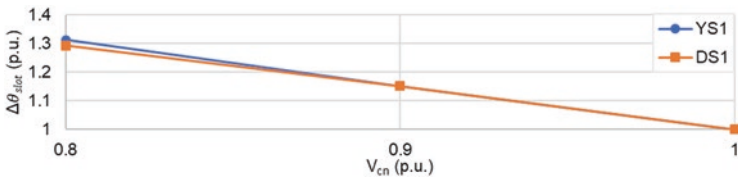


Fig. 14 Maximum temperature rise (p.u.) in the motor windings (p.u.) for different values of V_{cn} , at full-load (1445 rpm)

connection have a 0.91 p.u. of temperature rise, while the slots 34–36 in the delta connection have a 0.98 p.u. of temperature rise. This means that most likely the star connection could easily reduce the impact of voltage unbalance by dissipating the heat in the most affected slots nearby.

Moreover, as referred in [18], the star windings can have lower Joule losses due to the inexistence of the zero-sequence current (circulating currents in the delta circuit).

Finally, regarding the derating curves as a function of the percent voltage unbalance [17], shown in Fig. 15, it is possible to observe that the star connection shows a slightly better performance, especially in the cases with a higher voltage unbalance. The NEMA derating curve is also presented in Fig. 15, for reference.

Furthermore, it is possible to observe that the determined derating curves for star and delta connections differ from the NEMA derating curve, especially for lower values of voltage unbalance. This means that even with low values of voltage unbalance, the induction motor should not be running at full-load, otherwise it will cause

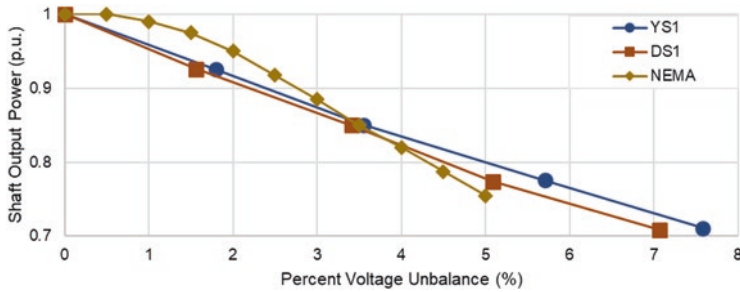


Fig. 15 Estimated derating curves for the tested motor for star and delta connections and the NEMA derating curve

an excessive winding temperature rise, potentially leading to a decrease of the motor lifetime.

4 Conclusions and Future Work

In this chapter, an experimental analysis of a SCIM under supply voltage unbalance is performed. By measuring the motor phase currents and voltages when one of the supply phase voltages is decreased down to as much as 80% of its nominal value, the tolerance of the motor to voltage unbalance in both star and delta connections, at no-load and full-load operation, can be assessed. It was found that for both no-load and full-load operation of the motor, an SVU would cause a higher deviation of the motor phase voltages for the star connection. However, regarding the deviation of the current and temperature rise in the stator slots for the tested motor, the star connection presented a better performance, especially in the no-load operation. Furthermore, despite the expected temperature rise difference between star and delta connections being lower when operating at full-load, the star connection is still expected to be the best solution, due to the inexistence of zero-sequence currents. Finally, regarding the derating curves, it was found, for the tested motor, that the star connection could operate at higher load levels for a given voltage unbalance.

In future work, more load levels will be evaluated (25%, 50%, and 75%). Additionally, the impact of the voltage unbalance in the motor efficiency will also be investigated for this particular motor.

Acknowledgments Prof. Edson Bortoni would like to thank the support of FAPEMIG, INERGE, CAPES, and CNPq, for their continued support in conducting the research.

References

1. H.W. Beaty, J.L. Kirtley, *Electric Motor Handbook* (McGraw-Hill, London, 1998)
2. A.E. Fitzgerald, C. Kingsley, S.D. Umans, *Electric Machinery* (McGraw-Hill, Boston, 2003)
3. F.J.T.E. Ferreira, M.V. Cistelegan, Simulating multi-connection, three-phase, squirrel-cage, induction motors by means of changing the per-phase equivalent circuit parameters, in 2008 18th International Conference on Electrical Machines, 2008, pp. 1–8
4. F.J.T.E. Ferreira, A.T. de Almeida, Novel multi-flux level, three-phase, squirrel-cage induction motor for efficiency and power factor maximization, in 2006 IEEE International Conference on Industrial Technology, 2006, pp. 214–221
5. F.J.T.E. Ferreira, Novel multflux, three-phase, dual-winding configurations, in 2018 XIII International Conference on Electrical Machines (ICEM), 2018, pp. 2511–2518
6. J.J. Grainger, W.D. Stevenson, W.D. Stevenson, *Power System Analysis* (McGraw-Hill, New York, 1994)
7. R.C. Dugan, R.C. Dugan, *Electrical Power Systems Quality* (McGraw-Hill, New York, 2003)
8. P.B. Cummings, J.R. Dunki-Jacobs, R.H. Kerr, Protection of induction motors against unbalanced voltage operation. *IEEE Trans. Ind. Appl.* **IA-21**(3), 778–792 (May 1985)
9. M. Al-Badri, P. Pillay, P. Angers, A novel technique for in situ efficiency estimation of three-phase IM operating with unbalanced voltages. *IEEE Trans. Ind. Appl.* **52**(4), 2843–2855 (July 2016)
10. C.-Y. Lee, B.-K. Chen, W.-J. Lee, Y.-F. Hsu, Effects of various unbalanced voltages on the operation performance of an induction motor under the same voltage unbalance factor condition, in 1997 IEEE Industrial and Commercial Power Systems Technical Conference. Conference Record, pp. 51–59
11. P. Pillay, P. Hofmann, M. Manyage, Derating of induction motors operating with a combination of unbalanced voltages and over or undervoltages. *IEEE Trans. Energy Convers.* **17**(4), 485–491 (Dec 2002)
12. W. Deprez, A. Dexters, S. Stevens, F. Parasiliti, R. Belmans, The combined effect of practical operating conditions and material choice on the performance of induction machines voltage unbalance & induction machines, in 5th International Conference on Energy Efficiency in Motor Driven Systems, 2007
13. F.J.T.E. Ferreira, On the star, delta and star-delta stator winding connections tolerance to voltage unbalance, in 2015 IEEE International Electric Machines & Drives Conference (IEMDC), 2015, pp. 1888–1894
14. F.J.T.E. Ferreira, B. Ge, E.C. Quispe, A.T. De Almeida, Star- and delta-connected windings tolerance to voltage unbalance in induction motors, in 2014 International Conference on Electrical Machines (ICEM), 2014, pp. 2045–2054
15. E.C. Quispe, I.D. López, F.J.T.E. Ferreira, V. Sousa, Unbalanced voltages impacts on the energy performance of induction motors. *Int. J. Electr. Comput. Eng.* **8**(3), 1412–1422 (2018)
16. O.C.N. Souto, J.C. De Oliveira, L.M. Neto, P.F. Ribeiro, Power quality impact on performance and associated costs of three-phase induction motors, in 8th International Conference on Harmonics and Quality of Power. Proceedings (Cat. No.98EX227), vol. 2, pp. 791–797
17. National Electrical Manufacturers Association, *NEMA Standards Publication MG 1-2016*
18. F.J.T.E. Ferreira, A.M. Silva, S.M.A. Cruz, A.T. De Almeida, Comparison of losses in star- and delta-connected induction motors with saturated core, in 2017 IEEE International Electric Machines and Drives Conference (IEMDC), 2017, pp. 1–8

Conserving Energy in Compressed Air System: Practical Case Studies from Indian Industry



Padmanabh Nagarkar and Prosanto Pal

1 Introduction

The energy and environmental impacts of air compressors are substantial. Studies have estimated that compressed air systems account for approximately 10% of total energy use in various countries, and typically are the largest energy-consuming equipment in industrial facilities [2].

India is one of the largest markets for air compressors, and the market is growing at a rapid pace. Leading international compressor manufacturers like Atlas Copco (Sweden), Ingersoll Rand (Ireland), Kaeser (Germany) have their presence in India. Air compressors are widely used by large industries as well as by small and medium enterprises (SMEs). Most large industries in India are mandated by law to get their plant operations, including compressed air systems, audited regularly to save energy [3]. However, there is no such regulation for SMEs and few of them can afford to engage the services of energy auditors to identify energy-saving options in their compressed air system.

This chapter focuses on energy saving in compressed air systems among SMEs. Like many economies, SMEs are the backbone of Indian industries. Most SMEs use compressed air inefficiently. Indian SMEs typically use air compressors ranging between 20 and 300 hp. (15–224 kW). The chapter focuses on oil-injected screw

Note: *The photos and line work incorporated in this chapter are purely indicative, symbolic, and web-based generic work which have been purely used here for explanatory and convenience purpose.*

P. Nagarkar (✉)
XL Consultants, Mumbai, India

P. Pal
TERI, Delhi, India
e-mail: prosanto@teri.res.in

compressors used among SMEs. The findings presented in the chapter are mainly based on empirical evidence gathered by the authors from their interactions with more than 100 SMEs in India.

We found that there is lot of ambiguity among SMEs about proper selection of air compressors and best operating practices (BOPs) in compressed air network. The chapter discusses practical insights gained from studies conducted on conserving energy in compressed air network used by small and medium scale industries. The following options for saving energy have been elaborated in the subsequent sections of the chapter:

- Leakages in compressed air system
- Wastage of power due to unloading
- Artificial demand
- Optimum pressure requirement in the plant
- Estimating receiver size
- Flow controller versus PM + VSD drive
- Suction air cooling

2 Leakages in Compressed Air System

Leakages in compressed air lead to huge wastage of power in industry. All the industries studied by the authors' required external technical assistance to quantify and plug air leakages.

The air leakages could be categorised into two categories: *primary leakages and secondary leakages*.

2.1 Primary Leakages

Primary leakages are the leakages through pipeline joints, filter regulator lubricator (FRL), tubing, etc. Typical Indian SMEs have a floor area of 50–100 m². The compressed air network is usually laid overhead with vertical drops to each machine. The following formula could be used to estimate the primary leakages.

$$\text{Primary leakages} = \frac{\text{Load time (in seconds)}}{\text{Load time (in seconds)} + \text{Unload time (in seconds)}} \times \text{FAD of compressor (in CFM)}$$

CFM = cubic feet per minute.

Another common problem is auto drain trap leakage.



The common problem in industries is moisture carryover in compressed air many a times, because of faulty auto drain traps.

Smaller nozzle timer-based ADTs choke; float types also choke. Electronic and level-based are costly and also fail frequently. The replacement cost is high.

The most reliable auto drain traps are timer-based and motorised with 12 mm opening. This has one disadvantage: if you keep drain interval short, lot of air is wasted, and if you keep drain interval long, water goes into the compressed air line.

In the air receiver, due to cooling at the surface of receiver, the water stays on the sides of the receiver, and due to gravity, it gradually falls and collects in the bottom dish.

The compressed air receivers, presently manufactured in India are based on IS 2825 (ASME Sec. VIII Div. 1) which is a code for unfired pressure vessels. It is a generalised code. The code doesn't address, compressed air receiver's one of the functions, that is, to remove moisture.

In compressed air system, moisture is collected at three major points.

1. In the moisture separator of the compressor: Sudden change in direction separates heavier water and lighter air.
2. In the Wet receiver: Every 10 °C. drop in compressed air temp. moisture quantity halves. Due to expansion and drop in compressed air temp, the moisture separates. If the auto drain trap of moisture separator is not functioning properly, the water separated goes to the wet receiver.
3. In air dryer: Refrigerated air dryer is a simple heat transfer mechanism. Drop in compressed air temp. removes moisture.

Separation of moisture from compressed air is first action, and second action is removal of this separated moisture, from main compressed air stream.

The second operation is when, normally, the failure chances are high, because of which the end user gets unwanted water.

We developed an attachment, to be connected to the receiver, called water accumulator. For a 5000 l. Receiver, accumulator capacity is 20 l (depending on the humidity and the compressor flow, this capacity varies.) it can accumulate water between 1 and 3 h. A good quality motorised auto drain trap (min. 12 mm opening) will ensure that only water is drained without loss of air. The 25 mm connection between accumulator and main receiver doesn't allow water accumulated, to go back to the main stream through the receiver.

Frequent operation and choking are main reasons of auto drain trap failures

Sr. no.	Without water accumulator	With water accumulator
1	All auto drain traps have some draw back Timer based with 4 mm opening – 1. If you keep short interval, there is a frequent operations and strainer choking 2. If you keep long interval, moisture goes in to the main line	You can keep 1–6 h interval, depending on the size of compressor
2	Motorised auto drain trap with 12 mm opening – Lot of air is lost along with water, and valve fails due to frequent operations	Motorised auto drain trap has 12 mm opening. No choking. No strainer required
3	No loss drain – Costly product. Failure due to dirt and dust	

2.2 Secondary Leakages

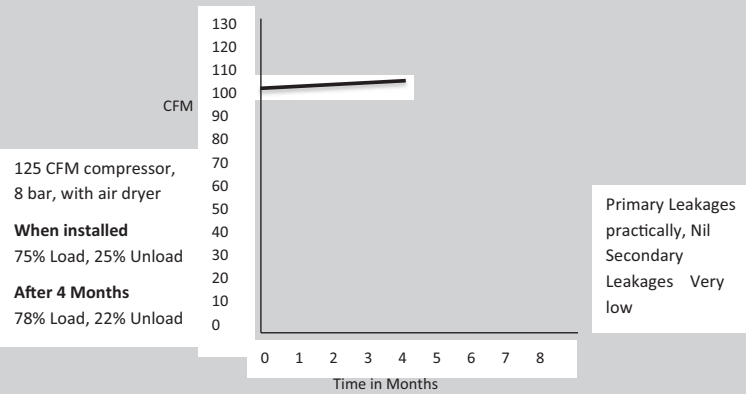
Secondary leakages refer to leakages through pneumatic cylinders and Solenoid valves, when the cylinder and Solenoid valves are in running condition. This is mainly due to leakages through the seals. Secondary leakages are a matter of concern especially when the factory has most of the compressed air being used for

pneumatic cylinders and the factory is not using air dryer. Secondary leakages normally occur due to poor lubrication, which in turn is caused by moist air directly going to the pneumatic cylinder and Solenoid valves. These leakages are more difficult to detect, and hence is more time consuming. However, they are important to detect, because from the energy point of view, these leakages increase over time. These leakages can be identified by simple soap bubble test or using good quality ultrasonic leak detectors.

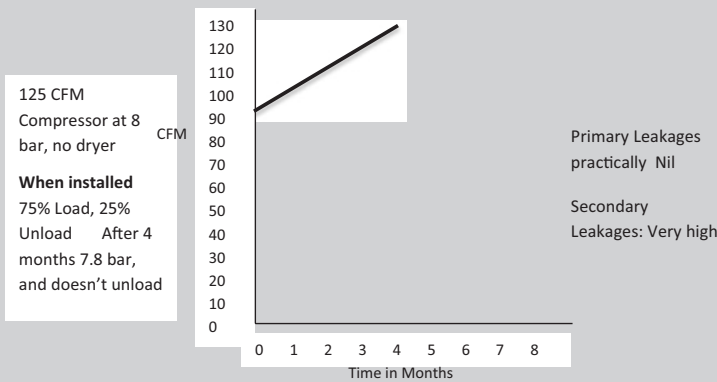
A comparative case-study of secondary air leakage in two plants, one using air dryer and other not using air dryer is given in Box 1. Both plants had identical pneumatic machines. Plant A was using a refrigerant type air dryer while Plant B was not.

Box 1 Case-study of secondary air leakage in two industries

Plant A – Seven packing lines each consuming 13 CFM (when new) and 13.5 CFM (after 4 months)



Plant B – Seven packing lines each line consuming 13 CFM (when new) 18 CFM (after 4 months)



The air compressor in Plant B was found to be consuming 20% more electrical energy to run the same number of packaging lines. There is virtually no maintenance, manpower, and spares required in Plant A against a technician regularly replacing the seal kits of pneumatic cylinders in Plant B.

2.3 Discussion

Auto drain trap leakages are a common problem. Water accumulator helps to arrest this leakage and allows only water to drain out. The leakage test is ideally carried out either during lunch break or on holidays when there is no productive use of compressed air. Auto drain traps should be closed before the test.

Normally, 3–5% air leakage, in total plant, is accepted as an industry norm. If the leakage is higher, detailed investigation is required. The primary leakages in the compressed air lines can be easily detected by a walk-through survey and identified leakages pointed out for corrective action by the maintenance team.

Air dryer is necessary with most of the air compressor installations, from energy conservation point of view. While primary compressed air leakages can be detected easily and plugged, it is much more difficult to identify secondary compressed air leakages. Many factory engineers sometimes do not appreciate the importance of dry air. Apart from preventing energy wastages due to secondary leakages, there are other advantages of using dry air, such as reduced corrosion of pipelines, improved comfort of workers, and so on.

The leakage test is best done by operating the air compressors when the plant is under shut down. The leakage points can easily be identified from the hissing sound made by the compressed air. The exact location can be pin-pointed by “tracing the pipeline” from where the sound is coming simply by feeling.

One can also use Ultrasonic detectors.

3 Wastage of Power Due to Unloading

Unloading power of air compressors leads to huge energy wastages in industries. The compressor unload data for 102 SMEs is given in Fig. 1.

Many of the units reported that in the day shift, compressor load is more than 70% but in second and third shift, compressor runs mostly unloaded. The variable speed drives (VSDs)¹ fitted externally were very costly and posed many problems like motor overheating in lower motor speeds (measured in revolutions per minute or RPM), the screw compressor throwing oil in to compressed air line due to low

¹VSD is also called variable frequency drive (VFD), adjustable speed drive (ASD) and adjustable frequency drive (AFD).

Fig. 1 Sample survey of air compressor unloading percentage among SMEs

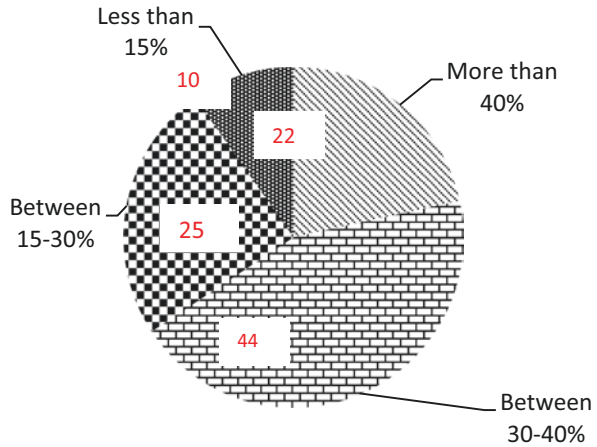


Table 1 Comparison of fixed-speed induction motor and VSD motor compressors

Fixed-speed induction motor compressor	Variable speed drive motor compressor
When compressed air reaches unloading pressure, the unloader closes the suction. There is no further compression; however, compressor consumes 30–40% of full load power which is a total waste	The motor speed is adjusted to the air demand. You just have to fix a pressure digit and compressor will speed up and down but maintains the pressure throughout
Generally, a pressure band is maintained, for example, say 7 bar unloading and 6.5 bar loading	You can fix a pressure digit. Say 6.7 bar. The compressor will continuously maintain 6.7 bar. This saving of 0.3 bar is also good energy saving. This reduces leakages and uncontrolled air consumption
The starting current is a kick, sometimes harmful to the compressor as well as electrical supply system	There is no starting kick. The compressor starts very smoothly
Number of start stops are limited depending on the motor HP	There is no limitation on number of starts
Take an example, where 120 HP compressor is running 30% unloaded. Considering service factor, the compressor full load power is 110 kW and unloaded power is 35 kW. In 24 h, there will be a power consumption of 2100 units	The same 120 HP compressor with SPM + VSD will consume 1700 units with a single pressure. this is about 20% of power saving

speed of screw etc. For SMEs many a times, screw compressor is the biggest motor in the plant and frequent starting and stopping created other electrical supply system problems.

Traditionally, SMEs use fixed-speed induction motor compressors. The advantages of using variable speed drive (VSD) motor compressors have not been disseminated widely among SMEs. Table 1 compares fixed-speed induction motor compressors with VSD motor compressors.

A better option from energy-efficiency view-point is to install screw compressors with built-in VSD. However, these compressors operate well with a load factor (the percentage of maximum capacity at which the compressor was operating) between 40% and 80%. The availability of permanent magnet (PM) VSD compressors has helped SMEs, particularly if there is low compressed air demand in night shifts.

3.1 Permanent Magnet VSD Compressors

PM VSD compressor is a relatively new concept and till now was not used in small and medium scale industries due to high cost. But now the costs have come down drastically, and most of the initial complaints like high electric motor failure, faced by PM + VSD compressor, has been resolved.

Figures 2 and 3 show cross-sections of AC induction motor and AC permanent magnet motor, respectively.

The advantages of PM Motor over induction motor are given in Table 2.

3.2 Discussion

PM + VSD is best for compressed air saving for SMEs. Figure 4 shows the energy cost saving of using PM + VSD compressor.

The green portion in the graph is air demand, which fluctuates depending upon consumption pattern of various compressed air consuming machines in the plant. The red line shows fixed speed induction motor compressor. It loads and unloads based on the signal received from the farthest end of the plant. The response time is very poor. One can increase the response time by installing a flow controller, additional receiver, bigger piping, etc.; however, there is no appreciable change in the curve.

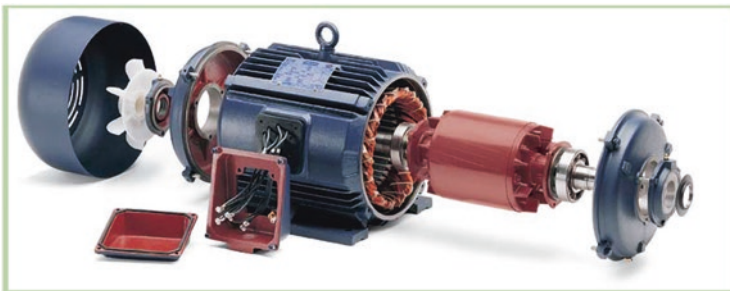


Fig. 2 Cross-section of AC induction motor

Fig. 3 Cross-section of AC permanent-magnet motor

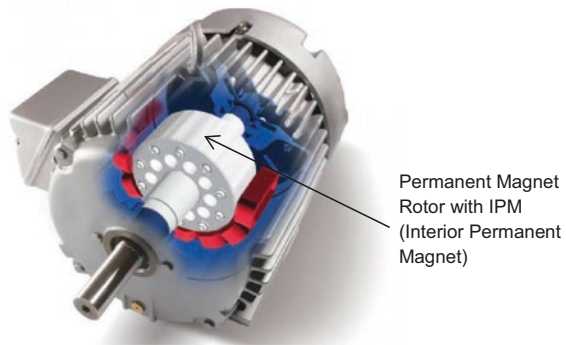


Table 2 Comparison of permanent magnet motor and induction motor

Permanent magnet motor	Induction motor – cage
Construction has a stator which has copper wires wound, and rotor is IPM (interior permanent magnet)	Construction has a stator which is wound with copper wires and rotor is having copper bars or copper wires
Efficiency = up to 98% (claimed by manufacturers)	Efficiency = up to 94–95% (claimed by manufacturers)
Compressor motor is a generally synchronous permanent magnet motor (SPM motor) Motors rotate at the same speed as the magnetic field produced by the stator windings; it is a synchronous machine	Rotor rotates at 2–3% lower RPM than stator winding alterations
Synchronous motor rotates at a rate locked to the frequency since it does not rely on current induction to produce the rotors magnetic field	Induction motors run with a slip. The rotor rotates slightly slower than AC alterations, in order to induce current in rotor windings
Rotor spins at the same speed as the motors internal rotating magnetic field	Rotors rotate considering the slip
Generally the speed ranges from 3000 to 5000 RPM. There are normally no bearings on the motor	Speed is 1500/3000 RPM
More efficient than induction motors so runs more coolly under the same load conditions	Motor overheating when separator element chokes, or due to lower voltage, is a common problem. Overheating degrades insulation
Permanent magnets produce more flux and resultant torque for their physical size	Induction produced by squirrel cage rotor, inherently limits power density
Overall size of PM motor is much smaller than induction motor	Induction motor is bigger in size
Overall for the same load pattern motor consumes 4–6% lesser power	High power consumption compared to SPM motor

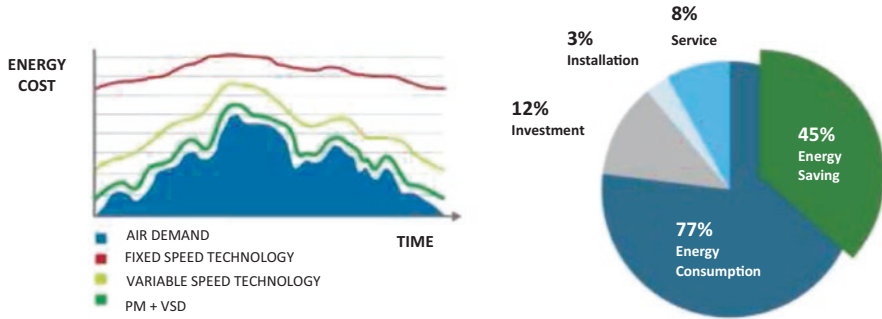


Fig. 4 Energy cost saving by using PM + VSD compressor

The second curve is that of standard variable speed drive, which is better than fixed-speed machine but not as efficient as PM + VSD. Third curve which is going parallel to the air demand is the best solution for SME. SMEs, which have a typical problem of low consumption in second shift and very low consumption in third shift, can save substantial energy by using PM + VSD compressor.

4 Artificial Demand

Amongst most of the compressor users, artificial demand is a subject which is not understood properly. The name itself, artificial demand, explains that it is unwanted higher pressure supplied to the plant which is unnecessary. Depending on the size of industry, its use of compressed air, initial design of piping and receiver sizing, the unproductive percentage can vary. There are some industries where unproductive use can be as high as 50% while some very well-maintained industries using energy-saving devices, such as flow controller, master controller VSD good piping, and proper receiver sizing, can have unproductive use as low as 5%.

Typically, up to 40% of compressed air has been found to be wasted due to artificial demand (producing more air than what is actually needed) as shown in Fig. 5.

Typical wastage of compressed air due to leakages, artificial demand, and improper use.

The main causes of artificial demand were found to be the following:

- On an average, artificial demand comes from running the compressors at too high a pressure – a simple but wrong solution to compensate for instantaneous peak demands arising in the plant.
- Many times, leaks are not plugged. Due to leaks, the extreme end user in the plant complains low pressure. Another wrong solution is to increase the compressor house pressure.
- Wrong size of piping, inadequate receiver sizing, and location results in pressure drop, due to which compressor house pressure is increased as compensation.

Fig. 5 Typical wastage of compressed air due to artificial demand

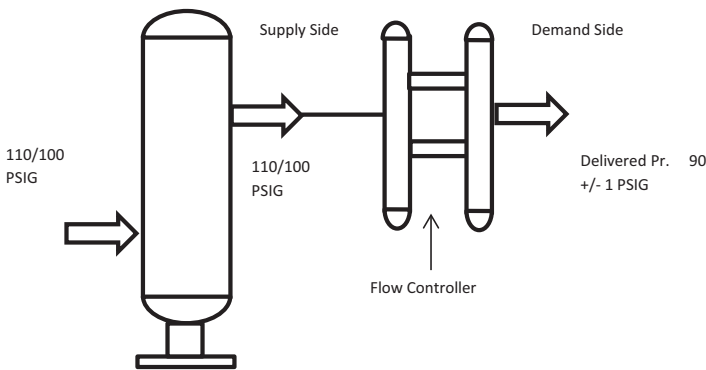
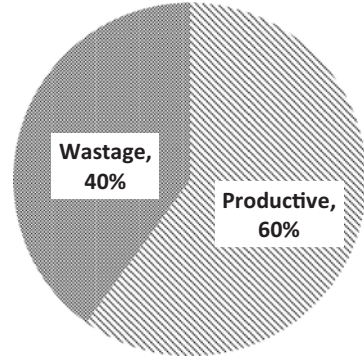


Fig. 6 Function of a flow controller

- Misuses of air, such as liquid agitation and equipment cooling, workers cleaning themselves contribute to further loss in pressure. Again pressure is increased in compressor house.

The result of all above is creation of artificial demand, causing the whole system to produce, consume, and waste more air than necessary. The result is predictable: more waste and higher energy bills.

4.1 Discussion

A flow controller helps eliminate artificial demand by allowing the air system to operate at the lowest possible pressure while ensuring that production processes flow efficiently and uninterrupted. The installation of flow controller will reduce the pressure in the network but at the same time will not allow it to fluctuate beyond +/- 1 psig (Figs. 6 and 7).

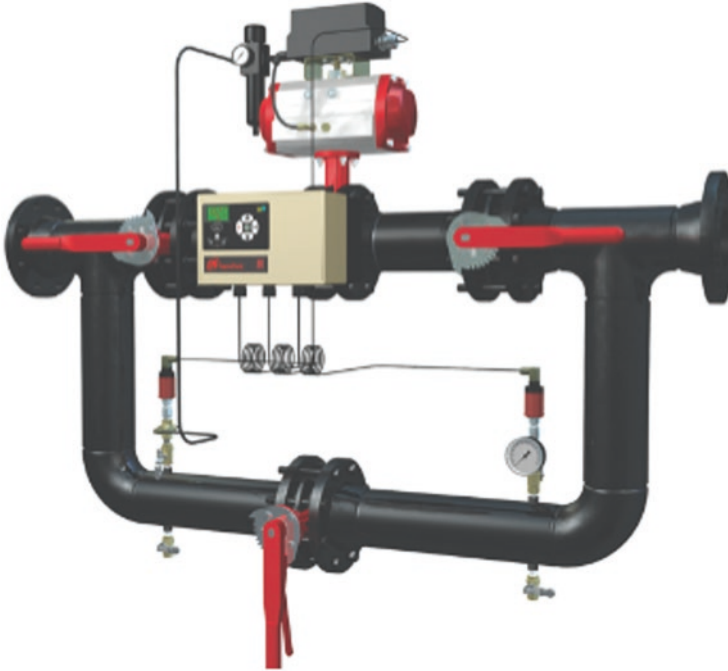


Fig. 7 Typical flow controller showing PID controller, control valve, sensor and solenoid valve

Flow controller is installed in the compressor house after treatment, that is, after air dryer and oil removal filters, and after air receiver. It controls the release of air from the air stored in the air receiver. There is the sensor at control valve outlet which gives commands to a diaphragm valve through a PID controller. Only that much air is released from the receiver that is required to maintain pressure band of ± 1 pounds per square inch (psi) in the plant. The principle is simple, when compressed air expands, the pressure decreases, and when air compresses, the pressure increases. Therefore, if more air is flowing away from the balance point, then pressure goes down and control valve opens to release more air from storage. If less air is flowing in to the balance point, the valve operates instantly to hold air back in storage.

The 'flow controller system' consists of the following.

1. A large capacity air receiver (size depends on system).
2. Flow controller to separate demand side and supply side of compressed air system. A flow controller consisting of the following sub-systems: proportional integral derivative (PID) controller, control valve, pressure transmitter, and solenoid valve. PID controller is a control loop feedback mechanism for modulated control. The pressure at outlet of flow controller is sensed and air flow is accordingly adjusted, to maintain the set point pressure. If set point pressure reduces, the flow controller will instantly take air from large air receiver and feed the

plant to maintain pressure. Similarly, when there is excess pressure in the net, PID gives command to the regulator to close the valve. The function of solenoid valve is to open control valve fully, if pressure drops below set point.

5 Optimum Pressure Requirement in the Plant

Before analysing any compressed air system, what is important is to find out what is the minimum pressure at which the plant can run satisfactorily. The pressure gauge shows a dampened pressure which is normally higher than minimum pressure acceptable, because analogue pressure gauge cannot indicate the dip. A sudden drop in pressure is often not reflected quickly enough on the dial of analogue pressure gauge. A better option is to install a *digital pressure data logger*, which will sense pressure in four decimals in psi and will log every 4 s.

The variation of compressed air pressure with time in a typical press shop for cutting gaskets is shown in Fig. 8.

Even when the operator observes a pressure of 90/85 psig in the dial of analogue pressure gauge, the actual pressure measured with a more accurate pressure data logger was found to dip to 79 psig. This means with a control flow, if the operator gets 80 +/- 1 psig, the product quality will not be affected. In fact, the product quality will be consistent because of the consistent pressure.

Hence, the first step to control air flow is to find out what is the minimum acceptable pressure profile. Once the profile is established, the additional receiver size may be estimated.

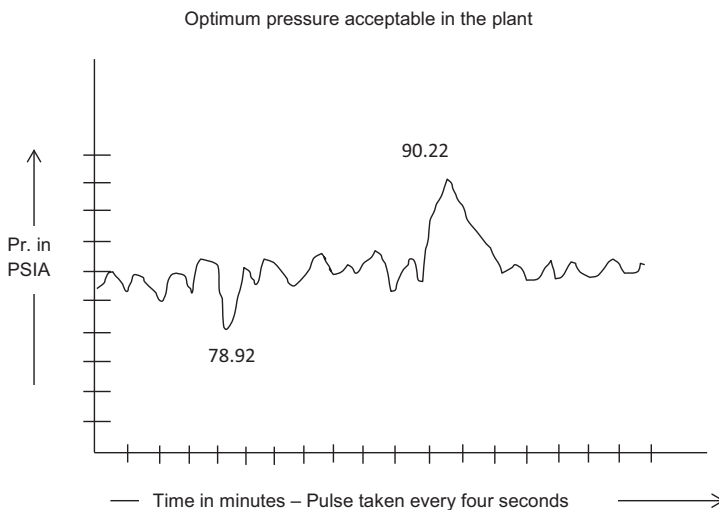


Fig. 8 Variation of compressed air pressure with time

Compressed air travels, at a limited velocity, inside a system determined by the pressure differential that exists. At 1 psig, this velocity is approx. 75 m/s, which means if compressor is more than 75 meter away, the operator will notice the change only after 1 s.

6 Estimating Receiver Size

Secondary receiver is very important to take care of peak demands, which arise intermittently. For area where the maximum pressure drop is observed, installing a secondary air receiver will help stabilise the pressure. The importance of sizing the receiver capacity optimally is shown in Fig. 9. It is presumed that piping dia. and looping is proper.

Ideal secondary air receiver will have a very low fluctuation of Pr. not beyond 0.2–0.3 bar.

If the Pr. variation is more, then we have a rule of thumb for SME.

The total receiver capacity can be calculated using the following formula.

$$\text{Secondary receiver capacity (in litre)} = \frac{(\text{Highest Pr.} - \text{Lowest Pr.}) \times \text{Compressor capacity in LPM}}{5}$$

For example, a 5660 LPM/7.5 bar compressor has a pressure variation from 7 to 5.1 bar at peak load.

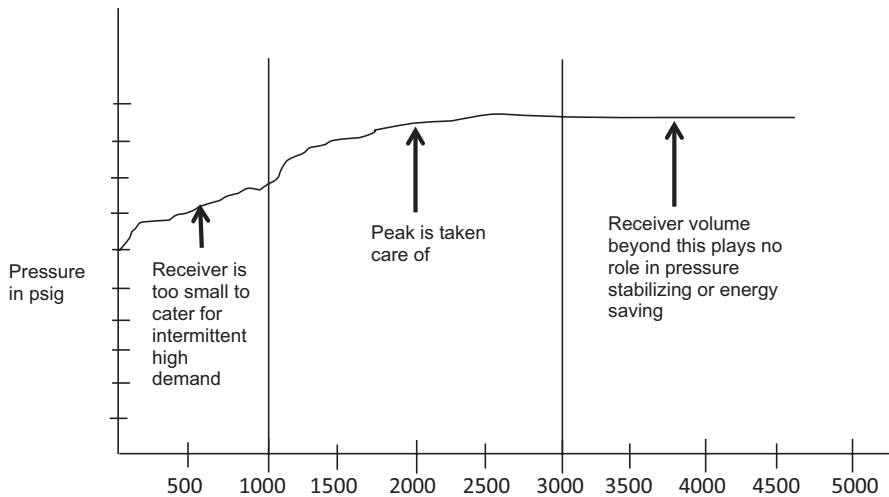


Fig. 9 Optimum receiver capacity (primary + secondary)

$$\text{Secondary storage capacity} = \frac{2.91 \times 5660}{5} = 3200 \text{ or say } 3000 \text{ l}$$

The above formula works for SMEs, which we have derived after taking trials; however, it may not work for large industries where the compressed air network is more complicated.

7 Flow Controller Versus VSD Drive in SMEs

We have observed that many of the SMEs have only one compressor running and one stand-by. 30% unloaded time is common. Piping leakages are reasonably under control but auto drain trap leakage is many a times neglected.

The flow controller is definitely a device, which gives a constant pressure, throughout the plant however, whether it will save energy substantially depends on the location. We have observed that many a places, flow controller is installed, worked for some time, but the moment there is some change in requirement of pressure or flow, the flow controller doesn't respond satisfactorily.

A flow controller is not a product which can be used as an accessory in a random fashion. To install a flow controller, the consumption pattern has to be studied very carefully and should be installed by an experienced engineer.

The disadvantages of flow controller for SMEs are the following:

1. Good-quality effective flow controllers consist of lot of electronic controls and costly valves. Hence, for SMEs it is not affordable.
2. Flow controllers require regular maintenance. The electronics is complicated.
3. Flow controllers require clean oil-free and moisture-free air, as control air.
4. For an SME using a single or two compressors, the flow controller is only going to result in increase in unloaded time. This saving is not more than 5–7%.

The only advantage of flow controllers is that they provide stabilized pressure (+/–1 psi) throughout the plant. However, there are very few manufacturing processes wherein +/–1 psi play a crucial role.

Instead of flow controller, a PM + VSD motor for SME is a better choice and is a high energy-saving modification.

Advantages of PM + VSD are as follows.

1. There is no unloaded power.
2. PM motor itself takes less power than induction motor.
3. Instead of a band of loading/unloading pressure, one can operate at a fixed pressure which is much lower than the unloading pressure.
4. It is always recommended to use a secondary receiver which helps in giving constant pressure in a peak demand. Secondary receiver helps to reduce time lag for increasing pressure for a VSD.

The overall effect will be energy saving to the tune of 30% by PM + VSD as against 5–7% by controller. For SMEs operating 16–24 h per day and running an induction motor compressor with 25–30% unloading time, PM + VSD is definitely a product which saves energy substantially.

A case-study on how artificial demand is tackled by replacing an existing flow controller with a secondary receiver coupled with PM + VSD compressor, as shown in Fig. 10.

8 Suction Air Cooling

Conventional wisdom and theoretical inputs suggest that lowering suction air temperature for any compressor will save substantial power. In fact thermodynamically, it can be proven that every 4 °C rise in inlet air temperature results in a higher energy consumption by 1% to achieve equivalent output. The energy saved in a compressor by cooling of the inlet air temperature is given in Table 3.

From above information, a maintenance engineers can assume that for a 600 CFM oil injected screw compressor, if suction temperature is reduced from 45 to 20 °C, then power will reduce by approximately 4.5% and volume output will increase by about 7%.

However, the three basic rotary types of compressors, which are oil-flooded, oil-free, and centrifugal, perform differently with suction cooling. Since most SMEs use oil-injected screw compressors, we studied them in more details. An experiment detailed in Table 4 was carried out in a running factory.

Although it may not be as accurate as in controlled laboratory, the actual reduction in power consumption was not found to be appreciable and definitely much less than 4% calculated theoretically. Thus, we find that at least in a running compressor, we don't find any appreciable change in either power or flow.

Table 3 Effect of intake air temperature on power consumption [1]

Inlet temperature (°C)	Relative air delivery (%)	Power saved (%)
10.0	102.0	+1.4
15.5	100.0	Nil
21.1	98.1	-1.3
26.6	96.3	-2.5
32.2	94.1	-4.0
37.7	92.8	-5.0
43.3	91.2	-5.8

Figures are Representative only

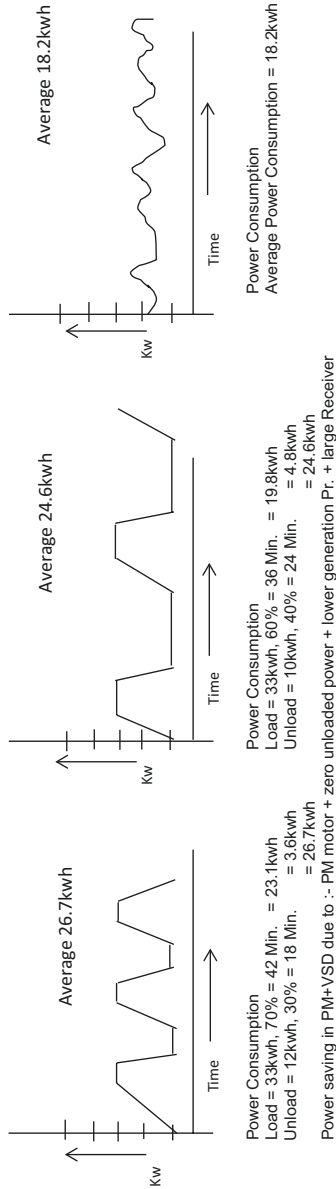
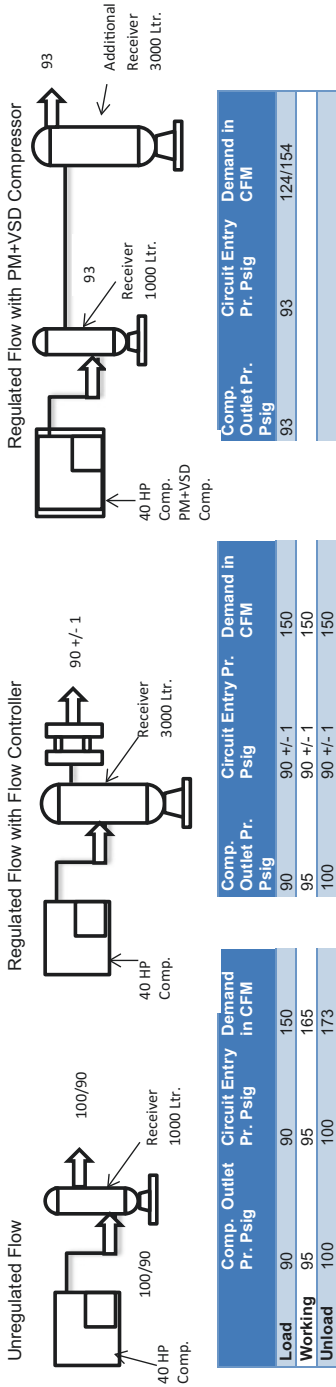


Fig. 10 Case study of replacing flow controller with PM- VSD compressor

Table 4 Variations in power consumption due to ambient air

Time of day	Ambient temp.	Air oil temp. at screw air end	Total package power KW	Pressure maintained at receiver in PSI	Precipitation rain fall	Capacity increment	Power variation
5 am	16 °C	84 °C	90.18	100.12	0	–	–
2 pm	33 °C	91 °C	90.20	100.08	0	Negligible	0.1%

8.1 Discussion

All three basic industrial rotary compressors, that is, oil-injected, oil-free, and centrifugal, have different performance due to suction cooling. As for oil-injected screw compressors, we did not find any change either in power or flow. More accurate laboratory tests are required, which only manufacturers can carry out for oil-injected screw compressors.

A very few engineers have experimented on oil-injected screw compressors in laboratories to find actual power saving by inlet suction cooling. We refer to a thesis on the same subject by a U.S. university and whose observations corroborate with our practical experience and readings [4].

In case of oil-injected screw compressors, the cold air from suction is entering already hot oil in the screw element. This oil continuously absorbs heat of compression and in turn oil is cooled in the oil cooler. The cold inlet only helps in reducing air oil temperature at screw air end discharge from 910 to 840 °C. Suction cooling definitely helps in reducing air oil temperature which gives a better life to oil and spare parts such as sealing rings, hoses. However, there is virtually no effect on power due to suction cooling.

We observed that apart from less spares and oil consumption, suction air cooling does not result in power savings in oil-injected screw compressors.

8.2 Case Study: Energy Saving of Replacing a Fixed Speed Induction Motor Compressor with a PM + VSD Air Compressor

An SME unit manufacturing sheet metal components was using four pneumatic presses. These presses consumed a total of 40 cfm of compressed air at 6.5 bar (g) pressure. Specification of the air compressor which was used by them and its operating conditions are given in Table 5.

The readings recorded during the walk-through audit of the compressor are given in Table 6.

There is scope to save energy by reducing the unload power consumption and reducing pressure fluctuations by keeping it constant at 6.5 bar. Incorporating a proper sized dryer and auto drain trap would increase the energy savings further.

Table 5 Compressor specifications and operating conditions

Make	ELGI Brand in India	Max. working pressure	8 Bar
Year of manufacturing	2017	Unloading/loading pressure	6/7 Bar
Motor kW	15	Total hours run	6707
FAD in CFM	95	No. of hours run per day	16 (300 days a year)

Table 6 Readings recorded during audit

Data	Reading	Remark
Air oil temp. on load	90 °C	Okay. Should be between 80 and 95 °C
Unloaded %	35% (loaded hours 4483/unloaded hours 2224)	High. Should be between 25 and 30%
Pressure drop dryer + filter	5 PSI	High. Should be ideally 3 psi. Could be due to undersized air dryer and oil removal filter. Proper sizing required
Auto drain trap	Leaking	Non-leaking auto drain traps required
Receiver size, primary + secondary	Primary 2000 l, no secondary receiver	–
Monthly average power consumption	11.06 kWh	

Table 7 Compressor specifications and operating conditions

Make	Brand in India	Max. working pressure	8 Bar
Year of manufacturing	2013	Unloading/loading pressure	6/7 Bar
Motor kW	30	Total hours run	22,100
FAD in CFM	160	No. of hours run per day	24 (300 days a year)

A 15 kW, PM + VSD air compressor was recommended to the SME. The new compressor delivered 6.5 bar constant pressure and monthly average electricity consumption of 7.8 kWh. Thus, an energy saving of 29% was achieved in the new air compressor.

8.3 Case Study: Energy Saving of Replacing a Fixed-Speed Induction Motor Compressor with a PM + VSD Air Compressor

An SME unit manufacturing blow moulding was using six blow moulding machines. These machines were manufacturing plastic containers from 10 to 250 l. The average air consumption was 125 cfm at 6.5 bar pressure. Specification of the air compressor which was used and the operating conditions are given in Table 7.

Table 8 Readings recorded during audit

Data	Reading	Remark
Air oil temp. on load	90 °C	Okay. Should be between 80 and 95 °C
Unloaded %	35% (loaded hours 4483/unloaded hours 2224)	High. Should be between 25 and 30%
Pressure drop dryer + filter	5 PSI	High. Should be ideally 3 psi. Could be due to undersized air dryer and oil removal filter. Proper sizing required
Auto drain trap	Leaking	Non-leaking auto drain traps required
Receiver size, primary + secondary	Primary 2000 l, no secondary receiver	–
Monthly average power consumption	11.06 kWh	

The readings recorded during the walk-through audit of the compressor are given in Table 8.

There is scope to save energy by reducing the unload power consumption and reducing pressure fluctuations by keeping it constant at 6.5 bar. Incorporating a proper sized dryer and auto drain trap would increase the energy savings further.

A 37 kW, PM + VSD air compressor was recommended to the SME (Considering expansion). The new compressor delivered 6.5 bar constant pressure and monthly average electricity consumption of 7.8 kWh. Thus, an energy saving of 25.3% was achieved in the new air compressor.

9 Conclusions

For a country like India, having tens of thousands of SMEs, conserving energy in compressed air system is very important. Most SMEs lack in-house expertise on optimum selection and operation of air compressors. A number of energy conservation opportunities in compressed air system were discussed in the chapter.

Air leakages are the biggest source of energy wastage in compressed air systems. Leakages should be controlled in the range of 3–5%. Regular tracing of the compressor line by hand or by leak detector is essential to plug leakages. Usefulness of air dryer is not well understood by SMEs. The use of air dryer helps in reducing secondary leakages. Energy wastages due to unload power consumption can be controlled by adopting energy-efficient PM + VSD compressors. A flow controller can be used to reduce artificial demand of running the compressors at a higher pressure to compensate for instantaneous peak demands arising in the plant. A sudden drop in pressure is often not reflected quickly enough on the dial of analogue pressure gauge. A better option is to install a digital pressure data logger, to sense and log the pressure accurately. Optimising the receiver size is important for energy saving. A simple method to estimate the receiver size has been given in the chapter.

A PM + VSD compressor can deliver constant pressure. It could lead to substantial energy savings, especially if operating hours of the compressor are high. Artificial demand in a plant can be tackled by replacing an existing flow controller with a secondary receiver coupled with PM + VSD compressor. Cooling of suction air helps in reducing air oil temperature which leads to longer life of the oil and spare parts such as sealing rings, hoses, etc. However, reducing the temperature of suction air may not significantly affect the power consumption of the air compressor.

There is an urgent need to raise the awareness in SMEs of saving energy in compressed air system. A nation-wide program, undertaken as a mission, aimed at providing technical assistance to SMEs on identification and implementation of energy-efficiency measures in their compressed air systems that will lead to very high energy savings, with consequent reduction of green-house gas (GHG) emissions.

References

1. BEE, *Guide Book for Energy Auditors and Managers* (Bureau of Energy Efficiency, New Delhi, 2003)
2. R. Saidur, N.A. Rahim, M. Hasanuzzamen, A review on compressed-air energy use and energy savings. *Renew. Sust. Energ. Rev.* **14**(4), 1135–1153 (2010)
3. The Gazette of India, 2018: Extraordinary Ministry of Power, Notification New Delhi, The 27 May, 2014 No. 1143. New Delhi, 27 May 2014
4. Ming Han Chua, *Experimental Investigation of Inlet Temperature on Input Power in an Oil-Flooded Rotary Screw Air Compressor*. University of Alabama, 2015

Optimizing Pump and Compressor Selection for Energy Efficiency Using True-Weighted Efficiency (TWE)



Trygve Dahl

1 Introduction

1.1 *Optimal Selection of Motor-Driven Fluid-Handling Equipment*

The US Department of Energy (DOE) published an influential report in 1998 stating that industrial motor systems are the largest single electrical energy consumer in the American economy, representing approximately 23% of all electricity sold in the United States in 1994 [1]. Furthermore, the DOE predicted that industrial motor system energy savings of 11–18% were possible using proven technologies. Improvements to major fluid-handling equipment such as pumps, fans, and air compressors that use these industrial motors represent up to 62% of the potential savings. This estimate does not include savings associated with improving the efficiency of the motors driving these systems, but the technical aspects of optimizing the application of pump, fan, and air compressor systems which are well-understood but not widely implemented.

The optimal selection of fluid-handling equipment (FHE) is a well-documented topic found in numerous papers and textbooks [2, 3]. Other studies involving the optimal selection of pumping equipment, which are applicable to compressors, blowers, and fans as well, are outlined in papers by the author [4–6]. Mechanical equipment selection must first satisfy the essential functional requirements required by the application. There are usually many satisfactory fluid-handling system (FHS) configurations that meet those requirements. The selection process includes considerations, such as the type of machine (pump, compressor, fan); configuration of the

T. Dahl (✉)
Intelliquip Inc., Bethlehem, PA, USA
e-mail: tdahl@intelliquip.com

machine, operating control strategy (variable speed, on-off, throttle control, bypass control); and type of prime mover (electric motor, engine, turbine). Those types of considerations are outlined in books on systems optimization or applications of variable speed motors and drives [7, 8]. Life Cycle Costing (LCC), goes beyond system optimization and considers the entire cost to purchase, install, operate, maintain, and then dispose of that equipment during its lifetime. A methodology to perform LCC for pumps is published by the Hydraulic Institute/Europump [9] and applicable to compressors, blowers, and fans [10]. For fluid-handling systems operating under continuous service or for significant time-periods, energy consumption is often the largest cost component of the LCC calculation. This chapter will focus on energy consumption as a key optimization criterion in the selection process for motor-driven pumps and compressors, hereafter referred to as fluid-handling equipment (FHE) or systems (FHS).

1.2 Energy Consumption

Energy consumption is determined by measuring or calculating power consumption over a specified period of time. For a single operating condition with constant input power, P , the energy consumption, E , over a specified time period, t , is calculated as follows:

$$E = P \cdot t \quad (1)$$

Fluid-handling equipment, such as pumps, compressors, blowers, and fans, generally operate at multiple conditions, along a single system curve or multiple system curves. These operating points occur at different flow and head (or pressure) conditions, with each operating for periods of time. A *Load Profile*, with the following characteristics, is used to describe the operating domain:

- Discrete operating points on the system curves, usually depicted as a percentage of a rated flow condition, $Q\%$.
- Time of operation at each operating point. The time of operation is usually determined over a fixed duration, often a 24 h or annual period. The percentage of time operating at each point is defined by $t\%$.
- One or more System Curves.

The performance characteristic and system curve interactions with the load profile are governed by the flow control method. Figures 1 and 2 illustrate a flow control curve, denoted as System Curve A, with four distinct operating conditions at 100%, 75%, 50%, and 25% of the duty point flow. Either a fixed speed (Fig. 1) or a variable speed (Fig. 2) control may be applied to achieve the desired flow control [11].

Since System Curve A is the desired flow control curve, a fixed-speed pump uses throttle control to achieve the four specified operating flows on that control curve A

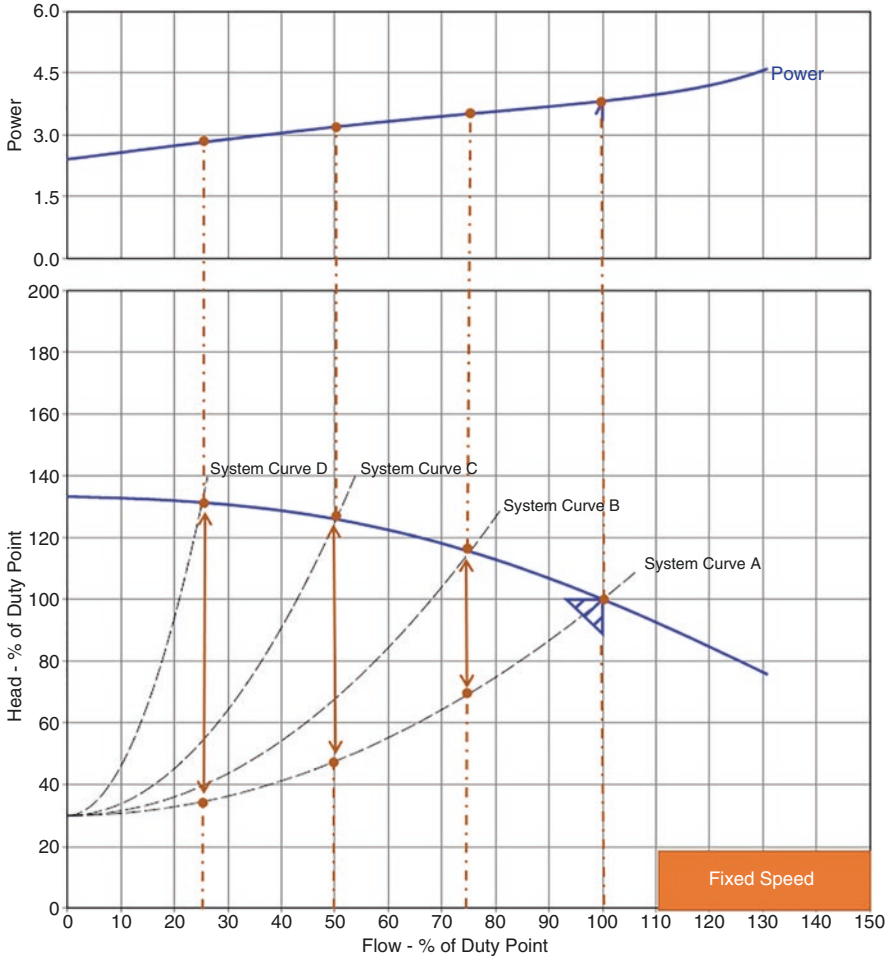


Fig. 1 Fixed-speed pump or compressor

(Fig. 1). This results in the three throttled system curves depicted as System Curve B, C, and D, respectively. The differential head (or pressure) loss due to throttling is depicted by the vertical arrows in the area between the Head (or pressure) Curve and the System Curve A in Fig. 1. Alternatively, variable speed control can satisfy the four operating conditions by adjusting the speed from 100% to 81%, to 65%, and then to 52% of the full speed to achieve all four-operating conditions in Fig. 2. The operating speeds are for illustration only, as the exact speed depends upon the performance characteristic of the turbomachine under evaluation.

Total system energy consumption, E_{total} , at multiple operating points $i = 1, 2, 3 \dots N$ is defined in equation form as:

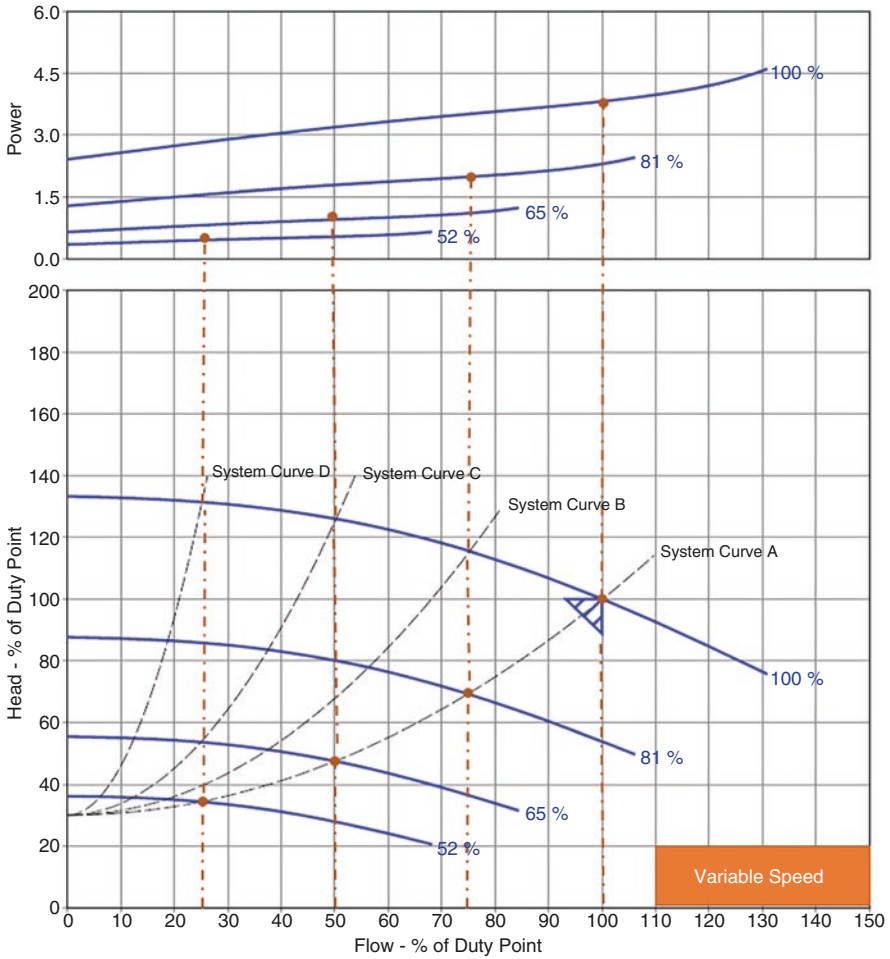


Fig. 2 Variable speed pump or compressor

$$E_{\text{total}} = \sum_{i=1}^N (E_i) = \sum_{i=1}^N (P_i \cdot t_i) \tag{2}$$

The lowest total energy consumption is an important evaluation criterion when comparing alternative FHS that also satisfy each of the other functional requirements. While calculating the total energy consumption over multiple different operating points is more precise than comparing models based on a single duty point efficiency, this calculation is not normally performed. Engineers typically use the design point efficiency as a preferred evaluation metric, as it is well-understood in the industry and readily comparable between different alternative FHS solutions. Unfortunately, there is no consistent or universally applied method for calculating efficiency involving multiple operating conditions.

2 Energy-Efficiency Standards and Regulations

The emphasis on energy-savings potential has inspired the development of new energy rating metrics in the last decade. These are published as new industry and government regulations in Europe and the United States that apply to specific classes of water pumps, fans, and industrial blowers. A few of these regulations and their applicable efficiency metrics are outlined below:

1. Ecodesign requirements for water pumps, EU Regulation No. 547/2012, was introduced in 2012 to establish minimum efficiency thresholds for rotodynamic water pumps in clean water services [12]. This regulation referenced a comprehensive empirical study of commercially available pumps, commissioned by the European Union (EU), leading to a Minimum Efficiency Index (MEI). The EU regulation establishes a minimum efficiency that all regulated pumps must achieve based on a fixed speed and three different operating conditions for each pump. Pumps that do not meet this requirement cannot be sold commercially.
2. In 2013, Europump, a European organization of pump manufacturers, recognized the need for an efficiency metric to rate each pump individually considering the multiple operating conditions associated with each pump system. Since total pump efficiency, η_1 , is a better indicator of total energy consumption than pump efficiency, η_2 , alone, consideration of the pump plus its motor and drive system was deemed necessary. Accordingly, Europump developed the Extended Product Approach, EPA [13]. The metric introduced in this approach is the Energy Efficiency Index, EEI, which is the ratio of the average power consumption of the actual pump operating under different operating conditions, $P_{1,avg}$, compared to the reference total power of the actual pump at its reference conditions of pump and motor efficiency, denoted as $P_{1,ref}$.

$$EEI = \frac{P_{1,avg}}{P_{1,ref}} \quad (3)$$

3. In the United States, the Department of Energy (DOE) also introduced new legislation in February 2016, establishing an Energy Conservation Standard and Test Procedure for certain clean water pumps [14]. This standard requires specific types of pumps sold in the United States, starting January 27, 2020 to meet a minimum Pump Energy Index, PEI. See also [15–18]. The PEI metric was inspired by the Ecodesign Regulations and the EEI but uses a different calculation procedure. The PEI is used to rate a basic pump model, where PEI is the ratio of the Pump Energy Rating, PER, for a given pump model compared to the standard Pump Energy Rating, PER_{STD} , for a comparable minimally compliant pump model. The standard considers pumps operating with either a Constant Load (CL) or a Variable Load (VL). The PEI formulas for PEI Constant Load, PEI_{CL} , and PEI Variable Load, PEI_{VL} , are shown below. Pumps that are regulated by the new standard must have a PEI value of 1.0 or less to be eligible for commercial sale after January 27, 2020.

$$PEI_{CL} = \frac{PER_{CL}}{PER_{STD}}; \quad (4)$$

$$PEI_{VL} = \frac{PER_{VL}}{PER_{STD}} \quad (5)$$

Fans and industrial blowers are also the subject of regulations as outlined in the following examples.

4. Minimum fan efficiency requirements were first considered in 2007. A 65% efficiency threshold was proposed for all fans. This approach was punitive towards certain classes of fans with a smaller fan diameter. Industry advocates and committees within the American Society of Heating, Refrigeration, and Air-Conditioning Engineers (ASHRAE), Air Movement and Control Association (AMCA), and the International Standard Organization (ISO) began work to develop a more informed method to classify fan efficiency. This led to a new metric known as the Fan Efficiency Grade (FEG). This metric established a minimum fan efficiency based on fan size (impeller diameter) [19]. The FEG was included in new industry standards introduced in ISO 12759 (Fans – Efficiency classification for fans) [20] followed in 2010 by AMCA 205 (Energy-Efficiency Classification for Fans) [21]. Then, ANSI/ASHRAE/IES published Standard 90.1 adopting AMCA 205 [22].
5. Coincident with these industry standards for fans, the Department of Energy (DOE) initiated the development of US regulations for electrically powered Residential Furnace Fans used in residential buildings for the purpose of circulating air through ducting [23]. Another new metric known as the Fan Efficiency Rating, FER, was introduced. The FER is a normalized estimate for annual energy consumption for a regulated furnace fan. The standard requires that all regulated furnace fans deliver a FER less than or equal to a minimum value, based on fan configuration. Manufacturers are required to comply with the standard for regulated products starting on July 3, 2019.
6. The DOE later extended the regulatory work for Furnace Fans to include Commercial and Industrial Fans and Blowers. This work is published as a notice of data availability (NODA) [24]. Published in this NODA, the DOE developed a new metric known as the Fan Efficiency Index, FEI. The FEI is defined as the fan energy rating (FER_{STD}) of a fan that exactly meets the efficiency level being analyzed, divided by the fan energy rating (FER) of a given fan model. The FER is defined as the weighted average electric input power of a fan over a specified load profile, in horsepower, measured at a given speed. A FEI value less than 1.0 would indicate that the fan does not meet the efficiency level being analyzed while a value greater than 1.0 indicates that the fan is more efficient than the minimum efficiency level analyzed. The FEI in equation form is shown below:

$$FEI = \frac{FER_{STD}}{FER} \quad (6)$$

In summary, these various standards and regulations introduced new ratings and efficiency metrics applied to specified models of pumps, compressors, blowers, or fans. For pumps, the rating could be designated as an EEI or a PEI, where values less than 1.0 are considered acceptable and lower values indicate lower energy consumption compared to standard pump models. While the EEI and the PEI are similar, they are not the same and are based on different calculation methods. For furnace fans, the ratings are also a useful efficiency rating. In one case, a larger FEG is better than a smaller FEG. Conversely, the DOE standard applies a FER, where a smaller FER is better, and must be less than a minimum value in order to be commercially sold. The NODA for Commercial and Industrial Fans and Blowers later introduces a FEI metric, where a value greater than 1 is considered better. The FEI rating is the inverse of the PEI metric for pumps, confusing engineers specifying pumps, fans, and blowers. Inasmuch as these ratings and metrics are unique and inconsistent across the different standards, they are essential benchmarks used to eliminate groups of inefficient equipment from commercial sale. However, these methods cannot be used to precisely determine the most energy-efficient FHS *for a specific system application and load case*, since these ratings are not *energy efficiency* metrics in the traditional sense but relative indicators of the efficiency of a model compared to a benchmark. This lack of a universal and easily understood efficiency metric inspired the development of the True-Weighted Efficiency metric.

3 TWE Method

True-Weighted Efficiency (TWE) addresses the industry need for a generalized efficiency metric that is reliably applied to any type of FHS application [11, 25]. A general introduction to the method and its derivation is as follows.

The general definition for the efficiency of a pump, fan, blower, or compressor is broadly defined as

$$\eta_c \text{ (or } \eta_h) = \frac{P_{\text{fluid}}}{P_{\text{input}}} \quad (7)$$

where η_c is the isentropic (or adiabatic) efficiency of a compressor and η_h is the hydraulic efficiency of the pump, P_{fluid} , is the useful energy input to the fluid per unit time. P_{input} is the power input to the rotor [3]. The determination of P_{fluid} is the isentropic (or adiabatic) power for a compressor or the hydraulic power for a pump. For larger pressure ratio compressors, polytropic power is often used in lieu of isentropic (or adiabatic) power. See [3] or [26] for details about the calculation of power and efficiency.

The power input to the rotor (or impeller) is always less than the power supplied to the rotating shaft because of external energy consumption in the bearings, seals, etc. Thus, the shaft power, P_2 , is related to the shaft efficiency, η_2 , as follows:

$$\eta_2 = \frac{P_{\text{fluid}}}{P_2} \tag{8}$$

The total input power is denoted as P_1 . For electric motor-driven systems, the input power is the electrical power input to an electric motor or the combination of electric motor and control system. This is also known as the *wire-to-water power*. Thus, the total input power, P_1 , is related to the total efficiency, η_1 , as follows:

$$\eta_1 = \frac{P_{\text{fluid}}}{P_1} \tag{9}$$

A pictorial description of the P_{fluid} , P_1 , and P_2 is shown in Fig. 3.

Energy consumption is a function of the power required over a specified period of time. For a single operating condition with a constant input power, P , the energy consumption, E , over a specified period of time, t , is defined as:

$$E = P \cdot t \tag{10}$$

TWE is thus derived using the conventional engineering efficiency ratio of useful energy output, E_{output} , versus energy input, E_{input} .

$$\text{TWE} = \frac{E_{\text{output}}}{E_{\text{input}}} \tag{11}$$

Furthermore, TWE is calculated as either the *True-Weighted Shaft Efficiency*, TWE_2 , or the *True-Weighted Total Efficiency*, TWE_1 . TWE_2 considers only shaft power consumption, P_2 , as typically depicted in a manufacturer’s characteristic performance curve. Alternatively, TWE_1 is based on total power, P_1 , that includes the additional power of the motor, drive, or control system that powers the shaft. Figure 3 depicts P_1 , P_2 , and P_{fluid} pictorially.

The general formula for True-Weighted Total Efficiency, TWE_1 , for $i = 1$ to N operating conditions is:

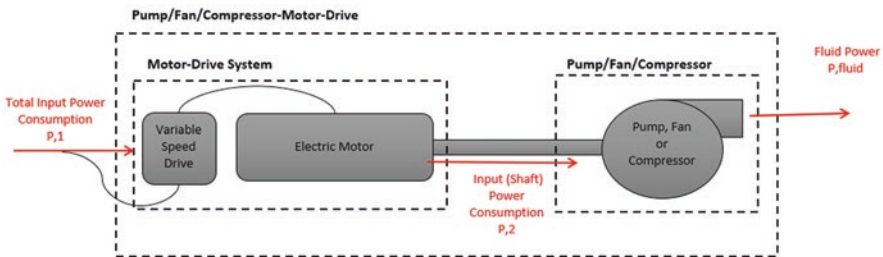


Fig. 3 Input, shaft, and fluid power in a pump/fan/compressor-motor-drive system

$$\text{TWE}_1 = \frac{E_{\text{fluid}}}{E_1} = \frac{\sum_{i=1}^N (P_{\text{fluid},i} \cdot t_i)}{\sum_{i=1}^N \left(\frac{P_{\text{fluid},i}}{\eta_{1,i}} \cdot t_i \right)} = \frac{\sum_{i=1}^N (P_{\text{fluid},i} \cdot t\%_i)}{\sum_{i=1}^N \left(\frac{P_{\text{fluid},i}}{\eta_{1,i}} \cdot t\%_i \right)} \quad (12)$$

True-Weighted Pump, Fan, or Compressor Efficiency, TWE_2 , is similarly defined as:

$$\text{TWE}_2 = \frac{E_{\text{fluid}}}{E_2} = \frac{\sum_{i=1}^N (P_{\text{fluid},i} \cdot t_i)}{\sum_{i=1}^N \left(\frac{P_{\text{fluid},i}}{\eta_{2,i}} \cdot t_i \right)} = \frac{\sum_{i=1}^N (P_{\text{fluid},i} \cdot t\%_i)}{\sum_{i=1}^N \left(\frac{P_{\text{fluid},i}}{\eta_{2,i}} \cdot t\%_i \right)} \quad (13)$$

In the special case of variable speed applications, a simplified TWE formula is developed solely on weighting factors and efficiency values. Weighting factors depend on the defined load case including the number of operating points, the percentage of operating time at each point, and the shape of the system curve. For the special case of four operating conditions (A, B, C, and D), the simplified TWE formula is written as follows:

$$\text{TWE} = \frac{1}{\frac{W_A}{\eta_A} + \frac{W_B}{\eta_B} + \frac{W_C}{\eta_C} + \frac{W_D}{\eta_D}} \quad (14)$$

A full derivation of the TWE method and a tabulation of weighting factors for different load profiles are found in [11]. The formula in Eq. (14) is also an improvement upon the PLEV (Part Load Efficiency Value) formula outlined in [11, 25].

4 Demonstration of the TWE Method

Fluid-handling equipment selection is a multi-dimensional optimization problem [2, 4, 6]. Candidate pump or compressor models (FHE) must first meet the functional requirements (FRs) of the application by satisfying the complete range of operating conditions, respecting operating speed limits, mechanical limits (shaft, bearings, pressure rating, vibration, etc.), adherence to industry specifications (API, ANSI, EN, Hydraulic Institute, ISO, AMCA, ASHRAE, etc.), general configuration and footprint dimensions, mean time between repairs (MTBR), and the operating control strategy. Candidates that satisfy the FRs are then evaluated according to a ranking or optimization scheme to determine the “best” choice.

There are three typical types of optimization strategies, each considering energy efficiency [27]. These three strategies are:

1. Maximum Design Point Efficiency
2. Maximum TWE
3. Minimum Evaluated Cost

These three strategies are illustrated in the following two case studies featuring motor-driven rotating equipment. Case Study A is based on a pump, while Case Study B is based on a turbocompressor.

4.1 Case Study A: Pump

Most pumping applications involve multiple operating conditions rather than operation at only a single design point. The TWE methodology is conveniently applied in these cases. The TWE method requires (a) a load case with a corresponding system or control curve and (b) a control method. The TWE method is illustrated using the following numerical load case.

- 100% duty condition defined as $Q_{100\%} = 75 \text{ m}^3/\text{h}$ (330.3 gpm) and $H_{100\%} = 30 \text{ m}$ (98.4 ft).
- Four Operating Conditions: A, B, C, and D with flowrates of 100%, 75%, 50%, and 25% of the 100% duty condition and corresponding operating times of 6%, 15%, 35%, and 44% respectively. This is a typical HVAC load profile as defined by Europump [13].
- An equivalent one-year uninterrupted operation 8760 h with a uniform energy cost of \$0.10/kWh.
- A parabolic-shaped system curve with the static head of 50% of the 100% duty head = $H_{\text{sh}0\%} = 15 \text{ m}$ (49.2 ft).
- Pump operating with a fixed or variable speed control method.

A web-based pump selection and optimization program is used to illustrate the numerical procedure in these strategies [28]. Most pump suppliers utilize either commercially available or proprietary pump selection programs. A list of search results of candidate pump selections are presented in Table 1. Each of the three different optimization strategies are described.

The most common efficiency-based optimization strategy is the *Maximum Design Point Efficiency Strategy*. Assuming all functional requirements (FRs) have been satisfied, the “best” or “optimal” pump selection is the one which delivers the highest overall design point efficiency. This strategy is often used because of the simplicity in selecting the best model using a single efficiency value obtained from a manufacturers catalog curve of selection software program. With reference to Table 1, the highest design point efficiency is model 100 × 80 × 200 IQ with an efficiency of 77.4% operating with a variable speed drive. The same pump can be supplied with a fixed-speed drive, but only delivers 67.3% efficiency using a direct fixed-speed drive.

The second optimization strategy is the *Maximum TWE Strategy*. This method is conveniently applied for pumping applications involving multiple operating conditions. With reference to Table 1, the model with the highest TWE is 80 × 50 × 200 IQ with a TWE of 68.8%. The 100 × 80 × 200 IQ is the next best choice delivering a slightly lower TWE of 67.5%. The TWE values are proportional to the 1-year

Table 1 List of pump candidates in Case Study A sorted by highest TWE

Size	Speed (rpm)	Design point efficiency (%)	TWE (%)	Initial purchase price, (C _i) US\$	Annual energy cost (C _e) US\$	Evaluated cost (C _{e,evaluated})1 Year US\$
80 × 50 × 200 IQ	2429 variable	65.0	68.8	\$3504	\$2463	\$5967
100 × 80 × 200 IQ	2139 variable	77.4	67.5	\$4245	\$2512	\$6757
100 × 80 × 250 IQ	1701 variable	71.5	65.2	\$4519	\$2596	\$7115
80 × 50 × 150 IQ	3033 variable	72.1	63.9	\$3342	\$2652	\$5994
100 × 80 × 200 IQ	2960 fixed	67.3	29.9	\$3345	\$5652	\$8997
80 × 50 × 200 IQ	2915 fixed	61.1	28.7	\$2604	\$5902	\$8506

Table 2 TWE calculation for the 80 × 50 × 200 IQ pump

Parameter	Operating condition				Total
	1	2	3	4	
Flow (%)	100	75	50	25	–
Flow (m ³ /h)	75	56.25	37.5	18.75	–
Operating time (%)	6	15	35	44	100
Operating time (h)	526	1314	3066	3854	8760
Energy cost, present value (\$)	0.1	0.1	0.1	0.1	–
Speed, rated (rpm)	2429	2024	1698	1482	–
Head (m)	30.01	23.45	18.82	15.95	–
Efficiency (%)	64.99	70.41	74.39	61.76	TWE = 68.82
Power, rated (kW)	9.42	5.09	2.58	1.32	–
Energy, hydraulic (kWh)	3216.70	4713.30	5884.70	3134.90	16,949.70
Energy, total (kWh)	4949.70	6694.50	7910.10	5075.90	24,630.20
Energy cost (\$)	\$494.97	\$669.45	\$791.01	\$507.59	\$2463.02

energy cost of \$2512 for 100 × 80 × 200 IQ compared to the more energy efficient 80 × 50 × 200 IQ with a 1 year energy cost of \$2463. Notice that both pumps are also available as fixed-speed options, but with much lower TWE values. This is a consequence of the fixed-speed control method that uses wasteful discharge throttling. In this example, fixed-speed control with discharge throttling has more than two times the annual energy cost compared to the same units operating with variable speed. A detailed TWE calculation for the 80 × 50 × 200 IQ is found in Table 2 and the accompanying performance curve in Fig. 4.

A few important observations can be made when contrasting the Maximum Design Point Efficiency Strategy with the Maximum TWE Strategy. First, the TWE

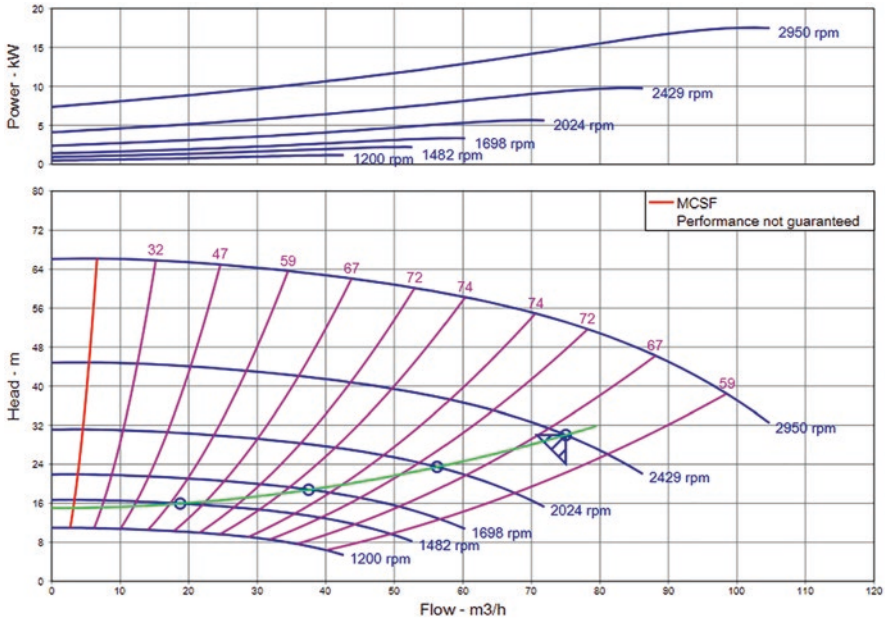


Fig. 4 Performance characteristic for the 80 × 50 × 200 IQ pump

is an efficiency metric that considers all the operating conditions in the calculation rather than the 100% design point alone. The TWE may be numerically larger or smaller than the design point efficiency. This is not a surprising result and reveals the importance of using the TWE method rather than the traditional Maximum Design Point Efficiency Strategy if the goal is to minimize energy consumption across multiple operating conditions. Second, the energy consumption for each candidate is inversely proportional to the TWE value, inherent in the principle of the TWE methodology. Therefore, the TWE of alternative pump selections will confidently indicate the proportional difference in energy consumption for both fixed or variable speed operation. This is not assured if one uses efficiency rankings such as the EEI, PEI, or PLEV [11, 25].

One of the disadvantages of the TWE Strategy is that additional calculations are needed (see Table 2) compared to the single point needed in the Maximum Design Point Strategy. This can be overcome using the simplified TWE formula found in Eq. 14. In this example, the Weighting Factors for this load case are: $W_A = 19.01\%$, $W_B = 27.84\%$, $W_C = 34.64\%$, $W_D = 18.51\%$. Then, a specifying engineer can easily calculate the TWE using the efficiency values for the four operating conditions, acquired from either Table 2 or graphically from Fig. 4 where $\eta_A = 64.99\%$, $\eta_B = 70.41\%$, $\eta_C = 74.39\%$, and $\eta_D = 61.76\%$. The TWE calculation is performed as follows, matching the previous result:

$$TWE = \frac{1}{\frac{W_A}{\eta_A} + \frac{W_B}{\eta_B} + \frac{W_C}{\eta_C} + \frac{W_D}{\eta_D}} = \frac{1}{\frac{19.01\%}{64.99\%} + \frac{27.84\%}{70.41\%} + \frac{34.64\%}{74.39\%} + \frac{18.51\%}{61.76\%}} = 68.8\% \quad (15)$$

The third optimization strategy, the *Minimum Evaluated Cost Strategy*, uses a Life Cycle Cost methodology as described in [9]. The goal in this strategy is to choose the design and operating concept with the lowest Life Cycle cost. However, during product selections, it is often difficult to consider all aspects of the LCC methodology, particularly installation and maintenance costs. Consequently, a simplified Life Cycle Cost (LCC) formula is used here that considers the equipment and energy costs directly attributed to the equipment selection (Fig. 3). With this strategy, the best choice satisfies all the functional requirements and has the lowest evaluated cost, $C_{\text{evaluated}}$. The simplified LCC equation is defined as:

$$C_{\text{evaluated}} = C_{\text{ic}} + C_e \quad (16)$$

where C_{ic} is the initial purchase price of the equipment and C_e is the energy cost to operate the equipment, directly related to the TWE, during the evaluated time period.

A summary of the $C_{\text{evaluated}}$ values for this case study are found in the last column in Table 1. In this case, the best choice is model $80 \times 50 \times 200$ IQ with a $C_{\text{evaluated}}$ of \$5967. This candidate was also the choice with the highest TWE while the lowest initial purchase price was fixed-speed model $80 \times 50 \times 150$ IQ. For short evaluation periods, the initial purchase price will dominate the evaluated cost calculation. As the evaluation period gets longer, the evaluated cost tends to be dominated by the ongoing energy costs, further emphasizing the impact of the energy cost evaluation.

4.2 Case Study B: Turbocompressor

Most compressor, fan, and blower applications also involve multiple operating conditions rather than operation at only a single design point. The TWE methodology is also applicable to this class of machine as outlined for a pump in Case Study A. This case study considers a variable speed turbocompressor with a typical performance curve as shown in Fig. 5. Here, an aeration system in a wastewater treatment plant application requires 0.60 bar differential pressure delivered with a maximum volumetric design flow of 20,000 m³/h along with a minimum flow condition of 25% of the design flow, 5000 m³/h, to satisfy off-peak loads. Unfortunately, the single turbocompressor performance shown in Fig. 5 is only capable of delivering approximately 6000 m³/h at its minimum surge flow condition and 18,200 m³/h at its maximum choke flow condition. Other models must be considered or operating multiple turbocompressors in parallel must be considered to satisfy this broad range of flow conditions. This is the subject of Case Study B.

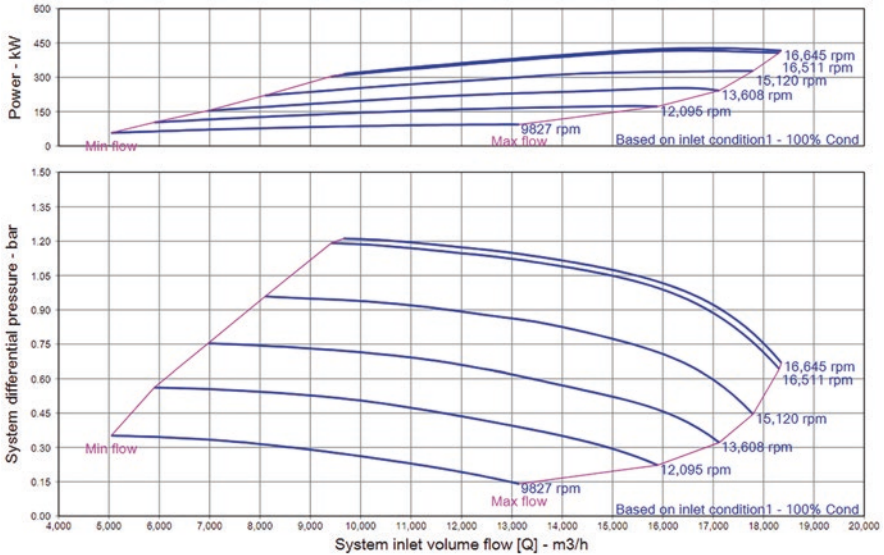


Fig. 5 Performance characteristic for turbocompressor (model IQT-80-A)

The numerical load case for Case Study B includes:

- 100% duty condition defined as $Q_{100\%} = 20,000 \text{ m}^3/\text{h}$ (11,772 cfm) and differential pressure $dP_{100\%} = 0.60 \text{ bar}$ (8.7 psi).
- Four Operating Conditions: A, B, C, and D with flowrates of 100%, 75%, 50%, and 25% of the 100% duty condition and equal operating times of 25% at each of the four conditions.
- An equivalent one-year uninterrupted operation 8760 h with a uniform energy cost of \$0.10/kWh.
- A constant pressure system curve with the static differential pressure equal to the $dP_{100\%} = 0.60 \text{ bar}$ condition.
- Turbocompressor operating with a variable speed and parallel operation.

Once again, a web-based turbocompressor selection and optimization program [28] is used to illustrate the numerical procedure in Case Study B. Search results of candidate turbocompressor selections are presented in the following table. Each of the three different optimization strategies are then described.

The *Maximum Design Point Efficiency Strategy* is applied first, optimized by model IQT-80A with two units operating and a design point efficiency of 77.0%. Using the *Maximum TWE Strategy*, the best choice is model IQT-190-A with a TWE value of 70.2%, as shown in the TWE list of values in Table 3. This method requires that all four operating conditions are satisfied while calculating the power and energy consumption at each operating condition. For this reason, model IQT-80-A does not have a calculated TWE value since this model cannot achieve the low flow, 5000 m³/h condition. Table 4 depicts the performance details and the numeric calculation of the TWE of 70.21% for model IQT-190-A operating with one, two, or

Table 3 List of turbocompressor candidates in Case Study B sorted by highest TWE

Size	Number of units operating	Design point efficiency	TWE	Initial purchase price, (C _{ic})	Annual energy cost (C _e)	Evaluated cost (C _{evaluated})1 Year
	(-)	(%)	(%)	US\$	US\$	US\$
IQT-80-A	2	77.0	-	\$225,000	-	-
IQT-190-A	3	71.1	70.2	\$525,000	\$217,905	\$742,905
IQT-120-A	4	70.2	70.2	\$560,000	\$218,015	\$778,015
IQT-180-A	3	70.1	69.2	\$480,000	\$220,971	\$700,971
IQT-190-A	2	65.3	67.9	\$350,000	\$225,570	\$575,570
IQT-180-A	2	63.8	66.6	\$320,000	\$229,512	\$549,512

Table 4 TWE calculation for the IQT-190-A turbocompressor with a total of three units available

Parameter	Operating condition				Total
	1	2	3	4	
Flow (%)	100	75	50	25	-
Flow (m ³ /h)	20,000	15,000	10,000	5000	-
Quantity of units operating	3	2	2	1	
Operating time (%)	25	25	25	25	100
Operating time (h)	2190	2190	2190	2190	8760
Energy cost, present value (\$)	0.1	0.1	0.1	0.1	-
Speed, rated (rpm)	15,597	15,968	15,086	15,086	-
Differential pressure (bar)	0.60	0.60	0.60	0.60	-
Isentropic efficiency (%)	80.06	79.34	78.31	78.31	
Total efficiency (%)	71.05	70.44	68.89	68.89	70.21
Power, rated (kW)	393	298	203	101	-
Energy, isentropic (kWh)	611,506	459,706	306,264	152,378	1,529,854
Energy, total (kWh)	860,670	652,620	444,570	221,190	2,179,050
Energy cost (\$)	\$86,067	\$65,262	\$44,457	\$22,119	\$217,905

three units in parallel. It shows the power consumption as a function of flowrate at a constant differential pressure of 0.60 bar for one, two, and three units in operation. It is apparent that one unit or two units can satisfy the 10,000 m³/h condition, while two or three units can satisfy the 15,000 m³/h condition. Since the objective of the Maximum TWE Strategy is to deliver the highest attainable TWE, two units rather than one unit operates at the 10,000 m³/h condition while three units, rather than two units, are operating at the 15,000 m³/h condition.

A few notable observations are repeated here in Case Study B as described earlier in Case Study A. First, the TWE metric includes all the operating conditions rather than the 100% design point alone, avoiding an inappropriate selection of

IQT-80-A rather than the fully compliant candidate, IQT-190-A with the highest TWE value. Second, the energy consumption for each candidate is inversely proportional to the TWE value, implicit in the TWE methodology. Therefore, comparing the TWE of alternative turbocompressor selections will confidently indicate the proportional difference in energy consumption between those models, which is not the case in using other metrics such as FEG, FER, or FEI. These non-TWE ratings are indicators of the energy efficiency of the model compared to a benchmark efficiency, not necessarily the actual application requirements.

The simplified TWE formula is also applicable in this variable speed application. The Weighting Factors for this load case are $W_A = 40\%$, $W_B = 30\%$, $W_C = 20\%$, $W_D = 10\%$ [11]. An engineer can then calculate the TWE using the efficiency values for the four operating conditions, acquired from Table 4 as $\eta_A = 71.05\%$, $\eta_B = 70.44\%$, $\eta_C = 68.89\%$, and $\eta_D = 68.89\%$. The TWE calculation is performed as follows, matching the result determined in Table 4.

$$\text{TWE} = \frac{1}{\frac{W_A}{\eta_A} + \frac{W_B}{\eta_B} + \frac{W_C}{\eta_C} + \frac{W_D}{\eta_D}} = \frac{1}{\frac{40\%}{71.05\%} + \frac{30\%}{70.44\%} + \frac{20\%}{68.89\%} + \frac{10\%}{68.89\%}} = 70.21\% \quad (17)$$

The third strategy, the *Minimum Evaluated Cost Strategy*, is numerically depicted by the $C_{\text{evaluated}}$ values in the last column in Table 3. Parallel operation of multiple turbocompressors must consider the benefit in adding the cost of an additional unit operating in parallel versus the lower energy cost consumed in that circumstance. Table 3 reveals examples of the IQT-190-A and the IQT-180-A available with two or three units. In the case of the IQT-190-A, the \$175,000 initial purchase price for one-unit results in an initial purchase price for two unit operation of \$350,000 and three unit operation of \$525,000. The incremental annual energy cost benefit in using three units is the difference between \$225,570 and \$217,905, or \$7665 per year. Buying three units versus two with a \$175,000 price difference to earn an annual energy cost savings of \$7665 is a steep cost penalty. The same circumstance applies to the IQT-180-A when comparing two or three units. The lower initial purchase price and only marginally higher annual energy cost establishes the IQT-180-A with two units operating in parallel as the best candidate with the lowest $C_{\text{evaluated}}$ of \$549,512 (Fig. 6).

Ironically, the best choice using a Minimum Evaluated Cost Strategy (IQT-180-A with two units operating) is the least attractive choice among the candidates using either the Maximum Design Point Efficiency Strategy or the Maximum TWE Strategy. This is due primarily to minor energy cost disadvantage of this unit and the substantial initial cost advantage of this candidate. There are other factors that are not considered in this simplified LCC formula such as the uptime and maintenance benefits of having an additional unit available as a standby, the time value of money, or consideration of maintenance or installation costs. All these factors are considered in a more detailed LCC evaluation, often performed by the purchaser of the equipment (i.e., the owner or specifying/consulting engineer).

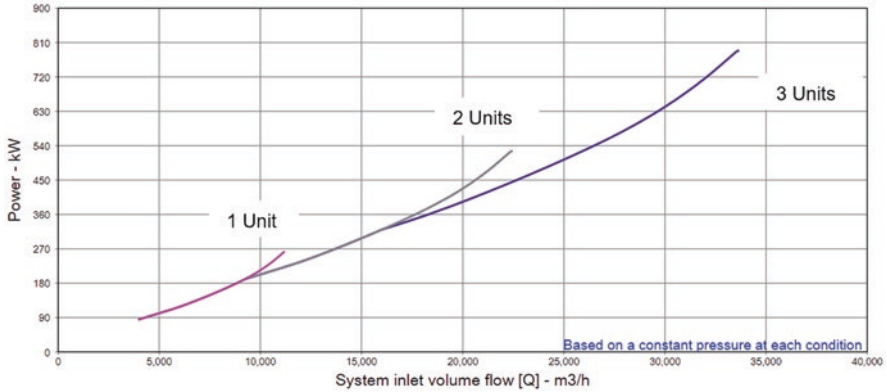


Fig. 6 Power vs. system flow for the IQT-190-A turbocompressor with multiple units operating

5 Summary

Motor-driven fluid-handling equipment such as pumps, compressors, fans, and blowers are expected to be energy efficient, either by legislation or by design. Legislation in the United States and in the European Union, among other world regions, are removing entire groups of low energy efficient products from the market by imposing energy-efficiency ratings in which regulated commercial products must comply. These energy-efficient fluid-handling machines, motors, and control systems are all having a positive effect in reducing energy consumption, cost, and their environmental impact. However, the industry needs a universal efficiency metric to help select the best model from among multiple candidates based on lowest energy consumption.

This chapter outlines a new energy-efficiency metric called True-Weighted Efficiency, TWE, that is shown to be applicable and conveniently applied to fluid-handling equipment. This method is demonstrated in two case studies and is known to be broadly applicable to many types of motor-driven fluid-handling equipment. TWE is a more robust efficiency metric than the maximum design point efficiency strategy. The TWE calculation is also incorporated into a simplified LCC strategy that considers a total evaluated cost of the equipment candidates.

The goal of this chapter is to inspire broad use of the TWE method by demonstrating that TWE is (1) an accurate and reliable measure of energy efficiency; (2) simple to describe, apply, and comprehend since it is based on the well-known principle of energy efficiency; and (3) conveniently calculated when adapted into existing equipment selection programs already pervasive in the industry or through manual calculations using the TWE formulas.

References

1. *United States Industrial Electric Motor Systems Market Opportunities Assessment*, US Department of Energy, December 1998. Can be downloaded at: <https://www.energy.gov/eere/amo/downloads/united-states-industrial-electric-motor-systems-market-opportunities-assessment>
2. T. Dahl, V. Patel, Chapter 14: Selecting and purchasing pumps, in *Pump Handbook*, 4th edn., (McGraw Hill Book Co., New York, 2008) ISBN 978-0-07-146044-6
3. S.L. Dixon, C.A. Hall, *Fluid Mechanics and Thermodynamics of Turbomachinery*, 7th edn. (Elsevier, Inc., 2014) ISBN 978-0124159549
4. T. Dahl, J. Ochs, *Preliminary Pump Selection and Configuration in an Engineered-to-Order Environment*. ASME Fluids Engineering Division Summer Meeting, FEDSM'97. June 22–26, 1997. FEDSM97-3336. Can be downloaded at: <https://intelliquip.com/wp-content/uploads/2018/05/FEDSM97-3336.pdf>
5. T. Dahl, *The Evolution of the Pump Business in the Information Age*. Proceedings of the ASME FEDSM'01, 2001 ASME Fluids Engineering Division Summer Meeting, May 29–June 1, 2001. FEDSM2001-18069. Can be downloaded at: <https://intelliquip.com/wp-content/uploads/2018/05/FEDSM2001-18069-1.pdf>
6. T. Dahl, *Development of a Design System for an Engineered-to-Order Product Line*. PhD Dissertation, Lehigh University, Bethlehem, PA. 1997
7. *Pump Systems Optimization: A Guide for Improved Energy Efficiency, Reliability, and Profitability* (Hydraulic Institute, 2018). ISBN 978-1935762744
8. *Application Guideline for Variable Speed Pumping* (Hydraulic Institute, 2017). ISBN 978-1-935762-59-1
9. *Pump Life Cycle Costs: A Guide to LCC Analysis for Pumping Systems* (Hydraulic Institute and Europump, 2001). ISBN 1-888952-58-0
10. A. Mahdavian, M. Mohamadian, *An Energy Efficient Approach for Flow Control of Parallel Blowers*. 11th International Conference on Environment and Electrical Engineering, IEEE, 18–25 May 2012. ISBN: 978-1-4577-1829-8
11. T. Dahl, *The Theory and Application of True Weighted Efficiency – A New Metric to Evaluate Pump Energy Efficiency Considering Multiple Operating Conditions*. Proceedings of the 47th Turbomachinery and 34th Pump Symposia, Houston TX, 17–20 Sept. 2018
12. Commission Regulation (EU) No 547/2012 of 25 June 2012 implementing Directive 2009/125/EC of the European Parliament and of the Council with regard to ecodesign requirements for water pumps. Can be downloaded at: <https://eur-lex.europa.eu/legal-content/EN/TXT/PDF/?uri=CELEX:32012R0547&from=IT>
13. *Europump, Extended Product Approach for Pumps: A Europump Guide*, Draft 27 October 2014. Can be downloaded at: [https://europump.net/uploads/Extended%20Product%20Approach%20for%20Pumps%20-%20A%20Europump%20guide%20\(27OCT2014\).pdf](https://europump.net/uploads/Extended%20Product%20Approach%20for%20Pumps%20-%20A%20Europump%20guide%20(27OCT2014).pdf)
14. Department of Energy 10 CFR 431 Subpart Y – Energy Conservation Standard and Test Procedure for Pumps. 2016. Can be downloaded at: <https://www.ecfr.gov/cgi-bin/text-idx?SID=c47d5f0d51131748848a5e8d41c2972b&mc=true&node=sp10.3.431.y&rgn=div6>
15. Department of Energy 10 CFR Parts 429 and 431 [Docket Number EERE-2011-BT-STD-0031] RIN 1904-AC54, Energy Conservation Program: Energy Conservation Standards for Pumps. Can be downloaded at: <https://www.energy.gov/sites/prod/files/2015/12/f28/Pumps%20ECS%20Final%20Rule.pdf>
16. HI 40.7-2015, *Hydraulic Institute Program Guide for Pump Test Laboratory Approval* (Hydraulic Institute 40.7, 2015)
17. HI 40.5-2016, *Program Guide for HI Energy Rating Program* (Hydraulic Institute 40.5, 2016)
18. HI 40.6-2016, *Methods for Rotodynamic Pump Efficiency Testing* (Hydraulic Institute 40.6, 2016)
19. J. Cermak, M. Ivanovich, Fan efficiency requirements for standard 90.1-2013. *ASHRAE J.*, April 2013

20. ISO 12759:2010 *Fans – Efficiency Classification for Fans*. Can be ordered from: <https://www.iso.org/standard/51665.html>
21. ANSI/AMCA 205-12 – Energy Efficiency Classification for Fans. Can be downloaded at: <https://webstore.ansi.org/Standards/AMCA/ANSIAMCA20512>
22. ANSI/ASHRAE/IES Standard 90.1-2016. Can be ordered from: <https://www.energycodes.gov/resource-center/training-courses/ansiashraeies-standard-901-2016>
23. Department of Energy 10 CFR Parts 429 and 430 [Docket Number EERE-2010-BT-STD-0011] RIN: 1904-AC22, Energy Conservation Program for Consumer Products: Energy Conservation Standards for Residential Furnace Fans
24. Department of Energy 10 CFR Part 431 [Docket No. EERE-2013-BT-STD-0006] RIN: 1904-AC55, Energy Conservation Standards for Commercial and Industrial Fans and Blowers: Availability of Provisional Analysis Tools
25. T. Dahl, *True Weighted Efficiency: A Different Method for Comparing Pumps* (Pumps and Systems, January 2018)
26. *Hydraulic Institute Rotodynamic (Centrifugal) Pumps – Definitions – Section 1.2.6* (Hydraulic Institute, 2014)
27. T. Dahl, *Optimizing Pump Selection for Energy Efficiency Across Multiple Operating Conditions using True Weighted Efficiency (TWE)*. Proceedings of the ASME-JSME-KSME 2019 Joint Fluids Engineering Conference, AJKFLUIDS2019, (Pending 28 July–1 August, 2019)
28. www.intelliquip.com